HEAD & NECK CANCER AND ESOPHAGEAL CANCER: FROM BIOSIGNATURES TO THERAPEUTICS

EDITED BY: Victor C. Kok, Cheng-Chia Yu and Jorge A. R. Salvador
PUBLISHED IN: Frontiers in Oncology

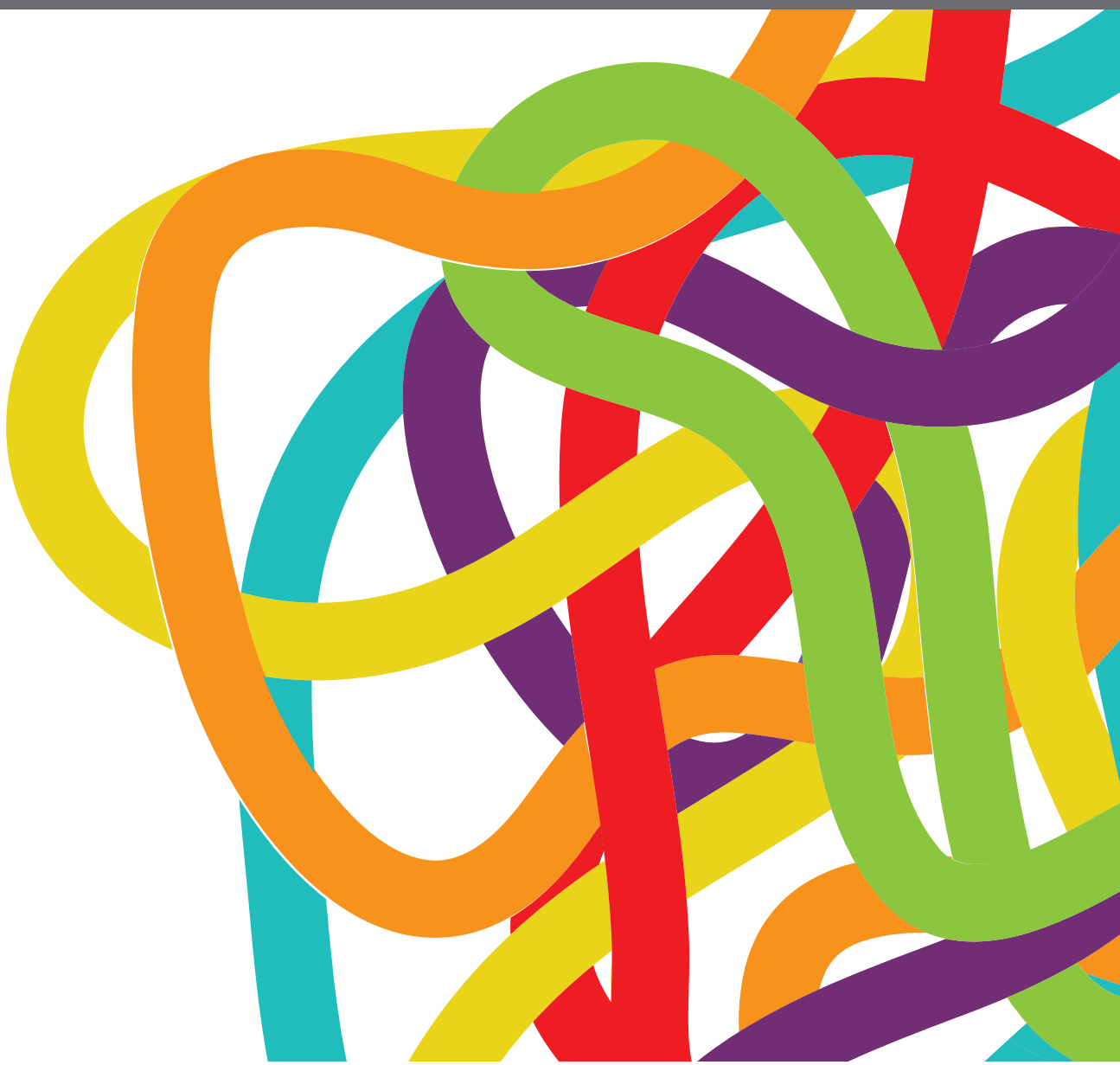

frontiers Research Topics

ISSN 1664-8714
ISBN 978-2-88966-759-8
DOI 10.3389/978-2-88966-759-8

About Frontiers

Frontiers is more than just an open-access publisher of scholarly articles: it is a pioneering approach to the world of academia, radically improving the way scholarly research is managed. The grand vision of Frontiers is a world where all people have an equal opportunity to seek, share and generate knowledge. Frontiers provides immediate and permanent online open access to all its publications, but this alone is not enough to realize our grand goals.

Frontiers Journal Series

The Frontiers Journal Series is a multi-tier and interdisciplinary set of open-access, online journals, promising a paradigm shift from the current review, selection and dissemination processes in academic publishing. All Frontiers journals are driven by researchers for researchers; therefore, they constitute a service to the scholarly community. At the same time, the Frontiers Journal Series operates on a revolutionary invention, the tiered publishing system, initially addressing specific communities of scholars, and gradually climbing up to broader public understanding, thus serving the interests of the lay society, too.

Dedication to Quality

Each Frontiers article is a landmark of the highest quality, thanks to genuinely collaborative interactions between authors and review editors, who include some of the world's best academicians. Research must be certified by peers before entering a stream of knowledge that may eventually reach the public - and shape society; therefore, Frontiers only applies the most rigorous and unbiased reviews.
Frontiers revolutionizes research publishing by freely delivering the most outstanding research, evaluated with no bias from both the academic and social point of view. By applying the most advanced information technologies, Frontiers is catapulting scholarly publishing into a new generation.

What are Frontiers Research Topics?

Frontiers Research Topics are very popular trademarks of the Frontiers Journals Series: they are collections of at least ten articles, all centered on a particular subject. With their unique mix of varied contributions from Original Research to Review Articles, Frontiers Research Topics unify the most influential researchers, the latest key findings and historical advances in a hot research area! Find out more on how to host your own Frontiers Research Topic or contribute to one as an author by contacting the Frontiers Editorial Office: frontiersin.org/about/contact

HEAD & NECK CANCER AND ESOPHAGEAL CANCER: FROM BIOSIGNATURES TO THERAPEUTICS

Topic Editors:
Victor C. Kok, Asia University, Taiwan
Cheng-Chia Yu, Chung Shan Medical University, Taiwan
Jorge A. R. Salvador, University of Coimbra, Portugal

Citation: Kok, V. C., Yu, C.-C., Salvador, J. A. R., eds. (2021). Head & Neck Cancer and Esophageal Cancer: From Biosignatures to Therapeutics. Lausanne: Frontiers Media SA. doi: 10.3389/978-2-88966-759-8

Table of Contents

frontiers in Oncology

EDITORIAL
published: 19 March 2021
doi: 10.3389/fonc.2021.666103

Editorial: Head & Neck Cancer and Esophageal Cancer: From Biosignatures to Therapeutics

Victor C. Kok[1,2]*, *Cheng-Chia Yu*[3,4] *and Jorge A.R. Salvador*[5]

[1] Division of Medical Oncology, Kuang Tien General Hospital Cancer Center, Taichung, Taiwan, [2] Department of Bioinformatics and Medical Engineering, Asia University Taiwan, Taichung, Taiwan, [3] Institute of Oral Sciences, Chung Shan Medical University, Taichung, Taiwan, [4] School of Dentistry, Chung Shan Medical University, Taichung, Taiwan, [5] Faculdade de Farmácia da Universidade de Coimbra, Pólo das Ciências da Saúde—Azinhaga de Santa Comba, Coimbra, Portugal

Keywords: head and neck squamous cancer cells, biosignatures, cancer biomarker detection, therapeutic developments, immune evasion

Head and neck cancers (excluding thyroid cancer) account for 4.9% of total cancers diagnosed worldwide (1). Optimizing better selection of different therapeutic strategies in head and neck cancer suffers from multiple unmet medical needs because of the critical anatomical site from which cancer arises, chemo- and radioresistance, lacking actionable driver mutations while showing both innate and acquired resistance to immune checkpoint blockade (Kok). Multifaceted cancer management cannot be successful without incorporating measurable and quantifiable biological biomarkers, such as specific enzyme concentration, imaging characteristics, gene phenotype, and metabolomic expression profiles. These biomarkers serve as indicators for cancer risk estimation, prognostication, and treatment monitoring in HNSCC and should be continually investigated.

P16 (INK4A) is an established prognostic biomarker in oropharyngeal cancer, and testing for it has been mandatory in this subgroup of cancer patients (2). Nevertheless, emerging evidence has also supported that P16 has similar prognostication in non-oropharyngeal cancer such as hypopharyngeal, laryngeal, and oral squamous cell carcinoma (OSCC) (3, 4). Over the past few years, rapid advances in genome analysis techniques have opened new possibilities for studying transcriptomes. In 2015, The Cancer Genome Atlas (TCGA) network demonstrated the somatic genome alterations from 279 HNSCC, revealing the genome alterations in P16-positive or smoking-related P16-negative HNSCC, as well as the therapeutic candidate alterations (5). Moreover, increasing evidence has suggested the significant role of aberrantly expressed microRNAs or long non-coding RNAs in head and neck cancer. Furthermore, molecular characterization of HNSCCs will better understand the carcinogenesis and cancer progression process and therapeutic implications. In this Research Topic, we have published studies providing new insights into genetic alterations or novel biological mechanisms underlying the carcinogenesis of head and neck cancer, molecular biomarkers, genomic (e.g., mRNA and long non-coding RNA), or metabolomic or expression profiles for head and neck cancer prognosis, emerging, candidate or novel biomarkers *in silico* or *in vivo* research, biomarkers indicative of resistance to chemotherapeutic or radiation therapy, prognostic or predictive outcome biomarkers, imaging biomarkers of hypoxia or stemness in head and neck cancer using positron emission tomography-computed tomography as an emerging imaging biomarker of occult neck lymph node metastasis in early-stage node-negative tongue cancer.

Unbalanced N^6-methyladenosine regulation, which affects RNA transcriptional modification, can be carcinogenic, which a paper in our Research Topic has investigated and confirmed its involvement

OPEN ACCESS

Edited and reviewed by:
Andreas Dietz,
Leipzig University, Germany

***Correspondence:**
Victor C. Kok
victorkok@asia.edu.tw

Specialty section:
This article was submitted to Head and Neck Cancer, a section of the journal Frontiers in Oncology

Received: *09 February 2021*
Accepted: *02 March 2021*
Published: *19 March 2021*

Citation:
Kok VC, Yu C-C and Salvador JAR (2021) Editorial: Head & Neck Cancer and Esophageal Cancer: From Biosignatures to Therapeutics. Front. Oncol. 11:666103. doi: 10.3389/fonc.2021.666103

in HNSCC (Zhou et al.). BRAF and its complex component, BCL11A, are known to be altered either as mutation, amplification, or deep deletion in approximately 5% of HNSCC (cBioPortal). Zhou et al. discovered that high levels of BCL11A found in laryngeal SCC tissues, as demonstrated in immunohistochemical staining, were associated with advanced lymph node metastasis and poor prognosis and positively correlated with MDM2 expression. Ambele et al. reported their discovery of a case of oral SCC presenting with high confidence BRAF:p.G469A:c.1406G>C somatic mutation. To investigate the homeobox A cluster (HOXA) gene family as a prognostic factor in laryngeal SCC, Li et al. found that HOXA2 and HOXA4 were downregulated whereas HOXA7 and HOXA9–13 were upregulated in laryngeal SCC. A study from central Taiwan investigated the association between the genotypes, the allelic frequency of long pentraxin 3 (PTX3, also known as TGF14) single-nucleotide variations, and the risk of oral cavity cancer in men (Yeh et al.). In the study, the combined effect of cigarette smoking and PTX3 polymorphism considerably increased the odds of late-stage oral cancer and lymph node metastases (Yeh et al.). Matrix metalloproteinases (MMPs) are implicated in carcinogenesis and cancer progression. It is interesting to note that the transcriptional expression of MMP25 is associated with earlier stage HNSCC, as demonstrated by an *in silico* study using The Cancer Genome Atlas dataset (Liang et al.). The authors have shown that the increased MMP25 expression correlates with increased immune infiltration levels in HNSCC, which significantly activated CD4+ memory T cells (Liang et al.). Resorting to metabolic reprogramming is a cancer hallmark of HNSCC, while increased glycolytic flux is a feature of cancer cells (the Warburg effect). Taking advantage of targeting the glycolysis in cancer cells, scientists have a strong rationale for pursuing glycolytic inhibitors in treating HNSCC. Hexokinase 2 (HK2) is the first enzyme of glycolysis. Li et al. discovered in their study that HNSCC is a glycolytic tumor, and HK2 inhibition does trigger a metabolic shift away from aerobic glycolysis toward mitochondrial metabolism. SMAD4 (also known as Deleted in Pancreatic Cancer-4, DPC4) is a tumor suppressor gene that mediates the TGF-β signaling. Low SMAD4 expression is associated with an approximately 5-fold increase of relapse during follow-up in a cohort of 122 HNSCC patients after adjusting for age, gender, and clinical stage (Lin et al.). Lin et al. leveraging next-generation sequencing analysis based on multiplex-PCR demonstrate that missense SMAD4 mutations could be a potential prognostic biomarker in patients with HNSCC.

Regarding radiological biomarkers development, our Research Topic has two relevant papers investigating the role of positron emission tomography-computerized tomography (PET-CT) scanning in the management of cT1-2N0M0 tongue cancer. In a prospectively enrolled cohort of patients, Zhao et al. found that PET-CT is useful in predicting occult lymph node metastasis; typically, when the SUV max is >9.0, it is significantly associated with worse locoregional control in this subgroup of cT1-2N0 tongue cancer patients. In their retrospective study, Zhu et al. suggested that neck dissection may be avoided when the PET-CT scan reveals no neck lymph node involvement.

We have two bioinformatics research papers using *in silico* methodology to deduce significant gene signatures in HNSCC. Li et al. utilized Weighted Gene Co-expression Network Analysis (WGCNA), differential gene expression analysis, and protein-protein interaction network construction to deduce ten hub genes related to survival from HNSCC. Yang and colleagues leveraged bioinformatics algorithms to establish a long non-coding RNA (lncRNA) signature associated with the prognosis of patients with HNSCC. The investigators ultimately demonstrated an eight lncRNA signature that may be useful in predicting the prognosis; furthermore, they showed that patients with high signature scores might have an abnormal immune function (Yang et al.).

Therapeutic development for HNSCC still requires more research effort to test for novel agents. We have five original articles on trying five chemicals or combinations in controlling HNSCCs. Five independent studies report pre-clinical evaluation of the anti-HNSCC activity of the following agents, hydroxygenkwanin, arsenic trioxide combined with cisplatin, pinostilbene hydrate, psorachromene, and taiwanin E.

Previous studies had revealed that hydroxygenkwanin (HGK), a flavonoid extracted from *Daphne genkwa* Sieb. et Zucc. exhibits anti-cancer effect. Huang and colleagues demonstrated that HGK might be an effective natural product for oral cancer therapy that inhibited cell growth dose-dependently in SAS and OCEM1 cells. They further showed the HGK induced the cell cycle arrest by flow cytometry and inhibited colony formation ability and cell movement. HGK induced intrinsic cell apoptosis pathway and caused cell cycle arrest through p21 activation (Huang et al.).

Hu and colleagues analyzed the inhibitory tumorigenicity of co-treatment with arsenic trioxide and cisplatin on head and neck cancer-initiating cells (HN-CICs) enriched from HNSCC cells. They observed that this drug combination strategy successfully synergized the cell death on HN-CICs with a Combination Index (CI) <1 by Chou-Talalay's analysis *in vitro* (Hu et al.). In addition, this therapeutic regimen also showed both preventive and therapeutic effects by *in vivo* xenograft assays.

Pinostilbene hydrate (PSH) significantly decreases the activity and expression of MMP-2 and markedly inhibits the abilities of cancer cell migration and invasion (Tseng et al.). Moreover, combined treatment of PSH with ERK1/2 inhibitor (U0126) caused significant elevation of the activity and the expression of MMP-2. Besides, PSH upregulated claudin-1 and E-cadherin expression levels while downregulating vimentin and N-cadherin on two nasopharyngeal carcinoma cell lines (Tseng et al.).

Psorachromene is an isoflavone component isolated from the fruit kernels of *P. corylifolia* L. with anti-inflammatory effects and no previous studies on its anti-cancer activity. Wang and colleagues studied the antitumor effects of psorachromene using cells and animal models of OSCC. Their results revealed that psorachromene significantly inhibited cell proliferation, migration, and invasiveness and increased chemotherapeutic agents' toxic effects against OSCC cells (Wang et al.).

Taiwanin E is a bioactive compound extracted from *Taiwania cryptomerioides* Hayata. Wang and colleagues studied the anti-cancer effect of taiwanin E against arecoline and 4-nitroquinoline-1-oxide-induced OSCC and elucidated the underlying intricacies. The results showed that taiwanin E significantly attenuated oral cancer cells' cell viability without significant cytotoxic effects for normal oral cells (N28) (Wang et al.).

In conclusions, we are humble to prepare this editorial after we have formally published the last paper included in this Research Topic because the road in search of the diagnostic, prognostic, and predictive biosignatures for specific settings in HNSCC is still a long way to go and therapeutic development to conquer this debilitating cancer is still flourishing. Nevertheless, colleagues worldwide have strong determinations to do good research on HNSCCs. Through the bit by bit of medical breakthrough, we will someday achieve great success in managing HNSCCs.

AUTHOR CONTRIBUTIONS

All authors contributed significantly as guest associate editor and provided feedback on the Editorial. All authors agree on the final manuscript and further publication. All authors contributed to the article and approved the submitted version.

ACKNOWLEDGMENTS

All three co-editors for this Research Topic would like to thank Prof. George D. Demetri, Prof. Ed Harlow, and Prof. Peter Howley, the renowned Harvard Medical School's High-Impact Cancer Research certificate program's Program Directors. During this program, the editors were inspired by the professors' teaching and decided to team up for carrying out this Research Topic project.

REFERENCES

1. Bray F, Ferlay J, Soerjomataram I, Siegel RL, Torre LA, Jemal A. Global cancer statistics 2018: GLOBOCAN estimates of incidence and mortality worldwide for 36 cancers in 185 countries. *CA Cancer J Clin* (2018) 68(6):394–424. doi: 10.3322/caac.21492
2. Weinberger PM, Yu Z, Haffty BG, Kowalski D, Harigopal M, Brandsma J, et al. Molecular classification identifies a subset of human papillomavirus–associated oropharyngeal cancers with favorable prognosis. *J Clin Oncol* (2006) 24(5):736–47. doi: 10.1200/jco.2004.00.3335
3. Wendt M, Romanitan M, Näsman A, Dalianis T, Hammarstedt L, Marklund L, et al. Presence of human papillomaviruses and p16 expression in hypopharyngeal cancer. *Head Neck* (2014) 36(1):107–12. doi: 10.1002/hed.23394
4. Shaughnessy JN, Farghaly H, Wilson L, Redman R, Potts K, Bumpous J, et al. HPV: a factor in organ preservation for locally advanced larynx and hypopharynx cancer? *Am J Otolaryngol* (2014) 35(1):19–24. doi: 10.1016/j.amjoto.2013.08.006
5. Leemans CR, Snijders PJF, Brakenhoff RH. The molecular landscape of head and neck cancer. *Nat Rev Cancer* (2018) 18(5):269–82. doi: 10.1038/nrc.2018.11

Conflict of Interest: The authors declare that the research was conducted in the absence of any commercial or financial relationships that could be construed as a potential conflict of interest.

frontiers in Oncology

ORIGINAL RESEARCH
published: 03 July 2019
doi: 10.3389/fonc.2019.00581

Functional Genetic Variant of Long Pentraxin 3 Gene Is Associated With Clinical Aspects of Oral Cancer in Male Patients

Chia-Ming Yeh[1,2,3], *Chiao-Wen Lin*[4,5], *Chun-Yi Chuang*[6,7], *Yu-Fan Liu*[8], *Chia-Hsuan Chou*[1], *Shun-Fa Yang*[1,9]* and *Mu-Kuan Chen*[1,2,3]*

[1] Institute of Medicine, Chung Shan Medical University, Taichung, Taiwan, [2] Cancer Research Center, Changhua Christian Hospital, Changhua, Taiwan, [3] Department of Otorhinolaryngology-Head and Neck Surgery, Changhua Christian Hospital, Changhua, Taiwan, [4] Institute of Oral Sciences, Chung Shan Medical University, Taichung, Taiwan, [5] Department of Dentistry, Chung Shan Medical University Hospital, Taichung, Taiwan, [6] School of Medicine, Chung Shan Medical University, Taichung, Taiwan, [7] Department of Otolaryngology, Chung Shan Medical University Hospital, Taichung, Taiwan, [8] Department of Biomedical Sciences, College of Medicine Sciences and Technology, Chung Shan Medical University, Taichung, Taiwan, [9] Department of Medical Research, Chung Shan Medical University Hospital, Taichung, Taiwan

OPEN ACCESS

Edited by:
Victor C. Kok,
Asia University, Taiwan

Reviewed by:
Jiiang-Huei Jeng,
National Taiwan University, Taiwan
Amanda Ewart Toland,
The Ohio State University, United States

***Correspondence:**
Shun-Fa Yang
ysf@csmu.edu.tw
Mu-Kuan Chen
53780@cch.org.tw

Specialty section:
This article was submitted to Head and Neck Cancer, a section of the journal Frontiers in Oncology

Received: *25 March 2019*
Accepted: *14 June 2019*
Published: *03 July 2019*

Citation:
Yeh C-M, Lin C-W, Chuang C-Y, Liu Y-F, Chou C-H, Yang S-F and Chen M-K (2019) Functional Genetic Variant of Long Pentraxin 3 Gene Is Associated With Clinical Aspects of Oral Cancer in Male Patients. Front. Oncol. 9:581. doi: 10.3389/fonc.2019.00581

Long pentraxin 3 (PTX3) is produced by various cell types and is correlated with tumor progression in various tumor types. However, the clinical significance of *PTX3* polymorphisms in oral cancer and their correlation with the risk of cancer are still unclear. In this study, we assessed the influence of *PTX3* gene polymorphisms and environmental factors on susceptibility to oral tumorigenesis. We recruited 865 cases with oral cancer and 1,189 controls. Four single-nucleotide variations of the *PTX3* gene (rs1840680, rs2305619, rs3816527, and rs2120243) were verified using a real-time polymerase chain reaction in control participants and cases with oral cancer. We found that rs3816527 in smokers was correlated with the development of late-stage cancer (odds ratio [OR], 2.328; 95% confidence interval [CI], 1.078–5.027) and increased lymph node metastasis (OR, 2.152; 95% CI, 1.047–4.422). Moreover, additional bioinformatics analysis results showed that the rs3816527 C allele variant to the A allele exhibited the strongest exonic splicing enhancer activity. In conclusion, our results suggested that *PTX3* rs3816527 plays a role in oral cancer development.

Keywords: long pentraxin 3, oral squamous cell carcinoma, single-nucleotide variation, metastasis, splicing, tumor progression

INTRODUCTION

The incidence of oral cancer in Asia and more particularly Taiwan increases annually. In addition to tobacco smoking and alcohol consumption, betel quid chewing is a major cause of oral cancer (1–4). Moreover, the annual number of deaths due to oral cancer among men is increasing rapidly (5). The global 5 year mortality rate of oral cancer is ∼50%. Although considerable progress has been made in surgery, chemotherapy, and radiotherapy, no considerable improvements have been made in the preceding 50 years (6).

TABLE 1 | Information on *PTX3* SNPs.

Variable	rs2120243	rs2305619	rs3816527	rs1840680
Chromosome	3:157429779	3:157437072	3:157437525	3:157438240
Exon	–	–	2	–
Nucleotide change	A>C	A>G	C>A	A>G
mRNA position	–	–	286	–
Function	TFBS	Intron variant	Non-synonymous	Intron variant
dbSNP allele	–	–	GCC ⟹ GAC	–
Protein residue	–	–	A [Ala] ⟹ D [Asp]	–
Allele frequencies	0.6744	0.6358	0.7845	0.6738

Allele frequencies were obtained from population databases gnomAD (https://gnomad.broadinstitute.org/) for East Asian population.

Pentraxins (PTXs) are a superfamily of conserved proteins that contain the pentraxin domain. Proteins of the pentraxin family are multifunctional and participate in acute immunological responses (7). PTX3, also known as TGF14, is a transmembrane molecule expressed in a variety of human tissues (8, 9). PTX3 is secreted by natural immune cells in response to inflammatory cytokines, such as interleukin-1 β (IL-1β) and tumor necrosis factor α (TNFα), or selected pathogen-associated molecular patterns (9–11). Therefore, *PTX3* may play a vital role at the crossroads of inflammation increase (12, 13), innate immunity (14–16), tissue repair stimulation (17, 18), and cancer (19–21). *PTX3* promotes cell migration and invasion in several cancers, and the expression of *PTX3* correlates with tumor progression in various human tumor types (19, 22–24).

Genetic variations contribute to susceptibility to common diseases such as cardiovascular disease, diabetes, inflammatory disease, and cancer (25–29). Single-nucleotide variations (SNVs) may be a causative genetic variant that can affect the expression and structure of proteins, thereby directly contributing to disease (30). The *PTX3* gene is located on chromosome 3 and contains three exons and two introns. Previous studies have described that SNVs in *PTX3* (rs2305619 and rs1840680) have functional significance. Results indicated that the A allele of *PTX3* SNVs (rs2305619 and rs1840680) is associated with higher plasma levels of PTX3 (31, 32). In addition, the A alleles of rs2305619 and rs1840680 are associated with susceptibility to *Pseudomonas aeruginosa* and *Mycobacterium tuberculosis* infections (33, 34). Carmo et al. also revealed that genetic variations in *PTX3* (rs2305619 and rs1840680) and plasma levels were associated with hepatocellular carcinoma (35). Moreover, Hakelius et al. indicated that PTX3 played a major role in non-malignant and oral cancer malignant disease processes (36). However, few studies have investigated the association of *PTX3* polymorphisms in oral cancer. Therefore, we investigated the relationship between four *PTX3* gene polymorphisms (rs1840680, rs2305619, rs3816527, and rs2120243; **Table 1**) and clinicopathological characteristics of patients with oral cancer to identify those with an increased risk of oral cancer.

Abbreviations: PTX3, long pentraxin 3; OSCC, oral squamous cell carcinoma; OR, odds ratio; SNV, single-nucleotide variation.

TABLE 2 | Distribution of demographic characteristics in 1,189 controls and 865 male individuals with oral cancer.

Variable	Controls (*N* = 1,189)	Cases (*N* = 865)	*p*-value
AGE (YRS)			
≦55	607 (51.0%)	454 (52.5%)	$p = 0.521$
>55	582 (49.0%)	411 (47.5%)	
BETEL QUID CHEWING			
No	991 (83.4%)	188 (21.7%)	$p < 0.001$*
Yes	198 (16.6%)	677 (78.3%)	
CIGARETTE SMOKING			
No	558 (46.9%)	99 (11.5%)	$p < 0.001$*
Yes	631 (53.1%)	766 (88.5%)	
ALCOHOL DRINKING			
No	954 (80.2%)	414 (47.9%)	$p < 0.001$*
Yes	235 (19.8%)	451 (52.1%)	
STAGE			
I+II		431 (49.8%)	
III+IV		434 (50.2%)	
TUMOR T STATUS			
T1+T2		496 (57.3%)	
T3+T4		369 (42.7%)	
LYMPH NODE STATUS			
N0		583 (67.4%)	
N1+N2+N3		282 (32.6%)	
METASTASIS			
M0		856 (99.0%)	
M1		9 (1.0%)	
CELL DIFFERENTIATION			
Well-differentiated		119 (13.8%)	
Moderately or poorly differentiated		746 (86.2%)	

Mann–Whitney U-test or Fisher's exact test was used between healthy controls and individuals with oral cancer. $^{*}p < 0.05$ *was considered statistically significant.*

MATERIALS AND METHODS

Study Population

The participants of this case–control study were 865 male cases with oral cancer of squamous cell carcinoma recruited from Changhua Christian Hospital in Changhua and Chung Shan Medical University Hospital in Taichung, Taiwan, between 2007 and 2017, and 1,189 cancer-free male controls selected from the Taiwan Biobank. The oral cancers of squamous cell carcinoma in this study were pre-specified to include any cancers that originated from buccal mucosa ($n = 314$; 36.3%), tongue ($n = 268$; 31.0%), gingiva ($n = 78$; 9.0%), palate ($n = 40$; 4.6%), floor of the mouth ($n = 25$; 2.9%), and other areas ($n = 140$; 16.2%). The Institutional Review Board of Chung Shan Medical University approved this study (CSMUH No: CS13214-1). All participants provided written informed consent. Personal characteristics and information, including demographic characteristics; tobacco smoking, betel quid chewing, and alcohol consumption habits; and the medical histories of the participants, were investigated using interviewer-administered questionnaires.

Determination of Genotypes

Genomic DNA from peripheral blood leukocytes was extracted using a QIAamp DNA Blood Mini Kit (Qiagen, Valencia, CA, USA) following the manufacturer's protocol (37). DNA was dissolved in ethylenediaminetetraacetic acid (EDTA) buffer (10 mM Tris, 1 mM EDTA; pH 7.8) and then quantified by measuring absorbance at 260 nm. Finally, the preparation was stored in a −20°C refrigerator and later analyzed using a real-time polymerase chain reaction (PCR) system. Allelic discrimination for the PTX3 SNV was performed using a TaqMan assay (ID C_12069244_10 for rs1840680, C_22275654_10 for rs2305619, C_3035766_30 for rs3816527, and C_11796613_20 for rs2120243) with an ABI StepOne Real-Time PCR System (Applied Biosystems). The genotypic frequencies of *PTX3* were further evaluated using the SDS v3.0 software program.

Bioinformatics Analysis

Several bioinformatics tools were used to assess the putative functional relevance of the rs3816527 PTX3 polymorphism. SNPinfo was used to predict the function of the rs351855 polymorphism. Splicing enhancement activity was analyzed using ESEfinder. We used the National Center for Biotechnology Information (NCBI) database to determine splicing types of PTX3. Furthermore, protein structure homology modeling of PTX3 was performed using SWISS-MODEL.

Statistical Analysis

The Mann–Whitney *U*-test was used to compare differences in demographic characteristics between healthy controls and cases with oral cancer. Multiple logistic regression models were used to determine the association between genotypic frequencies and oral cancer risk after adjustment for age, betel quid chewing, cigarette smoking, and alcohol consumption. Data were analyzed using SAS 9.1 statistical software. A $p < 0.05$ was considered significant.

RESULTS

Demographic Characteristics of the Participants

Table 2 displays the results of the statistical analysis of the participants' demographic characteristics. A total of 2,054

TABLE 3 | Genotyping and allelic frequency of *PTX3* single-nucleotide variations (SNVs) in individuals with oral cancer and controls.

Variable	Controls (*N* = 1,189 (%))	Cases (*N* = 865 (%))	OR (95% CI)	AOR (95% CI)
rs1840680				
GG	531 (44.7%)	375 (43.4%)	1.000 (reference)	1.000 (reference)
GA	532 (44.7%)	407 (47.0%)	1.083 (0.901–1.303)	1.056 (0.832–1.341)
AA	126 (10.6%)	83 (9.6%)	0.933 (0.686–1.268)	0.876 (0.591–1.297)
GA+AA	658 (55.3%)	490 (56.6%)	1.054 (0.884–1.258)	1.020 (0.812–1.281)
G allele	1594 (67.0%)	1157 (66.9%)	1.000 (reference)	1.000 (reference)
A allele	784 (33.0%)	573 (33.1%)	1.007 (0.883–1.149)	0.978 (0.825–1.159)
rs2305619				
GG	493 (41.5%)	346 (40.0%)	1.000 (reference)	1.000 (reference)
GA	550 (46.3%)	428 (49.5%)	1.109 (0.920–1.336)	1.126 (0.885–1.433)
AA	146 (12.2%)	91 (10.5%)	0.888 (0.661–1.194)	0.786 (0.537–1.151)
GA + AA	696 (58.5%)	519 (60.0%)	1.062 (0.889–1.270)	1.050 (0.835–1.322)
G allele	1536 (64.6%)	1120 (64.7%)	1.000 (reference)	1.000 (reference)
A allele	842 (35.4%)	610 (35.3%)	0.994 (0.873–1.131)	0.960 (0.812–1.135)
rs3816527				
AA	734 (61.7%)	511 (59.1%)	1.000 (reference)	1.000 (reference)
AC	402 (33.8%)	317 (36.6%)	1.133 (0.941–1.364)	1.191 (0.937–1.515)
CC	53 (4.5%)	37 (4.3%)	1.003 (0.649–1.549)	1.110 (0.633–1.947)
AC + CC	455 (38.3%)	354 (40.9%)	1.118 (0.934–1.337)	1.182 (0.938–1.490)
A allele	1870 (78.6%)	1339 (77.4%)	1.000 (reference)	1.000 (reference)
C allele	508 (21.4%)	391 (22.6%)	1.075 (0.926–1.248)	1.130 (0.931–1.371)
rs2120243				
CC	530 (44.6%)	385 (44.5%)	1.000 (reference)	1.000 (reference)
CA	542 (45.6%)	401 (46.4%)	1.019 (0.847–1.224)	1.062 (0.837–1.347)
AA	117 (9.8%)	79 (9.1%)	0.930 (0.679–1.273)	1.129 (0.753–1.692)
CA + AA	659 (55.4%)	480 (55.5%)	1.003 (0.841–1.196)	1.073 (0.855–1.347)
C allele	1602 (67.4%)	1171 (67.7%)	1.000 (reference)	1.000 (reference)
A allele	776 (32.6%)	559 (32.3%)	0.986 (0.863–1.125)	1.059 (0.893–1.257)

Adjusted odds ratios (aORs) with their 95% confidence intervals (CIs) were estimated using multiple logistic regression models after controlling for betel quid chewing, cigarette smoking, and alcohol consumption.

TABLE 4 | Association of the combined effect of *PTX3* gene polymorphisms and betel quid chewing with susceptibility to oral cancer among 1,397 smokers.

Variable	Controls ($n = 631$) (%)	Cases ($n = 766$) (%)	OR (95% CI)	*p*-value	AOR (95% CI)	*p*-value
rs1840680						
GG genotype & non-betel quid chewing	208 (33.0%)	53 (6.9%)	1.00 (reference)		1.000 (reference)	
GA or AA genotype or betel quid chewing	312 (49.4%)	356 (46.5%)	**4.478 (3.195–6.277)**	**$p < 0.001$**	**4.230 (2.998–5.969)**	**$p < 0.001$**
GA or AA genotype with betel quid chewing	111 (17.6%)	357 (46.6%)	**12.622 (8.725–18.259)**	**$p < 0.001$**	**10.504 (7.198–15.327)**	**$p < 0.001$**
rs2305619						
GG genotype & non-betel quid chewing	188 (29.8%)	44 (5.7%)	1.00 (reference)		1.000 (reference)	
GA or AA genotype or betel quid chewing	322 (51.0%)	349 (45.6%)	**4.631 (3.226–6.647)**	**$p < 0.001$**	**4.455 (3.081–6.441)**	**$p < 0.001$**
GA or AA genotype with betel quid chewing	121 (19.2%)	373 (48.7%)	**13.171 (8.944–19.395)**	**$p < 0.001$**	**11.271 (7.586–16.745)**	**$p < 0.001$**
rs3816527						
AA genotype & non-betel quid chewing	283 (44.8%)	66 (8.6%)	1.00 (reference)		1.000 (reference)	
AC or CC genotype or betel quid chewing	270 (42.8%)	449 (58.6%)	**7.130 (5.243–9.697)**	**$p < 0.001$**	**6.652 (4.857–9.112)**	**$p < 0.001$**
AC or CC genotype with betel quid chewing	78 (12.4%)	251 (32.8%)	**13.798 (9.538–19.960)**	**$p < 0.001$**	**11.827 (8.099–17.271)**	**$p < 0.001$**
rs2120243						
CC genotype & non-betel quid chewing	194 (30.8%)	54 (7.1%)	1.00 (reference)		1.000 (reference)	
CA or AA genotype or betel quid chewing	339 (53.7%)	363 (47.4%)	**3.847 (2.749–5.383)**	**$p < 0.001$**	**3.664 (2.600–5.162)**	**$p < 0.001$**
CA or AA genotype with betel quid chewing	98 (15.5%)	349 (45.5%)	**12.794 (8.787–18.628)**	**$p < 0.001$**	**10.755 (7.330–15.779)**	**$p < 0.001$**

Adjusted odds ratios (aORs) with their 95% confidence intervals (CIs) were estimated using multiple logistic regression models after controlling for age and alcohol drinking. P-values were adjusted for multiple comparisons by applying the Bonferroni correction. Bold values were considered statistically significant.

participants were enrolled, namely 865 male cases with oral cancer and 1,189 male controls. Results revealed significant differences in cigarette smoking ($p < 0.001$), betel quid chewing ($p < 0.001$), and alcohol consumption ($p < 0.001$) between the cases with oral cancer and the controls.

PTX3 Gene Polymorphisms in Cases With Oral Cancer and Controls

To investigate the association between *PTX3* gene polymorphisms and oral cancer risk, the genotypic, and allelic frequencies of *PTX3* in the individuals with oral cancer and the controls were established in this investigation (**Table 3**). After adjustment for betel quid chewing, cigarette smoking, and alcohol consumption, no significant difference was observed between the participants with oral cancer who had rs1840680, rs2305619, rs3816527, and rs2120243 polymorphisms of the *PTX3* gene and those with wild-type (WT) genes.

Combined Effects of Environmental Factors and *PTX3* Gene Polymorphisms on Oral Cancer

To determine the combined effects of environmental factors and *PTX3* gene SNVs on oral cancer susceptibility, we conducted further analysis on 1,397 smokers (**Table 4**). As presented in **Table 4**, participants with at least one A allele of rs1840680, one A allele of rs2305619, one C allele of rs3816527, or one A allele of rs2120243 exhibited 12.622-fold (95% CI: 8.725–18.259), 13.171-fold (95% CI: 8.944–19.395), 13.798-fold (95% CI: 9.538–19.960), and 12.794-fold (95% CI: 8.787–18.628) higher risks of oral cancer, respectively, compared with individuals with WT homozygotes who did not chew betel quid.

Effects of Polymorphic Genotypes of *PTX3* on Clinical Status of Oral Cancer

We analyzed the relationship between the combined effect of cigarette smoking and PTX3 variants on oral cancer development. As depicted in **Table 5**, individuals who possessed the CC allele of rs3816527 and smoked cigarettes were more prone to developing late-stage tumors (stage III/IV: OR, 2.328; 95% CI, 1.078–5.027; $p = 0.0314$) and lymph node metastasis (OR, 2.152; 95% CI, 1.047–4.422; $p = 0.0371$) compared with individuals who were homozygous for the WT allele of rs3816527 (**Table 5**).

Functional Connotation of the *PTX3* rs3816527 Locus

We investigated the functional connotation of the rs3816527 SNV on the *PTX3* gene. The function of *PTX3* rs3816527 was

TABLE 5 | Genotyping frequency of the *PTX3* rs3816527 polymorphism on clinical status of oral cancer among 766 smokers.

	Clinical Stage		**OR (95% CI)**	**AOR (95% CI)[a]**
***PTX3* rs3816527**	**Stage I/II (*n* = 379) *n* (%)**	**Stage III/IV (*n* = 387) *n* (%)**		
AA	235 (62.0%)	222 (57.3%)	1.000 (reference)	1.000 (reference)
AC	134 (35.4%)	143 (37.0%)	1.130 (0.838–1.523)	1.111 (0.823–1.500)
CC	10 (2.6%)	22 (5.7%)	**2.328 (1.078–5.027)[b]**	**2.424 (1.114–5.273)[d]**
	Tumor size			
PTX3 rs3816527	<underline<>T2 (*n* = 436) *n* (%)	> T2 (*n* = 330) *n* (%)		
AA	262 (60.1%)	195 (59.1%)	1.000 (reference)	1.000 (reference)
AC	157 (36.0%)	120 (36.4%)	1.027 (0.760–1.388)	1.034 (0.764–1.400)
CC	17 (3.9%)	15 (4.5%)	1.186 (0.578–2.432)	1.202 (0.582–2.483)
	Lymph node metastasis			
PTX3 rs3816527	No (*n* = 519) *n* (%)	Yes (*n* = 247) *n* (%)		
AA	312 (60.1%)	145 (58.7%)	1.000 (reference)	1.000 (reference)
AC	191 (36.8%)	186 (34.8%)	0.969 (0.702–1.337)	0.950 (0.687–1.312)
CC	16 (3.1%)	16 (6.5%)	**2.152 (1.047–4.422)[c]**	**2.183 (1.053–4.528)[e]**
	Cell differentiation			
PTX3 rs3816527	Well (*n* = 111) *n* (%)	Moderate/poor (*n* = 655) *n* (%)		
AA	70 (63.1%)	387 (59.1%)	1.000 (reference)	1.000 (reference)
AC	38 (34.2%)	239 (36.5%)	1.138 (0.743–1.743)	1.117 (0.728–1.713)
CC	3 (2.7%)	29 (4.4%)	1.748 (0.518–5.897)	1.750 (0.515–5.939)

[a]*Adjustment for the effects of betel quid chewing and alcohol consumption.*
[b]*p = 0.0314.*
[c]*p = 0.0371.*
[d]*p = 0.0256.*
[e]*p = 0.0359.*
Bold values were considered statistically significant.

performed using several bioinformatics tools, namely SNPinfo, the NCBI database, ESEfinder, and SWISS-MODEL. Data indicated that *PTX3* rs3816527 was located on the exonic splice enhancer sequence of the *PTX3* gene (**Figure 1A**). The C allele had stronger enhancement activity than did the A allele and may be more likely to promote the splicing modification of the *PTX3* gene (**Figure 1B**). Two splicing forms of *PTX3* existed in the NCBI database (**Figure 1C**).

DISCUSSION

Head and neck cancers are common worldwide. Approximately 90% of head and neck cancers are squamous cell carcinomas, of which ∼50% occur in the oral cavity (38, 39). In south Central Asia, oral cancer is the third most common type of cancer (40). Oral cancer is associated with the use of chronic stimuli such as tobacco smoking, alcohol consumption, and betel quid chewing in particular (3, 4, 41). PTX3 was recognized by proteomics as a critical candidate biomarker for liposarcoma (42), lung cancer (43), prostate cancer (44), and pancreatic cancer (22). For example, a high expression of PTX3 was found in pancreatic cancer cell lines and a direct relationship was found between tumor metastasis and PTX3 expression (22). Moreover, several studies have reported the role of *PTX3* in epithelial cancer progression due to EMT induction (45–48). A low expression of PTX3 has been associated with increased susceptibility to epithelial carcinogenesis (46). Previous studies have demonstrated that PTX3 mediated the induction of the EMT by reducing the expression of E-cadherin, increasing the expression of N-cadherin and vimentin, and promoting the migration of HK-2 cells (45). Moreover, results indicated that the expression of pentraxin family members was significantly associated with the poor prognosis of patients with pancreatic cancer (22). Furthermore, overexpression of PTX3 could promote the proliferation and invasion of cervical cancer *in vitro* and *in vivo* (24). However, few studies have discussed the role of PTX3 in oral cancer. In the present study, the combined effect of environmental factors and *PTX3* polymorphisms considerably increased the risk of oral cancer (**Table 4**). Moreover, patients with *PTX3* SNV rs3816527 with CC had the highest risk of tumors (**Table 5**).

The occurrence of cancer stems from the genetic and epigenetic alterations of the basic mechanisms of the normal cell cycle, such as replication control and cell death (49, 50). Most genes in the human genome consist of multiple introns and exons that are modified through splicing to form mature messenger ribonucleic acid and protein products (51, 52). Although alternative splicing (AS) provides cells with protein diversity, studies have found that pathological changes in splicing can contribute to the development of cancers. For instance, mutations and gene expression changes affect the splicing

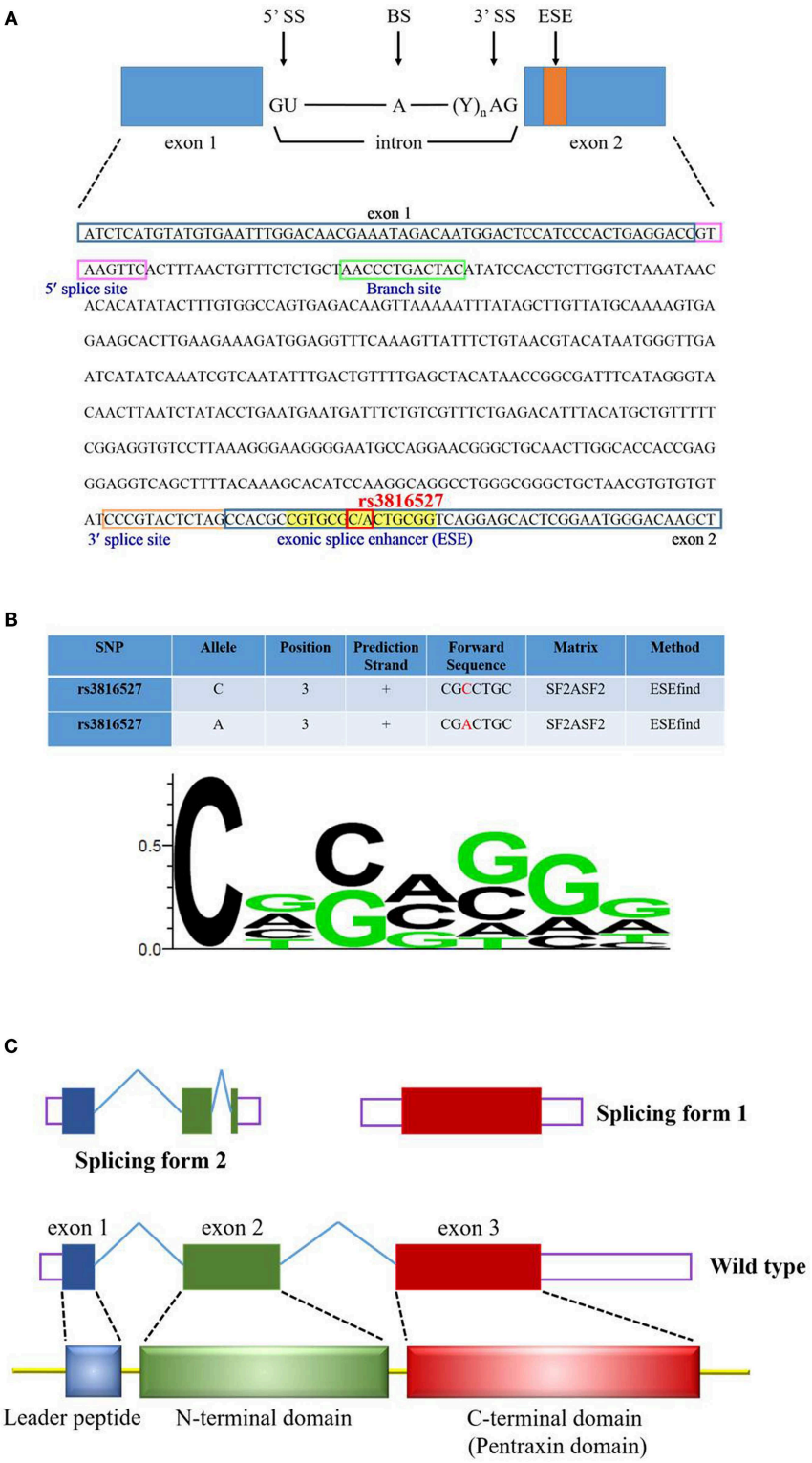

FIGURE 1 | Functional prediction profiling of *PTX3* SNV rs3816527. **(A)** The sequence of *PTX3* is from the NCBI reference sequences (RefSeq) (NM_002852.3). The cis-elements (5′ splice site, 3′ splice site, and branch site) and exonic splice enhancer (ESE) are indicated by various color squares. *PTX3* SNV rs3816527 is located on the ESE sequence. **(B)** The functional prediction of rs3816527 from SNPinfo web server is presented in this Figure. The relative frequency of the nucleotide for the ESE sequence is illustrated by the sequence logo. **(C)** *PTX3* gene consists of three exons. The first exon encodes the leader peptide, and the second and third exons encode N-terminal and C-terminal domains, respectively. Two common splicing forms of *PTX3* are accessed from the NCBI database.

regulatory sequences of key cancer-related genes (53) and the core or accessory components of spliceosome complexes (54–59).

PTX3 has two splice variants; one contains exon 1 or 2 (length of 453 bp) and the other contains exon 3 (length of 931 bp) (**Figure 1C**). ESEfinder analysis results revealed that the rs3816527 C allele had superior splicing enhancement activity for the A allele (**Figure 1B**). In addition, in the protein structure constructed by SWISS-MODEL, PTX3 was split into an N terminus and C terminus after splicing. Although the mechanism of action for this structure remains unclear, a molecular study indicated that the overexpression of PTX3 at the N terminus can considerably inhibit the oncogenic activity of transgenic adenocarcinoma mouse prostate-C2 transfectants, whereas C-terminal overexpression has only a minor effect on tumor growth (60).

We revealed an impact of *PTX3* gene variations on the development of oral cancer; however, there are some limitations in the study. As this study only included a discovery population and not a second independent study to replicate the findings, the associations between *PTX3* variations and oral cancer should be considered preliminary. The other concern is that we failed to exclude the possibility of potential selection bias and since the control group was enrolled among subjects without cancer on a hospital basis. In addition, determining the functional role of PTX3 in the development of oral cancer still requires further investigation.

In conclusion, our results suggest that the allelic effects of *PTX3* SNVs (rs1840680, rs2305619, rs3816527, and rs2120243) enhance the risk and progression of oral cancer in the presence of environmental factors such as tobacco smoking and betel quid chewing. This genetic association was observed most markedly in smokers. These results expose a novel genetic–environmental predisposition to oral cancer carcinogenesis.

DATA AVAILABILITY

The raw data supporting the conclusions of this manuscript will be made available by the authors, without undue reservation, to any qualified researcher.

ETHICS STATEMENT

The Institutional Review Board of Chung Shan Medical University approved this study (CSMUH No: CS13214-1). All participants provided informed consent.

AUTHOR CONTRIBUTIONS

C-MY, C-WL, S-FY, and M-KC contributed to conception, design and critically revised the manuscript. C-MY, S-FY, and M-KC contributed to conception and drafted the manuscript, C-YC, Y-FL, and C-HC contributed to performed experiments and analyzed data.

ACKNOWLEDGMENTS

This study was supported by grants from Ministry of Science and Technology, Taiwan (MOST-106-2314-B-371-005-MY3).

REFERENCES

1. Chiba I. Prevention of Betel Quid Chewers' Oral Cancer in the Asian-Pacific Area. *Asian Pac J Cancer Prev*. (2001) 2:263−9.
2. Jeng JH, Chang MC, Hahn LJ. Role of areca nut in betel quid-associated chemical carcinogenesis: current awareness and future perspectives. *Oral Oncol.* (2001) 37:477–92. doi: 10.1016/S1368-8375(01)00003-3
3. Su SC, Lin CW, Liu YF, Fan WL, Chen MK, Yu CP, et al. Exome sequencing of oral squamous cell carcinoma reveals molecular subgroups and novel therapeutic opportunities. *Theranostics.* (2017) 7:1088–99. doi: 10.7150/thno.18551
4. Yang SF, Huang HD, Fan WL, Jong YJ, Chen MK, Huang CN, et al. Compositional and functional variations of oral microbiota associated with the mutational changes in oral cancer. *Oral Oncol.* (2018) 77:1–8. doi: 10.1016/j.oraloncology.2017.12.005
5. Petti S, Scully C. How many individuals must be screened to reduce oral cancer mortality rate in the Western context? *Chall Oral Dis.* (2015) 21:949–54. doi: 10.1111/odi.12372
6. Miller C, Shay A, Tajudeen B, Sen N, Fidler M, Stenson K, et al. Clinical features and outcomes in young adults with oral tongue cancer. *Am J Otolaryngol.* (2019) 40:93–6. doi: 10.1016/j.amjoto.2018.09.022
7. Gewurz H, Zhang XH, Lint TF. Structure and function of the pentraxins. *Curr Opin Immunol.* (1995) 7:54–64. doi: 10.1016/0952-7915(95)80029-8
8. Garlanda C, Bottazzi B, Bastone A, Mantovani A. Pentraxins at the crossroads between innate immunity, inflammation, matrix deposition, and female fertility. *Ann Rev Immunol.* (2005) 23:337–66. doi: 10.1146/annurev.immunol.23.021704.115756
9. Lee GW, Lee TH, Vilcek J. TSG-14, a tumor necrosis factor- and IL-1-inducible protein, is a novel member of the pentaxin family of acute phase proteins. *J Immunol.* (1993) 150:1804–12.
10. Breviario F, d'Aniello EM, Golay J, Peri G, Bottazzi B, Bairoch A, et al. Interleukin-1-inducible genes in endothelial cells. Cloning of a new gene related to C-reactive protein and serum amyloid P component. *J Biol Chem.* (1992) 267:22190–7.
11. Vouret-Craviari V, Matteucci C, Peri G, Poli G, Introna M, Mantovani A. Expression of a long pentraxin, PTX3, by monocytes exposed to the mycobacterial cell wall component lipoarabinomannan. *Infect Immun.* (1997) 65:1345–50. doi: 10.1006/cyto.1997.0242
12. Bonavita E, Gentile S, Rubino M, Maina V, Papait R, Kunderfranco P, et al. PTX3 is an extrinsic oncosuppressor regulating complement-dependent inflammation in cancer. *Cell.* (2015) 160:700–14. doi: 10.1016/j.cell.2015.01.004
13. Daigo K, Mantovani A, Bottazzi B. The yin-yang of long pentraxin PTX3 in inflammation and immunity. *Immunol Lett.* (2014) 161:38–43. doi: 10.1016/j.imlet.2014.04.012
14. Jaillon S, Moalli F, Ragnarsdottir B, Bonavita E, Puthia M, Riva F, et al. The humoral pattern recognition molecule PTX3 is a key component of innate immunity against urinary tract infection. *Immunity.* (2014) 40:621–32. doi: 10.1016/j.immuni.2014.02.015
15. Kabbani D, Bhaskaran A, Singer LG, Bhimji A, Rotstein C, Keshavjee S, et al. Pentraxin 3 levels in bronchoalveolar lavage fluid of lung transplant recipients with invasive aspergillosis. *J Heart Lung Transpl.* (2017) 36:973–9. doi: 10.1016/j.healun.2017.04.007
16. Zhang J, Zhao GQ, Qu J, Lin J, Che CY, Yang XJ. Early expression of PTX3 in Aspergillus fumigatus infected rat cornea. *Inter J Ophthalmol.* (2018) 11:1084–9. doi: 10.18240/ijo.2018.07.02

17. Doni A, Garlanda C, Mantovani A. PTX3 orchestrates tissue repair. *Oncotarget*. (2015) 6:30435–6. doi: 10.18632/oncotarget.5453
18. Doni A, Musso T, Morone D, Bastone A, Zambelli V, Sironi M, et al. An acidic microenvironment sets the humoral pattern recognition molecule PTX3 in a tissue repair mode. *J Exp Med.* (2015) 212:905–25. doi: 10.1084/jem.20141268
19. Chang WC, Wu SL, Huang WC, Hsu JY, Chan SH, Wang JM, et al. PTX3 gene activation in EGF-induced head and neck cancer cell metastasis. *Oncotarget*. (2015) 6:7741–57. doi: 10.18632/oncotarget.3482
20. Garlanda C, Bottazzi B, Magrini E, Inforzato A, Mantovani A. PTX3, a humoral pattern recognition molecule in innate immunity, tissue repair, and cancer. *Physiol Rev.* (2018) 98:623–39. doi: 10.1152/physrev.00016.2017
21. Stallone G, Cormio L, Netti GS, Infante B, Selvaggio O, Fino GD, et al. Pentraxin 3: a novel biomarker for predicting progression from prostatic inflammation to prostate cancer. *Cancer Res.* (2014) 74:4230–8. doi: 10.1158/0008-5472.CAN-14-0369
22. Kondo S, Ueno H, Hosoi H, Hashimoto J, Morizane C, Koizumi F, et al. Clinical impact of pentraxin family expression on prognosis of pancreatic carcinoma. *Br J Cancer.* (2013) 109:739–46. doi: 10.1038/bjc.2013.348
23. Tung JN, Ko CP, Yang SF, Cheng CW, Chen PN, Chang CY, et al. Inhibition of pentraxin 3 in glioma cells impairs proliferation and invasion *in vitro* and *in vivo*. *J Neuro Oncol.* (2016) 129:201–9. doi: 10.1007/s11060-016-2168-z
24. Ying TH, Lee CH, Chiou HL, Yang SF, Lin CL, Hung CH, et al. Knockdown of Pentraxin 3 suppresses tumorigenicity and metastasis of human cervical cancer cells. *Sci Rep.* (2016) 6:29385. doi: 10.1038/srep29385
25. Eccles D, Tapper W. The influence of common polymorphisms on breast cancer. *Cancer Treat Res.* (2010) 155:15–32. doi: 10.1007/978-1-4419-6033-7_2
26. Hanahan D, Weinberg RA. The hallmarks of cancer. *Cell.* (2000) 100:57–70. doi: 10.1016/S0092-8674(00)81683-9
27. Hua KT, Liu YF, Hsu CL, Cheng TY, Yang CY, Chang JS, et al. 3'UTR polymorphisms of carbonic anhydrase IX determine the miR-34a targeting efficiency and prognosis of hepatocellular carcinoma. *Sci Rep.* (2017) 7:4466. doi: 10.1038/s41598-017-04732-3
28. Schmith VD, Campbell DA, Sehgal S, Anderson WH, Burns DK, Middleton LT, et al. Pharmacogenetics and disease genetics of complex diseases. *Cell Mol Life Sci.* (2003) 60:1636–46. doi: 10.1007/s00018-003-2369-4
29. Su SC, Hsieh MJ, Lin CW, Chuang CY, Liu YF, Yeh CM, et al. Impact of HOTAIR gene polymorphism and environmental risk on oral cancer. *J Dent Res.* (2018) 97:717–24. doi: 10.1177/0022034517749451
30. Sunyaev S, Ramensky V, Koch I, Lathe W 3rd, Kondrashov AS, Bork P. Prediction of deleterious human alleles. *Hum Mol Genet.* (2001) 10:591–7. doi: 10.1093/hmg/10.6.591
31. Barbati E, Specchia C, Villella M, Rossi ML, Barlera S, Bottazzi B, et al. Influence of pentraxin 3 (PTX3) genetic variants on myocardial infarction risk and PTX3 plasma levels. *PLoS ONE.* (2012) 7:e53030. doi: 10.1371/journal.pone.0053030
32. Diamond JM, Meyer NJ, Feng R, Rushefski M, Lederer DJ, Kawut SM, et al. Variation in PTX3 is associated with primary graft dysfunction after lung transplantation. *Am J Resp Crit Care Med.* (2012) 186:546–52. doi: 10.1164/rccm.201204-0692OC
33. Chiarini M, Sabelli C, Melotti P, Garlanda C, Savoldi G, Mazza C, et al. PTX3 genetic variations affect the risk of *Pseudomonas aeruginosa* airway colonization in cystic fibrosis patients. *Genes Immun.* (2010) 11:665–70. doi: 10.1038/gene.2010.41
34. Olesen R, Wejse C, Velez DR, Bisseye C, Sodemann M, Aaby P, et al. DC-SIGN (CD209), pentraxin 3 and vitamin D receptor gene variants associate with pulmonary tuberculosis risk in West Africans. *Genes Immun.* (2007) 8:456–67. doi: 10.1038/sj.gene.6364410
35. Carmo RF, Aroucha D, Vasconcelos LR, Pereira LM, Moura P, Cavalcanti MS. Genetic variation in PTX3 and plasma levels associated with hepatocellular carcinoma in patients with HCV. *J Viral Hepatit.* (2016) 23:116–22. doi: 10.1111/jvh.12472
36. Hakelius M, Reyhani V, Rubin K, Gerdin B, Nowinski D. Normal oral keratinocytes and head and neck squamous carcinoma cells induce an innate response of fibroblasts. *Anticanc Res.* (2016) 36:2131–7.
37. Su SC, Hsieh MJ, Liu YF, Chou YE, Lin CW, Yang SF. ADAMTS14 gene polymorphism and environmental risk in the development of oral cancer. *PLoS ONE.* (2016) 11:e0159585. doi: 10.1371/journal.pone.0159585
38. Boyle P, Levin B. *World Cancer Report 2008*. Lyon: IARC Press, International Agency for Research on Cancer (2008).
39. Jemal A, Siegel R, Ward E, Hao Y, Xu J, Thun MJ. Cancer statistics, 2009. *CA Cancer J Clin.* (2009) 59:225–49. doi: 10.3322/caac.20006
40. Petersen PE. The World Oral Health Report 2003: continuous improvement of oral health in the 21st century–the approach of the WHO Global Oral Health Programme. *Commun Dentist Oral Epidemiol. (2003)* 31(Suppl 1):3–23. doi: 10.1046/j..2003.com122.x
41. Su CW, Chien MH, Lin CW, Chen MK, Chow JM, Chuang CY, et al. Associations of genetic variations of the endothelial nitric oxide synthase gene and environmental carcinogens with oral cancer susceptibility and development. *Nitric Oxide Biol Chem.* (2018) 79:1–7. doi: 10.1016/j.niox.2018.06.005
42. Willeke F, Assad A, Findeisen P, Schromm E, Grobholz R, von Gerstenbergk B, et al. Overexpression of a member of the pentraxin family (PTX3) in human soft tissue liposarcoma. *Euro J Cancer.* (2006) 42:2639–46. doi: 10.1016/j.ejca.2006.05.035
43. Diamandis EP, Goodglick L, Planque C, Thornquist MD. Pentraxin-3 is a novel biomarker of lung carcinoma. *Clin Cancer Res.* (2011) 17:2395–9. doi: 10.1158/1078-0432.CCR-10-3024
44. Sardana G, Jung K, Stephan C, Diamandis EP. Proteomic analysis of conditioned media from the PC3, LNCaP, and 22Rv1 prostate cancer cell lines: discovery and validation of candidate prostate cancer biomarkers. *J Proteome Res.* (2008) 7:3329–38. doi: 10.1021/pr8003216
45. Hung TW, Tsai JP, Lin SH, Lee CH, Hsieh YH, Chang HR. Pentraxin 3 activates JNK signaling and regulates the epithelial-to-mesenchymal transition in renal fibrosis. *Cell Physiol Biochem.* (2016) 40:1029–38. doi: 10.1159/000453159
46. Ronca R, Di Salle E, Giacomini A, Leali D, Alessi P, Coltrini D, et al. Long pentraxin-3 inhibits epithelial-mesenchymal transition in melanoma cells. *Mol Cancer Therap.* (2013) 12:2760–71. doi: 10.1158/1535-7163.MCT-13-0487
47. Scimeca M, Antonacci C, Colombo D, Bonfiglio R, Buonomo OC, Bonanno E. Emerging prognostic markers related to mesenchymal characteristics of poorly differentiated breast cancers. *Tumour Biol.* (2016) 37:5427–35. doi: 10.1007/s13277-015-4361-7
48. Scimeca M, Antonacci C, Toschi N, Giannini E, Bonfiglio R, Buonomo CO, et al. Breast Osteoblast-like cells: a reliable early marker for bone metastases from breast cancer. *Clin Breast Cancer.* (2018) 18:e659–69. doi: 10.1016/j.clbc.2017.11.020
49. Feinberg AP, Koldobskiy MA, Gondor A. Epigenetic modulators, modifiers and mediators in cancer aetiology and progression. *Nat Rev Genet.* (2016) 17:284–99. doi: 10.1038/nrg.2016.13
50. Hanahan D, Weinberg RA. Hallmarks of cancer: the next generation. *Cell.* (2011) 144:646–74. doi: 10.1016/j.cell.2011.02.013
51. Pan Q, Shai O, Lee LJ, Frey BJ, Blencowe BJ. Deep surveying of alternative splicing complexity in the human transcriptome by high-throughput sequencing. *Nat Genet.* (2008) 40:1413–5. doi: 10.1038/ng.259
52. Wang ET, Sandberg R, Luo S, Khrebtukova I, Zhang L, Mayr C, et al. Alternative isoform regulation in human tissue transcriptomes. *Nature.* (2008) 456:470–6. doi: 10.1038/nature07509
53. Jung H, Lee D, Lee J, Park D, Kim YJ, Park WY, et al. Intron retention is a widespread mechanism of tumor-suppressor inactivation. *Nat Genet.* (2015) 47:1242–8. doi: 10.1038/ng.3414
54. Anczukow O, Rosenberg AZ, Akerman M, Das S, Zhan L, Karni R, et al. The splicing factor SRSF1 regulates apoptosis and proliferation to promote mammary epithelial cell transformation. *Nat Struct Mol Biol.* (2012) 19:220–8. doi: 10.1038/nsmb.2207
55. Jensen MA, Wilkinson JE, Krainer AR. Splicing factor SRSF6 promotes hyperplasia of sensitized skin. *Nat Struct Mol Biol.* (2014) 21:189–97. doi: 10.1038/nsmb.2756
56. Karni R, de Stanchina E, Lowe SW, Sinha R, Mu D, Krainer AR. The gene encoding the splicing factor SF2/ASF is a proto-oncogene. *Nat Struct Mol Biol.* (2007) 14:185–93. doi: 10.1038/nsmb1209
57. Quesada V, Conde L, Villamor N, Ordonez GR, Jares P, Bassaganyas L, et al. Exome sequencing identifies recurrent mutations of the splicing factor SF3B1 gene in chronic lymphocytic leukemia. *Nat Genet.* (2011) 44:47–52. doi: 10.1038/ng.1032

58. Wang L, Lawrence MS, Wan Y, Stojanov P, Sougnez C, Stevenson K, et al. SF3B1 and other novel cancer genes in chronic lymphocytic leukemia. *N Engl J Med.* (2011) 365:2497–506. doi: 10.1056/NEJMoa1109016
59. Yoshida K, Sanada M, Shiraishi Y, Nowak D, Nagata Y, Yamamoto R, et al. Frequent pathway mutations of splicing machinery in myelodysplasia. *Nature.* (2011) 478:64–9. doi: 10.1038/nature10496
60. Ronca R, Alessi P, Coltrini D, Di Salle E, Giacomini A, Leali D, et al. Long pentraxin-3 as an epithelial-stromal fibroblast growth factor-targeting inhibitor in prostate cancer. *J Pathol.* (2013) 230:228–38. doi: 10.1002/path.4181

Conflict of Interest Statement: The authors declare that the research was conducted in the absence of any commercial or financial relationships that could be construed as a potential conflict of interest.

frontiers in Oncology

REVIEW
published: 13 August 2019
doi: 10.3389/fonc.2019.00756

MicroRNAs as Therapeutic Targets in Nasopharyngeal Carcinoma

Sumei Wang[1,2,3]*, *François-Xavier Claret*[4,5] and *Wanyin Wu*[1,2]*

[1] Guangdong Provincial Key Laboratory of Clinical Research on Traditional Chinese Medicine Syndrome, Guangdong Provincial Hospital of Chinese Medicine, Guangzhou, China, [2] Department of Oncology, The Second Clinical College of Guangzhou University of Chinese Medicine, Guangzhou, China, [3] The Postdoctoral Research Station, Guangzhou University of Chinese Medicine, Guangzhou, China, [4] Department of Systems Biology, The University of Texas MD Anderson Cancer Center, Houston, TX, United States, [5] Experimental Therapeutic Academic Program and Cancer Biology Program, The University of Texas Graduate School of Biomedical Sciences at Houston, Houston, TX, United States

Nasopharyngeal carcinoma (NPC) is a malignancy of epithelial origin that is prone to local invasion and early distant metastasis. Although concurrent chemotherapy and radiotherapy improves the 5-year survival outcomes, persistent or recurrent disease still occurs. Therefore, novel therapeutic targets are needed for NPC patients. MicroRNAs (miRNAs) play important roles in normal cell homeostasis, and dysregulations of miRNA expression have been implicated in human cancers. In NPC, studies have revealed that miRNAs are dysregulated and involved in tumorigenesis, metastasis, invasion, resistance to chemo- and radiotherapy, and other disease- and treatment-related processes. The advantage of miRNA-based treatment approaches is that miRNAs can concurrently target multiple effectors of pathways involved in tumor cell differentiation and proliferation. Thus, miRNA-based cancer treatments, alone or combined with standard chemotherapy and/or radiotherapy, hold promise to improve treatment response and cure rates. In this review, we will summarize the dysregulation of miRNAs in NPC initiation, progression, and treatment as well as NPC-related signaling pathways, and we will discuss the potential applications of miRNAs as biomarkers and therapeutic targets in NPC patients. We conclude that miRNAs might be potential promising therapeutic targets in nasopharyngeal carcinoma.

Keywords: microRNA, Nasopharyngeal Carcinoma (NPC), therapeutic target, biomarker, application

OPEN ACCESS

Edited by:
Cheng-Chia Yu,
Chung Shan Medical University, Taiwan

Reviewed by:
Philippe Gorphe,
Institut Gustave Roussy, France
Pei-ling Hsieh,
China Medical University, Taiwan

***Correspondence:**
Sumei Wang
wangsumei198708@163.com
Wanyin Wu
wwanyin@126.com

Specialty section:
This article was submitted to Head and Neck Cancer, a section of the journal Frontiers in Oncology

Received: *01 April 2019*
Accepted: *26 July 2019*
Published: *13 August 2019*

Citation:
Wang S, Claret F-X and Wu W (2019) MicroRNAs as Therapeutic Targets in Nasopharyngeal Carcinoma. Front. Oncol. 9:756. doi: 10.3389/fonc.2019.00756

INTRODUCTION

Nasopharyngeal Carcinoma (NPC)

Nasopharyngeal carcinoma is a non-lymphomatous squamous cell carcinoma that arises from the epithelial lining of the nasopharynx. Local invasion and early distant metastasis are common in NPC. Etiologic factors for NPC include Epstein-Barr virus (EBV) infection, genetic predisposition, and environmental factors (1, 2). It is extremely difficult to detect early because of its deep location and lack of obvious clinical signs in its early stages. Concurrent chemotherapy and radiotherapy is a standard treatment for late-stage NPC (3). Nevertheless, despite the effectiveness of concurrent chemotherapy and radiotherapy in treating NPC, local or regional failure in the form of persistent or recurrent disease occurs in some patients. Therefore, novel biomarkers and therapeutic strategies to improve treatment outcomes are urgently required for NPC patients.

MicroRNAs (miRNAs)

MiRNAs are a class of endogenous non-coding RNA molecules that are typically 22–25 nucleotides long (4, 5). They are transcribed from intragenic or intergenic regions by RNA polymerase II into pri-miRNAs (at a length between 1 and 3 kb) (6), and further processed by the RNase III ribonucleases Drosha and DiGeorge syndrome critical region gene 8, *DGCR8*, complex in the nucleus into a hairpin intermediate pre-miRNA (consisting in a stem-loop structure of about 70 nucleotides) (7). The pre-miRNA is then transported from the nucleus to the cytoplasm by exportin 5 (8). After strand separation, the mature double-stranded miRNA, also known as the guide strand, is incorporated into an RNA-induced silencing complex (RISC), whole the passenger strand (miRNA*) is typically degraded. The RISC is the effector complex of the miRNA pathway and comprises miRNA, Argonaute proteins (Argonaute 1 to Argonaute 4) and other proteins. The mature strand is important for target recognition and for the incorporation of specific target mRNAs into RISC (8, 9). Each miRNA can potentially target many genes (about 500 on average), and about 60% of mRNAs have at least 1 evolutionarily conserved sequence that is believed to be targeted by miRNAs (10, 11).

Usually, miRNAs target the 3 prime untranslated region (3′UTR) of their target genes, most often causing mRNA deadenylation and degradation and subsequent translational repression (5, 12). However, other miRNA-mediated mechanisms of modulating mRNA expression have also been reported. Some miRNAs bind to the open reading frame or the 5′UTR of their target genes; in some cases, miRNAs have been shown to activate gene expression rather than suppress it (13). For example, Jopling et al. reported that miR-122 can bind to 5′UTR, inhibiting translation of its target genes (14). In 2008, another miRNA, miR-10a, was reported to enhance translation by binding to ribosomal protein mRNA at the 5′UTR (which is known to regulate translation) downstream of the conserved 5′TOP motif (13). In 2016, we demonstrated that miR-24 could bind to both 3′UTR and 5′UTR of *COPS5* (also named *JAB1* and COP9 signalosome subunit 5), leading to *COPS5* mRNA degradation and translational suppression (15). Besides, miRNAs can also regulate gene expression at the transcriptional level by binding directly to the DNA (16, 17). Moreover, proteins can also be targeted by miRNAs (18) (**Figure 1**).

Exosomal miRNAs

Exosomes are microvesicles that are 40–100 nm long. They originate in intracellular endosomal compartment and are secreted by cells into their microenvironment. Exosomes transport DNA fragments, proteins, mRNAs, and miRNAs from donor cells to recipient cells and are therefore crucial to intercellular communication. Exosomal miRNAs miR-21 and miR-29a are secreted by tumor cells and can bind to toll-like receptors on nearby immune cells, thus initiating an inflammatory response that promotes metastasis (19). Furthermore, miR-21 was observed at a higher level in exosomes from the serum of patients with esophageal squamous cell carcinoma than in serum from patients with benign diseases without systemic inflammation, and an association was found between exosomal miR-21 and the presence of metastasis with inflammation (20). In addition, exosomal miR-223 was reported to be elevated in breast cancer cells and promote breast cancer invasion (21). In NPC, exosomal miR-9 was found to inhibit angiogenesis through regulating PDK/AKT pathway (22). And exosomal miR-24-3p serves as a potential biomarker for NPC prognosis (23). Therefore, exosomal miRNAs are involved in the initiation and progression of cancers including NPC, and could be biomarkers for NPC patients.

EBV-Encoded miRNAs

EBV, a herpesvirus that infects the majority of the population worldwide asymptomatically (24), was the first human virus reported to encode miRNAs (25). More than 44 viral miRNAs are encoded from EBV. In NPC, EBV expresses EBNA1, LMP1, and LMP2A, EBERs, and BARTs (26). miR-BARTs, which are EBV-encoded miRNAs derived from BamH1-A rightward transcripts, are highly expressed in NPC and promote its development. A recent study showed that EBV-encoded miR-BARTS, including BART5-5p, BART7-3p, BART9-3p, and BART14-3p, downregulated the expression of a key DNA double-strand break repair gene, ataxia telangiectasia mutated (*ATM*), by targeting several sites on its 3′-UTR (27). Thus, those 4 EBV-encoded miRNAs work cooperatively to suppress *ATM* activity in response to DNA damage, contributing to NPC tumorigenesis. Those findings indicate that EBV-encoded miRNAs can be used as a novel therapeutic strategy for NPC.

THE MECHANISM OF miRNA REGULATION IN CANCERS

Genes encoding miRNAs are often located at or near fragile sites and in minimal regions of loss of heterozygosity, in minimal regions of amplification, and in common cancer-related breakpoints (28). Upregulated expression of miRNAs can be caused by genomic alterations such as translocations o amplification, and loss of function can be caused by alterations such as deletions, insertions, or mutations (29). For example, the mir-17-92 cluster, which is made up of mir-17, mir-18a, mir-19b,

Abbreviations: A20/TNFAIP3, tumor necrosis factor alpha-induced protein 3; ABCB1, ATP binding cassette subfamily B member 1; ATM, ataxia telangiectasia mutated; BRD7, bromodomain containing 7; CAPN4/CAPNS1, calpain small subunit 1; circRNA, circular RNA; COPS5, COP9 signalosome subunit 5; CXCL12, C-X-C motif chemokine ligand 12; CXCR4, C-X-C motif chemokine receptor 4; DGCR8, Drosha and DiGeorge syndrome critical region gene 8; E2F3, E2F transcription factor 3; EBV, Epstein-Barr virus; EMT, epithelial-mesenchymal transition; EZH2, enhancer of zeste homolog 2; *FGF5*, fibroblast growth factor 5; IL-17, interleukin-17; ITGA3, integrin subunit alpha 3; KLF12, Kruppel-like factor 12; LASP1, LIM and SH3 protein 1; lncRNA, long non-coding RNA; MALAT1, metastasis-associated lung adenocarcinoma transcript-1; AP3K5/ASK1, apoptosis signal-regulating kinase1; miRNA, microRNA; MIF, macrophage migration inhibitory factor; mTOR, mechanistic target of rapamycin kinase; NF-κB, nuclear factor κB; NPC, nasopharyngeal carcinoma; PDRG1, p53 and DNA damage regulated 1; PTEN, phosphatase and tensin homolog; RISC, RNA-induced silencing complex; RP, ribosomal protein; SP1, specificity protein 1; TIAM1, T cell lymphoma invasion and metastasis 1; TRIAP1, TP53-regulated inhibitor of apoptosis 1; TSGA10, testis-specific gene antigen 10; UTR, untranslated region; WNT2B, Wnt family member 2B; XIST, X inactivate-specific transcript.

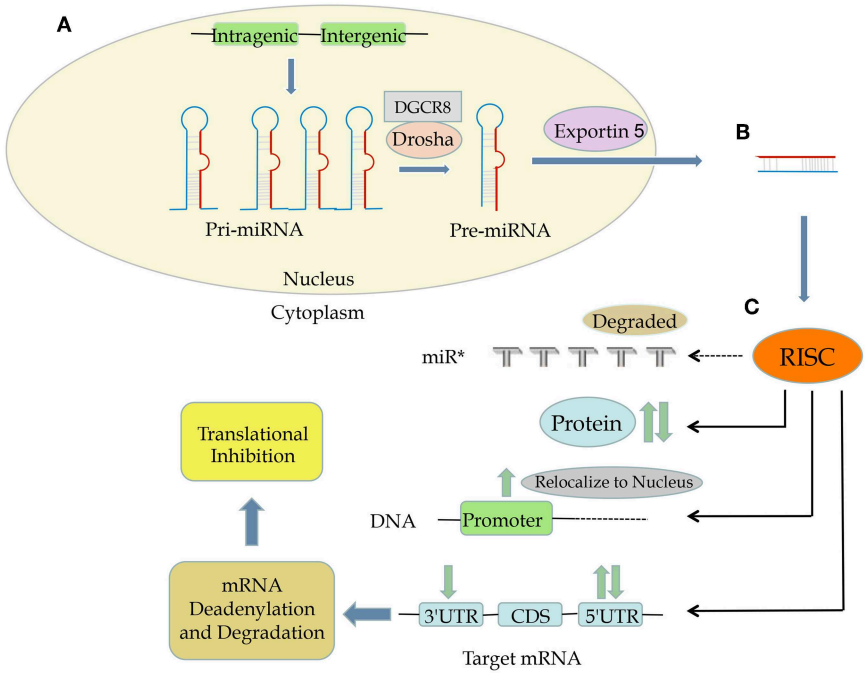

FIGURE 1 | The process and functions of miRNA. **(A)** Both intergenic and intragenic genes encode miRNAs. **(B)** Mature miRNAs are transcribed from pri-miRNA and then then pre-miRNA, translocated from nucleus to cytoplasm by exportin 5, and composed of RNA-induced silencing complex (RISC). **(C)** RISC can target mRNA at 3′UTR, CDS, and 5′UTR as well as DNA promoter sequences and even proteins, leading to upregulation or downregulation of a specific protein.

mir-19b-1, mir-201, and mir-92-1, resides in an 800 base-pair region of the non-coding gene *MIR17HG* (also called *C13orf25*), a genomic region known to be amplified in lymphomas (30). The mir-17-92 cluster is often overexpressed in hematological cancers (31, 32). In contrast, the mir-15a-mir-16-a cluster, which resides in the chromosome 13q14 region (between exons 2 and 5 of the non-coding gene *DLEU2*), is often downregulated in patients with chronic lymphocytic leukemia due to genomic deletion of this region (31, 33).

In addition to structural genetic alterations, epigenetic modulations, including DNA promoter hypermethylation and histone hypoacetylation, have been described in solid tumors (34). For example, miR-127 is downregulated because of promoter hypermethylation in human bladder cancer (34). Usually, hypermethylation of tumor-suppressive miRNAs leads to miRNA silencing, and hypomethylation of onco-miRNAs leads to their activation and to tumorigenesis (35). In addition, long non-coding RNAs (lncRNAs) can target miRNAs, resulting in in tumorigenesis and chemo- and radioresistance. For example, lncRNA FTH1P3 promotes ATP binding cassette subfamily B member 1 (ABCB1) protein expression by targeting miR-206, acting as a miRNA "sponge," leading to the activation of paclitaxel resistance in breast cancer (36). Circular RNAs (circRNAs) also can act as miRNA sponges to regulate miRNA expression. For example, circNT5E was recently reported to directly bind to miR-422a and inhibit its activity, promoting glioblastoma tumorigenesis (37).

The aberrant miRNA expression in cancer can also be caused by downstream miRNA processing. Merritt et al. reported that miRNA expression could be globally suppressed by short hairpin RNAs against Dicer and Drosha, 2 critical ribonucleases involved in miRNA processing (38). This miRNA suppression promotes cellular transformation and tumorigenesis.

The alteration of miRNA expression in cancers can also be caused by aberrant transcription factor activity, which leads to increased or decreased transcription from miRNA genes. The miR-34 miRNA family (comprising miR-34a, miR-34b, and miR-34c) is directly induced by the tumor suppressor p53. In cells with high levels of p53, miR-34 expression is elevated; furthermore, chromatin immunoprecipitation assays revealed that p53 can bind to the promoter of miR-34 (39, 40). The MYC oncoprotein downregulates transcription of tumor suppressor miRNAs such as let-7 and miR-29 family members. MYC can bind to conserved sequences of the miRNA promoter that it suppresses, and the suppression of miRNAs by MYC has been found to facilitate lymphomagenesis (41) (**Figure 2**).

miRNA DYSREGULATION IN NPC INITIATION

The function of miRNAs is largely influenced by the expression of their main targets. Some miRNAs promote tumorigenesis in some cell types and suppress it in others. The classification of a miRNA as an oncogene or a tumor suppressor, therefore, requires knowledge of the type of cell in which it acts. Typically, miRNAs do not cause a specific phenotype by aiming at a single target. Instead, miRNAs target multiple mRNAs concurrently and engage in complex interactions with the machinery that controls the transcriptome. In cancers, miRNAs often are

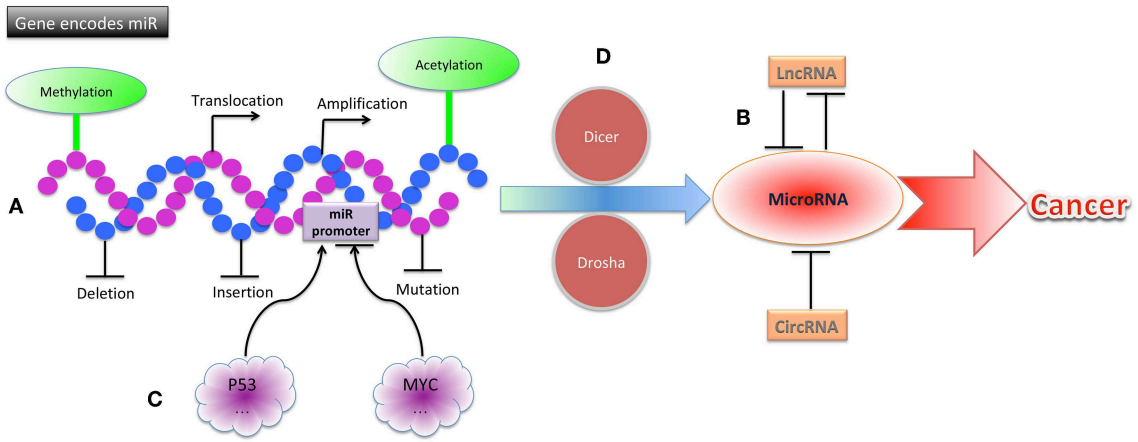

FIGURE 2 | The mechanisms of miRNA dysregulation in cancers. **(A)** Structural gene alterations, including translocation, amplification, deletion, insertion, and mutation contribute to miRNA dysregulation in cancers. **(B)** Epigenetic alterations, including methylation, acetylation, lncRNAs, and circRNAs contribute to miRNA dysregulation in cancers. **(C)** MiRNA promoters can be altered by p53, MYC, and other transcription factors, leading to cancer. **(D)** Alterations of proteins involved in miRNA processing, including Dicer, Drosha, and others, can result in cancer.

dysregulated and function collectively to mark differentiation states or individually as oncogenes or tumor suppressors. In NPC, miRNAs were reported to be expressed aberrantly and exert pivotal effects by altering the expression of their specific mRNA targets (42) (**Table 1**).

Onco-miRNAs in NPC

Tumor suppressor genes are usually inhibited by miRNAs directly, and such miRNAs are considered to be onco-miRNAs. For example, cell cycle inhibitor *CDKN1A* (also called *P21*) is believed to be directly targeted by miR-663 in NPC, leading to the promotion of NPC cell proliferation and tumorigenesis (43). An onco-miRNA, miR-125b, was found to be significantly upregulated in the NPC tissue compared with healthy nasopharyngeal mucosa, and this upregulation was correlated with poor survival outcomes; furthermore, high expression of miR-125b was identified as an independent predictor for shorter survival durations in NPC patients (44). The same study found that miR-125b promoted proliferation and inhibited apoptosis in NPC cells. A direct target of miR-125b, the tumor necrosis factor alpha-induced protein 3 gene *TNFAIP3* (formerly called *A20*), functions as a tumor suppressor in NPC and mediates miR-125b-promoted NPC tumorigenesis by activating the nuclear factor κB (NF-κB) signaling pathway. Together, these findings demonstrate that onco-miRNAs target tumor suppressor genes, leading to NPC initiation.

Tumor-Suppressive miRNAs in NPC

Oncogenes can be suppressed by miRNAs directly, and such miRNAs are considered to be tumor-suppressive miRNAs. For example, the C-X-C motif chemokine receptor 4 oncogene *CXCR4* can be directly targeted by tumor-suppressive miR-9, resulting in the inhibition of NPC pathogenesis. In NPC clinical specimens, miR-9 was observed to be downregulated (45). Interleukin-17 (IL-17), a proinflammatory cytokine, suppresses immune defense, and immune surveillance while promoting tumor growth. A study showed that IL-17 was targeted by miR-135a, resulting in the inhibition of NPC cell proliferation (46). In another study, overexpression of miR-320b was shown to suppress NPC cell proliferation and enhance mitochondrial fragmentation and apoptosis (47). In contrast, silencing miR-320b enhanced NPC tumor growth and inhibited cell apoptosis. The TP53-regulated inhibitor of apoptosis 1 gene, *TRIAP1*, has been found to be directly targeted by miR-320b, which mediates *TRIAP1*'s role in NPC cell proliferation inhibition and apoptosis induction. It has also been reported that miR-326/330-5p clusters can target cyclin D1 gene, *CCND1*, exerting their tumor-suppressive roles on NPC initiation (48). Some tumor-suppressive miRNAs target lncRNAs that function as oncogenes. For example, miR-25 expression was found to be upregulated in NPC cells, and its ectopic expression was shown to suppress NPC cell growth and motility by targeting metastasis-associated lung adenocarcinoma transcript-1 (*MALAT1*), a proto-oncogenic lncRNA (49). The tumor-suppressive miRNAs miR- 451 and miR-539-5p inhibit NPC initiation by targeting the macrophage migration inhibitory factor (*MIF*) and Kruppel-like factor 12 (*KLF12*) genes, respectively (50, 51). Finally, lentivirus can be used as a delivery system to overexpress specific tumor-suppressive miRNAs in NPC, resulting in the inhibition of NPC initiation. For example, lenti-miR-26a was shown to inhibit the tumorigenicity of NPC cells in nude mice significantly, providing a useful strategy for treating NPC patients (52).

miRNA DYSREGULATION IN NPC PROGRESSION

NPC is an aggressive disease that tends to spread locally and metastasize to regional lymph nodes and distant organs. Distant metastasis is the principal mode of treatment failure (53).

TABLE 1 | miRNA dysregulation in NPC initiation, progression and therapies.

miRNA	Target	Mechanism	Function	References
miR-663	*CDKN1A*	Promotes NPC cell proliferation	Onco-miRNA	(43)
miR-125b	*TNFAIP3*	Inhibits NPC cell apoptosis	Onco-miRNA	(44)
miR-9	*CXCR4*	Suppresses NPC pathogenesis	Suppressive miRNA	(45)
miR-135a	*IL-17*	Suppresses NPC cell proliferation	Suppressive miRNA	(46)
miR-320b	*TRIAP1*	Enhances NPC cell apoptosis	Suppressive miRNA	(47)
miR-326/330-5p clusters	*CCND1*	Suppresses NPC initiation	Suppressive miRNA	(48)
miR-25	*MALAT1*	Suppresses NPC cell growth	Suppressive miRNA	(49)
Exosomal miR-23a	*TSGA10*	Promotes NPC angiogenesis	Metastasis promoter	(54)
EBV-miR-BART1/7-3p	*PTEN*	Promotes EMT process	Metastasis promoter	(55, 56)
miR-29c	*TIAM1*	Suppresses NPC metastasis	Metastasis suppressor	(57)
miR-101	*ITGA3*	Inhibits NPC angiogenesis	Metastasis suppressor	(58)
miR-203a-3p	*LASP1*	Inhibits NPC metastasis	Metastasis suppressor	(59)
miR-630	*EZH2*	Inhibits NPC cell invasion	Metastasis suppressor	(60)
EBV-miR-BART6-3p	*MIR3936HG*	Suppresses NPC metastasis	Metastasis suppressor	(61)
miR-324-3p	*WNT2B*	Reduces NPC radioresistance	Radiosensitizer	(69)
miR-519d	*PDRG1*	Sensitizes NPC to IR	Radiosensitizer	(70)
miR-24	*COPS5/SP1*	Enhances NPC radiosensitivity	Radiosensitizer	(15)
miR-19b-3p	*TNFAIP3*	Increases NPC radioresistance	Radioresistant agent	(63)
miR-3188	*mTOR*	Suppresses NPC resistance of 5-FU	Chemosensitizer	(67)

CCND1, cyclin D1; CDKN1A, cyclin-dependent kinase inhibitor 1A; CXCR4, C-X-C motif chemokine receptor 4; IL-17, interleukin-17; MALAT1, metastasis-associated lung adenocarcinoma transcript 1; TNFAIP3, tumor necrosis factor alpha-induced protein 3; TRIAP1, TP53-regulated inhibitor of apoptosis 1; CXCL12, C-X-C motif chemokine ligand 12; EZH2, enhancer of zeste homolog 2; ITGA3, integrin subunit alpha 3; LASP1, LIM and SH3 protein 1; MIR3936HG, a long noncoding RNA; PTEN, phosphatase and tensin homolog; TIAM1, T cell lymphoma invasion and metastasis 1; TSGA10, testis-specific 10; 5-FU, fluorouracil; COPS5, COP9 signalosome subunit 5 (also called JAB1); MTOR, mechanistic target of rapamycin kinase; PDRG1, p53 and DNA damage regulated 1; SP1, specificity protein 1; WNT2B, Wnt family member 2B.

It is known that NPC metastasis is associated with miRNA dysregulation. The functions of miRNAs often are contradictory because they are determined by the cellular environment and the stage of the metastatic process. Therefore, identifying which miRNAs promote or suppress the metastatic process of NPC could lead to the development of new, efficient therapeutic agents to prevent or delay metastasis (**Table 1**).

Metastasis Promoter miRNAs in NPC

Mounting evidence implicates miRNAs in the modulation of angiogenesis, which is essential to the metastatic process. For instance, it has been reported that exosomal miR-23a overexpression promotes angiogenesis in NPC by directly targeting the testis-specific 10 gene, *TSGA10* (54). Furthermore, miR-23a overexpression in pre-metastatic NPC tissue was identified as a prognostic biomarker for early metastasis. In addition, EBV-encoded miR-BART1 has been shown to induce NPC metastasis by regulating pathways that depend on the phosphatase and tensin homolog gene, *PTEN* (55). Another EBV-encoded miRNA, miR-BART7-3p, was shown to promote the epithelial-mesenchymal transition (EMT) and metastasis of NPC cells by suppressing PTEN and consequently activating the PI3K/AKT/GSK-3β signaling pathway (56).

Metastasis Suppressor miRNAs in NPC

The tumor-suppressive miR-29c is also a metastasis suppressor that inhibits NPC cell migration, invasion, and metastasis by targeting the T cell lymphoma invasion and metastasis 1 gene, *TIAM1*, directly (57). In NPC patient samples and cell lines, miR-101 was found to be downregulated, and its ectopic expression significantly inhibited cell migration, invasion, and angiogenesis both *in vitro* and *in vivo*. The prometastatic gene integrin subunit alpha 3 (*ITGA3*) has been identified and validated as a target of miR-101 and shown to mediate the suppressive effects of miR-101 on NPC metastasis. Interestingly, the systemic delivery of lentivirus-mediated miR-101 in NPC suppressed lung metastatic colony formation with no noticeable toxic effects (58). Also, miR-203a-3p was found to be dysregulated and to act as a tumor suppressor in NPC. This miRNA suppresses NPC metastasis by targeting the LIM and SH3 protein 1 gene, *LASP1* (59).

Metastasis suppressor miRNAs can also target or be targeted by lncRNAs in NPC. For example, lncRNA *H19* has been found to be overexpressed in NPC tissue, and *H19* knockdown significantly suppressed invasion NPC cells. *H19* knockdown downregulated the expression of the enhancer of zeste homolog 2 gene, *EZH2*, which is upregulated in NPC and promotes invasion. *H19* does not bind directly to *EZH2* but instead modulates its expression by suppressing the activity of miR-630, which inhibits *EZH2* and interacts with *H19* in a sequence-specific manner. *H19* also suppresses E-cadherin expression and promotes invasion in NPC cells through the miR-630/EZH2 pathway (60). And He et al. demonstrated that EBV-miR-BART6-3p suppressed EBV-associated cancer cell migration and invasion by targeting lncRNA *MIR3936HG* (also known as *LOC553103*) and reversing the EMT process. And *MIR3936HG* knockdown by specific siRNAs was shown to phenocopy

the effect of EBV-miR-BART6-3p, while elevated *MIR3936HG* expression enhanced tumor cell migration and invasion to promote EMT (61).

miRNA DYSREGULATION-RELATED SIGNALING PATHWAYS IN NPC

Several signaling pathways are involved in miRNA dysregulation-related processes in NPC. For example, miR-125b was shown to promote NPC tumorigenesis by activating the NF-κB signaling pathway, which plays a critical role in NPC tumorigenesis and progression (44, 62). In addition, miR-19b-3p was found to be upregulated and to be an independent predictor for poor survival outcomes in NPC patients. MiR-19b-3b increased NPC cell radioresistance by targeting *TNFAIP3* and then activating the NF-κB signaling pathway (63).

The PTEN/AKT pathway plays an important role in NPC processes related to miRNA dysregulation. One study found that miR-141 was markedly elevated in NPC tissues and negatively correlated with both patient survival and the expression of the bromodomain containing 7 gene, *BRD7; BRD7* overexpression activated the PTEN/AKT pathway, but restoring miR-141 expression suppressed this activation and partially restored NPC cell proliferation and tumor growth. The BRD7/miR-141/PTEN/AKT axis therefore is important to NPC progression and could provide new treatment targets and diagnostic markers (64). In addition, EBV-encoded miRNAs miR-BART1 and miR-BART7-3p promote NPC metastasis by modulating the PTEN/PI3K/AKT signaling pathway (55, 56). PI3K signaling is also involved in miRNA dysregulation-related processes in NPC. A study of NPC tumor specimens found that tumor-suppressing protein PDCD4 suppresses the pPI3K/pAKT/c-JUN signaling pathway, which in turn modulates miR-374a's binding to *CCND1*, resulting in dysregulation of NPC cell growth, metastasis, and chemoresistance (65). In this study, miR-374a expression was positively correlated with PDCD4 expression and negatively correlated with *CCND1* expression. The PI3K/AKT/mTOR signaling pathway also significantly affects NPC tumorigenesis and development (66). For example, miR-3188 was shown to inhibit NPC cell cycle transition and proliferation, to sensitize cells to chemotherapy, and to extend survival in tumor-bearing mice, and to inactivate p-PI3K/p-AKT/c-JUN signaling by targeting mTOR directly, further suppressing the cell cycle through the p-PI3K/p-AKT/p-mTOR pathway (67).

miRNA DYSREGULATION IN NPC THERAPIES

Radiotherapy and chemotherapy are 2 main treatments for NPC. Mounting evidence shows that miRNAs are dysregulated during radio- or chemotherapy for NPC and may reduce or induce the sensitivity of NPC cells to radiotherapy or chemotherapy (**Table 1**).

miRNA Dysregulation in Radiotherapy

Radioresistance is the main reason for NPC treatment failure (68). Multiple studies have shown that miRNA expression in various cell types changed upon irradiation, as did the specific effects of various miRNAs on cellular radiosensitivity. It has been reported that miR-324-3p reduces NPC radioresistance by directly targeting the well-known oncogene Wnt family member 2B (*WNT2B*), inhibiting the gene's translation (69). Studies have also reported that miR-519d sensitizes NPC cells to radiation by directly targeting the 3′-UTR of *PDRG1* (p53 and DNA damage regulated 1) mRNA (70) and thatiR-24 increases radiosensitivity in NPC by targeting both *COPS5* and *SP1* (specificity protein 1) (15). In contrast, Huang et al. demonstrated that miR-19b-3p upregulation decreases—and downregulation increases—NPC sensitivity to radiation. The researchers also found that miR-19b-3p directly targeted *TNFAIP3*, and the gene's upregulation reversed miR-19b-3p's suppressive effects on NPC cell radiosensitivity. Thus, miR-19b-3p was shown to enhance radioresistance in NPC cells by activating the TNFAIP3/ NF-κB pathway (63). Together, these studies indicate the potential use of miRNAs as radiosensitizing agents in NPC treatment.

miRNAs Dysregulation in Chemotherapy

The importance of miRNAs in chemotherapy response has been demonstrated in multiple human cancers, including cancer of the tongue (71). In NPC, miR-3188 has been found to inhibit cell growth and resistance to fluorouracil by directly targeting the mechanistic target of rapamycin kinase gene, *MTOR*, and regulating the cell cycle (67). Another study showed that the metastasis suppressor miR-29c can also increase NPC cells' sensitivity to both radiotherapy and cisplatin-based chemotherapy (72). The above evidence shows that miRNAs mainly function as chemosensitizers in NPC.

miRNAS AS BIOMARKERS AND NOVEL THERAPEUTIC APPROACHES IN NPC

In the above sections, we showed that miRNAs are dysregulated during NPC initiation, progression, and therapy. In addition, several studies have reported that miRNA dysregulation is associated with the survival of NPC patients, and miRNAs may serve as independent biomarkers for NPC diagnosis, recurrence, and prognosis. Furthermore, a few molecularly targeted drugs have emerged as clinically active against advanced NPC in recent years (73), and the exploration of miRNAs as drugs or drug targets against other cancer types is already underway (29).

miRNAs as Biomarkers in NPC

Several miRNAs show potential as biomarkers in NPC. A recent meta-analysis indicated that increased miRNA expression led to a poor overall survival and increased the likelihood of death of NPC patients (74). The tumor and metastasis suppressor miR-29c has been shown to be downregulated in both the serum and tumor tissue of NPC patients, indicating its promise as a biomarker for NPC diagnosis, prognosis, and recurrence (75). Also, NPC patients were shown to have significantly higher serum levels of miR-663 compared with healthy individuals, and high levels were associated with worse 5-year overall and relapse-free survival outcomes in NPC patients (76). In addition, chemotherapy significantly lowered NPC patients' serum miR-663 levels. These results suggest a critical role for miR-663 as

a biomarker of NPC prognosis and response to chemotherapy. Recent studies showed that miR-31-5p was downregulated in present in NPC tissues and cell lines, acting as a tumor suppressive miRNA. And circulating miR-31-5p was identified to be a potential novel and non-invasive biomarker for the early diagnosis of NPC (77). The expression levels of tumor-educated platelet miR-34c-3p and miR-18a-5p are upregulated in NPC, which are promising novel liquid biopsy biomarkers for NPC diagnosis (78). In addition, miR-342-3p was significantly downregulated in NPC specimens and its low expression was significantly correlated with reduced overall survival of NPC patients, indicating miR-342-3p as a biomarker of NPC prognosis (79). All in all, the above results suggest miRNA can be a single biomarker for NPC diagnosis, prognosis, and response to therapy.

Additionally, miRNA signatures have been more and more identified to be novel biomarkers of NPC prognosis and prediction. For example, a two-miRNA signature of miR-548q and miR-483-5p were identified as potential biomarkers of NPC by comparing the plasma miRNA profiles of 31 NPC patients and 19 controls (80). And a three-miRNA signature including miR-548q, miR-630, and miR940 were increased in the plasma of NPC patients compared to those of controls. They are potential novel and useful biomarkers for NPC detection and diagnosis (81). The plasma level of miR-483-5p, miR-103, and miR-29a could be helpful to predict survival in patients with NPC (82). A four-miRNA signature of miR-22, miR-572, miR-638, and miR-1234 were identified to be prognostic biomarkers of NPC to the TNM staging system (83). Recently, a 8-miRNA signature including miR-188-5p, miR-1908, miR-3196, miR-3935, miR-4284, miR-4433-5p, miR-4665-3p, miR-513b, and 16-miRNA signature including miR-1224-3p, miR-1280, miR-155-5p, miR-1908, miR-1973, miR-296-5p, miR-361-3p, miR-425-5p, miR-4284, miR-4436b-5p, miR-4439, miR-4665-3p, miR-4706, miR-4740-3p, miR-5091, miR-513b are promising biomarkers for NPC diagnosis (84). Taker together, miRNAs can be as both single biomarkers and signatures for NPC detection, diagnosis, and prognosis (**Table 2**).

miRNAs as Therapeutic Approaches in NPC

One of the most appealing properties of miRNAs as therapeutic agents is their ability to simultaneously target more than 1 gene, making miRNAs extremely efficient for regulating distinct cell processes relevant to normal and malignant cell homeostasis. In NPC, miRNAs for gene therapy have been delivered using lentiviral vectors. For example, a previous study found that tumor suppressor miR-31-5pinhibited EBV-positive NPC tumorigenesis, and minicircle-oriP-miR-31, a novel EBNA1-specific miRNA delivery system, was constructed and shown to inhibit NPC cell proliferation and migration *in vitro* and to suppress xenograft growth and lung metastasis *in vivo*. The researchers also found that the WD repeat domain 5 gene, *WDR5*, is a target of miR-31-5p. The study proved that targeted delivery of miR-31-5p using a non-viral minicircle vector could serve as a novel therapeutic approach for NPC, indicating a promising miRNA therapy for NPC patients (85). More studies are still ongoing to apply miRNA therapy to patients with NPC.

CONCLUSIONS AND FUTURE DIRECTIONS

The need for novel therapeutic targets and agents for treating NPC patients is urgent, owing to NPC's anatomical location and resistance to both radiotherapy and chemotherapy. Large

TABLE 2 | miRNAs as biomarkers in NPC.

MiR	Expression in NPC	Biomarker	References
MiR-29c	Downregulated in NPC tissue	NPC diagnosis and prognosis	(75)
MiR-663	Upregualted in NPC serum	NPC prognosis and response to chemotherapy	(76)
MiR-31-5p	Downregulated in NPC tissue	NPC diagnosis	(77)
MiR-34c-3p	Upregualted in NPC tissue	NPC diagnosis	(78)
MiR-18a-5p	Upregualted in NPC tissue	NPC diagnosis	(78)
MiR-342-3p	Downregulated in NPC tissue	NPC prognosis	(79)
MiR signatures			
2-miRNA: miR-548q and miR-483-5p		NPC detection	(80)
3-miRNA: miR-548q, miR-630, and miR940		NPC detection and diagnosis	(81)
3-miRNA: miR-483-5p, miR-103, and miR-29a		NPC prognosis	(82)
4-miRNA: miR-22, miR-572, miR-638, and miR-1234		NPC prognosis	(83)
8-miRNA: miR-188-5p, miR-1908, miR-3196, miR-3935, miR-4284, miR-4433-5p, miR-4665-3p, miR-513b		NPC diagnosis	(84)
16-miRNA: miR-1224-3p, miR-1280, miR-155-5p, miR-1908, miR-1973, miR-296-5p, miR-361-3p, miR-425-5p, miR-4284, miR-4436b-5p, miR-4439, miR-4665-3p, miR-4706, miR-4740-3p, miR-5091, miR-513b		NPC diagnosis	(84)

numbers of miRNAs are dysregulated during the process of NPC initiation, progression, and therapy; therefore, miRNAs have been proposed as useful biomarkers to predict prognosis in and therapeutic approaches to cure patients with NPC. The advantages of using miRNAs as drugs antagonizing NPC is that 1 miRNA can target multiple targets and the same target can be targeted by many miRNAs, showing their comprehensive potential roles in the clinic. Based on the previous studies on miRNA dysregulations in NPC, how to use and take the advantages of miRNAs in clinic is to be solved. And due to the fact that miRNAs can regulate many mRNAs, the potential of toxic phenotypes and other off-target effects of miRNA treatment approaches is a major concern. As a result, more and more studies focusing on the toxic effects of targeting miRNAs are required before such therapies can be used safely in NPC patients.

AUTHOR CONTRIBUTIONS

SW was responsible for the writing and editing of the manuscript. F-XC was responsible for modifying the manuscript. WW provided some critical useful suggestions.

FUNDING

This work was supported by the Chinese medicine science and technology research project of Guangdong Provincial Hospital of Chinese Medicine (YN2016QJ03), the Guangdong Medical Science and Technology Research Foundation (A2018251), the doctoral research project of Guangdong Natural Science Foundation of China (2017A030310326), the China Postdoctoral Science Foundation Sixty-third Batches of Projects (2018M630941), the Guangzhou science and technology plan project (201804010149), the Major Research Projects in First-class Disciplines of Guangzhou University of Chinese Medicine (A1260619111001), and the Science and Technology Planning Project of Guangdong Province (2017B030314166).

ACKNOWLEDGMENTS

We thank Butt, Bryan F from the Department of Scientific Publications at The University of Texas MD Anderson Cancer Center for editorial support.

REFERENCES

1. Wei WI, Sham JS. Nasopharyngeal carcinoma. *Lancet*. (2005) 365:2041–54. doi: 10.1016/S0140-6736(05)66698-6
2. Le QT, Jones CD, Yau TK, Shirazi HA, Wong PH, Thomas EN, et al. A comparison study of different PCR assays in measuring circulating plasma epstein-barr virus DNA levels in patients with nasopharyngeal carcinoma. *Clin Cancer Res.* (2005) 11:5700–7. doi: 10.1158/1078-0432.CCR-05-0648
3. Chan AT, Gregoire V, Lefebvre JL, Licitra L, Felip E, Group E-E-EGW. Nasopharyngeal cancer: EHNS-ESMO-ESTRO Clinical Practice Guidelines for diagnosis, treatment and follow-up. *Ann Oncol.* (2010) 21(Suppl 5):v187–9. doi: 10.1093/annonc/mdq186
4. Lee RC, Feinbaum RL, Ambros V. The *C. elegans* heterochronic gene lin-4 encodes small RNAs with antisense complementarity to lin-14. *Cell.* (1993) 75:843–54. doi: 10.1016/0092-8674(93)90529-Y
5. Ambros V. The functions of animal microRNAs. *Nature.* (2004) 431:350–5. doi: 10.1038/nature02871
6. Lee Y, Kim M, Han J, Yeom KH, Lee S, Baek SH, et al. MicroRNA genes are transcribed by RNA polymerase II. *EMBO J.* (2004) 23:4051–60. doi: 10.1038/sj.emboj.7600385
7. Lee Y, Ahn C, Han J, Choi H, Kim J, Yim J, et al. The nuclear RNase III Drosha initiates microRNA processing. *Nature.* (2003) 425:415–9. doi: 10.1038/nature01957
8. Bohnsack MT, Czaplinski K, Gorlich D. Exportin 5 is a RanGTP-dependent dsRNA-binding protein that mediates nuclear export of pre-miRNAs. *RNA.* (2004) 10:185–91. doi: 10.1261/rna.5167604
9. Chendrimada TP, Gregory RI, Kumaraswamy E, Norman J, Cooch N, Nishikura K, et al. TRBP recruits the Dicer complex to Ago2 for microRNA processing and gene silencing. *Nature.* (2005) 436:740–4. doi: 10.1038/nature03868
10. Betel D, Wilson M, Gabow A, Marks DS, Sander C. The microRNA.org resource: targets and expression. *Nucleic Acids Res.* (2008) 36:D149–53. doi: 10.1093/nar/gkm995
11. Friedman RC, Farh KK, Burge CB, Bartel DP. Most mammalian mRNAs are conserved targets of microRNAs. *Genome Res.* (2009) 19:92–105. doi: 10.1101/gr.082701.108
12. Lal A, Navarro F, Maher CA, Maliszewski LE, Yan N, O'Day E, et al. miR-24 Inhibits cell proliferation by targeting E2F2, MYC, and other cell-cycle genes via binding to "seedless" 3'UTR microRNA recognition elements. *Mol Cell.* (2009) 35:610–25. doi: 10.1016/j.molcel.2009.08.020
13. Orom UA, Nielsen FC, Lund AH. MicroRNA-10a binds the 5'UTR of ribosomal protein mRNAs and enhances their translation. *Mol Cell.* (2008) 30:460–71. doi: 10.1016/j.molcel.2008.05.001
14. Jopling CL, Yi M, Lancaster AM, Lemon SM, Sarnow P. Modulation of hepatitis C virus RNA abundance by a liver-specific MicroRNA. *Science.* (2005) 309:1577–81. doi: 10.1126/science.1113329
15. Wang S, Pan Y, Zhang R, Xu T, Wu W, Zhang R, et al. Hsa-miR-24-3p increases nasopharyngeal carcinoma radiosensitivity by targeting both the 3'UTR and 5'UTR of Jab1/CSN5. *Oncogene.* (2016) 35:6096–6108. doi: 10.1038/onc.2016.147
16. Eiring AM, Harb JG, Neviani P, Garton C, Oaks JJ, Spizzo R, et al. miR-328 functions as an RNA decoy to modulate hnRNP E2 regulation of mRNA translation in leukemic blasts. *Cell.* (2010) 140:652–65. doi: 10.1016/j.cell.2010.01.007
17. Place RF, Li LC, Pookot D, Noonan EJ, Dahiya R. MicroRNA-373 induces expression of genes with complementary promoter sequences. *Proc Natl Acad Sci USA.* (2018) 115:E3325. doi: 10.1073/pnas.1803343115
18. Vasudevan S, Tong Y, Steitz JA. Switching from repression to activation: microRNAs can up-regulate translation. *Science.* (2007) 318:1931–4. doi: 10.1126/science.1149460
19. Fabbri M, Paone A, Calore F, Galli R, Croce CM. A new role for microRNAs, as ligands of Toll-like receptors. *RNA Biol.* (2013) 10:169–74. doi: 10.4161/rna.23144
20. Tanaka Y, Kamohara H, Kinoshita K, Kurashige J, Ishimoto T, Iwatsuki M, et al. Clinical impact of serum exosomal microRNA-21 as a clinical biomarker in human esophageal squamous cell carcinoma. *Cancer.* (2013) 119:1159–67. doi: 10.1002/cncr.27895
21. Yang M, Chen J, Su F, Yu B, Su F, Lin L, et al. Microvesicles secreted by macrophages shuttle invasion-potentiating microRNAs into breast cancer cells. *Mol Cancer.* (2011) 10:117. doi: 10.1186/1476-4598-10-117
22. Lu J, Liu QH, Wang F, Tan JJ, Deng YQ, Peng XH, et al. Exosomal miR-9 inhibits angiogenesis by targeting MDK and regulating PDK/AKT pathway in nasopharyngeal carcinoma. *J Exp Clin Cancer Res.* (2018) 37:147. doi: 10.1186/s13046-018-0814-3

23. Ye SB, Zhang H, Cai TT, Liu YN, Ni JJ, He J, et al. Exosomal miR-24-3p impedes T-cell function by targeting FGF11 and serves as a potential prognostic biomarker for nasopharyngeal carcinoma. *J Pathol.* (2016) 240:329–40. doi: 10.1002/path.4781
24. Lo AK, To KF, Lo KW, Lung RW, Hui JW, Liao G, et al. Modulation of LMP1 protein expression by EBV-encoded microRNAs. *Proc Natl Acad Sci USA.* (2007) 104:16164–9. doi: 10.1073/pnas.0702896104
25. Pfeffer S, Zavolan M, Grasser FA, Chien M, Russo JJ, Ju J, et al. Identification of virus-encoded microRNAs. *Science.* (2004) 304:734–6. doi: 10.1126/science.1096781
26. Raab-Traub N. Epstein-Barr virus in the pathogenesis of NPC. *Semin Cancer Biol.* (2002) 12:431–41. doi: 10.1016/S1044579X0200086X
27. Lung RW, Hau PM, Yu KH, Yip KY, Tong JH, Chak WP, et al. EBV-encoded miRNAs target ATM-mediated response in nasopharyngeal carcinoma. *J Pathol.* (2018) 244:394–407. doi: 10.1002/path.5018
28. Calin GA, Sevignani C, Dan Dumitru C, Hyslop T, Noch E, Yendamuri S, et al. Human microRNA genes are frequently located at fragile sites and genomic regions involved in cancers. *Proc Natl Acad Sci USA.* (2004) 101:2999–3004. doi: 10.1073/pnas.0307323101
29. Garzon R, Marcucci G, Croce CM. Targeting microRNAs in cancer: rationale, strategies and challenges. *Nat Rev Drug Discov.* (2010) 9:775–89. doi: 10.1038/nrd3179
30. Ota A, Tagawa H, Karnan S, Tsuzuki S, Karpas A, Kira S, et al. Identification and characterization of a novel gene, C13orf25, as a target for 13q31-q32 amplification in malignant lymphoma. *Cancer Res.* (2004) 64:3087–95. doi: 10.1158/0008-5472.CAN-03-3773
31. Calin GA, Ferracin M, Cimmino A, Di Leva G, Shimizu M, Wojcik SE, et al. A MicroRNA signature associated with prognosis and progression in chronic lymphocytic leukemia. *N Engl J Med.* (2005) 353:1793–801. doi: 10.1056/NEJMoa050995
32. Garzon R, Volinia S, Liu CG, Fernandez-Cymering C, Palumbo T, Pichiorri F, et al. MicroRNA signatures associated with cytogenetics and prognosis in acute myeloid leukemia. *Blood.* (2008) 111:3183–9. doi: 10.1182/blood-2007-07-098749
33. Calin GA, Dumitru CD, Shimizu M, Bichi R, Zupo S, Noch E, et al. Frequent deletions and down-regulation of micro- RNA genes miR15 and miR16 at 13q14 in chronic lymphocytic leukemia. *Proc Natl Acad Sci USA.* (2002) 99:15524–9. doi: 10.1073/pnas.242606799
34. Saito Y, Liang G, Egger G, Friedman JM, Chuang JC, Coetzee GA, et al. Specific activation of microRNA-127 with downregulation of the proto-oncogene BCL6 by chromatin-modifying drugs in human cancer cells. *Cancer Cell.* (2006) 9:435–43. doi: 10.1016/j.ccr.2006.04.020
35. Wang S, Wu W, Claret FX. Mutual regulation of microRNAs and DNA methylation in human cancers. *Epigenetics.* (2017) 12:187–97. doi: 10.1080/15592294.2016.1273308
36. Wang R, Zhang T, Yang Z, Jiang C, Seng J. Long non-coding RNA FTH1P3 activates paclitaxel resistance in breast cancer through miR-206/ABCB1. *J Cell Mol Med.* (2018) 22:4068–75. doi: 10.1111/jcmm.13679
37. Wang R, Zhang S, Chen X, Li N, Li J, Jia R, et al. CircNT5E acts as a sponge of microRNA-422a to promote glioblastoma tumorigenesis. *Cancer Res.* (2018) 78:4812–25. doi: 10.1158/0008-5472.CAN-18-0532
38. Merritt WM, Lin YG, Han LY, Kamat AA, Spannuth WA, Schmandt R, et al. Dicer, Drosha, and outcomes in patients with ovarian cancer. *N Engl J Med.* (2008) 359:2641–50. doi: 10.1056/NEJMoa0803785
39. He L, He X, Lim LP, de Stanchina E, Xuan Z, Liang Y, et al. A microRNA component of the p53 tumour suppressor network. *Nature.* (2007) 447:1130–4. doi: 10.1038/nature05939
40. Chang TC, Wentzel EA, Kent OA, Ramachandran K, Mullendore M, Lee KH, et al. Transactivation of miR-34a by p53 broadly influences gene expression and promotes apoptosis. *Mol Cell.* (2007) 26:745–52. doi: 10.1016/j.molcel.2007.05.010
41. Chang TC, Yu D, Lee YS, Wentzel EA, Arking DE, West KM, et al. Widespread microRNA repression by Myc contributes to tumorigenesis. *Nat Genet.* (2008) 40:43–50. doi: 10.1038/ng.2007.30
42. Chen HC, Chen GH, Chen YH, Liao WL, Liu CY, Chang KP, et al. MicroRNA deregulation and pathway alterations in nasopharyngeal carcinoma. *Br J Cancer.* (2009) 100:1002–11. doi: 10.1038/sj.bjc.6604948
43. Yi C, Wang Q, Wang L, Huang Y, Li L, Liu L, et al. MiR-663, a microRNA targeting p21(WAF1/CIP1), promotes the proliferation and tumorigenesis of nasopharyngeal carcinoma. *Oncogene.* (2012) 31:4421–33. doi: 10.1038/onc.2011.629
44. Zheng Z, Qu JQ, Yi HM, Ye X, Huang W, Xiao T, et al. MiR-125b regulates proliferation and apoptosis of nasopharyngeal carcinoma by targeting A20/NF-kappaB signaling pathway. *Cell Death Dis.* (2017) 8:e2855. doi: 10.1038/cddis.2017.211
45. Lu J, Luo H, Liu X, Peng Y, Zhang B, Wang L, et al. miR-9 targets CXCR4 and functions as a potential tumor suppressor in nasopharyngeal carcinoma. *Carcinogenesis.* (2014) 35:554–63. doi: 10.1093/carcin/bgt354
46. Wang LX, Kang ZP, Yang ZC, Ma RX, Tan Y, Peng XB, et al. MicroRNA-135a inhibits nasopharyngeal carcinoma cell proliferation through targeting interleukin-17. *Cell Physiol Biochem.* (2018) 46:2232–8. doi: 10.1159/000489591
47. Li Y, Tang X, He Q, Yang X, Ren X, Wen X, et al. Overexpression of mitochondria mediator gene TRIAP1 by miR-320b loss is associated with progression in nasopharyngeal carcinoma. *PLoS Genet.* (2016) 12:e1006183. doi: 10.1371/journal.pgen.1006183
48. Song P, Yin SC. Long non-coding RNA EWSAT1 promotes human nasopharyngeal carcinoma cell growth *in vitro* by targeting miR-326/-330-5p. *Aging.* (2016) 8:2948–60. doi: 10.18632/aging.101103
49. Hua WF, Zhong Q, Xia TL, Chen Q, Zhang MY, Zhou AJ, et al. RBM24 suppresses cancer progression by upregulating miR-25 to target MALAT1 in nasopharyngeal carcinoma. *Cell Death Dis.* (2016) 7:e2352. doi: 10.1038/cddis.2016.252
50. Liu N, Jiang N, Guo R, Jiang W, He QM, Xu YF, et al. MiR-451 inhibits cell growth and invasion by targeting MIF and is associated with survival in nasopharyngeal carcinoma. *Mol Cancer.* (2013) 12:123. doi: 10.1186/1476-4598-12-123
51. Sun KY, Peng T, Chen Z, Song P, Zhou XH. Long non-coding RNA LOC100129148 functions as an oncogene in human nasopharyngeal carcinoma by targeting miR-539-5p. *Aging.* (2017) 9:999–1011. doi: 10.18632/aging.101205
52. Lu JA, He ML, Wang L, Chen Y, Liu XO, Dong Q, et al. MiR-26a inhibits cell growth and tumorigenesis of nasopharyngeal carcinoma through repression of EZH2. *Cancer Res.* (2011) 71:225–33. doi: 10.1158/0008-5472.CAN-10-1850
53. Li ZL, Ye SB, OuYang LY, Zhang H, Chen YS, He J, et al. COX-2 promotes metastasis in nasopharyngeal carcinoma by mediating interactions between cancer cells and myeloid-derived suppressor cells. *Oncoimmunology.* (2015) 4:e1044712. doi: 10.1080/2162402X.2015.1044712
54. Bao L, You B, Shi S, Shan Y, Zhang Q, Yue H, et al. Metastasis-associated miR-23a from nasopharyngeal carcinoma-derived exosomes mediates angiogenesis by repressing a novel target gene TSGA10. *Oncogene.* (2018) 37:2873–89. doi: 10.1038/s41388-018-0183-6
55. Cai L, Ye Y, Jiang Q, Chen Y, Lyu X, Li J, et al. Epstein-Barr virus-encoded microRNA BART1 induces tumour metastasis by regulating PTEN-dependent pathways in nasopharyngeal carcinoma. *Nat Commun.* (2015) 6:7353. doi: 10.1038/ncomms8353
56. Cai LM, Lyu XM, Luo WR, Cui XF, Ye YF, Yuan CC, et al. EBV-miR-BART7-3p promotes the EMT and metastasis of nasopharyngeal carcinoma cells by suppressing the tumor suppressor PTEN. *Oncogene.* (2015) 34:2156–66. doi: 10.1038/onc.2014.341
57. Liu N, Tang LL, Sun Y, Cui RX, Wang HY, Huang BJ, et al. MiR-29c suppresses invasion and metastasis by targeting TIAM1 in nasopharyngeal carcinoma. *Cancer Lett.* (2013) 329:181–8. doi: 10.1016/j.canlet.2012.10.032
58. Tang XR, Wen X, He QM, Li YQ, Ren XY, Yang XJ, et al. MicroRNA-101 inhibits invasion and angiogenesis through targeting ITGA3 and its systemic delivery inhibits lung metastasis in nasopharyngeal carcinoma. *Cell Death Dis.* (2017) 8:e2566. doi: 10.1038/cddis.2016.486
59. Jiang N, Jiang X, Chen Z, Song X, Wu L, Zong D, et al. MiR-203a-3p suppresses cell proliferation and metastasis through inhibiting LASP1 in nasopharyngeal carcinoma. *J Exp Clin Cancer Res.* (2017) 36:138. doi: 10.1186/s13046-017-0604-3
60. Li X, Lin Y, Yang X, Wu X, He X. Long noncoding RNA H19 regulates EZH2 expression by interacting with miR-630 and promotes cell invasion in

nasopharyngeal carcinoma. *Biochem Biophys Res Commun.* (2016) 473:913–9. doi: 10.1016/j.bbrc.2016.03.150
61. He B, Li W, Wu Y, Wei F, Gong Z, Bo H, et al. Epstein-Barr virus-encoded miR-BART6-3p inhibits cancer cell metastasis and invasion by targeting long non-coding RNA LOC553103. *Cell Death Dis.* (2016) 7:e2353. doi: 10.1038/cddis.2016.253
62. Zhu DD, Zhang J, Deng W, Yip YL, Lung HL, Tsang CM, et al. Significance of NF-kappaB activation in immortalization of nasopharyngeal epithelial cells. *Int J Cancer.* (2016) 138:1175–85. doi: 10.1002/ijc.29850
63. Huang T, Yin L, Wu J, Gu JJ, Wu JZ, Chen D, et al. MicroRNA-19b-3p regulates nasopharyngeal carcinoma radiosensitivity by targeting TNFAIP3/NF-kappaB axis. *J Exp Clin Cancer Res.* (2016) 35:188. doi: 10.1186/s13046-016-0465-1
64. Liu Y, Zhao R, Wang H, Luo Y, Wang X, Niu W, et al. miR-141 is involved in BRD7-mediated cell proliferation and tumor formation through suppression of the PTEN/AKT pathway in nasopharyngeal carcinoma. *Cell Death Dis.* (2016) 7:e2156. doi: 10.1038/cddis.2016.64
65. Zhen Y, Fang W, Zhao M, Luo R, Liu Y, Fu Q, et al. miR-374a-CCND1-pPI3K/AKT-c-JUN feedback loop modulated by PDCD4 suppresses cell growth, metastasis, and sensitizes nasopharyngeal carcinoma to cisplatin. *Oncogene.* (2017) 36:275–85. doi: 10.1038/onc.2016.201
66. Wang F, Lu J, Peng X, Wang J, Liu X, Chen X, et al. Integrated analysis of microRNA regulatory network in nasopharyngeal carcinoma with deep sequencing. *J Exp Clin Cancer Res.* (2016) 35:17. doi: 10.1186/s13046-016-0292-4
67. Zhao M, Luo R, Liu Y, Gao L, Fu Z, Fu Q, et al. miR-3188 regulates nasopharyngeal carcinoma proliferation and chemosensitivity through a FOXO1-modulated positive feedback loop with mTOR-p-PI3K/AKT-c-JUN. *Nat Commun.* (2016) 7:11309. doi: 10.1038/ncomms11309
68. Liu SC, Tsang NM, Chiang WC, Chang KP, Hsueh C, Liang Y, et al. Leukemia inhibitory factor promotes nasopharyngeal carcinoma progression and radioresistance. *J Clin Invest.* (2013) 123:5269–83. doi: 10.1172/JCI63428
69. Li G, Liu Y, Su Z, Ren S, Zhu G, Tian Y, et al. MicroRNA-324-3p regulates nasopharyngeal carcinoma radioresistance by directly targeting WNT2B. *Eur J Cancer.* (2013) 49:2596–607. doi: 10.1016/j.ejca.2013.03.001
70. Xu T, Xiao D. Oleuropein enhances radiation sensitivity of nasopharyngeal carcinoma by downregulating PDRG1 through HIF1alpha-repressed microRNA-519d. *J Exp Clin Cancer Res.* (2017) 36:3. doi: 10.1186/s13046-016-0480-2
71. Sun L, Yao Y, Liu B, Lin Z, Lin L, Yang M, et al. MiR-200b and miR-15b regulate chemotherapy-induced epithelial-mesenchymal transition in human tongue cancer cells by targeting BMI1. *Oncogene.* (2012) 31:432–45. doi: 10.1038/onc.2011.263
72. Zhang JX, Qian D, Wang FW, Liao DZ, Wei JH, Tong ZT, et al. MicroRNA-29c enhances the sensitivities of human nasopharyngeal carcinoma to cisplatin-based chemotherapy and radiotherapy. *Cancer Lett.* (2013) 329:91–8. doi: 10.1016/j.canlet.2012.10.033
73. Lim WT, Ng QS, Ivy P, Leong SS, Singh O, Chowbay B, et al. A Phase II study of pazopanib in Asian patients with recurrent/metastatic nasopharyngeal carcinoma. *Clin Cancer Res.* (2011) 17:5481–9. doi: 10.1158/1078-0432.CCR-10-3409
74. Sabarimurugan S, Kumarasamy C, Baxi S, Devi A, Jayaraj R. Systematic review and meta-analysis of prognostic microRNA biomarkers for survival outcome in nasopharyngeal carcinoma. *PLoS ONE.* (2019) 14:e0209760. doi: 10.1371/journal.pone.0209760
75. Niu M, Gao D, Wen Q, Wei P, Pan S, Shuai C, et al. MiR-29c regulates the expression of miR-34c and miR-449a by targeting DNA methyltransferase 3a and 3b in nasopharyngeal carcinoma. *BMC Cancer.* (2016) 16:218. doi: 10.1186/s12885-016-2253-x
76. Liang S, Zhang N, Deng Y, Chen L, Zhang Y, Zheng Z, et al. Increased serum level of microRNA-663 is correlated with poor prognosis of patients with nasopharyngeal carcinoma. *Dis Markers.* (2016) 2016:7648215. doi: 10.1155/2016/7648215
77. Yi SJ, Liu P, Chen BL, Ou-Yang L, Xiong WM, Su JP. Circulating miR-31-5p may be a potential diagnostic biomarker in nasopharyngeal carcinoma. *Neoplasma.* (2019) 10:181109N847. doi: 10.4149/neo_2018_181109N847
78. Wang H, Wei X, Wu B, Su J, Tan W, Yang K. Tumor-educated platelet miR-34c-3p and miR-18a-5p as potential liquid biopsy biomarkers for nasopharyngeal carcinoma diagnosis. *Cancer Manag Res.* (2019) 11:3351–60. doi: 10.2147/CMAR.S195654
79. Cui Z, Zhao Y. microRNA-342-3p targets FOXQ1 to suppress the aggressive phenotype of nasopharyngeal carcinoma cells. *BMC Cancer.* (2019) 19:104. doi: 10.1186/s12885-018-5225-5
80. Zheng XH, Cui C, Ruan HL, Xue WQ, Zhang SD, Hu YZ, et al. Plasma microRNA profiling in nasopharyngeal carcinoma patients reveals miR-548q and miR-483-5p as potential biomarkers. *Chin J Cancer.* (2014) 33:330–8. doi: 10.5732/cjc.013.10246
81. Zhuo X, Zhou W, Li D, Chang A, Wang Y, Wu Y, et al. Plasma microRNA expression signature involving miR-548q, miR-630 and miR-940 as biomarkers for nasopharyngeal carcinoma detection. *Cancer Biomarkers.* (2018) 23:579–87. doi: 10.3233/CBM-181852
82. Wang HY, Yan LX, Shao Q, Fu S, Zhang ZC, Ye W, et al. Profiling plasma microRNA in nasopharyngeal carcinoma with deep sequencing. *Clin Chem.* (2014) 60:773–82. doi: 10.1373/clinchem.2013.214213
83. Liu N, Cui RX, Sun Y, Guo R, Mao YP, Tang LL, et al. A four-miRNA signature identified from genome-wide serum miRNA profiling predicts survival in patients with nasopharyngeal carcinoma. *Int J Cancer.* (2014) 134:1359–68. doi: 10.1002/ijc.28468
84. Wen W, Mai SJ, Lin HX, Zhang MY, Huang JL, Hua X, et al. Identification of two microRNA signatures in whole blood as novel biomarkers for diagnosis of nasopharyngeal carcinoma. *J Transl Med.* (2019) 17:186. doi: 10.1186/s12967-019-1923-2
85. Wu J, Tan X, Lin J, Yuan L, Chen J, Qiu L, et al. Minicircle-oriP-miR-31 as a novel EBNA1-specific miRNA therapy approach for nasopharyngeal carcinoma. *Hum Gene Ther.* (2017) 28:415–27. doi: 10.1089/hum.2016.136

Conflict of Interest Statement: The authors declare that the research was conducted in the absence of any commercial or financial relationships that could be construed as a potential conflict of interest.

frontiers in Oncology

CASE REPORT
published: 14 August 2019
doi: 10.3389/fonc.2019.00734

Pembrolizumab in a Patient With a Metastatic CASTLE Tumor of the Parotid

Lisa Lorenz[1†], Joscha von Rappard[1†], Walter Arnold[2†], Nicole Mutter[3], Udo Schirp[4], Andreas Scherr[5] and Andreas Werner Jehle[1,6]*

[1] Department of Internal Medicine, Hirslanden Klinik St. Anna, Lucerne, Switzerland, [2] Department of Pathology, Cantonal Hospital Lucerne, Lucerne, Switzerland, [3] Department of Oncology, Hirslanden Klinik St. Anna, Lucerne, Switzerland, [4] Institute of Radiology and Nuclear Medicine, Hirslanden Klinik St. Anna, Lucerne, Switzerland, [5] Department of Pneumology, Hirslanden Klinik St. Anna, Lucerne, Switzerland, [6] Transplantation Immunology and Nephrology, University Hospital Basel, Basel, Switzerland

OPEN ACCESS

Edited by:
Cheng-Chia Yu,
Chung Shan Medical University, Taiwan

Reviewed by:
Cesare Piazza,
National Tumor Institute (Italy), Italy
Prasanth Penumadu,
Jawaharlal Institute of Postgraduate Medical Education and Research (JIPMER), India

***Correspondence:**
Andreas Werner Jehle
andreas.jehle@hirslanden.ch;
andreas.jehle@unibas.ch

[†]These authors have contributed equally to this work

Specialty section:
This article was submitted to Head and Neck Cancer, a section of the journal Frontiers in Oncology

Received: 05 April 2019
Accepted: 22 July 2019
Published: 14 August 2019

Citation:
Lorenz L, von Rappard J, Arnold W, Mutter N, Schirp U, Scherr A and Jehle AW (2019) Pembrolizumab in a Patient With a Metastatic CASTLE Tumor of the Parotid. Front. Oncol. 9:734. doi: 10.3389/fonc.2019.00734

Carcinoma showing thymus-like elements (CASTLE) is a rare tumor, most commonly found in the thyroid gland. Here we report a case of CASTLE tumor localized to the parotid gland, recognized in retrospect after a late manifestation of symptomatic pleural carcinomatosis. The original tumor in the parotid gland was treated by surgery followed by radiotherapy. Ten years later, a metastatic disease with recurrent pleural effusions occurred. Pleural carcinomatosis was strongly positive for CD5, CD117, and p63 as was the original tumor of the parotid, which allowed the diagnosis of a CASTLE tumor. Additionally, the pleural tumor expressed high levels of programmed death ligand 1 (PD-L1), and the patient underwent treatment with the monoclonal PD-L1 inhibitor pembrolizumab achieving a partial remission. To the best of our knowledge, this is the first patient with a metastatic CASTLE tumor treated with a PD-L1 inhibitor.

Keywords: CASTLE, parotid, extrathyroidal, carcinoma, thymus-like, PD-L1, immunotherapy, checkpoint inhibitor

BACKGROUND

Carcinoma showing thymus-like differentiation (CASTLE) is a rare tumor usually of the thyroid gland or adjacent soft tissues of the neck (1). The entity was first described as an intrathyroidal epithelial thymoma by Miyauchi et al. (2) and later renamed as CASTLE by Chan and Rosai, who proposed that these tumors arise either from ectopic thymuses or from remnants of the branchial pouches that differentiate along the thymic line (3).

CASTLE tumors show not only structural similarity to thymic tissue but also express molecular markers of thymomas and thymic carcinomas (4, 5). In immunohistochemical staining, they are positive for CD5 in nearly all cases and positive for CD117 and p63, but negative for markers of thyroid carcinomas, such as thyroglobulin and calcitonin (5).

CASTLE tumors are indolent and slow-growing malignant neoplasms. In about 30–50% of cases, that describe the nodal status, lymph node involvement is reported and in 14–29% metastatic disease (6). Radical surgery is the treatment of choice for CASTLE, and radiotherapy is considered in patients with positive lymph node status. For advanced and metastatic disease, the standard

treatment is chemotherapy (6). However, because of the rarity of CASTLE, data on the effectiveness of adjuvant radiotherapy and chemotherapy is missing.

Immunotherapy has become a cornerstone in the treatment of several malignancies in the past few years and involves the use of immune checkpoint inhibitors including antibodies against programmed cell death protein 1 (PD-1), and programmed death ligand 1 (PD-L1) (7). When PD-1, which is primarily expressed on activated T cells, binds PD-L1 on tumor cells, the cytotoxic T-cell response is reduced. PD-L1 expression is associated with a better response to anti-PD-1 treatment in non-small cell lung cancer (8, 9) as well as in thymic carcinoma (10). Herein, we report what we believe is the first case of a metastatic CASTLE tumor systemically treated with the PD-L1 inhibitor pembrolizumab.

CASE PRESENTATION

A 79-year old woman was hospitalized on April 25, 2018, at which time she had progressive dyspnea over the past 5 weeks, productive cough, poor appetite, and weight loss of 5 kg over the last 6 months currently weighing 81 kg. Her medical history included an invasive ductal breast cancer pT1cN0M0 G2 ER 90%, PR 20% 20 years ago treated with lumpectomy, radiotherapy, and tamoxifen until 2004, and an undifferentiated cancer of the right parotid pT1 (17 mm) pN2 (1/2 positive in level I, 1/11 positive in level II, no extranodal extensions) pM0 diagnosed 2008 and treated with a total parotidectomy achieving R0 margins and a selective neck dissection levels II-IV followed by radiotherapy.

On physical examination, the patient was in mild respiratory distress. The pulmonary exam revealed dullness to percussion, decreased fremitus, and decreased breathing sounds in up to two-thirds of the left lung field. Oxygen saturation was 92% with the patient breathing ambient air, and arterial blood gases showed partial respiratory insufficiency. A chest X-ray confirmed a left-sided pleural effusion, and thoracentesis removed 1.5 liters of turbid fluid. Biochemical analysis of the fluid established an exudative etiology. Atypical cells with immunocytochemical positivity for p40, cytokeratin 5, and p63 in the cytopathology specimen were primarily suggestive of a non-small cell lung cancer, and a CT scan of the thorax showed a mass (4.2 × 2.2 × 2.8 cm) in the right upper lobe and extensive cardiophrenic, mediastinal, and hilar lymphadenopathy as well as enlarged lymph nodes along the left arteria mammaria interna. An FDG PET/CT scan confirmed these findings, and the scan revealed a hypermetabolic activity in mesenteric lymph nodes and at the left pleura (**Figures 1A,B**). Thoracoscopy and biopsy of the parietal pleura were performed. Surprisingly, histopathological examination revealed a non-small cell carcinoma (**Figure 2A**) expressing CD5 (**Figure 2B**), CD117 (**Figure 2C**), and p63 all indicating a carcinoma of thymic origin (5). With no signs of a thymic pathology, the histopathological diagnosis of CASTLE was established, and as additional immunostainings for CD5 (**Figure 3B**) and CD117 (**Figure 3C**) in the specimen of the parotid cancer diagnosed 2008 were positive also, a rare case of a CASTLE tumor of the parotid healed at the primary and neck sites, but with late metastatic dissemination was diagnosed.

As CD117 was highly overexpressed in the tumor, exons 9, 11, 13, 14, and 17 of the C-KIT gene were analyzed after extraction of genomic DNA by PCR using specific primers, but no common mutation was found consistent with previous reports (11, 12). Anticancer immunity and potential response to immunotherapy were assessed by PD-L1 staining of the pleural tumor, which showed a high expression level of 60% (**Figure 2D**).

The patient underwent talc pleurodesis and left partial pleurectomy for recurrent pleural effusions. Systemically, disseminated metastatic disease was treated with the monoclonal PD-L1 inhibitor pembrolizumab at a dose 200 mg every 3 weeks. Four months after the start of immunotherapy a follow-up FDG PET/CT study showed a partial remission with a moderate morphologic reduction of the tumor load, but a markedly reduced metabolic activity at all tumor sites (**Figures 1C,D**). Pembrolizumab treatment continued at a dose of 200 mg IV every 3 weeks. The patient showed a mild skin rash treated with low dose prednisolone (20 mg with tapering) for 2 weeks. No other adverse events associated with pembrolizumab were observed, and the therapy was tolerated well. At the last follow-up, the patient was in good clinical condition and had gained 3 kg of weight. On March 28th, 2019, a second follow-up FDG PET/CT showed no residual pleural effusion (not shown) and a further regression of lesions in the right lung and lymph nodes. Residual focal FDG-Uptake was seen in the left pleura (**Figures 1E,F**).

DISCUSSION

CASTLE is a rare malignant tumor, and in the majority of cases, the tumor is localized in the thyroid gland (6). Histologically, CASTLE resembles thymic carcinoma, and the current postulation is that these tumors arise from remnants of the branchial pouches with thymic differentiation, or ectopic thymuses (3, 13). This hypothesis is further supported by the observation that these tumors show positive immunostaining for CD5, CD117, and p63 reminiscent of thymomas and thymic carcinomas (4, 5). As Gao et al. (6) suggested the low number of reported cases of this disease may be related to the variable, and non-specific clinical manifestation and a conclusive diagnosis can only be maid by postsurgical pathological examination including immunohistochemical studies. A few extrathyroidal cases of CASTLE have been reported, and one of them localized to the right parotid and was classified as WHO stage III, pT1pN1cM0, and expressed CD5, CD117, P40, and P63 (14). The patient was treated with right total parotidectomy and ipsilateral selective neck dissection followed by adjuvant radiotherapy and remained disease free for more than 1 year after completing treatment on follow-up with MRI scan (14). In the case reported here, the diagnosis of the primary tumor in the parotid was made in

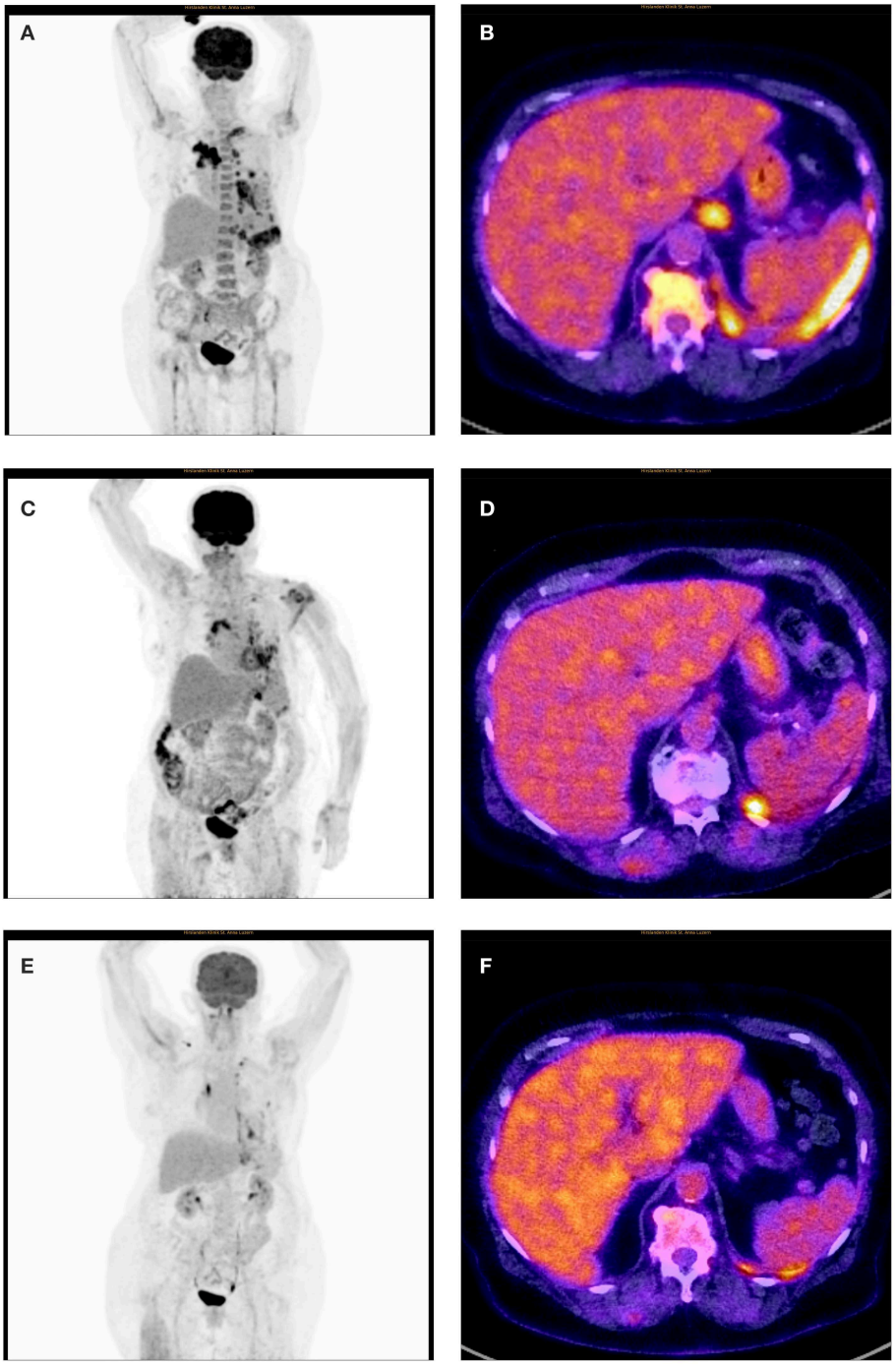

FIGURE 1 | Initial and follow-up FDG PET/CT: **(A)** Initial FDG-MIP with multiple hypermetabolic lesions in the upper lobe of the right lung, in mediastinal, hilar and upper mesenteric lymph nodes and at the left pleura. Increased turnover of the bone marrow. **(B)** Initial fusion FDG-PET/CT axial slice with pathologic high FDG-uptake in the left pleura, upper mesenteric lymph nodes, and bone marrow. Normal presentation of liver, spleen, and stomach. **(C)** Follow-up FDG-MIP after 4 months on pembrolizumab shows a generally reduced metabolism at all tumor locations. Normalization of the bone marrow turnover. Due to newly incipient traumatic injury at the left shoulder the patient could not lift up the left arm. **(D)** Fusion FDG-PET/CT axial slice after 4 months on pembrolizumab with residual FDG-uptake at the left pleura and in upper mesenteric lymph nodes. Normal presentation of the bone marrow. **(E)** Follow-up FDG-MIP after 11 months on pembrolizumab shows further regression of lesions in the upper lobe of the right lung as well as in mediastinal, hilar, and upper mesenteric lymph nodes (the focal lesions in the left mediastinum and supraclavicular right represent the central venous catheter). Residual focal FDG-Uptake in the left pleura. Normal turnover of the bone marrow. **(F)** Fusion FDG-PET/CT axial slice after 11 months on pembrolizumab with only little elevated FDG-uptake in the left pleura. The formerly upper mesenteric lymph node is healed up. Normal presentation of liver, spleen, stomach, and bone marrow.

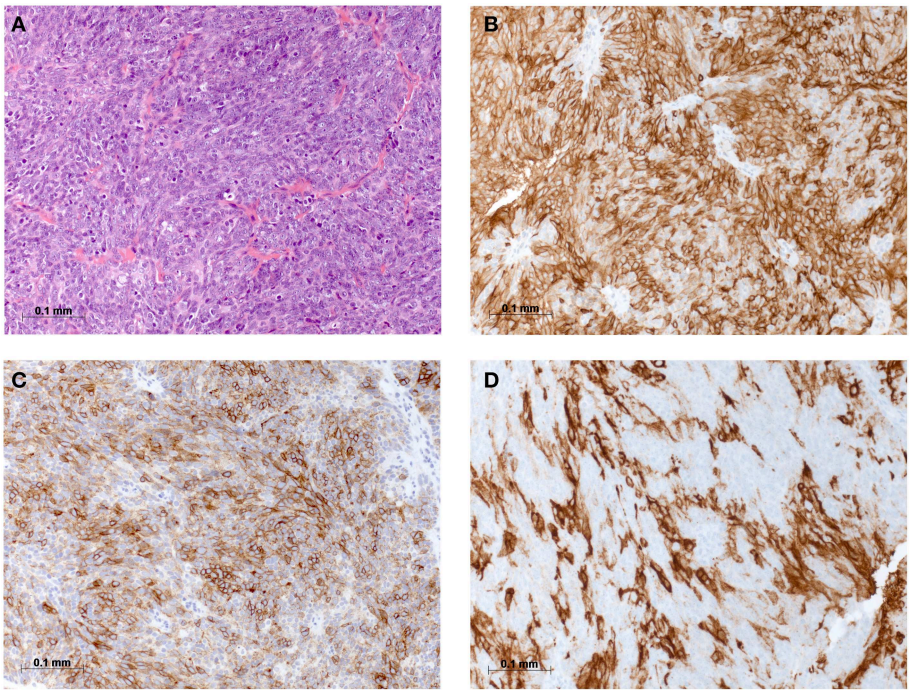

FIGURE 2 | Histomorphological and immunohistochemical analysis of parietal pleura, biopsy from 2018: **(A)** H & E staining, **(B)** Immunostaining for CD5, **(C)** Immunostaining for CD117, and **(D)** Immunostaining for PD-L1.

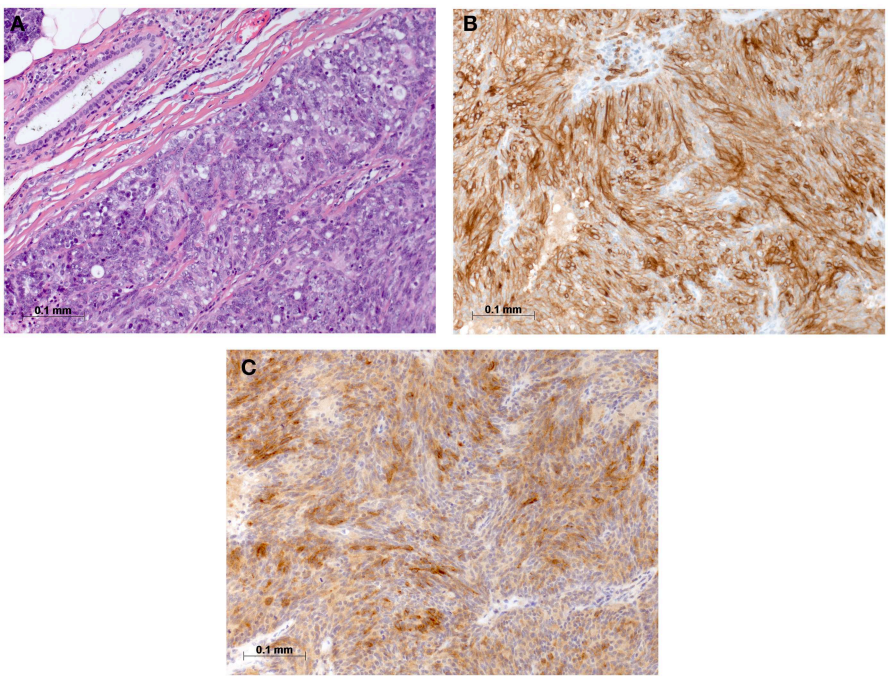

FIGURE 3 | Histomorphological and immunohistochemical analysis of parotid, tumor excisate from 2008: **(A)** H & E staining, **(B)** Immunostaining for CD5, and **(C)** Immunostaining for CD117.

retrospect after the disease was discovered in the pleural biopsy and after the parotid specimen was reanalyzed with additional staining for CD5 and CD117. We can not exclude the possibility of a metachronous CASTLE, but this seems unlikely due to the rarity of the disease. Also, we can not exclude with certainty that the lesion in the right upper lobe was a primary lung cancer with

metastasis of the collateral, left-sided pleura. But, this alternative diagnosis seems less likely in this non-smoking patient presenting with weight loss over 6 months and dyspnea due to the process in the left pleura with large, left-sided pleural effusion. Expression of CD5 and CD117 strongly support CASTLE with metastatic dissemination, though a minority of NSCLC are known to express CD5 and CD117 (15).

The parotid tumor pT1pN2pM0 diagnosed 2008 was treated as undifferentiated cancer with a total parotidectomy and a selective neck dissection levels II-IV followed by radiotherapy, a therapeutic approach typically used for CASTLE as well.

Chemotherapeutic regimens for advanced, metastatic CASTLE have been used based on those designed for thymic carcinomas (16) with the assumption that the tumor biology of CASTLE is similar to thymic carcinomas, but available data is very limited, and the benefit for patient survival unknown (6). For metastatic thymic carcinomas, the response rate to chemotherapy is <50% (17), and new effective therapies are awaited. Importantly, thymic carcinomas express high levels of PD-L1 (18), and recently, a first prospective study with the anti-PD-L1 antibody pembrolizumab in patients with no response to chemotherapy or recurrent, progressive disease was encouraging showing a positive correlation between response, progression-free survival, overall survival, and PD-L1 expression (10). To the best of our knowledge, expression levels of PD-L1 in CASTLE has not been investigated. In our patient 60% of tumor cells expressed PD-L1, and after intensive discussion in our interdisciplinary tumor board, a first line systemic therapy with pembrolizumab was initiated, which resulted in a partial response documented in a follow-up FDG PET/CT at 4 months. Except a skin rash no other adverse event potentially related to pembrolizumab was observed. At the last follow-up in March 2019 the patient was in good condition and a second follow-up FDG-PET/CT showed a sustained partial response.

CASTLE tumors may be found also in the parotid, have a slow and indolent course in spite of their undifferentiated histopathology, express PD-L1 and are therefore good targets for complementary immunotherapy when needed for recurrent/metastatic disease.

ETHICS STATEMENT

We received a written informed consent of the patient for the publication of this case report.

AUTHOR CONTRIBUTIONS

LL collected all data. LL and JvR wrote the first draft of the manuscript. WA performed histological analyses, provided images, and reviewed the manuscript. NM treated the patient and reviewed the manuscript. US provided FDG PET/CT images and reviewed the manuscript. AS reviewed the manuscript. AJ wrote the manuscript. All authors read and approved the submitted version of the manuscript.

REFERENCES

1. Youens KE, Bean SM, Dodd LG, Jones CK. Thyroid carcinoma showing thymus-like differentiation (CASTLE): case report with cytomorphology and review of the literature. *Diagn Cytopathol.* (2011) 39:204–9. doi: 10.1002/dc.21399
2. Miyauchi A, Kuma K, Matsuzuka F, Matsubayashi S, Kobayashi A, Tamai H, et al. Intrathyroidal epithelial thymoma - an entity distinct from squamous-cell carcinoma of the thyroid. *World J Surg.* (1985) 9:128–34. doi: 10.1007/BF01656263
3. Chan JK, Rosai J. Tumors of the neck showing thymic or related branchial pouch differentiation: a unifying concept. *Hum Pathol.* (1991) 22:349–67. doi: 10.1016/0046-8177(91)90083-2
4. Marx A, Chan JK, Coindre JM, Detterbeck F, Girard N, Harris NL, et al. The 2015 world health organization classification of tumors of the thymus: continuity and changes. *J Thoracic Oncol.* (2015) 10:1383–95. doi: 10.1097/JTO.0000000000000654
5. Ge W, Yao YZ, Chen G, Ding YT. Clinical analysis of 82 cases of carcinoma showing thymus-like differentiation of the thyroid. *Oncol Lett.* (2016) 11:1321–6. doi: 10.3892/ol.2015.4055
6. Gao R, Jia X, Ji T, Feng J, Yang A, Zhang G. Management and prognostic factors for thyroid carcinoma showing thymus-like elements (CASTLE): a case series study. *Front Oncol.* (2018) 8:477. doi: 10.3389/fonc.2018.00477
7. Hargadon KM, Johnson CE, Williams CJ. Immune checkpoint blockade therapy for cancer: an overview of FDA-approved immune checkpoint inhibitors. *Int Immunopharmacol.* (2018) 62:29–39. doi: 10.1016/j.intimp.2018.06.001
8. Garon EB, Rizvi NA, Hui R, Leighl N, Balmanoukian AS, Eder JP, et al. Pembrolizumab for the treatment of non-small-cell lung cancer. *N Engl J Med.* (2015) 372:2018–28. doi: 10.1056/NEJMoa1501824
9. Fehrenbacher L, Spira A, Ballinger M, Kowanetz M, Vansteenkiste J, Mazieres J, et al. Atezolizumab versus docetaxel for patients with previously treated non-small-cell lung cancer (POPLAR): a multicentre, open-label, phase 2 randomised controlled trial. *Lancet.* (2016) 387:1837–46. doi: 10.1016/S0140-6736(16)00587-0
10. Giaccone G, Kim C, Thompson J, McGuire C, Kallakury B, Chahine JJ, et al. Pembrolizumab in patients with thymic carcinoma: a single-arm, single-centre, phase 2 study. *Lancet Oncol.* (2018) 19:347–55. doi: 10.1016/S1470-2045(18)30062-7
11. Pan Y, Zhao X, Yang J, Deng J, Zhan Z, Luo Y, et al. Absence of gene mutations in KIT-positive carcinoma showing thymus-like elements of the thyroid. *Hum Pathol.* (2012) 43:350–5. doi: 10.1016/j.humpath.2011.05.003
12. Wang YF, Liu B, Fan XS, Rao Q, Xu Y, Xia QY, et al. Thyroid carcinoma showing thymus-like elements: a clinicopathologic, immunohistochemical, ultrastructural, and molecular analysis. *Am J Clin Pathol.* (2015) 143:223–33. doi: 10.1309/AJCPB7PS6QHWEFRK
13. Reimann JD, Dorfman DM, Nose V. Carcinoma showing thymus-like differentiation of the thyroid (CASTLE): a comparative study: evidence of thymic differentiation and solid cell nest origin. *Am J Surg Pathol.* (2006) 30:994–1001. doi: 10.1097/00000478-200608000-00010
14. Wong EHC, Tetter N, Tzankov A, Muller L. CASTLE tumor of the parotid: First documented case, literature review, and genetic analysis of the cancer. *Head Neck.* (2018) 40:E1–4. doi: 10.1002/hed.24985
15. Nakagawa K, Matsuno Y, Kunitoh H, Maeshima A, Asamura H, Tsuchiya R. Immunohistochemical KIT (CD117) expression in thymic epithelial tumors. *Chest.* (2005) 128:140–4. doi: 10.1378/chest.128.1.140

16. Hanamura T, Ito K, Uehara T, Fukushima T, Sasaki S, Koizumi T. Chemosensitivity in carcinoma showing thymus-like differentiation: a case report and review of the literature. *Thyroid*. (2015) 25:969–72. doi: 10.1089/thy.2015.0155
17. Kelly RJ, Petrini I, Rajan A, Wang Y, Giaccone G. Thymic malignancies: from clinical management to targeted therapies. *J Clin Oncol*. (2011) 29:4820–7. doi: 10.1200/JCO.2011.36.0487
18. Weissferdt A, Fujimoto J, Kalhor N, Rodriguez J, Bassett R, Wistuba, II, et al. Expression of PD-1 and PD-L1 in thymic epithelial neoplasms. *Modern Pathol*. (2017) 30:826–33. doi: 10.1038/modpathol.2017.6

Conflict of Interest Statement: The authors declare that the research was conducted in the absence of any commercial or financial relationships that could be construed as a potential conflict of interest.

frontiers in Oncology

ORIGINAL RESEARCH
published: 18 September 2019
doi: 10.3389/fonc.2019.00911

Anticancer Effect and Mechanism of Hydroxygenkwanin in Oral Squamous Cell Carcinoma

Yi-Chao Huang[1,2], *Po-Chuan Lee*[1], *Jane Jen Wang*[3] *and Yi-Chiung Hsu*[1]*

[1] *Department of Biomedical Sciences and Engineering, National Central University, Taoyuan, Taiwan,* [2] *Department of Medical Laboratory, Taoyuan Armed Forces General Hospital, Taoyuan, Taiwan,* [3] *The Department of Nursing, School of Nursing, National Taipei University of Nursing and Health Sciences, Taipei, Taiwan*

The incidence and mortality of oral squamous cell carcinoma (OSCC) are high, and the number of oral cancers had risen in the world. However, chemotherapy drugs have numerous side effects. There is an urgent requirement to develop a novel drug that can be used to treat oral cancer. Hydroxygenkwanin (HGK) is a nature flavonoid extracted from *Daphne genkwa Sieb. et Zucc. (Thymelaeaceae).* Previous studies had demonstrated that HGK exhibits anticancer effect, but the effect is still unclear in oral cancer. HGK inhibited cell growth dose-dependently in SAS and OCEM1 cells. The functional enrichment analysis showed the significant pathway in cellular movement, cell cycle and cellular growth and proliferation. We further demonstrated the HGK induced the cell cycle arrest by flow cytometry and inhibited colony formation ability and cell movement. The western blot showed that HGK induced cell cycle arrest through p21 activation and caused intrinsic cell apoptosis pathway. HGK inhibited the cell invasion and migration through down-regulation vimentin. HGK might be an effective natural product for oral cancer therapy.

Keywords: oral cancer, RNA sequencing, apoptosis, cell cycle, migration, invasion

OPEN ACCESS

Edited by:
Cheng-Chia Yu,
Chung Shan Medical University, Taiwan

Reviewed by:
Shih-Yin Chen,
China Medical University, Taiwan
Chia-Hung Yen,
Kaohsiung Medical University, Taiwan

***Correspondence:**
Yi-Chiung Hsu
syicncu@g.ncu.edu.tw

Specialty section:
This article was submitted to Head and Neck Cancer, a section of the journal Frontiers in Oncology

Received: *05 August 2019*
Accepted: *02 September 2019*
Published: *18 September 2019*

Citation:
Huang Y-C, Lee P-C, Wang JJ and Hsu Y-C (2019) Anticancer Effect and Mechanism of Hydroxygenkwanin in Oral Squamous Cell Carcinoma. Front. Oncol. 9:911. doi: 10.3389/fonc.2019.00911

INTRODUCTION

Oral cancer is a lethal disease worldwide with a 5-year survival rate of around 50% and oral squamous cell carcinoma (OSCC) accounts for 90% of all oral cancer types found in the mouth, tongue, and lips (1). The oral cancer is highly related to the exposure of risk factors such as betel nut chewing, smoking, alcohol drinking, and virus infection (2). From 2004 to 2015, the oral cancer incidence keeps increasing in Taiwan. Surgery, radiotherapy, and chemotherapy are the three main treatments intended to stop or eliminate the spread of oral cancer (3). However, chemotherapy compounds would cause normal cells damage. In order to reduce the side effect of treatment in oral cancer, identification of the new potentially anticancer compounds is necessary. Hydroxygenkwanin (HGK) is purification from *Daphne genkwa* plant. *Daphne genkwa* (*yuanhua* in Chinese), is one kind of Daphne plants (*Thymelaeaceae*) distributed in Europe, Taiwan and China. *Daphne genkwa* is a commonly used traditional Chinese medicine (TCM) known to have purgative and diuretic effects (4). The daphnane diterpenoid from the flowers of *Daphne genkwa*, has been demonstrated a potential anti-cancer effect in human non-small cell lung cancer (NSCLC) cells and anti-gioma (5, 6). The *Genkwa flos* flavonoids significantly decreased arthritis through antioxidant and hemorheological modulatory mechanisms in animal study (7). However, the systematic studies of HGK, the compound from *Daphnis Genkwa Flo*, in oral cancer is limited. We systematically study the gene expression profile in OECM1 and SAS cells treated with HGK. Furthermore, we investigate the anti-cancer mechanism of HGK in oral cancer cells.

MATERIALS AND METHODS

Cell Culture

HGK was purchased from Shanghai BS Bio-Tech Co., Ltd (Shanghai, China) and was dissolved in dimethyl sulfoxide (DMSO) (Merck, Darmstadt, Germany) as a stock solution of 100 mM and stored at −20°C before use. SAS is a human tongue squamous cell carcinoma from the Japanese Collection of Research Bioresources (Tokyo, Japan) (2). OECM1, a human gingival squamous carcinoma cells, derived according to previous study (2). Two cell lines were authenticated by short tandem repeat analysis and cultured in Dulbecco's modified Eagle's medium (DMEM) supplemented with 10% fetal bovine serum (FBS), 1.2 g/L sodium bicarbonate, 0.5 mM sodium pyruvate, and 2.5 mM L-glutamine. Chemical compounds, culture medium and FBS were purchased from Life Technologies (Grand Island, NY, USA).

Phenotypic Examination

Phenotypes including cell proliferation (MTT assay), clonogenic ability, migration, and invasion assay were done as described previously (2, 8).

RNA Sequencing

The total RNA samples are first treated with DNase I to degrade any possible DNA contamination. Then the mRNA is enriched by using the oligo (dT) magnetic beads. Mixed with the fragmentation buffer, the mRNA is fragmented into short fragments. Then the first strand of cDNA is synthesized by using random hexamer-primer. Buffer, dNTPs, RNase H and DNA polymerase I are added to synthesize the second strand. The double strand cDNA is purified with magnetic beads. End reparation and 3′-end single nucleotide A (adenine) addition is then performed. Finally, sequencing adaptors are ligated to the fragments. The fragments are enriched by PCR amplification. During the QC step, Agilent 2100 Bioanaylzer and ABI Step One Plus Real-Time PCR System are used to qualify and quantify of the sample library. The library products are ready for sequencing via Illumina HiSeq 4000 or other sequencer when necessary.

Differential Expression Analysis

Primary sequencing data that produced by Illumina Hiseq 4000 (San Diego, CA), called as raw reads, is subjected to quality control (QC) to determine if a resequencing step is needed (Using Trimmomativ v0.33). After QC, raw reads are filtered into clean reads which will be aligned to the reference sequences (mm10 for mouse) by Bowtie2 v2.2.6. QC of alignment

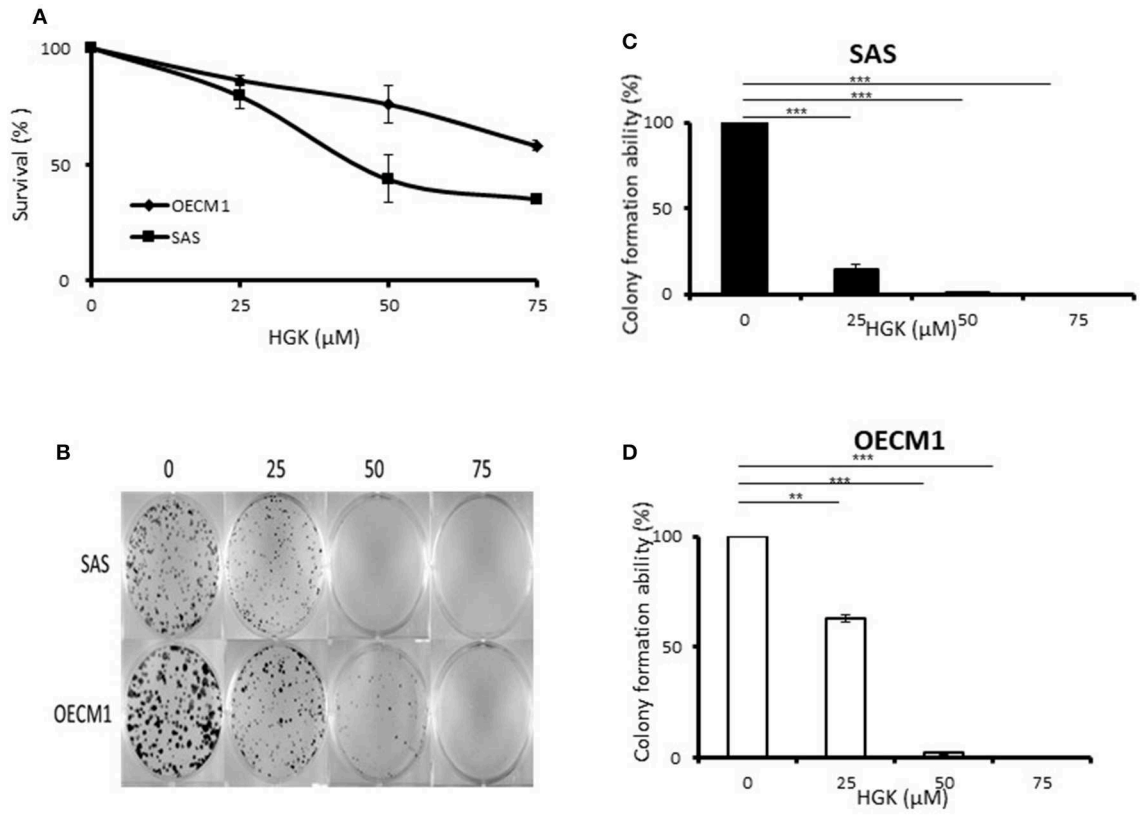

FIGURE 1 | Effects of HGK on the cell survival assay and colony formation of SAS and OECM1 cells. SAS and OECM1 cells were treated with HGK for 24 h in different concentrations (0, 25, 50, 75 μM). **(A)** MTT assay **(B)** The images showing colony formation assay in two cancer cells treated with HGK. **(C)** The quantitative analysis of colony numbers in SAS cells **(D)** in OECM1 cells. $^{**}P < 0.01$ and $^{***}P < 0.001$.

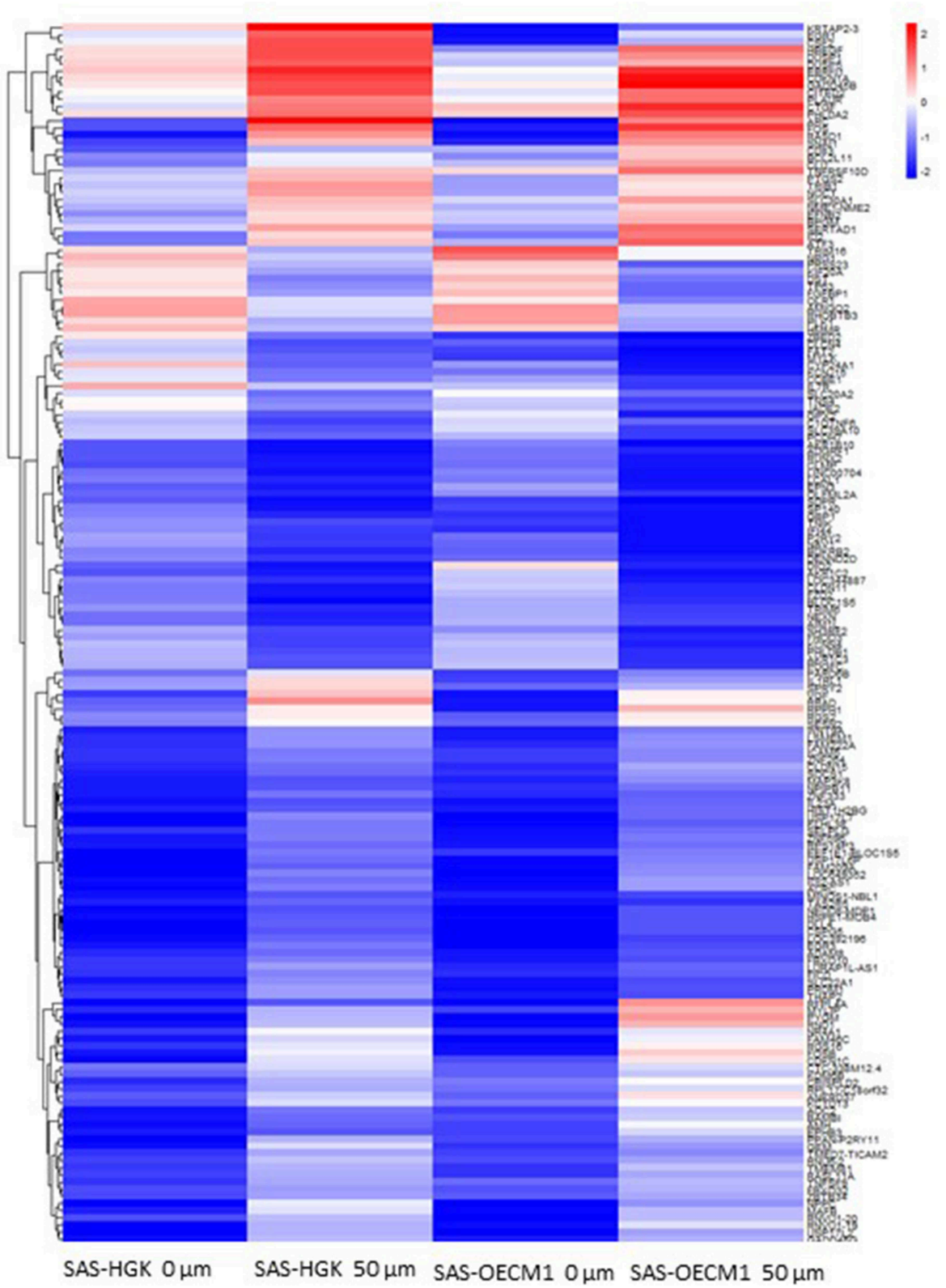

FIGURE 2 | Heatmap showing differential gene expression level with 50 μM HGK treatment for 24 h. Red indicating upregulation, and blue representing downregulation.

is performed to determine if resequencing is needed. The alignment data is utilized to calculate distribution of reads on reference genes and mapping ratio. Once all of the clean reads mapped to reference sequences, we're using "RSEM (RNA-seq by Expectation Maximization)" for calculating read raw count and normalized quantification from each sample. As we got the read quantification data, we could continue various different comparisons. The statistical tool we selected is "EBSeq v1.16.0" which may be used to identify DEGs (differential expressed genes). The RNAseq data were publicly available on NCBI's Sequence Read Archive (SRA) database (Bio-project: PRJNA559691).

Functional Enrichment

The pathway enrichment were analyzed by the Ingenuity Pathway Analysis (IPA) (QIAGEN company, Redwood City, CA, USA), and Gene set enrichment analysis (GSEA) (9).

TABLE 1 | Molecular and cellular functions analysis of differential gene expression in HGK-treated oral cancer cells.

Name	*p*-value range	#Molecules
Cellular movement	2.32E-04–2.39E-15	68
Cell death and survival	2.34E-04–7.60E-12	74
Cell cycle	2.35E-04–1.09E-11	87
Cellular growth and proliferation	2.35E-04–1.09E-11	78
DNA replication	2.80E-11–2.80E-11	22

Cell Cycle Analysis

Cell cycle analysis was performed as previously described (10). Briefly, cells were fixed in −20°C absolute ethanol for 4 h and resuspended in PBS having 20 μg/ml ribonuclease A. After incubating at 37°C for 30 min, propidium iodide 100 μg/ml was added to samples. Cell cycle was examined by flow cytometry (BD FACSCalibur TM system, Becton–Dickinson).

Western Blotting

Western blotting was performed as described previously (2). Antibodies against poly (ADP-ribose) polymerase (PARP) (Asp214), caspase 9, phosphor-H2A.X (ser139), E-cadherin, and Vimentin were purchased from Cell Signaling (Temecula, CA, USA). Anti-p21 and β-actin were purchased from Santa Cruz Biotechnology (Santa Cruz, CA, USA).

Statistics

Student's *t*-test was completed by the Statistical Package for the Social Sciences version 12.0 (SPSS, Inc). Differences between the variables were considered significant for p-values < 0.05.

RESULTS

Effects of HGK on the Cell Survival Assay and Colony Formation in SAS and OECM1 Cells

To determine the ability of HGK to inhibit cell growth and colony formation in two cell lines, cells were incubated in the absence or presence of increasing concentrations of HGK for 24 h. The growth and colony formation of SAS and OECM1 cells were reduced after exposure to 25–75 μM HGK for 24 h (**Figure 1**).

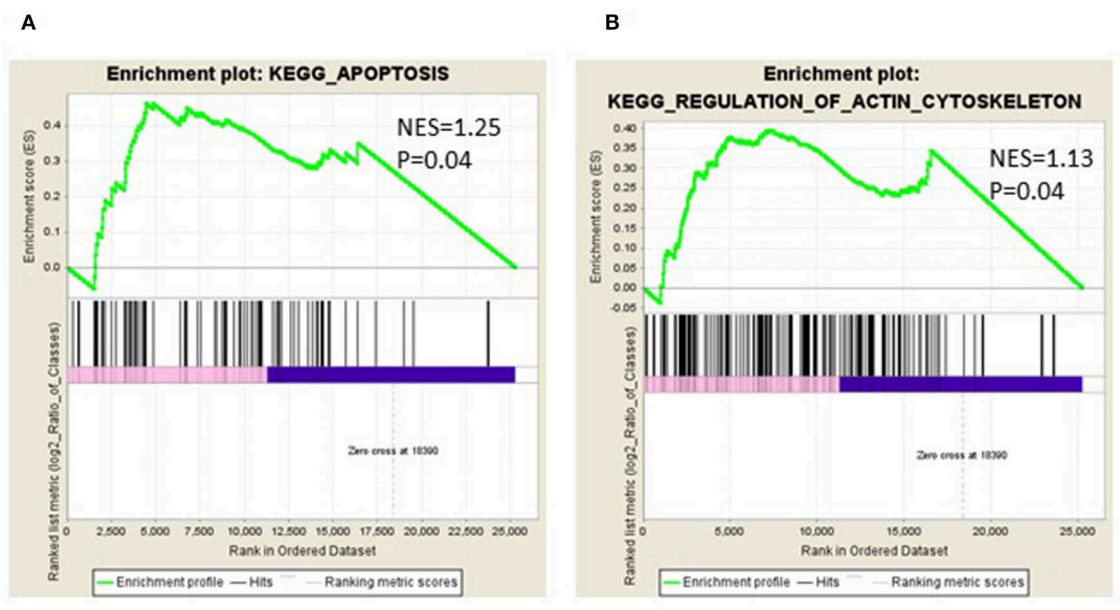

FIGURE 3 | Gene Set Enrichment Analysis (GSEA) enrichment plot involved in **(A)** apoptosis **(B)** in regulation of actin cytoskeleton.

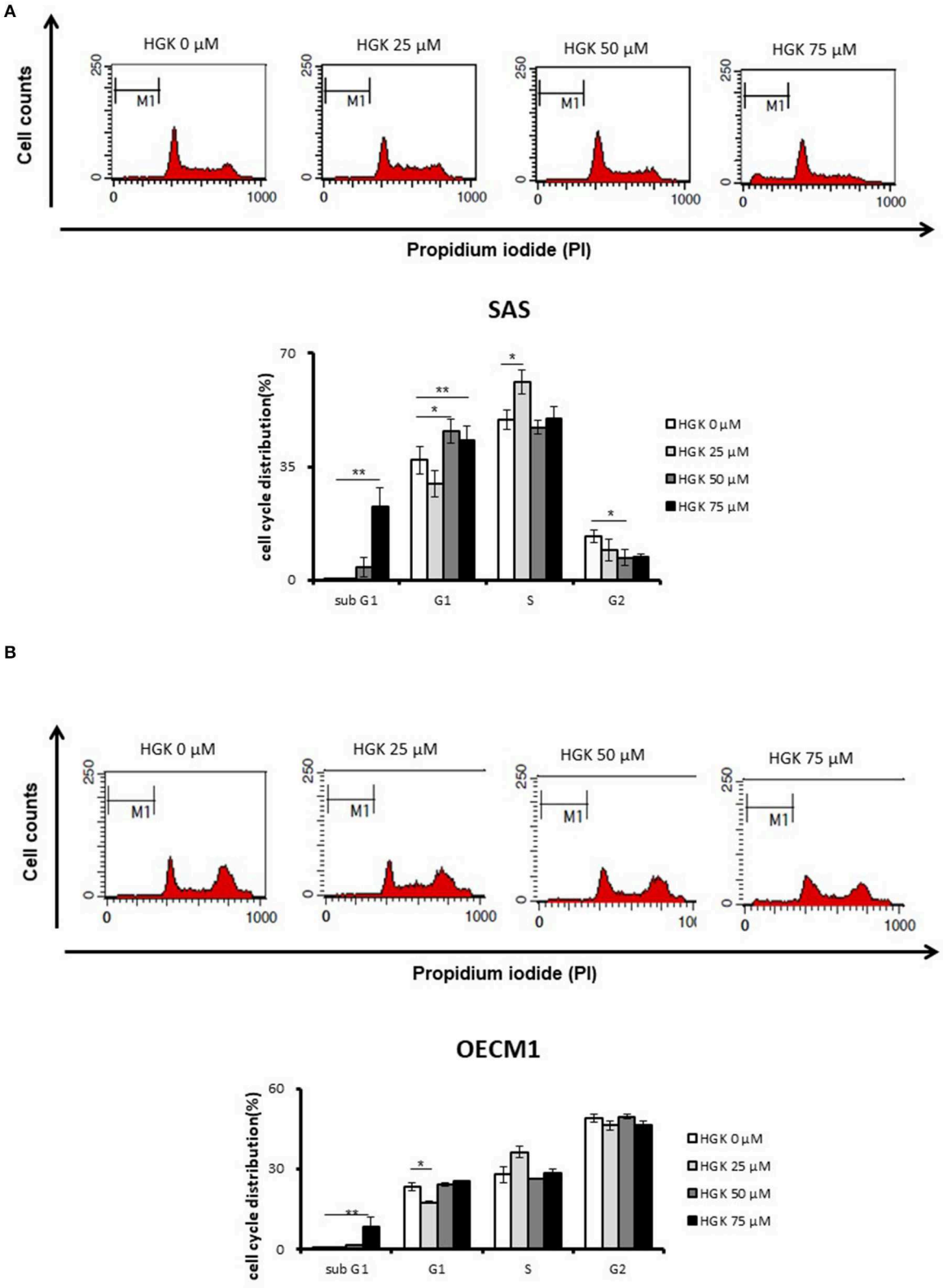

FIGURE 4 | Effects of HGK on the cell cycle progression in SAS and OECM1 cells. SAS cells **(A)** and OECM1 cell **(B)** were treated with 0, 25, 50, 75 μM for 24 h. The results are shown as the mean ± S.E. of three independent experiments. $^{*}P < 0.05$ and $^{**}P < 0.01$.

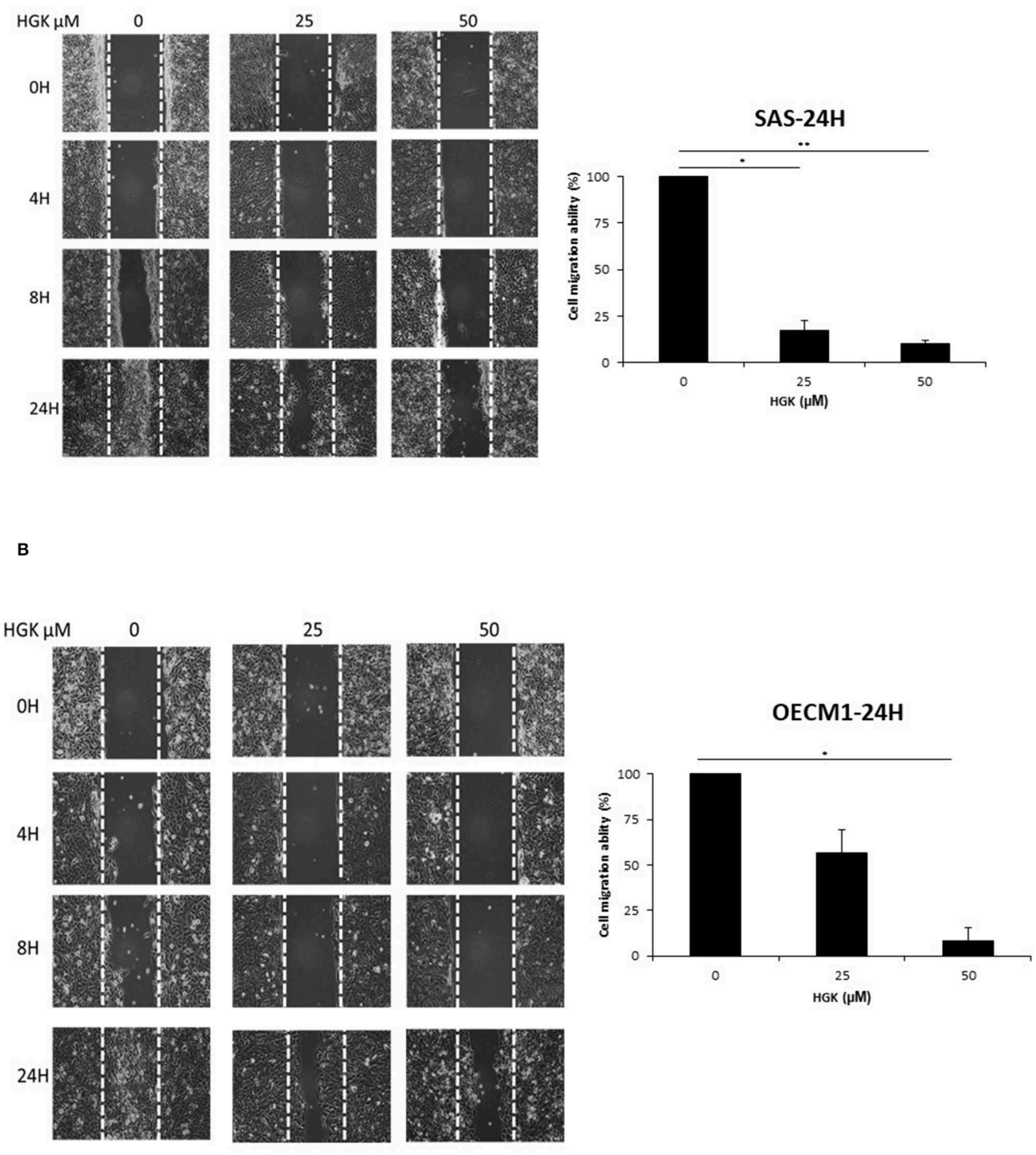

FIGURE 5 | Effects of HGK on cell migration in SAS **(A)** and OECM1 **(B)** cells. SAS and OECM1 cells were treated with 0, 25, 50, 75 μM HGK for 24 h. The results are shown as the mean ± S.E. of three independent experiments. $^{*}P < 0.05$ and $^{**}P < 0.01$.

The inhibition activity of HGK on cell survival assay and colony formation of SAS cells was more potent than on OECM1 cells.

Functional Enrichment Analysis of Differential Gene Expression Genes After HGK Treatment

We identified the differential gene expression genes from RNAseq data. A filtering criterion of FPKM value is more than 1 (11), and log2 fold change was greater than two in both SAS and OECM1 datasets. The sign of change must be consistent in both cell lines. A total of 274 genes were significant in the SAS dataset and 969 genes in the OECM1 dataset (**Table S1**). 170 genes were consistent change in both cell lines (**Figure 2**). **Table 1** showed the most significant molecular and cellular function of differential expression genes after HGK treatment in SAS and OECM1 cells. The final consistency 170 genes were listed in the **Table S2**. The cellular functions affected by HGK were involved in the cellular movement, cell cycle and cell proliferation (**Table 1**). GSEA shows a statistically significant difference between biological samples association with apoptosis and regulation of actin cytoskeleton functions

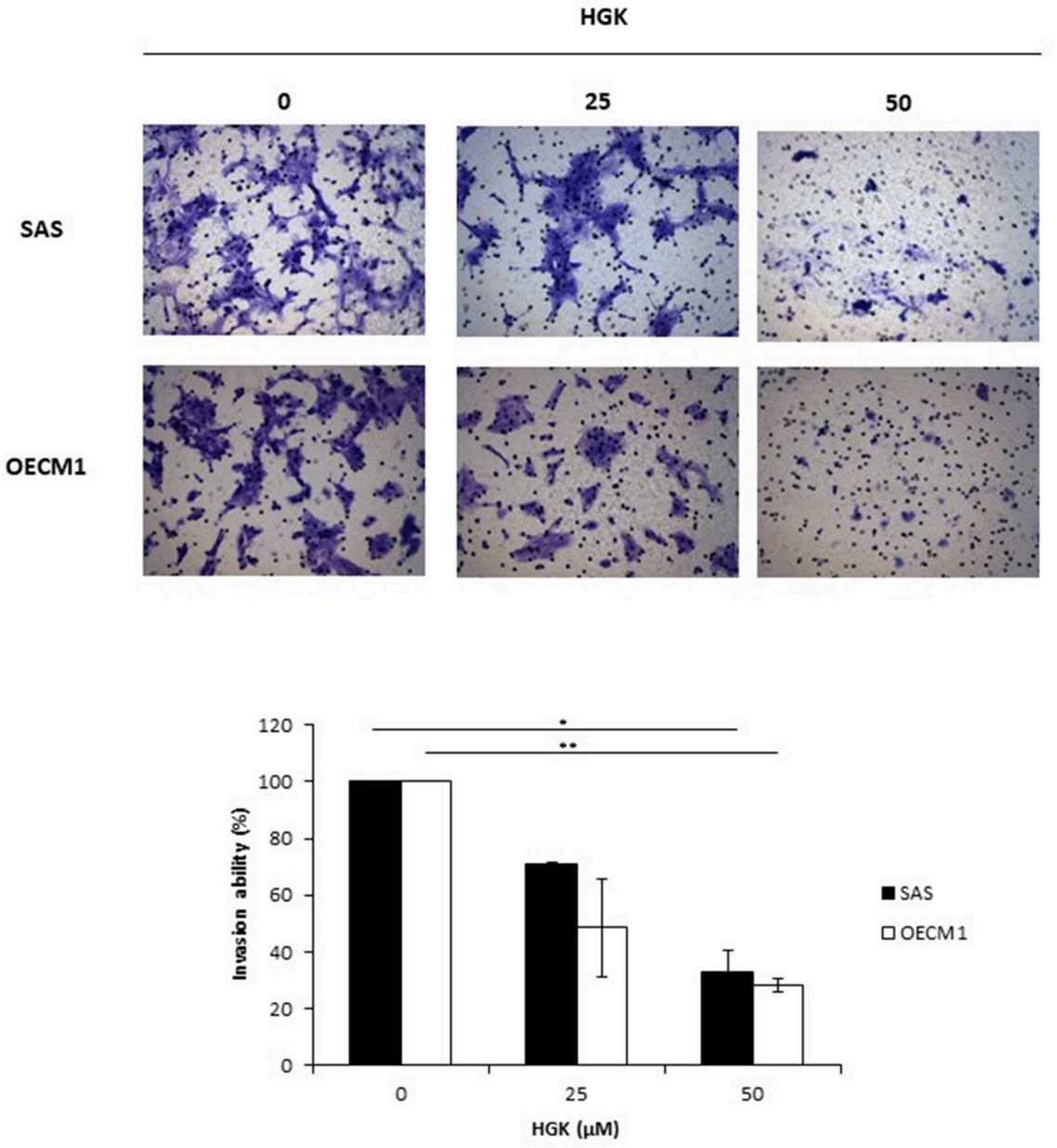

FIGURE 6 | Effects of HGK on cell invasion in SAS and OECM1 cells. SAS and OECM1 cells were treated with 0, 25, 50, 75 μM HGK for 24 h. The results are shown as the mean ± S.E. of three independent experiments. *$P < 0.05$ and **$P < 0.01$.

(**Figure 3**). Differential expression and pathway analysis in HGK treatment oral cancer cells indicated the cell cycle, cell survival and cell movement pathways were potential mechanisms.

Effects of HGK on the Cell Cycle Progression in SAS and OECM1 Cells

We further examine the HGK biological function according to the results of functional enrichment. For investigation of the effect of HGK on cell cycle progression, cells were stained by propidium iodide (PI) and measured by flow cytometry at 24 h following 25–75 μM HGK drug treatments. In **Figure 4**, as compare to control (0 μM), HGK dose dependently increased the percentage of sub G_0/G_1 phase SAS and OECM1 cells, and reduced the cells in G2/M phases of SAS cells but not OECM1 cells. 50 and 75 μM HGK increased the percentage of G_0/G_1 phase SAS cells, but 25 μM HGK reduced both of the cells in G_0/G_1 phases and concomitantly increased the percentage of S phase cells (**Figure 4**).

Effects of HGK on Cell Motion in SAS and OECM1 Cells

To investigate the HGK effect on SAS and OECM1 cell migration, we used wound healing assay. The cell migration was obviously reduced in SAS and OECM1 cells at 8 and 24 h after 25 and 50 μM HGK treatment (**Figure 5**). To investigate the HGK effect on SAS and OECM1 cell invasion, we used transwell invasion assay. As shown in **Figure 6**, the invasion was significantly reduced in 25 and 50 μM HGK treated- SAS and OECM1 cells.

Effects of HGK on Cell Cycle, Apoptosis, and EMT Regulatory Proteins in SAS and OECM1 Cells

In a previous result, we confirmed that HGK increased the percentage of SAS cells but not OECM1 cells in G0/G1 phase. In order to identify the molecular involved in the HGK effect of the G0/G1 phase, SAS and OECM1 cells were treated with 50 and 75 μM HGK for 24 h, and the cells were harvested for Western blotting. We observed the up-regulation of p21 in SAS cells after HGK treatment, but downregulation of p21 in OECM1 cells (**Figure 7**). p21 acts at the checkpoint in the cell cycle at the G1 phase. Western blot indicated that cell cycle regulated p21 might play an important role in in HGK-induced cell cycle arrest. HGK dose dependently increased the percentage of sub G_0/G_1 phase SAS and OECM1 cells (**Figure 4**). We further examined the apoptosis effect by using of H2AX Phosphorylation (12) and cleaved PARP cleaved caspase 9 (13). Western blot analyses of pH2AX, cl-PARP and cleaved caspase 9 in both HGK treated-SAS and OECM1 cells. The epithelial–mesenchymal transition (EMT) provides cells with migration and invasion abilities (14). We measured the e-cadherin (epithelial marker), and vimentin (mesenchymal markers) in HGK-treated cells. Vimentin showed significantly decreased between the HGK-treated and control groups, but not significant up-regulation of E-cadherin (**Figure 7**).

DISCUSSION

Natural compound and their related moieties played an important role in drug discovery and development (15). HGK

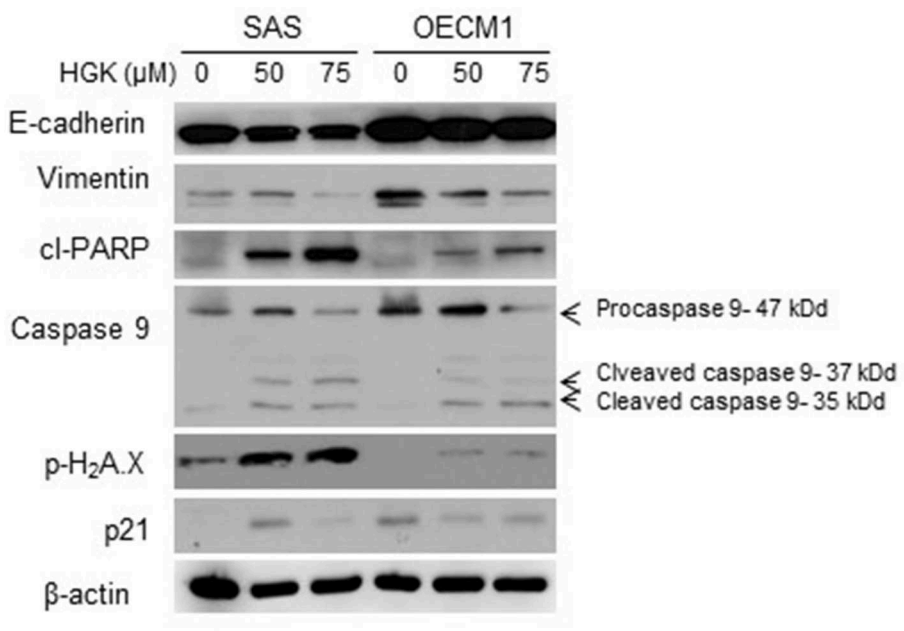

FIGURE 7 | Western blot analysis of cell cycle, apoptosis, and EMT regulatory proteins after treatment with HGK in SAS and OECM1 cells. β-actin was used as the internal marker.

was obtained from novel flavonoid extracted from *Daphne genkwa* and induced cancer cell toxicity, cell cycle arrest, apoptosis and EMT signaling pathways in different types of OSCC cell lines (OECM1 and SAS). We demonstrated that HGK significantly dose-dependently inhibited the rate of cell growth in OECM1 and SAS cells. SAS cells were higher sensitivity to HGK than OECM1 cells (**Figure 1**). The SAS cell line was high malignancy and metastasis derived from a poorly differentiated squamous cell carcinoma. The OECM-1 cell line was less malignancy established from a Taiwanese patient (16). Next-generation sequencing technologies are being widely applied in biomedical research (17). Systems for transcriptome profiling provided the insight into the specific biological pathways. Increases in G0/G1 phase cell cycle arrest with increasing doses of HGK treatments in SAS cells, but not OECM1 (**Figure 4**). Increase of the sub-G1 phase with various doses of HGK in both SAS and OECM1 cells. Western blot results showed that HGK activated the protein levels of p21in SAS cells, but decrease in OECM1 cells (**Figure 7**). The results were consistent with cell cycle analysis. The G1-S transition in cell cycle is driven mainly by cyclin-dependent kinase (CDK) 2 that is controlled by abundance of CDK inhibitors: p21 (18). p21 was a key cell cycle regulator that arrests cells in the G1 and G2 phases. Therefore, p21 proteins were involved in HGK-induced the cell cycle arrest in SAS cells. HGK induce the cell death of OSCC cells by apoptosis. The mechanisms of apoptosis are involving two main apoptotic pathways: the extrinsic and the intrinsic pathway (19). HGK induced cell apoptosis through the intrinsic pathway by activation of cleave Caspase 9, and cleave PARP (**Figure 7**). Histone H2AX phosphorylation was sensitive marker for DNA double-strand breaks (20). We demonstrated that HGK induce DNA damage in both two cell lines. Moreover, H2AX phosphorylation also an essential role in cell cycle arrest regulated by p21 and cell growth (21). HGK induced cell cycle arrest not only through p21 activation but also H2AX phosphorylation. Decrease of E-cadherin and gain of vimentin promoted tumor migration, leading to higher metastatic risk of head and neck squamous cell carcinoma patients (22). E-cadherin was an important therapeutic target for designing anti-tumor drugs (6). **Figure 7** showed that SAS1 and OECM1 cells did not loss the E-cadherin expression. Therefore, HGK inhibited the cell invasion and migration through down-regulation vimentin, not increase in E-cadherin.

In this study, we provided the bioinformatics analysis and biological functions experiments of HGK-treated oral cancer cells. Our results showed HGK had anti-cancer activities through multiple mechanisms including inhibition of cellular movement, cell cycle arrest and blocking cell proliferation in oral cancer cells. In conclusion, this study provided evidence that HGK was a potential natural anti-tumor compound for squamous cell carcinoma. However, further pharmacological and investigations *in vivo* are required.

DATA AVAILABILITY

The datasets generated in the study can be found in the SRA database (https://www.ncbi.nlm.nih.gov/sra) using the following accession numbers: STUDY: PRJNA559691, SAMPLE: OECM_HGK (SAMN12551609), EXPERIMENT: 7 (SRX6701569), RUN: OECM1-4_HHFT2DSXX_L4_R1.fastq.gz (SRR9953208), SAMPLE: OCEM_control (SAMN12551608), EXPERIMENT: 5 (SRX6701570), RUN: OECM1-3_HHFT2DSXX_L4_R1.fastq.gz (SRR9953207), SAMPLE: SAS_HGK (SAMN12551607), EXPERIMENT: 3 (SRX6701571), RUN: SAS-2_HHFT2DSXX_L4_R1.fastq.gz (SRR9953206), SAMPLE: SAS_control (SAMN12551606), EXPERIMENT: 1 (SRX6701572), RUN: SAS-1_HHFT2DSXX_L4_R1.fastq.gz (SRR9953205).

AUTHOR CONTRIBUTIONS

Y-CHu and P-CL performed the experiments and analyzed the data. Y-CHu, Y-CHs, and JW drafted the manuscript. Y-CHs contributed to conception and design of the study. All authors have read and approved the final manuscript.

FUNDING

This study was supported by grants from Ministry of Science and Technology, Taiwan (MOST-107-2314-B-008-002) and Taoyuan Armed Forces General Hospital, Taiwan (AFTYGH-10858). We thank Dr. Chi-Yuan Chen (Chang Gung University of Science and Technology) for providing technical support and intellectual discussions in this study.

SUPPLEMENTARY MATERIAL

The Supplementary Material for this article can be found online at: https://www.frontiersin.org/articles/10.3389/fonc.2019.00911/full#supplementary-material

Table S1 | The gene expression profiles in SAS and OECM1 treated with HGK.

Table S2 | The consistency expression genes.

REFERENCES

1. Markopoulos AK. Current aspects on oral squamous cell carcinoma. *Open Dent J.* (2012) 6:126–30. doi: 10.2174/1874210601206010126
2. Chen CY, Chiou SH, Huang CY, Jan CI, Lin SC, Hu WY, et al. Tid1 functions as a tumour suppressor in head and neck squamous cell carcinoma. *J Pathol.* (2009) 219:347–55. doi: 10.1002/path.2604
3. Hsu YY, Bai CH, Wang CC, Chen WL, Wu WT, Lai CH. Health disparities of employees in taiwan with major cancer diagnosis from 2004 to 2015: a nation- and population-based analysis. *Int J Environ Res Public Health*. (2019) 16:E1982. doi: 10.3390/ijerph16111982
4. Li S, Chou G, Hseu Y, Yang H, Kwan H, Yu Z. Isolation of anticancer constituents from flos genkwa (*Daphne genkwa* Sieb.et Zucc.) through bioassay-guided procedures. *Chem Cent J.* (2013) 7:159. doi: 10.1186/1752-153X-7-159

5. Kang JI, Hong JY, Lee HJ, Bae SY, Jung C, Park HJ, et al. Anti-tumor activity of yuanhuacine by regulating AMPK/mTOR signaling pathway and actin cytoskeleton organization in non-small cell lung cancer cells. *PLoS ONE*. (2015) 10:e0144368. doi: 10.1371/journal.pone.0144368
6. Song Y, Ye M, Zhou J, Wang ZW, Zhu X. Restoring E-cadherin expression by natural compounds for anticancer therapies in genital and urinary cancers. *Mol Ther Oncolytics*. (2019) 14:130–8. doi: 10.1016/j.omto.2019.04.005
7. Zhang CF, Zhang SL, He X, Yang XL, Wu HT, Lin BQ, et al. Antioxidant effects of Genkwa flos flavonoids on Freunds adjuvant-induced rheumatoid arthritis in rats. *J Ethnopharmacol*. (2014) 153:793–800. doi: 10.1016/j.jep.2014.03.046
8. Chen CY, Yang SC, Lee KH, Yang X, Wei LY, Chow LP, et al. The antitumor agent PBT-1 directly targets HSP90 and hnRNP A2/B1 and inhibits lung adenocarcinoma growth and metastasis. *J Med Chem*. (2014) 57:677–85. doi: 10.1021/jm401686b
9. Subramanian A, Tamayo P, Mootha VK, Mukherjee S, Ebert BL, Gillette MA, et al. Gene set enrichment analysis: a knowledge-based approach for interpreting genome-wide expression profiles. *Proc Natl Acad Sci USA*. (2005) 102:15545–50. doi: 10.1073/pnas.0506580102
10. Wang TH, Chan CW, Fang JY, Shih YM, Liu YW, Wang TV, et al. 2-O-Methylmagnolol upregulates the long non-coding RNA, GAS5, and enhances apoptosis in skin cancer cells. *Cell Death Dis*. (2017) 8:e2638. doi: 10.1038/cddis.2017.66
11. Mortazavi A, Williams BA, McCue K, Schaeffer L, Wold B. Mapping and quantifying mammalian transcriptomes by RNA-Seq. *Nat Methods*. (2008) 5:621–8. doi: 10.1038/nmeth.1226
12. Plesca D, Mazumder S, Almasan A. DNA damage response and apoptosis. *Methods Enzymol*. (2008) 446:107–22. doi: 10.1016/S0076-6879(08)01606-6
13. Kitazumi I, Tsukahara M. Regulation of DNA fragmentation: the role of caspases and phosphorylation. *FEBS J*. (2011) 278:427–41. doi: 10.1111/j.1742-4658.2010.07975.x
14. Lu W, Kang Y. Epithelial-mesenchymal plasticity in cancer progression and metastasis. *Dev Cell*. (2019) 49:361–74. doi: 10.1016/j.devcel.2019.04.010
15. Butler MS. The role of natural product chemistry in drug discovery. *J Nat Prod*. (2004) 67:2141–53. doi: 10.1021/np040106y
16. Chuang CY, Chang CP, Lee YJ, Lin WL, Chang WW, Wu JS, et al. PRMT1 expression is elevated in head and neck cancer and inhibition of protein arginine methylation by adenosine dialdehyde or PRMT1 knockdown downregulates proliferation and migration of oral cancer cells. *Oncol Rep*. (2017) 38:1115–23. doi: 10.3892/or.2017.5737
17. Han Y, Gao S, Muegge K, Zhang W, Zhou B. Advanced applications of RNA sequencing and challenges. *Bioinform Biol Insights*. (2015) 9(Suppl. 1):29–46. doi: 10.4137/BBI.S28991
18. Sherr CJ, Roberts JM. CDK inhibitors: positive and negative regulators of G1-phase progression. *Genes Dev*. (1999) 13:1501–12. doi: 10.1101/gad.13.12.1501
19. Elmore S. Apoptosis: a review of programmed cell death. *Toxicol Pathol*. (2007) 35:495–516. doi: 10.1080/01926230701320337
20. Sharma A, Singh K, Almasan A. Histone H2AX phosphorylation: a marker for DNA damage. *Methods Mol Biol*. (2012) 920:613–26. doi: 10.1007/978-1-61779-998-3_40
21. Fragkos M, Jurvansuu J, Beard P. H2AX is required for cell cycle arrest via the p53/p21 pathway. *Mol Cell Biol*. (2009) 29:2828–40. doi: 10.1128/MCB.01830-08
22. Nijkamp MM, Span PN, Hoogsteen IJ, van der Kogel AJ, Kaanders JH, Bussink J. Expression of E-cadherin and vimentin correlates with metastasis formation in head and neck squamous cell carcinoma patients. *Radiother Oncol*. (2011) 99:344–8. doi: 10.1016/j.radonc.2011.05.066

Conflict of Interest Statement: The authors declare that the research was conducted in the absence of any commercial or financial relationships that could be construed as a potential conflict of interest.

frontiers in Oncology

ORIGINAL RESEARCH
published: 18 September 2019
doi: 10.3389/fonc.2019.00898

Genome-Wide Identification of a Novel Eight-lncRNA Signature to Improve Prognostic Prediction in Head and Neck Squamous Cell Carcinoma

Bowen Yang[1,2†], *Jiming Shen*[1,2†], *Lu Xu*[1,2], *Ying Chen*[1,2], *Xiaofang Che*[1,2], *Xiujuan Qu*[1,2], *Yunpeng Liu*[1,2], *Yuee Teng*[1,2*] *and Zhi Li*[1,2*]

[1] *Department of Medical Oncology, First Hospital of China Medical University, Shenyang, China,* [2] *Key Laboratory of Anticancer Drugs and Biotherapy of Liaoning Province, First Hospital of China Medical University, Shenyang, China*

OPEN ACCESS

Edited by:
Ingeborg Tinhofer, Charité Medical University of Berlin, Germany

Reviewed by:
Cheng-Chia Yu, Chung Shan Medical University, Taiwan
Mathura Shanmugasundaram, Harvard Medical School, United States

***Correspondence:**
Zhi Li
zli@cmu.edu.cn
Yuee Teng
yeteng@cmu.edu.cn

†These authors have contributed equally to this work and share first authorship

Specialty section:
This article was submitted to Head and Neck Cancer, a section of the journal Frontiers in Oncology

Received: *26 March 2019*
Accepted: *28 August 2019*
Published: *18 September 2019*

Citation:
Yang B, Shen J, Xu L, Chen Y, Che X, Qu X, Liu Y, Teng Y and Li Z (2019) Genome-Wide Identification of a Novel Eight-lncRNA Signature to Improve Prognostic Prediction in Head and Neck Squamous Cell Carcinoma. Front. Oncol. 9:898. doi: 10.3389/fonc.2019.00898

Objectives: LncRNAs are essential survival prognostic indicators with important biological functions in tumorigenesis and tumor progression. This study aimed to establish a long non-coding RNA (lncRNA) signature that can effectively predict the prognosis of patients with head and neck squamous cell carcinoma (HNSCC) and explore the potential functions of these lncRNAs.

Materials and Methods: We re-annotated RNA sequencing and obtained exhaustive RNA-seq data of 269 patients with comprehensive clinical information from the GEO database. Then an 8-lncRNA signature capable of predicting the survival prognosis of HNSCC patients and a nomogram containing this signature were established. Weighted Co-expression Network Construction (WGCNA), Gene Set Enrichment Analysis (GSEA), and Gene Ontology (GO) enrichment were then applied to predict the possible biological functions of the signature and each individual lncRNA.

Results: Eight lncRNAs associated with survival in HNSCC patients, including AC010624.1, AC130456.4, LINC00608, LINC01300, MIR99AHG, AC008655.1, AC055758.2, and AC118553.1, were obtained by univariate regression, cox LASSO regression, and multivariate regression. Functionally, patients with high signature scores had abnormal immune functions via GSEA. AC010624.1 and AC130456.4 may participate in epidermal cell differentiation and skin development, and MIR99AHG in the formation of cellular structures. Other lncRNAs in the signature may also participate in important biological processes.

Conclusions: Therefore, we established an 8-lncRNA signature that can effectively guide clinical prediction of the prognosis of patients with HNSCC, and individuals with high signature scores may have abnormal immune function.

Keywords: head and neck squamous cell carcinoma (HNSCC), long non-coding RNA (lncRNA), prognostic signature, weighted co-expression network construction (WGCNA), gene set enrichment analysis (GSEA)

INTRODUCTION

Head and neck squamous carcinoma (HNSCC), the most common and malignant carcinoma affecting the head and neck region, is also the sixth common cancer worldwide (1, 2). In the past few decades, multidisciplinary therapy based on various combinations of surgery, chemotherapy, and radiotherapy has been applied for the management of HNSCC. In addition to the approved immune checkpoint inhibitors such as the second-line treatment (2016), no further progress has been made, resulting in ∼50% of HNSCC patients still dying from the disease (3–5). Meanwhile, the prognostic model currently used for HNSCC patients is based on clinicopathological parameters (CPPs), but many cases with the same clinical stage show different outcomes (5, 6). Prognostic signatures based on mRNAs could not be applied clinically (7, 8). Therefore, for HNSCC patients, an efficient prognostic model that can predict the survival prognosis of patients is urgently required.

Long non-coding RNAs (lncRNAs) are non-coding RNAs with more than 200 nucleotides in length. LncRNAs are important biomarkers for the diagnosis and prognosis of tumors because of higher tissue specificity and increased ease of detection compared with mRNAs (9–12). Accumulating evidence indicates lncRNAs play vital roles in the progression and tumorigenesis of tumors, including HNSCC (12–16). For example, LncRNA MIR31HG promotes cell proliferation and tumorigenesis by targeting HIF1A and P21. NEAT1 promotes laryngeal squamous cell cancer by regulating the miR-107/CDK6 pathway. Overexpression of lncRNA H19 promotes the occurrence of HNSCC (17–19). With the development of the high-throughput sequencing technology, more and more lncRNAs have been discovered, and lncRNA signatures associated with HNSCC prognosis have been established, but the functions of lncRNAs in most signatures remain unknown (20–23). Therefore, establishing an integrated lncRNA model associated with prognosis in HNSCC and predicting the functions of respective lncRNAs is of high importance for both patients and clinicians.

To identify lncRNAs associated with prognosis in HNSCC and guide clinical application, we integrated RNA-seq and clinical survival information of 269 patients from the GEO dataset and established a nomogram containing an 8-lncRNA signature. Functional enrichment was performed to predict the potential functions of the hub lncRNAs.

MATERIALS AND METHODS

Patient Information Collection and Study Design

All HNSCC patients were collected from GSE65858 public database (https://www.ncbi.nlm.nih.gov/geo/query/acc.cgi?acc=GSE65858). Here are two criteria used to select desired samples: (1) patients with mRNA expression data and clinical data were selected; (2) survival time of patients was more than 10 days. The platform of mRNA expression analysis of GSE65858 was Illumina HumanHT-12 V4.0 expression beadchip (GPL10558). All selected expression datasets were log2-transformed, then standardized.

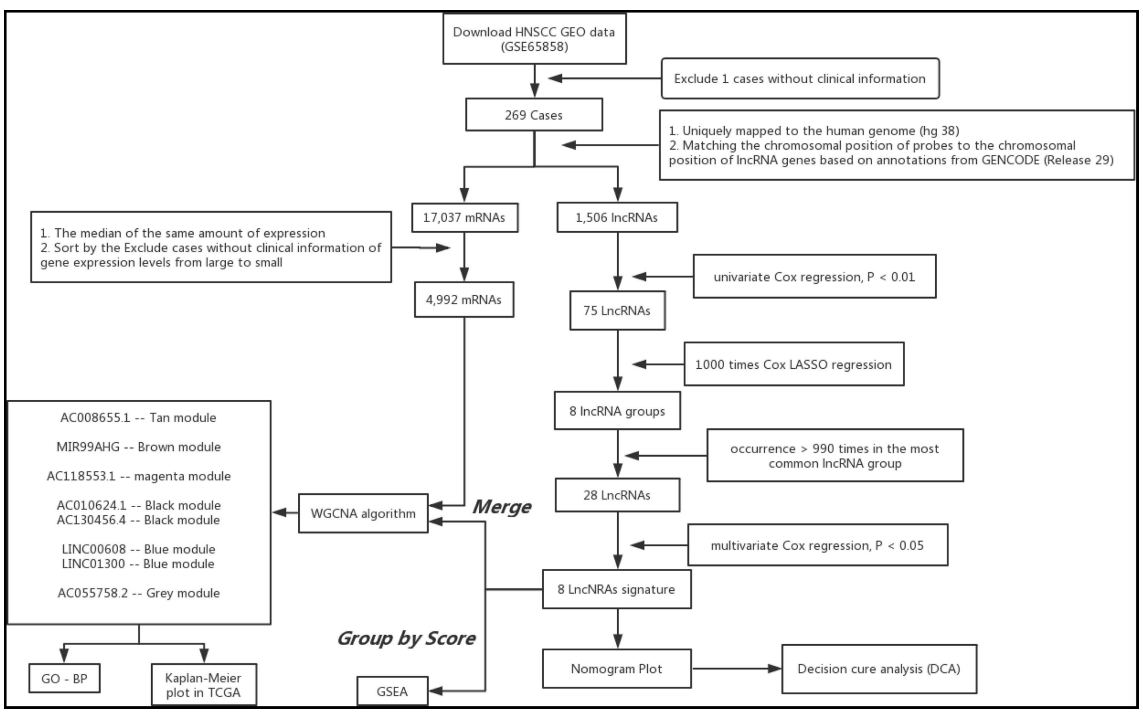

FIGURE 1 | Analysis of flowchart illustrates the exploration procedure for the HNSC prognostic lncRNAs and the related mechanisms.

Construction of lncRNA Expression Through Re-annotation

The Illumina probe sequences were obtained from the annotation file GPL10558 and uniquely mapped to the human genome (hg38) by NCBI blast without mismatch. Specific probes of lncRNAs were obtained by matching the chromosomal position of probes to the chromosomal position of lncRNA genes based on annotations from GENCODE (Release 29). For the case where different probes correspond to the same gene, the expression of the gene is taken as the median. LncRNAs were selected based on the following criteria according to the expression values and the calculated median and standard deviation (SD). First, lncRNAs with non-zero values in more than 75% of the cases were included. Second, the median and SD of the lncRNA was required to be larger than 1.

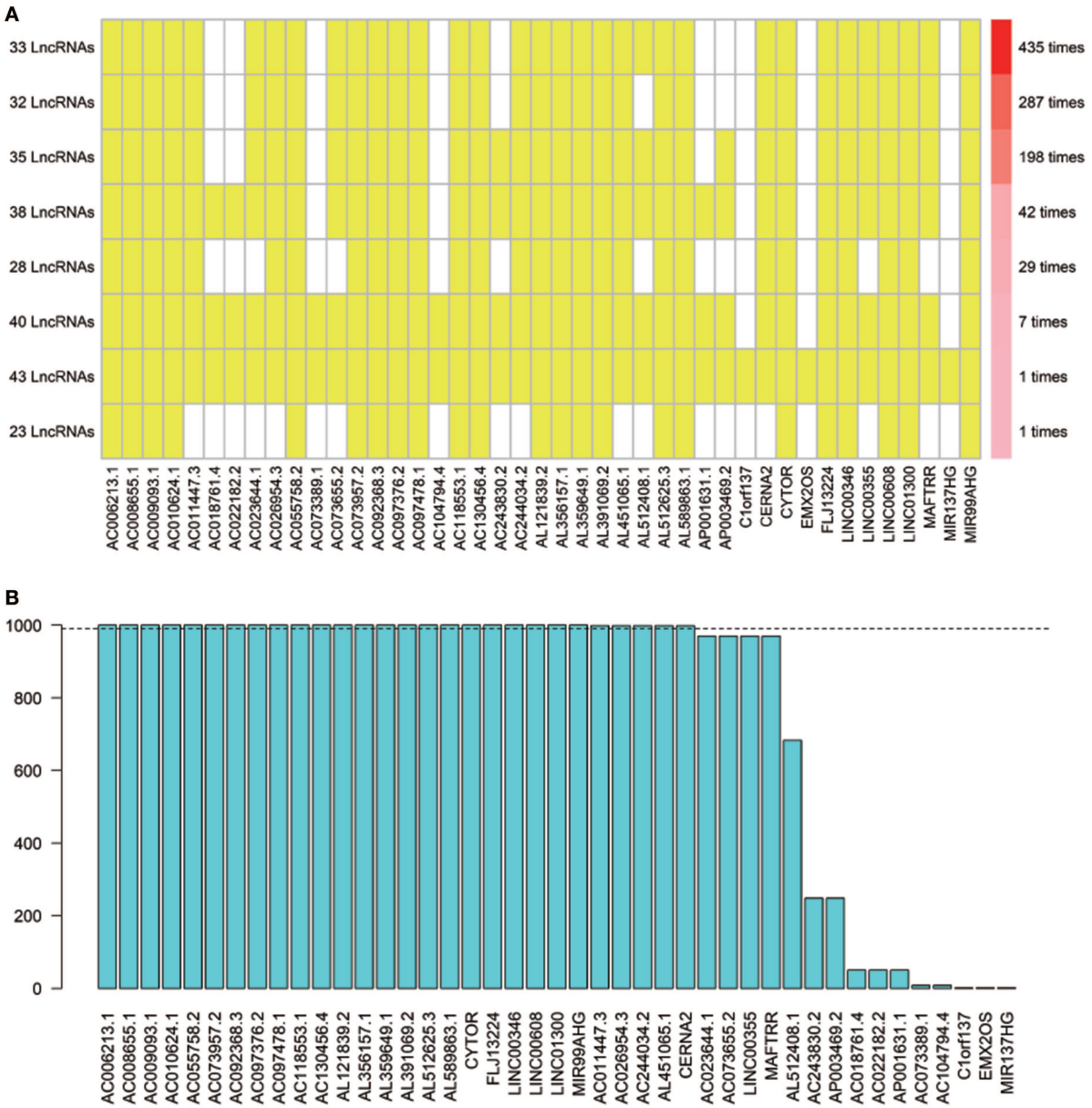

FIGURE 2 | The seed lncRNAs were extracted by 1,000 times Cox LASSO regression. **(A)** Highly consistency was demonstrated in the lncRNAs among the 8 extracted lncRNA sets. The left ordinate indicates the seed lncRNA set and the number of seeds lncRNAs found by every single iteration of LASSO. The right ordinate is the frequency of the seed lncRNA set disclosed through the 1,000 times Cox LASSO regression. The horizontal ordinate is the lncRNA name. The yellow block represents the occurrence of the particular lncRNA in the specific lncRNA set; **(B)** Totally 28 seed lncRNAs with >990 occurrences in the most common lncRNA set were filtered out for further analysis. The blue column indicates the frequency of each lncRNA occurs in the most common lncRNA set.

Cox Survival Analysis and Least Absolute Shrinkage and Selection Operator (LASSO) Regression With 10-fold Cross-Validation

The prognostic value of each lncRNA was firstly calculated in the univariate Cox analysis using R/survival package, and the lncRNAs with $P < 0.01$ were selected as seed lncRNAs for Cox LASSO regression with 10-fold cross-validation (CV). To identify the prognostic value of the lncRNAs, multivariate Cox regression was further performed using R/survival package based on each "significant" lncRNA disclosed in the above steps. A lncRNA with $P < 0.05$ was defined as significant. The corresponding hazard ratio (HR), 95% confidence interval (CI), and *P*-value were collected.

TABLE 1 | Descriptions of the eight lncRNAs.

Hg38_name	Ensembl_ID	Havana_gene	Gene_type	Chr	Start	End	Strand
MIR99AHG	ENSG00000215386.12	OTTHUMG00000074377.5	lincRNA	21	15928296	16645065	+
AC008655.1	ENSG00000267815.1	OTTHUMG00000183045.1	Antisense	19	50310022	50310539	–
AC010624.1	ENSG00000204666.3	OTTHUMG00000165525.1	Sense_overlapping	19	50050589	50066793	+
AC055758.2	ENSG00000244358.1	OTTHUMG00000159391.1	lincRNA	3	145939912	145961536	+
AC130456.4	ENSG00000260681.1	OTTHUMG00000177223.1	Antisense	16	19,410,729	19,411,662	–
AC118553.1	ENSG00000228084.1	OTTHUMG00000010804.1	Antisense	1	99968383	99969864	–
LINC00608	ENSG00000236445.4	OTTHUMG00000154665.5	Antisense	2	218975393	218989940	+
LINC01300	ENSG00000253595.5	OTTHUMG00000164482.1	Antisense	8	141340549	141344621	+

TABLE 2 | The correlations of the lncRNAs with patients' overall survival in HNSCC based on GSE65858 dataset using uni- and multi-variate Cox analysis.

Gene	Univariate cox			Multivariate cox		
	HR	95%CI	*P*-value	HR	95%CI	*P*-value
AC006213.1	0.02	0–0.25	0.002	0.14	0.01–2.15	0.16
AC008655.1	0.33	0.18–0.63	0.001	0.47	0.23–0.94	0.033*
AC009093.1	26.05	2.81–241.84	0.004	9.1	0.45–182.4	0.149
AC010624.1	0.01	0–0.23	0.003	0	0–0.1	0.001**
AC011447.3	0.53	0.24–1.17	0.117	0.45	0.16–1.26	0.129
AC026954.3	1.55	0.98–2.47	0.063	1.32	0.73–2.41	0.363
AC055758.2	0.04	0–0.74	0.031	0.02	0–0.67	0.029*
AC073957.2	14.28	1.07–190.83	0.044	9.94	0.54–184.8	0.123
AC092368.3	5.29	1.93–14.52	0.001	3.2	0.82–12.55	0.095
AC097376.2	0.04	0–0.46	0.01	0.36	0.02–6.28	0.482
AC097478.1	0.71	0.51–1	0.049	0.89	0.57–1.37	0.589
AC118553.1	0.02	0–0.22	0.001	0.03	0–0.4	0.008**
AC130456.4	5.02	1.3–19.41	0.019	22.51	4.02–126.25	0***
AC244034.2	0.17	0.04–0.65	0.01	0.99	0.19–4.99	0.986
AL121839.2	5.2	0.68–39.61	0.111	10.86	0.92–127.89	0.058
AL356157.1	12.25	2.18–68.67	0.004	2.51	0.2–32.17	0.479
AL359649.1	30.21	2.05–445.86	0.013	7.09	0.19–260.04	0.286
AL391069.2	0.03	0–0.36	0.005	0.07	0–1.06	0.055
AL451065.1	10.35	1.03–103.75	0.047	2.74	0.12–62.27	0.527
AL512625.3	11.94	1.26–113.15	0.031	8.72	0.57–133.69	0.12
AL589863.1	0.01	0–0.25	0.005	0.09	0–2.54	0.16
CERNA2	0.54	0.33–0.88	0.014	0.7	0.36–1.38	0.305
CYTOR	49.02	4.42–543.27	0.002	1.05	0.06–19.48	0.972
FLJ13224	0.01	0–0.32	0.008	0.03	0–1.13	0.058
LINC00346	21.89	2.24–213.51	0.008	8.91	0.41–196.03	0.165
LINC00608	0.04	0–0.74	0.03	0.01	0–0.27	0.006**
LINC01300	9.26	1.67–51.37	0.011	39.02	3.79–401.34	0.002**
MIR99AHG	0.19	0.05–0.69	0.012	0.23	0.05–0.97	0.046*

*$P < 0.05$, **$P < 0.01$, ***$P < 0.001$.

Development of an Individualized Prediction Model

The OS and Hazard ratios (HRs) were calculated by Kaplan–Meier algorithm and univariate Cox regression analysis, respectively. The log-rank method tested the differences between the survival curves. We used the following formula to construct a prognostic risk score model: $risk\ score = expGene1 \times \beta Gene1 + expGene2 \times \beta Gene2 + \exp Genen \times \beta Genen$ (exp, prognostic gene expression level; β, multivariate Cox regression model regression coefficients). The gene signature score as a predictor for HNSCC patients was analyzed in the model. We find out the significant variables through the univariate Cox regression analysis. Candidate variables with a P-value < 0.2 on univariate analysis were included in multivariable model. Finally, multivariable Cox regression model began with the clinical candidate predictors as follows: T stage, M stage, and Score. The nomogram model was built by the coefficients of the multivariable Cox regression model.

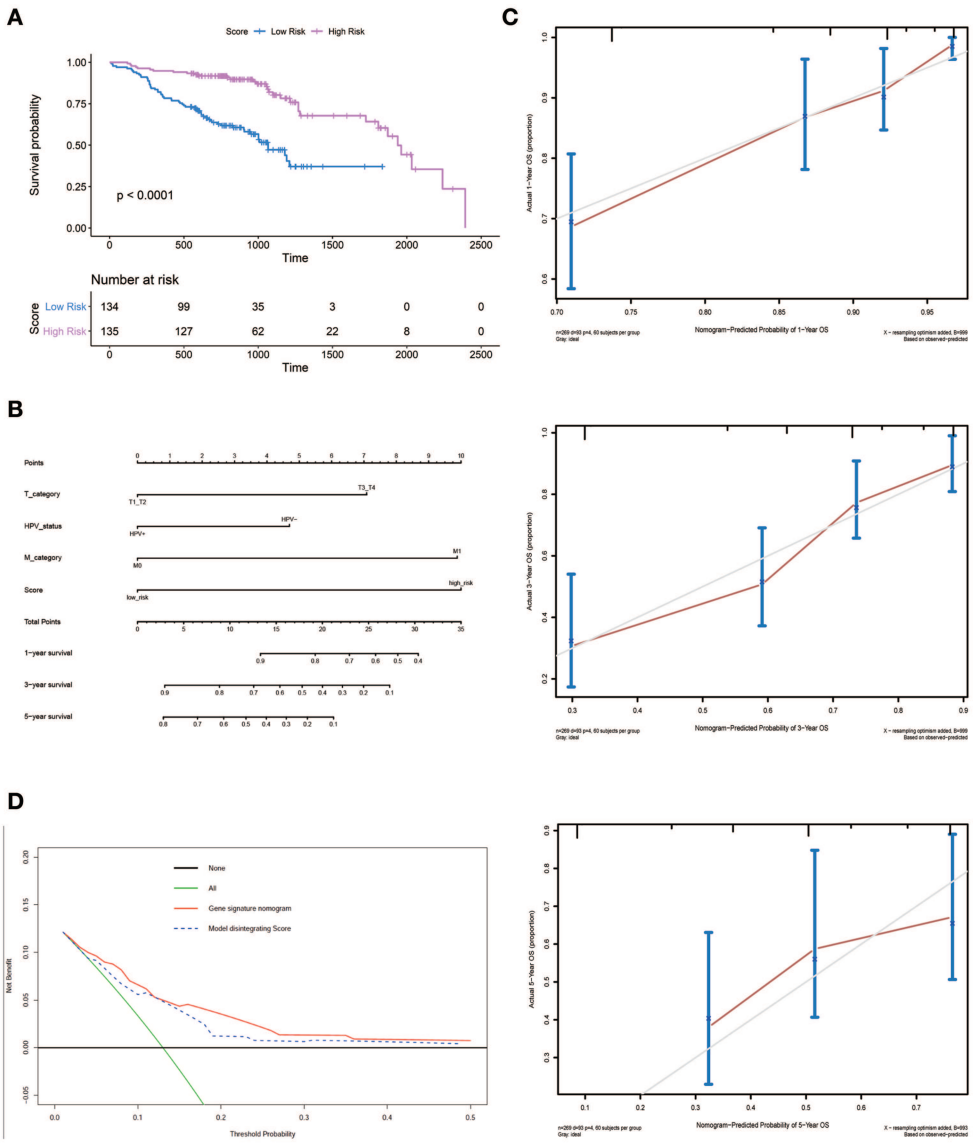

FIGURE 3 | Nomogram plot for patients with Head and Neck Squamous Cell Carcinoma. **(A)** Overall survival analysis on signature score in the GSE65858 dataset. **(B)** The gene nomogram was developed with signature score, T category, M category and HPV status. **(C)** Calibration curves of the gene nomogram. The y-axis represents the actual overall survival rate. The x-axis represents the predicted overall survival rate. The gray diagonal represents a perfect prediction of an ideal model. Dark red solid lines indicate the performance of the nomogram, where closer to the diagonal dashed line indicates a better prediction. **(D)** Decision curve analysis for the gene signature nomogram and the model without Score. The y-axis measures the net benefit. The red solid line represents the gene signature nomogram. The blue dashed line represents model without Score. The green line represents the assumption that all patients have died. Thin black line represents the assumption that no patients have died.

Clinical Use

The R-script stdca was (https://www.rdocumentation.org/packages/DecisionCurve/versions/1.4) used to do decision curve analysis (DCA) which can assess the clinical net benefit of different probability thresholds.

Gene Set Enrichment Analysis (GSEA)

The expression profile data were ranked according to the signature score, and the data were divided into high-risk group and low-risk group by the mean score. Then, we downloaded the h.all.v6.2.symbols.gmt (24) from the GSEA website, and analyzed our data using GSEA version 3.0.

Weighted Gene Co-expression Network Analysis

The "WGCNA" package in R was applied to performed co-expression network using the expression values of mRNA and lncRNAs screened above. Briefly, we constructed the weighted adjacency matrix using a power function based on a soft-thresholding parameter β. After that, the adjacency was transformed into topological overlap matrix (TOM), and average linkage hierarchical clustering was performed according to the TOM-based dissimilarity measure. In this study, we chose a minimum size (gene group) of 30 for the genes dendrogram and a cut-line (0.25) for module dendrogram and merged some modules.

Hub LncRNA and Module Function Annotation

To predict the molecular of each candidate lncRNA, lncRNA-related mRNAs were filtered out by WGCNA. The network visualization was performed by Cystoscope software version 3.5.1 (https://cytoscape.org/). An appropriate cutoff of p-values <0.05 and FDR <0.05 was used. The statistics and data visualization were performed by ClusterProfiler Package in RStudio.

Validation of MIR99AHG

We compared the expression of MIR99AHG and the relationship with overall survival in HNSCC and normal tissues with the available data from the gene expression profiling interactive analysis (GEPIA). GEPIA is an online tool that provides expression analysis functions for TCGA and GTEx data.

RESULTS

Patient Characteristics

The analysis procedure of the current study is shown in **Figure 1**. The basic characteristics of the patients are listed in **Table S1**. A total of 269 patients with HNSCC were retrieved from the GSE658585 dataset for further analysis. The male to female ratio was 4.72:1, and average age was 60.14 years. There were T3-4 (72.8%) and M0 (97.4%) cases; median survival time was 28 months, and 72.9% of all individuals had no HPV infection.

Identification of Eight lncRNAs for Predicting HNSCC Patient Survival

Using array re-annotation analysis, 1,506 lncRNAs were identified for prognostic significance in univariate Cox survival analysis, and 95 with $P < 0.01$ were filtered out and applied to 1,000 times Cox Lasso regression with 10-fold CV. A total of 8 lncRNA groups were disclosed, and high consistency among the lncRNA sets was demonstrated (**Figure 2A**). In the most common lncRNA set, 28 lncRNAs were uncovered to show >990 occurrences and extracted for further analysis (**Figure 2B**). Multivariate Cox analysis based on the 28 lncRNAs finally identified 8 lncRNAs, including AC008655.1, AC010624.1, AC055758.2, AC118553.1, AC130456.4, LINC00608, LINC01300, and MIR99AHG. The detailed information and the survival significance of the 8 lncRNAs are shown in **Tables 1**, **2**.

Development of the Gene Signature Prediction Model

The overall score of these 8 genes based on regression coefficients was as follows: signature score = (−0.9250632 × expression of AC008655.1) − (4.7457363 × expression of AC010624.1) − (4.1420857 × expression of AC055758.2) − (4.1541207 × expression of AC118553.1) + (1.8755252 × expression of AC130456.4) − (3.5253117 × expression of LINC00608) + (3.3913564 × expression of LINC01300) − (1.8634876 × expression of MIR99AHG).

TABLE 3 | Model discussion for 8 lncRNA HNSCC.

Characteristics	Model 1			Model 2		
	Hazard Ratio	95% CI	*P*-value	Hazard ratio	95% CI	*P*-value
HPV_status	0.53	0.31–0.9	0.018*	0.53	0.31–0.9	0.018*
M_category	3.29	1.41–7.63	0.006**	3.47	1.5–8.01	0.004**
N_category	1.18	0.66–2.1	0.576	1.27	0.71–2.26	0.425
T_category	2.42	1.28–4.58	0.007**	2.41	1.27–4.57	0.007**
Uicc_stage	1.03	0.37–2.88	0.949	0.92	0.33–2.57	0.874
Score				0.28	0.17–0.45	0***
C-index		0.68 (0.65–0.70)			0.75 (0.73–0.78)	

*$P < 0.05$, **$P < 0.01$, ***$P < 0.001$.

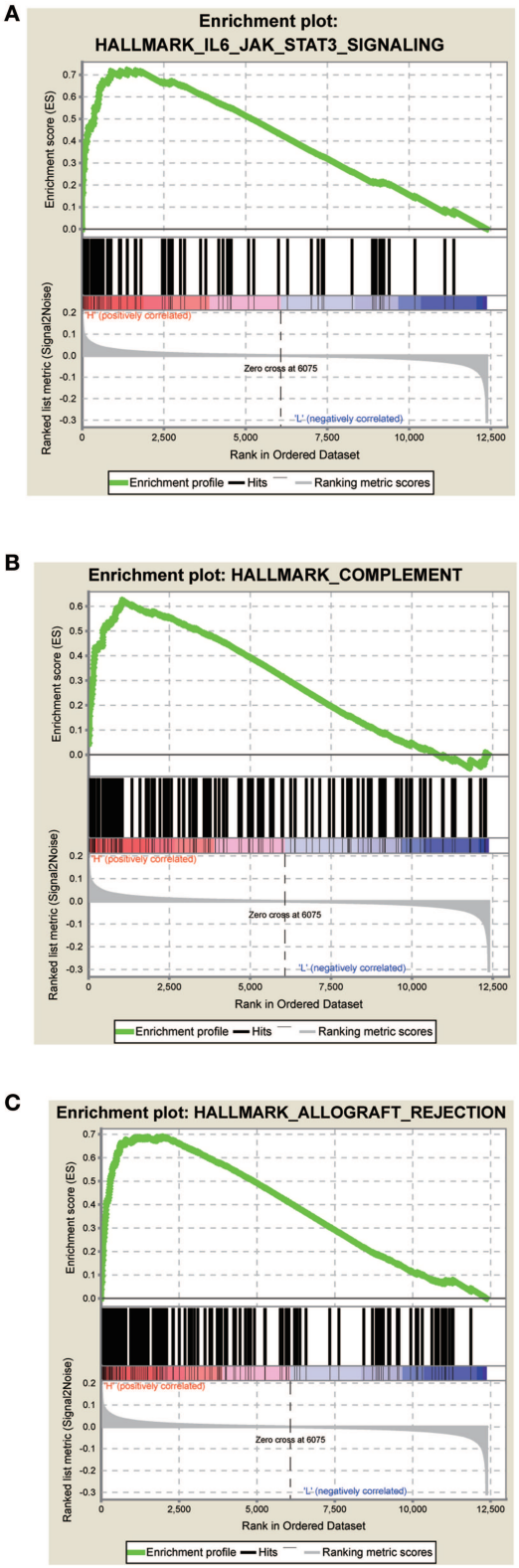

FIGURE 4 | Score correlated enrichment gene analysis with GSEA. **(A)** Hallmark IL6 JAK SATA3 SIGNALING ($P = 0.004$; FDR = 0.104; ES = 0.72); **(B)** HALLMARK COMPLEMENT ($P = 0.002$; FDR = 0.110; ES = 0.62); **(C)** HALLMARK ALLOGRAFT REJECTION ($P = 0.031$; FDR = 0.180; ES = 0.69).

An optimal cutoff value was selected to separate patients into low-risk and high-risk groups using the pROC package in R. **Figure 3A** shows that patients in the low-risk group had longer OS ($p < 0.0001$) than those of the high-risk group. Multivariate cox regression analysis included Score, Uicc_stage, T_category, N_category, M_category, and HPV_status as independent predictors. The results showed that factors with $P < 0.05$ were included in the prediction model (**Table 3**). Then, the model was also presented as a nomogram (**Figure 3B**). **Figure 3C** shows that calibration of the new prediction model was fitted; the results predicted by the model were basically consistent with the ideal results of the model incorporating the gene signature (C-index 0.75, 95% CI 0.73–0.78), which was more predictive than models not including it (C-index 0.68, 95% CI 0.65–0.71; **Table 3**).

Clinical Use

Figure 3D shows the DCAs for the prognostic prediction model and the model without the gene signature. The results showed that using the prognostic prediction model with the gene signature to predict the OS of patients could be of more benefit in the current model than the treat-all patients- or treat-none scheme. Compared with this model without the gene signature, the prognostic prediction model with the gene signature could bring greater benefits to patients.

GSEA of the Signature Score

The GSEA data showed that samples with high signature scores were mainly enriched in the hallmark of IL6 JAK SATA3 signaling, HALLMARK COMPLEMENT, and HALLMARK ALLOGRAFT REJECTION ($P < 0.05$; FDR < 0.2; **Figure 4**; **Table 4**).

Weighted Co-expression Network Construction (WGCNA)

A co-expression network was constructed using GSE65858, including 269 HNSCC samples with complete clinical data. The expression amounts of 5,000 genes including 4,992 mRNAs and 8 lncRNAs were analyzed for co-expression network constructing the "WGCNA" package. In the current study, to ensure a scale-free network, we selected $\beta = 5$ as the soft-thresholding power (**Figure 5A**) and identified a total of 13 modules (**Figure 5B**).

Identification of Hub lncRNAs in Modules and Function Annotation

Identifying modules most significantly related to clinical features is difficult. We found that the blue module was correlated with N category, T category, and Stage; N category showed the highest correlation ($P = 5.1e\text{-}62$; $r = 0.58$, **Figure 5C**).

To assess the functional involvement of the hub lncRNAs, their co-expression modules were determined via the WGCNA algorithm. We found AC010624.1 and AC130456.4 in the black module, LINC00608 and LINC01300 in the blue module, MIR99AHG in the brown module, AC008655.1 in the tan module, and AC118553.1 in the magenta module. All mRNAs in the modules, as well as mRNAs associated with the hub lncRNAs

TABLE 4 | Gene Set Enrichment Analysis (GSEA) group by score.

GS follow link to MSigDB	SIZE	ES	NES	NOM *p*-val	FDR *q*-val	FWER *p*-val	Rank at max	Leading edge
HALLMARK_IL6_JAK_STAT3_SIGNALING	66	0.72197646	1.6556728	0.004040404	0.104168214	0.065	1,383	Tags = 42%, list = 11%, signal = 48%
HALLMARK_COMPLEMENT	144	0.6246483	1.593254	0.002061856	0.1100425	0.138	1,045	Tags = 34%, list = 8%, signal = 37%
HALLMARK_ALLOGRAFT_REJECTION	146	0.6888915	1.5099503	0.031189084	0.18018493	0.287	1,987	Tags = 51%, list = 16%, signal = 60%

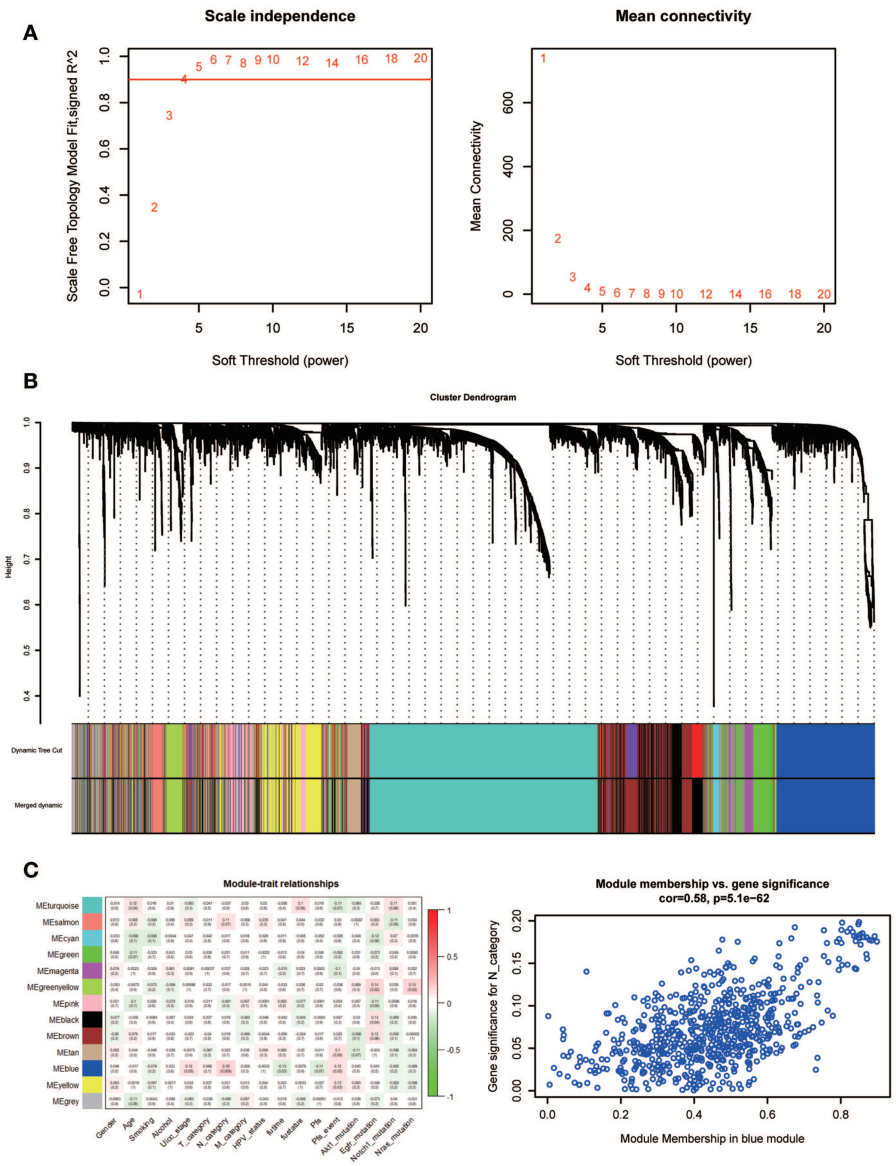

FIGURE 5 | Determination of soft-thresholding power in WGCNA. **(A)** Analysis of the scale-free fit index for various soft-thresholding powers (β) and analysis of the mean connectivity for various soft-thresholding powers. **(B)** Dendrogram of all differentially expressed genes clustered based on a dissimilarity measure. **(C)** Heatmap of the correlation between module eigengenes and clinical traits of HNSC. Scatter plot for correlation between gene module membership in the blue module and gene significance.

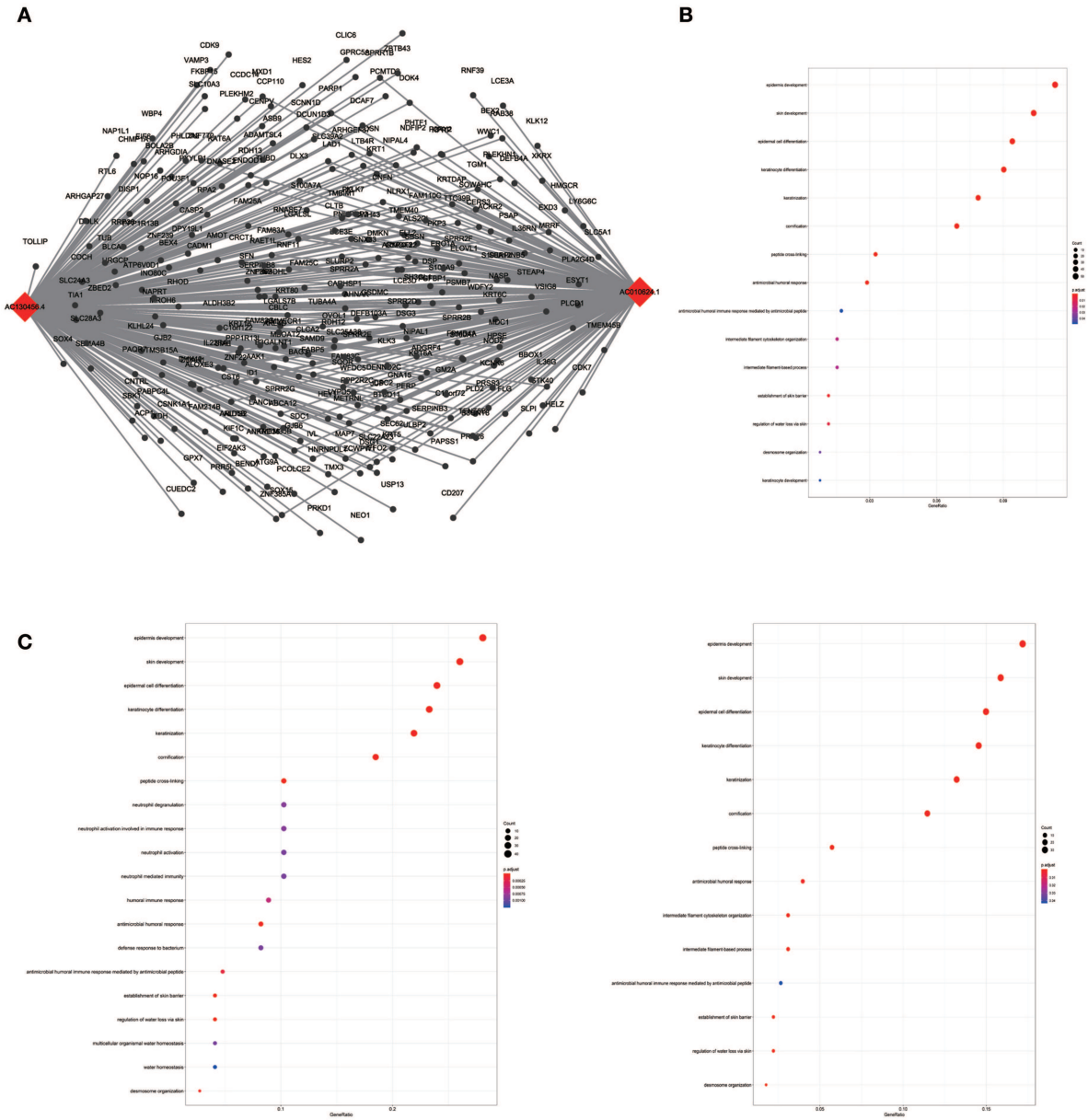

FIGURE 6 | LncRNA-mRNA network in Black module and functional enrichment. **(A)** The lncRNA-mRNA network in Black module, **(B)** GO-BP enrichment analysis (All genes in Black module), **(C)** GO-BP enrichment analysis (AC01 0624.1 related genes in Black module), and **(D)** GO-BP enrichment analysis (AC130456.4 related genes in Black module).

assessed by the ClusterProfiler Package in the R software, are shown in **Figures 6–10**.

Validation of Hub lncRNAs

All hub lncRNAs were selected for validation using the TCGA and GTEx datasets. In the TCGA database, MIR99AHG expression was associated with overall survival (**Figure 11A**), with a difference in expression between cancer and adjacent tissues (**Figure 11B**).

DISCUSSION

Using the mRNAs and lncRNAs selected after re-annotating the GSE65858 dataset of the GEO database, 8 prognosis-related lncRNAs including AC010624.1, AC130456.4, LINC00608, LINC01300, MIR99AHG, AC008655.1, AC055758.2, and AC118553.1 were obtained by univariate analysis, cox LASSO regression and multivariate analysis. Combined with clinical information, a nomogram containing an 8-lncRNA signature was established. Time-dependent calibration curves and decision

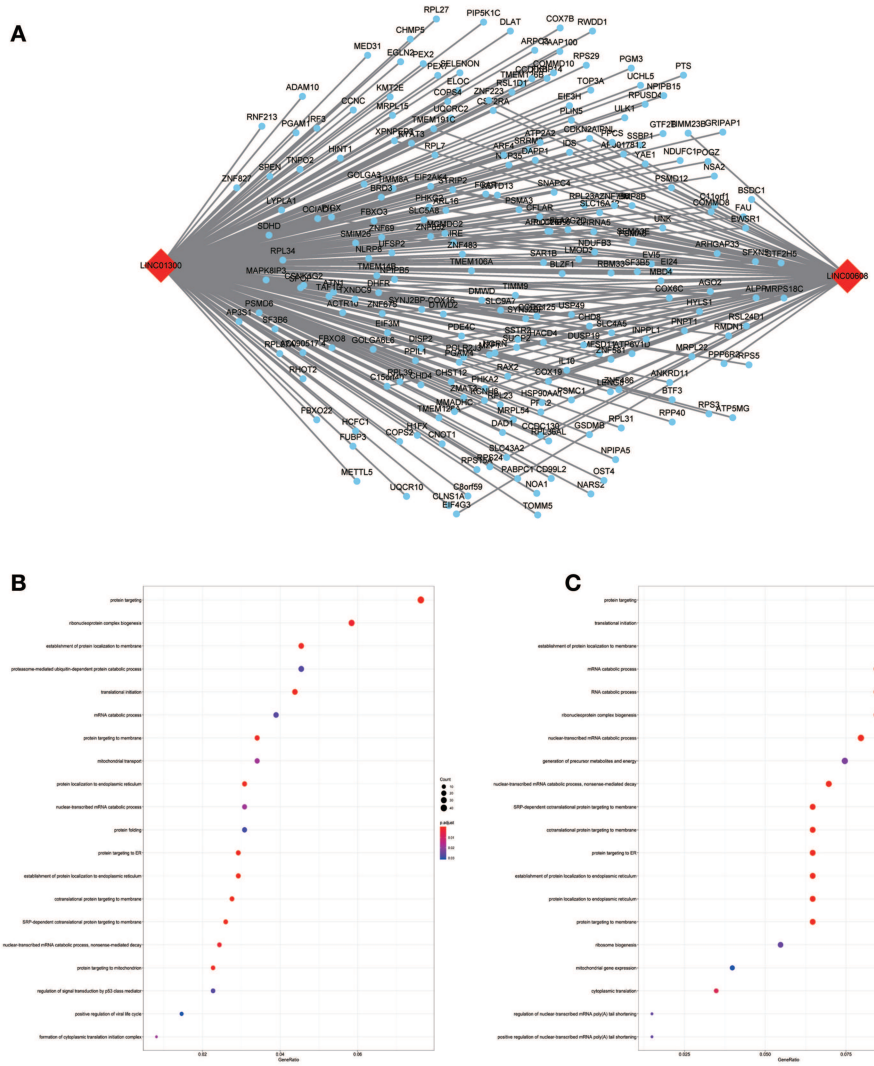

FIGURE 7 | LncRNA-mRNA network in Blue module and functional enrichment. **(A)** The lncRNA-mRNA network in Blue module, **(B)** GO-BP enrichment analysis (All genes in Blue module), **(C)** GO-BP enrichment analysis (LINC01300 related genes in Blue module).

curve analysis confirmed the prognostic significance and prediction superiority of the signature and nomogram. Further, GSEA of the signature score indicated that samples with high scores were mainly enriched in IL6/JAK/SATA3 signaling, complement, and allograft rejection, indicating HNSCC patients with poor prognosis might have dysfunctional immune systems. To identify the potential functions and involved biological processes of each lncRNA in the signature, WGCNA was performed. The black module containing AC010624.1 and AC130456.4, the blue comprising LINC00608 and LINC01300, the brown containing MIR99AHG, the tan encompassing AC008655.1, and the magenta containing AC118553.1 were obtained. GO enrichment analysis of all genes and lncRNA associated genes in modules was performed. Compared with previously established signatures (20–23), the current signature was more effective in predicting the prognosis of patients with HNSCC; more importantly, it indicated that the poor prognosis of high-score patients may be associated with changes in immune function. Furthermore, the possible biological functions of the lncRNAs contained in the signature were assessed, which provides new insights into possible treatment directions for HNSCC patients.

Previous studies have shown that the IL6/JAK/SATA3 pathway plays an important role in HNSCC (25–27), corroborating the current GSEA data. Drugs targeting the IL6/JAK/SATA3 pathway with low side effects are still under investigation (25–27). It can be inferred from the above signature that patients with high scores may benefit more from targeted drugs against the IL6/JAK/SATA3 pathway, which has a high guiding significance in future clinical applications. In addition, immune cells in the microenvironment such as M1/M2 macrophage, CD8+ T lymphocyte, NK cells, etc. can affect the

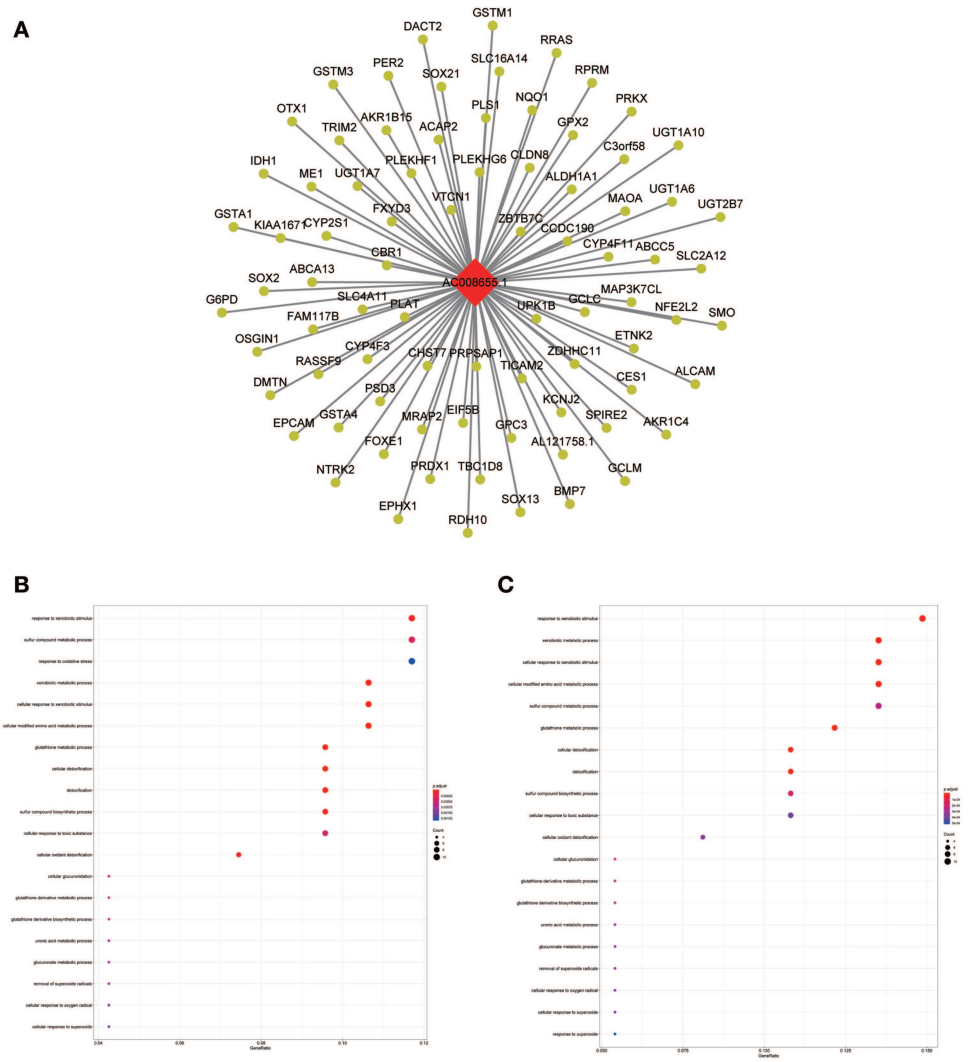

FIGURE 8 | LncRNA-mRNA network in Tan module and functional enrichment. **(A)** The lncRNA-mRNA network in Tan module, **(B)** GO-BP enrichment analysis (All genes in Tan module), and **(C)** GO-BP enrichment analysis (AC008655.1 related genes in Tan module).

tumor growth, progression, and cachexia of HNSCC by secreting IL-6. M2 macrophage can promote the proliferation of HNSCC, while CD8+ T lymphocyte, M1 macrophage, and NK cells can inhibit the progression of HNSCC via IL-6 (28). Therefore, we predicted the immune-related cells in the microenvironment of HNSCC through CIBERSORT and explored the relationship between lncRNAs in signature and these immune cells. It was found that lncRNA associated with good prognosis of HNSCC, such as AC010624.1 and MIR99AHG, was negatively correlated with NK cells resting and M2 macrophage (**Figures S1A–D**). Similarly, LINC01300 related to poor prognosis of HNSCC was negatively correlated with CD8+ T lymphocyte and M1 macrophage (**Figures S1E,F**). It provides a basis for the functional study of these lncRNAs in the IL6/JAK/STAT3 pathway and immune microenvironment, but the mechanism among lncRNAs and IL-6 remains to be explored. Besides, it had been reported HNSCC patients with high tumor mutational burden (TMB) appears worse prognosis (29). Our results showed AC010624.1 was negatively related with TMB, while LINC01300 was positively related with TMB (**Figures S1G,H**). LncRNAs in the signature play an important role in maintaining immune function in HNSCC, and the mechanisms need to be explored in the future.

WGCNA results showed that the black module containing AC010624.1 and AC130456.4 was closely related to EGFR mutation in clinical phenotypes, while GO enrichment data indicated that these two lncRNAs may both participate in epidermal cell differentiation and skin development, which is consistent with the potential function of the black module. EGFR is elevated in ∼90% of HNSCC patients and considered a negative prognostic factor for patients with HNSCC (30–32). Combining these findings, we hypothesized that

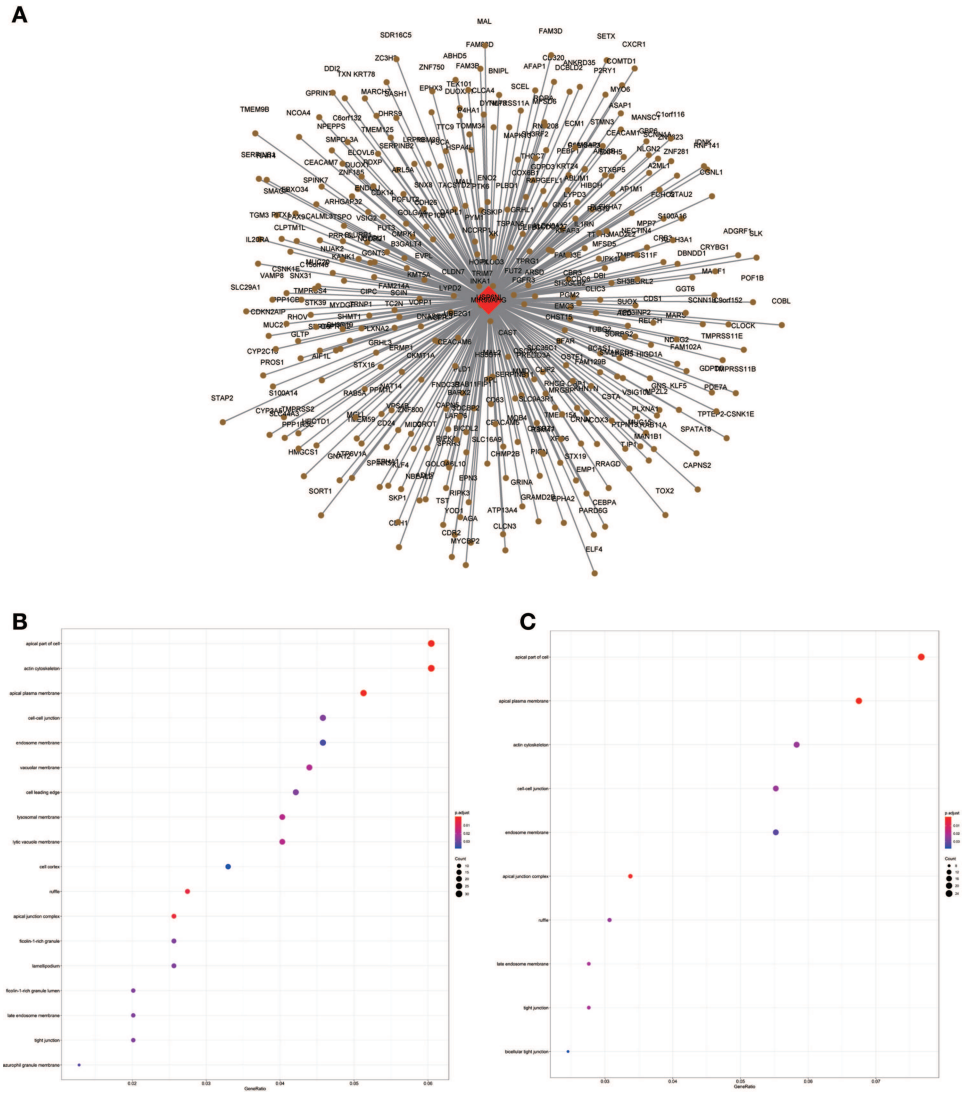

FIGURE 9 | LncRNA-mRNA network in Brown module and functional enrichment. **(A)** The lncRNA-mRNA network in Brown module, **(B)** GO-CC enrichment analysis (All genes in Brown module), and **(C)** GO-CC enrichment analysis (MIR99AHG related genes in Brown module).

AC010624.1 and AC130456.4 affect prognosis by participating in epidermal cell differentiation and skin development, which in turn affects EGFR mutation in patients with HNSCC. Whether and how AC010624.1 and AC130456.4 affect EGFR mutations deserves further investigation by molecular biology experiments.

Similarly, the brown module containing MIR99AHG was closely related to EGFR mutation in clinical phenotype. GO enrichment results indicated that the brown module was involved in the formation of cellular structures, such as the apical part of the cell, actin cytoskeleton, and apical plasma membrane, and MIR99AHG might also participate in this biological function. Previous studies have reported that MIR99AHG, also known as MONK, is a good prognostic indicator of breast cancer, lung squamous cell carcinoma, and colorectal cancer (33–36). Our results also supported these conclusions. We further investigated the potential biological process by which MIR99AHG acts and may affect EGFR gene mutation. There is a great need to further explore the role of MIR99AHG in the prognosis evaluation and treatment of HNSCC and other cancers. Finally, we used the TCGA database for validation. Patients with high MIR99AHG expression had better OS, and MIR99AHG was differentially expressed between HNSCC and adjacent tissues. In the future, the biological significance of MIR99AHG in HNSCC should be assessed.

The blue module containing LINC00608 and LINC01300 was associated with T and N stages, and GO enrichment results showed the blue module may be involved in protein processing and presentation. The potential functions of

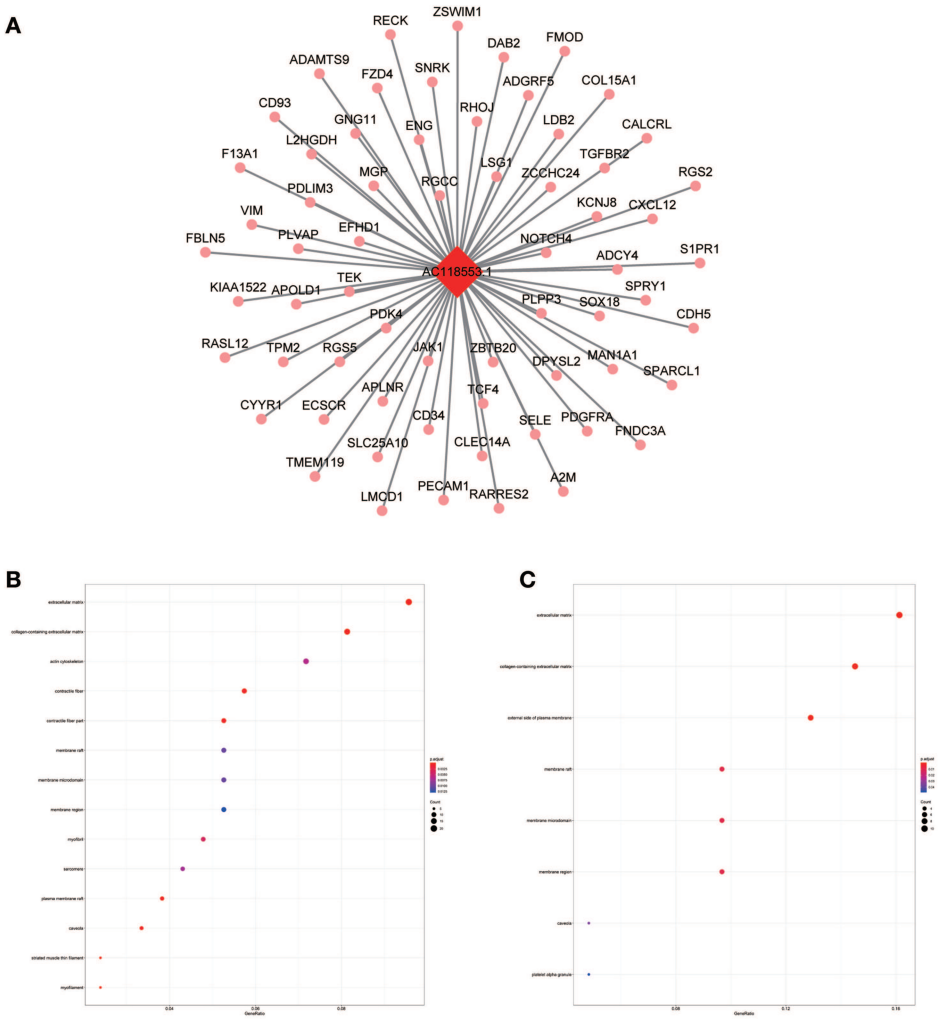

FIGURE 10 | LncRNA-mRNA network in Magenta module and functional enrichment. **(A)** The lncRNA-mRNA network in Magenta module, **(B)** GO-CC enrichment analysis (All genes in Magenta module), and **(C)** GO-CC enrichment analysis (AC118553.1 related genes in Magenta module).

both LINC00608 and LINC01300 were consistent with the blue module. The potential function enriched for AC008655.1 was the same as which the tan module, both of which might be related to the response to xenobiotics. The magenta module and AC118553.1 may be involved in the regulation of the extracellular matrix. LINC01300, AC008655.1, and AC118553.1 have not been previously reported. For the first time, we predicted the biological processes that may involve these lncRNAs, which deserve further investigation for predicting the prognosis of patients with HNSCC.

However, the limitations of this study should be mentioned. First, we did not apply an additional data set to validate the novel signature, which needs to be validated in large cohorts. Secondly, alcohol and tobacco consumptions are known prognostic factors of HNSCC (37–39), but the present signature did not fully consider the impact of these factors. This should be investigated in the future. Thirdly, HNSCC originated from different tissues, but the dataset we applied does not contain this information. Our signature lacked information of origination. Finally, we did not perform molecular biology experiments and clinical specimen validation to further explore the biological functions of hub lncRNAs involved in HNSCC.

In conclusion, we established an 8-lncRNA signature and a nomogram for predicting the prognosis of patients with HNSCC, and speculated that patients with a high signature score may have dysfunctional immune regulation, which may be a new direction of treatment for patients with HNSCC. Functional enrichment was performed to predict the potential functions of the lncRNAs contained in the signature, and for the first time, various biological functions and processes potentially altered by multiple lncRNAs were revealed. The 8-lncRNA signature is of great significance in evaluating patient prognosis and exploring new therapeutic targets for patients with HNSCC.

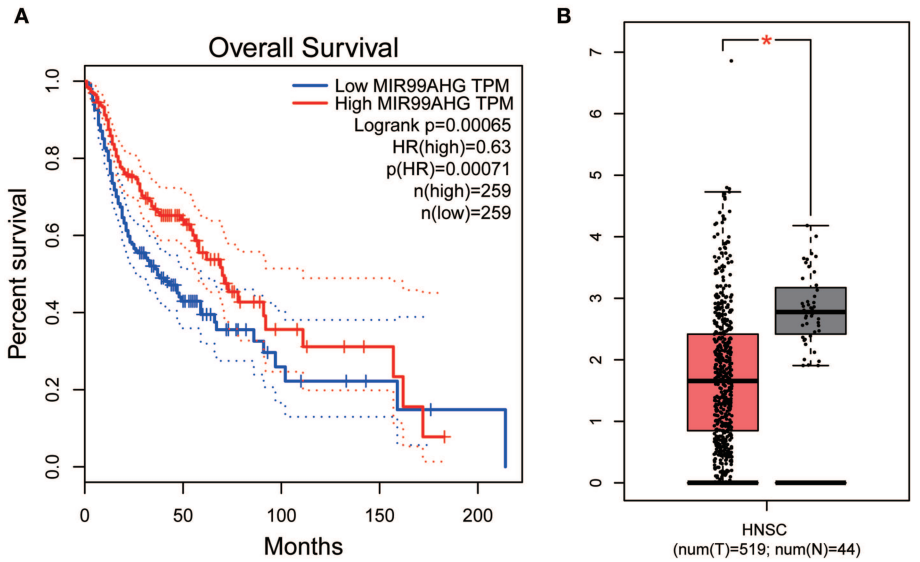

FIGURE 11 | Overall survival analyses and Gene expression difference analysis on MIR99AHG in the TCGA data set. **(A)** Kaplan-Meier curves of overall survival according to expression of MIR99AHG in TCGA-HNSC database. **(B)** Differentially expressed MIR99AHG in HNSC and normal tissues ($P < 0.05$).

DATA AVAILABILITY

Publicly available datasets were analyzed in this study. This data can be found here: https://www.ncbi.nlm.nih.gov/geo/query/acc.cgi?acc=GSE65858.

AUTHOR CONTRIBUTIONS

ZL conceived the study. BY conducted all statistical analyses. JS reviewed relevant literature and drafted the manuscript. LX, YC, XC, XQ, YL, and YT provided guidance to the study. All authors read and approved the final manuscript.

FUNDING

National Science and Technology Major Project of the Ministry of Science and Technology of China (No. 2017ZX09304025); National Natural Science Foundation of China (Nos. 81172535, 81302023). Science and Technology Plan Project of Liaoning Province (No. 2016007010); The Key Research and Development Program of Liaoning Province (No. 2018225060); The General Projects of Liaoning Province Colleges and Universities (No. LFWK201706).

SUPPLEMENTARY MATERIAL

The Supplementary Material for this article can be found online at: https://www.frontiersin.org/articles/10.3389/fonc.2019.00898/full#supplementary-material

Figure S1 | Relationship between lncRNA AC010624.1 and **(A)** CD8+ T lymphocyte, **(B)** M2 macrophage. Relationship between lncRNA MIR99AHG, and **(C)** CD8+ T lymphocyte, **(D)** NK cells resting. Relationship between lncRNA LINC01300 and **(E)** CD8+ T lymphocyte, **(F)** M1 macrophage. Relationship between lncRNA **(G)** AC010624.1, **(H)** LINC01300, **(I)** MIR99AHG and tumor mutational burden (TMB).

Table S1 | The basic characteristics of the patients.

REFERENCES

1. Leemans CR, Braakhuis BJ, Brakenhoff RH. The molecular biology of head and neck cancer. *Nat Rev Cancer.* (2011) 11:9–22. doi: 10.1038/nrc2982
2. Rothenberg SM, Ellisen LW. The molecular pathogenesis of head and neck squamous cell carcinoma. *J Clin Invest.* (2012) 122:1951–7. doi: 10.1172/JCI59889
3. Przybylski K, Majchrzak E, Weselik L, Golusinski W. Immunotherapy of head and neck squamous cell carcinoma (HNSCC). Immune checkpoint blockade. *Otolaryngol Pol.* (2018) 72:10–6. doi: 10.5604/01.3001.0012.4367
4. Cho J, Johnson DE, Grandis JR. Therapeutic implications of the genetic landscape of head and neck cancer. *Semin Radiat Oncol.* (2018) 28:2–11. doi: 10.1016/j.semradonc.2017.08.005
5. Marur S, Forastiere AA. Head and neck squamous cell carcinoma: update on epidemiology, diagnosis, and treatment. *Mayo Clin Proc.* (2016) 91:386–96. doi: 10.1016/j.mayocp.2015.12.017
6. Marur S, Forastiere AA. Head and neck cancer: changing epidemiology, diagnosis, and treatment. *Mayo Clin Proc.* (2008) 83:489–501. doi: 10.4065/83.4.489
7. Zhang ZL, Zhao LJ, Chai L, Zhou SH, Wang F, Wei Y, et al. Seven LncRNA-mRNA based risk score predicts the survival of head and neck squamous cell carcinoma. *Sci Rep.* (2017) 7:309. doi: 10.1038/s41598-017-00252-2
8. Guo W, Chen X, Zhu L, Wang Q. A six-mRNA signature model for the prognosis of head and neck squamous cell carcinoma. *Oncotarget.* (2017) 8:94528–38. doi: 10.18632/oncotarget.21786

9. Miranda-Castro R, de-Los-Santos-Alvarez N, Lobo-Castanon MJ. Long noncoding RNAs: from genomic junk to rising stars in the early detection of cancer. *Anal Bioanal Chem.* (2019). doi: 10.1007/s00216-019-01607-6
10. Yan X, Hu Z, Feng Y, Hu X, Yuan J, Zhao SD, et al. Comprehensive genomic characterization of long non-coding RNAs across human cancers. *Cancer Cell.* (2015) 28:529–40. doi: 10.1016/j.ccell.2015.09.006
11. Iyer MK, Niknafs YS, Malik R, Singhal U, Sahu A, Hosono Y, et al. The landscape of long noncoding RNAs in the human transcriptome. *Nat Genet.* (2015) 47:199–208. doi: 10.1038/ng.3192
12. Denaro N, Merlano MC, Russi EG, Lo Nigro C. Non coding RNAs in head and neck squamous cell carcinoma (HNSCC): a clinical perspective. *Anticancer Res.* (2014) 34:6887–96.
13. Sannigrahi MK, Sharma R, Panda NK, Khullar M. Role of non-coding RNAs in head and neck squamous cell carcinoma: a narrative review. *Oral Dis.* (2018) 24:1417–27. doi: 10.1111/odi.12782
14. Jathar S, Kumar V, Srivastava J, Tripathi V. Technological developments in lncRNA biology. *Adv Exp Med Biol.* (2017) 1008:283–323. doi: 10.1007/978-981-10-5203-3_10
15. Schmitt AM, Chang HY. Long noncoding RNAs in cancer pathways. *Cancer Cell.* (2016) 29:452–63. doi: 10.1016/j.ccell.2016.03.010
16. Dhamija S, Diederichs S. From junk to master regulators of invasion: lncRNA functions in migration, EMT and metastasis. *Int J Cancer.* (2016) 139:269–80. doi: 10.1002/ijc.30039
17. Wang R, Ma Z, Feng L, Yang Y, Tan C, Shi Q, et al. LncRNA MIR31HG targets HIF1A and P21 to facilitate head and neck cancer cell proliferation and tumorigenesis by promoting cell-cycle progression. *Mol Cancer.* (2018) 17:162. doi: 10.1186/s12943-018-0916-8
18. Wang P, Wu T, Zhou H, Jin Q, He G, Yu H, et al. Long noncoding RNA NEAT1 promotes laryngeal squamous cell cancer through regulating miR-107/CDK6 pathway. *J Exp Clin Cancer Res.* (2016) 35:22. doi: 10.1186/s13046-016-0297-z
19. Guan GF, Zhang DJ, Wen LJ, Xin D, Liu Y, Yu DJ, et al. Overexpression of lncRNA H19/miR-675 promotes tumorigenesis in head and neck squamous cell carcinoma. *Int J Med Sci.* (2016) 13:914–22. doi: 10.7150/ijms.16571
20. Wang P, Jin M, Sun CH, Yang L, Li YS, Wang X, et al. A three-lncRNA expression signature predicts survival in head and neck squamous cell carcinoma (HNSCC). *Biosci Rep.* (2018) 38:BSR20181528. doi: 10.1042/BSR20181528
21. Liu G, Zheng J, Zhuang L, Lv Y, Zhu G, Pi L, et al. A prognostic 5-lncRNA expression signature for head and neck squamous cell carcinoma. *Sci Rep.* (2018) 8:15250. doi: 10.1038/s41598-018-33642-1
22. Diao P, Song Y, Ge H, Wu Y, Li J, Zhang W, et al. Identification of 4-lncRNA prognostic signature in head and neck squamous cell carcinoma. *J Cell Biochem.* (2018) 120:10010–20. doi: 10.1002/jcb.28284
23. Cao W, Liu JN, Liu Z, Wang X, Han ZG, Ji T, et al. A three-lncRNA signature derived from the Atlas of ncRNA in cancer (TANRIC) database predicts the survival of patients with head and neck squamous cell carcinoma. *Oral Oncol.* (2017) 65:94–101. doi: 10.1016/j.oraloncology.2016.12.017
24. Aubry M, de Tayrac M, Etcheverry A, Clavreul A, Saikali S, Menei P, et al. From the core to beyond the margin: a genomic picture of glioblastoma intratumor heterogeneity. *Oncotarget.* (2015) 6:12094–109. doi: 10.18632/oncotarget.3297
25. Lee YS, Johnson DE, Grandis JR. An update: emerging drugs to treat squamous cell carcinomas of the head and neck. *Expert Opin Emerg Drugs.* (2018) 23:283–99. doi: 10.1080/14728214.2018.1543400
26. Gao J, Zhao S, Halstensen TS. Increased interleukin-6 expression is associated with poor prognosis and acquired cisplatin resistance in head and neck squamous cell carcinoma. *Oncol Rep.* (2016) 35:3265–74. doi: 10.3892/or.2016.4765
27. Choudhary MM, France TJ, Teknos TN, Kumar P. Interleukin-6 role in head and neck squamous cell carcinoma progression. *World J Otorhinolaryngol Head Neck Surg.* (2016) 2:90–7. doi: 10.1016/j.wjorl.2016.05.002
28. Plzak J, Boucek J, Bandurova V, Kolar M, Hradilova M, Szabo P, et al. The head and neck squamous cell carcinoma microenvironment as a potential target for cancer therapy. *Cancers.* (2019) 11:E440. doi: 10.3390/cancers11040440
29. Eder T, Hess AK, Konschak R, Stromberger C, Johrens K, Fleischer V, et al. Interference of tumour mutational burden with outcome of patients with head and neck cancer treated with definitive chemoradiation: a multicentre retrospective study of the German Cancer Consortium Radiation Oncology Group. *Eur J Cancer.* (2019) 116:67–76. doi: 10.1016/j.ejca.2019.04.015
30. Argiris A, Karamouzis MV, Raben D, Ferris RL. Head and neck cancer. *Lancet.* (2008) 371:1695–709. doi: 10.1016/S0140-6736(08)60728-X
31. Chung CH, Parker JS, Ely K, Carter J, Yi Y, Murphy BA, et al. Gene expression profiles identify epithelial-to-mesenchymal transition and activation of nuclear factor-kappaB signaling as characteristics of a high-risk head and neck squamous cell carcinoma. *Cancer Res.* (2006) 66:8210–8. doi: 10.1158/0008-5472.CAN-06-1213
32. Ang KK, Berkey BA, Tu X, Zhang HZ, Katz R, Hammond EH, et al. Impact of epidermal growth factor receptor expression on survival and pattern of relapse in patients with advanced head and neck carcinoma. *Cancer Res.* (2002) 62:7350–6. Available online at: https://cancerres.aacrjournals.org/content/62/24/7350.long
33. Ning P, Wu Z, Hu A, Li X, He J, Gong X, et al. Integrated genomic analyses of lung squamous cell carcinoma for identification of a possible competitive endogenous RNA network by means of TCGA datasets. *PeerJ.* (2018) 6:e4254. doi: 10.7717/peerj.4254
34. Liu R, Hu R, Zhang W, Zhou HH. Long noncoding RNA signature in predicting metastasis following tamoxifen treatment for ER-positive breast cancer. *Pharmacogenomics.* (2018) 19:825–35. doi: 10.2217/pgs-2018-0032
35. Huang F, Wen C, Zhuansun Y, Huang L, Chen W, Yang X, et al. A novel long noncoding RNA OECC promotes colorectal cancer development and is negatively regulated by miR-143-3p. *Biochem Biophys Res Commun.* (2018) 503:2949–55. doi: 10.1016/j.bbrc.2018.08.075
36. Emmrich S, Streltsov A, Schmidt F, Thangapandi VR, Reinhardt D, Klusmann J-H. LincRNAs MONC and MIR100HG act as oncogenes in acute megakaryoblastic leukemia. *Mol Cancer.* (2014) 13:171. doi: 10.1186/1476-4598-13-171
37. Farshadpour F, Kranenborg H, Calkoen EV, Hordijk GJ, Koole R, Slootweg PJ, et al. Survival analysis of head and neck squamous cell carcinoma: influence of smoking and drinking. *Head Neck.* (2011) 33:817–23. doi: 10.1002/hed.21549
38. Mayne ST, Cartmel B, Kirsh V, Goodwin WJ, Jr. Alcohol and tobacco use prediagnosis and postdiagnosis, and survival in a cohort of patients with early stage cancers of the oral cavity, pharynx, and larynx. *Cancer Epidemiol Biomark Prevent.* (2009) 18:3368–74. doi: 10.1158/1055-9965.EPI-09-0944
39. Gillison ML, D'Souza G, Westra W, Sugar E, Xiao W, Begum S, et al. Distinct risk factor profiles for human papillomavirus type 16-positive and human papillomavirus type 16-negative head and neck cancers. *J Natl Cancer Inst.* (2008) 100:407–20. doi: 10.1093/jnci/djn025

Conflict of Interest Statement: The authors declare that the research was conducted in the absence of any commercial or financial relationships that could be construed as a potential conflict of interest.

frontiers in Oncology

REVIEW
published: 18 September 2019
doi: 10.3389/fonc.2019.00894

Exosomes in Head and Neck Squamous Cell Carcinoma

Cheng Xiao[1], *Fang Song*[2], *Yu Long Zheng*[1], *Jiong Lv*[3], *Qiang Feng Wang*[1] *and Nong Xu*[1]*

[1] Department of Medical Oncology, College of Medicine, The First Affiliated Hospital, Zhejiang University, Hangzhou, China, [2] Department of Anesthesiology, College of Medicine, The First Affiliated Hospital, Zhejiang University, Hangzhou, China, [3] Department of Oral and Maxillofacial Surgery, College of Medicine, The First Affiliated Hospital, Zhejiang University, Hangzhou, China

Exosomes are small membranous vesicles that contain proteins, lipids, genetic material, and metabolites with abundant information from parental cells. Exosomes carry and deliver bioactive contents that can reprogram the functions of recipient cells and modulate the tumor microenvironment to induce pathological events through cell-to-cell communication and signal transduction. Tumor-derived exosomes (TDEs) in head and neck squamous cell carcinoma (HNSCC) are involved in most aspects of cancer initiation, invasion, progression, immunoregulation, therapeutic applications, and treatment resistance. In addition, HNSCC-derived exosomes can be used to obtain information on diagnostic and therapeutic biomarkers in circulating blood and saliva. Currently, the biology, mechanisms, and applications of TDEs in HNSCC are still unclear, and further research is required. In this review, we discuss various aspects of exosome biology, including exosomal components, exosomal biomarkers, and molecular mechanisms involved in immunoregulation, cancer metastasis, and therapy resistance. We also describe recent applications to update our understanding of exosomes in HNSCC.

Keywords: exosomes, head and neck squamous cell carcinoma, tumor microenvironment, biomarkers, therapy resistance

OPEN ACCESS

Edited by:
Cheng-Chia Yu, Chung Shan Medical University, Taiwan

Reviewed by:
Augusto Schneider, Universidade Federal de Pelotas, Brazil
Yin-Hwa Eva Shih, Asia University, Taiwan

***Correspondence:**
Nong Xu
nongxu@zju.edu.cn

Specialty section:
This article was submitted to Head and Neck Cancer, a section of the journal Frontiers in Oncology

Received: *25 May 2019*
Accepted: *27 August 2019*
Published: *18 September 2019*

Citation:
Xiao C, Song F, Zheng YL, Lv J, Wang QF and Xu N (2019) Exosomes in Head and Neck Squamous Cell Carcinoma. Front. Oncol. 9:894. doi: 10.3389/fonc.2019.00894

INTRODUCTION

Head and neck cancer (HNC) is one of the most widespread malignancies worldwide. Although continual progress has been made in the treatment of HNC, the 5-year overall survival rate of advanced HNC remains low at approximately 50% (1, 2). HNC frequently develops from mucosal surfaces of the mouth, including the oral cavity (tongue, lip, buccal, gingiva, and palate), oropharynx, larynx, and perioral skin carcinoma (3). More than 90% of HNCs are head and neck squamous cell carcinoma (HNSCC). The exact etiology of HNSCC remains unclear; however, tobacco and alcohol consumption are major risk factors for HNSCC, as demonstrated in epidemiological studies. Mucosal human papilloma virus (HPV) is also related to a subset of HNSCCs; ∼25.9% of HNSCCs are HPV positive, whereas the prevalence of HPV in oropharyngeal squamous cell carcinoma (SCC) is 34.1%, which is higher than that in oral SCC (4).

Exosomes, which were first discovered in 1983, are 30–150 nm mature double membrane multivesicular bodies (MVBs) originating from the endosomal pathway (5). Exosomes exist in the extracellular space and in liquids, such as blood, urine, and saliva (6). Exosomes are associated with many physiologic aspects of the disease via intercellular communication and signal transduction, indicating that exosomes have potential clinical applications as biomarkers

and therapeutic targets. Tumor-derived exosomes (TDEs) contain a cytomembrane, proteins, nucleic acids, lipids, and other substances from parental tumor cells (7). Moreover, exosomes are known to be involved in nearly all stages of cancer (8–11). Growing evidence has demonstrated that TDEs participate in the development, progression, and treatment of cancer by mediating intercellular communication and signal transduction (12, 13). The bioactive components of HNSCC-derived exosomes, such as microRNAs, transcription factors, and oncogenic proteins, play key roles in mediating tumorigenesis, tumor microenvironment reprogramming, immune tolerance, promoting metastasis, and therapy resistance. For example, intracellular annexin 1 (ANXA1) regulates epidermal growth factor receptor (EGFR) activity and alter the release of EGFR-containing TDEs in HNCs (14). Exosomes produced by hypoxic oral SCC cells deliver viral *miR-21* to normoxic cells, inducing the epithelial-mesenchymal transition (EMT) to promote cell migration and invasion (15). Another study showed that exosomal nuclear factor-κB-activating kinase-associated protein 1 (NAP1) derived from oral cancer promotes the cytotoxicity of natural killer (NK) cells via activation of the interferon regulatory factor (IRF-3) signaling pathway in recipient cells (16). In addition, *miR-34a-5p* in cancer-associated fibroblast (CAF)-derived exosomes in oral SCC stimulates the proliferation and metastasis of oral cancer cells through the AKT/glycogen synthease kinase-3β/β-catenin/Snail signaling cascade (17). A recent study demonstrated that thrombospondin 1 derived from oral SCC exosomes is also involved in the polarization of macrophages to M1-like tumor-associated macrophages and promotes the invasion of cancer cells (18). HNSCC-derived exosomes containing EphrinB1 may manipulate the tumor microenvironment through induction of tumor innervation (19). Additionally, Sento demonstrated that oral SCC-derived exosomes promote tumor growth by activating the phosphatidylinositol 3-kiase (PI3K)/AKT, mitogen-activated protein kinase (MAPK)/extracellular signal-regulated kinase (ERK), and c-Jun N-terminal kinase-1/signal transducer and activator of transcription (STAT) 2 pathways (20). Emerging evidence has supported the vital role of TDEs in the development, progression, and treatment of HNSCC.

In this review, we summarize many aspects of exosome biology and functions in HNSCC.

BIOGENESIS, FEATURES, AND COMPONENTS OF EXOSOMES

Inward Budding and MVB Formation

Different types of vesicles, including extracellular vesicles (EVs), MVBs, and exosomes, have been described and often labeled interchangeably in many previous studies. Although these different types of vesicles share overlapping features, they have distinct morphologies, properties, biogenesis mechanisms, and functional roles. Plasma membrane components and enclosing cytosolic components are incorporated into the invaginating membrane, resulting in the formation of early endosomes (21). Exosomes typically originate from inward budding from the membrane and are then released into the extracellular space via activation of Ca^{2+}-dependent or Rab-GTPases (22). Briefly, exosomes are generated from early endosomes, mature into MVBs, and are then secreted into the extracellular space upon fusion with the plasma membrane. First, exosomes start as early endosomes, which are formed by endocytosis of the plasma membrane. The biogenesis of exosomes and sorting of functional cargo is precisely regulated by certain mechanisms involving multiple factors. The most commonly described pathway for exosomes biogenesis is the endosomal sorting complex required for transport (ESCRT) machinery. Four types of ESCRTs (ESCRT-0–III) are involved in regulating MVB formation, vesicle budding, and protein cargo sorting (23). The ESCRT mechanism is initiated and sequestrated by ubiquitinated proteins to domains of the endosomal membrane via ubiquitin binding subunits of ESCRT-0 in the endosomal membrane, then interacting with the ESCRT-I and ESCRT-II complexes inducing membrane deformation into buds. Finally, the ESCRT-III complex separates from the MVBs membrane (23–25). However, the machinery that drives the load of protein cargo into ESCRT-dependent exosomes is still unclear.

Cells also utilize ESCRT-independent pathways, involving insphingosine-1-phosphate, ceramide, tetraspanin-enriched microdomains, and sphingomyelinase, for exosome production and release (26–28). These ESCRT-independent mechanisms may participate in promoting domain-induced budding, sorting of bioactive molecules into exosomes, segregation of cargo within the endosomal membrane, and exosome formation.

The ESCRT-dependent and -independent mechanisms of exosome release are based on the cell origin. In addition, membrane proteins of lysosomes and late endosomes may be important for the biogenesis and secretion of exosomes (29).

Regulated Secretion and Intercellular Interactions

Exosome secretion is involved in various signaling pathways. For example, the key regulatory role of RAB family proteins in trafficking intracellular exosomes was demonstrated by Colombo et al. (30). Another report showed that the Wnt pathway is particularly important for the dysregulation of exosome release in cancer cells (31). Additionally, the secretion of exosomes is mediated through exocytosis-associated molecular motors and cytoskeletal proteins (32). Spontaneous secretion of exosomes usually occurs at the steady state; however, some conditions are known to stimulate exosomes. Indeed, cell intrinsic signals are known to enhance the release of high levels of TDEs from cancer cells via activation of oncogenic signaling pathways or regulation of membrane fusion machinery (33). In addition, evidence suggests that microenvironmental conditions enhance exosome release from cancer cells (15, 34). Exosomes are then released into the extracellular environment through exocytosis or degraded by fusing with lysosomes. As previously described, Rab GTPases are essential regulators of exosome secretion. Furthermore, several studies have shown that soluble N-ethylmaleimide-sensitive component attachment protein receptor complexes, which are

involved in membrane fusion machinery, may affect the secretion of exosomes (35–37).

Ultimately, exosomes are internalized by recipient cells through receptor-mediated endocytosis, pinocytosis, phagocytosis, or fusion with the cell membrane, resulting in delivery of molecular and genetic components into the recipient cells (30). Exosomes target recipient cells after secretion into the extracellular space and then induce changes in downstream signaling pathways. The specificity of target recipient cells is dependent on the type of ligand/receptor pairs present on exosomes and recipient cells; and a study provides further insight that glycans are key players in the process of exosomes uptake (38). A schematic representation of exosome biogenesis and secretion pathways is shown in **Figure 1**.

FEATURES AND COMPONENTS OF EXOSOMES

Typical exosomes exhibit a particular biconcave or cup-like shape and are observed as spheroids under transmission electron microscopy (39). Exosome contents are rich in nucleic acids, cytosolic/endosome proteins, and cytoskeleton components, which have unique biological activities (40). The components of TDEs are distinct from those of exosomes released from healthy cells. TDEs deliver functional cargo, including oncogenes and oncogenic proteins that can exert biological activities. The functional cargoes, such as protein cargo, RNA cargo, and DNA cargo, of TDEs in the tumor microenvironment have an important role in promoting cancer progression and metastasis (**Figure 1**) (33). Protein cargoes, including different oncoproteins, immunomodulatory molecules, and growth factors, act as mediators of tumorigenesis. TDEs also contain abundant nucleic acids, such as microRNAs (miRNAs), mRNA, long noncoding RNAs, and DNAs, which deliver genetic information (41–43).

Many researchers have analyzed the functions of miRNAs in exosomes, and various specific miRNA cargoes and extracellular components have been detected in exosomes. These observations highlight the specificity of exosomal miRNAs, distinct miRNA signatures of exosomes, and various functions of exosomal miRNAs. A series of experiments have analyzed the function of the miRNAs in exosomes since their initial description (44). It has been reported that there was a selection of specific miRNA cargoes and extracellular exports in exosomes (30). These observations highlight the specificity of exosomal miRNAs, distinct miRNA signatures of exosomes, and various functions of exosomal miRNAs. Exosomal miRNAs are associated with a variety of pathological activities, including tumorigenesis, invasion, progression, angiogenesis, metastasis,

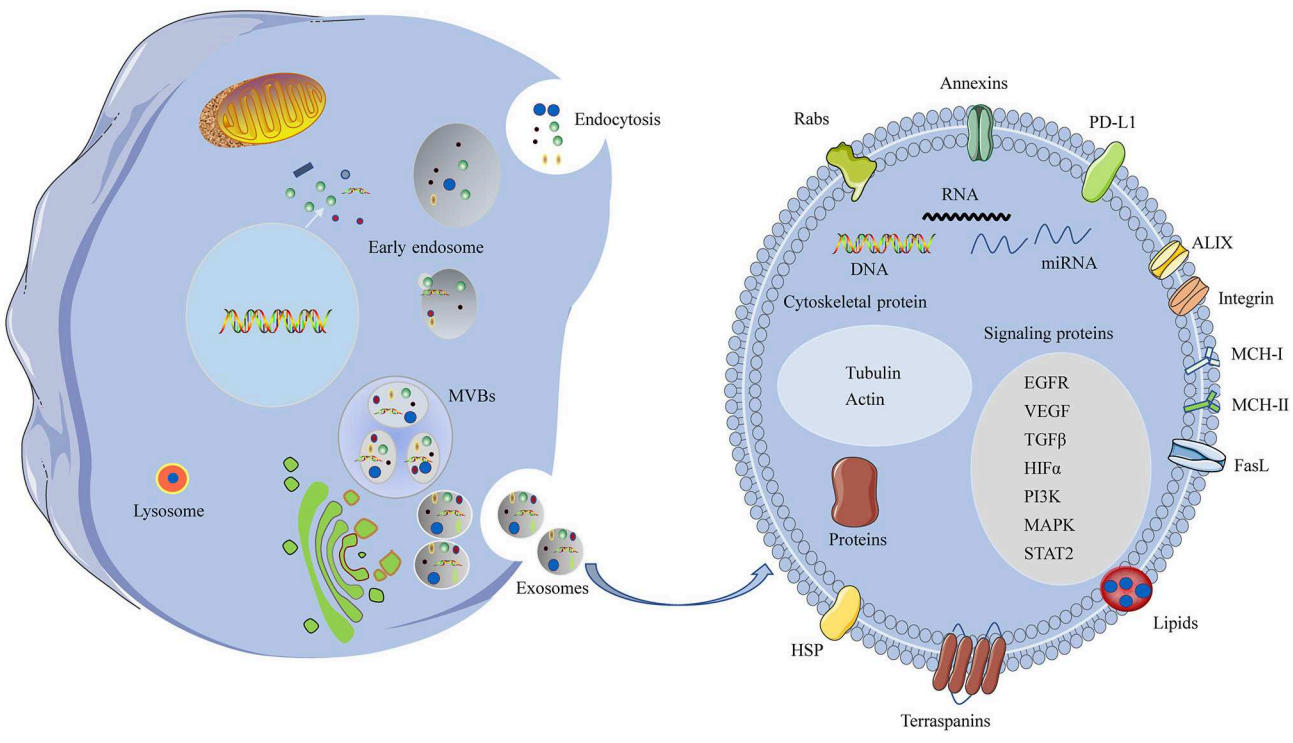

FIGURE 1 | A schematic representation of biogenesis and components of the HNSCC-derived exosomes. Invagination of the plasma membrane form early endosomes, followed by budding of payload into the endosomal membrane to form multivesicular endosomes (MVBs). Maturation of the late endosome through fusion with the plasma membrane and release of exosomes. Some of the late endosome fuse with lysosomes for lysosomal degradation. The HNSCC-derived exosomes contain various cellular ingredients, such as nucleic acids, lipid, and proteins, which act as key molecules of signaling transduction.

and chemoresistance. However, not all exosomal miRNAs are implicated in tumor-supportive mechanisms. miRNAs of exosomes are highly functional, with roles in intercellular communication and tumor microenvironment regulation, indicating that exosomal miRNAs play important roles in diagnostic and therapeutic applications.

In addition, exosomes contain ceramides, lipids, sphingolipids, cholesterol, and glycerophospholipids. Because exosomes originate from the fusion of endocytic compartments with the plasma membrane, the protein, lipid, and double lipid layer compositions can be used to identify exosomes. The most commonly identified markers are ALIX and tetraspanins, such as CD9, CD63, CD81, and CD82 (23).

FUNCTIONS OF EXOSOMES IN HNSCC

Exosomes have been identified as bioactive and informative nano-sized MVBs that influence many aspects of the development and progression of HNSCC. Here, we discuss recent findings of the mechanisms through which HNSCC-derived exosomes modulate the immune response, tumor microenvironment, cell-to-cell communication, and tumor invasion. We also describe exosomes as potential biomarkers and discuss their applications in cancer therapy and therapy resistance.

EXOSOMES AS POTENTIAL BIOMARKERS

In the clinical setting, some relevant biomarkers have been shown to influence treatments for patients with HNSCC. Several reports have shown that liquid biopsies, including biopsies of circulating tumor DNA, circulating tumor cells, and exosomal miRNAs, can have potential clinical applications in HNC (45). Moreover, HPV status is a prognostic factor in HNSCC; patients with HPV positivity have better responsiveness to chemotherapy and radiotherapy and are more susceptible to immune surveillance. In addition, miRNAs are independent prognostic markers for patients with HPV-negative HNSCC (46), and EGFR overexpression is associated with poorer prognosis and outcomes in HNSCC (47). However, further studies are needed to establish biomarkers for staging HNSCC and facilitating therapeutic decision-making.

Exosomes modulate various pathological activities to promote cancer cell growth, invasion, and distant metastasis. TDEs also carry valuable genomic and proteomic information and can provide information regarding alterations in genomic and proteomic profiles of exosomes from patients with cancer in response to anticancer therapies (48). Such proteomic and genetic components are well-protected within the lipid bilayer and can be preserved without significant loss of functional profiling. Therefore, exosomes may serve as promising markers for monitoring cancer progression and therapeutic responses (49).

TDEs can be obtained from blood or saliva of patients with HNSCC, indicating that TDEs may represent a real-time, non-invasive, clinically relevant biomarker of cancer progression, and treatment responses (45, 50–53). For example, the number of exosomes in the plasma has been shown to be a prognosis indicator for HNSCC. Gimzewski reported that elevated exosome numbers, exosome sizes, and interexosomes were detected in the saliva of patients with oral cancer (54). In addition, patients with HNSCC with advanced-stage disease and shorter overall survival usually exhibit elevated levels of exosomes in the plasma, indicating that plasma exosomes in HNSCC may have applications in monitoring tumor progression (52, 54). One previous study demonstrated that TDE signatures could serve as candidate biomarkers for early cancer diagnosis, monitoring, and surveillance in HPV-16-associated oropharyngeal (55). Moreover, a non-invasive method involving Fourier-transform infrared spectroscopy of salivary exosomes was shown to have high sensitivity and specificity in the diagnosis of oral cancer (56).

Non-coding RNAs from plasma exosomes have been extensively studied as potential biomarkers in HNSCC because they are derived from whole tumor cells and may therefore represent whole cellular RNAs (57, 58). Several studies have reported that cancer cells can selectively pack selected miRNAs into exosomes, and these selective exosomal miRNAs then act as tumor suppressors or oncogenes in HNSCC (59–61). Additionally, a hypoxic microenvironment can stimulate oral SCC to generate *miR-21*-rich exosomes, which are associated with lymph node metastasis (15). Serum exosomal *miR-21* and homeobox transcript antisense RNA (*HOTAIR*) are also significantly associated with the clinical characteristics of laryngeal SCC (59). In a previous study, elevated CAF-derived exosomal *miR-196a* levels were shown to be correlated with cisplatin resistance in HNSCC through targeting cyclin-dependent kinase (CDK) N1B and inhibitor of growth family member 5 (ING5), indicating that this miRNA may serve as a promising predictor of cisplatin resistance and poor survival in HNSCC (60). A study by Zhou and colleagues revealed that there were significant differences in expression between exosomal miRNAs and cellular miRNAs in laryngeal SCC (61). Furthermore, oral cancer-derived salivary exosomal *miR-512-3p* and *miR-412-3p* may serve as potential biomarkers (62). In another example, Inazawa and colleagues found that exosomal *miR-1246* induces cell motility and invasion through directly targeting differentially expressed in normal vs. neoplastic/MAPK-activating death domain-containing 2D in oral SCC (63). Collectively, these results suggested that exosomal miRNAs could serve as excellent diagnostic and prognostic biomarkers.

Analysis of exosomal proteins is a novel tool for developing exosomes as potential biomarkers for HNSCC. More than 80% of HNSCCs exhibit overexpression of EGFR in the membrane, and hyperactivity EGFR plays an important role in tumorigenesis development and drug-resistance mechanisms by activating various signaling pathways, including the PI3K/AKT, RAS/MEK/ERK, and Janus kinase (JAK)/STAT pathways, in HNSCC. A recent study showed that EGFR can be secreted from cells via the transport of exosomes and that these EGFR-containing exosomes have the ability to regulate autocrine VEGF production in endothelial cells (64). Exosomal EGFR mediates metastasis and tumor immunity in lung cancer (65). ANXA1,

a tumor suppressor in HNSCC, regulates EGFR activity and exosomal phospho-EGFR release, revealing that exosomal EGFR and phospho-EGFR may be prognostic biomarkers in HNSCC (14). Additionally, the levels of exosomal EGFR and phospho-EGFR are reduced after cetuximab treatment, indicating that exosomes can serve as biomarkers to monitor cetuximab treatment (66).

Analysis of exosome protein profiles showed that the characteristics and functions of exosomes from HPV-positive/-negative HNC differed significantly. HPV-positive exosomes had low p53 levels and did not contain cyclin D1, but did harbor p16, E6/E7, and the T-cell inhibitory protein PTPN11 (67). A recent study revealed that proteome analysis of salivary extracellular vesicles may yield prognostic biomarkers for oral SCC (68).

The microenvironment of HNSCC is highly immunosuppressive, and the programmed cell death (PD)-1/PD-ligand 1 (PD-L1) pathway plays an important role in HNSCC. High levels of PD-L1 are associated with poor outcomes in various types of cancer, including HNSCC. PD-1 checkpoint inhibitors were found to be safe and effective in platinum-refractory recurrent or metastatic HNSCC (69, 70). Furthermore, a study by Whiteside and colleagues indicated that PD-L1$^+$ exosomes in the plasma were related to immune suppression and disease progression. Additionally, blocking PD-L1$^+$ exosome signaling to PD-1$^+$ T cells attenuated immune suppression in patients with HNSCC (71). In another study, Ferris reported that JAK2/STAT1 signaling was involved in EGFR-mediated immune evasion in HNSCC and that therapies targeting this signaling pathway may be beneficial for blocking PD-L1 upregulation in HNSCC (72). Moreover, elevated heat-shock protein 90 levels in TDEs have been reported to serve as potential biomarkers for clinical stage and prognosis in patients with oral cancer (73). A recent study showed that plasma-derived exosomes were associated with disease progression of HNSCC after separation into CD3$^+$ and CD3$^-$ fractions (74). Furthermore, HNSCC-derived exosomes have been shown to exhibit synergistic interactions with invadopodia, indicating that exosomes play key roles in promoting cancer invasion (35). TDEs inducing transcriptome reprogramming can cause cancer-associated pathologies in HNSCC, including angiogenesis, immunoregulation, and metastasis; these functional differences in HNSCC may serve as candidate markers (75).

A growing body of evidence has shown that the characteristics of TDEs and exosomal components (e.g., exosomal miRNAs, exosomal proteins) may serve as potential noninvasive biomarkers for the detection, monitoring, and treatment of HNSCC (**Figure 2**). However, methods for TDE isolation and separation are complicated and time-consuming, and additional studies of TDEs as non-invasive biomarkers are needed.

ROLES IN REGULATING THE TUMOR MICROENVIRONMENT

Immune Cells

The tumor microenvironment is formed by stromal cells and is associated with malignant progression (76). Moreover, TDEs play important roles in regulating the tumor microenvironment of HNC (77). The immunological activities of exosomes are related to many aspects of immune regulation, including antigen presentation, immune activation, immune surveillance, and immune suppression. Tumor-infiltrating myeloid-derived suppressor cells (MDSCs), tumor-associated macrophages (TAMs), and regulatory T cells (Tregs) are known mediators of the immunosuppressive microenvironment and limit the efficacy of immune therapy in HNC (78). Exosomes that contain immunosuppressive molecules can facilitate immunosuppression in cancer, which helps cancer cells escape from immune responses, thereby promoting tumorigenesis (79, 80). Additionally, exosome-associated bioactive proteins and RNAs have been shown to regulate the immune system (81, 82). Exosomes may mediate immune suppression through

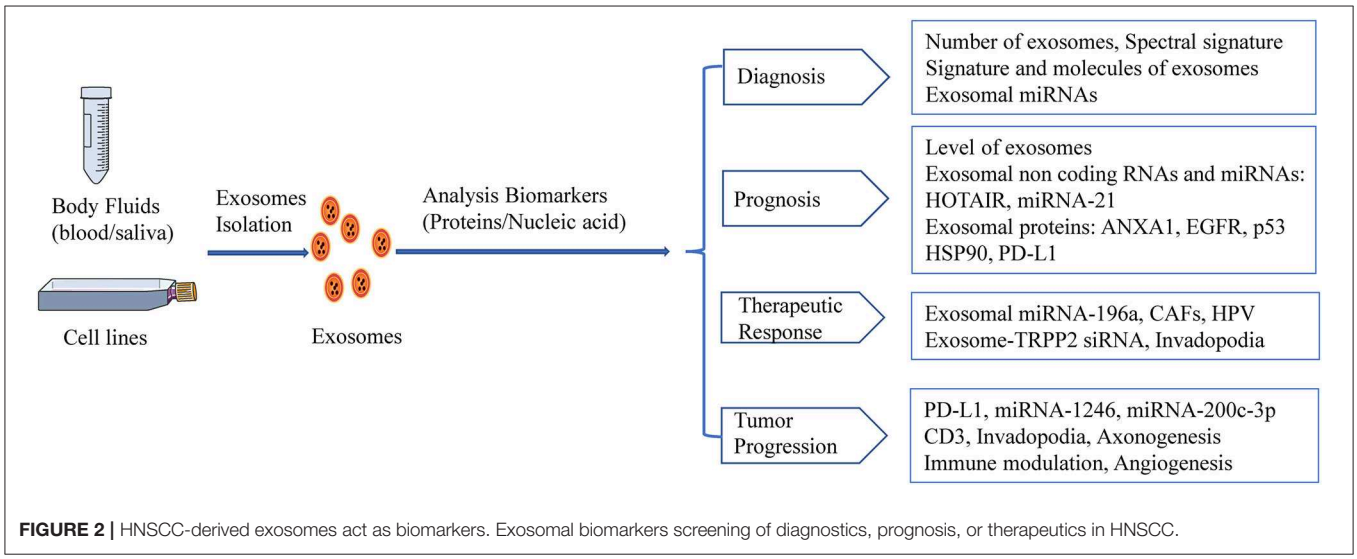

FIGURE 2 | HNSCC-derived exosomes act as biomarkers. Exosomal biomarkers screening of diagnostics, prognosis, or therapeutics in HNSCC.

directly/indirectly inhibiting the functions of T cells and NK cells and then altering the number or activity of immune suppressor cells, including MDSCs, Tregs, and HLA-DR cells (83). Exosomes are also involved in different soluble factors such as check-point receptor ligands (PD-L1), inhibitory cytokines (IL-10 and TGF-β1), death receptor ligands (FasL), ectoenzymes, and prostaglandin E2 responsible for antitumor immunity in the tumor microenvironment (84, 85). In lymphocytes and NK cells, exosomes are associated with disease stage and activity in patients with HNC, suggesting that plasma exosomes may be related to HNC progression (86). In cancer, exosome signaling may affect the immune system by inhibiting the maturity of antigen-presenting cells and TDEs that carry and transfer tumor antigens to antigen-presenting cells, thereby inducing T cell- or NK cell-dependent immune responses (87). In a similar study, TDEs containing FasL and tumor necrosis factor α were found to induce T-cell apoptosis, thereby establishing an immunosuppressive tumor microenvironment to support tumor progression (88). TDEs derived from multiple HNCC cell lines induce a suppressive phenotype in $CD8^+$ T cells through galectin-1, indicating that tumor-derived immunosuppressive exosomes may be potential therapeutic targets for preventing T-cell dysfunction and enhancing antitumor immune responses (89). As previously mentioned, the levels of oral SCC-derived $FasL^+$ microvesicles are correlated with tumor burden, and the $FasL^+$ microvesicles are involved in mediating apoptosis in activated T lymphocytes via receptor and mitochondrial pathways (51). A recent study showed that $CD4^+CD39^+$ Tregs produce adenosine by exposure to $CD39^+CD73^+$ exosomes from plasma in patients with HNSCC, thereby supporting tumor immune escape (90). Additionally, a recent study showed that oxygen pressure regulates the tumor microenvironment by altering exosomal miRNAs, which subsequently regulate the *miR-21*/phosphatase and tensin homolog (PTEN)/PD-L1 axis (91).

HPV-Positive and -Negative Exosomes

The molecular and functional profiles of exosomes from HPV-positive and -negative HNSCC are different. An early study demonstrated that HNSCC-derived exosomes have different effects on the immune system in HPV-positive and -negative HNSCC. However, there are no differences in suppressive $CD4^+$ and $CD8^+$ T cells between HPV-positive and -negative exosomes, although the responses of human monocyte-derived dendritic cells (DCs) and mature DCs to exosomes are different. HPV-positive exosomes promote DC maturation, whereas HPV-negative exosomes suppress DC maturation. HPV-negative exosomes suppress the expression of antigen processing machinery, whereas HPV-positive exosomes do not (67). HPV-positive exosomes that promote DC maturation may also stimulate antitumor immune responses, thereby improving clinical outcomes in patients with HPV-positive HNSCC (67). HPV has been shown to utilize host exosomes for cell-cell communication and to induce EGFR expression and AKT signaling in recipient cells. One study found that exosomal NAP1 derived from oral cancer cells can promote the activation of NK cells by increasing the expression and phosphorylation of IRF-3 (92).

Fibroblasts

CAFs are particularly important for regulating tumor progression. Mesenchymal stem cells reprogrammed by TDEs mediate pro-angiogenic activity and convert stromal cells into CAFs; these cells are a major component of the tumor microenvironment and play key roles in promoting tumor progression (93). HNC-derived CAFs are innately resistant to cisplatin. Indeed, a study by Zhang showed that exosomal *miR-196a* derived from HNC causes cisplatin resistance by targeting CDKN1B and ING5, highlighting the roles of CAF-derived exosomal *miR-196a* in promoting cell proliferation and inhibiting cell apoptosis in the HNC microenvironment (60). Moreover, high expression of microfibril associated protein 5 in CAF-derived exosomes may contribute to the proliferation and metastasis of oral SCC via activation of the MAPK and AKT signaling pathways (94). Additionally, TDEs have been shown to deliver caveolin-1 to the tumor microenvironment to mediate the EMT and CAFs in tongue SCC (95). In a similar study, CAF-derived exosomal *miR-34a-5p* was found to be associated with oral cancer cell proliferation and metastasis in oral SCC (17). Thus, TDEs are emerging as potent mediators of the tumor microenvironment in HNSCC (**Figure 3**).

ROLES OF TDES IN REGULATING CANCER PROGRESSION AND METASTASIS

Many studies have evaluated the roles of TDEs in cancer initiation and progression. Numerous molecules in TDEs have been implicated in the initiation and progression of cancer cells or the tumor microenvironment (96). Indeed, TDEs can transform epithelial cells into cancerous cells, thereby initiating tumorigenesis. Studies have shown that TDEs reprogram the functions of recipient cells and facilitate premetastatic niche transformation to promote metastasis through cell-cell communication or autocrine signals. Additionally, TDEs facilitate tumor progression by delivery of factors necessary for sustaining tumor growth via utilizing autocrine or juxtacrine signaling (97). Furthermore, many studies have shown that RNA from TDEs can promote metastasis (57). The shuttling of miRNA molecules may cause tumorigenesis, tumor progression, and mRNA entry into recipient cells, resulting in protein translation and metastasis (44). The EMT has been implicated in cancer cell progression and metastasis, and TDEs deliver functional complexes by membrane fusion with recipient cells and binding of the recipient cell membrane receptors to promote the EMT (98).

Exosomes derived from hypoxic oral SCC cells promote cell migration and invasion by delivering *miR-21* to normoxic cells in HNSCC (15). Nakashima conducted a study indicating that *miR-200c-3p* had invasive capacity in the human oral SCC microenvironment (99). Moreover, CAFs contribute to the proliferation and metastasis of oral cancer cells via

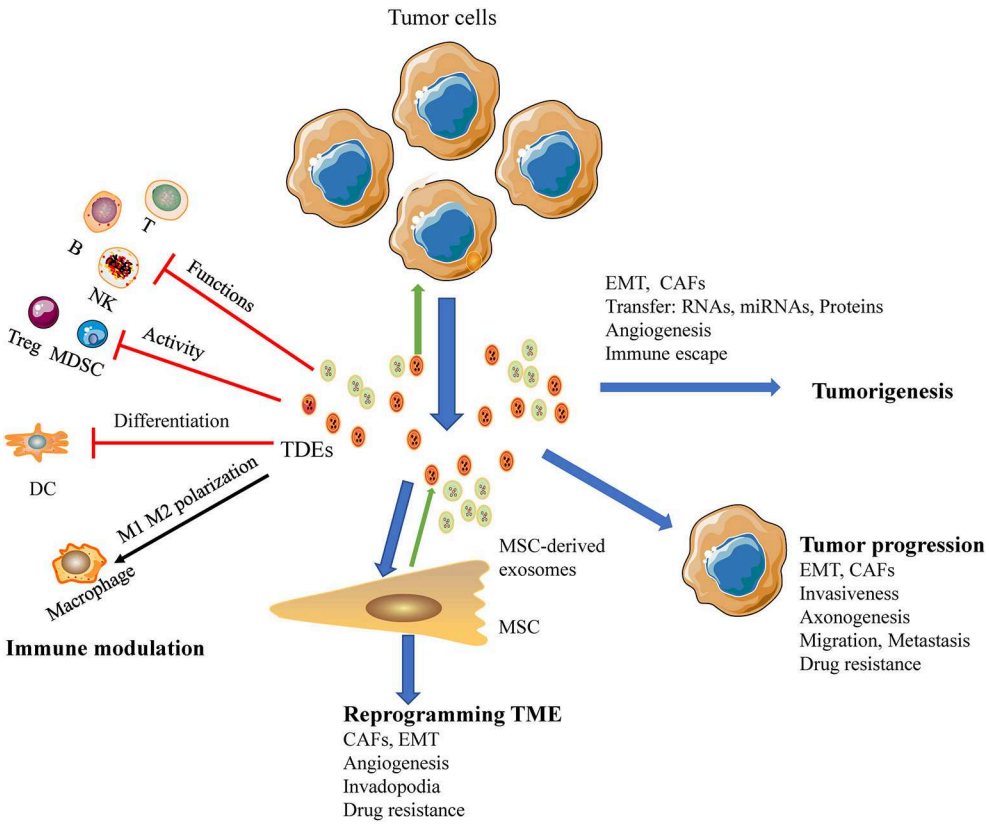

FIGURE 3 | A macroscopic view of the functions of HNSCC-derived exosomes in the tumor microenvironment. Exosomes reduce tumor immunosurveillance by interfering with the immune system: (a) inhibit the functions of immune cells; (b) suppress the activity of Tregs, MDSCs; (c) interference the differentiation of DC; (d) TAMs polarization. HNSCC-derived exosomes mediated metastasis via stimulating proliferation of endothelial cells, EMT, CAFs, and promote angiogenesis as well as re-programming of the stromal compartment. Also HNSCC-derived exosomes influence cancer progression, promoting cancer cell growth, and invasive behavior of cancer cells and development of therapy resistance.

exosome-mediated paracrine *miR-34a-5p* signaling (17). Several studies have reported the heterogeneity of transforming growth factor (TGF) β signaling in oral cavity SCC. TGFβ expressed on the surface of TDEs can differentiate fibroblasts into myofibroblasts, thereby promoting tumor progression and metastasis in oral cavity SCC (100). Additionally, exosomes target different organs via variations in integrin molecules expressed on the surface. Released exosomes can be delivered to distant organs to promote oncogenic activity by constructing a suitable premetastatic tumor microenvironment for tumor migration. Thus, TDEs contribute to the development of this premetastatic niche and induce metastatic potential in recipient cells. A recent study showed that exosomes can transport EGFR to the liver to remodel the liver microenvironment (101). TDEs can transfer oncogenic EGFR to endothelial cells, triggering upregulation of vascular endothelial growth factor (VEGF) and autocrine VEGF in endothelial cells exposed to cancer cell-related MVs (64). Moreover, oral cancer cell-derived MVs promote endothelial cell angiogenesis through the Shh/RhoA signaling pathway (102). Additional experiments have demonstrated that exosomal *miR-150* promotes tumorigenesis by upregulating VEGF, and another study showed that HNSCC-derived exosomes stimulate angiogenesis *in vitro* and *in vivo* through functional reprogramming of endothelial cells (103). These studies suggest that exosomal miRNA could affect the biology of endothelial cells; then the exosomal miRNA induces angiogenesis in HNC through different regulation pathways.

TDEs modulate the immune response in tumor microenvironment interactions implicated in cancer progression. Oral SCC-derived exosomes induced M1-like TAMs polarized and promoted tumor metastasis (18). And tumor released exosomes containing EphrinB1 potentiate induce axonogenesis will promote tumor innervation in HNSCC (19). And the delivery of miRNA-21-abundant exosomes promote EMT-mediated M2-like polarization of TAMs may promote tumor progression of HNSCC (104). Another study demonstrated that exosomes derived from irradiated HNSCC cells can modify cancer cell movement and promote migration of recipient cells through AKT-signaling (105). In an additional series of experiments, exosomes were recruited to the plasma membrane of invadopodia, and knockdown of Rab27a decreased exosome secretion and extracellular matrix digestion associated with maturing invadopodia (35). The mechanisms through which TDEs regulate cancer progression and metastasis are illustrated in **Figure 3**.

THERAPEUTIC APPLICATION

Exosomes are cell-derived nanoparticles that have unique properties, such as low immunogenicity, strong ability to cross physiological barriers, good biodistribution and bioavailability, and reduced immunogenicity. Thus, TDEs may have important roles as potential vehicles for anticancer drugs. In addition, exosomes can be remodeled through their parental cells or supplemented with desired biological activity (106). Exosomes have been designed as promising therapeutic agents in the treatment of various cancers (107–109). Because patients with metastatic HNSCC have a poor prognosis and do not typically respond well to traditional therapies, efficient targeted delivery of conventional chemotherapeutic drugs may be facilitated by innovative approaches to engineering drug delivery systems, such as exosomes.

Drug carrier exosomes have been isolated from various types of cells, including HEK-293 cells, immature DCs, macrophages, and cancer cells. Different therapeutic agents, including proteins, small interfering RNAs (siRNAs), miRNAs, and targeted drugs, can be incorporated into exosomes via electroporation, chemical-based transfection, modification of parental cells, or direct incubation, thereby increasing bioactivity and achieving targeted delivery in patients. The James Graham Brown Cancer Center initiated a phase I clinical trial to test the therapeutic effects of plant exosomes in HNC (NCT01668849). In various types of cancer, exosomes have been shown to shuttle miRNAs and soluble proteins as therapeutic molecules into recipient cells and tissues (107, 110). A hypoxic microenvironment promotes the generation of *miR-21*-rich exosomes by oral SCC in a hypoxia-inducible factor (HIF)-1a- and HIF-2a-dependent manner, and these *miR-21*-rich exosomes then mediate migration and invasion behaviors. Restoration of *miR-21* expression in HIF-1a- and HIF-2a-depleted exosomes rescues oral SCC migration and invasion (15). Moreover, hypoxic TDEs mediate MDSC function through the *miR-21*/PTEN/PD-L1 axis in oral SCC (91). These findings indicate the therapeutic value of exosome inhibition for oral SCC treatment.

Anti-EGFR nanobodies anchored on extracellular vesicles via glycosyl phosphatidylinositol may improve the targeting ability of extracellular vesicles, highlighting the potential applications of these extracellular vesicles as a drug delivery system and new tool in EGFR-expressing tumor cells (111). The blood-brain barrier restricts drugs from entering into the brain, which can reduce the therapeutic effects of brain cancer treatments. Brain endothelial cell-derived exosomes can deliver anticancer drugs across the blood-brain barrier for the treatment of brain cancer. Additionally, exosome-based drug carriers can mediate permeability across the blood-brain barrier, enabling the drug to target cancer cells (112).

The main rational approaches for inhibiting exosome-mediated tumor-promoting potential have focused on blocking exosome release and suppressing the communication of tumor cells with recipient cells. TDEs are known to be abundantly secreted from cancer cells, making them potential targets for anticancer therapy. Direct targeting of the exosome release process has also been studied for the treatment of cancer. Exosome-delivered transient receptor potential polycystic 2 (TRPP2) siRNA markedly suppresses TRPP2 expression and inhibits the EMT, suggesting that exosome-TRPP2 siRNA may be an effective RNA-based gene therapy in the treatment of HNC (113). Invadopodia also enhance exosome secretion; accordingly, silencing the expression of invadopodia may suppress TDE biogenesis and release (114). Another potential strategy for exosomal dysregulation is the inhibition of exosome uptake. Treatment with heparin blocks the uptake of exosomes by oral SCC cells, thereby attenuating exosome-induced cancer progression to inhibit the growth and progression of oral SCC cells (20). However, the use of these reagents for eliminating exosomes is currently limited to research use only because these reagents may also induce off-target effects. Further studies are needed to explore the translational implications of exosome-targeted reagents.

Owing to the potential presence of TDEs and the unique biomarkers associated with these vesicles, TDEs may also have applications as vaccine immunotherapies (115). Antigen-presenting exosomes from B lymphocytes and DCs containing MHCI/II complexes could stimulate $CD4^+$ and $CD8^+$ T cells as therapeutic HPV vaccines (116). Additionally, HPV oncogenes play vital roles in HPV-induced carcinogenesis, and silencing of endogenous HPV E6/E7 expression affects both the contents and levels of MVs released from HPV-positive cancer cells (117). These findings indicate that inhibition of endogenous HPV E6/E7 expression may have therapeutic applications. HPV vaccines based on endogenously engineered exosomes for HNC have been evaluated in several phase I clinical trials (118). However, additional studies are required to determine the feasibility and safety of TDEs as cancer vaccines. One of the major challenges in developing this approach is establishing scalable, reproducible methods for exosome production. MSCs may have uses in exosome production at a clinically applicable scale owing to their ability of produce large amounts of exosomes.

Collectively, these studies suggest that exosome-based strategies may have many benefits over conventional drug regimens; however, there are some limitations and challenges to the use of exosomes. First, because TDEs contain genetic components from cancer cells, cancer cells may not be suitable parental cells for exosome targeting in clinical applications. Additionally, efficient loading of exosomes without significant alterations to the structure and content of exosomal membranes may be difficult. Overall, these reports indicate that exosomes may function as exceptional gene delivery vectors that are safe, efficient, organ-/cell-specific, and nonimmunogenic. Nevertheless, significant efforts are required to before clinical applications are feasible.

ANTI-CANCER THERAPY RESISTANCE

Current therapy options for HNSCC include surgery, radiotherapy, chemotherapy, anti-EGFR-antibody treatment, and immunotherapy (119). However, drug resistance remains a major obstacle for achieving successful curative treatment of cancer. Drug resistance includes endogenous drug resistance,

innate drug resistance, and acquired drug resistance. Acquired drug resistance is a process through which cancer cells exposed to chemotherapy, radiation, or targeted therapy show reprogramming of their genome to acquire resistance to the therapy. Cancer cells may mitigate the effects of radiation and chemotherapy through different mechanisms (120, 121).

Given the important roles of exosomes in cellular communication and the tumor microenvironment, many studies have indicated that exosomes are involved in anticancer therapy resistance. In one mechanism, exosomes sequester cytotoxic drugs in intracellular vesicles and subsequently negate the effects of drugs within the cells (122). Owing to the nature of exosomes as mediators of cell-cell communication in the tumor microenvironment, these exosomes play important roles in therapy resistance by transferring various contents, such as miRNAs, mRNAs, DNAs, and proteins, to induce extrinsic therapy resistance (123). Similarly, exosomes also promote therapy resistance by transferring mRNAs, miRNAs, and other components. In addition, TDEs mediate therapy resistance by different mechanism, including improved DNA repair, anti-apoptotic signaling, or delivery of transporters to treatment-sensitive cells. As mediators of mesenchymal stem cells and the EMT, exosomes also promote tumor microenvironment-associated treatment resistance (123).

Exosomes derived from drug-resistant cancer cells mediate drug resistance through direct shuttling of drugs out of the cells (124). The AKT pathway is a frequently mutated oncogenic pathway in HNSCC and functions as a key regulator of radiation resistance and a major driver of cellular movement and migration (125). Exosomes derived from irradiated HNSCC cells trigger the AKT pathway to promote migration and increase chemotaxis in recipient cancer cells (105). Radiation therapy may increase the invasive and metastatic properties of HNSCC via release of an abundance of exosomes in hypoxic cancer tissue after radiotherapy (126–128). In patients with melanoma receiving PD-1 blockade therapy, the level of circulating exosomal PD-L1 correlates with tumor burden and response to therapy (129). The PD-1/PD-L1 immune checkpoint signaling axis exhibits remarkable responses in platinum-refractory recurrent or metastatic HNSCC; PD-L1-containing TDEs, which transfer functional PD-L1 and inhibit immune responses, may be regulators and biomarkers of resistance to PD-1 blockade therapy. In addition, exosomes derived from cisplatin-resistant HNSCC cells deliver *miR-21* to parental cells and induce cisplatin resistance, suggesting that these exosomes may function primarily through gene regulation (130). TDEs have been implicated in contributing to drug resistance in HNSCC (**Figure 3**).

FUTURE IMPLICATIONS

TDEs contain numerous bioactive cellular molecules and genetic characteristics, enabling them to alter the functions of recipient cells and the tumor microenvironment. Accordingly, TDEs play important regulatory roles in cancer. Indeed, TDEs are involved in many aspects of intercellular substance transmission and signal transfer, contributing to the initiation, development, metastasis, treatment resistance, and immunosuppression of HNSCC. In HNSCC, TDEs may serve as potential clinical biomarkers of progression or responses to therapy owing to their various functional contents (proteins, genes) and elements of the parental cancer cells. Nevertheless, exosomes have not yet been applied in the treatment of HNSCC. Further studies are needed to elucidate the molecular mechanisms involved in the release of exosomes and to explore the clinical applications of these vesicles. Understanding how cancer cells utilize TDEs to promote cancer growth and progression may lead to the development of novel therapies for HNSCC. Therefore, much work is needed to establish exosome-based therapies for the treatment of HNSCC.

AUTHOR CONTRIBUTIONS

CX, FS, and NX: review concept, review design, interpretation, manuscript preparation, and manuscript review. YZ, JL, and QW: manuscript preparation and manuscript review.

FUNDING

This study was funded by National Health and Family Planning Commission Research Fund & Zhejiang Provincial Medical Science and Technology Plan Project (No: KWJ-ZJ-1802).

REFERENCES

1. Bray F, Ferlay J, Soerjomataram I, Siegel RL, Torre LA, Jemal A. Global cancer statistics 2018: GLOBOCAN estimates of incidence and mortality worldwide for 36 cancers in 185 countries. *Cancer J Clin*. (2018) 68:394–424. doi: 10.3322/caac.21492
2. Ang KK, Harris J, Wheeler R, Weber R, Rosenthal DI, Nguyen-Tan PF, et al. Human papillomavirus and survival of patients with oropharyngeal cancer. *N Engl J Med*. (2010) 363:24–35. doi: 10.1056/NEJMoa0912217
3. Lydiatt WM, Patel SG, O'Sullivan B, Brandwein MS, Ridge JA, Migliacci JC, et al. Head and neck cancers-major changes in the American Joint Committee on cancer eighth edition cancer staging manual. *Cancer J Clin*. (2017) 67:122–37. doi: 10.3322/caac.21389
4. Kreimer AR, Clifford GM, Boyle P, Franceschi S. Human papillomavirus types in head and neck squamous cell carcinomas worldwide: a systematic review. *Cancer Epidemiol Biomark Prev*. (2005) 14:467–75. doi: 10.1158/1055-9965.EPI-04-0551
5. Pan BT, Johnstone RM. Fate of the transferrin receptor during maturation of sheep reticulocytes *in vitro*: selective externalization of the receptor. *Cell*. (1983) 33:967–78. doi: 10.1016/0092-8674(83)90040-5
6. Keller S, Ridinger J, Rupp AK, Janssen JW, Altevogt P. Body fluid derived exosomes as a novel template for clinical diagnostics. *J Transl Med*. (2011) 9:86. doi: 10.1186/1479-5876-9-86
7. Xin T, Greco V, Myung P. Hardwiring stem cell communication through tissue structure. *Cell*. (2016) 164:1212–25. doi: 10.1016/j.cell.2016.02.041
8. Steinbichler TB, Dudas J, Riechelmann H, Skvortsova, II. The role of exosomes in cancer metastasis. *Semin Cancer Biol*. (2017) 44:170–81. doi: 10.1016/j.semcancer.2017.02.006

9. Becker A, Thakur BK, Weiss JM, Kim HS, Peinado H, Lyden D. Extracellular vesicles in cancer: cell-to-cell mediators of metastasis. *Cancer Cell*. (2016) 30:836–48. doi: 10.1016/j.ccell.2016.10.009
10. Liu Y, Cao X. Organotropic metastasis: role of tumor exosomes. *Cell Res*. (2016) 26:149–50. doi: 10.1038/cr.2015.153
11. Zhang Y, Wang XF. A niche role for cancer exosomes in metastasis. *Nat Cell Biol*. (2015) 17:709–11. doi: 10.1038/ncb3181
12. Zhang HG, Grizzle WE. Exosomes: a novel pathway of local and distant intercellular communication that facilitates the growth and metastasis of neoplastic lesions. *Am J Pathol*. (2014) 184:28–41. doi: 10.1016/j.ajpath.2013.09.027
13. Wang Z, Chen JQ, Liu JL, Tian L. Exosomes in tumor microenvironment: novel transporters and biomarkers. *J Transl Med*. (2016) 14:297. doi: 10.1186/s12967-016-1056-9
14. Raulf N, Lucarelli P, Thavaraj S, Brown S, Vicencio JM, Sauter T, et al. Annexin A1 regulates EGFR activity and alters EGFR-containing tumour-derived exosomes in head and neck cancers. *Eur J Cancer*. (2018) 102:52–68. doi: 10.1016/j.ejca.2018.07.123
15. Li L, Li C, Wang S, Wang Z, Jiang J, Wang W, et al. Exosomes derived from hypoxic oral squamous cell carcinoma cells deliver miR-21 to normoxic cells to elicit a prometastatic phenotype. *Cancer Res*. (2016) 76:1770–80. doi: 10.1158/0008-5472.CAN-15-1625
16. Wang Y, Qin X, Zhu X, Chen W, Zhang J, Chen W. Oral cancer-derived exosomal NAP1 enhances cytotoxicity of natural killer cells via the IRF-3 pathway. *Oral Oncol*. (2018) 76:34–41. doi: 10.1016/j.oraloncology.2017.11.024
17. Li YY, Tao YW, Gao S, Li P, Zheng JM, Zhang SE, et al. Cancer-associated fibroblasts contribute to oral cancer cells proliferation and metastasis via exosome-mediated paracrine miR-34a-5p. *EBioMedicine*. (2018) 36:209–20. doi: 10.1016/j.ebiom.2018.09.006
18. Xiao M, Zhang J, Chen W, Chen W. M1-like tumor-associated macrophages activated by exosome-transferred THBS1 promote malignant migration in oral squamous cell carcinoma. *J Exp Clin Cancer Res*. (2018) 37:143. doi: 10.1186/s13046-018-0815-2
19. Madeo M, Colbert PL, Vermeer DW, Lucido CT, Cain JT, Vichaya EG, et al. Cancer exosomes induce tumor innervation. *Nat Commun*. (2018) 9:4284. doi: 10.1038/s41467-018-06640-0
20. Sento S, Sasabe E, Yamamoto T. Application of a persistent heparin treatment inhibits the malignant potential of oral squamous carcinoma cells induced by tumor cell-derived exosomes. *PLoS ONE*. (2016) 11:e0148454. doi: 10.1371/journal.pone.0148454
21. Abels ER, Breakefield XO. Introduction to extracellular vesicles: biogenesis, RNA cargo selection, content, release, and uptake. *Cell Mol Neurobiol*. (2016) 36:301–12. doi: 10.1007/s10571-016-0366-z
22. Blott EJ, Griffiths GM. Secretory lysosomes. *Nat Rev Mol Cell Biol*. (2002) 3:122–31. doi: 10.1038/nrm732
23. Colombo M, Moita C, van Niel G, Kowal J, Vigneron J, Benaroch P, et al. Analysis of ESCRT functions in exosome biogenesis, composition and secretion highlights the heterogeneity of extracellular vesicles. *J Cell Sci*. (2013) 126 (Pt 24):5553–65. doi: 10.1242/jcs.128868
24. Henne WM, Buchkovich NJ, Emr SD. The ESCRT pathway. *Dev Cell*. (2011) 21:77–91. doi: 10.1016/j.devcel.2011.05.015
25. Katzmann DJ, Babst M, Emr SD. Ubiquitin-dependent sorting into the multivesicular body pathway requires the function of a conserved endosomal protein sorting complex, ESCRT-I. *Cell*. (2001) 106:145–55. doi: 10.1016/S0092-8674(01)00434-2
26. Airola MV, Hannun YA. Sphingolipid metabolism and neutral sphingomyelinases. *Handb Exp Pharmacol*. (2013) 215:57–76. doi: 10.1007/978-3-7091-1368-4_3
27. Castro BM, Prieto M, Silva LC. Ceramide: a simple sphingolipid with unique biophysical properties. *Prog Lipid Res*. (2014) 54:53–67. doi: 10.1016/j.plipres.2014.01.004
28. Perez-Hernandez D, Gutierrez-Vazquez C, Jorge I, Lopez-Martin S, Ursa A, Sanchez-Madrid F, et al. The intracellular interactome of tetraspanin-enriched microdomains reveals their function as sorting machineries toward exosomes. *J Biol Chem*. (2013) 288:11649–61. doi: 10.1074/jbc.M112.445304
29. Zhu H, Guariglia S, Yu RY, Li W, Brancho D, Peinado H, et al. Mutation of SIMPLE in charcot-marie-tooth 1c alters production of exosomes. *Mol Biol Cell*. (2013) 24:1619–37, S1–3. doi: 10.1091/mbc.e12-07-0544
30. Colombo M, Raposo G, Thery C. Biogenesis, secretion, and intercellular interactions of exosomes and other extracellular vesicles. *Annu Rev Cell Dev Biol*. (2014) 30:255–89. doi: 10.1146/annurev-cellbio-101512-122326
31. Ekstrom EJ, Bergenfelz C, von Bulow V, Serifler F, Carlemalm E, Jonsson G, et al. WNT5A induces release of exosomes containing pro-angiogenic and immunosuppressive factors from malignant melanoma cells. *Mol Cancer*. (2014) 13:88. doi: 10.1186/1476-4598-13-88
32. Vlassov AV, Magdaleno S, Setterquist R, Conrad R. Exosomes: current knowledge of their composition, biological functions, and diagnostic and therapeutic potentials. *Biochim Biophys Acta*. (2012) 1820:940–8. doi: 10.1016/j.bbagen.2012.03.017
33. Bebelman MP, Smit MJ, Pegtel DM, Baglio SR. Biogenesis and function of extracellular vesicles in cancer. *Pharmacol Ther*. (2018) 188:1–11. doi: 10.1016/j.pharmthera.2018.02.013
34. Wang T, Gilkes DM, Takano N, Xiang L, Luo W, Bishop CJ, et al. Hypoxia-inducible factors and RAB22A mediate formation of microvesicles that stimulate breast cancer invasion and metastasis. *Proc Natl Acad Sci USA*. (2014) 111:E3234–42. doi: 10.1073/pnas.1410041111
35. Hoshino D, Kirkbride KC, Costello K, Clark ES, Sinha S, Grega-Larson N, et al. Exosome secretion is enhanced by invadopodia and drives invasive behavior. *Cell Rep*. (2013) 5:1159–68. doi: 10.1016/j.celrep.2013.10.050
36. Verweij FJ, Bebelman MP, Jimenez CR, Garcia-Vallejo JJ, Janssen H, Neefjes J, et al. Quantifying exosome secretion from single cells reveals a modulatory role for GPCR signaling. *J Cell Biol*. (2018) 217:1129–42. doi: 10.1083/jcb.201703206
37. Wei Y, Wang D, Jin F, Bian Z, Li L, Liang H, et al. Pyruvate kinase type M2 promotes tumour cell exosome release via phosphorylating synaptosome-associated protein 23. *Nat Commun*. (2017) 8:14041. doi: 10.1038/ncomms14041
38. Williams C, Pazos R, Royo F, Gonzalez E, Roura-Ferrer M, Martinez A, et al. Assessing the role of surface glycans of extracellular vesicles on cellular uptake. *Sci Rep*. (2019) 9:11920. doi: 10.1038/s41598-019-48499-1
39. Yellon DM, Davidson SM. Exosomes: nanoparticles involved in cardioprotection? *Circ Res*. (2014) 114:325–32. doi: 10.1161/CIRCRESAHA.113.300636
40. Thery C, Boussac M, Veron P, Ricciardi-Castagnoli P, Raposo G, Garin J, et al. Proteomic analysis of dendritic cell-derived exosomes: a secreted subcellular compartment distinct from apoptotic vesicles. *J Immunol*. (2001) 166:7309–18. doi: 10.4049/jimmunol.166.12.7309
41. Zhou W, Fong MY, Min Y, Somlo G, Liu L, Palomares MR, et al. Cancer-secreted miR-105 destroys vascular endothelial barriers to promote metastasis. *Cancer Cell*. (2014) 25:501–15. doi: 10.1016/j.ccr.2014.03.007
42. Melo SA, Sugimoto H, O'Connell JT, Kato N, Villanueva A, Vidal A, et al. Cancer exosomes perform cell-independent microRNA biogenesis and promote tumorigenesis. *Cancer Cell*. (2014) 26:707–21. doi: 10.1016/j.ccell.2014.09.005
43. Wilusz JE, Sunwoo H, Spector DL. Long noncoding RNAs: functional surprises from the RNA world. *Genes Dev*. (2009) 23:1494–504. doi: 10.1101/gad.1800909
44. Valadi H, Ekstrom K, Bossios A, Sjostrand M, Lee JJ, Lotvall JO. Exosome-mediated transfer of mRNAs and microRNAs is a novel mechanism of genetic exchange between cells. *Nat Cell Biol*. (2007) 9:654–9. doi: 10.1038/ncb1596
45. Nonaka T, Wong DTW. Liquid biopsy in head and neck cancer: promises and challenges. *J Dental Res*. (2018) 97:701–8. doi: 10.1177/0022034518762071
46. Hess J, Unger K, Maihoefer C, Schuttrumpf L, Wintergerst L, Heider T, et al. A five-microRNA signature predicts survival and disease control of patients with head and neck cancer negative for HPV infection. *Clin Cancer Res*. (2019) 25:1505–16. doi: 10.1158/1078-0432.CCR-18-0776
47. Xu MJ, Johnson DE, Grandis JR. EGFR-targeted therapies in the post-genomic era. *Cancer Metastasis Rev*. (2017) 36:463–73. doi: 10.1007/s10555-017-9687-8

48. Whiteside TL. The potential of tumor-derived exosomes for noninvasive cancer monitoring. *Expert Rev Mol Diagnos.* (2015) 15:1293–310. doi: 10.1586/14737159.2015.1071666
49. Wortzel I, Dror S, Kenific CM, Lyden D. Exosome-mediated metastasis: communication from a distance. *Dev Cell.* (2019) 49:347–60. doi: 10.1016/j.devcel.2019.04.011
50. Principe S, Hui AB, Bruce J, Sinha A, Liu FF, Kislinger T. Tumor-derived exosomes and microvesicles in head and neck cancer: implications for tumor biology and biomarker discovery. *Proteomics.* (2013) 13:1608–23. doi: 10.1002/pmic.201200533
51. Kim JW, Wieckowski E, Taylor DD, Reichert TE, Watkins S, Whiteside TL. Fas ligand-positive membranous vesicles isolated from sera of patients with oral cancer induce apoptosis of activated T lymphocytes. *Clin Cancer Res.* (2005) 11:1010–20.
52. Theodoraki MN, Hoffmann TK, Jackson EK, Whiteside TL. Exosomes in HNSCC plasma as surrogate markers of tumour progression and immune competence. *Clin Exp Immunol.* (2018) 194:67–78. doi: 10.1111/cei.13157
53. Zlotogorski-Hurvitz A, Dayan D, Chaushu G, Salo T, Vered M. Morphological and molecular features of oral fluid-derived exosomes: oral cancer patients versus healthy individuals. *J Cancer Res Clin Oncol.* (2016) 142:101–10. doi: 10.1007/s00432-015-2005-3
54. Sharma S, Gillespie BM, Palanisamy V, Gimzewski JK. Quantitative nanostructural and single-molecule force spectroscopy biomolecular analysis of human-saliva-derived exosomes. *Langmuir.* (2011) 27:14394–400. doi: 10.1021/la2038763
55. Kannan A, Hertweck KL, Philley JV, Wells RB, Dasgupta S. Genetic mutation and exosome signature of human papilloma virus associated oropharyngeal cancer. *Sci Rep.* (2017) 7:46102. doi: 10.1038/srep46102
56. Zlotogorski-Hurvitz A, Dekel BZ, Malonek D, Yahalom R, Vered M. FTIR-based spectrum of salivary exosomes coupled with computational-aided discriminating analysis in the diagnosis of oral cancer. *J Cancer Res Clin Oncol.* (2019) 145:685–94. doi: 10.1007/s00432-018-02827-6
57. Momen-Heravi F, Bala S. Emerging role of non-coding RNA in oral cancer. *Cell Signal.* (2018) 42:134–43. doi: 10.1016/j.cellsig.2017.10.009
58. Rabinowits G, Bowden M, Flores LM, Verselis S, Vergara V, Jo VY, et al. Comparative analysis of microRNA expression among benign and malignant tongue tissue and plasma of patients with tongue cancer. *Front Oncol.* (2017) 7:191. doi: 10.3389/fonc.2017.00191
59. Wang J, Zhou Y, Lu J, Sun Y, Xiao H, Liu M, et al. Combined detection of serum exosomal miR-21 and HOTAIR as diagnostic and prognostic biomarkers for laryngeal squamous cell carcinoma. *Med Oncol.* (2014) 31:148. doi: 10.1007/s12032-014-0148-8
60. Qin X, Guo H, Wang X, Zhu X, Yan M, Wang X, et al. Exosomal miR-196a derived from cancer-associated fibroblasts confers cisplatin resistance in head and neck cancer through targeting CDKN1B and ING5. *Genome Biol.* (2019) 20:12. doi: 10.1186/s13059-018-1604-0
61. Huang Q, Yang J, Zheng J, Hsueh C, Guo Y, Zhou L. Characterization of selective exosomal microRNA expression profile derived from laryngeal squamous cell carcinoma detected by next generation sequencing. *Oncol Rep.* (2018) 40:2584–94. doi: 10.3892/or.2018.6672
62. Gai C, Camussi F, Broccoletti R, Gambino A, Cabras M, Molinaro L, et al. Salivary extracellular vesicle-associated miRNAs as potential biomarkers in oral squamous cell carcinoma. *BMC Cancer.* (2018) 18:439. doi: 10.1186/s12885-018-4364-z
63. Sakha S, Muramatsu T, Ueda K, Inazawa J. Exosomal microRNA miR-1246 induces cell motility and invasion through the regulation of DENND2D in oral squamous cell carcinoma. *Sci Rep.* (2016) 6:38750. doi: 10.1038/srep38750
64. Al-Nedawi K, Meehan B, Kerbel RS, Allison AC, Rak J. Endothelial expression of autocrine VEGF upon the uptake of tumor-derived microvesicles containing oncogenic EGFR. *Proc Natl Acad Sci USA.* (2009) 106:3794–9. doi: 10.1073/pnas.0804543106
65. Huang SH, Li Y, Zhang J, Rong J, Ye S. Epidermal growth factor receptor-containing exosomes induce tumor-specific regulatory T cells. *Cancer Invest.* (2013) 31:330–5. doi: 10.3109/07357907.2013.789905
66. van Dommelen SM, van der Meel R, van Solinge WW, Coimbra M, Vader P, Schiffelers RM. Cetuximab treatment alters the content of extracellular vesicles released from tumor cells. *Nanomedicine.* (2016) 11:881–90. doi: 10.2217/nnm-2015-0009
67. Ludwig S, Sharma P, Theodoraki MN, Pietrowska M, Yerneni SS, Lang S, et al. Molecular and functional profiles of exosomes from HPV(+) and HPV(-) head and neck cancer cell lines. *Front Oncol.* (2018) 8:445. doi: 10.3389/fonc.2018.00445
68. Winck FV, Prado Ribeiro AC, Ramos Domingues R, Ling LY, Riano-Pachon DM, Rivera C, et al. Insights into immune responses in oral cancer through proteomic analysis of saliva and salivary extracellular vesicles. *Sci Rep.* (2015) 5:16305. doi: 10.1038/srep16305
69. Ferris RL, Blumenschein G Jr, Fayette J, Guigay J, Colevas AD, Licitra L, et al. Nivolumab for recurrent squamous-cell carcinoma of the head and neck. *N Engl J Med.* (2016) 375:1856–67. doi: 10.1056/NEJMoa1602252
70. Chow LQM, Haddad R, Gupta S, Mahipal A, Mehra R, Tahara M, et al. Antitumor activity of pembrolizumab in biomarker-unselected patients with recurrent and/or metastatic head and neck squamous cell carcinoma: results from the phase Ib KEYNOTE-012 expansion cohort. *J Clin Oncol.* (2016) 34:3838–45. doi: 10.1200/JCO.2016.68.1478
71. Theodoraki MN, Yerneni SS, Hoffmann TK, Gooding WE, Whiteside TL. Clinical significance of PD-L1(+) exosomes in plasma of head and neck cancer patients. *Clin Cancer Res.* (2018) 24:896–905. doi: 10.1158/1078-0432.CCR-17-2664
72. Concha-Benavente F, Srivastava RM, Trivedi S, Lei Y, Chandran U, Seethala RR, et al. Identification of the cell-intrinsic and -extrinsic pathways downstream of EGFR and IFNgamma that induce PD-L1 expression in head and neck cancer. *Cancer Res.* (2016) 76:1031–43. doi: 10.1158/0008-5472.CAN-15-2001
73. Ono K, Eguchi T, Sogawa C, Calderwood SK, Futagawa J, Kasai T, et al. HSP-enriched properties of extracellular vesicles involve survival of metastatic oral cancer cells. *J Cell Biochem.* (2018) 119:7350–62. doi: 10.1002/jcb.27039
74. Theodoraki MN, Hoffmann TK, Whiteside TL. Separation of plasma-derived exosomes into CD3((+)) and CD3((-)) fractions allows for association of immune cell and tumour cell markers with disease activity in HNSCC patients. *Clin Exp Immunol.* (2018) 192:271–83. doi: 10.1111/cei.13113
75. Qadir F, Aziz MA, Sari CP, Ma H, Dai H, Wang X, et al. Transcriptome reprogramming by cancer exosomes: identification of novel molecular targets in matrix and immune modulation. *Mol Cancer.* (2018) 17:97. doi: 10.1186/s12943-018-0846-5
76. Quail DF, Joyce JA. Microenvironmental regulation of tumor progression and metastasis. *Nat Med.* (2013) 19:1423–37. doi: 10.1038/nm.3394
77. Dayan D, Salo T, Salo S, Nyberg P, Nurmenniemi S, Costea DE, et al. Molecular crosstalk between cancer cells and tumor microenvironment components suggests potential targets for new therapeutic approaches in mobile tongue cancer. *Cancer Med.* (2012) 1:128–40. doi: 10.1002/cam4.24
78. Davis RJ, Van Waes C, Allen CT. Overcoming barriers to effective immunotherapy: MDSCs, TAMs, and Tregs as mediators of the immunosuppressive microenvironment in head and neck cancer. *Oral Oncol.* (2016) 58:59–70. doi: 10.1016/j.oraloncology.2016.05.002
79. Filipazzi P, Burdek M, Villa A, Rivoltini L, Huber V. Recent advances on the role of tumor exosomes in immunosuppression and disease progression. *Semin Cancer Biol.* (2012) 22:342–9. doi: 10.1016/j.semcancer.2012.02.005
80. Monypenny J, Milewicz H, Flores-Borja F, Weitsman G, Cheung A, Chowdhury R, et al. ALIX regulates tumor-mediated immunosuppression by controlling EGFR activity and PD-L1 presentation. *Cell Rep.* (2018) 24:630–41. doi: 10.1016/j.celrep.2018.06.066
81. van der Grein SG, Nolte-'t Hoen EN. "Small Talk" in the Innate immune system via RNA-containing extracellular vesicles. *Front Immunol.* (2014) 5:542. doi: 10.3389/fimmu.2014.00542
82. Aucher A, Rudnicka D, Davis DM. MicroRNAs transfer from human macrophages to hepato-carcinoma cells and inhibit proliferation. *J Immunol.* (2013) 191:6250–60. doi: 10.4049/jimmunol.1301728
83. Vincent-Schneider H, Stumptner-Cuvelette P, Lankar D, Pain S, Raposo G, Benaroch P, et al. Exosomes bearing HLA-DR1 molecules need dendritic cells to efficiently stimulate specific T cells. *Int Immunol.* (2002) 14:713–22. doi: 10.1093/intimm/dxf048
84. Whiteside TL. Exosomes and tumor-mediated immune suppression. *J Clin Invest.* (2016) 126:1216–23. doi: 10.1172/JCI81136

85. Shi L, Chen S, Yang L, Li Y. The role of PD-1 and PD-L1 in T-cell immune suppression in patients with hematological malignancies. *J Hematol Oncol.* (2013) 6:74. doi: 10.1186/1756-8722-6-74
86. Ludwig S, Floros T, Theodoraki MN, Hong CS, Jackson EK, Lang S, et al. Suppression of lymphocyte functions by plasma exosomes correlates with disease activity in patients with head and neck cancer. *Clin Cancer Res.* (2017) 23:4843–54. doi: 10.1158/1078-0432.CCR-16-2819
87. Wolfers J, Lozier A, Raposo G, Regnault A, Thery C, Masurier C, et al. Tumor-derived exosomes are a source of shared tumor rejection antigens for CTL cross-priming. *Nat Med*. (2001) 7:297–303. doi: 10.1038/85438
88. Zhang HG, Grizzle WE. Exosomes and cancer: a newly described pathway of immune suppression. *Clin Cancer Res*. (2011) 17:959–64. doi: 10.1158/1078-0432.CCR-10-1489
89. Maybruck BT, Pfannenstiel LW, Diaz-Montero M, Gastman BR. Tumor-derived exosomes induce CD8(+) T cell suppressors. *J Immunother Cancer*. (2017) 5:65. doi: 10.1186/s40425-017-0269-7
90. Schuler PJ, Saze Z, Hong CS, Muller L, Gillespie DG, Cheng D, et al. Human CD4+ CD39+ regulatory T cells produce adenosine upon co-expression of surface CD73 or contact with CD73+ exosomes or CD73+ cells. *Clin Exp Immunol*. (2014) 177:531–43. doi: 10.1111/cei.12354
91. Li L, Cao B, Liang X, Lu S, Luo H, Wang Z, et al. Microenvironmental oxygen pressure orchestrates an anti- and pro-tumoral gammadelta T cell equilibrium via tumor-derived exosomes. *Oncogene*. (2019) 38:2830–43. doi: 10.1038/s41388-018-0627-z
92. Zhou J, Li M, Lim WQ, Luo Z, Phua SZF, Huo R, et al. A transferrin-conjugated hollow nanoplatform for redox-controlled and targeted chemotherapy of tumor with reduced inflammatory reactions. *Theranostics.* (2018) 8:518–32. doi: 10.7150/thno.21194
93. Whiteside TL. Exosome and mesenchymal stem cell cross-talk in the tumor microenvironment. *Semin Immunol*. (2018) 35:69–79. doi: 10.1016/j.smim.2017.12.003
94. Principe S, Mejia-Guerrero S, Ignatchenko V, Sinha A, Ignatchenko A, Shi W, et al. Proteomic analysis of cancer-associated fibroblasts reveals a paracrine role for MFAP5 in human oral tongue squamous cell carcinoma. *J Proteome Res*. (2018) 17:2045–59. doi: 10.1021/acs.jproteome.7b00925
95. Vered M, Lehtonen M, Hotakainen L, Pirila E, Teppo S, Nyberg P, et al. Caveolin-1 accumulation in the tongue cancer tumor microenvironment is significantly associated with poor prognosis: an *in-vivo* and *in-vitro* study. *BMC Cancer*. (2015) 15:25. doi: 10.1186/s12885-015-1030-6
96. Milane L, Singh A, Mattheolabakis G, Suresh M, Amiji MM. Exosome mediated communication within the tumor microenvironment. *J Control Release*. (2015) 219:278–94. doi: 10.1016/j.jconrel.2015.06.029
97. Syn N, Wang L, Sethi G, Thiery JP, Goh BC. Exosome-mediated metastasis: from epithelial-mesenchymal transition to escape from immunosurveillance. *Trends Pharmacol Sci*. (2016) 37:606–17. doi: 10.1016/j.tips.2016.04.006
98. Blackwell RH, Foreman KE, Gupta GN. The role of cancer-derived exosomes in tumorigenicity & epithelial-to-mesenchymal transition. *Cancers*. (2017) 9:E105. doi: 10.3390/cancers9080105
99. Kawakubo-Yasukochi T, Morioka M, Hazekawa M, Yasukochi A, Nishinakagawa T, Ono K, et al. miR-200c-3p spreads invasive capacity in human oral squamous cell carcinoma microenvironment. *Mol Carcinogenesis*. (2018) 57:295–302. doi: 10.1002/mc.22744
100. Languino LR, Singh A, Prisco M, Inman GJ, Luginbuhl A, Curry JM, et al. Exosome-mediated transfer from the tumor microenvironment increases TGFbeta signaling in squamous cell carcinoma. *Am J Transl Res*. (2016) 8:2432–7.
101. Zhang H, Deng T, Liu R, Bai M, Zhou L, Wang X, et al. Exosome-delivered EGFR regulates liver microenvironment to promote gastric cancer liver metastasis. *Nat Commun*. (2017) 8:15016. doi: 10.1038/ncomms15016
102. Huaitong X, Yuanyong F, Yueqin T, Peng Z, Wei S, Kai S. Microvesicles releasing by oral cancer cells enhance endothelial cell angiogenesis via Shh/RhoA signaling pathway. *Cancer Biol Ther*. (2017) 18:783–91. doi: 10.1080/15384047.2017.1373213
103. Ludwig N, Yerneni SS, Razzo BM, Whiteside TL. Exosomes from HNSCC promote angiogenesis through reprogramming of endothelial cells. *Mol Cancer Res*. (2018) 16:1798–808. doi: 10.1158/1541-7786.MCR-18-0358
104. Hsieh CH, Tai SK, Yang MH. Snail-overexpressing cancer cells promote M2-like polarization of tumor-associated macrophages by delivering MiR-21-abundant exosomes. *Neoplasia*. (2018) 20:775–88. doi: 10.1016/j.neo.2018.06.004
105. Mutschelknaus L, Azimzadeh O, Heider T, Winkler K, Vetter M, Kell R, et al. Radiation alters the cargo of exosomes released from squamous head and neck cancer cells to promote migration of recipient cells. *Sci Rep*. (2017) 7:12423. doi: 10.1038/s41598-017-12403-6
106. Batrakova EV, Kim MS. Using exosomes, naturally-equipped nanocarriers, for drug delivery. *J Control Release*. (2015) 219:396–405. doi: 10.1016/j.jconrel.2015.07.030
107. Yim N, Ryu SW, Choi K, Lee KR, Lee S, Choi H, et al. Exosome engineering for efficient intracellular delivery of soluble proteins using optically reversible protein-protein interaction module. *Nat Commun*. (2016) 7:12277. doi: 10.1038/ncomms12277
108. Syn NL, Wang L, Chow EK, Lim CT, Goh BC. Exosomes in cancer nanomedicine and immunotherapy: prospects and challenges. *Trends Biotechnol*. (2017) 35:665–76. doi: 10.1016/j.tibtech.2017.03.004
109. Wu K, Xing F, Wu SY, Watabe K. Extracellular vesicles as emerging targets in cancer: recent development from bench to bedside. *Biochim Biophys Acta Rev Cancer*. (2017) 1868:538–63. doi: 10.1016/j.bbcan.2017.10.001
110. Li L, Piontek K, Ishida M, Fausther M, Dranoff JA, Fu R, et al. Extracellular vesicles carry microRNA-195 to intrahepatic cholangiocarcinoma and improve survival in a rat model. *Hepatology*. (2017) 65:501–14. doi: 10.1002/hep.28735
111. Kooijmans SA, Aleza CG, Roffler SR, van Solinge WW, Vader P, Schiffelers RM. Display of GPI-anchored anti-EGFR nanobodies on extracellular vesicles promotes tumour cell targeting. *J Extracell Vesicles*. (2016) 5:31053. doi: 10.3402/jev.v5.31053
112. Yang T, Martin P, Fogarty B, Brown A, Schurman K, Phipps R, et al. Exosome delivered anticancer drugs across the blood-brain barrier for brain cancer therapy in Danio rerio. *Pharm Res*. (2015) 32:2003–14. doi: 10.1007/s11095-014-1593-y
113. Wang C, Chen L, Huang Y, Li K, Jinye A, Fan T, et al. Exosome-delivered TRPP2 siRNA inhibits the epithelial-mesenchymal transition of FaDu cells. *Oncol Lett*. (2019) 17:1953–61. doi: 10.3892/ol.2018.9752
114. Murphy DA, Courtneidge SA. The 'ins' and 'outs' of podosomes and invadopodia: characteristics, formation and function. *Nat Rev Mol Cell Biol*. (2011) 12:413–26. doi: 10.1038/nrm3141
115. Sharma A, Khatun Z, Shiras A. Tumor exosomes: cellular postmen of cancer diagnosis and personalized therapy. *Nanomedicine*. (2016) 11:421–37. doi: 10.2217/nnm.15.210
116. Hao S, Bai O, Li F, Yuan J, Laferte S, Xiang J. Mature dendritic cells pulsed with exosomes stimulate efficient cytotoxic T-lymphocyte responses and antitumour immunity. *Immunology*. (2007) 120:90–102. doi: 10.1111/j.1365-2567.2006.02483.x
117. Honegger A, Leitz J, Bulkescher J, Hoppe-Seyler K, Hoppe-Seyler F. Silencing of human papillomavirus (HPV) E6/E7 oncogene expression affects both the contents and the amounts of extracellular microvesicles released from HPV-positive cancer cells. *Int J Cancer*. (2013) 133:1631–42. doi: 10.1002/ijc.28164
118. Di Bonito P, Accardi L, Galati L, Ferrantelli F, Federico M. Anti-cancer vaccine for HPV-associated neoplasms: focus on a therapeutic HPV vaccine based on a novel tumor antigen delivery method using endogenously engineered exosomes. *Cancers.* (2019) 11:E138. doi: 10.3390/cancers11020138
119. Cramer JD, Burtness B, Le QT, Ferris RL. The changing therapeutic landscape of head and neck cancer. *Nat Rev Clin Oncol.* (2019). doi: 10.1038/s41571-019-0227-z. [Epub ahead of print].
120. Meads MB, Gatenby RA, Dalton WS. Environment-mediated drug resistance: a major contributor to minimal residual disease. *Nat Rev Cancer*. (2009) 9:665–74. doi: 10.1038/nrc2714
121. Moitra K, Lou H, Dean M. Multidrug efflux pumps and cancer stem cells: insights into multidrug resistance and therapeutic development. *Clin Pharmacol Ther*. (2011) 89:491–502. doi: 10.1038/clpt.2011.14
122. Shedden K, Xie XT, Chandaroy P, Chang YT, Rosania GR. Expulsion of small molecules in vesicles shed by cancer cells: association with gene expression and chemosensitivity profiles. *Cancer Res.* (2003) 63:4331–7.

123. Steinbichler TB, Dudas J, Skvortsov S, Ganswindt U, Riechelmann H, Skvortsova II. Therapy resistance mediated by exosomes. *Mol Cancer.* (2019) 18:58. doi: 10.1186/s12943-019-0970-x
124. Namee NM, O'Driscoll L. Extracellular vesicles and anti-cancer drug resistance. *Biochim Biophys Acta Rev Cancer*. (2018) 1870:123–36. doi: 10.1016/j.bbcan.2018.07.003
125. Bussink J, van der Kogel AJ, Kaanders JH. Activation of the PI3-K/AKT pathway and implications for radioresistance mechanisms in head and neck cancer. *Lancet Oncol*. (2008) 9:288–96. doi: 10.1016/S1470-2045(08)70073-1
126. Pickhard AC, Margraf J, Knopf A, Stark T, Piontek G, Beck C, et al. Inhibition of radiation induced migration of human head and neck squamous cell carcinoma cells by blocking of EGF receptor pathways. *BMC Cancer.* (2011) 11:388. doi: 10.1186/1471-2407-11-388
127. Beck C, Piontek G, Haug A, Bas M, Knopf A, Stark T, et al. The kallikrein-kinin-system in head and neck squamous cell carcinoma (HNSCC) and its role in tumour survival, invasion, migration and response to radiotherapy. *Oral Oncol*. (2012) 48:1208–19. doi: 10.1016/j.oraloncology.2012.06.001
128. Mutschelknaus L, Peters C, Winkler K, Yentrapalli R, Heider T, Atkinson MJ, et al. Exosomes derived from squamous head and neck cancer promote cell survival after ionizing radiation. *PLoS ONE*. (2016) 11:e0152213. doi: 10.1371/journal.pone.0152213
129. Chen G, Huang AC, Zhang W, Zhang G, Wu M, Xu W, et al. Exosomal PD-L1 contributes to immunosuppression and is associated with anti-PD-1 response. *Nature*. (2018) 560:382–6. doi: 10.1038/s41586-018-0392-8
130. Liu T, Chen G, Sun D, Lei M, Li Y, Zhou C, et al. Exosomes containing miR-21 transfer the characteristic of cisplatin resistance by targeting PTEN and PDCD4 in oral squamous cell carcinoma. *Acta Biochim Biophys Sin*. (2017) 49:808–16. doi: 10.1093/abbs/gmx078

Conflict of Interest Statement: The authors declare that the research was conducted in the absence of any commercial or financial relationships that could be construed as a potential conflict of interest.

frontiers in Oncology

ORIGINAL RESEARCH
published: 24 September 2019
doi: 10.3389/fonc.2019.00950

Oncologic Outcomes of Patients With Sarcomatoid Carcinoma of the Hypopharynx

Liyuan Dai[1], Qigen Fang[1†], Peng Li[1], Fei Liu[2] and Xu Zhang[1]*

[1] Department of Head Neck and Thyroid, Affiliated Cancer Hospital of Zhengzhou University, Henan Cancer Hospital, Zhengzhou, China, [2] Department of Oral Medicine, The First Affiliated Hospital of Zhengzhou University, Henan Cancer Hospital, Zhengzhou, China

Objectives: Sarcomatoid carcinoma (SaCa) of the hypopharynx is rare, and its clinical pathologic characteristics and prognosis remain unknown. Therefore, the study aimed to analyze the oncologic outcomes of patients with SaCa of the hypopharynx.

Methods: Patients with SaCa of the hypopharynx who were surgically treated in the period from January 1985 to December 2018 were enrolled from two clinical centers. A matched pair study was also performed, and each patient with SaCa of the hypopharynx was matched with one patient with squamous cell carcinoma (SCC) of the hypopharynx. The main study endpoint was disease-specific survival (DSS).

Results: A total of 62 patients (all male) were enrolled. Compared to patients with traditional SCC of the hypopharynx, patients with SaCa of the hypopharynx were older and had higher rates of perineural invasion, lymphovascular invasion and cancer cachexia. The 5-year DSS rate was 20% in patients with SaCa compared to 34% in patients in the matched group, and the difference was significant ($p = 0.016$). According to the univariate analysis, tumor stage, lymph node stage, disease stage, and cachexia were associated with DSS. According to the Cox model, neck lymph node metastasis and disease stage were independent predictors for worse DSS.

Conclusion: The prognosis of patients with SaCa of the hypopharynx is dismal, and this type of SaCa is associated with more aggressive biological behavior than traditional SCC of the hypopharynx; neck lymph neck node metastasis and disease stage were the most important predictors of DSS.

Keywords: sarcomatoid carcinoma, cancer of the hypopharynx, spindle cell carcinoma, head and neck spindle cell carcinoma, prognosis

OPEN ACCESS

Edited by:
Cheng-Chia Yu, Chung Shan Medical University, Taiwan

Reviewed by:
Cesare Piazza, National Tumor Institute, Italy
Shilpi Sharma, Tata Memorial Hospital, India

****Correspondence:***
Qigen Fang
qigenfang@126.com

†Present address:
Qigen Fang, Department of Head Neck and Thyroid, Affiliated Cancer Hospital of Zhengzhou University, Henan Cancer Hospital, Zhengzhou, China

Specialty section:
This article was submitted to Head and Neck Cancer, a section of the journal Frontiers in Oncology

Received: *23 April 2019*
Accepted: *09 September 2019*
Published: *24 September 2019*

Citation:
Dai L, Fang Q, Li P, Liu F and Zhang X (2019) Oncologic Outcomes of Patients With Sarcomatoid Carcinoma of the Hypopharynx. Front. Oncol. 9:950. doi: 10.3389/fonc.2019.00950

INTRODUCTION

Since it was first reported by Virchow et al. (1) in 1864, sarcomatoid carcinoma (SaCa), a rare variant of squamous cell carcinoma (SCC), has been shown to be biphasic (2) and usually consists of both a conventional epithelial squamous cell component and a sarcomatous spindle cell component. Conventional SCC and sarcomatoid components have now been proven to arise monoclonally from a single stem cell (3–7). The disease is characterized by local recurrence and invasive growth, and is associated with poor prognosis. The tumor shows morphologic epithelial changes, where areas of squamous and spindle cell differentiation are observed (2–10).

The larynx is the most commonly involved site in SaCa of the head and neck region, followed by the oral cavity and hypopharynx (3). Cases of SaCa of the hypopharynx have only been described by a few authors (2, 3, 5–8, 11, 12); owing to the rarity of the disease, <50 cases have been reported, and detailed information regarding prognosis as well as prognostic factors for SaCa of the hypopharynx remain scarce. Therefore, we aimed to analyze the oncologic outcomes in SaCa of the hypopharynx by looking at outcomes occurring over a period of 30 years.

MATERIALS AND METHODS

The Zhengzhou University institutional research committee approved our study, all participants signed an informed consent agreement for medical research before initial treatment, and all experiments were performed in accordance with relevant guidelines and regulations.

The medical records of patients with primary spindle cell carcinoma or SaCa of the hypopharynx who were surgically treated from January 1985 to December 2018 were reviewed from two hospitals: Affiliated Cancer Hospital and The First Affiliated Hospital of Zhengzhou University. The two clinical centers had the same treatment principle for hypopharynx malignancies. Information regarding age, sex, operation record, treatment, pathologic report, and follow-up was collected and analyzed. Patients were restaged by the 7th edition AJCC classification. Cancer cachexia was defined as an unintentional weight loss of at least 5% of the premorbid weight occurring over 3–6 months (13). All the pathologic sections were re-evaluated by at least two head and neck pathologists for the accurate diagnosis of SaCa of the hypopharynx (**Figure 1**). Perineural invasion was considered to be present if tumor cells were identified within the perineural space and/or nerve bundle, and lymphovascular infiltration was positive if a tumor was noted within the lymphovascular channels (14). Drinkers were defined as those who consumed at least one alcoholic drink per day for at least 1 year, and smokers were defined as those who smoked on a daily basis or who had quit smoking for <5 years (15).

To compare the survival rates between patients with SaCa of the hypopharynx and those with SCC of the hypopharynx, patients with SCC of the hypopharynx were also reviewed during the same study period in the two hospitals. Each patient with SaCa of the hypopharynx was matched with one patient with SCC of the hypopharynx, and the matching process was performed according to age, sex, perineural invasion, lymphovascular invasion, and disease stage (15).

The propensity score matching was used to perform the pair matching process. A Pearson chi-square test or Fisher's exact test was used to compare the clinical pathologic variables between the two groups. Disease-specific survival (DSS) was the main study endpoint, and it was calculated by the Kaplan-Meier method. The factors that were significant in the univariable analysis were then analyzed in the Cox model to determine the independent risk factors. All statistical analyses were performed using SPSS 20.0. A p-value of <0.05 was considered significant.

RESULTS

There were 62 (all male) patients with SaCa of the hypopharynx enrolled in total: 25 (40.3%) patients from the Affiliated Cancer Hospital and 37 (59.7%) patients from the First Affiliated Hospital. The mean age was 65.3 years old, with a range from 51 to 76, and smoking and drinking were noted in 41 (66.1%) and 29 (46.8%) patients, respectively. Cachexia was noted in 37 (59.7%) patients. Tumor stages were distinguished as T1 in 10 (16.1%) patients, T2 in 20 (32.2%) patients, T3 in 16 (25.8%) patients, and T4 in 16 (25.8%) patients. A total of 45 (72.6%) patients underwent partial pharyngolaryngectomy, and 17 (27.4%) patients underwent total pharyngolaryngectomy. Thirty-seven (59.7%) patients underwent primary closure, 15 patients

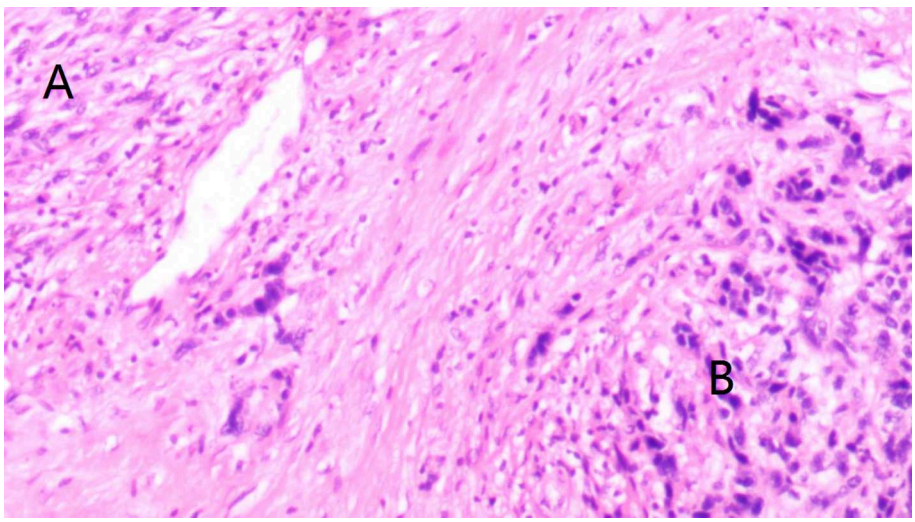

FIGURE 1 | Accurate diagnosis of sarcomatoid carcinoma (SaCa) of the hypopharynx showing morphologic epithelial changes, where areas of spindle cell **(A)** and squamous **(B)** differentiation are demonstrated (hematoxylin and eosin stain × 20).

(24.2%) underwent submental island flap reconstruction, and 10 patients (16.1%) underwent radial forearm flap reconstruction.

All patients underwent neck dissection, and a total of 59 selective neck dissections, 14 modified neck dissections, and five radical neck dissections were performed. Neck node metastasis was noted in 32 (51.6%) patients: N1 in 6 (18.8%, 6/32) patients, N2a in 10 (31.3%, 10/32) patients, N2b in 10 (31.3%, 10/32) patients, N2c in 3 (9.4%, 3/32) patients, and N3 in 3 (9.4%, 3/32) patients. The disease stages observed in patients were distinguished as I in 5 (8.1%) patients, II in 10 (16.1%) patients, III in 17 (27.4%) patients, and IV in 30 (48.4%) patients. Perineural invasion was reported in 23 (37.1%) patients, and lymphatic invasion was reported in 22 (35.5%) patients. A positive margin was demonstrated in 6 (9.7%) patients. Extracapsular extension of the node was reported in 17 (27.4%) patients. A total of 50 (80.6%) patients underwent postoperative radiotherapy, and 19 (30.6%) patients also received postoperative chemotherapy.

During the same period, there were 1,632 patients with traditional SCC of the hypopharynx. As described in **Table 1**, compared to traditional SCC of the hypopharynx, SaCa of the hypopharynx mainly affected male, older patients and was associated with a higher rate of perineural invasion; moreover, cancer cachexia was more common in patients with SaCa (all $p < 0.05$). No significant difference regarding tumor stage, neck lymph node stage, disease stage, lymphovascular invasion, or treatment was noted (all $p > 0.05$).

During our follow-up period with a mean time of 40.1 (range: 5–136) months, recurrence was noted in 49 (79.0%) patients: 22 (44.9%, 22/49) were cases of local recurrence, 14 (28.6%, 14/49) were cases of regional recurrence, 7 (14.3%, 7/49) were cases of loco-regional recurrence, and 6 (12.2%, 6/49) were cases of distant recurrence. Fifteen (30.6%, 15/49) patients experienced recurrence that was successfully salvaged by surgical treatment: 8 (53.3%, 8/15) patients underwent radical neck dissection, 5 (33.3%, 5/15) patients underwent total pharyngolaryngectomy, and 2 (13.3%, 2/15) patients underwent both radical neck dissection and total pharyngolaryngectomy. Forty-four (71.0%) patients died of the disease, and the 5- and 10-year DSS rates were 20 and 8%, respectively. After being matched, the two groups had no significant difference regarding age, sex, tumor stage, neck lymph node stage, disease stage, perineural invasion, lymphovascular invasion, or treatment (**Table 2**, all $p > 0.05$). In matched patients, the 5- and 10-year DSS rates were 34 and 28%, respectively, and the difference was significant ($p = 0.016$) (**Figure 2**).

With regard to the survival analysis in patients with SaCa, tumor stage, neck lymph node stage, disease stage, cachexia, and extracapsular extension were associated with the DSS rate according to the univariable analysis, and further Cox model analysis described that neck node stage and disease stage were the independent predictors for DSS rate (**Table 3**).

TABLE 1 | Comparison of clinical pathologic variables between patients with sarcomatoid carcinoma (SaCa) and patients with traditional hypopharynx squamous cell carcinoma (SCC).

	SaCa ($n = 62$)	SCC ($n = 1,632$)	p
Age			
≥65	47 (75.8%)	1,002 (61.4%)	
<65	15 (24.2%)	630 (38.6%)	0.022
Sex			
Male	62 (100%)	1,248 (76.5%)	
Female	0	384 (23.5%)	<0.001
Smokers			
Yes	41 (66.1%)	956 (58.6%)	
No	21 (33.9%)	676 (41.4%)	0.236
Drinkers			
Yes	29 (46.8%)	589 (36.1%)	
No	33 (53.2%)	1,043 (63.9%)	0.086
Cachexia			
Yes	37 (59.7%)	745 (45.6%)	
No	25 (40.3%)	887 (54.4%)	0.030
Tumor stage			
T1 + T2	30 (48.4%)	749 (45.9%)	
T3 + T4	32 (51.6%)	883 (54.1%)	0.699
Neck node stage			
N0	30 (48.4%)	715 (43.8%)	
N+	32 (51.6%)	917 (56.2%)	0.476
Disease stage			
I + II	15 (24.2%)	519 (31.8%)	
III + IV	47 (75.8%)	1113 (68.2%)	0.206
Perineural invasion[#]			
Yes	23 (37.1%)	287 (24.0%)	
No	39 (62.9%)	908 (76.0%)	0.020
Lymphovascular invasion*			
Yes	22 (35.5%)	248 (20.3%)	
No	40 (64.5%)	971 (79.7%)	0.004
Extracapsular spread[&]			
Yes	17 (27.4%)	333 (24.9%)	
No	45 (72.6%)	1004 (75.1%)	0.655
Treatment			
Surgery	12 (19.4%)	245 (15.0%)	
Surgery + radiotherapy	31 (50.0%)	822 (50.4%)	
Surgery + radiotherapy + chemotherapy	19 (30.6%)	565 (34.6%)	0.601

[#] *Status of perineural invasion in 437 patients with traditional SCC was unknown.*
**Status of lymphovascular invasion in 413 patients with traditional SCC was unknown.*
[&] *Status of extracapsular spread in 295 patients with traditional SCC was unknown.*
Gray value indicates significant variables.

DISCUSSION

Since SaCa was first reported in 1864 (1), a few studies have described its clinical and pathologic characteristics in the throat, the parotid gland and other subsites of the head and neck region (2–12). However, due to the rarity of the disease, <50 cases of SaCa of the hypopharynx have been previously reported (2–12), and the prognosis and prognostic factors remain unknown in SaCa of the hypopharynx; the current study was the first to present the clinical results of SaCa of the hypopharynx. SCC is the most common pathologic type found in head and neck cancer (16). Previous evidence has shown an evolution from

TABLE 2 | Comparison of clinical pathologic variables between patients with sarcomatoid carcinoma (SaCa) and matched patients with traditional hypopharynx squamous cell carcinoma (SCC).

	SaCa ($n = 62$)	SCC ($n = 62$)	$p^{\#}$
Age			
≥65	47 (75.8%)	47 (75.8%)	
<65	15 (24.2%)	15 (24.2%)	NS
Sex			
Male	62 (100%)	62 (100%)	
Female	0	0	NS
Smokers			
Yes	41 (66.1%)	37 (59.7%)	
No	21 (33.9%)	25 (40.3%)	NS
Drinkers			
Yes	29 (46.8%)	33 (53.2%)	
No	33 (53.2%)	29 (46.8%)	NS
Cachexia			
Yes	37 (59.7%)	37 (59.7%)	
No	25 (40.3%)	25 (40.3%)	NS
Tumor stage			
T1 + T2	30 (48.4%)	27 (43.5%)	
T3 + T4	32 (51.6%)	35 (56.5%)	NS
Neck lymph node stage			
N0	30 (48.4%)	34 (54.8%)	
N+	32 (51.6%)	28 (45.2%)	NS
Disease stage			
I + II	15 (24.2%)	15 (24.2%)	
III + IV	47 (75.8%)	47 (75.8%)	NS
Perineural invasion			
Yes	23 (37.1%)	23 (37.1%)	
No	39 (62.9%)	39 (62.9%)	NS
Lymphovascular invasion			
Yes	22 (35.5%)	22 (35.5%)	
No	40 (64.5%)	40 (64.5%)	NS
Extracapsular spread			
Yes	17 (27.4%)	14 (22.6%)	
No	45 (72.6%)	48 (77.4%)	NS
Treatment			
Surgery	12 (19.4%)	11 (17.7%)	
Surgery + radiotherapy	31 (50.0%)	33 (53.2%)	
Surgery + radiotherapy + chemotherapy	19 (30.6%)	18 (29.0%)	NS

[#]*NS, not significant.*

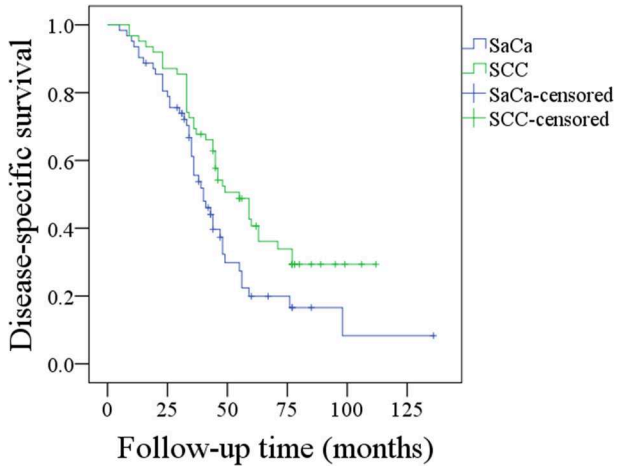

FIGURE 2 | Comparison of disease-specific survival between patients with sarcomatoid carcinoma (SaCa) of the hypopharynx and patients matched for squamous cell carcinoma (SCC) ($p = 0.016$).

TABLE 3 | Univariable and cox model analysis of predictors for the disease-specific survival in patients with hypopharynx sarcomatoid carcinoma.

Variables	Univariable	Cox model	
	p	*p*	Exp(B) (95% CI)
Age (<65 vs. ≥65)	0.185		
Smoke	0.385		
Alcohol	0.560		
Tumor stage (T1 + T2 vs. T3 + T4)	0.040	0.277	1.680 (0.402–7.011)
Node stage (N0 vs. N+)	<0.001	0.048	1.339 (1.011–4.697)
Disease stage (I+ II vs. III + IV)	0.013	0.002	2.090 (1.231–6.913)
Perineural invasion	0.175		
Lymphovascular invasion	0.403		
Cachexia	0.035	0.611	0.821 (0.287–4.341)
Extracapsular extension	0.021	0.058	1.339 (0.968–2.998)
Radiotherapy	0.689		
Chemotherapy	0.738		
Margin status	0.366		

Gray value indicates significant variables.

conventional epithelial cancer to SaCa as well as a malignant nature of the sarcomatoid component (7). There might be variations in survival between SaCa and conventional SCC. Our matched analysis supports the hypothesis that a significantly lower DSS rate is noted in patients with SaCa than in patients with SCC, and a similar finding was also reported by Chang et al. (8) in SaCa of the head and neck. However, it is prudent to conclude that the prognosis of SaCa of the hypopharynx is poorer than that of SCC of the hypopharynx: first, both studies had a limited sample size (62 cases and 18 cases), and second, even if the matching process had taken several confounding factors into consideration, the different radiation techniques and margin statuses were not analyzed between the two groups, owing to the long time span; these factors are typically independent negative prognostic predictors in head and neck cancer (17).

The detailed clinical pathologic characteristics of SaCa of the hypopharynx remain unclear. Gamez et al. (4) reported that the majority of patients with SaCa of the larynx were elderly males who presented with early-stage disease. Berthelet et al. (3) also reported a male prevalence and a low risk of lymph node metastasis in SaCa of the head and neck. Our findings partially supported these viewpoints: all patients were male, and

compared to patients with traditional SCC, patients with SaCa were older. However, hoarseness was apparent even in every patient with early-stage SCC of the larynx; however, there are typically no obvious symptoms that appear until advanced-stage cancer of the hypopharynx occurs, which might explain why most of our patients presented with advanced-stage disease. Cancer cachexia is a common concomitant phenomenon in SCC of the head and neck, and approximately one-third of patients have cachexia at diagnosis (18, 19). This finding is partially reflected by the degree of tumor malignancy (20); data demonstrate a higher degree of tumor malignancy in patients with SaCa than in our patients with traditional SCC of the hypopharynx and in previous reports (18, 19). Additionally, perineural invasion and lymphovascular invasion are two of the most important prognostic factors in SCC of the head and neck, and it has been noted that there are higher rates of perineural invasion and lymphovascular invasion in patients with SaCa. These findings suggest that the biological behavior of SaCa is more aggressive and might result in poorer survival than that of SCC.

The prognosis of patients with SaCa of the head and neck is typically dismal. In a report by Berthelet et al. (3), a total of 17 patients were enrolled for analysis, and the authors described that the median survival time was 32 months, with an actual survival of 72 and 42% at 2 and 5 years, respectively. In another paper focusing on outcomes in SaCa of the larynx, the authors reported that the 5-year overall survival, progression-free survival, and local control rates were 63, 46, and 72%, respectively (4). This finding apparently conflicts with our findings. The 5-year DSS rate was found to be only 20% in the current study; the first possible explanation for this finding is that advanced stage disease predominated in the current study, unlike in the abovementioned studies. Similarly, in a report published by Chang et al. (8), of the 78 included patients, 64% (50) were classified as having T3 or T4 tumors at the time of diagnosis, and the 5-year survival rate was 14%. Second, all the cases of disease in the current study involved localization in the hypopharynx, and cancer of the hypopharynx is usually associated with a poorer prognosis than cancers in other subsites of the head and neck (21).

Overall lymph node metastasis is typically uncommon in SaCa of the head and neck. Gamez et al. (4) reported that positive neck disease represented only 5% of the cases of SaCa of the larynx, and Niu et al. (10) reported that 5 (20%) patients had pathologic node metastasis out of the 15 patients undergoing neck dissection. However, in the current study, it was noted that 32 (51.6%) patients had neck metastatic disease, and this striking difference might be associated with the anatomic characteristics of the hypopharynx. There are abundant lymphatic vessels in the hypopharynx, and movements related to swallowing and speech can promote the occurrence of metastasis. Moreover, routine neck dissection was included in the primary treatment strategy in the two cancer centers, but in the abovementioned studies, elective neck dissection was more commonly performed, and this discrepancy might mask the true incidence of metastasis.

Prognostic factors have been evaluated for SaCa of the head and neck. Chang et al. (8) found that in a surgical intervention group, only a history of previous SCC produced good outcomes. The practice of neck dissection, the use of adjuvant therapies, or cancer stage did not affect the overall survival rate. Niu et al. described that in SaCa of the parotid gland, perineural nerve invasion was the only independent predictor for DSS (10). In the current study, neck lymph node metastasis was significantly associated with the DSS rate in SaCa of the hypopharynx. A higher neck lymph node metastasis stage and disease stage were associated with a higher risk of death, and a similar finding was also noted in SCC of the head and neck (22, 23).

The effectiveness of radiotherapy and chemotherapy for increasing local-regional and distant control in SCC of the head and neck has been widely accepted, but there is little evidence in the literature on the role of such adjuvant treatments for the treatment of SaCa. In a report by Chang et al. (8), 41 (64.1%) of the patients received radiotherapy, and the author found that no apparent survival benefit was associated with radiotherapy. In another paper focusing on SaCa of the larynx (24), the authors reported that compared to a 57.1% DSS rate with nonsurgical treatment, surgery led to a 5-year DSS rate of 84.1%, and adjuvant radiotherapy was not advised. Similarly, we also failed to note that postoperative adjuvant treatment could improve DSS. However, owing to the difference in the lymph node metastasis rate and pattern between cancer of the larynx and hypopharynx, the application of adjuvant radiotherapy cannot be easily excluded, and more studies are needed to clarify this question.

In summary, the prognosis of patients with SaCa of the hypopharynx is dismal, and SaCa of the hypopharynx is associated with more aggressive biological behavior than traditional SCC of the hypopharynx; neck lymph node stage and disease stage were the most important predictors for DSS.

DATA AVAILABILITY STATEMENT

All datasets generated for this study are included in the manuscript/supplementary files.

ETHICS STATEMENT

The Zhengzhou University institutional research committee approved our study and all participants signed an informed consent agreement for medical research before initial treatment. And all the related procedures were consistent with Ethics Committee regulations.

AUTHOR CONTRIBUTIONS

All authors contributed to data analysis, drafting, and revising the article, gave final approval of the version to be published, and agree to be accountable for all aspects of the work.

REFERENCES

1. Virchow R. *Die Krankhaften Geschwulste*. Berlin: Hirschwald (1864–1865).
2. Viswanathan S, Rahman K, Pallavi S, Sachin J, Patil A, Chaturvedi P, et al. Sarcomatoid (spindle cell) carcinoma of the head and neck mucosal region: a clinicopathologic review of 103 cases from a tertiary referral cancer centre. *Head Neck Pathol*. (2010) 4:265–75. doi: 10.1007/s12105-010-0204-4
3. Berthelet E, Shenouda G, Black MJ, Picariello M, Rochon L. Sarcomatoid carcinoma of the head and neck. *Am J Surg*. (1994) 168:455–8. doi: 10.1016/S0002-9610(05)80098-4
4. Gamez ME, Jeans E, Hinni ML, Moore E, Young G, Ma D, et al. Outcomes and patterns of failure of sarcomatoid carcinoma of the larynx: the Mayo Clinic experience. *Laryngoscope*. (2018) 128:373–7. doi: 10.1002/lary.26725
5. Rosko AJ, Birkeland AC, Wilson KF, Muenz DG, Bellile E, Bradford CR, et al. Tumor biomarkers in spindle cell variant squamous cell carcinoma of the head and neck. *Otolaryngol Head Neck Surg*. (2016) 155:106–12. doi: 10.1177/0194599816636612
6. Batsakis JG, Suarez P. Sarcomatoid carcinomas of the upper aerodigestive tracts. *Adv Anat Pathol*. (2000) 7:282–93. doi: 10.1097/00125480-200007050-00002
7. Choi HR, Sturgis EM, Rosenthal DI, Luna MA, Batsakis JG, El-Naggar AK. Sarcomatoid carcinoma of the head and neck: molecular evidence for evolution and progression from conventional squamous cell carcinomas. *Am J Surg Pathol*. (2003) 27:1216–20. doi: 10.1097/00000478-200309000-00004
8. Chang NJ, Kao DS, Lee LY, Chang JW, Hou MM, Lam WL, et al. Sarcomatoid carcinoma in head and neck: a review of 30 years of experience–clinical outcomes and reconstructive results. *Ann Plast Surg*. (2013) 71(Suppl. 1):S1–7. doi: 10.1097/SAP.0000000000000069
9. Huang SF, Chen IH, Liao CT, Chen TM, Lee KF. Sarcomatoid carcinoma of the parotid gland with apparent metastasis of epidermoid elements to cervical lymph nodes. *Acta Otolaryngol*. (2006) 126:667–71. doi: 10.1080/00016480500469560
10. Niu X. Sarcomatoid carcinoma in the parotid gland: a review of 30 years of experience. *Laryngoscope*. (2019) 129:1137–40. doi: 10.1002/lary.27474
11. Spencer MG, Elliott RIK, Wadsworth PV, Deutsch GP. Pseudosarcoma of the pharynx and larynx. *J Laryngol Otol*. (1983) 97:85–91. doi: 10.1017/S0022215100093853
12. Ampil FL. The controversial role of radiotherapy in spindle cell carcinoma (pseudosarcoma) of the head and neck. *Radiat Med*. (1985) 3:225–9.
13. Richey LM, George JR, Couch ME, Kanapkey BK, Yin X, Cannon T, et al. Defining cancer cachexia in head and neck squamous cell carcinoma. *Clin Cancer Res*. (2007) 13:6561–7. doi: 10.1158/1078-0432.CCR-07-0116
14. Fang Q, Li P, Qi J, Luo R, Chen D, Zhang X. Value of lingual lymph node metastasis in patients with squamous cell carcinoma of the tongue. *Laryngoscope*. (2019). doi: 10.1002/lary.27927. [Epub ahead of print].
15. Fang QG, Shi S, Liu FY, Sun CF. Squamous cell carcinoma of the oral cavity in ever smokers: a matched-pair analysis of survival. *J Craniofac Surg*. (2014)25:934–7. doi: 10.1097/SCS.0000000000000710
16. Liu F, Cheng GY, Fang QG, Sun Q. Natural history of untreated squamous cell carcinoma of the head and neck. *Clin Otolaryngol*. (2019) 44:200–3. doi: 10.1111/coa.13260
17. van der Veen J, Nuyts S. Can intensity-modulated-radiotherapy reduce toxicity in head and neck squamous cell carcinoma? *Cancers (Basel)*. (2017) 9:E135. doi: 10.3390/cancers9100135
18. Orell-Kotikangas H, Österlund P, Mäkitie O, Saarilahti K, Ravasco P, Schwab U, et al. Cachexia at diagnosis is associated with poor survival in head and neck cancer patients. *Acta Otolaryngol*. (2017) 137:778–85. doi: 10.1080/00016489.2016.1277263
19. Kwon M, Kim RB, Roh JL, Lee SW, Kim SB, Choi SH, et al. Prevalence and clinical significance of cancer cachexia based on time from treatment in advanced-stage head and neck squamous cell carcinoma. *Head Neck*. (2017) 39:716–23. doi: 10.1002/hed.24672
20. Gallagher IJ, Jacobi C, Tardif N, Rooyackers O, Fearon K. Omics/systems biology and cancer cachexia. *Semin Cell Dev Biol*. (2016) 54:92–103. doi: 10.1016/j.semcdb.2015.12.022
21. Sim F, Leidner R, Bell RB. Immunotherapy for head and neck cancer. *Oral Maxillofac Surg Clin North Am*. (2019) 31:85–100. doi: 10.1016/j.coms.2018.09.002
22. Fang QG, Shi S, Liu FY, Sun CF. Tongue squamous cell carcinoma as a possible distinct entity in patients under 40 years old. *Oncol Lett*. (2014) 7:2099–102. doi: 10.3892/ol.2014.2054
23. Fang QG, Shi S, Li ZN, Zhang X, Liua FY, Xu ZF, et al. Squamous cell carcinoma of the buccal mucosa: analysis of clinical presentation, outcome and prognostic factors. *Mol Clin Oncol*. (2013) 1:531–4. doi: 10.3892/mco.2013.86
24. Dubal PM, Marchiano E, Kam D, Dutta R, Kalyoussef E, Baredes S, et al. Laryngeal spindle cell carcinoma: a population-based analysis of incidence and survival. *Laryngoscope*. (2015) 125:2709–14. doi: 10.1002/lary.25383

Conflict of Interest: The authors declare that the research was conducted in the absence of any commercial or financial relationships that could be construed as a potential conflict of interest.

frontiers in Oncology

REVIEW
published: 15 October 2019
doi: 10.3389/fonc.2019.01084

Targeting the Immune Microenvironment in the Treatment of Head and Neck Squamous Cell Carcinoma

Hui-Ching Wang[1,2], *Leong-Perng Chan*[1,3] *and Shih-Feng Cho*[2,4]*

[1] Graduate Institute of Clinical Medicine, College of Medicine, Kaohsiung Medical University, Kaohsiung, Taiwan, [2] Division of Hematology and Oncology, Department of Internal Medicine, Kaohsiung Medical University Hospital, Kaohsiung Medical University, Kaohsiung, Taiwan, [3] Department of Otolaryngology-Head and Neck Surgery, Kaohsiung Medical University Hospital, Kaohsiung Medical University, Kaohsiung, Taiwan, [4] Faculty of Medicine, College of Medicine, Kaohsiung Medical University, Kaohsiung, Taiwan

Head and neck squamous cell carcinoma (HNSCC) is a highly aggressive solid tumor, with a 5-year mortality rate of ∼50%. The development of immunotherapies has improved the survival of patients with HNSCC, but, the long-term prognosis of patients with recurrent or metastatic HNSCC remains poor. HNSCC is characterized by intratumoral infiltration of regulatory T cells, dysfunctional natural killer cells, an elevated Treg/$CD8^+$ T cell ratio, and increased programmed cell death ligand 1 protein on tumor cells. This leads to an immunocompromised niche in favor of the proliferation and treatment resistance of cancer cells. To achieve an improved treatment response, several potential combination strategies, such as increasing the neoantigens for antigen presentation and therapeutic agents targeting components of the tumor microenvironment, have been explored and have shown promising results in preclinical studies. In addition, large-scale bioinformatic studies have also identified possible predictive biomarkers of HNSCC. As immunotherapy has shown survival benefits in recent HNSCC clinical trials, a comprehensive investigation of immune cells and immune-related factors/cytokines and the immune profiling of tumor cells during the development of HNSCC may provide more insights into the complex immune microenvironment and thus, facilitate the development of novel immunotherapeutic agents.

Keywords: head and neck cancer, microenvironment, biomarkers, immunotherapy, immunoresistance

OPEN ACCESS

Edited by:
Cheng-Chia Yu, Chung Shan Medical University, Taiwan

Reviewed by:
Yi Feng Wu, Buddhist Tzu Chi General Hospital, Taiwan
Chih-Yen Chien, Kaohsiung Chang Gung Memorial Hospital, Taiwan

***Correspondence:**
Shih-Feng Cho
sifong96@gmail.com

Specialty section:
This article was submitted to Head and Neck Cancer, a section of the journal Frontiers in Oncology

Received: *23 August 2019*
Accepted: *01 October 2019*
Published: *15 October 2019*

Citation:
Wang H-C, Chan L-P and Cho S-F (2019) Targeting the Immune Microenvironment in the Treatment of Head and Neck Squamous Cell Carcinoma. Front. Oncol. 9:1084. doi: 10.3389/fonc.2019.01084

INTRODUCTION

Head and neck cancer, 90% of which is squamous cell carcinoma (HNSCC), is the sixth most common cancer globally (1). HNSCC is composed of a heterogeneous group of tumors developing from the mucosa of the nasal and oral cavity, oropharynx, hypopharynx, or larynx (2). The major risk factors for HNSCC are smoking and alcohol consumption. Other risk factors include high risk human papillomavirus (HPV) infection, which is associated with oropharyngeal cancer increasingly worldwide (3). The areca nut chewing is linked to development of oral cancer in south Asia, Taiwan, and Pacific islanders. Treatment of HNSCC involves a multidisciplinary approach composed of surgery, radiotherapy, chemotherapy, and targeted therapy. However, the prognosis

of metastatic HNSCC remains extremely poor. A combination of cetuximab and chemotherapy (cisplatin and 5-fluorouracil) shows better clinical efficacy than conventional chemotherapy; however, the median overall survival time is ∼10 months (4). In recent years, the introduction of immune checkpoint inhibitors (ICIs) targeting the programmed death 1-programmed death ligand 1 (PD1-PDL1) pathway has resulted in further improvements in the outcome of patients with metastatic HNSCC, but the results remain unsatisfactory when compared with other malignancies, like melanoma and lung cancer (5, 6).

Accumulating data suggest that the tumor microenvironment (TME) plays an important role in the pathogenesis and development of treatment resistance in a variety of malignancies, including HNSCC. Several cell subtypes, including regulatory T cells (Tregs), cancer-associated fibroblasts, and macrophages, together with non-cellular components, like extracellular matrix (ECM), have been shown to be associated with immunocompromised status and the dysfunction of normal immune cells, like cytotoxic T cells or dendritic cells in the TME of HNSCC (7). HPV infection status and smoking are also related with distinct immune TMEs (8, 9).

To achieve improved treatment responses and clinical outcomes in the immunotherapy era, it is important to understand the complex immune TME of HNSCC. In this review, we describe major cell subtypes and cellular components and discuss their function. In addition, we summarize potential strategies to overcome TME-mediated treatment resistance.

TUMOR MICROENVIRONMENT OF HNSCC

The heterogeneity of molecular and cellular components has been reported in the TME of HNSCC (10, 11). However, the HNSCC TME is still characterized by some unique features, leading to immunosuppression and diminished anticancer immunity (**Table 1**). The TME is composed of stromal cells, immune cells, tumor cells, and cytokines, which mediate the interactions between these cells. HNSCC patients have decreased absolute T cell counts in the tumor and the circulation and the T cells have apoptotic features via the Fas/FasL signaling pathway and defective function (12, 16). The functional defects of tumor-infiltrating lymphocytes (TIL) include decreased expression of the CD3 zeta chain, decreased cytokine secretion, and loss of the ability to kill cancer cells (13–15). Tregs account for the major proportion of T cell components, which construct an immunosuppressive barrier, thus hindering the activity of effector T cells (Teffs) in the TME and interfering with the antitumor response to immunotherapy (26). A decrease in the number of immune cells with antigen-presenting machinery (such as dendritic cells) and in cytotoxic ability (such as natural killer cells) results in a profoundly immunodeficient tumor, which is common in HNSCC (16, 19, 27). Moreover, HNSCC tumors are characterized by desmoplastic stromal fibroblasts, which promote tumor invasion and progression via autocrine and paracrine factors (28, 29).

Communication within cancer cells, immune cells, and stromal cells via extracellular vesicles (EVs) is increasingly thought to be important (30). EVs not only deliver oncogenic proteins and non-coding RNA molecules to modulate tumor progression, but also modulate immune responses by inhibiting T cell proliferation and Th1 and Th17 differentiation (31). EVs promote suppressive immunity by activating Fas ligand (FasL), to induce $CD8^+$ T cell apoptosis and the polarization of THP-1 to tumor-associated macrophages (TAMs) of the M2 phenotype (32, 33). Although several studies have analyzed the TME, it remains difficult to define HNSCC as an immune-inflamed, immune-excluded, or immune-desert tumor, due to diverse intratumor/peritumor expression patterns and the distribution of immune cells and cytokines (34, 35). The antitumor immune response to immunotherapy in the TME depends on the balance of stromal components, intratumoral Teffs, and immune-suppressive cell populations.

Cellular Component of the HNSCC TME

Regulatory T Cells

Tregs are a subset of T cells that contribute to the immunosuppressive TME in HNSCC (21). Treg recruitment is mediated by chemokines and associated receptors, such as CCL28-CCR10 and CXCL12-CXCR4 (36, 37). Tregs are characterized by specific markers, such as of CD4; CD25; and the transcription factor, forkhead box P3 (FOXP3) (22). Tregs express high levels of cytotoxic T-lymphocyte-associated protein 4 (CTLA-4), which binds to CD80 and CD86 on antigen-presenting cells (APCs), leading to a reduced capacity to activate Teffs. Tregs exhibit their suppressor function by the consumption of interleukin-2 (IL-2), the secretion of granzyme and/or perforin to damage effector cells, and the production of immune-inhibitory cytokines and molecules, such as IL-10, IL-35, and transforming growth factor-β (38, 39). Tregs release large amounts of ATP and provide inhibitory signals to Teffs and APCs via the engagement of adenosine A_{2A} receptor ($A_{2A}R$) (40). In HNSCC, as in other malignancies, large numbers of Tregs infiltrate the TME. Intratumoral Tregs are more immunosuppressive than circulating Tregs, as evidenced by an increased expression of immune checkpoint molecules (23). A recent study identified a subset of Tregs with high levels of T-cell immunoglobulin and mucin domain-3 (TIM-3) expression from a population of $CD4^+CTLA\text{-}4^+CD25^{high}$ Treg cells. These high TIM-3-expressing Tregs are more immunosuppressive than Tregs with low levels of TIM-3 expression. After the administration of an anti-PD-1 monoclonal antibody, the expression of TIM-3 on this subgroup of T cells decreased (41). Another recent study demonstrated that Tregs are related to resistance to radiotherapy. The incorporation of an anti-CD25 antibody can overcome Treg-related treatment resistance (42). Several studies have demonstrated a negative prognostic impact of large numbers of Tregs in HNSCC (43, 44).

Myeloid-Derived Suppressor Cells

Myeloid-derived suppressor cells (MDSCs) can be divided into three major subtypes, $Ly6C^+$ monocytic MDSCs (M-MDSCs); $Ly6G^+$ granulocytic polymorphonuclear myeloid-derived suppressor cells (PMN-MDSCs); and early stage e-MDSCs, which consist of the former two subsets deficient in

TABLE 1 | Immune profilings of tumor microenvironment in HNSCC.

Characteristics	Functions and mechanisms	References
Decrease absolute T cell counts in tumor and circulation	Activation of Fas/FasL signaling pathway, leading to apoptosis of T cells	(12)
Dysregulation of T cell functions	1. Decreased HLA-DR expression on DCs and defective functions to stimulate allogeneic T cells 2. Decreased expression of the CD3 zeta chain (CD3ζ) 3. Decreased response to mitogens or IL-2 4. Absence of IL-2 and/or IFN-γ production	(13–15)
Downregulation of antigen processing machinery	Myeloid DCs is lower than lymphoid DCs	(16)
Increased Treg cell	1. Induce apoptosis of $CD8^+$ T cells 2. Inhibition of the proliferation of $CD4^+$ T cells	(12)
Increased MDSCs	Increased arginase-1 and iNOS driving immunosuppression partially by inactivating effector T cells	(17, 18)
Decreased NK cells	Impaired NK cell activity	(19)
Increased Activated, antigen-presenting and memory B cells		(20)
Increased expression of immune checkpoint ligand and receptors	A series of inhibitory immune checkpoints including PD-1, CTLA-4, TIM3, IDO, KIR, and TIGIT	(21–23)
Deficiencies or alterations of tumor HLA class I expression	Causing T-cell tolerance	(21)
Increased TGF-β, IL-6, and IL-10	Secreted by Tregs and MDSCs	(24, 25)
Aberrant activation of the transcription factors STAT3 and NF-kB	Related to IL-6 and TGF-β signaling, respectively	(24, 25)
Increase enzymes IDO-mediated degradation of the amino acid tryptophan	1. Deprivation of the tumor microenvironment of essential nutrients for T cell function 2. Activate Tregs to overcome immunogenic responses and promote tumorigenesis	(17, 18)

HLA, human leukocyte antigen; DC, dendritic cells; IL, interleukin; IFN, Interferon; DC, dendritic cells; MDSC, myeloid-derived suppressor cells; iNOS, inducible nitric oxide synthase; PD-1, Programmed death-1; CTLA-4, cytotoxic T-lymphocyte–associated antigen 4; TIM3, T-cell immunoglobulin and mucin domain-3; IDO, indoleamine 23-dioxygenase; KIR, killer cell immunoglobulin-like receptors; TIGIT, T cell immunoreceptor with Ig and ITIM domains; TGF, transforming growth factor; STAT3, Signal transducer and activator of transcription 3; NF-kB, nuclear factor kappa light chain enhancer of activated B cells.

myeloid lineage markers (45). The accumulation of MDSCs in the TME is associated with cancer progression and the inhibition of T cell activity and function (46). Various factors in the TME can induce the accumulation of MDSCs, including vascular endothelial growth factor (VEGF), IL-6, and granulocyte-macrophage colony-stimulating factor (GM-CSF) (20). In addition, MDSCs regulate the TME by increasing the production of nitric oxide, reactive oxygen species, inducible NO synthase, and arginase-1; depleting various amino acids, such as L-arginine, L-tryptophan, and L-cystein; inducing pro-angiogenic factors; and elevating the expression of PD-L1 (17, 18). In HNSCC, a recent study demonstrated that a higher frequency of PMN-MDSCs is associated with poorer survival. Specifically, a subset of $CD66b^+/CD11b^+/CD16^+$ mature PMN-MDSCs showed higher expression and activity of arginase I and demonstrated a greater suppressing effect on T cell proliferation and cytokine production than other MDSC subtypes. Moreover, high levels of $CD11b^+/CD16^+$ PMN-MDSCs, but not other PMN-MDSC subsets, are strongly correlated with adverse outcomes in HNSCC patients (47).

Cancer-Associated Fibroblasts

Cancer-associated fibroblasts (CAFs) construct the stroma of the TME to promote the growth of cancer cells. CAFs possess different characteristics dependent on their status. For example, the active form of CAFs displays typical markers, such as α-smooth muscle actin and fibroblast activation protein and promotes tumor proliferation, invasion, and metastasis (48–50). CAFs regulate the TME via secretion of various cytokines and growth factors, such as VEGF, epidermal growth factor, C-X-C motif chemokine ligands, and C-C motif chemokine ligands (CCLs) (51, 52). Most importantly, CAFs secrete matrix-metalloproteinases (MMPs), which are crucial regulators of the TME and are responsible for degradation of the ECM (53). CAFs can be transformed from diverse progenitor cells, including endothelial cells, resting fibroblasts, and epithelial cells, via mesothelial-mesenchymal transition or epithelial-mesenchymal transition (EMT) (54, 55). In the TME of HNSCC, CAFs can promote the proliferation, migration, and invasion of tumor cells (29). CAFs also have a metabolic relationship with tumor cells. CAFs secrete hepatocyte growth factor (HGF), which then activates c-met to promote the progression of HNSCC (56). Additionally, HNSCCs secrete basic fibroblast growth factor (bFGF) which increases the phosphorylation of p44/42 mitogen-activated protein kinase, leading to the secretion of HGF from CAFs. Notably, the secretion of bFGF is also mediated by CAF-secreted HGF. Inhibition of c-met and the FGF receptor can reduce tumor volume. CAFs are also associated with the development of cancer stem cells, which is associated with treatment resistance (57). CAF secretes periostin, which promotes a cancer stem cell-like phenotype via interaction with protein tyrosine kinase 7 (58). Another study also showed that CAFs secrete several proteins that promote the expression of stemness-associated genes in HNSCC cells.

Inhibition of these protein-associated pathways can suppress tumor growth (59).

Tumor-Associated Macrophages

TAMs have two distinct phenotypes, M1 and M2, with different morphological and biological characteristics (60, 61). The activated M1 phenotype promotes Th1 response and displays pro-inflammatory behaviors, whereas the activated M2 phenotype enhances Th2 response and mediates anti-inflammatory functions, which are more associated with tumor progression, invasion, metastasis, and the suppression of T cell immunity (61–63). Activated M2 macrophages demonstrate upregulated levels of IL-10, arginase-1, and peroxisome proliferator-activated receptor γ, which are known as markers of M2 TAMs (64–66). The M2 phenotype is induced by several cytokines, such as IL-4, IL-10, and IL-13. Activated M2 macrophages inhibit M1 TAMs and promote tissue remodeling through the production and secretion of anti-inflammatory cytokines, including IL-1 receptor antagonist, IL-10, transforming growth factor-β (TGF-β), VEGF, and tumor necrosis factor-α (TNF-α) (24, 25). In HNSCC, TAMs are recruited to the TME and directly contact SCC cells. A recent study showed that CCL18 derived from M2 macrophages is able to promote tumor metastasis by inducing EMT and stemness (67). Regarding clinical significance, a meta-analysis showed that high $CD68^+$ and $CD163^+$ TAM density is associated with poor cell differentiation and advanced disease status (68). Another meta-analysis showed that high stromal levels of $CD163^+$ TAMs are associated with poorer overall and progression-free survival (69).

Other Cellular Subtypes

Human natural killer (NK) cells are important in the innate immune system and can be classified into two subgroups according to the surface expression of CD56 and CD16. $CD56^{dim}/CD16^{bright}$ NK cells are predominantly responsible for natural cytotoxicity, whereas $CD56^{bright}/CD16^{dim}$ NK cells regulate immune reactions through the secretion of cytokines, such as interferon-γ and TNF-α (70, 71). The activation of NK cells induces the apoptosis of target cancer cell, through the exocytosis of perforin and granzymes, FasL and TNF-related apoptosis-inducing ligand (TRAIL) activation, or antibody-dependent cellular cytotoxicity (ADCC) (72, 73). The natural killer group 2D (NKG2D) receptors on immune cells, including NK and several T cell subsets, play an important role in immunosurveillance. By identifying and engaging the NKG2D ligand (NKG2DL) on tumor cells, NK and T cells can exert anti-tumor effects. In HNSCC, high plasma levels of shed NKG2DLs correlate with NK cell inhibition and disease progression (74).

Neutrophils are involved in the adaptive immunity response. Tumor-associated neutrophils (TANs) exhibit both pro- and anti-tumor characteristics. Similar to TAMs, TANs are also divided into two subgroups, N1 and N2 (75). Neutrophils eradicate cancer cells by releasing the antimicrobial and cytotoxic contents of their granules or by secreting immune mediators to recruit other antitumor effector cells. However, other factors from the tumor can shift neutrophils into a pro-tumor phenotype (76). Neutrophils with the pro-tumor N2 phenotype possess CXCR4, VEGF, and MMP-9 markers, which facilitate tumorigenesis, promote tumor growth, stimulate angiogenesis, and mediate immunosuppression (75).

Non-cellular Components in the TME

The ECM contains large composites of non-cellular factors, including structural proteins, growth factors, proteoglycans, and glycoproteins, which form the main structure of the TME (77). MMPs, which are mainly produced by the ECM, are a large family of proteins and peptide hydrolases that mediate the degradation of the ECM and facilitate the migration of cancer cells (78). MMPs also activate bFGF, VEGF, and TGF-β and promote angiogenesis (79, 80). Fibronectin is the major glycoprotein in the ECM and it plays a crucial role in interactions between other molecules, such as integrins, collagens, and fibrin (81, 82). Increased levels of fibronectin are associated with tumor invasion, progression, and resistance to treatment (83, 84). Other molecules are also involved in cell adhesion and proliferation and assist in supporting the surrounding TME.

HPV Infection and Smoking Are Associated With a Distinct Immune TME

HPV Infection

HPV infection plays a pivotal role in the immune modulation of HNSCC. In general, HPV-positive HNSCCs demonstrate relatively inflamed immunity compared with HPV-negative HNSCCs (**Table 2**). A TME with a prolonged viral infection induces anti-tumor immunity via the expression of tumor-associated antigens (TAAs) and tumor-specific antigens in immune cells and tumor cells (8). After cytotoxic therapies (radiotherapy or chemotherapy), the antigen-processing machinery (APM) promotes the expression of major histocompatibility complex (MHC) class I molecules to present the antigen peptide from dying tumor cells to T cells (89). In addition, an increase in the infiltration of NK cells and T cells, including $CD3^+$, $CD4^+$, and $CD8^+$ TILs, creates a vigorous TME that stimulates cellular immunity in HPV-positive HNSCCs (85, 86). Interestingly, HPV-positive oropharyngeal cancer demonstrates higher $CD4^+$, higher $CD8^+$, and lower $CD4^+/CD8^+$ ratio compared with HPV-negative HNSCC (85). Humoral immunity is also induced by the recruitment of $CD19^+/CD20^+$ B cells (87). Antigen presentation and cytotoxicity are promoted by gathering dendritic cells (DCs) and APCs (86). An increase in the number of intratumor and peritumor infiltrating immune cells results in a favorable prognosis and enhances the response to radiotherapy and immunotherapy (34). The interaction between HPV-negative oropharyngeal cancer cells and CAFs results in the secretion of chemokines via an IL-1/IL-1R-mediated mechanism, which is less prominent within the HPV-positive TME (88). Thus, the metabolic profiles are quite different between HPV-positive and HPV-negative HNSCCs.

The communication vesicles, EVs, also display different features depending on viral status. In HPV-positive cancers, exosomes carry viral proteins, genes, and TAAs (90, 91).

TABLE 2 | Different immune modulations between HPV-negative and HPV-positive HNSCC.

HPV negative HNSCC	HPV positive HNSCC	References
Lower $CD3^+$ T cells	Higher $CD3^+$ T cells	(85, 86)
Lower $CD4^+$ T cells	Higher $CD4^+$ T cells	(85, 86)
Lower $CD8^+$ T cells	Higher $CD8^+$ T cells	(85, 86)
Increased $CD4^+$/ $CD8^+$ ratio	Decreased $CD4^+$/ $CD8^+$ ratio	(85, 86)
Lower $CD45^+$ cells, $CD8^+$ cells, $CD8^+$ IFNγ^+ cells, and $CD8^+$IL-17^+ cells	Higher $CD45^+$ cells, $CD8^+$ cells, $CD8^+$ IFNγ^+ cells, and $CD8^+$IL-17^+ cells	(85, 86)
Lower $CD45^+$ lymphocytes and $CD19^+$/$CD20^+$ B cells	Higher $CD45^+$ lymphocytes and $CD19^+$/$CD20^+$ B cells	(87)
Higher Treg cells	Lower Treg cells	(85, 86)
Low $CD56^{dim}$ NK cells	High $CD56^{dim}$ NK cells	(85, 86)
Lower tumor-infiltrating APCs	higher tumor-infiltrating APCs	(86)
Lower myeloid and plasmacytoid DCs	Higher myeloid and plasmacytoid DCs	(86)
Lower DC signatures, including CD103, and CD11C	Higher DC signatures	(86)
Lower levels of chemokines	Higher levels of chemokines	(88)
Higher levels of Cox-2 and Tim-3 mRNA	Lower levels of Cox-2 and Tim-3 mRNA	(86)
Lower levels of PD-1 mRNA	Higher levels of PD-1 mRNA	(86)
Lower "T-cell exhaustion markers," including LAG3, PD-1, TIGIT, TIM3, and CD39	Higher "T-cell exhaustion markers"	(87)
Lower levels of cytotoxic mediators, including granzyme A, granzyme B, and perforin	Higher levels of cytotoxic mediators	(87)
Exosomes suppressed DC maturation and expression of APM components	Exosomes promoted DC maturation and did not suppress expression of APM components in mature DCs	(89)
Increased MAGEA1 and MAGEA3 gene expression	Increased CDKN2A gene expression	(87)

IFN, interferon; IL, interleukin; NK cells, natural killer cells; APC, antigen-presenting cell; DC, dendritic cells; Cox-2, cyclooxygenase-2; Tim-3, T-cell immunoglobulin and mucin domain-3; LAG-3, lymphocyte-activation gene 3; PD-1, Programmed death-1; TIGIT, T cell immunoreceptor with Ig and ITIM domains; APM, antigen processing machinery; MAGEA, melanoma-associated antigen; CDKN2A, cyclin-dependent kinase Inhibitor 2A.

However, these differences in EVs do not occur by influencing the T cell response. The functions of both $CD4^+$ and $CD8^+$ T cells are suppressed by these exosomes. The expression of co-stimulatory CD80 and CD83 molecules on immature DCs is up-regulated, but the expression of APM components is not suppressed in HPV-positive exosomes. In contrast, HPV(–) exosomes inhibit DC maturation and APM component expression (8). Moreover, HPV-negative tumors have a more active metabolic signature, with elevated expression of genes associated with glycolysis and oxidative phosphorylation (92). HPV-negative tumors are also characterized by increased MCT1 expression, which indicates that the regulation of lactate homoeostasis is more significant in promoting the invasion of HPV-negative HNSCCs (93).

Smoking

Smoking is a risk factor for the development of HNSCC and it promotes pro-inflammatory and immunosuppressive effects, which impact the TME of HNSCCs, to facilitate tumor development (94, 95). Smoking results in enrichment of immunogenic neoantigens which cause both pro- and anti-immunity effects in smoking-associated cancers, including lung cancer and HNSCC. In lung cancer, smoking leads to increased neoantigens and constructs an inflamed TME, which suggests higher response rates to ICIs in smokers. In contrast, the enhancement of immunogenic neoantigens by smoking forms a more immunosuppressive in TME in HNSCC by increased T cell apoptosis which is mediated through reactive oxygen and nitrogen species (94). In the TCGA database, enrichment scores from two Gene Expression Omnibus cohorts were higher in never-smoker and never-drinker (NSND) patients compared with smoker and drinker (SD) patients. To identify biological differences, gene set enrichment analysis of the TCGA dataset was performed and immunity-associated pathways were found to predominantly involve T-cell activation and differentiation in NSND patients. The TME in NSND patients is more immunoactive than the TME of SD patients, including an increased number of $CD8^+$ TIL cells; increased INF-γactivation; overexpression of immune checkpoint ligands and receptors, such as indoleamine 23-dioxygenase 1 (IDO1) and PD-L1; and higher scores in the pembrolizumab-response signature (96). Tobacco smoking attenuates the cytotoxicity of the TME by repressing $CD8^+$ T cells, NK cells, and DCs (9). Overall, smoking has a negative impact on immune responses, regardless of alcohol consumption.

MECHANISMS OF TME-MEDIATED DRUG RESISTANCE IN HNSCC

The mechanisms of resistance to epidermal growth factor receptor (EGFR) inhibitors have been known for decades and they include nuclear localization of EGFR, activation of other ErbB family receptors, mutant forms of the receptor (EGFRvIII), or cross-talk with other signaling pathways (97, 98). However, issues of resistant mechanisms to immunotherapy have been gradually emphasized recently. These include a lack of production, editing, and presentation of neo-antigens;

impaired intratumoral immune infiltration; impaired IFNγ signaling; immune factors within the TME; upregulation of alternative immune checkpoints; severe T-cell exhaustion; and T-cell epigenetic changes (99–102).

The downregulation of human leukocyte antigen (HLA) class I molecules and loss of β2-microglobulin expression interferes with antigen presentation to cytotoxic T cells (103). Specific oncogenic signaling pathways change the TME. Loss of the PTEN induces the expression of CCL2 and VEGF and blocks T-cell infiltration, leading to resistance to ICIs (104). Alterations in β-catenin/WNT signaling decrease CCL4 production and hinder the infiltration of DCs (105). During the development of ICI resistance, the TME shows an increase in the number of effector memory CD8 T cells ($CCR7^{-}CD45RA^{-}$), a lower CD4/CD8 ratio, and upregulation of TIM-3 on CD4 and CD8 T cells (100). Moreover, the major regulators of therapeutic response and resistance are Tregs and TAMs. In preclinical HNSCC mouse models, the Treg population is elevated during tumor rebound after combined treatment with ICI and radiation (26). Depletion of major histocompatibility complex class II-low TAMs increases chemotherapy-related DNA damage and apoptosis (106). Depletion of tumor-infiltrating Tregs using an anti-CD25 antibody, enhances the binding ability of activating Fc gamma receptors, increases Teff:Treg ratios, and improves the response to ICIs (107). High levels of alternative co-inhibitory receptors on T cells (e.g., CTLA-4, TIM-3, lymphocyte-activation gene 3, and V-domain Ig suppressor of T cell activation) and high levels of immune-suppressive cytokines or metabolites, causes T cell exhaustion, which also induces ICI resistance (108).

POTENTIAL STRATEGIES TO OVERCOME TME-MEDIATED DRUG RESISTANCE

Novel Therapeutic Agents or Combination Therapies

Due to the insufficient response elicited by immunotherapy alone, several mechanisms for the regulation of immunoresistant niches have been proposed, including defective immunorecognition, tumor insensitivity to T cell effector molecules, an immunosuppressive TME, and the compensatory regulation of multiple inhibitory and costimulatory immune checkpoints (**Figure 1**) (109). Combinations of diverse agents targeting distinct mechanisms have been investigated in recent years (**Table 3**).

Defective immunorecognition involves dysfunction of antigen presentation in tumor cells, anergy of tumor-specific cytotoxic T lymphocyte, and immunoediting. Radiotherapy and cytotoxic therapy (NCT02318771, NCT03040999, NCT03894891, NCT03162731, NCT02764593, NCT02938273) induce cell death to promote antigen presentation and trigger activation of the cGAS-STING pathway to enhance the T-cell response. Moreover, radiation adjusts the stromal TME (110). Cetuximab (NCT02764593, NCT03082534, NCT02938273) binds to EGFR

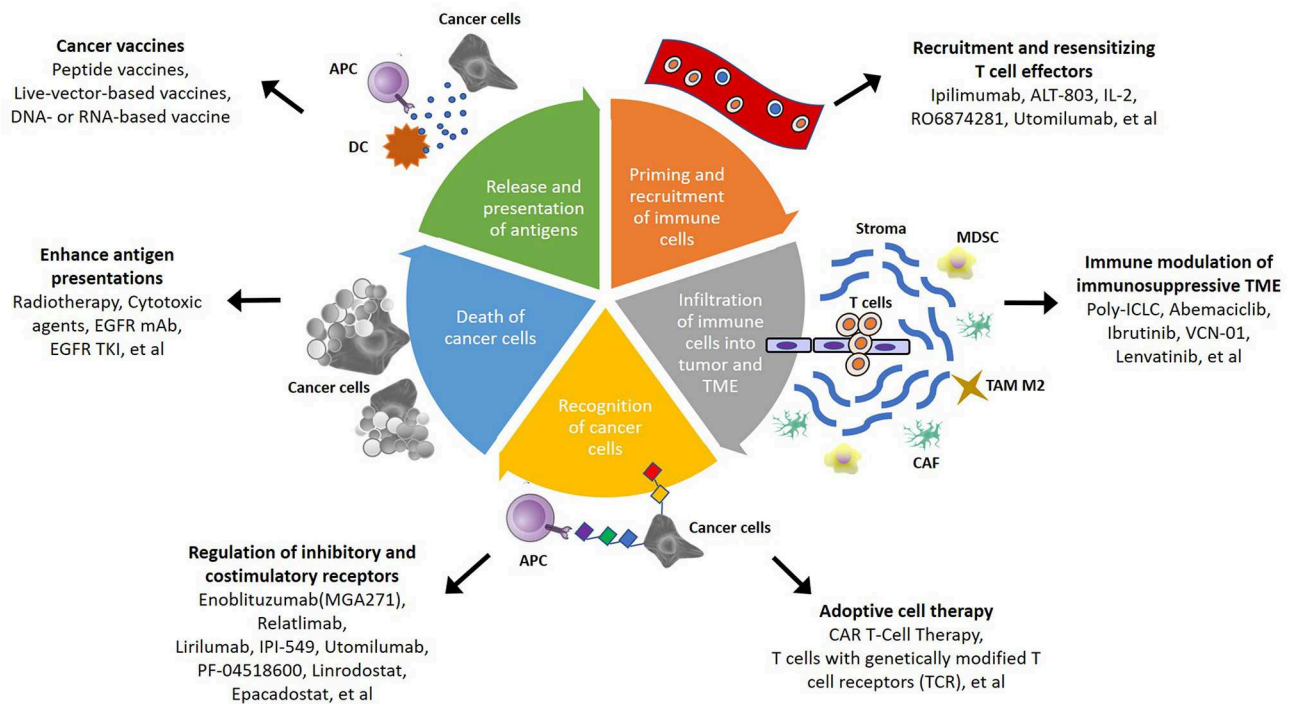

FIGURE 1 | Schematic summary of potential strategies to overcome immunosuppressive TME in head and neck squamous cell carcinoma (HNSCC). In cancer-immunity cycle, there are several therapeutic strategies that can be applied to overcome TME-mediated treatment resistance. The steps of immune responses involve priming and recruitment of immune cells, infiltration of immune cells into tumor, and TME, recognition and death of cancer cells, then release and presentation of antigen from cancer cells. Targeting different mechanism of immune response become more potential therapeutic approach in the future.

TABLE 3 | Combination therapy to enhance PD-1/PD-L1-based treatment efficacy.

Strategy	Treatments	Therapeutic modalities	Potential mechanisms	Phase	NCT ID status
Immunorecognition					
Enhance antigen presentations	Radiotherapy	• RT (1 fraction, 8 Gy) + Pembrolizumab • RT (5 fractions, 4 Gy) + Pembrolizumab • Pembrolizumab + RT (1 fraction, 8 Gy) + Pembrolizumab • Pembrolizumab + RT (5 fractions, 4 Gy) + Pembrolizumab	1. Induce cell death to promote antigen presentation 2. Trigger activation of cGAS-STING pathway to enhance T-cell response 3. Adjust stromal TME	1	NCT02318771 Active, not recruiting
	Radiotherapy Cytotoxic agents	• Pembrolizumab + Cisplatin + RT • Placebo + Cisplatin + RT		3	NCT03040999 Active, not recruiting
	Radiotherapy Cytotoxic agents	• Docetaxel + Cisplatin + Nivolumab + Radioimmunotherapy		2	NCT03894891 Recruiting
	Radiotherapy CTLA-4 inhibitor	• Nivolumab + Ipilimumab + RT		1	NCT03162731 Recruiting
	Radiotherapy Cytotoxic agents EGFR mAb	• Nivolumab + Cisplatin • Nivolumab + High-dose Cisplatin • Nivolumab + Cetuximab • Nivolumab + IMRT		1	NCT02764593 Active, not recruiting
	EGFR mAb	• Pembrolizumab + Cetuximab	1. Stimulate antibody-dependent cell-mediated cytotoxicity 2. Prime adaptive and innate cellular immunity 3. Competitively inhibit the binding of EGF and other ligands (TGF-α)	2	NCT03082534 Recruiting
		• Avelumab + Cetuximab + RT		1	NCT02938273 Active, not recruiting
	EGFR TKI	• Nivolumab + Afatinib	1. Downregulate PD-L1 expression 2. Reduce PD-L1 expression via inhibiting NF-κB 3. Block the immune escape by upregulating the expression of NKG2D ligands on tumor cells and NKG2D on NK cells 4. Enhance the susceptibility to NK cell-mediated lysis by induction of ULBP1 by inhibition of PKC pathwy	1	NCT03652233 Withdrawn
		• Pembrolizumab + Afatinib		2	NCT03695510 Not yet recruiting
Resensitizing T cell effectors	Interleukin	• ALT-803 + Pembrolizumab • ALT-803 + Nivolumab • ALT-803 + Atezolizumab • ALT-803 + Avelumab	1. IL-15 superagonist 2. promote $CD8^+$ T and NK cell expansion and function	2	NCT03228667 Recruiting
		• IL-2 + Pembrolizumab $^+$ Hypofractionated RT	1. Intralesional IL-2 2. increase PD-L1 expression and $CD8^+$ T cell infiltration	1/2	NCT03474497 Recruiting
		• RO6874281+ Atezolizumab	1. IL-2 Variant (IL-2v), engineered IL2v moiety with abolished binding to IL-2Ra 2. targeting Fibroblast Activation Protein-A 3. Activation of immune effector CD8 T and NK cells, reduce activity on Tregs	2	NCT03386721 Recruiting
Immune modulation of immunosuppressive TME					
DC/NK cells	Carboxymethylcellulose, polyinosinic-polycytidylic acid, and poly-L-lysine dsRNA	• IV Durvalumab + IV Tremelimumab + IT/IM Poly-ICLC	1. Synthetic dsRNA complex which directly activate DCs and trigger NK cells to kill tumor cells 2. Induce interferon-γ production	1/2	NCT02643303 Recruiting

(Continued)

TABLE 3 | Continued

Strategy	Treatments	Therapeutic modalities	Potential mechanisms	Phase	NCT ID status
Cell cycles	CDK4/6 inhibitor	• Abemaciclib + Nivolumab	Create an immune inflamed TMEs through T cell activation and tumor cell intrinsic effects	1/2	NCT03655444 Recruiting
Cytokines	BTK inhibitor	• Ibrutinib + Nivolumab • Ibrutinib + Cetuximab	1. Inhibit IL-2 inducible T-cell kinase (ITK) 2. Maintain balance between Th1/Th2 T cells	2	NCT03646461 Recruiting
HU	Stroma	• VCN-01 and Durvalumab	Tumor-selective replication-competent adenovirus expressing PH20 hyaluronidase	1	NCT03799744 Recruiting
VEGF	VEGF	• Lenvatinib + Pembrolizumab	1. Reduce tumor associated macrophages 2. Enhance the ratio of memory T cells	1b/2	NCT02501096 Recruiting
Regulation of inhibitory and costimulatory receptors					
Inhibitory receptor	B7-H3 (CD276)	• Enoblituzumab (MGA271) + Pembrolizumab	1. Synergistic antitumor activity 2. Engagement of both innate and adaptive immunity 3. Modulation of T-cell immunosuppression 4. Decrease the risk of auto-immune related AE	1	NCT02475213 Active, not recruiting
	LAG-3	• Relatlimab • Relatlimab + Nivolumab	1. Synergistic antitumor activity 2. Positively regulate effector T cell function	1/2	NCT01968109 Recruiting
	KIR	• Nivolumab • Nivolumab + Lirilumab • Nivolumab + Ipilimumab + Lirilumab	1. Block interaction between KIR2DL-1,-2,-3 inhibitory receptors and ligands 2. Promote effector T cell function 3. Reverse T cell exhaustion	1/2	NCT01714739 Active, not recruiting
	PI3K	• IPI-549 and Nivolumab	Transform macrophages from an immune-suppressive to an immune-activating phenotype	1	NCT02637531 Recruiting
	CTLA-4	• Nivolumab with Ipilimumab • Nivolumab	1. CTLA-4 inhibitor: induce a proliferative signature in a subset of memory T-cells 2. PD-1 inhibitor: modulate genes that are involved in T-cell or NK-cell effector functions 3. Increase in plasma cytokine or chemokine levels	2	NCT02919683 Recruiting
		• Nivolumab and Ipilimumab • Nivolumab and placebo		2	NCT02823574 Active, not recruiting
Stimulatory receptor	4-1BB (CD137) OX40 TLR9 agonist	• Cohort A5: Avelumab + Utomilumab (Human IgG2 4-1BB mAb) • Cohort F1: CMP-001(VLP-encapsulated TLR9 agonist) +Avelumab • Cohort F2: CMP-001 + Avelumab + Utomilumab • Cohort F3: CMP-001 + Avelumab+PF-04518600 (OX40 agonist)	1. Utomilumab: production of IFN-γ and IL-2; stimulate and increase NK cells and T cells 2. PF-04518600: co-stimulate effector T cells and deplete regulatory T cells, resulting in enhanced tumor immunity 3. CMP-001: release the oligonucleotide into APCs	1	NCT02554812 Recruiting
	4-1BB (CD137)	• PF-04518600 • PF-04518600 + Utomilumab (PF-05082566)		1	NCT02315066 Active, not recruiting
Other pathway	IDO1	• Nivolumab and Linrodostat (BMS986205) • Nivolumab	1. Inhibitor of indoleamine 2,3-dioxygenase 1, a cytosolic enzyme for oxidation of tryptophan into kynurenine. 2. Inhibition of IDO1–kynurenine–AhR signaling	2	NCT03854032 Recruiting

(Continued)

TABLE 3 | Continued

Strategy	Treatments	Therapeutic modalities	Potential mechanisms	Phase	NCT ID status
		• Nivolumab + Linrodostat • Cetuximab + Cisplatin/Carboplatin + Fluorouracil		3	NCT03386838 Withdrawn
		• Nivolumab + Epacadostat • Nivolumab + Epacadostat + Chemotherapy		1/2	NCT02327078 Active, not recruiting
		• Pembrolizumab + Epacadostat • Pembrolizumab • EXTREME regimen		3	NCT03358472 Active, not recruiting

RT, radiotherapy; Gy, gray; TME, tumor microenvironment; CTLA-4, cytotoxic T-lymphocyte–associated antigen 4; EGFR, epidermal growth factor receptor; mAb, monoclonal antibody; IMRT, intensity-modulated radiotherapy; EGF, epidermal growth factor; TGF, transforming growth factor; TKI, tyrosine kinase inhibitor; PD-L1, Programmed death-ligand 1; NK cells, Natural killer cells; IL, interleukin; DC, dendritic cells; IV, intravenous; IT, intratumoral; IM, intramuscular; dsRNA, double-stranded RNA; BTK, Bruton's tyrosine kinase; Th cells, T helper cells; HU, hyaluronidase; VEGF, vascular endothelial growth factor; AE, adverse event; LAG-3, lymphocyte-activation gene 3; KIR, killer cell immunoglobulin-like receptors; PI3K, phosphoinositide 3-kinases; IFN, Interferon; TLR9, Toll-like receptor 9; VLP, virus-like particle; APC, antigen-presenting cell; IDO1, indoleamine 23-dioxygenase 1; AhR, aryl hydrocarbon receptor.

and to the CD16 receptor on NK cells and DCs, resulting in innate and adaptive immune responses, including ADCC and T cell priming (111). Afatinib (NCT03652233, NCT03695510), an EGFR tyrosine kinase inhibitor, downregulates PD-L1 expression via the inhibition of NF-κB. However, afatinib hinders immune escape by increasing the expression of NKG2D ligands on tumor cells and NKG2D on NK cells (112). ALT-803 (NCT03228667), an IL-15 superagonist, promotes $CD8^+$ T cell and NK cell expansion and function and has demonstrated anti-tumor efficacy in preclinical models (113). Intralesional IL-2 (NCT03474497) increases PD-L1 expression and promotes $CD8^+$ T cell infiltration (114). RO6874281 (NCT03386721), an engineered IL2v moiety, maintains its affinity for IL-2Rβγ, thus activating effector CD8 T cells and NK cells and reducing Treg activity (115).

The immunosuppressive TME also contributes to the low sensitivity of HNSCC to ICIs. Modulating different components of the TME improves the efficacy of ICIs and enhances self-immunity. Poly-ICLC (NCT02643303), a carboxymethylcellulose, polyinosinic-polycytidylic acid, and poly-L-lysine dsRNA, is a synthetic dsRNA complex that directly activates DCs, triggers NK cells, and induces interferon-γ production (116). Abemaciclib (NCT03655444), a CDK4/6 inhibitor, creates an immune inflamed TME through T cell activation and intrinsic tumor cell effects (117). Ibrutinib (NCT03646461), a Bruton's tyrosine kinase inhibitor, inhibits IL-2 inducible T-cell kinase (ITK), to strengthen specific anti-tumor responses (118). ITK plays a crucial role in maintaining the balance between Th1 and Th2 T cells. VCN-01 (NCT03799744), a selective oncolytic adenovirus encoding the human glycosylphosphatidylinositol-anchored enzyme, PH20 hyaluronidase, shows potential anti-tumor effects. Replication of the injected adenovirus in tumor cells results in cell death and the infection of adjacent tumor cells. Hyaluronidase also degrades hyaluronic acid (HA), which is abundant in the ECM and inhibits tumor cell growth and metastasis (119). Lenvatinib (NCT02501096), a multikinase inhibitor of VEGFR 1–3, fibroblast growth factor receptors (FGFR) 1–4, platelet-derived growth factor α receptors, RET, and KIT, reduces the number of TAMs and increases the ratio of memory T cells (120).

The regulation of inhibitory and costimulatory receptors synergically enhances the immunological anti-tumor effect. Inhibitory receptors, including B7-H3, LAG-3, killer cell immunoglobulin-like receptors (KIRs), phosphoinositide 3-kinases (PI3Ks), and CTLA-4, are applied in combination therapies. Enoblituzumab (NCT02475213), an Fc optimized, humanized IgG1 monoclonal antibody, promotes binding to activating FcγR and recognizes B7-H3, which is highly expressed in HNSCC. Combination therapy may contribute to synergistic antitumor activity (121). Relatlimab (NCT01968109), an anti-LAG-3 monoclonal antibody, shows an additive antitumor effect when administered with ICIs. LAG3 negatively regulates Teff function and is a marker of T cell exhaustion (122). IPI-549 (NCT02637531), a selective PI3K-γ inhibitor, transforms macrophages from an immune-suppressive to an immune-activating phenotype, which may help overcome resistance to ICIs (123). The well-known dual blockade therapy consisting of anti-CTLA-4 and anti-PD-1 antibodies (NCT02919683, NCT02823574), stimulates distinct immune cells and results in an inflammatory TME to overcome cancer cells (124). Similarly, cooperation with stimulatory receptors increases clinical benefits and treatment efficacy. Utomilumab (NCT01307267, NCT02315066), a 4-1BB/CD137 agonist, stimulates the activity and number of NK cells and T cells (125). PF-04518600 (NCT01307267, NCT02315066), a selective anti-OX40 antibody, activates OX40 and increases the proliferation of memory and effector T-lymphocytes (126). CMP-001 (NCT01307267), a Toll-like receptor 9 (TLR9) agonist, comprises a CpG-A oligodeoxynucleotide packaged in particles. It activates tumor-associated plasmacytoid DCs, which construct an interferon-rich TME and results in anti-tumor $CD8^+$ T cell responses (127). IDO1, a major enzyme in tryptophan catabolism, is a target in clinical development, in combination with PD-1 ICIs (NCT03854032, NCT03386838,

NCT02327078, NCT03358472). IDO1 converts tryptophan to kynurenine, which then activates aryl hydrocarbon receptor (AhR), a ligand-activated transcription factor, in Tregs, DCs, and NK cells. Activation of AhR induces subsequent cascades in three different cell types. In Tregs, AhR results in the nuclear translocation and enhancement of FoxP3 transcripts and IL10, eventually increasing Treg populations. In DCs, AhR promotes the production of IL-10 and inhibits IFNβ signaling. In NK cells, AhR induces the production of both IL-10 and IFNγ. The IDO1-kynurenine-AhR axis demonstrates a positive feedback loop. These effects on immune cells help establish an immunosuppressive TME. The inhibition of IDO reverses immunosuppression and enhances the response to ICIs (128).

Cancer Vaccines

Cancer vaccines targeting HPV antigens and tumor-associated antigens enhance the immune response in HNSCC. Therapeutic vaccines include peptide vaccines, live-vector-based vaccines, and DNA- or RNA-based vaccines. Peptide vaccines derived from HPV antigens are taken up by DCs and displayed by either MHC class I, class II, or both molecules, after which they induce a T-cell mediated immune response. Several trials have investigated such drugs, including DPX-E7 (NCT02865135), GL-0817/GL-0810 (NCT00257738), P16_37-63 peptide (NCT01462838, NCT02526316), and ISA 101(NCT02426892). However, the response rates have been variable in relatively small populations of patients (129, 130). Live-vector-based vaccines are more immunogenic and induce strong pathogen-derived CD8 epitopes (131). Recent cancer vaccine modalities include DNA and RNA vaccines encoding selected tumor antigens or synthetic long peptide (SLP) vaccines co-delivering CD4 and CD8 epitopes (132). DNA or peptide vaccines targeting HPV E6 and E7 oncoproteins have demonstrated specific clinical efficacy in precancerous lesions and have shown promise in the treatment of HPV-related HNSCC. However, the development of vaccines against HPV-independent HNSCC has been less successful due to the difficulty in identifying available targets (133). Additional vaccine modalities are required to overcome the immunosuppressive TME in HNSCC.

Cell-Based Therapy

T cells, including TILs, T cells with genetically modified T cell receptors (TCRs), and T cells transfected with chimeric antigen receptors (CAR), are the main types of cell-based therapy (134). Sufficient numbers of TILs overcome the immunosuppressive TME by removing other exhausted immune cells and inhibitory factors, such as cytokines. Adoptive immunotherapy using CAR T cells has displayed promising outcomes in hematological malignancies, such as leukemia and multiple myeloma. The process of CAR T cell therapy includes retrieving T cells from the patient's blood or tumor, training and stimulating their expansion in an *in vitro* system, and injecting the expanded cells back into the patient to promote cancer elimination. The development of tumor antigen-specific TCRs, for example HPV-targeted TCRs in genetically modify T cells, is another approach for adoptive immunotherapy. These modified T cells possess high levels of immune-signaling initiators and show rapid recognition of intracellular antigens, which can initiate an immune response against cancer cells. A phase I/II trial targeting the HLA-A*02:01-restricted epitope of E6 (E6 TCR T cells) enrolled patients with HPV-positive and HLA-A*02:01-positive metastatic epithelial cancers and showed that a dose up to 2×10^{11} cells was safe for patients. Partial responses in 2 of 12 patients (both with anal cancer) were reported (135). A phase I trial of T4 CAR T cell immunotherapy in HNSCC demonstrated safe intratumoral administration of T4 T-cells that co-express: (i) T1E28ζ, a CAR containing an ErbB ligand coupled to a $CD28^{+}CD3\zeta$ endodomain and (ii) 4αβ, an IL-4-responsive chimeric cytokine receptor. Although a lymphopenia rate of 62% was observed, T4 manufacture was successful in 13/13 cases, yielding 2.5–7.5 Bn T cells (69 ± 13% transduced) (136). However, the development of adoptive cell therapy for HNSCC is still immature. There are still numerous difficulties and challenges including the identification of more specific peptide and genetic profiles of HNSCC cells. More precise knowledge of intracellular and extracellular neoantigens would help to identify potentially novel targets for cell therapy in HNSCC.

POTENTIAL BIOMARKERS IN HNSCC IMMUNOTHERAPY

Potential biomarkers in HNSCC have been discussed for many years, but there is still no consensus. Recent studies have tended to focus on specific biomarkers, including PD-L1 expression, HPV status, tumor immune infiltration, immune-associated signatures, gene expression profiles (GEPs), tumor mutational burden (TMB), the status of DNA mismatch repair, and smoking-related signatures. PD-L1 immunohistochemistry is the most frequently used marker in clinical practice. However, there are several challenges in the clinical application of these biomarkers. For example, PD-L1 is a heterogeneous marker with different intratumoral/temporal and primary/metastatic variations in expression (137). Different immunohistochemistry assays have been used, with different thresholds for positivity and different scoring criteria, including a tumor proportional score (TPS) and a combined proportional score (CPS) (138). HPV status also influences immunity within the TME and affects responses to immunotherapy (6). TILs, defined as $CD8^{+}$ T cells and Tregs, have demonstrated a possible role in distinguishing ICI responders from ICI non-responders (139). GEP and TMB, analyzed by microarray or next-generation sequencing platforms, have been investigated as predictive biomarkers for biological phenotypes and clinical outcomes in HNSCC. Some analyses have shown that TMB, CPS, and GEP can serve as independent predictive biomarkers for responsiveness to anti-PD-1/PD-L1 antibodies (140). Tumors with more mutations influencing the DNA damage response, for example those with mismatch repair deficiency (dMMR), have a higher TMB and are more sensitive to ICIs. This contributed to the FDA approval of pembrolizumab for patients with dMMR or MSI-H tumors, regardless of histology (141–143). Overall, while the interactions between the tumor, the immune system, and the microenvironment are complex, more

reliable predictive biomarkers are required to assess tumor responsiveness to immunotherapy.

PERSPECTIVES AND CONCLUSIONS

As ICI monotherapy shows a durable response in only a small subset of patients, combination therapy with anti-PD-1/PD-L1 antibodies has emerged as an alternative and has shown encouraging results in the treatment of HNSCC. In addition, the anti-tumor effects of ICIs can be reinforced by increasing antigen presentation via radiation or chemotherapy/target therapy, modulating TME, or collaborating with costimulatory and inhibitory receptors on tumor cells or immune cells. The niches around cancer cells are crucial for interference with the efficacy of checkpoint inhibitors and they determine whether a tumor is "immunoactive" or "immunosuppressive." Methods to overcome the immunotherapy resistance of the TME will become more crucial in the future. Multimodalities of treatment strategies aid in strengthening immunosurveillance and immunoediting. Studies to identify more specific targets for adoptive T cell therapies are ongoing. In addition, further studies designed to identify ideal biomarkers of individual tumors and to elucidate the mechanisms of immune escape are warranted.

AUTHOR CONTRIBUTIONS

H-CW, L-PC, and S-FC substantially contributed to the conception, drafting, editing, and final approval of this manuscript.

FUNDING

The presented study was supported by Grant No. S10518-3 from the Kaohsiung Medical University Hospital, Kaohsiung, Taiwan.

REFERENCES

1. Parkin DM, Bray F, Ferlay J, Pisani P. Global cancer statistics, 2002. *CA Cancer J Clin.* (2005) 55:74–108. doi: 10.3322/canjclin.55.2.74
2. Haddad RI, Shin DM. Recent advances in head and neck cancer. *N Engl J Med.* (2008) 359:1143–54. doi: 10.1056/NEJMra0707975
3. Hsu WL, Yu KJ, Chiang CJ, Chen TC, Wang CP. Head and neck cancer incidence trends in Taiwan, 1980 ~ 2014. *Int J Head Neck Sci.* (2017) 1:180–9. doi: 10.6696/IJHNS.2017.0103.05
4. Vermorken JB, Mesia R, Rivera F, Remenar E, Kawecki A, Rottey S, et al. Platinum-based chemotherapy plus cetuximab in head and neck cancer. *N Engl J Med.* (2008) 359:1116–27. doi: 10.1056/NEJMoa0802656
5. Ferris RL, Blumenschein GR, Fayette J, Guigay J, Colevas AD, Licitra LF, et al. Further evaluations of nivolumab (nivo) versus investigator's choice (IC) chemotherapy for recurrent or metastatic (R/M) squamous cell carcinoma of the head and neck (SCCHN): CheckMate 141. *Am Soc Clin Oncol.* (2016) doi: 10.1200/JCO.2016.34.15_suppl.6009
6. Chow LQ, Haddad R, Gupta S, Mahipal A, Mehra R, Tahara M, et al. Antitumor activity of pembrolizumab in biomarker-unselected patients with recurrent and/or metastatic head and neck squamous cell carcinoma: results from the phase Ib KEYNOTE-012 expansion cohort. *J Clin Oncol.* (2016) 34:3838–45. doi: 10.1200/JCO.2016.68.1478
7. Peltanova B, Raudenska M, Masarik M. Effect of tumor microenvironment on pathogenesis of the head and neck squamous cell carcinoma: a systematic review. *Mol Cancer.* (2019) 18:63. doi: 10.1186/s12943-019-0983-5
8. Ludwig S, Sharma P, Theodoraki MN, Pietrowska M, Yerneni SS, Lang S, et al. Molecular and functional profiles of exosomes from HPV (+) and HPV (–) head and neck cancer cell lines. *Front Oncol.* (2018) 8:445. doi: 10.3389/fonc.2018.00445
9. Stämpfli MR, Anderson GP. How cigarette smoke skews immune responses to promote infection, lung disease and cancer. *Nat Rev Immunol.* (2009) 9:377–84. doi: 10.1038/nri2530
10. Keck MK, Zuo Z, Khattri A, Stricker TP, Brown CD, Imanguli M, et al. Integrative analysis of head and neck cancer identifies two biologically distinct HPV and three non-HPV subtypes. *Clin Cancer Res.* (2015) 21:870–81. doi: 10.1158/1078-0432.CCR-14-2481
11. Hanna GJ, Liu H, Jones RE, Bacay AF, Lizotte PH, Ivanova EV, et al. Defining an inflamed tumor immunophenotype in recurrent, metastatic squamous cell carcinoma of the head and neck. *Oral Oncol.* (2017) 67:61–9. doi: 10.1016/j.oraloncology.2017.02.005
12. Duray A, Demoulin S, Hubert P, Delvenne P, Saussez S. Immune suppression in head and neck cancers: a review. *Clin Dev Immunol.* (2010) 2010:701657. doi: 10.1155/2010/701657
13. Reichert TE, Rabinowich H, Johnson JT, Whiteside TL. Mechanisms responsible for signaling and functional defects. *J Immunother.* (1998) 21:295–306. doi: 10.1097/00002371-199807000-00007
14. Whiteside TL. Immunobiology of head and neck cancer. *Cancer Metastasis Rev.* (2005) 24:95–105. doi: 10.1007/s10555-005-5050-6
15. Sakakura K, Chikamatsu K, Takahashi K, Whiteside TL, Furuya N. Maturation of circulating dendritic cells and imbalance of T-cell subsets in patients with squamous cell carcinoma of the head and neck. *Cancer Immunol Immunother.* (2006) 55:151–9. doi: 10.1007/s00262-005-0697-y
16. Pitt JM, Vétizou M, Daillère R, Roberti MP, Yamazaki T, Routy B, et al. Resistance mechanisms to immune-checkpoint blockade in cancer: tumor-intrinsic and-extrinsic factors. *Immunity.* (2016) 44:1255–69. doi: 10.1016/j.immuni.2016.06.001
17. Corzo CA, Cotter MJ, Cheng P, Cheng F, Kusmartsev S, Sotomayor E, et al. Mechanism regulating reactive oxygen species in tumor-induced myeloid-derived suppressor cells. *J Immunol.* (2009) 182:5693–701. doi: 10.4049/jimmunol.0900092
18. Noman MZ, Desantis G, Janji B, Hasmim M, Karray S, Dessen P, et al. PD-L1 is a novel direct target of HIF-1α, and its blockade under hypoxia enhanced MDSC-mediated T cell activation. *J Exp Med.* (2014) 211:781–90. doi: 10.1084/jem.20131916
19. Echarri M, Lopez-Martin A, Hitt R. Targeted therapy in locally advanced and recurrent/metastatic head and neck squamous cell carcinoma (LA-R/M HNSCC). *Cancers.* (2016) 8:27. doi: 10.3390/cancers8030027
20. Lechner MG, Liebertz DJ, Epstein AL. Characterization of cytokine-induced myeloid-derived suppressor cells from normal human peripheral blood mononuclear cells. *J Immunol.* (2010) 185:2273–84. doi: 10.4049/jimmunol.1000901
21. Lahl K, Loddenkemper C, Drouin C, Freyer J, Arnason J, Eberl G, et al. Selective depletion of Foxp3+ regulatory T cells induces a scurfy-like disease. *J Exp Med.* (2007) 204:57–63. doi: 10.1084/jem.20061852
22. Sakaguchi S, Miyara M, Costantino CM, Hafler DA. FOXP3+ regulatory T cells in the human immune system. *Nat Rev Immunol.* (2010) 10:490–500. doi: 10.1038/nri2785
23. Jie H, Gildener-Leapman N, Li J, Srivastava R, Gibson S, Whiteside T, et al. Intratumoral regulatory T cells upregulate immunosuppressive molecules in head and neck cancer patients. *Br J Cancer.* (2013) 109:2629–35. doi: 10.1038/bjc.2013.645
24. Sica A, Mantovani A. Macrophage plasticity and polarization: *in vivo* veritas. *J Clin Invest.* (2012) 122:787–95. doi: 10.1172/JCI59643
25. El-Rouby DH. Association of macrophages with angiogenesis in oral verrucous and squamous cell carcinomas. *J Oral Pathol Med.* (2010) 39:559–64. doi: 10.1111/j.1600-0714.2010.00879.x

26. Oweida A, Hararah MK, Phan A, Binder D, Bhatia S, Lennon S, et al. Resistance to radiotherapy and PD-L1 blockade is mediated by TIM-3 upregulation and regulatory T-cell infiltration. *Clin Cancer Res.* (2018) 24:5368–80. doi: 10.1158/1078-0432.CCR-18-1038
27. Kather JN, Suarez-Carmona M, Charoentong P, Weis CA, Hirsch D, Bankhead P, et al. Topography of cancer-associated immune cells in human solid tumors. *Elife.* (2018) 7:e36967. doi: 10.7554/eLife.36967
28. Kunz-Schughart LA, Knuechel R. Tumor-associated fibroblasts (part I): active stromal participants in tumor development and progression? *Histol Histopathol.* (2002) 17:599–621. doi: 10.14670/HH-17.599
29. Wheeler SE, Shi H, Lin F, Dasari S, Bednash J, Thorne S, et al. Tumor associated fibroblasts enhance head and neck squamous cell carcinoma proliferation, invasion, and metastasis in preclinical models. *Head Neck.* (2014) 36:385–92. doi: 10.1002/hed.23312
30. Xie C, Ji N, Tang Z, Li J, Chen Q. The role of extracellular vesicles from different origin in the microenvironment of head and neck cancers. *Mol Cancer.* (2019) 18:83. doi: 10.1186/s12943-019-0985-3
31. Whiteside TL. Immune modulation of T-cell and NK (natural killer) cell activities by TEXs (tumour-derived exosomes). *Biochem Soc Trans.* (2013) 41:245–51. doi: 10.1042/BST20120265
32. Kim JW, Wieckowski E, Taylor DD, Reichert TE, Watkins S, Whiteside TL. Fas ligand–positive membranous vesicles isolated from sera of patients with oral cancer induce apoptosis of activated T lymphocytes. *Clin Cancer Res.* (2005) 11:1010–20.
33. Al-Samadi A, Awad SA, Tuomainen K, Zhao Y, Salem A, Parikka M, et al. Crosstalk between tongue carcinoma cells, extracellular vesicles, and immune cells in *in vitro* and *in vivo* models. *Oncotarget.* (2017) 8:60123–34. doi: 10.18632/oncotarget.17768
34. Hegde PS, Karanikas V, Evers S. The where, the when, and the how of immune monitoring for cancer immunotherapies in the era of checkpoint inhibition. *Clin Cancer Res.* (2016) 22:1865–74. doi: 10.1158/1078-0432.CCR-15-1507
35. Canning M, Guo G, Yu M, Myint C, Groves M, Byrd K, et al. Heterogeneity of the head and neck squamous cell carcinoma immune landscape and its impact on immunotherapy. *Front Cell Dev Biol.* (2019) 7:52. doi: 10.3389/fcell.2019.00052
36. Facciabene A, Peng X, Hagemann IS, Balint K, Barchetti A, Wang LP, et al. Tumour hypoxia promotes tolerance and angiogenesis via CCL28 and T reg cells. *Nature.* (2011) 475:226–30. doi: 10.1038/nature10169
37. Zou L, Barnett B, Safah H, LaRussa VF, Evdemon-Hogan M, Mottram P, et al. Bone marrow is a reservoir for CD4+ CD25+ regulatory T cells that traffic through CXCL12/CXCR4 signals. *Cancer Res.* (2004) 64:8451–5. doi: 10.1158/0008-5472.CAN-04-1987
38. Togashi Y, Shitara K, Nishikawa H. Regulatory T cells in cancer immunosuppression—implications for anticancer therapy. *Nat Rev Clin Oncol.* (2019) 16:356–71. doi: 10.1038/s41571-019-0175-7
39. Jarnicki AG, Lysaght J, Todryk S, Mills KH. Suppression of antitumor immunity by IL-10 and TGF-beta-producing T cells infiltrating the growing tumor: influence of tumor environment on the induction of CD4+ and CD8+ regulatory T cells. *J Immunol.* (2006) 177:896–904. doi: 10.4049/jimmunol.177.2.896
40. Maj T, Wang W, Crespo J, Zhang H, Wang W, Wei S, et al. Oxidative stress controls regulatory T cell apoptosis and suppressor activity and PD-L1-blockade resistance in tumor. *Nat Immunol.* (2017) 18:1332–41. doi: 10.1038/ni.3868
41. Liu Z, McMichael EL, Shayan G, Li J, Chen K, Srivastava R, et al. Novel effector phenotype of Tim-3+ regulatory T cells leads to enhanced suppressive function in head and neck cancer patients. *Clin Cancer Res.* (2018) 24:4529–38. doi: 10.1158/1078-0432.CCR-17-1350
42. Oweida AJ, Darragh L, Phan A, Binder D, Bhatia S, Mueller A, et al. STAT3 Modulation of regulatory T cells in response to radiation therapy in head and neck cancer. *J Natl Cancer Inst.* (2019). doi: 10.1093/jnci/djz036. [Epub ahead of print].
43. Strauss L, Bergmann C, Gooding W, Johnson JT, Whiteside TL. The frequency and suppressor function of CD4+ CD25highFoxp3+ T cells in the circulation of patients with squamous cell carcinoma of the head and neck. *Clin Cancer Res.* (2007) 13:6301–11. doi: 10.1158/1078-0432.CCR-07-1403
44. Al-Qahtani D, Anil S, Rajendran R. Tumour infiltrating CD25+ FoxP3+ regulatory T cells (Tregs) relate to tumour grade and stromal inflammation in oral squamous cell carcinoma. *J Oral Pathol Med.* (2011) 40:636–42. doi: 10.1111/j.1600-0714.2011.01020.x
45. Ribechini E, Greifenberg V, Sandwick S, Lutz MB. Subsets, expansion and activation of myeloid-derived suppressor cells. *Med Microbiol Immunol.* (2010) 199:273–81. doi: 10.1007/s00430-010-0151-4
46. Gabrilovich DI. Myeloid-derived suppressor cells. *Cancer Immunol Res.* (2017) 5:3–8. doi: 10.1158/2326-6066.CIR-16-0297
47. Lang S, Bruderek K, Kaspar C, Höing B, Kanaan O, Dominas N, et al. Clinical relevance and suppressive capacity of human myeloid-derived suppressor cell subsets. *Clin Cancer Res.* (2018) 24:4834–44. doi: 10.1158/1078-0432.CCR-17-3726
48. Lim KP, Cirillo N, Hassona Y, Wei W, Thurlow JK, Cheong SC, et al. Fibroblast gene expression profile reflects the stage of tumour progression in oral squamous cell carcinoma. *J Pathol.* (2011) 223:459–69. doi: 10.1002/path.2841
49. Park JE, Lenter MC, Zimmermann RN, Garin-Chesa P, Old LJ, Rettig WJ. Fibroblast activation protein, a dual specificity serine protease expressed in reactive human tumor stromal fibroblasts. *J Biol Chem.* (1999) 274:36505–12. doi: 10.1074/jbc.274.51.36505
50. Wonganu B, Berger BW. A specific, transmembrane interface regulates fibroblast activation protein (FAP) homodimerization, trafficking and exopeptidase activity. *Biochim Biophys Acta.* (2016) 1858:1876–82. doi: 10.1016/j.bbamem.2016.05.001
51. Bello IO, Vered M, Dayan D, Dobriyan A, Yahalom R, Alanen K, et al. Cancer-associated fibroblasts, a parameter of the tumor microenvironment, overcomes carcinoma-associated parameters in the prognosis of patients with mobile tongue cancer. *Oral Oncol.* (2011) 47:33–8. doi: 10.1016/j.oraloncology.2010.10.013
52. Lotti F, Jarrar AM, Pai RK, Hitomi M, Lathia J, Mace A, et al. Chemotherapy activates cancer-associated fibroblasts to maintain colorectal cancer-initiating cells by IL-17A. *J Exp Med.* (2013) 210:2851–72. doi: 10.1084/jem.20131195
53. Glentis A, Oertle P, Mariani P, Chikina A, El Marjou F, Attieh Y, et al. Cancer-associated fibroblasts induce metalloprotease-independent cancer cell invasion of the basement membrane. *Nat Commun.* (2017) 8:924. doi: 10.1038/s41467-017-00985-8
54. Sandoval P, Jiménez-Heffernan JA, Rynne-Vidal Á, Pérez-Lozano ML, Gilsanz Á, Ruiz-Carpio V, et al. Carcinoma-associated fibroblasts derive from mesothelial cells via mesothelial-to-mesenchymal transition in peritoneal metastasis. *J Pathol.* (2013) 231:517–31. doi: 10.1002/path.4281
55. Iwano M, Plieth D, Danoff TM, Xue C, Okada H, Neilson EG. Evidence that fibroblasts derive from epithelium during tissue fibrosis. *J Clin Invest.* (2002) 110:341–50. doi: 10.1172/JCI0215518
56. Knowles LM, Stabile LP, Egloff AM, Rothstein ME, Thomas SM, Gubish CT, et al. HGF and c-Met participate in paracrine tumorigenic pathways in head and neck squamous cell cancer. *Clin Cancer Res.* (2009) 15:3740–50. doi: 10.1158/1078-0432.CCR-08-3252
57. Fiori ME, Di Franco S, Villanova L, Bianca P, Stassi G, De Maria R. Cancer-associated fibroblasts as abettors of tumor progression at the crossroads of EMT and therapy resistance. *Mol Cancer.* (2019) 18:70. doi: 10.1186/s12943-019-0994-2
58. Yu B, Wu K, Wang X, Zhang J, Wang L, Jiang Y, et al. Periostin secreted by cancer-associated fibroblasts promotes cancer stemness in head and neck cancer by activating protein tyrosine kinase 7. *Cell Death Dis.* (2018) 9:1082. doi: 10.1038/s41419-018-1116-6
59. Álvarez-Teijeiro S, García-Inclán C, Villaronga M, Casado P, Hermida-Prado F, Granda-Díaz R, et al. Factors secreted by cancer-associated fibroblasts that sustain cancer stem properties in head and neck squamous carcinoma cells as potential therapeutic targets. *Cancers.* (2018) 10:334. doi: 10.3390/cancers10090334
60. Murray PJ, Allen JE, Biswas SK, Fisher EA, Gilroy DW, Goerdt S, et al. Macrophage activation and polarization: nomenclature and experimental guidelines. *Immunity.* (2014) 41:14–20. doi: 10.1016/j.immuni.2014.06.008

61. Lin CN, Chien CY, Chuang HC. Are friends or foes? New strategy for head and neck squamous cell carcinoma treatment via immune regulation. *Int J Head Neck Sci.* (2017) 1:105–13. doi: 10.6696/IJHNS.2017.0102.03
62. Weber M, Büttner-Herold M, Hyckel P, Moebius P, Distel L, Ries J, et al. Small oral squamous cell carcinomas with nodal lymphogenic metastasis show increased infiltration of M2 polarized macrophages–an immunohistochemical analysis. *J Craniomaxillofac Surg.* (2014) 42:1087–94. doi: 10.1016/j.jcms.2014.01.035
63. Mantovani A, Biswas SK, Galdiero MR, Sica A, Locati M. Macrophage plasticity and polarization in tissue repair and remodelling. *J Pathol.* (2013) 229:176–85. doi: 10.1002/path.4133
64. Liu CY, Xu JY, Shi XY, Huang W, Ruan TY, Xie P, et al. M2-polarized tumor-associated macrophages promoted epithelial–mesenchymal transition in pancreatic cancer cells, partially through TLR4/IL-10 signaling pathway. *Lab Invest.* (2013) 93:844–54. doi: 10.1038/labinvest.2013.69
65. Rodriguez PC, Hernandez CP, Quiceno D, Dubinett SM, Zabaleta J, Ochoa JB, et al. Arginase I in myeloid suppressor cells is induced by COX-2 in lung carcinoma. *J Exp Med.* (2005) 202:931–9. doi: 10.1084/jem.20050715
66. Van Ginderachter JA, Meerschaut S, Liu Y, Brys L, De Groeve K, Ghassabeh GH, et al. Peroxisome proliferator-activated receptor gamma (PPARgamma) ligands reverse CTL suppression by alternatively activated (M2) macrophages in cancer. *Blood.* (2006) 108:525–35. doi: 10.1182/blood-2005-09-3777
67. She L, Qin Y, Wang J, Liu C, Zhu G, Li G, et al. Tumor-associated macrophages derived CCL18 promotes metastasis in squamous cell carcinoma of the head and neck. *Cancer Cell Int.* (2018) 18:120. doi: 10.1186/s12935-018-0620-1
68. Kumar AT, Knops A, Swendseid B, Martinez-Outschoorn UE, Harshyne L, Philp NJ, et al. Prognostic significance of tumor-associated macrophage content in head and neck squamous cell carcinoma: a meta-analysis. *Front Oncol.* (2019) 9:656. doi: 10.3389/fonc.2019.00656
69. Troiano G, Caponio VCA, Adipietro I, Tepedino M, Santoro R, Laino L, et al. Prognostic significance of CD68+ and CD163+ tumor associated macrophages in head and neck squamous cell carcinoma: a systematic review and meta-analysis. *Oral Oncol.* (2019) 93:66–75. doi: 10.1016/j.oraloncology.2019.04.019
70. Cooper MA, Fehniger TA, Caligiuri MA. The biology of human natural killer-cell subsets. *Trends Immunol.* (2001) 22:633–40. doi: 10.1016/S1471-4906(01)02060-9
71. Konjevic G, Jurisic V, Jovic V, Vuletic A, Martinovic KM, Radenkovic S, et al. Investigation of NK cell function and their modulation in different malignancies. *Immunol Res.* (2012) 52:139–56. doi: 10.1007/s12026-012-8285-7
72. Topham NJ, Hewitt EW. Natural killer cell cytotoxicity: how do they pull the trigger? *Immunology.* (2009) 128:7–15. doi: 10.1111/j.1365-2567.2009.03123.x
73. Wang W, Erbe AK, Hank JA, Morris ZS, Sondel PM. NK cell-mediated antibody-dependent cellular cytotoxicity in cancer immunotherapy. *Front Immunol.* (2015) 6:368. doi: 10.3389/fimmu.2015.00368
74. Weil S, Memmer S, Lechner A, Huppert V, Giannattasio A, Becker T, et al. Natural killer group 2D ligand depletion reconstitutes natural killer cell immunosurveillance of head and neck squamous cell carcinoma. *Front Immunol.* (2017) 8:387. doi: 10.3389/fimmu.2017.00387
75. Fridlender ZG, Sun J, Kim S, Kapoor V, Cheng G, Ling L, et al. Polarization of tumor-associated neutrophil phenotype by TGF-beta:"N1" versus "N2" TAN. *Cancer cell.* (2009) 16:183–94. doi: 10.1016/j.ccr.2009.06.017
76. Zhang X, Zhang W, Yuan X, Fu M, Qian H, Xu W. Neutrophils in cancer development and progression: roles, mechanisms, and implications. *Int J Oncol.* (2016) 49:857–67. doi: 10.3892/ijo.2016.3616
77. Levental KR, Yu H, Kass L, Lakins JN, Egeblad M, Erler JT, et al. Matrix crosslinking forces tumor progression by enhancing integrin signaling. *Cell.* (2009) 139:891–906. doi: 10.1016/j.cell.2009.10.027
78. Egeblad M, Werb Z. New functions for the matrix metalloproteinases in cancer progression. *Nat Rev Cancer.* (2002) 2:161–74. doi: 10.1038/nrc745
79. Bergers G, Brekken R, McMahon G, Vu TH, Itoh T, Tamaki K, et al. Matrix metalloproteinase-9 triggers the angiogenic switch during carcinogenesis. *Nat Cell Biol.* (2000) 2:737–44. doi: 10.1038/35036374
80. Tatti O, Vehviläinen P, Lehti K, Keski-Oja J. MT1-MMP releases latent TGF-beta1 from endothelial cell extracellular matrix via proteolytic processing of LTBP-1. *Exp Cell Res.* (2008) 314:2501–14. doi: 10.1016/j.yexcr.2008.05.018
81. Garcia AJ, Boettiger D. Integrin–fibronectin interactions at the cell-material interface: initial integrin binding and signaling. *Biomaterials.* (1999) 20:2427–33. doi: 10.1016/S0142-9612(99)00170-2
82. Brown AC, Dysart MM, Clarke KC, Stabenfeldt SE, Barker TH. Integrin α3β1 binding to fibronectin is dependent on the ninth type III repeat. *J Biol Chem.* (2015) 290:25534–47. doi: 10.1074/jbc.M115.656702
83. Lou X, Han X, Jin C, Tian W, Yu W, Ding D, et al. SOX2 targets fibronectin 1 to promote cell migration and invasion in ovarian cancer: new molecular leads for therapeutic intervention. *OMICS.* (2013) 17:510–8. doi: 10.1089/omi.2013.0058
84. Knowles LM, Gurski LA, Engel C, Gnarra JR, Maranchie JK, Pilch J. Integrin αvβ3 and fibronectin upregulate Slug in cancer cells to promote clot invasion and metastasis. *Cancer Res.* (2013) 73:6175–84. doi: 10.1158/0008-5472.CAN-13-0602
85. Matlung SE, Wilhelmina van Kempen PM, Bovenschen N, Baarle DV, Willems SM. Differences in T-cell infiltrates and survival between HPV+ and HPV-oropharyngeal squamous cell carcinoma. *Future Sci OA.* (2016) 2:FSO88. doi: 10.4155/fso.15.88
86. Partlová S, Bouček J, Kloudová K, Lukešová E, Zábrodský M, Grega M, et al. Distinct patterns of intratumoral immune cell infiltrates in patients with HPV-associated compared to non-virally induced head and neck squamous cell carcinoma. *Oncoimmunology.* (2015) 4:e965570. doi: 10.4161/21624011.2014.965570
87. Lechner A, Schlößer HA, Thelen M, Wennhold K, Rothschild SI, Gilles R, et al. Tumor-associated B cells and humoral immune response in head and neck squamous cell carcinoma. *Oncoimmunology.* (2019) 8:1535293. doi: 10.1080/2162402X.2018.1535293
88. Al-Sahaf S, Hunter KD, Bolt R, Ottewell PD, Murdoch C. The IL-1/IL-1R axis induces greater fibroblast-derived chemokine release in human papillomavirus-negative compared to positive oropharyngeal cancer. *Int J Cancer.* (2019) 144:334–44. doi: 10.1002/ijc.31852
89. Bloy N, Garcia P, Laumont CM, Pitt JM, Sistigu A, Stoll G, et al. Immunogenic stress and death of cancer cells: contribution of antigenicity vs adjuvanticity to immunosurveillance. *Immunol Rev.* (2017) 280:165–74. doi: 10.1111/imr.12582
90. Honegger A, Leitz J, Bulkescher J, Hoppe-Seyler K, Hoppe-Seyler F. Silencing of human papillomavirus (HPV) E6/E7 oncogene expression affects both the contents and the amounts of extracellular microvesicles released from HPV-positive cancer cells. *Int J Cancer.* (2013) 133:1631–42. doi: 10.1002/ijc.28164
91. Harden ME, Munger K. Human papillomavirus 16 E6 and E7 oncoprotein expression alters microRNA expression in extracellular vesicles. *Virology.* (2017) 508:63–9. doi: 10.1016/j.virol.2017.05.005
92. Fleming JC, Woo J, Moutasim K, Mellone M, Frampton SJ, Mead A, et al. HPV, tumour metabolism and novel target identification in head and neck squamous cell carcinoma. *Br J Cancer.* (2019) 120:356–67. doi: 10.1038/s41416-018-0364-7
93. Halestrap AP, Wilson MC. The monocarboxylate transporter family—role and regulation. *IUBMB Life.* (2012) 64:109–19. doi: 10.1002/iub.572
94. Desrichard A, Kuo F, Chowell D, Lee KW, Riaz N, Wong RJ, et al. Tobacco smoking-associated alterations in the immune microenvironment of squamous cell carcinomas. *J Natl Cancer Inst.* (2018) 110:1386–92. doi: 10.1093/jnci/djy060
95. Hernandez CP, Morrow K, Velasco C, Wyczechowska DD, Naura AS, Rodriguez PC. Effects of cigarette smoke extract on primary activated T cells. *Cell Immunol.* (2013) 282:38–43. doi: 10.1016/j.cellimm.2013.04.005
96. Foy JP, Bertolus C, Michallet MC, Deneuve S, Incitti R, Bendriss-Vermare N, et al. The immune microenvironment of HPV-negative oral squamous cell carcinoma from never-smokers and never-drinkers patients suggests higher clinical benefit of IDO1 and PD1/PD-L1 blockade. *Ann Oncol.* (2017) 28:1934–41. doi: 10.1093/annonc/mdx210
97. Sok JC, Coppelli FM, Thomas SM, Lango MN, Xi S, Hunt JL, et al. Mutant epidermal growth factor receptor (EGFRvIII) contributes to head and neck cancer growth and resistance to EGFR targeting. *Clin Cancer Res.* (2006) 12:5064–73. doi: 10.1158/1078-0432.CCR-06-0913

98. Hama T, Yuza Y, Suda T, Saito Y, Norizoe C, Kato T, et al. Functional mutation analysis of EGFR family genes and corresponding lymph node metastases in head and neck squamous cell carcinoma. *Clin Exp Metastasis.* (2012) 29:19–25. doi: 10.1007/s10585-011-9425-5
99. Bhatia S, Oweida A, Lennon S, Darragh LB, Milner D, Phan AV, et al. Inhibition of EphB4–Ephrin-B2 signaling reprograms the tumor immune microenvironment in head and neck cancers. *Cancer Res.* (2019) 79:2722–35. doi: 10.1158/0008-5472.CAN-18-3257
100. Koyama S, Akbay EA, Li YY, Herter-Sprie GS, Buczkowski KA, Richards WG, et al. Adaptive resistance to therapeutic PD-1 blockade is associated with upregulation of alternative immune checkpoints. *Nat Commun.* (2016) 7:10501. doi: 10.1038/ncomms10501
101. Gubin MM, Zhang X, Schuster H, Caron E, Ward JP, Noguchi T, et al. Checkpoint blockade cancer immunotherapy targets tumour-specific mutant antigens. *Nature.* (2014) 515:577–81. doi: 10.1038/nature13988
102. Jenkins RW, Barbie DA, Flaherty KT. Mechanisms of resistance to immune checkpoint inhibitors. *Br J Cancer.* (2018) 118:9–16. doi: 10.1038/bjc.2017.434
103. Zaretsky JM, Garcia-Diaz A, Shin DS, Escuin-Ordinas H, Hugo W, Hu-Lieskovan S, et al. Mutations associated with acquired resistance to PD-1 blockade in melanoma. *N Engl J Med.* (2016) 375:819–29. doi: 10.1056/NEJMoa1604958
104. Peng W, Chen JQ, Liu C, Malu S, Creasy C, Tetzlaff MT, et al. Loss of PTEN promotes resistance to T cell–mediated immunotherapy. *Cancer Discov.* (2016) 6:202–16. doi: 10.1158/2159-8290.CD-15-0283
105. Spranger S, Bao R, Gajewski TF. Melanoma-intrinsic β-catenin signalling prevents anti-tumour immunity. *Nature.* (2015) 523:231–5. doi: 10.1038/nature14404
106. Olson OC, Kim H, Quail DF, Foley EA, Joyce JA. Tumor-associated macrophages suppress the cytotoxic activity of antimitotic agents. *Cell Rep.* (2017) 19:101–13. doi: 10.1016/j.celrep.2017.03.038
107. Vargas FA, Furness AJ, Solomon I, Joshi K, Mekkaoui L, Lesko MH, et al. Fc-optimized anti-CD25 depletes tumor-infiltrating regulatory T cells and synergizes with PD-1 blockade to eradicate established tumors. *Immunity.* (2017) 46:577–86. doi: 10.1016/j.immuni.2017.03.013
108. O'Donnell JS, Long GV, Scolyer RA, Teng MW, Smyth MJ. Resistance to PD1/PDL1 checkpoint inhibition. *Cancer Treat Rev.* (2017) 52:71–81. doi: 10.1016/j.ctrv.2016.11.007
109. Syn NL, Teng MW, Mok TS, Soo RA. De-novo and acquired resistance to immune checkpoint targeting. *Lancet Oncol.* (2017) 18:e731–41. doi: 10.1016/S1470-2045(17)30607-1
110. Wang Y, Deng W, Li N, Neri S, Sharma A, Jiang W, et al. Combining immunotherapy and radiotherapy for cancer treatment: current challenges and future directions. *Front Pharmacol.* (2018) 9:185. doi: 10.3389/fphar.2018.00185
111. Ferris RL, Lenz HJ, Trotta AM, García-Foncillas J, Schulten J, Audhuy F, et al. Rationale for combination of therapeutic antibodies targeting tumor cells and immune checkpoint receptors: Harnessing innate and adaptive immunity through IgG1 isotype immune effector stimulation. *Cancer Treat Rev.* (2018) 63:48–60. doi: 10.1016/j.ctrv.2017.11.008
112. Liang H, Liu X, Wang M. Immunotherapy combined with epidermal growth factor receptor-tyrosine kinase inhibitors in non-small-cell lung cancer treatment. *Onco Targets Ther.* (2018) 11:6189–96. doi: 10.2147/OTT.S178497
113. Knudson KM, Hicks KC, Alter S, Schlom J, Gameiro SR. Mechanisms involved in IL-15 superagonist enhancement of anti-PD-L1 therapy. *J Immunother Cancer.* (2019) 7:82. doi: 10.1186/s40425-019-0551-y
114. Langan EA, Kümpers C, Graetz V, Perner S, Zillikens D, Terheyden P. Intralesional interleukin-2: a novel option to maximize response to systemic immune checkpoint therapy in loco-regional metastatic melanoma. *Dermatol Ther.* (2019) 32:e12901. doi: 10.1111/dth.12901
115. Soerensen MM, Ros W, Rodriguez-Ruiz ME, Robbrecht D, Rohrberg KS, Martin-Liberal J, et al. Safety, PK/PD, and anti-tumor activity of RO6874281, an engineered variant of interleukin-2 (IL-2v) targeted to tumor-associated fibroblasts via binding to fibroblast activation protein (FAP). *Am Soc Clin Oncol.* (2018) 36(Suppl. 15):e15155. doi: 10.1200/JCO.2018.36.15_suppl.e15155
116. Rady P, Cadet P, Bui T, Tyring S, Baron S, Stanton G, et al. Production of interferon gamma messenger RNA by cells of non-immune origin. *Cytokine.* (1995) 7:793–8. doi: 10.1006/cyto.1995.0095
117. Schaer D, Beckmann R, Dempsey J, Huber L, Forest A, Amaladas N, et al. The CDK4/6 inhibitor abemaciclib induces a T cell inflamed tumor microenvironment and enhances the efficacy of PD-L1 checkpoint blockade. *Cell Rep.* (2018) 22:2978–94. doi: 10.1016/j.celrep.2018.02.053
118. Sagiv-Barfi I, Kohrt HE, Czerwinski DK, Ng PP, Chang BY, Levy R. Therapeutic antitumor immunity by checkpoint blockade is enhanced by ibrutinib, an inhibitor of both BTK and ITK. *Proc Natl Acad Sci USA.* (2015) 112:E966–72. doi: 10.1073/pnas.1500712112
119. Hidalgo M, Gil M, Garcia-Carbonero R, Alvarez R, Laquente B, Moreno R, et al. First-in-human dose-escalation study of VCN-01, a selective oncolytic adenovirus with hyaluronidase activity in patients with advanced or metastatic cancer. *Eur J Cancer.* (2016) 69:S99–100. doi: 10.1016/S0959-8049(16)32895-7
120. Taylor MH, Rasco DW, Brose MS, Vogelzang NJ, Richey SL, Cohn AL, et al. A phase 1b/2 trial of lenvatinib plus pembrolizumab in patients with squamous cell carcinoma of the head and neck. *Am Soc Clin Oncol.* (2018) 36(Suppl. 15):6016. doi: 10.1200/JCO.2018.36.15_suppl.6016
121. Rizvi NA, Loo D, Baughman JE, Yun S, Chen F, Moore PA, et al. A phase 1 study of enoblituzumab in combination with pembrolizumab in patients with advanced B7-H3-expressing cancers. *Am Soc Clin Oncol.* (2016) 34(Suppl. 15):TPS3104. doi: 10.1200/JCO.2016.34.15_suppl.TPS3104
122. Lipson E, Long G, Tawbi H, Schadendorf D, Atkinson V, Maurer M, et al. 1302TiP CA224–047: a randomized, double-blind, phase II/III study of relatlimab (anti–LAG-3) in combination with nivolumab (anti–PD-1) versus nivolumab alone in previously untreated metastatic or unresectable melanoma. *Ann Oncol.* (2018) 29:mdy289.058. doi: 10.1093/annonc/mdy289.058
123. Sullivan RJ, Hong DS, Tolcher AW, Patnaik A, Shapiro G, Chmielowski B, et al. Initial results from first-in-human study of IPI-549, a tumor macrophage-targeting agent, combined with nivolumab in advanced solid tumors. *Am Soc Clin Oncol.* (2018) 36(Suppl. 15):3013. doi: 10.1200/JCO.2018.36.15_suppl.3013
124. Das R, Verma R, Sznol M, Boddupalli CS, Gettinger SN, Kluger H, et al. Combination therapy with anti–CTLA-4 and anti–PD-1 leads to distinct immunologic changes *in vivo*. *J Immunol.* (2015) 194:950–9. doi: 10.4049/jimmunol.1401686
125. Chin SM, Kimberlin CR, Roe-Zurz Z, Zhang P, Xu A, Liao-Chan S, et al. Structure of the 4–1BB/4–1BBL complex and distinct binding and functional properties of utomilumab and urelumab. *Nat Commun.* (2018) 9:4679. doi: 10.2210/pdb6mgp/pdb
126. Diab A, El-Khoueiry A, Eskens F, Ros W, Thompson J, Konto C, et al. A first-in-human (FIH) study of PF-04518600 (PF-8600) OX40 agonist in adult patients (pts) with select advanced malignancies. *Ann Oncol.* (2016) 27:359–78. doi: 10.1093/annonc/mdw378.08
127. Milhem M, Gonzales R, Medina T, Kirkwood JM, Buchbinder E, Mehmi I, et al. Abstract CT144: intratumoral toll-like receptor 9 (TLR9) agonist, CMP-001, in combination with pembrolizumab can reverse resistance to PD-1 inhibition in a phase Ib trial in subjects with advanced melanoma. *Cancer Res.* (2018) 78(Suppl. 13):CT144. doi: 10.1158/1538-7445.AM2018-CT144
128. Labadie BW, Bao R, Luke JJ. Reimagining IDO pathway inhibition in cancer immunotherapy via downstream focus on the tryptophan–kynurenine–aryl hydrocarbon axis. *Clin Cancer Res.* (2019) 25:1462–71. doi: 10.1158/1078-0432.CCR-18-2882
129. Massarelli E, William W, Johnson F, Kies M, Ferrarotto R, Guo M, et al. Combining immune checkpoint blockade and tumor-specific vaccine for patients with incurable human papillomavirus 16-related cancer: a phase 2 clinical trial. *JAMA Oncol.* (2019) 5:67–73. doi: 10.1001/jamaoncol.2018.4051
130. Schneider K, Grønhøj C, Hahn CH, von Buchwald C. Therapeutic human papillomavirus vaccines in head and neck cancer: a systematic review of current clinical trials. *Vaccine.* (2018) 36:6594–605. doi: 10.1016/j.vaccine.2018.09.027
131. Rice J, Ottensmeier CH, Stevenson FK. DNA vaccines: precision tools for activating effective immunity against cancer. *Nat Rev Cancer.* (2008) 8:108–20. doi: 10.1038/nrc2326

132. Krieg AM. CpG motifs in bacterial DNA and their immune effects. *Annu Rev Immunol.* (2002) 20:709–60. doi: 10.1146/annurev.immunol.20.100301.064842
133. Wang C, Dickie J, Sutavani RV, Pointer C, Thomas GJ, Savelyeva N. Targeting head and neck cancer by vaccination. *Front Immunol.* (2018) 9:830. doi: 10.3389/fimmu.2018.00830
134. Qureshi HA, Lee SM. Immunotherapy approaches beyond PD-1 inhibition: the future of cellular therapy for head and neck squamous cell carcinoma. *Curr Treat Options Oncol.* (2019) 20:31. doi: 10.1007/s11864-019-0630-9
135. Hinrichs CS, Doran SL, Stevanovic S, Adhikary S, Mojadidi M, Kwong ML, et al. A phase I/II clinical trial of E6 T-cell receptor gene therapy for human papillomavirus (HPV)-associated epithelial cancers. *Am Soc Clin Oncol.* (2017) 35(Suppl. 15):3009. doi: 10.1200/JCO.2017.35.15_suppl.3009
136. Papa S, Adami A, Metoudi M, Achkova D, van Schalkwyk M, Parente Pereira A, et al. A phase I trial of T4 CAR T-cell immunotherapy in head and neck squamous cancer (HNSCC). *Am Soc Clin Oncol.* (2018) 36(Suppl. 15):3046. doi: 10.1200/JCO.2018.36.15_suppl.3046
137. Okada S, Itoh K, Ishihara S, Shimada J, Kato D, Tsunezuka H, et al. Significance of PD-L1 expression in pulmonary metastases from head and neck squamous cell carcinoma. *Surg Oncol.* (2018) 27:259–65. doi: 10.1016/j.suronc.2018.04.007
138. Hirsch FR, McElhinny A, Stanforth D, Ranger-Moore J, Jansson M, Kulangara K, et al. PD-L1 immunohistochemistry assays for lung cancer: results from phase 1 of the blueprint PD-L1 IHC assay comparison project. *J Thorac Oncol.* (2017) 12:208–22. doi: 10.1016/j.jtho.2016.11.2228
139. Hanna GJ, Lizotte P, Cavanaugh M, Kuo FC, Shivdasani P, Frieden A, et al. Frameshift events predict anti–PD-1/L1 response in head and neck cancer. *JCI Insight.* (2018) 3:98811. doi: 10.1172/jci.insight.98811
140. Cristescu R, Mogg R, Ayers M, Albright A, Murphy E, Yearley J, et al. Pan-tumor genomic biomarkers for PD-1 checkpoint blockade–based immunotherapy. *Science.* (2018) 362:eaar3593. doi: 10.1126/science.aar3593
141. Chalmers ZR, Connelly CF, Fabrizio D, Gay L, Ali SM, Ennis R, et al. Analysis of 100,000 human cancer genomes reveals the landscape of tumor mutational burden. *Genome Med.* (2017) 9:34. doi: 10.1186/s13073-017-0424-2
142. Le DT, Durham JN, Smith KN, Wang H, Bartlett BR, Aulakh LK, et al. Mismatch repair deficiency predicts response of solid tumors to PD-1 blockade. *Science.* (2017) 357:409–13. doi: 10.1126/science.aan6733
143. Yarchoan M, Hopkins A, Jaffee EM. Tumor mutational burden and response rate to PD-1 inhibition. *N Engl J Med.* (2017) 377:2500–1. doi: 10.1056/NEJMc1713444

Conflict of Interest: The authors declare that the research was conducted in the absence of any commercial or financial relationships that could be construed as a potential conflict of interest.

frontiers in Oncology

ORIGINAL RESEARCH
published: 05 November 2019
doi: 10.3389/fonc.2019.01168

Psorachromene Suppresses Oral Squamous Cell Carcinoma Progression by Inhibiting Long Non-coding RNA GAS5 Mediated Epithelial-Mesenchymal Transition

Tong-Hong Wang[1,2,3†], *Yann-Lii Leu*[4,5,6†], *Chin-Chuan Chen*[1,4], *Tzong-Ming Shieh*[7], *Jang-Hau Lian*[8] *and Chi-Yuan Chen*[1,2*]

[1] Tissue Bank, Chang Gung Memorial Hospital, Tao-Yuan, Taiwan, [2] Research Center for Chinese Herbal Medicine, Graduate Institute of Health Industry Technology and Research Center for Food and Cosmetic Safety, College of Human Ecology, Chang Gung University of Science and Technology, Tao-Yuan, Taiwan, [3] Department of Hepato-Gastroenterology, Liver Research Center, Chang Gung Memorial Hospital, Tao-Yuan, Taiwan, [4] Graduate Institute of Natural Products, Chang Gung University, Tao-Yuan, Taiwan, [5] Chinese Herbal Medicine Research Team, Healthy Aging Research Center, Chang Gung University, Tao-Yuan, Taiwan, [6] Center for Traditional Chinese Medicine, Chang Gung Memorial Hospital, Tao-Yuan, Taiwan, [7] Department of Dental Hygiene, China Medical University, Taichung, Taiwan, [8] Genomic Medicine Core Laboratory, Chang Gung Memorial Hospital, Tao-Yuan, Taiwan

OPEN ACCESS

Edited by:
Cheng-Chia Yu,
Chung Shan Medical University, Taiwan

Reviewed by:
Yi Chiung Hsu,
National Central University, Taiwan
Hsifeng Tu,
National Yang-Ming University, Taiwan

***Correspondence:**
Chi-Yuan Chen
d49417002@gmail.com

[†] *These authors have contributed equally to this work*

Specialty section:
This article was submitted to Head and Neck Cancer, a section of the journal Frontiers in Oncology

Received: *23 August 2019*
Accepted: *17 October 2019*
Published: *05 November 2019*

Citation:
Wang T-H, Leu Y-L, Chen C-C, Shieh T-M, Lian J-H and Chen C-Y (2019) Psorachromene Suppresses Oral Squamous Cell Carcinoma Progression by Inhibiting Long Non-coding RNA GAS5 Mediated Epithelial-Mesenchymal Transition. Front. Oncol. 9:1168. doi: 10.3389/fonc.2019.01168

The extract of the seeds of *Psoralea corylifolia* Linn. (*P. corylifolia*) have been shown to display anti-tumor activity. However, the prospects of the active compounds from this plant in the treatment of oral squamous cell carcinoma (OSCC) remains unclear. In the present study, the antitumor effects of psorachromene, a flavonoid extracted from the seeds of *P. corylifolia*, were investigated using cells and animal models of OSCC; the downstream regulatory mechanisms were also elucidated. The results showed that psorachromene significantly repressed cell proliferation, migration, and invasiveness and increased the toxic effects of chemotherapeutic agents against OSCC cells. The repressive effects of psorachromene were attributable to the inhibition of EGFR-Slug signaling, and the induction of G2/M arrest and apoptosis in the OSCC cells. Additionally, we found that psorachromene induced the expression of tumor suppressor long non-coding ribonucleic acid (RNA) growth arrest-specific transcript 5 (GAS5) and the activation of its downstream anticancer mechanisms. Animal experiments also showed noticeable inhibition of tumor growth, without significant physiological toxicity. The findings indicate that psorachromene displays anti-tumor activity in OSCC, and warrants further investigation as a potential agent for clinical application.

Keywords: psorachromene, oral squamous cell carcinoma (OSCC), long non-coding RNA, growth arrest-specific transcript 5 (GAS5), epidermal growth factor receptor (EGFR)

INTRODUCTION

Oral cancer is the eleventh most common malignancy worldwide (1). In Taiwan, more than 4,700 people are diagnosed with oral cancer each year, and ∼2,200 people die from it. Among all types of oral cancer, oral squamous cell carcinoma (OSCC) is the most common, with an incidence of ∼90% (2). Smoking, drinking alcohol, and chewing tobacco or betel seeds are risk factors for OSCC (3–5).

Currently, the mainstay treatment for OSCC is surgical resection, with adjuvant chemotherapy or radiotherapy (6, 7). In addition, epidermal growth factor receptor (EGFR) and cyclooxygenase-2 (COX-2) inhibitors are also used in the treatment of OSCC (8, 9). However, the benefits of these therapies remain sub-optimal, and their side effects have a considerable impact on patients' quality of life. Therefore, oral cancer research continues to focus on the development of effective new treatment methods with minimal side effects.

Cancer-causing gene mutations are one of the major causes of OSCC (10–12). Previous studies have shown that over 75% of OSCC shows epidermal growth factor receptor (EGFR; also known as ErbB1 or HER1) overexpression; EGFR expression has shown a significantly positive association with the degree of malignancy (13–15). Therefore, inhibiting the growth of cancer cells by EGFR signaling inhibition is one of the current treatment strategies for OSCC (16, 17). Various EGFR inhibitors including anti-EGFR monoclonal antibodies (cetuximab and panitumumab) and small-molecule EGFR tyrosine kinase inhibitors (gefitinib, afatinib, and erlotinib) have been developed, and have demonstrated efficacy in OSCC (16, 18–20). However, only the monoclonal antibody cetuximab is currently approved for the treatment of OSCC; it has demonstrated significant inhibition of the progress of OSCC, with extension of survival (21, 22). Unfortunately, for reasons that are not fully clear, only ∼50% of patients respond to cetuximab (23, 24).

Traditional Chinese medicine (TCM) has long been used for the treatment of diseases in Asian countries (25, 26). Unlike Western medicine, TCM provides effective treatment options with relatively milder adverse effects (27–29). However, differences in the quality of TCM therapeutics and the levels of active ingredients usually result in variable therapeutic effects (30). In order to achieve more stable therapeutic effects, the active ingredients of many traditional Chinese medicinal materials have been purified and identified (31–33). The identified compounds can be used at lower doses with more specific therapeutic efficacy. Currently, many compounds extracted from TCM therapeutics, e.g., artemisinin, curcumin, resveratrol, and paclitaxel, which are used in the treatment of cancer have shown good efficacy (34–38). Among them, paclitaxel, camptothecin, and vinblastine, have also been approved for the treatment of various cancers, including lung cancer, liver cancer, and oral cancer (39).

Psoralea corylifolia L. is a TCM herb that is commonly used in Asian countries for the treatment of bacterial infections, inflammation, and cancer (40–44). *P. corylifolia* L. contains flavonoids such as bavachin, isobavachalcone, and neobavaisoflavone; polyphenols such as psoralidin, psoralen, and isopsoralen; and benzene ring compounds such as backuchiol; in addition, the herb has been found to have biological activity and various therapeutic effects (42). Psorachromene is an isoflavone component isolated from the fruit kernels of *P. corylifolia* L. (45). A few studies have investigated the mechanism of action of psorachromene. Recent reports indicate that psorachromene has anti-inflammatory effects that may inhibit inflammatory reactions caused by inducible NO synthase (iNOS) and cyclo-oxygenase (COX) expression induced by bacterial infection (46). However, there have been no studies on its anticancer effects. In this study, we investigated the anticancer activity of psorachromene in oral cancer, and studied its downstream regulatory mechanisms.

MATERIALS AND METHODS

Cell Lines and Culture Media

SAS is a human tongue squamous cell carcinoma cell line from the Japanese Collection of Research Bioresources (Tokyo, Japan) (47). OECM1 is a Taiwanese human gingival squamous carcinoma cell line; its derivation has been described in a previous study (47). Both cell lines were cultured in Dulbecco's modified Eagle's medium (DMEM) containing 10% fetal bovine serum (FBS), 1.2 g/L sodium bicarbonate, 0.5 mM sodium pyruvate, and 2.5 mM L-glutamine. The culture media, FBS, and chemical compounds were purchased from Life Technologies (Grand Island, NY, USA). The cells were cultured at 37°C in a humidified 5% CO_2 incubator.

Reagents and Antibodies

The crude materials of the *P. corylifolia* seed were purchased from Chuang Song Zong Pharmaceutical Co., Ltd (Kaohsiung, Taiwan). The dried seeds of *P. corylifolia* were infused in ethanol and were filtered to obtain the crude extract. The crude extract was partitioned in n-hexane/water (1:1). The n-hexane soluble extract was then fractionated by column chromatography on silica gel, eluting with n-hexane: ethylacetate to isolate psorachromene. The purity of psorachromene was determined by nuclear magnetic resonance analysis. Antibodies against vimentin, E-cadherin, slug, cleaved-PARP (cl-PARP, Asp214), and caspase 9 were obtained from Cell Signaling (Temecula, CA, USA). Antibodies against EGFR and β-actin were purchased from Santa Cruz Biotechnology (Santa Cruz, CA, USA). Prestained protein marker and TOOLSmart RNA extractor were purchased from BIOTOOLS (New Taipei City, Taiwan). The cisplatin and doxorubicin were purchased from Sigma-Aldrich (St. Louis, MO, USA), and the reagents for gel electrophoresis were purchased from Bio-Rad (Berkeley, CA, USA).

Cell Viability Assays

Cell viability was determined using the sulforhodamine B (SRB) assay by staining with trypan blue, as described previously (48, 49).

Terminal Deoxynucleotidyl Transferase dUTP Nick End Labeling (TUNEL) Assay

The apoptotic status of the treated cells was determined using a DeadEnd^{TM} Fluorometric TUNEL Assay Kit (Promega, Madison, WI) according to the manufacturers' protocol. In summary, the SAS cells were treated with psorachromene (50 μM) for 24 h and were then subjected to a terminal deoxynucleotidyl transferase dUTP nick end labeling (TUNEL) assay. The apoptotic cells (DAPI and TUNEL double stained cells) were enumerated using a fluorescence microscope (magnification, ×100). Cells in five different microscopic fields/dish were analyzed for each experiment.

Western Blotting

Cells were washed twice with phosphate-buffered saline (PBS), lysed in 200 μL of RIPA lysis buffer (Biotools Co. Ltd., Taiwan) containing protease inhibitors, and incubated on ice for 10 min. The samples were then centrifuged at 12,000 rpm for 30 min at 4°C, and the protein-containing supernatants were collected. The protein concentrations were determined using the Bio-Rad protein assay, and western blotting was performed as described previously (49).

Phenotypic Analysis for Clonogenic, Migration, and Invasion Ability

The clonogenic, migration, and invasion assays were performed as described previously (47).

Cell-Cycle Analysis

Cells were trypsinized, washed twice, and incubated in PBS containing 0.12% Triton X-100, 0.12 mmol/L EDTA, and 100 mg/mL ribonuclease A. Propidium iodide (50 μg/mL) was then added to each sample, and they were kept at 4°C for 20 min. Cell cycle distribution was then analyzed using flow cytometry (Beckman Coulter Epics Elite, Beckman, Inc.).

Whole-Transcriptome Sequencing

RNA extraction and whole-transcriptome sequencing was performed as described in a previous study (25).

Detection of lncRNA GAS5

RNA from the cells were isolated using a RNeasy mini kit (QIAGEN, Gaithersburg, MD, USA), according to the manufacturer's instructions. Two micrograms of RNA sample were subjected to reverse transcription (RT) using the reverse transcription kit (Applied Biosystems, Foster City, CA, USA). The expression of lncRNA GAS5 was detected by quantitative polymerase chain reaction (PCR) using the TaqMan gene expression assay (Applied Biosystems, Foster City, CA, USA), as described previously (50). Glyceraldehyde 3-phosphate dehydrogenase (GAPDH) was used as an internal control.

RNA Interference (RNAi)

Human lncRNA GAS5 were downregulated using a mixture of four small interfering RNAs (siRNAs) (ON-TARGETplus SMARTpool; Dharmacon, Lafayette, CO) as previously described (50). In summary, the four siRNAs targeting lncRNA GAS5 (GenBank accession no. NR_002578.2) covered the following: nucleotides 385-403 from the start codon (lncRNA GAS5-1: AGGCAGACCUGUUAUCCUA), nucleotides 248-266 (lncRNA GAS5-2: UGGAUGACUUGCUUGGGUA), nucleotides 567-585 (lncRNA GAS5-3: GAUGGAGUCUCAUGGCACA), and nucleotides 301-319 (lncRNA GAS5-4: AGGUAUGGAGAGUCGGCUU). Transfection was performed using the Dharmafect 1 transfection reagent (Dharmacon) according to the manufacturer's instructions.

In vivo Tumor Xenograft Study

The *in vivo* antitumor activity of psorachromene against SAS cells was studied using 6-week-old nude BALB/c nu/nu male mice. SAS cells (5×10^5) were subcutaneously implanted in the right flank of the mice on day 0. The mice were then randomized

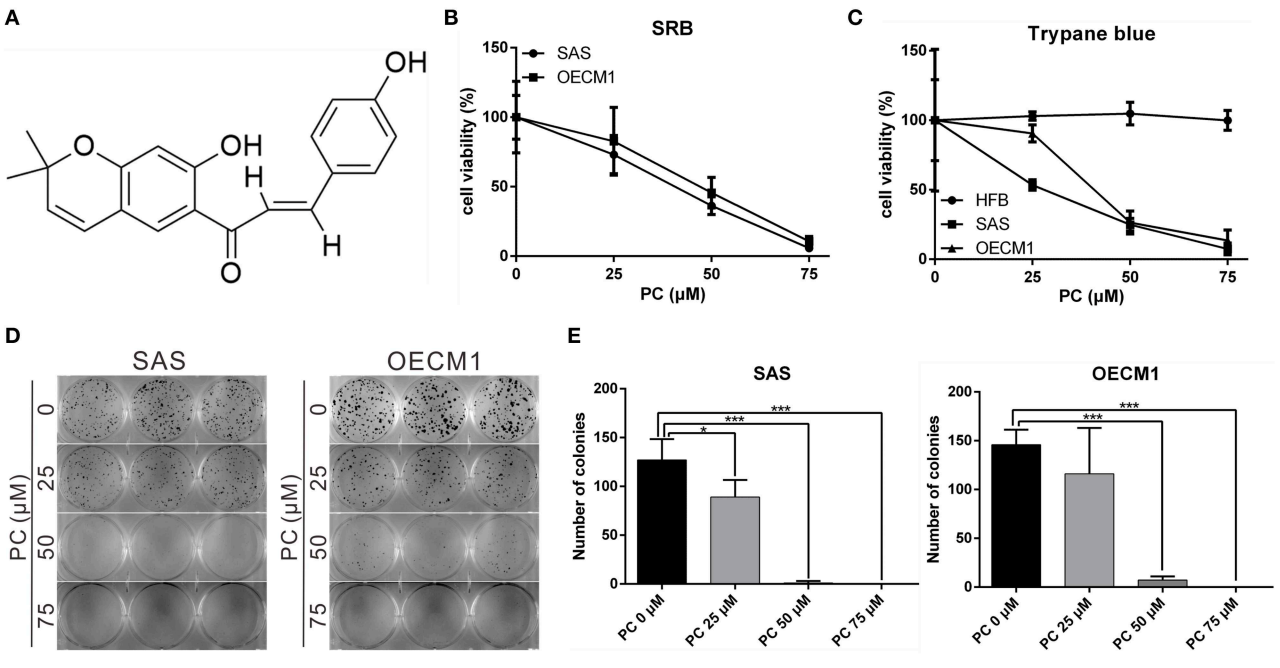

FIGURE 1 | Inhibition of the proliferation of OSCC cells by psorachromene. **(A)** Chemical structure of psorachromene. SAS and OECM1 cells were treated with different concentrations of psorachromene or vehicle (DMSO), and the cell proliferation status was analyzed using the SRB assay **(B)**, trypan blue staining assay **(C)**, and colony formation assay **(D,E)**. The results are the mean of three independent experiments. Significant differences vs. the control groups, $^{*}p < 0.05$, $^{***}p < 0.001$.

on day 7 into vehicle control and treatment groups of six animals each. Psorachromene and cisplatin were administered intraperitoneally thrice weekly, with 100 μL of psorachromene (25 mg/kg of body weight), cisplatin (2 mg/kg), or an equal volume of dimethyl sulfoxide (DMSO), which served as a control. The tumor volume was evaluated every 2 days using calipers, based on the following formula: tumor volume = length × width^2/2. Their body weights and food consumption were also determined to evaluate apparent signs of toxicity. The tumor-bearing mice were weighed and sacrificed on day 22 for assaying the tumor biology. All animal experiments were performed in accordance with the guidelines for the Animal Care Ethics Commission of the Chang Gung Memorial Hospital, under an approved animal protocol (IACUC approval no. 2018031301).

Immunohistochemistry

The tumors were fixed in formalin and embedded in paraffin. Consecutive 2-μm-thick sections were obtained from the paraffin-embedded tissue blocks, and were floated onto glass slides. The slide-mounted tissue sections were subjected to immunohistochemical staining as described previously (51).

Statistics

All data have been presented as means ± standard deviations (SD). The Student's *t*-test was employed for comparison, and all analyses were performed using the Statistical Package for the Social Sciences version 12.0 (SPSS, Inc.). Differences between the variables were considered significant for *p*-values of > 0.05.

RESULTS

Psorachromene Inhibited the Growth of OSCC Cells and Promoted Their Apoptosis

Psorachromene is a flavonoid extracted from the seeds of *P. corylifolia* L. (**Figure 1A**). In this study, we treated OSCC cells and human fibroblast cell lines with different concentrations of psorachromene and analyzed the cell proliferation status using Sulforhodamine B (SRB) assay to determine whether psorachromene has inhibitory activity on OSCC. The results showed that psorachromene could significantly inhibit the growth of SAS and OECM1 cells starting from concentrations of 25 μM; the inhibitory effect became more significant with increasing psorachromene concentrations (**Figure 1B**). Similar results were obtained on the trypan blue staining assay.

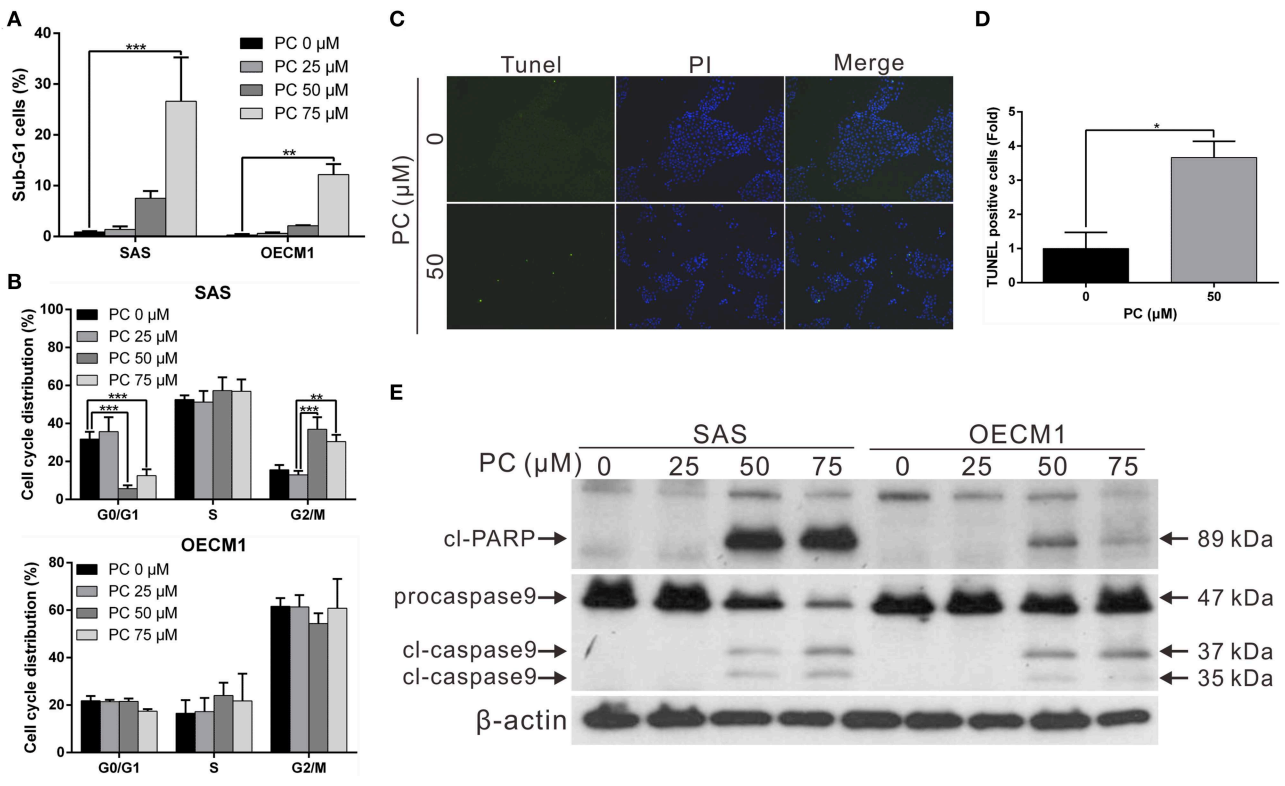

FIGURE 2 | Inhibition of cell cycle progression and promotion of apoptosis in OSCC cells by psorachromene. **(A,B)** Effect of psorachromene on cell cycle progression in SAS and OECM1 cells. The cells were treated with vehicles or different concentrations of psorachromene for 24 h. Cell cycle distribution was analyzed by flow cytometry. **(C)** SAS cells were treated with or without psorachromene, and cell apoptosis was determined using a terminal deoxynucleotidyl transferase dUTP nick end labeling (TUNEL) assay. Green punctate staining (white arrows) represents TUNEL-positive cells. Apoptotic cells were identified as DAPI and TUNEL double-stained cells. Magnification: 100×. Quantitative results seen in **(D)**. **(E)** Western blot analysis showing the effect on caspase 9 and PARP activity in OSCC cells after 48 h of psorachromene treatment. $^*p < 0.05$, $^{**}p < 0.01$, $^{***}p < 0.001$.

Psorachromene significantly inhibited the growth of SAS and OECM1 cells in a dose dependent manner. However, no inhibitory effect was observed on the growth of human fibroblast cell line HFB (**Figure 1C**). This indicated that psorachromene selectively inhibits the growth in OSCC cells without significant toxicity to normal cells. We also evaluated the impact of psorachromene on the colony forming ability of OSCC. The results showed significant inhibitory activity in a dose-dependent manner. At a concentration of 50 μM, psorachromene inhibited the colony forming ability of OSCC cells by more than 90% (**Figures 1D,E**), confirming its inhibitory activity on the growth of OSCC cells.

To determine the mechanism of inhibition of OSCC, we further compared the cell cycle progression between cells treated and not treated with psorachromene. Those treated with psorachromene were found to have been arrested in the G2 phase, their numbers in the sub-G1 phase were significantly higher compared to the control group (**Figures 2A,B**). These findings suggested that psorachromene inhibits cell cycle progression and promotes cell apoptosis. The results of the TUNEL assay also demonstrated that the number of apoptotic cells in the psorachromene treatment group were significantly higher compared with the control group (**Figures 2C,D**). Furthermore, the results of western blotting analysis confirmed the activation of caspase-9 and the cleavage of poly (ADP-ribose) polymerases (PARPs) by psorachromene, indicating that it promotes cell apoptosis by activating apoptosis-related proteins (**Figure 2E**).

Psorachromene Inhibits the Migration and Invasiveness of OSCC

Invasion and metastasis are the major contributors to the refractory nature of cancer. We conducted a wound-healing assay to evaluate whether psorachromene may affect cell migration; this was performed to further evaluate the potential of psorachromene in inhibiting metastasis and invasiveness in OSCC cells. The results showed that at a concentration of 25 μM, psorachromene significantly inhibited cell migration ability, and the inhibitory effects increased with the concentration of psorachromene. At a concentration of 75 μM, psorachromene inhibited the migration ability of SAS and OECM cells by 51.3 and 19.1%, respectively (**Figures 3A,B**). Furthermore, the invasion assay demonstrated that psorachromene may inhibit cell invasion by up to 83.7% at a concentration of 75 μM (**Figures 3C,D**).

Psorachromene Inhibits Epithelial-Mesenchymal Transition (EMT)

Epithelial-mesenchymal transition (EMT) is an important process in cancer cell metastasis, that weakens intercellular adhesions and facilitates metastasis. To determine whether

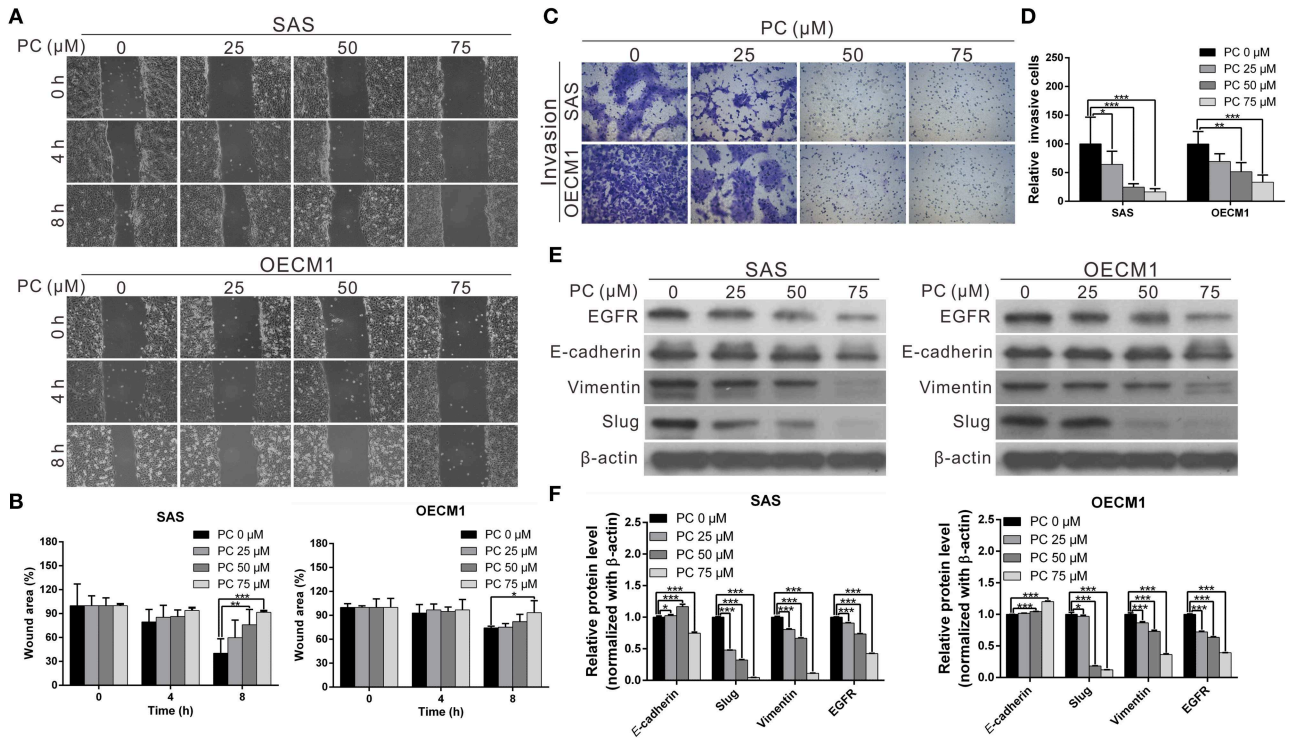

FIGURE 3 | Inhibition of cell metastasis ability in OSCC by psorachromene by inhibition of the progression of epithelial-mesenchymal transition. **(A)** The effect of psorachromene on the wound-healing ability of SAS and OECM1 cells. Quantitative results are seen in **(B)**. **(C,D)** The effect of psorachromene on the invasiveness of SAS and OECM1 cells. **(E)** Western blotting was used to examine the levels of EMT regulatory proteins in OSCC cells treated with psorachromene for 48 h. The quantified results are shown in (**F**). $^{*}p < 0.05$, $^{**}p < 0.01$, $^{***}p < 0.001$.

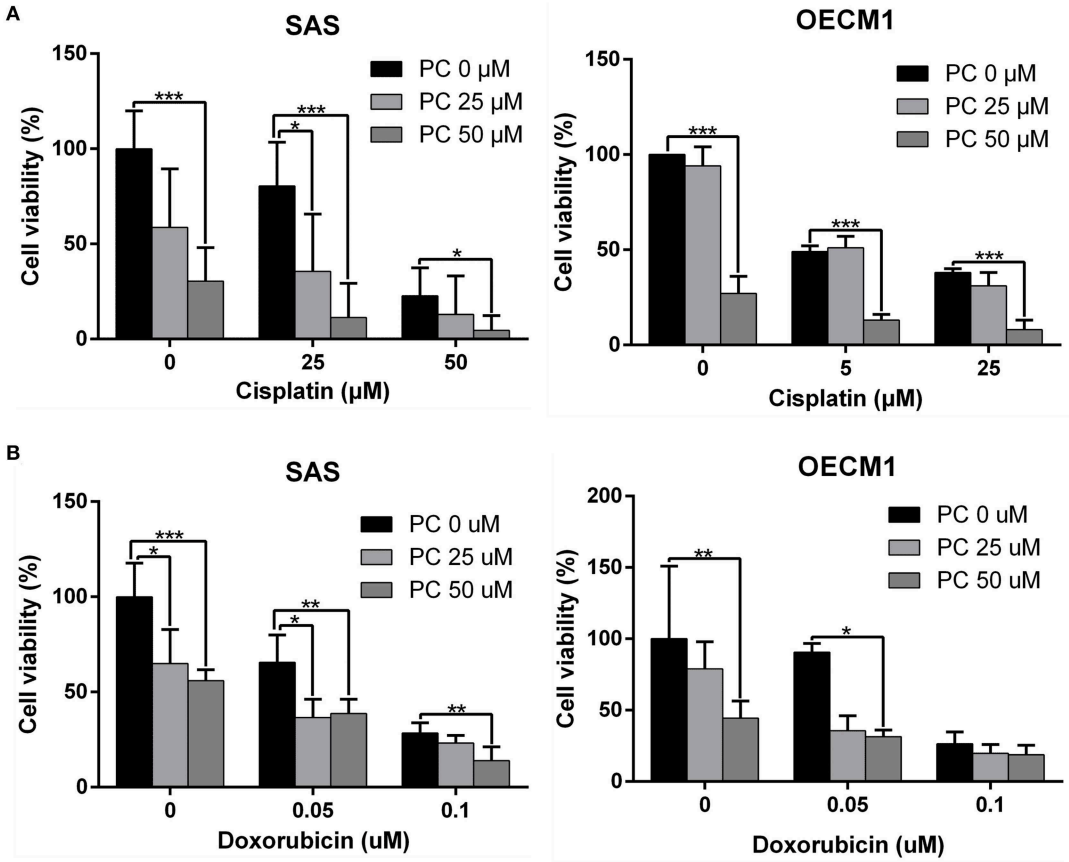

FIGURE 4 | Psorachromene combined with cisplatin and doxorubicin has additive effect. The effects of psorachromene combined with cisplatin and doxorubicin on proliferation of SAS **(A)** and OECM1 **(B)** cells. $^{*}p < 0.05$, $^{**}p < 0.01$, $^{***}p < 0.001$. All experiments were performed in triplicate.

psorachromene regulates EMT when inhibiting OSCC migration and invasion abilities, we performed western blotting to analyze the effects of psorachromene on EMT associated proteins. The results indicated that the expression of EMT-promoting proteins such as vimentin and slug was significantly lower in psorachromene-treated cells compared with the control group. However, the expression of E-cadherin did not change significantly (**Figures 3E,F**), suggesting that psorachromene may inhibit OSCC migration and invasion by inhibiting EMT.

Slug is a downstream gene regulated by the EGFR signaling pathway. We also evaluated whether psorachromene affects EGFR expression, and found its expression in psorachromene-treated cells to be significantly lower compared to the control group (**Figures 3E,F**). The results indicated that psorachromene may inhibit the expression of slug, and the progression of EMT by downregulating EGFR expression.

Psorachromene May Enhance the Therapeutic Effects of Cisplatin and Doxorubicin on OSCC

Cisplatin and doxorubicin are the commonly used chemotherapeutic drugs in the treatment of OSCC (52–54). In order to determine whether combining psorachromene with these drugs may improve their therapeutic effects on OSCC, we administered psorachromene, cisplatin, and doxorubicin alone, or in combination to the OSCC cells; we also evaluated its inhibitory effects on the growth of these cells. Cisplatin and doxorubicin alone had an inhibitory effect on OSCC; however, combination with psorachromene significantly enhanced the inhibition of OSCC. Compared to cisplatin or doxorubicin alone, the combination with psorachromene enhanced the toxicity on OSCC cells by up to 3.3-fold (**Figures 4A,B**). The combination index also demonstrated the additive effect of psorachromene in combination with cisplatin and doxorubicin (**Table 1**).

Psorachromene Inhibits Tumor Growth in Mice

The anticancer effects of psorachromene *in vivo* were verified using a mouse xenograft model; the effects of psorachromene on tumor growth in mice were similar to those of the cell experiments. The tumor growth rate was significantly reduced in mice treated with psorachromene. After 2 weeks of administering the drug, the tumor volume in the psorachromene-treated group was reduced by ∼75.5% compared with the control group (**Figures 5A,B**), and the tumor inhibitory effect was equivalent to that of the cisplatin-treated group (84.6%).

In addition, there were no significant differences in body weight between the psorachromene-treated and control groups (**Figure 5C**), indicating that psorachromene may not have significant physiological toxicity.

In addition, we analyzed the expression of EGFR and EMT-related proteins including slug, vimentin, and E-cadherin in murine tumor tissues using immunohistochemical staining, and found that psorachromene may significantly inhibit the expression of EGFR and EMT-promoting proteins (**Figure 5D**). The results of this experiment were identical to those of cellular experiments, suggesting that psorachromene may inhibit EMT.

Psorachromene May Inhibit the Activation of Signaling Pathways Associated With Cell Growth and Extracellular Structure Organization

To understand its anticancer mechanisms of action, we treated SAS and OECM1 cell lines with psorachromene, and performed whole-transcriptome sequencing to identify the genes and signaling pathways that may be regulated by psorachromene. Heatmap analysis showed that after psorachromene treatment, gene expression was significantly altered compared with the control group (**Figure 6A**). We further performed ingenuity pathway analysis, and found that psorachromene mainly regulates the LKB1 and ErbB/EGFR signaling pathways (**Figure 6B**), affects the energy metabolism of cells, and the composition and generation of the extracellular matrix, thereby inhibiting their growth and metastasis.

Psorachromene Exerts Anticancer Effects by Inducing the Expression of Long Non-coding RNA GAS5

Previous studies have confirmed that long non-coding RNAs (lncRNAs) play an important role in cell physiological regulation, and drug responses. To understand the role of lncRNAs in the anti-OSCC mechanisms of action of psorachromene, we analyzed the previously-mentioned transcriptome sequencing data, and found that 12 lncRNAs demonstrated a higher than 2-fold change in expression after psorachromene treatment, compared to the control group (**Figure 6C**). Among these lncRNAs, growth arrest-specific transcript 5 (GAS5) has recently been discovered to suppress cancer. It has been shown to inhibit the growth and metastasis of OSCC by regulating the miR-21/PTEN axis. To confirm the regulatory relation between psorachromene and GAS5, we performed real-time reverse transcriptase-PCR to determine the expression of GAS5 in OSCC cells. The results indicated that the expression of GAS5 in SAS and OECM1 cells treated with psorachromene was significantly higher than that of the control group (**Figure 6D**); this indicates that psorachromene may inhibit the growth and metastasis of OSCC by inducing GAS5 mediated anticancer mechanisms.

We performed a rescue assay to further verify the mentioned conditions. The results showed that psorachromene significantly inhibited the growth and migration of OSCC cells. After silencing GAS5 expression, we found that the inhibitory effects of psorachromene on OSCC cells were attenuated (**Figures 7A–D**); this indicated that the anti-OSCC action of psorachromene is partly achieved by regulating the lncRNA-GAS5 anticancer pathway.

TABLE 1 | The combination index.

	PC (μM)	DOX (μM)	CI
SAS	25	0.05	0.68011
	25	0.1	0.50582
	50	0.05	1.04119
	50	0.1	0.84218
OECM1	25	0.05	0.79836
	25	0.1	1.18195
	50	0.05	1.51916
	50	0.1	1.84227
	PC (μM)	**CIS (μM)**	**CI**
SAS	25	25	0.99174
	25	50	0.63005
	50	25	0.96329
	50	50	0.75840
OECM1	25	5	1.93719
	25	25	0.84726
	50	5	0.84689
	50	25	0.76593

DISCUSSION

Psorachromene is a flavonoid component of *P. corylifolia* L., accounting for 0.0016% of the total extract from the seeds of *P. corylifolia* L (55). Current understanding on the biological functions of psorachromene is limited. Only a few studies have reported on its anti-inflammatory activity, which may inhibit inducible nitric oxide synthase (iNOS) and COX expression induced by lipopolysaccharide (LPS), thereby inhibiting inflammatory reaction (46). However, no studies have evaluated its anticancer effects. In this study, we investigated the inhibitory activity of psorachromene on OSCC, and found that it significantly inhibited the growth, migration, and invasiveness of OSCC cells, and suppressed EMT by inducing the expression of lncRNA-GAS5. The results of our animal experiments also showed that it may significantly inhibit the growth of tumor cells and the expression of EMT-associated proteins. To the best our knowledge, this is the first study to demonstrate that psorachromene regulates lncRNAs to exert its antitumor effects.

Previous studies have shown that ∼80% of OSCC over-express EGFR; this leads to uncontrolled cell growth and enhances the metastatic ability of the cells (13, 56). It also enhances the resistance of OSCC to chemotherapeutic drugs including, cisplatin, 5-fluorouracil (5FU), and doxorubicin (57–59). Previous studies have also confirmed that the use of the EGFR inhibitor gefitinib in combination with cisplatin enhanced the therapeutic effects of the latter on

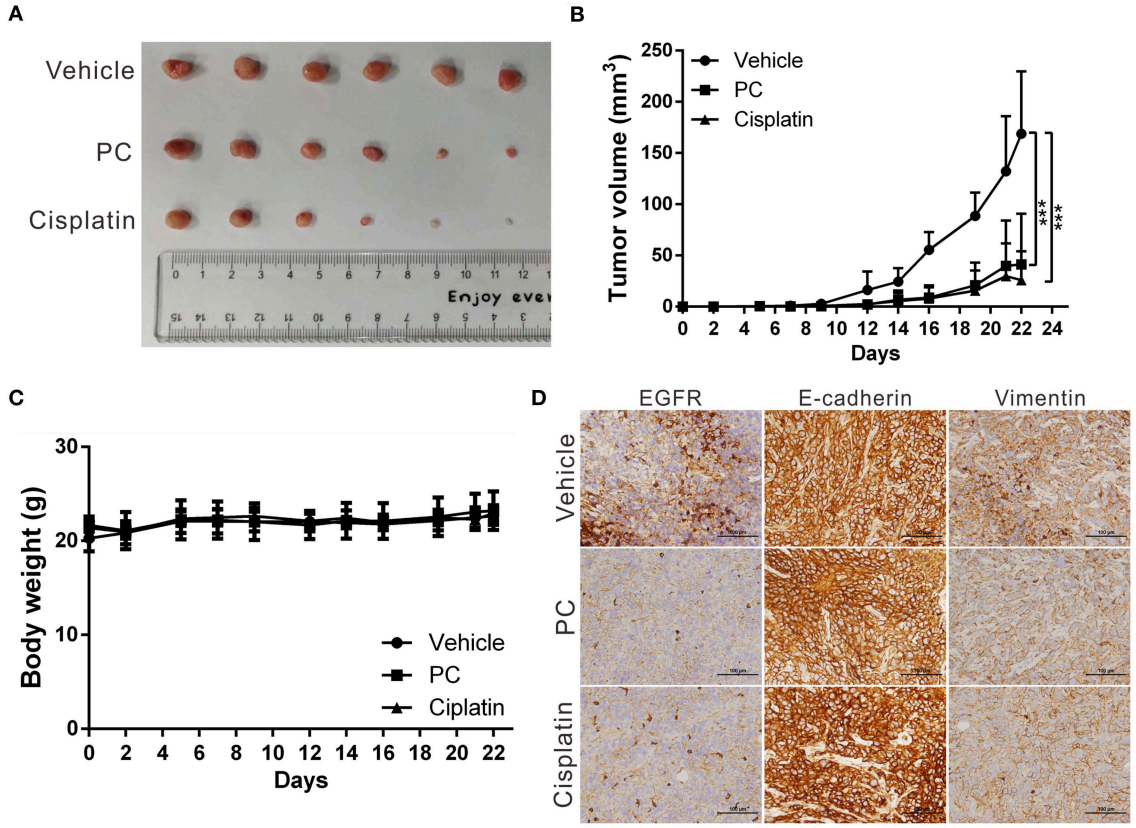

FIGURE 5 | Psorachromene inhibits tumor growth in mice. **(A)** A total of 5×10^6 SAS cells were inoculated into nude mice ($n = 6$). Representative images show the tumor xenografts at 3 weeks after implantation. Psorachromene significantly reduced tumor growth. **(B)** Tumor volumes were calculated every 3 days after injection. The volume of each tumor was calculated as follows: length $\times$ width^2 $\times$ 0.5. Bars indicate S.D. $^{***}p < 0.001$. **(C)** Body weights were calculated every 3 days after injection. **(D)** Immunohistochemical staining represents the effect of psorachromene on the expression of EGFR and EMT associated proteins in mice xenograft tumors. Magnification: 400×.

OSCC (20). This study demonstrated similar results. In addition to the inhibition of EGFR expression, psorachromene has synergistic activity with cisplatin and doxorubicin in the treatment of OSCC, with no significant physiological toxicities. Therefore, psorachromene has considerable potential for use as a therapeutic adjuvant in the treatment of OSCC.

To identify the genes and anticancer signaling pathways that may be regulated by psorachromene, we performed whole-transcriptome sequencing that examined the gene expression profiling of psorachromene in treated and untreated cells. The results showed that psorachromene mainly regulates the expression of genes associated with cell growth, extracellular matrix composition, and inflammation, among others, thereby inhibiting the growth and metastasis of OSCC cells; this was consistent with the results observed on cell functional assay. The inhibitory effect of psorachromene on the Erb-1 pathway indicates that it has considerable potential in the treatment of cancers that overexpress EGFR (including cancers of the breast and liver); it may also synergize with other anticancer drugs to enhance their therapeutic efficacy.

This study revealed that psorachromene induces lncRNA-GAS5 expression, which is a known anticancer lncRNA, and participates in the regulation of many important physiological processes, including cell growth, apoptosis, cell cycle progression, and EMT (60, 61). The low expression of GAS5 is closely related to the poor prognosis and chemoresistance of many cancers (62–65). Overexpression of GAS5 could enhance the inhibitory effect of Gefitinib on EGFR phosphorylation and its downstream signaling activation, while enhancing the sensitivity of lung cancer cells to EGFR-TKI (66). In addition, the chemotherapeutic drug, Lapatinib, can also enhance the response of breast cancer cells to trastuzumab by inducing GAS5 expression (67). Some studies have also suggested that GAS5 is significantly downregulated in OSCC cells, and that GAS5 expression may inhibit the growth and metastasis of OSCC by regulating the miR-21/PTEN axis (68). In this study, we found that psorachromene may induce GAS5 expression. It is speculated that the inhibitory effects of psorachromene on OSCC are partly attributable to GAS5-mediated anticancer mechanisms. Moreover, this result also shows the potential of psorachromene as a

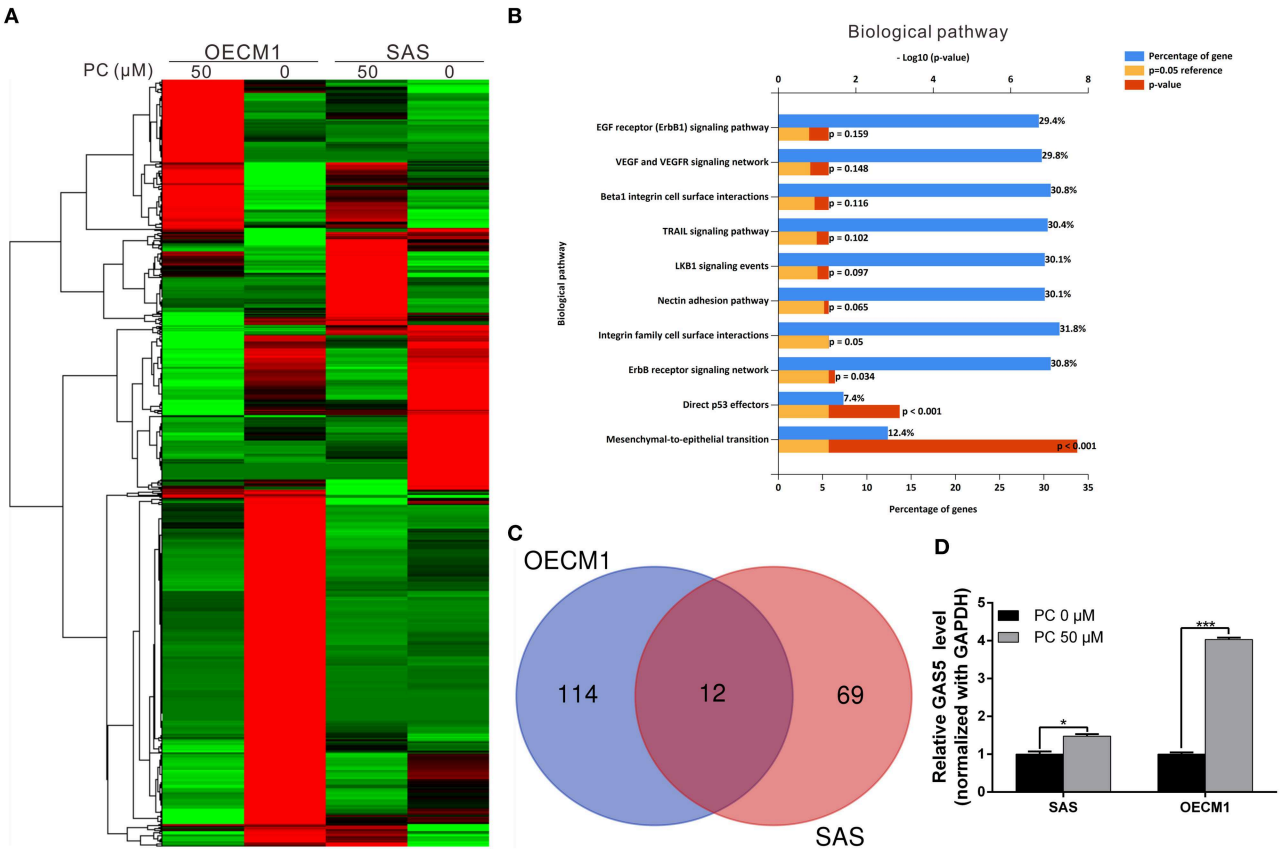

FIGURE 6 | Psorachromene-induced regulation of gene expression related to cell growth and extracellular structure organization. **(A)** Heatmap comparing significantly different expression of genes in SAS and OECM1 cells treated with or without psorachromene. The bar charts represent the enriched biological pathways **(B)** associated with the differentially expressed genes after psorachromene treatment. **(C)** The whole-transcriptome sequencing data shows that 12 lncRNAs manifested higher than a 2-fold change in expression after psorachromene treatment in both cell lines. **(D)** SAS and OECM1 cells were treated with psorachromene for 48 h, and GAS5 expression was analyzed using quantitative real-time RT-PCR. $^{*}p < 0.05$, $^{***}p < 0.001$.

therapeutic adjuvant that enhances the sensitivity of cancer cells to chemotherapeutic drugs by inducing the expression of GAS5.

Previous studies have demonstrated that long non-coding RNAs are involved in the regulation of a wide range of gene expression or protein stability. However, recent studies have shown that GAS5 does not regulate EGFR expression (66). We speculate that psorachromene regulates GAS5 and EGFR expression through two independent mechanisms; however, the detailed regulatory mechanism is yet to be delineated. In addition, the results of whole-transcriptome sequencing analysis showed that numerous lncRNAs are also regulated by psorachromene; the role of these lncRNAs in the anticancer mechanisms of psorachromene warrant further research.

In cell cycle analysis related to psorachromene treatment, the distribution of cell cycle between SAS and OECM1 cells is quite different. The inhibitory effect of psorachromene on SAS cells is better than that of OECM1. We speculated that the anti-OSCC effect of psorachromene may be induced by specific receptors. The genetic background difference between cells leads to the differences in receptor expression, which affect the anti-OSCC effect of psorachromene. However, the receptor that is targeted by psorachromene to achieve its anticancer mechanism and its detailed downstream regulation mechanism still need to be clarified to improve the clinical applicability of psorachromene.

The concentrations of psorachromene in *P. corylifolia* L. are not high; in addition, it has a simple structure. Therefore, psorachromene is mainly synthesized chemically for commercial formulations. Structural modifications may be introduced in the future to increase its anticancer activity and intracellular availability. In this study, we demonstrated the potential anticancer activity of psorachromene using cell and animal experiments; we also found that it affects certain relevant regulatory pathways. The small-molecule compounds that are commonly used in clinical practice only block specific carcinogenic pathways; in contrast, psorachromene has a wide range of targets. In addition, the animal experiments did not demonstrate significant differences in physiological toxicity compared to these molecules. In view of these findings, psorachromene holds

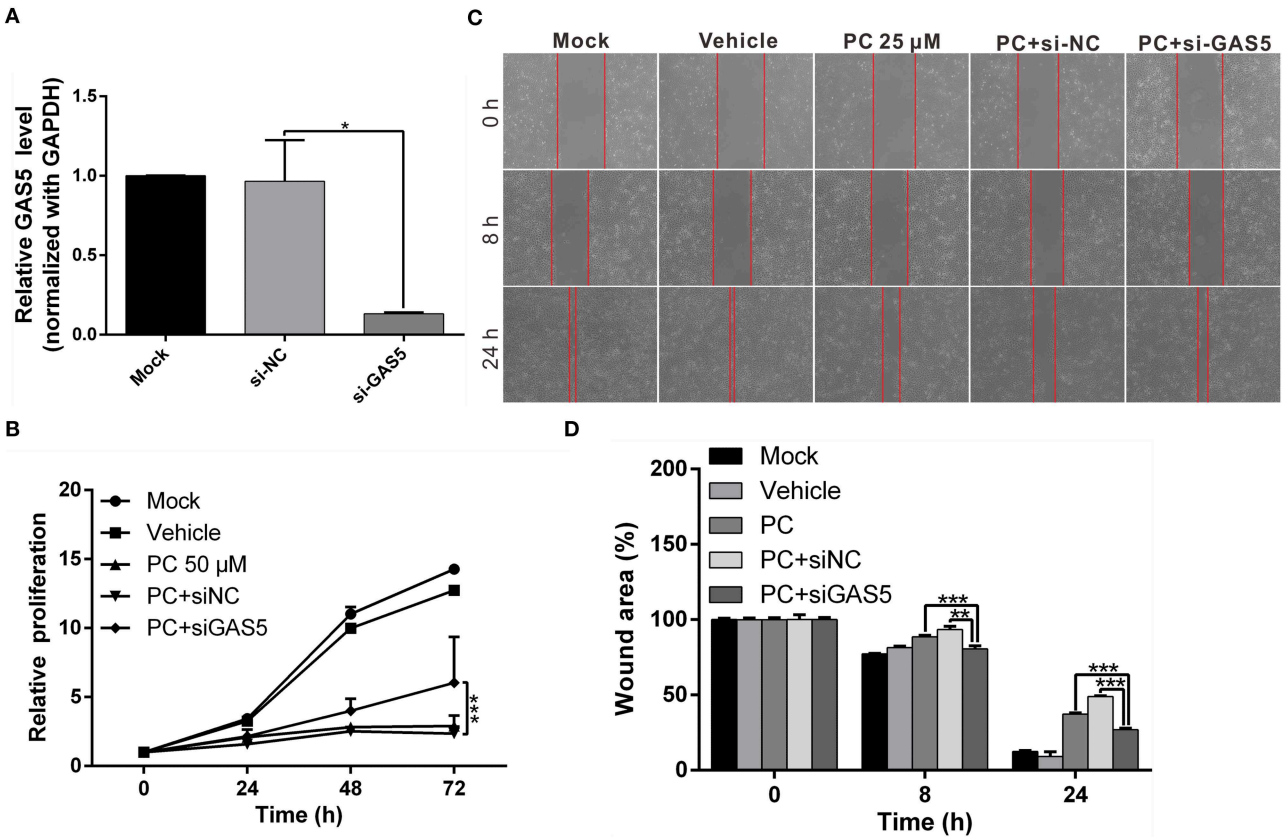

FIGURE 7 | The anticancer effect of psorachromene is exerted by inducing expression of lncRNA-GAS5. **(A)** Real-time PCR analysis shows the effect of siRNA treatments on the expression of GAS5 in OECM1 cells. GAPDH served as an internal control. **(B,C)** The inhibitory effects of psorachromene on cell proliferation and migration were significantly reversed by treatment with GAS5 siRNA (50 nM) in the OECM1 cells. The quantitative cell migration result was shown in **(D)**. $^{*}p < 0.05$, $^{**}p < 0.01$, $^{***}p < 0.001$.

promise as a new therapeutic agent for OSCC. Further studies with larger sample sizes are needed to validate our findings.

DATA AVAILABILITY STATEMENT

The data for this manuscript has been uploaded to: https://www.ncbi.nlm.nih.gov/bioproject/PRJNA562818.

ETHICS STATEMENT

The animal study was reviewed and approved by Animal Care Ethics Commission of the Chang Gung Memorial Hospital (IACUC approval no. 2018031301).

AUTHOR CONTRIBUTIONS

C-YC, T-HW, and Y-LL contributed to the conception and design of the study. C-YC, T-HW, Y-LL, C-CC, T-MS, and J-HL performed the experiments and statistical analyses. T-HW and C-YC prepared the first draft of the manuscript. All authors contributed to manuscript revision and have read and approved the submitted version.

FUNDING

This work was partially supported by the Ministry of Science and Technology, Taiwan (grant MOST 107-2314-B-182A-140-MY3) and the Chang Gung Medical Research Program of Taiwan (grant CMRPG3H1001 and CMRPF1H0012).

ACKNOWLEDGMENTS

The authors would like to thank the staff of the Tissue Bank and Genomic Medicine Core Laboratory at the Chang Gung Memorial Hospital, Lin-Kou, Taiwan for the excellent tissue processing and data analysis support.

REFERENCES

1. Ghantous Y, Abu Elnaaj I. Global incidence and risk factors of oral cancer. *Harefuah*. (2017) 156:645–9.
2. Bagan J, Sarrion G, Jimenez Y. Oral cancer: clinical features. *Oral Oncol.* (2010) 46:414–7. doi: 10.1016/j.oraloncology.2010.03.009
3. Nagler R, Dayan D. The dual role of saliva in oral carcinogenesis. *Oncology.* (2006) 71:10–7. doi: 10.1159/000100445
4. Chen YJ, Chang JT, Liao CT, Wang HM, Yen TC, Chiu CC, et al. Head and neck cancer in the betel quid chewing area: recent advances in molecular carcinogenesis. *Cancer Sci.* (2008) 99:1507–14. doi: 10.1111/j.1349-7006.2008.00863.x
5. Zygogianni AG, Kyrgias G, Karakitsos P, Psyrri A, Kouvaris J, Kelekis N, et al. Oral squamous cell cancer: early detection and the role of alcohol and smoking. *Head Neck Oncol.* (2011) 3:2. doi: 10.1186/1758-3284-3-2
6. Huang SH, O'sullivan B. Oral cancer: current role of radiotherapy and chemotherapy. *Med Oral Patol Oral Cir Bucal.* (2013) 18:e233–40. doi: 10.4317/medoral.18772
7. Gharat SA, Momin M, Bhavsar C. Oral squamous cell carcinoma: current treatment strategies and nanotechnology-based approaches for prevention and therapy. *Crit Rev Ther Drug Carrier Syst*. (2016) 33:363–400. doi: 10.1615/CritRevTherDrugCarrierSyst.2016016272
8. Hamakawa H, Nakashiro K, Sumida T, Shintani S, Myers JN, Takes RP, et al. Basic evidence of molecular targeted therapy for oral cancer and salivary gland cancer. *Head Neck.* (2008) 30:800–9. doi: 10.1002/hed.20830
9. Agnihotri NS, Astekar M. The role of novel prognostic markers PROX1 and FOXC2 in carcinogenesis of oral squamous cell carcinoma. *J Exp Ther Oncol.* (2018) 12:171–84.
10. Choi S, Myers JN. Molecular pathogenesis of oral squamous cell carcinoma: implications for therapy. *J Dent Res.* (2008) 87:14–32. doi: 10.1177/154405910808700104
11. Ramos-Garcia P, Ruiz-Avila I, Gil-Montoya JA, Ayen A, Gonzalez-Ruiz L, Navarro-Trivino FJ, et al. Relevance of chromosomal band 11q13 in oral carcinogenesis: an update of current knowledge. *Oral Oncol.* (2017) 72:7–16. doi: 10.1016/j.oraloncology.2017.04.016
12. Lindemann A, Takahashi H, Patel AA, Osman AA, Myers JN. Targeting the DNA damage response in OSCC with TP53 mutations. *J Dent Res.* (2018) 97:635–44. doi: 10.1177/0022034518759068
13. Kimura I, Kitahara H, Ooi K, Kato K, Noguchi N, Yoshizawa K, et al. Loss of epidermal growth factor receptor expression in oral squamous cell carcinoma is associated with invasiveness and epithelial-mesenchymal transition. *Oncol Lett.* (2016) 11:201–7. doi: 10.3892/ol.2015.3833
14. Xie X, Wang Z, Chen F, Yuan Y, Wang J, Liu R, et al. Roles of FGFR in oral carcinogenesis. *Cell Prolif.* (2016) 49:261–9. doi: 10.1111/cpr.12260
15. Huang SF, Chien HT, Cheng SD, Chuang WY, Liao CT, Wang HM. EGFR copy number alterations in primary tumors, metastatic lymph nodes, and recurrent and multiple primary tumors in oral cavity squamous cell carcinoma. *BMC Cancer.* (2017) 17:592. doi: 10.1186/s12885-017-3586-9
16. Soria JC, Felip E, Cobo M, Lu S, Syrigos K, Lee KH, et al. Afatinib versus erlotinib as second-line treatment of patients with advanced squamous cell carcinoma of the lung (LUX-Lung 8): an open-label randomised controlled phase 3 trial. *Lancet Oncol.* (2015) 16:897–907. doi: 10.1016/S1470-2045(15)00006-6
17. Fujiwara T, Eguchi T, Sogawa C, Ono K, Murakami J, Ibaragi S, et al. Carcinogenic epithelial-mesenchymal transition initiated by oral cancer exosomes is inhibited by anti-EGFR antibody cetuximab. *Oral Oncol.* (2018) 86:251–7. doi: 10.1016/j.oraloncology.2018.09.030
18. Cohen RB. Current challenges and clinical investigations of epidermal growth factor receptor (EGFR)- and ErbB family-targeted agents in the treatment of head and neck squamous cell carcinoma (HNSCC). *Cancer Treat Rev.* (2014) 40:567–77. doi: 10.1016/j.ctrv.2013.10.002
19. Brands RC, Muller-Richter UD, De Donno F, Seher A, Mutzbauer G, Linz C, et al. Co-treatment of wild-type EGFR head and neck cancer cell lines with afatinib and cisplatin. *Mol Med Rep.* (2016) 13:2338–44. doi: 10.3892/mmr.2016.4786
20. Khalil A, Jameson MJ. The EGFR inhibitor gefitinib enhanced the response of human oral squamous cell carcinoma to cisplatin *in vitro*. *Drugs R D.* (2017) 17:545–55. doi: 10.1007/s40268-017-0204-x
21. Rabinowits G, Haddad RI. Overcoming resistance to EGFR inhibitor in head and neck cancer: a review of the literature. *Oral Oncol.* (2012) 48:1085–9. doi: 10.1016/j.oraloncology.2012.06.016
22. Lopez-Verdin S, Lavalle-Carrasco J, Carreon-Burciaga RG, Serafin-Higuera N, Molina-Frechero N, Gonzalez-Gonzalez R, et al. Molecular markers of anticancer drug resistance in head and neck squamous cell carcinoma: a literature review. *Cancers.* (2018) 10:E376. doi: 10.3390/cancers10100376
23. Perri F, Longo F, Ionna F, Caponigro F. Recent results of cetuximab use in the treatment of squamous cell carcinoma of the head and neck. *Onco Targets Ther*. (2009) 2:243–50. doi: 10.2147/OTT.S6056
24. Naruse T, Yanamoto S, Matsushita Y, Sakamoto Y, Morishita K, Ohba S, et al. Cetuximab for the treatment of locally advanced and recurrent/metastatic oral cancer: an investigation of distant metastasis. *Mol Clin Oncol.* (2016) 5:246–52. doi: 10.3892/mco.2016.928
25. Chen CY, Chen CC, Shieh TM, Hsueh C, Wang SH, Leu YL, et al. Corylin suppresses hepatocellular carcinoma progression via the inhibition of epithelial-mesenchymal transition, mediated by long noncoding RNA GAS5. *Int J Mol Sci.* (2018) 19:E380. doi: 10.3390/ijms19020380
26. An W, Lai H, Zhang Y, Liu M, Lin X, Cao S. Apoptotic pathway as the therapeutic target for anticancer traditional chinese medicines. *Front Pharmacol.* (2019) 10:758. doi: 10.3389/fphar.2019.00758
27. He DY, Dai SM. Anti-inflammatory and immunomodulatory effects of paeonia lactiflora pall., a traditional chinese herbal medicine. *Front. Pharmacol.* (2011) 2:10. doi: 10.3389/fphar.2011.00010
28. Ji L, Tong X, Wang H, Tian H, Zhou H, Zhang L, et al. Efficacy and safety of traditional chinese medicine for diabetes: a double-blind, randomised, controlled trial. *PLoS ONE.* (2013) 8:e56703. doi: 10.1371/journal.pone.0056703
29. Jiao L, Dong C, Liu J, Chen Z, Zhang L, Xu J, et al. Effects of Chinese medicine as adjunct medication for adjuvant chemotherapy treatments of non-small cell lung cancer patients. *Sci Rep.* (2017) 7:46524. doi: 10.1038/srep46524
30. Zhang A, Sun H, Wang X. Potentiating therapeutic effects by enhancing synergism based on active constituents from traditional medicine. *Phytother Res.* (2014) 28:526–33. doi: 10.1002/ptr.5032
31. Xu L, Zhao W, Wang D, Ma X. Chinese medicine in the battle against obesity and metabolic diseases. *Front Physiol.* (2018) 9:850. doi: 10.3389/fphys.2018.00850
32. Jiang Z, Gao W, Huang L. Tanshinones, critical pharmacological components in *Salvia miltiorrhiza*. *Front Pharmacol.* (2019) 10:202. doi: 10.3389/fphar.2019.00202
33. Zhu H, Liu C, Hou J, Long H, Wang B, Guo D, et al. Gastrodia elata blume polysaccharides: a review of their acquisition, analysis, modification, and pharmacological activities. *Molecules.* (2019) 24:E2436. doi: 10.3390/molecules24132436
34. Ye MX, Li Y, Yin H, Zhang J. Curcumin: updated molecular mechanisms and intervention targets in human lung cancer. *Int J Mol Sci*. (2012) 13:3959–78. doi: 10.3390/ijms13033959
35. Terlikowska KM, Witkowska AM, Zujko ME, Dobrzycka B, Terlikowski SJ. Potential application of curcumin and its analogues in the treatment strategy of patients with primary epithelial ovarian cancer. *Int J Mol Sci.* (2014) 15:21703–22. doi: 10.3390/ijms151221703
36. Hong M, Tan HY, Li S, Cheung F, Wang N, Nagamatsu T, et al. Cancer stem cells: the potential targets of Chinese medicines and their active compounds. *Int J Mol Sci.* (2016) 17:E893. doi: 10.3390/ijms17060893
37. Houh YK, Kim KE, Park S, Hur DY, Kim S, Kim D, et al. The effects of artemisinin on the cytolytic activity of natural killer (NK) cells. *Int J Mol Sci.* (2017) 18:E1600. doi: 10.3390/ijms18071600
38. Slezakova S, Ruda-Kucerova J. Anticancer activity of artemisinin and its derivatives. *Anticancer Res.* (2017) 37:5995–6003. doi: 10.21873/anticanres.12046
39. Cragg GM, Pezzuto JM. Natural products as a vital source for the discovery of cancer chemotherapeutic and chemopreventive agents. *Med Princ Pract.* (2016) 25(Suppl 2):41–59. doi: 10.1159/000443404
40. Kim YJ, Lim HS, Lee J, Jeong SJ. Quantitative analysis of *Psoralea corylifolia* Linne and its neuroprotective and anti-neuroinflammatory effects in HT22 hippocampal cells and BV-2 microglia. *Molecules.* (2016) 21:E1076. doi: 10.3390/molecules21081076

41. Li CC, Wang TL, Zhang ZQ, Yang WQ, Wang YF, Chai X, et al. Phytochemical and pharmacological studies on the genus psoralea: a mini review. *Evid Based Complement Alternat Med*. (2016) 2016:8108643. doi: 10.1155/2016/8108643
42. Zhang X, Zhao W, Wang Y, Lu J, Chen X. The chemical constituents and bioactivities of *Psoralea corylifolia* Linn.: a review. *Am J Chin Med*. (2016) 44:35–60. doi: 10.1142/S0192415X16500038
43. Hung YL, Fang SH, Wang SC, Cheng WC, Liu PL, Su CC, et al. Corylin protects LPS-induced sepsis and attenuates LPS-induced inflammatory response. *Sci Rep*. (2017) 7:46299. doi: 10.1038/srep46299
44. Alam F, Khan GN, Asad M. *Psoralea corylifolia* L.: ethnobotanical, biological, and chemical aspects: a review. *Phytother Res*. (2018) 32:597–615. doi: 10.1002/ptr.6006
45. Choi YH, Yon GH, Hong KS, Yoo DS, Choi CW, Park WK, et al. *In vitro* BACE-1 inhibitory phenolic components from the seeds of *Psoralea corylifolia*. *Planta Med*. (2008) 74:1405–8. doi: 10.1055/s-2008-1081301
46. Kim DH, Li H, Han YE, Jeong JH, Lee HJ, Ryu JH. Modulation of inducible nitric oxide synthase expression in LPS-stimulated BV-2 microglia by prenylated chalcones from *Cullen corylifolium* (L.) medik. through Inhibition of I-kappaBalpha degradation. *Molecules*. (2018) 23:E109. doi: 10.3390/molecules23010109
47. Chen CY, Chiou SH, Huang CY, Jan CI, Lin SC, Hu WY, et al. Tid1 functions as a tumour suppressor in head and neck squamous cell carcinoma. *J Pathol*. (2009) 219:347–55. doi: 10.1002/path.2604
48. Chen CY, Yang SC, Lee KH, Yang X, Wei LY, Chow LP, et al. The antitumor agent PBT-1 directly targets HSP90 and hnRNP A2/B1 and inhibits lung adenocarcinoma growth and metastasis. *J Med Chem*. (2014) 57:677–85. doi: 10.1021/jm401686b
49. Chen CY, Jan CI, Pi WC, Wang WL, Yang PC, Wang TH, et al. Heterogeneous nuclear ribonucleoproteins A1 and A2 modulate expression of Tid1 isoforms and EGFR signaling in non-small cell lung cancer. *Oncotarget*. (2016) 7:16760–72. doi: 10.18632/oncotarget.7606
50. Wang TH, Chan CW, Fang JY, Shih YM, Liu YW, Wang TV, et al. 2-O-Methylmagnolol upregulates the long non-coding RNA, GAS5, and enhances apoptosis in skin cancer cells. *Cell Death Dis*. (2017) 8:e2638. doi: 10.1038/cddis.2017.66
51. Chen CC, Chen CY, Ueng SH, Hsueh C, Yeh CT, Ho JY, et al. Corylin increases the sensitivity of hepatocellular carcinoma cells to chemotherapy through long noncoding RNA RAD51-AS1-mediated inhibition of DNA repair. *Cell Death Dis*. (2018) 9:543. doi: 10.1038/s41419-018-0575-0
52. Chu Q, Amano O, Kanda Y, Kunii S, Wang Q, Sakagami H. Tumor-specific cytotoxicity and type of cell death induced by gefitinib in oral squamous cell carcinoma cell lines. *Anticancer Res*. (2009) 29:5023–31.
53. Sivanantham B, Sethuraman S, Krishnan UM. Combinatorial effects of curcumin with an anti-neoplastic agent on head and neck squamous cell carcinoma through the regulation of EGFR-ERK1/2 and apoptotic signaling pathways. *ACS Comb Sci*. (2016) 18:22–35. doi: 10.1021/acscombsci.5b00043
54. Iocca O, Farcomeni A, Di Rocco A, Di Maio P, Golusinski P, Pardinas Lopez S, et al. Locally advanced squamous cell carcinoma of the head and neck: a systematic review and Bayesian network meta-analysis of the currently available treatment options. *Oral Oncol*. (2018) 80:40–51. doi: 10.1016/j.oraloncology.2018.03.001
55. Khushboo PS, Jadhav VM, Kadam VJ, Sathe NS. *Psoralea corylifolia* Linn.-"Kushtanashini." *Pharmacogn Rev*. (2010) 4:69–76. doi: 10.4103/0973-7847.65331
56. Sarkis SA, Abdullah BH, Abdul Majeed BA, Talabani NG. Immunohistochemical expression of epidermal growth factor receptor (EGFR) in oral squamous cell carcinoma in relation to proliferation, apoptosis, angiogenesis and lymphangiogenesis. *Head Neck Oncol*. (2010) 2:13. doi: 10.1186/1758-3284-2-13
57. Yamano Y, Uzawa K, Saito K, Nakashima D, Kasamatsu A, Koike H, et al. Identification of cisplatin-resistance related genes in head and neck squamous cell carcinoma. *Int J Cancer*. (2010) 126:437–49. doi: 10.1002/ijc.24704
58. Celentano A, Mccullough M, Cirillo N. Glucocorticoids reduce chemotherapeutic effectiveness on OSCC cells via glucose-dependent mechanisms. *J Cell Physiol*. (2019) 234:2013–20. doi: 10.1002/jcp.27227
59. Maji S, Shriwas O, Samal SK, Priyadarshini M, Rath R, Panda S, et al. STAT3- and GSK3beta-mediated Mcl-1 regulation modulates TPF resistance in oral squamous cell carcinoma. *Carcinogenesis*. (2019) 40:173–83. doi: 10.1093/carcin/bgy135
60. Ma C, Shi X, Zhu Q, Li Q, Liu Y, Yao Y, et al. The growth arrest-specific transcript 5 (GAS5): a pivotal tumor suppressor long noncoding RNA in human cancers. *Tumour Biol*. (2016) 37:1437–44. doi: 10.1007/s13277-015-4521-9
61. Ghaforui-Fard S, Taheri M. Growth arrest specific transcript 5 in tumorigenesis process: an update on the expression pattern and genomic variants. *Biomed Pharmacother*. (2019) 112:108723. doi: 10.1016/j.biopha.2019.108723
62. Pickard MR, Williams GT. Regulation of apoptosis by long non-coding RNA GAS5 in breast cancer cells: implications for chemotherapy. *Breast Cancer Res Treat*. (2014) 145:359–70. doi: 10.1007/s10549-014-2974-y
63. Guo LJ, Zhang S, Gao B, Jiang Y, Zhang XH, Tian WG, et al. Low expression of long non-coding RNA GAS5 is associated with poor prognosis of patients with thyroid cancer. *Exp Mol Pathol*. (2017) 102:500–4. doi: 10.1016/j.yexmp.2017.05.008
64. Yang Y, Shen Z, Yan Y, Wang B, Zhang J, Shen C, et al. Long non-coding RNA GAS5 inhibits cell proliferation, induces G0/G1 arrest and apoptosis, and functions as a prognostic marker in colorectal cancer. *Oncol Lett*. (2017) 13:3151–8. doi: 10.3892/ol.2017.5841
65. Avgeris M, Tsilimantou A, Levis PK, Tokas T, Sideris DC, Stravodimos K, et al. Loss of GAS5 tumour suppressor lncRNA: an independent molecular cancer biomarker for short-term relapse and progression in bladder cancer patients. *Br J Cancer*. (2018) 119:1477–86. doi: 10.1038/s41416-018-0320-6
66. Dong S, Qu X, Li W, Zhong X, Li P, Yang S, et al. The long non-coding RNA, GAS5, enhances gefitinib-induced cell death in innate EGFR tyrosine kinase inhibitor-resistant lung adenocarcinoma cells with wide-type EGFR via downregulation of the IGF-1R expression. *J Hematol Oncol*. (2015) 8:43. doi: 10.1186/s13045-015-0140-6
67. Li W, Zhai L, Wang H, Liu C, Zhang J, Chen W, et al. Downregulation of LncRNA GAS5 causes trastuzumab resistance in breast cancer. *Oncotarget*. (2016) 7:27778–86. doi: 10.18632/oncotarget.8413
68. Zeng B, Li Y, Jiang F, Wei C, Chen G, Zhang W, et al. LncRNA GAS5 suppresses proliferation, migration, invasion, and epithelial-mesenchymal transition in oral squamous cell carcinoma by regulating the miR-21/PTEN axis. *Exp Cell Res*. (2019) 374:365–73. doi: 10.1016/j.yexcr.2018.12.014

Conflict of Interest: The authors declare that the research was conducted in the absence of any commercial or financial relationships that could be construed as a potential conflict of interest.

frontiers in Oncology

CASE REPORT
published: 12 November 2019
doi: 10.3389/fonc.2019.01204

Enabling Precision Medicine for Rare Head and Neck Tumors: The Example of BRAF/MEK Targeting in Patients With Metastatic Ameloblastoma

Maxime Brunet[1], *Emmanuel Khalifa*[2] *and Antoine Italiano*[1,3,4]*

[1] Department of Medicine, Institut Bergonié, Bordeaux, France, [2] Department of Tumor Genetics, Institut Bergonié, Bordeaux, France, [3] Faculty of Médicine, University of Bordeaux, Bordeaux, France, [4] INSERM, ACTION U1218, Bordeaux, France

Background: Ameloblastoma is a rare head and neck tumor characterized by a high incidence of BRAF mutation providing a rationale for the use of BRAF inhibitors in patients with advanced disease.

Methods: We report the case of a 26-year old female presenting with metastatic ameloblastoma. A molecular screening of the tumor revealed a BRAF V600E mutation.

Results: The patient started treatment with dabrafenib and trametinib and experienced complete response which is still ongoing 30 weeks after treatment onset.

Conclusions: The complete response observed here illustrate the role of molecular profiling in complicate clinical situation of rare head and neck cancer and the potential benefit of BRAF-targeted therapy in ameloblastoma carrying *BRAF* V600E mutation.

Keywords: ameloblastoma, BRAF, targeted therapeutic drugs, rare tumor, precision oncology

OPEN ACCESS

Edited by:
Cheng-Chia Yu,
Chung Shan Medical University, Taiwan

Reviewed by:
Thorsten Fuereder,
Medical University of Vienna, Austria
Julia Chang,
National Taiwan University, Taiwan

***Correspondence:**
Antoine Italiano
a.italiano@bordeaux.unicancer.fr

Specialty section:
This article was submitted to Head and Neck Cancer, a section of the journal Frontiers in Oncology

Received: *27 April 2019*
Accepted: *23 October 2019*
Published: *12 November 2019*

Citation:
Brunet M, Khalifa E and Italiano A (2019) Enabling Precision Medicine for Rare Head and Neck Tumors: The Example of BRAF/MEK Targeting in Patients With Metastatic Ameloblastoma. Front. Oncol. 9:1204. doi: 10.3389/fonc.2019.01204

INTRODUCTION

Precision oncology aims to tailor the therapeutic strategy based on tumor's molecular alterations. Previous studies have suggested the validity of such approach in rare and ultra-rare tumor subtypes, including rare head and neck cancers; with the identification of targetable alterations in up to 93% of cases (1). Ameloblastomas are rare tumors, which often have a benign course. Metastatic evolution is extremely rare and there is no standard of care for patients in this setting.

CASE REPORT

In November 2018, a 26-year old female was referred for hemoptysis and cough of several weeks' duration. Her past medical history was significant for the diagnosis, at the age of 13 years, of an ameloblastoma of the right mandible (tooth 48) treated by surgery with clear margins and no evidence of locoregional relapse since then. A CT scan was performed which showed numerous bilateral nodules. The patient underwent a CT-guided percutaneous lung biopsy of one of these nodules. Histological examination was in favor of lung metastasis of ameloblastoma.

The patient was enrolled in our molecular screening program after signature of informed consent (Bergonié Institut Profiling study, NCT02534649) and gave also written informed consent for the publication of this case report. Next-generation sequencing of the metastatic tumor sample was performed as previously described and revealed the presence of a *BRAF* gene V600E mutation [**Figure 1**; (2)]. Given the lack of validated standard treatment for advanced ameloblastoma, the molecular tumor board recommended initiation of a BRAF-targeted therapy. The patient started treatment with dabrafenib (150 mg BID) combined with trametinib (2 mg QD). The first TEP-CT

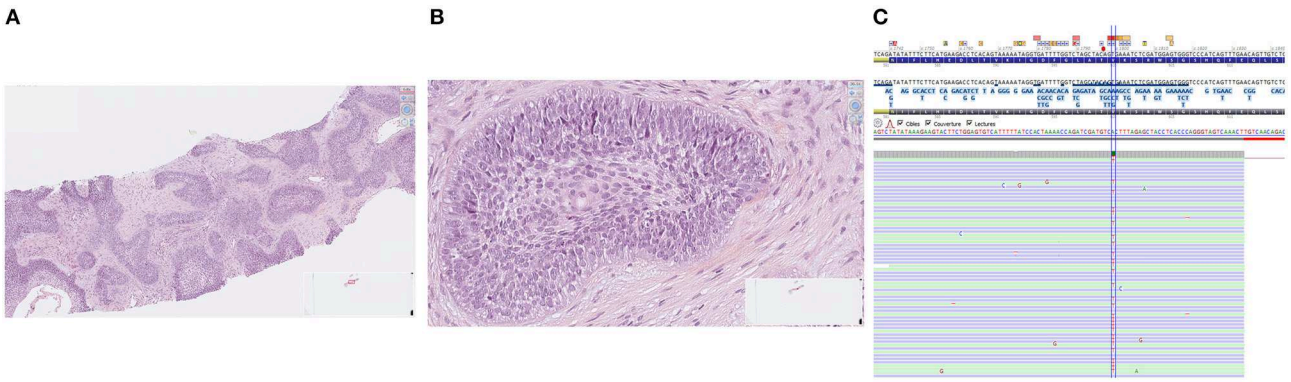

FIGURE 1 | Histological features of ameloblastoma (**A**: low magnification, **B**: high magnification) and BRAF V600E gene mutation assessed by next-generation sequencing **(C)**.

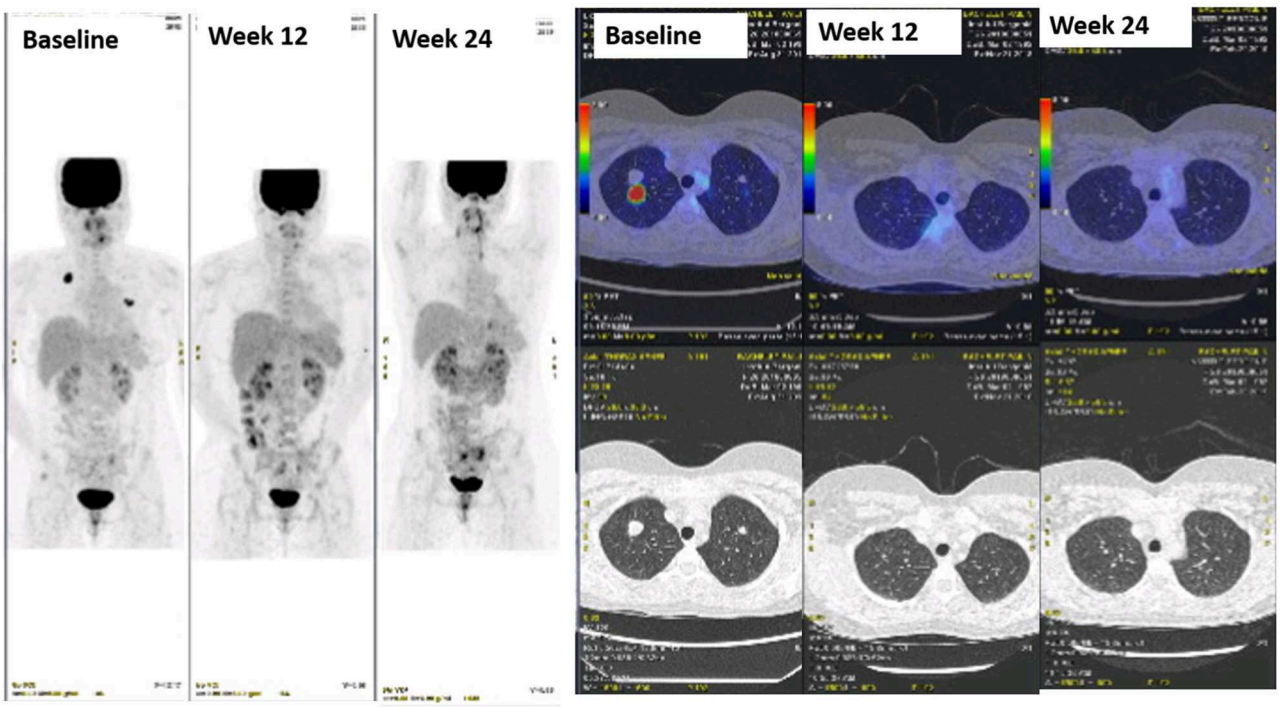

FIGURE 2 | Sustained complete response to dabrafenib + trametinib in a patient with ameloblastoma metastatic to the lungs.

scan performed 12 weeks after treatment onset showed competed response according to RECIST and PERCIST criteria (**Figure 2**). The patient is still doing well and in complete remission 30 weeks after treatment initiation.

DISCUSSION

The ameloblastoma is a histologically almost always benign odontogenic tumor of the jaw bones with a potential of locoregional recurrence (3). Distant metastases are extremely rare.

Anecdotal response has been reported with platinum salts agents but there is no standard of care in this setting (4). A seminal study investigating the molecular landscape of ameloblastomas revealed that ameloblastomas are characterized by the a frequent incidence of BRAF V600E mutations particularly in tumors located in the mandibular region while mutations of the SMO gene (39%) were predominant in maxillary tumors (82%) (5). This study and others provided a rationale to investigate BRAF targeting in patients with advance ameloblastoma. Previous case reports have suggested the clinical activity of BRAF inhibitor such as vemurafenib in patients with advanced ameloblastoma (**Table 1**). We opted here for the combination of a BRAF and MEK inhibitors. Indeed, several studies performed in melanomas, and other BRAF-driven malignancy, showed that acquired resistance to

TABLE 1 | Clinical reports of BRAF-targeting in advanced ameloblastoma.

References	Clinical setting	Tumor stage	Treatment	Outcome
Fernandes et al. (6)	29 years old female	Locally advanced	Vemurafenib	Partial response PFS not reached at 11 months after treatment onset
Tan et al. (7)	85 years old male	Locally advanced	Dabrafenib	Partial response
Faden and Algazi (8)	83 years old male	Locally advanced	Dabrafenib	Partial response PFS not reached at 12 months
Kaye et al. (9)	40 years old male	Metastatic	Dabrafenib + trametinib	Partial response Not reached at 5 months after treatment onset

BRAF inhibitors frequently develops through reactivation of the mitogen-activated protein kinase (MAPK) pathway, resulting in limited progression-free survival (10) In addition, the use of BRAF inhibitors as single agent may induce the development of secondary skin tumors, originating from a paradoxical activation of the MAPK pathway in cells without a *BRAF* mutation (10). In melanomas, combining a BRAF inhibitor with a MEK inhibitor addresses the limitations of single-agent BRAF inhibitors and results in a significant delay in the emergence of resistance, with a longer overall than with BRAF inhibitor alone, as well as a decreased incidence of BRAF-inhibitor–induced skin tumors (10). The toxicity of such a combination profile is generally good with the most common adverse events being rash, pyrexia, asthenia, headache, nausea, and arthralgia (11). The complete response observed here illustrate the role of molecular profiling in complicate clinical situation of rare head and neck cancer and the potential benefit of BRAF-targeted therapy in ameloblastoma carrying *BRAF* V600E mutation.

DATA AVAILABILITY STATEMENT

All datasets generated for this study are included in the article/supplementary material.

ETHICS STATEMENT

This study was approved by the institutional review board of Institut Bergonié.

AUTHOR CONTRIBUTIONS

AI: conception and design. EK and AI: collection and assembly of data. All authors: data analysis, interpretation, manuscript writing, and final approval of manuscript.

FUNDING

This study was funded by the Fondation MSD Avenir (Grant: HEART study).

REFERENCES

1. Kato S, Kurasaki K, Ikeda S, Kurzrock R. Rare tumor clinic: the University of California San Diego Moores Cancer Center experience with a precision therapy approach. *Oncologist*. (2018) 23:171–8. doi: 10.1634/theoncologist.2017-0199
2. Cousin S, Grellety T, Toulmonde M, Auzanneau C, Khalifa E, Laizet Y, et al. Clinical impact of extensive molecular profiling in advanced cancer patients. *J Hematol Oncol.* (2017) 10:45. doi: 10.1186/s13045-017-0411-5
3. Sciubba J. Odontogenic tumors. In: Barnes L, Eveson J, Reichart P, Sidransky D, editors. *World Health Organization Classification of Tumors, Pathology and Genetics of Head and Neck Tumors*. Lyon: IARC Press (2005). p. 287–93.
4. McClary AC, West RB, McClary AC, Pollack JR, Fischbein NJ, Holsinger CF, et al. Ameloblastoma: a clinical review and trends in management. *Eur Arch Otorhinolaryngol.* (2016) 273:1649–61. doi: 10.1007/s00405-015-3631-8
5. Sweeney RT, McClary AC, Myers BR, Biscocho J, Neahring L, Kwei KA, et al. Identification of recurrent SMO and BRAF mutations in ameloblastomas. *Nat Genet.* (2014) 46:722–5. doi: 10.1038/ng.2986
6. Fernandes GS, Girardi DM, Bernardes JPG, Fonseca FP, Fregnani ER. Clinical benefit and radiological response with BRAF inhibitor in a patient with recurrent ameloblastoma harboring V600E mutation. *BMC Cancer.* (2018) 18:887. doi: 10.1186/s12885-018-4802-y
7. Tan S, Pollack JR, Kaplan MJ, Colevas AD, West RB. BRAF inhibitor treatment of primary BRAF-mutant ameloblastoma with pathologic assessment of response. *Oral Surg Oral Med Oral Pathol Oral Radiol.* (2016) 122:e5–7. doi: 10.1016/j.oooo.2015.12.016
8. Faden DL, Algazi A. Durable treatment of ameloblastoma with single agent BRAFi Re: Clinical and radiographic response with combined BRAF-targeted therapy in stage 4 ameloblastoma. *J Natl Cancer Inst.* (2016) 109:djw190. doi: 10.1093/jnci/djw190
9. Kaye FJ, Ivey AM, Drane WE, Mendenhall WM, Allan RW. Clinical and radiographic response with combined BRAF-targeted therapy in stage 4 ameloblastoma. *J Natl Cancer Inst.* (2014) 107:378. doi: 10.1093/jnci/dju378
10. Torres-Collado AX, Knott J, Jazirehi AR. Reversal of resistance in targeted therapy of metastatic melanoma: lessons learned from vemurafenib ($BRAF^{V600E}$-Specific Inhibitor). *Cancers.* (2018) 10:E157. doi: 10.3390/cancers10060157
11. Knispel S, Zimmer L, Kanaki T, Ugurel S, Schadendorf D, Livingstone E. The safety and efficacy of dabrafenib and trametinib for the treatment of melanoma. *Expert Opin Drug Saf.* (2018) 17:73–87. doi: 10.1080/14740338.2018.1390562

Conflict of Interest: The authors declare that the research was conducted in the absence of any commercial or financial relationships that could be construed as a potential conflict of interest.

frontiers in Oncology

REVIEW
published: 21 November 2019
doi: 10.3389/fonc.2019.01275

Susceptibility of Multiple Primary Cancers in Patients With Head and Neck Cancer: Nature or Nurture?

Wei-long Zhang[1†], *Zhuo-li Zhu*[1†], *Mei-chang Huang*[1], *Ya-Jie Tang*[2], *Ya-ling Tang*[1*] and *Xin-hua Liang*[1*]

[1] State Key Laboratory of Oral Diseases, National Clinical Research Center for Oral Diseases, West China Hospital of Stomatology, Sichuan University, Chengdu, China, [2] State Key Laboratory of Microbial Technology, Shandong University, Qingdao, China

Multiple primary cancers (MPCs) are major obstacles to long-term survival in head and neck cancer (HNSCC), however, the molecular mechanism underlying multiple carcinogenesis remains unclear. "Field cancerization" is a classical theory to elaborate the malignant progression of MPCs. Apart from environmental and immune factors, genetic factors may have great potential as molecular markers for MPCs risk prediction. This review focuses on inherited and acquired gene mutations in MPCs, including germ-line mutation, single-nucleotide polymorphism, chromosomal instability, microsatellite instability and DNA methylation. And definition and prognosis of MPCs have also been discussed. These may pave the way for the early detection, prevention and effective treatment of MPCs in HNSCC.

Keywords: head and neck cancer, multiple primary cancer, field cancerization, cancer-associated fibroblasts, genetic factor, biomarker

OPEN ACCESS

Edited by:
Jorge A. R. Salvador,
University of Coimbra, Portugal

Reviewed by:
Cesare Piazza,
National Tumor Institute, Italy
Thorsten Fuereder,
Medical University of Vienna, Austria

***Correspondence:**
Ya-ling Tang
tangyaling@scu.edu.cn
Xin-hua Liang
lxh88866@scu.edu.cn

[†]*These authors have contributed equally to this work*

Specialty section:
This article was submitted to Head and Neck Cancer, a section of the journal Frontiers in Oncology

Received: *05 September 2019*
Accepted: *04 November 2019*
Published: *21 November 2019*

Citation:
Zhang W, Zhu Z, Huang M, Tang Y-J, Tang Y and Liang X (2019) Susceptibility of Multiple Primary Cancers in Patients With Head and Neck Cancer: Nature or Nurture? Front. Oncol. 9:1275. doi: 10.3389/fonc.2019.01275

INTRODUCTION

Head and neck squamous cancer (HNSCC) ranks sixth among the most prevalent malignancies in the world (1). It is estimated that HNSCC accounts for 64,690 new cases and 13,740 deaths in the United states in 2018 (2). Although significant improvements have been made in the therapeutic modalities, the prognosis of HNSCC remains stagnant in the past decades, with a 5-year survival of only 50% (3). The dismal prognosis has always been attributed to local recurrences, distant metastasis, and development of multiple primary cancers (MPCs).

MPCs are defined as two or more primary cancers occurring in an individual synchronously or metachronously, neither extensions, recurrences nor metastases of each other (International Agency for Research on Cancer), which accounts for approximately one-third of deaths in HNSCC (4, 5). MPCs are also named as second primary malignancies (SPMs), secondary primary tumors (SPTs), second primary cancers (SPCs), and multiple primary tumors (MPTs) (6). Several risk factors, including smoking exposure, alcohol consumption, human papilloma virus (HPV), and hepatitis C virus (HCV), have been suggested to be associated with the development of MPCs (7–10). However, researches revealed that a major proportion of MPCs could not be fully explained by these environmental factors, and genetic factors, such as single-nucleotide polymorphism (SNP), chromosomal instability (CIN), microsatellite instability (MSI), and epigenetic alterations, may contribute to the susceptibility of MPCs in HNSCC (11).

MPCs have been considered to be a clinical quandary both in diagnosis and treatment. It is challenging for the oncologists to distinguish MPCs from a metastasis or local recurrence merely on the basis of clinical and pathological information. Furthermore, this classification leaves a profound effect on the choice of treatment as well as patients' prognosis. Recently, there are a number of novel screening strategies for MPCs prediction, such as genetic markers, and the role of genetic alterations in the development of MPCs after index HNSCC were not fully elucidated (12). Here, we conducted this review to summarize the mechanisms and relevant genetic alterations of MPCs, which might provide benefit in the detection, prevention, and treatment of MPCs in HNSCC.

DEFINITION AND PROGNOSIS OF MPCs

In 1932, Warren and Gates published the classical clinical criteria of SPT, being (1) each of the malignancies must have been verified by histologic examination, (2) the malignancies must be anatomical separate by normal mucosa, and (3) exclude the possibility that the second malignancy represents a metastasis of the index tumor (13). However, this clinical definition carries the risk of misclassification and inability to differentiate between an SPT, a recurrence and a metastasis (14). For example, what distance should lie between the malignancies? How to define the normal mucosa, by naked eye or histologic examination? How to distinguish the SPT from a metastasis or a recurrence? To solve this dilemma, Braakhuis et al. proposed a new classification on the basis of molecular profiles of the tumors and the genetically altered mucosal field between the tumors (14). Tumors displaying distinct molecular profiles or sharing a common pattern attributed to chance are defined as SPTs, while those possessing similar molecular aberration are defined as local recurrences (14).

It is widely accepted that MPCs are the leading obstacle to long-term survival among HNSCC patients (15). According to a retrospective study conducted by Shiga et al., patients with synchronous SPMs displayed a poorer 5-year overall survival rate than those with metachromous SPMs in Japan (16). In line with this result, Bugter et al. claimed that the 5-yearsurvival rate for synchronous and metachronous primary cancer patients was 25 and 85%, respectively (17). The higher proportion of high-stage tumor in the synchronous primary cancer patients and unadjusted treatment protocol may account for this discrepancy.

However, accumulating evidence has demonstrated that HPV-positive HNSCC patients were accompanied by a decreased risk for SPT than HPV-negative HNSCC patients (18–20). HPV has been established as an emerging carcinogen in a subset of HNSCCs, particularly in the oropharynx (21). HPV-positive HNSCCs differ from HPV-negative HNSCCs induced by tobacco and alcohol epidemiologically, clinically, and biologically (22–24). The putative reasons for this phenomenon are as follows: (1) HPV-positive HNSCCs exhibited higher sensitivity to radiotherapy and chemotherapy (25); (2) HPV-positive HNSCCs often arise in an environment with lower exposure to tobacco and displayed fewer smoking-related genetic abnormalities, which is less associated with smoking-related SPTs (26–28); (3) Saito et al. suggested that field cancerization effect would not be observed in HPV-positive HNSCCs, since HPV viral DNA integration was limited to the cancerous tissue (29). However, the concrete mechanisms between HPV-positive HNSCCs and SPTs are remained to be elucidated in the future.

The dismal clinical outcome of MPCs in HNSCC emphasizes on the importance of early diagnosis and prevention. These genetic alterations could serve as molecular makers to guide the early diagnosis, prevention and treatment of HNSCC patients in several aspects. Firstly, these molecular markers could be readily obtained by the primary tumor samples without bringing additional invasion to patients (30). Secondly, genetic markers could select the high-risk individuals for MPCs, which should be under strict cancer surveillance and proper preventive procedures. Given the discrepancies between HPV-positive and HPV-negative HNSCC, Jain et al. proposed that future screening procedures for MPCs may be adjusted by HPV and smoking status (31). Thirdly, in-depth understanding of the role of these molecular markers in MPCs may pave the way for targeted gene therapies. In addition, genetic markers could be utilized to distinguish MPCs from a local recurrence or a metastasis. For example, Mercer et al. showed that microsatellite PCR facilitated the discrimination between second primary cancer and metastatic HNSCC (32). Daher et al. employed combined HPV typing and TP53 mutational profiling successfully identified the accurate origin of lung tumors in 32 HNSCC patients, in which only 13 cases were diagnosed correctly on the basis of clinical and morphological data alone (33). Apart from physical and pathological information, genetic profiles analysis could be an effective tool to distinguish MPCs from a recurrence. Gasparotto et al. suggested that 3 clinically diagnosed recurrences and 2 lung lesions were actually MPTs by comparing the p53 mutation status of primary tumors and corresponding recurrences/metastases in HNSCC patients (34). Microsatellite analysis indicated that 6 tumors showing clonally-related patterns with primary tumors were recurrences, while 17 tumors with clonally-unrelated patterns were SPTs in 23 HNSCC patients with genetic changes (35).

MECHANISM OF MPCs

The concrete molecular mechanism underlying multiple carcinogenesis remains unclear. "Field cancerization" theory has often been applied to explain the occurrence of MPCs (**Figure 1**). The stem cell receives one (or more) genetic hit (**Figure 1A**), probably a mutation of *p53* gene, and gives rise to a patch with genetically altered daughter cells [(36); **Figure 1B**]. Then a subsequent genetic alteration induces the patch to spread in a lateral direction and substitutes the normal epithelial cells to form a field [(36); **Figure 1C**]. As the field expands at the expense of normal epithelial cells, additional genetic alterations take place and promote the progression from field to an overt carcinoma (**Figure 1D**). The second tumor of monoclonal origin develops by implantation, intraepithelial migration or sub-mucosal spread of primary cancer cells (**Figure 1E**), while the polyclonal

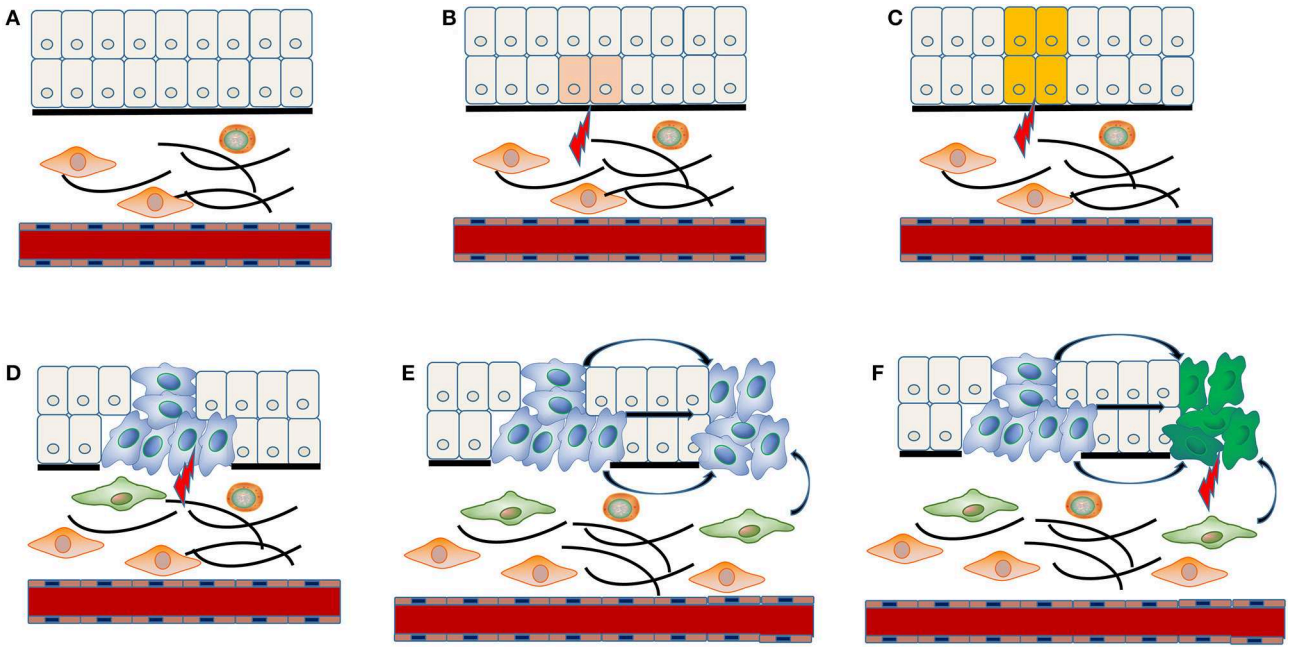

FIGURE 1 | "Field cancerization" theory in the MPCs of HNSCC. The stem cell receives first genetic hit **(A)**, and gives rise to a patch with genetically altered daughter cells **(B)**. Then a patch develops into a field by expanding in a lateral direction under the indduction of a second genetic hit **(C)**. Additional genetic alterations take place and convert the field to an overt carcinoma **(D)**. The implantation, intraepithelial migration or sub-mucosal spread of primary cancer cells lead to the development of a SPT with monoclonal origin **(E)**, while the final genetic hit induces the occurrence of a SPT with polyclonal origin **(F)**.

second tumor forms under the induction of final genetic hit [(14, 37); **Figure 1F**].

Failure of immune surveillance also contributed to the occurrence of SPTs in HNSCC (**Figure 2**). Patients with decreased T-cell numbers in the circulation were predisposed to infections, disease recurrence, or a second malignancy (38). Kuss et al. reported that CD4+ and CD8+ T cells were significantly reduced in the SPT group relative to normal control group in HNSCCs (38). And patients with recurrences or SPTs showed a 25% lower number of CD4+ T cells than those with primary disease (38). The TCR associated CD3 zeta chain plays a critical role in the signal transduction of T-cell activation, the absence of which impairs T-cell signaling and consequently leads to immune dysfunction (39). Kuss et al. concluded that individuals with SPTs or recurrences exhibited lowest zeta-chain expression, which might exert long-lasting negative effects on the anti-tumor immune response (40). Decreased expression of HLA class I molecules is considered to be an effective strategy for malignant cells to evade host immunosurveillance (41). Grandis et al. suggested that the number of HLA allelic loss increased the risk of developing a new primary tumor (41). Collectively, decreased T-cell numbers, CD3 zeta chain and HLA class I molecules may be associated with the development of SPT, which may provide new opportunities for cancer immunotherapy in HNSCC.

In addition, cancer-associated fibroblasts (CAFs) may play an unneglectable role in the development of field cancerization [(42); **Figure 2**]. Ge et al. proposed that migratory cancer-associated fibroblasts (CAFs), also named myofibroblast, may appear beneath the cluster of genetic altered epithelial cells, and ultimately lead to the malignant transformation of these cells (42). Angadi et al. demonstrated that myofibroblasts were present in the stroma around the oral squamous cell carcinoma (OSCC) cell as well as the connective tissue below the histologically normal mucosa adjacent to OSCC by immunochemistry, which validates Ge's hypothesis further (43). Chan et al. indicated that cancer-associated fibroblasts promoted field cancerization by elevating the expression of reactive oxygen species (ROS) in the microenvironment (44). CAFs from squamous cell carcinoma reduced the expression of Smad3 and cJUN to suppress the activity of glutathione peroxidase 1 (GPX1), one key enzyme affecting hydrogen peroxide detoxification. Suppression of GPX1 leads to elevation of extracellular hydrogen peroxide, which facilitates the conversion of normal fibroblast to CAF phenotype, and promotes the tumor-forming capacity and invasiveness. Till now, there is no more available evidences on the role of tumor microenvironment in MPCs, including macrophages, myeloid-derived suppressor cells (MDSCs) and etc., which warrants further investigation in the future.

MPCs AND INHERITED MUTATIONS

MPCs and Germ-Line Mutations

Germ-line mutation of tumor suppressor genes has been considered to be a potential driver of MPCs. *p53* gene, known as the "the guardian of the genome," is an well-known tumor

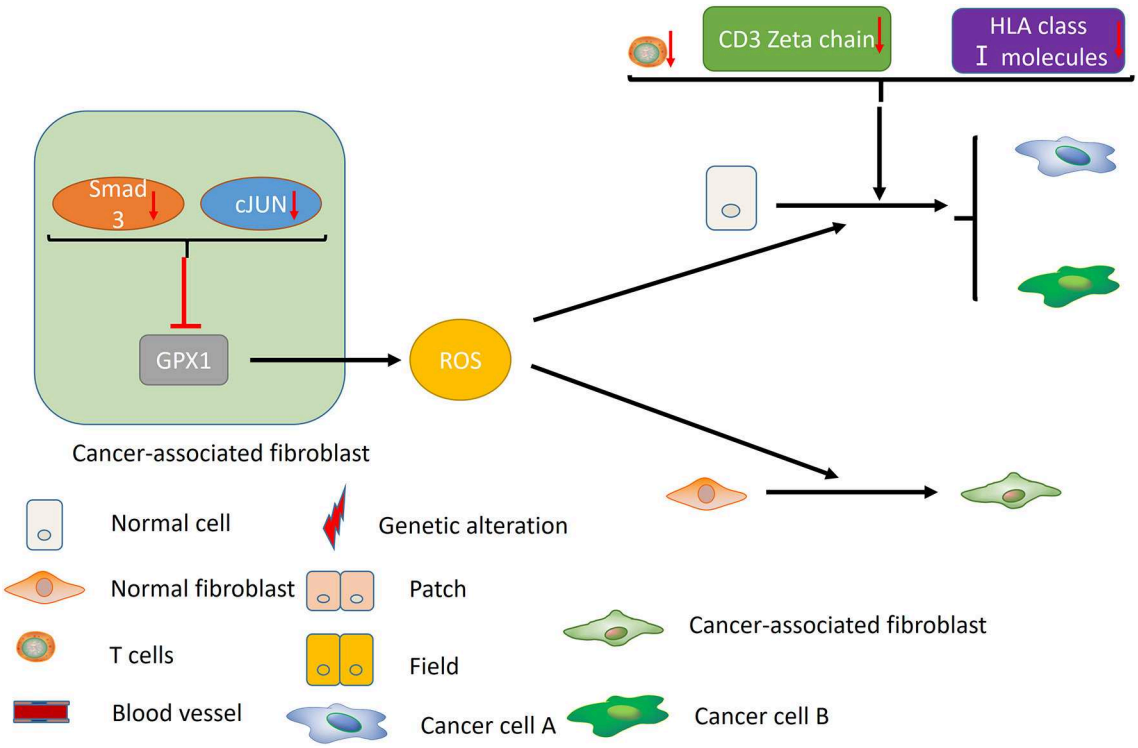

FIGURE 2 | Immune factors and CAFs contribute to the development of MPCs. Decreased T-cell numbers, CD3 zeta chain and HLA class I molecules may promote the development of MPCs by inducing immunosuppression. In the CAFs, reduced expression of Smad3 and cJUN suppress the activity of GPX1, leading to the elevation of extracellular hydrogen peroxide. High hydrogen peroxide level in the microenvironment induces the conversion of normal fibroblast to CAF phenotype, and promotes the occurrence of MPCs.

suppressor gene which has been involved in the cell cycle control and DNA repair (45). It is estimated that *p53* gene was mutated in approximately 50% of HNSCC patients (46). In 1999, Gallo and his colleagues employed polymerase chain reaction single-strand conformation polymorphism (PCR-SSCP) analysis and DNA sequencing to examine the *p53* germ-line mutations in 24 HNSCC patients who developed MPCs and their first-degree relatives. As a consequence, only one missense mutation in exon 6 as well as two same-sense mutations in exon 6 and 8 have been detected (47). So the authors proposed that *p53* gene might not be the only target responsible for the multiple genetic alterations of field cancerization (47).

CDKN2A, a tumor suppressor gene exerting an important role in the regulation of cell cycle, is associated with the occurrence of HNSCC. Cabanillas et al. proposed that germ-line mutations of *CDKN2A* gene may serve as a common feature of HNSCC (30). However, Jefferies et al. screened full coding sequence of *CDKN2A* gene and failed to detect any germ-line mutations in 40 HNSCC patients with a SPC, which suggested that germ-line mutations of *CDKN2A* contributed less to the susceptibility of MPCs (48).

Mismatch genes, such as *hMLHI*, contribute greatly to the MPCs of gastrointestinal cancers. Nevertheless, its germ-lime mutations don't seem to be an major event in the carcinogenesis of HNSCC or MPTs (49). Piccinin et al. analyzed the mutations of *hMLHI* gene by PCR-SSCP and sequencing in 67 HNSCC patients, 22 MPTs and 45 controls, and no somatic or germ-lime mutations of hMLHI have been identified (49).

Based on the above, it seems that germ-line mutations of certain tumor suppressor genes and DNA repair genes, including *p53*, *CDKN2A*, and *hMLHI*, exert a minor influence on the genetic predisposition of MPCs after index HNSCC.

MPCs and SNPs

It is estimated that SNP accounts for up to 90% of genetic variability (50). Researchers have demonstrated that genetic polymorphisms of various genes were correlated with the risk of MPCs in HNSCC. Based on their functions, these genes could be classified into four categories: tumor suppressor genes, oncogenes, DNA repair genes and carcinogen metabolism-related genes, which were listed in detail as follows.

SNPs of Tumor Suppressor Genes

p53 makes a substantial contribution to the regulation of cell cycle, cellular apoptosis and anti-cancer properties (45). *p53* mutations have been shown to be correlated with the occurrence of primary HNSCC as well as SPMs (51). The polymorphism of *p53* commonly occurred at the codon 72, with a substitution of proline for arginine, which might promote the carcinogenesis by disturbing the apoptosis process and cell cycle (52). Several

studies indicated that *p53* codon 72 polymorphism may play a minor role in the development of HNSCC (53, 54). However, Li et al. showed that patients with *p53* 72Arg/Pro and the combined *p53* 72Arg/Pro + Pro/Pro genotypes exhibited a significantly greater risk of SPMs in a cohort of 1271 HNSCC patients, compared with *p53* 72Arg/Arg genotype (51). The authors speculated that *p53* codon 72 polymorphism may influence the SPM risk by modifying the response to DNA-damaging treatments (51). Despite the inherited limitations of patient selection and clinical outcome collection, these results indicated that *p53* codon 72 polymorphism could serve as a genetic marker to evaluate the risk of SPMs in HNSCC.

Functionally, tumor suppressor gene *p14* and *p73* belong to the *p53*-related gene family. $p14^{ARF}$ gene maps to 9p21 and encodes proteins of $p16^{INK4a}$ and $p14^{ARF}$, thus playing an important role in maintaining genomic stability via *p53* and *Rb* pathways (6). Direct interaction between $p14^{ARF}$ and *MDM2* impedes the protesomal degradation of p53, resulting in an abnormal cell cycle regulation and cellular apoptosis (55). Genetic Alterations of $p14^{ARF}$ have been considered to be rare in the development of HNSCC. Gruttgen et al. evaluated the p14 expression with immunochemistry, and concluded that loss of $p14^{ARF}$ merely occurred in 15 of 100 HNSCC patients (56). Zhang et al. stated that $p14^{ARF}$-rs3088440 and rs3731217 polymorphisms were correlated with a moderately increased risk of SPMs in HNSCC (6). Compared with those without $p14^{ARF}$ variant genotypes, HNSCC patients with both variant genotypes had a 3-fold increased risk for developing SPMs (6). Therefore, $p14^{ARF}$ polymorphisms could serve as a risk marker for SPMs in HNSCC patients (6).

p73 displays a similar function as *p53* in the regulation of cell cycle, apoptosis and DNA repair by inducing apoptosis or G1 cell cycle arrest (57). It has been assumed that *p73* compensated for the absence of *p53* induced by mutations (58). Previous studies have revealed that genetic abnormalities of *p73*, such as its G4C14-to-A4T14 polymorphism, were associated the risk of HNSCC (59, 60). Li et al. investigated the role of *p73* G4C14-to-A4T14 polymorphism in SPMs in a cohort of 1384 HNSCC patients, and advocated that patients carrying *p73* GC/AT heterozygotes or the combined *p73* GC/AT+AT/AT genotypes had a significantly lower SPM susceptibility, compared to those with *p73* GC/GC genotype. The *p73* GC/AT+AT/AT genotypes conferred a pronounced protection over SPMs in several subgroups, for example, older patients, men, minorities, ever smoker, and ever drinkers, further supporting the role of *p73* polymorphism as a genetic marker of MPCs in HNSCC patients (61).

FAS belongs to the death receptor family and interacts with its ligand, *FASLG,* to modulate the extrinsic apoptosis pathway, cellular homeostasis and immune escape of tumor cells (62, 63). Genetic alterations of the *FAS/FASLG* signaling pathway may lead to immune evasion, thus facilitating tumorigenesis including SPM (64). *FAS*-1377G>A, *FAS*−670A>G, *FASLG*-844C>T, and *FASLG*-124 A>G are four well-known SNPs in the FAS/FASLG signaling pathway. Zhang et al. reported that subjects with both the *FAS*-1377 AA and *FAS*-670 (GG + AG) genotypes were associated with an increased risk of HNSCC, but not for those with *FASLG* variant genotypes (65). But things are really different when it comes to the incidence of MPCs. It has been demonstrated that patients carrying *FAS*-670 AG+GG genotypes or *FASLG*-844 CT+TT genotypes were significantly associated with mounting risk of SPMs compared with the wild-type homozygous genotypes, which makes *FAS* and *FASLG* polymorphisms a potential marker for HNSCC patients at high SPM risk (64). Additionally, the risk of SPM was augmented in a dose-response manner for those with increasing number of risk genotypes (64).

p21 and p27 are two CDK inhibitors which participate in the regulation of DNA repair, cell cycle, and apoptosis (66). It has been demonstrated that SNPs in *p21* and *p27* were associated with risk of HNSCC (67, 68). HNSCC patients carrying *p27* 109 TG/GG, *p21* 98 CA/AA, and *p21* 70 CT/TT variant genotypes had a worse survival and an increased SPM risk than those with *p27*109 TT, *p21* 98 CC, and *p21* 70 CC genotypes, respectively (69). Moreover, patients with *p27* (T109G) and *p21* (C98A and C70T) polymorphisms were 2.4 times more susceptible to develop MPCs than those without variant genotypes (69). These results indicated that *p27* T109G and *p21* (C98A and C70T) polymorphisms seem to modulate the susceptibility of SPMs in HNSCC.

Accumulating evidences have established that SNPs of tumor suppressor genes made a considerable contribution to the formation of MPCs in HNSCC, which makes SNPs of tumor suppressor genes a potential molecular marker to predict the risk of MPCs in HNSCC.

SNPs of Oncogenes

Murine double minute 2 (*MDM2*), also known as an E3 ubiquitin ligase, is the central antagonist of the tumor suppressor *p53* (70). MDM2 negatively regulates the activity of *p53* by suppressing its transcriptional activity and promoting its degradation, thus contributing to the carcinogenic process (71). The overexpression and genetic alterations of *MDM2* have been commonly reported in HNSCC (72). Two SNPs in its promoter region, *MDM2*-rs2279744 and *MDM2*-rs937283, may alter MDM2 expression at transcriptional level and subsequently modulate the risk of HNSCC (71). With respect to SPM, Jin et al. reported that *MDM2*-rs2279744 and *MDM2*-rs937283 increased the susceptibility of SPM in HNSCC by 90 and 20%, respectively (73).

Analogous to *MDM2* in structure, murine double minute 4 (*MDM4*) is also a negative regulator of *p53*. Several studies suggested that high *MDM4* expression may substitute for *p53* mutations, and *MDM4* overexpression was a common event in the HNSCC patients (74). Three *MDM4* SNPs, rs11801299G>A, rs1380576C>G, and rs10900598G>T, have been identified in HNSCC patients. Yu et al. proposed that individuals with combined 1-3 risk genotypes of *MDM4* SNPs exhibited significantly increased risk of oropharyngeal cancer (75). In a cohort of 1283 HNSCC patients, Jin et al. concluded that *MDM4*-rs11801299, *MDM4*-rs1380576, and *MDM4*-rs10900598 enhanced the incidence of SPMs in index HNSCC cases by 10, 10, and 40%, respectively (73). Collectively, *MDM2* and *MDM4* polymorphisms may increase the susceptibility of SPMs

in HNSCC to some extent, which may improve the precision of risk estimates of SPMs.

SNPs of DNA Repair Genes

The MRN complex, composed of *MRE11*, *RAD50,* and *Nbs1*, plays a critical role in the double-strand break repair and telomere maintenance (76). To evaluate the role of *MRE11* and *RAD50* genes in HNSCC, Ziółkowska-Suchanek et al. conducted a case and control study of 358 HNSCC patients. Their results suggested that common variants of *MRE11* and *RAD50* genes contributed little to the occurrence of HNSCC and SPTs located in the head and neck region (77). *XRCC3*, short for X-ray repair cross-complementing group 3, is another important gene which participates in the double-strand break repair (78). Several studies revealed that *XRCC3* C18067T polymorphism may play a minor role in the etiology of primary HNSCC as well as MPTs. (78, 79).

The X-ray repair cross-complementing group 1 (*XRCC1*) exerts on a vital role in the DNA single-strand break repair pathway (80). *XRCC1* Arg194Trp, *XRCC1* Arg280His, and *XRCC1* Arg399Gln are the three most common examined SNPs in the *XRCC1* gene (81, 82). Lou et al. suggested that *XRCC1* Arg194Trp, *XRCC1* Arg280His, and *XRCC1* Arg399Gln posed limited effect on the HNSCC risk in a meta-analysis with 29 studies (83). Similarly, no significant associations have been presented between *XRCC1* gene SNPs and the incidence of MPT in the HNSCC patients (79).

Apart from double-strand and single-strand repair pathway, the host can protect the genome from damage induced by various environmental carcinogens by means of nucleotide excision repair (NER) pathway (84). Seven SNPs of the *NER* genes involved in the HNSCC are listed as follows: *XPC* Ala499Val, *XPC* Lys939Gln, *XPD* Asp312Asn, *XPD* Lys751Gln, *XPG* His1104Asp, *ERCC1* C8092A, and *XPA* G23A. Zafereo et al. declared that no significant association between aforementioned seven SNPs and the SPM susceptibility, independently or collectively, has been found in a recessive model (84).

All in all, no significant associations between SNPs of DNA repair genes and MPC risk have been found so far. On the basis of above evidences, it is plausible that SNPs of DNA repair genes might not play a major role in the development of MPCs in the HNSCC subjects.

SNPs of Carcinogen Metabolism-Related Genes

Glutathione peroxidase I (GPX1), a selenium-dependent enzyme, participates in the detoxification of activated oxygen species (85). Genetic alterations or polymorphism in the coding region of *GPX1* gene might be involved in the development of cancer. A significant correlation has been observed between *GPX1* expression and T-stage as well as index tumor sites in HNSCC patients (86). The *GPX1* polymorphism represents three possible alleles, namely ALA5, ALA6, and ALA7. Jefferies et al. evaluated the association between *GPX1* genetic polymorphisms and HNSCC patients who developed SPTs in a case-control study. A significant difference in allele frequencies of *GPX1* ALA*6 and ALA*7 was observed between the SPT cases and controls, which indicated that polymorphisms of *GPX1* gene may be a molecular marker for the development of SPTs in HNSCC (85).

CYP1A1 and *CYP2E1* are two main genes associated with the carcinogen metabolic activation. Rydzanicz et al. reported that HNSCC patients with *CYP1A1* genotype *1/*4 and allele *4 represented a 4.1- and 2.6-fold risk of developing MPT, respectively (79). However, no significant correlations has been established between SNPs of *CYP2E1* gene and the incidence of MPT, which suggested a limited role of *CYP2E1* in the susceptibility of MPTs in HNSCC (79).

Glutathione S transferase (GST) plays a critical role in the detoxication and elimination of various carcinogens (87). *GSTM1*, *GSTT1*, and *GSTM3* gene are three members of the GST family in human (87). Studies reported that the *GSTT1* null genotype and polymorphism in *GSTM3* gene were not correlated with a statistically significant increased risk for SPTs or tobacco-related SPTs (79, 88). Inversely, a significant association was observed between the polymorphism in *GSTM1* gene and development of SPTs or tobacco-related SPTs (88).

N-acetyltransferase 2 (*NAT2*) gene participates in the metabolism of aromatic, heterocyclic amines and hydrazines (89). Evidence from 23 case and control studies indicated that *NAT2* polymorphisms could increase the incidence of HNSCC by 23% and serve as a risk factor of HNSCC in Asians (90). With respect to MPCs, *NAT2**7B was significantly correlated with an increased risk for SPTs in patients after index HNSCC (79).

According to the available evidences, a significant association has been observed between MPCs and SNPs of carcinogen metabolism-related genes, such as *CYP1A1*, *GSTM1,* and *NAT2*. However, well-designed, large-scale, multi-center studies are still warranted to verify these conclusions in the future.

MPCs AND ACQUIRED MUTATIONS

MPCs and CIN

CIN comprises altered DNA copy number and loss or rearrangement of the chromosomes, resulting in the loss or gain of function of certain genes (91). Piccinin et al. evaluated the LOH status at 1p, 3p, 9p, 13q, and 19p. However, no significant differences have been observed between the MPCs group and single cancer group, which suggested that chromosomal instability may not account for the propensity to develop SPMs in the upper aerodigestive tract (49).

MPCs and MSI

MSI, a major hallmark of genetic instability, originates from deficient DNA mismatch repair (92). It is mostly observed and studied in the hereditary non-polyposis colorectal cancer, which is characterized by MPCs of different organs, such as gastrointestinal, endometrial and urinary tract (93). So, MSI is considered to be a major determinant in the development of MPCs. Piccinin et al. analyzed the MSI on five chromosomes in 67 HNSCC patients, 22 MPCs and 45 controls, and revealed that no significant differences existed between MSI and MPCs cases (49). This implied that except for MSI, other systems concerning the genome integrity might be responsible for the

TABLE 1 | Genetic factors, genes, and potential biomarkers of multiple primary cancer of HNSCC.

Factors	Genes	Potential biomarkers
Germline mutation	*p53*, *CDKN2A*, *hMLHI*	Unidentified
SNP	Tumor suppressor genes: *p53*, *p1p14*, *p73*, *FAS/FASLG*, *p21*, *p27*	*p53*, *p1p14*, *p73*, *FAS/FASLG*, *p21*, *p27*
	Oncogenes: *MDM2*, *MDM4*	*MDM2*, *MDM4*
	DNA repair genes: *MRE11*, *RAD50*, *NBN*, *XRCC3*, *XRCC1*, *XPC*, *XPD*, *XPG*, *ERCC1*, *XPA*	Unidentified
	Carcinogen Metabolism-related genes: *GPX1*, *CYP1A1*, *CYP2E1*, *GSTT1*, GSTM1, *GSTM3*, *NAT2*	*GPX1*, *CYP1A1*, *GSTM1*, *NAT2*
CIN	Unidentified	Unidentified
MSI	Unidentified	Unidentified
Epigenetic alterations	*CCNA1*, *DCC*, *TIMP3*	*CCNA1*, *TIMP3*

carcinogenesis of HNSCC and tumor multiplicity of the head and neck region (49).

MPCs and DNA Methylation

DNA methylation is a well-categorized change of epigenetic alterations in tumors, which is capable of silencing the classic tumor suppressor genes (94). DNA methylation could disrupt the tumor suppressor gene function by obstructing its promoter region and impeding the transcriptional process (95). Longo et al. have detected *CCNA1*, *DCC*, and *TIMP3* hypermethylation in the exfoliated cell samples of HNSCC patients (96). To investigate the relationship between hypermethylation and MPCs in HNSCC, Rettori et al. examined the methylation patterns of 19 genes in 70 HNSCC cases (97), revealing that *CCNA1* and *TIMP3* hypermethylation were significantly connected with formation of SPT in HNSCC. Hypermethylation of *CCNA1* and *TIMP3* might be a promising genetic marker to predict the incidence of SPT in HNSCC subjects, providing the basis for the use of preventive measures and adjuvant treatment.

CONCLUSIONS

The dismal prognosis of HNSCC has always been attributed to the occurrence of MPCs. "Field cancerization," induced by carcinogens and CAFs, is proposed to elaborate the development of MPCs. Apart from environmental and immune factors, genetic factors may play a major role in the risk of MPCs. In summary, SNPs of tumor suppressor genes, oncogenes and carcinogen metabolism-related genes, together with DNA methylation, may serve as potential molecular markers of MPCs risk (**Table 1**). SNP chips and next-generation sequencing technology will enables us to access the strength of these "nature" components of MPCs, resulting in early diagnosis and better survival in HNSCC patients. However, there is still a long way to go before the clinical application of these genetic markers. HNSCC is a genetically heterogeneous disease with a wide range of genetic alterations (98), so a panel of genetic markers with the most accuracy and specificity need to be selected. On the other hand, large-scale, well-designed, and multi-center studies are warranted to examine their clinical relevance.

AUTHOR CONTRIBUTIONS

All authors listed have made a substantial, direct and intellectual contribution to the work, and approved it for publication.

FUNDING

This work was supported by National Natural Science Foundation of China grants (Nos. 81672672, 81572650, 81772891, 81502357, and 81972542) and by State Key Laboratory of Oral Diseases Special Funded Projects.

REFERENCES

1. Whaley JT, Indelicato DJ, Morris CG, Hinerman RW, Amdur RJ, Mendenhall WM, et al. Ewing tumors of the head and neck. *Am J Clin Oncol.* (2010) 33:321–6. doi: 10.1097/COC.0b013e3181aaca71
2. Siegel RL, Miller KD, Jemal A. Cancer statistics, 2018. *CA Cancer J Clin.* (2018) 68:7–30. doi: 10.3322/caac.21442
3. Leemans CR, Braakhuis BJ, Brakenhoff RH. The molecular biology of head and neck cancer. *Nat Rev Cancer.* (2011) 11:9–22. doi: 10.1038/nrc2982
4. Simpson MC, Massa ST, Boakye EA, Antisdel JL, Stamatakis KA, Varvares MA, et al. Primary cancer vs competing causes of death in survivors of head and neck cancer. *JAMA Oncol.* (2018) 4:257–9. doi: 10.1001/jamaoncol.2017.4478
5. van der Schroeff MP, van de Schans SA, Piccirillo JF, Langeveld TP, Baatenburg de Jong RJ, Janssen-Heijnen ML. Conditional relative survival in head and neck squamous cell carcinoma: permanent excess mortality risk for long-term survivors. *Head Neck.* (2010) 32:1613–8. doi: 10.1002/hed.21369
6. Zhang Y, Sturgis EM, Zafereo ME, Wei Q, Li G. p14ARF genetic polymorphisms and susceptibility to second primary malignancy in patients with index squamous cell carcinoma of the head and neck. *Cancer.* (2011) 117:1227–35. doi: 10.1002/cncr.25605
7. Do KA, Johnson MM, Lee JJ, Wu XF, Dong Q, Hong WK, et al. Longitudinal study of smoking patterns in relation to the development of smoking-related secondary primary tumors in patients with upper aerodigestive tract malignancies. *Cancer.* (2004) 101:2837–42. doi: 10.1002/cncr.20714
8. Leon X, Del Prado Venegas M, Orus C, Kolanczak K, Garcia J, Quer M. Metachronous second primary tumours in the aerodigestive tract in patients with early stage head and neck squamous cell carcinomas. *Eur Arch Otorhinolaryngol.* (2005) 262:905–9. doi: 10.1007/s00405-005-0922-5
9. Nagao Y, Sata M. High incidence of multiple primary carcinomas in HCV-infected patients with oral squamous cell carcinoma. *Med Sci Monit.* (2009) 15:CR453–9.
10. Xu CC, Biron VL, Puttagunta L, Seikaly H. HPV status and second primary tumours in oropharyngeal squamous cell carcinoma. *J Otolaryngol Head Neck Surg.* (2013) 42:36. doi: 10.1186/1916-0216-42-36
11. Foulkes WD, Brunet JS, Sieh W, Black MJ, Shenouda G, Narod SA. Familial risks of squamous cell carcinoma of the head and neck: retrospective case-control study. *BMJ.* (1996) 313:716–21. doi: 10.1136/bmj.313.7059.716

12. Bunbanjerdsuk S, Vorasan N, Saethang T, Pongrujikorn T, Pangpunyakulchai D, Mongkonsiri N, et al. Oncoproteomic and gene expression analyses identify prognostic biomarkers for second primary malignancy in patients with head and neck squamous cell carcinoma. *Mod Pathol.* (2019) 32:943–56. doi: 10.1038/s41379-019-0211-2
13. Warren S, Gates O. Multiple primary malignant tumors: a survey of the literature and statistical study. *Am J Cancer.* (1932) 16:1358–414.
14. Braakhuis BJ, Tabor MP, Leemans CR, van der Waal I, Snow GB, Brakenhoff RH. Second primary tumors and field cancerization in oral and oropharyngeal cancer: molecular techniques provide new insights and definitions. *Head Neck.* (2002) 24:198–206. doi: 10.1002/hed.10042
15. León X, Quer M, Orús C, Venegas MdP. Can cure be achieved in patients with head and neck carcinomas? The problem of second neoplasm. *Expert Rev Anticancer Ther.* (2001) 1:125–33. doi: 10.1586/14737140.1.1.125
16. Shiga K, Tateda M, Katagiri K, Nakanome A, Ogawa T, Asada Y, et al. Distinct features of second primary malignancies in head and neck cancer patients in Japan. *Tohoku J Exp Med.* (2011) 225:5–12. doi: 10.1620/tjem.225.5
17. Bugter O, van Iwaarden DLP, Dronkers EAC, de Herdt MJ, Wieringa MH, Verduijn GM, et al. Survival of patients with head and neck cancer with metachronous multiple primary tumors is surprisingly favorable. *Head Neck.* (2019) 41:1648–55. doi: 10.1002/hed.25595
18. Ang KK, Harris J, Wheeler R, Weber R, Rosenthal DI, Nguyen-Tan PF, et al. Human papillomavirus and survival of patients with oropharyngeal cancer. *N Engl J Med.* (2010) 363:24–35. doi: 10.1056/NEJMoa0912217
19. Huang SF, Li HF, Liao CT, Wang HM, Chen IH, Chang JT, et al. Association of HPV infections with second primary tumors in early-staged oral cavity cancer. *Oral Dis.* (2012) 18:809–15. doi: 10.1111/j.1601-0825.2012.01950.x
20. Martel M, Alemany L, Taberna M, Mena M, Tous S, Bague S, et al. The role of HPV on the risk of second primary neoplasia in patients with oropharyngeal carcinoma. *Oral Oncol.* (2017) 64:37–43. doi: 10.1016/j.oraloncology.2016.11.011
21. Weinberger PM, Yu Z, Haffty BG, Kowalski D, Harigopal M, Brandsma J, et al. Molecular classification identifies a subset of human papillomavirus–associated oropharyngeal cancers with favorable prognosis. *J Clin Oncol.* (2006) 24:736–47. doi: 10.1200/JCO.2004.00.3335
22. D'Souza G, Kreimer AR, Viscidi R, Pawlita M, Fakhry C, Koch WM, et al. Case-control study of human papillomavirus and oropharyngeal cancer. *N Engl J Med.* (2007) 356:1944–56. doi: 10.1056/NEJMoa065497
23. Benson E, Li R, Eisele D, Fakhry C. The clinical impact of HPV tumor status upon head and neck squamous cell carcinomas. *Oral Oncol.* (2014) 50:565–74. doi: 10.1016/j.oraloncology.2013.09.008
24. Rampias T, Sasaki C, Psyrri A. Molecular mechanisms of HPV induced carcinogenesis in head and neck. *Oral Oncol.* (2014) 50:356–63. doi: 10.1016/j.oraloncology.2013.07.011
25. Fakhry C, Westra WH, Li S, Cmelak A, Ridge JA, Pinto H, et al. Improved survival of patients with human papillomavirus-positive head and neck squamous cell carcinoma in a prospective clinical trial. *J Natl Cancer Inst.* (2008) 100:261–9. doi: 10.1093/jnci/djn011
26. Licitra L, Perrone F, Bossi P, Suardi S, Mariani L, Artusi R, et al. High-risk human papillomavirus affects prognosis in patients with surgically treated oropharyngeal squamous cell carcinoma. *J Clin Oncol.* (2006) 24:5630–6. doi: 10.1200/JCO.2005.04.6136
27. Klussmann JP, Mooren JJ, Lehnen M, Claessen SM, Stenner M, Huebbers CU, et al. Genetic signatures of HPV-related and unrelated oropharyngeal carcinoma and their prognostic implications. *Clin Cancer Res.* (2009) 15:1779–86. doi: 10.1158/1078-0432.CCR-08-1463
28. Martinez I, Wang J, Hobson KF, Ferris RL, Khan SA. Identification of differentially expressed genes in HPV-positive and HPV-negative oropharyngeal squamous cell carcinomas. *Eur J Cancer.* (2007) 43:415–32. doi: 10.1016/j.ejca.2006.09.001
29. Saito Y, Ebihara Y, Ushiku T, Omura G, Kobayashi K, Ando M, et al. Negative human papillomavirus status and excessive alcohol consumption are significant risk factors for second primary malignancies in Japanese patients with oropharyngeal carcinoma. *Jpn J Clin Oncol.* (2014) 44:564–9. doi: 10.1093/jjco/hyu042
30. Cabanillas R, Astudillo A, Valle M, de la Rosa J, Álvarez R, Durán NS, et al. Novel germline CDKN2A mutation associated with head and neck squamous cell carcinomas and melanomas. *Head Neck.* (2013) 35:E80–4. doi: 10.1002/hed.21911
31. Jain KS, Sikora AG, Baxi SS, Morris LG. Synchronous cancers in patients with head and neck cancer: risks in the era of human papillomavirus-associated oropharyngeal cancer. *Cancer.* (2013) 119:1832–7. doi: 10.1002/cncr.27988
32. Mercer RR, Lucas NC, Simmons AN, Zander DS, Tsongalis GJ, Funkhouser WK, et al. Molecular discrimination of multiple primary versus metastatic squamous cell cancers of the head/neck and lung. *Exp Mol Pathol.* (2009) 86:1–9. doi: 10.1016/j.yexmp.2008.11.003
33. Daher T, Tur MK, Brobeil A, Etschmann B, Witte B, Engenhart-Cabillic R, et al. Combined human papillomavirus typing and TP53 mutation analysis in distinguishing second primary tumors from lung metastases in patients with head and neck squamous cell carcinoma. *Head Neck.* (2018) 40:1109–19. doi: 10.1002/hed.25041
34. Gasparotto D, Maestro R, Barzan L, Vukosavljevic T, Doglioni C, Sulfaro S, et al. Recurrences and second primary tumours in the head and neck region: differentiation by p53 mutation analysis. *Ann Oncol.* (1995) 6:933–9. doi: 10.1093/oxfordjournals.annonc.a059362
35. Ronchetti D, Arisi E, Neri A, Pruneri G, Digiuni B, Sambataro G, et al. Microsatellite analyses of recurrence or second primary tumor in head and neck cancer. *Anticancer Res.* (2005) 25:2771–5.
36. Braakhuis BJ, Tabor MP, Kummer JA, Leemans CR, Brakenhoff RH. A genetic explanation of Slaughter's concept of field cancerization: evidence and clinical implications. *Cancer Res.* (2003) 63:1727–30.
37. Simple M, Suresh A, Das D, Kuriakose MA. Cancer stem cells and field cancerization of oral squamous cell carcinoma. *Oral Oncol.* (2015) 51:643–51. doi: 10.1016/j.oraloncology.2015.04.006
38. Kuss I, Hathaway B, Ferris RL, Gooding W, Whiteside TL. Decreased absolute counts of T lymphocyte subsets and their relation to disease in squamous cell carcinoma of the head and neck. *Clin Cancer Res.* (2004) 10:3755–62. doi: 10.1158/1078-0432.CCR-04-0054
39. Atienza JA, Dasanu CA. Incidence of second primary malignancies in patients with treated head and neck cancer: a comprehensive review of literature. *Curr Med Res Opin.* (2012) 28:1899–909. doi: 10.1185/03007995.2012.746218
40. Kuss I, Saito T, Johnson JT, Whiteside TL. Clinical significance of decreased zeta chain expression in peripheral blood lymphocytes of patients with head and neck cancer. *Clin Cancer Res.* (1999) 5:329–34.
41. Grandis JR, Falkner DM, Melhem MF, Gooding WE, Drenning SD, Morel PA. Human leukocyte antigen class I allelic and haplotype loss in squamous cell carcinoma of the head and neck: clinical and immunogenetic consequences. *Clin Cancer Res.* (2000) 6:2794–802.
42. Ge L, Meng W, Zhou H, Bhowmick N. Could stroma contribute to field cancerization? *Med Hypotheses.* (2010) 75:26–31. doi: 10.1016/j.mehy.2010.01.019
43. Angadi PV, Patil PV, Kale AD, Hallikerimath S, Babji D. Myofibroblast presence in apparently normal mucosa adjacent to oral squamous cell carcinoma associated with chronic tobacco/areca nut use: evidence for field cancerization. *Acta Odontol Scand.* (2014) 72:502–8. doi: 10.3109/00016357.2013.871648
44. Chan JS, Tan MJ, Sng MK, Teo Z, Phua T, Choo CC, et al. Cancer-associated fibroblasts enact field cancerization by promoting extratumoral oxidative stress. *Cell Death Dis.* (2017) 8:e2562. doi: 10.1038/cddis.2016.492
45. Lane DP. Cancer. p53, guardian of the genome. *Nature.* (1992) 358:15–6. doi: 10.1038/358015a0
46. Brachman DG, Graves D, Vokes E, Beckett M, Haraf D, Montag A, et al. Occurrence of p53 gene deletions and human papilloma virus infection in human head and neck cancer. *Cancer Res.* (1992) 52:4832–6.
47. Gallo O, Sardi I, Pepe G, Franchi A, Attanasio M, Giusti B, et al. Multiple primary tumors of the upper aerodigestive tract: is there a role for constitutional mutations in the p53 gene? *Int J Cancer.* (1999) 82:180–6. doi: 10.1002/(SICI)1097-0215(19990719)82:2<180::AID-IJC5>3.0.CO;2-P
48. Jefferies S, Edwards S, Hamoudi R, A'Hern R, Foulkes W, Goldgar D, et al. No germline mutations in CDKN2A (p16) in patients with squamous cell cancer of the head and neck and second primary tumours. *Br J Cancer.* (2001) 85:1383. doi: 10.1054/bjoc.2001.2068
49. Piccinin S, Gasparotto D, Vukosavljevic T, Barzan L, Sulfaro S, Maestro R, et al. Microsatellite instability in squamous cell carcinomas of the head and neck

related to field cancerization phenomena. *Br J Cancer.* (1998) 78:1147–51. doi: 10.1038/bjc.1998.644
50. Skierucha M, Milne AN, Offerhaus GJ, Polkowski WP, Maciejewski R, Sitarz R. Molecular alterations in gastric cancer with special reference to the early-onset subtype. *World J Gastroenterol.* (2016) 22:2460–74. doi: 10.3748/wjg.v22.i8.2460
51. Li F, Sturgis EM, Chen X, Zafereo ME, Wei Q, Li G. Association of p53 codon 72 polymorphism with risk of second primary malignancy in patients with squamous cell carcinoma of the head and neck. *Cancer.* (2010) 116:2350–9. doi: 10.1002/cncr.25072
52. Bergamaschi D, Samuels Y, Sullivan A, Zvelebil M, Breyssens H, Bisso A, et al. iASPP preferentially binds p53 proline-rich region and modulates apoptotic function of codon 72-polymorphic p53. *Nat Genet.* (2006) 38:1133–41. doi: 10.1038/ng1879
53. Mojtahedi Z, Hashemi SB, Khademi B, Karimi M, Haghshenas MR, Fattahi MJ, et al. p53 codon 72 polymorphism association with head and neck squamous cell carcinoma. *Braz J Otorhinolaryngol.* (2010) 76:316–20. doi: 10.1590/S1808-86942010000300008
54. Hamel N, Black MJ, Ghadirian P, Foulkes WD. No association between P53 codon 72 polymorphism and risk of squamous cell carcinoma of the head and neck. *Br J Cancer.* (2000) 82:757–9. doi: 10.1054/bjoc.1999.0993
55. Lowe SW, Sherr CJ. Tumor suppression by Ink4a-Arf: progress and puzzles. *Curr Opin Genet Develop.* (2003) 13:77–83. doi: 10.1016/S0959-437X(02)00013-8
56. Gruttgen A, Reichenzeller M, Junger M, Schlien S, Affolter A, Bosch FX. Detailed gene expression analysis but not microsatellite marker analysis of 9p21 reveals differential defects in the INK4a gene locus in the majority of head and neck cancers. *J Pathol.* (2001) 194:311–7. doi: 10.1002/path.906
57. Flores ER, Tsai KY, Crowley D, Sengupta S, Yang A, McKeon F, et al. p63 and p73 are required for p53-dependent apoptosis in response to DNA damage. *Nature.* (2002) 416:560–4. doi: 10.1038/416560a
58. Zheng T, Wang J, Chen X, Meng X, Song X, Lu Z, et al. Disruption of p73-MDM2 binding synergizes with gemcitabine to induce apoptosis in HuCCT1 cholangiocarcinoma cell line with p53 mutation. *Tumour Biol.* (2010) 31:287–95. doi: 10.1007/s13277-010-0035-7
59. Li G, Sturgis EM, Wang LE, Chamberlain RM, Amos CI, Spitz MR, et al. Association of a p73 exon 2 G4C14-to-A4T14 polymorphism with risk of squamous cell carcinoma of the head and neck. *Carcinogenesis.* (2004) 25:1911–6. doi: 10.1093/carcin/bgh197
60. Galli P, Cadoni G, Volante M, De Feo E, Amore R, Giorgio A, et al. A case-control study on the combined effects of p53 and p73 polymorphisms on head and neck cancer risk in an Italian population. *BMC Cancer.* (2009) 9:137. doi: 10.1186/1471-2407-9-137
61. Li F, Sturgis EM, Zafereo ME, Liu Z, Wang LE, Wei Q, et al. p73 G4C14-to-A4T14 polymorphism and risk of second primary malignancy after index squamous cell carcinoma of head and neck. *Int J Cancer.* (2009) 125:2660–5. doi: 10.1002/ijc.24570
62. Blaes J, Thome CM, Pfenning PN, Rubmann P, Sahm F, Wick A, et al. Inhibition of CD95/CD95L (FAS/FASLG) signaling with APG101 prevents invasion and enhances radiation therapy for glioblastoma. *Mol Cancer Res.* (2018) 16:767–76. doi: 10.1158/1541-7786.MCR-17-0563
63. Reichmann E. The biological role of the Fas/FasL system during tumor formation and progression. *Semin Cancer Biol.* (2002) 12:309–15. doi: 10.1016/S1044-579X(02)00017-2
64. Lei D, Sturgis EM, Wang LE, Liu Z, Zafereo ME, Wei Q, et al. FAS and FASLG genetic variants and risk for second primary malignancy in patients with squamous cell carcinoma of the head and neck. *Cancer Epidemiol Biomarkers Prev.* (2010) 19:1484–91. doi: 10.1158/1055-9965.EPI-10-0030
65. Zhang Z, Wang LE, Sturgis EM, El-Naggar AK, Hong WK, Amos CI, et al. Polymorphisms of FAS and FAS ligand genes involved in the death pathway and risk and progression of squamous cell carcinoma of the head and neck. *Clin Cancer Res.* (2006) 12:5596–602. doi: 10.1158/1078-0432.CCR-05-1739
66. Llanos S, Garcia-Pedrero JM, Morgado-Palacin L, Rodrigo JP, Serrano M. Stabilization of p21 by mTORC1/4E-BP1 predicts clinical outcome of head and neck cancers. *Nat Commun.* (2016) 7:10438. doi: 10.1038/ncomms10438
67. Li G, Liu Z, Sturgis EM, Shi Q, Chamberlain RM, Spitz MR, et al. Genetic polymorphisms of p21 are associated with risk of squamous cell carcinoma of the head and neck. *Carcinogenesis.* (2005) 26:1596–602. doi: 10.1093/carcin/bgi105
68. Li G, Sturgis EM, Wang LE, Chamberlain RM, Spitz MR, El-Naggar AK, et al. Association between the V109G polymorphism of the p27 gene and the risk and progression of oral squamous cell carcinoma. *Clin Cancer Res.* (2004) 10:3996–4002. doi: 10.1158/1078-0432.CCR-04-0089
69. Wang Z, Sturgis EM, Zhang F, Lei D, Liu Z, Xu L, et al. Genetic variants of p27 and p21 as predictors for risk of second primary malignancy in patients with index squamous cell carcinoma of head and neck. *Mol Cancer.* (2012) 11:17. doi: 10.1186/1476-4598-11-17
70. Li Q, Lozano G. Molecular pathways: targeting Mdm2 and Mdm4 in cancer therapy. *Clin Cancer Res.* (2013) 19:34–41. doi: 10.1158/1078-0432.CCR-12-0053
71. Yu H, Huang YJ, Liu Z, Wang LE, Li G, Sturgis EM, et al. Effects of MDM2 promoter polymorphisms and p53 codon 72 polymorphism on risk and age at onset of squamous cell carcinoma of the head and neck. *Mol Carcinog.* (2011) 50:697–706. doi: 10.1002/mc.20806
72. Whibley C, Pharoah PD, Hollstein M. p53 polymorphisms: cancer implications. *Nat Rev Cancer.* (2009) 9:95–107. doi: 10.1038/nrc2584
73. Jin L, Sturgis EM, Zhang Y, Huang Z, Wei P, Guo W, et al. Genetic variants in p53-related genes confer susceptibility to second primary malignancy in patients with index squamous cell carcinoma of head and neck. *Carcinogenesis.* (2013) 34:1551–7. doi: 10.1093/carcin/bgt096
74. Valentin-Vega YA, Barboza JA, Chau GP, El-Naggar AK, Lozano G. High levels of the p53 inhibitor MDM4 in head and neck squamous carcinomas. *Hum. Pathol.* (2007) 38:1553–62. doi: 10.1016/j.humpath.2007.03.005
75. Yu H, Wang LE, Liu Z, Wei S, Li G, Sturgis EM, et al. Polymorphisms of MDM4 and risk of squamous cell carcinoma of the head and neck. *Pharmacogenet Genomics.* (2011) 21:388–96. doi: 10.1097/FPC.0b013e32834632e4
76. Lamarche BJ, Orazio NI, Weitzman MD. The MRN complex in double-strand break repair and telomere maintenance. *FEBS Lett.* (2010) 584:3682–95. doi: 10.1016/j.febslet.2010.07.029
77. Ziolkowska-Suchanek I, Mosor M, Wierzbicka M, Rydzanicz M, Baranowska M, Nowak J. The MRN protein complex genes: MRE11 and RAD50 and susceptibility to head and neck cancers. *Mol Cancer.* (2013) 12:113. doi: 10.1186/1476-4598-12-113
78. Shen H, Sturgis EM, Dahlstrom KR, Zheng Y, Spitz MR, Wei Q. A variant of the DNA repair gene XRCC3 and risk of squamous cell carcinoma of the head and neck: a case-control analysis. *Int J Cancer.* (2002) 99:869–72. doi: 10.1002/ijc.10413
79. Rydzanicz M, Wierzbicka M, Gajecka M, Szyfter W, Szyfter K. The impact of genetic factors on the incidence of multiple primary tumors (MPT) of the head and neck. *Cancer Lett.* (2005) 224:263–78. doi: 10.1016/j.canlet.2005.01.015
80. Whitehouse CJ, Taylor RM, Thistlethwaite A, Zhang H, Karimi-Busheri F, Lasko DD, et al. XRCC1 stimulates human polynucleotide kinase activity at damaged DNA termini and accelerates DNA single-strand break repair. *Cell.* (2001) 104:107–17. doi: 10.1016/S0092-8674(01)00195-7
81. Laantri N, Jalbout M, Khyatti M, Ayoub WB, Dahmoul S, Ayad M, et al. XRCC1 and hOGG1 genes and risk of nasopharyngeal carcinoma in North African countries. *Mol Carcinog.* (2011) 50:732–7. doi: 10.1002/mc.20754
82. Csejtei A, Tibold A, Koltai K, Varga Z, Szanyi I, Gobel G, et al. Association between XRCC1 polymorphisms and head and neck cancer in a Hungarian population. *Anticancer Res.* (2009) 29:4169–73.
83. Lou Y, Peng WJ, Cao DS, Xie J, Li HH, Jiang ZX. DNA repair gene XRCC1 polymorphisms and head and neck cancer risk: an updated meta-analysis including 16344 subjects. *PLoS ONE.* (2013) 8:e74059. doi: 10.1371/journal.pone.0074059
84. Zafereo ME, Sturgis EM, Liu Z, Wang LE, Wei Q, Li G. Nucleotide excision repair core gene polymorphisms and risk of second primary malignancy in patients with index squamous cell carcinoma of the head and neck. *Carcinogenesis.* (2009) 30:997–1002. doi: 10.1093/carcin/bgp096
85. Jefferies S, Kote-Jarai Z, Goldgar D, Houlston R, Frazer-Williams M-J, A'Hern R, et al. Association between polymorphisms of the GPX1 gene and second primary tumours after index squamous cell cancer of the head and neck. *Oral Oncol.* (2005) 41:455–61. doi: 10.1016/j.oraloncology.2004.09.012

86. Dequanter D, Dok R, Koolen L, Vander Poorten V, Nuyts S. Prognostic significance of glutathione peroxidase levels (GPx1) in head and neck cancers. *Front Oncol.* (2017) 7:84. doi: 10.3389/fonc.2017.00084
87. Singh H, Sachan R, Devi S, Pandey SN, Mittal B. Association of GSTM1, GSTT1, and GSTM3 gene polymorphisms and susceptibility to cervical cancer in a North Indian population. *Am J Obstet Gynecol.* (2008) 198:303 e1–6. doi: 10.1016/j.ajog.2007.09.046
88. Minard CG, Spitz MR, Wu X, Hong WK, Etzel CJ. Evaluation of glutathione S-transferase polymorphisms and mutagen sensitivity as risk factors for the development of second primary tumors in patients previously diagnosed with early-stage head and neck cancer. *Cancer.* (2006) 106:2636–44. doi: 10.1002/cncr.21928
89. Walker K, Ginsberg G, Hattis D, Johns DO, Guyton KZ, Sonawane B. Genetic polymorphism in N-Acetyltransferase (NAT): population distribution of NAT1 and NAT2 activity. *J Toxicol Environ Health B Crit Rev.* (2009) 12:440–72. doi: 10.1080/10937400903158383
90. Zhang L, Xiang Z, Hao R, Li R, Zhu Y. N-acetyltransferase 2 genetic variants confer the susceptibility to head and neck carcinoma: evidence from 23 case-control studies. *Tumour Biol.* (2014) 35:3585–95. doi: 10.1007/s13277-013-1473-9
91. McClelland SE. Role of chromosomal instability in cancer progression. *Endocr Relat Cancer.* (2017) 24:T23–31. doi: 10.1530/ERC-17-0187
92. Yamamoto H, Imai K. Microsatellite instability: an update. *Arch Toxicol.* (2015) 89:899–921. doi: 10.1007/s00204-015-1474-0
93. Yamashita K, Arimura Y, Kurokawa S, Itoh F, Endo T, Hirata K, et al. Microsatellite instability in patients with multiple primary cancers of the gastrointestinal tract. *Gut.* (2000) 46:790–4. doi: 10.1136/gut.46.6.790
94. Jones PA, Baylin SB. The fundamental role of epigenetic events in cancer. *Nat Rev Genet.* (2002) 3:415–28. doi: 10.1038/nrg816
95. Garinis GA, Patrinos GP, Spanakis NE, Menounos PG. DNA hypermethylation: when tumour suppressor genes go silent. *Hum Genet.* (2002) 111:115–27. doi: 10.1007/s00439-002-0783-6
96. Longo AL, Rettori MM, de Carvalho AC, Kowalski LP, Carvalho AL, Vettore AL. Evaluation of the methylation profile of exfoliated cell samples from patients with head and neck squamous cell carcinoma. *Head Neck.* (2014) 36:631–7. doi: 10.1002/hed.23345
97. Rettori MM, de Carvalho AC, Longo AL, de Oliveira CZ, Kowalski LP, Carvalho AL, et al. TIMP3 and CCNA1 hypermethylation in HNSCC is associated with an increased incidence of second primary tumors. *J Transl Med.* (2013) 11:316. doi: 10.1186/1479-5876-11-316
98. Wiseman SM, Stoler DL, Anderson GR. The role of genomic instability in the pathogenesis of squamous cell carcinoma of the head and neck. *Surg Oncol Clin N Am.* (2004) 13:1–11. doi: 10.1016/S1055-3207(03)00118-2

Conflict of Interest: The authors declare that the research was conducted in the absence of any commercial or financial relationships that could be construed as a potential conflict of interest.

frontiers in Oncology

ORIGINAL RESEARCH
published: 03 December 2019
doi: 10.3389/fonc.2019.01364

Pinostilbene Hydrate Inhibits the Migration and Invasion of Human Nasopharyngeal Carcinoma Cells by Downregulating MMP-2 Expression and Suppressing Epithelial–Mesenchymal Transition Through the Mitogen-Activated Protein Kinase Signaling Pathways

Pao-Yu Tseng[1†], *Yen-Tze Liu*[2,3,4,5†], *Chia-Chieh Lin*[5], *Yi-Ching Chuang*[5], *Yu-Sheng Lo*[5], *Yi-Ting Hsi*[5], *Ming-Ju Hsieh*[3,4,5,6*] *and Mu-Kuan Chen*[1*]

[1] *Department of Otorhinolaryngology, Head and Neck Surgery, Changhua Christian Hospital, Changhua, Taiwan,* [2] *Department of Family Medicine, Changhua Christian Hospital, Changhua, Taiwan,* [3] *Institute of Medicine, Chung Shan Medical University, Taichung, Taiwan,* [4] *Department of Holistic Wellness, Mingdao University, Changhua, Taiwan,* [5] *Oral Cancer Research Center, Changhua Christian Hospital, Changhua, Taiwan,* [6] *Graduate Institute of Biomedical Sciences, China Medical University, Taichung, Taiwan*

Background: Nasopharyngeal carcinoma (NPC) is one of the most common head and neck cancers in East and Southeast Asia. During the past decades, advances in radiotherapy and chemotherapy had shown the improvement in tumor control with fewer side effects. Nevertheless, metastasis of NPC causes treatment failure and is often associated with poor clinical outcome and cancer mortality.

Hypothesis/Purpose: Pinostilbene hydrate (PSH) was recently demonstrated to have anti-metastatic properties on human oral cancers. However, the effects of PSH on NPC cells remain unknown.

Methods and Results: This study aims to investigate the anti-cancer ability of PSH on human NPC by wound healing, transwell assays, zymography assay, and Western blot assay to explore the possible underlying mechanisms. PSH significantly reduced the migrated distance of NPC cells in a dose-dependent manner and the abilities of cancer cell migration and invasion were markedly inhibited. The activity and the expression of MMP-2 were also significantly decreased after treatment with PSH. Furthermore, combined treatment of PSH with ERK1/2 inhibitor (U0126) caused significant elevation of the activity and the expression of MMP-2. Additionally, PSH upregulated the expression levels of E-cadherin and Claudin-1 while downregulating that of N-cadherin and vimentin on both NPC cell lines.

Conclusion: Our research illustrates that PSH inhibits the migration and invasion of human NPC cells. After exposure to PSH on NPC, the expression of MMP-2 is

OPEN ACCESS

Edited by:
Jan Baptist Vermorken, University of Antwerp, Belgium

Reviewed by:
Cheng-Chia Yu, Chung Shan Medical University, Taiwan
Chih-Hsin Tang, China Medical University, Taiwan

***Correspondence:**
Ming-Ju Hsieh
170780@cch.org.tw
Mu-Kuan Chen
53780@cch.org.tw

[†]These authors have contributed equally to this work

Specialty section:
This article was submitted to Head and Neck Cancer, a section of the journal Frontiers in Oncology

Received: *11 June 2019*
Accepted: *18 November 2019*
Published: *03 December 2019*

Citation:
Tseng P-Y, Liu Y-T, Lin C-C, Chuang Y-C, Lo Y-S, Hsi Y-T, Hsieh M-J and Chen M-K (2019) Pinostilbene Hydrate Inhibits the Migration and Invasion of Human Nasopharyngeal Carcinoma Cells by Downregulating MMP-2 Expression and Suppressing Epithelial–Mesenchymal Transition Through the Mitogen-Activated Protein Kinase Signaling Pathways. Front. Oncol. 9:1364. doi: 10.3389/fonc.2019.01364

downregulated and EMT is suppressed through MAPK signaling pathways. These observations suggest that PSH could be a potential anti-metastatic agent for patients with NPC.

Keywords: pinostilbene hydrate, MMP-2, epithelial–mesenchymal transition, MAPK, nasopharyngeal carcinoma

INTRODUCTION

Nasopharyngeal carcinoma (NPC), a malignant epithelial tumor arising from the lining of the nasopharynx, is commonly found at the fossa of Rosenmüller. It has a distinct geographical and ethnic distribution. Many of new cases were reported in east and southeast parts of Asia (1). Worldwide, an estimated 87,000 incident cases and 51,000 deaths occur annually, accounting for about 0.6% of the global cancer burden (1). In Taiwan, the age-adjusted incidence rate of NPC per 100,000 person-years is 8.18 for men and 2.35 for women (2), in contrast to <1 in North America and Europe for both sexes (1). Many risk factors are associated with NPC, including Epstein-Barr virus (EBV) infection (3), host genetic susceptibility in endemic regions (4–6), dietary exposure to salted fish and environment factors (7, 8). Depending on the histological appearance, the World Health Organization (WHO) subtypes NPC as keratinizing squamous cell carcinoma (SCC), non-keratinizing carcinoma and basaloid SCC. Non-keratinizing carcinoma is further sub-categorized into differentiated or undifferentiated tumors (9). In regions with endemic NPC, undifferentiated carcinoma comprises over 95% of cases and the vast majority are associated with EBV infection (10, 11).

During the past decades, advances in population screening, diagnostic imaging, intensity-modulated radiotherapy (IMRT) and systemic agents have driven the improvement in disease control and survival (12, 13). The primary treatment for early stage patients is definitive radiotherapy and the addition of chemotherapy for locally advanced cases has shown a benefit in overall survival (12, 14). However, the metastatic potentiality of NPC remains the major reason of treatment failure for patients; the 5- and 8-years distant metastatic rates were reported as 14.5 and 16.4% in the era of IMRT (15). Furthermore, around 15% of cases were found to have distant metastases at initial staging in endemic NPC (16). Therefore, an effort must be made to optimize the management of tumor invasion and migration in order to achieve a better clinical outcome.

Cancer metastasis is a complex process; it involves the translocation of a cancer cell to a distant organ and the colonization of tumor cells at distant site (17). The metastatic dissemination consists of a series of sequential, interrelated steps: cancer cells invade the host stroma and surrounding tissue, enter the lymphatic channels and blood systems (intravasation), survive in the circulation and translocate to distant organs through the bloodstream, exit from the bloodstream (extravasation), survive the foreign microenvironment of distant tissues, and finally proliferate within the organ parenchyma into a macroscopic metastatic tumor (colonization) (17, 18).

Invasion of ECM is another critical process in cancer metastasis; both chemokine signaling and interactions between cancer cells and physical components of the metastatic niche are involved (17, 19). The matrix metalloproteinases (MMPs), a family of zinc-dependent endopeptidases that consist of more than 20 human MMPs, are the most prominent proteinases associated with cancer progression. Numerous studies had found the upregulated activity of MMPs in head and neck SCC and a negative association between the MMP level and the prognosis (20–24). Therefore, to understand how MMPs work in metastasis of NPC may help us to find more ways of tumor control.

People are increasing their interests in studying naturally extracted compounds or their analogs as one of anti-cancer agents. Resveratrol (*trans*-3,5,4′-trihydroxystilbene), existing in grapes, berries and red wine, is one of the well-studied agents with potential roles in both cancer prevention and treatment (25, 26). Resveratrol also showed synergistic effects with 5-fluoruracyl and cisplatin in the adjuvant therapy which increased the chemosensitization of cancers (27, 28). While resveratrol is unstable in the environment, it is very sensitive to air and light. For years, many derivatives of resveratrol were investigated and studies demonstrated that methylated resveratrol derivatives were more effective in the treatment of cancer with better bioavailability and bioactivity (29–31). Pinostilbene (3,4'-dihydroxy-5-methoxystilbene) is one of the naturally occurring methylated derivatives of resveratrol; it was reported to exert a potent neuroprotective effect against parkinsonism mimetic 6-hydroxydopamine-induced neurotoxicity in SH-SY5Y cells (31) and inhibitory effects on human colon cancer cells (32). More recently, study also found the antimetastatic effects of pinostilbene hydrate (PSH) on human oral SCC by downregulation of MMP-2 through mitogen-activated protein kinase (MAPK) signaling pathway (33). However, anti-cancer ability of PSH on NPC cells remains unknown. Here we try to evaluate the effects of PSH on NPC-039 and NPC-BM cells and discuss the possible involved mechanisms.

MATERIALS AND METHODS

Reagents

Pinostilbene hydrate (3, 4′-Dihydroxy-5-methoxy-trans-stilbene hydrate, PSH) (≥95% purity) was purchased from Sigma-Aldrich (St. Louis, MO, USA) and dissolved in pure grade dimethyl sulfoxide (DMSO). Antibodies against MMP-2, protein kinase B (PKB, also known as AKT), phospho-AKT (p-AKT), p38, phospho-p38 (p-p38), extracellular signal-regulated kinase 1/2 (ERK 1/2), phospho-ERK 1/2 (p-ERK1/2), c-Jun N-terminal

Abbreviations: NPC, Nasopharyngeal carcinoma; PSH, Pinostilbene hydrate; ERKs, Extracellular signal–regulated kinases; JNKs, c-Jun N-terminal kinases; MAPK, Mitogen-activated protein kinases.

kinase 1/2 (JNK 1/2), phospho-JNK1/2 (p-JNK1/2), E-cadherin, Claudin-1, Vimentin, and N-cadherin were purchased from cell Signaling Technology (Danvers, MA, USA) and stored at −20°C. β-actin was bought from Novus Biologicals (Littleton, CO, USA). 3-(4, 5-dimethylthiazol-2-yl)-2, 5-diphenyltetrazolium bromide (MTT) were obtained from Sigma-Aldrich (St Louis, MO, USA) and stored at 4°C. Specific ERK1/2 inhibitor (U0126) and JNK1/2 inhibitor (SP600125) were purchased from Santa Cruz Biotechnology (Santa Cruz, CA, USA) and stored at −20°C.

Cell Culture

The human NPC cell lines NPC-BM and NPC-039 were provided by doctor Jen-Tsun Lin, Hematology and Oncology, Changhua Christian Hospital. The human nasopharyngeal normal primary cell line was obtained from Celprogen (Torrance, CA). The cells were cultured in RPMI 1640 Medium (Gibco BRL, Grand Island, NY, USA) supplemented with 10% fetal bovine serum (FBS), 1% penicillin/streptomycin, 1.5 g/l sodium bicarbonate, 1 mM glutamine, and 1 mM sodium pyruvate (Sigma, St. Louis, MO) at 37°C in one atmosphere with 5% CO_2.

Cell Viability (MTT Assay)

The cell viability was determined by MTT assay. NPC-039 and NPC-BM (1×10^4 cells/well) were seeded in 24-well plates and treated with various concentrations of PSH (0, 20, 40, and 80 μM) for 24 h. Then the medium was removed and the cells were incubated with MTT reagent 500 μl (0.5 mg/mL) at 37°C in 5% CO_2 for 4 h. After removing the supernatant, DMSO was added to dissolve the formed formazan crystals. At last, the absorbance of the converted dye was measured using an enzyme-linked immunosorbent assay (ELISA) plate reader at a wavelength of 595 nm to determine the cell viability.

Wound Healing Assay

NPC-039 and NPC-BM cells were seeded on 6-well plates at 5×10^5 cells/well and incubated for 24 h. Then the cells were wounded by scratching with a 200-μl sterile pipette tip. After being washed twice, the cells were treated with PSH (0, 20, 40, and 80 μM) for 24 h. Then the cell migration was observed and photographed at the appropriate fields by using a phase-contrast microscope. The wound closure was monitored for 6 h. The cell-free area in the dish was measured by an inverted microscope (OlympusIX71, Tokyo, Japan) and the cell migrated distance was calculated by ImageJ software. Experiments were performed for at least three times.

Cell Migration and Invasion Assays

Cell migration and invasion assays were performed as previously described (33, 34). NPC-039 and NPC-BM cells were incubated with different concentrations of PSH (0, 20, 40, and 80 μM) for 24 h. For migration assay, the lower chamber was filled with 600 μL of medium supplemented with 10% FBS in advance. Then the treated cells were seeded to the upper compartment of Transwell (Greiner Bio-One, North Carolina, USA) and incubated at 37°C for 16 h. For invasion assay, the treated cells were seeded in a matrigel (25 mg/50 mL, 60 μl; BD Biosciences, MA) coated upper compartment of chamber with growth medium placed in underneath chamber and incubated for 24 h. The non-migratory cells were removed after incubation for 24 h. Finally, the membrane was fixed with methanol and stained with 10% Giemsa for 2 h. The migratory cell number was quantified by randomly counting at more than three independent visual fields under the light microscope.

Assessment of MMP-2 Activity

NPC-039 and NPC-BM cells were plated in 24-well plates and treated with different concentrations of PSH (0, 20, 40, and 80 μM) for 24 h. Then the cultured medium was collected, mixed with a loading buffer and subjected to 0.1% gelatin−8% sodium dodecyl sulfate-polyacrylamide gel electrophoresis (SDS-PAGE). After the proteins were electrophoretically separated, the gels were washed for 30 min twice in 2.5% Triton X-100 and incubated in reaction buffer (40 mM Tris-HCL, pH 8.0, 0.02% NaN_3, 10 mM $CaCl_2$) at 37°C for overnight. Subsequently, the gel was stained with Coomassie Brilliant Blue R-250 as described previously (33, 34) and the zones corresponding to proteolytic activity of MMP-2 were analyzed by ImageJ software.

Western Blot Analysis

The treated cells were harvested and lysed in ice-cold RIPA buffer to extract all proteins. The protein concentrations were detected using the bicinchoninic acid (BCA) assay. Equal amounts of proteins were separated by 10% polyacrylamide gel and transferred onto a polyvinylidene fluoride (PVDF) membrane (EMD Millipore). After blocking in 5% non-fat milk with TBS-T buffer (20 mM Tris, 137 mM NaCl, pH 7.4) at room temperature for 1 h, membranes were incubated with diluted primary antibody (dilution of 1:1,000) and β-actin at 4°C with gentle shaking for overnight. Then washing with TBS-T for three times, membranes were incubated with the appropriate horseradish peroxidase-conjugated secondary antibody at room temperature for 1 h, rewashing with TBS-T for three times, the blots were visualized using an enhanced chemiluminescence (ECL) reagent (EMD Millipore) and autoradiography. β-actin was used as a loading control. The relative photographic density was quantified by ImageQuant LAS 4000 mini Biomolecular Imager (GE Healthcare Bio-Sciences AB, Björkgatan 30 751 84 Uppsala, Sweden). The relative density was quantitated with gel documentation and analysis (AlphaImager 2000; Alpha Innotech Corporation, San Leandro, CA, USA).

Statistical Analysis

Statistical analysis was performed using SigmaStat 2.0 (Jandel Scientific, San Rafael, CA). Data were presented as the mean ± standard deviation (SD) of at least three independent experiments. Student's *t*-test was used for comparison among different groups. $P < 0.05$ was considered as statistically significant.

RESULTS

Effects of PSH on the Viability of Human NPC Cells

To examine the cytotoxicity of PSH on NPC cell lines, the cells were evaluated by MTT assay. The chemical structure of PSH is shown in **Figure 1A**. NPC-039, NPC-BM, and human nasopharyngeal normal primary cell lines were treated with various concentrations of PSH (0, 20, 40, and 80 μM) for 24 h. The growth-inhibitory effects were observed (**Figures 1B–D**). Comparing with the control group, PSH significantly inhibited the cell viability when NPC-039 and NPC-BM were incubated with 80 μM of PSH. No significant cytotoxic effects were observed on both cell lines when treated with other concentrations of PSH. A concentration range of 0–80 μM of PSH was then chosen for subsequent experiments.

Inhibitory Effects of PSH on Motility, Migration, and Invasion of NPC Cell Lines

To determine the role of PSH on motility of NPC cells, the wound healing assay was performed. The results showed a significant reduction in migrated distance for both cell lines after exposure to PSH (**Figures 2A–D**). PSH markedly inhibited the wound gap closure in a dose-dependent manner. To evaluate the effects of PSH in migration and invasion of NPC-039 and NPC-BM cells, transwell assays were used. As shown in **Figure 2**, the abilities of cancer cell migration (**Figures 2E,F**) and invasion (**Figures 2G,H**) were significantly decreased by PSH on both cell lines in a dose-dependent manner. These results indicated that PSH played a negative role in migration and invasion of human NPC cells.

PSH Downregulated MMP-2 Activity and Expression on NPC Cells

Degradation of ECM by extracellular proteinases is crucial to the invasion and migration of cancer cells (35, 36) and MMPs are the most famous proteinases associated with tumorigenesis. We investigated the activity of MMP-2 in PSH treated human NPC cells through the gelatin zymography assay. After exposure to PSH (0, 20, 40, and 80 μM) for 24 h, significantly reduced activity of MMP-2 in a dose-dependent manner was noticed on NPC-039 and NPC-BM cells (**Figures 3A–D**). Furthermore, the expression of MMP-2 was examined by Western blot assay. With higher dose of PSH administration on both cell lines, the expression level of MMP-2 became lower (**Figures 3E–H**). PSH significantly downregulated the activity and expression of MMP-2 in human NPC cells.

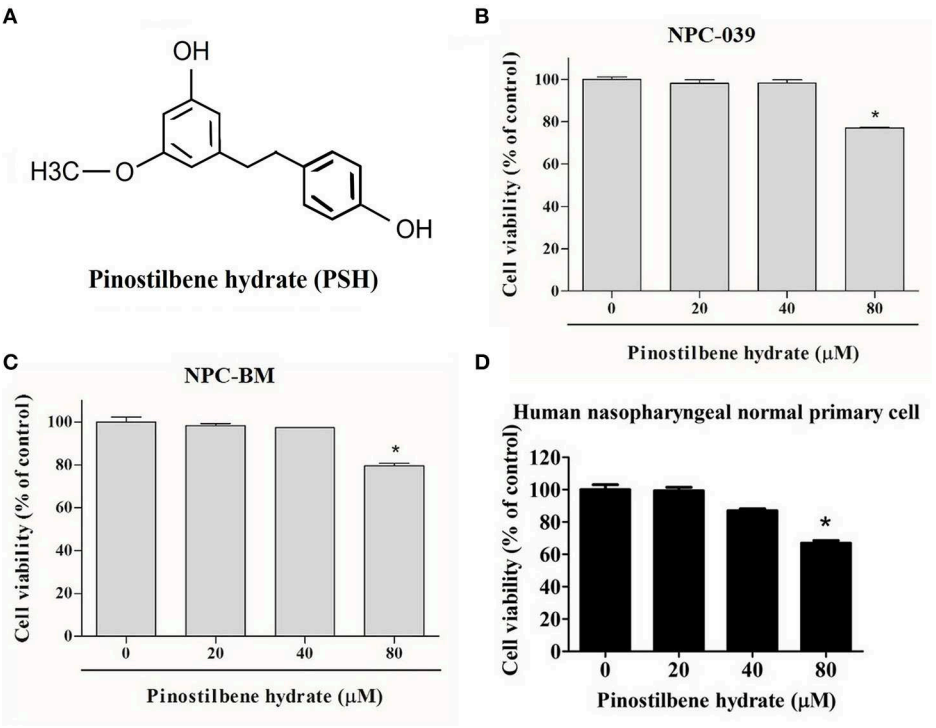

FIGURE 1 | Effects of PSH on the viability of human NPC cells. NPC-039 and NPC-BM cells were treated with various concentrations of PSH (0, 20, 40, and 80 μM) for 24 h. The cell viability was determined by MTT assay. **(A)** Chemical structure of pinostilbene hydrate (PSH). The cytotoxicity was observed on **(B)** NPC-039, **(C)** NPC-BM, and **(D)** human nasopharyngeal normal primary cell lines. PSH significantly inhibited the cell viability of NPC-039 and NPC-BM cells after treatment with 80 μM of PSH. The values are the mean ± SD of at least three independent experiments. $^*p < 0.05$.

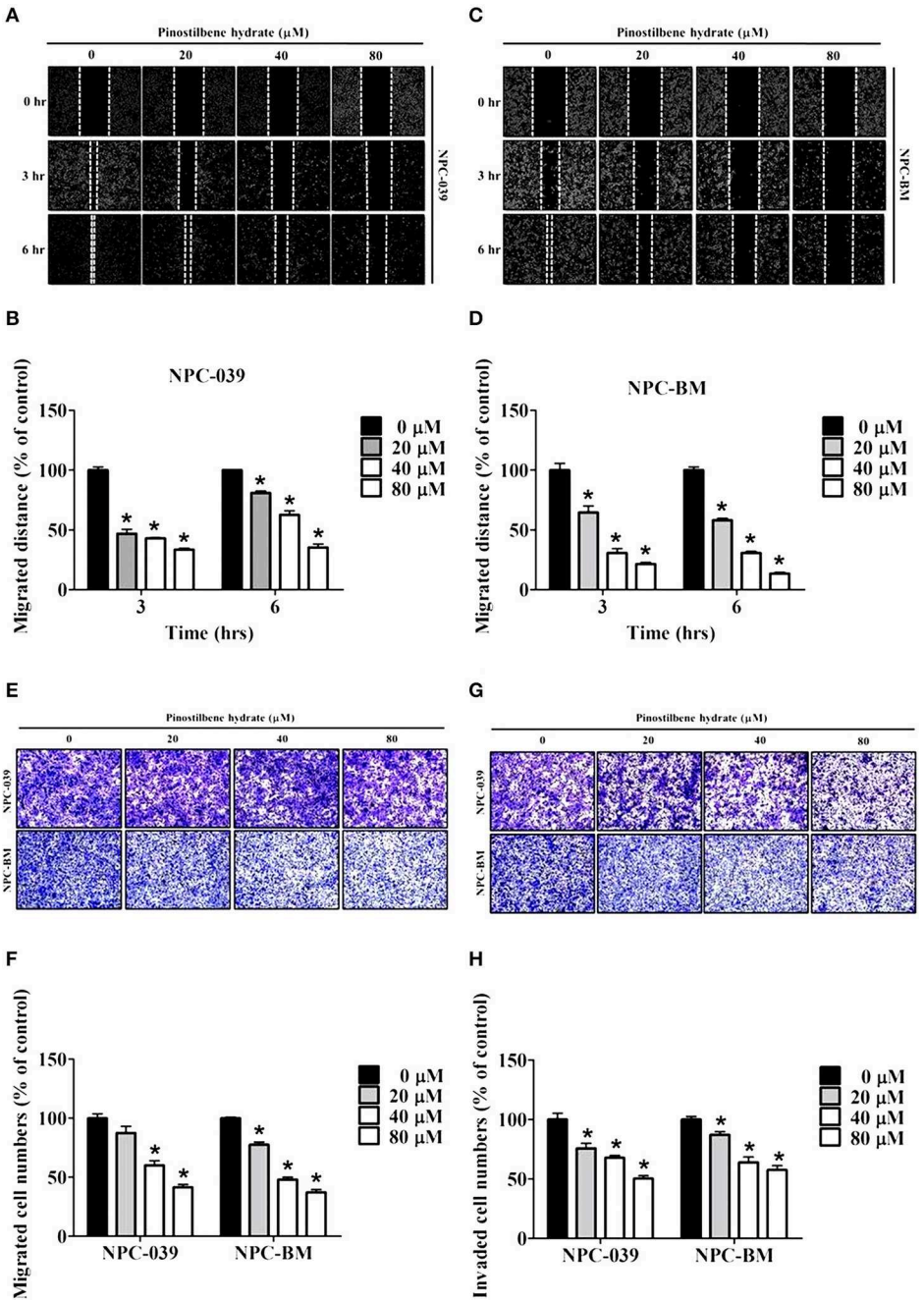

FIGURE 2 | Effects of PSH on motility, migration, and invasion of NPC cell lines. NPC cells were treated with various concentrations of PSH (0, 20, 40, and 80 μM) for 24 h. The migrated distance was determined by the wound healing assay on NPC-039 **(A,B)** and NPC-BM **(C,D)** cell lines. PSH significantly reduced the migrated distance of NPC cells when pictured at 3 and 6 h in a dose-dependent manner. To evaluate the effects of PSH in migration **(E,F)** and invasion **(G,H)** transwell assays were used. The abilities of cell migration and invasion were markedly inhibited by PSH on both cell lines in a dose-dependent manner. The values are the mean ± SD of at least three independent experiments. *$p < 0.05$.

PSH Reduced the Activity of MMP-2 via the MAPK Signaling Pathways on NPC-039 and NPC-BM Cell Lines

Previous studies indicated that the MAPK pathways were involved in the regulation of MMP-2 expression on oral cancer cells (33, 37). To evaluate the associated mechanisms in NPC, we directly measured the expression and the phosphorylation of AKT, ERK1/2, JNK1/2, p38 on NPC cells in response to PSH by Western blot analysis. The findings revealed that PSH promoted the expression of p-ERK1/2 and p-JNK1/2,

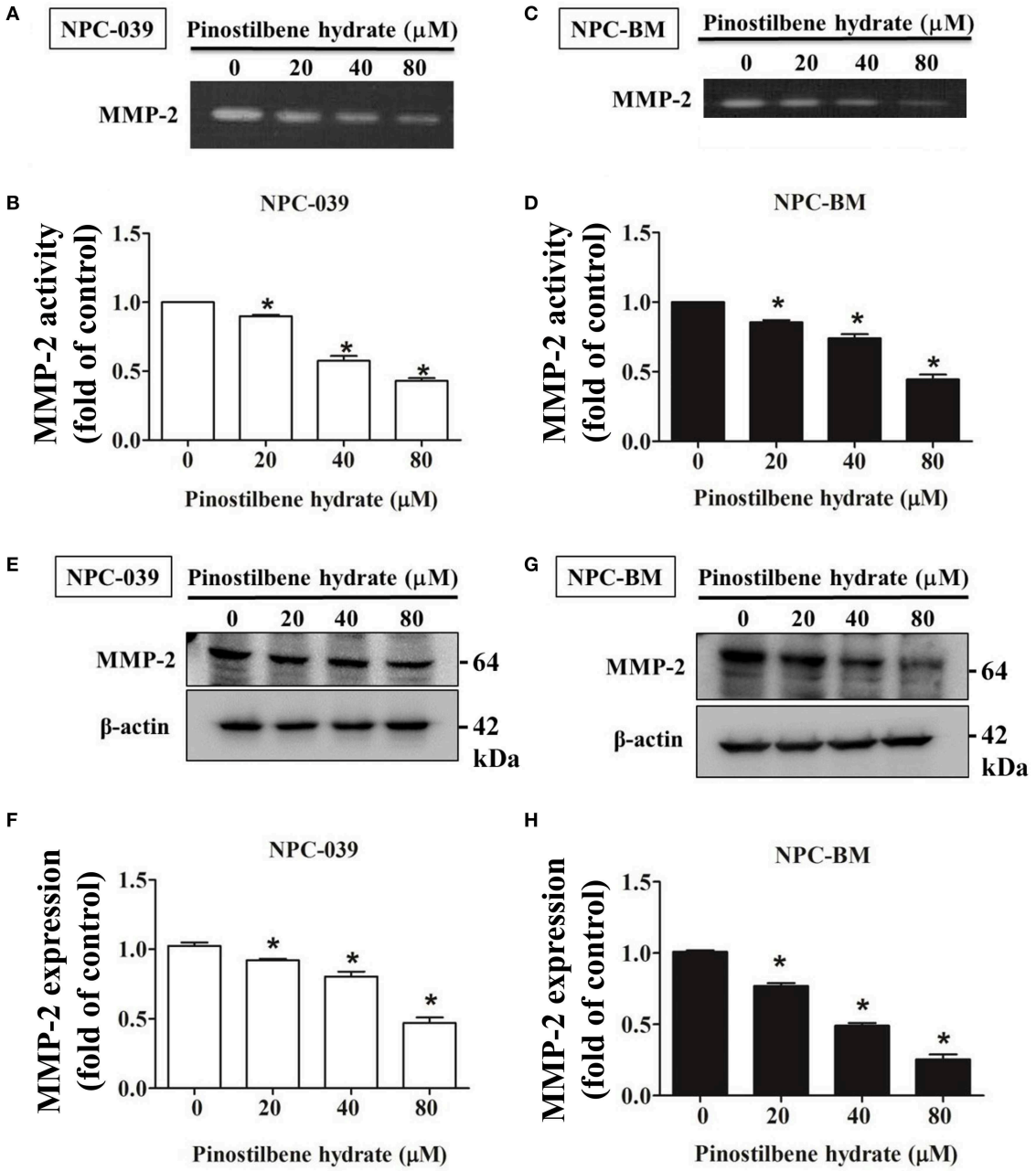

FIGURE 3 | PSH downregulated the activity and expression of MMP-2 in NPC cells. The activity of MMP-2 in PSH treated human NPC cells was examined by the gelatin zymography assay. Significant decreased activity of MMP-2 in a dose-dependent manner was noticed on NPC-039 **(A,B)** and NPC-BM cell lines **(C,D)**. **(E–H)** The expression of MMP-2 level was detected by Western blot assay. PSH significantly reduced the expression of MMP-2 in a dose-dependent manner on both cell lines. β-actin was used as a loading control. The values are the mean ± SD of at least three independent experiments. $^*p < 0.05$.

but not p-AKT and p-p38, on NPC-039 and NPC-BM cell lines in a dose-dependent manner **(Figures 4A–C)**. To further clarify whether PSH regulated the activity of MMP-2 through MAPK signaling pathways, cells were pretreated with or without specific ERK1/2 inhibitor (U0126) or JNK1/2 inhibitor (SP600125) for 1 h followed by treatment with PSH (0 and 80 μM) for 24 h. The activity of MMP-2 was then determined by gelatin zymography as previously described in methods. The results showed a significant elevation in activity of MMP-2 on 80 μM PSH treated NPC cells with exposure to U0126 or SP600125 when compared with PSH treatment only **(Figures 4D–G)**. In addition, a combined treatment of PSH with U0126, but not SP600125, also significantly contributed to the increased expression of MMP-2 level on both cell lines

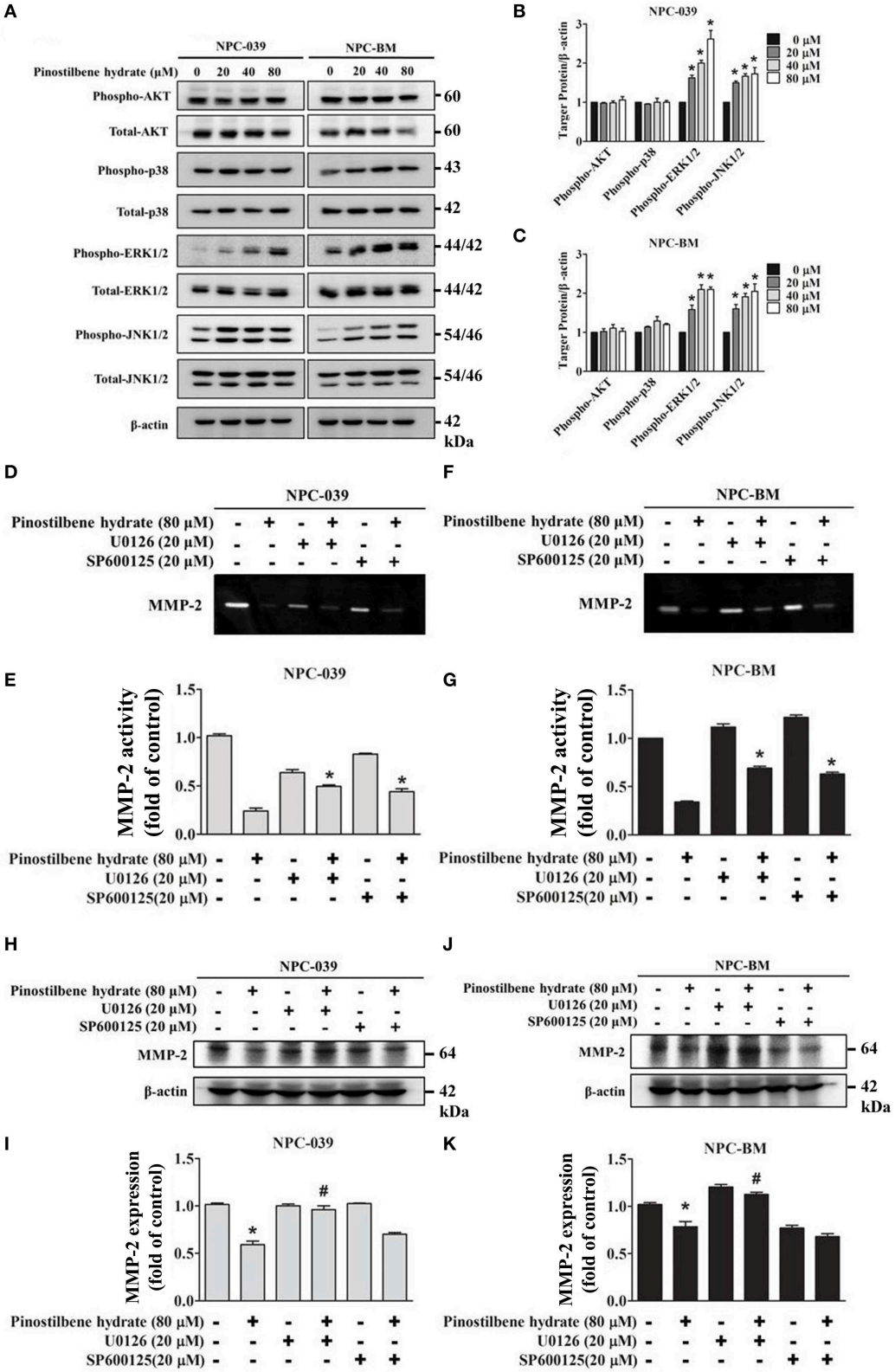

FIGURE 4 | PSH regulated the activity of MMP-2 via the MAPK signaling pathways on NPC-039 and NPC-BM cell lines. **(A)** Cells were treated with different concentrations of PSH (0–80 μM) for 24 h. The p-AKT, p-ERK1/2, p-JNK1/2, and p-p38 were analyzed by Western blot with their respective antibodies. The total

(Continued)

FIGURE 4 | protein of AKT, ERK1/2, JNK1/2, and p38 is also shown. **(B,C)** PSH significantly promoted the expression of p-ERK1/2 and p-JNK1/2 on NPC-039 and NPC-BM cell lines in a dose-dependent manner. Values represent the mean ± SD of at least three independent experiments. $^{*}P < 0.05$, compared with the control (0 μM). **(D–G)** The cells were pretreated with or without ERK1/2 inhibitor (U0126) or JNK1/2 inhibitor (SP600125) followed by treatment with PSH (0 and 80 μM) for 24 h significantly upregulated activity of MMP-2 in combined treatment of PSH with U0126 or SP600125 was noted. $^{*}P < 0.05$, compared with 80 μM PSH treated only group. **(H–K)** A co-treatment of PSH with U0126, but not SP600125, significantly contributed to the elevated expression of MMP-2 level on both cell lines. $^{*}P < 0.05$, compared with the control. $^{\#}P < 0.05$, compared with 80 μM PSH treated only group.

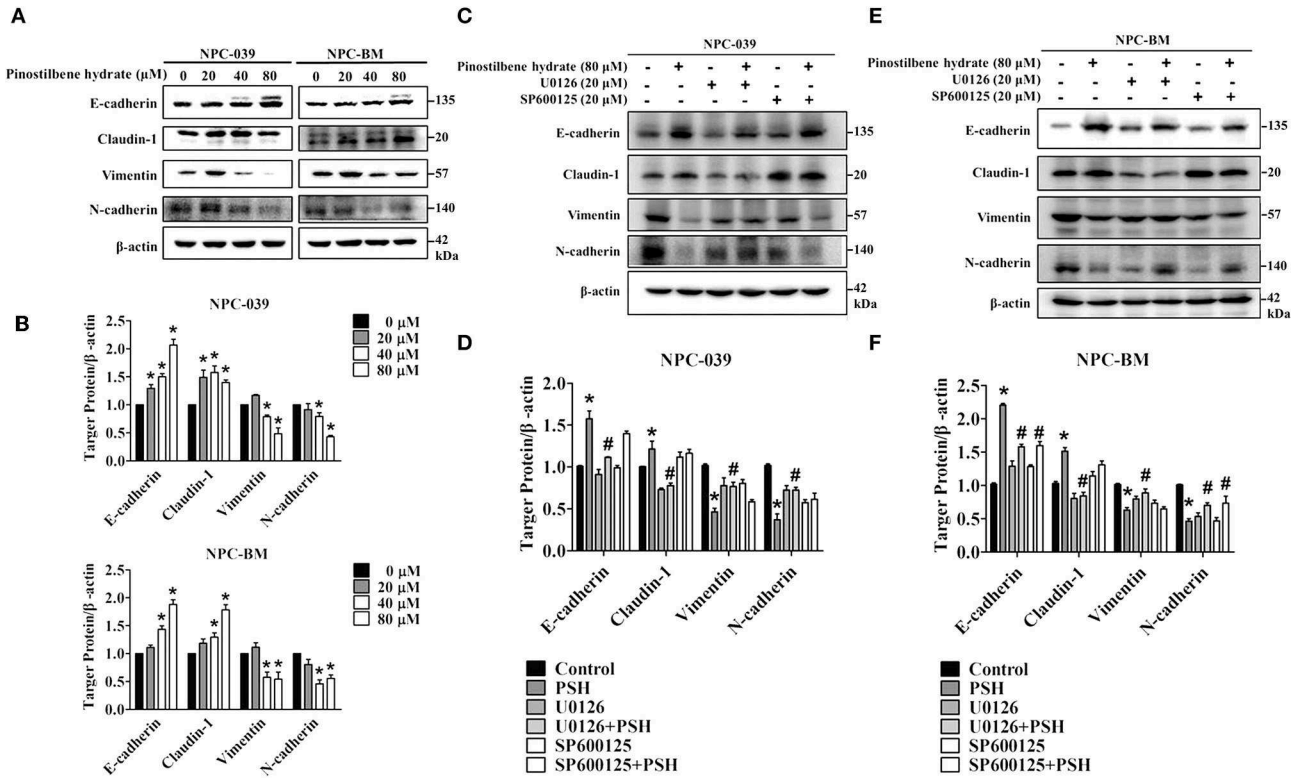

FIGURE 5 | PSH suppressed EMT on NPC cells via the MAPK signaling pathways. **(A,B)** Cells were treated with PSH (0–80 μM) for 24 h. The expression levels of epithelial marker proteins (E-cadherin, Claudin-1) and mesenchymal marker proteins (vimentin, N-cadherin) were analyzed by Western blot. PSH upregulated the expression of E-cadherin and Claudin-1 while downregulating that of N-cadherin and vimentin on both NPC cell lines. $^{*}P < 0.05$, compared with the control (0 μM). **(C,D)** Combined treatment of PSH with U0126 in NPC-039 cells showed significant increased levels of vimentin and N-cadherin with decreased levels of E-cadherin and Claudin-1 when compared with 80 μM PSH treatment only group. $^{*}P < 0.05$, compared with the control. $^{\#}P < 0.05$, compared with 80 μM PSH treated only group. **(E,F)** Relative to the group treated with 80 μM PSH alone, a co-treatment of PSH with U0126 or SP600125 in NPC-BM cell lines elevated the expression levels of mesenchymal markers and suppressed the expression of epithelial marker proteins. $^{*}P < 0.05$, compared with the control. $^{\#}P < 0.05$, compared with 80 μM PSH treated only.

(**Figures 4H–K**). Therefore, the phosphorylation of ERK1/2 was involved in the regulation of MMP-2 in NPC cells with PSH administration.

PSH Suppressed EMT in NPC Cells via the MAPK Signaling Pathways

EMT is also one important process in cancer metastasis. We thus examined the influence of PSH on EMT markers in NPC cell lines. After incubation with various concentrations of PSH (0, 20, 40, and 80 μM) for 24 h, the expression levels of epithelial marker proteins (E-cadherin, Claudin-1) and mesenchymal marker proteins (vimentin, N-cadherin) were analyzed by Western blot assay (**Figures 5A,B**). The findings indicated that PSH upregulated the expression levels of E-cadherin and Claudin-1 while downregulating that of N-cadherin and vimentin on both NPC cell lines ($^{*}P < 0.05$). To further clarify the association between PSH-suppressed EMT and MAPK signaling pathways, cells were pretreated with or without U0126 or SP600125 for 1 h followed by treatment with PSH (0 and 80 μM) for 24 h. The EMT markers were then determined again. In NPC-039 cells, co-treatment with PSH and U0126 showed significant elevated levels of vimentin and N-cadherin with decreased levels of E-cadherin and Claudin-1 as compared with 80 μM PSH treatment only (**Figures 5C,D**). Similar results were also noted in NPC-BM cells; co-treatment of PSH with U0126 or SP600125 increased the expression levels of mesenchymal marker proteins while suppressing the levels of epithelial marker proteins relative to the group treated with 80 μM PSH alone (**Figures 5E,F**). These

data revealed that PSH could suppress EMT in human NPC cells through the MAPK pathways.

DISCUSSION

NPC is a radiosensitive tumor and definitive radiotherapy or chemoradiotherapy forms the main treatment for non-metastatic NPC. The introduction of IMRT and the addition of systemic agents to radiotherapy partly contribute to the improvement in disease control and survival (12, 14). However, the great potentiality of systemic dissemination in NPC patients is troublesome and the outcomes for metastatic cases are heterogeneous and can be very poor (12, 15). In previous study, the anti-metastatic effect of PSH on human oral SCC by downregulation of MMP-2 through MAPK pathways was reported (33). Here, we further examined the effects of PSH on two NPC cell lines and discussed the possible mechanisms. Our results suggested that PSH inhibited the migration and invasion of NPC cells by downregulating MMP-2 expression and suppressing EMT through the MAPK signaling pathways.

Cancer metastasis is a complicated process; both EMT and the invasion of ECM play crucial roles during the metastatic dissemination (17, 18). The MMPs are proteinases that involve the ECM invasion, cancer migration and signaling pathways that control cell growth and angiogenesis (35, 36). Among MMPs, MMP-2 and MMP-9 are collagenase that can selectively degrade type IV collagen, a major component of ECM; overexpression of MMP-2 or MMP-9 is associated with more lymph node metastases, distant metastases and poor survival in head and neck SCC (21–24). Furthermore, Wong and colleague reported that a high pro-MMP2 level was correlated with poor survival in patients with undifferentiated NPC (38). Liu et al. demonstrated an increased MMP-9 level as an unfavorable prognostic factor for NPC; patients with elevated MMP-9 level had a significantly shorter overall survival (OS) time and higher MMP-9 level was positively associated with the status of lymph node metastasis and clinical stage (39). Therefore, MMPs inhibitor had become one of molecular targeted therapy in development for treatment of NPC (40). One study had shown zoledronic acid (MMP inhibitor) combined with chemotherapy could improve progression-free survival (PFS) and OS in NPC patients with bone metastases (41).

In the present study, the cell viability of NPC-039 and NPC-BM cells were significantly decreased after exposure to 80 μM of PSH for 24 h (**Figures 1B,C**). A significant reduction in migrated distance was also observed through the wound healing assay; PSH markedly suppressed the wound gap closure in a dose-dependent manner (**Figures 2A–D**). In addition, the ability of cancer cell migration and invasion were inhibited by PSH on both NPC cell lines (**Figures 2E–H**). These results indicated that PSH played a negative role in the migration and invasion of human NPC cells and PSH could be a potential anti-metastatic drug for NPC. Various studies had shown the anti-metastatic effects of certain agent on NPC or oral cancers through the downregulation of MMP-2 or MMP-9 via the MAPK signaling pathways (33, 34, 37, 42). We thus used the gelatin zymography assay and Western blot to analyze the effects of PSH on MMPs in NPC cells. Our findings showed PSH reduced the activity and the expression of MMP-2 in a dose-dependent manner on NPC cells (**Figure 3**). We then further evaluated the mechanisms that involved PSH mediated MMP-2 expression in NPC. The levels of MAPK pathway proteins were examined after treatment with PSH. Our data revealed PSH promoted the expression of p-ERK1/2 and p-JNK1/2, but not p-AKT and p-p38, in human NPC cells (**Figures 4A–C**). Moreover, co-treatment with PSH and ERK1/2 inhibitor (U0126) or JNK1/2 inhibitor (SP600125) contributed to the upregulated activity of MMP-2 in NPC when compared with PSH treatment only group (**Figures 4D–G**). Therefore, MAPK signaling pathways were involved in PSH mediated MMP-2 regulation in NPC and blocking the ERK or JNK pathway might interfere the anti-metastatic ability of PSH to NPC cells.

EMT is also recognized as an important step in the metastasis of malignancies and the level of E-cadherin was negatively correlated with the clinical prognosis in NPC (40, 43–45). Nowadays demethylation of E-cadherin gene is considered to be a potential therapeutic strategy for patients with NPC (46). Some studies demonstrated the inhibitory effects on migration and invasion of NPC cells by suppressing EMT (47, 48). We then observed the influence of PSH on EMT markers in NPC-039 and NPC-BM cells by Western blot assay. After exposure to PSH, expression levels of the epithelial markers E-cadherin and Claudin-1 increased, while that of the mesenchymal markers N-cadherin and vimentin decreased (**Figures 5A,B**). Furthermore, combined treatment with PSH and U0126 or SP600125 showed significantly elevated levels of mesenchymal markers with decreased levels of epithelial markers relative to the group treated with PSH alone (**Figures 5C–F**). Taken together, PSH suppressed the EMT process in NPC cells; the addition of ERK 1/2 inhibitor or JNK1/2 inhibitor reversed this ability and induced NPC cells to regain EMT characteristics which restored the invasiveness of NPC cells. These data suggested that PSH might suppress EMT in human NPC cell lines through the MAPK pathways.

Our results demonstrated that PSH downregulated the activity and the expression of MMP-2 on both NPC-039 and NPC-BM cell lines. A significant reduced migrated distance under the wound healing assay and marked inhibitory effects on the migration and invasion of NPC cells were also observed. After exposure to PSH, the expression of epithelial markers increased, while that of mesenchymal markers decreased, which suggested the ability of PSH to reverse the EMT process in NPC. We also found the associations of MAPK pathways with PSH mediated MMP-2 downregulation and EMT suppression in NPC; ERK and JNK pathways were involved in these molecular mechanisms. In conclusion, PSH inhibited the migration and invasion of human NPC cells *in vitro* by downregulating MMP-2 and suppressing EMT through MAPK signaling pathways. Data obtained from our study indicated that PSH could be a potential anti-metastatic agent for patients with NPC, though more detailed studies may be needed for further application.

DATA AVAILABILITY STATEMENT

All datasets generated for this study are included in the article/supplementary material.

AUTHOR CONTRIBUTIONS

P-YT, M-JH, and M-KC: study conception and design. C-CL, Y-CC, Y-SL, and Y-TH: acquisition, analysis, and interpretation of data. P-YT, Y-TL, and M-JH: drafting/revision of the work for intellectual content and context. M-KC: final approval and overall responsibility for the published work. All authors read and approved the final manuscript.

FUNDING

This study was supported by grants from National Science Council, Taiwan (MOST 108-2314-B-371-010) and Changhua Christian Hospital (108-CCH-IRP-041, 108-CCH-IRP-002, 108-CCH-ICO-145). The authors of the manuscript do not have a direct financial relation with the commercial identity mentioned in this paper.

REFERENCES

1. Ferlay J, Soerjomataram I, Dikshit R, Eser S, Mathers C, Rebelo M, et al. Cancer incidence and mortality worldwide: sources, methods and major patterns in GLOBOCAN 2012. *Int J Cancer*. (2015) 136:E359–86. doi: 10.1002/ijc.29210
2. Huang WY, Lin CL, Lin CY, Jen YM, Lo CH, Sung FC, et al. Survival outcome of patients with nasopharyngeal carcinoma: a nationwide analysis of 13 407 patients in Taiwan. *Clin Otolaryngol*. (2015) 40:327–34. doi: 10.1111/coa.12371
3. Andersson-Anvret M, Forsby N, Klein G, Henle W. Relationship between the Epstein-Barr virus and undifferentiated nasopharyngeal carcinoma: correlated nucleic acid hybridization and histopathological examination. *Int J Cancer*. (1977) 20:486–94. doi: 10.1002/ijc.2910200403
4. Bei JX, Jia WH, Zeng YX. Familial and large-scale case-control studies identify genes associated with nasopharyngeal carcinoma. *Semin Cancer Biol*. (2012) 22:96–106. doi: 10.1016/j.semcancer.2012.01.012
5. Hildesheim A, Wang CP. Genetic predisposition factors and nasopharyngeal carcinoma risk: a review of epidemiological association studies, 2000-2011: Rosetta Stone for NPC: genetics, viral infection, and other environmental factors. *Semin Cancer Biol*. (2012) 22:107–16. doi: 10.1016/j.semcancer.2012.01.007
6. Lin DC, Meng X, Hazawa M, Nagata Y, Varela AM, Xu L, et al. The genomic landscape of nasopharyngeal carcinoma. *Nat Genet*. (2014) 46:866–71. doi: 10.1038/ng.3006
7. Ward MH, Pan WH, Cheng YJ, Li FH, Brinton LA, Chen CJ, et al. Dietary exposure to nitrite and nitrosamines and risk of nasopharyngeal carcinoma in Taiwan. *Int J Cancer*. (2000) 86:603–9. doi: 10.1002/(SICI)1097-0215(20000601)86:5<603::AID-IJC1>3.0.CO;2-H
8. Guo X, Johnson RC, Deng H, Liao J, Guan L, Nelson GW, et al. Evaluation of nonviral risk factors for nasopharyngeal carcinoma in a high-risk population of Southern China. *Int J Cancer*. (2009) 124:2942–7. doi: 10.1002/ijc.24293
9. Stelow EB, Wenig BM. Update from the 4th edition of the World Health Organization classification of head and neck tumours: nasopharynx. *Head Neck Pathol*. (2017) 11:16–22. doi: 10.1007/s12105-017-0787-0
10. Nicholls JM. Nasopharyngeal carcinoma: classification and histologic appearances. *Adv Anat Pathol*. (1997) 4:71–84. doi: 10.1097/00125480-199703000-00001
11. Niedobitek G, Hansmann ML, Herbst H, Young LS, Dienemann D, et al. Epstein-Barr virus and carcinomas: undifferentiated carcinomas but not squamous cell carcinomas of the nasopharynx are regularly associated with the virus. *J Pathol*. (1991) 165:17–24. doi: 10.1002/path.1711650105
12. Chua MLK, Wee JTS, Hui EP, Chan ATC. Nasopharyngeal carcinoma. *Lancet*. (2016) 387:1012–24. doi: 10.1016/S0140-6736(15)00055-0
13. Lam WKJ, Chan JYK. Recent advances in the management of nasopharyngeal carcinoma. *F1000Res*. (2018) 7:F1000. doi: 10.12688/f1000research.15066.1
14. Blanchard P, Lee A, Marguet S, Leclercq J, Ng WT, Ma J, et al. Chemotherapy and radiotherapy in nasopharyngeal carcinoma: an update of the MAC-NPC meta-analysis. *Lancet Oncol*. (2015) 16:645–55. doi: 10.1016/S1470-2045(15)70126-9
15. Li AC, Xiao WW, Shen GZ, Wang L, Xu AA, Cao YQ, et al. Distant metastasis risk and patterns of nasopharyngeal carcinoma in the era of IMRT: long-term results and benefits of chemotherapy. *Oncotarget*. (2015) 6:24511–21. doi: 10.18632/oncotarget.4312
16. Tang LQ, Chen QY, Fan W, Liu H, Zhang L, Guo L, et al. Prospective study of tailoring whole-body dual-modality [18F]fluorodeoxyglucose positron emission tomography/computed tomography with plasma Epstein-Barr virus DNA for detecting distant metastasis in endemic nasopharyngeal carcinoma at initial staging. *J Clin Oncol*. (2013) 31:2861–9. doi: 10.1200/JCO.2012.46.0816
17. Chaffer CL, Weinberg RA. A perspective on cancer cell metastasis. *Science*. (2011) 331:1559–64. doi: 10.1126/science.1203543
18. Fidler IJ. The pathogenesis of cancer metastasis: the 'seed and soil' hypothesis revisited. *Nat Rev Cancer*. (2003) 3:453–8. doi: 10.1038/nrc1098
19. Blaha L, Zhang C, Cabodi M, Wong JY. A microfluidic platform for modeling metastatic cancer cell matrix invasion. *Biofabrication*. (2017) 9:045001. doi: 10.1088/1758-5090/aa869d
20. Kusukawa J, Sasaguri Y, Morimatsu M, Kameyama T. Expression of matrix metalloproteinase-3 in stage I and II squamous cell carcinoma of the oral cavity. *J Oral Maxillofac Surg*. (1995) 53:530–4. doi: 10.1016/0278-2391(95)90065-9
21. Hong SD, Hong SP, Lee JI, Lim CY. Expression of matrix metalloproteinase-2 and−9 in oral squamous cell carcinomas with regard to the metastatic potential. *Oral Oncol*. (2000) 36:207–13. doi: 10.1016/S1368-8375(99)00088-3
22. Riedel F, Gotte K, Schwalb J, Bergler W, Hormann K. Expression of 92-kDa type IV collagenase correlates with angiogenic markers and poor survival in head and neck squamous cell carcinoma. *Int J Oncol*. (2000) 17:1099–105. doi: 10.3892/ijo.17.6.1099
23. Shimada T, Nakamura H, Yamashita K, Kawata R, Murakami Y, Fujimoto N, et al. Enhanced production and activation of progelatinase A mediated by membrane-type 1 matrix metalloproteinase in human oral squamous cell carcinomas: implications for lymph node metastasis. *Clin Exp Metastasis*. (2000) 18:179–88. doi: 10.1023/A:1006749501682
24. Yoshizaki T, Maruyama Y, Sato H, Furukawa M. Expression of tissue inhibitor of matrix metalloproteinase-2 correlates with activation of matrix metalloproteinase-2 and predicts poor prognosis in tongue squamous cell carcinoma. *Int J Cancer*. (2001) 95:44–50. doi: 10.1002/1097-0215(20010120)95:1<44::AID-IJC1008>3.0.CO;2-M
25. Shrotriya S, Agarwal R, Sclafani RA. A perspective on chemoprevention by resveratrol in head and neck squamous cell carcinoma. *Adv Exp Med Biol*. (2015) 815:333–48. doi: 10.1007/978-3-319-09614-8_19
26. Varoni EM, Lo Faro AF, Sharifi-Rad J, Iriti M. Anticancer molecular mechanisms of resveratrol. *Front Nutr*. (2016) 3:8. doi: 10.3389/fnut.2016.00008
27. Buhrmann C, Shayan P, Kraehe P, Popper B, Goel A, Shakibaei M. Resveratrol induces chemosensitization to 5-fluorouracil through up-regulation of intercellular junctions, Epithelial-to-mesenchymal transition and apoptosis in colorectal cancer. *Biochem Pharmacol*. (2015) 98:51–68. doi: 10.1016/j.bcp.2015.08.105
28. Ma L, Li W, Wang R, Nan Y, Wang Q, Liu W, et al. Resveratrol enhanced anticancer effects of cisplatin on non-small cell lung cancer cell lines by

inducing mitochondrial dysfunction and cell apoptosis. *Int J Oncol*. (2015) 47:1460–8. doi: 10.3892/ijo.2015.3124
29. Tolomeo M, Grimaudo S, Di Cristina A, Roberti M, Pizzirani D, Meli M, et al. Pterostilbene and 3′-hydroxypterostilbene are effective apoptosis-inducing agents in MDR and BCR-ABL-expressing leukemia cells. *Int J Biochem Cell Biol*. (2005) 37:1709–26. doi: 10.1016/j.biocel.2005 03.004
30. Mikstacka R, Przybylska D, Rimando AM, Baer-Dubowska W. Inhibition of human recombinant cytochromes P450 CYP1A1 and CYP1B1 by trans-resveratrol methyl ethers. *Mol Nutr Food Res*. (2007) 51:517–24. doi: 10.1002/mnfr.200600135
31. Chao J, Li H, Cheng KW, Yu MS, Chang RC, Wang M. Protective effects of pinostilbene, a resveratrol methylated derivative, against 6-hydroxydopamine-induced neurotoxicity in SH-SY5Y cells. *J Nutr Biochem*. (2010) 21:482–9. doi: 10.1016/j.jnutbio.2009. 02.004
32. Sun Y, Wu X, Cai X, Song M, Zheng J, Pan C, et al. Identification of pinostilbene as a major colonic metabolite of pterostilbene and its inhibitory effects on colon cancer cells. *Mol Nutr Food Res*. (2016) 60:1924–32. doi: 10.1002/mnfr.201500989
33. Hsieh MJ, Chin MC, Lin CC, His YT, Lo YS, Chuang YC, et al. Pinostilbene hydrate suppresses human oral cancer cell metastasis by downregulation of matrix metalloproteinase-2 through the mitogen-activated protein kinase signaling pathway. *Cell Physiol Biochem*. (2018) 50:911–23. doi: 10.1159/000494476
34. Ho HY, Lin CW, Chien MH, Reiter RJ, Su SC, Hsieh YH, et al. Melatonin suppresses TPA-induced metastasis by downregulating matrix metalloproteinase-9 expression through JNK/SP-1 signaling in nasopharyngeal carcinoma. *J Pineal Res*. (2016) 61:479–92. doi: 10.1111/jpi.12365
35. Egeblad M, Werb Z. New functions for the matrix metalloproteinases in cancer progression. *Nat Rev Cancer*. (2002) 2:161–74. doi: 10.1038/nrc745
36. Kessenbrock K, Plaks V, Werb Z. Matrix metalloproteinases: regulators of the tumor microenvironment. *Cell*. (2010) 141:52–67. doi: 10.1016/j.cell.2010.03.015
37. Huang YW, Chuang CY, Hsieh YS, Chen PN, Yang SF, Shih Hsuan L, et al. Rubus idaeus extract suppresses migration and invasion of human oral cancer by inhibiting MMP-2 through modulation of the Erk1/2 signaling pathway. *Environ Toxicol*. (2017) 32:1037–46. doi: 10.1002/tox.22302
38. Wong TS, Kwong DL, Sham JS, Wei WI, Kwong YL, Yuen AP. Clinicopathologic significance of plasma matrix metalloproteinase-2 and−9 levels in patients with undifferentiated nasopharyngeal carcinoma. *Eur J Surg Oncol*. (2004) 30:560–4. doi: 10.1016/j.ejso.2004.02.007
39. Liu Z, Li L, Yang Z, Luo W, Li X, Yang H, et al. Increased expression of MMP9 is correlated with poor prognosis of nasopharyngeal carcinoma. *BMC Cancer*. (2010) 10:270. doi: 10.1186/1471-2407-10-270
40. Liu MT, Chen MK, Huang CC, Huang CY. Prognostic value of molecular markers and implication for molecular targeted therapies in nasopharyngeal carcinoma: an update in an era of new targeted molecules development. *World J Oncol*. (2015) 6:243–61. doi: 10.14740/wjon610w
41. Jin Y, An X, Cai YC, Cao Y, Cai XY, Xia Q, et al. Zoledronic acid combined with chemotherapy bring survival benefits to patients with bone metastases from nasopharyngeal carcinoma. *J Cancer Res Clin Oncol*. (2011) 137:1545–51. doi: 10.1007/s00432-011-1027-8
42. Hsin CH, Huang CC, Chen PN, Hsieh YS, Yang SF, Ho YT, et al. Rubus idaeus inhibits migration and invasion of human nasopharyngeal carcinoma cells by suppression of MMP-2 through modulation of the ERK1/2 pathway. *Am J Chin Med*. (2017) 45:1557–72. doi: 10.1142/S0192415X17500847
43. Huang GW, Mo WN, Kuang GQ, Nong HT, Wei MY, Sunagawa M, et al. Expression of p16, nm23-H1, E-cadherin, and CD44 gene products and their significance in nasopharyngeal carcinoma. *Laryngoscope*. (2001) 111:1465–71. doi: 10.1097/00005537-200108000-00025
44. Li Z, Ren Y, Lin SX, Liang YJ, Liang HZ. Association of E-cadherin and beta-catenin with metastasis in nasopharyngeal carcinoma. *Chin Med J*. (2004) 117:1232–9.
45. Galera-Ruiz H, Rios MJ, Gonzalez-Campora R, De Miguel M, Carmona MI, Moreno AM, et al. The cadherin-catenin complex in nasopharyngeal carcinoma. *Eur Arch Otorhinolaryngol*. (2011) 268:1335–41. doi: 10.1007/s00405-010-1464-z
46. Ran Y, Wu S, You Y. Demethylation of E-cadherin gene in nasopharyngeal carcinoma could serve as a potential therapeutic strategy. *J Biochem*. (2011) 149:49–54. doi: 10.1093/jb/mvq128
47. Wang D, Wu C, Liu D, Zhang L, Long G, Hu G, et al. Ginsenoside Rg3 inhibits migration and invasion of nasopharyngeal carcinoma cells and suppresses epithelial mesenchymal transition. *Biomed Res Int*. (2019) 2019:8407683. doi: 10.1155/2019/8407683
48. Yu D, An X, Fan W, Wang X, He Y, Li B. PNUTS mediates ionizing radiation-induced CNE-2 nasopharyngeal carcinoma cell migration, invasion, and epithelial-mesenchymal transition via the PI3K/AKT signaling pathway. *Onco Targets Ther*. (2019) 12:1205–14. doi: 10.2147/OTT.S188571

Conflict of Interest: The authors declare that the research was conducted in the absence of any commercial or financial relationships that could be construed as a potential conflict of interest.

frontiers in Oncology

ORIGINAL RESEARCH
published: 06 December 2019
doi: 10.3389/fonc.2019.01379

SMAD4 Somatic Mutations in Head and Neck Carcinoma Are Associated With Tumor Progression

Li-Han Lin[1], *Kuo-Wei Chang*[2,3], *Hui-Wen Cheng*[1] *and Chung-Ji Liu*[3,4]*

[1] Department of Medical Research, MacKay Memorial Hospital, Taipei, Taiwan, [2] Department of Stomatology, Taipei Veterans General Hospital, Taipei, Taiwan, [3] School of Dentistry, Institute of Oral Biology, National Yang-Ming University, Taipei, Taiwan, [4] Department of Oral and Maxillofacial Surgery, Taipei MacKay Memorial Hospital, Taipei, Taiwan

As the incidence and the mortality rate of head and neck squamous cell carcinoma (HNSCC) is increasing worldwide, gaining knowledge about the genomic changes which happen in the carcinogenesis of HNSCC is essential for the diagnosis and therapy of the disease. *SMAD4* (DPC4) is a tumor suppressor gene. It is located at chromosome 18q21.1 and a member of the SMAD family. Which mediates the TGF-β signaling pathway, thereby controlling the growth of epithelial cells. In the study presented here, we analyzed tumor samples by multiplex PCR-based next-generation sequencing (NGS) and found deleterious mutations of *SMAD4 in* 4.1% of the tumors. Knock-down experiments of endogenous and exogenous SMAD4 expression demonstrated that SMAD4 is involved in the migration and invasion of HNSCC cells. Functional analysis of a missense mutation in the MH1 domain of SMAD4 may be responsible for the loss of function in suppressing tumor progression. Missense *SMAD4* mutations, therefore, could be useful prognostic determinants for patients affected by HNSCCs. This report is the first study where NGS analysis based on multiplex-PCR is used to demonstrate the imminent occurrence of missense *SMAD4* mutations in HNSCC cells. The gene analysis that we performed may support the identification of *SMAD4* mutations as a diagnostic marker or even as a potential therapeutic target in head and neck cancer. Moreover, the analytic strategy proposed for the detection of mutations in the *SMAD4* gene may be validated as a platform to assist mutation screening.

Keywords: head and neck cancer, loss of heterozygosity, *SMAD4*, somatic mutation, survival

OPEN ACCESS

Edited by:
Cheng-Chia Yu,
Chung Shan Medical University, Taiwan

Reviewed by:
Chih Yuan Fang,
Taipei Medical University, Taiwan
ChihYu Peng,
Erasmus Medical Center, Netherlands

***Correspondence:**
Chung-Ji Liu
liucjliu3229@gmail.com

Specialty section:
This article was submitted to Head and Neck Cancer, a section of the journal Frontiers in Oncology

Received: *12 September 2019*
Accepted: *22 November 2019*
Published: *06 December 2019*

Citation:
Lin L-H, Chang K-W, Cheng H-W and Liu C-J (2019) SMAD4 Somatic Mutations in Head and Neck Carcinoma Are Associated With Tumor Progression. Front. Oncol. 9:1379. doi: 10.3389/fonc.2019.01379

INTRODUCTION

Head and neck squamous cell carcinomas (HNSCC), which include oral squamous cell carcinomas, are the sixth most prevalent malignancy worldwide (1, 2). The pathogenesis of HNSCC is affected by many molecular factors, among them e.g., mutations in *TP53*, and genes related to *PIK3CA and* Notch family signaling (3–9). The role which these factors are playing in the progression of the tumors remains unclear to a wide extent (3, 4, 6, 10, 11). Although the knowledge on head and neck carcinogenesis has improved a lot in the past 40 years and many innovations in surgery as well as chemo- and radiotherapy have been made, the survival rates for many HNSCC types

have not improved considerably (2). Recent developments in high-throughput, next-generation parallel sequencing technologies are facilitating sensitive detection, and quantification of genetic alterations. New insights in the molecular basis of HNSCC progression have been provided by whole-exome sequencing (WES) (8, 12, 13). The analysis of WES data which was obtained from The Cancer Genome Atlas (TCGA) (6, 14) pointed to novel genes with significant mutations and underlined the complex molecular pathogenesis of HNSCC, which includes a high degree of heterogeneity between tumors (15).

SMAD4 is a transcription factor of the SMAD family which takes part in TGF-β signaling. SMAD4 stands for SMA- and MAD-related protein 4, other names are SMAD family member 4, Deleted in Pancreatic Cancer-4 (DPC4) and Mothers against decapentaplegic homolog 4, SMAD4 is present in all metazoans and is highly conserved between species (16). As the main effector of TGF-β signaling, SMAD4 has been found to be non-functional in more than half of adenocarcinomas of the pancreatic duct (17–19), and to varying degrees, in several other types of cancers (20–24). In many studies that have been conducted in the past 20 years it was found that the loss of SMAD4 function alone does not initiate a tumor, but it may promote the progression of tumors which have been initiated by other molecular defects, like the activation of KRas activation in the case of pancreatic duct adenocarcinoma and the inactivation of APC in colorectal cancer (20, 24). The loss of SMAD4 is playing a crucial role in the response to DNA damage with the consequence of increased genomic instability. This is very prominent in skin cancer and suggests a distinct role of SMAD4 in the progression of various types of tumors (25).

Screening large genes with multiples exons for mutations by traditional Sanger sequencing is slow, labor intensive and costly. Next-generation sequencing (NGS) in contrast allows the direct analysis of mutations in monogenic diseases at low cost without pre-screening. Novel DNA variants that have been identified by NGS still may be corroborated by Sanger sequencing before reporting them.

In this study, we performed NGS analysis based on multiplex PCR NGS for the investigation of *SMAD4* mutations in HNSCC.

We found that mutations of *SMAD4*, as well as its expression level, are linked to the progression of HNSCC and affect patient survival. Moreover, we investigated the role of deleterious *SMAD4* mutations to elucidate their role in HNSCC neoplasms.

MATERIALS AND METHODS

Patients

This study was approved by the Institutional Review Board of Mackay Memorial Hospital (approval number: 15MMHIS104). All patients provided written informed consent. Tumor samples were obtained from 122 patients undergoing HNSCC surgery (**Supplementary Table 1**). Cells were isolated from tissue sections by laser capture microdissection (LCM) following established protocols (3, 4). Additionally, 10 mL of whole blood was collected in the morning after fasting in Vacutainer tubes containing EDTA as the anticoagulant (Becton Dickson, Franklin Lakes, NJ, USA) from each patient. None of the patients included in this study had received radiotherapy or adjuvant chemotherapy before surgery. DNA was extracted from blood and cancerous tissue as reported previously (26).

SMAD4 Mutation Analysis by PCR-Based NGS

Individual primer sets for 10 long PCR reactions were designed with Primer3 (version 0.4.0) (ELIXIR, funded by the European Commission) to amplify the entire coding sequence (exons 2–12) for human *SMAD4* (**Supplementary Table 2** and **Supplementary Figure 1A**). Amplicon concentrations were determined with the Qubit dsDNA HS Assay kit on a Qubit 2.0 fluorometer (Life Technologies, Carlsbad, CA, USA). PCR reactions were carried out using the KAPA LongRange HotStart kit (Kapa Biosystems, Wilmington, MA, USA). For library generation, long PCR products of each sample were pooled and then purified using Agencourt Ampure XP beads (Beckman Coulter, Pasadena, CA, USA). Indexed libraries of the pooled PCR products were prepared using the Illumina Nextera XT library preparation kit and then sequenced on the Illumina MiSeq system, following the manufacturer's instructions. Variant call format files were generated using the MiSeq Reporter software (version 2.3.32). The variants were further filtered on the basis of the following criteria: (1) DP <30, (2) genotype quality <30, (3) number of mismatches within a 40-bp window ≤ 3, (4) mutant allele frequency of at least 10% in tumors and $<1\%$ in normal cells, and (5) MAF in the 1000 Genomes Project and dbSNP137 $> 1\%$. The Integrative Genomics Viewer (IGV) was used to determine the read counts of the target amplicons and to confirm the detected variants. The mutation spectrum and lollipop figures for *SMAD4* were generated with the OncoPrinter and MutationMapper tools available at cBioPortal (27, 28).

Mutation Point Validation

To validate the somatic mutations which were identified in the multiplex PCR-based NGS results, conventional Sanger sequencing was applied. Individual primer sets were designed in Primer3 (version 0.4.0), they have been listed in **Supplementary Table 3**. For Sanger sequencing, PCR reactions were performed with a standard hot start kit. Amplicons were sequenced with the ABI BigDye Terminator Cycle Sequencing kit on an ABI 3730xl DNA analyzer (Applied Biosystems, Foster City, CA, USA).

Immunohistochemistry

SMAD4 protein was visualized in tissue sections by immunohistochemistry, following previously reported protocols (29). In brief, 5-μm-thick tissue sections were dewaxed, rehydrated, and then incubated with monoclonal mouse anti-human SMAD4 antibody (sc-7966, 1:100 dilution; Santa Cruz Biotechnology, Santa Cruz, CA, USA) in a humidification chamber at 4°C overnight. After rinsing with PBS, standard immunohistochemical staining was done using streptavidin-biotin complex system (Dako Corp.) with aminoethylcarbazole as the chromogen and subsequently counterstained with hematoxylin and mounted with Clearmount

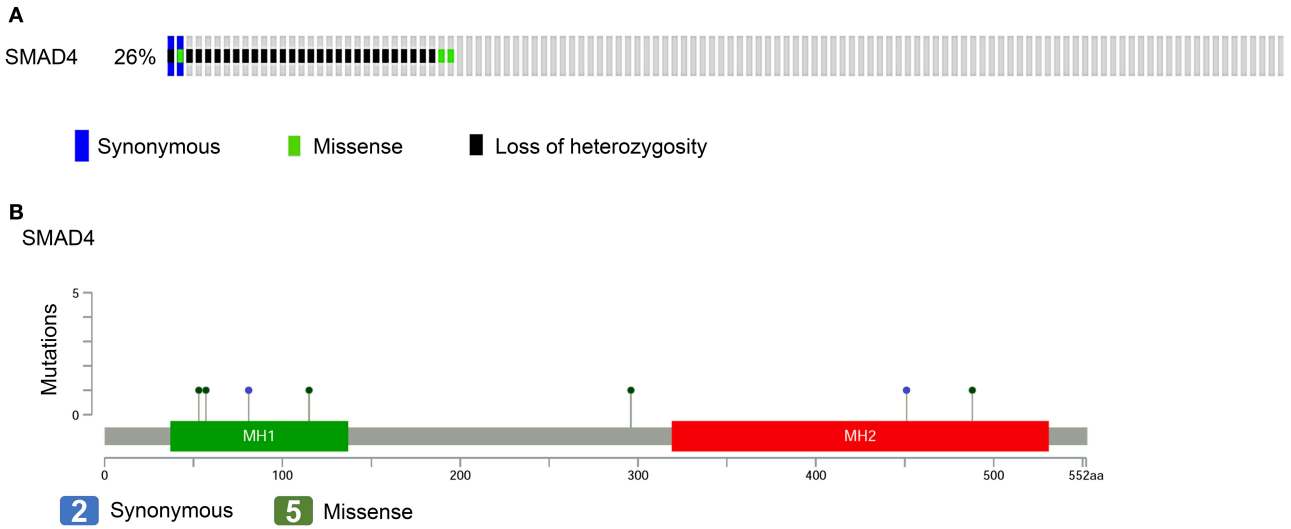

FIGURE 1 | *SMAD4* mutations in patients with HNSCC. **(A)** Frequency of *SMAD4* LOH, mutations, or both. Each column represents one patient. Colored boxes designate LOH status and mutation types. **(B)** Distribution of mutations in the sequence coding for *SMAD4*. Colored ovals represent mutation types, colored boxes represent domains. Colored boxes represent mutation types.

(Zymed Laboratories, Inc.). The primary antibody used was a Preimmune mouse IgG was used as a negative control. Normal epithelium adjacent to the tumor served as the internal positive control. Tumors containing ≥50% and <50% positive cancer cells were classified to have high and low SMAD4 expression (30).

Cell Culture, Reagents, and Phenotypic Assays

In this study, the HNSCC cell lines SAS, OECM-1, HSC3, FaDu, SCC25, OC3, and OC4 were used. Normal human oral keratinocytes (NOKs); served as controls. The cells were cultured as described previously (31). Our cell lines were authenticated by Mission Biotech (Nangang, Taipei, Taiwan) on August 8, 2017, using the Promega StemElite ID System and analyzed on ABI PRISM 3730 Genetic Analyzer with GeneMapper (version 3.7). si-*SMAD4* and scramble control (si-control) oligonucleotides were purchased from Santa Cruz Biotech (Santa Cruz). For transfection, TransFectin Lipid Reagent (BioRad Lab., Hercules, CA, USA) was used. sh-SMAD4 vectors (TRCN0000010321) and a sh-Luc control vector (TRCN0000072249), packaged in lentiviruses, were purchased from National RNAi Core (Academia Sinica, Taipei, Taiwan). The cells were infected and selected using puromycin (Sigma-Aldrich) at 5.0 μg/mL for 7 days to establish stable subclones. Phenotypic events, including proliferation, migration, and invasion, were analyzed as previously described (10, 32).

Analysis of SMAD4 Mutations in HNSCC Cell Lines

All coding exons of *SMAD4* in SAS, OECM-1, HSC3, FaDu, SCC25, OC3, and OC4 cells were amplified by PCR and then sequenced using the ABI BigDye Terminator Cycle Sequencing kit on an ABI 3730xl DNA analyzer (Applied Biosystems). The variants with MAF > 1% in the 1000 Genomes Project and dbSNP137 were filtered.

Constructs

The *SMAD4* cDNA sequence was amplified from the cDNA of SAS cells with the primers *SMAD4*_Forward and *SMAD4*_Reverse, introducing BamHI and EcoRI sites for directional cloning. The PCR product then was subcloned into the pBabe puro vector. The p.H132Y, p.P296T, and p.A488V mutations were introduced into *SMAD4* cDNA with the Q5 Site-Directed Mutagenesis kit (New England BioLabs, Ipswich, MA, USA) with the primers H132Ymut, P296Tmut, and A488Vmut. We named the resulting mutants p.H132Y, p.P296T, and p.A488V, respectively. **Supplementary Table 3** lists the primers used in this section.

Loss of Heterozygosity Analysis at the *SMAD4* Locus

Three polymorphic markers close to the *SMAD4* locus (D18S363, D18S474, and D18S46) were used to analyze the loss of heterozygosity status (LOH) of *SMAD4*. These markers are described in **Supplementary Table 3**. As templates, samples of genomic DNA (∼100 ng) were extracted from HNSCCs and matching normal tissues. The PCR reaction (20 μL) contained 5× Phusion HF buffer, 200 μM of each dNTP, 0.25 μM of each marker, and 0.3 μl (0.6 units) of Phusion High-Fidelity DNA Polymerase (Thermo Fisher Scientific, Vilnius, Lithuania). Amplification was performed under the following conditions: 98°C for 5 min, followed by 35 cycles at 98°C for 20 s, 60°C for 15 s, and 72°C for 30 s. The final extension was at 72°C for 7 min. The PCR product (0.5 μL) was mixed with 0.5 μL of GeneScan-600 LIZ dye Size Standard (Applied Biosystems) in 10 μL of Hi-Di formamide (Applied Biosystems), denatured

for 3 min at 95°C, and then cooled on ice. The samples were separated by capillary electrophoresis with an ABI PRISM 96-capillary 3730xl DNA Analyzer (Applied Biosystems) and the results were analyzed using GeneMapper (version 3.7; Applied Biosystems). LOH was evaluated using the following formula: LOH = (height of tumor allele 2/height of tumor allele 1)/(height of normal allele 2/height of normal allele 1). As described previously (33). When the height of the tumor alleles decreased by >40%, the calculated LOH became >1.49 or <0.5; thus, we considered this ratio to indicate LOH positivity (**Supplementary Figure 1B**). Homozygous cases were considered non-informative for LOH.

Western Blotting

Western Blot analysis was performed as previously described (29). Equal amounts of protein (30 μg) were loaded per lane. As primary antibodies anti-SMAD4 (diluted 1:500, Santa Cruz) and anti-GAPDH (diluted 1:5,000, Santa Cruz) antibodies were employed. For detection, an HRP-conjugated horse anti-mouse IgG was used as the secondary antibody (diluted 1:5,000; Cell signaling; Cell Signaling Technology, Danvers, MA, USA).

Statistical Analysis

Data are presented as the mean ± SEM. Chi-square and *t*-tests were used. Overall survival (OS) was defined as the time between

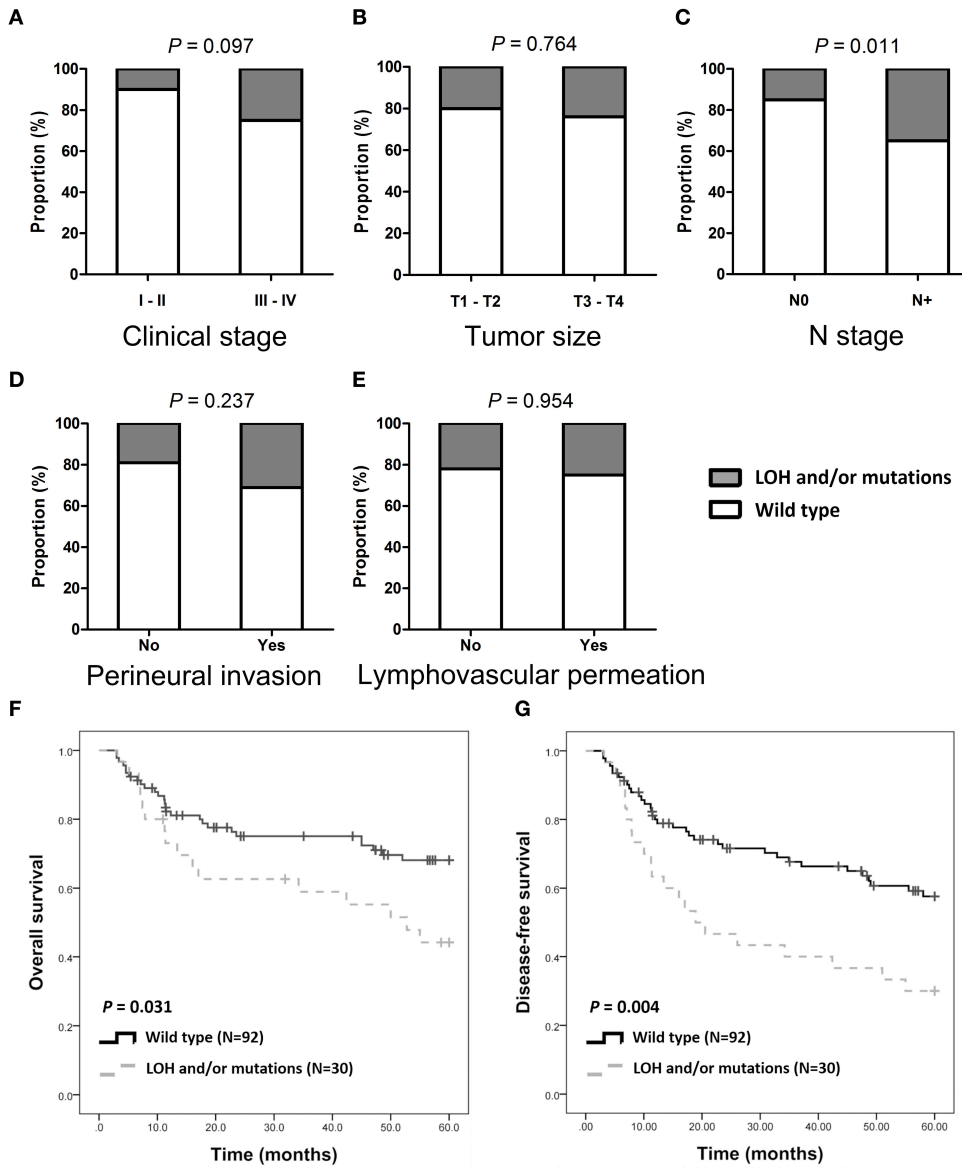

FIGURE 2 | *SMAD4* LOH and mutations and clinical/pathological parameters. **(A–E)** Histograms are showing the association of *SMAD4* LOH with mutation status and clinical stages **(A)**, tumor size **(B)**, N stage **(C)**, perineural invasion **(D)**, and lymphovascular permeation **(E)**. **(F,G)** Kaplan–Meier analysis according to *SMAD4* LOH and mutation status for OS **(F)** and DFS **(G)**.

the date of first diagnosis and the date of death or final follow-up. Disease-free survival (DFS) was defined as the time from the date of first diagnosis until the date of first recurrence or death. Patients without evidence of disease recurrence were censored at the final follow-up or death. Kaplan–Meier analysis was used to compare OS and DFS between the two groups. The multivariate Cox Proportional Hazards Model was used to assess the association of both OS and DFS with *SMAD4* LOH, mutation status, and immunoexpression. Statistical significance was assumed to be indicated by $^{*}P < 0.05$, $^{**}P < 0.01$, and $^{***}P < 0.001$ respectively. Cross-comparisons showing no statistically significant differences were not considered in further analysis.

RESULTS

Somatic Mutations and LOH in *SMAD4*

For the evaluation of the performance of SMAD4 in clinical assessments, 122 HNSCC samples were analyzed by multiplex PCR-based NGS and LOH analysis. We identified seven somatic mutations in the samples by NGS; of these, two were synonymous and five were missense mutations (**Figures 1A,B**, **Supplementary Table 4**). No hotspot region was found for *SMAD4* mutations. The missense mutation p.Ala488Val, previously has been reported by Lee et al. (chr18:48604641) (34). Three polymorphic biomarkers (D18S474, D18S46, and D18S363) which are surrounding the *SMAD4* locus were used to analyze LOH status. Percent LOH was 15.57% (19/122), 13.93% (17/122), and 13.11% (16/122) in D18S363, D18S46, and D18S474, respectively. In 28 (22.95%) patients, LOH was detected in at least one of the three markers (**Figure 1A**), whereas LOH was noted in two or all three markers in 17 (13.93%) patients.

Of the 122 patients, 32 (26.2%) had SMAD4 LOH, mutations, or both, and the remaining 90 demonstrated no mutations or LOH (**Figure 1A**). The frequency of *SMAD4* LOH was higher in patients with lymph node metastasis, mutations, or both compared to those where no metastasis was observed ($P = 0.011$, **Figure 2C**). No significant differences were observed in the clinical stage, tumor size, perineural invasion, or lymphovascular permeation (**Figures 2A–E**, **Supplementary Table 5**). The Kaplan–Meier analysis indicated that patients with *SMAD4* LOH, mutations, or both had a significantly poorer OS and DFS than those with wild-type *SMAD4* ($P = 0.031$ and 0.004, respectively; **Figures 2F,G**, respectively). Both univariate and adjusted multivariate Cox regression analyses revealed poor OS and DFS in patients with *SMAD4* LOH, mutations, or both (OS hazard ratio [HR]: 1.95, $P = 0.034$; OS adjusted HR: 2.08, $P = 0.024$; DFS HR: 2.08, $P = 0.008$, DFS adjusted HR: 1.97, $P = 0.016$; **Table 1**).

SMAD4 Expression in HNSCC Patients

SMAD4 was detected in the cytoplasm and in the nuclei of basal and parabasal cells in normal oral epithelium which was adjacent to tumors (**Figure 3A**, top left). In tumor tissues, SMAD4 immunoreactivity varied from weak (**Figure 3A**, middle) to intense (**Figure 3A**, right). Low SMAD4 expression significantly correlated with the clinical stage ($P = 0.004$), tumor size ($P = 0.020$), and lymph node metastasis ($P = 0.041$; **Figures 3B–G** and **Supplementary Table 6**). No differences were observed in SMAD4 expression in association with the LOH and mutation status, perineural invasion, and lymphovascular permeation. The Kaplan–Meier analysis revealed significantly poorer OS and DFS in patients when SMAD4 expression was low, compared to those with high SMAD4 expression ($P = 0.033$ and $P = 0.026$, respectively; **Figures 3H,I**, respectively). DFS was shorter in patients with when SMAD4 expression was low, as revealed by both univariate and adjusted multivariate Cox regression analysis. (HR: 4.43, $P = 0.043$ and HR: 4.54, $P = 0.046$, respectively; **Table 1**). Univariate Cox regression analysis showed that OS was poorer in patients with low SMAD4 expression (HR: 4.30, $P = 0.047$). However, after the multivariate Cox regression analysis, the correlation between SMAD4 expression and OS became only slightly significant (HR: 4.09, $P = 0.063$).

Association Between SMAD4 Knockdown and Increased HNSCC Invasiveness

The protein levels of SMAD4 in NOKs and HNSCC cells were determined by Western Blotting. As shown in **Figure 4A**, four of the seven (57.1%) tested HNSCC cell lines had decreased or no protein expression of SMAD4, compared to NOKs. Interestingly, in SAS and OC3 cells the endogenous SMAD4 expression relative to the NOKs was elevated. No SMAD4 protein could be detected in FaDu cells (**Figure 4A**). These findings are in agreement with the already described homozygous deletion of *SMAD4* in FaDu cells (35). The remaining two HNSCC cell lines (OC3 and HSC3 cells) were sequenced and two missense mutations were found (**Supplementary Table 7**) No mutation or LOH was found in OC4, OECM1, SAS, or SCC25 cells. OC3 and HSC3 which have missense mutation were excluded from further phenotype studies.

To further elucidate the oncogenic role of *SMAD4* in HNSCC, we established stable *SMAD4*-knockdown SAS and SCC25 subclones. The knockdown effect was confirmed through Western blotting (**Figure 4B**). Cell proliferation was not affected by the knockdown of *SMAD4* (**Figures 4C,F**), but HNSCC cell migration and invasion were significantly increased (**Figures 4D,E,G,H**). To corroborate this result, we transfected SAS and SCC25 cells with si-*SMAD4* oligonucleotides (**Supplementary Figure 2**). Western blotting confirmed the si-*SMAD4* knockdown effect on *SMAD4* expression (**Supplementary Figure 2A**). Migration and invasion of HNSCC cells were significantly increased during the transient knockdown, but their proliferation behavior did not change (**Supplementary Figures 2B–D**). These results indicate that the mobility and invasiveness of HNSCC cells were enhanced by the knockdown of *SMAD4*.

Association Between Mutations of *SMAD4* With Increased Invasiveness in HNSCC

To characterize the effects of *SMAD4* on the phenotype, the full-length coding region of *SMAD4* was amplified from SAS cells and cloned to generate the *SMAD4* construct. In the tumor

TABLE 1 | Univariate and Multivariate analysis of disease-free survival rate in HNSCC patients.

Variables	HR (95%CI)	*P*	Adjusted HR (95%CI)	*P*
Overall survival				
SMAD4 LOH and mutations				
Wild type	Reference		Reference	
LOH and/or mutations	1.95 (1.05–3.62)	0.034*	2.08 (1.10–3.92)	0.024*
SMAD4 expression				
High	Reference		Reference	
Low	4.30 (1.02–18.15)	0.047*	4.09 (0.93–18.00)	0.063
Disease-free survival				
SMAD4 LOH and mutations				
Wild type	Reference		Reference	
LOH and/or mutations	2.08 (1.21–3.57)	0.008*	1.97 (1.14–3.42)	0.016*
SMAD4 expression				
High	Reference		Reference	
Low	4.43 (1.05–18.69)	0.043*	4.54 (1.03–20.12)	0.046*

Adjusted for age, gender, and clinical stage.
HR, hazard ratio; CI, confidence interval.

samples, three missense mutations were found (p.His132Tyr, p.Pro296Thr, and p.Ala488Val, **Supplementary Table 4**). These mutations are localized in the MH1, Linker, and MH2 domains, respectively (**Figure 5A**). By Sanger sequencing, we confirmed them as somatic mutations (**Supplementary Figure 1C**). We further made constructs for these mutations to be able to express these mutant proteins for further study. FaDu and OECM1 cells (which have no or only low*SMAD4* expression) were transfected with the *SMAD4* vector and the mutant constructs. Western blotting was used to detect *SMAD4* expression levels (**Figures 5B,C**). The exogenous *SMAD4* expression reduced the migration and invasion of FaDu and OECM1 cells (**Figures 5E,F,H,I**). When the mutant p.H132Y was transfected, the phenotypes repressed by *SMAD4* overexpression was abolished. The proliferation rates of the transfected cell lines were not affected (**Figures 5D,G**). However, transfection with p.P296T and p.A488V mutant constructs did not abolish the rescuing effects of *SMAD4* overexpression on invasion and migration in HNSCC cells.

DISCUSSION

Varying rates of *SMAD4* mutations have been detected in a wide range of cancers by large-scale exome sequencing. Compared with 35% of pancreatic cancer and 12% of colon cancer cases (20, 36–38), *SMAD4* mutation in other types of cancers has occurred at lower rates. In COSMIC cohort studies, point mutations of *SMAD4* were identified in 0.21, 2.24, 2.46, and 8.86% of kidney, lung, esophagus, and biliary tract cancers, respectively (24, 38–44). In general, 2.5 to 4% of the HNSCC tumors demonstrate the somatic mutation of *SMAD4*, making *SMAD4* the fourth mutated gene in different types of cancers (8). In the study presented here, somatic *SMAD4* mutations were found in 4.1% of HNSCC tumors we analyzed. This study is the first where somatic *SMAD4* mutations in HNSCC were detected by multiplex PCR-based NGS. Besides, IGV was used to reconfirm all mutations. Sanger sequencing confirmed three specific non-sense mutations. Thus, despite *SMAD4* is a large gene that is coding for a 552-amino acid polypeptide with a molecular weight of 60.439 Da, the current NGS-based strategy can be a reliable method for *SMAD4* screening. No hotspot for mutations in the *SMAD4* gene has been reported previously and we have not detected any was it observed in our study (8); therefore, allele-specific approaches that are targeting only common mutations (45, 46) are not suitable for the exploration of *SMAD4* mutations in HNSCC. We have designed the multiplex PCR assay to generate *SMAD4* amplicon libraries for sequencing. This includes protein-coding regions as well as conserved splice sites. Because this approach is highly scalable, it may provide advantages over Sanger sequencing regarding its potential application in routine clinical diagnostics, also because the labor required for analyzing individual samples for somatic *SMAD4* mutations is low.

SMAD proteins have two evolutionarily conserved regions separated by a linker region, MAD homology 1 and 2 (MH1 and MH2, respectively). The MH1 domain at the N/terminus is responsible for sequence-specific DNA binding (47, 48), the roles of the MH2 domain are heteromerization and transactivation (49, 50). Besides, the MH2 region partially interferes with the DNA-binding function of the MH1 region (47, 50, 51). Mutations in the domain between L43 and R135 may reduce the ability of *SMAD4* to bind DNA considerably, as a β-hairpin protein motif within this region is responsible for the interaction with DNA. Our results demonstrate that the whole MH1 domain is very sensitive to changes in its overall primary structure and that tumorigenic mutations within the area of L43 and R135 interfere with its capability to bind DNA (52). Kim et al. were the first to document a non-sense mutation of *SMAD4* (GAA526TAA) in two cell lines derived from the same HNSCC patient (53). Reiss et al. reported a homozygous deletion which includes the *SMAD4* gene locus in FaDu cells (54). Others have furthermore identified the *SMAD4* mutation in this HNSCC cell line (35, 55). The results of our Western Blotting experiments verified that this mutation

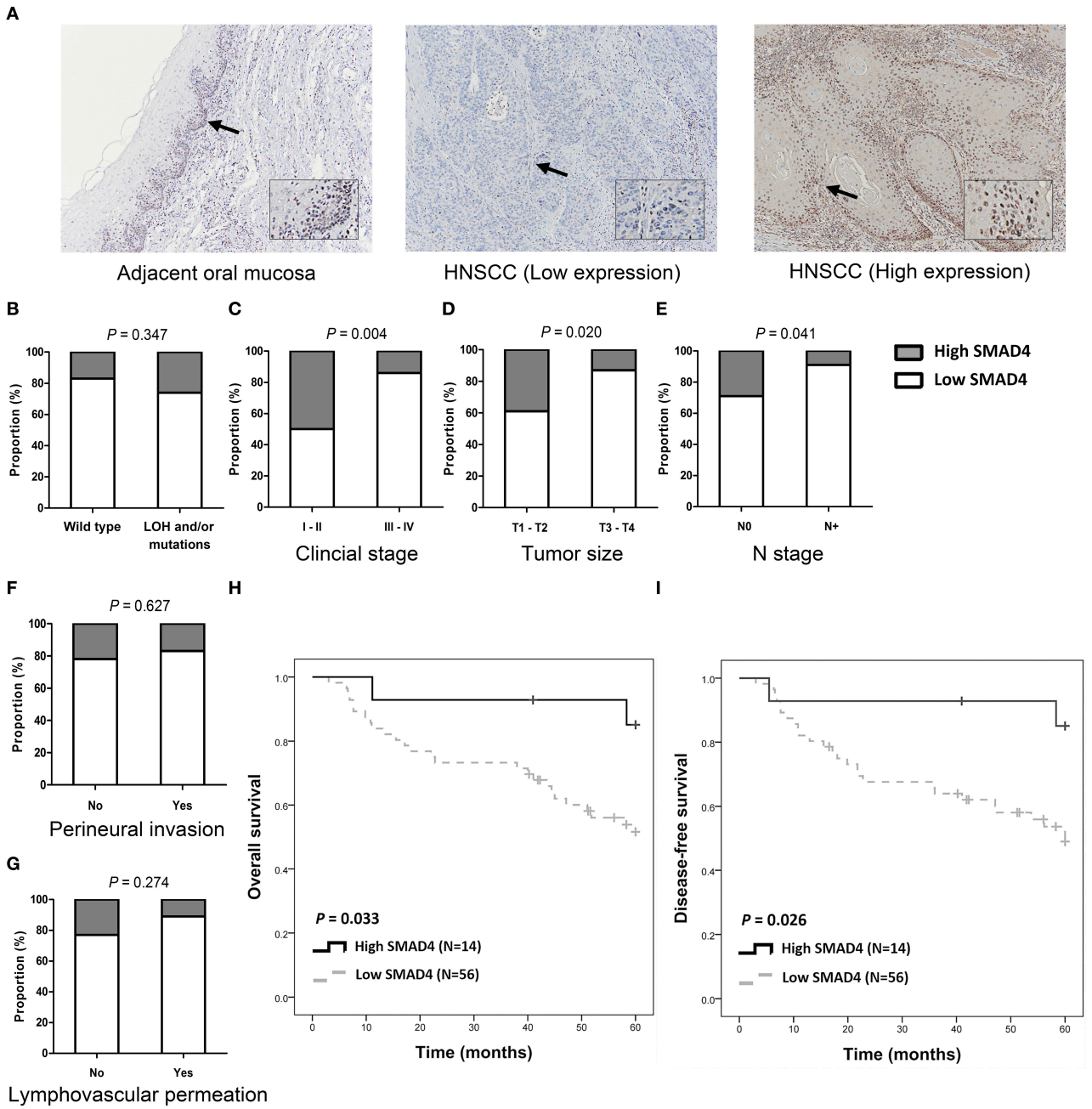

FIGURE 3 | SMAD4 immunoexpression and clinicopathological parameters. **(A)** Immunohistochemistry for SMAD4 in adjacent normal-appearing mucosa (left) and HNSCC tumor tissue (middle and right), as indicated. Tumor tissue showing low (middle), and high (right) SMAD4 staining. Arrows indicate enlarged area. Inset images enlarged by 300% relative to original image. **(B–G)** Histograms showing the association of SMAD4 immunoexpression with *SMAD4* LOH and mutation status **(B)**, clinical stage **(C)**, tumor size **(D)**, N stage **(E)**, perineural invasion **(F)**, and lymphovascular permeation **(G)**. **(H,I)** Kaplan–Meier analysis according to SMAD4 immunoexpression for OS **(H)** and DFS **(I)**.

which results in a nonsense mutation causes the complete loss of *SMAD4* expression. This finding is consistent with previous observations that the majority of missense mutations outside of codons 330–370 inactivate SMAD4 through the degradation of the protein (56). These data are pointing out the important role *SMAD4* is playing in HNSCC carcinogenesis (35). In this study, p.P296T and p.A488V mutant constructs did not abolish the rescuing effects of *SMAD4* overexpression on the migration and invasion in HNSCC cells, suggesting that these mutations may have other functions, warranting further research.

The loss of SMAD4 protein contributes to an increase in genomic instability in the tumor epithelia. This effect, together with blocking the growth inhibition and apoptosis which normally are induced by TGF-β but enhancing of

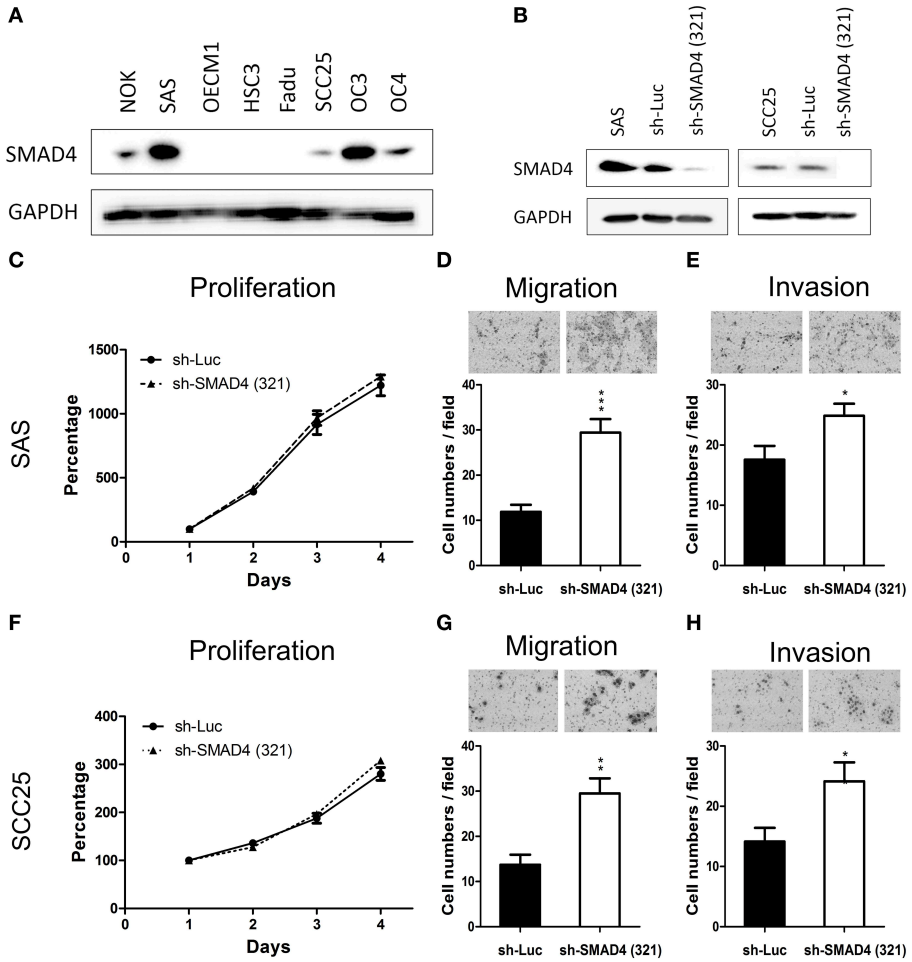

FIGURE 4 | Association of *SMAD4* knockdown with oncogenic phenotypes in HNSCC cells. **(A)** Western blotting for SMAD4 expression in NOK cells and the seven HNSCC cell lines investigated. In SAS and SCC25 cells, *SMAD4* expression levels are higher compared to other cell lines. **(B)** Western blotting on extracts from sh-Luc cell subclone (control) and sh-SMA1D4 (321) cell subclone, which was established from the construct TRCN0000010321. **(C–E)** SAS and **(F–H)** SCC25 cells: proliferation (**C,F**, respectively), migration (**D,G**, respectively), and invasion (**E,H**, respectively).

TGF-β-mediated inflammation, could give way to the expansion of genetic defects cells during HNSCC tumorigenesis (57). *SMAD4* expression may be a determinant of sensitivity/resistance to EGFR/MAPK or EGFR/JNK inhibition in HPV-negative HNSCC tumors (58). However, the studies on SMAD4 loss have reported highly inconsistent results (30, 59, 60). Hernandez et al. developed a *SMAD4* fluorescence *in situ* hybridization assay to measure chromosomal *SMAD4* loss at the single-cell level in primary HNSCC samples and in and patient-derived xenografted (PDX) HNSCC tumors (61). They found a heterozygous loss of *SMAD4* in 35% of primary HNSCCs and 41.3% of PDX tumors. Moreover, in 4.3% of the PDX tumors, the loss of *SMAD4* was homozygous. Hernandez et al. also revealed intertumor and intratumor heterogeneities of *SMAD4* chromosomal loss in HNSCCs (60, 61). In the study presented here, LCM was used to purify the cancerous tissue because LCM makes it possible to approximate the true gene profile of pure cancer cell subpopulations in the context of their actual tissue environment (3, 4). Combining LCM and NGS may be used to detect changes in the karyotype of neoplastic lesions of the oral epithelium.

Analyzing a region of chromosome 18q which has been found to be frequently lost in pancreatic cancers led to the identification of *SMAD4* and the elucidation of its role in tumorigenesis (44), which was supported by the observation that germ-line *SMAD4* mutations cause juvenile polyposis (JP), a condition which is characterized by the formation of intestinal polyps at young age and a cumulative lifetime risk for gastrointestinal cancer of 50% (62). Breast cancers with mutations in the *SMAD4* gene (63) are as sensitive to PARP inhibitors as *BRCA*-mutant breast or ovarian cancers. Similar challenges exist for lung cancers with *SMAD4* (64), but a phenotype where *SMAD4* has been lost has not yet been observed.

A convenient tool to confirm the oncogenic effects of mutated genes in question is the controlled expression of mutant constructs. The current study revealed that mutant *SMAD4* can promote HNSCC tumorigenesis via cell migration and invasion. These data are concordant with the results of our clinical analysis,

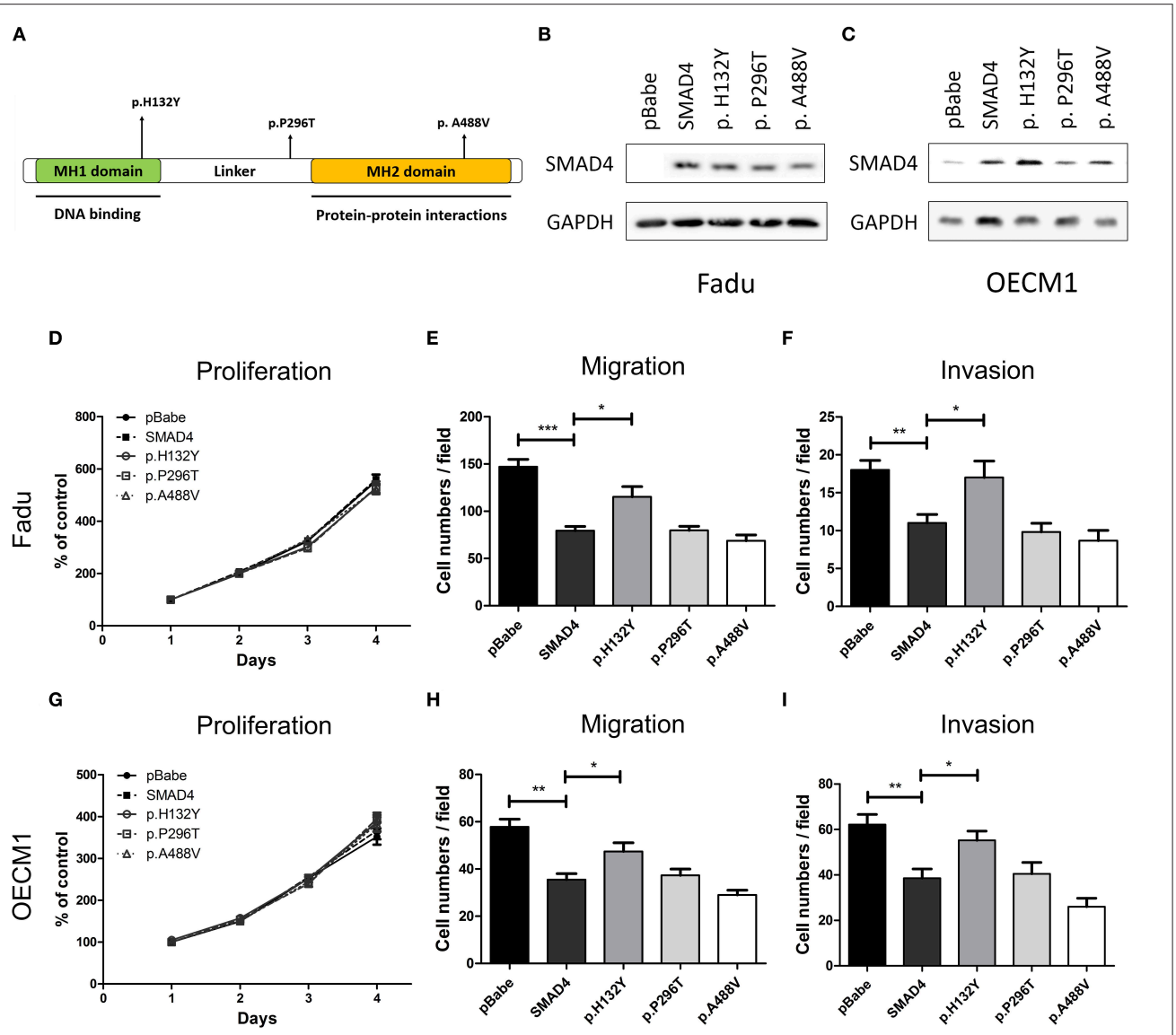

FIGURE 5 | Association of SMAD4 expression with oncogenic phenotypes in HNSCC cells. **(A)** Illustration of various *SMAD4* constructs. Vertical arrows indicate the position of various mutations that were generated for this study. **(B,D–F)** FaDu and **(C,G–I)** OECM1 cells. Results of the Western blotting analysis. The cells were transfected with the vectors, and Western blotting was performed using an anti-SMAD4 antibody to detect the expression of exogenous SMAD4 proteins (**B,C**, respectively): Proliferation (**D,G**, respectively), migration (**E,H**, respectively), and invasion (**F,I**, respectively).

demonstrating more aggressive behavior and the potential for nodal metastasis of tumors with *SMAD4* mutations. The mechanisms that cause diverse *SMAD4* mutations, particularly missense mutations, confer loss-of-function to *SMAD4*.

In HNSCC, the region on chromosome 18q where *SMAD4* is located is frequently lost at the genetic level in HNSCC (65). In esophageal cancer, the loss of SMAD4 correlates with the invasion depth and the pathologic stage (59) as well as with regional metastases and with decreased survival (30).In animal models for HNSCC, *SMAD4* haploid insufficiency promoted tumor development (57). The loss of *SMAD4* is contributing to increased genomic instability in the tumor epithelia. Defects in the signaling of *SMAD* family proteins are associated with an increased tendency for metastatic spread and regional or distant recurrence of HNSCC (66). Thus, inactivation of TGF-β/SMAD signaling is frequently observed in HNSCC, and the inactivation of these signaling pathways might adversely affect patient outcomes. However, the location at which *SMAD4* is downregulated in human HNSCCs and the causal role of *SMAD4* LOH HNSCC development and progression remain unknown. We are the first to demonstrate that LOH and lower expression of SMAD4 can cause regional nodal metastasis and reduce the OS and DFS of HNSCC.

The inactivation of SMAD4 signaling is also associated with poorer prognosis in patients with adenocarcinoma of the pancreas and cancers of the esophagus (23, 43, 67). When *SMAD4* expression is lost in colorectal cancers (CRCs), it is associated with advanced stage disease, the presence of lymph

node metastasis, and poor prognosis (38, 67, 68). However, Kouvidou et al. failed to illustrate this relationship in colon cancer (69). Bacman et al. observed that missing nuclear expression of *SMAD4* does not correlate with tumor grade or with the clinical outcome in colon cancer (70). Similar to CRCs, poor HNSCC-related patient outcomes are associated with 18q LOH (71, 72). SMAD4 depletion in an HNSCC cell line induces cetuximab resistance and results in worse survival in an orthotopic mouse model *in vivo*. JNK and MAPK activation as mediators of cetuximab resistance and provide the foundation for the concomitant EGFR and JNK/MAPK inhibition as a potential strategy for overcoming cetuximab resistance in HNSCCs with SMAD4 loss (58). However, in other studies, 18q loss did not appear to affect the survival of patients with HNSCCs (73, 74). This study indicates that LOH with *SMAD4* mutations may significantly decrease the survival of patients with HNSCCs.

Our analysis results demonstrated an inverse correlation between somatic *SMAD4* mutations and the downregulation of *SMAD4* in HNSCCs, following other studies. Furthermore, the results of our studies demonstrate that *SMAD4* loss due to mutations and downregulation results in increased tumor progression and recurrence rates. Moreover, *SMAD4* mutation and loss, as well as low *SMAD4* expression, worsened the OS. These factors may have led to the substantial differences between our and TCGA database's mutation profiles. Although the disparities warrant further resolution, the presented findings are congruent with those reported for other malignancies (75–77).

To summarize, HNSCC is highly heterogeneous at both the cellular and the genetic levels. The current findings show clearly that *SMAD4* expression is suppressing the progression of HNSCC. Somatic mutations in *SMAD4* and its expression determine the recurrence of HNSCC and go along with poor prognosis. Therefore, the proposed analysis of the genetic status may facilitate the identification of mutations in the *SMAD4* gene as a novel diagnostic marker or therapeutic target in HNSCC and other head and neck cancers.

DATA AVAILABILITY STATEMENT

The data in this manuscript was submitted to Short Reads Archive under the BioProject accession PRJNA588804 and SRA Run Selector project (https://www.ncbi.nlm.nih.gov/Traces/study/?acc=PRJNA588804&o=acc_s%3Aa).

ETHICS STATEMENT

The studies involving human participants were reviewed and approved by MacKay Memorial Hospital. The patients/participants provided their written informed consent to participate in this study.

AUTHOR CONTRIBUTIONS

C-JL: study design. C-JL, L-HL, and K-WC: data analysis. H-WC and L-HL: lab work. C-JL and K-WC: paper preparation.

FUNDING

This study was supported by grants from MacKay Memorial Hospital (MMH-E-105-12 and MMH-E-108-12) and the Ministry of Science and Technology, Taiwan (MOST 108-2314-B-195−002-MY2 and MOST 105-2314-B-195-005-MY3).

ACKNOWLEDGMENTS

This manuscript was edited by Wallace Academic Editing.

SUPPLEMENTARY MATERIAL

The Supplementary Material for this article can be found online at: https://www.frontiersin.org/articles/10.3389/fonc.2019.01379/full#supplementary-material

Supplementary Figure 1 | Identification of *SMAD4* mutations in HNSCC. **(A)** Schematic of five amplicons (blue arrows) covering exons 2–12 of *SMAD4* for sequencing. **(B)** Representative fluorescent electropherograms for LOH marker D18S363 (left), D18S474 (middle), and D18S46 (right). Samples of genomic DNA that were extracted from tumors and matching normal tissues were used as templates. **(C)** Representative Sanger sequencing analysis of mutations p.His132Tyr, p.Pro296Thr, and p.Ala488Val. Upper panels, blood samples; lower panels, cancer samples. The arrows depict wild-type or mutated nucleotides.

Supplementary Figure 2 | Effect of si-*SMAD4* transfection in HNSCC cells. **(A)** Western blotting for OC4 (left) and OECM1 (right) treated with 20 and 40-nM si-*SMAD4* or control oligonucleotides for 48 h: **(B)** proliferation, **(C)** migration, and **(D)** invasion.

Supplementary Table 1 | Clinicopathological characteristics of the HNSCC patients ($n = 122$).

Supplementary Table 2 | List of long PCR primers used for amplification of *SMAD4* gene.

Supplementary Table 3 | List of PCR primers used for PCR, sequencing, and construction, site directed mutagenesis, and *SMAD4* LOH.

Supplementary Table 4 | List of *SMAD4* mutations in HNSCC tumors.

Supplementary Table 5 | Clinical parameters and *SMAD4* LOH and/or mutations in HNSCC patients ($n = 122$).

Supplementary Table 6 | Clinical parameter and *SMAD4* expression in OSCC patients ($n = 70$).

Supplementary Table 7 | List of *SMAD4* mutations in HNSCC cell lines.

REFERENCES

1. Ferlay J, Soerjomataram I, Dikshit R, Eser S, Mathers C, Rebelo M, et al. Cancer incidence and mortality worldwide: sources, methods and major patterns in GLOBOCAN 2012. *Int J Cancer*. (2015) 136:E359–86. doi: 10.1002/ijc.29210
2. Gupta S, Kong W, Peng Y, Miao Q, Mackillop WJ. Temporal trends in the incidence and survival of cancers of the upper aerodigestive tract in Ontario and the United States. *Int J Cancer*. (2009) 125:2159–65. doi: 10.1002/ijc.24533
3. Liu CJ, Lin SC, Chen YJ, Chang KM, Chang KW. Array-comparative genomic hybridization to detect genomewide changes in microdissected primary and metastatic oral squamous cell carcinomas. *Mol Carcinog*. (2006) 45:721–31. doi: 10.1002/mc.20213
4. Liu CJ, Liu TY, Kuo LT, Cheng HW, Chu TH, Chang KW, et al. Differential gene expression signature between primary and metastatic head

and neck squamous cell carcinoma. *J Pathol.* (2008) 214:489–97. doi: 10.1002/path.2306
5. Lin SC, Chen YJ, Kao SY, Hsu MT, Lin CH, Yang SC, et al. Chromosomal changes in betel-associated oral squamous cell carcinomas and their relationship to clinical parameters. *Oral Oncol.* (2002) 38:266–73. doi: 10.1016/S1368-8375(01)00054-9
6. Cancer Genome Atlas Research N, Weinstein JN, Collisson EA, Mills GB, Shaw KR, Ozenberger BA, et al. The cancer genome atlas pan-cancer analysis project. *Nat Genet.* (2013) 45:1113–20. doi: 10.1038/ng.2764
7. Chang KW, Sarraj S, Lin SC, Tsai PI, Solt D. P53 expression, p53 and Ha-ras mutation and telomerase activation during nitrosamine-mediated hamster pouch carcinogenesis. *Carcinogenesis.* (2000) 21:1441–51. doi: 10.1093/carcin/21.5.441
8. Agrawal N, Frederick MJ, Pickering CR, Bettegowda C, Chang K, Li RJ, et al. Exome sequencing of head and neck squamous cell carcinoma reveals inactivating mutations in NOTCH1. *Science.* (2011) 333:1154–7. doi: 10.1126/science.1206923
9. Croce CM. Oncogenes and cancer. *N Engl J Med.* (2008) 358:502–11. doi: 10.1056/NEJMra072367
10. Liu CJ, Tsai MM, Hung PS, Kao SY, Liu TY, Wu KJ, et al. miR-31 ablates expression of the HIF regulatory factor FIH to activate the HIF pathway in head and neck carcinoma. *Cancer Res.* (2010) 70:1635–44. doi: 10.1158/0008-5472.CAN-09-2291
11. Gaykalova DA, Mambo E, Choudhary A, Houghton J, Buddavarapu K, Sanford T, et al. Novel insight into mutational landscape of head and neck squamous cell carcinoma. *PLoS ONE.* (2014) 9:e93102. doi: 10.1371/journal.pone.0093102
12. Stransky N, Egloff AM, Tward AD, Kostic AD, Cibulskis K, Sivachenko A, et al. The mutational landscape of head and neck squamous cell carcinoma. *Science.* (2011) 333:1157–60. doi: 10.1126/science.1208130
13. Pickering CR, Zhang J, Yoo SY, Bengtsson L, Moorthy S, Neskey DM, et al. Integrative genomic characterization of oral squamous cell carcinoma identifies frequent somatic drivers. *Cancer Discov.* (2013) 3:770–81. doi: 10.1158/2159-8290.CD-12-0537
14. Cancer Genome Atlas N. Comprehensive genomic characterization of head and neck squamous cell carcinomas. *Nature.* (2015) 517:576–82. doi: 10.1038/nature14129
15. Kandoth C, McLellan MD, Vandin F, Ye K, Niu B, Lu C, et al. Mutational landscape and significance across 12 major cancer types. *Nature.* (2013) 502:333–9. doi: 10.1038/nature12634
16. Massague J. TGFbeta signalling in context. *Nat Rev Mol Cell Biol.* (2012) 13:616–30. doi: 10.1038/nrm3434
17. Wilentz RE, Iacobuzio-Donahue CA, Argani P, McCarthy DM, Parsons JL, Yeo CJ, et al. Loss of expression of Dpc4 in pancreatic intraepithelial neoplasia: evidence that DPC4 inactivation occurs late in neoplastic progression. *Cancer Res.* (2000) 60:2002–6. Retrieved from: https://cancerres.aacrjournals.org/content/60/7/2002
18. Gu G, Dubauskaite J, Melton DA. Direct evidence for the pancreatic lineage: NGN3+ cells are islet progenitors and are distinct from duct progenitors. *Development.* (2002) 129:2447–57. Retrieved from: https://dev.biologists.org/content/129/10/2447.long
19. Kawaguchi Y, Cooper B, Gannon M, Ray M, MacDonald RJ, Wright CV. The role of the transcriptional regulator Ptf1a in converting intestinal to pancreatic progenitors. *Nat Genet.* (2002) 32:128–34. doi: 10.1038/ng959
20. Miyaki M, Iijima T, Konishi M, Sakai K, Ishii A, Yasuno M, et al. Higher frequency of Smad4 gene mutation in human colorectal cancer with distant metastasis. *Oncogene.* (1999) 18:3098–103. doi: 10.1038/sj.onc.1202642
21. Liao X, Hao Y, Zhang X, Ward S, Houldsworth J, Polydorides AD, et al. Clinicopathological characterization of SMAD4-mutated intestinal adenocarcinomas: a case-control study. *PLoS ONE.* (2019) 14:e0212142. doi: 10.1371/journal.pone.0212142
22. Ding Z, Wu CJ, Chu GC, Xiao Y, Ho D, Zhang J, et al. SMAD4-dependent barrier constrains prostate cancer growth and metastatic progression. *Nature.* (2011) 470:269–73. doi: 10.1038/nature09677
23. Haeger SM, Thompson JJ, Kalra S, Cleaver TG, Merrick D, Wang XJ, et al. Smad4 loss promotes lung cancer formation but increases sensitivity to DNA topoisomerase inhibitors. *Oncogene.* (2016) 35:577–86. doi: 10.1038/onc.2015.112
24. Zhao M, Mishra L, Deng CX. The role of TGF-beta/SMAD4 signaling in cancer. *Int J Biol Sci.* (2018) 14:111–23. doi: 10.7150/ijbs.23230
25. Yang L, Mao C, Teng Y, Li W, Zhang J, Cheng X, et al. Targeted disruption of Smad4 in mouse epidermis results in failure of hair follicle cycling and formation of skin tumors. *Cancer Res.* (2005) 65:8671–8. doi: 10.1158/0008-5472.CAN-05-0800
26. Hung PS, Chang KW, Kao SY, Chu TH, Liu CJ, Lin SC. Association between the rs2910164 polymorphism in pre-mir-146a and oral carcinoma progression. *Oral Oncol.* (2012) 48:404–8. doi: 10.1016/j.oraloncology.2011.11.019
27. Gao J, Aksoy BA, Dogrusoz U, Dresdner G, Gross B, Sumer SO, et al. Integrative analysis of complex cancer genomics and clinical profiles using the cBioPortal. *Sci Signal.* (2013) 6:pl1. doi: 10.1126/scisignal.2004088
28. Cerami E, Gao J, Dogrusoz U, Gross BE, Sumer SO, Aksoy BA, et al. The cBio cancer genomics portal: an open platform for exploring multidimensional cancer genomics data. *Cancer Discov.* (2012) 2:401–4. doi: 10.1158/2159-8290.CD-12-0095
29. Chen YF, Yang CC, Kao SY, Liu CJ, Lin SC, Chang KW. MicroRNA-211 enhances the oncogenicity of carcinogen-induced oral carcinoma by repressing TCF12 and increasing antioxidant activity. *Cancer Res.* (2016) 76:4872–86. doi: 10.1158/0008-5472.CAN-15-1664
30. Natsugoe S, Xiangming C, Matsumoto M, Okumura H, Nakashima S, Sakita H, et al. Smad4 and transforming growth factor beta1 expression in patients with squamous cell carcinoma of the esophagus. *Clin Cancer Res.* (2002) 8:1838–42. Retrieved from: https://clincancerres.aacrjournals.org/content/8/6/1838.long
31. Lin SC, Lin LH, Yu SY, Kao SY, Chang KW, Cheng HW, et al. FAT1 somatic mutations in head and neck carcinoma are associated with tumor progression and survival. *Carcinogenesis.* (2018) 39:1320–30. doi: 10.1093/carcin/bgy107
32. Hung PS, Tu HF, Kao SY, Yang CC, Liu CJ, Huang TY, et al. miR-31 is upregulated in oral premalignant epithelium and contributes to the immortalization of normal oral keratinocytes. *Carcinogenesis.* (2014) 35:1162–71. doi: 10.1093/carcin/bgu024
33. Demopoulos K, Arvanitis DA, Vassilakis DA, Siafakas NM, Spandidos DA. MYCL1, FHIT, SPARC, p16(INK4) and TP53 genes associated to lung cancer in idiopathic pulmonary fibrosis. *J Cell Mol Med.* (2002) 6:215–22. doi: 10.1111/j.1582-4934.2002.tb00188.x
34. Lee S, Cho YS, Shim C, Kim J, Choi J, Oh S, et al. Aberrant expression of Smad4 results in resistance against the growth-inhibitory effect of transforming growth factor-beta in the SiHa human cervical carcinoma cell line. *Int J Cancer.* (2001) 94:500–7. doi: 10.1002/ijc.1494
35. Qiu W, Schonleben F, Li X, Su GH. Disruption of transforming growth factor beta-Smad signaling pathway in head and neck squamous cell carcinoma as evidenced by mutations of SMAD2 and SMAD4. *Cancer Lett.* (2007) 245:163–70. doi: 10.1016/j.canlet.2006.01.003
36. Rozenblum E, Schutte M, Goggins M, Hahn SA, Panzer S, Zahurak M, et al. Tumor-suppressive pathways in pancreatic carcinoma. *Cancer Res.* (1997) 57:1731–4.
37. Yatsuoka T, Sunamura M, Furukawa T, Fukushige S, Yokoyama T, Inoue H, et al. Association of poor prognosis with loss of 12q, 17p, and 18q, and concordant loss of 6q/17p and 12q/18q in human pancreatic ductal adenocarcinoma. *Am J Gastroenterol.* (2000) 95:2080–5. doi: 10.1111/j.1572-0241.2000.02171.x
38. Chang YC, Chang JG, Liu TC, Lin CY, Yang SF, Ho CM, et al. Mutation analysis of 13 driver genes of colorectal cancer-related pathways in Taiwanese patients. *World J Gastroenterol.* (2016) 22:2314–25. doi: 10.3748/wjg.v22.i7.2314
39. Martin D, Abba MC, Molinolo AA, Vitale-Cross L, Wang Z, Zaida M, et al. The head and neck cancer cell oncogenome: a platform for the development of precision molecular therapies. *Oncotarget.* (2014) 5:8906–23. doi: 10.18632/oncotarget.2417
40. India Project Team of the International Cancer Genome C. Mutational landscape of gingivo-buccal oral squamous cell carcinoma reveals new recurrently-mutated genes and molecular subgroups. *Nat Commun.* (2013) 4:2873. doi: 10.1038/ncomms3873
41. Kim KT, Kim BS, Kim JH. Association between FAT1 mutation and overall survival in patients with human papillomavirus-negative head and

neck squamous cell carcinoma. *Head Neck.* (2016) 38(Suppl. 1):E2021–9. doi: 10.1002/hed.24372
42. Chen SJ, Liu H, Liao CT, Huang PJ, Huang Y, Hsu A, et al. Ultra-deep targeted sequencing of advanced oral squamous cell carcinoma identifies a mutation-based prognostic gene signature. *Oncotarget.* (2015) 6:18066–80. doi: 10.18632/oncotarget.3768
43. Blackford A, Serrano OK, Wolfgang CL, Parmigiani G, Jones S, Zhang X, et al. SMAD4 gene mutations are associated with poor prognosis in pancreatic cancer. *Clin Cancer Res.* (2009) 15:4674–9. doi: 10.1158/1078-0432.CCR-09-0227
44. Hahn SA, Schutte M, Hoque AT, Moskaluk CA, da Costa LT, Rozenblum E, et al. DPC4, a candidate tumor suppressor gene at human chromosome 18q21.1. *Science.* (1996) 271:350–3. doi: 10.1126/science.271.5247.350
45. Nakaya K, Yamagata HD, Arita N, Nakashiro KI, Nose M, Miki T, et al. Identification of homozygous deletions of tumor suppressor gene FAT in oral cancer using CGH-array. *Oncogene.* (2007) 26:5300–8. doi: 10.1038/sj.onc.1210330
46. Chosdol K, Misra A, Puri S, Srivastava T, Chattopadhyay P, Sarkar C, et al. Frequent loss of heterozygosity and altered expression of the candidate tumor suppressor gene 'FAT' in human astrocytic tumors. *BMC Cancer.* (2009) 9:5. doi: 10.1186/1471-2407-9-5
47. Kim J, Johnson K, Chen HJ, Carroll S, Laughon A. Drosophila Mad binds to DNA and directly mediates activation of vestigial by Decapentaplegic. *Nature.* (1997) 388:304–8. doi: 10.1038/40906
48. Zawel L, Dai JL, Buckhaults P, Zhou S, Kinzler KW, Vogelstein B, et al. Human Smad3 and Smad4 are sequence-specific transcription activators. *Mol Cell.* (1998) 1:611–7. doi: 10.1016/S1097-2765(00)80061-1
49. Shi Y, Hata A, Lo RS, Massague J, Pavletich NP. A structural basis for mutational inactivation of the tumour suppressor Smad4. *Nature.* (1997) 388:87–93. doi: 10.1038/40431
50. Dai JL, Turnacioglu KK, Schutte M, Sugar AY, Kern SE. Dpc4 transcriptional activation and dysfunction in cancer cells. *Cancer Res.* (1998) 58:4592–7.
51. Hata A, Lo RS, Wotton D, Lagna G, Massague J. Mutations increasing autoinhibition inactivate tumour suppressors Smad2 and Smad4. *Nature.* (1997) 388:82–7. doi: 10.1038/40424
52. Jones JB, Kern SE. Functional mapping of the MH1 DNA-binding domain of DPC4/SMAD4. *Nucleic Acids Res.* (2000) 28:2363–8. doi: 10.1093/nar/28.12.2363
53. Kim SK, Fan Y, Papadimitrakopoulou V, Clayman G, Hittelman WN, Hong WK, et al. DPC4, a candidate tumor suppressor gene, is altered infrequently in head and neck squamous cell carcinoma. *Cancer Res.* (1996) 56:2519–21.
54. Reiss M, Santoro V, de Jonge RR, Vellucci VF. Transfer of chromosome 18 into human head and neck squamous carcinoma cells: evidence for tumor suppression by Smad4/DPC4. *Cell Growth Differ.* (1997) 8:407–15.
55. Ikediobi ON, Davies H, Bignell G, Edkins S, Stevens C, O'Meara S, et al. Mutation analysis of 24 known cancer genes in the NCI-60 cell line set. *Mol Cancer Ther.* (2006) 5:2606–12. doi: 10.1158/1535-7163.MCT-06-0433
56. Thiagalingam S, Lengauer C, Leach FS, Schutte M, Hahn SA, Overhauser J, et al. Evaluation of candidate tumour suppressor genes on chromosome 18 in colorectal cancers. *Nat Genet.* (1996) 13:343–6. doi: 10.1038/ng0796-343
57. Bornstein S, White R, Malkoski S, Oka M, Han G, Cleaver T, et al. Smad4 loss in mice causes spontaneous head and neck cancer with increased genomic instability and inflammation. *J Clin Invest.* (2009) 119:3408–19. doi: 10.1172/JCI38854
58. Ozawa H, Ranaweera RS, Izumchenko E, Makarev E, Zhavoronkov A, Fertig EJ, et al. SMAD4 loss is associated with cetuximab resistance and induction of MAPK/JNK activation in head and neck cancer cells. *Clin Cancer Res.* (2017) 23:5162–75. doi: 10.1158/1078-0432.CCR-16-1686
59. Fukuchi M, Masuda N, Miyazaki T, Nakajima M, Osawa H, Kato H, et al. Decreased Smad4 expression in the transforming growth factor-beta signaling pathway during progression of esophageal squamous cell carcinoma. *Cancer.* (2002) 95:737–43. doi: 10.1002/cncr.10727
60. Xie W, Aisner S, Baredes S, Sreepada G, Shah R, Reiss M. Alterations of Smad expression and activation in defining 2 subtypes of human head and neck squamous cell carcinoma. *Head Neck.* (2013) 35:76–85. doi: 10.1002/hed.22924
61. Hernandez AL, Wang Y, Somerset HL, Keysar SB, Aisner DL, Marshall C, et al. Inter- and intra-tumor heterogeneity of SMAD4 loss in head and neck squamous cell carcinomas. *Mol Carcinog.* (2019) 58:666–73. doi: 10.1002/mc.22958
62. Zbuk KM, Eng C. Hamartomatous polyposis syndromes. *Nat Clin Pract Gastroenterol Hepatol.* (2007) 4:492–502. doi: 10.1038/ncpgasthep0902
63. Zhong D, Morikawa A, Guo L, Colpaert C, Xiong L, Nassar A, et al. Homozygous deletion of SMAD4 in breast cancer cell lines and invasive ductal carcinomas. *Cancer Biol Ther.* (2006) 5:601–7. doi: 10.4161/cbt.5.6.2660
64. Nagatake M, Takagi Y, Osada H, Uchida K, Mitsudomi T, Saji S, et al. Somatic *in vivo* alterations of the DPC4 gene at 18q21 in human lung cancers. *Cancer Res.* (1996) 56:2718–20.
65. Snijders AM, Schmidt BL, Fridlyand J, Dekker N, Pinkel D, Jordan RC, et al. Rare amplicons implicate frequent deregulation of cell fate specification pathways in oral squamous cell carcinoma. *Oncogene.* (2005) 24:4232–42. doi: 10.1038/sj.onc.1208601
66. Xie W, Bharathy S, Kim D, Haffty BG, Rimm DL, Reiss M. Frequent alterations of Smad signaling in human head and neck squamous cell carcinomas: a tissue microarray analysis. *Oncol Res.* (2003) 14:61–73. doi: 10.3727/000000003108748612
67. Jia X, Shanmugam C, Paluri RK, Jhala NC, Behring MP, Katkoori VR, et al. Prognostic value of loss of heterozygosity and sub-cellular localization of SMAD4 varies with tumor stage in colorectal cancer. *Oncotarget.* (2017) 8:20198–212. doi: 10.18632/oncotarget.15560
68. Xie W, Rimm DL, Lin Y, Shih WJ, Reiss M. Loss of Smad signaling in human colorectal cancer is associated with advanced disease and poor prognosis. *Cancer J.* (2003) 9:302–12. doi: 10.1097/00130404-200307000-00013
69. Kouvidou C, Latoufis C, Lianou E, Kouvatseas G, Kakouri E, Anagnostakis D, et al. Expression of Smad4 and TGF-beta2 in colorectal carcinoma. *Anticancer Res.* (2006) 26:2901–7. Retrieved from: http://ar.iiarjournals.org/content/26/4B/2901
70. Bacman D, Merkel S, Croner R, Papadopoulos T, Brueckl W, Dimmler A. TGF-beta receptor 2 downregulation in tumour-associated stroma worsens prognosis and high-grade tumours show more tumour-associated macrophages and lower TGF-beta1 expression in colon carcinoma: a retrospective study. *BMC Cancer.* (2007) 7:156. doi: 10.1186/1471-2407-7-156
71. Pearlstein RP, Benninger MS, Carey TE, Zarbo RJ, Torres FX, Rybicki BA, et al. Loss of 18q predicts poor survival of patients with squamous cell carcinoma of the head and neck. *Genes Chromosomes Cancer.* (1998) 21:333–9. doi: 10.1002/(SICI)1098-2264(199804)21:4<;333::AID-GCC7>;3.0.CO;2-#
72. Kelker W, Van Dyke DL, Worsham MJ, Christopherson PL, James CD, Conlon MR, et al. Loss of 18q and homozygosity for the DCC locus: possible markers for clinically aggressive squamous cell carcinoma. *Anticancer Res.* (1996) 16:2365–72.
73. Choi HR, Roberts DB, Johnigan RH, Sturgis EM, Rosenthal DI, Weber RS, et al. Molecular and clinicopathologic comparisons of head and neck squamous carcinoma variants: common and distinctive features of biological significance. *Am J Surg Pathol.* (2004) 28:1299–310. doi: 10.1097/01.pas.0000138003.46650.dc
74. Ng IO, Xiao L, Lam KY, Yuen PW, Ng M. Microsatellite alterations in squamous cell carcinoma of the head and neck—clustering of loss of heterozygosity in a distinct subset. *Oral Oncol.* (2000) 36:484–90. doi: 10.1016/S1368-8375(00)00040-3
75. Morris LG, Kaufman AM, Gong Y, Ramaswami D, Walsh LA, Turcan S, et al. Recurrent somatic mutation of FAT1 in multiple human cancers leads to aberrant Wnt activation. *Nat Genet.* (2013) 45:253–61. doi: 10.1038/ng.2538
76. Wang L, Lyu S, Wang S, Shen H, Niu F, Liu X, et al. Loss of FAT1 during the progression from DCIS to IDC and predict poor clinical outcome in breast cancer. *Exp Mol Pathol.* (2016) 100:177–83. doi: 10.1016/j.yexmp.2015.12.012
77. Yu J, Li H. The expression of FAT1 is associated with overall survival in children with medulloblastoma. *Tumori.* (2017) 103:44–52. doi: 10.5301/tj.5000570

Conflict of Interest: The authors declare that the research was conducted in the absence of any commercial or financial relationships that could be construed as a potential conflict of interest.

frontiers in Oncology

ORIGINAL RESEARCH
published: 17 December 2019
doi: 10.3389/fonc.2019.01309

Taiwanin E Induces Cell Cycle Arrest and Apoptosis in Arecoline/4-NQO-Induced Oral Cancer Cells Through Modulation of the ERK Signaling Pathway

Shih-Hao Wang[1,2], Hsi-Chin Wu[3], Khan Farheen Badrealam[4], Yueh-Hsiung Kuo[2,5,6], Yun-Peng Chao[7], Hsi-Hsien Hsu[8,9], Da-Tian Bau[4], Vijaya Padma Viswanadha[10], Yi-Hui Chen[11], Pei-Jei Lio[12], Chung-Jen Chiang[12†] and Chih-Yang Huang[2,4,13,14,15*†]*

[1] Department of Otolaryngology, Ditmanson Medical Foundation, Chiayi Christian Hospital, Chiayi, Taiwan, [2] Department of Biotechnology, Asia University, Taichung, Taiwan, [3] School of Medicine, China Medical University, Taichung, Taiwan, [4] Graduate Institute of Biomedicine, China Medical University and Hospital, Taichung, Taiwan, [5] Department of Chinese Pharmaceutical Sciences and Chinese Medicine Resources, China Medical University, Taichung, Taiwan, [6] Chinese Medicine Research Center, China Medical University, Taichung, Taiwan, [7] Department of Chemical Engineering, Feng Chia University, Taichung, Taiwan, [8] Division of Colorectal Surgery, Mackay Memorial Hospital, Taipei, Taiwan, [9] Mackay Medicine, Nursing and Management College, Taipei, Taiwan, [10] Department of Biotechnology, Bharathiar University, Coimbatore, India, [11] Department of M-Commerce and Multimedia Applications, Asia University, Taichung, Taiwan, [12] Department of Medical Laboratory Science and Biotechnology, China Medical University, Taichung, Taiwan, [13] Cardiovascular and Mitochondria Related Diseases Research Center, Hualien Tzu Chi Hospital, Hualien, Taiwan, [14] Center of General Education, Buddhist Tzu Chi Medical Foundation, Tzu Chi University of Science and Technology, Hualien, Taiwan, [15] Department of Medical Research, China Medical University Hospital, China Medical University, Taichung, Taiwan

Taiwanin E is a bioactive compound extracted from *Taiwania cryptomerioides* Hayata. In this research endeavor, we studied the anti-cancer effect of Taiwanin E against arecoline and 4-nitroquinoline-1-oxide-induced oral squamous cancer cells (OSCC), and elucidated the underlying intricacies. OSCC were treated with Taiwanin E and analyzed through MTT assay, Flow cytometry, TUNEL assay, and Western blotting for their efficacy against OSCC. Interestingly, it was found that Taiwanin E significantly attenuated the cell viability of oral cancer cells (T28); however, no significant cytotoxic effects were found for normal oral cells (N28). Further, Flow cytometry analysis showed that Taiwanin E induced G1cell cycle arrest in T28 oral cancer cells and Western blot analysis suggested that Taiwanin E considerably downregulated cell cycle regulatory proteins and activated p53, p21, and p27 proteins. Further, TUNEL and Western blot studies instigated that it induced cellular apoptosis and attenuated the p-PI3K/p-Akt survival mechanism in T28 oral cancer cells seemingly through modulation of the ERK signaling cascade. Collectively, the present study highlights the prospective therapeutic efficacy of Taiwanin E against arecoline and 4-nitroquinoline-1-oxide-induced oral cancer.

Keywords: Taiwanin E, oral cancer, apoptosis, cell cycle arrest, therapeutics

OPEN ACCESS

Edited by:
Victor C. Kok,
Asia University, Taiwan

Reviewed by:
Mohammad Asad,
Albert Einstein College of Medicine, United States
Mohammad Javed Equbal,
Texas A&M University Commerce, United States

***Correspondence:**
Chung-Jen Chiang
cjchiang@mail.cmu.edu.tw
Chih-Yang Huang
cyhuang@mail.cmu.edu.tw

† These authors have contributed equally to this work

Specialty section:
This article was submitted to Head and Neck Cancer, a section of the journal Frontiers in Oncology

Received: *20 July 2019*
Accepted: *11 November 2019*
Published: *17 December 2019*

Citation:
Wang S-H, Wu H-C, Badrealam KF, Kuo Y-H, Chao Y-P, Hsu H-H, Bau D-T, Viswanadha VP, Chen Y-H, Lio P-J, Chiang C-J and Huang C-Y (2019) Taiwanin E Induces Cell Cycle Arrest and Apoptosis in Arecoline/4-NQO-Induced Oral Cancer Cells Through Modulation of the ERK Signaling Pathway. Front. Oncol. 9:1309. doi: 10.3389/fonc.2019.01309

INTRODUCTION

Over the years, complementary and alternative medicine therapies have garnered great attention all across the globe (1, 2). Accumulating evidences has highlighted the efficacy of various small molecule compounds/phytochemicals as effective therapeutic entities against various diseases and pathological conditions, including cancer (3–6). Previous reports from our group have ascertained the potential of several bioactive compounds against cancer together with providing an insight into their mechanisms of action (7–11).

Taiwania (*Taiwania cryptomerioides* Hayata) represents one of the most economically relevant plant species endemic to Taiwan. Numerous bioactive compounds have been derived from this plant species. Many of them have been demonstrated to exhibit potent activity against bacteria, fungi, termites, mites, and cancers (12–15). To this end, recently, we have provided convincing evidence for the efficacy of Taiwanin A against arecoline and 4-nitroquinoline-1-oxide-induced oral cancer (16–18). Nevertheless, to the best of our knowledge, the effect of Taiwanin E against oral cancer and the underlying mechanism remains poorly understood.

Despite advancement in the allied field of biomedical sciences, the repercussions that may arise from cancer represent a significant human toll. According to statistics, globally, oral cancer is amongst 10 most common cancers. Oral squamous cell carcinoma (OSCC) is the most common malignant epithelial neoplasm that can afflict the oral cavity. It is thought that more than 90% malignancies arising from the head and neck tissue section are OSCC (19). Despite the availability of treatment strategies, including surgery, radiation, and chemotherapy, the overall survival rate of patients remains poor (20, 21). Taking these into consideration, in the current research endeavor, we have studied the effect of Taiwanin E against oral cancer and elucidated the underlying mechanism for their efficacy against oral cancer.

Interestingly, it was found that Taiwanin E significantly attenuated the cell viability of oral cancer cells (T28) in a dose- and time-dependent fashion; nevertheless, no cytotoxic effects were found for normal oral cells (N28). Moreover, it was observed that Taiwanin E induces G1 cell cycle arrest in T28 cells, as was evident through Flow cytometry studies, and, further, Western blot analysis suggested that Taiwanin E considerably downregulated cell cycle regulatory proteins and activated p53, p21, and p27 proteins. In addition, TUNEL staining showed that Taiwanin E induced apoptosis in T28 oral cancer cells. Furthermore, it was found that the cell survival proteins, such as p-PI3K, p-Akt, and the antiapoptotic protein Bcl-xL, were considerably reduced following treatment with Taiwanin E; nevertheless, the pro-apoptotic proteins, such as Bax, Cyt C, and c Cas 3, were, however, considerably enhanced. Further, understanding the underlying intricacies; mechanistically, it was found that Taiwanin E modulated the expression of ERK and resulted in cellular apoptosis in T28 oral cancer cells. Taken together, the data convincingly ascertained the promising candidature of Taiwanin E against oral cancer.

MATERIALS AND METHODS

Chemicals and Reagents

All chemicals and reagents were procured from Sigma Aldrich Co. (MO, USA) unless otherwise mentioned.

Purification of Taiwanin E

Taiwanin E was obtained from freshly cut wood of *Taiwania cryptomerioides* Hayata. The procedures for isolation, purification, and characterization of Taiwanin E was performed following our previously published reports with slight modifications (22, 23). Finally, the as-purified Taiwanin E was dissolved in DMSO, filtered through 0.22 μm fluoropore filter (Millipore, MA, USA), and employed for subsequent studies.

Establishment of Cell Model for Oral Cancer

An OSCC model was established following the protocol described in our previous studies (16, 17). Basically, carcinogenesis was induced in C57BL/6J Narl male mice by daily oral administration of 0.5 mg/mL arecoline (Sigma Aldrich, MO, USA) and 0.2 mg/mL of 4-NQO (Sigma Aldrich, MO, USA) for 28 days. Thereafter, primary oral squamous carcinoma cells were derived from tumor (T28) tissue following 28 weeks of administration. In addition, primary oral squamous cells were also derived from a paired control group, i.e., non-tumor normal (N28), tissue, and these were used as normal control cells.

All the animal experimentation protocols performed in the study were strictly in accordance with the Animal Care and Use Committee of the China Medical University, Taichung, Republic of China (Taiwan).

N28 and T28 cells were cultured in Dulbecco's minimum essential medium (D7777) (Sigma Aldrich, MO, USA) supplemented with 10% charcoal-treated FBS (Characterized Fetal Bovine Serum, HyClone Inc., Utah, USA), 1% penicillin/streptomycin (Invitrogen Corp., California, USA), L-Glutamine, and $NaHCO_3$.

For treatment, cells were seeded in triplicate in cell culture plates and treated with varying concentrations of Taiwanin E (0, 1, 5, and 10 μM) for different time intervals (0, 3, 6, 12, 24, and 48 h), and thereafter, the cells were harvested and analyzed for respective parameters. For activator experiments, cells were treated with Taiwanin E (10 μM) and co-treated with increasing concentrations of ERK activator (0.5, 1.0, 2.5, and 5.0 μM) for 24 h. Thereafter, they were analyzed by MTT assay and Western blotting, following the standard procedures as described below.

Cell Viability Assay

Cell viability was assessed as reported in our previous studies (16). Basically, cells were seeded in triplicate in cell culture plates and treated with increasing concentrations of Taiwanin E (0, 1, 5, and 10 μM) for a 24 h time interval. In addition, cells were treated with Taiwanin E (10 μM) for different time intervals (0, 3, 6, 12, 24, and 48 h). Following incubation with Taiwanin E for varying concentrations and time periods, the cells were thereafter treated with 0.5 mg/mL of MTT reagent and incubated for 4 h in dark conditions. Finally, the formazan crystals were dissolved

in 500 μL of DMSO (dimethyl sulfoxide), and the absorbance was acquired at 570 nm on a multi-well ELIZA plate reader. Cell viability was represented as the percentage of control.

Cell Cycle Analysis

Cell cycle study was performed with flow cytometry. Briefly, T28 oral cancer cells (1×10^5 cells/well) were seeded in tissue culture plates; thereafter, they were treated with varying doses of Taiwanin E (0, 1, 5, and 10 μM) for 24 h and treated with Taiwanin E (10 μM) for different time intervals (0, 3, 6, 12, 24, and 48 h). Following treatment, cells were harvested and subsequently fixed in chilled ethanol overnight at 4°C. Consequently, cells were washed with PBS, centrifuged at 600 ×g for 5 min and thereafter resuspended in PBS containing 10 mg/ml RNase A and incubated with 30 mg/ml of PI for 30 min at RT. Finally, the samples were acquired with flow cytometry (Becton Dickinson, CA, USA).

Western Blot Analysis

Western blot was executed as reported previously (16, 24). In brief, cells were lysed in RIPA lysis buffer containing 50 mM Tris, pH 7.5, 150 mM NaCl, 1% NP-40, 0.1% SDS, 0.5% sodium deoxycholate, phosphatase inhibitor cocktail, and a proteinase inhibitor cocktail and thereafter centrifuged at 12,000 × g for 30 min at 4°C to obtain the cell lysate (25). After this, the supernatants were obtained, and protein concentration was estimated through a Bio-RAD protein quantification reagent following the Bradford method. Thereafter, the samples were resolved through 8–12% sodium dodecyl sulfate polyacrylamide gel electrophoresis (SDS-PAGE) and blotted onto polyvinylidene difluoride (PVDF) membranes (Millipore, MA, USA). The membranes were thereafter blocked with blocking solution (5% skimmed milk in TBST) for 1 h at RT. Following the blocking steps, the membranes were washed with TBST thrice and finally incubated with primary antibodies against β-actin, Cyclin B1, Cyclin D1, Cyclin E, p21, p27, JNK, p-ERK, p-JNK, p38, Cytochrome C, Bcl-xL, and Bax from Santa Cruz (CA, USA); pS473-Akt, p-PI3K, cleaved caspase-3, pP53, and p-p38 from Cell Signaling (CA, USA); and ERK from BD Biosciences (CA, USA). Following the washing procedures, the membranes were then subsequently incubated with secondary antibodies for 1 h at RT. Finally, the Antigen–Antibody molecular intricacies were assessed with enhanced chemiluminescence (ECL) horseradish peroxidase (HRP) substrate (Millipore, MA, USA), and the signals were acquired by LAS 3,000 imaging system (Fujifilm, Tokyo, Japan). Membranes were stripped and reprobed with other antibodies for the subsequent detection of other proteins.

TUNEL Assay

Cellular apoptosis was analyzed by *in situ* terminal deoxynucleotide transferase-mediated dUTP nick end-labeling (TUNEL) assay following manufacturer-recommended procedures (26). In brief, cells were cultured in 24-well culture plates and treated with Taiwanin E, and, thereafter, the cells were harvested, washed with 1×PBS (Gibco BRL, Paisley, UK), and incubated with TUNEL assay reagents at RT for stipulated time intervals. After this, the samples were examined with flow cytometry (Becton Dickinson, CA, USA).

Statistical Analysis

Results are represented as mean ± SD. Statistical analysis was done with Graph Pad Prism5 statistical software (Graph-Pad, CA, USA). Multiple comparisons were assessed through ANOVA. p Values of ≤ 0.05 were regarded as statistically significant. All experiments were performed in triplicate in a blinded manner. Results were quantified with Image J software (NIH, Bethesda, MD, USA) and processed through Adobe Photoshop.

RESULTS

The Effect of Taiwanin E on Cell Viability and the Cell Cycle Process of Oral Cancer Cells Following Dose-Dependent Treatment

Normal oral cells N28 and cancer cells T28 were treated with increasing concentrations of Taiwanin E for a 24 h time interval; thereafter, cell viability was ascertained by MTT assay. MTT data showed that Taiwanin E exhibited cytotoxic effects on T28 oral cancer cells, especially at 10 μM concentration, whereas no cytotoxic effects were observed for N28 normal oral cells (**Figure 1A**). In addition, it was observed that Taiwanin E exhibited significant cytotoxicity against other squamous cell carcinoma cell lines SCC9 and SCC25 (data not shown). Considering the results, we further examined whether Taiwanin E treatment could modulate cell cycle progression in oral cancer cells T28. To this end, cells were treated with increasing concentrations of Taiwanin E for 24 h; thereafter, they were analyzed through flow cytometry. As evident from **Figure 1**, it was found that there were considerable increase in the G1 population (60.07% at 5 μM, 67.80% at 10 μM) in Taiwanin E-treated T28 cells as compared to control cells, wherein only 58.03% of cells were in the G1 population (**Figure 1B**). The data from the study suggested an accumulation in the G1 phase of the cell cycle following treatment with Taiwanin E.

The Effect of Taiwanin E on Cell Viability and the Cell Cycle Process of Oral Cancer Cells Following Time-Dependent Treatment

Further, N28 and T28 cells were treated with Taiwanin E (10 μM) for different time periods from 0 to 48 h, and cell viability was determined through MTT assay; interestingly, it was observed that Taiwanin E exhibited cytotoxic effects on T28 cells in a time-dependent manner. However, no such effects were observed for normal N28 oral cells (**Figure 2A**). Further, we also determined the effect of treatment of Taiwanin E for different time interval (0–48 h) on the cell progression; it was found that there were considerable increases in the G1 population in a time-dependent fashion (**Figure 2B**) (27).

Collectively, these results suggested that Taiwanin E exhibited cytotoxic manifestations toward tumor oral cells T28 in a dose- and time-dependent fashion; however, no cytotoxic effects were

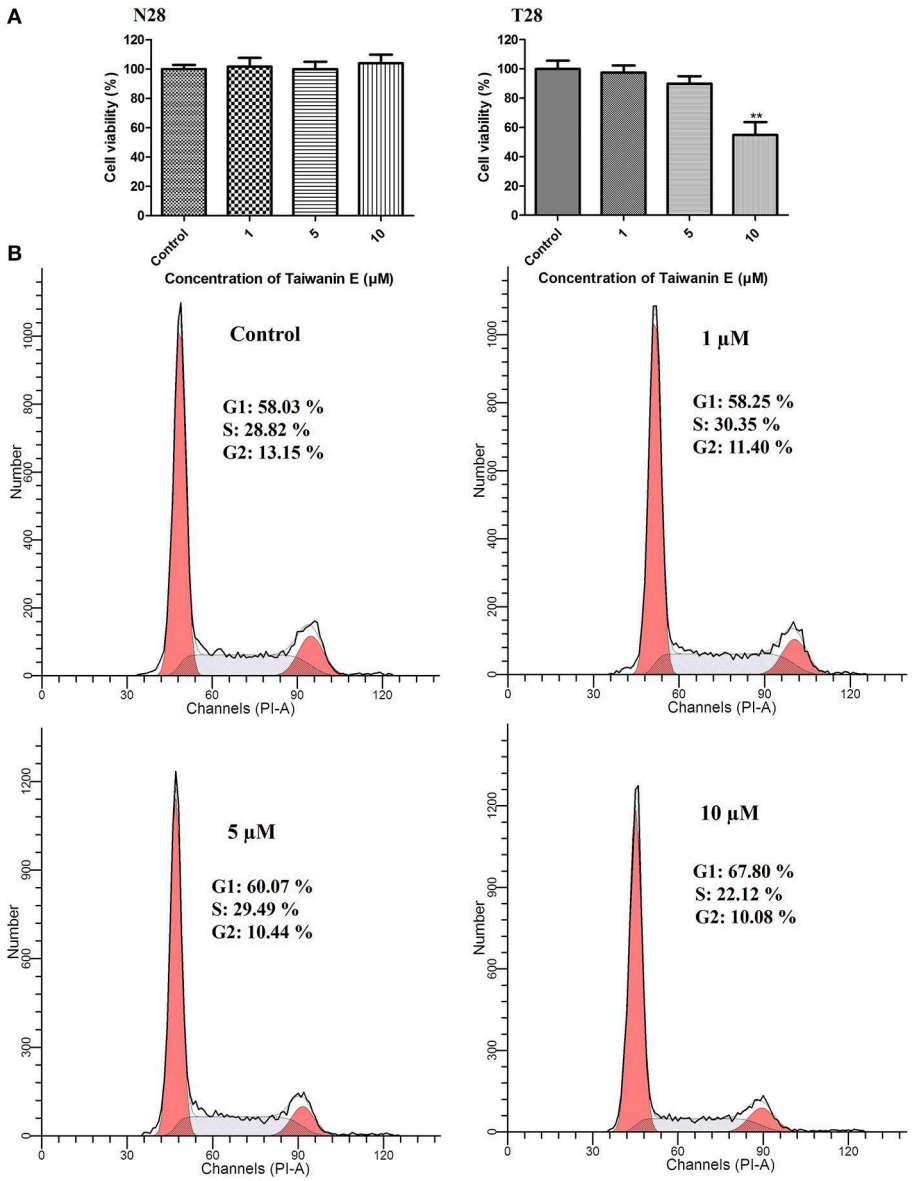

FIGURE 1 | Effect of Taiwanin E on cell viability and cell cycle progression of oral cells. Normal oral cells N28 and Cancer oral cells T28 were treated with varying concentrations of Taiwanin E (0, 1, 5, and 10 μM) for 24 h. The cell viability of N28 cells and T28 cells was assessed with MTT assay **(A)**. $^{**}p < 0.01$ represents significant differences compared with control. T28 cells were treated with varying concentrations of Taiwanin E (0, 1, 5, and 10) μM for 24 h, and the DNA content was assessed through flow cytometry. Results were represented as percentages of the cell population in G1, S, and G2 phases of the cell cycle **(B)**.

observed for normal oral cells N28. Moreover, Taiwanin E treatment in T28 cells modulated their normal regulation of cell cycle progression. Nevertheless, no significant effects were observed for normal oral cells N28 (data not shown).

The Effect of Taiwanin E on Cell Cycle-Related Proteins of Oral Cancer Cells

We further investigated whether Taiwanin E affects cell cycle-related proteins in T28 oral cancer cells. To this end, cells were treated with Taiwanin E (10 μM) for different time periods from 0 to 48 h and thereafter analyzed through Western blotting. Interestingly, it was found that the cell cycle regulatory proteins, such as cyclin B1, cyclin D1, and cyclin E, were considerably decreased (**Figure 3A**), whereas p53, p21, and p27 protein levels were substantially increased following treatment with Taiwanin E (**Figure 3B**).

The Effect of Taiwanin E on the Induction of Apoptosis in Oral Cancer Cells

We further investigated whether Taiwanin E could induce cellular apoptosis in T28 oral cancer cells. As evident through TUNEL assay, considerable apoptosis was observed following treatment with Taiwanin E (**Figure 4A**). To gain further insight

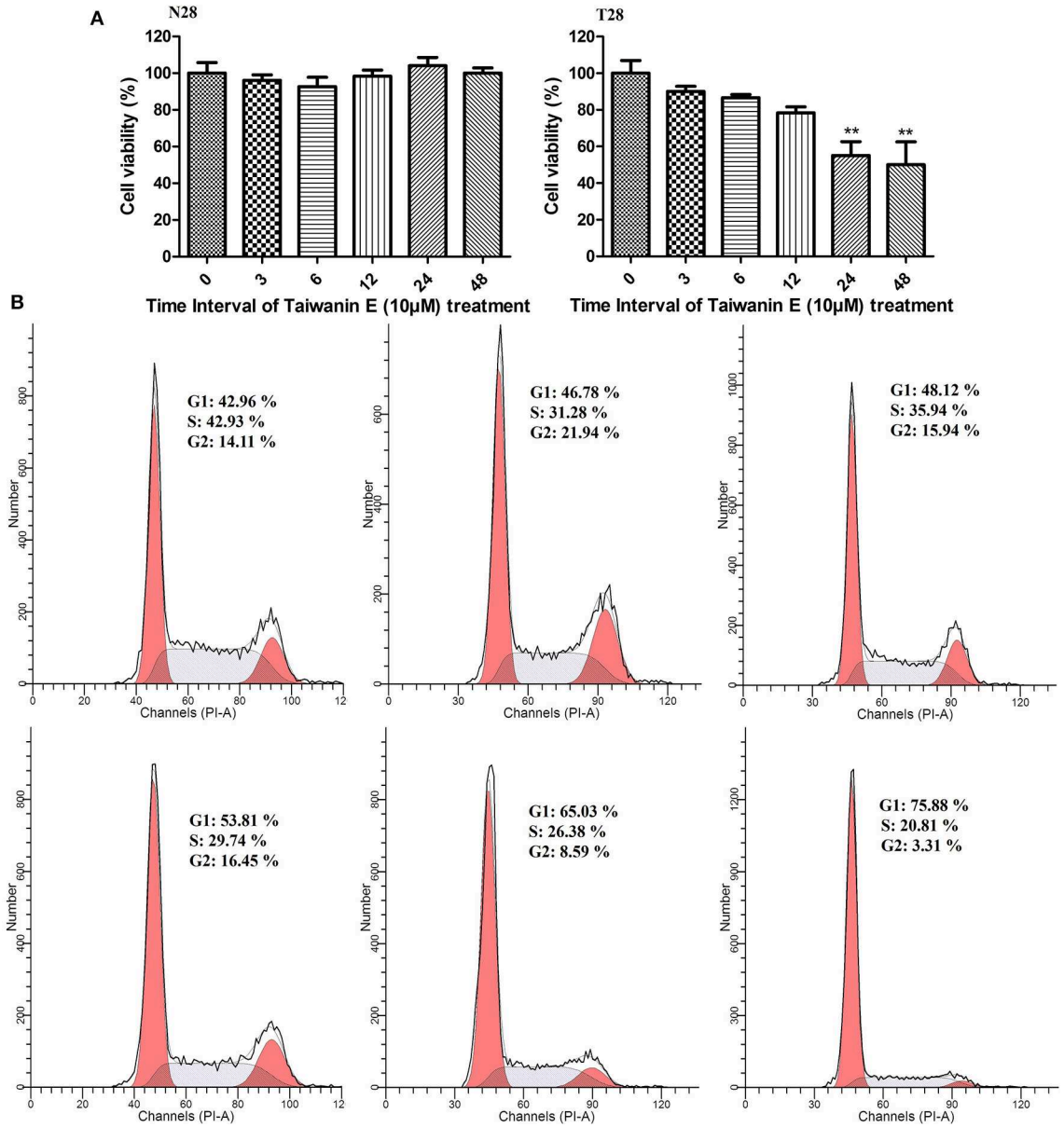

FIGURE 2 | Effect of Taiwanin E on cell viability and cell cycle progression of oral cells. Normal oral cells N28 and cancer oral cells T28 were treated with Taiwanin E (10 μM) for different time intervals. The cell viability of N28 cells and T28 cells was assessed with MTT assay **(A)**. $^{**}p < 0.01$ represents significant differences compared with control. T28 cells were treated with Taiwanin E (10 μM) for different time interval, and the DNA content was assessed through flow cytometry. Results were represented as a percentage of the cell population in G1, S, and G2 phases of the cell cycle **(B)**.

into the effect of Taiwanin E on T28 oral cancer cells, we examined the protein levels of p-PI3K, p-Akt, Bcl-xL, Bax, cytochrome C, and cleaved caspase 3. Intriguingly, it was observed that T28 cells, when treated with Taiwanin E, showed a significant decrement in survival-related proteins, including p-PI3K, p-Akt, and anti-apoptotic protein Bcl-xL, in a time-dependent manner; contrastingly, the levels of Bax, Cyt C, and cleaved-caspase 3 were considerably decreased accordingly (**Figure 4B**).

The Effect of Taiwanin E on the MAPK Signaling Cascade in Oral Cancer Cells

Further, the effect of Taiwanin E on the MAPK signaling cascade was investigated. As could be seen from the figure, following treatment with Taiwanin E, a considerable reduction in the p-ERK1/2 was observed; no significant effects, however, were observed for p-JNK and p-p38 proteins (**Figure 5**). Collectively, these results showed that Taiwanin E considerably regulated the MAPK signaling cascade.

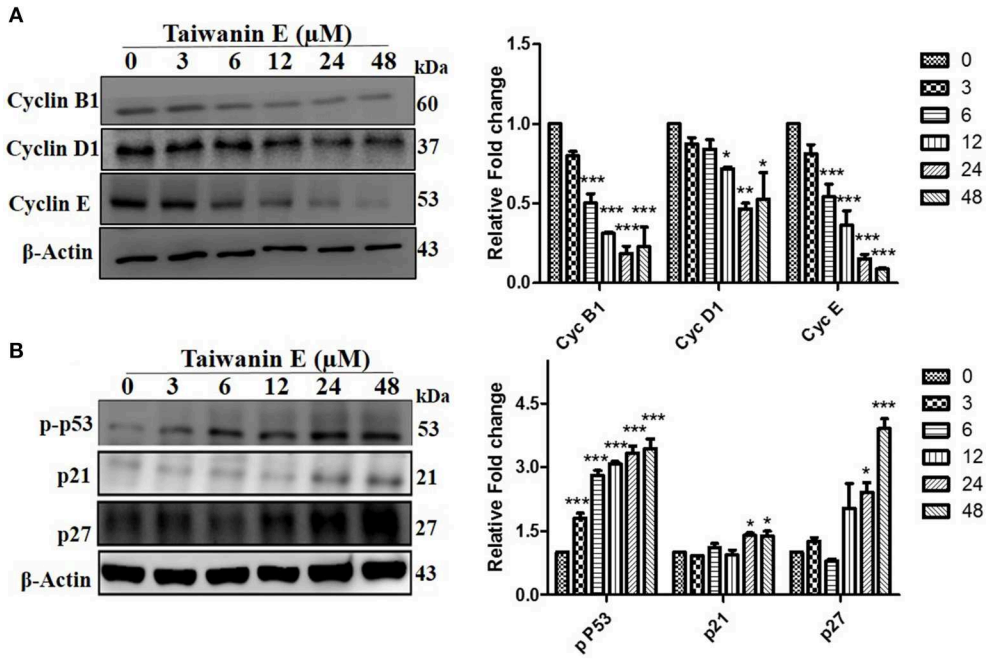

FIGURE 3 | Effect of Taiwanin E on cell cycle-related proteins in oral cancer cells. T28 cells were treated with Taiwanin E (10 μM) for different time intervals and thereafter analyzed through Western blotting. Samples were assessed for the expression of Cyclin B1, Cyclin D1, and Cyclin E **(A)** and p53, p21, and p27 **(B)**, respectively. Graphs represent mean values of three independent experiment in T28 cells. $^{*}p < 0.05$, $^{**}p < 0.01$, and $^{***}p < 0.001$ represent significant differences compared with control.

The Effects of Taiwanin E on ERK in Oral Cancer Cells

To further investigate the underlying intricacies of modulation of ERK in the efficacy of Taiwanin E, the effect of the ERK activator on T28 cell proliferation was ascertained. Intriguingly, it was observed that ERK activator co-treatment with Taiwanin E in T28 cells considerably reversed the effect of Taiwanin E in a dose-dependent fashion (**Figure 6A**). In addition, we further examined whether the ERK activator co-treatment could interfere with the signal transduction pathway of cellular apoptosis. Interestingly, the results showed that co-treatment with the ERK activator considerably increased Bcl-xL protein levels and reduced Cyt C protein levels (**Figure 6**). These results highlighted the role of ERK in the efficacy of Taiwanin E against T28 oral cancer cells.

Collectively, it could be envisaged that Taiwanin E considerably modulated ERK, which eventually led to the inhibition of cancer cell survival, induced cell cycle arrest at G1, and apoptosis in T28 oral cancer cells. Collectively, the data convincingly demonstrated that Taiwanin E may potentially become an effective small molecular drug against oral cancer in the near future.

DISCUSSION

Various bioactive compounds (lignans, flavones, sesquiterpenoids, diterpenoids, cyclitols, steroids, etc.) derived from Taiwania has been shown to be effective against various debilitating diseases. Accumulating evidences have shown their efficacy against various forms of cancers, including A-549 lung carcinoma, MCF-7 breast adenocarcinoma, and HT-29 colon adenocarcinoma (22). In this research endeavor, we investigated the anti-cancer effect of Taiwanin E against arecoline and 4-nitroquinoline-1-oxide-induced OSCC and elucidated the underlying mechanism thereof. Basically, OSCC were treated with Taiwanin E and analyzed for their bioactivities against OSCC. Collectively, the data of the present study suggest that Taiwanin E significantly attenuated the cell viability of oral cancer cells (T28) in a dose- and time-dependent fashion. Moreover, it was observed that Taiwanin E induced G1 cell cycle arrest in T28 cells, as was evident through Flow cytometry studies, and further Western blot analysis suggested that Taiwanin E considerably downregulated cell cycle regulatory proteins, including Cyclin B1, Cyclin D1, and Cyclin E, and activated p53, p21, and p27 proteins, respectively. Furthermore, TUNEL staining showed that Taiwanin E induced considerable apoptosis in T28 cells, and, in addition, it was found that the cell survival proteins, such as p-PI3K and p-Akt and the anti-apoptotic protein Bcl-xL, were considerably reduced following treatment with Taiwanin E The pro-apoptotic proteins, such as Bax, Cyt C, and c Cas-3, were, however, considerably enhanced. Furthermore, in understanding the underlying intricacies mechanistically, it was found that Taiwanin E seemingly modulated ERK and thereby attenuated cell survival and induced cellular apoptosis in T28 oral cancer cells.

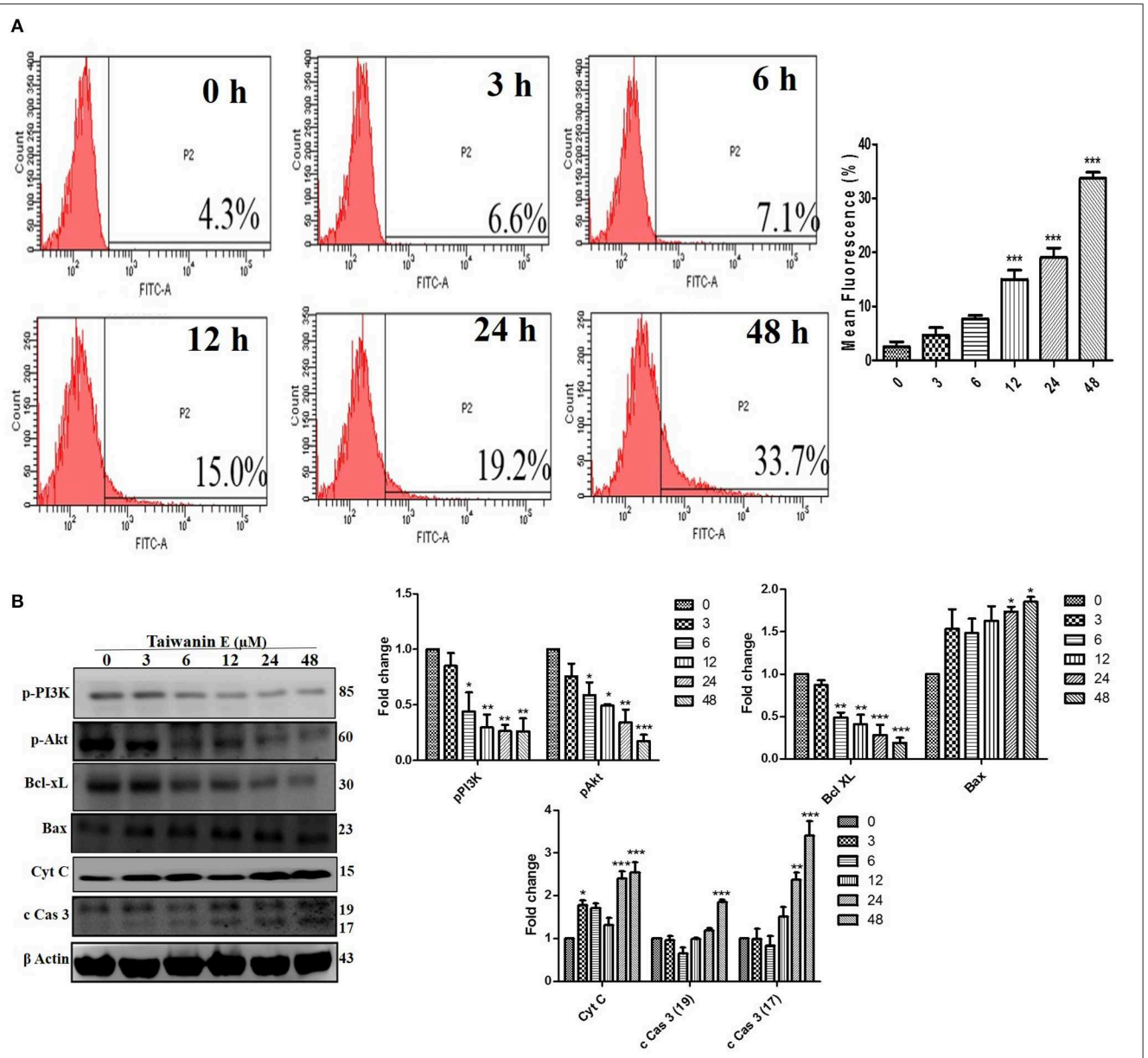

FIGURE 4 | Effect of Taiwanin E on the induction of cellular apoptosis in oral cancer cells. T28 cells were treated with Taiwanin E (10 μM) for different time periods The samples were stained with a TUNEL kit and analyzed through flow cytometry **(A)**. T28 cells were treated with Taiwanin E (10 μM) for different time periods. Cell lysates were analyzed for the expressions of p-PI3K, p-Akt, Bcl-xL, Bax, Cyt C, and c Cas 3 through Western blotting **(B)**. Graphs represents the mean value of three separate experiment in the T28 cells. *$p < 0.05$, **$p < 0.01$, and ***$p < 0.001$ represent significant differences compared with control group.

It is widely accepted that alteration in cell cycle progression causes severe cellular damage which eventually leads to apoptosis. It was found that Taiwanin E induces cell cycle arrest in OSCC in a dose and time dependent fashion. Analyzing the molecular intricacies underlying Taiwanin E-induced cell cycle arrest, it was observed that Taiwanin E treatment downregulated the expression of cell cycle regulatory proteins; in addition, Taiwanin E regulated the p53 tumor suppressor and increased the protein expression of p21 and p27. This is in concordance with the study by Shyur et al., wherein they demonstrated that Taiwanin A isolated from *Taiwania cryptomerioides* Hayata upregulated p53, phosphorylated p53, p21, and p27, and, contrastingly, downregulated the G(2)/M checkpoint mediators cyclins, leading to the induction of G(2)/M cell-cycle arrest in MCF-7 cells (13).

As a matter of fact, the apoptotic pathways are regulated through the orchestrated communication of diverse pro-apoptotic and anti-apoptotic signaling mediators. Essentially, the pro-apoptotic signaling mediators lead to the modulation of mitochondrial potential and subsequent release of mediators, which eventually triggers a cascade of events that lead to apoptosis. The data of the present study demonstrated that Taiwanin E treatment increased the amount of pro-apoptotic

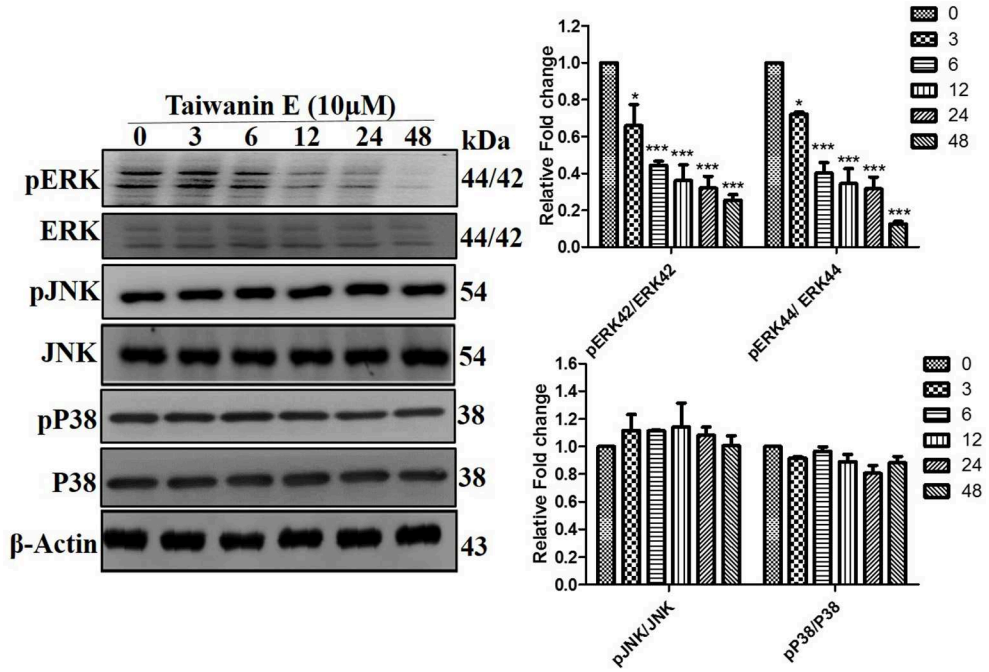

FIGURE 5 | Taiwanin E modulate the ERK signaling cascade in oral cancer cells. T28 cells were treated with Taiwanin E (10 μM) for different time periods. Thereafter, cell lysates were analyzed for the expression of ERK, pERK, JNK, pJNK, p38, and p-p38 through Western blotting. Graphs represents mean values of three independent experiment in T28 cells. $^{*}p < 0.05$ and $^{***}p < 0.001$ represent significant differences compared with control.

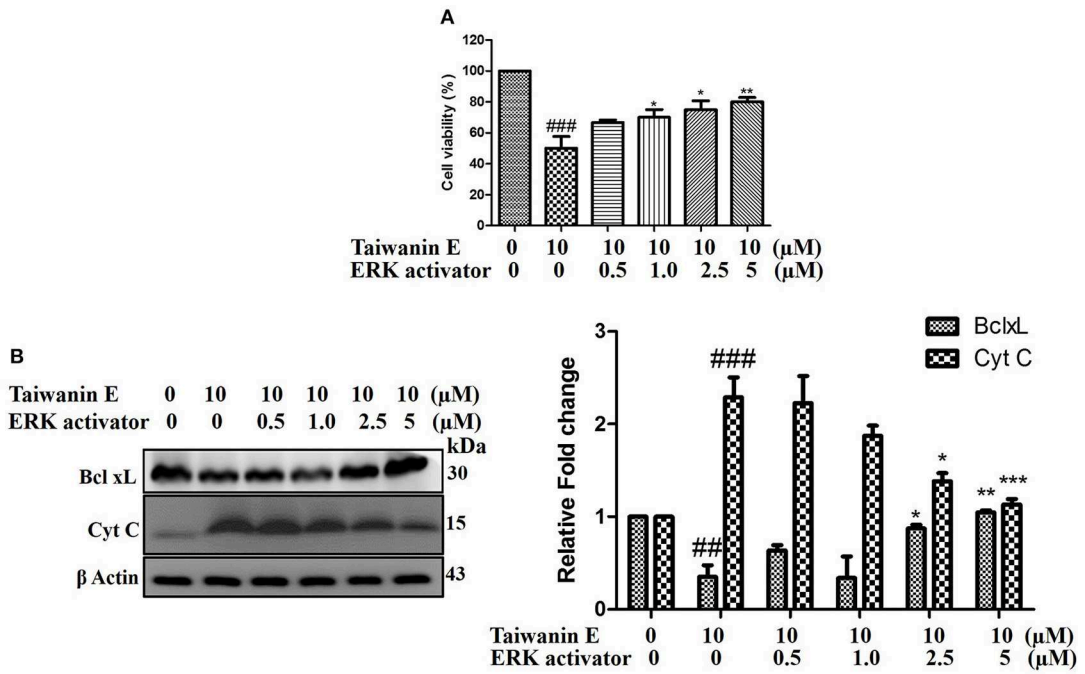

FIGURE 6 | Effect of Taiwanin E on ERK activation in oral cancer cells. T28 cells were co-treated with ERK activator and Taiwanin E for 24 h. Thereafter, cell viability was analyzed through MTT assay **(A)**. T28 cells were co-treated with ERK activator and Taiwanin E for 24 h. Thereafter, cell lysates were analyzed through Western blotting for the expression of Bcl-xL and Cyt C proteins through Western blotting **(B)**. Graphs represent mean value of three separate experiment in T28 cells. $^{\#\#}p < 0.01$ and $^{\#\#\#}p < 0.001$ represent significant differences compared with control group, whereas $^{*}p < 0.05$, $^{**}p < 0.01$, and $^{***}p < 0.001$ represent significant differences compared with the Taiwanin E-treated group.

proteins. Bax released cytochrome C from the mitochondria, induced Caspase activation, and downregulated the survival protein p-PI3K, p-Akt, and anti-apoptotic Bcl-xL, which is certainly suggestive of their promising anti-cancer potential against OSCC.

MAPK/ERK signaling cascades are crucial pathways that plays an imperative role in the orchestration of normal cell proliferation, survival, and differentiation. It is widely accepted that aberrant regulation of MAPK has been involved in various human diseases, including cancer. Thus, the MAPK/ERK signaling network has been the focus of various research endeavors in order to ascertain novel target-based approaches for cancer therapeutics (28). Intriguingly, our study demonstrated that Taiwanin E modulated ERK signaling for therapeutic efficacy (28). This is in concordance with the reports, wherein authors have implicated the role of the ERK signaling mediator in the efficacy of the anti-cancer compounds. To this end, Wang et al. reported that Geraniin inhibited migration and invasion of human osteosarcoma cancer cells, seemingly through the regulation of the PI3K/Akt and ERK1/2 signaling pathways (29). Furthermore, Fong et al., while demonstrating the efficacy of BPIQ-induced cell migration and apoptosis in human non-small cell lung cancer (NSCLC) cells, highlighted that MAPK kinases, in particular ERK mediators, were responsible for their anti-cancer potential (30). In addition, Kuo et al. have explicitly demonstrated that the a related compound of Taiwanin E, i.e., a novel derivative of Taiwanin A, inhibited dual key proliferation signaling transduction pathways in a Triple-Negative Breast Cancer model (31).

Collectively, keeping in mind the fact that various phytochemicals, such as taxol (from *Taxus brevifolia*) and camptothecin derivatives (from *Camptotheca acuminate*), are widely explored for cancer treatment, and, as Taiwanin E displayed lower cytotoxicity against normal oral cells, it could be envisaged as a promising drug to treat oral cancer in the near future, thus warranting future investigation.

DATA AVAILABILITY STATEMENT

The datasets generated for this study are available on request to the corresponding author.

AUTHOR CONTRIBUTIONS

S-HW and C-YH contributed toward the conception and design of the study. S-HW, H-CW, and KB performed the experiments and data analysis. KB, C-JC, and C-YH contributed to the manuscript writing, editing, and proofreading. Y-HK, Y-PC, H-HH, D-TB, VV, Y-HC, and P-JL supported the experiment design, data analysis, and the manuscript writing and proofreading.

FUNDING

This work was financially supported by the Taiwan Ministry of Health and Welfare Clinical Trial Center MOHW105-TDU-B-212-133019 and MOHW108-TDU-B-212-133004. KB acknowledges the support of MOST 107-2811-b-039-513, Taiwan, in the form of a postdoctoral fellowship.

REFERENCES

1. Chrysant SG, Chrysant GS. Herbs used for the treatment of hypertension and their mechanism of action. *Curr Hypertension Rep*. (2017) 19:77. doi: 10.1007/s11906-017-0775-5
2. Chiang JT, Badrealam KF, Shibu MA, Cheng SF, Shen CY, Chang CF, et al. Anti-apoptosis and anti-fibrosis effects of eriobotrya japonica in spontaneously hypertensive rat hearts. *Int J Mol Sci*. (2018) 19:E1638. doi: 10.3390/ijms19061638
3. Hedigan K. Cancer: herbal medicine reduces chemotherapy toxicity. *Nat Rev Drug Discov*. (2010) 9:765. doi: 10.1038/nrd3280
4. Efferth T, Li PC, Konkimalla VS, Kaina B. From traditional Chinese medicine to rational cancer therapy. *Trends Mol Med*. (2007) 13:353–61. doi: 10.1016/j.molmed.2007.07.001
5. Li-Weber M. Targeting apoptosis pathways in cancer by Chinese medicine. *Cancer Lett*. (2013) 332:304–12. doi: 10.1016/j.canlet.2010.07.015
6. Newman DJ, Cragg GM. Natural products as sources of new drugs over the last 25 years. *J Nat Prod*. (2007) 70:461–77. doi: 10.1021/np068054v
7. Abdelfadil E, Cheng YH, Bau DT, Ting WJ, Chen LM, Hsu HH, et al. Thymoquinone induces apoptosis in oral cancer cells through p38beta inhibition. *Am J Chinese Med*. (2013) 41:683–96. doi: 10.1142/S0192415X1350047X
8. Chen MC, Huang CY, Hsu SL, Lin E, Ku CT, Lin H, et al. Retinoic acid induces apoptosis of prostate cancer DU145 cells through Cdk5 overactivation. *Evid-Based Compl Altern Med*. (2012) 2012:580736. doi: 10.1155/2012/580736
9. Tsai KH, Hsien HH, Chen LM, Ting WJ, Yang YS, Kuo CH, et al. Rhubarb inhibits hepatocellular carcinoma cell metastasis via GSK-3-beta activation to enhance protein degradation and attenuate nuclear translocation of beta-catenin. *Food Chem*. (2013) 138:278–85. doi: 10.1016/j.foodchem.2012.10.038
10. Dung TD, Chang HC, Binh TV, Lee MR, Tsai CH, Tsai FJ, et al. Zanthoxylum avicennae extracts inhibit cell proliferation through protein phosphatase 2A activation in HA22T human hepatocellular carcinoma cells *in vitro* and *in vivo*. *Int J Mol Med*. (2012) 29:1045–52. doi: 10.3892/ijmm.2012.938
11. Dung TD, Chang HC, Chen CY, Peng WH, Tsai CH, Tsai FJ, et al. Zanthoxylum avicennae extracts induce cell apoptosis through protein phosphatase 2A activation in HA22T human hepatocellular carcinoma cells and block tumor growth in xenografted nude mice. *Int J Mol Med*. (2011) 28:927–36. doi: 10.3892/ijmm.2012
12. Ho PJ, Chou CK, Kuo YH, Tu LC, Yeh SF. Taiwanin a induced cell cycle arrest and p53-dependent apoptosis in human hepatocellular carcinoma HepG2 *Cells Life Sci*. (2007) 80:493–503. doi: 10.1016/j.lfs.2006.10.017
13. Shyur LF, Lee SH, Chang ST, Lo CP, Kuo YH, Wang SY. Taiwanin A inhibits MCF-7 cancer cell activity through induction of oxidative stress, upregulation of DNA damage checkpoint kinases, and activation of p53 and FasL/Fas signaling pathways. *Phytomedicine*. (2010) 18:16–24. doi: 10.1016/j.phymed.2010.06.005
14. Chang ST, Cheng SS, Wang SY. Antitermitic activity of essential oils and components from Taiwania (Taiwania cryptomerioides). *J Chem Ecol*. (2001) 27:717–24. doi: 10.1023/a:1010397801826
15. Chang ST, Chen PF, Wang SY, Wu HH. Antimite activity of essential oils and their constituents from Taiwania cryptomerioides. *J Med Entomol*. (2001) 38:455–7. doi: 10.1603/0022-2585-38.3.455
16. Tsai CY, Fang HY, Shibu MA, Lin YM, Chou YC, Chen YH, et al. Taiwanin C elicits apoptosis in arecoline and 4-nitroquinoline-1-oxide-induced oral squamous cell carcinoma cells and hinders proliferation via epidermal

growth factor receptor/PI3K suppression. *Environ Toxicol*. (2019) 34:760–67. doi: 10.1002/tox.22742
17. Hsieh CH, Hsu HH, Shibu MA, Day CH, Bau DT, Ho CC, et al. Down-regulation of beta-catenin and the associated migration ability by Taiwanin C in arecoline and 4-NQO-induced oral cancer cells via GSK-3beta activation. *Mol Carcinogen*. (2017) 56:1055–67. doi: 10.1002/mc.22570
18. Lin KH, Shibu MA, Kuo YH, Chen YC, Hsu HH, Bau DT, et al. Taiwanin C selectively inhibits arecoline and 4-NQO-induced oral cancer cell proliferation via ERK1/2 inactivation. *Environ Toxicol*. (2017) 32:62–9. doi: 10.1002/tox.22212
19. Murugan AK, Munirajan AK, Tsuchida N. Ras oncogenes in oral cancer: the past 20 years. *Oral Oncol*. (2012) 48:383–92. doi: 10.1016/j.oraloncology.2011.12.006
20. Silverman S Jr. Demographics and occurrence of oral and pharyngeal cancers. The outcomes, the trends, the challenge. *J Am Dental Assoc*. (2001) 132 (Suppl.):7s–11s. doi: 10.14219/jada.archive.2001.0382
21. Yu GP, Mehta V, Branovan D, Huang Q, Hashibe M, Zhang ZF, et al. Improved survival among patients with base of tongue and tonsil cancer in the United States. *Cancer Causes Control*. (2012) 23:153–64. doi: 10.1007/s10552-011-9864-y
22. Chang ST, Wang DS, Wu CL, Shiah SG, Kuo YH, Chang CJ. Cytotoxicity of extractives from Taiwania cryptomerioides heartwood. *Phytochemistry*. (2000) 55:227–32. doi: 10.1016/S0031-9422(00)00275-2
23. Hsu HH, Kuo WW, Day CH, Shibu MA, Li SY, Chang SH, et al. Taiwanin E inhibits cell migration in human LoVo colon cancer cells by suppressing MMP-2/9 expression via p38 MAPK pathway. *Environ Toxicol*. (2017) 32:2021–31. doi: 10.1002/tox.22379
24. Chao CN, Lai CH, Badrealam KF, Lo JF, Shen CY, Chen CH, et al. CHIP attenuates lipopolysaccharide-induced cardiac hypertrophy and apoptosis by promoting NFATc3 proteasomal degradation. *J Cell Physiol*. (2019) 234:20128–138. doi: 10.1002/jcp.28614
25. Khan BF, Hamidullah, Dwivedi S, Konwar R, Zubair S, Owais M. Potential of bacterial culture media in biofabrication of metal nanoparticles and the therapeutic potential of the as-synthesized nanoparticles in conjunction with artemisinin against MDA-MB-231 breast cancer cells. *J Cell Physiol*. (2018) 234:6951–64. doi: 10.1002/jcp.27438
26. Zhang X, Bommareddy A, Chen W, Khalifa S, Kaushik RS, Fahmy H, et al. Sarcophine-diol, a chemopreventive agent of skin cancer, inhibits cell growth and induces apoptosis through extrinsic pathway in human epidermoid carcinoma A431 Cells. *Transl Oncol*. (2009) 2:21–30. doi: 10.1593/tlo.08190
27. He X, Maimaiti M, Jiao Y, Meng X, Li H. Sinomenine Induces G1-Phase Cell Cycle Arrest and apoptosis in malignant glioma cells via downregulation of sirtuin 1 and induction of p53 acetylation. *Technol Cancer Res Treat*. (2018) 17:1533034618770305. doi: 10.1177/1533034618770305
28. Roberts PJ, Der CJ. Targeting the Raf-MEK-ERK mitogen-activated protein kinase cascade for the treatment of cancer. *Oncogene*. (2007) 26:3291–310. doi: 10.1038/sj.onc.1210422
29. Wang Y, Wan D, Zhou R, Zhong W, Lu S, Chai Y. Geraniin inhibits migration and invasion of human osteosarcoma cancer cells through regulation of PI3K/Akt and ERK1/2 signaling pathways. *Anti-Cancer Drugs*. (2017) 28:959–66. doi: 10.1097/CAD.0000000000000535
30. Fong Y, Wu CY, Chang KF, Chen BH, Chou WJ, Tseng CH, et al. Dual roles of extracellular signal-regulated kinase (ERK) in quinoline compound BPIQ-induced apoptosis and anti-migration of human non-small cell lung cancer cells. *Cancer Cell Int*. (2017) 17:37. doi: 10.1186/s12935-017-0403-0
31. Kuo YH, Chiang EI, Chao CY, Rodriguez RL, Chou PY, Tsai SY, et al. Dual inhibition of key proliferation signaling pathways in triple-negative breast cancer cells by a novel derivative of Taiwanin A. *Mol Cancer Therapeutics*. (2017) 16:480–93. doi: 10.1158/1535-7163.MCT-16-0011

Conflict of Interest: The authors declare that the research was conducted in the absence of any commercial or financial relationships that could be construed as a potential conflict of interest.

The handling Editor declared a shared affiliation, though no other collaboration, with several of the authors C-YH and Y-HC.

frontiers in Oncology

ORIGINAL RESEARCH
published: 20 December 2019
doi: 10.3389/fonc.2019.01450

SIX1 Activates STAT3 Signaling to Promote the Proliferation of Thyroid Carcinoma via EYA1

Deguang Kong[1], Anping Li[2], Yu Liu[3], Qiuxia Cui[4], Kun Wang[5], Dan Zhang[5], Jianing Tang[4], Yaying Du[5], Zhisu Liu[1], Gaosong Wu[4] and Kongming Wu[2]**

[1] Department of General Surgery, Zhongnan Hospital of Wuhan University, Wuhan, China, [2] Department of Medical Oncology, The Affiliated Cancer Hospital of Zhengzhou University and Henan Cancer Hospital, Zhengzhou, China, [3] Department of Geriatrics, Tongji Hospital of Tongji Medical College, Huazhong University of Science and Technology, Wuhan, China, [4] Department of Thyroid and Breast Surgery, Zhongnan Hospital of Wuhan University, Wuhan, China, [5] Department of Thyroid and Breast Surgery, Tongji Hospital of Tongji Medical College, Huazhong University of Science and Technology, Wuhan, China

As a critical member of the Retinal Determination Gene Network (RDGN), SIX1 has been regarded as a tumor promoter in various types of cancer. However, its role in papillary thyroid carcinoma (PTC) has never been investigated. In this study, thyroid carcinoma tissue microarray staining was employed to identify the expression patterns of SIX1 and its co-activator EYA1. Papillary thyroid cancer cell lines, BCPAP, and TPC-1 cells were used to investigate the potential mechanism of SIX1 *in vitro* and *in vivo*. Flow cytometry analysis, MTT assay, the growth curve assay, colony formation assay, EdU incorporation and xenograft assay were performed to demonstrate the role of SIX1 in the malignant change of PTC cells. Western blot and Real-time PCR were used to detect the interaction among the SIX1, EYA1, and STAT3 signaling. In comparison with normal tissue, high expressions of SIX1 and EYA1 were associated with a malignant tumor. Importantly, SIX1 strongly correlated with EYA1 in thyroid carcinoma tissue microarray. Functional assays indicated SIX1 increased EYA1 expression by stabilizing EYA1 at the post-transcriptional level. Besides, SIX1 promoted the proliferation and invasion of thyroid carcinoma via activation of STAT3 signaling and its downstream targets in an EYA1-dependent manner. SIX1 can integrate with EYA1 to contribute to PTC development via activation of the classical STAT3 signaling. These data suggested targeting the abnormal activation of the SIX1/EYA1 complex may represent a novel therapeutic strategy for advanced PTC patients.

Keywords: SIX1, EYA1, STAT3 signal, thyroid papillary carcinoma, tumor growth

OPEN ACCESS

Edited by:
Cheng-Chia Yu,
Chung Shan Medical University, Taiwan

Reviewed by:
Yan Wang,
Capital Medical University, China
Chia-Hwa Lee,
Taipei Medical University, Taiwan

****Correspondence:***
Gaosong Wu
wugaosongtj@163.com
Kongming Wu
wukm_lab@163.com

Specialty section:
This article was submitted to Head and Neck Cancer, a section of the journal Frontiers in Oncology

Received: *30 April 2019*
Accepted: *04 December 2019*
Published: *20 December 2019*

Citation:
Kong D, Li A, Liu Y, Cui Q, Wang K, Zhang D, Tang J, Du Y, Liu Z, Wu G and Wu K (2019) SIX1 Activates STAT3 Signaling to Promote the Proliferation of Thyroid Carcinoma via EYA1. Front. Oncol. 9:1450. doi: 10.3389/fonc.2019.01450

INTRODUCTION

The incidence of thyroid cancer is rapidly increasing in recent two decades, and it has become the most common endocrine malignancy worldwide (1, 2). As the predominant pathological type of thyroid carcinoma, papillary thyroid carcinoma (PTC) accounts for more than 80% of the total (3). For most of PTC patients, conventional surgical thyroidectomy with radioactive iodine ablation and thyrotropin hormone-suppressive levothyroxine can obtain a satisfactory outcome (4). However, about 10% of cases suffer from a locally advanced or metastatic disease at diagnosis, which

are the most frequent causes of thyroid cancer-related death (5). Understanding the molecular basis of thyroid cancer is essential for developing effective strategies for advanced PTC patients (6).

The development of therapeutic agents that target tumor driver genes is the fundament for precision medicine (7). Exciting discoveries like the genetic duet of *BRAF* ^{V600E} and *RAS* mutations have led to significant progress in targeted therapies. Several *BRAF* tyrosine kinase inhibitors are either approved or undergoing investigation for patients with malignancies carrying *BRAF* mutations (8). However, the complexity in molecular subtypes of PTCs is still a challenge in exploring novel biomarker for guiding personal treatment in advanced stage (9). Meanwhile, alterations of critical signaling pathways in thyroid development like MAPK and PI3K-AKT can initiate tumorigenesis and promote tumor metastasis (10). Targeting the aberrant expression of development related genes or signaling may provide an opportunity for the molecular-based treatment of thyroid cancer.

In this respect, the *retinal determination gene network* (RDGN) family is required for organismal development in mammalian (11). This regulatory network mainly consists of *dachshund* (*dac*/Dach), the Six family transcription factor *sine oculis* (*so*/Six) and a tyrosine phosphatase *eyes absent* (*eya*/Eya). The balance of Dach/Eya/Six network governs the tissue differentiation (11). Recently, the abnormal activation SIX1 and EYA family have been proved to be involved in the development of multiple cancers. SIX1 promoted malignant transformation of mammary epithelial cells, including increased proliferation and anchorage independent growth by activating cyclin A1 (12). Via activation of TGF-β and MAPK signal, SIX1 enhanced the accumulation of cancer stem cells (CSCs) as well as induced epithelial-mesenchymal transition (EMT), and even switched the role of TGF-β/SMAD signal from tumor suppressors to oncogenic proteins in breast cancer (13–16). SIX1 can inhibit p53 by upregulating microRNA-27a-3p and downregulating ribosomal protein L26 (RPL26) to diminish the p53-mediated tumor suppression across different cancer types (7). Most recent study found the microRNA-548a-3p/SIX1 axis strongly linked aerobic glycolysis to carcinogenesis (17). SIX1 and EYA can integrate with other signal pathways to modulate the apoptosis, cell proliferation and tumor growth (18). To date, the profiles of SIX1 and EYA1 have been independently identified as a prognostic biomarker in breast cancer (13, 19). However, the functional relationship of SIX1 and EYA1 in thyroid cancer remains to be discovered.

Abnormal re-activation of embryological genes can trigger the tumorigenesis. A previous study has indicated that the Eya1 and Six1 were required for the morphogenesis of mammalian thyroid (20). Given these observations, the role of SIX1 and EYA1 in tumorigenesis and progression of PTC deserves further investigation. In this study, we explored the role of SIX1 in PTC through *in vitro* and *in vivo* experiments, which implicated SIX1 coordinated with EYA1 to drive neoplastic growth and invasion via activation of the classical STAT3 signaling.

MATERIALS AND METHODS

PTC Tissue Microarray and Immunohistochemistry

Commercially available tissue microarray (TMA) slides (TH8010 and TH802a, US Biomax, Inc.) were purchased for immunohistochemistry (IHC) analysis. Specific primary antibodies against SIX1 (Sigma, USA) and EYA1 (Proteintech, China) were used for IHC with a 2-step protocol (21). Whole slide image capture was performed on the EVOS auto cell image system (Life technology, USA). For semi-quantitative evaluation of protein level in tissue, the staining intensity was graded as previously described (22). The immunohistochemical score were assessed by two experienced pathologists without knowledge of patients' characteristics. Scores were calculated on intensity and percentage of positive staining tumor cell nuclei or cytoplasm in the whole tissue stains were evaluated according to Fromowitz Standard. Briefly, the staining intensity was graded as follows: no staining, 0; weakly positive, 1; moderately positive, 2; and strongly positive, 3. The percentage of positive cells was into four grades: 0–25% staining, 1; 26–50% staining, 2; 51–75% staining, 3; and 76–100% staining, 4. The multiplication of the intensity and percentage scores was used to calculate the final staining score. For quantification, all stains were assessed at 200× magnifications and at least three fields from each core were counted.

Cells Culture and Transfection

Human papillary thyroid cancer cell lines BCPAP, NPA and TPC-1 were provided by Dr. Du (Tongji Hospital of Tongji Medical College) and cultured in recommended condition. Cell line authenticity was confirmed by Short Tandem Repeat (STR) DNA profiling (the STR profiles were shown in **Supplementary Materials**). All experiments were performed using cell lines from passage 6 to 25. Cells were seeded at 50% confluence in 6 cm plate on the day before transduction. HEK 293T cells were transfected with pLV vector or pLV-SIX1 expression plasmid with package plasmids by Lipofectamine™ 2000 (Invitrogen, Carlsbad CA, USA). The supernatant was collected and polybrene (1:1,000) was added into the supernatant. The mixed supernatant was applied to recipient cells for infection. The expression of SIX1 was verified by quantitative reverse transcription-PCR (qRT-PCR) and Western blot. For small interfering RNA (siRNA)-mediated downregulation of EYA1, BCPAP-Vector and BCPAP-SIX1 cells were seeded in 6-well plates and transfected with siRNA or scramble control (Ribobio Company, Guangzhou, China) duplexes using Lipofectamine™ 2000 (Invitrogen, Carlsbad CA, USA). EYA1 siRNA: (sense) 5′-CAGGAAAUAAUUCACUCACAAdTdT-3′; (antisense) 5′-UUGUGAGUGAAUUAUUUCCUGdTdT- 3′.

Western Blot Analysis

Cell and tissue lysates were extracted using ice-cold RIPA buffer and measured using a bicinchoninic acid (BCA) protein assay kit (Promoter, China). Proteins were resolved on 10% SDS-polyacrylamide gels and transferred to PVDF membranes. The antibodies used in Western blot were as

follows: SIX1, EYA1, C-MYC (Santa Cruz, USA), STAT3 (Cell Signaling Technology, USA), p-STAT3 (Tyr705) (Cell Signaling Technology, USA), BCL-XL (Cell Signaling Technology, USA), Caspase 3 (Proteintech, China), Cleaved PARP1 (Ruiying Bio, China), Cleaved Caspase 9 (Ruiying Bio, China), β-tublin (Cell Signaling Technology, USA), GAPDH (Cell Signaling Technology, USA) and VINCULIN (Sigma, USA).

Quantitative Reverse Transcription-PCR (qRT-PCR)

RNA was prepared from PTC cells with the TRIzol reagent (Invitrogen, USA). cDNA was reversed from 1 μg total RNA using a reverse transcription kit (TOYOBO, Japan). RT-qPCR was performed with the SYBR® Green Real-time PCR Master Mix Kit (TOYOBO, Japan). Gene expression was normalized to GAPDH. The primer sequences for real-time RT-PCR were as follows: SIX1: (forward) 5′-ACAAGAACGAGAGCG TACTCA-3′, (reverse) 5′-CTCCACGTAATGCGCCTTCA-3′; EYA1: (forward) 5′-GTTCATCTGGGACTTGGA-3′, (reverse) 5′-GCTTAGGTCCTGTCCGTT-3′; GAPDH: (forward) 5′-CAATGACCCCTTCATTGACC-3′, (reverse) 5′-GATCTCGC TCCTGGAAGATG-3′.

Cell Proliferation Assays

For MTT assay, 2,000 cells were seeded into 96-well plates and analyzed by adding MTT (tetrazolium bromide, 5 mg/mL, GE Healthcare) as previously described (22). To measure the growth curve, 2.5×10^3 cells were seeded in 24-well culture plates and the numbers of viable cells were serially counted for 6–7 days. Colony formation assay was performed as previously described (23). Two weeks later, cells were fixed with 4% paraformaldehyde and stained by 0.5% crystal violet for visualization and counting on the plate.

Cell-Cycle Analysis

About 3×10^5 cells were seeded into a 6 cm Petri dish. After 24 h incubation, the cells were collected and fixed with 75% cold ethanol at −20°C overnight. DNA was incubated with 200 μL RNase A (1 mg/mL) and 500 μL propidium iodide (PI, 100 μg/mL) for 30 min at room temperature in the dark and analyzed by using the FACSort flow cytometer (Becton, Dickinson Company, USA). The data were analyzed with ModFit LT V2.0 software (Becton, Dickinson Company, USA).

Transwell Migration and Invasion Assay

Transwell chambers (pore size 8.0 μm) (Corning Inc., USA) were either uncoated (migration assay) or coated (invasion assay) with Matrigel as previously described (23). All experiments were conducted in triplicate.

Annexin V-FITC/PI Assay

The apoptosis was determined by the Annexin V-FITC/PI apoptosis detection kit (BD Biosciences, USA). Briefly, cells were treated with 200 μM H_2O_2 (Sigma, USA) for 24 h. The cells were collected, and then resuspended in 200 μL of binding buffer. After incubation of Annexin V-FITC and PI for 15 min at room temperature, 300 μL binding buffer was added to the cells and the results were analyzed by flow cytometry (Beckman-Coulter Inc., USA). The experiment was repeated in triplicate.

Ethynyl-20-deoxyuridine (EdU) Incorporation Assay

EdU incorporation assay was performed with EdU assay kit (Ribobio, China). Briefly, 1×10^3 cells per well were culture in 96-well plates for 48 h, and then 50 μM of EdU was added to each well and cultured for additional 2 h. The cells were fixed with 4% formaldehyde for 15 min and treated with 0.5% Triton X-100 for 20 min. After washing with PBS, 100 μl of 1 × Apollo reaction cocktail was added and incubated for 30 min. After staining with 100 μl of Hoechst 33342 for 30 min, the cells were visualized under EVOS cell image system. The results were analyzed by Image-Pro Plus 6.0 software (Media Cybernetics, USA). All experiments were done in triplicate and three independent repeating experiments were performed.

Immunofluorescent Labeling of SIX1 and EYA1

Cells were seeded in a 24-well plate (5×10^4cells/well) and cultured for 48 h, then fixed with 4% paraformaldehyde. Next, cells were permeabilized with 0.1% Triton X-100 and blocked using 5% goat serum for 30 min. Cells were further incubated overnight with primary antibodies against SIX1 (anti-mouse, 1:100, Santa Cruz, USA), EYA1 (anti-rabbit, 1:100, Proteintech, China). Next day, cells were incubated with either Alexa Fluor 594 or Alexa Fluor 488 for 1 h. Nuclei were visualized with DAPI stain. The stained cells were examined with EVOS cell image system.

Tumor Formation Assay

Five- to 6-week-old female NOD/SCID mice were purchased from Beijing HFK Bioscience Limited Company and maintained under the Specific Pathogen-Free (SPF) conditions at Laboratory Animal Centre. All the protocols were reviewed and approved by the Institutional Ethics Committee and performed in accordance with national guidelines. All mice were randomly divided into two groups: TPC1-shControl ($n = 20$) and TPC1-shSIX1 ($n = 20$). Cells were counted and serially diluted in 100 ml of 1:1 PBS/Matrigel, and injected subcutaneously. The mice were monitored every 3 days. At 3 weeks post-injection, all mice were euthanized and analyzed for tumor formation. Tumors were collected for further Western Blot analysis.

Statistical Analysis

GraphPad Prism 6.0 software was used for the statistical analyses. The IHC scores were tested whether the data matched normal distribution or not. If it was, then the difference between groups were conducted by using parametric statistics (*Student t*-test), otherwise performing non-parametric statistics (*Mann-Whitney* test). The correlations between clinicopathological and immunohistochemical variables were calculated according to *Person* χ^2-test. Cell culture experiments differences between the groups were evaluated by the *Student t*-test, including EdU assays, MTT activity, growth curve assays, colony formation

assay, Transwell migration, and invasion assays, Annexin V-FITC/PI assays, PCR and western blot assays. All data were expressed as mean ± standard error. $P < 0.05$ were considered statistically significant.

RESULTS

Both SIX1 and EYA1 Were Increased in PTC Patients

To identify the expression pattern of SIX1 and EYA1 in human thyroid tissue as well as tumor, we performed IHC analysis by using two tissue microarrays (TH8010 and TH802a). After excluding the duplicated reports ($n = 6$) and detached sample ($n = 9$), two tissue microarrays contained 145 samples, including normal thyroid tissue ($n = 10$), atypical adenoma ($n = 1$), oncocytoma ($n = 4$), colloid adenoma ($n = 15$), fetal adenoma ($n = 10$), follicular adenoma ($n = 10$), follicular carcinoma (FTC, $n = 18$), medullary carcinoma (MTC, $n = 5$), papillary carcinoma (PTC, $n = 66$), and anaplastic carcinoma (ATC, $n = 6$). The IHC score for each type was shown in **Figure 1A**. In comparison with normal tissue, SIX1 and EYA1 kept low expression in benign tumor and no statistic difference was found for either SIX1 or EYA1 between groups. However, a significant increase in SIX1 and EYA1 was detected in malignant tumor, including FTC ($p = 0.011$, $p = 0.038$; respectively), MTC ($p = 0.006$, $p = 0.043$; respectively), PTC ($p < 0.001$, $p < 0.001$; respectively) and ATC samples ($p = 0.002$, $p < 0.001$; respectively) (**Figure 1A**). The representative images of IHC staining for normal and cancerous tissue were shown in **Figure 1B**. Intriguingly, SIX1 was tightly linked to EYA1 in malignant tumor. The analysis from Spearman correlation based on all malignant sample in these tissue microarrays indicated that SIX1 had a strongly positive relationship with EYA1 (**Figure 1C**). BRAF mutation is the most common mutation in PTC (8). To test whether there was relationship between SIX1/EYA1 and $BRAF^{V600E}$ mutation, the GEO database (GSE54958) was applied to analyze. There was no difference in the expression of SIX1/EYA1 and $BRAF^{V600E}$ mutation (Data not shown).

Since PTC is the most common type of thyroid carcinoma and also occupied the majority of the tissue microarrays in this study, we next examined the association of SIX1 and EYA1

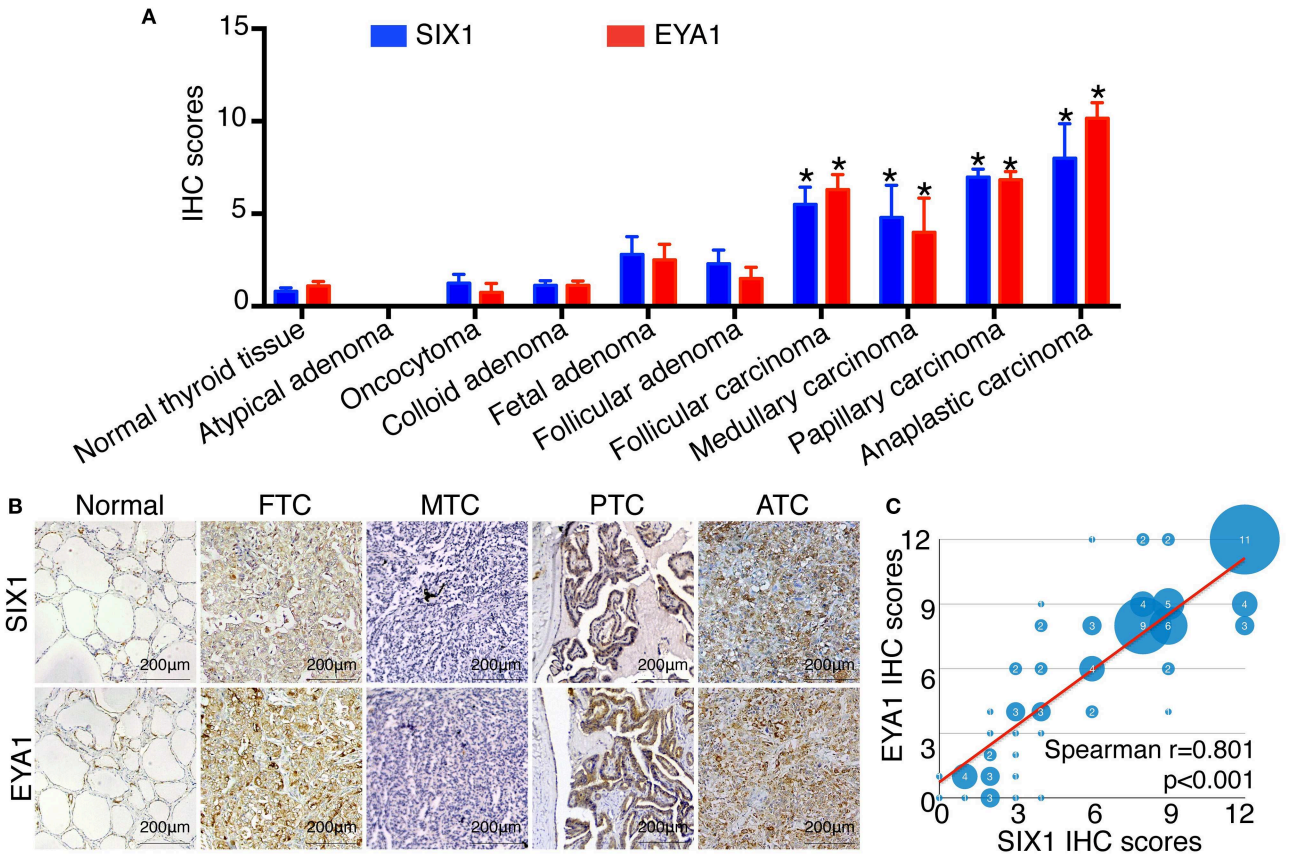

FIGURE 1 | The expression of SIX1 and EYA1 in PTC tissues. The semi quantitative results displayed as median ± stand error **(A)**. The relative expression of SIX1 and EYA1 in thyroid carcinoma tissue microarray, including normal thyroid tissue, atypical adenoma, oncocytoma, colloid adenoma, fetal adenoma, follicular adenoma, follicular carcinoma, medullary carcinoma, papillary carcinoma, and anaplastic carcinoma, *represents a statistical difference was found compared with normal tissue. **(B)** Representative immunohistochemistry images of SIX1 and EYA1 expression in normal thyroid, papillary thyroid carcinoma (PTC), follicular thyroid carcinoma (FTC), medullary thyroid carcinoma (MTC), and anaplastic thyroid cancer (ATC). **(C)** The positive relationship between SIX1 and EYA1 in thyroid malignant carcinoma.

TABLE 1 | Association between SIX1/EYA1 expression and clinicopathologic factors in papillary carcinoma (TH8010 + TH802a).

Characteristics	SIX1 expression			EYA1 expression		
	Low (≤6)	High (>6)	*p*	Low (≤6)	High (>6)	*p*
Sex			0.481*			0.177*
Male	4	8		3	9	
Female	24	30		25	29	
Age (y)	38.96 ± 2.429	49.63 ± 2.662	0.006†	39.5 ± 2.434	49.24 ± 2.7	0.012†
Tumor size			0.347*			0.145*
≤4 cm (T1 + T2)	12	12		13	11	
>4 cm (T3 + T4)	16	26		15	27	
Lymph node metastasis			0.043*			0.030*
Absent	23	23		24	22	
Present	4	14		4	14	
Stage			0.015*			0.015*
I + II	24	22		24	22	
III + IVA	4	16		4	16	

**Person chi-square test.*
† Independent-sample t-test.

expression with clinicopathological parameters. Based on the semi-quantitative criteria, we defined IHC score over 6 (>6) was higher and scores under 6 (≤6) was lower expression. We found that the levels of SIX1 and EYA1 expression were significantly associated with age, lymph node metastasis (two sample missed this information, tissue ID: Etg030430 and Etg030007) and clinical stage, but not tumor size (**Table 1**). Based on these data, high expressions of SIX1 and EYA1 are closely correlated with thyroid malignant tumor. SIX1 may cooperate with EYA1 and play a key role in lymph node metastasis via a BRAF-independent manner.

SIX1 Increased the Proportion of Cells in S Phase in PTC Cell Lines

Since SIX1 is a DNA-specific transcriptional factor, whereas EYA1 basically acts as a co-factor to increase SIX1-dependent function (11), we mainly focused on the functional role of SIX1 in thyroid cancer for first. The base line expressions of SIX1 were detected by western blot in PTC cell lines, including BCPAP, TPC-1, and NPA, with HEK 293T cell as a positive control. The results showed that SIX1 were barely expressed in BCPAP cells, whereas highly enriched in TPC-1 cells (**Figure 2A**). The next step was establishing the thyroid cell lines with either overexpression or knockdown of SIX1 by employing lentivirus-mediated gene transfer system. BCPAP cells stably overexpressing SIX1 were successfully transduced by pLV-SIX1 (BCPAP-SIX1) and pLV empty vector (BCPAP-Vector). Meanwhile, lentivirus shRNA expression vector for SIX1 or scramble control were transduced into TPC-1 cells (**Figure 2B**).

To assess the role of SIX1 in cell cycle regulation, propidium iodide staining and flow cytometry were performed. Overexpression of SIX1 significantly decreased the percentage of cells in the G0/G1 phase (78.47 ± 2.37% vs. 67.31 ± 1.56%, $p = 0.017$) and increased the subpopulation in the S phases (16.33 ± 2.44% vs. 27.68 ± 1.72%, $p = 0.019$) in BCPAP cells (**Figures 2C,D**). Conversely, knockdown SIX1 in TPC-1 cells induced a significant increase of G0/G1 phase (53.73 ± 0.87% vs. 64.79 ± 1.46%, $p = 0.003$) and a decrease in the S-phase population (34.42 ± 0.61% vs. 22.77 ± 1.32%, $p = 0.001$) compared with control group (**Figures 3A,B**). To further evaluate the effect of SIX1 in cell cycle regulation, EdU incorporation assay was examined. In accordance with results of flow cytometry, the proportion of EdU positive cells was increased by 2.84-folds induced by SIX1 overexpressing in BCPAP cells (**Figure 2E**). And the number of EdU positive cells in TPC-1-shSIX1 group was reduced by 40% in comparison with TPC1-shControl (**Figure 3C**). Taken together, these data demonstrate that SIX1 promoted cell cycle progression in thyroid cancer cells.

SIX1 Overexpression Induced Proliferation, Cell Migration, and Invasion in PTC

To examine the effect of SIX1 on PTC cellular proliferation, MTT assays, cell growth curve, and colony formation assays were performed to assess the proliferative ability. MTT assays showed the tumor cell growth rate significantly increased after ectopic expression of SIX1 (**Figure 2F**) and decreased after silencing the endogenous SIX1 expression (**Figure 3D**), which were in accord with the findings from cell growth curve (**Figures 2G, 3E**). Transfecting the exogenous *SIX1* gene into BCPAP cells can increase both colony number and size (**Figure 2H**), and SIX1 knockdown otherwise resulted in approximately 50% colony growth inhibition in the TPC-1 cells (**Figure 3F**). Furthermore, cell migration and invasion were significantly increased in BCPAP cells with SIX1 overexpression (**Figure 2I**) and decreased by half in TPC-1 cells after knockdown of SIX1 (**Figure 3G**). These data suggested that SIX1 induced the oncogenic properties of PTC.

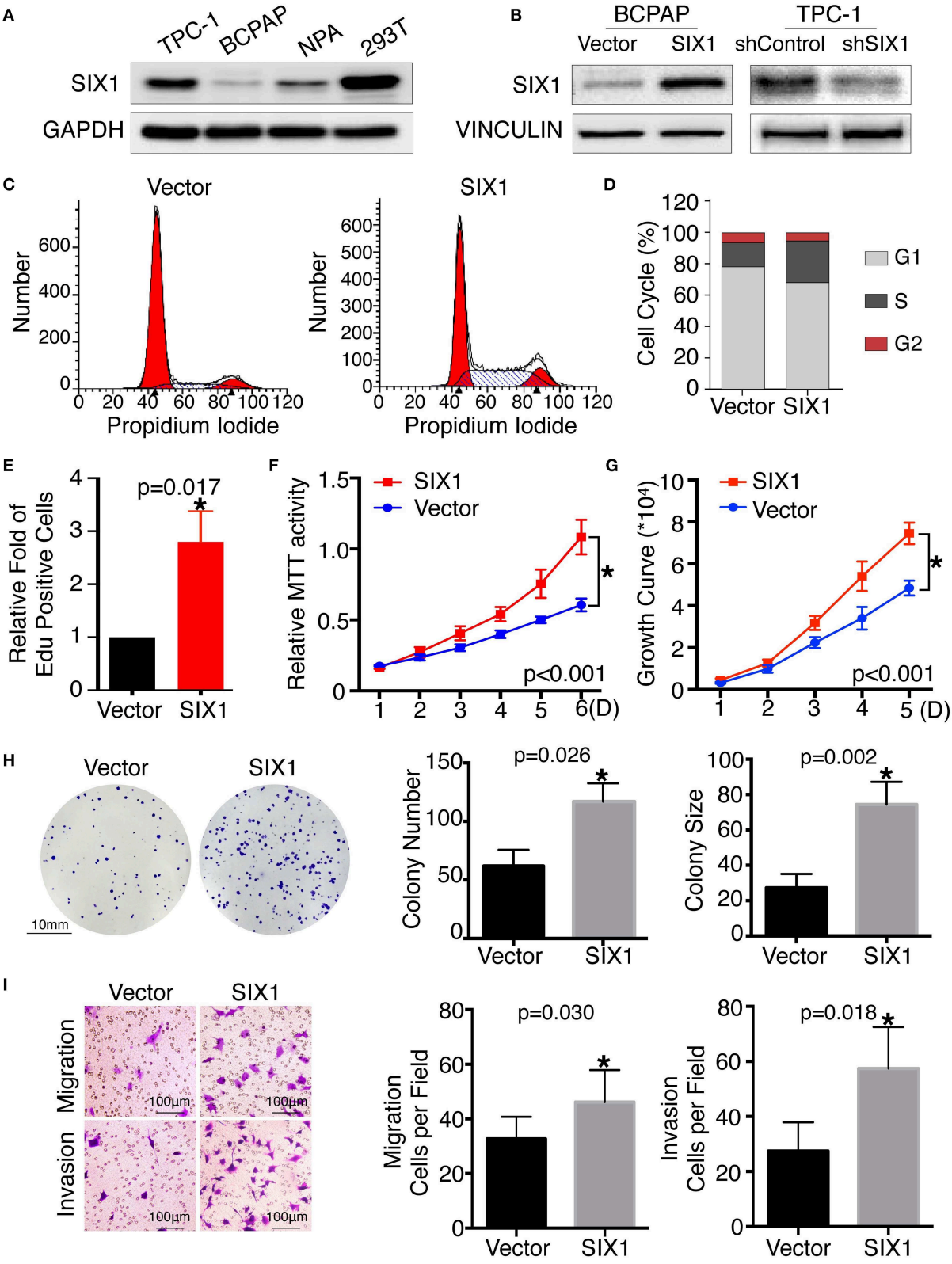

FIGURE 2 | Ectopic expression of SIX1 increased the proportion of cells in S phase and promoted proliferation, migration and invasion in BCPAP cell lines. Protein abundance of SIX1 in PTC cell lines by western blot analysis **(A)**. Western blot analysis confirmed the efficiency of ectopic expressing SIX1 in BCPAP cells or silencing SIX1 in TPC-1 cells **(B)**. Representative images of cell cycle plot **(C)** and quantitative results ($n = 3$) **(D)**. Quantitative results of EdU staining of cells with SIX1

(Continued)

FIGURE 2 | overexpression ($n = 3$) **(E)**. MTT assays of BCPAP cells with ectopic expression of SIX1 ($n = 5$) **(F)**. Growth curve assays of BCPAP cells with ectopic expression of SIX1 ($n = 5$) **(G)**. Representative images of colony formation assays of BCPAP cells with ectopic expression of SIX1 and quantitative results ($n = 3$) **(H)**. The representative images of migration and invasion assay in BCPAP cells with SIX1 overexpression and quantitative analysis ($n = 3$) **(I)**. *$p < 0.05$.

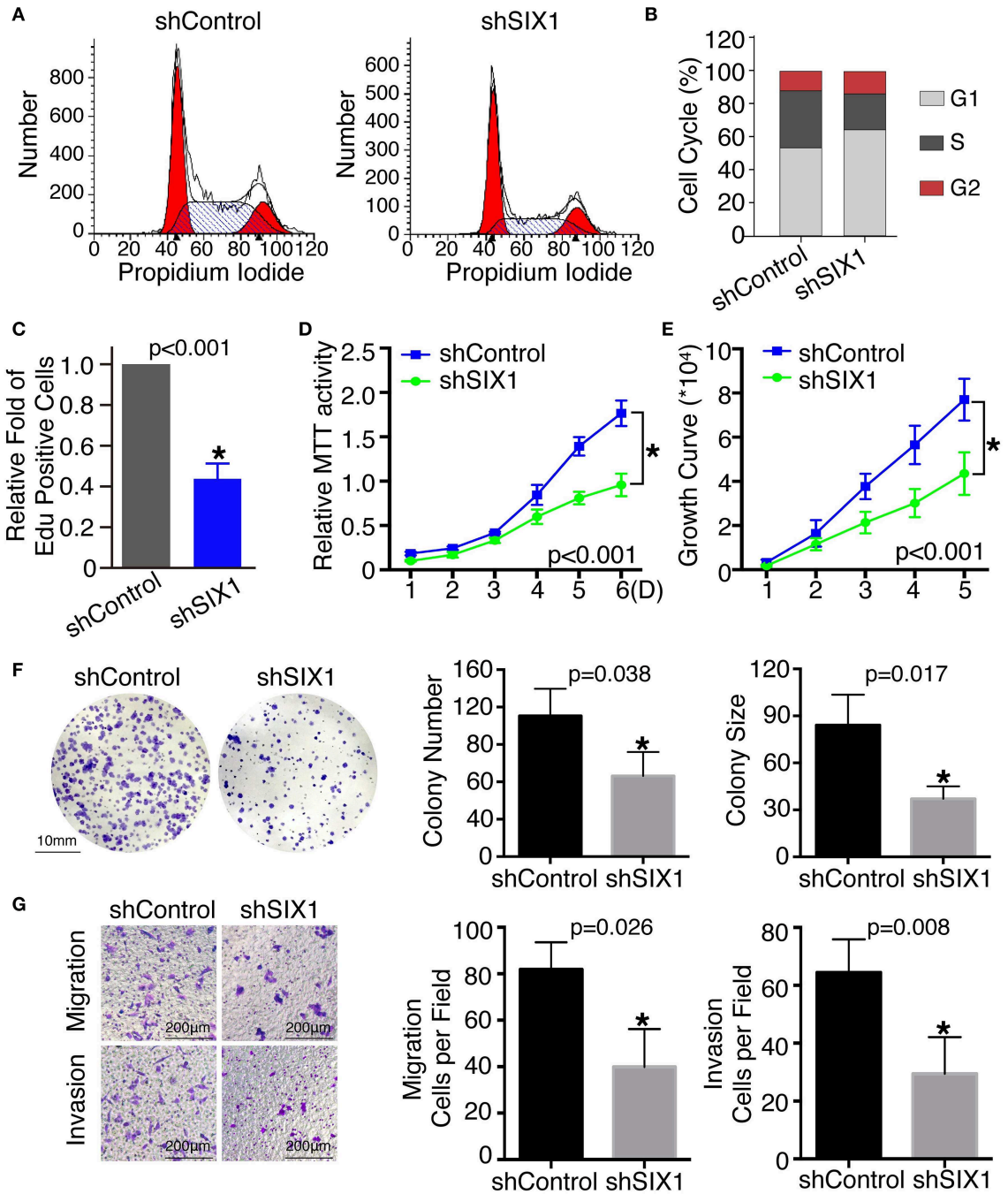

FIGURE 3 | Knockdown SIX1 decreased the proportion of cells in S phase and inhibited proliferation, migration, and invasion in TPC-1 cell lines. Representative images of cell cycle plot **(A)** and quantitative results ($n = 3$) **(B)**. Quantitative results of EdU staining of cells with SIX1 knockdown ($n = 3$) **(C)**. MTT assays of TPC-1 cells after silencing SIX1 ($n = 5$) **(D)**. Growth curve assays of TPC-1 cells after silencing SIX1 ($n = 5$) **(E)**. Representative images of colony formation assays of TPC-1 cells after silencing SIX1 and quantitative results ($n = 3$) **(F)**. The representative images of migration and invasion assay in TPC-1 cells after silencing SIX1 and quantitative analysis ($n = 3$) **(G)**. *$p < 0.05$.

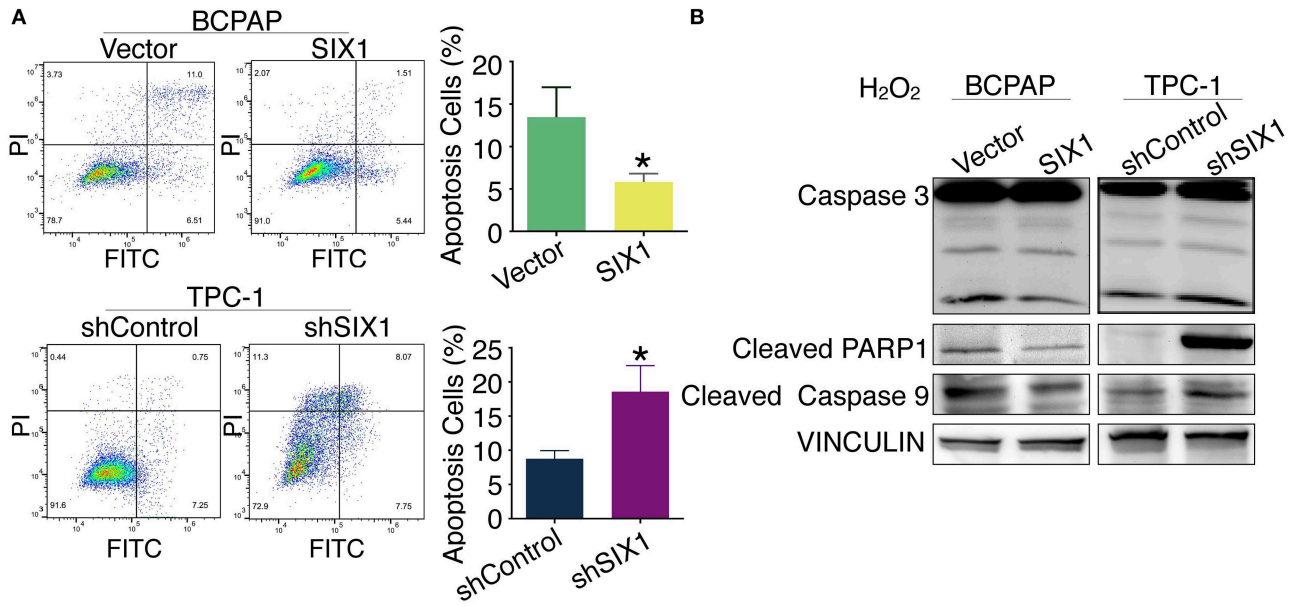

FIGURE 4 | SIX1 attenuated H_2O_2-induced apoptosis in PTC cell lines. PTC cell lines were incubated for 24 h, and then exposed to 200 μM H_2O_2 for 24 h. Annexin V-FITC/PI assay was used to evaluate the apoptosis. Representative image of apoptosis assay and quantitative analysis ($n = 3$) **(A)**. The protein expression of caspase 3, cleaved PARP1 and cleaved caspase 9 in PTC cell lines was detected by Western blotting **(B)**. *$p < 0.05$.

SIX1 Protected PTC Cells Against H_2O_2-Induced Apoptosis

Increased proliferation and reduced apoptosis are the fundamental feature of cancer cells. Next, we evaluated whether SIX1 protected PTC cell lines from apoptosis assessed by Annexin V-FITC/PI staining. Flow cytometric analysis results indicated that H_2O_2 induced apoptosis in PTC cell lines. The proportion of apoptotic cells in BCPAP-SIX1 group was significantly reduced from 13.46 to 5.82% in comparison with BCPAP-Vector ($p = 0.022$) (**Figure 4A**). The proportion of apoptotic cells in TPC1-shSIX1 group was increased significantly from 8.75 to 18.56% in comparison with TPC1-shControl ($p = 0.0133$) (**Figure 4A**). The protein expression levels of caspase 3, cleaved PARP1 and cleaved caspase 9 were detected by Western blotting. The results showed that SIX1 significantly attenuated H_2O_2-induced upregulation of cleaved Caspase 3, cleaved PARP1 and cleaved Caspase 9 protein expression (**Figure 4B**).

STAT3 Signal Is Responsible for the SIX1-Induced Proliferation of PTC Cells in an EYA1-Dependent Manner

Although there is a consensus that EYA functions as a co-activator in SIX1-associated malignant properties, little is known about whether and how SIX1 modulates EYA1 expression. Immunofluorescence assay showed the positive relationship and co-localization of SIX1 and EYA1 (**Figure 5A**). Moreover, we carried out qRT-PCR to examine the mRNA change. However, the mRNA of *EYA1* did not change when *SIX1* was overexpressed in BCPAP or *SIX1* was knocked down in TPC-1 cells (**Figure 5B**), indicating that SIX1 induces the protein abundance of EYA1 at post-transcriptional level, rather than directly involves in the transcriptional regulation of EYA1 mRNA.

Cell cycle proteins regulated by SIX1 might be responsible for the proliferation in PTC. To address the underlying mechanisms, cell cycle elements were screened by western blot. SIX1 significantly promoted the abundance of C-MYC (**Figure 5C**). Since C-MYC is the downstream target of STAT3 signaling and other group has reported SIX1 can induce p-STAT3 expression in human keratinocytes (24), we hypothesized that SIX1 might promote C-MYC abundance via activation of STAT3 signaling. Ectopic expression of SIX1 could significantly upregulate the expression of p-STAT3 (Try705) as well as its downstream target BCL-XL. As expected, knockdown SIX1 in TPC-1 cell showed the opposite (**Figure 5C**).

To further determine whether EYA1 was required for the SIX1-induced STAT3 signaling activation. siRNA was used to transiently knock down EYA1 in BCPAP-vector and BCPAP-SIX1 cells. Intriguingly, the upregulation of p-STAT3, C-MYC, and BCL-XL induced by SIX1 was abolished after silencing EYA1. Additionally, knocking down EYA1 in BCPAP-Vector cells diminished endogenous expression of STAT3 signal and its downstream targets (**Figure 5D**). We evaluated the effects of EYA1 knock-down in TPC-1 cells which had higher endogenous expression of SIX1. The expressions of SIX1, p-STAT3, C-MYC, and BCL-XL abundance were down regulated after silencing EYA1 by siRNA in TPC-1 cells (**Figure 5E**).

Next, we compared the functional significance of SIX1/EYA1 interaction. Both colony formation assay and MTT showed that the proliferation ability was significantly reduced when

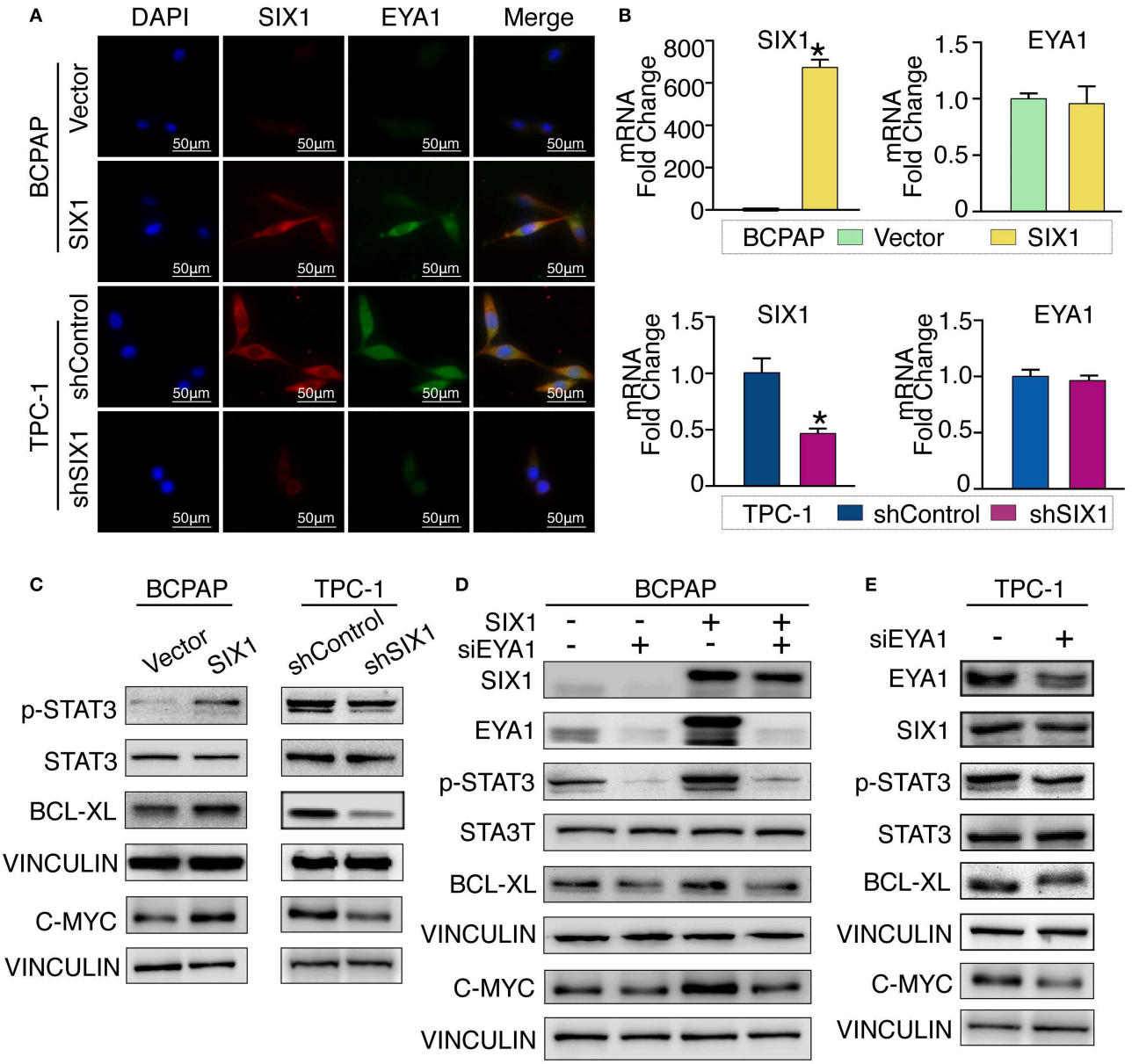

FIGURE 5 | SIX1 activated STAT3 signaling pathway to promote PTC cells proliferation via EYA1. Immunofluorescence show the co-localization of SIX1 (red) and EYA1 (green) **(A)**. The relative mRNA level of SIX1 and EYA1 in PTC cell lines with SIX1 overexpression or silencing **(B)**. Western blot analysis of indicated protein from PTC cells with SIX1 overexpression or silencing **(C)**. Western blot analysis of indicated protein from BCPAP cells with SIX1 and/or EYA1 silencing **(D)**. Western blot analysis of indicated protein from TPC-1 cells with EYA1 silencing **(E)**. $^*p < 0.05$.

EYA1 was knocked down in SIX1-overexpressing BCPAP cells (**Figures 6A,B,E**). In agreement, SIX1-induced DNA synthesis was inhibited by knock down EYA1, as evaluated by EdU incorporation assay (**Figures 6G,H**). On the other side, colony formation assay and MTT demonstrated that knockdown endogenous EYA1 can inhibit TPC-1 cell growth (**Figures 6C,D,F**). Together, these data suggest that the activation of STAT3 signaling induced by SIX1 is dependent on the presence of EYA1 in PTC cells.

Silencing SIX1 Suppressed Tumor Growth as Well as STAT3 Signal Activation *in vivo*

To test whether blocking the expression of SIX1 abolished the PTC cell proliferation *in vivo*, 2×10^6 TPC1-shControl or TPC1-shSIX1 cells were injected, respectively, into the subcutaneous fat of immunodeficient mice. Downregulation of the endogenous SIX1 by shRNA in TPC-1 cells not only showed a trend of slowing down the tumor associated weight loss (**Figure 7A**), but also significantly reduced the volume as well as the weight of

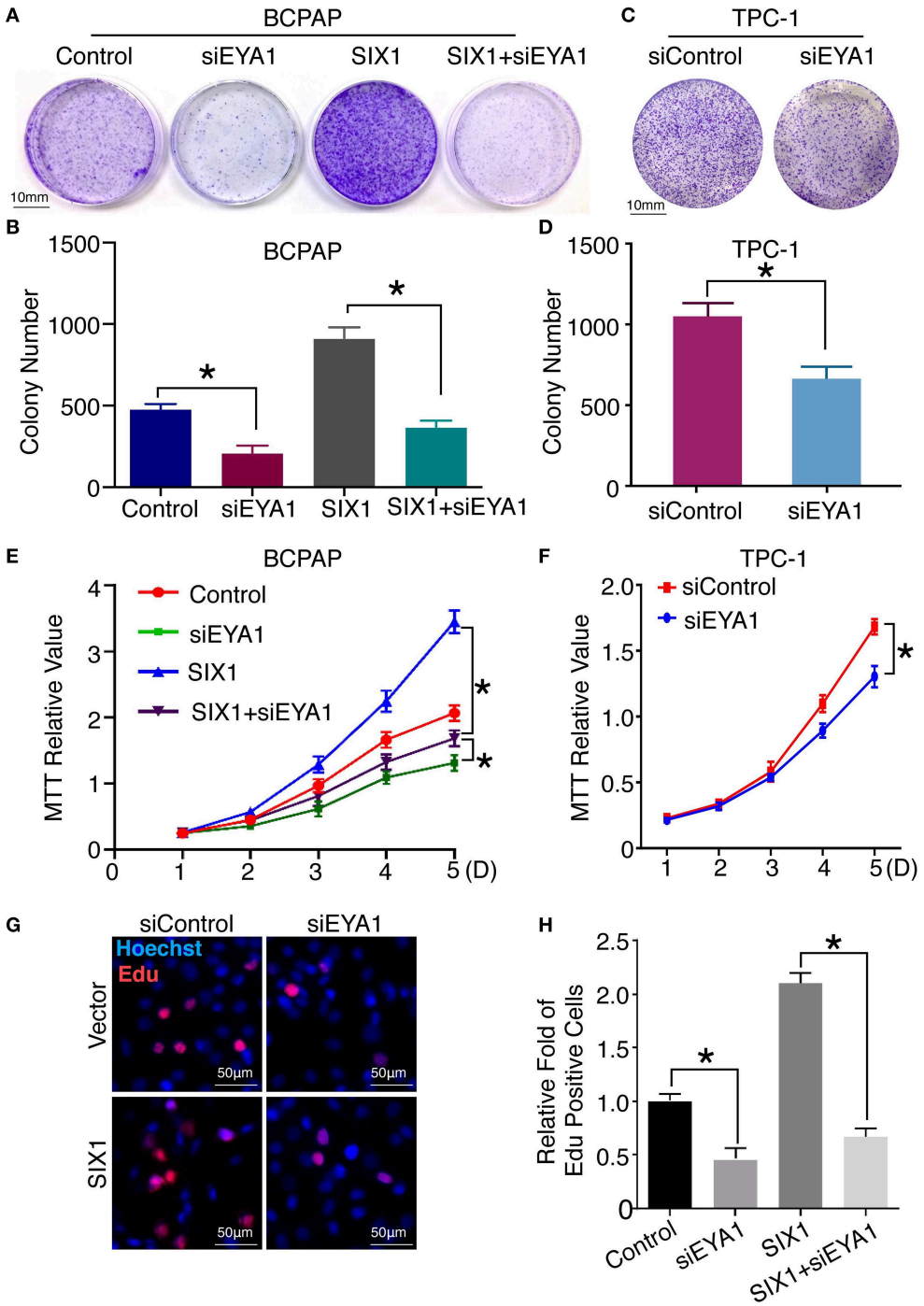

FIGURE 6 | Interaction of SIX1 and EYA1 determined PTC cells proliferation. Representative image of colony formation from BCPAP cells with SIX1 overexpression and/or siEYA1 **(A)** and quantitative analysis ($n = 3$) **(B)**. Representative image of colony formation from TPC-1 cells with siEYA1 **(C)** and quantitative analysis ($n = 3$) **(D)**. MTT assay of BCPAP cells with SIX1 overexpression and/or siEYA1 ($n = 5$) **(E)**. MTT assay of TPC-1 cells with siEYA1($n = 5$) **(F)**. Representative images of EdU assay of BCPAP cells with SIX1 overexpression and/or siEYA1 **(G)** and quantitative analysis ($n = 3$) **(H)**. *$p < 0.05$.

xenografted tumors (**Figures 7B–D**). At the time of sacrifice, xenograft tumors were harvested and examined by western blot. Consistent with these findings *in vitro,* the tumors in TPC1-shSIX1 group retained SIX1 lower-expression *in vivo* and the levels of EYA1, p-STAT3 (Try705) and C-MYC were significantly decreased compared with shControl group (**Figures 7E,F**). Taken together, these results highlight the potential for targeting SIX1 in the comprehensive therapy for PTC patients.

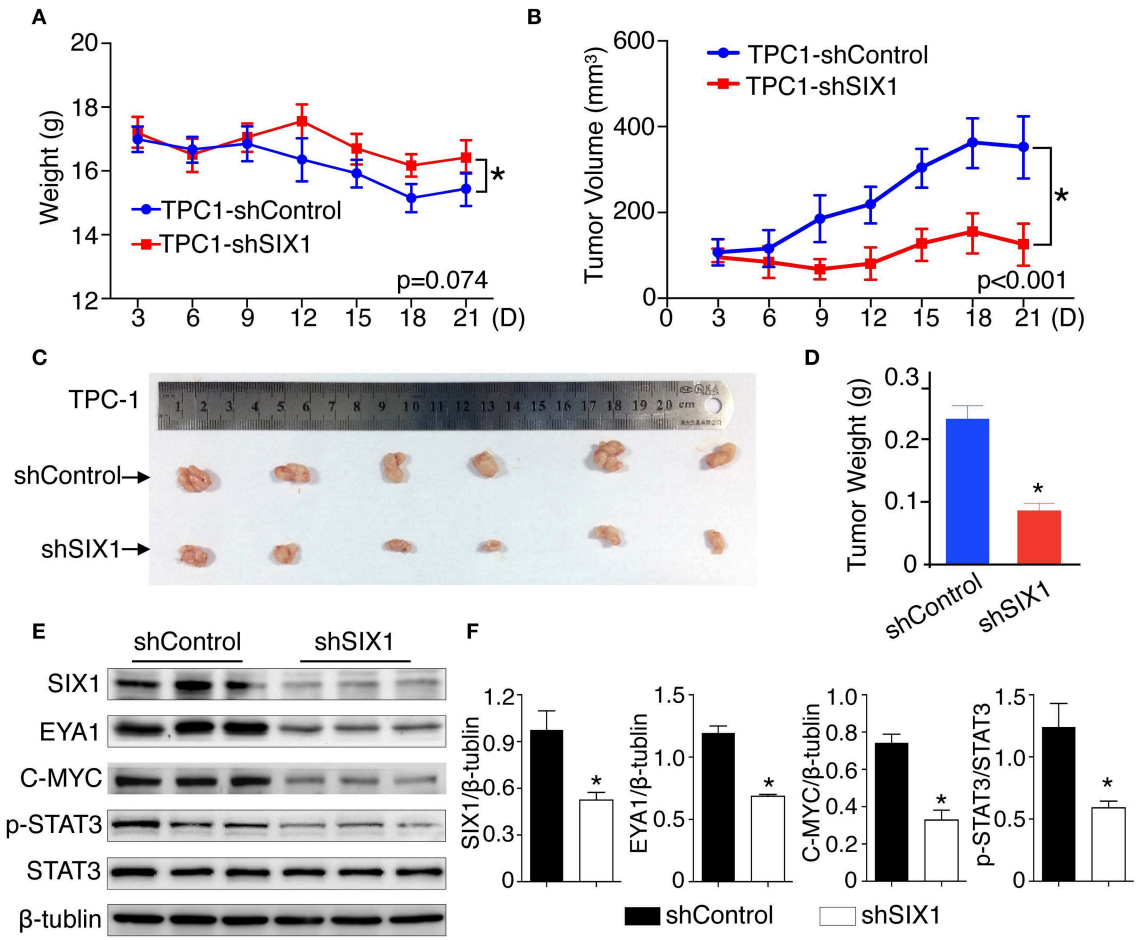

FIGURE 7 | Silencing SIX1 suppressed tumor growth as well as STAT3 signal *in vivo*. TPC-1 cells with SIX1 silencing or vector control were implanted into immunodeficiency mice, the body weight **(A)** and tumor volume **(B)** was monitored ($n = 20$). Representative tumor image **(C)** and quantitative analysis ($n = 20$) **(D)** were showed. Western blot analysis of total protein from tumor tissue **(E)** and relative quantitative analysis ($n = 3$) **(F)**. *$p < 0.05$.

DISCUSSION

Exciting outcome of molecular targeting therapy is driving the need for better understanding the tumor biological features of each patient (7). Recent evidence has linked RDGN family with the progression of various cancers, indicating it might be a potential therapeutic target for precision medicine (11–18, 25). In the present study, our results first showed that SIX1 protein elevated in thyroid malignant tumor. In papillary thyroid carcinoma, high expressions of SIX1 and EYA1 were associated with advanced age, lymph node metastasis and clinical stage. Functional assays suggested SIX1 not only enhanced PTC proliferation, but also provided significant protection against apoptosis, which relied on the activation of STAT3 signaling. The analysis of patients' samples indicated EYA1 was positively correlated with SIX1. Not only the ectopic expression of SIX1 increased EYA1, but also STAT3 signaling activation induced by SIX1 depended on EYA1.

Although Six1 had intrinsic transcriptional domain, its activation required Eya family to be the co-activator (26). Co-transfection of Six/*so* and Eya/*eya* induced a huge synergistic activation of the downstream targets, whereas Six or Eya alone showed a low level of transcription. Therefore, it generally recognized that Six1-Eya function as a transcriptional complex (11). However, the coordinated mechanism between SIX1 and EYAs in human is largely elusive. Current studies are mainly focused on the functional association between SIX1 and EYAs. It has been reported SIX1 bound to EYA by a single amphipathic helical structure, an essential part for SIX1-associated metastatic phenotypes (27). One significant finding in our study was that SIX1 induced EYA1 protein expression in PTC and modulated its abundance at the post-transcriptional level. Recent evidence indicated that cyclin-dependent kinase 6 (CDK6) bound to and promoted degradation of the EYA2 protein, and SIX1 partially stabilized EYA2 against CDK6 induced degradation (28), which is in support of our finding. Our results also showed EYA1 was necessary for STAT3 signaling activation as well as the cellular

proliferation induced by SIX1. Based on these data, it indicates SIX1 might stabilize the EYA1 protein rather than activate the gene transcription directly, suggesting a reciprocal regulation between SIX1 and EYA family.

Another intriguing finding is STAT3 signaling is involved in the regulation of SIX1 in PTC. This is consistent with a previous report demonstrating that SIX1 can increase the phosphorylation of STAT3 in HPV16-immortalized human keratinocytes (24). Given the role of STAT3 signaling in regulating cell proliferation, vascular formation and immune response associated with cancer progression, it is important to explore novel targets that inhibit the ectopic activation of STAT3 signaling (29). By activating pro-proliferative and pro-survival genes, including C-MYC and Cyclin D1, and anti-apoptotic BCL-2 or BCL-XL, STAT3 mediated tumorigenesis by protecting cells from apoptotic stress, and promoting cell-cycle progression and inflammation response in multiple cancers (30). STAT3 phosphorylated on Try705 in the carboxyl-terminal transactivation domain is regarded as the key to amplify STAT3 signal. In thyroid, STAT3 pathway was found to be involved in the onset and invasion of tumor (31). STAT3 interacted with the sonic hedgehog (SHH) pathway, which can predict the prognosis or guiding the personal therapy against PTC (32). Ekpe-Adewuy et al. revealed that growth factor receptor-alpha (PDGFRα) promoted EMT of PTC cells via provoking STAT3 signal pathway (33). Our study found SIX1 activated STAT3 signaling in an EYA1-dependent manner by increased the level of phospho-Try705. *In vitro* experiments indicated that SIX1 increased the phosphorylation of STAT3, leading to an increasing of C-MYC and BCL-XL to promote cell proliferation and anti-apoptosis. In addition, the activation of STAT3 signaling induced by SIX1 relied on EYA1. Silencing EYA1 expression abolished the SIX1-medicated STAT3 signaling activation in cell proliferation. Our mouse xenograft model also confirmed that decreased SIX1 abundance was associated with significantly reduced tumor volume and suppression of STAT3 signaling. These findings suggest that STAT3 signaling plays a crucial role in the functional significance of SIX1 in thyroid cancer, and it may raise a possibility that JAK/STAT3 inhibitors can be treated in those PTC patients with high expression of SIX1.

Our study indicated that SIX1 and EYA1 might be used as malignancy hallmarks in papillary thyroid cancer. Higher levels of SIX1 and EYA1 were found correlated with advanced age and lymph node metastasis, which are well-known poor prognostic factors in PTC. Although the tumor size showed no significant relationship with SIX1 or EYA1 expression, the functional assays identified that overexpression of SIX1 contribute to the proliferation of PTC cells, whereas knockdown SIX1 showed the opposite. Moreover, the success of lipid nanoparticles (LNP)-formulated siRNA targeting VEGF and kinesin spindle protein (KSP) in cancer patients with liver metastasis raised a hope that silencing SIX1 expression using shRNA or miRNA maybe a potential cancer treatment strategy (34). For example, microRNA-185 translationally represses SIX1 and thereby sensitizes SIX1-overexpressing cancer cells to TRAIL-induced apoptosis (35). It is known that EYAs mediate the transcriptional activation of SIX1 (27). Our study also showed that EYA1 is responsible for SIX1-induced STAT3 signaling activation, indicating disruption of EYA1 function may suppress the SIX1-mediate tumor growth in PTC. To date, Benzbromarone and its derivative, Benzarone were also found to be well-recognized EYA inhibitors (36). The major metabolite of Benzbromarone, 6-hydroxy Benzbromarone, is a more powerful inhibitor of EYAs, and may block tumor growth by inhibiting angiogenesis (37). Therefore, a combination treatment with either SIX1 or EYA1 inhibitors may provide benefit in a properly selected group of PTC patients.

DATA AVAILABILITY STATEMENT

All datasets generated for this study are included in the article/**Supplementary Material**.

ETHICS STATEMENT

This study was approved by the Institutional Review Board of Tongji Hospital.

AUTHOR CONTRIBUTIONS

GW and KWu developed the hypothesis and designed the experiments. DK, AL, YL, QC, KWa, DZ, JT, and YD performed the experiments. DK prepared the manuscript. ZL contributed to the pathology review and interpretation.

FUNDING

This study was supported by the National Natural Science Foundation of China (No. 81572608, 81874120), Wuhan Science and Technology Bureau (No. 2017060201010170), and the young thyroid doctors' research projects supported by China International Medical Foundation in 2015 (No. 2016026).

SUPPLEMENTARY MATERIAL

The Supplementary Material for this article can be found online at: https://www.frontiersin.org/articles/10.3389/fonc.2019.01450/full#supplementary-material

Supplementary Data Sheet 1 | STR profile of BCPAP.

Supplementary Image 1 | STR profile of TPC-1.

REFERENCES

1. Mao Y, Xing M. Recent incidences and differential trends of thyroid cancer in the USA. *Endocr Relat Cancer.* (2016) 23:313–22. doi: 10.1530/ERC-15-0445
2. Tufano RP, Noureldine SI, Angelos P. Incidental thyroid nodules and thyroid cancer: considerations before determining management. *JAMA Otolaryngol Head Neck Surg.* (2015) 141:566–72. doi: 10.1001/jamaoto.2015.0647
3. Zhang S, Wang Y, Chen M, Sun L, Han J, Elena VK, et al. CXCL12 methylation-mediated epigenetic regulation of gene expression in

papillary thyroid carcinoma. *Sci Rep.* (2017) 7:44033. doi: 10.1038/srep44033
4. Haugen BR, Alexander EK, Bible KC, Doherty GM, Mandel SJ, Nikiforov YE, et al. 2015 American thyroid association management guidelines for adult patients with thyroid nodules and differentiated thyroid cancer: the american thyroid association guidelines task force on thyroid nodules and differentiated thyroid cancer. *Thyroid.* (2016) 26:1–133. doi: 10.1089/thy.2015.0020
5. Valerio L, Pieruzzi L, Giani C, Agate L, Bottici V, Lorusso L, et al. Targeted therapy in thyroid cancer: state of the art. *Clin Oncol.* (2017) 29:316–24. doi: 10.1016/j.clon.2017.02.009
6. Lan X, Xu J, Chen C, Zheng C, Wang J, Cao J, et al. The landscape of circular RNA expression profiles in papillary thyroid carcinoma based on RNA sequencing. *Cell Physiol Biochem.* (2018) 47:1122–32. doi: 10.1159/000490188
7. Biankin AV, Piantadosi S, Hollingsworth SJ. Patient-centric trials for therapeutic development in precision oncology. *Nature.* (2015) 526:361–70. doi: 10.1038/nature15819
8. Jiao X, Zhang H, Xu X, Yu Y, Zhang H, Zhang J, et al. S100A4 knockout sensitizes anaplastic thyroid carcinoma cells harboring BRAFV600E/Mt to vemurafenib. *Cell Physiol Biochem.* (2018) 49:1143–62. doi: 10.1159/000493296
9. Xing M. Molecular pathogenesis and mechanisms of thyroid cancer. *Nat Rev Cancer.* (2013) 13:184–99. doi: 10.1038/nrc3431
10. Jin Z, Cheng X, Feng H, Kuang J, Yang W, Peng C, et al. Apatinib inhibits angiogenesis via suppressing Akt/GSK3beta/ANG signaling pathway in anaplastic thyroid cancer. *Cell Physiol Biochem.* (2017) 44:1471–84. doi: 10.1159/000485583
11. Liu Y, Han N, Zhou S, Zhou R, Yuan X, Xu H, et al. The DACH/EYA/SIX gene network and its role in tumor initiation and progression. *Int J Cancer.* (2016) 138:1067–75. doi: 10.1002/ijc.29560
12. Coletta RD, Christensen KL, Micalizzi DS, Jedlicka P, Varella-Garcia M, Ford HL. Six1 overexpression in mammary cells induces genomic instability and is sufficient for malignant transformation. *Cancer Res.* (2008) 68:2204–13. doi: 10.1158/0008-5472.CAN-07-3141
13. Iwanaga R, Wang CA, Micalizzi DS, Harrell JC, Jedlicka P, Sartorius CA, et al. Expression of Six1 in luminal breast cancers predicts poor prognosis and promotes increases in tumor initiating cells by activation of extracellular signal-regulated kinase and transforming growth factor-beta signaling pathways. *Breast Cancer Res.* (2012) 14:R100. doi: 10.1186/bcr3219
14. Micalizzi DS, Christensen KL, Jedlicka P, Coletta RD, Barón AE, Harrell JC, et al. The Six1 homeoprotein induces human mammary carcinoma cells to undergo epithelial-mesenchymal transition and metastasis in mice through increasing TGF-beta signaling. *J Clin Invest.* (2009) 119:2678–90. doi: 10.1172/JCI37815
15. Micalizzi DS, Wang CA, Farabaugh SM, Schiemann WP, Ford HL. Homeoprotein Six1 increases TGF-beta type I receptor and converts TGF-beta signaling from suppressive to supportive for tumor growth. *Cancer Res.* (2010) 70:10371–80. doi: 10.1158/0008-5472.CAN-10-1354
16. Xu H, Zhang Y, Altomare D, Pena MM, Wan F, Pirisi L, et al. Six1 promotes epithelial-mesenchymal transition and malignant conversion in human papillomavirus type 16-immortalized human keratinocytes. *Carcinogenesis.* (2014) 35:1379–88. doi: 10.1093/carcin/bgu050
17. Li L, Liang Y, Kang L, Liu Y, Gao S, Chen S, et al. Transcriptional regulation of the Warburg effect in cancer by SIX1. *Cancer Cell.* (2018) 33:368–85.e367. doi: 10.1016/j.ccell.2018.01.010
18. Kong D, Liu Y, Liu Q, Han N, Zhang C, Pestell RG, et al. The retinal determination gene network: from developmental regulator to cancer therapeutic target. *Oncotarget.* (2016) 7:50755–65. doi: 10.18632/oncotarget.9394
19. Wu K, Li Z, Cai S, Tian L, Chen K, Wang J, et al. EYA1 phosphatase function is essential to drive breast cancer cell proliferation through cyclin D1. *Cancer Res.* (2013) 73:4488–99. doi: 10.1158/0008-5472.CAN-12-4078
20. Xu PX, Zheng W, Laclef C, Maire P, Maas RL, Peters H, et al. Eya1 is required for the morphogenesis of mammalian thymus, parathyroid and thyroid. *Development.* (2002) 129:3033–44.
21. Liu Q, Li A, Yu S, Qin S, Han N, Pestell RG, et al. DACH1 antagonizes CXCL8 to repress tumorigenesis of lung adenocarcinoma and improve prognosis. *J Hematol Oncol.* (2018) 11:53. doi: 10.1186/s13045-018-0597-1
22. Chu Q, Han N, Yuan X, Nie X, Wu H, Chen Y, et al. DACH1 inhibits cyclin D1 expression, cellular proliferation and tumor growth of renal cancer cells. *J Hematol Oncol.* (2014) 7:73. doi: 10.1186/s13045-014-0073-5
23. Liu Y, Zhou R, Yuan X, Han N, Zhou S, Xu H, et al. DACH1 is a novel predictive and prognostic biomarker in hepatocellular carcinoma as a negative regulator of Wnt/β-catenin signaling. *Oncotarget.* (2015) 6:8621–34. doi: 10.18632/oncotarget.3281
24. Xu HW, Pirisi L, Creek KE. Six1 overexpression at early stages of HPV16-mediated transformation of human keratinocytes promotes differentiation resistance and EMT. *Virology.* (2015) 474:144–53. doi: 10.1016/j.virol.2014.10.010
25. Towers CG, Guarnieri AL, Micalizzi DS, Harrell JC, Gillen AE, Kim J, et al. The Six1 oncoprotein downregulates p53 via concomitant regulation of RPL26 and microRNA-27a-3p. *Nat Commun.* (2015) 6:10077. doi: 10.1038/ncomms10077
26. Blevins MA, Towers CG, Patrick AN, Zhao R, Ford HL. The SIX1-EYA transcriptional complex as a therapeutic target in cancer. *Expert Opin Ther Targets.* (2015) 19:213–25. doi: 10.1517/14728222.2014.978860
27. Patrick AN, Cabrera JH, Smith AL, Chen XS, Ford HL, Zhao R. Structure-function analyses of the human SIX1-EYA2 complex reveal insights into metastasis and BOR syndrome. *Nat Struct Mol Biol.* (2013) 20:447–53. doi: 10.1038/nsmb.2505
28. Kohrt D, Crary J, Zimmer M, Patrick AN, Ford HL, Hinds PW, et al. CDK6 binds and promotes the degradation of the EYA2 protein. *Cell Cycle.* (2014) 13:62–71. doi: 10.4161/cc.26755
29. Frank DA. STAT3 as a central mediator of neoplastic cellular transformation. *Cancer Lett.* (2007) 251:199–210. doi: 10.1016/j.canlet.2006.10.017
30. Furtek SL, Backos DS, Matheson CJ, Reigan P. Strategies and approaches of targeting STAT3 for cancer treatment. *ACS Chem Biol.* (2016) 11:308–18. doi: 10.1021/acschembio.5b00945
31. Zhang J, Gill A, Atmore B, Johns A, Delbridge L, Lai R, et al. Upregulation of the signal transducers and activators of transcription 3 (STAT3) pathway in lymphatic metastases of papillary thyroid cancer. *Int J Clin Exp Pathol.* (2011) 4:356–62.
32. Dong W, Cui J, Tian X, He L, Wang Z, Zhang P, et al. Aberrant sonic hedgehog signaling pathway and STAT3 activation in papillary thyroid cancer. *Int J Clin Exp Med.* (2014) 7:1786–93.
33. Ekpe-Adewuyi E, Lopez-Campistrous A, Tang X, Brindley DN, McMullen TP. Platelet derived growth factor receptor alpha mediates nodal metastases in papillary thyroid cancer by driving the epithelial-mesenchymal transition. *Oncotarget.* (2016) 7:83684–700. doi: 10.18632/oncotarget.13299
34. Tabernero J, Shapiro GI, LoRusso PM, Cervantes A, Schwartz GK, Weiss GJ, et al. First-in-humans trial of an RNA interference therapeutic targeting VEGF and KSP in cancer patients with liver involvement. *Cancer Discov.* (2013) 3:406–17. doi: 10.1158/2159-8290.CD-12-0429
35. Imam JS, Buddavarapu K, Lee-Chang JS, Ganapathy S, Camosy C, Chen Y, et al. MicroRNA-185 suppresses tumor growth and progression by targeting the Six1 oncogene in human cancers. *Oncogene.* (2010) 29:4971–9. doi: 10.1038/onc.2010.233
36. Tadjuidje E, Wang TS, Pandey RN, Sumanas S, Lang RA, Hegde RS. The EYA tyrosine phosphatase activity is pro-angiogenic and is inhibited by benzbromarone. *PLoS ONE.* (2012) 7:e34806. doi: 10.1371/journal.pone.0034806
37. Pandey RN, Wang TS, Tadjuidje E, McDonald MG, Rettie AE, Hegde RS. Structure-activity relationships of benzbromarone metabolites and derivatives as EYA inhibitory anti-angiogenic agents. *PLoS ONE.* (2013) 8:e84582. doi: 10.1371/journal.pone.0084582

Conflict of Interest: The authors declare that the research was conducted in the absence of any commercial or financial relationships that could be construed as a potential conflict of interest.

frontiers in Oncology

SYSTEMATIC REVIEW
published: 05 February 2020
doi: 10.3389/fonc.2019.01561

When the Loss Costs Too Much: A Systematic Review and Meta-Analysis of Sarcopenia in Head and Neck Cancer

Xin Hua [1,2†], Shan Liu [3†], Jun-Fang Liao [4†], Wen Wen [1,2†], Zhi-Qing Long [1,2], Zi-Jian Lu [1,5], Ling Guo [1,5†] and Huan-Xin Lin [1,2*†]*

[1] State Key Laboratory of Oncology in South China, Collaborative Innovation Center for Cancer Medicine, SunYat-sen University Cancer Center, Guangzhou, China, [2] Department of Radiotherapy, Sun Yat-sen University Cancer Center, Guangzhou, China, [3] Department of Radiation Oncology, Sichuan Cancer Hospital & Institute, Sichuan Cancer Center, School of Medicine, University of Electronic Science and Technology of China, Chengdu, China, [4] Department of Radiation Oncology, National Cancer Center/National Clinical Cancer Research Center for Cancer/Cancer Hospital & Shenzhen Hospital, Chinese Academy of Medical Sciences and Peking Union Medical College, Shenzhen, China, [5] Guangdong Key Laboratory of Nasopharyngeal Carcinoma Diagnosis and Therapy, Department of Nasopharyngeal Carcinoma, Sun Yat-sen University Cancer Center, Guangzhou, China

OPEN ACCESS

Edited by:
Jorge A. R. Salvador, Faculty of Pharmacy, University of Coimbra, Portugal

Reviewed by:
Edgar K. Selzer, Medical University of Vienna, Austria
Ik Jae Lee, Gangnam Severance Hospital, South Korea
Yeona Cho, Yonsei University College of Medicine, South Korea, in collaboration with reviewer IL

***Correspondence:**
Ling Guo
guoling@sysucc.org.cn
Huan-Xin Lin
linhx@sysucc.org.cn

[†] These authors have contributed equally to this work

Specialty section:
This article was submitted to Head and Neck Cancer, a section of the journal Frontiers in Oncology

Received: 08 July 2019
Accepted: 23 December 2019
Published: 05 February 2020

Citation:
Hua X, Liu S, Liao J-F, Wen W, Long Z-Q, Lu Z-J, Guo L and Lin H-X (2020) When the Loss Costs Too Much: A Systematic Review and Meta-Analysis of Sarcopenia in Head and Neck Cancer. Front. Oncol. 9:1561. doi: 10.3389/fonc.2019.01561

Purpose: Whether or not skeletal muscle mass (SMM) depletion, known as sarcopenia, has significant negative effects on the prognosis of patients with head and neck cancer (HNC) is both new and controversial. In this meta-analysis, we aimed to determine the prognostic significance of sarcopenia in HNC.

Methods: We searched PubMed, the Cochrane Library, Embase, and Web of Science, which contain trial registries and meeting proceedings, to identify related published or unpublished studies. We used the Newcastle–Ottawa Scale (NOS) to appraise the risk of bias of the included retrospective studies. Pooled hazard ratios (HR) and the I^2 statistic were estimated for the impact of sarcopenia on overall survival (OS) and relapse-free survival (RFS).

Results: We analyzed data from 11 studies involving 2,483 patients (39.4% on average of whom had sarcopenia). Based on the univariate analysis data, the sarcopenia group had significantly poorer OS compared to the non-sarcopenia group [HR = 1.97, 95% confidence interval (CI): 1.71–2.26, I^2 = 0%]. In the cutoff value subgroup, group 1, defined as skeletal muscle index (SMI) of 38.5 cm^2/m^2 for women and 52.4 cm^2/m^2 for men (HR = 2.41, 95% CI: 1.72–3.38, I^2 = 0%), had much poorer OS. In the race subgroup, the results were consistent between the Asia (HR = 2.11, 95% CI: 1.59–2.81) and non-Asia group (HR = 1.92, 95% CI: 1.64–2.25). The sarcopenia group also had significantly poorer RFS (HR = 1.74, 95% CI: 1.43–2.12, I^2 = 0%).

Conclusions: Presence of pre-treatment sarcopenia has a significant negative impact on OS and RFS in HNC compared with its absence. Further well-conducted studies with detailed stratification are needed to complement our findings.

Keywords: head and neck cancer, sarcopenia, meta-analysis, prognostic factor, skeletal muscle mass (SMM)

INTRODUCTION

Head and neck cancer (HNC) is a complex heterogeneous disease; numerous covariates affect its survival outcomes. According to National Comprehensive Cancer Network (NCCN) guidelines, radiotherapy (RT) with or without chemotherapy is the main treatment method for locally advanced HNC (1). Due to the local toxic effects of RT and chemoradiotherapy, patients with HNC may experience significant progressive weight loss and muscle mass depletion, which eventually lead to poor prognosis (2–4). Although weight loss is commonly used in clinical settings to screen for the risk of adverse outcomes in HNC, there are no universally recognized clear and reliable conclusions on the association of skeletal muscle mass (SMM) depletion and prognosis in HNC.

The main factors affecting treatment outcome are tumor characteristics and host-related factors (including age, sex, and nutritional status). Patients with HNC have a much higher risk of malnutrition than patients with other malignancies (5). Cancer patients with malnutrition typically lose lean body mass and muscle mass, while fat mass may remain or even increase (6). Muscle mass depletion, known as sarcopenia, can theoretically affect the treatment tolerance and prognosis of patients with HNC.

Sarcopenia is officially defined as generalized and progressive low SMM and function, and is related to physical disability and functional impairment (7). Sarcopenia in HNC can be quantified by the cross-sectional area in square centimeters (cm^2) divided by the squared height in meters (m^2) at the third lumbar (L3) or cervical (C3) vertebra level using computed tomography (CT) imaging (8). Recent studies have shown that sarcopenia is associated with increased risk of complications after tumor therapy and reduced disease-free survival (DFS) and overall survival (OS) (9–12). Sarcopenia and its effect on treatment-related complications and the clinical prognosis of HNC have recently attracted research attention. However, underestimation of the importance of sarcopenia continues to evolve when compared to the large number of studies that have been focused on different patient- and disease-related variables affecting the prognosis of patients with HNC (13–16).

Currently, whether sarcopenia in HNC can act as a prognostic factor is both little well-known and controversial (17, 18). Accordingly, we conducted this meta-analysis to investigate the prevalence of sarcopenia in patients with HNC and to determine its impact on clinical prognosis.

METHODS

Search Strategy

The prospective registration number of this meta-analysis on PROSPERO was CRD42019128406. This study was approved by the Ethics Committee of Sun Yat-sen University Cancer Center. Databases such as PubMed, the Cochrane Library, Embase, and Web of Science, which contain trial registries and meeting proceedings, were searched before August 30, 2019. In each database, we used the same search term: ("sarcopenia" or "fragility" or "sarcopenic" or "muscle index" or "muscle mass" or "muscle depletion" or "muscular atrophy") and ("head and neck cancer" or "head and neck neoplasm" or "HNSCC"). The language restriction was English; there were no other filters.

Study Selection

At the full-text screening step, two reviewers (X.H. and S.L.) assessed the relevant literature independently for inclusion. The κ statistic was used for inter-rater reliability (19). The inclusion criteria were as follows: (1) cohort and case–control study; (2) studied patients with HNC(s); (3) reported SMM or function measurement; and (4) reported prognostic data such as OS, progression-free survival (PFS), or DFS. Studies were excluded if data on the impact of sarcopenia on survival outcomes were unavailable.

Data Extraction

The two reviewers (S.L. and X.H.) extracted data from primary texts and Supplementary Appendixes independently and summarized them in a standardized data abstraction form. The extracted items are partly listed in **Table 1**. The results were reconciled and a third reviewer (J.F.L.) was consulted if there were discrepancies. In the case of missing data, the authors of the study in question were contacted via e-mail. If the authors did not reply, data from the published articles were used.

Risk of Bias Assessment

Two reviewers (W.W. and Z.Q.L.) assessed the bias independently. We used the modified Newcastle–Ottawa Scale (NOS) (35), which involves patient selection, study group comparability, and assessment of outcomes, to appraise the methodological quality of the included retrospective studies. The quality of each cohort study was scored 0–9, and case–control studies were scored 0–10; studies with scores of at least 6 were deemed good quality (19).

Meta-Analysis

We calculated and subsequently pooled in standard meta-analyses and hazard ratios (HRs) with corresponding 95% confidence intervals (95% CIs) for survival outcomes. HR and its 95% CI were directly used if these values were reported; otherwise, the natural logarithm of the HR (lnHR) and standard error of the lnHR [se(lnHR)] were calculated to determine the pooled HRs and 95% CIs according to the method of Parmar et al. (36) and Tierney et al. (37). The χ^2 and I^2 tests were used to appraise statistical heterogeneity between studies, with significance set at $P < 0.10$. The random-effects model was consistently used to maintain a conservative conclusion. Exploratory subgroup analyses were also performed. Potential publication bias was quantitatively assessed by funnel plot and quantified by the Egger test (38) and the trim-and-fill method (39) using Stata 14.0 (Stata Corp, College Station, TX, USA). The meta-analyses were performed using Review Manager 5.3 (Cochrane Collaboration, Oxford, UK).

TABLE 1 | Characteristics of included studies.

Author year	Country	Cancer	Stage	No. of patients	Age	Follow-up (months)	Sarcopenia assessment	Cut point (cm^2/m^2)			Sarcopenia (%)	Treatment	Outcome	Adjusted major confounders	NOS score
								Female	Male	Methods					
Ganju et al. (20)	America	Head and neck excluding p16+ oropharynx cancer	AJCC 7th III–IVB	246	60 (19–88)	35.1 (1–83)	*L3 SMI	41	43 or 53 by BMI	Martin et al. (12)	58	CCRT/IC+ CCRT, Surgery+	OS PFS	Baseline BMI, Age, Sex, Race, Site, Stage, Smoke, Treatment	**7**
Stone et al. (21)	America	Head and neck	AJCC I–IVB	260	61.1 (±11)	ND	L3 SMI	38.5	52.4	Prado et al. (6)	55.4	Surgery ± RT/CRT	OS	Baseline BMI, Stage, Smoke, ALB, HPV, Treatment	**7**
Bril et al. (22)	Netherlands	Larynx and Hypopharynx	AJCC 6/7th 0–IV	235	64.7 (±9.1)	62.4	*L3 SMI	43.2	43.2	Wendrich et al. (23)	46.4	Surgery ± pre Chemo/RT ± adjuvant treatment	OS	Baseline BMI, Sex, Smoke, Site, Treatment	**7**
Jung et al. (24)	Korea	Head and neck	AJCC 7th III–IV	258	64 (56–73)	53.6 (26.3–70.5)	L3 SMI	38.5	52.4	Prado et al. (6), Mourtzakis et al. (25)	6.6	Surgery ± RT/CCRT	OS DFS	Baseline Age, CCI, ALB, Site, HPV-P16, Smoke, Treatment	**7**
† Van Rijn–Dekker et al. (26)	Netherlands	HNSCC	AJCC I–IVB	750	ND	ND	*L3 SMI	30.6	42.4	Lowest gender-specific quartile	25	Chemo/RT	OS DFS	Baseline Age, WHO score, stage, site	**6**
Cho et al. (17)	Korea	Head and neck	AJCC III–IVB	221	59 (18–94)	30 (1–110)	L3 SMI	31	49	Go et al. (27), Kim et al. (28)	48.0	RT/ CCRT/ IC+CCRT	OS, PFS	Univariate analysis	**7**
‡ Fattouh et al. (29)	America	HNSCC	AJCC 6/7th M0	113	ND	≥60	L3 SMI	38.5	52.4	Prado et al. (30), Mokdad et al. (31)	64.6	Chemo/RT, Surgery+	OS	Baseline BMI, Age, Sex, Stage, Treatment	**8**
Grossberg et al. (18)	ND	HNSCC	AJCC 7th M0	190	57.7 (±9.4)	68.6	L3 SMI	38.5	52.4	Prado et al. (6), Parsons et al. (32)	35.3	RT/CCRT/IC+ CCRT, Surgery+	OS,	Baseline BMI, Age, Sex, Smoke, Site, Stage, Treatment, HIV, Diabetes, Cardiovascular disease	**8**
Nishikawa et al. (33)	Japan	HNSCC	M0	85	66 (28–89)	29.6 (1–40.7)	L3 SMI	30.3	46.7	Prado et al. (6)	46.0	RT/ CCRT/ BioRT/Surgery, NACT+	OS	Baseline weight loss, ALB, CRP	**6**
Tamaki et al. (34)	Japan	SCC of oropharyngeal	AJCC II–IVC	113	Non-sarcopenia 57.63 (±10.25); sarcopenia 63.5 (±12.91)	0–120	L3 SMI	41	41or 43	Martin et al. (12)	28.3	CCRT/surgery ± adjuvant treatment	OS DFS	Baseline BMI, HPV-P16, Sex, Smoke, Alcohol	**6**
Wendrich et al. (23)	Dutch	HNSCC	AJCC III-IV (locally advanced)	112	54.5 (±9.4)	15–90	*L3 SMI	43.2	43.2	Non-gender-specific optimal stratification	54.5	CCRT	OS	Univariate analysis	**6**

**L3 SMI was calculated by C3 SMI using the method from Swartz et al. (8).*

† Research as a conference meeting paper and the author provided information about sarcopenia (%).

‡ Research does not have a univariate analyzed OS data.

AJCC, American Joint Committee on Cancer; BMI, body mass index; HNSCC, head and neck squamous cell carcinoma; CCRT, concurrent chemoradiotherapy; IC, induction chemotherapy; L3, the third lumbar vertebra; No., number; ND, no description; OS, overall survival; DFS, disease-free survival; DSS, disease-specific survival; M, metastasis; NOS, Newcastle–Ottawa Scale; PFS, progression-free survival; RT, radiation therapy; SMI, skeletal muscle index. Bold represents the value of NOS-Score.

RESULTS

Search Strategy

After the initial literature search on August 30, 2019, 11 studies (17, 18, 20–24, 26, 29, 33, 34), including one nested case–control study (29) and a meeting abstract (26), assessing 2,483 patients were pooled in the present meta-analysis. Of the patients involved, an average of 39.4% had sarcopenia (979 patients and 1,504 patients had and did not have sarcopenia, respectively, according to different cutoff values; **Figure 1**). The kappa coefficient was 0.842 (**Figure S1**).

Characteristics of the Studies

Table 1 summarizes the characteristics of the 11 retrospective studies. Four studies (17, 24, 33, 34) were from Asia, i.e., Japan and Korea. All studies included patients with non-metastatic clinical stage, except the cohort of Tamaki et al. (34), which included four patients with stage IVC disease. All studies used the SMI, quantified by the cross-sectional area in cm^2 divided by m^2 at the L3 or the C3, and then calculated the L3 vertebra level mainly using CT imaging. There were different sarcopenia cutoff definitions (6, 12, 25, 27, 28, 30–32); three studies (22, 23, 26) used self-defined definitions to obtain optimum stratification. Sarcopenia prevalence ranged from 6.6 to 64.6%. The HRs from nine studies were adjusted for major confounders such as baseline body mass index (BMI) etc. The quality of all included studies was fair (**Table S1**). All studies had low risk of bias, with NOS scores of 6–8. HR and 95% CI data from two studies (17, 23) were extracted and estimated from survival curves using indirect methods. Lastly, no authors except Van Rijn-Dekker (26) replied to our query e-mails; therefore, we used only the available published data.

Overall Survival

The meta-analysis of the univariate and multivariate data of the influence of the SMI on OS using the random-effects model is depicted in (**Figures 2A,B**). The sarcopenia group had significantly poorer OS compared to the non-sarcopenia group (in **Figure 2A** HR = 1.97, 95% CI: 1.71–2.26, $I^2 = 0\%$ and $P = 0.46$; in **Figure 2B** HR = 2.15, 95% CI: 1.66–2.79, $I^2 = 50\%$ and $P = 0.04$). **Table 2** shows the exploratory subgroup analyses. In the primary SMI subgroup, the L3 SMI calculated from the C3 SMI showed results consistent with the L3 primary SMI (HR = 1.90, 95% CI: 1.60–2.25; HR = 2.12, 95% CI: 1.66–2.71, respectively). In the three subgroups according to cutoff values, group 1, defined as SMI of 38.5 cm^2/m^2 for women and 52.4 cm^2/m^2 for men, had much poorer OS (HR = 2.41, 95% CI: 1.72–3.38, $I^2 = 0\%$). Sarcopenia had a similar impact on the Asia and non-Asia subgroups (HR = 2.11, 95% CI: 1.59–2.81; HR = 1.92, 95% CI: 1.64–2.25, respectively). There was no difference between the high-quality group with NOS $\geq$ 7 and intermediate-quality group with NOS = 6 (HR = 2.13, 95% CI: 1.74–2.60; HR = 1.83, 95% CI: 1.48–2.26, respectively). As the χ^2 test *P*-value of 0.46 and an I^2 of 0% indicated consistency between the studies (**Figure 2A**), we did not perform sensitivity analysis except for multivariate meta-analysis for OS (**Table S2**).

Relapse-Free Survival

We defined RFS as the interval between diagnosis to the detection of first progression, death from any cause, or last follow-up that

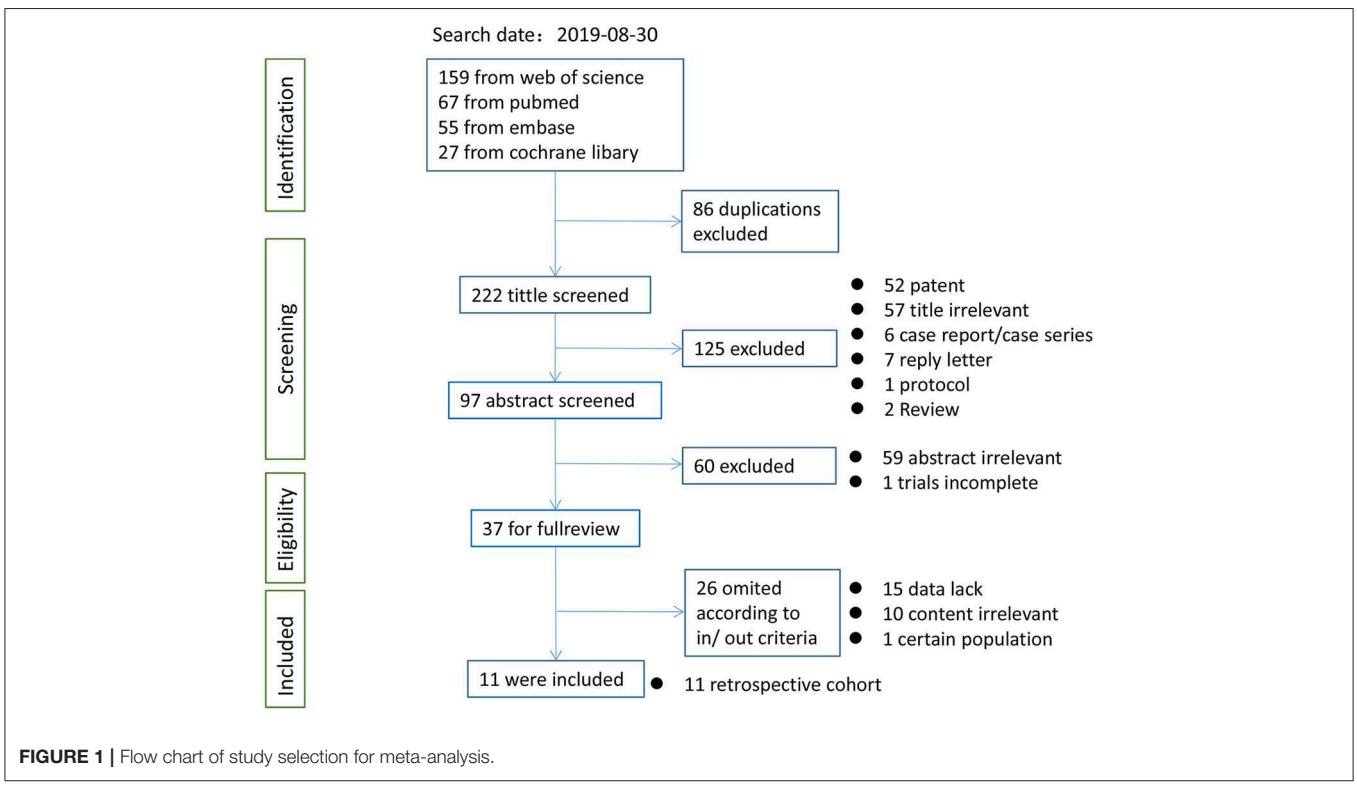

FIGURE 1 | Flow chart of study selection for meta-analysis.

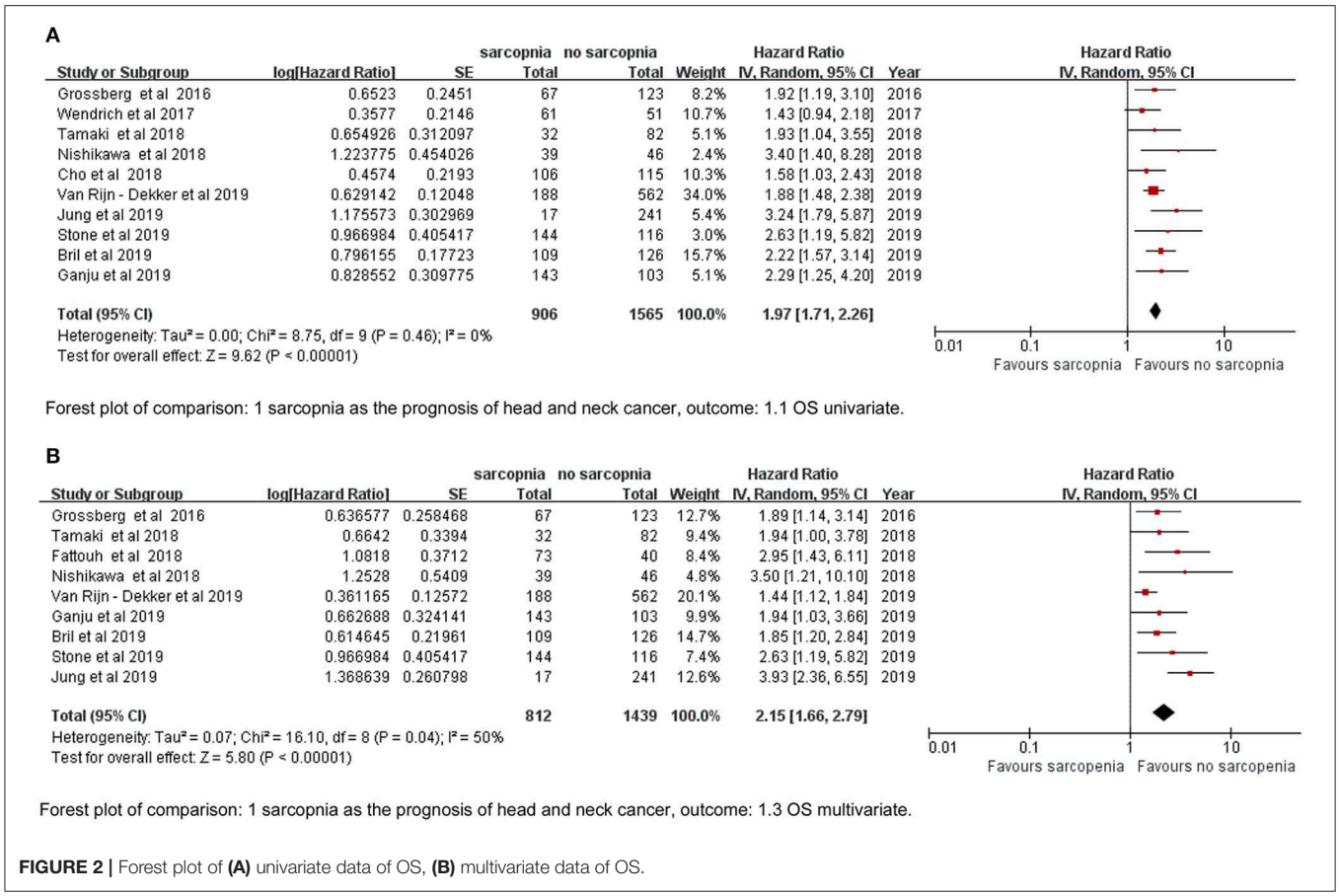

FIGURE 2 | Forest plot of **(A)** univariate data of OS, **(B)** multivariate data of OS.

represented PFS in the study by Cho et al. (17) and DFS by Tamaki et al. (34). The sarcopenia group had significantly poorer RFS based on both univariate and multivariate data (HR = 1.74, 95% CI: 1.43–2.12, $P < 0.00001$, $I^2 = 0\%$; HR = 1.68, 95% CI: 1.27–2.23, $P = 0.003$, $I^2 = 14\%$; **Figures 3A,B**).

Publication Bias

The publication bias test results are not separately reported (**Figures S2**, **S3**). In accordance with the funnel plot in **Figure S3**, Egger's test indicated a high likelihood of reporting bias ($P = 0.035$); however, the trim-and-fill method indicated that three hypothetical studies were filled in while the final conclusion remained unchanged (**Figure S2**).

DISCUSSION

Sarcopenia, known as the loss of SMM and function, is common in patients with various solid cancers with incidence ranging from 11 to 74% (40, 41). Following digestive cancer, patients with HNCs have a higher risk of experiencing malnutrition than patients with other cancer types (5, 42), due to the impact of the special tumor location and more serious treatment toxicity on the food intake. Accordingly, several recent studies have further explored the predictive value of sarcopenia in treatment-related complications and the prognosis of survival in HNC. Wendrich et al. (23) found that sarcopenia increased the risk of chemotherapy dose-limiting toxicity (CDLT) in patients with LA-HNSCC receiving chemoradiotherapy (44.3 vs. 13.7%, $P < 0.001$). Achim et al. (43) showed that up to 77% of patients with laryngeal cancer had preoperative sarcopenia and that sarcopenia was an independent predictor for all complications of total laryngectomy. Wendrich et al. (23) did not find a significant OS reduction for low SMM ($P = 0.187$). Grossberg et al. (18) found that, in patients with HNSCC, pre-RT SM depletion was no longer prognostic when BMI was included in the multivariate analysis. Indeed, obese patients without sarcopenia have significantly better prognosis than obese patients with sarcopenia (sarcopenia obesity) (6, 44). Therefore, as a nutrition-related indicator, whether sarcopenia independently affects the prognosis of HNC is appealing.

This is the first meta-analysis to report quantitative assessment of SMI and prognosis in HNC. The pooled HRs show that pre-treatment sarcopenia is significantly associated with poorer OS and RFS. The univariate HRs for survival outcomes were used to derive conclusions because we believed and observed that the multivariate meta-analysis that negative results did not participate in could be a source of publication bias.

We found relatively significant heterogeneity ($I^2 = 50\%$) in the multivariate meta-analysis for OS (**Figure 2B**). It appears that results by Jung et al. (24) and Van Rijn-Dekker et al. (26) are debatable (**Table S2**). The former had a much higher risk than any other research (HR = 3.93, 95% CI; 2.36–6.55). Interestingly,

TABLE 2 | Subgroup analyses of the prognostic effect on OS of the sarcopenia vs. non-sarcopenia group in head and neck cancer.

Variable	Subgroups	Availability		Effect		Heterogeneity	
		Studies (*N*)	Patients (*N*)	HR (95% CI)	*P*-values	I^2 (%)	P^*_{inter}
Race	Asian	4	678	2.11 [1.59, 2.81]	<0.00001	39	0.5
	Non-Asian	6	1,793	1.92 [1.64, 2.25]	<0.0001	0	
Stage	Locally advanced	4	837	1.92 [1.35, 2.73]	0.0003	49	0.95
	Non-metastasis	5	1,520	2.04 [1.71, 2.42]	<0.0001	0	
	Contained M1	1	114	1.94 [1.04, 3.55]	0.04	–	
Primary SMI	L3	6	1,128	2.12 [1.66, 2.71]	<0.00001	7	0.47
	C3	4	1,343	1.90 [1.60, 2.25]	<0.00001	0	
†Cutoff	Group1	3	708	2.41 [1.72, 3.38]	<0.0001	0	0.45
	Group2	3	1,056	1.87 [1.47, 2.38]	<0.00001	14	
	Group3	4	707	1.92 [1.53, 2.41]	<0.00001	0	
NOS quality	NOS ≥ 7	6	1,410	2.13 [1.74, 2.60]	<0.0001	0	0.3
	NOS = 6	4	1,061	1.83 [1.48, 2.26]	<0.00001	8	
HR data extract	Directly	8	2,138	2.11 [1.81, 2.47]	<0.00001	0	0.05
	Indirectly	2	333	1.50 [1.11, 2.03]	0.008	0	

*P_{inter} represents the significance of heterogeneity between subgroups calculated by Revman software.
†Cutoff value in Group 1: 38.5 cm^2/m^2 for women and 52.4 cm^2/m^2 for men; Group 2: 30.3–31 cm^2/m^2 for women and 42.4–49 cm^2/m^2 for men; Group 3: 41–43.2 cm^2/m^2 for women and 41–43.2 cm^2/m^2 for men.
N, number; HR, hazards ratio; NOS, Newcastle–Ottawa Scale.

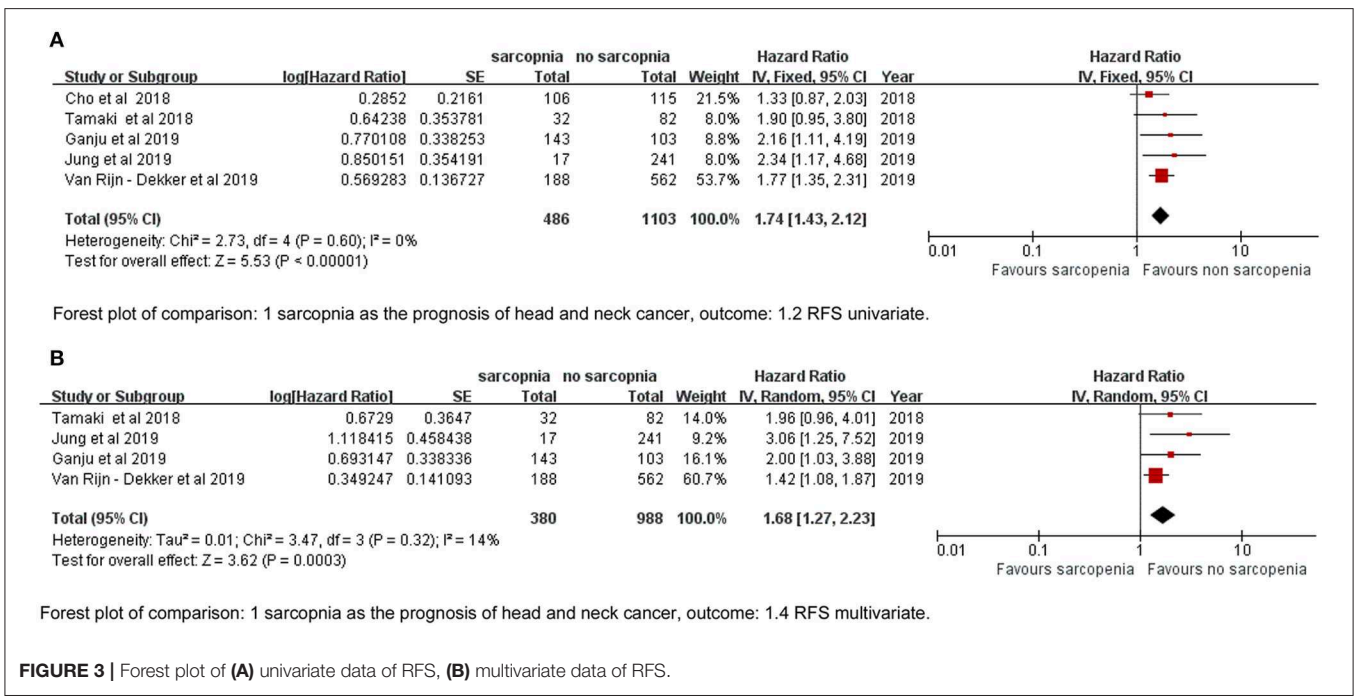

FIGURE 3 | Forest plot of **(A)** univariate data of RFS, **(B)** multivariate data of RFS.

the cutoff value they used was the same as that from three other included articles (18, 21, 29) (**Table 1**), but the incidence rate of sarcopenia was only 6.6%; the possible reasons for this are as follows: (a) 6.6% is for sarcopenia with visceral obesity in their study, (b) the locally advanced cancer stage is the distinguishing property, or (c) there might be potential bias that affected the incidence. The study by Van Rijn-Dekker et al., which will soon be published in full, was a meeting abstract that investigated a large-scale cohort of 750 patients with HNSCC, the incidence of sarcopenia was also low, i.e., as 25%, and the result was conservative and narrow (HR = 1.44, 95% CI: 1.12–1.84). In their e-mail reply, the cutoff was set by the lowest sex-specific quartile categorized in our Group 2 cutoff subgroup. Group 2 was less good enough to report a prognostic effect of sarcopenia than Group 1, which is based on log-rank statistics to separate patients with sarcopenia (6) (**Table 2**), so we agree that setting a

cutoff for sarcopenia by using the log-rank test may be better. It is common to obtain the head and neck CT in HNC, and we also did not observe significant intergroup heterogeneity between the primary site of SMI definition subgroups (C3 or L3) (**Table 2**). We suggest that more studies should explore the effect and cutoff value of neck muscles on HNC prognosis.

In our review, sarcopenia had a similar impact on the Asia and non-Asia subgroups, which suggest that sarcopenia could be widely used. Sarcopenia was not a prognostic factor for p16+ oropharyngeal cancer (34, 45), and maybe different tumor types that caused a wide range of prognosis have specific influence on sarcopenia; thus, it is imperative for further studies on particular and rare types of tumors other than p16+ oropharyngeal cancer to determine the prognostic value of sarcopenia. As for the set of cutoff value, the low intergroup heterogeneity indicates that different cutoffs could all be used (**Table 2**). Therefore, a unitary cutoff is not reasonable, and it can be inferred that using different races, tumor-node-metastasis (TNM) clinical stages, tumor types, age groups, and other features to form the appropriate multi-factor model can identify patients with poor prognosis as accurately as possible.

Our study also aims to turn its attention to the routine evaluation and intervention of sarcopenia for HNC. Many strategies can be attempted to prevent and treat sarcopenia. Among them, lifestyle modification, specific dietary habits, and therapeutic measures have been recommended. Protein supplementation and regular resistance exercise are the mainstream treatments of sarcopenia: to increase muscle mass and help augment muscle strength (46, 47). In addition, drugs that can block the cytokines associated with the muscle atrophy signaling pathways [such as myostatin/activin, interleukin (IL)-6, and tumor necrosis factor (TNF)-α] or medications that induce signals of muscle hypertrophy (such as growth hormone agonists, ghrelin, and anabolic steroids) may be useful for sarcopenia accompanied by visceral obesity (48).

Due to the retrospective nature of the included studies, the present meta-analysis has several limitations. First, only some of those articles included the treatment variable, which is a significant prognostic factor for survival outcomes, into their multivariate analysis, and no matching methods were used, so there might have been interaction effects. Second, there were little data about stratifying the impact of pre-treatment sarcopenia on survival according to clinical stages, which is commonly used for identifying higher-risk groups. For example, Van Rijn-Dekker et al. (26) found that sarcopenia is not a prognostic factor in early-stage HNSCC. Third, because Fattouh et al. (29) only reported the positive HR in their multivariate analysis, the univariate meta-analysis included 10/11 of eligible primary studies; however, according to the principle of Cox regression, there is little chance that the conclusion of the meta-analysis will be affected. Finally, the reasons for the different statistical significance between Egger's test and the trim-and-fill method might derive from the low number of included studies; however, these studies are relatively new, and we did not receive replies from the authors of three conference articles with positive (49, 50) and negative (51) results, which requires further evaluation after their official publication.

CONCLUSION

The presence of pre-treatment sarcopenia has a significant negative impact on OS and RFS in HNC compared with its absence. Further well-conducted studies with detailed stratification are needed to complement our findings.

DATA AVAILABILITY STATEMENT

Please contact author for data requests.

AUTHOR CONTRIBUTIONS

XH, SL, and J-FL collected, extracted, and analyzed the data and wrote the paper. WW, Z-QL, and Z-JL performed quality assessment and analyzed the data. LG and H-XL conceived and designed this study. All authors reviewed the paper, read, and approved the final manuscript.

FUNDING

This work was partly supported by the National Natural Science Foundation of China (Nos. 81772877, 81773103, and 81572848).

SUPPLEMENTARY MATERIAL

The Supplementary Material for this article can be found online at: https://www.frontiersin.org/articles/10.3389/fonc.2019.01561/full#supplementary-material

Table S1 | NOS score of included retrospective studies.

Table S2 | Sensitivity analysis (one study was omitted in each round) of multivariate meta-analysis of OS between the sarcopenia and non-sarcopenia groups.

Figure S1 | Kappa coefficient value for 38 eligible studies at full text step. Kappa value 0.0–0.20 (slight), 0.21–0.40 (fair), 0.41–0.60 (moderate), 0.61–0.80 (substantial), and 0.81–1 (almost perfect).

Figure S2 | Egger's test for OS and trim-and-fill method. For Egger's test, if the test of H0: $P > 0.1$, there is no publication bias; for the trim-and-fill method, if the final conclusion from the estimated pooled HR and 95%CI remains unchanged, publication bias has little influence on the authenticity of the final conclusion.

Figure S3 | Funnel plot of univariate meta-analysis for OS.

REFERENCES

1. Noguchi M, Kakuma T, Uemura H, Nasu Y, Kumon H, Hirao Y, et al. A randomized phase II trial of personalized peptide vaccine plus low dose estramustine phosphate (EMP) versus standard dose EMP in patients with castration resistant prostate cancer. *Cancer Immunol Immun.* (2010) 59:1001–9. doi: 10.1007/s00262-010-0822-4
2. Jager-Wittenaar H, Dijkstra PU, Vissink A, Langendijk JA, van der Laan BF, Pruim J, et al. Changes in nutritional status and dietary intake during

and after head and neck cancer treatment. *Head Neck.* (2011) 33:863–70. doi: 10.1002/hed.21546
3. Jackson W, Alexander N, Schipper M, Fig L, Feng F, Jolly S. Characterization of changes in total body composition for patients with head and neck cancer undergoing chemoradiotherapy using dual-energy x-ray absorptiometry. *Head Neck.* (2014) 36:1356–62. doi: 10.1002/hed.23461
4. Langius JA, Bakker S, Rietveld DH, Kruizenga HM, Langendijk JA, Weijs PJ, et al. Critical weight loss is a major prognostic indicator for disease-specific survival in patients with head and neck cancer receiving radiotherapy. *Br J Cancer.* (2013) 109:1093–9. doi: 10.1038/bjc.2013.458
5. Pressoir M, Desne S, Berchery D, Rossignol G, Poiree B, Meslier M, et al. Prevalence, risk factors and clinical implications of malnutrition in French comprehensive cancer centres. *Br J Cancer.* (2010) 102:966–71. doi: 10.1038/sj.bjc.6605578
6. Prado CM, Lieffers JR, McCargar LJ, Reiman T, Sawyer MB, Martin L, et al. Prevalence and clinical implications of sarcopenic obesity in patients with solid tumours of the respiratory and gastrointestinal tracts: a population-based study. *Lancet Oncol.* (2008) 9:629–35. doi: 10.1016/S1470-2045(08)70153-0
7. Cruz-Jentoft AJ, Bahat G, Bauer J, Boirie Y, Bruyere O, Cederholm T, et al. Sarcopenia: revised European consensus on definition and diagnosis. *Age Ageing.* (2019) 48:16–31. doi: 10.1093/ageing/afy169
8. Swartz JE, Pothen AJ, Wegner I, Smid EJ, Swart KM, de Bree R, et al. Feasibility of using head and neck CT imaging to assess skeletal muscle mass in head and neck cancer patients. *Oral Oncol.* (2016) 62:28–33. doi: 10.1016/j.oraloncology.2016.09.006
9. Miyamoto Y, Baba Y, Sakamoto Y, Ohuchi M, Tokunaga R, Kurashige J, et al. Sarcopenia is a negative prognostic factor after curative resection of colorectal cancer. *Ann Surg Oncol.* (2015) 22:2663–8. doi: 10.1245/s10434-014-4281-6
10. Kuroki LM, Mangano M, Allsworth JE, Menias CO, Massad LS, Powell MA, et al. Pre-operative assessment of muscle mass to predict surgical complications and prognosis in patients with endometrial cancer. *Ann Surg Oncol.* (2015) 22:972–9. doi: 10.1245/s10434-014-4040-8
11. Voron T, Tselikas L, Pietrasz D, Pigneur F, Laurent A, Compagnon P, et al. Sarcopenia impacts on short- and long-term results of hepatectomy for hepatocellular carcinoma. *Ann Surg.* (2015) 261:1173–83. doi: 10.1097/SLA.0000000000000743
12. Martin L, Birdsell L, Macdonald N, Reiman T, Clandinin MT, McCargar LJ, et al. Cancer cachexia in the age of obesity: skeletal muscle depletion is a powerful prognostic factor, independent of body mass index. *J Clin Oncol.* (2013) 31:1539–47. doi: 10.1200/JCO.2012.45.2722
13. Du E, Mazul AL, Farquhar D, Brennan P, Anantharaman D, Abedi-Ardekani B, et al. Long-term survival in head and neck cancer: impact of site, stage, smoking, and human papillomavirus status. *Laryngoscope.* (2019) 129:2506–13. doi: 10.1002/lary.27807
14. Giraldi L, Leoncini E, Pastorino R, Wunsch-Filho V, de Carvalho M, Lopez R, et al. Alcohol and cigarette consumption predict mortality in patients with head and neck cancer: a pooled analysis within the International Head and Neck Cancer Epidemiology (INHANCE) consortium. *Ann Oncol.* (2017) 28:2843–51. doi: 10.1093/annonc/mdx486
15. Iyengar NM, Kochhar A, Morris PG, Morris LG, Zhou XK, Ghossein RA, et al. Impact of obesity on the survival of patients with early-stage squamous cell carcinoma of the oral tongue. *Cancer.* (2014) 120:983–91. doi: 10.1002/cncr.28532
16. Rietbergen MM, Brakenhoff RH, Bloemena E, Witte BI, Snijders PJ, Heideman DA, et al. Human papillomavirus detection and comorbidity: critical issues in selection of patients with oropharyngeal cancer for treatment De-escalation trials. *Ann Oncol.* (2013) 24:2740–5. doi: 10.1093/annonc/mdt319
17. Cho Y, Kim JW, Keum KC, Lee CG, Jeung HC, Lee IJ. Prognostic significance of sarcopenia with inflammation in patients with head and neck cancer who underwent definitive chemoradiotherapy. *Front Oncol.* (2018) 8:457. doi: 10.3389/fonc.2018.00457
18. Grossberg AJ, Chamchod S, Fuller CD, Mohamed AS, Heukelom J, Eichelberger H, et al. Association of body composition with survival and locoregional control of radiotherapy-treated head and neck squamous cell carcinoma. *JAMA Oncol.* (2016) 2:782–9. doi: 10.1001/jamaoncol.2015.6339
19. Talwar B, Donnelly R, Skelly R, Donaldson M. Nutritional management in head and neck cancer: United Kingdom National Multidisciplinary Guidelines. *J Laryngol Otol.* (2016) 130:S32–40. doi: 10.1017/S0022215116000402
20. Ganju RG, Morse R, Hoover A, TenNapel M, Lominska CE. The impact of sarcopenia on tolerance of radiation and outcome in patients with head and neck cancer receiving chemoradiation. *Radiother Oncol.* (2019) 137:117–24. doi: 10.1016/j.radonc.2019.04.023
21. Stone L, Olson B, Mowery A, Krasnow S, Jiang A, Li R, et al. Association between sarcopenia and mortality in patients undergoing surgical excision of head and neck cancer. *JAMA Otolaryngol Head Neck Surg.* (2019) 145:647–54. doi: 10.1001/jamaoto.2019.1185
22. Bril SI, Pezier TF, Tijink BM, Janssen LM, Braunius WW, de Bree R. Preoperative low skeletal muscle mass as a risk factor for pharyngocutaneous fistula and decreased overall survival in patients undergoing total laryngectomy. *Head Neck.* (2019) 41:1745–55. doi: 10.1002/hed.25638
23. Wendrich AW, Swartz JE, Bril SI, Wegner I, de Graeff A, Smid EJ, et al. Low skeletal muscle mass is a predictive factor for chemotherapy dose-limiting toxicity in patients with locally advanced head and neck cancer. *Oral oncol.* (2017) 71:26–33.. doi: 10.1016/j.oraloncology.2017.05.012
24. Jung AR, Roh JL, Kim JS, Kim SB, Choi SH, Nam SY, et al. Prognostic value of body composition on recurrence and survival of advanced-stage head and neck cancer. *Eur J Cancer.* (2019) 116:98–106. doi: 10.1016/j.ejca.2019.05.006
25. Mourtzakis M, Prado CM, Lieffers JR, Reiman T, McCargar LJ, Baracos VE. A practical and precise approach to quantification of body composition in cancer patients using computed tomography images acquired during routine care. *Appl Physiol Nutr Metab.* (2008) 33:997–1006. doi: 10.1139/H08-075
26. Van Rijn-Dekker I, Van den Bosch L, Van den Hoek A, Bijl H, Dieters M, Van Aken E, et al. Impact of sarcopenia on survival and late toxicity in head and neck cancer patients treated with RT. *Radiother Oncol.* (2019) 133:S197–8. doi: 10.1016/S0167-8140(19)30813-8
27. Go SI, Park MJ, Song HN, Kang MH, Park HJ, Jeon KN, et al. Sarcopenia and inflammation are independent predictors of survival in male patients newly diagnosed with small cell lung cancer. *Support Care Cancer.* (2016) 24:2075–84. doi: 10.1007/s00520-015-2997-x
28. Kim YS, Lee Y, Chung YS, Lee DJ, Joo NS, Hong D, et al. Prevalence of sarcopenia and sarcopenic obesity in the Korean population based on the Fourth Korean National Health and Nutritional Examination Surveys. *J Gerontol A Biol Sci Med Sci.* (2012) 67:1107–13. doi: 10.1093/gerona/gls071
29. Fattouh M, Chang GY, Ow TJ, Shifteh K, Rosenblatt G, Patel VM, et al. Association between pretreatment obesity, sarcopenia, and survival in patients with head and neck cancer. *Head Neck.* (2018) 41:707–14. doi: 10.1002/hed.25420
30. Prado CM, Baracos VE, McCargar LJ, Reiman T, Mourtzakis M, Tonkin K, et al. Sarcopenia as a determinant of chemotherapy toxicity and time to tumor progression in metastatic breast cancer patients receiving capecitabine treatment. *Clin Cancer Res.* (2009) 15:2920–6. doi: 10.1158/1078-0432.CCR-08-2242
31. Mokdad AH, Ford ES, Bowman BA, Dietz WH, Vinicor F, Bales VS, et al. Prevalence of obesity, diabetes, and obesity-related health risk factors, 2001. *JAMA.* (2003) 289:76–9. doi: 10.1001/jama.289.1.76
32. Parsons HA, Baracos VE, Dhillon N, Hong DS, Kurzrock R. Body composition, symptoms, and survival in advanced cancer patients referred to a phase I service. *PLoS ONE.* (2012) 7:e29330. doi: 10.1371/journal.pone.0029330
33. Nishikawa D, Hanai N, Suzuki H, Koide Y, Beppu S, Hasegawa Y. The impact of skeletal muscle depletion on head and neck squamous cell carcinoma. *ORL.* (2018) 80:1–9. doi: 10.1159/000485515
34. Tamaki A, Manzoor NF, Babajanian E, Ascha M, Rezaee R, Zender CA. Clinical significance of sarcopenia among patients with advanced oropharyngeal cancer. *Otolaryngol Head Neck Surg.* (2018) 160:480–7. doi: 10.1177/0194599818793857
35. Wells G, Shea BJ, O'Connell D, Peterson J, Welch V, Losos M. The Newcastle-Ottawa Scale (NOS) for assessing the quality of nonrandomised studies in meta-analyses. Available online at: http://www.ohri.ca/programs/clinical_epidemiology/oxford.asp
36. Parmar MK, Torri V, Stewart L. Extracting summary statistics to perform meta-analyses of the published literature for survival endpoints. *Stat Med.*

(1998) 17:2815–34. doi: 10.1002/(sici)1097-0258(19981230)17:24<2815::aid-sim110>3.0.co;2-8
37. Tierney JF, Stewart LA, Ghersi D, Burdett S, Sydes MR. Practical methods for incorporating summary time-to-event data into meta-analysis. *Trials.* (2007) 8:16. doi: 10.1186/1745-6215-8-16
38. Egger M, Davey Smith G, Schneider M, Minder C. Bias in meta-analysis detected by a simple, graphical test. *BMJ.* (1997) 315:629–34. doi: 10.1136/bmj.315.7109.629
39. Duval S, Tweedie R. Trim and fill: a simple funnel-plot-based method of testing and adjusting for publication bias in meta-analysis. *Biometrics.* (2000) 56:455–63. doi: 10.1111/j.0006-341X.2000.00455.x
40. Shachar SS, Williams GR, Muss HB, Nishijima TF. Prognostic value of sarcopenia in adults with solid tumours: A meta-analysis and systematic review. *Eur J Cancer.* (2016) 57:58–67. doi: 10.1016/j.ejca.2015.12.030
41. Chang KV, Chen JD, Wu WT, Huang KC, Hsu CT, Han DS. Association between loss of skeletal muscle mass and mortality and tumor recurrence in hepatocellular carcinoma: a systematic review and meta-analysis. *Liver Cancer.* (2018) 7:90–103. doi: 10.1159/000484950
42. Gorenc M, Kozjek NR, Strojan P. Malnutrition and cachexia in patients with head and neck cancer treated with (chemo) radiotherapy. *Rep Pract Oncol Radiother.* (2015) 20:249–58. doi: 10.1016/j.rpor.2015.03.001
43. Achim V, Bash J, Mowery A, Guimaraes AR, Li R, Schindler J, et al. prognostic indication of sarcopenia for wound complication after total laryngectomy. *JAMA Otolaryngol Head Neck Surg.* (2017) 143:1159. doi: 10.1001/jamaoto.2017.0547
44. Ozola Zalite I, Zykus R, Francisco Gonzalez M, Saygili F, Pukitis A, Gaujoux S, et al. Influence of cachexia and sarcopenia on survival in pancreatic ductal adenocarcinoma: a systematic review. *Pancreatology.* (2015) 15:19–24. doi: 10.1016/j.pan.2014.11.006
45. Ganju RG, Morse R, Tennapel MJ, Hoover A, Kakarala K, Shnayder L, et al. Skeletal muscle gauge measured at the c3 vertebral body predicts for outcomes in men with P16-positive oropharynx cancer. *Int J Radiat Oncol Biol Phys.* (2019) 105:E420. doi: 10.1016/j.ijrobp.2019.06.1528
46. Freiberger E, Sieber C, Pfeifer K. Physical activity, exercise, and sarcopenia – future challenges. *Wien Med Wochenschr.* (2011) 161:416–25. doi: 10.1007/s10354-011-0001-z
47. Morley JE, Argiles JM, Evans WJ, Bhasin S, Cella D, Deutz NE, et al. Nutritional recommendations for the management of sarcopenia. *J Am Med Dir Assoc.* (2010) 11:391–6. doi: 10.1016/j.jamda.2010.04.014
48. Cohen S, Nathan JA, Goldberg AL. Muscle wasting in disease: molecular mechanisms and promising therapies. *Nat Rev Drug Discov.* (2015) 14:58–74. doi: 10.1038/nrd4467
49. Chamchod S, Fuller CD, Grossberg AJ, Mohamed AS, Heukelom J, ichelberger H, et al. sarcopenia/cachexia is associated with reduced survival and locoregional control in head and neck cancer patients receiving radiotherapy: results from quantitative imaging analysis of lean body mass. *Oncology.* (2015) 29(4 Suppl 1):205153.
50. Inokuchi H, Okano K, Takehana K, Tsutsui K, Hiraoka M. Prognostic impact of quantitative imaging analysis of lean body mass after chemoradiation therapy for patients with advanced nasopharyngeal cancer. *Int J Radiat Oncol Biol Phys.* (2018) 100:1342. doi: 10.1016/j.ijrobp.2017.12.094
51. Kabarriti R, Ohri N, Bontempo A, Romano M, Modi C, Viswanathan S, et al. The impact of dietary regimen compliance and sarcopenia in head and neck cancer patients treated with definitive radiation therapy. *Int J Radiat Oncol Biol Phys.* (2015) 93:E332–3. doi: 10.1016/j.ijrobp.2015.07.1395

Conflict of Interest: The authors declare that the research was conducted in the absence of any commercial or financial relationships that could be construed as a potential conflict of interest.

frontiers in Oncology

ORIGINAL RESEARCH
published: 27 February 2020
doi: 10.3389/fonc.2020.00112

Differentiation of Thyroid Nodules Difficult to Diagnose With Contrast-Enhanced Ultrasonography and Real-Time Elastography

Xuehua Xi[1†], Luying Gao[2†], Qiong Wu[2,3†], Shibao Fang[3], Jingzhu Xu[4], Ruyu Liu[2], Xiao Yang[2], Shenling Zhu[2], Ruina Zhao[2], Xingjian Lai[2], Xiaoyan Zhang[2], Bo Zhang[1,2] and Yuxin Jiang[2*]*

[1] Department of Ultrasound, China–Japan Friendship Hospital, Beijing, China, [2] Department of Ultrasound, Peking Union Medical College Hospital, Chinese Academy of Medical Sciences & Peking Union Medical College, Beijing, China, [3] Department of Ultrasound, Affiliated Hospital of Qingdao University, Qingdao, China, [4] Department of General Surgery, Peking Union Medical College Hospital, Chinese Academy of Medical Sciences & Peking Union Medical College, Beijing, China

OPEN ACCESS

Edited by:
Jorge A. R. Salvador,
University of Coimbra, Portugal

Reviewed by:
Prasanth Penumadu,
Jawaharlal Institute of Postgraduate Medical Education and Research (JIPMER), India
Shilpi Sharma,
Narayana Superspeciality Hospital, Gurugram, India

***Correspondence:**
Bo Zhang
thyroidus@163.com
Yuxin Jiang
jiangyuxinxh@163.com

[†]These authors have contributed equally to this work and share first authorship

Specialty section:
This article was submitted to Head and Neck Cancer, a section of the journal Frontiers in Oncology

Received: 07 September 2019
Accepted: 21 January 2020
Published: 27 February 2020

Citation:
Xi X, Gao L, Wu Q, Fang S, Xu J, Liu R, Yang X, Zhu S, Zhao R, Lai X, Zhang X, Zhang B and Jiang Y (2020) Differentiation of Thyroid Nodules Difficult to Diagnose With Contrast-Enhanced Ultrasonography and Real-Time Elastography. Front. Oncol. 10:112. doi: 10.3389/fonc.2020.00112

According to the 2015 American Thyroid Association (ATA), referred risk stratification and thyroid nodules with intermediate- and low-suspicion patterns are difficult to diagnose. The objective of this study is to evaluate the diagnostic performance of contrast-enhanced ultrasonography (CEUS) and elastosonography (ES) for the differentiation of these thyroid nodules. From November 2011 to June 2016, a total of 163 thyroid nodules with intermediate- and low-suspicion patterns in 150 consecutive patients at our hospital were studied before surgery. With surgical pathology as the standard, the diagnostic value of CEUS and ES was analyzed. There were 29 (17.8%) malignant lesions and 134 (82.2%) benign lesions. The enhancement patterns of CEUS, the echogenicity, and the elastography were significantly different between malignant and benign lesions ($P < 0.05$). Heterogenous enhancement was more common in malignant nodules, and the sensitivity, specificity, positive predictive value, negative predictive value, and odds ratio were 51.7, 88.1, 48.4, 89.4, and 10.1%, respectively. The diagnostic accuracy of CEUS was better than the conventional ultrasound [area under the curve (AUC), 0.729 vs. 0.616, $P = 0.021$]. The enhancement patterns of CEUS were helpful in the differential diagnosis of thyroid nodules with intermediate and low suspicion.

Keywords: thyroid carcinoma, contrast-enhanced ultrasonography, elastosonography, American Thyroid Association, intermediate- and low-suspicion patterns

INTRODUCTION

The 2015 American Thyroid Association Management Guidelines for Adult Patients with Thyroid Nodules and Differentiated Thyroid Cancer (1) (2015 ATA guidelines) proposed a risk stratification of thyroid nodules based on a series of studies on the ultrasonographic features of thyroid nodules. The guide classifies the sonographic appearance of the vast majority of thyroid nodules into the following categories of ultrasound patterns: high suspicion, intermediate suspicion, low suspicion, very low suspicion, and benign. Intermediate suspicion (malignancy risk 10–20%) nodules are hypoechoic solid nodules with smooth regular margins and without malignant features

such as microcalcifications, extrathyroidal extension, or a taller-than-wide shape. Low-suspicion (malignancy risk, 5–10%) nodules are isoechoic or hyperechoic solid nodules or partially cystic nodules with eccentric uniformly solid areas without malignant features. These nodules have similar ultrasound features as nodules suspicious of follicular lesions in the "British Thyroid Association Guidelines for the Management of Thyroid Cancer" (2) (BTA guidelines). Despite the fact that the malignancy risk is not relatively high, differentiating malignant from benign lesions by conventional ultrasonography (CUS) is challenging.

Contrast-enhanced ultrasonography (CEUS) has been widely used to evaluate the microvessel perfusion of thyroid nodules. Elastosonography (ES) quantifies the firmness of the tissue and displays it as a color map on which the hardness of the tissues can be reflected. Many studies have concluded that the accuracy of the diagnosis of thyroid nodules can be increased by combining CEUS and ES with CUS (3–5). However, the value of CEUS and ES in evaluating nodules with intermediate- and low-suspicion patterns is unclear.

METHODS

This study was approved by the ethics committee of Peking Union Medical College Hospital (PUMCH), and informed consent was obtained from all patients before CEUS and ES.

Patients

A total of 604 patients with thyroid nodules admitted to PUMCH from November 2011 to June 2016 who met the following criteria were included in this study: (a) CUS indicated that the thyroid nodule was of intermediate or low suspicion according to the 2015 ATA guidelines for referred risk stratification, and (b) the largest diameter of the nodule was larger than 5 mm in size. The exclusion criteria were as follows: (a) patients who did not undergo surgery, (b) patients younger than 18 years of age, (c) women during pregnancy or lactation, and (d) patients who could not tolerate the intravenous injection of contrast agents because of heart, lung, kidney, or other vital organ dysfunction or severe allergies. A total of 163 thyroid nodules in 150 consecutive patients (mean age, 47.9; range, 18–83 years) were included. Two nodules in eight patients each and three nodules in three patients each were included. In six of those eight patients, the two nodules were located in different lobes. In two other patients, the two nodules were not near each other, although they were in the same lobe. In three patients, two of the three nodules were located in the same lobe, and the other was located in a different lobe. CUS, CEUS, and ES were performed in all patients, and the ultrasound-guided fine needle aspiration (FNA) was performed in nine patients before surgery.

Ultrasound Examination

All ultrasound (US) examinations were performed with a 5- to 12-MHz liner probe (iU22; Philips Medical System, Bothell, WA, United States). The CUS examination was performed with the standard equipment settings for thyroid glands. Standard machine settings for CEUS were used, and the contrast medium used was SonoVue (Bracco Imaging, Milan, Italy). With a 20- or 22-gauge peripheral intravenous cannula, SonoVue was injected intravenously as a bolus at a dose of 1.2 ml, followed by 5 ml of normal saline as a flush. The timer on the US machine was then started, and each contrast imaging acquisition lasted more than 2 min after the bolus injection; the imaging was digitally stored. During real-time elastography (RTE), the probe was positioned perpendicular to the skin, and no compression was applied at the skin above the targeted thyroid nodule. When there were two nodules in a patient, CEUS was performed on the second nodule after the first injected contrast agent was completely cleaned in the whole gland. CUS, RTE, and CEUS images and cine clips were analyzed by two radiologists with more than 5 years of experience in thyroid US. They were blinded to the patients' clinical data and pathological results. In cases of discrepancies between the two readers, a consensus was reached after discussion.

TABLE 1 | Clinical characteristics of nodules with intermediate and low suspicion.

Clinical characteristics	Malignant group ($n = 29$)	Benign group ($n = 121$)	*P*-value
Age (years)	44.0 ± 11.9	48.7 ± 11.8	0.706
Sex			0.054
Female	17 (58.6)	91 (75.2)	
Male	12 (41.4)	30 (24.8)	
Mixed with HT	1 (3.4)	19 (15.7)	0.081
Size (cm)*	2.1 ± 1.5	2.6 ± 1.4	0.675

HT, Hashimoto thyroiditis.
**For 163 nodules.*

TABLE 2 | Comparison of fine needle aspiration (FNA) cytopathology and histological pathology of nine nodules.

Nodule number	FNA cytopathology	Histological pathology
1	A small amount of thyroid follicular epithelial cells and no tumor cells	Thyroid atypical adenoma
2	Thyroid follicular epithelial cells and no tumor cells	Thyroid adenoma
3	Suspicious for a follicular neoplasm	Thyroid follicular carcinoma
4	Thyroid follicular epithelial cells and no tumor cells	Thyroid follicular carcinoma
5	No exception of follicular adenoma	Nodular goiter with adenomatous hyperplasia
6	Thyroid follicular adenoma	Nodular goiter with adenomatous hyperplasia
7	Tumor-like lesion from thyroid follicular epithelial cells. Tumor or adenomatous change cannot be distinguished because no specific capsule was seen.	Nodular hashimoto thyroiditis
8	Consistent with thyroid follicular neoplasm, and thyroid adenoma was considered	Nodular goiter with adenomatous hyperplasia
9	Thyroid follicular epithelial cells and no tumor cells	Nodular goiter

The CUS features of all thyroid nodules were recorded according to the halo, echogenicity, internal component, echotexture (homogenous or heterogenous), calcifications, and vascularity. Halos were classified as absent, regularly thin, or irregular (including thick halos, incomplete halos, and halos of different widths). Echogenicity was classified as hypoechogenicity, isoechogenicity, hyperechogenicity, or marked hyperechogenicity relative to the surrounding normal parenchyma. The internal component of a nodule was classified as solid (defined as composed entirely or nearly entirely of soft tissue, with only a few tiny cystic spaces) (6), predominantly solid, and predominantly cystic. Calcifications, when present, were categorized as microcalcifications, disrupted rim calcifications, and other types of calcifications. Microcalcifications were defined as calcifications that were ≤1 mm in diameter and visualized as tiny hyperechoic foci. Disrupted rim calcifications were defined as interrupted peripheral calcifications in association with a soft tissue rim outside the calcification. When a nodule had both microcalcifications and other types of calcifications, it was classified as having microcalcifications. The vascularity of nodules was classified into five types by Frates (7) as follows: 0 for no visible flow, 1 for minimal internal flow without a peripheral ring, 2 for a peripheral ring of flow (defined as >25% of the nodule's circumference) with minimal or no internal flow, 3 for a peripheral ring of flow with a small to moderate amount of internal flow, and 4 for extensive internal flow with or without a peripheral ring. We regarded type 4 as increased intranodular vascularity. CEUS characteristics included peak intensity (categorized as low, equal, or high) and enhanced pattern (categorized as homogenous, heterogenous, or ring enhancing). Elastography score elasticity was classified in five different patterns, adding elastography score (ESS) 0 to the version of Asteria criteria (8): ESS 0, red and blue, or blue and green, or red and green are layered distribution in cystic nodules or predominantly cystic nodules; ESS 1, homogenously in green (soft); ESS 2, predominantly in green with few blue areas/spots; ESS 3, predominantly in blue with a few green areas/spots; and ESS 4, completely in blue (hard).

TABLE 3 | Ultrasound (US) characteristics of benign and malignant thyroid nodules with intermediate and low suspicion.

US characteristics	Malignant nodules ($n = 29$)	Benign nodules ($n = 134$)	*P*-value
Halo			0.183
Absent	17 (58.6)	58 (43.3)	
Regular and thin	8 (27.6)	62 (46.3)	
Irregular	4 (13.8)	14 (10.4)	
Internal component			0.157
Solid	20 (69.0)	74 (55.2)	
Predominantly solid	9 (31.0)	47 (35.1)	
Predominantly cystic	0 (–)	13 (9.7)	
Echogenicity			0.033
Hyperechogenicity	1 (3.4)	18(13.4)	
Isoechogenicity	5 (17.2)	53 (39.6)	
Hypoechogenicity	20 (69.0)	57 (42.5)	
Marked hypoechogenicity	3 (10.3)	6 (4.5)	
Homogeneity			0.762
Homogenous	7 (24.1)	36 (26.9)	
Heterogenous	22 (75.9)	98 (73.1)	
Calcification			0.746
Absent	18 (62.1)	95 (70.9)	
Microcalcification	1 (3.4)	3 (2.2)	
Disrupted rim calcification	0 (0)	0 (0)	
Other types of calcification	10 (34.5)	36 (26.9)	
Vascularity type			0.429
Type 0	0 (0)	0 (0)	
Type 1	2 (6.9)	0 (-)	
Type 2	3 (10.3)	1 (0.7)	
Type 3	4 (13.8)	27 (20.1)	
Type 4	20 (69.0)	106 (79.1)	
Risk stratification			<0.001
Intermediate suspicion	21 (72.4)	45 (33.6)	
Low suspicion	8 (27.6)	89 (66.4)	

Review of Histopathology

An experienced pathologist who was blinded to the clinical information reviewed the histopathology of all the specimens. The papillary thyroid carcinomas (PTCs) were divided into classical PTC and follicular variants of the PTC (FVPTC).

Statistical Analysis

The statistical analysis was performed with the SPSS statistical package (Version 19.0, SPSS Chicago, IL, United States)

TABLE 4 | Contrast-enhanced ultrasonography (CEUS) and elastosonography (ES) characteristics of malignant and benign thyroid nodules.

CEUS and ES characteristics	Malignant nodules ($n = 29$)	Benign nodules ($n = 134$)	*P*-value
Enhanced pattern			<0.001
Ring enhancing	11 (37.9)	89 (66.4)	
Homogenous	2 (6.9)	24 (17.9)	
Heterogenous	15 (51.7)	16 (11.9)	
No enhancement	1 (3.4)	5 (3.7)	
Peak intensity*			0.289
High	10 (34.5)	55 (41.0)	
Equal	9 (31.0)	51 (38.1)	
Low	9 (31.0)	21 (15.7)	
Elastography score†			0.015
0	1 (3.8)	13 (9.7)	
1	0 (–)	12 (9.0)	
2	11 (42.3)	68 (50.7)	
3	9 (34.6)	36 (26.9)	
4	5 (19.2)	5 (3.7)	

**The peak intensity of two nodules was not determined because the nodules were too large and the surrounding thyroid parenchyma could not be displayed in the same plane for reference.*

†*The ES of the three nodules was not determined because the nodules were too close to the carotid artery and the results were unreliable.*

and MedCalc 11.4.2.0 software (MedCalc Software, Ostend, Belgium). The quantitative data were expressed as the mean ± standard deviation. The Student's *t*-test was used for comparing the groups. The χ^2 test or Fisher's exact test was used to compare categorical data. The sensitivity, specificity, positive predictive value (PPV), negative predictive value (NPV), and accuracy were calculated through a comparison with the pathological findings. A receiver operating characteristic (ROC) curve analysis was used to compare CEUS, ES, and CUS. A $P < 0.05$ was considered statistically significant.

RESULTS

Clinical Characteristics

The clinical characteristics are summarized in **Table 1**. The age, gender, nodule size, and incidence of coexistence with Hashimoto thyroiditis (HT) did not significantly differ between the benign and malignant groups ($P > 0.05$). The results of the cytopathology and histopathology of the nine nodules that underwent FNA are summarized in **Table 2**. Histological pathology demonstrated that 29 lesions (17.8%) were malignant, and 134 lesions (82.2%) were benign. One hundred one nodular goiters (75.4%) constituted the majority of benign lesions, 18 of the 134 lesions were adenomatous nodules (ANs). The remainder of the benign lesions consisted of six follicular adenomas (FAs, 25.4%) and nine HTs (6.7%). Of the malignant lesions, 21 cases were PTCs, with 17 classical variant and 4 follicular variants, 7 cases were follicular carcinomas (FCs), and 1 case was medullary carcinoma (MC). Cervical lymph node metastasis was confirmed in one FC and six PTCs. Metastatic lesions were found in cervical striated muscles and fibrous connective tissues in another FC.

US Characteristics

The CUS characteristics are summarized in **Table 3**. No significant difference was observed in the US features of absent or irregular halos (a solid internal component, a heterogenous echo

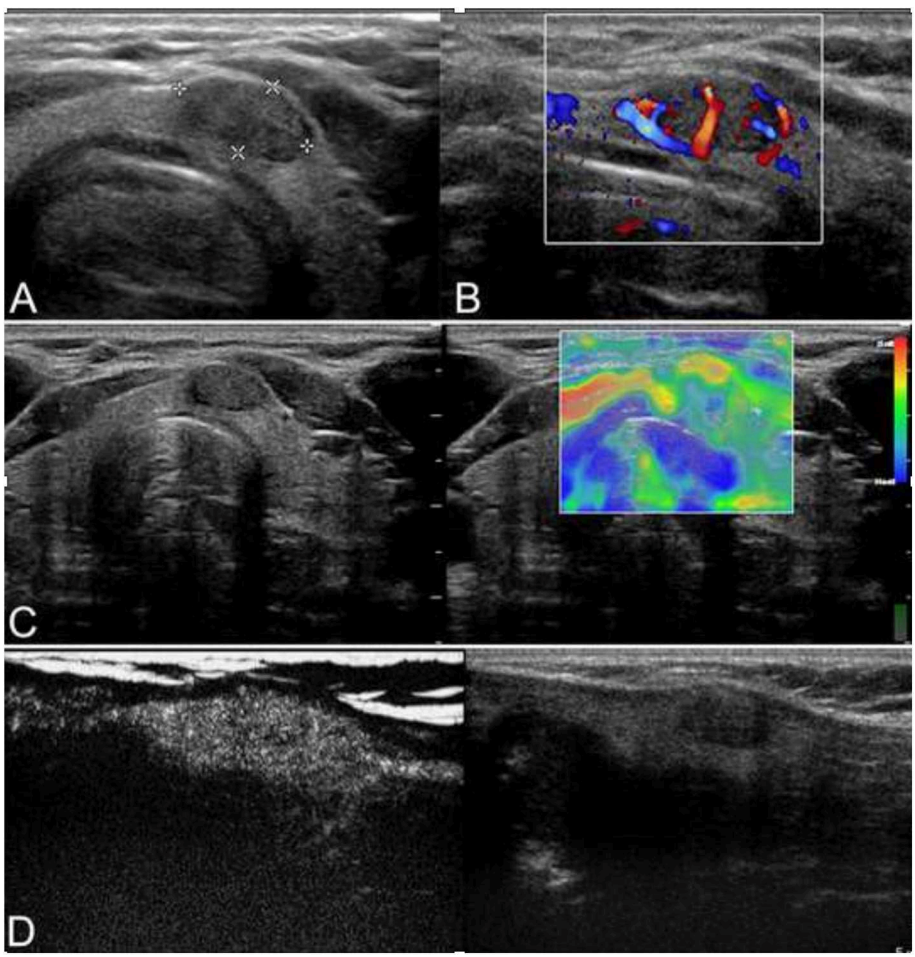

FIGURE 1 | Ultrasound of a 42-year-old man who incidentally detected a thyroid nodule is shown. **(A)** Conventional ultrasonography (CUS) showed that there was a solid hypoechoic nodule with a regular margin in the isthmus of the thyroid. The nodule was of intermediate suspicion. **(B)** Color Doppler showed intranodular and peripheral vascularity. **(C)** The elastography score was 2, indicating that the nodule was soft. **(D)** Contrast-enhanced ultrasonography (CEUS) revealed heterogenous enhancement. The nodule was a papillary thyroid carcinoma (PTC) confirmed by histological pathology.

texture, and microcalcification or disrupted rim calcification between benign and malignant lesions). Moderate or abundant blood flow (Frates type 3 or 4) was detected in the majority of the nodules with intermediate- and low-suspicion patterns. The difference in increased intranodular vascularity (Frates type 4) between benign and malignant lesions was not statistically significant ($P > 0.05$). Of the malignant nodules, two PTCs showed peripheral vascularity without intranodular vascularity, and four PTCs showed partial hypervascularity with perforating vessels into the nodule. Regular peripheral and intranodular vascularity was found in the other 15 malignant lesions.

The CEUS characteristics and ES of the nodules are shown in **Table 4** and **Figures 1–4**. Heterogenous enhancement was significantly ($P < 0.001$) associated with a malignant outcome with a 10.1 odds ratio [OR; 95% confidence interval (CI) ranging from 3.9 to 25.7]. The sensitivity, specificity, positive predictive value, and negative predictive value were 51.7, 88.1, 48.4, and 89.4%, respectively. The enhancement patterns of 12 PTCs and 2 FCs and 1 MC were heterogenous, 2 PTCs were homogenous, 1 PTC had no enhancement, and the remaining 6 PTCs and 5 FCs exhibited a ring-enhancing pattern. Among the benign nodules, 89 cases (66.4%) showed a ring-enhancing pattern; 24 cases (17.9%) showed homogenous enhancement, including 18 nodular goiters and 3 HT; and 16 cases (11.9%) showed heterogenous enhancement, including 10 nodular goiter, 2 FAs, and 4 HTs. The intensity of enhancement was not significantly different ($P = 0.289$). Most of the nodules showed soft texture in elasticity imaging, and the difference in the ES between the benign and malignant groups was significant ($P = 0.015$).

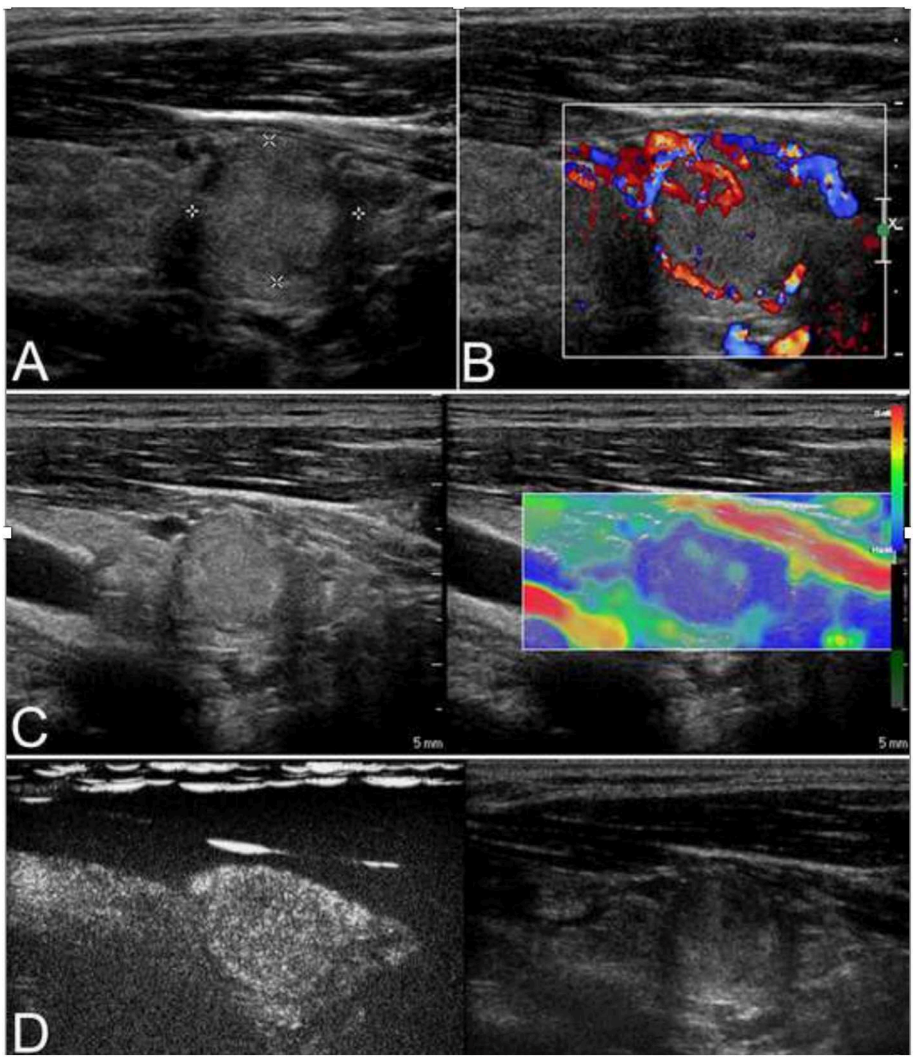

FIGURE 2 | This case is a 27-year-old man with an follicular carcinoma (FC) nodule. **(A)** Conventional ultrasonography (CUS) showed a solid hyperechoic nodule in the left lobe that was associated with a regular thin halo and an inside area that was hypoechoic, which is indicative of low suspicion. **(B)** Abundant intranodular and peripheral vascularity was detected. **(C)** The elastography score was 2, indicating a soft stiffness. **(D)** Contrast-enhanced ultrasonography (CEUS) revealed heterogenous enhancement.

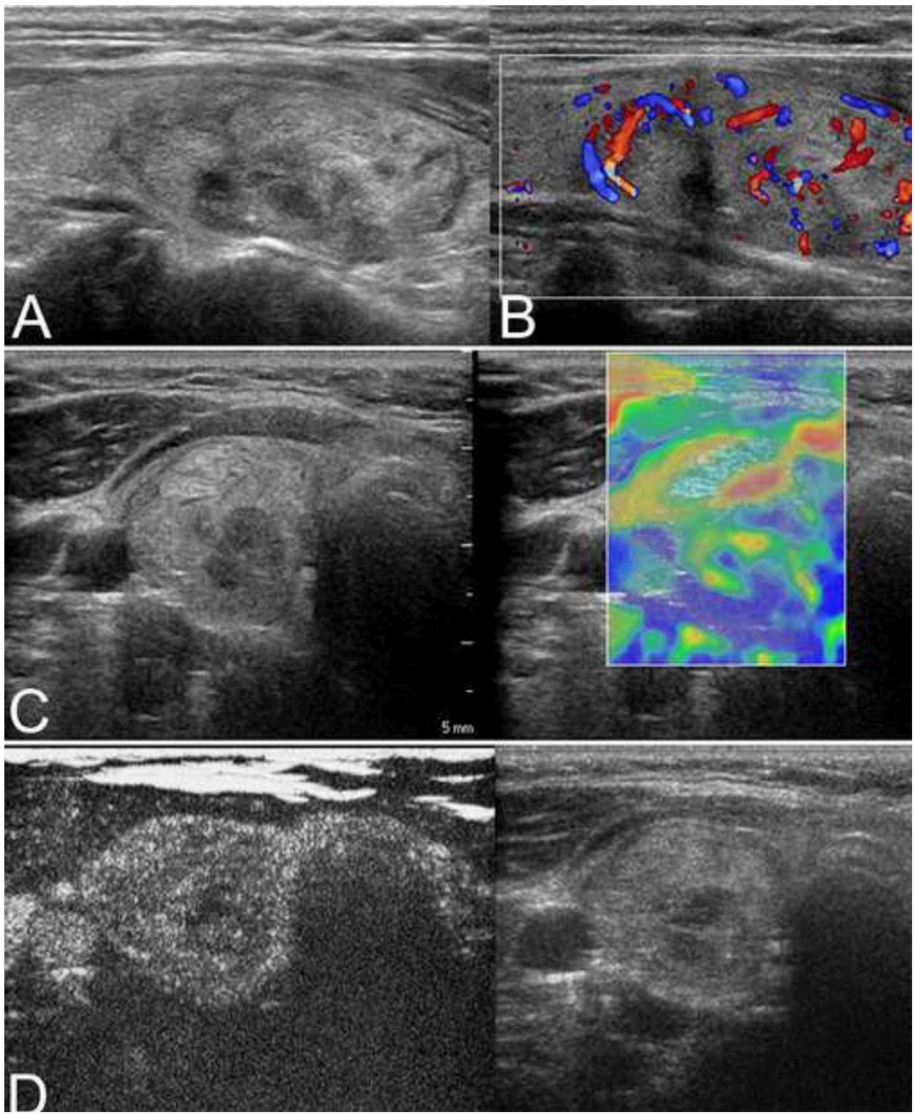

FIGURE 3 | (A) The isoechoic solid nodule with a regular thin halo was evaluated as low suspicion by conventional ultrasonography (CUS) in a 38-year-old man. **(B)** Color Doppler showed intranodular and peripheral vascularity. **(C)** The elastography score was 3, indicating a hard stiffness. **(D)** Contrast-enhanced ultrasonography (CEUS) revealed ring enhancement. The nodule was a follicular adenoma.

Diagnostic Performance of the CEUS and ES

Sensitivity, specificity, PPV, NPV, accuracy, and area under the curve (AUC) of CUS were 69.0, 57.5, 26.0, 89.5, 59.5, and 0.61% (95% CI, 0.53–0.69), respectively. Nodules with the CEUS patterns of heterogenous enhancement was considered malignant. The sensitivity, specificity, PPV, NPV, accuracy, and AUC for CEUS were 51.7, 88.1, 48.4, 89.4, 81.6, and 0.73% (95% CI, 0.65–0.80), respectively. The ROC curves demonstrated that the best cutoff value for ES was 3. The sensitivity, specificity, PPV, NPV, accuracy, and AUC for ES were 53.8, 69.4, 25.5, 88.6, 66.9, and 0.62% (95% CI, 0.54–0.69), respectively (**Table 5**). The CEUS showed a higher AUC than CEUS and ES (0.729 vs. 0.616, $P = 0.021$; 0.729 vs. 0.608, $P = 0.046$). We added this in *Result* and *Abstract* and emphasized in red color (lines 37 and 88–99).

DISCUSSION

High-resolution neck ultrasonography is the most important method for the evaluation of a thyroid nodule. The latest ATA guidelines have proposed criteria for risk stratification that categorizes the thyroid nodules and stratify the risk of malignancy. However, the differential diagnosis of nodules with intermediate and low suspicion is difficult. In the "British Thyroid Association Guidelines for the Management of Thyroid Cancer" (2), these nodules are defined as suspicious of follicular lesions on ultrasound and classified as indeterminate/equivocal.

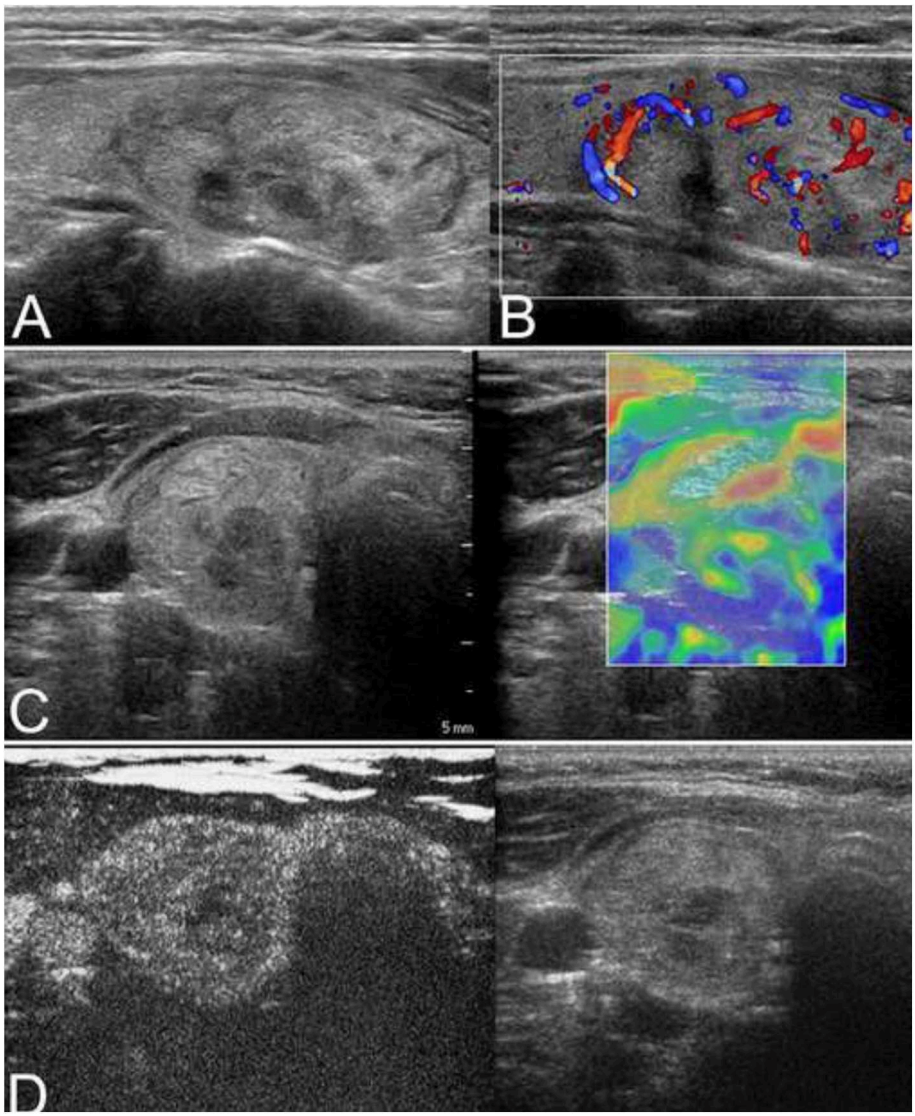

FIGURE 4 | A nodular goiter with adenomatous hyperplasia in a 59-year-old woman is shown. **(A)** Conventional ultrasonography (CUS) showed that the solid hyperechoic nodule in the right lobe was heterogenous in echotexture and had regular margins, indicative of low suspicion. **(B)** Color Doppler showed intranodular and peripheral vascularity. **(C)** The elastography score was 2, indicating a soft stiffness. **(D)** Contrast-enhanced ultrasonography (CEUS) revealed ring-enhancement.

A total of 71.4% of the nodules were thyroid tumors with a follicular growth pattern. Our study showed that the enhancement pattern was a significant factor for differentiating benign and malignant nodules with intermediate and low suspicion. Some researchers have revealed that age, sex, and tumor size are predictive parameters of malignancy in follicular neoplasms of the thyroid (diagnosed by intraoperative frozen section or FNA) (9, 10). The male gender, ages <45 years, and nodules larger than 4 cm were risk factors for malignancy. In our study, 15.7% of women and 28.6% of men had malignant nodules. Sixteen patients (10.7%) younger than 45 years of age and 13 patients (8.7%) older than 45 years of age were diagnosed with malignant lesions, with no statistically significant differences observed. Of the 29 malignant nodules, only 3 (10.3%) were larger than 4 cm. Therefore, using sex, age, and nodule size as the predictive malignant parameters may result in missed diagnoses and misdiagnoses.

Conventional ultrasound features such as a solid internal component, hypoechogenicity, irregular margins, a taller-than-wide shape, and microcalcification are predictive of thyroid carcinoma (11, 12). However, these features are classical malignant characteristics for non-follicular neoplasms. Koike et al. (13) found that the sensitivity of preoperative US diagnosis was 18.2% for follicular neoplasms. Multiple logistic regression analyses revealed that conventional ultrasound could not identify FC and FA (13). The results of this study were similar to these previous results.

TABLE 5 | Diagnostic efficiency of the contrast-enhanced ultrasonography (CEUS), elastosonography (SE) and conventional ultrasonography (CUS).

	Se (%)	Sp (%)	PPV (%)	NPV (%)	Ac (%)	AUC (95% CI)*
CUES	51.7	88.1	48.4	89.4	81.6	0.729 (0.653–0.796)
SE	53.8	69.4	25.5	88.6	66.9	0.616 (0.536–0.692)
CUS	69.0	57.5	26.0	89.5	59.5	0.608 (0.528–0.685)

CEUS, contrast-enhanced ultrasonography; ES, elastosonography; CUS, conventional ultrasonography; Se, sensitivity; Sp, specificity; PPV, positive predictive value; NPV, negative predictive value; AUC, area under the curve; CI, confidence interval.

CEUS can reflect the state of microcirculation perfusion of nodules. Three meta-analyses showed that both the sensitivity and specificity of CEUS were more than 85% (14–16). Most research have suggested that a heterogenous enhancement pattern is a reliable index for predicting malignancy and that a ring-enhancement pattern is a feature of benign nodules. Our study has revealed that the predictivity of malignancy of ATA risk stratification is improved by adding CEUS. The malignancy risk of the intermediate and low suspicious nodules is 5–20%. The risk can increase to 38.5% when the nodule shows heterogenous enhancement. Despite the low sensitivity (51.7%), it has a very high specificity and OR for malignancy. Of the 29 malignant nodules, 12 PTCs and 2 FCs and MC presented with heterogenous enhancement, which might be due to the more heterogenous growth of malignant nodules and the more imbalanced blood distribution, with the coexistence of areas of rich and poor microvasculature. In addition, malignant nodules contain regions of complicated morphological collagen degeneration, which have either no small vessels or vessels whose caliber is so small that microbubbles cannot enter, resulting in heterogenous enhancement. However, the other six PTCs and five FCs presented with ring enhancement. Two FVPTC nodules were 3.8 and 4.0 cm in ultrasound images, but the pathological size of the cancer area was only 0.4 and 0.5 cm, respectively, with the surrounding tissue presenting with nodular goiter. This finding may result in a benign enhancement pattern. The reason that malignant nodules showed ring enhancement may be that the nodules were surrounded by vessels or that vessels existed in the capsule of the nodule, which is consistent with the color Doppler features.

Elastosonography provided an estimation of tissue stiffness. In our study, only 14 malignant nodules were hard, with 3–4 elastography scores. The other 15 malignant nodules were relatively soft. This result was different from most studies, which reported that malignant thyroid nodules were often stiff. The most likely reason is that the constitution of the cases was vastly different. In this study, 24.1% of the malignant nodules were FCs, and 13.8% of the nodules were FVPTCs. Pathological changes in these nodules showed that follicular cells containing colloid were abundant, making the texture soft. Therefore, real-time elastography was not able to distinguish benign and malignant nodules with intermediate and low suspicion.

FNA is the best preoperative diagnostic method for thyroid nodules but is indeterminate in 15–20% of the cases especially when follicular neoplasms are involved. When a follicular neoplasm is suspected, the histological possibilities include an AN, FA, or FC. FVPTC will also sometimes fall into this category when the nuclear features are more subtle. These features cannot be distinguished by the use of cytology alone because the evaluation of morphology is subjective (17, 18) and the sample is too limited to represent the entire heterogenous lesion. In addition, the presence of capsule or vessel invasion for diagnosing FC cannot be evaluated by FNA (19). One FC in this study was suspicious for a follicular neoplasm, and the other FC exhibited only thyroid follicular epithelial cells and no tumor cells. Another lesion that was suspicious for FC by FNA was a nodular goiter with adenomatous hyperplasia confirmed by surgical pathology.

A limitation of our study is selective bias. This study is a retrospective study, and the subjects included were patients undergoing surgery. Whether the results are applicable to all clinical conditions remains to be verified. In addition, the strain ratio was not evaluated with ES. Further large studies using more indicators are needed to obtain a more accurate value.

CONCLUSIONS

The CEUS enhancement pattern is helpful for differentiating between benign and malignant nodules with an intermediate or low suspicion. Heterogenous enhancement is associated with malignant nodules, a finding that could modify the clinical decision to avoid the misdiagnosis of FC in some patients. CUS characteristics, other qualitative CEUS indices, ES, and FNA have limited value.

DATA AVAILABILITY STATEMENT

All datasets generated for this study are included in the article/supplementary material.

ETHICS STATEMENT

This prospective study was approved by the ethics committee of Peking Union Medical College Hospital, and informed consent was obtained. The patients/participants provided their written informed consent to participate in this study. Written informed consent was obtained from the individual(s) for the publication of any potentially identifiable images or data included in this article.

AUTHOR CONTRIBUTIONS

BZ and YJ conceived and designed the study. JX, RL, and RZ collected the data. XY and SZ performed the analysis. XL and XZ prepared all the figures and tables. XX, LG and QW were major contributors in writing the manuscript. SF edited the manuscript. All authors read and approved the final manuscript.

FUNDING

This study was supported by a grant from the National Natural Science Foundation of China (No. 81541131), the Capital Development Research Foundation (CD 2016-2-40110), and the International Science and Technology Cooperation Program of China (2015DFA30440).

REFERENCES

1. Haugen BR, Alexander EK, Bible KC, Doherty GM, Mandel SJ, Nikiforov YE, et al. 2015 American thyroid association management guidelines for adult patients with thyroid nodules and differentiated thyroid cancer: the American thyroid association guidelines task force on thyroid nodules and differentiated thyroid cancer. *Thyroid*. (2016) 26:1–133. doi: 10.1089/thy.2015.0020
2. Perros P, Boelaert K, Colley S, Evans C, Evans RM, Gerrard Ba G, et al. Guidelines for the management of thyroid cancer. *Clin Endocrinol*. (2014) 811:1–122. doi: 10.1111/cen.12515
3. Giusti M, Campomenosi C, Gay S, Massa B, Silvestri E, Monti E, et al. The use of semi- quantitative ultrasound elastosonography in combination with conventional ultrasonography and contrast-enhanced ultrasonography in the assessment of malignancy risk of thyroid nodules with indeterminate cytology. *Thyroid Res*. (2014) 7:9. doi: 10.1186/s13044-014-0009-8
4. Cantisani V, Consorti F, Guerrisi A, Guerrisi I, Ricci P, Di Segni M, et al. Prospective comparative evaluation of quantitative-elastosonography (Q-elastography) and contrast-enhanced ultrasound for the evaluation of thyroid nodules: preliminary experience. *Eur J Radiol*. (2013) 82:1892–8. doi: 10.1016/j.ejrad.2013.07.005
5. Liang XN, Guo RJ, Li S, Zheng ZM, Liang HD. Binary logistic regression analysis of solid thyroid nodules imaged by high-frequency ultrasonography, acoustic radiation force impulse, and contrast-enhanced ultrasonography. *Eur Rev Med Pharmacol Sci*. (2014) 18:3601–10.
6. Grant EG, Tessler FN, Hoang JK, Langer JE, Beland MD, Berland LL, et al. Thyroid ultrasound reporting lexicon: white paper of the ACR thyroid imaging, reporting and data system (TIRADS) committee. *J Am Coll Radiol*. (2015) 12:1272–9. doi: 10.1016/j.jacr.2015.07.011
7. Frates MC, Benson CB, Doubilet PM, Cibas ES, Marqusee E. Can color doppler sonography aid in the prediction of malignancy of thyroid nodules? *J Ultrasound Med*. (2003) 22:127–31. doi: 10.7863/jum.2003.22.2.127
8. Asteria C, Giovanardi A, Pizzocaro A, Cozzaglio L, Morabito A, Somalvico F, et al. US- elastography in the differential diagnosis of benign and malignant thyroid nodules. *Thyroid*. (2008) 18:523–31. doi: 10.1089/thy.2007.0323
9. Paramo JC, Mesko T. Age, tumor size, and in-office ultrasonography are predictive parameters of malignancy in follicular neoplasms of the thyroid. *Endocr Pract*. (2008) 14:447–51. doi: 10.4158/EP.14.4.447
10. Baloch ZW, Fleisher S, LiVolsi VA, Gupta PK. Diagnosis of "follicular neoplasm": a gray zone in thyroid fine-needle aspiration cytology. *Diagn Cytopathol*. (2002) 26:41–4. doi: 10.1002/dc.10043
11. Kwak JY, Han KH, Yoon JH, Moon HJ, Son EJ, Park SH, et al. Thyroid imaging reporting and data system for US features of nodules: a step in establishing better stratification of cancer risk. *Radiology*. (2011) 260:892–9. doi: 10.1148/radiol.11110206
12. Choi YJ, Yun JS, Kim DH. Clinical and ultrasound features of cytology diagnosed follicular neoplasm. *Endocr J*. (2009) 56:383–9. doi: 10.1507/endocrj.K08E-310
13. Koike E, Noguchi S, Yamashita H, Murakami T, Ohshima A, Kawamoto H, et al. Ultrasonographic characteristics of thyroid nodules: prediction of malignancy. *Arch Surg*. (2001) 136:334–7. doi: 10.1001/archsurg.136.3.334
14. Yu D, Han Y, Chen T. Contrast-enhanced ultrasound for differentiation of benign and malignant thyroid lesions: meta-analysis. *Otolaryngol Head Neck Surg*. (2014) 151:909–15. doi: 10.1177/0194599814555838
15. Ma X, Zhang B, Ling W, Liu R, Jia H, Zhu F, et al. Contrast-enhanced sonography for the identification of benign and malignant thyroid nodules: systematic review and meta-analysis. *J Clin Ultrasound*. (2016) 44:199–209. doi: 10.1002/jcu.22311
16. Sun B, Lang L, Zhu X, Jiang F, Hong Y, He L. Accuracy of contrast-enhanced ultrasound in the identification of thyroid nodules: a meta-analysis. *Int J Clin Exp Med*. (2015) 8:12882—9.
17. Olson MT, Boonyaarunnate T, Aragon Han P, Umbricht CB, Ali SZ, Zeiger MA. A tertiary center's experience with second review of 3885 thyroid cytopathology specimens. *J Clin Endocrinol Metab*. (2013) 98:1450–7. doi: 10.1210/jc.2012-3898
18. Olson MT, Clark DP, Erozan YS, Ali SZ. Spectrum of risk of malignancy in subcategories of atypia of undetermined significance. *Acta Cytol*. (2011) 55:518–25. doi: 10.1159/000333232
19. Wang CC, Friedman L, Kennedy GC, Wang H, Kebebew E, Steward DL, et al. A large multicenter correlation study of thyroid nodule cytopathology and histopathology. *Thyroid*. (2011) 21:243–51. doi: 10.1089/thy.2010.0243

Conflict of Interest: The authors declare that the research was conducted in the absence of any commercial or financial relationships that could be construed as a potential conflict of interest.

frontiers in Oncology

REVIEW
published: 28 February 2020
doi: 10.3389/fonc.2020.00268

Current Understanding of the Mechanisms Underlying Immune Evasion From PD-1/PD-L1 Immune Checkpoint Blockade in Head and Neck Cancer

Victor C. Kok [1,2]*

[1] Department of Medical Oncology, Kuang Tien General Hospital Cancer Center, Taichung, Taiwan, [2] Department of Bioinformatics and Medical Engineering, Asia University Taiwan, Taichung, Taiwan

Starting in 2014, large phase III clinical trials began to disclose the study results of using programmed death (PD)-1 immune checkpoint inhibitors (ICIs) (pembrolizumab, nivolumab) and PD-ligand (L)1 (atezolizumab, durvalumab, avelumab) ICIs immunotherapy in patients with advanced head and neck squamous cell carcinoma (HNSCC). In the recurrent and metastatic (R/M), cisplatin-refractory setting, nivolumab achieved a 2.2-fold increase of the median 1-year overall survival as compared with investigators' choice of salvage chemotherapy (36.0 vs. 16.6%). A paradigm shift to the winning regimen, pembrolizumab combined with platinum and infusional fluorouracil, has outperformed the past gold standard of cetuximab-based platinum and fluorouracil combination in terms of overall survival (median, 13.6 vs. 10.1 mo) when administered as the first-line treatment for R/M HNSCC. Nevertheless, many patients still did not respond to the PD-1/PD-L1 checkpoint inhibitor treatment, indicating innate, adapted, or quickly acquired resistance to the immunotherapy. The mechanisms of resistance to ICIs targeting the PD-1/PD-L1 signaling pathway in the context of HNSCC are the focus of this review. The past 5 years have seen improved understanding of the mechanisms underlying checkpoint inhibition resistance in tumor cells, such as: tumor cell adaption with malfunction of the antigen-presenting machinery via class I human leukocyte antigen (HLA), reintroduction of cyclin D–cyclin-dependent kinase (CDK) 4 complex to cell cycles, enrichment of CD44+ cancer stem-like cells, or development of inactivating mutation in IKZF1 gene; impairment of T-cell functions and proliferation through mutations in the interferon-γ-regulating genes, suppression of the stimulator of interferon genes (STING) pathway, or resulted from constitutional nutritional iron deficiency state; metabolic reprogramming by cancer cells with changes in metabolites such as GTP cyclohydrolase 1, tetrahydrobiopterin, kynurenine, indoleamine 2,3-dioxygenase, and arginase 1; defective dendritic cells, CD-69 sufficient state; and the upregulation or activation of the alternative immune checkpoints, including lymphocyte activation gene-3 (LAG3), T-cell

OPEN ACCESS

Edited by:
Vincent Vander Poorten, KU Leuven, Belgium

Reviewed by:
Sylvie Rottey, Ghent University, Belgium
Gyorgy B. Halmos, University Medical Center Groningen, Netherlands

***Correspondence:**
Victor C. Kok
victorkok@asia.edu.tw

Specialty section:
This article was submitted to Head and Neck Cancer, a section of the journal Frontiers in Oncology

Received: *19 December 2019*
Accepted: *17 February 2020*
Published: *28 February 2020*

Citation:
Kok VC (2020) Current Understanding of the Mechanisms Underlying Immune Evasion From PD-1/PD-L1 Immune Checkpoint Blockade in Head and Neck Cancer. Front. Oncol. 10:268. doi: 10.3389/fonc.2020.00268

immunoglobulin and ITIM domain (TIGIT)/CD155 pathway, T-cell immunoglobulin mucin-3 (TIM-3), and V domain-containing Ig suppressor of T-cell activation (VISTA). Several potential biomarkers or biosignatures, which could predict the response or resistance to the PD-1/PD-L1 checkpoint immunotherapy, are also discussed.

Keywords: PD-1/PD-L1 signaling pathway, HNSCC, immune checkpoint blockade, cancer immunotherapy, innate resistance, adapted resistance, immune evasion, head and neck cancer

INTRODUCTION

Scope of Problems

Head and neck cancers encompass a group of malignancies arising from several anatomical mucosal sites, including the nasal cavity, paranasal sinuses, nasopharynx, oropharynx, hypopharynx, larynx and lips, and oral cavity. According to GLOBOCAN epidemiological estimates of incidence and mortality of cancer worldwide, in 2018, there were ∼835,000 new cases of cancer arising from the lips, oral cavity, naso-, oro-, and hypo-pharynx and larynx; with the number of deaths in the same year being ∼431,000 (1). The majority (95%) of histopathological types of head and neck cancer is squamous cell carcinoma (HNSCC) (2). Virus-related nasopharyngeal carcinoma will be included in this review because of its immunogenicity and encouraging trial outcomes (3, 4). The tumorigenesis can separate head and neck cancers into virus-related (Epstein-Barr virus-related nasopharyngeal carcinoma (NPC) and human papillomavirus (HPV)-positive oropharyngeal HNSCC) cancer and non-viral (HPV-negative) HNSCC, the latter being related to smoking, alcohol, and betel quid consumption in etiology.

Early-stage and locally advanced stage HNSCC should be treated with curative intent incorporating radical surgical resection or radical radiotherapy combined with chemotherapy. More than 65% of previously treated HNSCC will develop local recurrence or distant metastasis (5). It is very challenging for the head and neck cancer team to manage patients with unresectable locally advanced stage, relapsed or metastatic (R/M) HNSCC, mainly because of the high propensity for intrinsic, spatial, and acquired resistance to chemotherapeutic agents, radiotherapy, and anti-epidermal growth factor receptor monoclonal antibodies. The current first-line regimen for R/M HNSCC adopted a new paradigm in 2019, when the results of the randomized controlled trial, comparing pembrolizumab combined with platinum and infusional 5-fluorouracil to the past gold-standard regimen of cetuximab plus the same chemotherapy combination, confirmed an overall survival benefit (hazard ratio, HR, for death at 0.65, 95% confidence interval, CI, 0.53–0.80) favoring the pembrolizumab-based treatment arm (**Table 1**). Pembrolizumab is an anti-programmed cell death (PD)-1 monoclonal antibody, previously known as MK-3475, and subsequently, lambrolizumab (8).

Abbreviations: APOBEC, Apolipoprotein B mRNA editing enzyme, catalytic polypeptide-like; BDSC, Bone marrow-derived stromal cell; BMSC, Bone marrow-derived suppressor cell; CPS, Combined positive score; HNSCC, Head and neck squamous cell carcinoma; ICB, Immune checkpoint blockade; ICP, Immune checkpoint; IDO1, Indoleamine 2,3-dioxygenase-1; IKZF1, IKAROS family zinc finger 1; JAK, Janus kinase; MDSC, Myeloid-derived suppressor cell; MMR, Mismatched Repair; ORR, Overall Response Rate; PD-L1, Programmed death-ligand 1; PFS, Progression-free survival; R/M, Relapsed/metastatic; STAT, signal transducer and activator of transcription; STING, Stimulator of Interferon Genes; TCGA, The Cancer Genome Atlas (program); TIGIT, T-cell immunoglobulin and ITIM domain; Tim-3, T cell immunoglobulin and mucin-domain containing-3; TMB, Tumor mutation burden; TME, Tumor microenvironment; VISTA, V domain-containing Ig suppressor of T-cell activation.

The Rationale of Anti-PD-1/PD-Ligand (L)1 Immunotherapy for R/M HNSCC

One of the hallmarks of cancer is the ability of cancer cells to evade immune destruction (9). PD-1 is a co-inhibitory receptor on the cell surface of cytotoxic T lymphocytes. The ligation of PD-1 and PD-L1 or PD-L2 on tumor cells or antigen-presenting cells (APCs) elicits an immunosuppressive response, which implements subsequent metabolic reprogramming in T cells, decreases effector T cells and memory T cells, and increases Treg and exhausted T cell abundance (10). For the past few years, the abundance of PD-L1 protein in the HNSCC tumor, with its microenvironment sphere, has been the focus of numerous studies (2, 11–17). Observe the oral cavity squamous cell carcinoma (OCSCC) as an example, the prevalence of PD-L1 positivity has been reported in 45-87% of cases, depending on the cut-off value for positivity, whether cytoplasmic staining was counted as positive, and inclusion of the proportion of HPV+ cancer cases (2, 11). The PD-1/PD-L1 axis applies immunosuppressive signals, inducing anergy of cytotoxic T-cells; thus, the blockade of this ligation (analogous to releasing the brake) becomes a strong rationale for anti-PD-1 immunotherapy for R/M HNSCC.

The Recent Development of Anti-PD-1/PD-L1 Monoclonal Antibody-Based Treatment for R/M HNSCC

Table 2 attempts to summarize the recent relevant clinical trials investigating PD-1 or PD-L1 blockade in R/M HNSCC or NPC. Usually, NPC does not belong to the classical HNSCC membership due to unique tumor pathogenesis and different treatment protocols. However, anti-PD-1 therapy for NPC will be shown in this review to give our readers a broader picture of the immunotherapy comparing classical HNSCCs to NPC. The same would apply to HPV-positive oropharyngeal cancer. Overall response rate (ORR), progression-free survival (PFS), duration of response (DoR), and overall survival (OS) are shown if these results are available in the published paper. To date, only the following two anti-PD-1 monoclonal antibodies, pembrolizumab and nivolumab, and two anti-PD-L1 monoclonal antibodies, durvalumab, and atezolizumab (anti-PD-L1), have been tested in

TABLE 1 | Summary of data demonstrating the evolving new paradigms of systemic treatment for R/M HNSCC over 12 years.

Outcomes	Platinum + 5-FU (6)	Cetuximab + Platinum + 5-FU (6)	Pembrolizumab + Platinum + 5-FU (7)*
No. of patients	$n = 200$	$n = 222$	$n = 281$
Overall Response Rate (95% CI)	20% (15–25%)	36% (29–42%)	36.4% (not given)
Progression-Free Survival (mo.)	3.3 (2.9–4.3)	5.6 (5.0–6.0)	HR = 0.84 (95% CI, 0.69–1.02)*
Overall Survival in mo. (95% CI)	7.4 (6.4–8.3)	10.1 (8.6–11.2)	13.6 (not given)
Hazard ratio for OS (95% CI)	0.80 (0.64–0.99)		
		0.65 (0.53–0.80)	

**Results shown here represent the subgroup of patients whose Combined Positive Score (CPS) for PD-L1 was ≥1. The exact figure for progression-free survival was not given in the Abstract.*

R/M HNSCC (**Table 2**). As yet, there is only one published phase I study regarding avelumab, a PD-L1 inhibitor, in R/M HNSCC (27–29).

The efficacy of anti-PD-1 and anti-PD-L1 for R/M HNSCC, regardless of its use at as salvage therapy, in the second-line, or even in the first-line while combined with platinum plus infusional 5-fluorouracil, the ORRs were fairly poor across the board. When used in the first-line combined with PF chemotherapy for R/M HNSCC, the response rate was reported as 36.4% (7). Nearly 64% of the patients' tumors demonstrated either primary or adaptive resistance [cancer cells salvaged themselves by resorting to immunoediting and thus, further created an immunosuppressive tumor microenvironment (TME)] (30) to the combination immunochemotherapy.

This review serves to present the recent research findings with implications on the mechanisms of immune evasion from the anti-PD1 or anti-PD-L1 immune checkpoint blockade.

METHODS

Methodology for the Literature Search

A dynamic PubMed literature search until September 14, 2019, using the Medical Subject Headings and the Boolean search terms, was used to retrieve articles indexed under keywords, such as "head and neck cancer," "head and neck squamous cell carcinoma," "HNSCC," "oral cavity squamous cell carcinoma," "OCSCC," "immunotherapy," "pembrolizumab," "nivolumab," "atezolizumab," "durvalumab," "avelumab," "immune escape," "immune evasion," "resistance," "relapsed or metastatic," "unresected locally advanced," "mechanism," "PD-L1," "PD-1," "immune checkpoint inhibitor," "immunoediting," "tumor microenvironment," "immunosuppressive," and "adapted resistance." The American Society of Clinical Oncology Meeting Abstract database was also searched for the relevant trials. Also, a hand search from the "Similar Articles" inside the PubMed panel was performed to retrieve related articles.

In the EndNote software, "Find Duplicates" function was activated to remove duplicated papers. "Find Full Text" was then activated to download those articles available for download. The Harvard Medical School digital library, "BrowZine," was then used to complete all full-text downloads for the EndNote library. Review articles represented most retrieved articles in the library, and only a few of them would be cited in this review. Whereas, articles with primary research data from innovative experiments and clinical trials would be selected.

RESULTS AND DISCUSSION

HNSCC Cancer Cells Remodel and Shape an Immunosuppressive TME

Within the tumor microenvironment, there exists a plethora of cytokines, and various infiltrating immune cells, such as CD8+ T cells and APCs, including dendritic cells, anti-tumoral M1 macrophages, pro-tumoral M2 macrophages [tumor-associated macrophages (TAM), myeloid-derived suppressor cells (MDSC), cancer-associated fibroblasts (CAFs), and regulatory T cells (Tregs) (**Figure 1**)]. Like the immunosuppressive lymphocytic Tregs, MDSC functions as myeloid regulatory cells (MRC) and is further separated into monocytic-MDSC and polymorphonuclear-MDSC (31). A study by Takahashi and colleagues identified that CAFs stimulate and polarize the increase of CD68+ and CD163+ pro-tumoral macrophages in the TME (32).

Primary Resistance to ICIs in HNSCC

A Birmingham research group developed a 54-gene hypoxia-immune classifier to prognosticate patients with HNSCC, and uncovered that tumors that are high-hypoxia/low-immune are associated with "immune-desert" microenvironmental profiles (33). Hypoxia within a tumor microenvironment will increase the immune-inhibitory PD-L1 generation through the hypoxia-inducible factor (HIF)-1α signaling (33, 34). An immune desert tumor microenvironment promotes immune evasion for cancer cells. These cold tumors respond poorly to single-agent PD-1/PD-L1 immune checkpoint (ICP) immunotherapy. The JAK family of kinases (JAK1/2/3, TYK2) is involved in PD-L1 induction in tumor, stromal, and immune cells (35). A group of investigators from Foundation Medicine Inc., Cambridge, Boston, showed that in a preclinical study focusing on endometrial carcinoma and stomach adenocarcinoma, somatic mutation of JAK1 with loss of function (meaning loss of JAK1-mediated interferon response) results in immune evasion, particularly in microsatellite instability-high (MSI-H) tumors with high total mutational burden (TMB) (35).

TABLE 2 | Summary of clinical trial results of PD-1 or PD-L1 blockade in R/M HNSCC and NPC showing overall response rate (ORR), duration of response (DoR), progression-free survival (PFS), and overall survival (OS).

1st Author/ published year/ (References)/EudraCT No.	Phase of study/Study Name/No. pts	Key immunotherapy drug	Biomarker	Failed treatment previously	Treatment outcomes
Chow/2016/(18)/2012-005771-14	Phase Ib/KEYNOTE-012 Expansion Cohort/*n* = 132	Pembrolizumab at a fixed dose, 200 mg Q3W	Irrespective of biomarker status	57% failed two or more lines of chemo	6-mo. PFS = 23%; 6-mo. OS = 59%. ORR = 22% in PD-L1+ tumors. Duration of response = not reached (range, ≥ 2 to ≥ 11 mo.)
Bauml/2017/(19)/2014-002447-18	Phase II/KEYNOTE-055/*n* = 171	Pembrolizumab	82% PD-L1 positive (CPS ≥ 1%)	75% failed platinum and cetuximab or more	ORR = 16% (95% CI, 11% to 23%). Duration of response = 8 mo. (2+ to 12+ mo.); Median PFS = 2.1 mo., and median OS = 8 mo.
Hsu/2017/(13)/ 2013-004507-39	Phase Ib/KEYNOTE-028/*n* = 27 NPC	Pembrolizumab	Dako 22C3 positive ≥ 1%	70.4% failed three or more lines	ORR = 25.9% (95% CI, 11.1 to 46.3)
Cohen/2019/(20)/2014-001749-26	Phase III/KEYNOTE-040/*n* = 247 (pembro. arm)	Pembrolizumab at a fixed-dose, 200 mg Q3W	PD-L1 tumor proportion score (≥ 50% vs. < 50%)	Failed platinum-containing chemo	ORR = 14·6% (95% CI, 10.4–19.6); Duration of response = 18.4 mo (95% CI 5.8–18.4); Median PFS = 2·1 mo (95% CI 2.1–2.3); Median OS = 8.4 mo. (95% CI 6.4–9.4).
Rischin/2019/(7)/2014-003698-41	Phase III/KEYNOTE-048/*n* = 882 (entire)	Pembrolizumab vs. pembrolizumab + PF vs. cetuximab + PF	CPS for PD-L1 protein expression.	First-line for R/M HNSCC	In the CPS ≥ 1 group, ORR = 36.4% and median OS = 13.6 mo. (in pembrolizumab + PF) vs. ORR, 35.7%; OS, 10.4 mo. (in cetuximab + PF); HR = 0.65, 95% CI, 0.53–0.80).
Ferris/2016/(21); Ferris/2018/(22)/ 2013-003622-86	Phase III/CHECKMATE-141/*n* = 240 (nivo. arm)	Nivolumab 3 mg/kg Q2W	Dako positive ≥ 1%, ≥ 5%, vs. ≥ 10%.	Failed within 6 mo. of platinum therapy	ORR = 13.3% (9.3–18.3); OS = 7.7 mo. (5.7–8.8). 24-mo. OS = 16.9%.
Colevas/2018/(23)/2011-001422-23	Phase Ia/PCD4989g/*n* = 32	Atezolizumab	Responses observed irrespective of HPV or PD-L1 status.	Heavily pretreated	ORR = 22% (95% CI, 9–40%); PFS = 2.6 mo. (0.5–48.4 mo.); Median OS = 6.0 mo (range 0.5–51.6+ mo).
Segal/2019/(24)/not available	Phase I/II expansion/*n* = 62	Durvalumab 10 mg/kg Q2W for 12 mo	32.3% had tumor cell PD-L1 expression ≥ 25%	Failed median of 2 prior systemic treatments (range, 1-13)	ORR = 6.5% (15.0% for PD-L1 ≥ 25%, 2.6% for < 25%); TTP = 2.7 months (range, 1.2-5.5); PFS = 1.4 mo; OS = 8.4 mo. OS rate = 62% at 6 mo and 38% at 12 mo (42% for PD-L1 ≥ 25%, 36% for < 25%).
Siu/2018/(25)/not available	Phase II randomized, open-label/CONDOR/*n* = 67	Durvalumab (10 mg/kg Q2W) monotherapy	PD-L1–low/negative	Failed 1 platinum-containing regimen	ORR = 9.2% (3.46-19.02)
Siu/2018/(25)/not available	Phase II randomized, open-label/ CONDOR/*n* = 133	Durvalumab + tremelimumab (anti-CTLA-4)	PD-L1–low/negative	Failed 1 platinum-containing regimen	ORR = 7.8% (3.78-13.79%)
Bahig/2019/(26)/not available	Phase I-II/*n* = 35 (non-NPC)	Durvalumab (1500 mg Q4W) + tremelimumab (75 mg Q4W × 4 doses) + SBRT to metastases at cycles 2 and 3 of immunotherapy	Biomarker-unselected	Patients with ≥ 2 extracranial metastatic lesions.	Ongoing study
Elbers/2019(27)/not available	Phase I/*n* = 9 (cisplatin-unfit)	Cetuximab-radiotherapy + avelumab (concurrent 10 mg/kg Q2W + 4 months maintenance)	None	Unfit for cisplatin but with an indication for concurrent bioradiotherapy	At 12 (median, 95% CI, 8–26) months follow-up, recurrence occurred in 4/8 patients (50%).
Merlano/2018/(28)/2017-000353-39	Phase Ib-II/CONFRONT/*n* =	Avelumab 10 mg/kg Q2W + Cyclophosphamide 50 mg daily + 8 Gy radiotherapy day 8.	None	Failed at least therapy with platinum, fluorouracil, and cetuximab	Ongoing study.

EudraCT, European Union Drug Regulating Authorities Clinical Trials; NPC, nasopharyngeal carcinoma; SBRT, stereotactic body radiotherapy; CPS, Combined Positive Score.

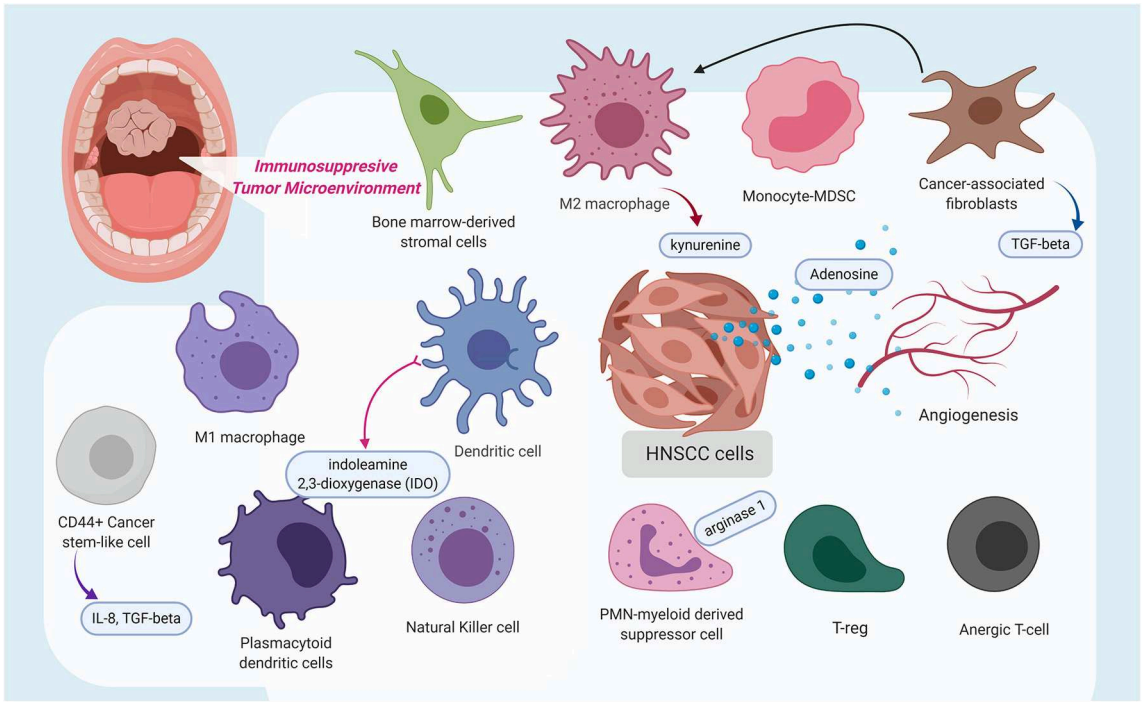

FIGURE 1 | This schematic diagram highlights the immunosuppressive tumor microenvironment (TME) in which a variety of immune cells are polarized to possess pro-tumoral features, stimulated cancer-associated fibroblasts, which release transforming growth factor-β, and even angiogenesis contribute to the immunosuppressive state. Additionally, several molecules, such as kynurenine, adenosine, indoleamine 2,3-dioxygenase, arginase 1, interleukin (IL)-8, and IL-10, were identified to contribute to a pro-tumoral immunosuppressive TME or at extreme, an immune-desert. The figure was created with BioRender.com and was exported under a paid subscription.

Soft tissue infections or deep neck infection in the head and neck region can occur in patients with locally advanced HNSCC. Antibiotic usage around the time of ICI treatment could dampen the effects of PD-1/PD-L1 blockade (36–39), as antibiotics usage for head and neck soft tissue infection will disrupt the integrity of the gut microbiome. A recent study demonstrates that disruptions in the gut microbiome composition, also known as dysbiosis, is one of the mechanisms of primary resistance to ICI therapy (36). Experiments using fecal microbiota transplantation in avatar mice demonstrate that a combination of *A. muciniphila* and *E. hirae* would increase the CCR9- or CXCR3-expressing central memory T cells in the mesenteric lymph nodes and induce dendritic cells to secrete IL-12, a Th1 cytokine essential to elicit immunogenicity during PD-1/PD-L1 blockade (36). However, the actual mechanisms by which the intestinal flora modulate ICP immunotherapy is still unclear.

An immunosuppressive tumor microenvironment can also result from immune modulatory effects of CAF (32), TAM (40), and MDSC (41) (**Figure 1**). In addition, extracellular signals from angiogenesis can also drive immune suppression by directly suppressing APCs and immune effector cells, or by augmenting the effect of Tregs, MDSC, and TAM. Reciprocally, the above-mentioned immune suppressive cells can also drive angiogenesis (**Figure 1**), rendering a vicious cycle of disrupted immune activation (42).

What Does HNSCC Possess to Avoid Immunosurveillance or Destruction via the PD-1/PD-L1 Immune Checkpoint (ICP) Blockade?

To understand the tumor microenvironment of the oral cavity SCC using the infiltrating lymphocyte repertoires as an example, several studies identified considerable antigen-experienced CD4+ and CD8+ cells, Tregs, and PD-1-expressing and Tim-3-expressing T cells, as well as lymphoid follicles with germinal center-like structures (11, 43–48). These immunosuppressive characteristics are indicative of T-cell exhaustion. **Table 2** shows that ∼60% of patients with R/M HNSCC would not respond to the PD-1/PD-L1 ICP therapy. This means that even the "release of the brakes" through blocking the ligation of PD-1/PD-L1, cannot adequately allow the cytotoxic T cells to mount an attack of significant proportions on cancer cells, which would prevent tumor shrinkage or induce mixed responses amongst measurable tumor sites. The potential mechanisms being recognized for causing acquired immune escape from the PD-1/PD-L1 ICP in the setting of head and neck cancer are summarized in **Table 3**.

There are currently four areas of research on the molecular resistance mechanisms underlying the selective pressure from PD-1/PD-L1 ICB (**Table 3**). In this review, they are categorized as tumor cell adaption, impairment of T cell functions and proliferation, changes in metabolite- and cytokine-rich tumor

TABLE 3 | Mechanisms of immune escape that are implicated in HNSCC.

Potential mechanisms	HPV+ or HPV-	Component in the immunity against cancer	References
TUMOR CELLS ADAPTION			
Antigen presenting machinery (APM) via class I HLA	No data	Activated CD8+ immunologic pressure could induce transcriptional loss of HLA class one loci; deleterious alterations in *JAK1/2* and β2-microglobulin.	(49–52)
Downregulation of the transporter associated with antigen processing (TAP)-1/2 heterodimer		APM component downregulated by the IFN-γ-phosphorylated STAT1-mediated signaling pathway; results in escaping recognition by tumor antigen-specific cytotoxic T lymphocytes.	(53, 54)
JAK mutation	Both	Leads to loss of sensitivity to IFN-γ signals.	(35)
Cyclin D–CDK4 kinase re-introduction	No data	Destabilizes PD-L1 and controls the PD-L1 abundance in tumor cells.	(55)
Enrichment of CD44+ cancer stem-like cells	No data	Activates immunosuppressive network through cytokine release.	(54)
IKZF1-inactivating mutations	No data	Genomic alterations of the master regulator IKZF1 correlates with low immune recruitment.	(56)
IMPAIRED T-CELL FUNCTIONS AND PROLIFERATION			
Nutritional iron deficiency state	Both	Affects T-cell proliferation	(57–59)
Mutations in interferon-γ-regulating genes	Both	Exhausted "Immune Class" enriched with M2 macrophages, WNT/TGF-β activation	(60, 61)
Suppression of stimulator of interferon genes (STING) pathway	HPV+	Dampens the antitumor immune response.	(62)
Inhibition of STAT1 phosphorylation	Both	Enhanced T-cell exhaustion and accumulation of MDSCs	(63)
CHANGES IN METABOLITE- AND CYTOKINE-RICH TUMOR MICROENVIRONMENTS			
Defective dendritic cells (DC)	Both	Defective cytokine- and STAT-mediated regulation of DC.	(64–66)
CD69-sufficient state	Both	Leads to effector T-cell exhaustion.	(67)
Genetic inactivation of GTP cyclohydrolase 1 (GCP1)	No data	Drastically impairs T-cell maturation.	(58)
Metabolite tetrahydrobiopterin (BH4) inhibited by kynurenine	No data	Will impair T cell function.	(58)
Indoleamine 2,3-dioxygenase-1 (IDO1); Tryptophan metabolite, kynurenine (Kyn) level	Both	IDO1 inhibits T cell proliferation, restricts tumor immune infiltration, and retards antitumor immune responses. Kyn released from ϕ, and myeloid cells activate T-reg cells.	(12, 68, 69)
Cancer-associated fibroblasts secrete TGF-β	Both	Results in restraining CD8+ T effector cells infiltrating into microenvironment. TGF-β1 also decreases the number of dendritic cells in the draining lymph nodes.	(32, 70–73)
Arginase 1 expression on microenvironment myeloid cells	Both	Arg1 leads to L-arginine depletion depriving T cells and NK cells of essential nutrients required for proliferation.	(74)
CD38-upregulation	Both	CD38 inhibits CD8+ T-cell function via adenosine receptor signaling.	(75, 76)
Ectonucleotidases CD39/CD73 axis	Both	CD39 is considered a tumor-specific dysfunction marker. Tregs use the axis to diminish anti-cancer killing.	(76–79)
Polymorphonuclear myeloid-derived suppressor cells (PMN-MDSC) activation	Both	Through the nitric oxide pathway, PMN-MDSCs impair proliferation and expression molecules in activated T cells.	(41)
Nucleotide-binding domain leucine-rich repeat and pyrin domain containing receptor 3 (NLRP3) inflammasome activation	Both	Leads to downstream interleukin (IL)-1β release. NLRP3 inflammasome/IL-1β axis increases MDSCs, Tregs and TAMs creating an immunosuppressive microenvironment.	(80)
ACTIVATION OF AND DEPENDENCE ON ALTERNATIVE IMMUNE CHECKPOINTS			
Lymphocyte activation gene-3 (LAG3) (=CD223) upregulation	More in HPV+	Induces a state of functional exhaustion in effector T-cells.	(81, 82)
T-cell immunoglobulin and ITIM domain (TIGIT)/CD155 pathway activation	Both	Augments TIGIT+ T-regs, a unique T-reg subset, leading to active suppression of anti-tumor immune response and T-cell exhaustion.	(82–85)
T-cell immunoglobulin mucin-3 (TIM-3) upregulation	Both	TIM-3 is considered a tumor-specific dysfunction marker. It dampens effector T-cell functions in the microenvironment.	(44, 48, 77, 86)
V domain-containing Ig suppressor of T-cell activation (VISTA)	Both	Leads to T-cell exhaustion and T-reg recruitment in the microenvironment.	(87, 88)

Investigated mechanisms of acquired immune escape from PD-1/PD-L1 checkpoint blockade relevant to head and neck cancer.

microenvironments, and activation of and dependence on alternative immune checkpoints.

Tumor Cell Adaption

Tumor cell adaption occurs through various processes, namely with modification of molecules causing immune escape via malfunction of the antigen-presenting machinery via class I HLA, reintroduction of cyclin D–CDK4 kinase heterodimers to cell cycles (55), enrichment of CD44+ cancer stem-like cells (54), JAK mutation (35), or development of inactivating mutation in IKZF1 gene, the master regulator of immune infiltrates recruitment (56).

Speckle-type POZ protein (SPOP) is an E3 ubiquitin ligase adaptor protein mediating poly-ubiquitination and proteasome-mediated degradation of several proteins, such as PD-L1 (55, 89). SPOP mutations or copy number variation can act as a tumor suppressor or progressor depending on the different context in different cancer types. In head and neck cancer, TCGA dataset, <2% of patient tumors exhibited mutated or altered SPOP, which was associated with non-significant reduction of the relative risk of relapse or disease progression (relative risk = 0.4, 95% confidence interval, 0.06–2.61) (**Supplementary Table 1**). Recent research identified that cyclin D-CDK4 kinase reintroduction in CAF would destabilize PD-L1 molecules via the cullin 3-SPOP pathway (55). Whereas, loss of function mutations of SPOP will increase the level of PD-L1 and tumor-infiltrating lymphocytes, as observed in mouse models. CDK4/6 inhibitor treatment will theoretically increase PD-L1 levels thus potentiating the ICB treatment (55).

In the milieu of the HNSCC immune microenvironment (**Figure 1**), there exists a kind of CD44+ stem-like cell, whose immunosuppressive capabilities have been demonstrated to be more effective than CD44-negative stem cells to inhibit the effector T-cell population while simultaneously inducing immunosuppressive Tregs and MDSC (54).

Genes function as a master regulator to control the expression of downstream genes by controlling transcription factors. IKZF1 is such a master regulator that could lead to enhanced recruitment of immune infiltrate and tumor sensitivity to ICP inhibitors in several cancer types. Genomic alterations of this gene could negatively affect immunogenicity and tumor response to ICB (56).

Results from genomic studies of HNSCC demonstrate that the immune evasion genetic pathways are different between HPV-negative and HPV-positive HNSCCs (24). The HLA mutations are uncommonly found with <10% prevalence rate in HPV-negative HNSCCs, whereas, the HPV-positive tumors will have more common HLA and Beta2-microglobulin (B2M) mutations and TRAF3 loss (90). B2M is a light chain incorporated with the MHC Class I heavy chain to form a capable antigen-presenting machinery complex. B2M deficiency in tumor cells, which results in defective cell surface HLA Class I complex or subsequent acquired loss of B2M while under immunotherapy, has been recognized as a crucial immune escape mechanism as demonstrated in various solid tumor models (91).

Impairment in T Cell Functions and Proliferation

Potential mechanisms of intrinsic or adaptive resistance rest upon T-cell functions and proliferation, which is the most essential weapon the human body utilizes to destroy cancer cells. T-cell functions and proliferation can be impaired through mutations in interferon-γ-regulating genes, suppression of the Stimulator of Interferon genes (STING) pathway or result from constitutional nutritional iron deficiency states (57–59, 62). It is noted that HPV-antigen expression levels in the tumor microenvironment would enhance cytotoxic T lymphocyte dysregulation (77).

Changes in Metabolite- and Cytokine-Rich Tumor Microenvironments

The other well-known hallmark of cancer is metabolic reprogramming by cancer cells. The tumor extracellular microenvironment contains a vibrant display of metabolites and cytokines released from different cell types aiming to create an immunosuppressive environment for the proliferation of tumor cells. **Table 3** highlights several notable changes in metabolite-rich and cytokine-rich tumor stroma with consequences of dampening anti-cancer immunity. Defective cytokine- and STAT-mediated regulation of dendritic cells (DCs) leads to defective DCs. CD-69 sufficient state will cause effector T-cell exhaustion. The actual mechanism is still elusive; however, it is apparent that CD-69 expressed on leucocytes is responsible for cell retention in the tumor microenvironment and the CD-69 expression on T-cells is associated with the expression of PD-1 and Tim-3 in T-cells (67).

The function of metabolites GTP cyclohydrolase 1 (GCH1) and tetrahydrobiopterin (BH4) has been identified to be able to increase T-cell proliferation and promote their maturation. GCH1 is the first rate-limiting enzyme in the *de novo* BH4-synthesis pathway. Whereas, metabolite kynurenine has been found to activate Treg cells, and the enzyme indoleamine 2,3-dioxygenase (IDO) inhibits T cell proliferation and restricts tumor infiltration. Arginase 1 (Arg1) depletes L-arginine, depriving the essential nutrients that T cells and NK cells need to proliferate. The alterations of these metabolites will adversely impact anti-cancer immunity through various molecular mechanisms.

Activation of and Dependence on Alternative Immune Checkpoints

The fourth group of mechanisms underlying the resistance to PD-1-PD-L1 blockade includes activation of and dependence on alternative immune checkpoints. These alternative immune checkpoints other than PD-L1 include lymphocyte activation gene-3 (LAG3) (=CD223) upregulation, T-cell immunoglobulin and ITIM domain (TIGIT)/CD155 pathway activation, T-cell immunoglobulin mucin-3 (TIM-3) upregulation, and V domain-containing Ig suppressor of T-cell activation (VISTA). The past two decades have seen research identify the G-protein-coupled adenosine receptors mediating downregulation of the inflammatory tumor microenvironment creating

an immunosuppressive milieu. Adenosine and adenosine triphosphate (ATP) are the most abundant metabolites within a cell and in the extracellular space, which acts as an autocrine and paracrine messenger. While ATP acts as an accelerator to promote proinflammatory activities, adenosine, via the Gs-coupled A2a and A2b receptors, suppresses various immune cells, including T lymphocytes, NK cells, neutrophils, dendritic cells, and macrophages (75, 76, 78, 92–95).

There are several vital molecules interplaying within the *adenosine receptor signaling*. The molecule, CD73, is an ecto-5-nucleotidase, which will dephosphorylate extracellular AMP to immunosuppressive adenosine (78, 79, 94). As a ubiquitous membranous ectozyme, CD38, cleaves NAD(+) and NADP(+), generating cyclic ADP ribose (cADPR), NAADP, and ADPR, which are directly involved in the calcium signaling essential for a cell (96). Current evidence suggests that one of the significant mechanisms in acquired immune escape from PD-1/PD-L1 inhibition is CD38 upregulation. CD38 promotes adenosine production through the **CD38-CD203a-CD73 axis**. Studies discovered that the tumor cells hijacked and leveraged the adenosine receptor signaling pathway by upregulating the activities of CD38, to develop resistance to PD-1/PD-L1 immunotherapy through inhibition of CD8+ T-cell function. Upregulation of CD38 is induced by tumor-derived soluble mediators, all-trans retinoic acid (ATRA) and IFNβ, in the tumor microenvironment.

Prediction of Response to Anti-PD-1 Immunotherapy in HNSCC

The development of predictive precision oncology aiming to discover and validate biomarkers that can predict the response from PD-1/PD-L1 immunotherapy has evolved relentlessly in the past years. **Table 4** highlights the current discovery of biomarker predictors for immunotherapy response in patients who received PD-1/PD-L1 ICB. The eagerly awaited issues to be solved in predictive biomarker development are to achieve adequate clinical evidence about the discriminative capacity (power) of each biomarker. While the evidence is being investigated through clinical studies, **Table 4** aims to demonstrate some potentially investigated or helpful biomarkers related to the field of HNSCC. These include the combined positive score (CPS) for PD-L1 protein expression, mismatch repair (MMR)-deficient status, apolipoprotein B mRNA editing enzyme, catalytic polypeptide-like (APOBEC)-driven mutations status, the molecular exhausted immune class, molecular active immune class, the interferon-γ signature (6-genes), the expanded immune signature (18-genes), the condition of somatic frameshift events in tumor suppressor genes, the total mutational burden (TMB), and the microenvironment infiltrating arginase 1 (Arg1)+/CD68+ macrophage-mediated immune evasion state.

The immunohistochemistry combined positive score (CPS) for quantifying the PD-L1 expression in a tumor sample has been adopted to predict tumor response to ICB treatment. This score is calculated as the number of PD-L1+ tumor cells, lymphocytes, and macrophages, divided by the total number of viable tumor cells, and multiplying by 100. In various trials, CPS $\geq$ 1% predicts immunotherapy response. The caveat of using CPS at the 1% cutoff to select HNSCC patients for PD-1 ICB is that intratumor heterogeneity should be considered. Rasmussen et al. have prospectively investigated the intratumor heterogeneity in PD-L1 expression in HNSCC in 28 patients with a total of 33 whole surgical specimens (98). With 1% cut off, 52% of the six random core biopsies from each surgical specimen was concordant with CPS. Defining a tumor as positive if just a single-one of the core biopsies was positive using CPS at 1% cut-off, the negative predictive value of a single negative core biopsy was 0% (98).

DNA mismatch repair (MMR) genes, hMLH1 and hMSH2, once inactivated, can accumulate thousands of mutations in simple repeats in genomic DNA and develop microsatellite instability (MSI). A defective MMR system results in both MSI and high tumor mutation burden (TMB-high), which further generates neoantigens to be identified by APCs to mount an effective cytotoxic killing of tumor cells. It has been estimated that MSI is present in ∼40% of patients with HNSCC (106). The frequency of MSI in an endemic betel-quid chewing region is about the same as the otherwise non-endemic regions, having a rate of 37.9% (107). Despite the fact that these TMB-high cancers are more immunogenic, unlike those immunogenic-desert tumors, half of the TMB-high patients still do not respond to anti-PD-1 immunotherapy (108). Subsequently, a study looking at the mutational landscape of MSI-high discovered that the extent of immunotherapy response is specifically associated with a mutational load accumulating the insertion-deletion (indel) mutations (99). The authors emphasize that there is a greater impact of frameshifting indel mutations over the more general missense mutations, in eliciting anti-PD-1 immunotherapy response.

Generally speaking, TMB was defined as the total number of somatic, coding, base substitution, and indel mutations counted per megabase (Mb) of genome interrogated (109). In terms of the mutational burden as assessed by real-time gene sequencing, HNSCC exhibits median mutations/Mb of 5.0 with 10.1% (95% CI, 8.5%−11.9%) having $>$ 20 mutations/Mb (109). In a group of 81 patients with HNSCC, higher TMB, as demonstrated by the targeted massively parallel tumor sequencing, predicted PD-1/PD-L1 ICB response ($P < 0.01$) (105).

T Cell-Inflamed Gene Signature

IFN-γ signaling (expanded immune) signature consists of the following 18 genes: *CD3D, CCL5, CD3D, CD3E, IL2RG, CIITA, GZMK, CXCL9, CXCR6, TAGAP, CD2, HLA-E, IDO1, LAG3, NKG7, GZMB, STAT1,* and *CXCL10* (60). Typically, the core IFN-γ gene signature comprises six genes, i.e., *IDO1, CXCL9, CXCL10, HLA-DRA, STAT1,* and *IFNG* (60). In a retrospective analysis of the correlation of the 18-gene signature score (as a continuous variable) with the best of response (BOR) and PFS for 43 patients with HNSCC of the KEYNOTE-012 cohort (18, 110), strong statistical significance ($P = 0.015$ and $P < 0.001$, respectively) was obtained. The 18-gene IFN-γ signature profile derived from the NanoString platform is under development as a clinical-grade companion diagnostic incorporated into the future or ongoing pembrolizumab trials (111).

TABLE 4 | Response prediction to anti-PD-1 immunotherapy in HNSCC.

Gene alterations or signature	Testing platform	Response to anti-PD-1 checkpoint blockade	References
Combined Positive Score (CPS) for PD-L1 protein Expression	Immunohistochemistry on formalin-fixed paraffin-embedded tissue samples	CPS = number of PD-L1+ tumor cells, lymphocytes, and macrophages, divided by the total number of viable tumor cells, and multiplying by 100. In various trials, CPS $\geq$ 1 predicts response.	(7, 19, 97, 98)
MMR-deficient	Quantification of genomic MSI level (MSI intensity)	Higher insertion-deletion (Indel) load predicts response.	(99)
Apolipoprotein B mRNA editing enzyme, catalytic polypeptide-like (APOBEC)-driven mutations	APOBEC enrichment scores.	Upregulated as an innate immune response particularly in HPV+ tumors. APOBEC3 mutation leads to driver mutation in *PI3KCA*.	(100–102)
Molecular exhausted immune class	Gene expression pattern analyzed by non-negative matrix factorization algorithm	Portends a worse prognosis than active immune class in overall survival.	(61)
Molecular active immune class		Better prognosis (overall survival) than exhausted class. May predict immune responses.	(61)
Interferon-γ signature (6-genes)	NanoString nCounter mRNA	Low signature score did not respond to pembrolizumab.	(103)
Expanded immune signature (18-genes)	NanoString nCounter mRNA	Low signature score did not respond to pembrolizumab.	(103)
Somatic frameshift events in tumor suppressor genes	Targeted massively parallel sequencing	More frequently seen in HPV- responders.	(104, 105)
Total mutational burden (TMB)	Targeted massively parallel sequencing	Predicts response in HPV- HNSCC.	(104, 105)
Microenvironment infiltrating arginase 1 (Arg1)+/CD68+ macrophage-mediated immune evasion	Enzyme-Linked Immunosorbent Assay (ELISA)	Plasma Arg1 level (ng/mL) to predict immune evasion (cutoff to be determined)	(74)

An enriched proinflammatory M1 macrophage signature, enhanced cytolytic activity, abundant tumor-infiltrating lymphocytes, high human papillomavirus (HPV) infection, and favorable prognosis were associated with active immune class (all, $P < 0.05$).

A bioinformatics study using a non-negative matrix factorization algorithm of the RNA sequencing profiles of 522 patients with HNSCC collected in the TCGA identified an immune class (61). This immune class was determined based on the enriched inflammatory response, enhanced cytolytic activity, and active interferon-γ signaling. There are two subclasses within the immune class, namely, the exhausted immune class, with a poor prognosis, and the active immune class, with a favorable prognosis. The active immune class was highlighted to have enriched anti-tumoral M1 macrophage polarization, stronger cytolytic activity, abundant tumor-infiltrating lymphocytes, and higher HPV infection rates (61). The research findings are relevant to the clinical application on selecting patients with active immune signatures for immunotherapy.

Finally, IFN-gamma signaling depends on the integrity of the JAK/STAT pathway. An orthotopic head and neck squamous cell carcinoma model experiment using Stat1 deficient [Stat1(−/−)] mice observed enhanced T-cell exhaustion and accumulation of MDSCs, creating a tumor-permissive microenvironment in Stat1 deficient mice (63).

Based on current research findings, if tumor samples are discovered possessing any of the aforementioned genetic aberrations or signatures indicating a hot immune tumor, a treatment recommendation incorporating the blockade of the PD-1/PD-L1 axis is justified. The status of recommendation on selecting a predictive biomarker will be refined when new evidence or data is available to suggest otherwise.

CONCLUSIONS

Hnsccs have more immunosuppressive tumor microenvironments although the initial research indicated that HNSCCs are amongst the top malignancies ranked from high to low by the neoantigen loads and total tumor burdens. Although a new treatment paradigm has been established placing pembrolizumab + platinum and infusional fluorouracil as the new standard as the first line for R/M HNSCC, ∼64% of patients will not benefit from the significant tumor regression criteria, indicating innate, adaptive resistance to the blockade of PD-1/PD-L1 ligation. This review assimilated the research findings after an extensive literature review and presents the potential mechanisms of immune escape from the PD-1/PD-L1 checkpoint inhibition into four aspects as follows: tumor cell adaption, impairment of T-cell functions and proliferation, changes in metabolite- and cytokine-rich tumor microenvironments, and activation of the alternative immune checkpoints. There are no easy methods for immunotherapy response prediction in HNSCC. Even the widely accepted criteria of the combined positivity score for PD-L1 protein expression, commonly adopted in several clinical trials to stratify patients with HNSCC by the degree of immunogenicity, may have a negative predictive value of zero percent if just one core-biopsy was examined, questioning the usefulness of this immunohistochemistry test in unresectable patients.

Targeted massively parallel sequencing and NanoString nCounter mRNA analysis showing the results of total mutational burden or certain immune signatures present promising tests with the potential to discriminate between immune responsive or unresponsive patients with HNSCC, thus requiring further research to confirm their utility in predictive precision immuno-oncology. Every patient with HNSCC contemplating ICI therapy, theoretically, should be considered for several tests, namely TMB, MSI, PD-L1/L2 genome amplification, viral antigens, and next-generation sequencing, to identify actionable targets to combine with ICI therapy.

AUTHOR CONTRIBUTIONS

The sole author of this work performed all aspects related to a review article, such as research idea conception, research strategy planning, literature search, retrieval and selection, extensive analysis of data, drafting the manuscript, drawing figures, creating tables, and finally approved this manuscript for publishing.

ACKNOWLEDGMENTS

The author is grateful that part of this review has been critically reviewed as a Capstone Project Topic Review by an anonymous expert in the field of Harvard Medical School, Boston, in the High-Impact Cancer Research: Cancer Biology and Therapeutics program. A significant amount of time was dedicated to the Capstone Project during the 1 year program. The author of this review took part in the program as a student and this review is a result of these activities.

SUPPLEMENTARY MATERIAL

The Supplementary Material for this article can be found online at: https://www.frontiersin.org/articles/10.3389/fonc.2020.00268/full#supplementary-material

REFERENCES

1. Bray F, Ferlay J, Soerjomataram I, Siegel RL, Torre LA, Jemal A. Global cancer statistics 2018: GLOBOCAN estimates of incidence and mortality worldwide for 36 cancers in 185 countries. *CA Cancer J Clin.* (2018) 68:394-424. doi: 10.3322/caac.21492
2. Straub M, Drecoll E, Pfarr N, Weichert W, Langer R, Hapfelmeier A, et al. CD274/PD-L1 gene amplification and PD-L1 protein expression are common events in squamous cell carcinoma of the oral cavity. *Oncotarget.* (2016) 7:12024–34. doi: 10.18632/oncotarget.7593
3. Martorelli D, Houali K, Caggiari L, Vaccher E, Barzan L, Franchin G, et al. Spontaneous T cell responses to Epstein-Barr virus-encoded BARF1 protein and derived peptides in patients with nasopharyngeal carcinoma: bases for improved immunotherapy. *Int J Cancer.* (2008) 123:1100–7. doi: 10.1002/ijc.23621
4. Wu TS, Wang LC, Liu SC, Hsu TY, Lin CY, Feng GJ, et al. EBV oncogene N-LMP1 induces CD4 T cell-mediated angiogenic blockade in the murine tumor model. *J Immunol.* (2015) 194:4577–87. doi: 10.4049/jimmunol.1400794
5. Chow LQM. Head and neck cancer. *N Engl J Med.* (2020) 382:60–72. doi: 10.1056/NEJMra1715715
6. Vermorken JB, Mesia R, Rivera F, Remenar E, Kawecki A, Rottey S, et al. Platinum-based chemotherapy plus cetuximab in head and neck cancer. *N Engl J Med.* (2008) 359:1116–27. doi: 10.1056/NEJMoa0802656
7. Rischin D, Harrington K, Greil R, Soulieres D, Tahara M, de Castro G, et al. Protocol-specified final analysis of the phase 3 KEYNOTE-048 trial of pembrolizumab (pembro) as first-line therapy for recurrent/metastatic head and neck squamous cell carcinoma (R/M HNSCC). *J Clin Oncol.* (2019) 37:6000.
8. Hamid O, Robert C, Daud A, Hodi FS, Hwu WJ, Kefford R, et al. Safety and tumor responses with lambrolizumab (anti-PD-1) in melanoma. *N Engl J Med.* (2013) 369:134–44. doi: 10.1056/NEJMoa1305133
9. Hanahan D, Weinberg RA. Hallmarks of cancer: the next generation. *Cell.* (2011) 144:646–74. doi: 10.1016/j.cell.2011.02.013
10. Bardhan K, Anagnostou T, Boussiotis VA. The PD1:PD-L1/2 pathway from discovery to clinical implementation. *Front Immunol.* (2016) 7:550. doi: 10.3389/fimmu.2016.00550
11. Badoual C, Hans S, Merillon N, Van Ryswick C, Ravel P, Benhamouda N, et al. PD-1-expressing tumor-infiltrating T cells are a favorable prognostic biomarker in HPV-associated head and neck cancer. *Cancer Res.* (2013) 73:128–38. doi: 10.1158/0008-5472.CAN-12-2606
12. Foy JP, Bertolus C, Michallet MC, Deneuve S, Incitti R, Bendriss-Vermare N, et al. The immune microenvironment of HPV-negative oral squamous cell carcinoma from never-smokers and never-drinkers patients suggests higher clinical benefit of IDO1 and PD1/PD-L1 blockade. *Ann Oncol.* (2017) 28:1934–41. doi: 10.1093/annonc/mdx210
13. Hsu C, Lee SH, Ejadi S, Even C, Cohen RB, Le Tourneau C, et al. Safety and antitumor activity of pembrolizumab in patients with programmed death-ligand 1-positive nasopharyngeal carcinoma: results of the KEYNOTE-028 study. *J Clin Oncol.* (2017) 35:4050–6. doi: 10.1200/JCO.2017.73.3675
14. Kim HS, Lee JY, Lim SH, Park K, Sun JM, Ko YH, et al. Association between PD-L1 and HPV status and the prognostic value of PD-L1 in oropharyngeal squamous cell carcinoma. *Cancer Res Treat.* (2016) 48:527–36. doi: 10.4143/crt.2015.249
15. Mletzko S, Pinato DJ, Robey RC, Dalla Pria A, Benson P, Imami N, et al. Programmed death ligand 1 (PD-L1) expression influences the immune-tolerogenic microenvironment in antiretroviral therapy-refractory Kaposi's sarcoma: a pilot study. *Oncoimmunology.* (2017) 6:e1304337. doi: 10.1080/2162402x.2017.1304337
16. Ritprajak P, Azuma M. Intrinsic and extrinsic control of expression of the immunoregulatory molecule PD-L1 in epithelial cells and squamous cell carcinoma. *Oral Oncol.* (2015) 51:221–8. doi: 10.1016/j.oraloncology.2014.11.014
17. Vassilakopoulou M, Avgeris M, Velcheti V, Kotoula V, Rampias T, Chatzopoulos K, et al. Evaluation of PD-L1 expression and associated tumor-infiltrating lymphocytes in laryngeal squamous cell carcinoma. *Clin Cancer Res.* (2016) 22:704–13. doi: 10.1158/1078-0432.CCR-15-1543
18. Chow LQM, Haddad R, Gupta S, Mahipal A, Mehra R, Tahara M, et al. Antitumor activity of pembrolizumab in biomarker-unselected patients with recurrent and/or metastatic head and neck squamous cell carcinoma: results from the phase Ib KEYNOTE-012 expansion cohort. *J Clin Oncol.* (2016) 34:3838–45. doi: 10.1200/JCO.2016.68.1478
19. Bauml J, Seiwert TY, Pfister DG, Worden F, Liu SV, Gilbert J, et al. Pembrolizumab for platinum- and cetuximab-refractory head and neck cancer: results from a single-arm, phase II study. *J Clin Oncol.* (2017) 35:1542–9. doi: 10.1200/JCO.2016.70.1524
20. Cohen EEW, Soulieres D, Le Tourneau C, Dinis J, Licitra L, Ahn MJ, et al. Pembrolizumab versus methotrexate, docetaxel, or cetuximab for recurrent or metastatic head-and-neck squamous cell carcinoma (KEYNOTE-040): a randomised, open-label, phase 3 study. *Lancet.* (2019) 393:156–67. doi: 10.1016/s0140-6736(18)31999-8

21. Ferris RL, Blumenschein G, Jr., Fayette J, Guigay J, Colevas AD, Licitra L, et al. Nivolumab for recurrent squamous-cell carcinoma of the head and neck. *N Engl J Med.* (2016) 375:1856–67. doi: 10.1056/NEJMoa1602252
22. Ferris RL, Blumenschein G Jr., Fayette J, Guigay J, Colevas AD, Licitra L, et al. Nivolumab vs investigator's choice in recurrent or metastatic squamous cell carcinoma of the head and neck: 2-year long-term survival update of CheckMate 141 with analyses by tumor PD-L1 expression. *Oral Oncol.* (2018) 81:45-51. doi: 10.1016/j.oraloncology.2018.04.008
23. Colevas AD, Bahleda R, Braiteh F, Balmanoukian A, Brana I, Chau NG, et al. Safety and clinical activity of atezolizumab in head and neck cancer: results from a phase I trial. *Ann Oncol.* (2018) 29:2247–53. doi: 10.1093/annonc/mdy411
24. Segal NH, Ou SI, Balmanoukian A, Fury MG, Massarelli E, Brahmer JR, et al. Safety and efficacy of durvalumab in patients with head and neck squamous cell carcinoma: results from a phase I/II expansion cohort. *Eur J Cancer.* (2019) 109:154-61. doi: 10.1016/j.ejca.2018.12.029
25. Siu LL, Even C, Mesia R, Remenar E, Daste A, Delord JP, et al. Safety and efficacy of durvalumab with or without tremelimumab in patients with PD-L1-low/negative recurrent or metastatic HNSCC: the phase 2 CONDOR randomized clinical trial. *JAMA Oncol.* (2018) 5:195-203. doi: 10.1001/jamaoncol.2018.4628
26. Bahig H, Aubin F, Stagg J, Gologan O, Ballivy O, Bissada E, et al. Phase I/II trial of durvalumab plus tremelimumab and stereotactic body radiotherapy for metastatic head and neck carcinoma. *BMC Cancer.* (2019) 19:68. doi: 10.1186/s12885-019-5266-4
27. Elbers JBW, Al-Mamgani A, Tesseslaar MET, van den Brekel MWM, Lange CAH, van der Wal JE, et al. Immuno-radiotherapy with cetuximab and avelumab for advanced stage head and neck squamous cell carcinoma: Results from a phase-I trial. *Radiother Oncol.* (2019) 142:79-84. doi: 10.1016/j.radonc.2019.08.007
28. Merlano MC, Merlotti AM, Licitra L, Denaro N, Fea E, Galizia D, et al. Activation of immune responses in patients with relapsed-metastatic head and neck cancer (CONFRONT phase I-II trial): multimodality immunotherapy with avelumab, short-course radiotherapy, and cyclophosphamide. *Clin Transl Radiat Oncol.* (2018) 12:47-52. doi: 10.1016/j.ctro.2018.08.001
29. Yu Y, Lee NY. JAVELIN head and neck 100: a phase III trial of avelumab and chemoradiation for locally advanced head and neck cancer. *Future Oncol.* (2019) 15:687–94. doi: 10.2217/fon-2018-0405
30. Sharma P, Hu-Lieskovan S, Wargo JA, Ribas A. Primary, adaptive, and acquired resistance to cancer immunotherapy. *Cell.* (2017) 168:707–23. doi: 10.1016/j.cell.2017.01.017
31. Cassetta L, Baekkevold ES, Brandau S, Bujko A, Cassatella MA, Dorhoi A, et al. Deciphering myeloid-derived suppressor cells: isolation and markers in humans, mice and non-human primates. *Cancer Immunol Immunother.* (2019) 68:687–97. doi: 10.1007/s00262-019-02302-2
32. Takahashi H, Sakakura K, Kudo T, Toyoda M, Kaira K, Oyama T, et al. Cancer-associated fibroblasts promote an immunosuppressive microenvironment through the induction and accumulation of protumoral macrophages. *Oncotarget.* (2017) 8:8633–47. doi: 10.18632/oncotarget.14374
33. Brooks JM, Menezes AN, Ibrahim M, Archer L, Lal N, Bagnall CJ, et al. Development and validation of a combined hypoxia and immune prognostic classifier for head and neck cancer. *Clin Cancer Res.* (2019) 25:5315–28. doi: 10.1158/1078-0432.CCR-18-3314
34. Barsoum IB, Smallwood CA, Siemens DR, Graham CH. A mechanism of hypoxia-mediated escape from adaptive immunity in cancer cells. *Cancer Res.* (2014) 74:665–74. doi: 10.1158/0008-5472.CAN-13-0992
35. Albacker LA, Wu J, Smith P, Warmuth M, Stephens PJ, Zhu P, et al. Loss of function JAK1 mutations occur at high frequency in cancers with microsatellite instability and are suggestive of immune evasion. *PLoS ONE.* (2017) 12:e0176181. doi: 10.1371/journal.pone.0176181
36. Routy B, Le Chatelier E, Derosa L, Duong CPM, Alou MT, Daillere R, et al. Gut microbiome influences efficacy of PD-1-based immunotherapy against epithelial tumors. *Science.* (2018) 359:91–7. doi: 10.1126/science.aan3706
37. Elkrief A, El Raichani L, Richard C, Messaoudene M, Belkaid W, Malo J, et al. Antibiotics are associated with decreased progression-free survival of advanced melanoma patients treated with immune checkpoint inhibitors. *Oncoimmunology.* (2019) 8:e1568812. doi: 10.1080/2162402x.2019.1568812
38. Lalani AA, Xie W, Braun DA, Kaymakcalan M, Bosse D, Steinharter JA, et al. Effect of antibiotic use on outcomes with systemic therapies in metastatic renal cell carcinoma. *Eur Urol Oncol.* (2019). doi: 10.1016/j.euo.2019.09.001. [Epub ahead of print].
39. Zhao S, Gao G, Li W, Li X, Zhao C, Jiang T, et al. Antibiotics are associated with attenuated efficacy of anti-PD-1/PD-L1 therapies in Chinese patients with advanced non-small cell lung cancer. *Lung Cancer.* (2019) 130:10-7. doi: 10.1016/j.lungcan.2019.01.017
40. Sakakura K, Takahashi H, Kaira K, Toyoda M, Murata T, Ohnishi H, et al. Relationship between tumor-associated macrophage subsets and CD47 expression in squamous cell carcinoma of the head and neck in the tumor microenvironment. *Lab Invest.* (2016) 96:994–1003. doi: 10.1038/labinvest.2016.70
41. Raber PL, Thevenot P, Sierra R, Wyczechowska D, Halle D, Ramirez ME, et al. Subpopulations of myeloid-derived suppressor cells impair T cell responses through independent nitric oxide-related pathways. *Int J Cancer.* (2014) 134:2853–64. doi: 10.1002/ijc.28622
42. Rahma OE, Hodi FS. The intersection between tumor angiogenesis and immune suppression. *Clin Cancer Res.* (2019) 25:5449–57. doi: 10.1158/1078-0432.Ccr-18-1543
43. Kato R, Yamasaki M, Urakawa S, Nishida K, Makino T, Morimoto-Okazawa A, et al. Increased Tim-3(+) T cells in PBMCs during nivolumab therapy correlate with responses and prognosis of advanced esophageal squamous cell carcinoma patients. *Cancer Immunol Immunother.* (2018) 67:1673–83. doi: 10.1007/s00262-018-2225-x
44. Liu Z, McMichael EL, Shayan G, Li J, Chen K, Srivastava R, et al. Novel effector phenotype of Tim-3(+) regulatory T cells leads to enhanced suppressive function in head and neck cancer patients. *Clin Cancer Res.* (2018) 24:4529–38. doi: 10.1158/1078-0432.CCR-17-1350
45. Quan H, Fang L, Pan H, Deng Z, Gao S, Liu O, et al. An adaptive immune response driven by mature, antigen-experienced T and B cells within the microenvironment of oral squamous cell carcinoma. *Int J Cancer.* (2016) 138:2952–62. doi: 10.1002/ijc.30019
46. Shayan G, Srivastava R, Li J, Schmitt N, Kane LP, Ferris RL. Adaptive resistance to anti-PD1 therapy by Tim-3 upregulation is mediated by the PI3K-Akt pathway in head and neck cancer. *Oncoimmunology.* (2016) 6:e1261779. doi: 10.1080/2162402X.2016.1261779
47. Linedale R, Schmidt C, King BT, Ganko AG, Simpson F, Panizza BJ, et al. Elevated frequencies of CD8 T cells expressing PD-1, CTLA-4 and Tim-3 within tumour from perineural squamous cell carcinoma patients. *PLoS ONE.* (2017) 12:e0175755. doi: 10.1371/journal.pone.0175755
48. Oweida A, Hararah MK, Phan A, Binder D, Bhatia S, Lennon S, et al. Resistance to radiotherapy and PD-L1 blockade is mediated by TIM-3 upregulation and regulatory T-cell infiltration. *Clin Cancer Res.* (2018) 24:5368–80. doi: 10.1158/1078-0432.CCR-18-1038
49. Concha-Benavente F, Srivastava R, Ferrone S, Ferris RL. Immunological and clinical significance of HLA class I antigen processing machinery component defects in malignant cells. *Oral Oncol.* (2016) 58:52-8. doi: 10.1016/j.oraloncology.2016.05.008
50. Gettinger S, Choi J, Hastings K, Truini A, Datar I, Sowell R, et al. Impaired HLA class i antigen processing and presentation as a mechanism of acquired resistance to immune checkpoint inhibitors in lung cancer. *Cancer Discov.* (2017) 7:1420–35. doi: 10.1158/2159-8290.Cd-17-0593
51. Ogino T, Shigyo H, Ishii H, Katayama A, Miyokawa N, Harabuchi Y, et al. HLA class I antigen down-regulation in primary laryngeal squamous cell carcinoma lesions as a poor prognostic marker. *Cancer Res.* (2006) 66:9281–9. doi: 10.1158/0008-5472.CAN-06-0488
52. Paulson KG, Voillet V, McAfee MS, Hunter DS, Wagener FD, Perdicchio M, et al. Acquired cancer resistance to combination immunotherapy from transcriptional loss of class I HLA. *Nature Commun.* (2018) 9:3868. doi: 10.1038/s41467-018-06300-3
53. Leibowitz MS, Andrade Filho PA, Ferrone S, Ferris RL. Deficiency of activated STAT1 in head and neck cancer cells mediates TAP1-dependent escape from cytotoxic T lymphocytes. *Cancer Immunol Immunother.* (2011) 60:525–35. doi: 10.1007/s00262-010-0961-7
54. Chikamatsu K, Takahashi G, Sakakura K, Ferrone S, Masuyama K. Immunoregulatory properties of CD44+ cancer stem-like cells in squamous

cell carcinoma of the head and neck. *Head Neck.* (2011) 33:208–15. doi: 10.1002/hed.21420
55. Zhang J, Bu X, Wang H, Zhu Y, Geng Y, Nihira NT, et al. Cyclin D-CDK4 kinase destabilizes PD-L1 via cullin 3-SPOP to control cancer immune surveillance. *Nature.* (2018) 553:91–5. doi: 10.1038/nature25015
56. Chen JC, Perez-Lorenzo R, Saenger YM, Drake CG, Christiano AM. IKZF1 enhances immune infiltrate recruitment in solid tumors and susceptibility to immunotherapy. *Cell Syst.* (2018) 7:92–103.e4. doi: 10.1016/j.cels.2018.05.020
57. Cassat JE, Skaar EP. Iron in infection and immunity. *Cell Host Microbe.* (2013) 13:509–19. doi: 10.1016/j.chom.2013.04.010
58. Cronin SJF, Seehus C, Weidinger A, Talbot S, Reissig S, Seifert M, et al. The metabolite BH4 controls T cell proliferation in autoimmunity and cancer. *Nature.* (2018) 563:564–8. doi: 10.1038/s41586-018-0701-2
59. Hung N, Shen CC, Hu YW, Hu LY, Yeh CM, Teng CJ, et al. Risk of cancer in patients with iron deficiency anemia: a nationwide population-based study. *PLoS ONE.* (2015) 10:e0119647. doi: 10.1371/journal.pone.0119647
60. Ayers M, Lunceford J, Nebozhyn M, Murphy E, Loboda A, Kaufman DR, et al. IFN-gamma-related mRNA profile predicts clinical response to PD-1 blockade. *J Clin Investig.* (2017) 127:2930–40. doi: 10.1172/JCI91190
61. Chen YP, Wang YQ, Lv JW, Li YQ, Chua MLK, Le QT, et al. Identification and validation of novel microenvironment-based immune molecular subgroups of head and neck squamous cell carcinoma: implications for immunotherapy. *Ann Oncol.* (2019) 30:68–75. doi: 10.1093/annonc/mdy470
62. Cadwell K, Wu L, Cao J, Cai WL, Lang SM, Horton JR, et al. KDM5 histone demethylases repress immune response via suppression of STING. *PLoS Biology.* (2018) 16:e2006134. doi: 10.1371/journal.pbio.2006134.
63. Ryan N, Anderson K, Volpedo G, Hamza O, Varikuti S, Satoskar AR, et al. STAT1 inhibits T cell exhaustion and myeloid derived suppressor cell accumulation to promote anti-tumor immune responses in head and neck squamous cell carcinoma. *Int J Cancer.* (2019) 146:1717–1729. doi: 10.1002/ijc.32781
64. Barry KC, Hsu J, Broz ML, Cueto FJ, Binnewies M, Combes AJ, et al. A natural killer-dendritic cell axis defines checkpoint therapy-responsive tumor microenvironments. *Nat Med.* (2018) 24:1178–91. doi: 10.1038/s41591-018-0085-8
65. Chrisikos TT, Zhou Y, Slone N, Babcock R, Watowich SS, Li HS. Molecular regulation of dendritic cell development and function in homeostasis, inflammation, and cancer. *Mol Immunol.* (2019) 110:24-39. doi: 10.1016/j.molimm.2018.01.014
66. Versteven M, Van den Bergh JMJ, Marcq E, Smits ELJ, Van Tendeloo VFI, Hobo W, et al. Dendritic cells and programmed death-1 blockade: a joint venture to combat cancer. *Front Immunol.* (2018) 9:394. doi: 10.3389/fimmu.2018.00394
67. Mita Y, Kimura MY, Hayashizaki K, Koyama-Nasu R, Ito T, Motohashi S, et al. Crucial role of CD69 in anti-tumor immunity through regulating the exhaustion of tumor-infiltrating T cells. *Int Immunol.* (2018) 30:559–67. doi: 10.1093/intimm/dxy050
68. Laimer K, Troester B, Kloss F, Schafer G, Obrist P, Perathoner A, et al. Expression and prognostic impact of indoleamine 2,3-dioxygenase in oral squamous cell carcinomas. *Oral Oncol.* (2011) 47:352–7. doi: 10.1016/j.oraloncology.2011.03.007
69. Platten M, Nollen EAA, Rohrig UF, Fallarino F, Opitz CA. Tryptophan metabolism as a common therapeutic target in cancer, neurodegeneration and beyond. *Nat Rev Drug Discov.* (2019) 18:379–401. doi: 10.1038/s41573-019-0016-5
70. Holmgaard RB, Schaer DA, Li Y, Castaneda SP, Murphy MY, Xu X, et al. Targeting the TGFbeta pathway with galunisertib, a TGFbetaRI small molecule inhibitor, promotes anti-tumor immunity leading to durable, complete responses, as monotherapy and in combination with checkpoint blockade. *J Immunother Cancer.* (2018) 6:47. doi: 10.1186/s40425-018-0356-4
71. Mariathasan S, Turley SJ, Nickles D, Castiglioni A, Yuen K, Wang Y, et al. TGFbeta attenuates tumour response to PD-L1 blockade by contributing to exclusion of T cells. *Nature.* (2018) 554:544–8. doi: 10.1038/nature25501
72. Tauriello DVF, Palomo-Ponce S, Stork D, Berenguer-Llergo A, Badia-Ramentol J, Iglesias M, et al. TGFbeta drives immune evasion in genetically reconstituted colon cancer metastasis. *Nature.* (2018) 554:538–43. doi: 10.1038/nature25492
73. Weber F, Byrne SN, Le S, Brown DA, Breit SN, Scolyer RA, et al. Transforming growth factor-beta1 immobilises dendritic cells within skin tumours and facilitates tumour escape from the immune system. *Cancer Immunol Immunother.* (2005) 54:898–906. doi: 10.1007/s00262-004-0652-3
74. Steggerda SM, Bennett MK, Chen J, Emberley E, Huang T, Janes JR, et al. Inhibition of arginase by CB-1158 blocks myeloid cell-mediated immune suppression in the tumor microenvironment. *J Immunother Cancer.* (2017) 5:101. doi: 10.1186/s40425-017-0308-4
75. Chen L, Diao L, Yang Y, Yi X, Rodriguez BL, Li Y, et al. CD38-mediated immunosuppression as a mechanism of tumor cell escape from PD-1/PD-L1 blockade. *Cancer Discov.* (2018) 8:1156–75. doi: 10.1158/2159-8290.CD-17-1033
76. Mittal D, Vijayan D, Smyth MJ. Overcoming acquired PD-1/PD-L1 resistance with CD38 blockade. *Cancer Discov.* (2018) 8:1066–8. doi: 10.1158/2159-8290.CD-18-0798
77. Krishna S, Ulrich P, Wilson E, Parikh F, Narang P, Yang S, et al. Human papilloma virus specific immunogenicity and dysfunction of CD8(+) T cells in head and neck cancer. *Cancer Res.* (2018) 78:6159–70. doi: 10.1158/0008-5472.Can-18-0163
78. Leone RD, Sun IM, Oh MH, Sun IH, Wen J, Englert J, et al. Inhibition of the adenosine A2a receptor modulates expression of T cell coinhibitory receptors and improves effector function for enhanced checkpoint blockade and ACT in murine cancer models. *Cancer Immunol Immunother.* (2018) 67:1271–84. doi: 10.1007/s00262-018-2186-0
79. Deng W-W, Li Y-C, Ma S-R, Mao L, Yu G-T, Bu L-L, et al. Specific blockade CD73 alters the "exhausted" phenotype of T cells in head and neck squamous cell carcinoma. *Int J Cancer.* (2018) 143:1494–504. doi: 10.1002/ijc.31534
80. Chen L, Huang C-F, Li Y-C, Deng W-W, Mao L, Wu L, et al. Blockage of the NLRP3 inflammasome by MCC950 improves anti-tumor immune responses in head and neck squamous cell carcinoma. *Cell Mol. Life Sci.* (2018) 75:2045–58. doi: 10.1007/s00018-017-2720-9
81. Andrews LP, Marciscano AE, Drake CG, Vignali DA. LAG3 (CD223) as a cancer immunotherapy target. *Immunol Rev.* (2017) 276:80–96. doi: 10.1111/imr.12519
82. Gameiro SF, Ghasemi F, Barrett JW, Koropatnick J, Nichols AC, Mymryk JS, et al. Treatment-naive HPV+ head and neck cancers display a T-cell-inflamed phenotype distinct from their HPV- counterparts that has implications for immunotherapy. *Oncoimmunology.* (2018) 7:e1498439. doi: 10.1080/2162402x.2018.1498439
83. Mandal R, Senbabaoglu Y, Desrichard A, Havel JJ, Dalin MG, Riaz N, et al. The head and neck cancer immune landscape and its immunotherapeutic implications. *JCI Insight.* (2016) 1:e89829. doi: 10.1172/jci.insight.89829
84. Shayan G, Kansy BA, Gibson SP, Srivastava RM, Bryan JK, Bauman JE, et al. Phase Ib study of immune biomarker modulation with neoadjuvant cetuximab and TLR8 stimulation in head and neck cancer to overcome suppressive myeloid signals. *Clin Cancer Res.* (2018) 24:62–72. doi: 10.1158/1078-0432.Ccr-17-0357
85. Wu L, Mao L, Liu JF, Chen L, Yu GT, Yang LL, et al. Blockade of TIGIT/CD155 signaling reverses T-cell exhaustion and enhances antitumor capability in head and neck squamous cell carcinoma. *Cancer Immunol Res.* (2019) 7:1700–13. doi: 10.1158/2326-6066.Cir-18-0725
86. Koyama S, Akbay EA, Li YY, Herter-Sprie GS, Buczkowski KA, Richards WG, et al. Adaptive resistance to therapeutic PD-1 blockade is associated with upregulation of alternative immune checkpoints. *Nat Commun.* (2016) 7:10501. doi: 10.1038/ncomms10501
87. Kondo Y, Ohno T, Nishii N, Harada K, Yagita H, Azuma M. Differential contribution of three immune checkpoint (VISTA, CTLA-4, PD-1) pathways to antitumor responses against squamous cell carcinoma. *Oral Oncol.* (2016) 57:54-60. doi: 10.1016/j.oraloncology.2016.04.005
88. Wu L, Deng WW, Huang CF, Bu LL, Yu GT, Mao L, et al. Expression of VISTA correlated with immunosuppression and synergized with CD8 to predict survival in human oral squamous cell carcinoma. *Cancer Immunol Immunother.* (2017) 66:627–36. doi: 10.1007/s00262-017-1968-0

89. Zhang XJ, Jin Y, Song JL, Deng F. MiR-373 promotes proliferation and metastasis of oral squamous cell carcinoma by targeting SPOP. *Eur Rev Med Pharmacol Sci.* (2019) 23:5270–6. doi: 10.26355/eurrev_201906_18193
90. Hammerman PS, Hayes DN, Grandis JR. Therapeutic insights from genomic studies of head and neck squamous cell carcinomas. *Cancer Discov.* (2015) 5:239–44. doi: 10.1158/2159-8290.CD-14-1205
91. Bernal M, Ruiz-Cabello F, Concha A, Paschen A, Garrido F. Implication of the beta2-microglobulin gene in the generation of tumor escape phenotypes. *Cancer Immunol Immunother.* (2012) 61:1359–71. doi: 10.1007/s00262-012-1321-6
92. Mediavilla-Varela M, Castro J, Chiappori A, Noyes D, Hernandez DC, Allard B, et al. A Novel antagonist of the immune checkpoint protein adenosine A2a receptor restores tumor-infiltrating lymphocyte activity in the context of the tumor microenvironment. *Neoplasia.* (2017) 19:530–6. doi: 10.1016/j.neo.2017.02.004
93. Young A, Mittal D, Stagg J, Smyth MJ. Targeting cancer-derived adenosine: new therapeutic approaches. *Cancer Discov.* (2014) 4:879–88. doi: 10.1158/2159-8290.CD-14-0341
94. Hausler SF, Montalban del Barrio I, Strohschein J, Chandran PA, Engel JB, Honig A, et al. Ectonucleotidases CD39 and CD73 on OvCA cells are potent adenosine-generating enzymes responsible for adenosine receptor 2A-dependent suppression of T cell function and NK cell cytotoxicity. *Cancer Immunol Immunother.* (2011) 60:1405–18. doi: 10.1007/s00262-011-1040-4
95. Ohta A, Gorelik E, Prasad SJ, Ronchese F, Lukashev D, Wong MK, et al. A2A adenosine receptor protects tumors from antitumor T cells. *Proc Natl Acad Sci USA.* (2006) 103:13132–7. doi: 10.1073/pnas.0605251103
96. Malavasi F, Deaglio S, Funaro A, Ferrero E, Horenstein AL, Ortolan E, et al. Evolution and function of the ADP ribosyl cyclase/CD38 gene family in physiology and pathology. *Physiol Rev.* (2008) 88:841–86. doi: 10.1152/physrev.00035.2007
97. Cohen EEW, Bell RB, Bifulco CB, Burtness B, Gillison ML, Harrington KJ, et al. The Society for Immunotherapy of Cancer consensus statement on immunotherapy for the treatment of squamous cell carcinoma of the head and neck (HNSCC). *J Immunother Cancer.* (2019) 7:184. doi: 10.1186/s40425-019-0662-5.
98. Rasmussen JH, Lelkaitis G, Hakansson K, Vogelius IR, Johannesen HH, Fischer BM, et al. Intratumor heterogeneity of PD-L1 expression in head and neck squamous cell carcinoma. *Br J Cancer.* (2019) 120:1003–6. doi: 10.1038/s41416-019-0449-y
99. Mandal R, Samstein RM, Lee KW, Havel JJ, Wang H, Krishna C, et al. Genetic diversity of tumors with mismatch repair deficiency influences anti-PD-1 immunotherapy response. *Science.* (2019) 364:485–91. doi: 10.1126/science.aau0447
100. Faden DL, Ding F, Lin Y, Zhai S, Kuo F, Chan TA, et al. APOBEC mutagenesis is tightly linked to the immune landscape and immunotherapy biomarkers in head and neck squamous cell carcinoma. *Oral Oncol.* (2019) 96:140-7. doi: 10.1016/j.oraloncology.2019.07.020
101. Faden DL, Thomas S, Cantalupo PG, Agrawal N, Myers J, DeRisi J. Multi-modality analysis supports APOBEC as a major source of mutations in head and neck squamous cell carcinoma. *Oral Oncol.* (2017) 74:8-14. doi: 10.1016/j.oraloncology.2017.09.002
102. Gillison ML, Akagi K, Xiao W, Jiang B, Pickard RKL, Li J, et al. Human papillomavirus and the landscape of secondary genetic alterations in oral cancers. *Genome Res.* (2019) 29:1–17. doi: 10.1101/gr.241141.118
103. Ayers M, Lunceford J, Nebozhyn M, Murphy E, Loboda A, Albright A, et al. Relationship between immune gene signatures and clinical response to PD-1 blockade with pembrolizumab (MK-3475) in patients with advanced solid tumors. *J Immunother Cancer.* (2015) 3(Suppl. 2):P80. doi: 10.1186/2051-1426-3-s2-p80
104. Georgiadis A, Durham JN, Keefer LA, Bartlett BR, Zielonka M, Murphy D, et al. Noninvasive detection of microsatellite instability and high tumor mutation burden[[Inline Image]] in cancer patients treated with PD-1 blockade. *Clin Cancer Res.* (2019) 25:7024–34. doi: 10.1158/1078-0432.CCR-19-1372
105. Hanna GJ, Lizotte P, Cavanaugh M, Kuo FC, Shivdasani P, Frieden A, et al. Frameshift events predict anti-PD-1/L1 response in head and neck cancer. *JCI Insight.* (2018) 3:98811. doi: 10.1172/jci.insight.98811
106. Demokan S, Suoglu Y, Demir D, Gozeler M, Dalay N. Microsatellite instability and methylation of the DNA mismatch repair genes in head and neck cancer. *Ann Oncol.* (2006) 17:995–9. doi: 10.1093/annonc/mdl048
107. Lin JC, Wang CC, Jiang RS, Wang WY, Liu SA. Microsatellite alteration in head and neck squamous cell carcinoma patients from a betel quid-prevalent region. *Sci Rep.* (2016) 6:22614. doi: 10.1038/srep22614
108. Le DT, Durham JN, Smith KN, Wang H, Bartlett BR, Aulakh LK, et al. Mismatch repair deficiency predicts response of solid tumors to PD-1 blockade. *Science.* (2017) 357:409–13. doi: 10.1126/science.aan6733
109. Chalmers ZR, Connelly CF, Fabrizio D, Gay L, Ali SM, Ennis R, et al. Analysis of 100,000 human cancer genomes reveals the landscape of tumor mutational burden. *Genome Med.* (2017) 9:34. doi: 10.1186/s13073-017-0424-2
110. Seiwert TY, Burtness B, Mehra R, Weiss J, Berger R, Eder JP, et al. Safety and clinical activity of pembrolizumab for treatment of recurrent or metastatic squamous cell carcinoma of the head and neck (KEYNOTE-012): an open-label, multicentre, phase 1b trial. *Lancet Oncol.* (2016) 17:956–65. doi: 10.1016/s1470-2045(16)30066-3.
111. Wallden B, Pekker I, Popa S, Dowidar N, Sullivan A, Hood T, et al. Development and analytical performance of a molecular diagnostic for anti-PD1 response on the nCounter Dx Analysis System. *J Clin Oncol.* (2016) 34(15_suppl):3034. doi: 10.1200/JCO.2016.34.15_suppl.3034

Conflict of Interest: The author declares that the research was conducted in the absence of any commercial or financial relationships that could be construed as a potential conflict of interest.

frontiers in Oncology

ORIGINAL RESEARCH
published: 03 March 2020
doi: 10.3389/fonc.2020.00176

Regulatory Role of Hexokinase 2 in Modulating Head and Neck Tumorigenesis

Wan-Chun Li[1,2,3], Chien-Hsiang Huang[1], Yi-Ta Hsieh[1], Tsai-Ying Chen[1], Li-Hao Cheng[1], Chang-Yi Chen[1], Chung-Ji Liu[1,2,4,5], Hsin-Ming Chen[6], Chien-Ling Huang[7], Jeng-Fan Lo[1,2,3,8] and Kuo-Wei Chang[1,2,3,8]*

[1] *Institute of Oral Biology, School of Dentistry, National Yang-Ming University, Taipei, Taiwan,* [2] *Department of Dentistry, School of Dentistry, National Yang-Ming University, Taipei, Taiwan,* [3] *Cancer Progression Research Center, National Yang-Ming University, Taipei, Taiwan,* [4] *Department of Oral and Maxillofacial Surgery, MacKay Memorial Hospital, Taipei, Taiwan,* [5] *Department of Medical Research, MacKay Memorial Hospital, Taipei, Taiwan,* [6] *School of Dentistry and Department of Dentistry, National Taiwan University Medical College and National Taiwan University Hospital, Taipei, Taiwan,* [7] *Department of Health Technology and Informatics (HTI), The Hong Kong Polytechnic University (PolyU), Kowloon, Hong Kong,* [8] *Department of Stomatology, Taipei Veterans General Hospital, Taipei, Taiwan*

To support great demand of cell growth, cancer cells preferentially obtain energy and biomacromolecules by glycolysis over mitochondrial oxidative phosphorylation (OxPhos). Among all glycolytic enzymes, hexokinase (HK), a rate-limiting enzyme at the first step of glycolysis to catalyze cellular glucose into glucose-6-phosphate, is herein emphasized. Four HK isoforms, HK1-HK4, were discovered in nature. It was shown that HK2 expression is enriched in many tumor cells and correlated with poorer survival rates in most neoplastic cells. HK2-mediated regulations for cell malignancy and mechanistic cues in regulating head and neck tumorigenesis, however, are not fully elucidated. Cellular malignancy index, such as cell growth, cellular motility, and treatment sensitivity, and molecular alterations were determined in HK2-deficient head and neck squamous cell carcinoma (HNSCC) cells. By using various cancer databases, HK2, but not HK1, positively correlates with HNSCC progression in a stage-dependent manner. A high HK2 expression was detected in head and neck cancerous tissues compared with their normal counterparts, both in mouse and human subjects. Loss of HK2 in HNSCC cells resulted in reduced cell (*in vitro*) and tumor (*in vivo*) growth, as well as decreased epithelial-mesenchymal transition–mediated cell movement; in contrast, HK2-deficient HNSCC cells exhibited greater sensitivity to chemotherapeutic drugs cisplatin and 5-fluorouracil but are more resistant to photodynamic therapy, indicating that HK2 expression could selectively define treatment sensitivity in HNSCC cells. At the molecular level, it was found that HK2 alteration drove metabolic reprogramming toward OxPhos and modulated oncogenic Akt and mutant TP53-mediated signals in HNSCC cells. In summary, the present study showed that HK2 suppression could lessen HNSCC oncogenicity and modulate therapeutic sensitivity, thereby being an ideal therapeutic target for HNSCCs.

Keywords: head and neck cancer, hexokinase 2, cellular malignancy, metabolic shift, therapeutic efficacy

OPEN ACCESS

Edited by:
Victor C. Kok,
Asia University, Taiwan

Reviewed by:
Lo-Lin Tsai,
Taipei Medical University, Taiwan
Pei-ling Hsieh,
China Medical University, Taiwan

****Correspondence:***
Wan-Chun Li
wcli@ym.edu.tw

Specialty section:
This article was submitted to Head and Neck Cancer, a section of the journal Frontiers in Oncology

Received: *26 November 2019*
Accepted: *31 January 2020*
Published: *03 March 2020*

Citation:
Li W-C, Huang C-H, Hsieh Y-T, Chen T-Y, Cheng L-H, Chen C-Y, Liu C-J, Chen H-M, Huang C-L, Lo J-F and Chang K-W (2020) Regulatory Role of Hexokinase 2 in Modulating Head and Neck Tumorigenesis. Front. Oncol. 10:176. doi: 10.3389/fonc.2020.00176

INTRODUCTION

Most cancers have acquired the same set of functional capabilities during tumorigenesis including sustained proliferative signal, evaded growth suppressors, resisted cell death, sustained angiogenesis, and deregulated cellular energetics (1). In the aspect of energy production, glucose is a major source of bioenergetics and biomolecules used to maintain cellular homeostasis. Glucose molecules could be metabolized by glycolysis to generate pyruvate in cells; the pyruvate could be either oxidatively metabolized to generate up to 38 ATPs through the process of oxidative phosphorylation (OxPhos) or be reductively converted into organic acids or alcohols by fermentation producing only 2 ATP (2). In general, normal cells in non-malignant tissues developed an evolutionary choice of "Pasteur effect" to allow a system to fine tune cell metabolism in unfavorable environment (3, 4). On the contrary, cancer cells exhibited a unique metabolic system by taking advantage of aerobic glycolysis for demands of energy and biomolecules regardless of oxygen status; in this way, cancer cells preferentially drive their metabolism away from OxPhos toward glycolysis, so-called Warburg effect (5).

Previous studies have sought to target different cancer-specific metabolic pathways, in particular glycolysis, for development of antitumor treatments (6–9). There are three irreversible reactions in glycolysis. It is well-known that the glycolytic rate is limited by the phosphorylation state of glycolytic enzymes hexokinases (HKs), because at the first step of glycolysis, HKs catalyze the intake glucose into glucose-6-phosphate (G-6-P) (10). Hexokinase–mediated catalysis is ATP dependent and a key determinant for the direction and magnitude of glucose flux within cells; thus, it would more efficient to target glucose metabolism in cancer cells by cutting down this earliest step of glucose flux (11). Four HK isoforms including HK1, HK2, HK3, and HK4 encoded by different genes were found in nature. Among them, HK1 is ubiquitously expressed in most mammalian tissues, and HK2 is detected in adipose, skeletal, and cardiac muscles, whereas HK3 and HK4 show relatively low expression in mammalian tissues (12). In the aspect of protein structure, two catalytic domains, both in N- and C-terminal portions, are detected in HK2, resulting in greater glycolytic rate compared with HK1-mediated glycolysis, whereas only one catalytic domain was found at the carboxyl terminal part in HK1 protein (13). In clinic, HK2 is rarely expressed in normal tissues as a high level of HK2 expression was detected in many solid tumors (14) and is associated with elevated progression, poorer overall survival, and treatment resistance in breast cancer (both primary and metastatic kinds) (15–18), bladder cancer (19), cervical squamous cell carcinoma (20), colorectal cancer (21), epithelial ovarian tumors (22), glioblastoma multiforme (23), hepatocellular carcinoma (24), laryngeal squamous cell carcinoma (25), lung cancer (26), neuroblastoma (27), neuroendocrine tumor (28), pancreatic cancer (29), and prostate cancer (30), making it an excellent target for development of anticancer therapy. Moreover, given its selective expression in tumors, HK2 has drawn increasing attention on its clinical implications forming the basis of fluorodeoxyglucose F-18 positron emission tomography imaging, a widely used clinical procedure to detect tumors. Indeed, a recent meta-analysis provides evidence that HK2 could be a marker to predict the risk of all-cause mortality and cancer progression in patients with tumors of the digestive system (31).

Numbers of molecular cues including signal transducer and activator of transcription 3 (32–35), protein kinase B (PKB), also known as Akt (19, 36–38), mammalian target of rapamycin (38–40), and PH domain leucine-rich repeat protein phosphatase (41), as well as autophagy (42, 43), have been found to control HK2-mediated metabolic alterations, thereby regulating tumor identity. Moreover, HK2 contains an N-terminal hydrophobic domain allowing it to bind to outer mitochondrial membrane voltage-dependent anion channel (VDAC) protein, thereby resulting in Bax-mediated apoptosis. HK2–VDAC interaction could also provide kinetic benefits in HK2 exhibiting greater affinity to ATP over G-6-P, suggesting that HK2 could regulate oncogenicity via modulation of mitochondrial physiology (44–47). More recent studies further discovered that p53-inducible protein TIGAR (Tp53-induced Glycolysis and Apoptosis Regulator), Akt, and ER stress sensor kinase could regulate mitochondrial HK2 localization (48–51). Interestingly, mitochondrial TIGAR–HK2 complex upregulated HK2 and hypoxia-inducible factor 1 activity limiting reactive oxygen species production and protecting from tumor cell death under hypoxic condition implying that p53 could be an essential key regulator for HK2-mediated oncogenesis (26, 30, 48). In addition to signaling factors, HK2 regulated by epigenetic mediators including microRNAs (32, 52–55), long non-coding RNAs (56–58), and histone/DNA methylation (59) are also important to modulate HK2-mediated tumorigenicity. Taken together, HK2 seems to be a master promoting factor in controlling carcinogenesis in different cancers; to date, however, the role of HK2 in controlling head and neck squamous cell carcinoma (HNSCC) development was rarely focused. The present study was therefore conceived to determine cellular, molecular, and physiological alterations of HNSCC cells in response to HK2 silencing.

MATERIALS AND METHODS

Basic Reagents, Cells, and Animal and Human Protocols

All experimental reagents including 4-nitroquinoline 1-oxide (4-NQO), 3-(4,5-Dimethylthiazol-2-yl)-2,5-diphenyltetrazolium bromide (MTT), cisplatin (CDDP), and 5-fluorouracil (5-FU) were purchased from Sigma. The HNSCC cell lines, clinical human HNSCC tissues, and animal procedure were obtained and described elsewhere (60, 61).

Establishment of HK2 Silencing HNSCC Cells

Three plasmids encoding small hairpin RNAs (shRNAs) targeting HK2 gene were purchased from the National RNAi Core Facility (NRCF), Academia Sinica, Taipei, Taiwan. The targeting sequences were as listed: 5-GCCTGGCTAACTTCATGGATA-3 (A), 5-CCGTAACATTCTCATCGATTT-3 (B), and 5-GCTTGA AGATTAGGTACTATC-3 (C) (NRCF). The control nucleotide

sequence of shRNA was 5-GCGGTTGCCAAGAGGTTCCAT-3, which was the random sequence that targets luciferase (shLuc) mRNA. Lentiviral vectors containing shHK2/shLuc were generated in 293T cells.

Cellular and Molecular Assays

Cell growth (MTT and trypan blue exclusion assays), cell cycle, annexin V–fluorescein isothiocyanate–based cell apoptosis, Transwell-based cell migration/invasion, drug resistance (IC50 determination), quantitative real-time polymerase chain reaction (qRT-PCR), Western blot, aldehyde dehydrogenase (ALDH) activity, immunostaining analysis, human phospho-antibody array, and XF Metabolic Assay analyses were performed as previously described at Instrumentation Resource Center, National Yang Ming University (61, 62). Primers for qRT-PCR analysis (**Supplementary Table 1**) and antibodies used for protein assays (**Supplementary Table 2**) are listed. ImageJ (National Institute of Health, Bethesda, Maryland, United States) was used for quantification.

Aminolevulinic Acid–Photodynamic Therapy Treatment

5-Aminolevulinic acid (ALA) 1 mM was made by diluting 1 M ALA stock with serum-free medium and neutralized to pH 7.2 with NaOH immediately before use. The total number of 5×10^5 cells were incubated with 1 mM ALA for 3 h, and the medium was replaced with 100 μL phosphate-buffered saline to prevent thermal injury by the light. The cells were then exposed to various doses of light source (30.33 mW/cm²) with a 635-nm wavelength emission of red light. After exposure, cells are replaced with culture medium and cultured for 24 h. Relative viable cells were determined by the MTT method.

Measurement of Lactate, ATP, and PDH Activity

Extracellular lactate, intracellular ATP level, and pyruvate dehydrogenase (PDH) activity were determined previously (62). Cell number or genomic DNA content was used to normalize detections.

Xenografic Model

The HNSCC cells 1×10^6 to 4×10^6 and 1 μL of each medium were mixed and subcutaneously injected into the back of nude mice. Tumor volume and size were recorded.

Statistical Analysis

All analyses were statistically determined using Microsoft Excel 2013 (Microsoft, Redmond, WA, United States)/Prism 5 (GraphPad, San Diego, CA, United States). All quantifications are presented as mean ± SEM. A significant difference was defined as $p < 0.05$.

RESULTS

HK2 Expression Defines HNSCC Progression in Clinic

By taking advantage of The Cancer Genomic Atlas–based UALCAN, Firebrowse, and The Human Protein Atlas (www.proteinatlas.org) databases (63–65), it was found that HK2 transcript, in comparison with HK1, is enriched in most primary tumor tissues compared with their normal counterparts (**Figures 1A,B**). Further analysis for HK1 and HK2 expression in HNSCCs indicated that (i) HK2 expression, but not HK1, is positively correlated with tumor stages and grades (**Figures 1C,D**); (ii) HK2 level, but not HK1, is upregulated in HPV$^-$ HNSCC tissues (**Figure 1E**); and (iii) HK2 expression, but not HK1, is increased in early metastatic HNSCCs [with one to three axillary lymph nodes (N1)] (**Figure 1F**). Furthermore, immunohistochemical analysis showed that HK2 is strongly detected in 4-NQO–induced mouse tongue neoplastic lesions compared with normal oral epithelium (**Figure 1G**), as well as human oral squamous cell carcinoma (**Figure 1H**). Surprisingly, differential HK1 level could better stratify cancer-specific survival rates than HK2 in HNSCC patients (**Supplementary Figure 1**), suggesting that HK1 and HK2 might play differential roles during HNSCC tumorigenesis. Taken together, these analyses suggest that HK2 serves as a rather early prognostic indicator in the majority of HNSCC population.

HK2 Loss Modulates HNSCC Cell Growth and Motility

In consistent with former findings in other cancer tissues, HK2, both in mRNA and protein level, is highly expressed in tested HNSCC cell lines (**Supplementary Table 3**) compared to normal human oral keratinocytes (NHOKs) (**Figure 2A** and **Supplementary Figure 2**). A wide spectrum of cellular alterations and their potential underlying regulatory cues in response to HK2 loss were next focused on. As shRNA-mediated HK2-deficient HNSCC cells were successfully established without apparent morphological change (**Figures 2B,C** and **Supplementary Figure 3**), it was demonstrated that, by using both trypan blue exclusion (**Figure 2D**) and MTT (**Figure 2E**) assays, HK2-silencing resulted in decreased cell growth in HNSCC cells. Further analysis found no significant cell cycling change and cell apoptosis (data now shown) in HK2-silencing HNSCC cells compared with control cells, suggesting that HK2 could possibly control cell growth via self-protective machinery, such as autophagy (42, 43). *In vivo* growth for HK2-silencing tumors was also analyzed, and it was shown that HK2 loss resulted in significantly smaller xenografic tumors compared with control tumors (**Figure 2F**).

Potential impact of HK2 loss in regulating cell motility was also analyzed by using Transwell-based assays (62). The results indicated that HK2 deficiency led to significant decrease of cell migration and invasion in OECM-1 and HSC3 clones (**Figures 3A,B**). At cellular and molecular levels, lactate level, cytoskeletal organization and epithelial–mesenchymal transition (EMT) could modulate cell motility (66–68). While a slight, but not significant, increase in extracellular lactate production was detected in HK2-silencing HNSCC cells (**Supplementary Figure 4**), immunofluorescence staining analysis implied that lamellipodia-like F-actin (dot-lined in **Figure 3C**) was predominantly found in HK2-deficient

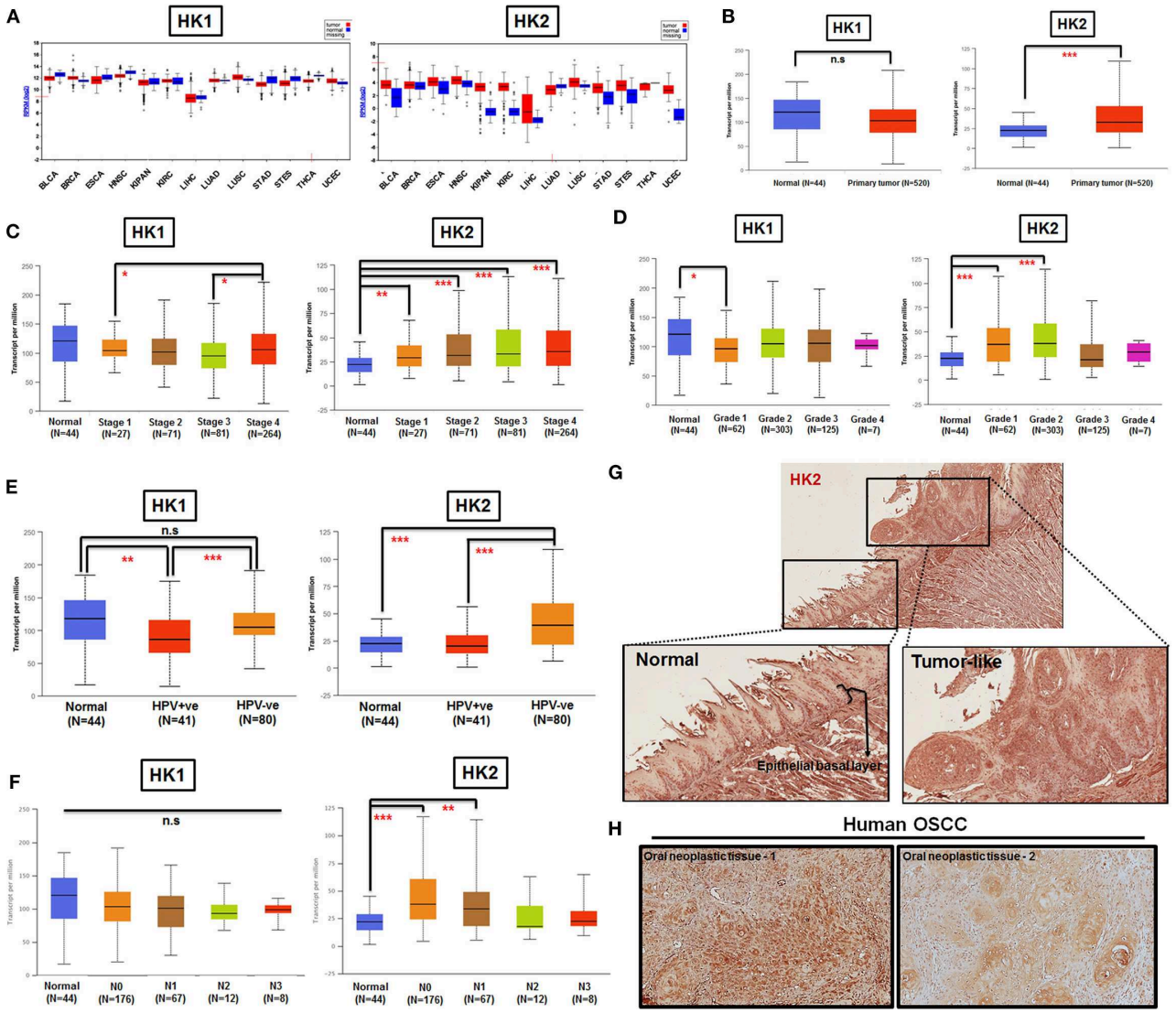

FIGURE 1 | HK2 level positively correlates with HNSCC progression in clinic. **(A)** HK1, but not HK2, mRNA expression is enriched in most human tumors by using Firebrowser database. BCLA, bladder urothelial carcinoma; BRCA, breast invasive carcinoma; ESCA, esophageal carcinoma; HNSCC, head and neck squamous cell carcinoma; KIPAN, Pan-kidney cohort (KICH+KIRC+KIRP); KIRC, kidney renal clear cell carcinoma; LIHC, liver hepatocellular carcinoma; LUAD, lung adenocarcinoma; LUSC, lung squamous cell carcinoma; STAD, stomach adenocarcinoma; STES, stomach and esophageal carcinoma; THCA, Thyroid carcinoma; UCEC, uterine corpus endometrial carcinoma. **(B)** Statistical analysis for HK1 and HK2 mRNA levels in normal and primary HNSCC tissues as well as tumor tissues, classified by clinical **(C)** stages, **(D)** grade, **(E)** HPV infection status, and **(F)** nodal metastasis status from UALCAN database. Immunohistochemical analysis for HK2 in **(G)** in 12-week 4-NQO–treated mouse tongue and **(H)** human oral squamous cell carcinoma (hOSCC) tissues. Data are shown as mean ± SEM. ***$p < 0.001$, **$p < 0.01$, *$p < 0.05$, and n.s., non-significant.

HNSCC cells in comparison with control cells those contain more evident filopodia-like protrusions. Interestingly, as shRNA-mediated HK2 manipulation seems to heterogeneously silence HK2 protein, HNSCC cells with greater HK2 loss (white arrows in **Figure 3C**) showed more and compacted F-actin staining signals compared with cells with less HK2 expression (yellow arrows in **Figure 3C**), revealing that HK2 loss potentially reduces F-actin level in a single-cell basis. Moreover, increased epithelial marker E-cadherin accompanied with decreased mesenchymal markers N-cadherin, Snail, and Twist was detected in mRNA level (**Figure 3D**), further supporting the important role of EMT in HK2-mediated cell motility alteration. The role of HK2 in regulating tumor metastasis *in vivo* was further defined in a previously established primary and metastatic xenografic tumor model (60). By using microarray analysis, it was found that HK2, but not HK1 and HK3, is enriched in highly migrating cells in this model (**Figure 3E**). In brief, multiple molecular factors play key roles in regulating cell movement upon HK2 loss.

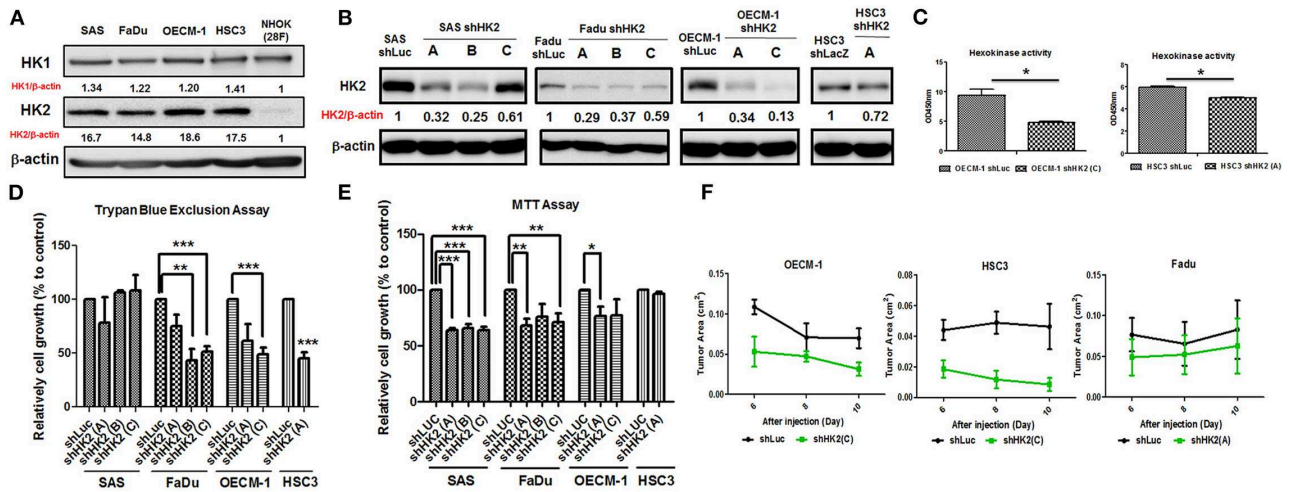

FIGURE 2 | Differential HNSCC cell growth and HNSCC-bearing xenografic tumor growth in response to HK2 loss. Respective Western blot analysis for HK1 and HK2 protein expression in **(A)** HNSCC and NHOK cells and **(B)** shRNA-mediated HK2-silencing HNSCCC cells. **(C)** Colorimetric hexokinase activity assay showed functional deficient in HK2-silencing OECM-1 and HSC3 cells. Cell growth was examined in HK2-silencing HNSCC cells using **(D)** trypan exclusion and **(E)** MTT assays. **(F)** HK2 loss downregulated HNSCC-bearing xenografic tumor growth. shLuc vector is used as a control plasmid. Data are shown as mean ± SEM ($N \geq 3$). ***$p < 0.001$, **$p < 0.01$, and *$p < 0.05$.

HK2 Expression Determines Treatment Resistance in HNSCCs Through Regulations of Stemness and Differentiation

The sensitivity for chemotherapeutic drugs, CDDP and 5-FU, as well as for photodynamic therapy (PDT), in HK2-silencing HNSCC cells was next examined. The results showed a common pattern of decreased half maximal inhibitory concentration (IC50) level for CDDP and 5-FU in HK2-deficient HNSCC cells compared with control cells (**Figure 4A**). Photodynamic therapy is an approved adjuvant treatment to lessen the disease mass of various premalignant and malignant lesions, including HNSCCs (69, 70). Photodynamic therapy–mediated cell apoptosis could be induced under numbers of physiological and pathological conditions, and one of the main advantages of PDT treatment is the higher selectivity to target transformed cells over normal cells (71). As HK2 loss could potentially reduce cell malignancy in HNSCC cells, it is expected that HK2-silencing HNSCC cells are less sensitive to PDT treatment (**Figure 4B**). At molecular level, previous study has shown that HK2 is essential for tumor initiation and survival in Kras-driven mouse lung cancer and ErbB2-driven mouse breast cancer, indicating that HK2 could be important to regulate cancer stemness (24). Moreover, it was also shown that elevated stemness could be a key factor underlying chemoresistance in HNSCCs (72). Consistent with this notion, stemness indicators Nanog and Oct4 mRNA (**Figure 4C**) and ALDH activity (**Figure 4D**) were downregulated in HK2-silencing HNSCC cells. Further analysis showed that HK2 protein is enriched in stem-like/high-grade sphere cells (**Figure 4E**), and strikingly, HK2 loss resulted in significantly less sphere number in selective medium used to culture head and neck cancer–initiating cells (**Figure 4F**). On the other hand, epithelial differentiation marker involucrin in OECM-1 cells with greater HK2 loss (clone C) was highly detected (**Figure 4G**), further supporting that HK2 change could regulate stemness and differentiation status, which modulate treatment sensitivity in HNSCC cells.

Molecular Alterations and Metabolic Shift in HK2-Silencing HNSCC Cells

HK2-mediated metabolic and molecular regulators for HNSCC malignancy were next examined. Metabolic reprogramming was recently proposed, suggesting that cancer cells could adapt to unfavorable metabolic stresses (73). Numbers of investigations have been reported showing metabolic shift upon HK2 changes in non-HNSCC cells (32, 40, 50, 54); in agreement with these findings, Seahorse analysis showed that HK2 loss led to increased basal and maximal mitochondrial respiration (**Figures 5A,B**), implying HK2-silencing HNSCC cells were metabolically programmed, being more dependent on mitochondrial metabolism. This statement could be further supported by the results showing a greater extracellular acidification rate (ECAR) upon addition of ATPase inhibitor oligomycin (**Figure 5C**) and increased PDH activity (**Figure 5D**) in HK2-silencing HNSCC cells. Unexpectedly, HK2 deficiency–mediated decreased cell growth did not result from reduction of cellular ATP level (**Figure 5E**), suggesting that bioenergetics could be dispensable for metabolism-mediated cell growth. Using a high-throughput human protein array, it was discovered that Akt (S473), TP53 (S15, S46, and S392), and p27 (T198) proteins were downregulated in HK2-silencing OECM-1 cells

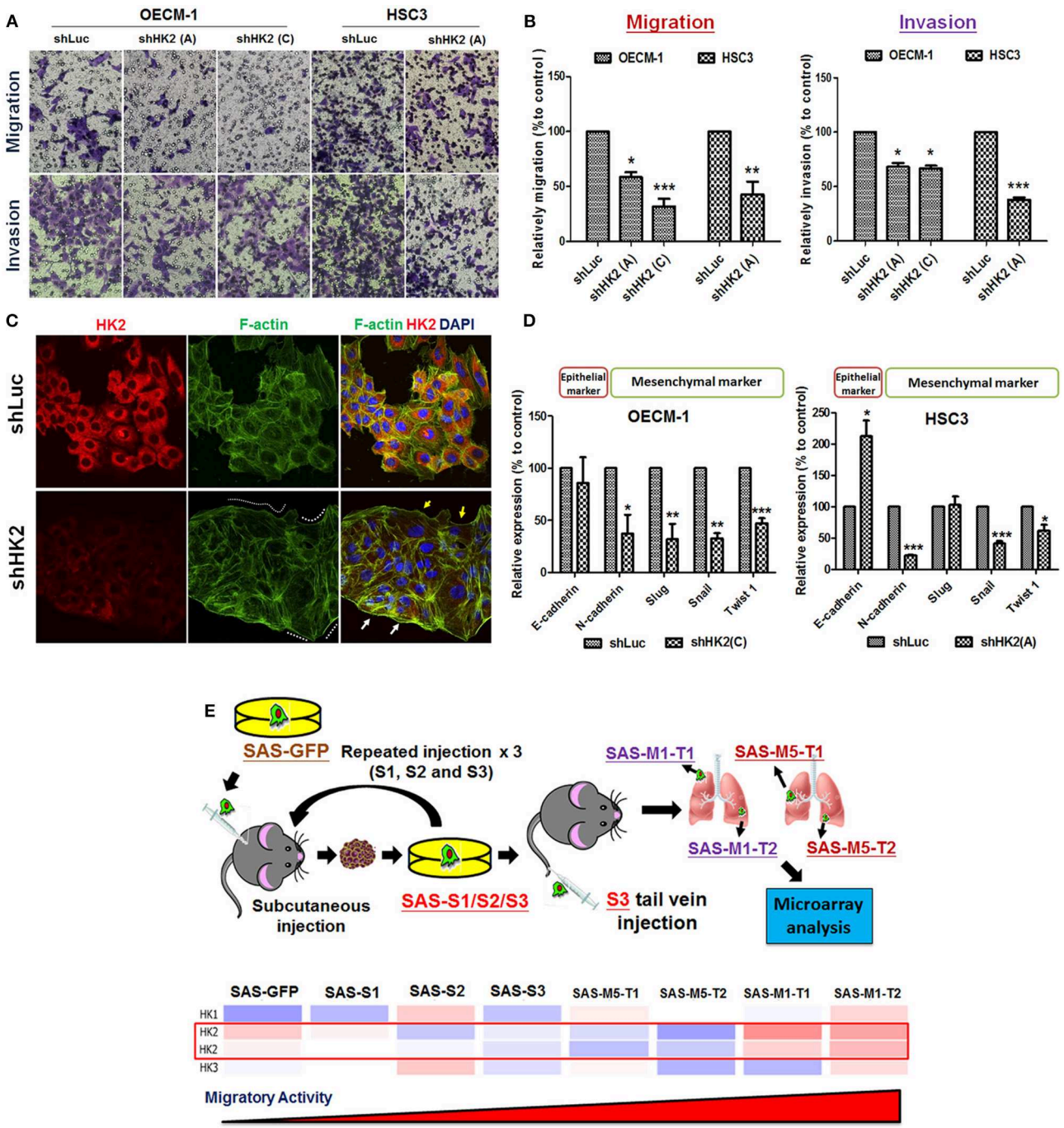

FIGURE 3 | Cell motility changes in HK2-silencing HNSCC Cells. **(A,B)** Transwell cell migration and invasion assays were performed in HK2-silencing HNSCC cells. HK2 knockdown led to significantly less migration and invasion in HNSCC cells. The changes of cell motility could result from **(C)** rearrangement of lamellipodia-like (dot-lined) and filopodia-like F-actin structures. HK2-silencing OECM-1 cells showed heterogeneous population, whereas cells with higher HK2 expression exhibited more condense F-actin structure (white arrows), while cells with less HK2 expression displayed little F-actin staining; and **(D)** altered EMT-associated mRNA expression. **(E)** Microarray analysis showed an increasing HK2, but not HK1 and HK3, mRNA expression in *in situ* injected (S1/2/3) and distant metastatic (M1/M5) HNSCC derived tumors. Data are presented as mean ± SEM ($N \geq 3$). ***$p < 0.001$, **$p < 0.01$, and *$p < 0.05$.

(**Figure 5F**). Western blot analysis further confirmed that Akt activity, but not another common oncogenic signaling factor Erk1/2, was deceased in HK2-deficient OECM-1 and HSC3 cells (**Figure 5G**).

DISCUSSION

In the present study, it was shown that HK2 loss downregulated cell growth, EMT-mediated cell movement,

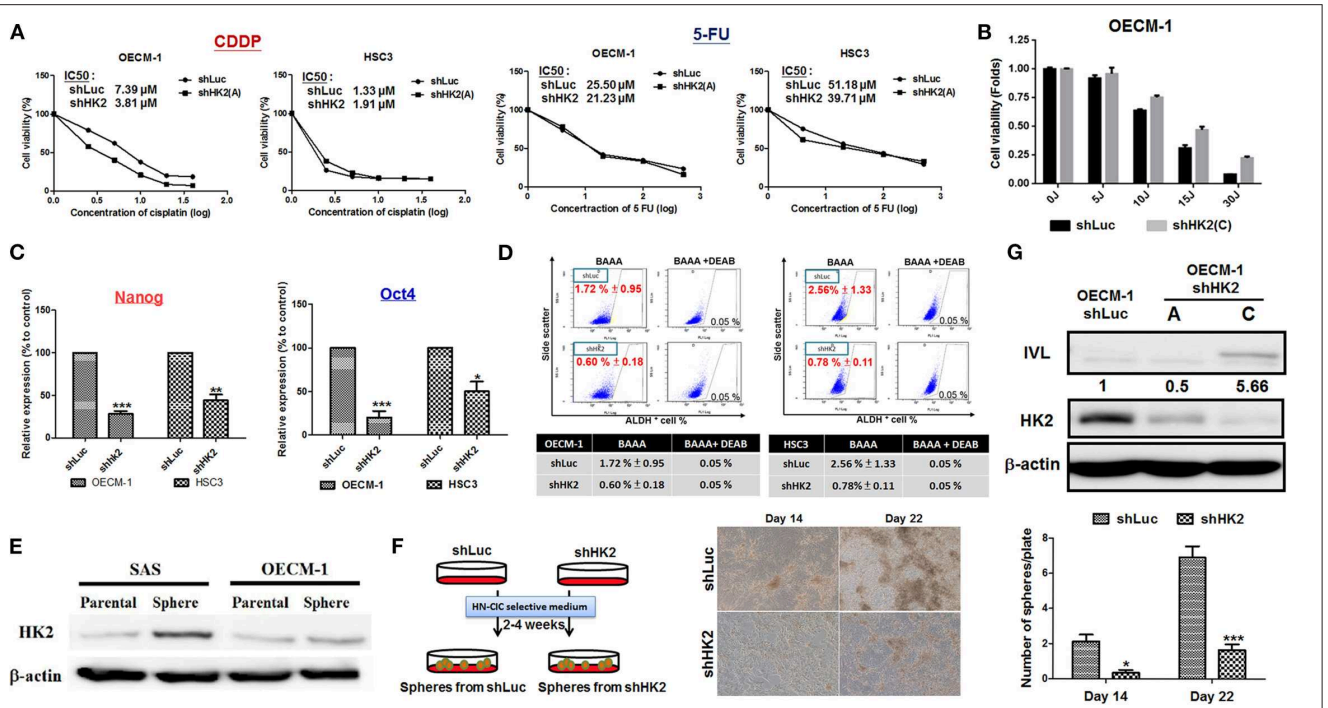

FIGURE 4 | HK2 loss modulated therapeutic sensitivity in HNSCC Cells. **(A)** Decreased IC50 for clinical chemotherapeutic agent CDDP and 5-FU, whereas **(B)** greater resistance in response to photodynamic therapy was detected in HK2-deficient HNSCC cells. This effect is probably regulated via decreased **(C)** Nanog/Oct4 mRNA expression and/or **(D)** ALDH activity. While **(E)** HK2 is highly expressed in SAS and OECM-1 derived sphere cells compared with parental cells, **(F)** HK2 loss resulted in decease of sphere formation. **(G)** Upregulation for cellular differentiation marker involucrin (IVL) protein was detected by Western blot analysis in HK2-silencing HNSCC cells. Data are presented as mean ± SEM ($N \geq 3$). ***$p < 0.001$, **$p < 0.01$, and *$p < 0.05$.

and stemness/differentiation-related treatment sensitivity; in addition, altered bioenergetics and modulation of oncogenic signaling molecules including Akt and phosphorylated TP53 could underlie HK2-mediated regulations in HNSCC cells (**Figure 5H**). Overall findings concluded that targeting HK2 could be an ideal therapeutic strategy in treating HNSCCs. One interesting discovery from the current study is that in HNSCC cells HK2-mediated malignant suppression is likely through glycolytic manipulation based on the following data: (i) HK2 is highly expressed in HNSCC cells implying that HNSCCs are "glycolytic" tumor; (ii) HK2 inhibition triggers metabolic shift away from glycolysis toward mitochondrial metabolism and (iii) it is found that mitochondria are swelling and lack cristae in HNSCC cells compared with human oral fibroblasts (**Supplementary Figure 5**). This finding agreed with previous investigations showing that HK2-mediated metabolic modulation is a key machinery to control cancerous characteristics (41, 54, 74, 75), even though it is required to further define the potential impact of mitochondrial HK2 (49, 51) in controlling tumorigenesis in HNSCC cells in the current experimental setting.

Another interesting finding is the potential involvement of phosphorylated TP53 and p27 proteins in HK2-mediated regulations for HNSCC oncogenicity. Based on protein array analysis, HK2 loss resulted in decreased phosphorylated TP53 at transactivation domain (S15 and S46) and C-terminal domain (S392) in OECM-1 cells. While previous sequencing analysis for TP53 gene in OECM-1 cells showed that OECM-1 cells carry mutant TP53 (P139R/V239L) (62), phosphorylation on S15, S46, and S392 of TP53 could be oncogenic in OECM-1 cells. This statement could be supported by previous studies showing that S15 phosphorylation of TP53 contributed mutant TP53 stability, thereby prolonging cell viability in ovarian cancer cells (76), and S392 phosphorylation in mutant TP53 could lead to tumor progression in esophageal squamous cell carcinoma (77). While it was reported that T198 phosphorylation of cell cycle regulator p27 promotes cyclin D1–CDK4–p27 complex assembly (78), as well as increases p27-RhoA–mediated cell motility (79), HK2 silencing–mediated T198 p27 loss could be a potential underlying cue in controlling HNSCC cell growth and migration. Further elucidation for roles of different TP53 phosphorylation sites in both wild-type and mutant HNSCC cells in regulating tumorigenicity is expected.

With extensive studies, including the present investigation, showing that HK2 is a master promoting factor in different stages of carcinogenesis (**Supplementary Table 4**), much efforts were put in exploring HK-mediated tumor inhibitors, despite that no potent drugs targeting HK2 are yet available in clinic (80–84). Taking the most promising HK2-targeting drug, 3-bromopyruvate (3-BP), as an example, although single treatment of 3-BP, at the appropriate dose and formulation, could effectively destroy glycolytic tumors and seems to be

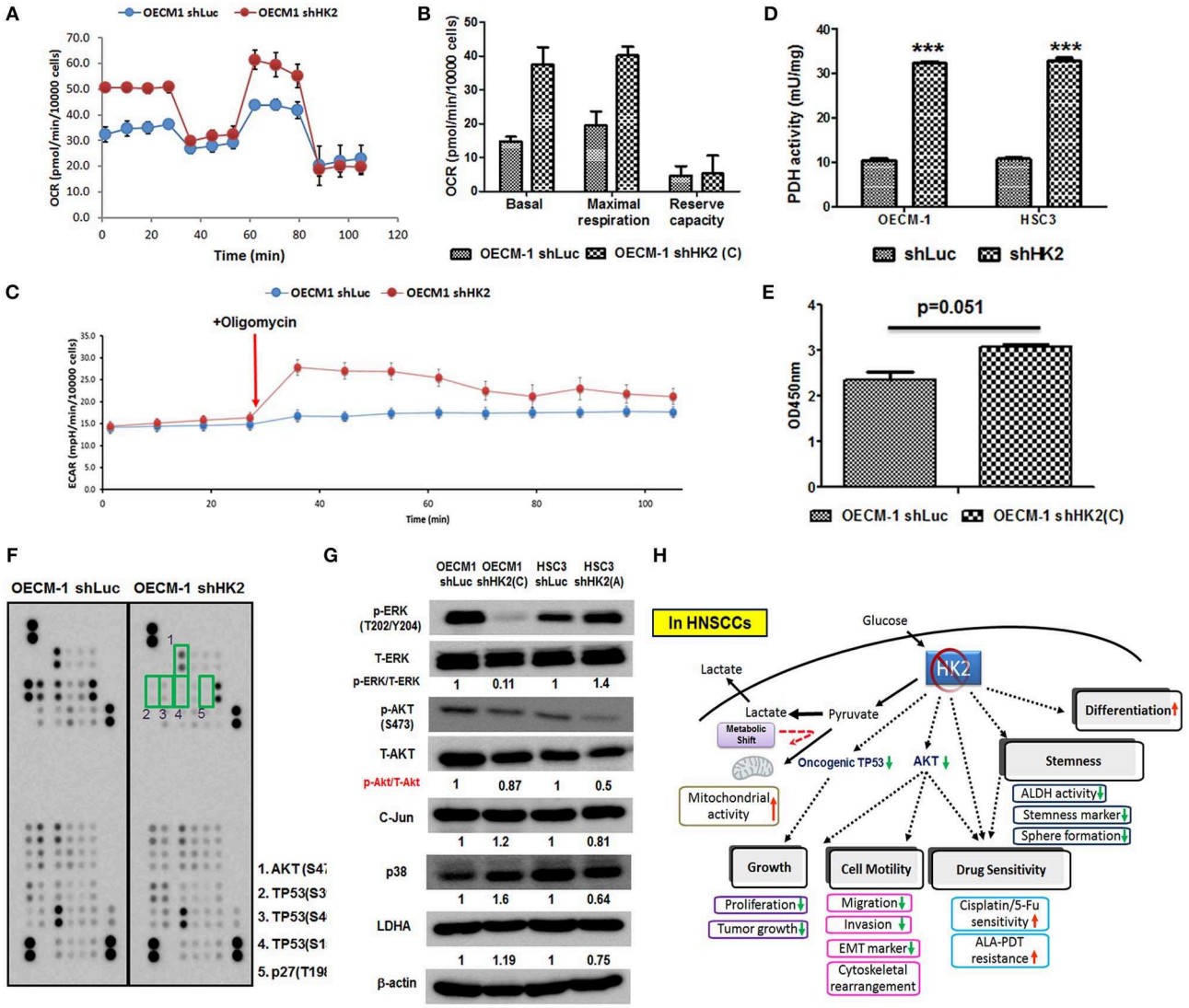

FIGURE 5 | Metabolic and molecular changes in HK2-silencing HNSCC cells. **(A,B)** Seahorse metabolic analysis showed an elevated basal respiration and maximal respiration in HK2 deficient OECM-1 cells. **(C)** Sharp increase of ECAR upon addition of ATPase inhibitor oligomycin and **(D)** increased pyruvate dehydrogenase activity reflected that HK2 loss triggers HNSCC cells toward mitochondrial metabolism. **(E)** ATP level was slightly increased in HK2-silencing OECM-1 cells. **(F)** Human protein array analysis for phosphorylated proteins differentially expressed in HK2-silencing OECM-1 cells was performed. Green boxes indicated oncogenic phosphorylated molecules: (1) Akt (S473), (2) TP53 (S392), (3) TP53 (S46), (4) TP53 (S15), and (5) p27 (T198). **(G)** Western blot analysis confirmed that phosphorylated PKB/Akt proteins is downregulated in HK2-silencing HNSCC cells. p38, P38 mitogen-activated protein kinase; LDHA, lactate dehydrogenase A. **(H)** Graphic summary of HK2-mediated regulations in HNSCC cells. Data are presented as mean ± SEM ($N > 3$). ***$P < 0.001$.

non-toxic to all sorts of vertebrates, certain failure cases were still reported in clinical test (83). It is noteworthy that 3-BP administration also resulted in great pain and inflammation in an HNSCC patient enrolled in a 3-BP trial at the Dayspring Cancer Clinic (http://www.dayspringcancerclinic.com). In addition to a demand of a larger clinical cohort, to achieve better outcomes by using 3-BP or other HK2 inhibitors, as stated in **Supplementary Table 4**, to cure cancer in clinic, a very recent article suggested that simultaneous or sequential treatment of 3-BP and other conventional therapeutic agents needs to be tested for optimal tumor-killing ability, and/or localized delivery of 3-BP directly into tumor tissues should be considered without affecting normal cells (85). Based on current findings, a more systemic study to test synergic antiproliferative effects of different HK2 inhibitors, not only for 3-BP but also for other known small molecules (listed in **Supplementary Table 4**), and their underlying molecular mechanisms in combination of treatments of chemotherapeutic drugs, radiotherapy, and targeted therapy (such as EGFR antagonist cetuximab), needs to be conducted, both *in vitro* and *in vivo*. In addition to BP-3, it is hoped that other inexpensive and safe anticancer HK2 inhibitors could also be

discovered, successfully pass clinical trials, and soon be available in global market.

DATA AVAILABILITY STATEMENT

The datasets generated for this study are available on request to the corresponding author.

ETHICS STATEMENT

The studies involving human participants were reviewed and approved by Institutional Review Boards (IRB) of MacKay Memorial Hospital and National Taiwan University Hospital, Taiwan. The patients/participants provided their written informed consent to participate in this study. This animal study was reviewed and approved by Institutional Animal Care and Use Committee (IACUC), National Yang-Ming University.

AUTHOR CONTRIBUTIONS

W-CL devised and coordinated the study. C-HH, Y-TH, T-YC, L-HC, and C-YC performed experiments. C-HH conducted animal experiments. C-HH and Y-TH performed statistical analysis. C-JL, H-MC, C-LH, J-FL, and K-WC provided samples and critical discussion. W-CL wrote the manuscript. All authors read and approved the final manuscript.

FUNDING

This work was supported by grants from Ministry of Science and Technology, Taiwan (Grant Nos. NSC-102-2314-B-010-010-, Most-103-2314-B-010-024-MY3, and MOST-106-2314-B-010-005-MY3), Yen Tjing Ling Medical Foundation (Grant No. CI-106-13) and a grant from Ministry of Education, Aiming for the Top University Plan as well as the Higher Education Sprout Project by the Ministry of Education (MOE) in Taiwan.

ACKNOWLEDGMENTS

We thank the National RNAi Core Facility at Academia Sinica in Taiwan for providing shRNA reagents. We thank Dr. Jude Clapper for review and English revision for the manuscript.

SUPPLEMENTARY MATERIAL

The Supplementary Material for this article can be found online at: https://www.frontiersin.org/articles/10.3389/fonc.2020.00176/full#supplementary-material

REFERENCES

1. Hanahan D, Weinberg RA. The hallmarks of cancer. *Cell*. (2000) 100:57–70. doi: 10.1016/S0092-8674(00)81683-9
2. Nijsten MW, van Dam GM. Hypothesis: using the Warburg effect against cancer by reducing glucose and providing lactate. *Med Hypotheses*. (2009) 73:48–51. doi: 10.1016/j.mehy.2009.01.041
3. Dang CV. Links between metabolism and cancer. *Genes Dev*. (2012) 26:877–90. doi: 10.1101/gad.189365.112
4. Racker E. History of the Pasteur effect and its pathobiology. *Mol Cell Biochem*. (1974) 5:17–23. doi: 10.1007/BF01874168
5. Warburg O. On the origin of cancer cells. *Science*. (1956) 123:309–14. doi: 10.1126/science.123.3191.309
6. Hsieh YT, Chen YF, Lin SC, Chang KW, Li WC. Targeting Cellular Metabolism Modulates Head and Neck Oncogenesis. *Int J Mol Sci*. (2019) 20:E3960. doi: 10.3390/ijms20163960
7. Vander Heiden MG Targeting cancer metabolism: a therapeutic window opens. *Nat Rev Drug Discov*. (2011) 10:671–84. doi: 10.1038/nrd3504
8. Vander Heiden MG, De Berardinis RJ. Understanding the Intersections between Metabolism and Cancer Biology. *Cell*. (2017) 168:657–669. doi: 10.1016/j.cell.2016.12.039
9. Hamanaka RB, Chandel NS. Targeting glucose metabolism for cancer therapy. *J Exp Med*. (2012) 209:211–5. doi: 10.1084/jem.20120162
10. Gatenby RA, Gillies RJ. Why do cancers have high aerobic glycolysis? *Nat Rev Cancer*. (2004) 4:891–9. doi: 10.1038/nrc1478
11. Lunt SY, Vander Heiden MG. Aerobic glycolysis: meeting the metabolic requirements of cell proliferation. *Annu Rev Cell Dev Biol*. (2011) 27:441–64. doi: 10.1146/annurev-cellbio-092910-154237
12. Wilson JE. Isozymes of mammalian hexokinase: structure, subcellular localization and metabolic function. *J Exp Biol*. (2003) 206, 2049–57. doi: 10.1242/jeb.00241
13. Roberts DJ and Miyamoto S. Hexokinase II integrates energy metabolism and cellular protection: akting on mitochondria and TORCing to autophagy. *Cell Death Differ*. (2015) 22:248–57. doi: 10.1038/cdd.2014.173
14. Liu Y, Wu K, Shi L, Xiang F, Tao K, Wang G. Prognostic significance of the metabolic marker hexokinase-2 in various solid tumors: a meta-analysis. *PLoS ONE*. (2016) 11:e0166230. doi: 10.1371/journal.pone.0166230
15. Bacci M, Giannoni E, Fearns A, Ribas R, Gao Q, Taddei ML, et al. Morandi: miR-155 drives metabolic reprogramming of ER+ breast cancer cells following long-term estrogen deprivation and predicts clinical response to aromatase inhibitors. *Cancer Res*. (2016) 76:1615–26. doi: 10.1158/0008-5472.CAN-15-2038
16. van't LJ Veer, Dai H, van de Vijver MJ, He YD, Hart AA, Mao M, et al. Gene expression profiling predicts clinical outcome of breast cancer. *Nature*. (2002) 415:530–6. doi: 10.1038/415530a
17. Liu X, Miao W, Huang M, Li L, Dai X, Wang Y. Elevated hexokinase II expression confers acquired resistance to 4-hydroxytamoxifen in breast cancer cells. *Mol Cell Proteomics*. (2019) 18:2273–2284. doi: 10.1074/mcp.RA119.001576
18. Palmieri D, Fitzgerald D, Shreeve SM, Hua E, Bronder JL, Weil RJ, et al. Analyses of resected human brain metastases of breast cancer reveal the association between up-regulation of hexokinase 2 and poor prognosis. *Mol Cancer Res*. (2009) 7:1438–45. doi: 10.1158/1541-7786.MCR-09-0234
19. Yang X, Cheng Y, Li P, Tao J, Deng X, Zhang X, et al. A lentiviral sponge for miRNA-21 diminishes aerobic glycolysis in bladder cancer T24 cells via the PTEN/PI3K/AKT/mTOR axis. *Tumour Biol*. (2015) 36:383–91. doi: 10.1007/s13277-014-2617-2
20. Huang X, Liu M, Sun H, Wang F, Xie X, Chen X, et al. HK2 is a radiation resistant and independent negative prognostic factor for patients with locally advanced cervical squamous cell carcinoma. *Int J Clin Exp Pathol*. (2015) 8:4054–63.
21. Iwamoto M, Kawada K, Nakamoto Y, Itatani Y, Inamoto S, Toda K, et al. Regulation of 18F-FDG accumulation in colorectal cancer cells with mutated KRAS. *J Nucl Med*. (2014) 55:2038–44. doi: 10.2967/jnumed.114.142927
22. Jin Z, Gu J, Xin X, Li Y, Wang H. Expression of hexokinase 2 in epithelial ovarian tumors and its clinical significance in serous ovarian cancer. *Eur J Gynaecol Oncol*. (2014) 35:519–24.
23. Wolf A, Agnihotri S, Micallef J, Mukherjee J, Sabha N, Cairns R, et al. Hexokinase 2 is a key mediator of aerobic glycolysis and promotes tumor

growth in human glioblastoma multiforme. *J Exp Med*. (2011) 208:313–26. doi: 10.1084/jem.20101470
24. Kwee SA, Hernandez B, Chan O, Wong L. Choline kinase alpha and hexokinase-2 protein expression in hepatocellular carcinoma: association with survival. *PLoS ONE*. (2012) 7:e46591. doi: 10.1371/journal.pone.0046591
25. Chen J, Zhang S, Li Y, Tang Z, Kong W. Hexokinase 2 overexpression promotes the proliferation and survival of laryngeal squamous cell carcinoma. *Tumour Biol*. (2014) 35:3743–53. doi: 10.1007/s13277-013-1496-2
26. Wang H, Wang L, Zhang Y, Wang J, Deng Y, Lin D. Inhibition of glycolytic enzyme hexokinase II (HK2) suppresses lung tumor growth. *Cancer Cell Int*. (2016) 16: 38. doi: 10.1186/s12935-016-0313-6
27. Botzer LE, Maman S, Sagi-Assif O, Meshel T, Nevo I, Yron I. Hexokinase 2 is a determinant of neuroblastoma metastasis. *Br J Cancer*. (2016) 114:759–66. doi: 10.1038/bjc.2016.26
28. Binderup T, Knigge UP, Federspiel B, Sommer P, Hasselby JP, Loft A. Gene expression of glucose transporter 1 (GLUT1), hexokinase 1 and hexokinase 2 in gastroenteropancreatic neuroendocrine tumors: correlation with F-18-fluorodeoxyglucose positron emission tomography and cellular proliferation. *Diagnostics*. (2013) 3:372–84. doi: 10.3390/diagnostics3040372
29. Ogawa H, Nagano H, Konno M, Eguchi H, Koseki J, Kawamoto K, et al. The combination of the expression of hexokinase 2 and pyruvate kinase M2 is a prognostic marker in patients with pancreatic cancer. *Mol Clin Oncol*. (2015) 3:563–571. doi: 10.3892/mco.2015.490
30. Wang L, Xiong H, Wu F, Zhang Y, Wang J, Zhao L, et al. Hexokinase 2-mediated Warburg effect is required for PTEN- and p53-deficiency-driven prostate cancer growth. *Cell Rep*. (2014) 8:1461–74. doi: 10.1016/j.celrep.2014.07.053
31. Wu J, Hu L, Wu F, Zou L, He T. Poor prognosis of hexokinase 2 overexpression in solid tumors of digestive system: a meta-analysis. *Oncotarget*. (2017) 8:32332–44. doi: 10.18632/oncotarget.15974
32. Jiang S, Zhang LF, Zhang HW, Hu S, Lu MH, Liang S, et al. A novel miR-155/miR-143 cascade controls glycolysis by regulating hexokinase 2 in breast cancer cells. *EMBO J*. (2012) 31:1985–98. doi: 10.1038/emboj.2012.45
33. Li M, Jin R, Wang W, Zhang T, Sang J, Li N, et al. STAT3 regulates glycolysis via targeting hexokinase 2 in hepatocellular carcinoma cells. *Oncotarget*. (2017) 8:24777–84. doi: 10.18632/oncotarget.15801
34. Li J, Liu T, Zhao L, Chen W, Hou H, Ye Z, et al. Ginsenoside 20(S)Rg3 inhibits the Warburg effect through STAT3 pathways in ovarian cancer cells. *Int J Oncol*. (2015) 46:775–81. doi: 10.3892/ijo.2014.2767
35. Li Z, Li X, Wu S, Xue M, Chen W. Long non-coding RNA UCA1 promotes glycolysis by upregulating hexokinase 2 through the mTOR-STAT3/microRNA143 pathway. *Cancer Sci*. (2014) 105:951–5. doi: 10.1111/cas.12461
36. Li W, Ma X, Li N, Liu H, Dong Q, Zhang J, et al. Resveratrol inhibits hexokinases II mediated glycolysis in non-small cell lung cancer via targeting Akt signaling pathway. *Exp Cell Res*. (2016) 349:320–327. doi: 10.1016/j.yexcr.2016.11.002
37. Liu CC, Chou KT, Hsu JW, Lin JH, Hsu TW, Yen DH, et al. High metabolic rate and stem cell characteristics of esophageal cancer stem-like cells depend on the Hsp27-AKT-HK2 pathway. *Int J Cancer*. (2019) 145:2144–2156. doi: 10.1002/ijc.32301
38. Gao X, Han H. Jolkinolide B inhibits glycolysis by downregulating hexokinase 2 expression through inactivating the Akt/mTOR pathway in non-small cell lung cancer cells. *J Cell Biochem*. (2018) 119:4967–4974. doi: 10.1002/jcb.26742
39. Kim JE, He Q, Chen Y, Shi C, Yu K. mTOR-targeted therapy: differential perturbation to mitochondrial membrane potential and permeability transition pore plays a role in therapeutic response. *Biochem Biophys Res Commun*. (2014) 447:184–91. doi: 10.1016/j.bbrc.2014.03.124
40. deWaal D, Nogueira V, Terry AR, Patra KC, Jeon SM, Guzman G, et al. Hexokinase-2 depletion inhibits glycolysis and induces oxidative phosphorylation in hepatocellular carcinoma and sensitizes to metformin. *Nat Commun*. (2018) 9:446. doi: 10.1038/s41467-017-02733-4
41. Xiong X, Wen YA, Mitov MI, CO M, Miyamoto S, Gao T. PHLPP regulates hexokinase 2-dependent glucose metabolism in colon cancer cells. *Cell Death Discov*. (2017) 3:16103. doi: 10.1038/cddiscovery.2016.103
42. Jiao L, Zhang HL, Li DD, Yang KL, Tang J, Li X, et al. Regulation of glycolytic metabolism by autophagy in liver cancer involves selective autophagic degradation of HK2 (hexokinase 2). *Autophagy*. (2018) 14:671–684. doi: 10.1080/15548627.2017.1381804
43. Zhang XY, Zhang M, Cong Q, Zhang MX, Zhang MY, Lu YY, et al. Hexokinase 2 confers resistance to cisplatin in ovarian cancer cells by enhancing cisplatin-induced autophagy. *Int J Biochem Cell Biol*. (2018) 95:9–16. doi: 10.1016/j.biocel.2017.12.010
44. Arora KK, Pedersen PL. Functional significance of mitochondrial bound hexokinase in tumor cell metabolism. Evidence for preferential phosphorylation of glucose by intramitochondrially generated ATP. *J Biol Chem*. (1988) 263:17422–8.
45. Mathupala SP, Ko YH, Pedersen PL. Hexokinase II: cancer's double-edged sword acting as both facilitator and gatekeeper of malignancy when bound to mitochondria. *Oncogene*. (2006) 25:4777–86. doi: 10.1038/sj.onc.1209603
46. Zhang D, Yip YM and Li L. *In silico* construction of HK2-VDAC1 complex and investigating the HK2 binding-induced molecular gating mechanism of VDAC1. *Mitochondrion*. (2016) 30:222–8. doi: 10.1016/j.mito.2016.08.009
47. Nagdas S, Kashatus JA, Nascimento A, Hussain SS, Trainor RE, Pollock SR, et al. Drp1 promotes KRas-driven metabolic changes to drive pancreatic tumor growth. *Cell Rep*. (2019) 28:45–59.e5. doi: 10.1016/j.celrep.2019.07.031
48. Cheung EC, Ludwig RL, Vousden KH. Mitochondrial localization of TIGAR under hypoxia stimulates HK2 and lowers ROS and cell death. *Proc Natl Acad Sci USA*. (2012) 109:20491–6. doi: 10.1073/pnas.1206530109
49. Neary CL, Pastorino JG. Akt inhibition promotes hexokinase 2 redistribution and glucose uptake in cancer cells. *J Cell Physiol*. (2013) 228:1943–8. doi: 10.1002/jcp.24361
50. Gao F, Li M, Liu WB, Zhou ZS, Zhang R, Li JL, et al. Epigallocatechin gallate inhibits human tongue carcinoma cells via HK2mediated glycolysis. *Oncol Rep*. (2015) 33:1533–9. doi: 10.3892/or.2015.3727
51. Hou X, Liu Y, Liu H, Chen X, Liu M, Che H, et al. PERK silence inhibits glioma cell growth under low glucose stress by blockage of p-AKT and subsequent HK2's mitochondria translocation. *Sci Rep*. (2015) 5:9065. doi: 10.1038/srep09065
52. Gregersen LH, Jacobsen A, Frankel LB, Wen J, Krogh A, Lund AH. MicroRNA-143 down-regulates Hexokinase 2 in colon cancer cells. *BMC Cancer*. (2012) 12:232. doi: 10.1186/1471-2407-12-232
53. Yoshino H, Enokida H, Itesako T, Kojima S, Kinoshita T, Tatarano S, et al. Tumor-suppressive microRNA-143/145 cluster targets hexokinase-2 in renal cell carcinoma. *Cancer Sci*. (2013) 104:1567–74. doi: 10.1111/cas.12280
54. Guo W, Qiu Z, Wang Z, Wang Q, Tan N, Chen T, et al. MiR-199a-5p is negatively associated with malignancies and regulates glycolysis and lactate production by targeting hexokinase 2 in liver cancer. *Hepatology*. (2015) 62:1132–44. doi: 10.1002/hep.27929
55. Qin Y, Cheng C, Lu H, Wang Y. MiR-4458 suppresses glycolysis and lactate production by directly targeting hexokinase2 in colon cancer cells. *Biochem Biophys Res Commun*. (2016) 469:37–43. doi: 10.1016/j.bbrc.2015.11.066
56. Song J, Wu X, Liu F, Li M, Sun Y, Wang Y, et al. Long non-coding RNA PVT1 promotes glycolysis and tumor progression by regulating miR-497/HK2 axis in osteosarcoma. *Biochem Biophys Res Commun*. (2017) 490:217–224. doi: 10.1016/j.bbrc.2017.06.024
57. Fan L, Huang C, Li J, Gao T, Lin Z, Yao T. Long noncoding RNA urothelial cancer associated 1 regulates radioresistance via the hexokinase 2/glycolytic pathway in cervical cancer. *Int J Mol Med*. (2018) 42:2247–59. doi: 10.3892/ijmm.2018.3778
58. Ma Y, Hu M, Zhou L, Ling S, Li Y, Kong B. Long non-coding RNA HOTAIR promotes cancer cell energy metabolism in pancreatic adenocarcinoma by upregulating hexokinase-2. *Oncol Lett*. (2019) 18:2212–9. doi: 10.3892/ol.2019.10551
59. Lee HG, Kim H, Son T, Jeong Y, Kim SU, Dong SM, et al. Regulation of HK2 expression through alterations in CpG methylation of the HK2 promoter during progression of hepatocellular carcinoma. *Oncotarget*. (2016) 7:41798–810. doi: 10.18632/oncotarget.9723
60. Chen YS, Huang WL, Chang SH, Chang KW, Kao SY, Lo JF, et al. Enhanced filopodium formation and stem-like phenotypes in a novel metastatic head and neck cancer cell model. *Oncol Rep*. (2013) 30:2829–37. doi: 10.3892/or.2013.2772
61. Liu CJ, Chang WJ, Chen CY, Sun FJ, Cheng HW, Chen TY, et al. Dynamic cellular and molecular modulations of diabetes mediated head

and neck carcinogenesis. *Oncotarget*. (2015) 6:29268–84. doi: 10.18632/oncotarget.4922
62. Chen TY, Hsieh YT, Huang JM, Liu CJ, Chuang LT, Huang PC, et al. Determination of pyruvate metabolic fates modulates head and neck tumorigenesis. *Neoplasia*. (2019) 21:641–52. doi: 10.1016/j.neo.2019.04.007
63. Deng M, Bragelmann J, Kryukov I, Saraiva-Agostinho N, Perner S. FirebrowseR: an R client to the broad institute's firehose pipeline. *Database*. (2017) 2017:160. doi: 10.1093/database/baw160
64. Chandrashekar DS, Bashel B, Balasubramanya SAH, Creighton CJ, Ponce-Rodriguez I, Chakravarthi B, et al. UALCAN: a portal for facilitating tumor subgroup gene expression and survival analyses. *Neoplasia*. (2017) 19:649–58. doi: 10.1016/j.neo.2017.05.002
65. Uhlen M, Zhang C, Lee S, Sjostedt E, Fagerberg L, Bidkhori G, et al. A pathology atlas of the human cancer transcriptome. *Science*. (2017) 357:eaan2507. doi: 10.1126/science.aan2507
66. San-Millan, Brooks GA. Reexamining cancer metabolism: lactate production for carcinogenesis could be the purpose and explanation of the Warburg Effect. *Carcinogenesis*. (2017) 38:119–33. doi: 10.1093/carcin/bgw127
67. Fife CM, McCarroll JA, Kavallaris M. Movers and shakers: cell cytoskeleton in cancer metastasis. *Br J Pharmacol*. (2014) 171:5507–23. doi: 10.1111/bph.12704
68. Brabletz T, Kalluri R, Nieto MA, Weinberg RA. EMT in cancer. *Nat Rev Cancer*. (2018) 18:128–134. doi: 10.1038/nrc.2017.118
69. Seshadri M, Spernyak JA, Mazurchuk R, Camacho SH, Oseroff AR, Cheney RT, et al. Tumor vascular response to photodynamic therapy and the antivascular agent 5,6-dimethylxanthenone-4-acetic acid: implications for combination therapy. *Clin Cancer Res*. (2005) 11:4241–50. doi: 10.1158/1078-0432.CCR-04-2703
70. Nokes B, Apel M, Jones C, Brown G, Lang JE. Aminolevulinic acid (ALA): photodynamic detection and potential therapeutic applications. *J Surg Res*. (2013) 181:262–71. doi: 10.1016/j.jss.2013.02.002
71. Fayter D, Corbett M, Heirs M, Fox D, Eastwood A. A systematic review of photodynamic therapy in the treatment of pre-cancerous skin conditions, barrett's oesophagus and cancers of the biliary tract, brain, head and neck, lung, oesophagus and skin. *Health Technol Assess*. (2010) 14:1–288. doi: 10.3310/hta14370
72. Kulsum S, Sudheendra HV, Pandian R, Ravindra DR, Siddappa G, R N, et al. Cancer stem cell mediated acquired chemoresistance in head and neck cancer can be abrogated by aldehyde dehydrogenase 1 A1 inhibition. *Mol Carcinog*. (2017) 56:694–711. doi: 10.1002/mc.22526
73. Keibler MA, Wasylenko TM, Kelleher JK, Iliopoulos O, Vander Heiden MG, Stephanopoulos G. Metabolic requirements for cancer cell proliferation. *Cancer Metab*. (2016) 4:16. doi: 10.1186/s40170-016-0156-6
74. Gershon TR, Crowther AJ, Liu H, Miller CR, Deshmukh M. Cerebellar granule neuron progenitors are the source of Hk2 in the postnatal cerebellum. *Cancer Metab*. (2013) 1:15. doi: 10.1186/2049-3002-1-15
75. Li LQ, Yang Y, Chen H, Zhang L, Pan D, Xie WJ. MicroRNA-181b inhibits glycolysis in gastric cancer cells via targeting hexokinase 2 gene. *Cancer Biomark*. (2016) 17:75–81. doi: 10.3233/CBM-160619
76. Sonego M, Schiappacassi M, Lovisa S, Dall'Acqua A, Bagnoli M, Lovat F, et al. Stathmin regulates mutant p53 stability and transcriptional activity in ovarian cancer. *EMBO Mol Med*. (2013) 5:707–22. doi: 10.1002/emmm.201201504
77. Matsumoto M, Furihata M, Kurabayashi A, Sasaguri S, Araki K, Hayashi H, et al. Prognostic significance of serine 392 phosphorylation in overexpressed p53 protein in human esophageal squamous cell carcinoma. *Oncology*. (2004) 67:143–50. doi: 10.1159/000081001
78. Larrea MD, Liang J, Da Silva T, Hong F, Shao SH, Han K, et al. Phosphorylation of p27Kip1 regulates assembly and activation of cyclin D1-Cdk4. *Mol Cell Biol*. (2008) 28:6462–72. doi: 10.1128/MCB.02300-07
79. Larrea MD, Hong F, Wander SA, da Silva TG, Helfman D, Lannigan D, et al. RSK1 drives p27Kip1 phosphorylation at T198 to promote RhoA inhibition and increase cell motility. *Proc Natl Acad Sci USA*. (2009) 106:9268–73. doi: 10.1073/pnas.0805057106
80. Dai W, Wang F, Lu J, Xia Y, He L, Chen K, et al. By reducing hexokinase 2, resveratrol induces apoptosis in HCC cells addicted to aerobic glycolysis and inhibits tumor growth in mice. *Oncotarget*. (2015) 6:13703–17. doi: 10.18632/oncotarget.3800
81. Geng C, Li J, Ding F, Wu G, Yang Q, Sun Y, et al. Curcumin suppresses 4-hydroxytamoxifen resistance in breast cancer cells by targeting SLUG/Hexokinase 2 pathway. *Biochem Biophys Res Commun*. (2016) 473:147–53. doi: 10.1016/j.bbrc.2016.03.067
82. Li W, Zheng M, Wu S, Gao S, Yang M, Li Z, et al. Benserazide, a dopadecarboxylase inhibitor, suppresses tumor growth by targeting hexokinase 2. *J Exp Clin Cancer Res*. (2017) 36:58. doi: 10.1186/s13046-017-0530-4
83. Lis P, Dylag M, Niedzwiecka K, Ko YH, Pedersen PL, Goffeau A. The HK2 Dependent "Warburg effect" and mitochondrial oxidative phosphorylation in Cancer: targets for effective therapy with 3-Bromopyruvate. *Molecules*. (2016) 21:E1730. doi: 10.3390/molecules21121730
84. Lin H, Zeng J, Xie R, Schulz MJ, Tedesco R, Qu J, et al. Discovery of a Novel 2,6-disubstituted glucosamine series of potent and selective hexokinase 2 inhibitors. *ACS Med Chem Lett*. (2016) 7:217–22. doi: 10.1021/acsmedchemlett.5b00214
85. Abdel-Wahab F, Mahmoud W, Al-Harizy RM. Targeting glucose metabolism to suppress cancer progression: prospective of anti-glycolytic cancer therapy. *Pharmacol Res*. (2019) 150:104511. doi: 10.1016/j.phrs.2019.104511

Conflict of Interest: The authors declare that the research was conducted in the absence of any commercial or financial relationships that could be construed as a potential conflict of interest.

frontiers in Oncology

ORIGINAL RESEARCH
published: 11 March 2020
doi: 10.3389/fonc.2020.00217

Apatinib Inhibits Cell Proliferation and Induces Autophagy in Human Papillary Thyroid Carcinoma via the PI3K/Akt/mTOR Signaling Pathway

Xiangrui Meng[1†], Huijuan Wang[2†], Jingzhu Zhao[2], Linfei Hu[2], Jingtai Zhi[2], Songfeng Wei[2], Xianhui Ruan[2], Xiukun Hou[2], Dapeng Li[2], Jun Zhang[2], Weiwei Yang[3], Biyun Qian[4], Yu Wu[2,5], Yuan Zhang[6], Zhaowei Meng[7], Lizhao Guan[8], Huilai Zhang[1], Xiangqian Zheng[2]* and Ming Gao[2]**

[1] Key Laboratory of Cancer Prevention and Therapy, Department of Lymphoma, National Clinical Research Center for Cancer, Tianjin's Clinical Research Center for Cancer, Tianjin Medical University Cancer Institute and Hospital, Tianjin, China, [2] Key Laboratory of Cancer Prevention and Therapy, Department of Thyroid and Neck Tumor, National Clinical Research Center for Cancer, Tianjin's Clinical Research Center for Cancer, Tianjin Medical University Cancer Institute and Hospital, Tianjin, China, [3] Department of Otolaryngology-Head and Neck Surgery, Tianjin First Center Hospital, Tianjin, China, [4] Department of Epidemiology, School of Public Health, Shanghai Jiao Tong University, Shanghai, China, [5] Department of Head and Neck Surgery, Fujian Cancer Hospital, Fujian Medical University Cancer Hospital, Fujian, China, [6] Department of Head and Neck Surgery, Jiangsu Cancer Hospital, Jiangsu Institute of Cancer Research, Nanjing Medical University Affiliated Cancer Hospital, Nanjing, China, [7] Department of Nuclear Medicine, Tianjin Medical University General Hospital, Tianjin, China, [8] Department of Biochemistry and Molecular Biology, School of Basic Medical Sciences, Tianjin Medical University, Tianjin, China

Background: Patients with metastatic radioiodine-refractory papillary thyroid carcinoma (PTC) have limited treatment options and a poor prognosis. There is an urgent need to develop new drugs targeting PTC for clinical application. Apatinib, a novel small-molecule tyrosine kinase inhibitor (TKI), is highly selective for vascular endothelial growth factor receptor-2 (VEGFR2) and exhibits antitumor effects in a variety of solid tumors. Although apatinib has been shown to be safe and efficacious in radioiodine-refractory differentiated thyroid cancer, the mechanism underlying its antitumor effect is unclear. In this report, we explored the effects of apatinib on PTC *in vitro* and *in vivo*.

Methods: VEGFR2 expression levels were evaluated by immunohistochemistry (IHC), qPCR, and western blotting (WB). The effects of apatinib on cell viability, colony formation, and migration in the Transwell assay were assessed *in vitro*, and its effect on tumor growth rate was assessed *in vivo*. In addition, the levels of proteins in signaling pathways were determined by WB. Finally, the autophagy level was assessed by WB, immunofluorescence (IF), and transmission electron microscopy.

Results: We found that high VEGFR2 expression is associated with tumor size, T stage, and lymph node metastasis in patients with PTC and that apatinib inhibits PTC cell growth, promotes apoptosis, and induces cell cycle arrest through the PI3K/Akt/mTOR signaling pathway. Moreover, apatinib induces autophagy, and pharmacological inhibition of autophagy or small interfering RNA (siRNA)-mediated targeting of autophagy-associated gene 5 (ATG5) can further increase PTC cell apoptosis.

OPEN ACCESS

Edited by:
Jorge A. R. Salvador, University of Coimbra, Portugal

Reviewed by:
Jianfeng Huang, Sanford Burnham Prebys Medical Discovery Institute, United States
Wenmin Xia, University of California, San Diego, United States
Haixia Guan, The First Affiliated Hospital of China Medical University, China

***Correspondence:**
Huilai Zhang
zhlwgq@126.com
Xiangqian Zheng
xiangqian_zheng@163.com
Ming Gao
headandneck2008@126.com

[†]These authors have contributed equally to this work

Specialty section:
This article was submitted to Head and Neck Cancer, a section of the journal Frontiers in Oncology

Received: *13 August 2019*
Accepted: *07 February 2020*
Published: *11 March 2020*

Citation:
Meng X, Wang H, Zhao J, Hu L, Zhi J, Wei S, Ruan X, Hou X, Li D, Zhang J, Yang W, Qian B, Wu Y, Zhang Y, Meng Z, Guan L, Zhang H, Zheng X and Gao M (2020) Apatinib Inhibits Cell Proliferation and Induces Autophagy in Human Papillary Thyroid Carcinoma via the PI3K/Akt/mTOR Signaling Pathway. Front. Oncol. 10:217. doi: 10.3389/fonc.2020.00217

Conclusion: Our data suggest that apatinib can induce apoptosis and autophagy via the PI3K/Akt/mTOR signaling pathway for the treatment of PTC and that autophagy is a potential novel target for future therapy in resistant PTC.

Keywords: apatinib, papillary thyroid carcinoma, PI3K, apoptosis, autophagy

INTRODUCTION

Thyroid cancer is the most common endocrine system tumor, and 53,990 new cases were predicted in 2018 (1). Standard treatments for papillary thyroid carcinoma (PTC), the most common type of thyroid cancer, include surgery, thyroid-stimulating hormone suppression, and radioiodine treatment. With these standard treatments, most patients have a good prognosis; however, 5% of patients present with radioiodine-refractory thyroid cancer and distant metastasis (2, 3). Currently, few treatment options are available for these patients. Therefore, new therapeutic strategies are urgently needed for PTC patients with advanced disease.

With an improved understanding of the molecular mechanisms of thyroid cancer, several important tumorigenic factors have been identified as new targets for antitumor therapy (4–6). A series of antitumor drugs, especially multiple targeted tyrosine kinase inhibitors (TKIs), have been developed for clinical treatment. Among them, sorafenib and vandetanib have been approved as standard therapies for advanced PTC (7, 8). In addition, an increasing number of TKIs are undergoing clinical trials. Apatinib is a new oral TKI that inhibits vascular endothelial growth factor receptor-2 (VEGFR2) with high selectivity. Apatinib has been approved as a safe and effective drug for patients with advanced gastric cancer for whom standard chemotherapy has failed (9, 10). In addition, apatinib has shown antitumor effects in various types of solid tumors in a number of ongoing phase II and III clinical trials (11, 12). Lin et al. (13) reported that apatinib showed promising efficacy in a small number of patients with radioiodine-refractory differentiated thyroid cancer. However, the antitumor mechanism of apatinib in PTC is unclear.

Drug resistance, a perpetual theme in the field of cancer treatment, is associated with multiple mechanisms. A series of studies have shown that autophagy activity plays an important role in TKI resistance. Autophagy is a catabolic process that is prevalent in eukaryotic cells that provides energy to support metabolism and survival by degrading proteins and organelles and maintains cell homeostasis (14). Accumulating evidence associates autophagy with adaptive drug resistance in multiple tumors. Patients with chronic lymphocytic leukemia who presented a higher level of autophagy were reported to exhibit a shorter survival time after treatment with imatinib than those who presented a lower level of autophagy, and imatinib treatment was more efficacious in patients with a higher level of autophagy. The same phenomenon was observed in the treatment of differentiated thyroid cancer with vemurafenib (15). Vemurafenib, a selective RAF inhibitor, did not achieve good results in the treatment of B-Raf mutant thyroid cancer, and the mechanism of drug resistance was shown to be related to autophagy induced by vemurafenib. Therefore, autophagy inhibition has become a potential target for TKI-resistant cancers.

In this study, we found that apatinib had an antitumor effect on PTC *in vitro* and *in vivo*. We also discovered that apatinib could induce protective autophagy. Notably, we investigated the relationship between apoptosis and autophagy induced by apatinib and inferred that targeting apatinib-induced autophagy has potential therapeutic benefit in the treatment of PTC.

Abbreviations: PTC, papillary thyroid carcinoma; VEGFR2, vascular endothelial growth factor receptor-2; ATG5, autophagy-associated gene 5; TKIs, tyrosine kinase inhibitors.

MATERIALS AND METHODS

Reagents

Apatinib was kindly provided by Jiangsu Hengrui Medicine Company (Jiangsu, China). The following primary antibodies were used: anti-VEGFR2, anti-Akt, anti-phospho-Akt (anti-p-Akt), anti-mTOR, anti-phospho-mTOR (anti-p-mTOR), anti-P70S6K, anti-phospho-P70S6K (anti-p-P70S6K), anti-ULK1, anti-phospho-ULK1 [anti-p-ULK1 (Ser 757)], anti-cyclin D1, anti-Bcl-2, anti-cleaved caspase3, anti-P21, anti-Bax, anti-ATG5, anti-P62/SQSTM1, anti-LC3B, and anti-Ki-67 antibodies (Cell Signaling Technology, Danvers, MA, USA), and anti-GAPDH and anti-cleaved PARP antibodies (GeneTex, Irvine, CA, USA). Hydroxychloroquine (HCQ) and SC79 were purchased from Selleck Chemicals (Houston, TX, USA).

Cell Lines and Cell Culture

Four PTC cell lines (BCPAP, K1, KTC-1, and TPC-1 cells), two ATC cell lines (CAL-62 and 8505C cells), and one normal follicular epithelial cell line (Nthy-oris-3 cells; N9) were used in this study. K-1, TPC-1, and N9 cells were purchased from American Type Culture Collection (ATCC, USA), and the other cell lines were purchased from the Type Culture Collection of the Chinese Academy of Sciences (Shanghai, China). All the cell lines used in our experiments were routinely authenticated with short tandem repeat DNA profiling analysis by us or the investigator from which we received the cells, and the passage number of the cells used for experiments was ∼20–30 in our laboratory. The cells were cultured in RPMI-1640 or DMEM supplemented with 10% FBS and 1% antibiotics (penicillin and streptomycin). All the cells were maintained in a humidified incubator at 37°C with 5% CO_2. All culture reagents were purchased from Gibco (Grand Island, NY, USA).

Clinical Data and Tissue Samples

A total of 187 patients diagnosed with PTC between January 2013 and June 2013 at Tianjin Medical University Cancer were enrolled in the study. Paraffinized blocks of cancer tissue were used to generate tissue microarrays (TMAs), with a random selection of 43 adjacent normal thyroid follicular tissues used as a control. Fresh cancer and adjacent normal thyroid follicular tissue specimens were collected from 22 PTC patients. All patients provided informed consent. This study was performed with the approval of the Tianjin Medical University Institutional Review Board.

Animals

Twenty 4-week-old female NSG mice weighing 20 to 22 g purchased from SPF Biotechnology (Beijing, China) were used for the K-1 cell xenografts. All mice were housed under pathogen-free conditions. All animal experiments were carried out with the approval of the Ethics Committee of the Tianjin Medical University Cancer Institute and Hospital.

Immunohistochemistry

The 3 μm sections on the TMA and from the paraffin block were subjected to immunohistochemical staining for

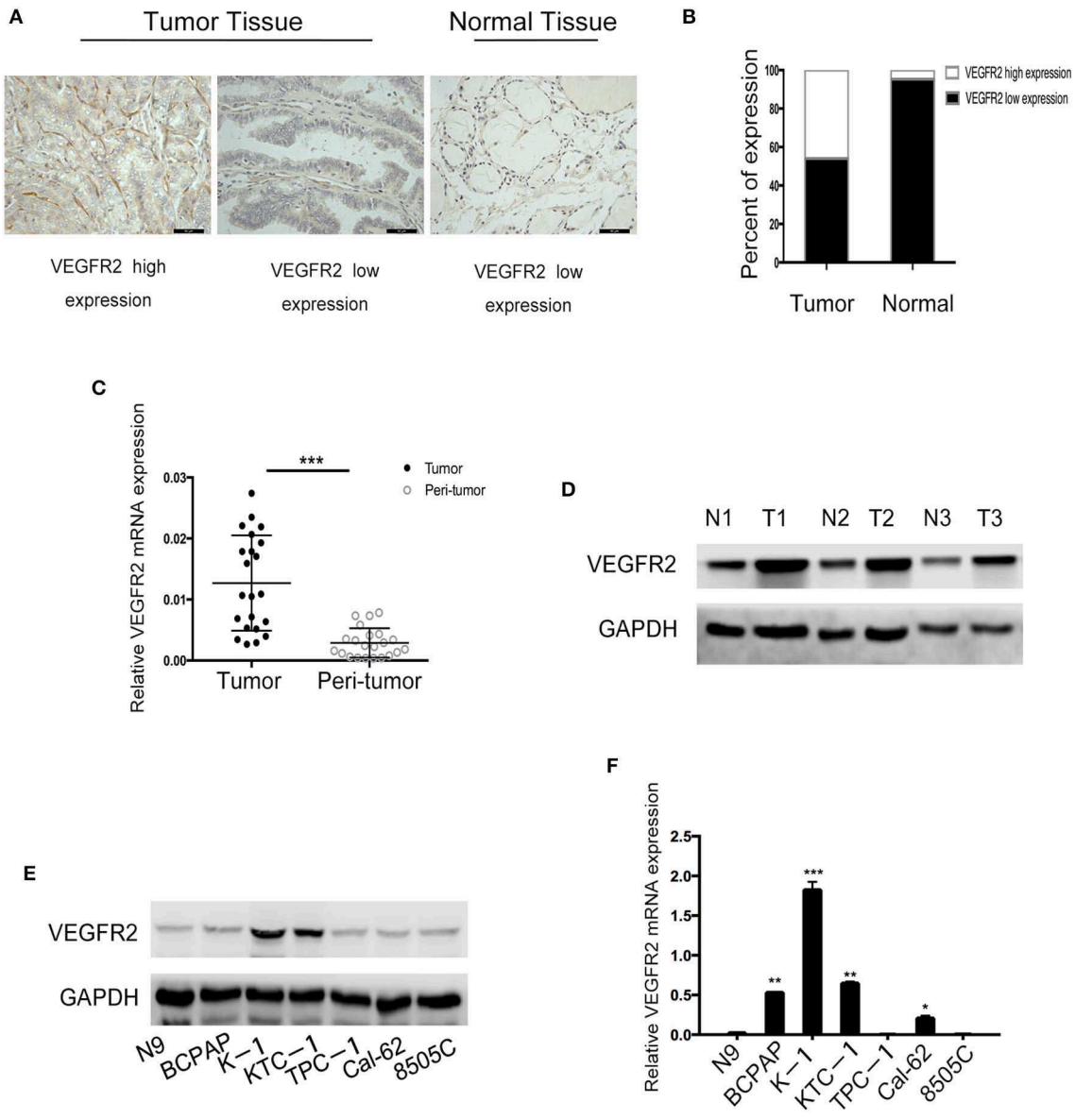

FIGURE 1 | VEGFR2 expression is elevated in PTC. **(A)** Immunohistochemical staining of a TMA containing PTC and normal thyroid follicular tissue specimens for VEGFR2. **(B)** VEGFR2 expression in PTC and normal thyroid follicular tissue. **(C)** VEGFR2 mRNA levels in PTC and normal thyroid follicular tissue. **(D)** Western blot assay showing increased VEGFR2 expression in PTC tissue compared to normal thyroid tissue. **(E)** Western blot assay of VEGFR2 expression in thyroid cell lines. **(F)** VEGFR2 mRNA levels in thyroid cell lines. Data are expressed as the mean ± SD (*$P < 0.05$, **$P < 0.01$, ***$P < 0.001$ vs. N9 cells).

VEGFR2, cleaved caspase3, and Ki-67 according to standard immunohistochemistry (IHC) protocol. Signals were amplified using a DAB substrate kit. Images were taken with an Olympus BX51 microscope. The results were evaluated independently by two experienced pathologists and scored with the H-score method.

RNA Extraction and Quantitative RT-PCR

Total RNA was extracted from tissues and cells by using a TRIzol reagent (Invitrogen, Carlsbad, CA, USA), and total RNA was reverse-transcribed to cDNA using PrimeScript RT Master Mix (TaKaRa, Tokyo, Japan). To quantify VEGFR2 and actin mRNA levels, quantitative RT-PCR was performed on the reverse-transcribed products with SYBR Premix Ex Taq II (TakaRa, Tokyo, Japan) and specific primers. The sequences of the primers were as follows: 5′-GTGATCGGAAATGACACTGGAG-3′ and 5′-CATGTTGGTCACTAACAGAAGCA-3′.

Cell-Viability and Colony-Formation Assays

The cell counting kit-8 (CCK8, Dojindo, Japan) assay was used as previously described to assess cell viability. The IC50 was calculated from survival curves using GraphPad Prism 7.0. For the colony-formation assay, cells were seeded at 500 cells per well in 6-well plates on the day before the experiment and then cultured in a medium containing apatinib at different concentrations for 2 weeks. Cell colonies were stained with 0.1% crystal violet before being photographed.

Cell Apoptosis and Cell Cycle Analyses

Cells were treated with apatinib at different concentrations for 24 h, collected by trypsinization, washed twice with PBS, and stained with staining solution from an Annexin V/FITC detection kit. The samples were analyzed by flow cytometry according to the kit's instructions.

Cells were treated with apatinib at different concentrations for 24 h, collected by trypsinization, and washed twice with PBS. The harvested cells were fixed with 70% cold ethanol at −20°C overnight and stained with a propidium iodide (PI) solution containing RNase. Samples were analyzed by flow cytometry.

Protein Extraction and Western Blotting (WB)

Proteins were extracted from different cells by using protease and phosphatase inhibitors according to the manufacturer's instructions, and the protein concentration was quantified using the BCA method. Equal amounts of protein were resolved by 8%−12% SDS-PAGE and transferred to PVDF membranes. Primary antibodies against the following proteins were used: VEGFR2, Akt, p-Akt, mTOR, p-mTOR, P70S6K, p-P70S6K, ULK1, p-ULK1 (Ser 757), cleaved PARP, Bcl-2, Bax, cleaved caspase3, cyclin D1, P21, P62, ATG5, and LC3B.

TABLE 1 | VEGFR2 expression in thyroid cancer and normal thyroid follicular tissue.

VEGFR2 expression	Tumor tissue	Normal tissue	χ^2	*p*-value
Low	101 (54%)	41 (95.4%)		
High	86 (46%)	2 (4.6%)	23.571	0.000

Immunofluorescence (IF) Staining

Cells were cultivated on coverslips, incubated with 5 μM apatinib for 24 h, fixed in 4% paraformaldehyde for 20 min, and then permeabilized with 0.2% Triton X-100 for 5 min. After being blocked with 5% BSA for 1 h, the cells were incubated with anti-LC3B primary antibody overnight at 4°C. Then, the cells were washed, incubated with secondary antibody, and stained with 4',6-diamidino-2-phenylindole (DAPI) (Solarbio, Beijing, China). Cells mounted on coverslips were observed by confocal microscopy.

Cells were incubated with apatinib with or without HCQ in the above steps.

Transmission Electron Microscopy

The ultrastructure of autophagosomes in the treated cells was identified by transmission electron microscopy as described previously (16).

RNA Interference

Small interfering RNA (siRNA) targeting ATG5 was designed and synthesized by GenePharma (Shanghai, China). K-1 cells were transfected with ATG5 siRNA with Lipofectamine 2000 according to the manufacturer's instructions. The total protein was extracted 48 h after transfection as described previously (17).

TABLE 2 | Relationship between clinicopathological features and VEGFR2 expression in PTC ($n = 187$).

Clinicopathological feature	VEGFR2 expression		χ^2	*p*-value
	Low	High		
Age				
<55	81 (52.6%)	73 (47.4%)	0.702	0.402
≥55	20 (60.6%)	13 (39.4%)		
Gender				
Male	22 (41.5%)	31 (58.5%)	4.654	0.031
Female	79 (59.0%)	55 (41.0%)		
Tumor size				
>1	47 (40.2%)	70 (59.8%)	24.102	0.000
≤1	54 (77.1%)	16 (22.9%)		
Multifocality				
Absent	65 (50.8%)	63 (49.2%)	1.703	0.192
Present	36 (61.0%)	23 (39.0%)		
T stage				
I–II	98 (58.0%)	71 (42.0%)	11.182	0.001
III–IV	3 (16.7%)	15 (83.3%)		
Lymph node metastasis				
Absent	70 (76.9%)	21 (23.1%)	37.464	0.000
Present	31 (32.3%)	65 (67.7%)		
TNM stage				
I–II	98 (56.3%)	76 (43.6%)	5.382	0.02
III–IV	3 (23.1%)	10 (76.9%)		

Xenograft Model

All mice were housed under pathogen-free conditions. All animal experiments were carried out with the approval of the Ethics Committee of the Tianjin Medical University Cancer Institute and Hospital. K1 cells (5×10^6 in 0.1 ml of serum-free medium/mouse) were injected subcutaneously into the right buttock of each mouse. When the tumor grew to 3 $\times$ 3 mm^2, the mice were randomly assigned to four groups, and the five mice in each group were administered dimethyl sulfoxide (DMSO), apatinib (100 mg/kg/day orally), HCQ (60 mg/kg/day interperitoneally), or a combination of apatinib and HCQ for 28 days. The mice were then monitored for an additional 14 days. The tumors were measured every 4 days with digital calipers.

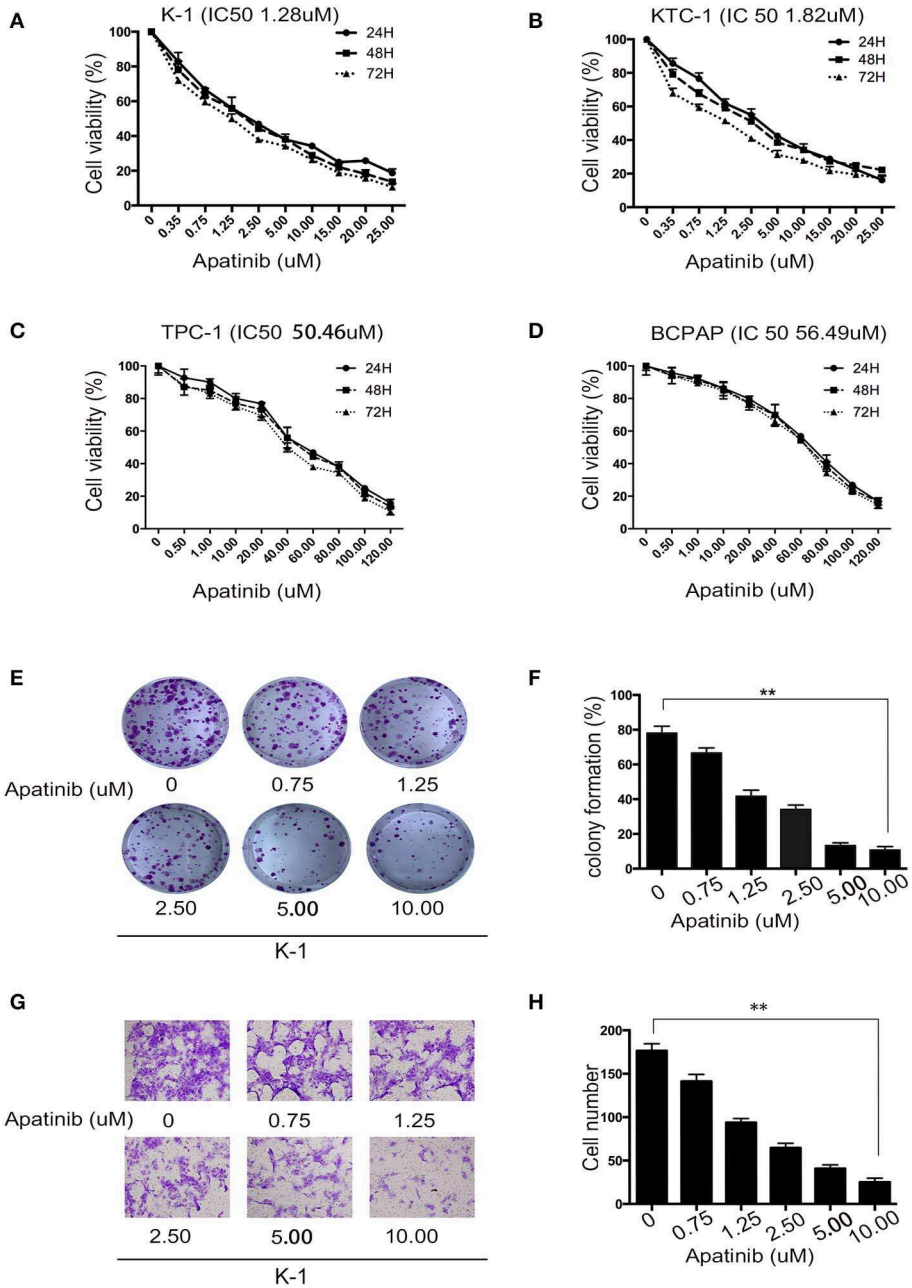

FIGURE 2 | Apatinib inhibits the proliferation and migration of PTC cell lines. **(A–D)** K-1, KTC-1, TPC-1, and BCPAP cells were incubated with apatinib at various concentrations for 24, 48, and 72 h. Then, cell viability was detected by CCK8 assay, and the IC50 values of apatinib at 24 h are shown in brackets behind the name of the cell line. **(E,F)** Apatinib inhibited the long-term proliferation of K-1 cells, as measured by colony-formation assay. **(G,H)** Apatinib suppressed the migration of K-1 cells, and the migration index was measured by Transwell assay. Each experiment was performed three times. Data are expressed as the mean ± SD (*$P < 0.05$, **$P < 0.01$, ***$P < 0.001$).

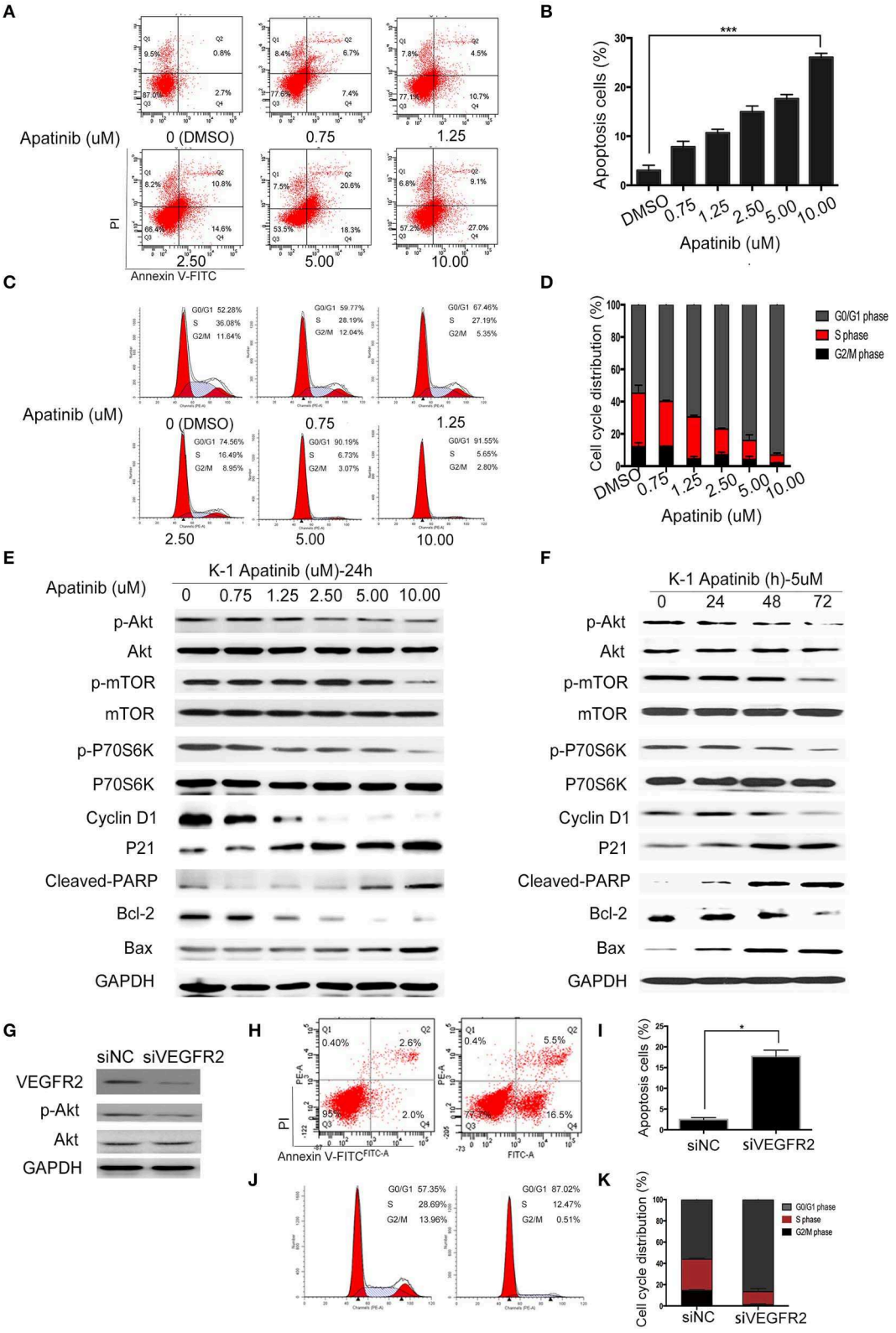

FIGURE 3 | Apatinib induces apoptosis and cell cycle arrest *in vitro.* **(A,B)** Annexin V-FITC/PI staining to detect apoptosis in PTC cells induced by apatinib at various concentrations. Apoptotic cells were analyzed by flow cytometry; (AnV+) (PI–) cells were considered early apoptotic, while (AnV+) (PI+) cells were considered late

(Continued)

FIGURE 3 | apoptotic. **(C,D)** Apatinib at various concentrations caused G0/G1 arrest in PTC cells. After PI staining, the cell cycle distribution was assessed by flow cytometry. **(E,F)** The expression of proteins related to apoptosis, the cell cycle, and cell signaling pathways was determined by western blotting. **(G)** K-1 cells were transfected with VEGFR2 siRNA, the protein expression level of VEGFR2; p-Akt and Akt were detected by western blot. **(H,I)** After VEGFR2 was downregulated, the percentage of apoptotic cells were analyzed by flow cytometry; (AnV+) (PI–) cells were considered early apoptotic, while (AnV+) (PI+) cells were considered late apoptotic. **(J,K)** After VEGFR2 was downregulated, the cell cycle distribution was assessed by flow cytometry. Data are expressed as the mean ± SD (*$P < 0.05$, **$P < 0.01$, ***$P < 0.001$).

Statistical Analysis

GraphPad Prism version 7.0 (La Jolla, CA, USA) was used for statistical analyses. Differences among variants were assessed by the chi-square test, and comparisons between groups were analyzed by one-way ANOVA. *P*-values indicating significant differences are shown in the figures as follows: ***$p < 0.001$, **$p < 0.01$, *$p < 0.05$.

RESULTS

VEGFR2 Expression Was Elevated in PTC

VEGFR2 expression was evaluated in 187 cases of PTC and 43 adjacent normal thyroid follicular epithelial tissues through IHC. The expression of VEGFR2 at the plasma membrane and in the cytoplasm was detected. We observed that most signals were detected from cancer cells (numerous true papillae and ground glass nuclei compared with follicular epithelial cells), as shown in **Figure 1A**. VEGFR2 expression was higher in thyroid cancer tissue than in normal thyroid follicular tissue (**Figure 1B** and **Table 1**). Meanwhile, a high level of VEGFR2 expression was associated with tumor size, T stage, lymph node metastasis, and tumor node metastasis (TNM) stage (**Table 2**). To further explore VEGFR2 expression in PTC, RT-PCR was used to detect VEGFR2 mRNA levels in fresh specimens from 22 PTC patients; these mRNA levels were obviously higher in PTC tissues than in normal thyroid follicular tissues (**Figure 1C**). Three of the 22 patients were randomly selected for an analysis of VEGFR2 protein expression in tissue by WB, the results of which showed that VEGFR2 expression was higher in cancer tissue than in normal tissue (**Figure 1D**). Next, we examined VEGFR2 protein and mRNA levels in seven thyroid cell lines, including normal thyroid follicular epithelial cells, PTC cell lines, and anaplastic thyroid cancer cell lines. VEGFR2 expression in the K-1 and KTC-1 PTC cell lines was higher than that in the other cell lines (**Figures 1E,F**). These data suggest that VEGFR2 expression is elevated in PTC.

Apatinib Inhibited the Proliferation and Migration of PTC Cell Lines

To assess the effects of apatinib on the growth of PTC cells, we used the K-1, KTC-1, TPC-1, and BCPAP cell lines. We treated the cell lines with apatinib at increasing concentrations for 24, 48, and 72 h and used the CCK8 assay to determine cell viability. Apatinib effectively inhibited the growth of PTC cells in a dose-dependent manner (**Figures 2A–D**). The IC50 values for apatinib in K-1 and KTC-1 cells, which highly expressed VEGFR2, were 1.28 and 1.82 μM, respectively, at 24 h. The IC50 value for apatinib in TPC-1 and BCPAP cells, which exhibited low VEGFR2 expression, were 50.46 and 56.49 μM at 24 h, respectively. Based on these results, we used the K-1 and KTC-1 cell lines for further investigation. To further examine the effects of apatinib on PTC cell proliferation, a colony-formation assay was performed with K-1 and KTC-1 cells. Apatinib reduced the colony-formation ability of K-1 (**Figures 2E,F**) and KTC-1 cells (**Figures S1A,B**) in a dose-dependent manner. These data confirmed that apatinib suppressed the proliferation of PTC cells *in vitro*.

To examine the effects of apatinib on the migration and invasion of PTC cells, Transwell assays were carried out with K-1 and KTC-1 cells. We found that apatinib inhibited the migration and invasion of K-1 (migration assay shown in **Figures 2G,H**; invasion assay shown in **Figures S1E,F**) and KTC-1 (migration assay shown in **Figures S1C,D**; invasion assay shown in **Figures S1G,H**) cells in a dose-dependent manner. These data suggested that apatinib inhibits PTC cell migration and invasion.

Apatinib Induced Apoptosis and Cell Cycle Arrest in PTC Cells

To confirm the effect of apatinib on PTC cells, K-1 and KTC-1 cells were treated with apatinib at various concentrations for 24 h, stained with Annexin V/FITC and PI, and analyzed by flow cytometry. The results confirmed that apatinib induced apoptosis in both K-1 (**Figures 3A,B**) and KTC-1 (**Figures S2A,B**) cells in a concentration-dependent manner. Moreover, PTC cells treated with apatinib at various concentrations for 24 h in G0/G1 phase of the cell cycle accumulated, as shown in **Figures 3C,D** and **Figures S2C,D**. To ascertain the mechanism of this effect, we examined the expression of proteins related to cell signaling (Akt, mTOR, and P70S6K), the cell cycle (cyclin D1 and P21), and apoptosis signaling (cleaved PARP, Bax, and Bcl-2) by WB. Apatinib decreased cyclin D1 expression and increased P21 expression in a dose- and time-dependent manner. Meanwhile, apatinib upregulated cleaved PARP and Bax levels and downregulated Bcl-2 levels in a dose- and time-dependent manner. Apatinib also downregulated p-Akt, p-mTOR, and p-P70S6K levels, shown in **Figures 3E,F** and **Figures S3A–C**. To verify whether the antitumor effect of apatinib is governed by the VEGFR2-mediated pathways, we knocked down in K-1 cells using siRNA. K-1 cells were transfected with VEGFR2 siRNA for 24 h. As shown in **Figure 3G**, VEGFR2 siRNA inhibited the expression of VEGFR2 and p-Akt. Compared with the control group, VEGFR2 downregulated group-induced apoptosis and cell cycle arrest, shown in **Figures 3H–K**. Therefore, all the data confirmed that apatinib can regulate the PI3K/Akt/mTOR signaling pathway and induce apoptosis and cell cycle arrest in PTC cells.

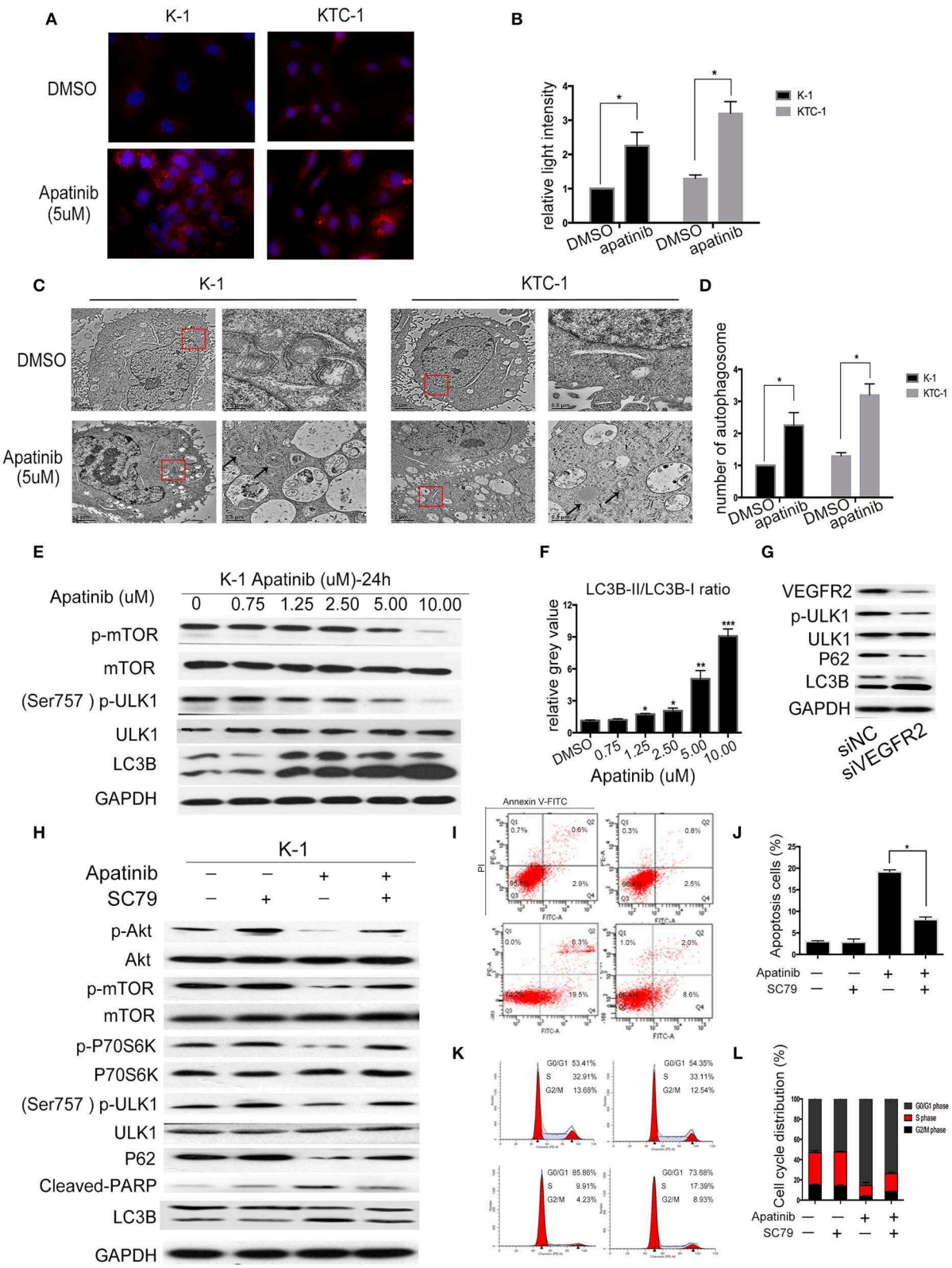

FIGURE 4 | Apatinib induces autophagy in PTC cell lines via the Akt/mTOR signaling pathway. **(A,B)** Immunofluorescence images of K-1 and KTC-1 cells treated with or without 5 μM apatinib for 24 h. Original images were taken at 400× magnification. There were more LC3B puncta in the apatinib-treated group than in the control

(Continued)

FIGURE 4 | group. **(C,D)** Transition electron microscopy images of K-1 and KTC-1 cells treated with or without apatinib for 24 h. More autophagic vacuoles (AVs) were observed in the apatinib-treated group than in the control group. Arrows: autophagosomes. **(E)** The expression of proteins related to cell signaling pathways and autophagy. **(F)** The relative gray value of LC3B-II/LC3B-I. **(G)** K-1 cells were transfected with VEGFR2 siRNA, the protein expression level of VEGFR2; p-ULK1, ULK1, P62, and LC3B were detected by western blot. **(H)** K-1 cells were treated with apatinib with or without SC79 for 24 h. The expression of proteins related to apoptosis, the cell cycle, and cell signaling pathways was determined by western blotting. **(I,J)** K-1 cells were treated as **(H)**; the percentage of apoptotic cells was analyzed by flow cytometry; (AnV+) (PI–) cells were considered early apoptotic, while (AnV+) (PI+) cells were considered late apoptotic. **(K,L)** K-1 cells were treated as **(H)**; the cell cycle distribution was assessed by flow cytometry. Data are expressed as the mean ± SD (*$P < 0.05$, **$P < 0.01$, ***$P < 0.001$).

Apatinib Induced Autophagy in PTC Cell Lines via the Akt/mTOR Signaling Pathway

Autophagy is a double-edged sword in tumors, as it can cause tumor survival or death. A number of studies have found that the mechanism of TKI resistance is closely related to autophagy. Therefore, we next examined whether apatinib causes autophagy in PTC. First, we measured the expression of LC3B, a key marker in the initial stage of autophagy, using an IF assay. As shown in **Figures 4A,B**, apatinib-treated cells showed LC3B accumulation. Furthermore, we used transmission electron microscopy to assess the formation of autophagic vacuoles (autophagosomes). As shown in **Figures 4C,D**, the formation of autophagosomes in apatinib-treated cells was dramatically increased compared with that in untreated cells. Finally, we performed WB to measure protein expression, and as shown in **Figures 4E,F**, after treatment with apatinib at various concentrations, the expression of p-mTOR and p-ULK1 decreased, while that of LC3B increased, further confirming that apatinib induces autophagy in PTC cells.

To explore whether apatinib-induced autophagy is governed by the VEGFR2-mediated pathways, we knocked down in K-1 cells using siRNA. K-1 cells were transfected with VEGFR2 siRNA for 24 h. As shown in **Figure 4G**, after VEGFR2 was downregulated, the expression of VEGFR2, p-ULK1, and P62 were decreased, and the expression of LC3B was increased. The data suggested that apatinib-induced autophagy was governed by VEGFR2-mediated pathways. Many recent reports (18, 19) have indicated that the PI3K/Akt/mTOR signaling pathway negatively regulates autophagy and apoptosis in many tumors. As shown in **Figure 3**, apatinib could regulate the Akt/mTOR signaling pathway and induce apoptosis. To further investigate whether the Akt/mTOR signaling pathway is involved in apatinib-induced autophagy in PTC cells, we treated K-1 cells with apatinib and SC79, an agonist of AKT. As shown in **Figure 4H**, the expression of p-Akt, p-mTOR, p-P70S6K, p-ULK1, and P62 was increased in cells treated with both SC79 and apatinib compared with apatinib-treated cells, and the expression of cleaved PARP and LC3B was decreased, suggesting that apoptosis and autophagy were inhibited. Meanwhile, flow cytometry data showed that cells treated with both apatinib and SC79 have a lower apoptotic rate and a lower cell cycle arrest rate than cells treated with the apatinib signal group, shown in **Figures 4I–L**. Thus, activation of the Akt pathway could rescue the apoptosis and autophagy induced by apatinib. Taken together, these results confirmed that apatinib induces apoptosis and autophagy in PTC cells via the PI3K/Akt/mTOR signaling pathway.

Inhibition of Autophagy Sensitized PTC Cells to Apatinib

To determine whether LC3B accumulation induced by apatinib is due to inhibited autophagosome degradation or enhanced autophagosome formation, we treated K-1 cells with DMSO or apatinib with/without HCQ. HCQ inhibits the final stage of autophagy, preventing the degradation of autophagosomes by increasing lysosomal pH. As shown in **Figures 5A,B**, among both K-1 and KTC-1 cells, LC3B expression was decreased in the cotreated group compared with the apatinib-treated group. Similarly, among K-1 and KTC-1 cells, compared with the apatinib-treated groups, the cotreated groups showed increased autophagic vacuole formation (**Figures 5C,D**). These data suggested that autophagy was inhibited by HCQ treatment.

To explore the role of apatinib-induced autophagy in PTC cells, we treated K-1 cells with DMSO, apatinib, HCQ, or both apatinib and HCQ and found that combination treatment was the most effective at inducing apoptosis, as evidenced by the significantly higher ratio of apoptotic cells than that in the group treated with apatinib alone (**Figures 5E,F**), and the same result was observed in the KTC-1 cell line (**Figures S4A,B**). In apatinib-treated cells, LC3B-II expression increased, and the expression of P62, a substrate of autophagosome degradation, decreased. In the cotreatment group, LC3B-II and P62 expression levels were further increased; as shown in **Figure 5G**, autophagy was inhibited in the cotreated group, which exhibited increased cleaved PARP and Bax expression levels and decreased Bcl-2 expression levels. Taken together, these results suggested that apatinib-induced autophagy was cytoprotective and that inhibiting autophagy could increase apoptosis.

To further determine whether HCQ functions by inhibiting autophagy rather than through an unknown mechanism, we inhibited autophagy using genetic tools. ATG5, a key gene in the formation of autophagic vacuoles, was knocked down in K-1 cells using siRNA. K-1 cells were transfected with ATG5 siRNA for 24 h and then treated with or without apatinib for another 24 h. As shown in **Figures 5H–J**, ATG5 siRNA inhibited the expression of ATG5 and LC3B, suggesting that autophagy had been inhibited. Compared with the group treated with negative control siRNA, the group treated with ATG5 siRNA and the apatinib combination treatment group showed significant increased cleaved PARP levels. Overall, these results demonstrated that autophagy inhibitors enhance the efficacy of apatinib in PTC cells.

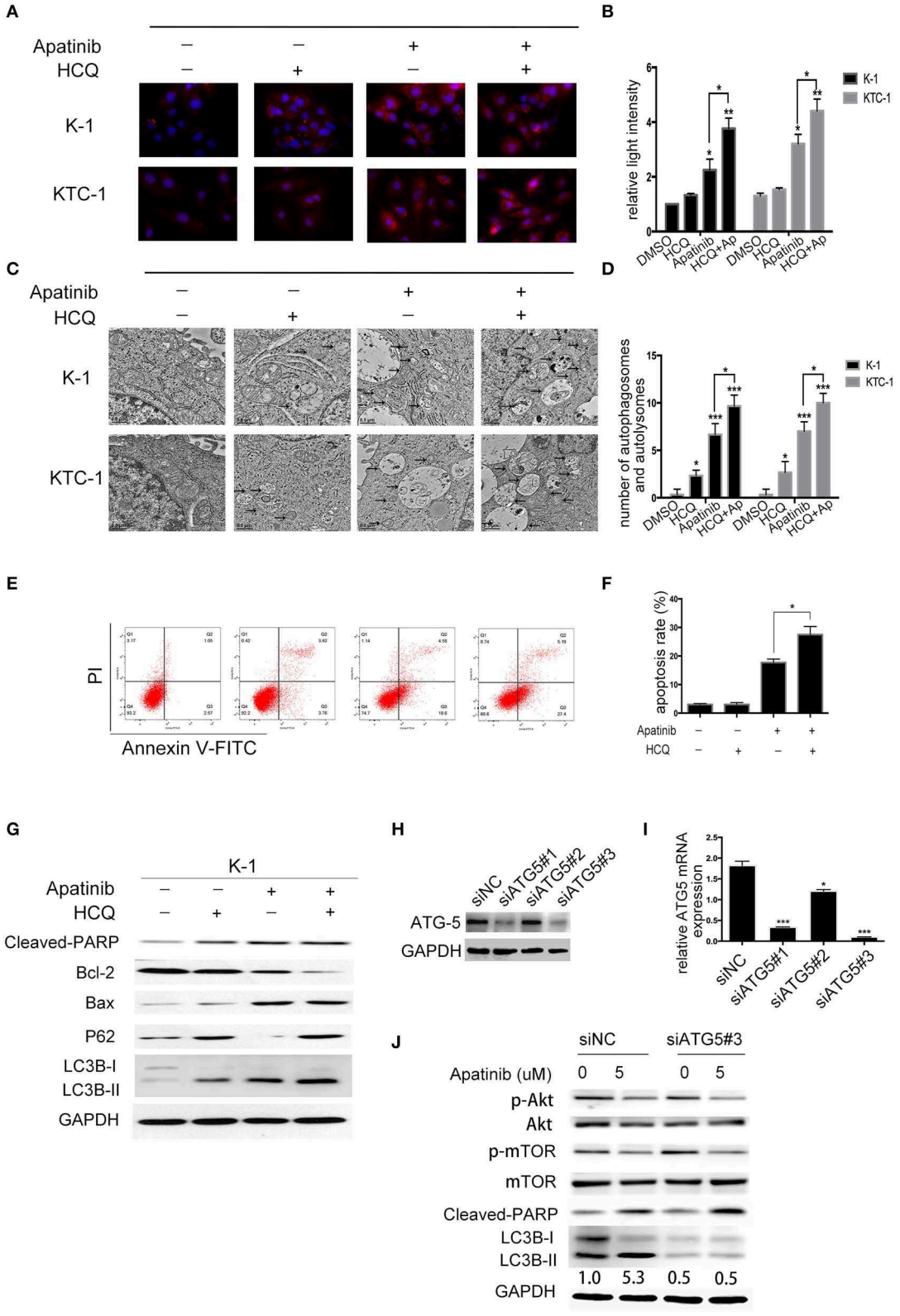

FIGURE 5 | Inhibition of autophagy enhances apatinib-induced apoptosis in PTC cells. **(A, B)** Representative immunofluorescence images of K-1 and KTC-1 cells treated with DMSO, HCQ, apatinib, or a combination of apatinib and HCQ. **(C, D)** Representative transition electron microscopy images of K-1 and KTC-1 cells

(Continued)

FIGURE 5 | treated with DMSO, HCQ, apatinib, or a combination of apatinib and HCQ. Arrows: autophagosomes and autolysosomes. **(E, F)** Inhibition of autophagy with HCQ enhanced the apoptosis of apatinib-treated PTC cells. **(G)** The expression levels of autophagy- and apoptosis-related proteins were detected by western blotting after the treatment of K-1 cells with apatinib with or without HCQ. **(H)** K-1 cells were transfected with ATG5 siRNA, the protein expression levels of ATG5. **(I)** K-1 cells were transfected with ATG5 siRNA, the mRNA expression levels of ATG5. **(J)** After ATG5 downregulation, the expression levels of p-Akt, p-mTOR, cleaved PARP, and LC3B in K-1 cells with or without apatinib treatment were determined by western blotting. Data are expressed as the mean ± SD (*$P < 0.05$, **$P < 0.01$, ***$P < 0.001$).

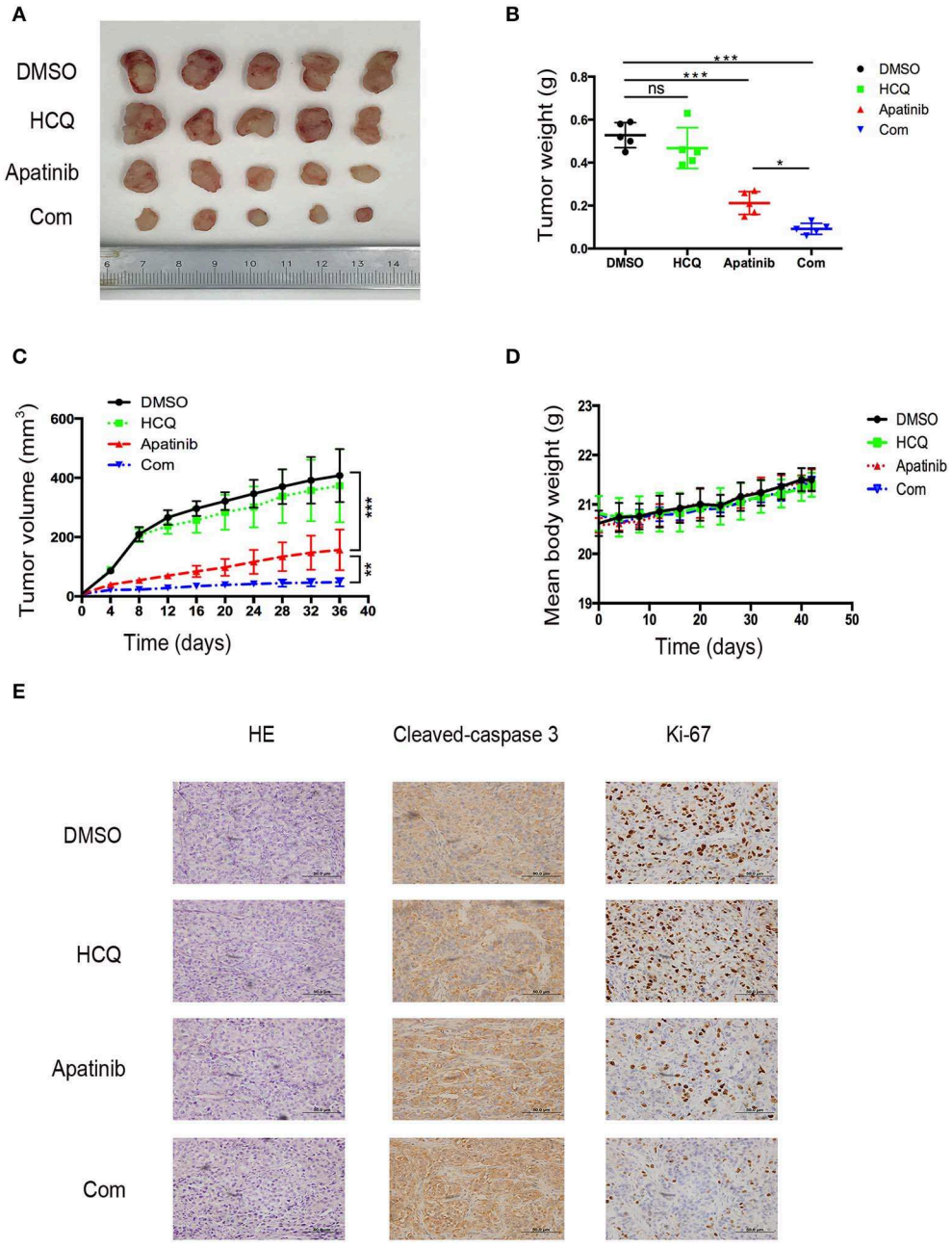

FIGURE 6 | Inhibition of autophagy enhanced the suppression of PTC growth by apatinib *in vivo*. **(A)** Images of tumors dissected from mice in the four groups (DMSO control group, HCQ single-treatment group, apatinib single-treatment group, and apatinib and HCQ combined treatment group) inoculated with K-1 cells. **(B)** Tumor weights in the four groups. **(C)** Tumor volumes in the four groups. **(D)** Mouse weights in the four groups. **(E)** HE and IHC staining to detect cleaved caspase 3 and Ki-67 in the four groups. Data are expressed as the mean ± SD (*$P < 0.05$, **$P < 0.01$, ***$P < 0.001$).

Inhibition of Autophagy Enhanced the Suppression of PTC Growth Induced by Apatinib *in vivo*

To confirm the effect of apatinib-induced apoptosis and autophagy on PTC *in vivo*, we used K-1 cells to generate an *in vivo* xenograft model. The xenograft mice were divided into the following four groups: group A (a DMSO control group), group B (a HCQ single-treatment group), group C (an apatinib single-treatment group), and group D (an apatinib and HCQ combination treatment group). Based on our results, the DMSO control group and the HCQ single-treatment group did not show significant differences in tumor volume or tumor weight. In contrast, the apatinib single-treatment group showed significantly decreased tumor volume and tumor weight compared with the DMSO control group and the HCQ single-treatment group, and tumor volume and weight were significantly different in the HCQ combination treatment group and the apatinib single-treatment group. Moreover, Ki-67 expression in the combined treatment group was significantly decreased, and cleaved caspase3 expression was increased, implying that apoptosis was enhanced in these tumors. These results demonstrated that apatinib-mediated suppression of tumor growth and blockade of autophagy could improve the antitumor effect on PTC *in vivo*, as shown in **Figure 6**. Taken together, these results suggested that autophagy inhibitors enhance the efficacy of apatinib in PTC and that given their low toxicity, these inhibitors can be an effective curative therapy in PTC.

DISCUSSION

PTC is the most common type of thyroid cancer and has a favorable prognosis. However, a small proportion of PTC patients develop metastatic disease and are resistant to conventional therapies, including thyrotropin-suppressive therapy and radioactive iodine; the outlook in these patients is therefore dim, as current treatment options for these patients are limited. Apatinib is a novel TKI highly selective for VEGFR2 with good antitumor effects in various types of solid tumors. Apatinib was shown to be safe and highly efficacious in a small number of patients with radioiodine-refractory differentiated thyroid cancer (13). In this report, we investigated the potential therapeutic effect of apatinib on PTC and the mechanism of apatinib *in vitro* and *in vivo*.

Apatinib was reported to suppress angiogenesis in anaplastic thyroid carcinoma by blocking the Akt/GSK3/ANG pathway (20–22); however, the effect of apatinib in PTC is unclear. In this report, we discovered that apatinib could inhibit PTC cell growth and migration and the induction of apoptosis. The PI3K/Akt signaling pathway plays an important role in a variety of tumors, including thyroid cancer, and is closely related to tumorigenesis, proliferation, invasion, apoptosis, and autophagy. Our data showed that p-Akt levels were decreased after apatinib treatment in a dose- and time-dependent manner.

Thus, we suggest that apatinib promotes apoptosis through the PI3K/Akt/mTOR signaling pathway. Autophagy is a ubiquitous cellular mechanism for the maintenance of homeostasis. In tumor cells, autophagy plays a dual role as it can promote death or survival. Some studies have confirmed that TKI resistance is associated with increased autophagic activity (23–25). In this report, we found that apatinib induced autophagy in PTC, as it does in other types of tumors. Moreover, we used HCQ, an autophagy inhibitor, in combination with apatinib to inhibit autophagic flux and increase apoptosis, further confirming that apatinib-induced autophagy is a protective mechanism in tumor cells. Moreover, the same results were obtained in ATG5-knockdown PTC cells, and these results were further confirmed at the genetic level. The Akt signaling pathway closely interacts with mTOR to influence autophagy, and in this study, we found that after apatinib treatment, the levels of p-mTOR, p-P70S6K, and p-ULK1 were decreased. Moreover, apatinib cotreatment with SC79, an activator of Akt, reduced apoptosis and autophagy. Thus, we demonstrated that apatinib can induce apoptosis and autophagy via the PI3K/Akt/mTOR signaling pathway and that this pathway might be a novel mechanism of drug resistance. Furthermore, the blockade of autophagy could enhance the sensitivity of PTC to apatinib.

In summary, our data show that apatinib exerted antitumor effects in PTC by suppressing tumor growth, promoting apoptosis, and inhibiting migration through the PI3K/Akt/mTOR signaling pathway. Additionally, apatinib could induce autophagy. Importantly, apatinib-induced autophagy was cytoprotective in PTC cells, and the blockade autophagy could improve apoptosis *in vitro* and *in vivo*. Thus, these findings reinforce our research findings and the clinical application of apatinib and indicate that autophagy is a new molecular therapeutic target in PTC. Combination treatment with apatinib and an autophagy inhibitor may be a useful therapeutic strategy for refractory PTC, and our data provide support for future clinical trials of autophagy inhibitors.

DATA AVAILABILITY STATEMENT

All datasets generated for this study are included in the article/**Supplementary Material**.

ETHICS STATEMENT

The studies involving human participants were reviewed and approved by Ethics Committee of Tianjin Cancer Institute and Hospital. The patients/participants provided their written informed consent to participate in this study. The animal study was reviewed and approved by Ethics Committee of Tianjin Cancer Institute and Hospital. Written informed consent was obtained from the individual(s) for the publication of any potentially identifiable images or data included in this article.

AUTHOR CONTRIBUTIONS

Conceptualization: XZ. Data curation and investigation: XM and HW. Formal analysis: JZhao and LH. Funding acquisition: XZ, JZhi, SW, XR, DL, YZ, ZM, WY, and LG. Methodology: BQ and MG. Project administration: HZ and MG. Resources: XZ and

MG. Software: XH, JZhang, YW, HZ, XZ, and MG. Writing—original draft and writing—review and editing: XM.

FUNDING

This work was partially supported by grants from the National Natural Science Foundation of China (grant nos. 81472580, 81872169, 81502322, and 81702629), Tianjin Key Research and Development Program Science and Technology Support Key Projects (grant no. 17YFZCSY00690), the Tianjin Tumor Hospital Foundation for Clinical Trials, China (No. C1701), and the Jiangsu Provincial Key Research Development Program (BE2016796).

SUPPLEMENTARY MATERIAL

The Supplementary Material for this article can be found online at: https://www.frontiersin.org/articles/10.3389/fonc.2020.00217/full#supplementary-material

REFERENCES

1. Siegel RL, Miller KD, Jemal A. Cancer statistics. *CA Cancer J Clin.* (2018) 68:7–30. doi: 10.3322/caac.21442
2. Tuttle RM, Haddad RI, Ball DW, Byrd D, Dickson P, Duh QY, et al. Thyroid carcinoma, version 2.2014. *J Natl Compr Canc Netw.* (2014) 12:1671–80. doi: 10.6004/jnccn.2014.0169
3. Antonelli A, Fallahi P, Ferrari SM, Carpi A, Berti P, Materazzi G, et al. Dedifferentiated thyroid cancer: a therapeutic challenge. *Biomed Pharmacother.* (2008) 62:559–63. doi: 10.1016/j.biopha.2008.07.056
4. Bible KC, Ryder M. Evolving molecularly targeted therapies for advanced-stage thyroid cancers. *Nat Rev Clin Oncol.* (2016) 13:403–16. doi: 10.1038/nrclinonc.2016.19
5. Spitzweg C, Bible KC, Hofbauer LC, Morris JC. Advanced radioiodine-refractory differentiated thyroid cancer: the sodium iodide symporter and other emerging therapeutic targets. *Lancet Diabetes Endocrinol.* (2014) 2:830–42. doi: 10.1016/S2213-8587(14)70051-8
6. Harris PJ, Bible KC. Emerging therapeutics for advanced thyroid malignancies: rationale and targeted approaches. *Expert Opin Investig Drugs.* (2011) 20:1357–75. doi: 10.1517/13543784.2011.614230
7. Schlumberger M, Tahara M, Wirth LJ, Robinson B, Brose MS, Elisei R, et al. Lenvatinib versus placebo in radioiodine-refractory thyroid cancer. *N Engl J Med.* (2015) 372:621–30. doi: 10.1056/NEJMoa1406470
8. Brose MS, Nutting CM, Jarzab B, Elisei R, Siena S, Bastholt L, et al. Sorafenib in radioactive iodine-refractory, locally advanced or metastatic differentiated thyroid cancer: a randomised, double-blind, phase 3 trial. *Lancet.* (2014) 384:319–28. doi: 10.1016/S0140-6736(14)60421-9
9. Li J, Qin S, Xu J, Guo W, Xiong J, Bai Y, et al. Apatinib for chemotherapy-refractory advanced metastatic gastric cancer: results from a randomized, placebo-controlled, parallel-arm, phase II trial. *J Clin Oncol.* (2013) 31:3219–25. doi: 10.1200/JCO.2013.48.8585
10. Li J, Qin S, Xu J, Xiong J, Wu C, Bai Y, et al. Randomized, double-blind, placebo-controlled phase iii trial of apatinib in patients with chemotherapy-refractory advanced or metastatic adenocarcinoma of the stomach or gastroesophageal junction. *J Clin Oncol.* (2016) 34:1448–54. doi: 10.1200/JCO.2015.63.5995
11. Hu X, Zhang J, Xu B, Jiang Z, Ragaz J, Tong Z, et al. Multicenter phase II study of apatinib, a novel VEGFR inhibitor in heavily pretreated patients with metastatic triple-negative breast cancer. *Int J Cancer.* (2014) 135:1961–9. doi: 10.1002/ijc.28829
12. Hu X, Cao J, Hu W, Wu C, Pan Y, Cai L, et al. Multicenter phase II study of apatinib in non-triple-negative metastatic breast cancer. *BMC Cancer.* (2014) 14:820. doi: 10.1186/1471-2407-14-820
13. Lin Y, Wang C, Gao W, Cui R, Liang J. Overwhelming rapid metabolic and structural response to apatinib in radioiodine refractory differentiated thyroid cancer. *Oncotarget.* (2017) 8:42252–61. doi: 10.18632/oncotarget.15036
14. Rabinowitz JD, White E. Autophagy and metabolism. *Science.* (2010) 330:1344–8. doi: 10.1126/science.1193497
15. Wang W, Kang H, Zhao Y, Min I, Wyrwas B, Moore M, et al. Targeting autophagy sensitizes BRAF-Mutant thyroid cancer to vemurafenib. *J Clin Endocrinol Metab.* (2017) 102:634–43. doi: 10.1210/jc.2016-1999
16. Shen Y, Yang J, Zhao J, Xiao C, Xu C, Xiang Y. The switch from ER stress-induced apoptosis to autophagy via ROS-mediated JNK/p62 signals: a survival mechanism in methotrexate-resistant choriocarcinoma cells. *Exp Cell Res.* (2015) 334:207–18. doi: 10.1016/j.yexcr.2015.04.010
17. Fan Q, Meng X, Liang H, Zhang H, Liu X, Li L, et al. miR-10a inhibits cell proliferation and promotes cell apoptosis by targeting BCL6 in diffuse large B-cell lymphoma. *Protein Cell.* (2016) 7:899–912. doi: 10.1007/s13238-016-0316-z
18. Viola G, Bortolozzi R, Hamel E, Moro S, Brun P, Castagliuolo I, et al. MG-2477, a new tubulin inhibitor, induces autophagy through inhibition of the Akt/mTOR pathway and delayed apoptosis in A549 cells. *Biochem Pharmacol.* (2012) 83:16–26. doi: 10.1016/j.bcp.2011.09.017
19. Harashima N, Inao T, Imamura R, Okano S, Suda T, Harada M. Roles of the PI3K/Akt pathway and autophagy in TLR3 signaling-induced apoptosis and growth arrest of human prostate cancer cells. *Cancer Immunol Immunother.* (2012) 61:667–76. doi: 10.1007/s00262-011-1132-1
20. Jin Z, Cheng X, Feng H, Kuang J, Yang W, Peng C, et al. Apatinib inhibits angiogenesis via suppressing Akt/GSK3beta/ANG signaling pathway in anaplastic thyroid cancer. *Cell Physiol Biochem.* (2017) 44:1471–84. doi: 10.1159/000485583
21. Manfredi GI, Dicitore A, Gaudenzi G, Caraglia M, Persani L, Vitale G. PI3K/Akt/mTOR signaling in medullary thyroid cancer: a promising molecular target for cancer therapy. *Endocrine.* (2015) 48:363–70. doi: 10.1007/s12020-014-0380-1
22. Motti ML, Califano D, Troncone G, De Marco C, Migliaccio I, Palmieri E, et al. Complex regulation of the cyclin-dependent kinase inhibitor p27kip1 in thyroid cancer cells by the PI3K/AKT pathway: regulation of p27kip1 expression and localization. *Am J Pathol.* (2005) 166:737–49. doi: 10.1016/S0002-9440(10)62295-X
23. Liu K, Ren T, Huang Y, Sun K, Bao X, Wang S, et al. Apatinib promotes autophagy and apoptosis through VEGFR2/STAT3/BCL-2 signaling in osteosarcoma. *Cell Death Dis.* (2017) 8:e3015. doi: 10.1038/cddis.2017.422
24. Calabretta B, Salomoni P. Inhibition of autophagy: a new strategy to enhance sensitivity of chronic myeloid leukemia stem cells to tyrosine kinase inhibitors. *Leuk Lymphoma.* (2011) 52(Suppl. 1):54–9. doi: 10.3109/10428194.2010.546913
25. Li YY, Lam SK, Mak JC, Zheng CY, Ho JC. Erlotinib-induced autophagy in epidermal growth factor receptor mutated non-small cell lung cancer. *Lung Cancer.* (2013) 81:354–61. doi: 10.1016/j.lungcan.2013.05.012

Conflict of Interest: The authors declare that the research was conducted in the absence of any commercial or financial relationships that could be construed as a potential conflict of interest.

frontiers in Oncology

ORIGINAL RESEARCH
published: 20 March 2020
doi: 10.3389/fonc.2020.00375

BCL11A Promotes the Progression of Laryngeal Squamous Cell Carcinoma

Jian Zhou[1,2,3], Liang Zhou[2,3], Duo Zhang[2,3], Wei-Jing Tang[2,3], Di Tang[2,3], Xiao-Ling Shi[2,3], Yue Yang[2,3], Lin Zhou[1], Fei Liu[1], Yong Yu[4], Pentao Liu[4], Lei Tao[2,3] and Li-Ming Lu[1]**

[1] Shanghai Institute of Immunology, Shanghai Jiaotong University School of Medicine, Shanghai, China, [2] Department of Otolaryngology, Eye, Ear, Nose and Throat Hospital, Fudan University, Shanghai, China, [3] Shanghai Key Clinical Disciplines of Otorhinolaryngology, Shanghai, China, [4] Wellcome Trust Sanger Institute, Cambridge, United Kingdom

Background: We report functional and clinical data uncovering the significance of B-cell lymphoma/leukemia 11A (BCL11A) in laryngeal squamous cell carcinoma (LSCC).

Methods: We examined BCL11A expression in a cohort of LSCC patients and evaluated the association between BCL11A expression and clinicopathological features. We investigated the consequences of overexpressing BCL11A in the LSCC cell line on proliferation, migration, invasion, cell cycle, chemosensitivity, and growth *in vivo*. We explored the relationship between BCL11A and MDM2 in LSCC and tumorigenesis pathways by using the Human Cancer PathwayFinder Array.

Results: High levels of BCL11A were found in LSCC tissues and were more frequently associated with advanced lymphatic metastasis stages with poor prognoses. BCL11A overexpression enhanced LSCC proliferation *in vitro* and *vivo*. A positive correlation between MDM2 and BCL11A expression was identified.

Conclusions: These data uncover important functions of BCL11A in LSCC and identify BCL11A as a prognostic biomarker and potential therapeutic target in LSCC.

Keywords: BCL11A, LSCC, proto-oncogene, MDM2, prognosis

OPEN ACCESS

Edited by:
Jan Baptist Vermorken, University of Antwerp, Belgium

Reviewed by:
Yanan Sun, Harbin Medical University, China
Zifan Wu, Zhongshan People's hospital (ZSPH), China

***Correspondence:**
Lei Tao
doctortaolei@163.com
Li-Ming Lu
lulunew2003@163.com

Specialty section:
This article was submitted to Head and Neck Cancer, a section of the journal Frontiers in Oncology

Received: *15 June 2019*
Accepted: *03 March 2020*
Published: *20 March 2020*

Citation:
Zhou J, Zhou L, Zhang D, Tang W-J, Tang D, Shi X-L, Yang Y, Zhou L, Liu F, Yu Y, Liu P, Tao L and Lu L-M (2020) BCL11A Promotes the Progression of Laryngeal Squamous Cell Carcinoma. Front. Oncol. 10:375. doi: 10.3389/fonc.2020.00375

INTRODUCTION

Laryngeal squamous cell carcinoma (LSCC) is the eleventh most common tumor in males. The most deep-rooted risk factors for LSCC are alcohol abuse and tobacco use (1). The LSCC has a poor prognosis, with a 5 year survival rate <50%. The aforementioned is mostly attributed to regional and local recurrences, especially in patients with stage III or IV disease (2). Studies are needed to increase our understanding of the pathogenesis and prognosis of LSCC.

The *Bcl11a* gene encodes a C2H2 zinc finger transcription factor, which acts as a retroviral insertion site (Evi9) in myeloid leukemia in BXH-2 mice (3, 4). The gene was initially recognized in a rare $t_{(2;14)}$ (p16; q32.3) translocation in aggressive B-cell chronic lymphocytic leukemia, and it is usually co-amplified with the proto-oncogene REL in classical Hodgkin's lymphoma and non-Hodgkin's lymphoma (5, 6). The role of BCL11A in solid melanomas has not been widely studied. Khaled et al. studied the BCL11A oncogene in triple-negative breast tumors and reported that its overexpression promoted cancer development (7). Jiang et al. revealed that BCL11A protein expression levels were markedly upregulated in non-small-cell lung cancer (NSCLC) tissues, particularly in large cell cancer and squamous cell cancer (SCC). A multivariate analysis demonstrated that BCL11A was an independent prognostic factor for both overall survival and disease-free survival (8). To address these issues, we determined BCL11A expression in

LSCC and investigated its clinical significance by associating clinicopathologic parameters with BCL11A expression in LSCC patients. We further dissected the cellular and molecular mechanisms underlying BCL11A function in LSCC.

MATERIALS AND METHODS

Patient Population

Sixty-nine LSCC patients were recruited for this study. All of them had undergone total laryngectomy, with or without chemotherapy from November 2013 to September 2014 in the Otolaryngology Head and Neck Surgery Department of the Eye, Ear, Nose and Throat Hospital, Fudan University. Of 69 patients entered in this research, suitable tissues for Tissue Microarrays (TMA) were available for all 69 patients. All patients were categorized on the basis of UICC stage classification using specimens. All cases were collected according to study protocols permitted by the Ethics Committee of Fudan University, and all the participants offered written informed consent before the commencement of the research. The following data were recorded: patient's age, T stage, N stage, carcinoma stage, drinking status (non-drinker, drinker), smoking status (non-smoker, smoker), and tumor recurrence. Non-smokers were defined as those who smoked $\leq$10 packs/y, and smokers were defined as those who smoked $>$10 packs/y. All patients followed up for 2 years. Progression-free survival was defined as the time from registration to local or distant recurrence. Failure was recorded on the occasion of recurrent cancer or if the primary tumor was never wholly gone.

Cell Culture Conditions

Human laryngeal cancer cell line AMC-HN-8 cells were obtained from the Asian Medical Center, Ulsan University College of Medicine approximately 8 years ago. The cells were cultured in RPMI-1640 (Gibco, CA, U.S.A.), supplemented with streptomycin (100 μg/ml; Beyotime), penicillin (100 units/ml; Beyotime, China) and 10% fetal bovine serum (Gibco), in a 5% CO_2 incubator at 37°C.

Establishment of Stable Cell Lines With Overexpression of BCl11A

The lentiviral vectors expressing the Bcl11A-FLAG sequence (Bcl11A-OE) and the NCs were provided by Hanyin Co. (Shanghai). The primers were as follows:

Bcl11a-F: 5′ GACTAGTGCCACCATGTCTCGCCGCAAG CAAGG3′; Bcl11a-R: 5′ CGGGATCCTCACTTGTCGTCAT CGTCCTTGTAGTCGAACTTAAGGGCTCTCGAGCTT-3′.

Amplified flag-tagged Bcl11a was cloned into a pHY-LV-OE2.2 vector. Recombinant lentiviruses (Bcl11A-OE and NC) (Hanyin Co.) were then arranged and titered to 10^9 TU/ml. To establish stable cell lines, cells were plated in six-well plates and infected with the virus and polybrene the next day. Positive clones were then incubated with puromycin for 14 d. Bcl11A overexpression was verified by Western blot and qRT-PCR analyses.

Cell Proliferation Assays

The proliferation effects of AMC-HN-8-NC and AMC-HN-8-BCL11A cells were measured by CCK-8 assay. The cells were plated into 96-well plates, with 100 μl (1×10^4/ml) in each well in the exponential growth phase. The cells were then placed in an incubator at 37°C for 5 d, then 10 μl CCK-8 was added to every well then incubated for 1 h. The absorbance of every unit was assessed at 450 and 650 nm using a standard enzyme-linked immunosorbant assay. The absorbance values at A450 and A650 were calculated, and the results were measured in triplicate.

Colony Formation Assay

Cells were plated at 800 cells per well in six-well plates ($n = 2$). After 15 d of culture, the cells were stained with crystal violet, photographed and scored.

Transwell Migration Assays

In the transwell migration assays, 8.0 μm pore polyethylene terephthalate track-etched membrane cell culture inserts (FALCON) were used. A total volume of 600 μl of RPMI-1640 medium (Gibco), supplemented with 20% serum, was loaded into the lower chamber of a 24-well plate. Then, 1×10^5 cells in 100 μl of medium were added to the upper chamber, and the cells were allowed to migrate for 24 h at 37°C. Five random fields per insert were imaged at ×200 magnification. The migrated cells were calculated by ImageJ (NIH Image, NIH).

Invasion Assays

In the invasion assays, 8 μm transwells were coated with 1 mg/ml of Matrigel (BD Pharmingen). The medium (100 μl) containing the cells (2×10^5) was added to the higher unit, and the cells were allowed to migrate for 24 h in a 37°C incubator. All the experiments were performed in triplicate. The rest of the experimental methods were the same as those used in the migration assays.

Investigation of Cell Cycle Phase Using Flow Cytometry

The AMC-HN-8 cells were trypsinized, washed with PBS and then fixed by icy 70% ethanol for 24 h. The cells were stained with 1 ml of PI (0.1 mg/ml with 0.1% Triton X-100; Sangon Biotech) and cultured in the dark for half an hour. The cells were evaluated using a flow cytometer (FACSCalibur, Becton-Dickinson).

Immunochemistry

The tumor tissues were dissected, fixed and embedded in paraffin. The tissue microarray analysis (TMA) was completed with tumors by using multiple representative 1 mm cores from each tumor. Immunohistochemistry staining with haematoxylin/eosin (H&E) of 4–5 μm paraffin sections was performed. The primary antibodies were mouse monoclonal anti-human anti-BCL11A (Clone: EPR 14943-44, 1:100 dilution, Abcam, London, U.K.) and anti-MDM2 (Clone: SMP 14, 1:50 dilution, Abcam). Each tumor was assigned a score based on the staining intensity (no staining = 0, weak staining = 1, moderate staining = 2, and strong staining = 3). The extent of staining was classified as follows: 81–100% = 4, 51–80% = 3, 11–50% = 2, 1–10%

= 1, and 0% = 0 (9). The final score was determined by multiplying the intensity scores by the scores for the positively stained cells, with a maximum score of 12 and a minimum score of 0. Scores ≥ 6 were categorized as high expression, and scores lower than this were classified as low expression. The numbers of positively stained BCL11A and MDM2 cells were estimated by two independent researchers who were blinded to the clinical characteristics.

qRT-PCR Assays

Whole RNA was extracted by TRIzol (Invitrogen, CA, U.S.A.). The total RNA (1 μg) was used for cDNA synthesis by a reverse transcription kit (Takara, Japan) in a 20 μl reaction mixture containing 5 μM of random hexamers, 0.1 μM of a specific primer and 2.5 μM of an oligo (dT) primer. The assay was executed on an Applied Biosystems 7500 Fast System. The expression levels of the target gene RNAs were standardized to that of GAPDH. The BCL11A primer pair was as follow:F:ACAA ACGGAAACAATGCAATGG, R:TTTCATCTCGATTGGTGAA GGG.

Cancer PathwayFinder PCR Array

The RNA was extracted from the AMC-HN-8-BCL11A cells and AMC-HN-8-NC cells in the exponential growth phase using TRIzol (Invitrogen). The gene expression of 84 genes in nine biological tumorigenesis pathways was measured using the Human Cancer Pathway-Finder RT^2 Profiler PCR Array (SABiosciences) according to established guidelines and evaluated using the MX3005P Real-Time PCR System (Stratagene). Only genes with 1.5-fold variation or greater were selected for further research. The data were confirmed using a combination of qPCR and Western blot assays.

Western Blot Analysis

The total cell extracts were processed by denaturing proteins with SDS loading buffer (Beyotime, China). Equivalent amounts of protein were separated by 12% SDS-polyacrylamide gel electrophoresis, transferred to polyvinylidene fluoride membranes (Millipore Corporation, MA, and U.S.A.) and then blocked for 30 min in Tris-buffered saline with Tween 20 (TBST) and 5% non-fat milk. The blots were incubated at 4°C overnight in a series of antibodies diluted in TBST buffer: BCL11A (Clone: EPR 14943-44, Abcam, London, U.K.) and MDM2 primary antibodies (1:5,000), baculoviral IAP repeat containing 3 (BIRC3) antibody (Clone: E 40, 1:1000 dilution, Abcam), β-2-microglobulin (B2M) antibody (Clone: EP2978Y, 1:5000 dilution, Abcam), STMN1 antibody (Clone: EP1573, 1:50000 dilution, Abcam), SNAI2 antibody (ab75629, 1:50000 dilution, Abcam), haem oxygenase 1 (HMOX1) antibody (Clone: HO-1-1, 1:1000 dilution, Abcam), and protein phosphatase 1 regulatory inhibitor subunit 15A (PPP1R15A) antibody (ab 9869, 1:1000 dilution, Abcam). After washing with TBST, the membranes were incubated in secondary antibodies (1:4,000; KPL, MD, USA) and then analyzed by a chemiluminescence detection kit (Thermo Scientific, Inc., NJ, USA).

Xenograft Studies

The tumor growth of the AMC-HN-8-NC and AMC-HN-8-BCL11A cell lines (1×10^6 cells per cell line) was determined following a subcutaneous injection of cells into the left flank of 6-week-old male nude mice (Department of Laboratory Animal Science, Fudan University), with five animals in each group. The tumor size was analyzed (mm^3) by means of the formula: $0.5 \times (L \times W^2)$. The tumor specimens were fixed using 4% paraformaldehyde for paraffin embedding. Paraffin sections were stained with H&E according to established guidelines. All animal studies were approved by the Animal Center, Eye Ear Nose and Throat Hospital, Fudan University.

Statistical Analysis

The associations between BCL11A and MDM2 status and the recorded clinicopathological characteristics were assessed using a two-sample *t*-test, with $\chi 2$ tests used for categorical variables. A two-tailed *P*-value of 0.05 or less was considered statistically noteworthy. All the data were investigated by SPSS version 19.0 (IBM, Portsmouth, U.K.).

RESULTS

BCL11A Was Highly Expressed in LSCC Patients

Of 69 patients enrolled in this study, immunohistological examination revealed that 52 (75.4%) tumors were classified as high BCL11A expression, while 15 (37.5%) paracancer tissues expressed high BCL11A ($p < 0.01$) (**Figures 1A,B**) (**Table 1**). Although age, smoking and alcohol did not differ significantly between groups, most of the BCL11A high-expression patients were diagnosed in the advanced clinical N1/N2 lymph node metastasis stage ($p = 0.023$) (**Table 2**).

In accordance with previous studies, high expression of BCL11A was associated with significantly higher loco-regional recurrence or mortality (hazard ratio: 12; 95% CI, 1.43–100.8, $P = 0.009$) (**Table 2**).

High BCL11A Levels Promoted LSCC Development

BCL11A, a transcription factor and component of the BRAF complex, has been shown to be involved in regulating cell proliferation, apoptosis and transformation (10). We next investigated the cellular and molecular mechanisms of high levels of BCL11A in LSCC. We started by testing whether BCL11A overexpression affects LSCC cells *in vitro*. We examined the LSCC cell line AMC-HN-8 and found that it expressed low levels of BCL11A (**Figure 1C**). The AMC-HN-8 cell line has been extensively used to study LSCC (11), and we chose to test BCL11A overexpression in AMC-HN-8 cells. The effects of BCL11A overexpression (**Figures 1D,E**) were confirmed at the RNA and protein levels.

BCL11A Promoted LSCC Cell Proliferation *in vitro*

BCL11A overexpression promoted proliferation in AMC-HN-8 cells (**Figure 2A**). Furthermore, the BCL11A-overexpressing

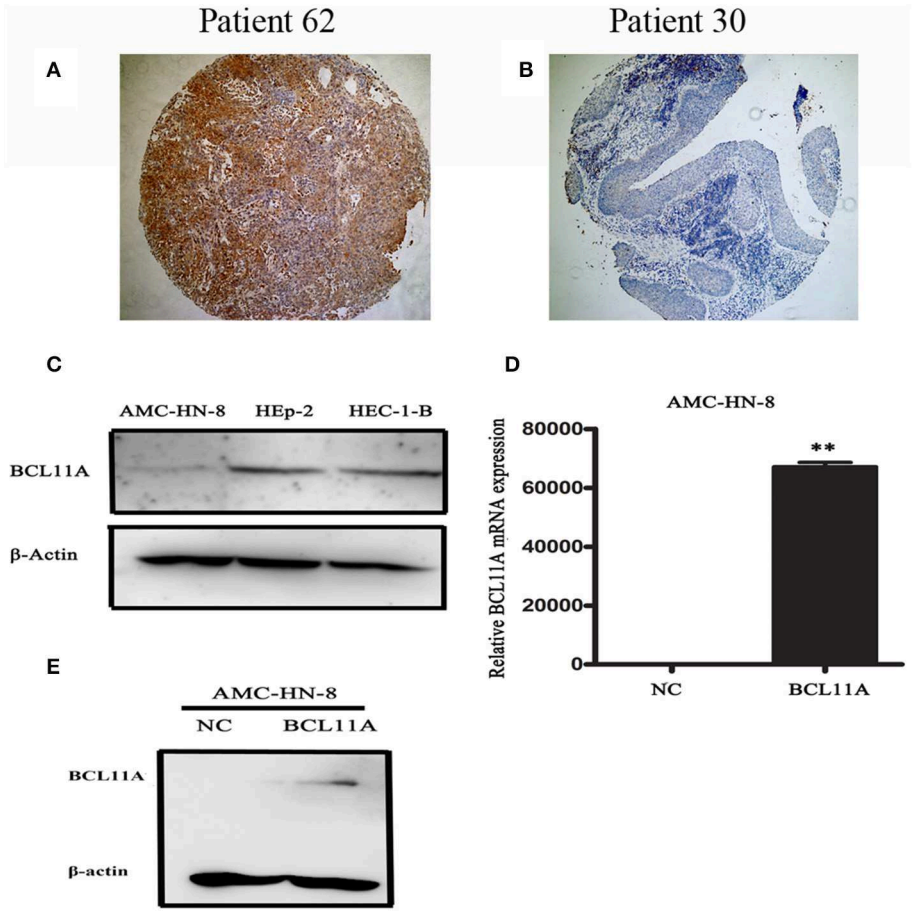

FIGURE 1 | Representative images of BCL11A-positive staining in LSCC cells **(A)** and BCL11A– negative staining in LSCC sections **(B)**. **(C)** A Western blot revealed low expression in the AMC-HN-8 cells. HEC-1-B was used as the positive control for BCL11A expression. **(D,E)** BCL11A overexpression in the AMC-HN-8 cells confirmed by qRT-PCR and Western blot analyses. $^{**}P < 0.01$.

TABLE 1 | Relationship between BCL11A expression and tissue types.

Tissue type	No.	Low	High (%)	OR (95% CI)	*P*-value
Paracancer tissue	40	25	15 (37.5%)		
Carcinoma	69	17	52 (75.4%)	5.1 (2.20–11.84)	<0.01

AMC-HN-8 cells formed more colonies than did the parental cells (**Figures 2B,C**). These results revealed that one important function of BCL11A is to promote LSCC cell proliferation.

Effects of BCL11A Expression on LSCC Cell Migration and Invasion

We next investigated the effect of BCL11A on cell migration and invasion in LSCC cell lines. Transwell assays showed that overexpression of BCL11A significantly increased the migration and invasion capacity of AMC-HN-8 cells (**Figures 3A–D**). The results indicated that overexpression of BCL11A seemed to increase the migration and invasion of these cells.

Change in the Chemosensitivity of Cisplatin After BCL11A Overexpression

We next addressed whether changes in BCL11A in AMC-HN-8 cells could have an impact on chemosensitivity to cisplatin. Overexpression of BCL11A in AMC-HN-8 cells significantly increased their survival or inhibited chemosensitivity to cisplatin (**Figure 4A**). The results show that BCL11A-high tumors could be more resistant to chemotherapies such as cisplatin.

Impact of BCL11A on the Cell Cycle

Overexpression of BCL11A had no significant effect on cell cycle kinetics (**Figure 4B**).

BCL11A Promoted LSCC Growth *in vivo*

The substantial effects of BCL11A expression changes on cell proliferation, cell invasion and chemo-sensitivity prompted us to investigate the consequences of BCL11A expression changes *in vivo*. LSCC cells overexpressing BCL11A were injected into immunocompromised recipient mice to induce tumor development. The tumors in the mice injected with the BCL11A-overexpressing AMC-HN-8 cells were larger and

TABLE 2 | Relationship between BCL11A expression and clinicopathological characteristics.

Parameter	No.	Low (%)	High (%)	OR (95% CI)	*P*-value
AGE					
<60	19	5 (26.3%)	14 (73.7%)	1.13 (0.34–3.79)	0.842
≥60	50	12 (24%)	38 (76%)		
SMOKING					
Never	20	3 (15%)	17 (85%)	0.44 (0.11–1.75)	0.235
Former or current	49	14 (28.6%)	35 (71.4%)		
ALCOHOL					
Never	34	5 (14.7%)	29 (85.3%)	0.33 (0.10–1.07)	0.093
Former or current	35	12 (34.3%)	23 (65.7%)		
LYMPHATIC METASTASIS					
N0	31	12 (38.7%)	19 (61.3%)	4.2 (1.27–12.65)	0.023
N1–2	38	5 (13.2%)	33 (86.8%)		
PATHOLOGICAL STAGE					
Initial (I + II)	14	6 (42.9%)	8 (57.1%)	3 (0.86–10.45)	0.076
Advanced (III+IV)	55	11 (20%)	44 (80%)		
SURVIVAL STATUS (17 PATIENTS WERE LOST TO FOLLOW)					
Survivors	36	16 (44.4%)	20 (55.6%)	12 (1.43–100.8)	0.009
Deceased or recurrence	16	1(6.3%)	15 (93.7%)		

heavier ($P < 0.05$ for both; **Figures 5A–D**). These *in vivo* results demonstrate that BCL11A has important functions for LSCC *in vivo* tumor development.

Correlation of BCL11A and MDM2 in LSCC

It has been shown in breast cancer cells that BCL11A positively regulates MDM2 expression (12). To evaluate the potential association of BCL11A and MDM2 in LSCC, we evaluated BCL11A and MDM2 co-expression by immunochemistry in the same tissue microarrays (TMA) from 69 LSCC patients (**Figures 6A–D**). Each tumor was assigned a BCL11A and MDM2 expression score based on the staining intensity and staining extent. A significant direct correlation was identified between the expression of BCL11A and MDM2 in the samples ($r = 0.442$; $P = 0.001$; **Figure 6E**). Experimentally, overexpression of BCL11A in AMC-HN-8 cells increased the MDM2 protein level (**Figure 6F**). Clinically, the LSCC cases that simultaneously expressed high BCL11A and MDM2 levels exhibited high rates of mortality or recurrence compared to the other patient subgroups (11/23 vs. 5/29). These data suggest that one function of BCL11A in LSCC is the regulation of MDM2.

Regulation of Tumorigenesis Molecules After BCL11A Overexpression

To identify other molecules or pathways that were regulated by BCL11A in LSCC, the Human Cancer PathwayFinder PCR Array analysis of nine different biological pathways (cell cycle, angiogenesis, cell senescence, DNA damage and repair, apoptosis, epithelial-to-mesenchymal transition, metabolism, hypoxia, telomeres and telomerase) (12) was performed (**Figures 6G–I**). The results revealed significant expression changes in several genes, including B2M, HMOX1, SNAI2, STMN1, BIRC3, and PPP1R15A in the AMC-HN-8 cells overexpressing BCL11A (**Figure 6J**). The Western blot analysis verified the expression changes of these proteins, except for STMN1 (**Figure 6K**). The altered gene expression of these molecules could represent additional mechanisms underlying the activity of BCL11A in LSCC.

DISCUSSION

The BCL11A gene, which spans over 102 kb on chromosome 2p16, is associated with various cancers (6, 13). It was initially observed in B-cell chronic lymphocytic leukemia, and it is considered a proto-oncogene of malignant hematological diseases (3, 14). Khaled et al. demonstrated that BCL11A was a new breast tumor gene and an important factor in normal mammary epithelial development (7). Other research indicated that the expression of BCL11A was reduced in bone marrow and brain, lymphoid and fetal liver tissue (15, 16).

BCL11A was also reported to be amplified in lung squamous cell cancer (SCC), with amplification more common among SCC samples of NSCLC without metastases (17). Jiang et al. reported the possible role of BCL11A in identifying and predicting the prognosis of NSCLC patients, particularly those with early-stage SCC. In their study, BCL11A was specifically overexpressed in tumor tissues rather than paracancer tissues. In the present study, BCL11A was also specifically overexpressed at the protein level in LSCC tissues rather than paracancer tissues. These findings are also consistent with the results of Zhang et al. (18), who observed that BCL11A-XL was markedly overexpressed in large cell lung cancer and squamous cell lung cancer.

Khaled et al. reported that knockdown of BCL11A expression in TNBC cells in a mouse model markedly decreased cancer

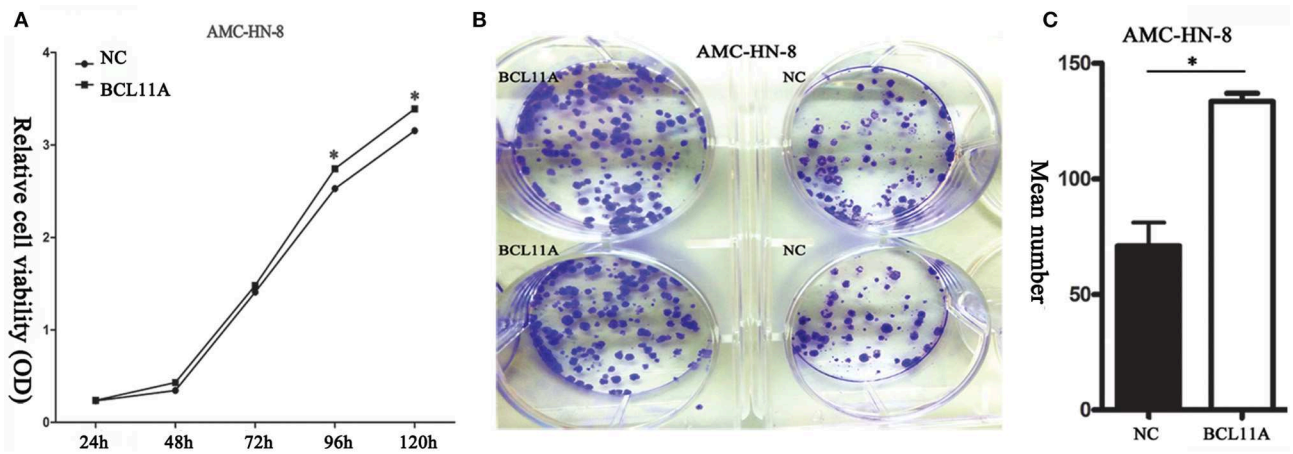

FIGURE 2 | (A) BCL11A overexpression increased AMC-HN-8 cell proliferation. **(B)** Overexpression of BCL11A in the AMC-HN-8 cells significantly increased their colony-forming abilities. **(C)** Quantitative comparison of the colonies formed from the parental AMC-HN-8 cells (NC) and the BCL11A overexpression (BCL11A) ones. $^{*}P < 0.05$.

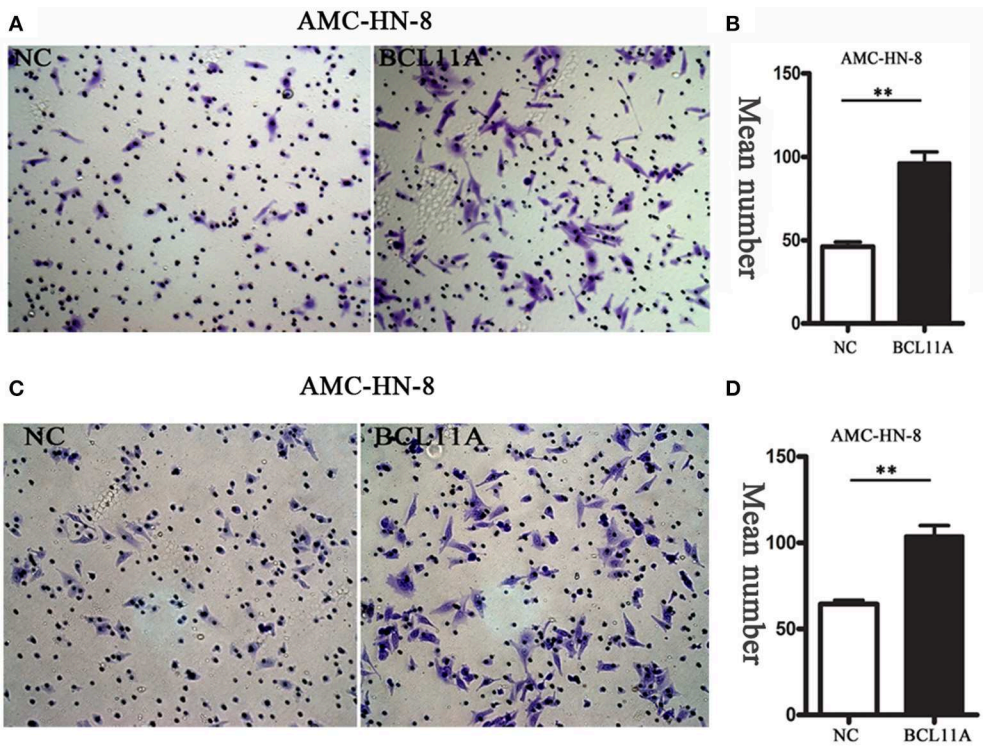

FIGURE 3 | The migration/ invasion ability of LSCC cells with overexpression in the transwell assay. **(A)** Increased migration capability of BCL11A-overexpression AMC-HN-8 cells detected by the transwell assay. Images showing the migrated AMC-HN-8 cells on the lower surface of the transwell membranes. Magnification ×200. **(B)** The numbers of migrated AMC-HN-8 cells in five random fields under the microscope (mean ± SD, $n = 5$). **(C)** Increased invasion capability of BCL11A-overexpression AMC-HN-8 cells. Images showing the invaded BCL11A-overexpresing AMC-HN-8 cells on lower surface of the transwell membranes in different groups. Magnification ×200. **(D)** The number of invaded BCL11A-overexpressing AMC-HN-8 in five random fields under the microscope (mean ± SD, $n = 5$). $^{**}P < 0.01$.

development (7). In this study, BCL11A overexpression in the AMC-HN-8 LSCC cell line increased LSCC proliferation and invasion *in vitro* and promoted the growth of LSCC xenografts *in vivo*. Overexpression of BCL11A had no noteworthy effects on cell cycle kinetics (**Figure 4B**), which is similar to the results presented by Khaled et al. (7). They also reported that the

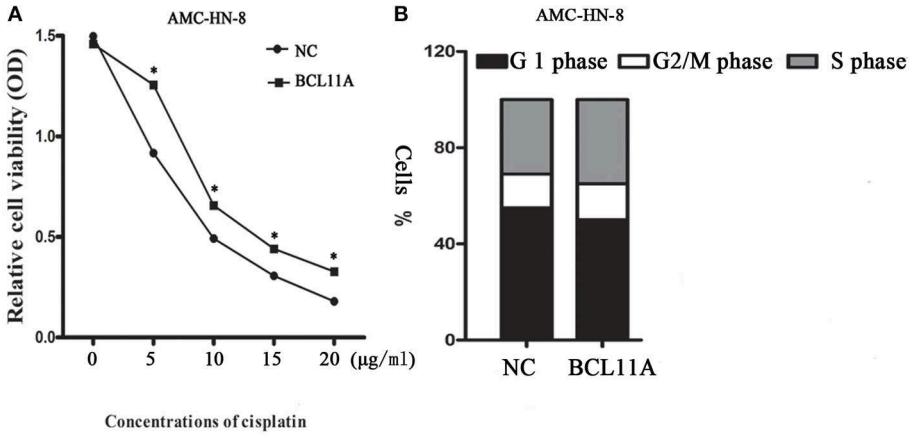

FIGURE 4 | (A) Influence of different concentrations of cisplatin on the cytotoxicity of negative controls (NC) AMC-HN-8 and overexpression BCL11A AMC-HN-8 cell strains. **(B)** Cell cycle investigation, showing that overexpression did not affect cell cycle kinetics in the two cell lines. The data are the mean ± s.d. ($n = 3$).*$P < 0.05$.

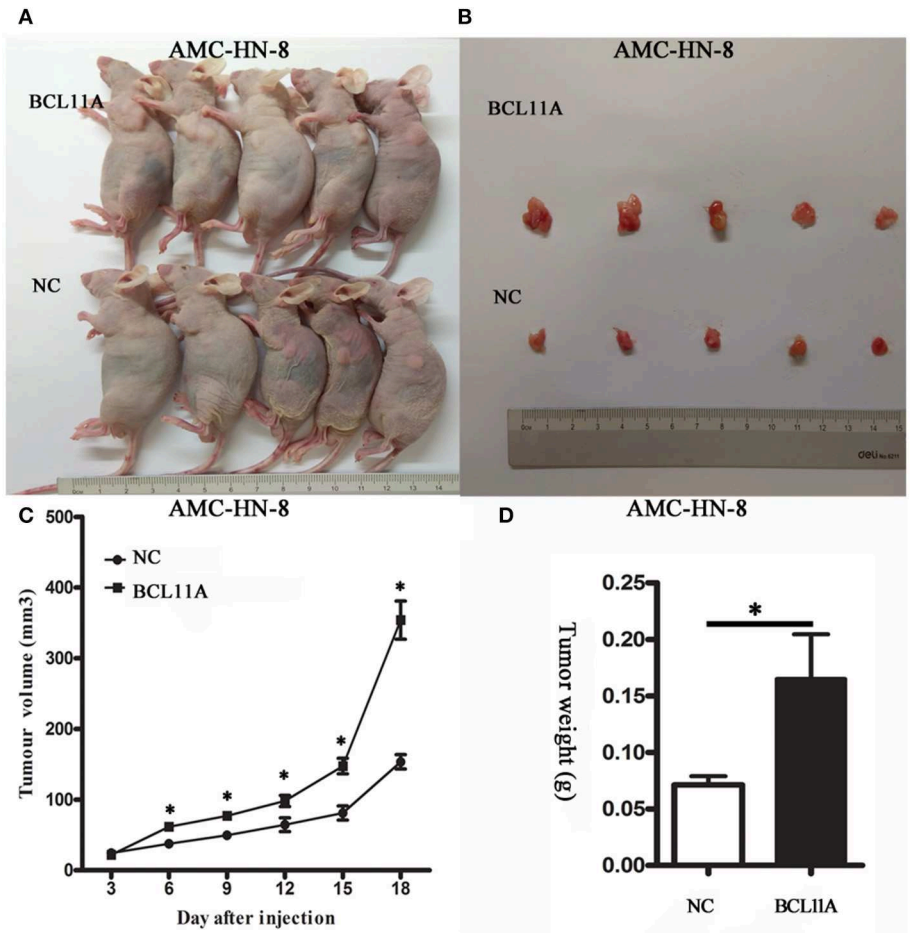

FIGURE 5 | BCL11A regulated AMC-HN-8 cell growth *in vivo*. **(A)** Images of mice with xenograft tumors of BCL11A-overexpression AMC-HN-8 cells and the control cells (NC); **(B)** Image of tumors isolated from nude mice. **(C)** Growth curves of the xenografts in the BCL11A-overexpression AMC-HN-8 cell group and control cells (NC) ($n = 5$, mean ± SEM). **(D)** Comparison of the weight of the xenografts in the BCL11A-overexpression AMC-HN-8 cells and control cells (NC) harvested 18 d after injection of the cells ($n = 5$, mean ± SEM). *$P < 0.05$.

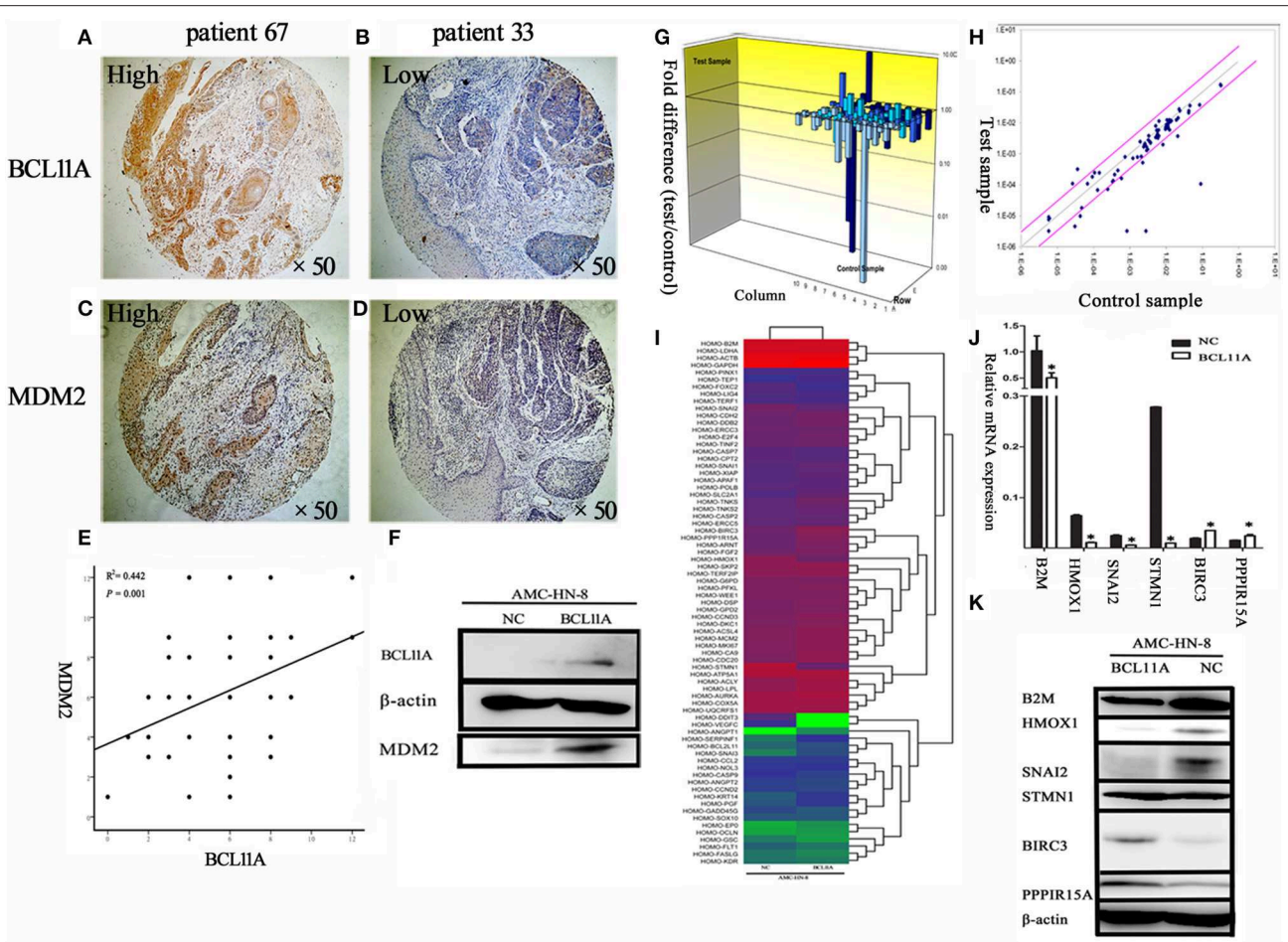

FIGURE 6 | (A–D) Co-expression of BCL11A and MDM2 in some LSCCs, as shown by immunohistochemistry. **(E)** Linear regression analysis of BCL11A vs. MDM2 expression levels (immunohistochemistry scores in the same TMA). **(F)** The Western blot showed that MDM2 was up-regulated in the BCL11A overexpression AMC-HN-8 cell line at the protein level. **(G)** PCR microarray investigation of human cancer pathway genes in the BCL11A-overexpression AMC-HN-8 cells. 3D profile graph displays the fold change in the expression of each gene in the BCL11A-overexpression AMC-HN-8 cells vs. that of the control cells. Columns pointing up (with z-axis values > 1) indicate up-regulation of gene expression, and the columns pointing down (with z-axis values < 1) denote down-regulation of gene expression. **(H)** The corresponding scatter plots display the validity of the test and expression level of every gene in the BCL11A-overexpression AMC-HN-8 cells vs. that of the control cells ($n = 3$). **(I)** Heat map of the 84 probe sets in BCL11A-overexpression AMC-HN-8 cells vs. that of the control cells. **(J)** Six selected genes in the BCL11A-overexpression AMC-HN-8 cells showed a significant change at the mRNA level vs. that of the control cells. **(K)** Western blot verification of the gene expression changes. *$P < 0.05$.

survival rates of triple-negative breast cancer patients with either copy number gains or high expression of BCL11A were poorer than those of the remainder of the group. In addition to lower survival rates, the patients with copy number gains of BCL11A had a higher rate of metastasis and relapse. In our study, LSCC patients with high expression of BCL11A were significantly more likely to suffer loco-regional recurrence or to become moribund than those with low expression of BCL11A (hazard ratio: 12, $P = 0.009$) (**Table 2**). Furthermore, the vast majority of patients with high expression of BCL11A were diagnosed with advanced clinical N1/N2 lymphatic metastasis ($P = 0.023$) (**Table 2**). Previous studies of four other tumor patient data sets reported a similar tendency (19–22). On the other hand, some studies have shown that BCL11A is an independent prognostic factor for both disease-free survival and overall survival (8, 18). The role of BCL11A expression as a biomarker in the clinic requires additional exploration.

It was reported that BCL11A can also upregulate MDM2 expression, which hinders p53 activities (23). These molecular changes happen frequently in solid cancers. Yu et al. reported that Mdm2 was downregulated in Bcl11a-deficient B cells. ChIP tests showed that Bcl11a was bound to Mdm2. Furthermore, overexpressing Mdm2 rescued both apoptosis and proliferation defects caused by Bcl11a knockdown in B cells. In addition, Bcl11a deletion resulted in p53 accumulation in lymphocytes, likely due to reduced Mdm2/Mdm4 (24). In the current study, as shown by the BCL11A and MDM2 immunochemistry scores in the LSCC TMA, there was a significant correlation between BCL11A and MDM2 expression ($r = 0.442$; $P = 0.001$; **Figure 6E**). In the LSCC cell line, overexpression of BCL11A

caused high expression of MDM2 (**Figure 6F**). However, the relevance of MDM2 expression highly depends on p53 status, and further research will be focused on the relationship between P53 status and MDM2.

We applied the Cancer PathwayFinder PCR array to identify additional genes regulated by BCL11A in LSCC. Among the upregulated genes in the AMC-HN-8-BCL11A cells, some genes are classified as involving apoptosis, DNA damage, and DNA repair; BIRC3 promotes resistance of cancer cells to apoptosis (25, 26). Another gene, PPP1R15A, was previously shown to be involved in apoptosis or cell growth (27). Among the downregulated genes in the AMC-HN-8-BCL11A cells, some genes were associated with the epithelial-to-mesenchymal transition and hypoxia, including B2M, which is a Class I MHC protein that regulates the proliferation of normal cells and carcinoma cells (28). HMOX1, the inducible isoform of the rate-limiting enzyme in haem degradation, neutralizes inflammatory and oxidative injury. HMOX-1 deficiency results in high levels of endothelial damage and prolonged inflammation (29, 30). In addition, SNAI2, which represses E-cadherin (CDH1), was also downregulated. In renal cell tumors, SNAI2-positive renal cell tumors were reported to be associated with lower-stage tumors and a better prognosis than SNAI2-negative tumors (31).

CONCLUSIONS

This study investigated the proto-oncogene BCL11A in LSCC. The results revealed that BCL11A was upregulated in some clinical LSCC tissue samples at the protein level. The statistical analyses showed that BCL11A expression was strongly associated with lymph node status and the survival of LSCC patients. We demonstrated experimentally that BCL11A regulated cell proliferation, cell invasion/migration and chemosensitivity in LSCC cells *in vitro* and in LSCC xenografts *in vivo*. BCL11A also upregulated the expression of MDM2, which is frequently co-expressed in LSCC.

DATA AVAILABILITY STATEMENT

The raw data supporting the conclusions of this article will be made available by the authors, without undue reservation, to any qualified researcher.

ETHICS STATEMENT

The studies involving human participants were reviewed and approved by the Ethics Committee of Fudan University. The patients/participants provided their written informed consent to participate in this study. The animal study was reviewed and approved by the Ethics Committee of Fudan University.

AUTHOR'S NOTE

We demonstrated that BCL11A expression was strongly associated with lymph node status and the survival of LSCC patients and BCL11A regulated cell proliferation, cell invasion/migration and chemosensitivity in LSCC cells *in vitro* and LSCC xenografts *in vivo*. BCL11A also up-regulated the expression of MDM2, which is frequently co-expressed in LSCC. Our results uncovered important functions of BCL11A in LSCC and identify BCL11A as a prognostic biomarker and potential therapeutic target in LSCC.

AUTHOR CONTRIBUTIONS

LT and L-ML designed and conceived the experiments. JZ, LiaZ, DZ, W-JT, DT, X-LS, and YueY collected samples. JZ, LinZ, FL, and YonY completed the experiment. JZ, LiaZ, and PL analyzed the experimental data. JZ and DZ finished the paper.

FUNDING

This work was sponsored by The National Natural Science Foundation of China (Grant numbers: 30972691, 30801283, 81671579, and 31370904), Shanghai Sailing Program (Grant number: 19YF1405900), The Technology Project of Shanghai (Grant numbers: 11JC1410802, 09QA1401000, 10QA1405900, and 14411961900), Shanghai's health system of talents training plan (Grant numbers: XYQ2011055 and XYQ2011015), Shanghai Pujiang Program (15PJD021); Program for scientific and technological innovation from the Science and Technology Commission of Shanghai Municipality (18140903800 and 15401900500); Shuguang Planning of Shanghai Municipal Education Commission of (16SG14); Program of Shanghai translational Medicine Collaborative Innovation Center cooperation (TM201522 and TM201721), the National Key Research and Development Program (2017YFA0104500).

ACKNOWLEDGMENTS

We thank the staff of Shanghai Institute of Immunology, Wellcome Trust Sanger Institute, for their technical support and expertise.

REFERENCES

1. Jemal A, Bray F, Center MM, Ferlay J, Ward E, Forman D. Global cancer statistics. *CA Cancer J Clin*. (2011) 61:69–90. doi: 10.3322/caac.20107
2. Alhamarneh O, Agada F, Madden L, Stafford N, Greenman J. Serum IL10 and circulating CD4(+) CD25(high) regulatory T cell numbers as predictors of clinical outcome and survival in patients with head and neck squamous cell carcinoma. *Head Neck*. (2011) 33:415–23. doi: 10.1002/hed.21464
3. Nakamura T, Yamazaki Y, Saiki Y, Moriyama M, Largaespada DA, Jenkins NA, et al. Evi9 encodes a novel zinc finger protein that physically interacts with BCL6, a known human B-cell proto-oncogene product. *Mol Cell Biol*. (2000) 20:3178–86. doi: 10.1128/MCB.20.9.3178-3186.2000
4. Ng SY, Yoshida T, Zhang J, Georgopoulos K. Genome-wide lineage-specific transcriptional networks underscore Ikaros-dependent lymphoid priming in hematopoietic stem cells. *Immunity*. (2009) 30:493–507. doi: 10.1016/j.immuni.2009.01.014

5. Fell HP, Smith RG, Tucker PW. Molecular analysis of the t(2;14) translocation of childhood chronic lymphocytic leukemia. *Science.* (1986) 232:491–4. doi: 10.1126/science.3961491
6. Satterwhite E, Sonoki T, Willis TG, Harder L, Nowak R, Arriola EL, et al. The BCL11 gene family: involvement of BCL11A in lymphoid malignancies. *Blood.* (2001) 98:3413–20. doi: 10.1182/blood.V98.12.3413
7. Khaled WT, Choon Lee S, Stingl J, Chen X, Raza Ali H, Rueda OM, et al. BCL11A is a triple-negative breast cancer gene with critical functions in stem and progenitor cells. *Nat Commun.* (2015) 6:5987. doi: 10.1038/ncomms6987
8. Jiang BY, Zhang XC, Su J, Meng W, Yang XN, Yang JJ, et al. BCL11A overexpression predicts survival and relapse in non-small cell lung cancer and is modulated by microRNA-30a and gene amplification. *Mol Cancer.* (2013) 12:61. doi: 10.1186/1476-4598-12-61
9. Koo CL, Kok LF, Lee MY, Wu TS, Cheng YW, Hsu JD, et al. Scoring mechanisms of p16INK4a immunohistochemistry based on either independent nucleic stain or mixed cytoplasmic with nucleic expression can significantly signal to distinguish between endocervical and endometrial adenocarcinomas in a tissue microarray study. *J Transl Med.* (2009) 7:25. doi: 10.1186/1479-5876-7-25
10. Kasaian K, Wiseman SM, Walker BA, Schein JE, Zhao Y, Hirst M, et al. The genomic and transcriptomic landscape of anaplastic thyroid cancer: implications for therapy. *BMC Cancer.* (2015) 15:984. doi: 10.1186/s12885-015-1955-9
11. Wan G, Zhou L, Xie M, Chen H, Tian J. Characterization of side population cells from laryngeal cancer cell lines. *Head Neck.* (2010) 32:1302–9. doi: 10.1002/hed.21325
12. Winter SC, Buffa FM, Silva P, Miller C, Valentine HR, Turley H, et al. Relation of a hypoxia metagene derived from head and neck cancer to prognosis of multiple cancers. *Cancer Res.* (2007) 67:3441–9. doi: 10.1158/0008-5472.CAN-06-3322
13. Chen Z, Luo HY, Steinberg MH, Chui DH. BCL11A represses HBG transcription in K562 cells. *Blood Cells Mol Dis.* (2009) 42:144–9. doi: 10.1016/j.bcmd.2008.12.003
14. Weniger MA, Pulford K, Gesk S, Ehrlich S, Banham AH, Lyne L, et al. Gains of the proto-oncogene BCL11A and nuclear accumulation of BCL11A(XL) protein are frequent in primary mediastinal B-cell lymphoma. *Leukemia.* (2006) 20:1880–2. doi: 10.1038/sj.leu.2404324
15. Kuo TY, Hsueh YP. Expression of zinc finger transcription factor Bcl11A/Evi9/CTIP1 in rat brain. *J Neurosci Res.* (2007) 85:1628–36. doi: 10.1002/jnr.21300
16. Sankaran VG, Menne TF, Xu J, Akie TE, Lettre G, Van Handel B, et al. Human fetal hemoglobin expression is regulated by the developmental stage-specific repressor BCL11A. *Science.* (2008) 322:1839–842. doi: 10.1126/science.1165409
17. Boelens MC, Kok K, van der Vlies P, van der Vries G, Sietsma H, Timens W, et al. Genomic aberrations in squamous cell lung carcinoma related to lymph node or distant metastasis. *Lung Cancer.* (2009) 66:372–8. doi: 10.1016/j.lungcan.2009.02.017
18. Zhang N, Jiang BY, Zhang XC, Xie Z, Su J, Zhang Q, et al. The BCL11A-XL expression predicts relapse in squamous cell carcinoma and large cell carcinoma. *J Thorac Dis.* (2015) 7:1630–6. doi: 10.3978/j.issn.2072-1439.2015.09.39
19. Desmedt C, Piette F, Loi S, Wang Y, Lallemand F, Haibe-Kains B, et al. Strong time dependence of the 76-gene prognostic signature for node-negative breast cancer patients in the TRANSBIG multicenter independent validation series. *Clin Cancer Res.* (2007) 13:3207–14. doi: 10.1158/1078-0432.CCR-06-2765
20. Hatzis C, Pusztai L, Valero V, Booser DJ, Esserman L, Lluch A, et al. A genomic predictor of response and survival following taxane-anthracycline chemotherapy for invasive breast cancer. *JAMA.* (2011). 305:1873–81. doi: 10.1001/jama.2011.593
21. Ma XJ, Wang Z, Ryan PD, Isakoff SJ, Barmettler A, Fuller A, et al. A two-gene expression ratio predicts clinical outcome in breast cancer patients treated with tamoxifen. *Cancer Cell.* (2004) 5:607–16. doi: 10.1016/j.ccr.2004.05.015
22. Schmidt M, Bohm D, von Torne C, Steiner E, Puhl A, Pilch H, et al. The humoral immune system has a key prognostic impact in node-negative breast cancer. *Cancer Res.* (2008) 68:5405–13. doi: 10.1158/0008-5472.CAN-07-5206
23. Pulford K, Banham AH, Lyne L, Jones M, Ippolito GC, Liu H, et al. The BCL11AXL transcription factor: its distribution in normal and malignant tissues and use as a marker for plasmacytoid dendritic cells. *Leukemia.* (2006) 20:1439–41. doi: 10.1038/sj.leu.2404260
24. Yu Y, Wang J, Khaled W, Burke S, Li P, Chen X, et al. Bcl11a is essential for lymphoid development and negatively regulates p53. *J Exp Med.* (2012) 209:2467–83. doi: 10.1084/jem.20121846
25. Petersen SL, Wang L, Yalcin-Chin A, Li L, Peyton M, Minna J, et al. Autocrine TNFalpha signaling renders human cancer cells susceptible to Smac-mimetic-induced apoptosis. *Cancer Cell.* (2007) 12:445–56. doi: 10.1016/j.ccr.2007.08.029
26. Petersen SL, Peyton M, Minna JD, Wang X. Overcoming cancer cell resistance to Smac mimetic induced apoptosis by modulating cIAP-2 expression. *Proc Natl Acad Sci USA.* (2010) 107:11936–41. doi: 10.1073/pnas.1005667107
27. Tan J, Yang X, Zhuang L, Jiang X, Chen W, Lee PL, et al. Pharmacologic disruption of Polycomb-repressive complex 2-mediated gene repression selectively induces apoptosis in cancer cells. *Genes Dev.* (2007) 21:1050–63. doi: 10.1101/gad.1524107
28. D'Urso CM, Wang ZG, Cao Y, Tatake R, Zeff RA, Ferrone S. Lack of HLA class I antigen expression by cultured melanoma cells FO-1 due to a defect in B2m gene expression. *J Clin Invest.* (1991) 87:284–92. doi: 10.1172/JCI114984
29. Kawashima A, Oda Y, Yachie A, Koizumi S, Nakanishi I. Heme oxygenase-1 deficiency: the first autopsy case. *Hum Pathol.* (2002) 33:125–130. doi: 10.1053/hupa.2002.30217
30. Yachie A, Toma T, Mizuno K, Okamoto H, Shimura S, Ohta K, et al. Heme oxygenase-1 production by peripheral blood monocytes during acute inflammatory illnesses of children. *Exp Biol Med.* (2003) 228:550–6. doi: 10.1177/15353702-0322805-26
31. Mikami S, Katsube K, Oya M, Ishida M, Kosaka T, Mizuno R, et al. Expression of Snail and Slug in renal cell carcinoma: E-cadherin repressor Snail is associated with cancer invasion and prognosis. *Lab Invest.* (2011) 91:1443–58. doi: 10.1038/labinvest.2011.111

Conflict of Interest: The authors declare that the research was conducted in the absence of any commercial or financial relationships that could be construed as a potential conflict of interest.

frontiers in Oncology

ORIGINAL RESEARCH
published: 31 March 2020
doi: 10.3389/fonc.2020.00368

Expression Profile and Prognostic Values of *HOXA* Family Members in Laryngeal Squamous Cell Cancer

Jinyun Li[1], *Meng Ye*[1] *and Chongchang Zhou*[2]*

[1] Department of Oncology and Hematology, The Affiliated Hospital of Medical School of Ningbo University, Ningbo, China,
[2] Department of Otorhinolaryngology Head and Neck Surgery, Ningbo Medical Center Lihuili Hospital, Ningbo, China

The homeobox A cluster (*HOXA*) gene family, comprising 11 members, is involved in a wide spectrum of biological functions in human cancers. However, there is little research on the expression profile and prognostic values of *HOXA* genes in laryngeal squamous cell cancer (LSCC). Based on updated public resources and integrative bioinformatics analysis, we assessed the expression profile and prognostic values of the *HOXA* family members. Expression and methylation data on *HOXA* family members were obtained from The Cancer Genome Atlas (TCGA). The prognostic values of *HOXA* members and clinical features were identified. A gene set enrichment analysis (GSEA) was conducted to explore the mechanism underlying the involvement of *HOXA* members in LSCC. The associations between tumor immune infiltrating cells (TIICs) and the *HOXA* family members were evaluated using the Tumor Immune Estimation Resource (TIMER) database. *HOXA2* and *HOXA4* were downregulated and *HOXA7* and *HOXA9–13* were upregulated in LSCC. Upregulation of *HOXA10*, *HOXA11,* and *HOXA13*, along with two clinical characteristics (M stage and gender), were associated with a poor LSCC prognosis based on the results of univariate and multivariate Cox proportional hazards regression analyses. Although there were no significant correlations between TIICs and *HOXA* members, the GSEA results indicated that *HOXA* members participate in multiple biological processes underlying tumorigenesis. This study comprehensively analyzed the *HOXA* members, providing insights for further investigation of the *HOXA* family members as potential targets in LSCC.

Keywords: *HOXA* family, TCGA, prognosis, GSEA, LSCC

OPEN ACCESS

Edited by:
Jorge A. R. Salvador, University of Coimbra, Portugal

Reviewed by:
Hong-Quan Duong, Hanoi University of Public Health, Vietnam
Maria Cossu Rocca, European Institute of Oncology (IEO), Italy

***Correspondence:**
Chongchang Zhou
zhou900709900709@163.com

Specialty section:
This article was submitted to Head and Neck Cancer, a section of the journal Frontiers in Oncology

Received: *29 November 2019*
Accepted: *02 March 2020*
Published: *31 March 2020*

Citation:
Li J, Ye M and Zhou C (2020) Expression Profile and Prognostic Values of HOXA Family Members in Laryngeal Squamous Cell Cancer. Front. Oncol. 10:368. doi: 10.3389/fonc.2020.00368

INTRODUCTION

Laryngeal cancer is one of the most common malignancies in the head and neck region, and laryngeal squamous cell cancer (LSCC) accounts for more than 95% of cases (1). Despite progress regarding comprehensive therapeutic strategies to treat LSCC, the prognosis of LSCC remains unsatisfactory, as 30–40% of patients die within 5 years of diagnosis with advanced LSCC (2). Identification of reliable biomarkers for LSCC prognosis could facilitate individualized treatment.

The *HOX* gene family is one of the families of homeobox genes that function as developmental regulatory genes (3). In mammals, there are 39 HOX genes in four gene clusters named *HOXA*, *HOXB*, *HOXC,* and *HOXD* (4). The *HOXA* cluster comprises 11 genes (including *HOXA1*, *HOXA2*, *HOXA3*, *HOXA4*, *HOXA5*, *HOXA6*, *HOXA7*, *HOXA9*, *HOXA10*, *HOXA11,* and *HOXA13*), which

encode proteins that contain the DNA-binding homeobox motif (5). The molecular functions of the *HOXA* family cover a wide spectrum of biological processes, including differentiation, proliferation, migration and cell death. A substantial body of scientific evidence indicates that the expression of particular *HOXA* genes is dysregulated in certain types of carcinomas, which contributes to carcinogenesis (6–10). For instance, *HOXA1* mRNA and protein expression is upregulated in breast cancer, and forced expression of *HOXA1* in human breast cancer cells resulted in increased cell proliferation and doxorubicin resistance (11, 12). Aberrantly expressed *HOXA6* and *HOXA13* were also observed in breast cancer (13). In colorectal cancer, *HOXA13* was expressed more in normal colons than in malignant colons, and it was more highly expressed on the left side of the normal colon compared to the right side, indicating that differential *HOXA* gene expression occurs in an organized manner (10). Additionally, several studies have reported that *HOXA9* and *HOXA10* can serve as predictive biomarkers of poor survival in glioblastoma multiforme (GBM) (14–16).

Collectively, the differential expression and prognostic values of the *HOXA* family members have been noticed in various types of cancers. Studying the differential expression of *HOXA* genes in LSCC provides an opportunity to advance our understanding of LSCC development and to develop new therapeutic agents. In this study, based on updated public resources and integrative bioinformatics analysis, the expression profile and prognostic values of the *HOXA* family members were comprehensively assessed.

MATERIALS AND METHODS

The Cancer Genome Atlas (TCGA) mRNA Expression Data of the *HOXA* Family

The TCGA program was conducted by the National Cancer Institute and National Human Genome Research Institute to molecularly characterize over 20,000 primary cancer samples and matched normal samples spanning 33 cancer types, including 528 cases of primary head and neck squamous carcinoma (HNSC), two cases of metastatic HNSC and 74 adjacent normal control samples. A total of 111 cases of laryngeal squamous cell cancer (LSCC) and 12 normal controls were included in the current study, after matching clinical parameters (including gender, age, smoking history, alcohol consumption, tumor (T) stage, node (N) stage, metastasis (M) stage, clinical stage and primary cancer sites). Subsequently, we used the Genomic Data Commons (GDC) Data Transfer Tool recommended by TCGA to download high-throughput sequencing (HTSeq) Fragments Per Kilobase of transcript per Million mapped reads (FPKM) data on the *HOXA* family.

Comparison of the mRNA Expression of the HOXA Family in LSCC and Normal Tissues

Using Perl 5.26 software, the mRNA expression levels of the *HOXA* family were obtained from the HTSeq level 3 data on genome mRNA expression. The differential expression of the *HOXA* family in LSCC tissues compared to normal tissues was analyzed utilized the *limma* package in R 3.6.0 software. The results were visualized using the *pheatmap* package.

Correlation Between mRNA Expression and Methylation of the *HOXA* Family in LSCC

We used the GDC Data Transfer Tool recommended by TCGA to download data from Illumina HumanMethylation 450K on the methylation levels of cg sites in the gene promoter regions of differentially expressed *HOXA* members in LSCC tissues. Thereafter, we utilized the *corrplot* package to further explore the correlation between methylation and *HOXA* expression in LSCC. The information on cg sites from Illumina HumanMethylation 450K were annotated using the annotation file from the official Illumina website (https://support.illumina.com/downloads/~infinium_humanmethylation450_product_files.html).

Survival Analysis of *HOXA* Members in LSCC

The prognostic values of the *HOXA* members were investigated using the following two steps: (1) the associations between *HOXA* members, as well as each clinical parameter, and overall survival among LSCC patients were assessed using univariate Cox proportional hazards regression analyses and (2) using multivariate Cox proportional hazards regression analysis, the independent prognostic values of the *HOXA* members were then obtained by controlling for the significant clinical parameters from step 1. All the analyses were performed using the *survival* package in R 3.6.0 software.

Associations Between Tumor Immune Infiltrating Cells (TIICs) and the *HOXA* Family Using the Tumor Immune Estimation Resource (TIMER) Database

Tumor cells and TIICs interact through multiple genes and pathways during cancer progression. To explore the correlations between TIICs and *HOXA* members, we utilized the TIMER platform (https://cistrome.shinyapps.io/timer/), which is an online tool for assessing the specific gene(s) associated with TIICs (17). In TIMER, the TIICs include B-cells, $CD4^+$ T-cells, $CD8^+$ T-cells, dendritic cells, macrophages and neutrophils.

Gene Set Enrichment Analysis (GSEA)

To evaluate the potential mechanism underlying the involvement of *HOXA* members in the carcinogenesis of LSCC, we performed GSEA (version 4.0.1; http://software.broadinstitute.org/gsea/index.jsp) to identify the to identify the pathways related to the differential *HOXA* expression in the TCGA LSCC tissues (18). The annotated gene set file c2.cp.kegg.v7.0.symbols.gmt (from the Msig database) was used as the reference. GSEA was performed using a

random combination number of 1,000 permutations and a false discovery rate (FDR) <0.05 to identify the significantly enriched pathways.

Statistical Analysis

The HTSeq FPKM mRNA data from the TCGA database was handled using Perl 5.26 software. The *limma* package was applied to analyze the expression of *HOXA* members in LSCC tissues, the *corrplot* package was used for the correlation between methylation and expression of *HOXA* members, the *survival* package was used for the analysis of prognostic values, the *ggplot* package was used to plot forest plots related to the multivariate Cox proportional hazards regression analysis.

RESULTS

Expression Status of *HOXA* Members in LSCC Tissues

First of all, the mRNA expression data on *HOXA* members (*HOXA1–13*) from 111 LSCC samples and 12 normal control samples, which originated from TCGA, were obtained using Perl software. Pearson's correlation of *HOXA* family genes were calculated and used to assess whether these genes were correlated with each other using the *corrplot* package. As shown in **Figure 1**, the *HOXA* family genes were correlated to a significant degree.

Thereafter, the differentially expressed *HOXA* members were analyzed using the *limma* package and visualized

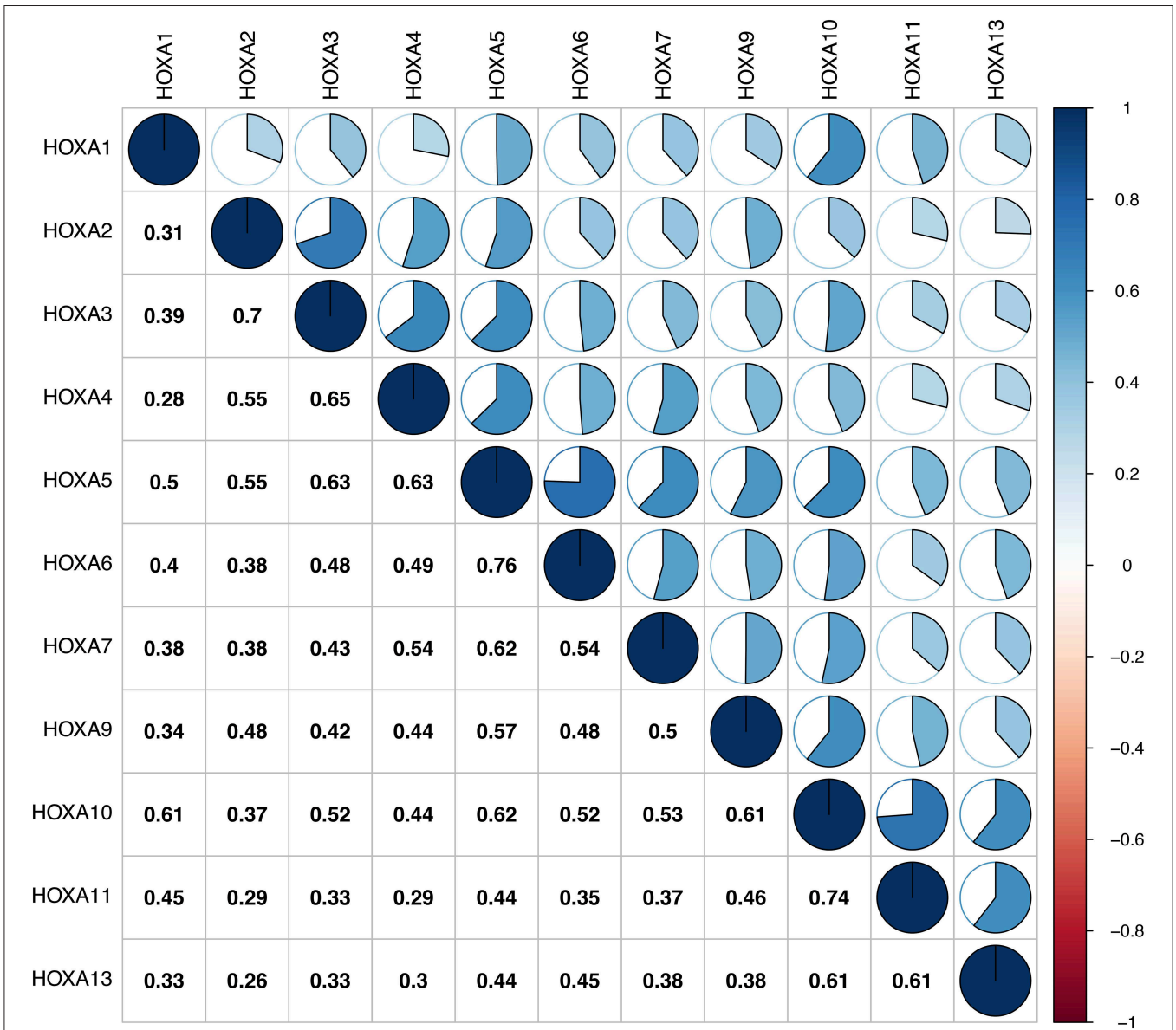

FIGURE 1 | Associations between *HOXA* family members.

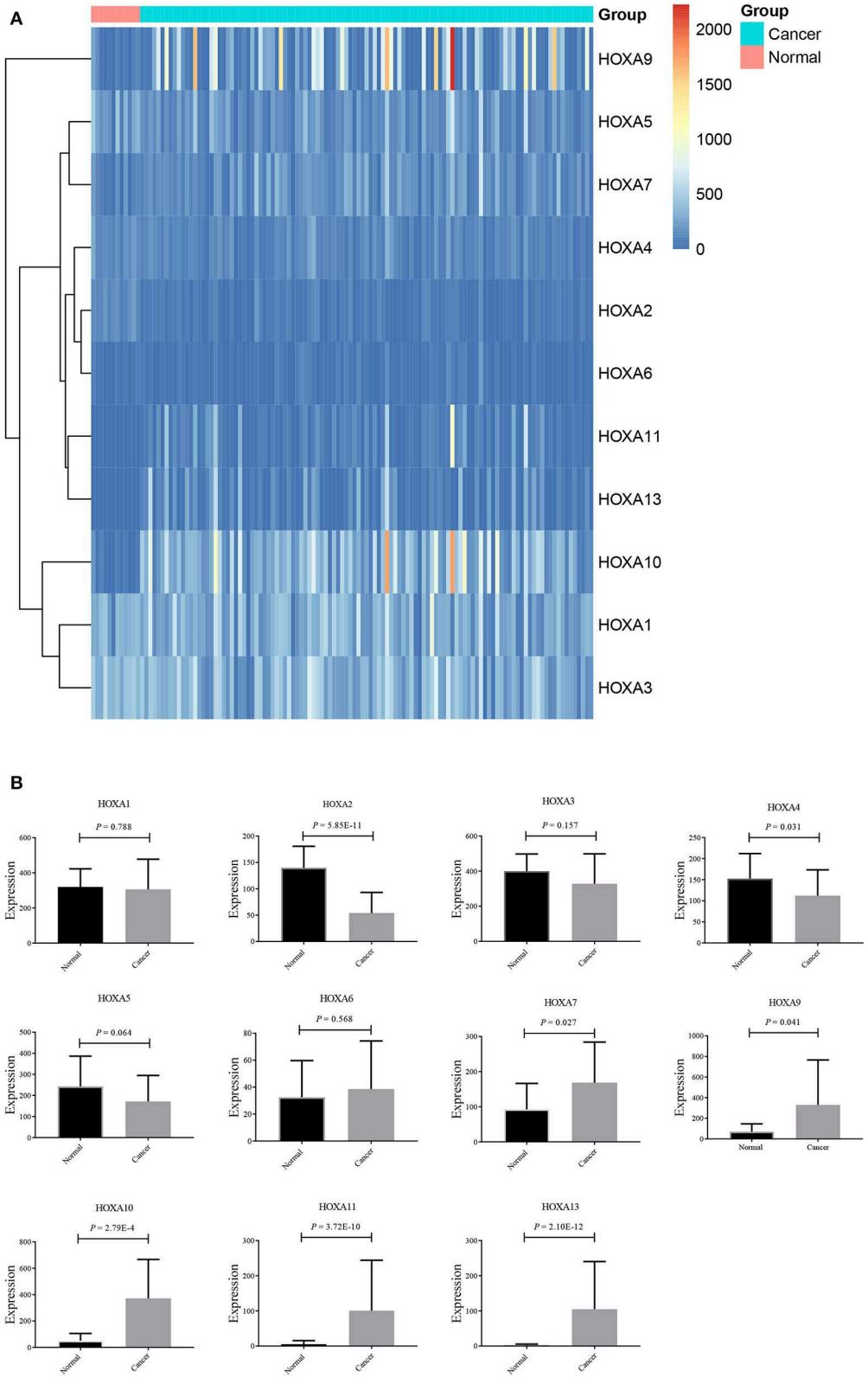

FIGURE 2 | Expression profile of *HOXA* members in LSCC represented by a heatmap **(A)**, and histograms **(B)**.

using the *pheatmap* package, as shown in **Figure 2A**. As shown in **Figure 2B**, *HOXA2* and *HOXA4* were significantly downregulated in LSCC tissues compared to control tissues, while *HOXA7*, *HOXA9*, *HOXA10*, *HOXA11,* and *HOXA13* were significantly upregulated in LSCC tissues. There were no significant differences in *HOXA1*, *HOXA3*, *HOXA5,* and *HOXA6* expression between LSCC and control tissues.

Correlation of HOXA Expression and Methylation in LSCC

Methylation of gene promoter regions is one of the most common mechanisms that influences gene expression during the progression of human cancer. We identified seven differentially expressed *HOXA* members in LSCC (downregulated *HOXA2* and *HOXA4* and upregulated *HOXA7*, *HOXA9*, *HOXA10*, *HOXA11,* and *HOXA13*). The Pearson's correlation results showed that six of seven differentially expressed *HOXA* members (including *HOXA4*, *HOXA7*, *HOXA9*, *HOXA10*, *HOXA11,* and *HOXA13*) was negative associated with methylation level (**Figure S1**), and only five of the 32 assessed CG sites in the promoter region of *HOXA2* exhibited negative correlation with *HOXA2* expression in LSCC (**Figure 3**). These results indicated the inverse correlation between expression and methylation level of *HOXA* members in LSCC.

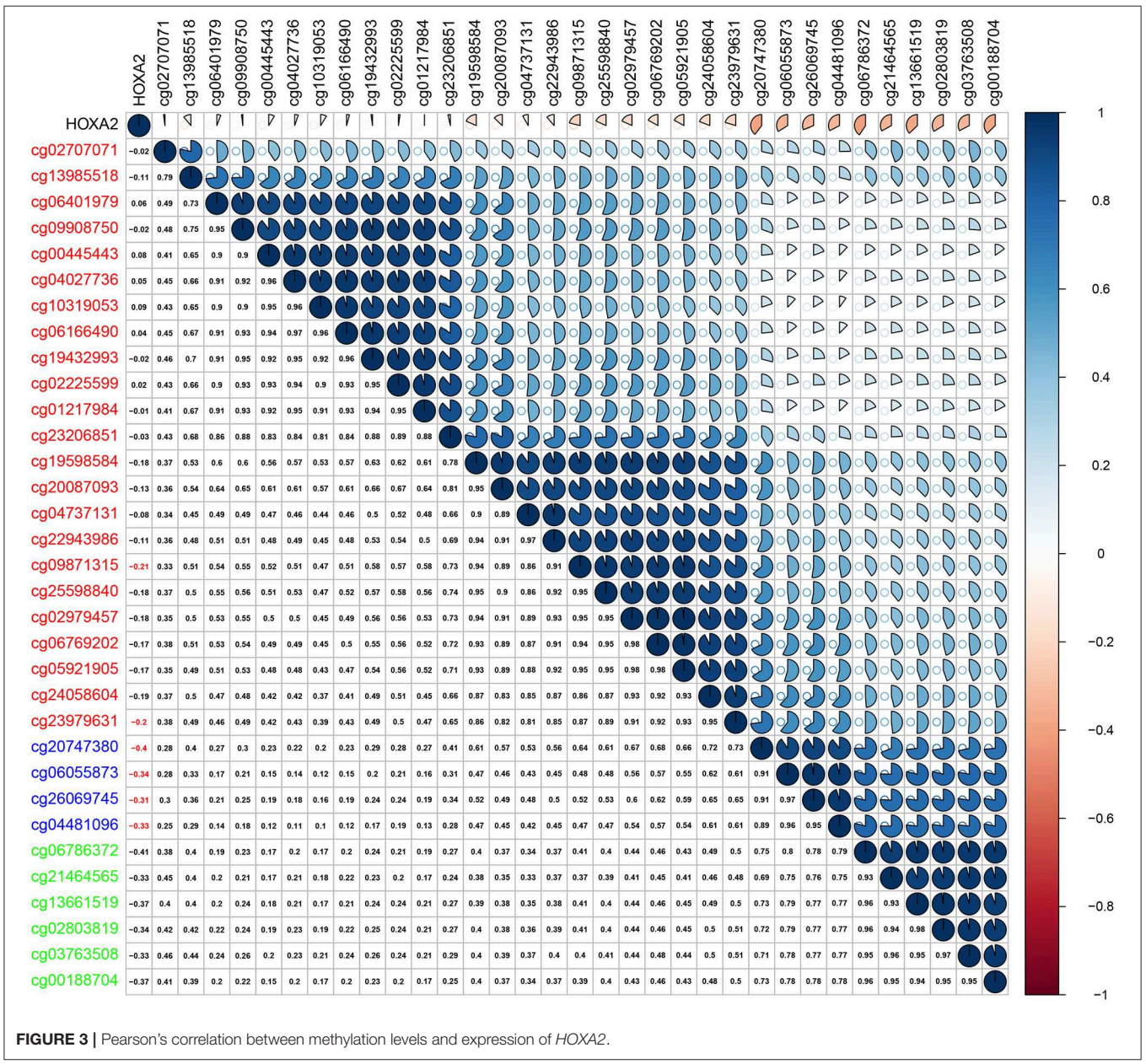

FIGURE 3 | Pearson's correlation between methylation levels and expression of *HOXA2*.

Prognostic Values of *HOXA* Members in LSCC

Subsequently, the prognostic values of *HOXA* members were analyzed. First, the predictive capabilities of differentially expressed *HOXA* members (*HOXA2*, *HOXA4*, *HOXA7*, *HOXA9*, *HOXA10*, *HOXA11,* and *HOXA13*) and clinical features were assessed by univariate Cox proportional hazards regression analyses. The results showed that the expression of three *HOXA* members (*HOXA10*, *HOXA11,* and *HOXA13*) and two clinical features (M stage and male) were associated with poor outcome of LSCC patients (hazard ratio [HR] for *HOXA10*: 1.379 (1.081–1.759); HR for *HOXA11*: 1.179 (1.000–1.391); HR for *HOXA13*: 1.129 (0.999–1.277); HR for M stage: 8.225 (1.901–35.594); and HR for male: 3.367 [1.708–6.639]) (**Table 1**). Second, the independent prognostic values of *HOXA10*, *HOXA11,* and *HOXA13* were assessed using multivariate Cox proportional hazards regression analysis to control for the prognostic effects of the clinical features. The results showed that the expression of *HOXA10*, *HOXA11,* and *HOXA13* and two clinical parameters (M stage and gender) were independent prognostic biomarkers of LSCC outcome. The results of the multivariate Cox proportional hazards regression analysis are exhibited in forest plots in **Figure 4**.

Correlations Between TIICs and *HOXA* Members

Considering the increasing evidence on the associations between immunological features and prognosis in cancer, we further

TABLE 1 | Univariate Cox proportional hazards regression analyses of *HOXA* members and clinical features in LSCC.

Parameter	Univariate analysis		
	Hazard ratio	95% CI	*P*
Age	1.004	0.969–1.041	0.811
Smoking history	0.659	0.366–1.185	0.164
Alcohol consumption	0.668	0.377–1.1827	0.166
M stage	8.225	1.901–35.594	**0.005**
N stage	1.305	0.744–2.289	0.354
T stage	0.702	0.348–1.4145	0.322
Stage	0.894	0.379–2.108	0.797
Gender	3.367	1.708–6.639	**4.564E−04**
Grade	0.886	0.581–1.351	0.572
HOXA1 expression	1.384	1.042–1.837	**0.025**
HOXA2 expression	1.059	0.828–1.356	0.646
HOXA3 expression	1.238	0.932–1.647	0.140
HOXA4 expression	1.174	0.857–1.608	0.317
HOXA5 expression	1.143	0.885–1.477	0.304
HOXA6 expression	1.105	0.915–1.334	0.299
HOXA7 expression	1.149	0.93–1.419	0.198
HOXA9 expression	1.115	0.993–1.252	0.065
HOXA10 expression	1.379	1.081–1.759	**0.0097**
HOXA11 expression	1.179	1.000–1.391	**0.0498**
HOXA13 expression	1.129	0.999–1.277	**0.051**

Bold means P < 0.05.

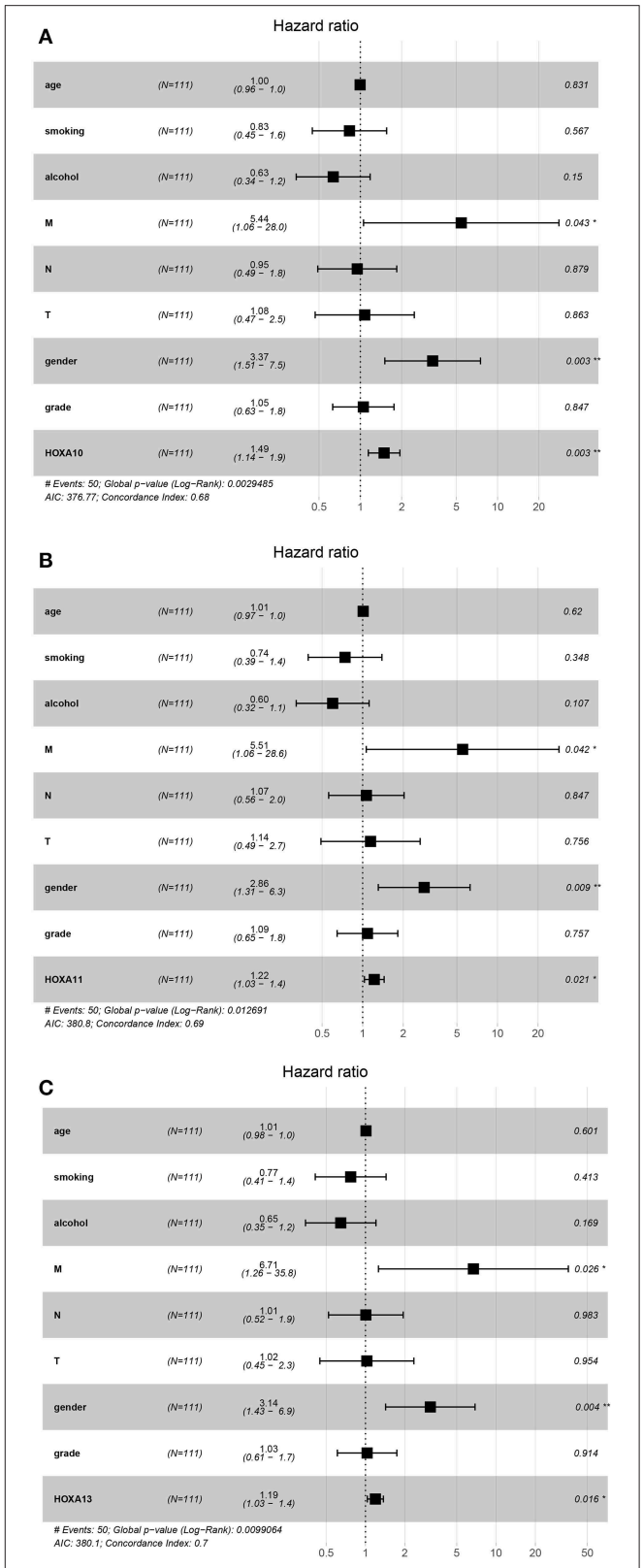

FIGURE 4 | Forest plots of the results of multivariate Cox regression analyses of significant prognostic factors: *HOXA10* **(A)**, *HOXA11* **(B)**, and *HOXA13* **(C)**. *stands for $P < 0.05$; **stands for $P < 0.01$.

explored the correlations between TIICs and *HOXA* members. The TIMER database is a public resource used to explore the associations between certain gene products and immune cells around tumor cells. The first column in **Figure 5** shows scatterplots of the expression of *HOXA* members against tumor purity. *HOXA* members with high expression in the microenvironment cells are expected to have a negative association with tumor purity, while *HOXA* members with high expression in tumor cells are expect to have a positive association with tumor purity (17). In accordance with our aforementioned findings, *HOXA7*, *HOXA10*, and *HOXA13* were highly expressed in LSCC tissues, with positive associations with tumor purity (**Figure 5**). However, there were no significant correlations between TIICs and *HOXA* members (**Figure S2**).

Potential Mechanism Underlying the Effects of Prognostic *HOXA* Members on LSCC Carcinogenesis

A GSEA of differentially expressed *HOXA* members with statistical prognostic value was conducted to evaluate the potential biological mechanism by which differential expression of *HOXA10*, *HOXA11*, and *HOXA13* affects the carcinogenesis of LSCC. The GSEA indicated that high expression of *HOXA10* was related to "WNT signaling pathway," "pathway in cancer," "basal cell carcinoma," "cell cycle," "mismatch repair," and "DNA replication" (**Figure 6A**), high expression of *HOXA11* was related to "DNA replication," "mismatch repair," and "nucleotide excision repair" (**Figure 6B**) and high expression of *HOXA13* was related to "colorectal cancer" and "WNT signaling pathway" (**Figure 6C**).

DISCUSSION

Homeobox genes were first identified in the fruit fly Drosophila (19). A total of 39 *HOX* genes are located on various chromosomes, which are clustered into four clusters, namely *HOXA*, *HOXB*, *HOXC* and *HOXD* (4). The genes in these four cluster each encode a 61-amino acid homeodomain, and these genes are key components of master regulatory pathways during normal embryonic development (3). A typical characteristic of the homeodomain is its DNA-binding nature; the proteins function as transcription factors by binding to the promoters of various target genes (20). Increasing evidence has shown that the protein products of *HOXA* genes not only act as transcriptional factors promoting carcinogenesis but also serve as tumor-suppressor factors, based on their aberrant expression patterns in certain organs. Increasing published or public genomic data and multiple online platforms provide us the opportunity for exploring the expression profiles of families of genes in human cancers and their clinical practice value. This study demonstrated the distinct expression profile and methylation profile, prognostic values and biological processes related to *HOXA* members in LSCC.

Previous research has shown that, according to expression data, *HOXA* genes contribute to the development of human cancers. Reverse transcriptase-polymerase chain reaction (RT-PCR) showed that *HOXA7* and *HOXA9* mRNAs were significantly overexpressed in esophageal squamous cell carcinoma tissues compared to non-cancerous surrounding tissues (21), while *HOXA9* was epigenetically downregulated in lung cancer (22). *HOXA13* expression increased in breast cancer (13), whereas it was downregulated in colorectal cancer (10). However, the expression of the entire *HOXA* family in LSCC was not previously comprehensively investigated. This *in silico* study demonstrated the expression profile of *HOXA* members in LSCC and showed that *HOXA2* and *HOXA4* were downregulated in LSCC tissues compared to normal control tissues. In contrast, *HOXA7*, *HOXA9*, *HOXA10*, *HOXA11,* and *HOXA13* were upregulated in LSCC tissues compared to normal control tissues. Unfortunately, no significant differences in the mRNA expression of *HOXA1*, *HOXA3*, *HOXA5,* and *HOXA6* were identified in LSCC tissues compared to normal control tissues.

According to the Pearson's correlation between *HOXA* mRNA expression and the methylation level of cg sites in the promoter regions in LSCC, among the seven differentially expressed *HOXA* members (*HOXA2*, *HOXA4*, *HOXA7*, *HOXA9*, *HOXA10*, *HOXA11,* and *HOXA13*), most expression levels, particularly regarding *HOXA4* and *HOXA9*, are affected by the methylation level. These results are in accordance with previous findings showing a negative correlation between *HOXA4* methylation and expression in patients with acute myeloid leukemia (23).

Several reports have identified *HOXA* gene signatures in GBM, and high expression of *HOXA9* and *HOXA10* were reported to be predictors of poor outcome in patients with GBM (14, 15). Moreover, it was reported that novel methylation markers in *HOXA9* also served as an independent indicator of prognosis in invasive bladder cancer (24). Additionally, multiple highly expressed *HOXA* members were reported to be significantly correlated with poor overall survival in patients with acute myeloid leukemia (25). In this study, univariate Cox proportional hazards regression analyses were performed to analyze the prognostic values of *HOXA* members in LSCC. In fact, four *HOXA* members were significantly associated with poor clinical outcomes in LSCC (*HOXA1*, *HOXA10*, *HOXA11,* and *HOXA13*). Thus, although no significant differential expression of *HOXA1* was found in LSCC, the univariate Cox proportional hazards regression showed that *HOXA1* expression was significantly associated with prognosis. The predictive potential of *HOXA* has also been reported in breast cancer (12). In breast cancer, *HOXA1* knockdown inhibited cell proliferation and increased apoptosis and cell cycle arrest by influencing the aberrant expression of several cell cycle and apoptosis-associated proteins, comprising cyclin D1, B-cell lymphoma 2 (Bcl-2) and Bcl-2-like protein 4 (12). Thus, although *HOXA1* was not differentially expressed in LSCC, the prognostic value of *HOXA1* has been highlighted in various human cancers, including in LSCC. Exploration of the *HOXA1*-related mechanisms is still required.

In hepatocellular carcinoma cells, *HOXA10* knockdown induced cell cycle arrest at the G0/G1 phase and apoptosis by reducing the expression of Cyclin D1 and Survivin (26). Decreased expression of *HOXA10* accelerated the acetylation

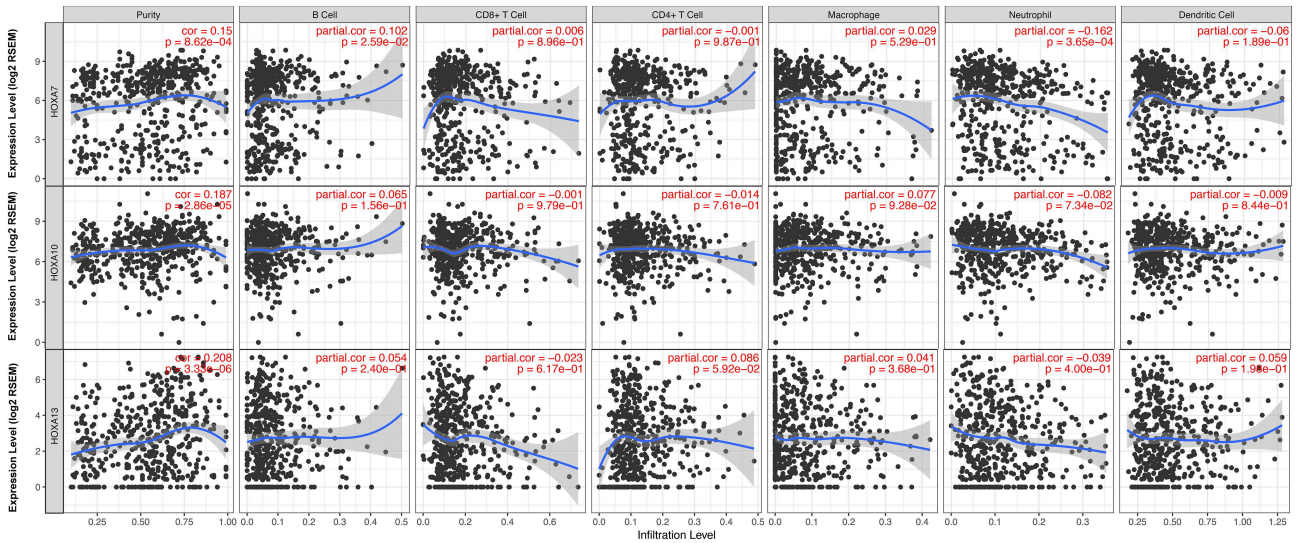

FIGURE 5 | Correlations between tumor infiltrating immune cells (TIICs; B cells, CD4+ T cells, CD8+ T cells, neutrophils, macrophages, and dendritic cells) and *HOXA* members (including *HOXA7*, *HOXA10*, and *HOXA13*) in LSCC. Tumor purity is shown in the panels on the left.

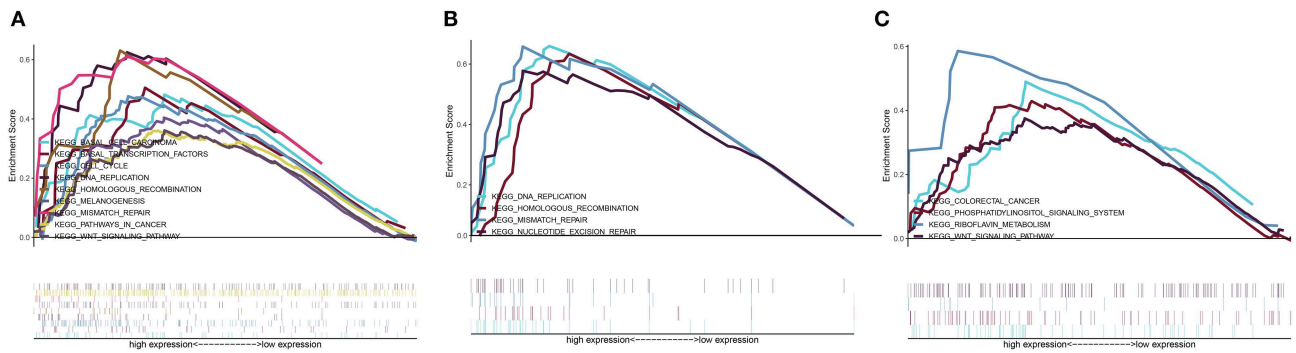

FIGURE 6 | Cancer-related Kyoto Encyclopedia of Genes and Genomes (KEGG) pathways associated with *HOXA10* **(A)**, *HOXA11* **(B)**, and *HOXA13* **(C)** based on a gene set enrichment analysis (GSEA).

of p53 (Lys382) and suppressed the transcription of histone deacetylase 1 (HDAC1; a potential deacetylase for p53) to activate p53 transcription (26). Additionally, *HOXA10* might promote cell proliferation by elevating Bcl-2 expression and inhibiting apoptosis in gastric cancer, and high expression of *HOXA10* predicted poor overall survival in gastric cancer patients (27). In this study, we found high expression of *HOXA10* in LSCC tissues. Both univariate and multivariate Cox proportional hazards regression analyses affirmed the prognostic value of *HOXA10* in the prediction of poor outcome in LSCC patients.

Overexpression of *HOXA11* has been observed in ovarian cancer (28), bladder cancer (29), renal cell carcinoma (29) and lung cancer (30), while downregulation of *HOXA11* has been observed in gastric cancer (31) and glioblastoma (32). In glioblastoma, overexpression of *HOXA11* confers a tumor suppressive effect, reduces treatment resistance and contributes to a favorable prognosis (32). However, overexpression of *HOXA11* showed a poor association with overall survival in lung cancer (33). *HOXA11* was significantly downregulated in cisplatin-resistant lung adenocarcinoma cell lines compared with parent cell lines, and *in vitro* experiments showed that overexpression of *HOXA11* increased cisplatin sensitivity by inhibiting Akt/β-catenin signaling (34). Our results showed high expression of *HOXA11* in LSCC, which was associated with unfavorable outcomes in LSCC patients. However, given that there is little relevant research on the topic, the biological and prognostic values of *HOXA11* warrant further intensive investigation. It may be useful to systematically explore the prognostic value of *HOXA11* using meta-analysis.

HOXA13 is expressed more in normal colons than in malignant colons. Additionally, *HOXA13* was differentially expressed based on location, with higher expression on the left side of the normal colon compared to the right side (10). Differential expression of *HOXA13* was also reported in breast

cancer (13), gastric cancer (35), prostate carcinoma (36) and thyroid cancer (37). *HOXA13* knockdown significantly restored the epithelial characteristics and reduced the mesenchymal characteristics of the cancer cells via the transforming growth factor (TGF)-β signaling pathway (35). Moreover, *HOXA13* expression negatively affects cisplatin sensitivity in human esophageal squamous cells and overall survival in patients with esophageal squamous cell carcinoma (38). Our results showed that multiple cancer-associated pathways were identified in LSCC tissues with high expression of *HOXA13*, and high expression of *HOXA13* in LSCC predicted poor overall survival.

CONCLUSION

This *in silico* study demonstrated the expression profile of *HOXA* family members in LSCC and the biological and prognostic values of the *HOXA* family in LSCC, providing insights for further investigation of *HOXA* members as potential targets in LSCC.

DATA AVAILABILITY STATEMENT

The data that support the findings of this study are openly available in The Cancer Genome Atlas (TCGA) program at https://portal.gdc.cancer.gov/.

AUTHOR CONTRIBUTIONS

JL and CZ designed the research study and analyzed the data from public database. JL, MY, and CZ were involved in data analysis. CZ was responsible for writing of manuscript. JL and MY contributed to the revised manuscript. All authors reviewed the manuscript.

FUNDING

This work was supported by the Ningbo Health Branding Subject Fund (No. PPXK2018-02).

SUPPLEMENTARY MATERIAL

The Supplementary Material for this article can be found online at: https://www.frontiersin.org/articles/10.3389/fonc.2020.00368/full#supplementary-material

Figure S1 | Pearson's correlation between methylation levels and expression of all differentially expressed HOXA members in LSCC [including *HOXA2* **(A)**, *HOXA4* **(B)**, *HOXA7* **(C)**, *HOXA9* **(D)**, *HOXA10* **(E)**, *HOXA11* **(F)**, and *HOXA13* **(G)**].

Figure S2 | Correlations between tumor infiltrating immune cells (TIICs; B cells, CD4+ T cells, CD8+ T cells, neutrophils, macrophages, and dendritic cells) and all *HOXA* members in LSCC.

REFERENCES

1. Siegel RL, Miller KD, Jemal A. Cancer statistics, 2019. *CA Cancer J Clin.* (2019) 69:7–34. doi: 10.3322/caac.21551
2. Thompson LD. Laryngeal dysplasia, squamous cell carcinoma, and variants. *Surg Pathol Clin.* (2017) 10:15–33. doi: 10.1016/j.path.2016.10.003
3. Gehring WJ, Hiromi Y. Homeotic genes and the homeobox. *Annu Rev Genet.* (1986) 20:147–73. doi: 10.1146/annurev.ge.20.120186.001051
4. Ruddle FH, Bartels JL, Bentley KL, Kappen C, Murtha MT, Pendleton JW. Evolution of hox genes. *Annu Rev Genet.* (1994) 28:423–42. doi: 10.1146/annurev.ge.28.120194.002231
5. Sanchez-Herrero E. Hox targets and cellular functions. *Scientifica.* (2013) 2013:738257. doi: 10.1155/2013/738257
6. Maeda K, Hamada J, Takahashi Y, Tada M, Yamamoto Y, Sugihara T, et al. Altered expressions of HOX genes in human cutaneous malignant melanoma. *Int J Cancer.* (2005) 114:436–41. doi: 10.1002/ijc.20706
7. Makiyama K, Hamada J, Takada M, Murakawa K, Takahashi Y, Tada M, et al. Aberrant expression of HOX genes in human invasive breast carcinoma. *Oncol Rep.* (2005) 13:673–9. doi: 10.3892/or.13.4.673
8. Abe M, Hamada J, Takahashi O, Takahashi Y, Tada M, Miyamoto M, et al. Disordered expression of HOX genes in human non-small cell lung cancer. *Oncol Rep.* (2006) 15:797–802. doi: 10.3892/or.15.4.797
9. Hassan NM, Hamada J, Murai T, Seino A, Takahashi Y, Tada M, et al. Aberrant expression of HOX genes in oral dysplasia and squamous cell carcinoma tissues. *Oncol Res.* (2006) 16:217–24. doi: 10.3727/000000006783981080
10. Kanai M, Hamada J, Takada M, Asano T, Murakawa K, Takahashi Y, et al. Aberrant expressions of HOX genes in colorectal and hepatocellular carcinomas. *Oncol Rep.* (2010) 23:843–51. doi: 10.3892/or_00000706
11. Zhang X, Zhu T, Chen Y, Mertani HC, Lee KO, Lobie PE. Human growth hormone-regulated HOXA1 is a human mammary epithelial oncogene. *J Biol Chem.* (2003) 278:7580–90. doi: 10.1074/jbc.M212050200
12. Liu J, Liu J, Lu X. HOXA1 upregulation is associated with poor prognosis and tumor progression in breast cancer. *Exp Ther Med.* (2019) 17:1896–902. doi: 10.3892/etm.2018.7145
13. Hur H, Lee JY, Yun HJ, Park BW, Kim MH. Analysis of HOX gene expression patterns in human breast cancer. *Mol Biotechnol.* (2014) 56:64–71. doi: 10.1007/s12033-013-9682-4
14. Murat A, Migliavacca E, Gorlia T, Lambiv WL, Shay T, Hamou MF, et al. Stem cell-related "self-renewal" signature and high epidermal growth factor receptor expression associated with resistance to concomitant chemoradiotherapy in glioblastoma. *J Clin Oncol.* (2008) 26:3015–24. doi: 10.1200/JCO.2007.15.7164
15. Costa BM, Smith JS, Chen Y, Chen J, Phillips HS, Aldape KD, et al. Reversing HOXA9 oncogene activation by PI3K inhibition: epigenetic mechanism and prognostic significance in human glioblastoma. *Cancer Res.* (2010) 70:453–62. doi: 10.1158/0008-5472.CAN-09-2189
16. Gaspar N, Marshall L, Perryman L, Bax DA, Little SE, Viana-Pereira M, et al. MGMT-independent temozolomide resistance in pediatric glioblastoma cells associated with a PI3-kinase-mediated HOX/stem cell gene signature. *Cancer Res.* (2010) 70:9243–52. doi: 10.1158/0008-5472.CAN-10-1250
17. Li T, Fan J, Wang B, Traugh N, Chen Q, Liu JS, et al. TIMER: a web server for comprehensive analysis of tumor-infiltrating immune cells. *Cancer Res.* (2017) 77:e108–10. doi: 10.1158/0008-5472.CAN-17-0307
18. Subramanian A, Tamayo P, Mootha VK, Mukherjee S, Ebert BL, Gillette MA, et al. Gene set enrichment analysis: a knowledge-based approach for interpreting genome-wide expression profiles. *Proc Natl Acad Sci USA.* (2005) 102:15545–50. doi: 10.1073/pnas.0506580102
19. Lewis EB. A gene complex controlling segmentation in *Drosophila*. *Nature.* (1978) 276:565–70. doi: 10.1038/276565a0
20. Errico MC, Felicetti F, Bottero L, Mattia G, Boe A, Felli N, et al. The abrogation of the HOXB7/PBX2 complex induces apoptosis in melanoma through the miR-221&222-c-FOS pathway. *Int J Cancer.* (2013) 133:879–92. doi: 10.1002/ijc.28097
21. Chen KN, Gu ZD, Ke Y, Li JY, Shi XT, Xu GW. Expression of 11 HOX genes is deregulated in esophageal squamous cell carcinoma. *Clin Cancer Res.* (2005) 11:1044–9. Available online at: https://clincancerres.aacrjournals.org/content/clincanres/11/3/1044.full.pdf
22. Rauch T, Wang Z, Zhang X, Zhong X, Wu X, Lau SK, et al. Homeobox gene methylation in lung cancer studied by genome-wide analysis with a

microarray-based methylated CpG island recovery assay. *Proc Natl Acad Sci USA*. (2007) 104:5527–32. doi: 10.1073/pnas.0701059104
23. Musialik E, Bujko M, Kober P, Grygorowicz MA, Libura M, Przestrzelska M, et al. Promoter DNA methylation and expression levels of HOXA4, HOXA5 and MEIS1 in acute myeloid leukemia. *Mol Med Rep*. (2015) 11:3948–54. doi: 10.3892/mmr.2015.3196
24. Kim YJ, Yoon HY, Kim JS, Kang HW, Min BD, Kim SK, et al. HOXA9, ISL1 and ALDH1A3 methylation patterns as prognostic markers for nonmuscle invasive bladder cancer: array-based DNA methylation and expression profiling. *Int J Cancer*. (2013) 133:1135–42. doi: 10.1002/ijc.28121
25. Chen SL, Qin ZY, Hu F, Wang Y, Dai YJ, Liang Y. The role of the HOXA gene family in acute myeloid leukemia. *Genes*. (2019) 10:621. doi: 10.3390/genes10080621
26. Zhang Y, Chen J, Wu SS, Lv MJ, Yu YS, Tang ZH, et al. HOXA10 knockdown inhibits proliferation, induces cell cycle arrest and apoptosis in hepatocellular carcinoma cells through HDAC1. *Cancer Manag Res.* (2019) 11:7065–76. doi: 10.2147/CMAR.S199239
27. Song C, Han Y, Luo H, Qin Z, Chen Z, Liu Y, et al. HOXA10 induces BCL2 expression, inhibits apoptosis, and promotes cell proliferation in gastric cancer. *Cancer Med.* (2019) 8:5651–61. doi: 10.1002/cam4.2440
28. Cheng W, Liu J, Yoshida H, Rosen D, Naora H. Lineage infidelity of epithelial ovarian cancers is controlled by HOX genes that specify regional identity in the reproductive tract. *Nat Med.* (2005) 11:531–7. doi: 10.1038/nm1230
29. Cantile M, Cindolo L, Napodano G, Altieri V, Cillo C. Hyperexpression of locus C genes in the HOX network is strongly associated *in vivo* with human bladder transitional cell carcinomas. *Oncogene*. (2003) 22:6462–8. doi: 10.1038/sj.onc.1206808
30. Zhang R, Zhang TT, Zhai GQ, Guo XY, Qin Y, Gan TQ, et al. Evaluation of the HOXA11 level in patients with lung squamous cancer and insights into potential molecular pathways via bioinformatics analysis. *World J Surg Oncol.* (2018) 16:109. doi: 10.1186/s12957-018-1375-9
31. Cui Y, Gao D, Linghu E, Zhan Q, Chen R, Brock MV, et al. Epigenetic changes and functional study of HOXA11 in human gastric cancer. *Epigenomics*. (2015) 7:201–13. doi: 10.2217/epi.14.92
32. Se YB, Kim SH, Kim JY, Kim JE, Dho YS, Kim JW, et al. Underexpression of HOXA11 is associated with treatment resistance and poor prognosis in glioblastoma. *Cancer Res Treat.* (2017) 49:387–98. doi: 10.4143/crt.2016.106
33. Yang X, Deng Y, He RQ, Li XJ, Ma J, Chen G, et al. Upregulation of HOXA11 during the progression of lung adenocarcinoma detected via multiple approaches. *Int J Mol Med.* (2018) 42:2650–64. doi: 10.3892/ijmm.2018.3826
34. Zhang Y, Yuan Y, Li Y, Zhang P, Chen P, Sun S. An inverse interaction between HOXA11 and HOXA11-AS is associated with cisplatin resistance in lung adenocarcinoma. *Epigenetics*. (2019) 14:949–60. doi: 10.1080/15592294.2019.1625673
35. He YX, Song XH, Zhao ZY, Zhao H. HOXA13 upregulation in gastric cancer is associated with enhanced cancer cell invasion and epithelial-to-mesenchymal transition. *Eur Rev Med Pharmacol Sci.* (2017) 21:258–65. Available online at: https://www.europeanreview.org/article/12092
36. Javed S, Langley SE. Importance of HOX genes in normal prostate gland formation, prostate cancer development and its early detection. *BJU Int.* (2014) 113:535–40. doi: 10.1111/bju.12269
37. Cantile M, Scognamiglio G, La Sala L, La Mantia E, Scaramuzza V, Valentino E, et al. Aberrant expression of posterior HOX genes in well differentiated histotypes of thyroid cancers. *Int J Mol Sci.* (2013) 14:21727–40. doi: 10.3390/ijms141121727
38. Shi Q, Shen L, Dong B, Fu H, Kang X, Dai L, et al. Downregulation of HOXA13 sensitizes human esophageal squamous cell carcinoma to chemotherapy. *Thorac Cancer*. (2018) 9:836–46. doi: 10.1111/1759-7714.12758

Conflict of Interest: The authors declare that the research was conducted in the absence of any commercial or financial relationships that could be construed as a potential conflict of interest.

frontiers in Oncology

ORIGINAL RESEARCH
published: 07 April 2020
doi: 10.3389/fonc.2020.00471

Lingual Lymph Node Metastasis in cT1-2N0 Tongue Squamous Cell Carcinoma: Is It an Indicator for Elective Neck Dissection

Wenli Yang, Minglei Sun, Qiaoyan Jie, Haixia Zhou, Peng Zhang* and Juanfang Zhu**

Department of Stomatology, The First Affiliated Hospital of Zhengzhou University, Zhengzhou, China

Objective: Accurate predictors for occult metastasis in cT1-2N0 tongue squamous cell carcinoma (SCC) remains scarce, the main goal in current study was to evaluate whether there is significant association between lingual lymph node (LLN) metastasis and occult lymph node metastasis as well as whether there is prognostic value of LLN metastasis in early stage tongue SCC.

Methods: Patients with surgically treated primary cT1-2N0 tongue SCC were prospectively enrolled from January 2010 to December 2018. LLNs were dissected independently for pathologic analysis. The main study endpoints were locoregional control survival (LRC) and disease-specific survival (DSS). The Chi-square test and multivariate regression analysis were used to assess the predictors for occult metastasis. The Kaplan-Meier approach and Cox model were used to analyze the potential prognostic factors.

Results: A total of 317 patients were enrolled for analysis. Eighty-eight patients had occult metastasis with a prevalence of 27.8%. LLNs presented in 89 patients, in which 43 patients had LLN metastasis. In the 43 patients with positive LLNs, 20 patients had occult metastasis, in 274 patients with negative LLNs or no LLNs, 68 patients had occult metastasis, the difference was significant ($p = 0.012$). Further multivariate regression analysis confirmed the independence of LLN metastasis in predicting the occult metastasis. In patients without LLNs, the 5-year LRC rate was 79%, in patients with negative LLNs, the 5-year LRC rate was 78%, in patients with positive LLNs, the 5-year LRC rate was 62%, the difference was significant ($p = 0.024$). In patients without LLNs, the 5-year DSS rate was 84%, in patients with negative LLNs, the 5-year DSS rate was 74%, in patients with positive LLNs, the 5-year DSS rate was 51%, the difference was significant ($p < 0.001$), further Cox model confirmed the independence of LLN metastasis in affecting the LRC and DSS.

Conclusions: LLN metastasis is significantly associated with occult neck lymph node metastasis, and decrease the LRC and DSS in early stage tongue SCC.

Keywords: lingual lymph node, occult metastasis, early stage tongue squamous cell carcinoma, squamous cell carcinoma, elective neck dissection

OPEN ACCESS

Edited by:
Victor C. Kok,
Asia University, Taiwan

Reviewed by:
Han-Sin Jeong,
Sungkyunkwan University,
South Korea
Zhenning Li,
University at Buffalo, United States

****Correspondence:***
Wenli Yang
yangwenli7412540@163.com
Peng Zhang
sunqiangsqs456@163.com
Juanfang Zhu
zzyouzi@163.com

Specialty section:
This article was submitted to Head and Neck Cancer, a section of the journal Frontiers in Oncology

Received: *27 July 2019*
Accepted: *16 March 2020*
Published: *07 April 2020*

Citation:
Yang W, Sun M, Jie Q, Zhou H, Zhang P and Zhu J (2020) Lingual Lymph Node Metastasis in cT1-2N0 Tongue Squamous Cell Carcinoma: Is It an Indicator for Elective Neck Dissection. Front. Oncol. 10:471. doi: 10.3389/fonc.2020.00471

INTRODUCTION

Tongue squamous cell carcinoma (SCC) is the most common oral cavity malignancy (1, 2), its prognosis has not improved significantly despite advances in diagnosis and treatment, neck lymph node metastasis is one of the most important prognostic factors (3, 4), but unfortunately these positive lymph nodes are usually occult or subclinical at the initial treatment in early stage tongue SCC. Owing to a wide range of occult metastasis rate (5, 6), either elective neck dissection (END) or the watchful waiting policy has been the favored treatment for cT1-2N0 tongue SCC (7, 8). Investigators favoring for END comment that END allows more accurate disease stage and decision of the need for adjuvant therapies, and resection of metastatic lymph nodes could potentially reduce the recurrence risk (9, 10), however, the main concern according to the traditional watchful waiting policy is the associated surgical complication including shoulder dysfunction and over-treatment for those patients having no pathologic metastases (11). Considering there is no accurate diagnostic procedure for staging the neck preoperatively, the elective management of the neck in cT1-2N0 tongue SCC has been the subject of much debate during the past three decades and continues to be controversial.

Lingual lymph nodes (LLNs) were firstly introduced by Rouviere et al. (12). These authors have divided LLNs into two groups: the lateral lingual nodes are lateral to the genioglossus or the hyoglossus muscles, and the median lingual node resides between the medial side of the genioglossus muscle and the lingual septum (12, 13). A number of researchers have reported the phenomenon of LLN metastasis in primary or recurrent oral SCC by cases reports (14–22), but whether there is significant association between LLN metastasis and occult lymph node metastasis as well as whether there is prognostic value of LLN metastasis in early stage tongue SCC remain unknown. Therefore, the current study aimed to clarify these questions.

METHODS

The Zhengzhou University institutional research committee approved our study, and all participants provided written informed consent for medical research prior to enrollment in the study. All experiments were performed in accordance with relevant guidelines and regulations.

From January 2010 to December 2018, patients with primary cT1-2N0 tongue SCC according to the 7th AJCC classification were prospectively investigated. The only inclusion criteria was that patients underwent surgical treatment for primary cancer disease; patients who lost their visits were excluded for analysis. Information including age, sex, adverse pathologic characteristics, and follow-up of enrolled patients was collected and analyzed. All patients had underwent a neck dissection. Drinkers were defined as those who consumed at least one alcoholic drink per day for at least 1 year (2, 3), smokers were defined as those smoked on a daily basis or had quit smoking for less than 5 years (2, 3). cT1-2 was defined as a maximum diameter of tumors <2 cm or a diameter ranging from 2 to 4 cm, patients were considered to have cN0 disease if they had no evidence of nodal metastasis on clinical examination, ultrasound, or radiographic imaging (23, 24).

All pathologic sections were reviewed by at least two pathologists, and perineural invasion was considered to be present if tumor cells were identified within the perineural space and/or nerve bundle; lymphovascular infiltration was positive if tumor cells were noted within the lymphovascular channels (23). The pathologic depth of invasion (DOI) was measured from the level of the adjacent normal mucosa to the deepest point of tumor infiltration, regardless of the presence or absence of ulceration (24).

All patients underwent radical primary tumor excision with a minimum margin of 1 cm, the muscle of the mouth floor was preserved in highest measure, the adipose tissue in the mouth floor including the sublingual gland was separated from the primary tumor, and then dissected for any possible lymph nodes (**Figure 1**) for postoperative pathology analysis independently, END (levelI-III) was routinely performed for tongue SCC patients with the exception of very early-stage disease in our cancer center. Indication for adjuvant treatment included perineural invasion, lymphovascular invasion, positive margin, and cervical lymph node metastasis. All patients were regularly followed every 3 months within the first 2 years after

FIGURE 1 | Lingual lymph node (white row).

the operation and every 6 months within the third to fifth year after the operation. If there was any doubt regarding disease recurrence, active interference was performed. (25).

The association between neck occult metastasis and clinical pathologic variables was firstly evaluated by the Chi-square test, and then by multivariate regression analysis for detecting the independent predictor. The main study endpoints were locoregional control (LRC) and disease specific survival (DSS), and the survival time was calculated from date of surgery to the date of an event or latest follow-up. The Kaplan-Meier approach (log-rank test) was used to calculate the LRC and DSS rates. The factors which were significant in univariate analysis were then analyzed in the multivariate proportional hazard Cox model for determining the independent prognostic factors. All statistical analyses were performed on SPSS 20.0, and a $p < 0.05$ was considered significant.

RESULTS

There were 317 patients (227 male and 90 female) enrolled in total, the mean age was 58.3 (range: 28–78) years. Smoker and drinker were noted in 189 (59.6%) and 130 (41.0%) patients, respectively. Clinical tumor stages were distributed as T1 in 143 (45.1%) patients and T2 in 174 (54.9%) patients, respectively. Perineural invasion and lymphovascular invasion were noted in 46 (14.5%) and 33 (10.4%) patients, respectively. Pathologic tumor grade was distributed as well in 122 (38.4%) patients, moderate in 143 (45.1%) patients, and poor in 52 (16.4%) patients. The mean pathologic DOI was 6.9 (range: 3.0–15.8) mm. Negative margin was achieved in all patients (100%). There were 65 (20.5%) patients underwent flap reconstruction for tongue restoration including 25 platysma myocutaneous flaps, 17 submental island flaps, 15 radial forearm flaps, and eight anterolateral thigh flaps.

LLNs were reported in 89 (28.1%) patients, the mean number of LLNs was 1.4 (range: 1–3), 43 of the 89 patients had pathologic LLN metastasis, the mean number of positive LLNs was 1.3 (range: 1–3), the overall LLN metastasis rate was 13.6% (43/317). As described by **Table 1**, the LLN metastasis was significantly associated with cervical lymph node metastasis and tumor stage.

Occult neck lymph node metastasis occurred in 88 (27.8%) patients. There was no extracapsular spread. Seventy-eight patients had isolate level I metastasis, nine patients had simultaneous level I and II metastasis, and 1 patient had simultaneous level I, II, and III metastasis. In 43 patients with positive LLNs, 20 patients had occult metastasis, in 46 patients with negative LLNs, 12 patients had occult metastasis, in 228 patients with no LLNs, 56 patients had occult metastasis, the difference was significant ($p = 0.012$). The sensitivity of positive LLN to predict positive occult neck node metastasis was 22.7% (95% CI, 14.5–32.9%), and the positive test likelihood ratio was 2.3 (95% CI, 1.3–3.9). The Chi-square test also reported the significant association between occult metastasis and tumor stage, pathologic DOI, and pathologic tumor grade (all $p < 0.05$). Further multivariate regression described the factors of tumor stage ($p = 0.005$, 2.445[1.247–6.332]), pathologic DOI ($p = 0.033$, 2.118[1.684–5.226]), LLN status ($p = 0.041$, 1.984[1.247–3.222]), and pathologic tumor grade ($p = 0.008$, 3.221[1.647–7.669]) independently increased the risk of occult neck lymph node metastasis (**Table 2**).

TABLE 1 | Association between clinical pathologic variables and lingual lymph node metastasis.

Variables	Lingual lymph node status		*p*
	Positive ($n = 43$)	Negative or none ($n = 274$)	
Age			
<40	7	23	
≥40	36	251	0.101
Sex			
Male	33	194	
Female	10	80	0.422
Smoking			
Yes	23	166	
No	20	108	0.378
Drinking			
Yes	15	115	
No	28	159	0.380
Tumor stage			
T1	12	131	
T2	31	143	0.015
DOI*			
<5 mm	15	132	
≥5 mm	28	142	0.104
PI#			
Yes	8	38	
No	35	236	0.412
LVI%			
Yes	5	28	
No	38	246	0.779
Occult metastasis			
Negative	23	206	
Positive	20	68	0.003
Tumor grade			
Well	13	109	
Moderate	20	123	
Poor	10	42	0.313

, depth of invasion; #, perineural invasion; %, lymphovascular invasion.

Table 3 analyzed the cervical metastasis pattern according to the status of the LLNs, and it described that there might be a trending of more extensive metastasis if there was LLN metastasis.

After follow-up with mean time of 37.5 (range: 2–93) months, 100 patients received adjuvant radiotherapy, and 10 patients also received adjuvant chemotherapy, locoregional recurrence occurred in 58 patients, disease-specific death occurred in 43 patients.

The 5-year LRC rate was 77%. In patients without LLNs, the 5-year LRC rate was 79%, in patients with negative LLNs,

TABLE 2 | Association between clinical pathologic variables and occult neck lymph node metastasis.

Variables	Occult metastasis		X^2	Multivariate regression	
	+ (*n* = 88)	− (*n* = 229)	p	p	RR[95% CI]
Age					
<40	7	23			
≥40	81	206	0.569		
Sex					
Male	63	164			
Female	25	65	0.996		
Smoking					
Yes	53	136			
No	35	93	0.107		
Drinking					
Yes	35	95			
No	53	134	0.781		
Tumor stage					
T1	25	118			
T2	63	111	<0.001	0.005	2.445[1.247–6.332]
DOI*					
<5 mm	32	115			
≥5 mm	56	114	0.027	0.033	2.118[1.684–5.226]
PI#					
Yes	15	31			
No	73	198	0.427		
LVI%					
Yes	13	20			
No	75	209	0.115		
LLN&					
No	56	172			
Negative	12	34			
Positive	20	23	0.012	0.041	1.984[1.247–3.222]
Tumor grade					
Well	26	96			
Moderate	40	103			
Poor	22	30	0.018	0.008	3.221[1.647–7.669]

**, depth of invasion; #, perineural invasion; %, lymphovascular invasion; &, lingual lymph node.*

TABLE 3 | Cervical metastasis pattern according to the status of lingual lymph node (LLN) status.

Level metastasis	LLN status		
	Positive	Negative	None
I	20	12	56
II	2	2	6
III	1	0	0

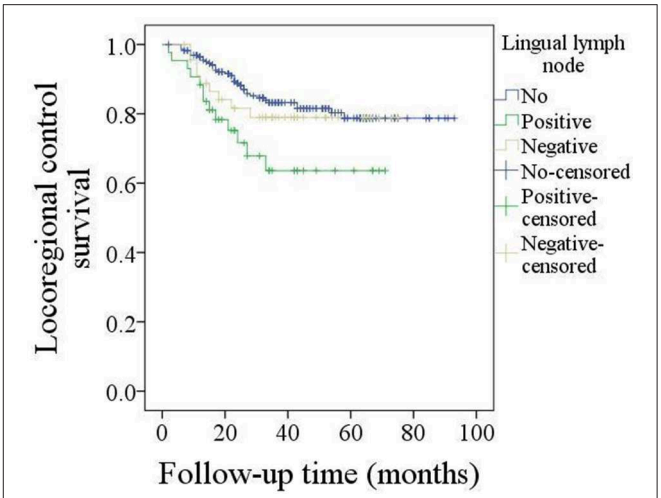

FIGURE 2 | Comparison of locoregional control survival in patients with different lingual lymph node status ($p = 0.024$).

TABLE 4 | Prognostic factors for the locoregional control in patients with cT1-2N0 tongue squamous cell carcinoma.

Variables	Univariate analysis	Cox model	
	p	*P*	HR[95%CI]
Age (<40 vs. ≥40)	0.547		
Sex	0.336		
Smoking	0.147		
Drinking	0.225		
Tumor stage (T1 vs. T2)	0.005	0.174	3.664[0.786–12.004]
Neck node stage (N0 vs. N+)	0.001	<0.001	4.222[1.782–9.664]
DOI* (<5 vs. ≥5 mm)	0.026	0.013	2.643[1.844–6.449]
Perineural invasion	0.014	0.008	2.847[1.471–7.552]
Lymphovascular invasion	0.008	0.085	3.412[0.925–9.227]
Pathologic tumor grade	0.111		
Well			
Moderate			
Poor			
LLN status	0.024		
No			
Negative		0.845	1.235[0.158–2.111]
Positive		0.015	1.999[1.325–4.668]
Adjuvant treatment	0.521		

the 5-year LRC rate was 78%, in patients with positive LLNs, the 5-year LRC rate was 62%, the difference was significant ($p = 0.024$, **Figure 2**). As described by **Table 4**, the factors of tumor stage, LLN status, neck lymph node metastasis, perineural invasion, lymphovascular invasion, and pathologic DOI were associated with the locoregional control, further Cox model confirmed the independence of LLN status, neck lymph node metastasis, perineural invasion, and pathologic DOI in predicting the LRC survival.

The 5-year DSS rate was 78%. In patients without LLNs, the 5-year DSS rate was 84%, in patients with negative LLNs, the 5-year DSS rate was 74%, in patients with positive LLNs, the 5-year DSS rate was 51%, the difference was significant ($p < 0.001$, **Figure 3**). As described by **Table 5**, the factors

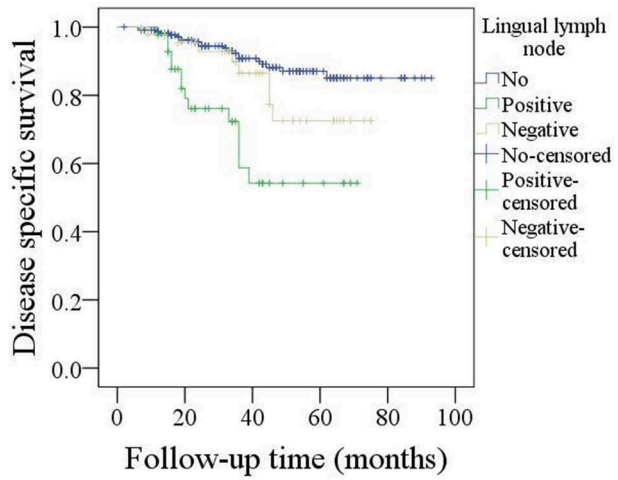

FIGURE 3 | Comparison of disease specific survival in patients with different lingual lymph node status ($p < 0.001$).

TABLE 5 | Prognostic factors for the disease specific survival in patients with cT1-2N0 tongue squamous cell carcinoma.

Variables	Univariate analysis	Cox model	
	p	P	HR[95%CI]
Age (<40 vs. ≥40)	0.254		
Sex	0.631		
Smoking	0.215		
Drinking	0.334		
Tumor stage (T1 vs. T2)	0.088		
Neck node stage (N0 vs. N+)	0.002	<0.001	2.222[1.258–5.331]
DOI* (<5 vs. ≥5 mm)	0.015	0.003	3.524[1.631–8.552]
Perineural invasion	0.263		
Lymphovascular invasion	0.014	0.005	2.338[1.726–5.434]
Pathologic tumor grade	0.021		
Well			
Moderate		0.015	2.114[1.235–4.002]
Poor		<0.001	4.669[1.978–9.224]
LLN status	<0.001		
No			
Negative		0.098	1.735[0.896–3.425]
Positive		<0.001	1.845[1.137–3.987]
Adjuvant treatment	0.521		

of LLN status, lymphovascular invasion, neck lymph node metastasis, pathologic tumor grade, and pathologic DOI were associated with the DSS, further Cox model confirmed the independence of LLN status, neck lymph node metastasis, pathologic tumor grade, and pathologic DOI in predicting the DSS.

DISCUSSION

The most important finding in current study was that the LLN metastasis was significantly associated with the risk of occult metastasis as well as the prognosis in early stage tongue SCC. It could provide benefit in decision making regarding neck management in cT1-2N0 tongue SCC, and also it suggested more advanced treatment would be required in despite of the neck lymph node status.

The presence of neck lymph node metastasis was an important prognostic factor for head and neck SCC (1–3). END was usually an important part in primary operation, but owing to the wide range of occult metastasis rate in cT1-2N0 tongue SCC (10), the neck management of cT1-2N0 tongue SCC has been debated over the years remaining its controversy. Although there was high quality literature including D'Cruz et al. (26) and Ren et al. (27) showed the benefit associated with routine neck dissection, the ideal treatment for patients with cT1-2N0 tongue SCC must be balanced between and the possible surgical morbidity and optimal oncological outcomes. The common principle was that N0 necks should be treated electively when the occult metastatic rate was more than 20% (28). In current study, the overall occult metastasis rate was 27.8%, but the occult metastasis rate was just 17.5% for T1 disease, all patients underwent END. Therefore, there was a number of patients were over-treated, there were at least three aspects for explaining this phenomenon: firstly, the high requirement of routine follow-up of wait-and-see policy was usually out of our patients' ability, as described by our previous studies (13, 25), patients in our cancer hospital usually came from low income family and remote districts; secondly, there was abundant evidence indicating that there was often a low salvage rate on disease recurrence in patients who do not have prophylactic therapy of the clinically N0 neck (1–5), thirdly, also the most important one, there were no reliable predictors for occult neck lymph node metastasis from previous studies.

A number of researchers had aimed to explore the potential predictors for the occult neck lymph node metastasis. Tumor budding was defined as the presence of small clusters of cancer cells or isolated single cancer cell, it suggested a more aggressive biologic behavior and carried more possibility of migrating to the adjacent stroma. Xie et al. (29) described the tumor budding intensity was significantly associated with occult lymph node metastasis. Systemic inflammatory response could promote tumor cell proliferation, microvascular regeneration, and tumor metastasis, further, the peripheral neutrophil-to-lymphocyte ratio (NLR) was an accurate and reliable inflammatory marker. High NLR is thought to be significantly associated with worse survival in solid cancers (28). Abbate et al. (30) firstly presented there was higher risk for occult neck lymph node metastasis when pre-treatment NLR was greater than 2.93. Loganathan et al. (31) recently reported END should be considered when the tumor thickness exceeds 5 mm based on the significant relationship between tumor thickness and occult neck lymph node metastasis. Other analyzed variables included perineural invasion, lymphovascular invasion, and pathologic DOI (32, 33). However, data regarding the these pathologic factors usually could not be obtained preoperatively or during operation, and pretreatment NLR were nonspecific parameters because they could be influenced by concomitant conditions, such as infections or inflammation. Therefore, more accurate indicators

were needed. In current study it was noted that LLN metastasis was related to additional nearly 2-fold risk of occult metastasis, and might promote more extensive metastasis. The status of LLNs was easily obtained by frozen section, it might act as a useful indicator for END in early stage tongue SCC. LLNs were not included in any N groups in TNM stage system, the lymph pathway draining to the LLNs passes through the medial side of the submandibular gland parahyoid area and connects to the middle internal jugular lymph nodes (13, 19). Saito et al. (19) firstly described the feasibility of LLN acting as the sentinel lymph node in tongue SCC by imaging methods, current study would support this comment. However, we must considered the fact that the sensitivity and positive test likelihood ratio of positive LLN to predict occult metastasis was a little poor, it was insufficient for deciding neck management, we should not rely solely on the LLN positivity to justify the neck lymph node dissection, more other parameters were needed to increase its reliability.

Prognostic factors for tongue SCC were extensively analyzed, common predictors for worse prognosis included high tumor stage, poor pathologic tumor grade, perineural invasion, lymphovascular invasion, high pathologic DOI, neck lymph node metastasis, high NLR, and so on (2, 3, 13, 14). But the significance of LLN metastasis was rarely assessed. Jia et al. (14) recently reported all the patients with LLN metastases had an advanced neck lymph node classification in their 111 patients, the incidence and metastasis of the LLNs were associated with pathological classifications of SCC of the tongue and the floor of the mouth. Similar finding was also noted in a prospective study by Fang et al. (13), the authors also described LLN metastasis was uncommon, but it could decreased the LRC in advanced tongue SCC. But whether there was similar phenomenon in early stage tongue SCC remained unclear. We were the first to present LLN metastasis significantly decreased the LRC and DSS. In a letter to the editors, Calabrese et al. (34) stated that LLN metastasis could worsen the prognosis and may act as the same way as level I lymph node metastasis. Our findings may support this hypothesis; however, we do not have such data, more studies were needed to clarify this question.

There are some limitations in current study: firstly, the statistical power was reduced by our relatively small sample size. Secondly, there might be more interesting findings found in the future if the follow-up time was longer. Thirdly, lingual lymph nodes were partially dissected by surgeons, and because of our subjective knowledge, there might be bias for detecting the LLNs (35).

CONCLUSIONS

In summary, LLN metastasis is relatively uncommon in early stage tongue SCC, but it is significant associated with the occurrence of occult neck lymph node metastasis, and it apparently decrease the LRC and DSS.

DATA AVAILABILITY STATEMENT

All data generated or analyzed during this study are included in this published article and the primary data could be achieved from the corresponding author.

ETHICS STATEMENT

The studies involving human participants were reviewed and approved by Zhengzhou University. The patients/participants provided their written informed consent to participate in this study.

AUTHOR CONTRIBUTIONS

WY, QJ, and PZ: study design and manuscript writing. QJ and PZ: studies selecting and data analysis. WY, MS, HZ, QJ, and JZ: study quality evaluating. WY, JZ, MS, HZ, QJ, and PZ: manuscript revising. All authors have read and approved the final manuscript.

FUNDING

This study was funded by Key scientific research projects of colleges and universities in Henan Province (No. 20B320031).

REFERENCES

1. Farhood Z, Simpson M, Ward GM, Walker RJ, Osazuwa-Peters N. Does anatomic subsite influence oral cavity cancer mortality? A SEER database analysis. *Laryngoscope.* (2019) 129:1400–6. doi: 10.1002/lary.27490
2. Fang QG, Shi S, Liu FY, Sun CF. Tongue squamous cell carcinoma as a possible distinct entity in patients under 40 years old. *Oncol Lett.* (2014) 7:2099–102. doi: 10.3892/ol.2014.2054
3. Fang QG, Shi S, Liu FY, Sun CF. Squamous cell carcinoma of the oral cavity in ever smokers: a matched-pair analysis of survival. *J Craniofac Surg.* (2014) 25:934–7. doi: 10.1097/SCS.0000000000000710
4. Afzali P, Ward BB. Management of the neck in oral squamous cell carcinoma: background, classification, and current philosophy. *Oral Maxillofac Surg Clin North Am.* (2019) 31:69–84. doi: 10.1016/j.coms.2018.09.004
5. Yuen AP, Wei WI, Wong YM, Tang KC. Elective neck dissection versus observation in the treatment of early oral tongue carcinoma. *Head Neck.* (1997) 19:583–8. doi: 10.1002/(SICI)1097-0347(199710)19:7<583::AID-HED4>3.0.CO;2-3
6. Mücke T, Mitchell DA, Wagenpfeil S, Ritschl LM, Wolff K-D, Kanatas A. Incidence and outcome for patients with occult lymph node involvement in T1 and T2 oral squamous cell carcinoma: a prospective study. *BMC Cancer.* (2014) 14:346. doi: 10.1186/1471-2407-14-346
7. Feng Z, Li JN, Li CZ, Guo CB. Elective neck dissection versus observation in the management of early tongue carcinoma with clinically node-negative neck: a retrospective study of 229 cases. *J Craniomaxillofac Surg.* (2014) 42:806–10. doi: 10.1016/j.jcms.2013.11.016
8. Cao Y, Wang T, Yu C, Guo X, Li C, Li L. Elective neck dissection versus wait-and-watch policy for oral cavity squamous cell carcinoma in early stage: a

systematic review and meta-analysis based on survival data. *J Oral Maxillofac Surg.* (2019) 77:2154–67. doi: 10.1016/j.joms.2019.03.015
9. Lim YC, Lee JS, Koo BS, Kim SH, Kim YH, Choi EC. Treatment of contralateral N0 neck in early squamous cell carcinoma of the oral tongue: elective neck dissection versus observation. *Laryngoscope.* (2006) 116:461–5. doi: 10.1097/01.mlg.0000195366.91395.9b
10. Abu-Ghanem S, Yehuda M, Carmel NN, Leshno M, Abergel A, Gutfeld O, et al. Elective neck dissection vs observation in early-stage squamous cell carcinoma of the oral tongue with no clinically apparent lymph node metastasis in the neck: a systematic review and meta-analysis. *JAMA Otolaryngol Head Neck Surg.* (2016) 142:857–65. doi: 10.1001/jamaoto.2016.1281
11. Fakih AR, Rao RS, Borges AM, Patel AR. Elective versus therapeutic neck dissection in early carcinoma of the oral tongue. *Am J Surg.* (1989) 158:309–13. doi: 10.1016/0002-9610(89)90122-0
12. Rouviere H. *Anatomy of the Human Lymphatic System.* Ann Arbor, MI: Edward Brothers (1938).
13. Fang Q, Li P, Qi J, Luo R, Chen D, Zhang X. Value of lingual lymph node metastasis in patients with squamous cell carcinoma of the tongue. *Laryngoscope.* (2019) 129:2527–30. doi: 10.1002/lary.27927
14. Jia J, Jia MQ, Zou HX. Lingual lymph nodes in patients with squamous cell carcinoma of the tongue and the floor of the mouth. *Head Neck.* (2018) 40:2383–8. doi: 10.1002/hed.25340
15. Ando M, Asai M, Ono T, Nakanishi Y, Asakage T, Yamasoba T. Metastases to the lingual nodes in tongue cancer: a pitfall in a conventional neck dissection. *Auris Nasus Larynx.* (2010) 37:386–9. doi: 10.1016/j.anl.2009.10.001
16. Dutton JM, Graham SM, Hoffman HT. Metastatic cancer to the floor of mouth: the lingual lymph nodes. *Head Neck.* (2002) 24:401–5. doi: 10.1002/hed.10026
17. Han W, Yang X, Huang X, Hu Q, Wang Z. Metastases to lingual lymph nodes from squamous cell carcinoma of the tongue. *Br J Oral Maxillofac Surg.* (2008) 46:376–8, doi: 10.1016/j.bjoms.2007.12.002
18. Zhang T, Ord RA, Wei WI, Zhao J. Sublingual lymph node metastasis of early tongue cancer: report of two cases and review of the literature. *Int J Oral Maxillofac Surg.* (2011) 40:597–600. doi: 10.1016/j.ijom.2010.12.009
19. Saito M, Nishiyama H, Oda Y, Shingaki S, Hayashi T. The lingual lymph node identified as a sentinel node on CT lymphography in a patient with cN0 squamous cell carcinoma of the tongue. *Dentomaxillofac Radiol.* (2012) 41:254–8. doi: 10.1259/dmfr/61883763
20. Woolgar JA. Histological distribution of cervical lymph node metastases from intraoral/oropharyngeal squamous cell carcinomas. *Br J Oral Maxillofac Surg.* (1999) 37:175–80. doi: 10.1054/bjom.1999.0036
21. Umeda M, Minamikawa T, Shigeta T, Oguni A, Kataoka T, Takahashi H, et al. Metastasis to the lingual lymph node in patients with squamous cell carcinoma of the floor of the mouth: a report of two cases. *Kobe J Med Sci.* (2010) 55:E67–72.
22. Ozeki S, Tashiro H, Okamoto M, Matsushima T. Metastasis to the lingual lymph node in carcinoma of the tongue. *J Maxillofac Surg.* (1985) 13:277–81. doi: 10.1016/S0301-0503(85)80064-3
23. Skulsky SL, O'Sullivan B, McArdle O, Leader M, Roche M, Conlon PJ, et al. Review of high-risk features of cutaneous squamous cell carcinoma and discrepancies between the American Joint Committee on Cancer and NCCN Clinical Practice Guidelines In Oncology. *Head Neck.* (2017) 39:578–94. doi: 10.1002/hed.24580
24. Lydiatt WM, Patel SG, O'Sullivan B, Brandwein MS, Ridge JA, Migliacci JC, et al. Head and Neck cancers-major changes in the American Joint Committee on cancer eighth edition cancer staging manual. *CA Cancer J Clin.* (2017) 67:122–37. doi: 10.3322/caac.21389
25. Dai L, Fang Q, Li P, Wu J, Zhang X. Secondary squamous cell carcinoma of the oral cavity after nasopharyngeal carcinoma. *Cancer Res Treat.* (2020) 52:109–16. doi: 10.4143/crt.2019.202
26. D'Cruz AK, Vaish R, Kapre N, Dandekar M, Gupta S, Hawaldar R, et al. Elective versus therapeutic neck dissection in node-negative oral cancer. *N Engl J Med.* (2015) 373:521–9. doi: 10.1056/NEJMoa1506007
27. Ren ZH, Xu JL, Li B, Fan TF, Ji T, Zhang CP. Elective versus therapeutic neck dissection in node-negative oral cancer: evidence from five randomized controlled trials. *Oral Oncol.* (2015) 51:976–81. doi: 10.1016/j.oraloncology.2015.08.009
28. Weiss MH, Harrison LB, Isaacs RS. Use of decision analysis in planning a management strategy for the stage N0 neck. *Arch Otolaryngol Head Neck Surg.* (1994) 120:699–702. doi: 10.1001/archotol.1994.01880310005001
29. Xie N, Wang C, Liu X, Li R, Hou J, Chen X, et al. Tumor budding correlates with occult cervical lymph node metastasis and poor prognosis in clinical early-stage tongue squamous cell carcinoma. *J Oral Pathol Med.* (2015) 44:266–72. doi: 10.1111/jop.12242
30. Abbate V, Dell'Aversana Orabona G, Salzano G, Bonavolontà P, Maglitto F, Romano A, et al. Pre-treatment neutrophil-to-lymphocyte ratio as a predictor for occult cervical metastasis in early stage (T1-T2 cN0) squamous cell carcinoma of the oral tongue. *Surg Oncol.* (2018) 27:503–7. doi: 10.1016/j.suronc.2018.06.002
31. Loganathan P, Sayan A, Hsu DWK, Paraneetharan S, Ilankovan V. Squamous cell carcinoma of the anterior tongue: is tumour thickness an indicator for cervical metastasis? *Int J Oral Maxillofac Surg.* (2017) 46:407–12. doi: 10.1016/j.ijom.2016.11.003
32. Lim SC, Zhang S, Ishii G, Endoh Y, Kodama K, Miyamoto S, et al. Predictive markers for late cervical metastasis in stage I and II invasive squamous cell carcinoma of the oral tongue. *Clin Cancer Res.* (2004) 10(1 Pt 1):166–72. doi: 10.1158/1078-0432.CCR-0533-3
33. Sparano A, Weinstein G, Chalian A, Yodul M, Weber R. Multivariate predictors of occult neck metastasis in early oral tongue cancer. *Otolaryngol Head Neck Surg.* (2004) 131:472–6. doi: 10.1016/j.otohns.2004.04.008
34. Calabrese L, Renne G, De Cicco C, Chiesa F. Metastatic cancer to the floor of mouth: the lingual lymph nodes. *Head Neck.* (2003) 25:341–2. doi: 10.1002/hed.10259
35. Fang Q, Liu F, Seng D. Oncologic outcome of parotid mucoepidermoid carcinoma in pediatric patients. *Cancer Manag Res.* (2019) 11:1081–5. doi: 10.2147/CMAR.S192788

Conflict of Interest: The authors declare that the research was conducted in the absence of any commercial or financial relationships that could be construed as a potential conflict of interest.

frontiers in Oncology

ORIGINAL RESEARCH
published: 09 April 2020
doi: 10.3389/fonc.2020.00386

Significance of PET-CT for Detecting Occult Lymph Node Metastasis and Affecting Prognosis in Early-Stage Tongue Squamous Cell Carcinoma

Guo Zhao[1], *Jianli Sun*[1], *Kai Ba*[1]* *and Yunxiang Zhang*[2]

[1] Department of Oral Medicine, The First Affiliated Hospital of Zhengzhou University, Zhengzhou, China, [2] Department of Endodontics, Kaifeng Stomatology Hospital, Kaifeng, China

Objective: We aimed to clarify the significance of PET-CT for detecting occult lymph node metastasis and for affecting prognosis in early-stage tongue squamous cell carcinoma (SCC).

Methods: Patients with surgically treated primary cT1-2N0 tongue SCC who agreed to undergo a preoperative PET-CT scan were prospectively enrolled. The primary study outcomes were occult neck lymph node metastasis and locoregional control (LRC). The Kaplan-Meier method was used to analyze the LRC rate, and then the factors that were significant in the Kaplan-Meier method were assessed in the Cox model to determine the independent factors.

Results: A total of 135 patients were included, and the median maximum standardized uptake value (SUV max) of the primary tumor was 9.0. When analyzing the PET-CT results, 18 patients were recognized as having neck lymph node metastasis, and 12 patients were proven to have pathologic lymph nodes. A total of 117 patients did not have neck lymph node metastasis reported by PET-CT, and five patients were proven to have pathologic lymph nodes. The sensitivity and specificity of PET-CT for predicting occult metastasis were 70.6 and 94.9%, respectively. In patients with an SUV max $\leq$9.0, the 5-year LRC rate was 95%; in patients with an SUV max >9.0, the 5-year LRC rate was 85%, and the difference was significant. Further Cox model analyses confirmed the independence of the SUV max for predicting LRC.

Conclusion: PET-CT has a high specificity for predicting occult lymph node metastasis, and an SUV max >9.0 is significantly associated with worse LRC in cT1-2N0 tongue SCC.

Keywords: PET-CT, occult lymph node metastasis, early-stage tongue squamous cell carcinoma, tongue squamous cell carcinoma, oral squamous cell carcinoma

OPEN ACCESS

Edited by:
Victor C. Kok,
Asia University, Taiwan

Reviewed by:
Davide Lombardi,
University of Brescia, Italy
Peng Li,
University at Buffalo, United States

***Correspondence:**
Kai Ba
k.ba@msn.com

Specialty section:
This article was submitted to Head and Neck Cancer, a section of the journal Frontiers in Oncology

Received: *07 November 2019*
Accepted: *04 March 2020*
Published: *09 April 2020*

Citation:
Zhao G, Sun J, Ba K and Zhang Y (2020) Significance of PET-CT for Detecting Occult Lymph Node Metastasis and Affecting Prognosis in Early-Stage Tongue Squamous Cell Carcinoma. Front. Oncol. 10:386. doi: 10.3389/fonc.2020.00386

INTRODUCTION

Tongue squamous cell carcinoma (SCC) is a common malignancy in the oral cavity, and complete resection is the standard treatment procedure (1, 2). Owing to the wide range of occult lymph node metastasis rates, there is controversy regarding the best neck management. It is important for us to detect patients who are at high risk of neck lymph node metastasis preoperatively.

Current researchers have demonstrated the role of perineural invasion, lymphovascular invasion, depth of invasion, neutrophil-to-lymphocyte ratio, and so on in predicting occult lymph node metastasis (3–6), but the significance of PET-CT for determining occult lymph node metastasis has rarely been discussed. Zhang et al. (7) described that the overall sensitivity and specificity of PET-CT in cT1-2 oral SCC were 21.4 and 98.4%, respectively, with a negative predictive value of 99.1%. Myers et al. (8) demonstrated an estimated overall sensitivity of PET-CT for the N0 neck of 78% with a specificity of 100%. On the other hand, cancer cells use glucose as an energy source, and tumors with strong growth potential and invasiveness are highly likely to take up FDG (9), as indicated by the maximum standardized uptake value (SUV max). Previous authors have depicted the prognostic role of the SUV max in head and neck SCC; however, all these studies included all subsites or analyzed large-volume tumors together with small-volume tumors. Considering that different biological behaviors exist between tongue SCC and SCC at other sites, in the current study, we aimed to clarify the significance of PET-CT for detecting occult lymph node metastasis and affecting prognosis in early-stage tongue squamous cell carcinoma.

PATIENTS AND METHODS

The Zhengzhou University Institutional Research Committee approved our study (No. 201845YZ), and all patients signed informed consent agreements for medical research before the initial treatment. All methods were performed in accordance with the relevant guidelines and regulations.

From January 2010 to December 2018, consecutive patients with primary early stage (cT1-2N0) tongue SCC were prospectively enrolled. The only inclusion criterion was that the patient agreed to undergo a PET-CT examination preoperatively. Clinical pathologic and follow-up data, including age, sex, smoking status, drinking status, pathologic TNM stage based on the AJCC 8th edition, perineural invasion (PNI), lymphovascular invasion (LVI), extracapsular extension (ECS), depth of invasion (DOI), and SUV max of the primary tumor, were recorded in the enrolled patients.

Smokers/drinkers were defined as patients who smoked/drank at diagnosis or who had stopped for <1-year (10, 11). All pathologic sections were reviewed by at least two head and neck pathologists. PNI was considered to be present if tumor cells were identified within the perineural space and/or nerve bundle; LVI was positive if tumors were noted within the lymphovascular channels (12). The pathologic DOI was measured from the level of the adjacent normal mucosa to the deepest point of tumor infiltration, regardless of the presence or absence of ulceration (13). cT1-2 was defined by a maximum tumor diameter of <2 cm or ranging from 2 to 4 cm. Patients were considered cN0 if they had no evidence of nodal metastasis on a clinical exam, ultrasound, or radiographic imaging (not including PET-CT) (9). The cut-off value of the SUV max was set according to the median value (14).

Several PET/CT scanners were used to perform the PET-CT scans (GE Healthcare, Milwaukee, America). Patients fasted for at least 6 h before the PET-CT scan. The procedure was postponed when glucose levels were >200 mg/dL. Each patient received 10–20 mCi of [^{18}F] FDG dose, based on his or her weight. Axial PET and diagnostic CT images were obtained from the calvarial vertex through the upper thighs after urinary voiding. Emission images were obtained after a radiopharmaceutical injection 1 h later. There was no contrast medium used during the CT scan. The images were reconstructed in the thickness of a 2.5 mm slice. The SUV max was measured for both the primary tumor and regional lymph nodes. For every suspicious lesion, the isocontour region of interest centered on the maximum value pixel was drawn automatically with workstation tools generating the SUV max of the region. An SUV max cut-off of 2.5 MBq/g was used for FDG-avid lymph nodes and primary tumors on PET-CT.

In our cancer center, systemic examinations, including ultrasound, CT, and MRI, were routinely performed. PET-CT was selectively suggested, and complete resection of the primary tumor with a margin of at least 1 cm, including the adipose tissue in the mouth floor as well as the sublingual gland and neck dissection (level 1–3), was routinely performed in every patient with any stage of tongue SCC. Adjuvant treatment was suggested if there was neck lymph node metastasis, PNI, LVI, or a positive margin. All patients were regularly followed up with every 3 months within the first 2- years after the operation and every 6 months within the third to fifth years after the operation. If there was suspicion of disease recurrence, active interference was performed.

The primary study outcomes were occult neck lymph node metastasis and locoregional control (LRC). The 4-fold table method was used to analyze the association between PET-CT and occult lymph node metastasis. The survival time was calculated from the date of surgery to the date of the first event of local, regional, or locoregional recurrence or to the latest follow-up. The Kaplan-Meier method was used to analyze the LRC rate, and then the factors that were significant in the Kaplan-Meier method were assessed in the Cox model to determine the independent factors. All statistical analyses were performed using SPSS 20.0, all reported p-value was two-sided, and $p < 0.05$ was considered to be significant.

RESULTS

There were 135 patients (109 males and 26 females) enrolled in total, and the mean age was 54.5 (range: 30–76) years. There were 76 (56.3%) smokers and 55 (40.7%) drinkers. The median SUV max was 9.0 (range: 2.3–29.7). Clinical tumor stages were characterized as cT1 in 57 (42.2%) cases and cT2 in 78 (57.8%) cases. 5 cT1 tumors were corrected into pT2 tumors after operation. PNI and LVI were noted in 18 (13.3%) and 15 (11.1%) patients, respectively. The mean DOI was 6.0 (range: 1.0–9.5) mm. Tumor differentiation was well in 53 (39.3%) cases, moderate in 70 (51.9%) cases, and poor in 12 (8.9%) cases. Negative margins were achieved in all patients.

Occult neck lymph node metastasis was reported in five of the 57 patients with cT1 disease with a rate of 8.8% and in 12 of the 78 patients with cT2 disease with a rate of 15.4%. ECS was reported in three (3/17, 17.6%) patients. The total number of positive lymph nodes was 23.

When analyzing the PET-CT results, 18 patients were recognized as having neck lymph node metastasis, and 12 patients were proven to have pathologic lymph nodes. A total of 117 patients did not have neck lymph node metastasis reported by PET-CT, and five patients were proven to have pathologic lymph nodes. The sensitivity and specificity of PET-CT for predicting occult metastasis were 70.6 and 94.9%, respectively.

The mean follow-up time was 53.9 (range: 6–95) months. Twenty five patients underwent adjuvant radiotherapy, while three patients also received adjuvant chemotherapy. Thirteen patients suffered from disease recurrence: four cases locally, five cases regionally, and four cases locoregionally. Eight patients were successfully salvaged with surgical treatment. In patients with an SUV max ≤9.0, there were three cases of recurrence, and the 5-year LRC rate was 95%. In patients with an SUV max >9.0, there were ten cases of recurrence, and the 5-year LRC rate was 85%; the difference was significant (**Figure 1**, $p = 0.043$). Further Cox model analyses confirmed the independence of the SUV max for predicting LRC (**Table 1**).

DISCUSSION

The most important finding in the current study was that PET-CT had a high specificity for predicting occult lymph node metastasis, and an SUV max >9.0 was significantly associated with worse LRC in patients with early-stage tongue SCC. These results can provide better guidance regarding decision making in terms of neck dissection and can help determine which patients would need adjuvant radiotherapy.

Neck lymph node metastasis is the most important prognostic factor in oral SCC, and neck management for early-stage tongue SCC is a key issue. A few authors who support routine neck dissection depicted that it could be beneficial for accurately staging the neck and identifying patients who require adjuvant therapy as well as improving survival (15). However, some authors have reported that the rate of occult neck lymph node metastasis varies, and a considerable number of patients have been over-treated (16). This controversy prompted the effort to determine the possible predictors for occult lymph node metastasis. Larson et al. (17) aimed to clarify the contribution of adverse pathologic characteristics to clinical outcomes in small tongue SCC and concluded that, even though PNI and LVI occurred, the prevalence of occult lymph node metastasis was very low in small disease with a DOI ≤ 4.0 mm. Wu et al. (18) described that a DOI larger than 4 mm and a stable growth pattern in the invasive front were independent risk factors for occult lymph node metastasis in cT1-2N0 tongue SCC. A similar finding was also reported by Faisal et al. (19): 179 patients with early-stage tongue SCC were divided into three groups according to the AJCC cutoff points in the 8th edition according to depth(group A: 1–5 mm, group B: 6–10 mm, and group C: > 10 mm). The authors noted that the risk of local recurrence and nodal metastasis in group A was 15 and 23%, in group B was 20 and 34%, and in group C was 40 and 53%, respectively. However, all these studies were retrospective, and the analyzed predictors, including DOI, PNI, and LVI, usually remained unknown during the frozen section, which would greatly limit their clinical application.

Cancer cells utilize glucose as energy in general, and PET-CT has been widely used to detect the primary site and metastasized lymph nodes. Additionally, a number of researchers have clarified the role of PET-CT in evaluating neck status. Chaukar et al. (20) previously compared the diagnostic accuracy of staging a cN0 neck among ultrasound, contrast enhanced CT, and PET-CT in 70 oral SCC patients. The authors reported that the PET-CT scan

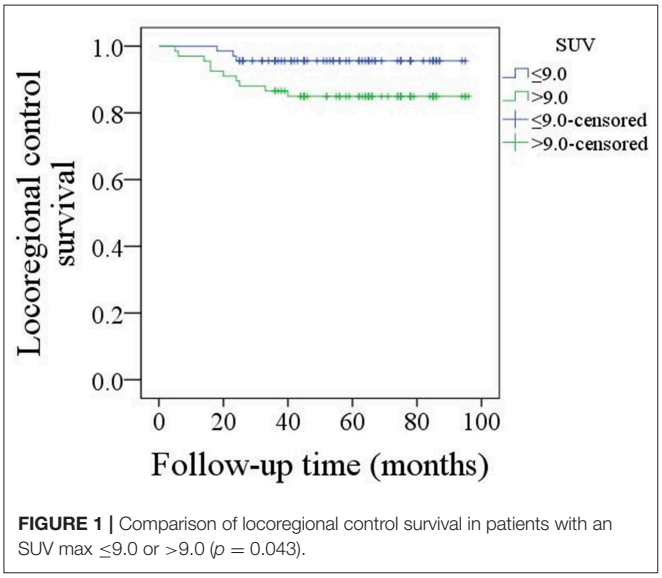

FIGURE 1 | Comparison of locoregional control survival in patients with an SUV max ≤9.0 or >9.0 ($p = 0.043$).

TABLE 1 | Univariate and Cox model analyses of risk factors for the locoregional control survival in patients with cT1-2N0 tongue squamous cell carcinoma.

Variables	Univariate	Cox model	
	Log-rank test	*p*	HR [95% CI]
Age (<40 vs. ≥40)	0.458		
Gender	0.336		
Smoking	0.478		
Drinking	0.221		
SUV max (≤9.0 vs. >9.0)	0.043	0.034	2.445 [1.226–4.998]
Pathologic tumor stage	0.012	<0.001	3.668 [1.479–9.336]
Pathologic neck lymph node stage	0.024	0.421	4.612 [0.741–9.667]
Perineural invasion	0.089		
Extracapsular extension	0.642		
Lymphovascular invasion	0.031	0.042	2.889 [1.365–4.416]
Tumor differentiation	0.009		
Well			
Moderate		0.097	2.579 [0.947–5.667]
Poor		0.016	3.978 [1.741–8.665]
Radiotherapy	0.116		

had a poor specificity of 54.1% owing to the high false-positive rate, and the CT scan showed the best accuracy with 80.2% with a specificity of 85.4% and sensitivity of 73.6%. The authors concluded this strange finding was contributed in part by the epidemic of chronic granulomatous diseases in India. Currently, more and more researchers are describing a convincing result. Bae et al. (21) enrolled 178 oral SCC patients with negative neck palpation findings, and found the sensitivity for the detection of occult metastasis was higher for PET-CT than that for CT/MRI imaging on a per-patient (69.1% vs. 35.7%), per-level (62.1% vs. 29.3%), and per-side (70.5% vs. 36.4%) basis. Gordin et al. (22) found that PET-CT had a sensitivity of 89% and a specificity of 95% for predicting neck lymph node metastasis in head and neck SCC. A similar finding was also reported by Jeong et al. (23) and Roh et al. (24); however, all these studies included SCCs of all subsites, and small-volume cancers were analyzed together with large-volume cancers. The prevalence of neck lymph node metastasis is significantly associated with tumor stage, but the role of PET-CT in early-stage tongue SCC has rarely been discussed. Zhang et al. (7) might have been the first to report that the overall sensitivity and specificity of PET-CT for predicting occult lymph node metastasis were 21.4 and 98.4%, respectively. This finding was partially consistent with our results. The high specificity found in both studies is possibly attributed to the low occult lymph node metastasis rate. The significant conflict of sensitivity between the two studies might be explained by the following aspects: the different economic status that exists between China and other Western countries might cause differences in oral hygiene, and it is well-known that infectious lymph nodes and inflammation lead to false-positive PET-CT outcomes. The findings of the two studies might suggest that if there is a negative result according to PET-CT, there may be a very high possibility of no occult lymph node metastasis. Some may argue, then, that active observation is an option for early-stage tongue SCC. There have been conflicting results regarding the comparison between elective neck dissection and active observation in cT1-2N0 tongue SCC (15, 16). Another uncommon tool that has been used is sentinel lymph node biopsy (SLNB). Recently, Cramer et al. (25) compared the survival difference between SLNB and elective neck dissection groups; the authors reported that neck dissection was avoided in 63.8% of patients receiving SLNB, the two groups had similar overall survival, and decreases in perioperative morbidity and hospital stay were seen in patients with SLNB. Alex et al. (26) described that SLNB was easily performed with a high success rate, and it had a relatively high specificity and a low false-negative rate. Similar findings were also reported by Holden et al. (27) and Den Toom et al. (28). Both SLNB and PET-CT had high value for predicting nodal metastasis in oral SCC. However, in China, SLNB is not widely used for oral SCC. Although the risk is low, SLNB is invasive. Klode et al. (29) noted that SLNB was much more sensitive than PET-CT for discovering small lymph node metastases in malignant melanoma; however, in cervical cancer patients, Papadia et al. (30) demonstrated that, compared to SLNB, PET-CT represented a "safety net" that helped the surgeon identify metastatic lymph nodes, especially in patients with large tumors. On the other hand, even though our unpublished data showed that PET-CT-guided neck dissection could achieve similar disease control to routine neck dissection, the cost utility as well as the actual applicability of PET-CT remains unknown, and further studies are needed to clarify these questions.

The prognosis of tongue SCC has been frequently analyzed. The widely accepted prognostic factors include tumor stage, neck lymph node stage, PNI, LVI, margin status, and so on (1–3, 5). However, the significance of the SUV max remains unclear. The SUV max is partially related to the malignant grade of tumor cells, reflecting proliferation ability. Hasegawa et al. (31) described that an SUV max >8.0 indicated a higher tumor stage, neck lymph node metastasis, the presence of PNI and LVI, and a higher Ki-67 index. Further survival analysis also confirmed that worse disease-free survival was indicated by an SUV max >8.0. Yokobori et al. (32) reported that patients with T2 stage disease had a higher SUV max than patients with T1 stage disease, and patients with a higher SUV max tended to have a higher frequency of PNI, microvessel density, and expression of LAT1. This finding was consistent with our results, suggesting that the SUV max might be used as a marker of adjuvant treatment in future studies.

The main limitation in the current study might be that it seems to provide the questionable message that PET-CT is suitable for all patients with low-stage oral tongue SCC, which slightly contradicts most recently published guidelines; however, what we wish to demonstrate is that PET-CT is an alternative in select patients. It is also a reliable method for guiding cN0 neck management in early-stage tongue squamous cell carcinoma.

In summary, PET-CT has a high specificity for predicting occult lymph node metastasis, and an SUV max >9.0 is significantly associated with worse LRC in cT1-2N0 tongue SCC.

DATA AVAILABILITY STATEMENT

All data generated or analyzed during this study are included in this published article, and the primary data can be provided by the corresponding author.

ETHICS STATEMENT

The studies involving human participants were reviewed and approved by The Zhengzhou University institutional research committee. The patients/participants provided their written informed consent to participate in this study.

AUTHOR CONTRIBUTIONS

All the authors contributed to study design, manuscript writing, study selection, data analysis, study quality evaluating, and manuscript revising. All authors have read and approved the final manuscript.

ACKNOWLEDGMENTS

This study was supported by National Natural Science Foundation of China (Grant No. 81500826).

REFERENCES

1. Fang Q, Li P, Qi J, Luo R, Chen D, Zhang X. Value of lingual lymph node metastasis in patients with squamous cell carcinoma of the tongue. *Laryngoscope.* (2019) 129:2527–30. doi: 10.1002/lary.27927
2. Dai L, Fang Q, Li P, Wu J, Zhang X. Secondary squamous cell carcinoma of the oral cavity after nasopharyngeal carcinoma. *Cancer Res Treat.* (2020) 52:109–16. doi: 10.4143/crt.2019.202
3. Massey C, Dharmarajan A, Bannuru RR, Rebeiz E. Management of N0 neck in early oral squamous cell carcinoma: a systematic review and meta-analysis. *Laryngoscope.* (2019) 129:E284–98. doi: 10.1002/lary.27627
4. Morand GB, Ikenberg K, Vital DG, Cardona I, Moch H, Stoeckli SJ, et al. Preoperative assessment of CD44-mediated depth of invasion as predictor of occult metastases in early oral squamous cell carcinoma. *Head Neck.* (2019) 41:950–8. doi: 10.1002/hed.25532
5. Tam S, Amit M, Zafereo M, Bell D, Weber RS. Depth of invasion as a predictor of nodal disease and survival in patients with oral tongue squamous cell carcinoma. *Head Neck.* (2019) 41:177–84. doi: 10.1002/hed.25506
6. Abbate V, Dell'Aversana Orabona G, Salzano G, Bonavolontà P, Maglitto F, Romano A, et al. Pre-treatment neutrophil-to-lymphocyte ratio as a predictor for occult cervical metastasis in early stage (T1-T2 cN0) squamous cell carcinoma of the oral tongue. *Surg Oncol.* (2018) 27:503–7. doi: 10.1016/j.suronc.2018.06.002
7. Zhang H, Seikaly H, Biron VL, Jeffery CC. Utility of PET-CT in detecting nodal metastasis in cN0 early stage oral cavity squamous cell carcinoma. *Oral Oncol.* (2018) 80:89–92. doi: 10.1016/j.oraloncology.2018.04.003
8. Myers LL, Wax MK, Nabi H, Simpson GT, Lamonica D. Positron emission tomography in the evaluation of the N0 neck. *Laryngoscope.* (1999) 108:232–6. doi: 10.1097/00005537-199802000-00014
9. Arya S, Rane P, Deshmukh A. Oral cavity squamous cell carcinoma: role of pretreatment imaging and its influence on management. *Clin Radiol.* (2014) 69:916–30. doi: 10.1016/j.crad.2014.04.013
10. Ouyang PY, Su Z, Mao YP, Liang XX, Liu Q, Xie FY. Prognostic impact of family history in southern Chinese patients with undifferentiated nasopharyngeal carcinoma. *Br J Cancer.* (2013) 109:788–94. doi: 10.1038/bjc.2013.343
11. Fang QG, Shi S, Liu FY, Sun CF. Squamous cell carcinoma of the oral cavity in ever smokers: a matched-pair analysis of survival. *J Craniofac Surg.* (2014) 25:934–7. doi: 10.1097/SCS.0000000000000710
12. Skulsky SL, O'Sullivan B, McArdle O, Leader M, Roche M, Conlon PJ, et al. Review of high-risk features of cutaneous squamous cell carcinoma and discrepancies between the American Joint Committee on Cancer and NCCN Clinical Practice Guidelines In Oncology. *Head Neck.* (2017) 39:578–94. doi: 10.1002/hed.24580
13. Lydiatt WM, Patel SG, O'Sullivan B, Brandwein MS, Ridge JA, Migliacci JC, et al. Head and neck cancers-major changes in the American Joint Committee on cancer eighth edition cancer staging manual. *CA Cancer J Clin.* (2017) 67:122–37. doi: 10.3322/caac.21389
14. Halfpenny W, Hain SF, Biassoni L, Maisey MN, Sherman JA, McGurk M. FDG PET. A possible prognostic factor in head and neck cancer. *Br J Cancer.* (2002) 86:512–6. doi: 10.1038/sj.bjc.6600114
15. Abu-Ghanem S, Yehuda M, Carmel NN, Leshno M, Abergel A, Gutfeld O, et al. Elective neck dissection vs observation in early-stage squamous cell carcinoma of the oral tongue with no clinically apparent lymph node metastasis in the neck: a systematic review and meta-analysis. *JAMA Otolaryngol Head Neck Surg.* (2016) 142:857–65. doi: 10.1001/jamaoto.2016.1281
16. Otsuru M, Ota Y, Yanamoto S, Okura M, Umeda M, Kirita T, et al. A multicenter retrospective study of elective neck dissection for T1-2N0M0 tongue squamous cell carcinoma: analysis using propensity score-matching. *Ann Surg Oncol.* (2019) 26:555–63. doi: 10.1245/s10434-018-07089-7
17. Larson AR, Kemmer J, Formeister E, El-Sayed I, Ha P, George J, et al. Beyond depth of invasion: adverse pathologic tumor features in early oral tongue squamous cell carcinoma. *Laryngoscope.* (2019) doi: 10.1002/lary.28241
18. Wu K, Wei J, Liu Z, Yu B, Yang X, Zhang C, et al. Can pattern and depth of invasion predict lymph node relapse and prognosis in tongue squamous cell carcinoma. *BMC Cancer.* (2019) 19:714. doi: 10.1186/s12885-019-5859-y
19. Faisal M, Abu Bakar M, Sarwar A, Adeel M, Batool F, Malik KI, et al. Depth of invasion (DOI) as a predictor of cervical nodal metastasis and local recurrence in early stage squamous cell carcinoma of oral tongue (ESSCOT). *PLoS ONE.* (2018) 13:e0202632. doi: 10.1371/journal.pone.0202632
20. Chaukar D, Dandekar M, Kane S, Arya S, Purandare N, Rangarajan V, et al. Relative value of ultrasound, computed tomography and positron emission tomography imaging in the clinically node-negative neck in oral cancer. *Asia Pac J Clin Oncol.* (2016) 12:e332–8. doi: 10.1111/ajco.12255
21. Bae MR, Roh JL, Kim JS, Lee JH, Cho KJ, Choi SH, et al. 18F-FDG PET/CT versus CT/MR imaging for detection of neck lymph node metastasis in palpably node-negative oral cavity cancer. *J Cancer Res Clin Oncol.* (2020). 146:237–44. doi: 10.1007/s00432-019-03054-3
22. Gordin A, Golz A, Keidar Z, Daitzchman M, Bar-Shalom R, Israel O. The role of FDG-PET/CT imaging in head and neck malignant conditions: impact on diagnostic accuracy and patient care. *Otolaryngol Head Neck Surg.* (2007) 137:130–7. doi: 10.1016/j.otohns.2007.02.001
23. Jeong HS, Baek CH, Son YI, Ki Chung M, Kyung Lee D, Young Choi J, et al. Use of integrated 18F-FDG PET/CT to improve the accuracy of initial cervical nodal evaluation in patients with head and neck squamous cell carcinoma. *Head Neck.* (2007) 29:203–10. doi: 10.1002/hed.20504
24. Roh JL, Park JP, Kim JS, Lee JH, Cho KJ, Choi SH, Nam SY, Kim SY. 18F fluorodeoxyglucose PET/CT in head and neck squamous cell carcinoma with negative neck palpation findings: a prospective study. *Radiology.* (2014). 271:153–61. doi: 10.1148/radiol.13131470
25. Cramer JD, Sridharan S, Ferris RL, Duvvuri U, Samant S. Sentinel lymph node biopsy versus elective neck dissection for stage I to II oral cavity cancer. *Laryngoscope.* (2019) 129:162–9. doi: 10.1002/lary.27323
26. Alex JC. The application of sentinel node radiolocalization to solid tumors of the head and neck: a 10-year experience. *Laryngoscope.* (2004) 114:2–19. doi: 10.1097/00005537-200401000-00002
27. Holden AM, Sharma D, Schilling C, Gnanasegaran G, Odell EW, Sassoon I, et al. Biopsy of the sentinel lymph node in oral squamous cell carcinoma: analysis of error in 100 consecutive cases. *Br J Oral Maxillofac Surg.* (2018) 56:615–20. doi: 10.1016/j.bjoms.2018.06.019
28. Den Toom IJ, Heuveling DA, Flach GB, van Weert S, Karagozoglu KH, van Schie A, et al. Sentinel node biopsy for early-stage oral cavity cancer: the VU University Medical Center experience. *Head Neck.* (2015) 37:573–8. doi: 10.1002/hed.23632
29. Klode J, Dissemond J, Grabbe S, Hillen U, Poeppel T, Boeing C. Sentinel lymph node excision and PET-CT in the initial stage of malignant melanoma: a retrospective analysis of 61 patients with malignant melanoma in American Joint Committee on Cancer stages I and II. *Dermatol Surg.* (2010) 36:439–45. doi: 10.1111/j.1524-4725.2010.01479.x
30. Papadia A, Gasparri ML, Genoud S, Bernd K, Mueller MD. The combination of preoperative PET/CT and sentinel lymph node biopsy in the surgical management of early-stage cervical cancer. *J Cancer Res Clin Oncol.* (2017) 143:2275–81. doi: 10.1007/s00432-017-2467-6
31. Hasegawa O, Satomi T, Kono M, Watanabe M, Ikehata N, Chikazu D. Correlation analysis between the SUVmax of FDG-PET/CT and clinicopathological characteristics in oral squamous cell carcinoma. *Odontology.* (2019) 107:237–3. doi: 10.1007/s10266-018-0379-9
32. Yokobori Y, Toyoda M, Sakakura K, Kaira K, Tsushima Y, Chikamatsu K. (18)F-FDG uptake on PET correlates with biological potential in early oral squamous cell carcinoma. *Acta Otolaryngol.* (2015). 135:494–9. doi: 10.3109/00016489.2014.969385

Conflict of Interest: The authors declare that the research was conducted in the absence of any commercial or financial relationships that could be construed as a potential conflict of interest.

frontiers in Oncology

ORIGINAL RESEARCH
published: 15 April 2020
doi: 10.3389/fonc.2020.00463

Combinatorial Low Dose Arsenic Trioxide and Cisplatin Exacerbates Autophagy via AMPK/STAT3 Signaling on Targeting Head and Neck Cancer Initiating Cells

Wei-Chun Hu[1†], *Wan-Huai Teo*[1†], *Tung-Fu Huang*[2,3,4], *Te-Chang Lee*[5] *and Jeng-Fan Lo*[1,6,7,8*]

[1] *Institute of Oral Biology, National Yang-Ming University, Taipei, Taiwan,* [2] *School of Medicine, National Yang-Ming University, Taipei, Taiwan,* [3] *Department of Orthopedics and Traumatology, Taipei Veterans General Hospital, Taipei, Taiwan,* [4] *Department of Exercise and Health Science, National Taipei University of Nursing and Health Sciences, Taipei, Taiwan,* [5] *Institute of Biomedical Sciences, Academia Sinica, Taipei, Taiwan,* [6] *Department of Dentistry, School of Dentistry, National Yang-Ming University, Taipei, Taiwan,* [7] *Cancer Progression Research Center, National Yang-Ming University, Taipei, Taiwan,* [8] *Department of Dentistry, Taipei Veterans General Hospital, Taipei, Taiwan*

OPEN ACCESS

Edited by:
Cheng-Chia Yu,
Chung Shan Medical University, Taiwan

Reviewed by:
Pei-Ling Hsieh,
China Medical University, Taiwan
Shih-Feng Cho,
Kaohsiung Medical University, Taiwan

****Correspondence:***
Jeng-Fan Lo
jflo@ym.edu.tw

[†]These authors have contributed equally to this work

Specialty section:
This article was submitted to Head and Neck Cancer, a section of the journal Frontiers in Oncology

Received: *31 December 2019*
Accepted: *16 March 2020*
Published: *15 April 2020*

Citation:
Hu W-C, Teo W-H, Huang T-F, Lee T-C and Lo J-F (2020) Combinatorial Low Dose Arsenic Trioxide and Cisplatin Exacerbates Autophagy via AMPK/STAT3 Signaling on Targeting Head and Neck Cancer Initiating Cells. Front. Oncol. 10:463. doi: 10.3389/fonc.2020.00463

Head and neck squamous cell carcinoma (HNSCC) is a highly lethal disease with high-level of epidemic both in the world and Taiwan. Previous studies support that head and neck cancer-initiating cells (HN-CICs), a subpopulation of cancer cells with enhanced stemness properties, contribute to therapy resistance and tumor recurrence. Arsenic trioxide (As_2O_3; ATO) has shown to be an effective anti-cancer drug targeting acute promyelocytic leukemia (APL). Combinatorial treatment with high dose of ATO and cisplatin (CDDP) exert synergistic apoptotic effects in cancer cell lines of various solid tumors, however, it may cause of significant side effect to the patients. Nevertheless, none has reported the anti-cancerous effect of ATO/CDDP targeting HN-CICs. In this study, we aim to evaluate the low dose combination of ATO with conventional chemo-drugs CDDP treatment on targeting HN-CICs. We first analyzed the inhibitory tumorigenicity of co-treatment with ATO and chemo-drugs on HN-CICs which are enriched from HNSCC cells. We observed that ATO/CDDP therapeutic regimen successfully synergized the cell death on HN-CICs with a Combination Index (CI) <1 by Chou-Talalay's analysis *in vitro*. Interestingly, the ATO/CDDP regimen also induced exaggerated autophagy on HN-CICs. Additionally, this drug combination strategy also empowered both preventive and therapeutic effect by *in vivo* xenograft assays. Finally, we provide the underlying molecular mechanisms of ATO-based therapeutic regimen on HN-CICs. Together, low dose of combinatorial ATO/CDDP regimen induced cell death as well as exacerbated autophagy via AMPK-STAT3 mediated pathway in HN-CICs.

Keywords: head and neck cancer-initiating cells, arsenic trioxide, combination index, autophagy, synergistic effects

BACKGROUND

Head and neck cancer (HNC), a disease with a major worldwide burden. About 95% of HNC is squamous cell carcinoma (HNSCC) which make up the sixth most common cause of cancer death. It is responsible for 300,000 deaths annually (1). HNSCC is considered one of the most common cancers leading to significant mortality and morbidity in Taiwan. Treatment for HNSCC usually involves therapies with surgery, radiation, or chemotherapy alone or concurrent chemotherapy/radiation. However, the overwhelming majority of HNSCC patients' survival outcomes still remain poor. The 5-year overall survival rate of HNSCC's patients is about 40–50% (2), thus, illustrating the urgent need to develop novel therapeutic options to prolong the patients survival.

In the past decade, the hierarchical model of cancer stem cells (CSCs) or cancer initiating cells (CICs) has raised an intense topic in cancer biology or treatment. The CICs are a subpopulation of cancer cells with differentiation ability to maintain the bulk cells population of the tumor with heterogeneous phenotypes and to trigger tumor-initiating activity. Besides, the self-renewal ability of CICs also attributes to the cancer relapse, drug resistance and radio-resistance (3). Most of the therapeutic agents are capable of eliminating the more rapidly proliferating bulk cells, however, the CICs may lay dormant after the therapies (4). After the interruption of treatment, CICs may remerge as they are intrinsically resistant to the therapy agents or they have required mutations that confer resistance to the therapy agents (5). Previously, we have successfully enriched HN-CICs by spheroid cultivation (6), and have identified a subset of HN-CICs with low intracellular reactive oxygen species levels (ROS^{Low}) which sustain the stemness properties and tumorigenicity (7). The HN-CICs have demonstrated chemo-resistant phenotype. Interestingly, this subpopulation cells also can be enriched in cisplatin-resistance cell line (7). Thus, development of novel therapeutic agents to target HN-CICs is required, and it would benefit for future HNSCC therapy.

Arsenic Trioxide As_2O_3 (ATO) has been used in traditional Chinese medicine as pharmaceutical agents for over 2400 years (8). It has shown promising results in the treatment of hematopoietic malignancies (9, 10). In year 2000, Food and Drug Administration (11) have approved arsenic trioxide ($Trisenox^{TM}$) for treatment of acute promyelocytic leukemia (APL) (12). Studies have shown that ATO was an effective therapeutic agent in APL with 63.8 to 93% high remission rate and could prolong patients' survival rate (13). A number of studies also have revealed a pro-apoptotic activity of ATO in solid tumors, including breast cancer, gastric cancer, hepatocellular carcinomas and sarcoma (14–17). Although ATO is able to improve the disease outcome, of note, ATO also introduces to common side effects such as gastrointestinal disorders, cough, fatigue, skin rash, myelosuppression and the most burden are the liver function failure and cardiac toxicity (18). Previous studies have revealed that ATO has been correlated to many anticancer mechanisms, such as promoting tumor cell differentiation, inhibition of tumor cell growth and induce cells apoptosis. ATO also shows to reduce chemo-resistance in tumor cells via inducing the apoptosis mechanism (19). ATO has been reported to induce partial differentiation and apoptosis in APL cells (20, 21). Although ATO anti-cancer activity has utterly studied in various solid tumors such as hepatocellular carcinoma (HCC), colorectal cancer (CRC), breast cancer and gliomas, it's only effective in APL treatment and less successful in other malignancies. Clinically, high dose of ATO is required to accomplish the anti-cancer activity in solid tumors in comparison with hematological malignancies (22). Instead of attempting on ATO single treatment, researchers are looking toward the combinatorial therapeutic regimen. It has been reported that ATO enhances the therapeutic efficacy of cisplatin treatment on both oral and ovarian cancers (23, 24). ATO treatment has been carried out in HNSCC (25, 26), however the results indicating that high doses of single ATO is required to eliminate the cancer cells. Impractical high doses usage of ATO will cause strong side effects in heart and vascular toxicity. Concerning these side effects, the combination regimens of ATO treatments are applied to various cancers (27).

ATO can induce autophagy cell death in various solid tumors (28). Autophagy is referred to an intracellular degradation system in cytoplasmic components and act as cytoprotective to overcome various stress condition. The interplay of autophagy and cancer is complicate and remain controversy. There are evidences implicating that autophagy may play a role as a tumor suppressor (29), while some suggest that it may promote tumorigenesis (30). Interestingly, our previous finding shows that YMGK-1 from *Antrodia cinnamomea* successfully eliminates HN-CICs via autophagy mediated cell death (31).

In this study, we performed a combinatorial low dose ATO/cisplatin (CDDP) treatment targeting the HN-CICs as well as HNSCC cisplatin-resistant cells ($HNSCC\text{-}CisPt^{R}$). We examined the cytotoxicity effects of low dose ATO/CDDP treatment both *in vitro* and *in vivo* assays. The experimental results revealed that the combinatorial of low dose ATO/CDDP treatment has a great potential to promote cell death in HN-CICs. In addition, we further investigated the cellular mechanism underlying ATO-base therapeutic regimen induced cell death. We found that ATO/CDDP not only induced cell differentiation but also exaggerated autophagy mediated cell death. The combinatorial low dose of ATO/CDDP treatment provided a potential therapeutic application, which can efficiently eradicate the HN-CICs.

MATERIALS AND METHODS

Cell Lines Cultivation and Enrichment of HN-CICs From HNSCCs

The oral cavity HNSCC cell lines, SAS obtained from Japanese Collection Research Bioresources (Tokyo, Japan), OECM1 provided by Prof. Ching-Liang Meng of National Defense Medical College, (Taipei, Taiwan) and $SAS\text{-}CisPt^{R}$ cells were used in this study. SAS, $SAS\text{-}CisPt^{R}$ and OECM1 cells were cultured in DMEM and RPMI supplemented with 10% FBS (GIBCO, Mexico), respectively (6, 7). The enrichment of HN-CICs were performed by cultivating both cell lines in tumor sphere

condition medium consisting of serum-free DMEM/F12 medium (GIBCO, UK), N2 supplement (GIBCO, USA), 10 ng/mL human recombinant basic fibroblast growth factor (bFGF), and 10 ng/mL Epidermal Growth Factor (EGF) (PEPROTECH, USA). The cells were plated at a density of 7.5×10^4 live cells per 100 mm dishes as per experimental requirement. The cells were monitored and the medium was changed every other day until the tumor sphere cells were formed in about 4 weeks. All cells were cultured under the condition of 37°C with 5% CO_2 (6).

Western Blot

Protein extracts were prepared from cells by using RIPA buffer, and the protein concentration was measured by protein assay kit (Bio-Rad, USA). Protein extracts were denatured in sample buffer and subjected to SDS-PAGE gel electrophoresis. The electrophoretic proteins were then transferred to the nitrocellulose (NC) membrane. Nitrocellulose membranes were blocked in 5% skimmed milk and probed with primary antibodies. NC membrane were then washed and incubated with HRP-conjugated secondary anti-rabbit IgG or anti-mouse IgG at room temperature in TBST containing 5% milk for 1 h. After extensive washes in TBST, the signals were visualized by the enhanced chemiluminescence system as described by the manufacturer (Millipore, Germany) in conjunction with in LAS-4000 image analyzer (GE Healthcare, Japan). The immunoblotting signals from anti-Beta-actin (BA3R, Thermo Fisher Scientific, USA) or anti-GAPDH (GA1R, Thermo Fisher Scientific, USA) antibodies were used as a loading control.

Annexin V Apoptotic Assay

Apoptotic cells were detected with an Annexin V-FITC kit (Calbiochem, Darmstadt, Germany). 1×10^6 cells were stained with Annexin V–FITC and analyzed by FACS Calibur apparatus (Becton Dickinson, USA).

Anchorage Independent Growth Assay

Each well (35 mm) of a six-well culture dish was coated with 2 ml bottom agar (Sigma-Aldrich, USA) mixture [DMEM, 10% (v/v) FCS, 0.6% (w/v) agar]. After the bottom layer was solidified, 1 ml top agar-medium mixture [DMEM, 10% (v/v) FCS, 0.3% (w/v) agar] containing 1×10^4 cells with ATO or CDDP single treatment and ATO/CDDP combined treatment was added, and the dishes were incubated at 37°C for 15 days. The colonies were counted over five fields per well for 15 fields in triplicate experiments.

Subcutaneous Xenografts in Nude Mice

All the animal practices in this study were approved and treated in accordance with the Institutional Animal Care and Use Committee (IACUC No. 1020504) of National Yang-Ming University, Taipei, Taiwan. HN-CICs cells were subcutaneously injected into BALB/c nude mice (6–8 weeks). Tumor volume (TV) was calculated using the following formula: TV (cm^3) = (Length × Width ^{2})/2.

Inmmunohistochemistry

After deparaffinization and rehydration, the tissue sections were processed with antigen retrieval by boiling the slides in sodium citrate buffer (10 mM, pH 6.0). The slides were immersed in 3% H_2O_2 for 10 min and washed thrice with PBST. The tissue sections were then blocked with serum (Vestastain Elite ABC kit, Vector Laboratories, USA) for 30 min, followed by incubating with the primary antibody, in PBS solution at room temperature for 2 h in a container. Tissue slides were washed with PBS and incubated with biotin-labeled secondary antibody for 30 min, followed by 30 min streptavidin-horse radish peroxidase conjugates incubation. The slides were washed thrice with PBS. Subsequently, the tissue sections were immersed with AEC substrate kit as described by the manufacturer (Dako Corporation, USA) for 10 min. Hematoxylin was applied for counter-staining. Finally, the tumor sections were mounted with Gurr® (BDH Laboratory Supplies, U.K.) and examined under a microscope.

RESULTS

Combinatorial Low Dose ATO/CDDP Treatment Synergistically Promotes Cell Death in HN-CICs and Diminishes the Stemness Properties

In order to evaluate the anti-cancerous efficacy of low dose combinatorial treatment with ATO/CDDP, we performed the co-treatment on HN-CICs by combining different doses of ATO with different doses of conventional chemo-drug, CDDP. Annexin V/PI double staining was used to examine the apoptotic effects by ATO/CDDP co-treatment. The flow cytometry analyses indicated that the cell number of Annexin V/PI positive staining under the co-treatment of ATO/CDDP was substantially higher than that of HN-CICs with single treatment (**Figure 1A**). Cells treated with low dose of ATO (3 μM) in combination with 8 μM CDDP revealed strong cell death. These results indicate that low dose of combinatorial ATO/CDDP can promote cell death of HN-CICs. However, we found that co-treatment of ATO/CDDP did not cause cell death in normal human keratinocyte cells (NHOK) (**Supplementary 1**). In additional, either SAS-CICs or OECM1-CICs showed more resistant to ATO single treatment when compared with parental cell lines (data not shown). To determine the synergistic effects of the combinatorial ATO/CDDP treatment, we performed the Chou-Talalay's method analyses, and the combination index value (CI value) was calculated by using CompuSyn software. As shown in **Figure 1B** and **Table S1**, most of combinational regimens were reside on synergism sections (CI < 1). For the following experiments conducted we used the combinatorial ATO/CDDP dosages with synergism. Additionally, the protein level of stemness markers such as Nanog and Oct4 was downregulated in ATO/CDDP co-treated SAS derived HN-CICs (SAS-CICs) in comparison to that of the untreated cells or cisplatin/ATO single treated cells (**Figure 1C**). The above mentioned findings indicate that the stemness properties of SAS-CICs were abrogated after the ATO/CDDP combinatorial treatment.

ATO/CDDP Treatment Re-sensitizes the Cisplatin-Resistance Cell Line

As we have demonstrated that HN-CICs are more chemoresistant (7). Here, we would like to investigate whether combinatorial

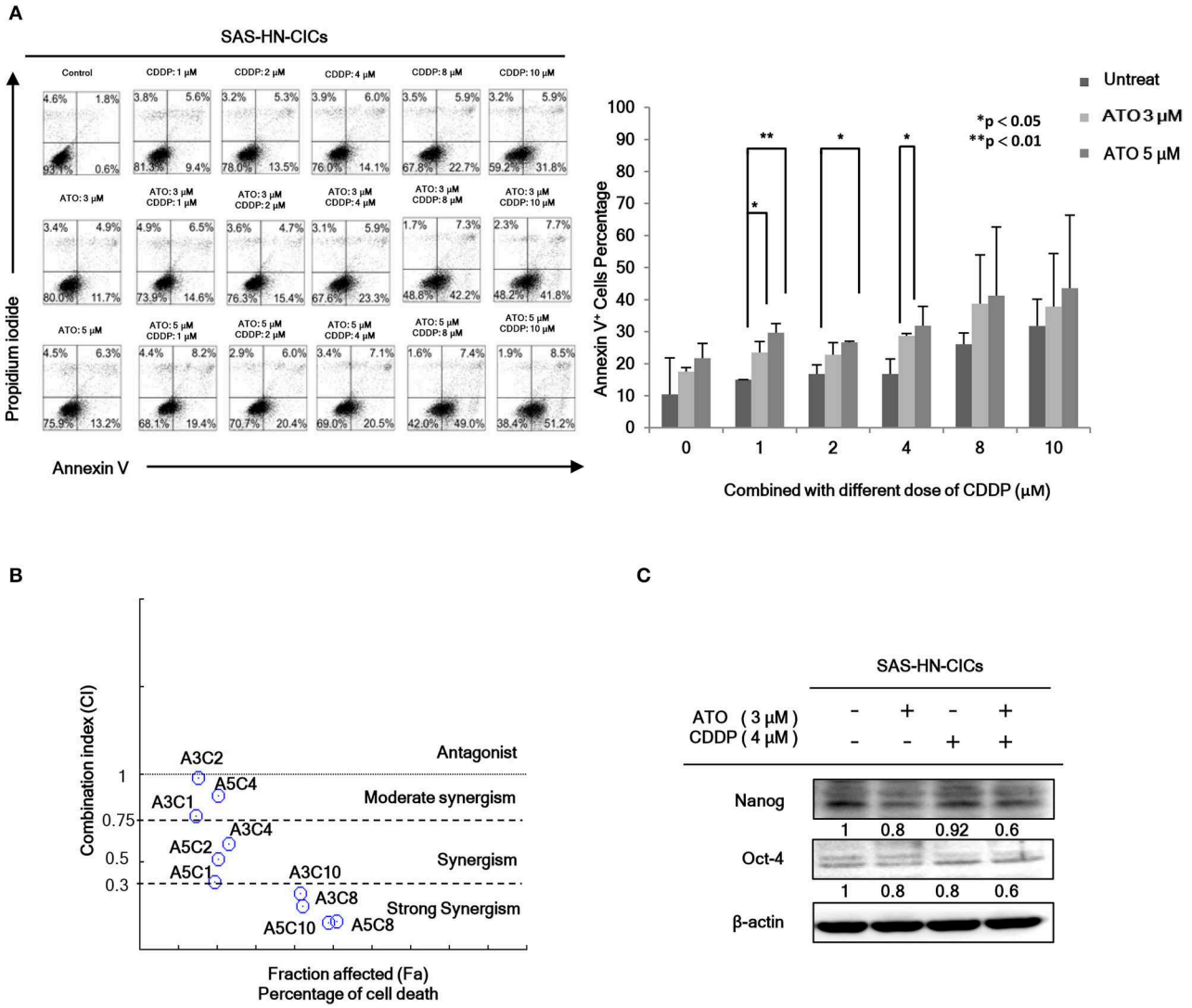

FIGURE 1 | Synergistic effect of combinatorial low dose ATO/CDDP treatment on promoting cell death and diminishing the stemness properties of HN-CICs. **(A)** HN-CICs treated with ATO/CDDP, ATO, and CDDP alone for 24 h, respectively. The cell death was examined by Annexin V/PI staining. Statistical analysis was performed by student's *t*-tests. $^{*}p < 0.05$ and $^{**}p < 0.01$. **(B)** Synergistic effect of combination ATO/CDDP on HN-CICs was calculated by using Chou–Talalay analysis. Different doses of combination ATO/CDDP treatment induced cell death of HN-CICs (percentage) and combination index (CI value), Y axis. Each point represents different doses of combination ATO/CDDP CI value. CI values were generated by using Compusyn Software, X axis indicates the effects (Fa, fractioned effected, % inhibition), and symbols represent CI values derived from actual data points (CI = 1, activity; CI > 1, antagonism; CI < 1, synergy). **(C)** Immunoblot assay to examine the expression of the stemness markers, Nanog and Oct-4, of HN-CICs after single or combined treatment of ATO (3 μM) or CDDP (4 μM) on HN-CICs for 48 h, respectively. β-actin signal was used as loading control.

low dose ATO/CDDP treatment can re-sensitize the chemo-resistant cells by co-treating the Cisplatin resistant SAS-CisPt^{R} cells (7) which possessing the HN-CICs characters with ATO/CDDP regimen. The combinatorial low dose ATO/CDDP treatment not only re-sensitized to CDDP but also induced cell death on the treated SAS-CisPt^{R} cells (**Figure 2A**). Consistent to SAS-CICs results, the stemness properties of SAS-CisPt^{R} cells were also diminished after the combined treatment with ATO/CDDP (**Figure 2B**).

ATO/CDDP Treatment Induces Autophagic Cell Death and Promotes Cell Differentiation in HN-CICs

According to our previous research, autophagy mediated cell death can be a major molecular mechanism to induce cell death in HN-CICs (31). In fact, the role of ATO in promoting cellular autophagy are reported in other cancer cell line (27). Initially, we found that the cell death numbers were increased when HN-CICs were treated with low dose ATO/CDDP through

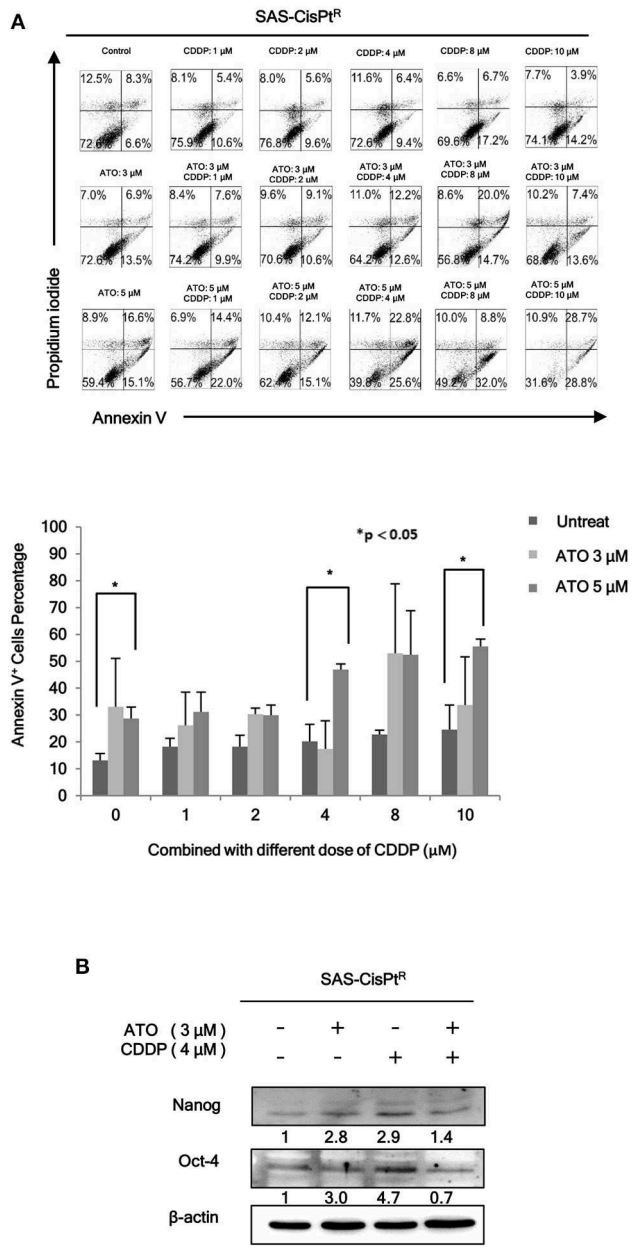

FIGURE 2 | Low dose ATO/CDDP co-treatment re-sensitizing the SAS-CisPt^R cells. **(A)** Cell death of the SAS-CisPt^R cells treated with single or combined ATO and CDDP for 24 h was examined by Annexin V/PI staining. Statistical analyses were performed by student's *t*-tests. $^*p < 0.05$. **(B)** Immunoblot analyses were used to detected the expression profile of stemness markers, Nanog and Oct-4, of SAS-CisPt^R cells after single or combined treatment of ATO (3 μM) or CDDP (4 μM), respectively. β-actin signal was used as loading control.

Annexin V/PI double staining analyses. However, this induced cell death caused by ATO/CDDP co-treatment was reversed when the autophagic cell death inhibitor, 3-Methyladenine (3-MA), was simultaneously co-treated (**Figure 3A**). Further, we determined the protein LC-3B I/II ratio, a autophagic marker, by immunoblotting assay (**Figure 3B**). ATO single treatment induced expression of autophagy marker, LC-3B-II. The expression of LC-3B-II was further elevated in cells under ATO/CDDP treatment, interestingly, addition of 3-MA also reversed the expression of LC-3B-II. Moreover, the expression of both apoptotic markers [poly (ADP ribose) polymerase (PARP1) and cleaved-caspase3] was also significantly increased, and this induction of apoptotic markers can be reversed by 3-MA co-treatment. We also observed the elevated protein level of the differentiation markers (cytokeratin 18 and involucrin) in ATO/CDDP combinatorial treated cells compared to the protein level of single treated or untreated cells (**Figure 3C**). Taken together, these results suggest that low dose of combinatorial ATO/CDDP promotes cell death by exaggerating autophagy to promote both cell apoptosis and differentiation.

Combinatorial Low Dose ATO/CDDP Suppresses the Malignancy of HN-CICs *in vitro* and *in vivo*

To further characterize the anti-cancerous effects of ATO/CDDP combined treatment in HN-CICs, we first performed anchorage independent growth assay. The colony number of the untreated cells was similar to that of the ATO or CDDP singly treated HN-CICs (**Figure 4A**). However, combined treatment with 2 or 4 μM ATO and CDDP significantly reduced the colony number (**Figure 4A**). These results indicate that low dose of ATO combined treatment with CDDP impairs malignancy and self-renewal ability of HN-CICs. To further elucidate the anti-cancerous growth effects of the combined treatment of ATO/CDDP *in vivo*, we used xenograft mouse models to analyze the attenuated tumorigeneity of HN-CICs by ATO/CDDP regimen treatment. Here, we carried out two animal models, the first one was administrated as the cancer preventive model (**Figure 4B**). To do so, the 8-week old nude mice were first subcutaneously injected with HN-CICs which were pre-treated with single or combined regimen of ATO/CDDP. The size of tumor generated from the pre-treated HN-CICs was measured continuously after cell inoculation (**Figure 4C**). We observed that HN-CICs under single treatment with ATO or CDDP did not significantly affect their tumor growth ability but delay the tumor initiating timing of HN-CICs during tumor formation. However, HN-CICs pretreated with ATO/CDDP regimen showed dramatic loss of tumor initiating ability. Secondly, we performed the cancer therapeutic model (**Figure 4D**). Nude mice were first injected with enriched HN-CICs. When mice bearing HN-CICs derived tumor, with primary tumor growing to around 0.1 cm^3, they were administrated with single ATO, CDDP or combinatorial regimen. In the therapeutic model, we found that the effect of cisplatin single treatment was similar to the placebo group on day 36 (**Figure 4E**). Additionally, ATO single treatment compared to CDDP single and placebo treatment showed an anti-cancerous effect but without the statistical significance. Unsurprisingly, we observed that the combined ATO/CDDP treatment had significant effect on inhibiting tumor growth. The above mentioned results implicate that combinatorial of low dose ATO/CDDP has a therapeutic potential on targeting

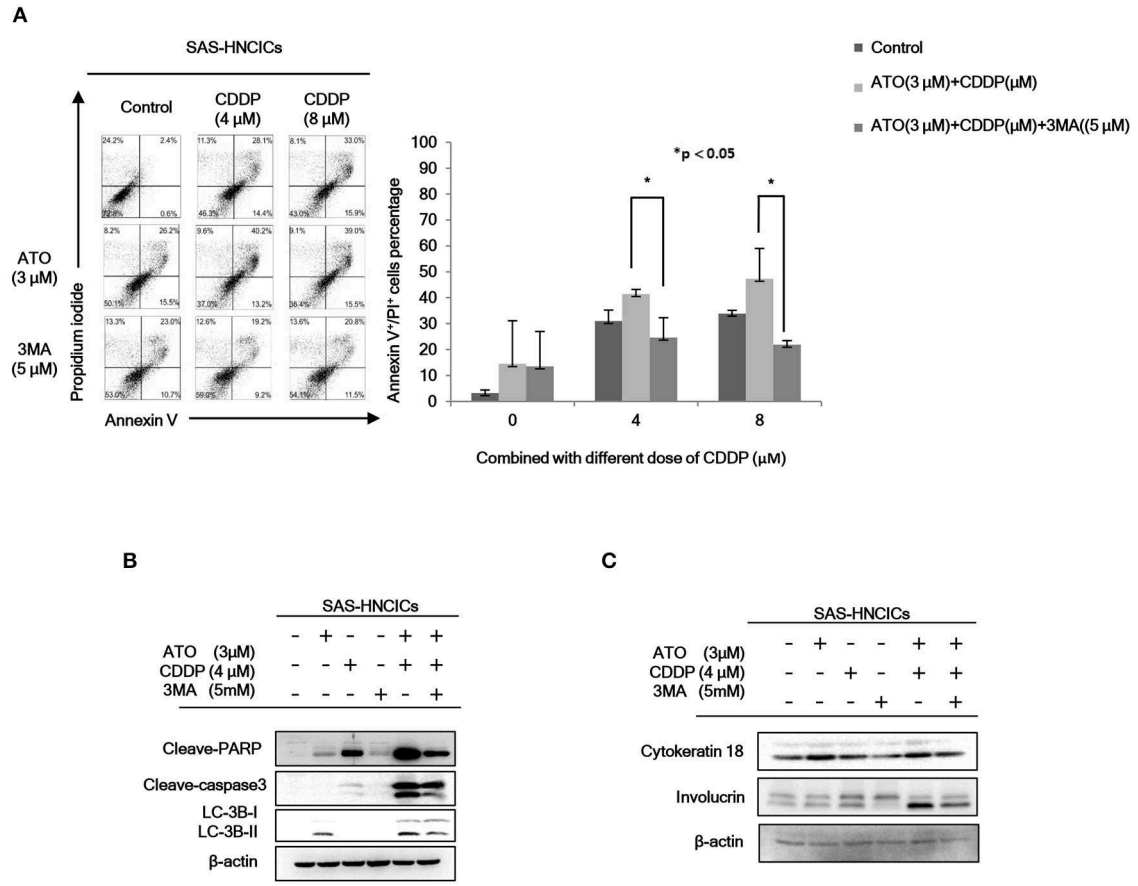

FIGURE 3 | Low dose ATO/CDDP co-treatment inducing autophagy and differentiation in HN-CICs. **(A)** SAS-CICs cells were treated with different doses of ATO, CDDP and/or 3-Methylamphetamine (3-MA) for 24 h and analyzed by annexin V/PI staining. The bar chart revealed the amount of Annexin V^+/PI^+ cells. **(B)** Immunoblot analyses indicated expression of autophagy related markers such as PARP, cleaved caspase3 and LC3B. **(C)** SAS-CICs cells were treated with single or combined treatment of ATO (3 μM), CDDP (4 μM), and/or 3-MA (5 mM) for 48 h. Immunoblot analyses were used to detected the expression profile of epithelial differentiation marker such as Cytokeratin 18 and Involucrin. β-actin signal was used as loading control. Statistical analyses were performed by student's *t*-tests. $^*p < 0.05$.

HN-CICs. To further verify the cell death response to drug treatment, we performed TUNEL assay to detect the dying cells of tumor mass with drug treatment (**Figure 4F**). The TUNEL signal was highly displayed in the combined ATO/CDDP administrated tumor sections. We also observed a strong cytokeratin 18 staining, and a mild decrease of NANOG signal on IHC staining of ATO/ CDDP combined treated tumor sections (**Figure 4G**). Taken together, the results suggest that low dose of ATO/CDDP therapy is able to suppress tumor growth by inducing cell death and abolishing cancer stemness in xenografted mouse model.

The Molecular Mechanisms of ATO-Based Therapeutic Regimen Promote Cell Death in HN-CICs

According to our previous studies, dysregulation of autophagy could be the main molecular mechanism to induce the cell death in HN-CICs (31, 32). Further, we showed that ATO/CDDP treatment induced autophagic cell death and promotes cell differentiation in HN-CICs. Hence, we first examined the autophagy signaling pathway to uncover this molecular mechanism whether it is dysregulated in inducing cell death by ATO/CDDP regimen treatment. When the combination treatment applied, we observed a decrease of phospho-PI3K and phospho-mTOR in both SAS-HNCICs (**Figure 5A**) and SAS-$CisPt^R$ (**Figure 5C**) but not in OECM1-CICs by immunoblot analyses (**Figure 5B**). Additionally, the ATO/CDDP combined treatment suppressed the expression of phospho-STAT3 in SAS-CICs, OECM1-CICs, and SAS-$CisPt^R$. Interestingly, a significant elevation of p-AMPK was observed in these SAS-CICs, OECM1-CICs and SAS-$CisPt^R$ cells under ATO/CDDP treatment. Together, the dysregulation of autophagy of HN-CICs are regulated through AMPK, STAT3 signaling pathways under ATO/CDDP treatment.

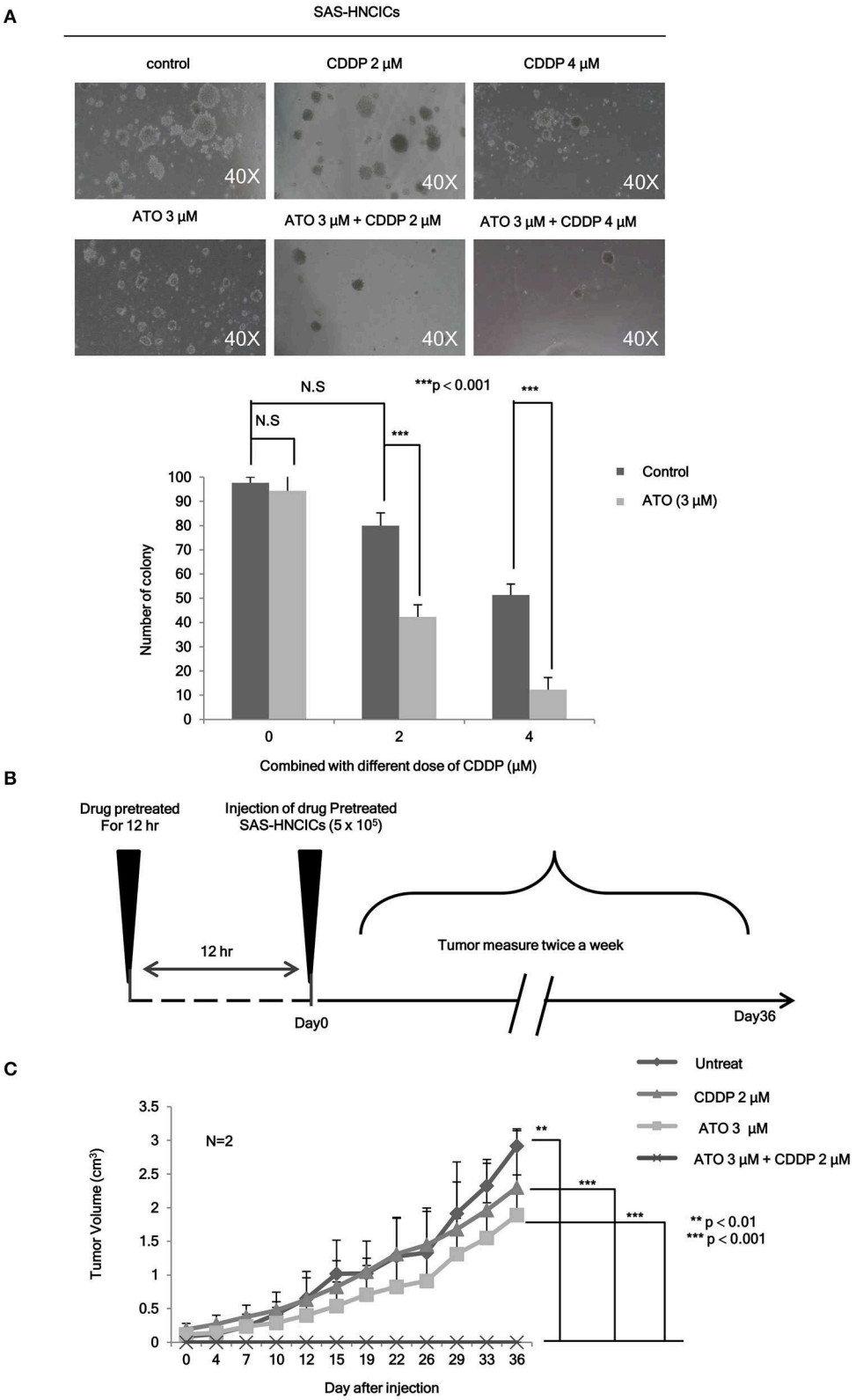

FIGURE 4 | Continued

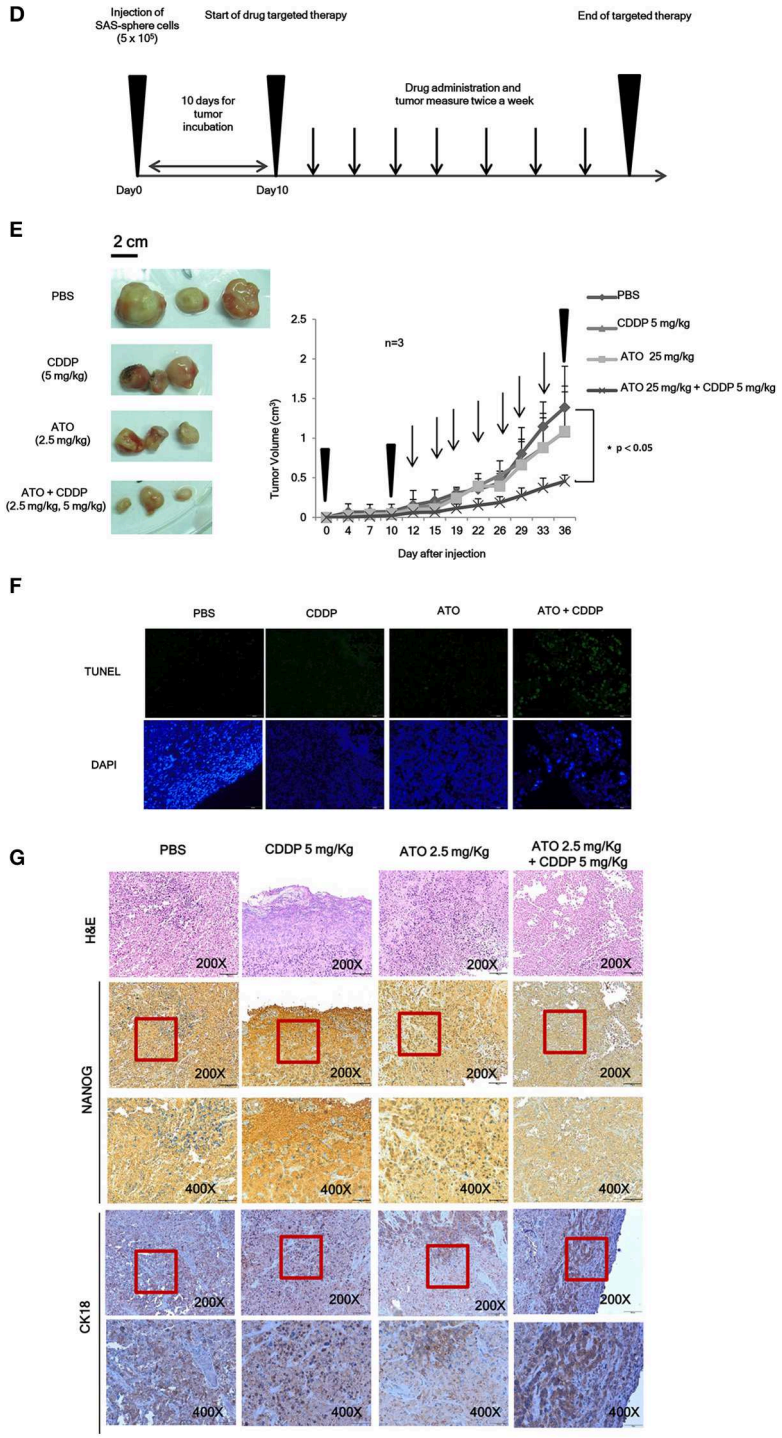

FIGURE 4 | Low dose ATO/CDDP treatment suppressing the malignancy of HN-CICs both *in vitro* and *in vivo*. **(A)** SAS-CICs cells were treated with single or combined treatment of ATO and CDDP for 12 h. The treated cells were then plated on soft agar for 15 days. The colony formation ability of the SAS-CICs cell under distinct condition was collected as shown in the representative images. The bar graphs showed the amounts of colonies with a diameter $\geq$ 100 μm over 5 fields per assay. The data are the mean ± SD from three independent experiments and analyzed by Student's *t*-test (*$p < 0.05$). **(B)** The schematic of preventive model;

(Continued)

FIGURE 4 | SAS-CICs cells were singly or combinatorically pretreated with ATO (3 μM) and of CDDP (2 μM) for 12 h. These cells were subcutaneously injected into the back of nude mice. **(C)** The tumor growth generated from the treated SAS-CICs cells was recorded and analyzed. **(D)** The schematic of therapeutic model was used to demonstrate the anti-tumorous ability of low doses ATO/CDDP regimen. SAS-CICs cells were first subcutaneously inoculated onto the back of nude mice. When the tumor size reached around 0.1 cm^3, ATO (2.5 mg/kg) and CDDP (5 mg/kg) were either singly or combinatorically intraperitoneal injected into the nude mice. PBS was used as placebo. **(E)** The mice were sacrificed on day 36, and the images of the generated tumors were collected. Tumor growth curves were also recorded and analyzed. **(F)** TUNEL assay was performed to analyze the cell death among the collected xenograft tumors. DAPI dye was used as counter staining. **(G)** Xenograft tumors generated from SAS-CICs cells treated with ATO/CDDP regimen were collected. Subsequently, immunohistochemistry staining was performed to detect the expression of stemness marker (Nanog) and differentiation marker (CK18). H&E; hematoxylin and eosin stain.

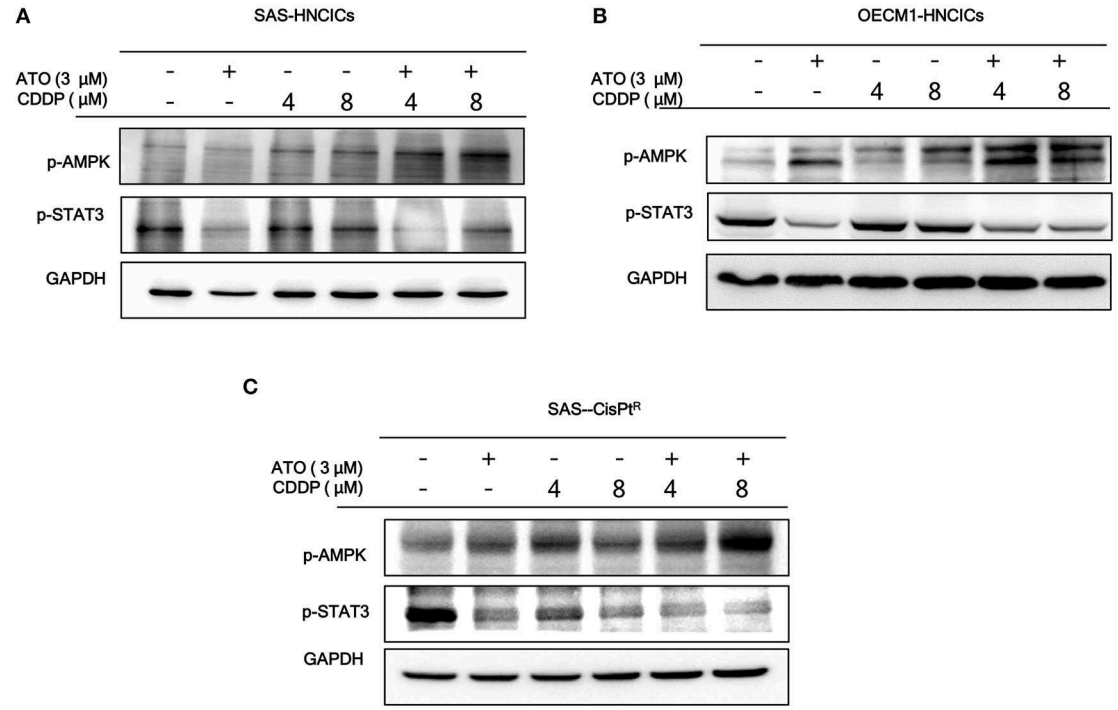

FIGURE 5 | The molecular targets of ATO/CDDP regimen. **(A)** SAS-CICs, **(B)** OECM1-CICs, and **(C)** SAS-CisPtR administrated with single or combined treatment of ATO and CDDP treated were harvested and analyzed by immunoblot assay by targeting the cancerous related molecules, p-AMPK and p-STAT3. GAPDH was used as loading control.

DISCUSSION

Arsenic trioxide is well-known of its anti-cancer activity to treat acute promyelocytic leukemia (APL) patients (33). In previous studies, 0.16 mg/kg/day ATO is administered to APL patient; the treatment course takes about 6 weeks and the dosage of ATO is nearly 6–8 μM in the plasma (34). In the conventional ATO therapy, it requires a high dose to induce the apoptotic effect. In this study, we have successfully demonstrated a low dose of combinatorial ATO/CDDP treatment synergistically induced the exaggerated autophagy mediated cell death in HN-CICs. The CI analysis indicates that the combinatorial effect of ATO/CDDP exhibits a wide range of synergism (CI < 1) in HN-CICs, ranging from 0.15 to 0.98. Further, we found that the low dose ATO (3 μM) combined with 4 μM cisplatin effectively induced apoptotic cell death in HN-CICs (**Figure 1A**). This combinational regimen also inhibited the HN-CICs self-renewal ability. Importantly, we observed the inhibitory tumorigenicity of HN-CICs in the therapeutic nude mice model *in vivo* which was administrated with low dose ATO/CDDP. Moreover, the combinatorial low doses of both ATO and CDDP in our study were effective even in the cisplatin-resistant cells.

HNSCC patients are still facing the relapse after therapy (35). This may due to the conventional treatments cannot efficiently eliminate CICs, which are involved in the tumor progression, metastasis, and chemo/radio resistance (36). Recent clinical studies showed that conventional chemotherapeutics generally affect proliferative cells, potentially eliminate proliferating cancer cells but not targeting the slow dividing cells CICs (37). CICs have exhibited quiescent slow-cycling phenotype and have been shown to be involved in tumor progression, cancer recurrence and metastasis because of their therapeutic resistance (31, 38). Thus, in this study we focused on ATO/CDDP combinatorial therapy targeting the HN-CICs. This ATO-based therapeutic regimen seems to promote the HN-CICs differentiation (**Figures 3C**, **4G**) as we observed the enhanced

expression of differentiation markers Cytokeratin 18 and Involucrin. It has been reported, ATO can diminish stemness properties in leukemia or hepatocellular carcinoma derived cancer initiating cells (39, 40). In addition, Tomuleasa et al. have reported that low concentration of ATO lead to differentiation in glioblastoma multiforme (GBM) stem-like cells (41). Cisplatin is a standard therapeutic agent of HNSCC through specifically targeting highly proliferation cells (2, 11, 42). Indeed, cumulative evidence suggested CDDP could not suppress the high stemness properties of cancer cells. Together, the combinatorial low dose ATO/CDDP regimen seems to facilitate HN-CICs differentiation into highly proliferated cells and subsequently underwent cell apoptosis.

We observed the induced autophagy when the ATO/CDDP was applied to HN-CICs. The expression of LC3 II (**Figure 3B**), a well-known marker for autophagy, was enhanced in this combinatorial treated HN-CICs. Similar results are seen in our early discovery that exaggerated induction of autophagy abolishes the stemness properties of HN-CICs, in the mean times, loss of stemness properties of HN-CICs can promote the cell differentiation ability (31). During the cancer progression and metastasis stage, autophagy emerges as a pro-tumoral role in order to eliminate the ROS-induced metabolic stress (43, 44). Intriguingly, we observed a consistency of up-regulation of p-AMPK in combinatorial treated cells. AMPK is a conserve energy-sensing kinase. AMPK is activated in response to metabolic stress and shortage of energy. Once activated, AMPK globally promotes catabolic processes. In accordance, AMPK has be linked to the regulation of autophagy (45, 46). Here, we showed that the activation of AMPK seems to increase the autophagic flux in ATO/CDDP treated cells (**Figure 5**). In this case, the excessive autophagy in these treated cells reverse the protective role of pro-tumoral but promoting the CICs to undergo autophagic cell death.

Another crucial issue of current HNSCC therapeutic is an emerging of drug resistance. This is most likely due to the existence of CICs which are resistant to chemo-drugs. Our previous publications (7, 32) have demonstrated that CDDP-resistance cells (SAS-CisPt^R) consist of highly stemness properties. The combination of ATO/CDDP regimen synergistically induced cell death in SAS-CisPt^R cells (**Figure 2A**). Although the dose used to diminish the SAS-CisPt^R cell lines was higher than the dose used in HN-CICs, the dosage is relatively lower than clinical administrated dosage. The anti-tumorous effect of the combined ATO/CDDP treatment to ovarian cancer (24) or oral squamous cell carcinoma (OSCC) (23) has been studied by others. However, the used dose of ATO/CDDP is higher than that in our current study. Furthermore, we had successfully eradicated both the HN-CICs and SAS-CisPtR cells by using low dose of ATO/CDDP regimen.

Cisplatin induced drug resistance effects are connected with mTOR signaling up-regulated (47). Our results also revealed that the treatment of ATO/CDDP in HN-CICs could reverse the cisplatin induced mTOR upregulation in SAS-CICs and OECM1-CICs (**Figure 5**). Phosphatidylinositol 3-kinase (PI3K)/mammalian target of rapamycin (mTOR) pathway is a well-known signaling for controlling cell survival through autophagy regelation. This crucial survival pathway can affect cells proliferation, angiogenesis, metabolism, and differentiation. Interesting, our result revealed that the phosphorylated PI3K expression only suppressed in SAS derived HN-CICs and SAS-CisP^R but not in OECM1-CICs under ATO/CDDP regimen treatment. This may refer to the conversed sensitivity of PI3K between SAS-CICs and OECM1-CICs. In other autophagy inhibitor study also perform different PI3K effects during their drug treatment (48). Together, the upstream of mTOR signal may not derive from PI3K in OECM1 cells. Finally, SAS-CisPt^R cells did not decrease mTOR under ATO/CDDP treatment. However, PI3K signaling is becoming more sensitive in CDDP single and ATO/CDDP combined treatment in this resistance line. This phenotype may refer to drug-resistance of SAS-CisPt^R cells. To overcome cisplatin cytotoxicity, this cell line obtained other mTOR upstream signaling to maintain cell survive but not derived fromPI3K. However, we still can successfully promote cell death in these cells via ATO/CDDP treatment (**Figure 2**). The PI3K/mTOR

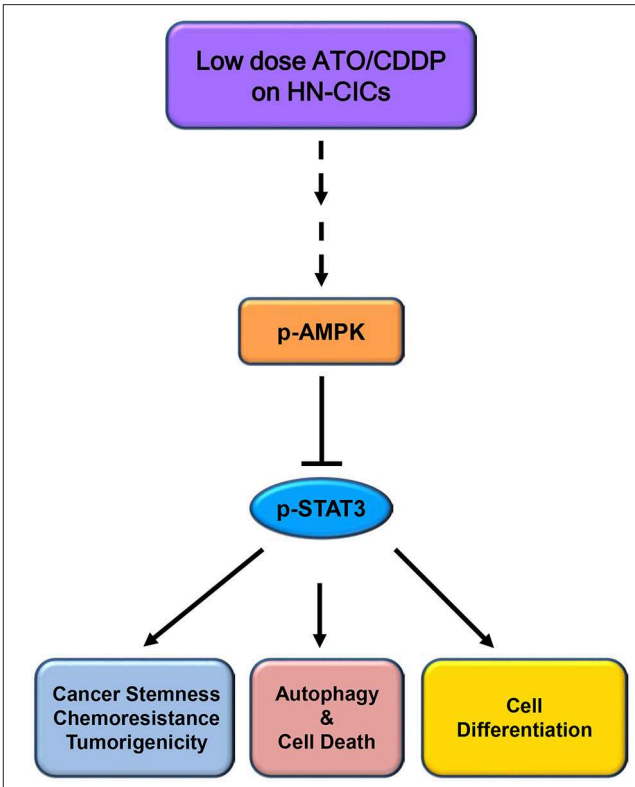

FIGURE 6 | Schematic of molecular signaling targeted by low dose ATO/CDDP regimen. Overall, the low dose ATO/CDDP regimen diminishes the stemness properties, and promotes cell differentiation in HN-CICs. Exaggerated autophagy mediated cell death is induced by the low dose ATO/CDDP regimen to inhibit the tumorigenicity of HN-CICs. Tumor suppressor AMPK expression increased may participate in this molecular mechanism regulation. However, this therapeutic regimen direct or indirect targets are still unknown; (----) refers to unknown relationship or factors.

is shown in dysregulation pathway in various cancer cells (49). Recently in glioblastoma stem-like cells research, mTOR pathway is link to the self-renewal ability and tumorigenicity of CICs. In addition, cellular key energy sensor kinase AMP activated protein (AMPK) was reported that it could promote autophagy by mTOR inactivation. In our data also suggested ATO-based therapeutic regimen can induced AMPK activity.

High concentrations of ATO can activate Jun N-terminal kinase (JNK) (50). In addition, in adipocyte study that JNK/STAT3 signaling can be suppressed by AMPK (51). In breast CICs study, STAT3 has been suggested as a specific marker, which can mediate the Nanog regulation. In our previous publication, YMGKI-2 showed to restore the chemosensitivity and promoting differentiation in CICs through targeting the Src/STAT3/c-Myc pathway (31, 32). Taken together, these evidences support that STAT3 play a critical role in HN-CICs. STAT3 signaling is constitutively activated in various cancer types (32, 52, 53). Its diverse pro-tumoral role has been widely reported. Thus, STAT3 signaling has been chosen as cancer therapeutic target. STAT3 has been proposed as CDDP sensitivity converse key factor (54). There are reports showing some potential molecules could affect the JAK-STAT3 cancerous pathway (55) to promote cell apoptosis effects. Fascinatingly, our data revealed the ATO single treatment, or ATO combined with CDDP could significantly block STAT3 activity in HN-CICs.

CONCLUSION

Overall, the low dose combinatorial treatment of ATO/CDDP provokes a synergistic cell death effect in both HN-CICs and SAS-CisPt^R cells. Although the proposed dosage is lower than the clinical dosage, it could effectively diminish the HN-CICs. Strikingly, with this low dose combinatorial ATO/CDDP, we showed either both *in vitro* and *in vivo* study, the tumorigenesis was inhibited. Finally, the ATO/CDDP treated HN-CICs and/or SAS-CisPt^R cells underwent cell differentiation, autophagy, and cell death might through the activation of p-AMPK and inhibition of STAT3 signaling pathway (**Figure 6**).

DATA AVAILABILITY STATEMENT

All datasets generated for this study are included in the article/**Supplementary Material**.

ETHICS STATEMENT

The animal study was reviewed and approved by All the experimental procedures regarding animal handling were approved by the Institutional Animal Care and Use Committee (IACUC) of the National Yang-Ming University (IACUC No. 1020504).

AUTHOR CONTRIBUTIONS

W-CH, W-HT, and J-FL: study design and manuscript drafting. W-CH and W-HT: experimental work. T-FH, T-CL, and J-FL: reviewed the manuscript and discussed results.

FUNDING

This study was supported by grants from National Yang-Ming University (108CRC-T402) and the Ministry of Science and Technology, Taiwan (MOST 108-2811-B-010-534, MOST 104-2314-B-010-047-MY3, MOST 107-2314-B-010-024-MY3, and MOST 108-2314-B-010-009-MY3).

SUPPLEMENTARY MATERIAL

The Supplementary Material for this article can be found online at: https://www.frontiersin.org/articles/10.3389/fonc.2020.00463/full#supplementary-material

REFERENCES

1. Jemal A, Bray F, Center MM, Ferlay J, Ward E, Forman D. Global cancer statistics. *CA Cancer J Clin*. (2011) 61:69–90. doi: 10.3322/caac.20107
2. Leemans CR, Braakhuis BJ, Brakenhoff RH. The molecular biology of head and neck cancer. *Nat Rev Cancer*. (2011) 11:9–22. doi: 10.1038/nrc2982
3. De Angelis ML, Francescangeli F, La Torre F, Zeuner A. Stem cell plasticity and dormancy in the development of cancer therapy resistance. *Front Oncol*. (2019) 9:626. doi: 10.3389/fonc.2019.00626
4. Baillie R, Tan ST, Itinteang T. Cancer stem cells in oral cavity squamous cell carcinoma: a review. *Front Oncol*. (2017) 7:112. doi: 10.3389/fonc.2017.00112
5. McCubrey JA, Chappell WH, Abrams SL, Franklin RA, Long JM, Sattler JA, et al. Targeting the cancer initiating cell: the Achilles' heel of cancer. *Adv Enzyme Regul*. (2011) 51:152–62. doi: 10.1016/j.advenzreg.2010.09.002
6. Chiou SH, Yu CC, Huang CY, Lin SC, Liu CJ, Tsai TH, et al. Positive correlations of Oct-4 and Nanog in oral cancer stem-like cells and high-grade oral squamous cell carcinoma. *Clin Cancer Res*. (2008) 14:4085–95. doi: 10.1158/1078-0432.CCR-07-4404
7. Chang CW, Chen YS, Chou SH, Han CL, Chen YJ, Yang CC, et al. Distinct subpopulations of head and neck cancer cells with different levels of intracellular reactive oxygen species exhibit diverse stemness, proliferation, and chemosensitivity. *Cancer Res*. (2014) 74:6291–305. doi: 10.1158/0008-5472.CAN-14-0626
8. Rao Y, Li R, Zhang D. A drug from poison: how the therapeutic effect of arsenic trioxide on acute promyelocytic leukemia was discovered. *Sci China Life Sci*. (2013) 56:495–502. doi: 10.1007/s11427-013-4487-z
9. Au WY, Li CK, Lee V, Yuen HL, Yau J, Chan GC, et al. Oral arsenic trioxide for relapsed acute promyelocytic leukemia in pediatric patients. *Pediatr Blood Cancer*. (2012) 58:630–2. doi: 10.1002/pbc.23306
10. Carney DA. Arsenic trioxide mechanisms of action–looking beyond acute promyelocytic leukemia. *Leuk Lymph*. (2008) 49:1846–51. doi: 10.1080/10428190802464745
11. Safdari Y, Khalili M, Farajnia S, Asgharzadeh M, Yazdani Y, Sadeghi M. Recent advances in head and neck squamous cell carcinoma–a review. *Clin Biochem*. (2014) 47:1195–202. doi: 10.1016/j.clinbiochem.2014.05.066
12. Lengfelder E, Hofmann WK, Nowak D. Impact of arsenic trioxide in the treatment of acute promyelocytic leukemia. *Leukemia*. (2012) 26:433–42. doi: 10.1038/leu.2011.245
13. Kitamura K, Kiyoi H, Yoshida H, Tobita T, Takeshita A, Ohno R, et al. New retinoids and arsenic compounds for the treatment of refractory acute

promyelocytic leukemia: clinical and basic studies for the next generation. *Cancer Chemother Pharmacol*. (1997) 40:S36–41.
14. Zhang YC, Zhou YQ, Yan B, Shi J, Xiu LJ, Sun YW, et al. Secondary acute promyelocytic leukemia following chemotherapy for gastric cancer: a case report. *World J Gastroenterol*. (2015) 21:4402–7. doi: 10.3748/wjg.v21.i14.4402
15. Wang Y, Wang L, Yin C, An B, Hao Y, Wei T, et al. Arsenic trioxide inhibits breast cancer cell growth via microRNA-328/hERG pathway in MCF-7 cells. *Mol Med Rep*. (2015) 12:1233–8. doi: 10.3892/mmr.2015.3558
16. Luo Q, Li Y, Lai Y, Zhang Z. The role of NF-kappaB in PARP-inhibitor-mediated sensitization and detoxification of arsenic trioxide in hepatocellular carcinoma cells. *J Toxicol Sci*. (2015) 40:349–63. doi: 10.2131/jts.40.349
17. Chiu HW, Tseng YC, Hsu YH, Lin YF, Foo NP, Guo HR, et al. Arsenic trioxide induces programmed cell death through stimulation of ER stress and inhibition of the ubiquitin-proteasome system in human sarcoma cells. *Cancer Lett*. (2015) 356(Pt. B):762–72. doi: 10.1016/j.canlet.2014.10.025
18. Soignet SL, Frankel SR, Douer D, Tallman MS, Kantarjian H, Calleja E, et al. United States multicenter study of arsenic trioxide in relapsed acute promyelocytic leukemia. *J Clin Oncol*. (2001) 19:3852–60. doi: 10.1200/JCO.2001.19.18.3852
19. Zhai B, Jiang X, He C, Zhao D, Ma L, Xu L, et al. Arsenic trioxide potentiates the anti-cancer activities of sorafenib against hepatocellular carcinoma by inhibiting Akt activation. *Tumour Biol*. (2015) 36:2323–34. doi: 10.1007/s13277-014-2839-3
20. Soignet SL, Maslak P, Wang ZG, Jhanwar S, Calleja E, Dardashti LJ, et al. Complete remission after treatment of acute promyelocytic leukemia with arsenic trioxide. *N Engl J Med*. (1998) 339:1341–8. doi: 10.1056/NEJM199811053391901
21. Gianni M, Koken MH, Chelbi-Alix MK, Benoit G, Lanotte M, Chen Z, et al. Combined arsenic and retinoic acid treatment enhances differentiation and apoptosis in arsenic-resistant NB4 cells. *Blood*. (1998) 91:4300–10.
22. Subbarayan PR, Ardalan B. In the war against solid tumors arsenic trioxide needs partners. *J Gastrointest Cancer*. (2014) 45:363–71. doi: 10.1007/s12029-014-9617-8
23. Nakaoka T, Ota A, Ono T, Karnan S, Konishi H, Furuhashi A, et al. Combined arsenic trioxide-cisplatin treatment enhances apoptosis in oral squamous cell carcinoma cells. *Cell Oncol*. (2014) 37:119–29. doi: 10.1007/s13402-014-0167-7
24. Zhang N, Wu ZM, McGowan E, Shi J, Hong ZB, Ding CW, et al. Arsenic trioxide and cisplatin synergism increase cytotoxicity in human ovarian cancer cells: therapeutic potential for ovarian cancer. *Cancer Sci*. (2009) 100:2459–64. doi: 10.1111/j.1349-7006.2009.01340.x
25. Seol JG, Park WH, Kim ES, Jung CW, Hyun JM, Kim BK, et al. Effect of arsenic trioxide on cell cycle arrest in head and neck cancer cell line PCI-1. *Biochem Biophys Res Commun*. (1999) 265:400–4. doi: 10.1006/bbrc.1999.1697
26. Kotowski U, Heiduschka G, Brunner M, Erovic BM, Martinek H, Thurnher D. Arsenic trioxide enhances the cytotoxic effect of cisplatin in head and neck squamous cell carcinoma cell lines. *Oncol Lett*. (2012) 3:1326–30. doi: 10.3892/ol.2012.643
27. Pastorek M, Gronesova P, Cholujova D, Hunakova L, Bujnakova Z, Balaz P, et al. Realgar. (As4S4) nanoparticles and arsenic trioxide. (As2O3) induced autophagy and apoptosis in human melanoma cells *in vitro*. *Neoplasma*. (2014) 61:700–9. doi: 10.4149/neo_2014_085
28. Toepfer N, Childress C, Parikh A, Rukstalis D, Yang W. Atorvastatin induces autophagy in prostate cancer PC3 cells through activation of LC3 transcription. *Cancer Biology Ther*. (2011) 12:691–9. doi: 10.4161/cbt.12.8.15978
29. Zeng X, Kinsella TJ. Impact of autophagy on chemotherapy and radiotherapy mediated tumor cytotoxicity: "To Live or not to Live". *Front Oncol*. (2011) 1:30. doi: 10.3389/fonc.2011.00030
30. Perera RM, Stoykova S, Nicolay BN, Ross KN, Fitamant J, Boukhali M, et al. Transcriptional control of autophagy–lysosome function drives pancreatic cancer metabolism. *Nature*. (2015) 524:361–5. doi: 10.1038/nature 14587
31. Chang C-W, Chen C-C, Wu M-J, Chen Y-S, Chen C-C, Sheu S-J, et al. Active component of *Antrodia cinnamomea* mycelia targeting head and neck cancer initiating cells through exaggerated autophagic cell death. *Evid Based Complement Altern Med*. (2013) 2013:946451. doi: 10.1155/2013/946451
32. Chang CW, Chen YS, Chen CC, Chan IO, Chen CC, Sheu SJ, et al. Targeting cancer initiating cells by promoting cell differentiation and restoring chemosensitivity via dual inactivation of STAT3 and src activity using an active component of antrodia cinnamomea mycelia. *Oncotarget*. (2016) 7:73016–31. doi: 10.18632/oncotarget.12194
33. Mi JQ, Chen SJ, Zhou GB, Yan XJ, Chen Z. Synergistic targeted therapy for acute promyelocytic leukaemia: a model of translational research in human cancer. *J Intern Med*. (2015) 278:627–42. doi: 10.1111/joim. 12376
34. Shen ZX, Chen GQ, Ni JH, Li XS, Xiong SM, Qiu QY, et al. Use of arsenic trioxide. (As2O3) in the treatment of acute promyelocytic leukemia (APL): II. Clinical efficacy and pharmacokinetics in relapsed patients. *Blood*. (1997) 89:3354–60.
35. Siegel RL, Miller KD, Jemal A. Cancer statistics, 2015. *CA Cancer J Clin*. (2015) 65:5–29. doi: 10.3322/caac.21254
36. Frank NY, Schatton T, Frank MH. The therapeutic promise of the cancer stem cell concept. *J Clin Invest*. (2010) 120:41–50. doi: 10.1172/JCI41004
37. Moore N, Lyle S. Quiescent, slow-cycling stem cell populations in cancer: a review of the evidence and discussion of significance. *J Oncol*. (2011) 2011:396076. doi: 10.1155/2011/3 96076
38. Koukourakis MI, Giatromanolaki A, Tsakmaki V, Danielidis V, Sivridis E. Cancer stem cell phenotype relates to radio-chemotherapy outcome in locally advanced squamous cell head-neck cancer. *Br J Cancer*. (2012) 106:846–53. doi: 10.1038/bjc.2012.33
39. Ito K, Bernardi R, Morotti A, Matsuoka S, Saglio G, Ikeda Y, et al. PML targeting eradicates quiescent leukaemia-initiating cells. *Nature*. (2008) 453:1072–8. doi: 10.1038/nature 07016
40. Li L, Liu Y, Guo Y, Liu B, Zhao Y, Li P, et al. Regulatory MiR-148a-ACVR1/BMP circuit defines a cancer stem cell-like aggressive subtype of hepatocellular carcinoma. *Hepatology*. (2015) 61:574–84. doi: 10.1002/hep.27543
41. Tomuleasa C, Soritau O, Kacso G, Fischer-Fodor E, Cocis A, Ioani H, et al. Arsenic trioxide sensitizes cancer stem cells to chemoradiotherapy. A new approach in the treatment of inoperable glioblastoma multiforme. *J BUON*. (2010) 15:758–62.
42. Li H, Zhu X, Zhang Y, Xiang J, Chen H. Arsenic trioxide exerts synergistic effects with cisplatin on non-small cell lung cancer cells via apoptosis induction. *J Exp Clin Cancer Res*. (2009) 28:110. doi: 10.1186/1756-9966-28-110
43. Guo JY, Chen H-Y, Mathew R, Fan J, Strohecker AM, Karsli-Uzunbas G, et al. Activated Ras requires autophagy to maintain oxidative metabolism and tumorigenesis. *Genes Dev*. (2011) 25:460–70. doi: 10.1101/gad.2016311
44. Guo JY, Karsli-Uzunbas G, Mathew R, Aisner SC, Kamphorst JJ, Strohecker AM, et al. Autophagy suppresses progression of K-ras-induced lung tumors to oncocytomas and maintains lipid homeostasis. *Genes Dev*. (2013) 27:1447–61. doi: 10.1101/gad.219642.113
45. Luo Z, Zang M, Guo W. AMPK as a metabolic tumor suppressor: control of metabolism and cell growth. *Fut Oncol*. (2010) 6:457–70. doi: 10.2217/fon.09.174
46. Sanli T, Steinberg GR, Singh G, Tsakiridis T. AMP-activated protein kinase (AMPK) beyond metabolism: a novel genomic stress sensor participating in the DNA damage response pathway. *Cancer Biol Ther*. (2014) 15:156–69. doi: 10.4161/cbt.26726
47. Yang H, Gao Y, Fan X, Liu X, Peng L, Ci X. Oridonin sensitizes cisplatin-induced apoptosis via AMPK/Akt/mTOR-dependent autophagosome accumulation in A549 cells. *Front Oncol*. (2019) 9:769. doi: 10.3389/fonc.2019.00769
48. Cheng MF, Lin SR, Tseng FJ, Huang YC, Tsai MJ, Fu YS, et al. The autophagic inhibition oral squamous cell carcinoma cancer growth of 16-hydroxy-cleroda-3,14-dine-15,16-olide. *Oncotarget*. (2017) 8:78379–96. doi: 10.18632/oncotarget. 18987
49. Zhou J, Wulfkuhle J, Zhang H, Gu P, Yang Y, Deng J, et al. Activation of the PTEN/mTOR/STAT3 pathway in breast cancer stem-like cells is required for viability and maintenance. *Proc Natl Acad Sci USA*. (2007) 104:16 158–63. doi: 10.1073/pnas.0702596104

50. Wen J, Cheng HY, Feng Y, Rice L, Liu S, Mo A, et al. P38 MAPK inhibition enhancing ATO-induced cytotoxicity against multiple myeloma cells. *Br J Haematol*. (2008) 140:169–80. doi: 10.1111/j.1365-2141.2007.06895.x
51. Mancini SJ, White AD, Bijland S, Rutherford C, Graham D, Richter EA, et al. Activation of AMP-activated protein kinase rapidly suppresses multiple pro-inflammatory pathways in adipocytes including IL-1 receptor-associated kinase-4 phosphorylation. *Mol Cell Endocrinol*. (2017) 440:44–56. doi: 10.1016/j.mce.2016.11.010
52. Chang L, Gong F, Cai H, Li Z, Cui Y. Combined RNAi targeting human Stat3 and ADAM9 as gene therapy for non-small cell lung cancer. *Oncol Lett*. (2016) 11:1242–50. doi: 10.3892/ol.2015.4018
53. Zheng M, Cao MX, Yu XH, Li L, Wang K, Wang SS, et al. STAT3 Promotes invasion and aerobic glycolysis of human oral squamous cell carcinoma via inhibiting FoxO1. *Front Oncol*. (2019) 9:1175. doi: 10.3389/fonc.2019.01175
54. Fang L, Gao L, Xie L, Xiao G. GC7 enhances cisplatin sensitivity via STAT3 signaling pathway inhibition and eIF5A2 inactivation in mesenchymal phenotype oral cancer cells. *Oncol Rep*. (2018) 39:1283–91. doi: 10.3892/or.2017.6161
55. Luo F, Xu Y, Ling M, Zhao Y, Xu W, Liang X, et al. Arsenite evokes IL-6 secretion, autocrine regulation of STAT3 signaling, and miR-21 expression, processes involved in the EMT and malignant transformation of human bronchial epithelial cells. *Toxicol Appl Pharmacol*. (2013) 273:27–34. doi: 10.1016/j.taap.2013.08.025

Conflict of Interest: The authors declare that the research was conducted in the absence of any commercial or financial relationships that could be construed as a potential conflict of interest.

frontiers in Oncology

ORIGINAL RESEARCH
published: 30 April 2020
doi: 10.3389/fonc.2020.00683

Amplification of 3q26.2, 5q14.3, 8q24.3, 8q22.3, and 14q32.33 Are Possible Common Genetic Alterations in Oral Cancer Patients

Melvin A. Ambele[1,2]*, *Andre van Zyl*[3], *Michael S. Pepper*[2], *Marlene B. van Heerden*[1] and *Willie F. P. van Heerden*[1]

[1] Department of Oral Pathology and Oral Biology, Faculty of Health Sciences, School of Dentistry, University of Pretoria, Pretoria, South Africa, [2] Department of Immunology, and SAMRC Extramural Unit for Stem Cell Research and Therapy, Faculty of Health Sciences, Institute for Cellular and Molecular Medicine, University of Pretoria, Pretoria, South Africa, [3] Specialist in Oral Medicine and Periodontics, Private Practice, Stellenbosch, South Africa

The lack of clinical biomarkers for head and neck cancer subtypes limits early diagnosis and monitoring of disease progression. This study investigates genetic alterations in clinically identical tumor, tumor-adjacent dysplastic epithelium (TADE) and normal epithelium (NE) in five oral cancer patients to identify differences and commonalities between oral cancer, TADE and NE. A VELscope®Vx device was used to identify TADE and NE surrounding a clinical tumor for analysis of genetic alterations using the OncoScan® assay. One of the tumor samples examined was an "M" class tumor with a high confidence *BRAF*:p.G469A:c.1406G>C somatic mutation, which is the first to be reported in oral cancer. Another tumor showed mosaicism in genetic alterations, indicating the presence of multiple clones. Overall, each patient's tumor, TADE and NE showed a distinct genetic profile which indicates intertumoral clonal/genetic diversity. Interestingly, four tumors showed gain of 3q26.2, 5q14.3, 8q24.3, 8q22.3, 14q32.33 and loss/LOH in 9p21.3 while all TADE had LOH on 22q11.23. In addition, some genetic alterations progressed from NE through TADE into tumor in individual patients. Furthermore, no molecular event was identified that is common to all NE and/or TADE that progressed into tumor. This pilot study demonstrates the presence of genetic heterogeneity in oral tumorigenesis, and suggests that there might exist some common genetic alterations between tumors and TADE. However, this observation would need to be further investigated and validated in a larger cohort of oral cancer patients for its potential role in oral tumorigenesis.

Keywords: oral squamous cell carcinomas, head and neck cancer, genomic heterogeneity, intratumor clonal heterogeneity, intertumoral clonal diversity, OncoScan® FFPE assay, VELscope®Vx device

OPEN ACCESS

Edited by:
Victor C. Kok,
Asia University, Taiwan

Reviewed by:
Anu R. I.,
MVR Cancer Centre and Research Institute, India
Shu-Chun Lin,
National Yang-Ming University, Taiwan

***Correspondence:**
Melvin A. Ambele
melvin.ambele@up.ac.za

Specialty section:
This article was submitted to Head and Neck Cancer, a section of the journal Frontiers in Oncology

Received: *04 October 2019*
Accepted: *14 April 2020*
Published: *30 April 2020*

Citation:
Ambele MA, van Zyl A, Pepper MS, van Heerden MB and van Heerden WFP (2020) Amplification of 3q26.2, 5q14.3, 8q24.3, 8q22.3, and 14q32.33 Are Possible Common Genetic Alterations in Oral Cancer Patients. Front. Oncol. 10:683. doi: 10.3389/fonc.2020.00683

INTRODUCTION

The Globocan 2018 statistics reported 887,659 new cases of head and neck cancer (lip & oral cavity; 354,864, salivary gland; 52,799, oropharynx; 92,887, nasopharynx; 129,079, hypopharynx; 80,608 and larynx; 177,422 cases) with 453,307 deaths worldwide (http://gco.iarc.fr/today/fact-sheets-cancers). Significant genomic instability and resultant clonal diversity are hallmark characteristics

of head and neck squamous cell carcinoma (HNSCC). Heterogeneity in phenotype, etiology, biology and clinical presentation are common features of HNSCC, and this may account for the dismal 5-year survival rates which are as low as 50% in all patients, despite treatment. Except for tumor human papilloma virus (HPV) status, the molecular risk factors investigated in HNSCC have yielded limited clinical utility. Risk stratification for HNSCC is based largely on the tumor anatomical site, stage and histological characteristics (1). Of interest is oral squamous cell carcinoma (OSCC) that develops through a multistep process involving the accumulation of multiple genetic mutations. This process is influenced both by genetic predisposition and environmental risk factors such as tobacco, alcohol, and HPV infection (2). Differences in tumor evolution and progression as well as resistance to therapy in oral cancer can be attributed to intratumoral clonal heterogeneity and intertumoralal clonal diversity, which are seen in clinical cases of oral cancer and other cancers of the head and neck region (1, 3–6). Understanding the molecular mechanisms of clonal heterogeneity within a tumor and clonal diversity between tumors may lead to better treatment outcomes in affected patients.

Field cancerization is to date the most acceptable molecular progression model for OSCC development. The model was proposed by Slaughter et al. and linked the presence of dysplastic changes in tumor-adjacent epithelium of oral cancer specimens with local recurrence and multifocal areas of cancer development process in many cells as a result of exposure to a carcinogen such as tobacco (7). A previous study in our group has also demonstrated this concept of field cancerization in OSCC with heterozygosity in p16 expression (8). Genetic alterations, mainly loss of heterozygosity (LOH) or deletion in chromosomal regions 9p (*CDKN2A*) (2, 9), 3p (*FHIT* & *RSSFIA*) (10, 11), and 17p (*TP53*) (2) have been observed in relatively high proportions of dysplastic lesions and are considered early events in oral carcinogenesis. Losses at 13q and 8p are observed more frequently in carcinomas than in dysplasia, and are associated with late stages of oral carcinogenesis (2, 12).

Inactivation of tumor suppressor genes (TSGs) by loss of heterozygosity (LOH) or deletion and/or the activation of oncogenes by gene amplification are the two major types of genetic alterations most often associated with OSCC tumorigenesis (1, 12, 13). In this study, a VELscope®Vx Handpiece (LED Dental Inc, Canada) was used to identify tumor-adjacent dysplastic epithelium (TADE) and normal epithelium (NE) surrounding a clinically detected cancer. The Affymetrix OncoScan® FFPE assay was then used to investigate the genetic alterations in these specimens with the aim of identifying common molecular events in all tumor, TADE and NE samples. Significant findings could be further explored in a larger cohort of oral cancer patients for their potential role in early to late stages of oral tumorigenesis.

MATERIALS AND METHODS

Clinical Diagnosis of Oral Cancer Patients

Patients with OSSC were referred to the Pretoria Oral and Dental Hospital. Each patient was seen in a specialist clinic where the primary lesion was identified, and a scalpel biopsy was done for histological confirmation of the OSSC. Written informed consent was obtained from all five patients and the study was approved by the Faculty of Health Sciences Research Ethics Committee (Reference number 44/2010).

VELscope® Screening of Oral Cancer Patients and Tissue Collection

The VELscope®Vx Handpiece (LED Dental Inc, Canada) is a portable device with a 40–460 nm light source that has been shown to be effective at identifying lesions at risk of developing cancer in clinically normal mucosa (14). This device has a sensitivity of 98% and a specificity of 100% for identification of oral dysplasia and cancer (15). VELscope® is a diagnostic aid that when applied, results in pale green autofluorescence of normal mucosa and shows loss of fluorescence with abnormal tissue. This fluorescence is viewed through the narrow-band filter built into the eyepiece (16). It has also been shown to be effective at identifying lesions at risk of developing cancer in clinically normal mucosa as seen under normal light (14). One study showed that VELscope® is able to identify LOH at 3p and 9p in mucosa surrounding a clinically detected cancer, with margins as wide as 25 mm (17). Hence, each patient received a comprehensive intra-oral clinical examination with the use of the VELscope® to identify TADE and NE sites (**Figure 1**) for tissue sampling.

DNA Extraction, Quantification, and OncoScan® FFPE Assay

Formalin fixed paraffin embedded (FFPE) specimens of tumor, TADE and NE were prepared from hemi-glossectomy specimens (**Figure 2**) with different histological classification (**Figure 3**). Genomic DNA (gDNA) was extracted from each FFPE sample (tumor, TADE and NE) using the QIAamp DNA FFPE Tissue kit (QIAGEN GmbH, Hilden, Germany) according to the manufacturer's protocol. DNA was quantified using a Quant-iT™ PicoGreen® dsDNA Assay Kit (Life Technologies) following the manufacturer's recommended protocol. Eighty nanogram gDNA was prepared for each sample and run on the Affymetrix OncoScan® FFPE assay kit (Affymetrix; Thermo Fisher Scientific company) according to the manufacturers' instructions (18). The Affymetrix OncoScan® FFPE assay is a molecular analytical tool that works efficiently on formalin-fixed paraffin-embedded (FFPE) samples. It provides a comprehensive coverage of whole genome copy number alterations, LOH and somatic mutations of genes that have been implicated in cancer and tumor progression by utilizing the molecular inversion Probe (MIP) technology (18). Briefly, to each 80 ng of gDNA sample, copy number variation and somatic mutations MIP mixes was added followed by denaturation for 5 min at 95°C and an overnight annealing for 17 h at 58°C. The product of each sample was split into two wells to which dATP (A) and dTTP (T) (A/T) was added into one well while dGTP (G) and dCTP (C) (G/C) was added to the other well to perform a gap fill reaction according to the manufacture's manual. A cocktail of exonucleases supplied with the OncoScan® kit was used to digest gDNA and uncircularized MIP. Cleavage enzymes supplied with the OncoScan® kit

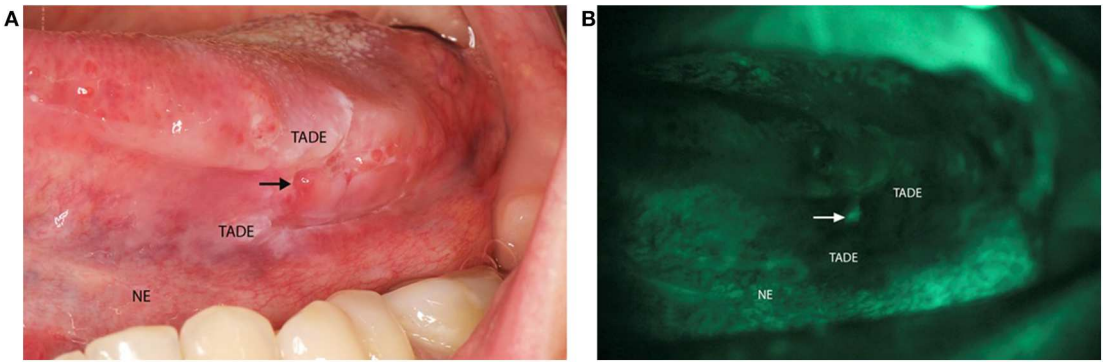

FIGURE 1 | Clinical photo of VELscope® oral cancer screening of a patient. **(A)** Image of a patient with a squamous cell carcinoma on the left side of the tongue presenting as an ulcer (arrow). The tumor adjacent dysplastic epithelium (TADE) that showed loss of fluorescence with the VELscope® is present around the ulcer with the distant clinical normal epithelium (NE) that did not show loss of fluorescence. **(B)** Photograph of the VELscope® analysis showing the ulcer (arrow) with surrounding TADE with loss of autofluorescence and NE showing normal autofluorescence. (Number of patients screened = 5).

were then used to linearize the circular MIP that had been gap filled by A/T or G/C nucleotides followed by a PCR amplification. A second round of PCR amplification was then performed using Haeii enzyme supplied with the OncoScan® kit to cleave amplicons from the previous PCR reaction. The cleaved fragments were then hybridized onto the OncoScan® assay array overnight for 17 h according the manufacturer's protocol. The arrays were then washed and stained using the Affymetrix GeneChip® Fluidics Station 450 and scanned on the Affymetrix GeneChip® Scanner 3000 7G. Each scanned array generates array images known as a DAT file that were automatically converted into fluorescence intensity (CEL) files by the Affymetrix® GeneChip® Command Console® (AGCC) software version 4. CEL files were imported onto the Affymetrix OncoScan™ Console software version 1.3 and processed to generate OSCHP files which were analyzed using Chromosome Analysis Suite (ChAS) for copy number alterations (CNAs) and LOH in approximately 900 cancer genes as well as for 74 clinically actionable somatic mutations in nine cancer genes (*BRAF*, *EGFR*, *IDH1*, *IDH2*, *KRAS*, *NRAS*, *PIK3CA*, *PTEN*, and *TP53*) (18).

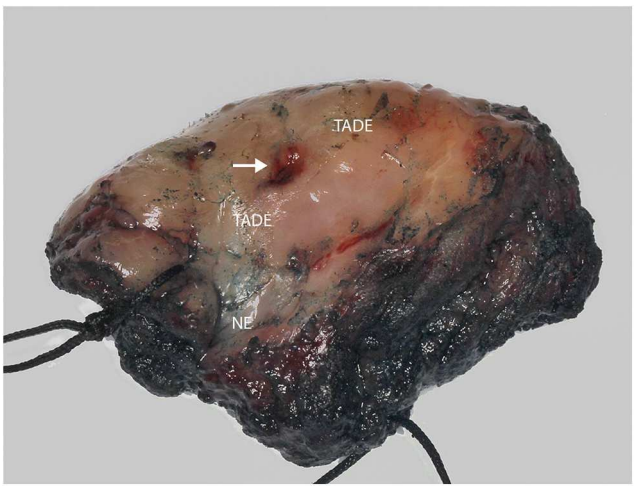

FIGURE 2 | Photograph of hemi-glossectomy specimen. Image showing the carcinoma (arrow) as well as the TADE and NE areas (as determined previously using the VELscope®, number of patients screened = 5).

RESULTS

Sample Size and Classification

Fifteen clinical specimens consisting of 5 tumors, 5 TADE and 5 distant NE from five oral cancer patients were examined in this pilot study for genetic changes such as copy number alterations (CNAs), loss of heterozygosity (LOH) and other somatic mutations (SMs). Of the five tumor samples, four were characterized by high CNAs (referred to as C class tumors) and showed a progressive development of genomic instability characterized by LOH and CNAs from NE through TADE to tumor. One patient's tumor was characterized by a high confidence somatic mutation with few CNAs (referred to as an M class tumor) (19) when compared to the TADE and NE in the same patient.

Genetic Alterations Reveal Both Intratumoral Clonal Heterogeneity and Intertumoral Clonal Diversity

Tumor 1 showed a characteristic HNSCC mutation profile including the amplification of 3q26/28 (*TP63*, *SOX2*, *PIK3CA*), *FGFR1*, 11q13 (*CCND1*, *FADD*, *CTTN*), *E2F1*, *PTK2*, loss of *NSD1* and LOH in *CDKN2A* and *TP53* (20). The TADE and NE showed mutations in certain chromosomal regions that do not contain any of the well described HNSCC associated gene mutations. However, some observed molecular events such as the size of a Cn-LOH on 5q14.3 in NE, increased in TADE and changed to a CNL-LOH in the tumor. Also, Cn-LOH on 16q21 in NE and TADE changed to a CNL-LOH in the tumor. Extensive functional studies would be important to validate the significance of these two events in the development and progression of this tumor.

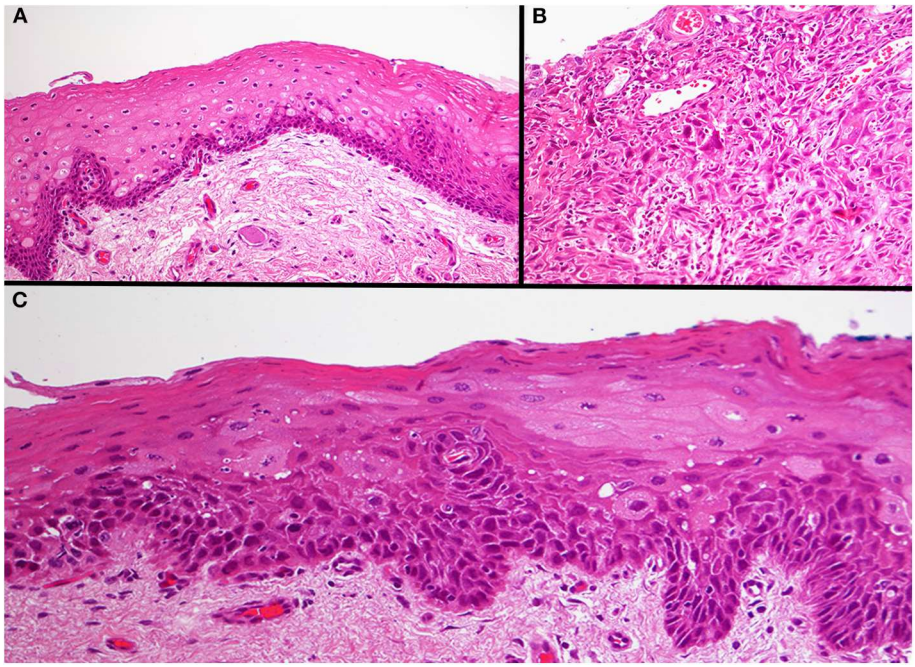

FIGURE 3 | Photomicrograph of the three different areas. Histology of the normal epithelium showing basal cell hyperplasia with no atypia **(A)**. The base of the tumor ulcer consisted of a poorly differentiated squamous cell carcinoma **(B)**. The tumor adjacent dysplastic epithelium (TADE) that showed loss of fluorescence with the VELscope® showed the presence of moderate epithelial dysplasia **(C)**. Original magnification X200.

Tumor 2 is an "M" class tumor (tumor driven by mutation rather than CNAs) typified by a high confidence *BRAF*:p.G469A:c.1406G>C somatic mutation with less genomic instability compared to the TADE and NE. This somatic mutation resulted from the substitution of glycine (G) by alanine (A) at position 469 in *BRAF*. This mutation has been reported in non-small-cell lung cancer (21–23) and in colorectal cancer (24) but not in oral cancer. Loss in *FHIT* and *RB1* were the only well described HNSCC associated mutations (25) detected in TADE and which were absent from both the tumor and NE, suggesting this TADE is an independent clone and not related to the tumor. Interestingly, the size of a loss on 3p26.3 in NE that increased in this TADE would be important to investigate further for possible role in early genetic event in the NE, since a loss in this region has been suggested to be an independent prognostic factor in OSCC patients (26, 27).

Tumor 3 showed mosaicism in CNAs which is indicative of a highly heterogenous tumor with multiple clones. This tumor showed mosaicism in the amplification of *TP63*, *PIK3CA*, *SOX2*, *FADD*, *CTTN*, *CCND1*, *NOTCH1*, *E2F1*, *HRAS*, *BIRC2*, *EGFR*, *MYC*, *PTK2*, loss in *FHIT* and *CDKN2A*, and LOH in *NSD1*, *FAT1* and *APC*. All these mutations constitute a combination of distinct mutation profiles for various molecular sub-types of HNSCC of different etiology (1, 13, 25). Genetic alterations in TADE and NE did not involve any well described HNSCC associated mutations.

Tumor 4 showed amplification of *PIKC3A*, *SOX2*, *TP63*, *EGFR*, *PTK2*, *NOTCH 1, 2 & 3*, *AJUBA*, *TRAF3*, *ERBB2*, *MYC,* and *KMT2D*, loss of *CDKN2A*, *FAT1*, *APC*, *RB1*, *KLK12*, *SMAD4*, and *PTEN*, and LOH of *FHIT*, *CDKN2A*, *CASP8*, *TP53* and *NFE2L2*, which have all been reported in HNSCC (1, 13). TADE and NE had no detectable HNSCC associated mutations. However, the size of a LOH at 3p21.31 in NE and TADE increased in the tumor. In addition, the size of a homozygous deletion of 19p13.2 in NE and TADE that increased in the tumor; this warrants further investigation as it may have played a role in oral cancer development and progression in this patient.

Tumor 5 had a high confidence *PIK3CA*:p.H1047R:c.3140A>G somatic mutation resulting from the substitution of histidine (H) by arginine (R) at position 1047 of the *PIK3CA* gene. This somatic mutation has previously been detected in HNSCC patients (28). This tumor also showed additional mutations such as amplification of *TP63*, *SOX2*, *PIK3CA*, *FADD*, *CTTN*, *CCND1*, *EGFR*, *FGFR1*, *CASP8*, *SMAD4*, *TP53*, *NFE2L2*, *NOTCH1, 2,& 3*, *MYC*, *PTK2*, *AJUBA*, *TRAF3*, *ERBB2*, *NRAS*, *KRAS*, *HRAS*, *FAT1*, *KEAP1*, *E2F1,* and *SMAD2*, loss of *RASSF1*, *FHIT*, *CDKN2A*, *KMT2D*, *RB1*, *APC*, *CSMD1*, *PTPRD*, *MET*, *CUL3*, and *NSD1* and a LOH of *TP53*, *NOTCH1*, *APC*, *RB1*, *CSMD1*, *PTPRD*, *CUL3*, *NSD1*, *CDKN2A*, *FHIT,* and *RASSF1*, which have been reported in HNCSS (1, 13, 25). Mutations detected in TADE and NE were not those that have been well described to be associated with HNSCC.

Identification of Molecular Events Common to Histologically Identical Samples From all Patients

We examined the mutation profile of the three groups of histologically identical sample types (tumor, TADE, and NE)

from all five patients in an attempt to identify genetic alterations that are unique to each sample in the different groups (inter-patient heterogeneity) as well as those that are common to all samples in each group, which could potentially be explored in a larger cohort study of oral cancer patients for their clinical significance.

Tumor

With the exception of tumor 2, all tumor samples showed characteristic mutations of HNSCC including amplification of 3q26.2 (*TP63*, *SOX2*, *PIK3CA*) (1), 5q14.3 (*APC*) (13, 29, 30), 8q24.3 (*PTK2*) (25), 8q22.3 (*LRP12*) (27) as well as loss and/or LOH of 9p21.3 (*CDKN2A*) (1, 31). Other characteristic HNSCC mutations such as loss of 4q35.1 (*FAT1*) (1, 31), 5q35.2 (*NSD1*) (1, 31), LOH of 17p13.2 (*TP53*) (1, 31), and amplification of 7p11.2 (*EGFR*) (1, 31), 8q24.21 (*MYC*) (1, 25, 32) and 11q13.3 (*CCND1*, *FADD*, *CTTN*) (1) were detected in three tumors. Interestingly, we also found genetic alterations not previously described in HNSCC such as amplification of 14q32.33 (*LINC00221*) and 20q11.22 in 4 tumors, and loss and/or LOH of 5q23.2, 5q35.1 and loss of 3p24.1 (*NEK10*) in three tumors. There were many other undescribed detectable genetic alterations present in at least 3 tumor samples (**Table S1**). Despite some common molecular features of HNSCC detected in all tumor samples, the type of alteration (gain, loss or LOH) detected in some of the affected chromosomal locations and in certain HNSCC associated genes, differ from one tumor to another, thereby making each tumor genetically distinct (**Table 1**).

Tumor-Adjacent Dysplastic Epithelium (TADE)

Except for TADE 2, all TADE showed fewer CNAs compared to their respective tumor samples. The number of genetic alterations that were common to at least 3 TADE were fewer and different from those found among tumor samples (**Table 2**). Interestingly, a LOH event on 22q11.23 (*GSTTP1*, *LOC391322*, *GSTT1*, *GSTTP2*) was present in all 5 TADE. Other alterations detected in at least 3 TADE includes amplification of 1p13.3 (*GSTM2*, *GSTM1*, *GSTM5*), 14q32.33 (*LINC00221*) and LOH of 3p21.1 (*NEK4*) and 3p21.31. *NEK4* has not been reported in HNSCC tumorigenesis and this gene is known to regulate cell entry into replicative senescence as well as the response to double strand DNA damage (33). Thus, LOH of *NEK4* in OSCC should be functionally investigated further as it could be suggestive of a putative TSG in the development of dysplastic lesions in the oral mucosal. Genetic alterations of a specific type (gain, loss or LOH) in affected chromosomal locations/genes were consistent among TADE unlike in tumor samples. Notwithstanding the limited number of mutations found to be common among TADE, there were alterations that were present and/or absent in a subset of TADE thereby resulting in each patient's TADE having a unique genetic profile (**Table 2**).

Normal Epithelium (NE)

In all patients, NE had fewer CNAs compared to their respective TADE. Only two genetic alterations were common to at least two out of the five NE (**Table 3**). Surprisingly, one of the genetic events—loss and/or LOH of 3p21.3—was common in all the five NE. Inactivating mutations in this region have been a consistent finding in cancers, especially HNSCC, and have been associated with early development of dysplastic lesions in HNSCC (13, 27, 34–43). The clinical significance of this genetic event in NE is unknown and warrants further investigation.

Is There a Marker for Progression in Oral Cancer Tumorigenesis?

We examined genetic alterations present in NE and/or TADE that were also found in tumor and as such could denote progression through clonal expansion from a single progenitor clone. Such progressive genetic alterations from NE and/or TADE to tumor could be suggestive of an early marker for oral cancer development and/or progression. We could not find a single genetic event that was common to all five NE and/or TADE which progressed to tumor. This demonstrates a high level of genetic diversity among all five patients' samples. Nevertheless, the activating mutation of the novel putative oncogene *LINC00221* (14q32.33) and the inactivating mutation of the novel putative TSG *NEK4* (3p21.1) that were detected in TADE1 & 5, were retained as they progressed into their respective tumors.

DISCUSSION

Genetic heterogeneity in HNSCC has been described in tumors from various anatomical sites analyzed using different techniques (3, 5, 44). This pilot study reports analysis of the genome of tumor, TADE and NE from five patients with OSCC with the aim of identifying molecular events in tumor, TADE and NE samples, which could be explored further in a larger cohort study of oral cancer patients for their significance in oral tumorigenesis. Tumor from each patient showed a unique interpatient mutation profile. Differences in the types of genetic alterations (gain, loss and/or LOH) at the same chromosomal location and in some HNSCC associated genes observed in tumor samples are indicative of intertumoral genetic diversity. Tumor 2 showed a high confidence *BRAF*:p.G469A:c.1406G>C somatic mutation (classified as "M" class tumor), which is the first to be reported in oral cancer. This tumor sample showed less genomic instability compared to TADE and NE. "M" class tumors have previously been observed in oral cancer (1, 19). Except for tumor 2, all tumors were characterized by high CNAs classified as "C" class tumors. Tumor 3 showed mosaicism in CNAs, which is indicative of intratumoral clonal heterogeneity. Lack of uniformity in the mutational landscape of all 5 tumors suggests intertumoral clonal/genetic diversity. Except for tumor 2, all tumors showed focal deletion of 3p and amplification of 5p and 8q which contain genes not previously described to be associated with HNSCC. Furthermore, amplification of 14q32.33 (*LINC00221*) and 20q11.22 in all 4 tumors and a loss and/or LOH of 5q23.2, 5q35.1 and 3p24.1 (*NEK10*) in three tumors are interesting findings which would require more detailed functional studies to evaluate their possible role as putative oncogenes and TSGs, respectively, in these regions. *NEK10*, not previously described in HNSCC tumorigenesis, has been reported to mediate G2/M cell cycle arrest (45) and could be a potential TSG in oral cancer.

TABLE 1 | Genetic alterations on the same chromosomal location common to at least three tumors.

Chromosome cytoband start location	Types of alteration in tumor				
	Tumor 1	**Tumor 2**	**Tumor 3**	**Tumor 4**	**Tumor 5**
1q31.1	–	LOH	–	Gain	Gain
3p26.3 (26, 27)	–	–	Loss	Loss	Loss
4q31.2	–	–	Loss	Gain	Gain
4q35.1 (*FAT1*) (1, 31)	–	–	Loss	Loss	Gain
5q11.2	Loss	–	–	Loss	Loss
6p25.2	LOH	–	Gain	Gain	LOH
7p11.2 (*EGFR*) (1, 31)	–	–	Gain	Gain	Gain
9p23	LOH	Gain	Gain	Loss	LOH
11q13.3 (*CCND1*, *FADD*, *CTTN*) (1)	Gain	–	Gain	–	Gain
12q24.12 (*ALDH2*)	LOH	LOH	–	Gain	–
13q13.1	Loss	–	–	LOH	Loss
15q11.2	Gain	–	Loss	Loss	Gain
16p13.3	LOH	–	Loss	Gain	Gain
17p13.2 (*TP53*) (1, 31)	LOH	–	–	LOH	Gain + LOH
20q11.21	Gain	–	Gain	–	Gain
22q11.23 (*GSTT1*)	–	–	Gain	Gain	Gain

The same chromosomal location revealed intertumoral genetic diversity of all five tumors based on either (a) a discrepancy in the genetic alterations (gain, loss, or LOH) or (b) the presence/absence of a genetic alteration only in certain tumors.

TABLE 2 | Genetic alterations on the same chromosomal location common to at least two TADE.

Chromosome cytoband start location	Types of alteration in TADE				
	TADE 1	**TADE 2**	**TADE 3**	**TADE 4**	**TADE 5**
1p13.3 (*GSTM1*) (46)	–	Gain	–	Gain	Gain
3p21.1 (*NEK4*)	LOH	LOH	–	–	LOH
3p21.31 (*RASSF1*)	LOH	Loss	–	LOH	–
14q32.33 (*LINC00221*)	Gain	Gain	–	–	Gain
22q11.23 (*GSTT1*) (47)	LOH	LOH	Gain + LOH	LOH	Gain +LOH

All 5 TADE showed differences in genetic alteration (LOH, gain, gain + LOH, or none) at the same loci.

TABLE 3 | Genetic alterations common to at least two NE.

Chromosome cytoband start location	Types of alteration in NE				
	NE 1	**NE 2**	**NE 3**	**NE 4**	**NE 5**
3p21.3	LOH	Loss + LOH	LOH	Loss + LOH	LOH
5q23.3	–	LOH	LOH	–	–
11p11.12	LOH	–	–	–	Gain

Genetic alterations detected were mostly loss and LOH on chromosomes 3p, 5q, and 11p which could be used to distinguish between individual patient's NE.

Interestingly, TADE from all 5 patients showed inactivating mutations of 22q11.23 (*GSTTP1*, *LOC391322*, *GSTT1*, *GSTTP2*). The clinical significance of this genetic alteration in all five patients is unknown. However, given the presence of a traditional risk factor (tobacco consumption) in all patients, further studies are warranted.

Surprisingly, all five NE showed inactivating mutations of 3p21.3, known to contain TSGs or resident cancer genes. Alterations in this region are one of the most consistent genetic events reported not only in HNSCC but also in other cancer types (13, 27, 34–43). The presence of this genetic alteration in NE of all patients is therefore very surprising; could it possibly be that this particular region of the human genome is naturally very unstable? Further investigation of NE in both healthy individuals and oral cancer patients would be beneficial in understanding this genomic region and its associated genetic alterations.

CONCLUSION

Amplification of 3q26.2, 5q14.3, 8q24.3, 8q22.3, 14q32.33, 20q11.22 together with a loss/LOH on 9p21.3 was detected in four out of the five oral cancer samples, and a LOH on 22q11.23 detected in all five TADE. Furthermore, no molecular event was identified that is common to all NE and/or TADE that progressed into tumor. The small sample size limits the clinical significance of these findings. We therefore recommend further studies in a larger cohort of oral cancer patients to determine their significance in oral cancer biology.

DATA AVAILABILITY STATEMENT

The datasets generated for this study are available on request to the corresponding author.

ETHICS STATEMENT

The studies involving human participants were reviewed and approved by University of Pretoria Faculty of Health Sciences Research Ethics Committee (Reference number 44/2010). The patients/participants provided their written informed consent to participate in this study.

AUTHOR CONTRIBUTIONS

MA performed the OncoScan® assay, data analysis, interpretation, and wrote the first draft of the manuscript. AZ conceptualized the study, performed clinical examination of patients, the Velscope® screening, data interpretation, and edited the manuscript, MP contributed to the study design, data interpretation, edited the manuscript, and provided funding for the study. MH prepared FFPE specimen of all tissues, performed DNA isolation, and edited the manuscript. WH conceptualized the study, performed clinical examination of patients, data interpretation, edited the manuscript, and provided funding for the study.

FUNDING

This work was funded by the Cancer Association of South Africa (WFPvH) and the South African Medical Research Council (MSP—Flagship and Extramural Stem Cell Unit).

ACKNOWLEDGMENTS

The authors would like to thank the five oral cancer subjects that consented and participated in this study and Izak Storm at BIOCOM Africa and Jo Mcbride at the Centre for Proteomic & Genomic Research, Cape Town for their technical support with the OncoScan® assay.

SUPPLEMENTARY MATERIAL

The Supplementary Material for this article can be found online at: https://www.frontiersin.org/articles/10.3389/fonc.2020.00683/full#supplementary-material

REFERENCES

1. The Cancer Genome Atlas N, Lawrence MS, Sougnez C, Lichtenstein L, Cibulskis K, Lander E, et al. Comprehensive genomic characterization of head and neck squamous cell carcinomas. *Nature.* (2015) 517:576. doi: 10.1038/nature14129
2. Califano J, van der Riet P, Westra W, Nawroz H, Clayman G, Piantadosi S, et al. Genetic progression model for head and neck cancer: implications for field cancerization. *Cancer Res.* (1996) 56:2488–92. doi: 10.1016/S0194-5998(96)80631-0
3. Mroz EA, Rocco JW. Intra-tumor heterogeneity in head and neck cancer and its clinical implications. *World J Otorhinolaryngol Head Neck Surg.* (2016) 2:60–7. doi: 10.1016/j.wjorl.2016.05.007
4. Zhang XC, Xu C, Mitchell RM, Zhang B, Zhao D, Li Y, et al. Tumor evolution and intratumor heterogeneity of an oropharyngeal squamous cell carcinoma revealed by whole-genome sequencing. *Neoplasia.* (2013) 15:1371–8. doi: 10.1593/neo.131400
5. Sarode G, Sarode SC, Tupkari J, Patil S. Is oral squamous cell carcinoma unique in terms of intra- and inter-tumoral heterogeneity? *Transl Res Oral Oncol.* (2017) 2:2057178X17703578. doi: 10.1177/2057178X17703578
6. Klussmann JP. Head and neck cancer - new insights into a heterogeneous disease. *Oncol Res Treat.* (2017) 40:318–9. doi: 10.1159/000477255
7. Slaughter DP, Southwick HW, Smejkal W. Field cancerization in oral stratified squamous epithelium; clinical implications of multicentric origin. *Cancer.* (1953) 6:963–8. doi: 10.1002/1097-0142(195309)6:5<963::AID-CNCR2820060515>3.0.CO;2-Q
8. Ambele MA, Pepper MS, van Heerden MB, van Heerden WFP. Heterozygosity of p16 expression in an oral squamous cell carcinoma with associated loss of heterozygosity and copy number alterations. *Head Neck.* (2019) 41:E62–5. doi: 10.1002/hed.25566
9. Mao L, Lee JS, Fan YH, Ro JY, Batsakis JG, Lippman S, et al. Frequent microsatellite alterations at chromosomes 9p21 and 3p14 in oral premalignant lesions and their value in cancer risk assessment. *Nat Med.* (1996) 2:682–5. doi: 10.1038/nm0696-682
10. Masayesva BG, Ha P, Garrett-Mayer E, Pilkington T, Mao R, Pevsner J, et al. Gene expression alterations over large chromosomal regions in cancers include multiple genes unrelated to malignant progression. *Proc Natl Acad Sci USA.* (2004) 101:8715–20. doi: 10.1073/pnas.0400027101
11. Garnis C, Baldwin C, Zhang L, Rosin MP, Lam WL. Use of complete coverage array comparative genomic hybridization to define copy number alterations on chromosome 3p in oral squamous cell carcinomas. *Cancer Res.* (2003) 63:8582−5.
12. Choi S, Myers JN. Molecular pathogenesis of oral squamous cell carcinoma: implications for therapy. *J Dental Res.* (2008) 87:14–32. doi: 10.1177/154405910808700104
13. Kasamatsu A, Uzawa K, Usukura K, Koike K, Nakashima D, Ishigami T, et al. Loss of heterozygosity in oral cancer. *Oral Sci Int.* (2011) 8:37–43. doi: 10.1016/S1348-8643(11)00027-9
14. Poh CF, Ng SP, Williams PM, Zhang L, Laronde DM, Lane P, et al. Direct fluorescence visualization of clinically occult high-risk oral premalignant disease using a simple hand-held device. *Head Neck.* (2007) 29:71–6. doi: 10.1002/hed.20468
15. Lane PM, Gilhuly T, Whitehead P, Zeng H, Poh CF, Ng S, et al. Simple device for the direct visualization of oral-cavity tissue fluorescence. *J Biomed Opt.* (2006) 11:024006. doi: 10.1117/1.2193157
16. Lingen MW, Kalmar JR, Karrison T, Speight PM. Critical evaluation of diagnostic aids for the detection of oral cancer. *Oral Oncol.* (2008) 44:10–22. doi: 10.1016/j.oraloncology.2007.06.011
17. Poh CF, Zhang L, Anderson DW, Durham JS, Williams PM, Priddy RW, et al. Fluorescence visualization detection of field alterations in tumor

margins of oral cancer patients. *Clin Cancer Res.* (2006) 12:6716–22. doi: 10.1158/1078-0432.CCR-06-1317
18. Foster JM, Oumie A, Togneri FS, Vasques FR, Hau D, Taylor M, et al. Cross-laboratory validation of the OncoScan(R) FFPE Assay, a multiplex tool for whole genome tumour profiling. *BMC Med Genom.* (2015) 8:5. doi: 10.1186/s12920-015-0079-z
19. Ciriello G, Miller ML, Aksoy BA, Senbabaoglu Y, Schultz N, Sander C. Emerging landscape of oncogenic signatures across human cancers. *Nat Genet.* (2013) 45:1127–33. doi: 10.1038/ng.2762
20. Hanahan D, Weinberg RA. Hallmarks of cancer: the next generation. *Cell.* (2011) 144:646–74. doi: 10.1016/j.cell.2011.02.013
21. Cardarella S, Ogino A, Nishino M, Butaney M, Shen J, Lydon C, et al. Clinical, pathologic, and biologic features associated with BRAF mutations in non-small cell lung cancer. *Clin Cancer Res.* (2013) 19:4532–40. doi: 10.1158/1078-0432.CCR-13-0657
22. Davies H, Bignell GR, Cox C, Stephens P, Edkins S, Clegg S, et al. Mutations of the BRAF gene in human cancer. *Nature.* (2002) 417:949–54. doi: 10.1038/nature00766
23. Paik PK, Arcila ME, Fara M, Sima CS, Miller VA, Kris MG, et al. Clinical characteristics of patients with lung adenocarcinomas harboring BRAF mutations. *J Clin Oncol.* (2011) 29:2046–51. doi: 10.1200/JCO.2010.33.1280
24. Rizzo S, Bronte G, Fanale D, Corsini L, Silvestris N, Santini D, et al. Prognostic vs predictive molecular biomarkers in colorectal cancer: is KRAS and BRAF wild type status required for anti-EGFR therapy? *Cancer Treat Rev.* (2010) 36 (Suppl. 3):S56–61. doi: 10.1016/S0305-7372(10)70021-9
25. Leemans CR, Braakhuis BJ, Brakenhoff RH. The molecular biology of head and neck cancer. *Nat Rev Cancer.* (2011) 11:9–22. doi: 10.1038/nrc2982
26. Uchida K, Oga A, Nakao M, Mano T, Mihara M, Kawauchi S, et al. Loss of 3p26.3 is an independent prognostic factor in patients with oral squamous cell carcinoma. *Oncol Rep.* (2011) 26:463–9. doi: 10.3892/or.2011.1327
27. Vincent-Chong VK, Salahshourifar I, Woo KM, Anwar A, Razali R, Gudimella R, et al. Genome wide profiling in oral squamous cell carcinoma identifies a four genetic marker signature of prognostic significance. *PLoS ONE.* (2017) 12:e0174865. doi: 10.1371/journal.pone.0174865
28. Janku F, Wheler JJ, Naing A, Falchook GS, Hong DS, Stepanek VM, et al. PIK3CA mutation H1047R is associated with response to PI3K/AKT/mTOR signaling pathway inhibitors in early-phase clinical trials. *Cancer Res.* (2013) 73:276–84. doi: 10.1158/0008-5472.CAN-12-1726
29. Largey JS, Meltzer SJ, Sauk JJ, Hebert CA, Archibald DW. Loss of heterozygosity involving the APC gene in oral squamous cell carcinomas. *Oral Surg Oral Med Oral Pathol.* (1994) 77:260–3. doi: 10.1016/0030-4220(94)90295-X
30. Rivero ER, Horta MC, Silva Guerra EN, Ferraz AR, Nunes FD. Loss of heterozygosity of the APC gene in oral squamous cell carcinoma. *Pathol Res Pract.* (2008) 204:793–7. doi: 10.1016/j.prp.2008.05.003
31. Leemans CR, Snijders PJF, Brakenhoff RH. The molecular landscape of head and neck cancer. *Nat Rev Cancer.* (2018) 18:269–82. doi: 10.1038/nrc.2018.11
32. Rodrigo JP, Lazo PS, Ramos S, Alvarez I, Suarez C. MYC amplification in squamous cell carcinomas of the head and neck. *Arch Otolaryngol Head Neck Surg.* (1996) 122:504–7. doi: 10.1001/archotol.1996.01890170038008
33. Nguyen CL, Possemato R, Bauerlein EL, Xie A, Scully R, Hahn WC. Nek4 regulates entry into replicative senescence and the response to DNA damage in human fibroblasts. *Mol Cell Biol.* (2012) 32:3963–77. doi: 10.1128/MCB.00436-12
34. Ghosh S, Ghosh A, Maiti GP, Alam N, Roy A, Roy B, et al. Alterations of 3p21.31 tumor suppressor genes in head and neck squamous cell carcinoma: Correlation with progression and prognosis. *Int J Cancer.* (2008) 123:2594–604. doi: 10.1002/ijc.23834
35. Angeloni D. Molecular analysis of deletions in human chromosome 3p21 and the role of resident cancer genes in disease. *Brief Funct Genom Proteom.* (2007) 6:19–39. doi: 10.1093/bfgp/elm007
36. Marsit CJ, Hasegawa M, Hirao T, Kim DH, Aldape K, Hinds PW, et al. Loss of heterozygosity of chromosome 3p21 is associated with mutant TP53 and better patient survival in non-small-cell lung cancer. *Cancer Res.* (2004) 64:8702–7. doi: 10.1158/0008-5472.CAN-04-2558
37. Wang K, Ling T, Wu H, Zhang J. Screening of candidate tumor-suppressor genes in 3p21.3 and investigation of the methylation of gene promoters in oral squamous cell carcinoma. *Oncol Rep.* (2013) 29:1175–82. doi: 10.3892/or.2012.2213
38. Dasgupta S, Chakraborty SB, Roy A, Roychowdhury S, Panda CK. Differential deletions of chromosome 3p are associated with the development of uterine cervical carcinoma in Indian patients. *Mol Pathol.* (2003) 56:263–9. doi: 10.1136/mp.56.5.263
39. Martin CL, Reshmi SC, Ried T, Gottberg W, Wilson JW, Reddy JK, et al. Chromosomal imbalances in oral squamous cell carcinoma: examination of 31 cell lines and review of the literature. *Oral Oncol.* (2008) 44:369–82. doi: 10.1016/j.oraloncology.2007.05.003
40. Hogg RP, Honorio S, Martinez A, Agathanggelou A, Dallol A, Fullwood P, et al. Frequent 3p allele loss and epigenetic inactivation of the RASSF1A tumour suppressor gene from region 3p21.3 in head and neck squamous cell carcinoma. *Eur J Cancer.* (2002) 38:1585–92. doi: 10.1016/S0959-8049(01)00422-1
41. Maestro R, Gasparotto D, Vukosavljevic T, Barzan L, Sulfaro S, Boiocchi M. Three discrete regions of deletion at 3p in head and neck cancers. *Cancer Res.* (1993) 53:5775–9.
42. Chakraborty SB, Sabbir MG, Roy A, Sengupta A, Panda CK. Multiple deletions in chromosome 3p are associated with the development of head and neck squamous cell carcinoma. *Int J Human Genet.* (2003) 3:79–87. doi: 10.1080/09723757.2003.11885832
43. Chakraborty SB, Dasgupta S, Roy A, Sengupta A, Ray B, Roychoudhury S, et al. Differential deletions in 3p are associated with the development of head and neck squamous cell carcinoma in Indian patients. *Cancer Genet Cytogenet.* (2003) 146:130–8. doi: 10.1016/S0165-4608(03)00127-4
44. Mroz EA, Tward AD, Hammon RJ, Ren Y, Rocco JW. Intra-tumor genetic heterogeneity and mortality in head and neck cancer: analysis of data from the Cancer Genome Atlas. *PLoS Med.* (2015) 12:e1001786. doi: 10.1371/journal.pmed.1001786
45. Moniz LS, Stambolic V. Nek10 mediates G2/M cell cycle arrest and MEK autoactivation in response to UV irradiation. *Mol Cell Biol.* (2011) 31:30–42. doi: 10.1128/MCB.00648-10
46. Zhang X, Huang M, Wu X, Kadlubar S, Lin J, Yu X, et al. GSTM1 copy number and promoter haplotype as predictors for risk of recurrence and/or second primary tumor in patients with head and neck cancer. *Pharmacogenom Personal Med.* (2013) 6:9–17. doi: 10.2147/PGPM.S35949
47. Singh M, Shah PP, Singh AP, Ruwali M, Mathur N, Pant MC, et al. Association of genetic polymorphisms in glutathione S-transferases and susceptibility to head and neck cancer. *Mutat Res.* (2008) 638:184–94. doi: 10.1016/j.mrfmmm.2007.10.003

Conflict of Interest: The authors declare that the research was conducted in the absence of any commercial or financial relationships that could be construed as a potential conflict of interest.

frontiers in Oncology

REVIEW
published: 12 May 2020
doi: 10.3389/fonc.2020.00619

Functional Landscape of Dysregulated MicroRNAs in Oral Squamous Cell Carcinoma: Clinical Implications

Ruma Dey Ghosh[1]*, *Arun Pattatheyil*[2] and *Susanta Roychoudhury*[3]

[1] Tata Translational Cancer Research Center, Tata Medical Center, Kolkata, India, [2] Department of Head and Neck Surgical Oncology, Tata Medical Center, Kolkata, India, [3] Saroj Gupta Cancer Centre and Research Institute, Kolkata, India

MicroRNA (miRNA) dysregulation is associated with the pathogenesis of oral squamous cell carcinoma (OSCC), and its elucidation could potentially provide information on patient outcome. A growing body of translational research on miRNA biology is focusing on precision oncology, aiming to decode the miRNA regulatory network in the development and progression of cancer. Tissue-specific expression and stable presence in all body fluids are unique features of miRNAs, which could be potentially exploited in the clinical setting. Recent understanding of miRNA properties has led them to be useful, attractive, and potential tools either as biomarkers (distinct miRNA expression signature) for diagnosis and prognostic outcomes or as targets for novel therapeutic entities, enabling personalized treatment for OSCC. In this review, we discuss recent research on different aspects of alterations in miRNA profiles along with their clinical significance and strive to identify probable potential miRNA biomarkers for diagnosis and prognosis of OSCC. We also discuss the current understanding and scope of development of miRNA-based therapeutics against OSCC.

Keywords: dysregulated miRNA, miRNA biomarker, non-invasive biomarker, miRNA-based therapy, oral squamous cell carcinoma

OPEN ACCESS

Edited by:
Jorge A. R. Salvador, University of Coimbra, Portugal

Reviewed by:
Cesare Piazza, Istituto Nazionale dei Tumori (IRCCS), Italy
Agnieszka Sobecka, Poznan University of Medical Sciences, Poland

***Correspondence:**
Ruma Dey Ghosh
deyrumai@yahoo.co.in;
ruma.deyghosh@tmckolkata.com

Specialty section:
This article was submitted to Head and Neck Cancer, a section of the journal Frontiers in Oncology

Received: *19 September 2019*
Accepted: *03 April 2020*
Published: *12 May 2020*

Citation:
Ghosh RD, Pattatheyil A and Roychoudhury S (2020) Functional Landscape of Dysregulated MicroRNAs in Oral Squamous Cell Carcinoma: Clinical Implications. Front. Oncol. 10:619. doi: 10.3389/fonc.2020.00619

INTRODUCTION

Oral squamous cell carcinoma (OSCC) is the second most common cancer reported in India. According to recent Globacon-2018 data, ∼120,000 new cases of OSCC are detected every year in India (1, 2). It is the leading cause of cancer-associated death in the Indian male population. Annually, more than 72,000 deaths are attributed to this disease in this country (3). OSCC originates in mucosal epithelial cells of the oral cavity (4, 5). Tobacco (smoking/smokeless) and alcohol are the primary risk factors for OSCC. Chewing of areca nut, betel leaf, poor oral health hygiene, and human papillomavirus (HPV) infection are also important risk factors for OSCC. Treatment in the early stages of the disease offers the best chance of cure (4, 5). Surgery is the first line of treatment, whereas radiotherapy and chemotherapy are used as adjuvant therapies (6, 7). Treatment strategies mainly depend on the location of the primary tumor, identification of high-risk features by histopathology, stage of tumor, and comorbidities. The 5-year survival rate of patients with oral cancer is around 50%. Poor outcomes are attributed to disease recurrence (both second primaries and locoregional recurrence) and distant metastasis. Despite availability of risk information from histopathology, the pattern and timing of relapse and metastasis are difficult

to predict. About 86% of the recurrence occurs within 24 months after primary treatment (7). Prognostic information is mainly derived from anatomic location; tumor stage; tumor thickness; and histological characteristics like cellular heterogeneity, degree of differentiation, depth of invasion, presence of nodal metastases, margin status, neural invasion, and pattern of invasion (6).

Biomarkers are quantifiable indicators associated with the specific disease conditions that facilitate decision-making by clinicians with respect to the most effective clinical interventions. In conventional practice, extra nodal extension (ENE), perineural invasion (PNI), and lymphovascular invasion (LVI) are considered histopathological biomarkers associated with poor disease prognosis (6, 7). Given that the genetics of OSCC is highly heterogeneous and complex, so far, no known molecular biomarker (except HPV positivity) has been used to subclassify OSCC accurately. Currently, only one epidermal growth factor receptor (EGFR)-specific targeted-immunotherapy with cetuximab antibody is available for the management of this cancer. Therefore, in the current scenario, early detection of the disease with identification of distinct prognostic subgroups to facilitate advanced treatment strategies is required for effective management of OSCC. Genomic, epigenomic, proteomic, and metabolomic high-throughput approaches have recently been used to discover and validate tumor biomarkers individually and/or in panels (8–13). Since microRNAs (miRNAs) are highly stable in tissues as well as in circulation, they are considered potential biomarkers for cancer detection and prognostication (14–18). Here, we review potential candidate miRNAs for their possible use as molecular biomarkers to improve the diagnosis and prognostication of OSCC and to stratify such patients into distinct prognostic subgroups. In this review, we have voyaged through various dysregulated miRNAs reported to be responsible for the pathogenesis, progression, and specific outcomes of OSCC. Their functional associations with overall therapeutic management, responsiveness, recurrence, and metastasis of OSCC are also elaborated upon.

BASICS OF MicroRNAs: ALTERED miRNA FUNCTION CAN FINE-TUNE CELL-FATE DECISION VIA ALTERED GENE AND PROTEIN EXPRESSION

Mature miRNAs are endogenous, single-stranded, evolutionarily conserved, non-coding RNAs ∼19–26 nucleotides long; discovered by Lee et al. (19). miRNAs preferentially interact with complementary seed sequences in the 3′ untranslated regions (UTRs) of their target mRNAs. miRNA binding sites may also be present in the 5′ UTRs and coding sequences of target mRNAs (20). miRNA-mediated gene silencing is a fundamental biological process for cellular homeostasis, executed through translational inhibition followed by mRNA deadenylation and decay (21–23). Circulating cell-free miRNAs also play an important role in intracellular/intercellular communication through miRNA-mediated gene silencing (17, 24). As a result, miRNA expression profiles in tissues and circulation are associated with several pathophysiological conditions, including cancers (17, 25). Dysregulation in miRNA expression profile was first reported in leukemia (26). Therefore, a distinct miRNA expression signature that distinguishes normal tissues from cancer tissues could be a new "hallmark of cancer," which regulates almost all other cancer hallmarks defined earlier (18, 27, 28).

Functional dysregulation of mature miRNAs is associated with various kinds of pathological conditions. Dysregulation of miRNA expression and function may be due to one or more of the following: (1) altered miRNA biogenesis process: (a) epigenetic (methylation and histone modifications) alterations of miRNA genes, (b) altered activities of transcription factors, and (c) altered expression of miRNA-processing enzymes (Drosha, Dicer, etc.); (2) chromosomal instability, genomic instability, and presence of mutations in miRNA genes; (3) single-nucleotide polymorphisms (SNPs), deletions, and duplications in miRNA genes (pri-, pre-, and mature miRNA regions) as well as in the binding sequences on target mRNAs; (4) loss of miRNA-binding sites on target mRNAs; and (5) redirecting of the miRNA-induced silencing complex (miRISC) to multiple competitive miRNA-binding sites present in competing endogenous RNAs (ceRNAs), which act as miRNA sponges and inhibit their functions (17, 23, 28–30). All ceRNAs are naturally occurring, endogenous regulatory molecules, like long non-coding RNAs (lncRNAs), circular RNAs, pseudogenes, and some protein-coding mRNAs (29, 30). Notably, in miRNA-mediated regulatory networks, one miRNA can regulate many genes and a single gene can be regulated by many miRNAs (23).

The above-described processes ultimately lead to activation of some oncogenic genes/proteins and, at the same time, deactivation of some tumor suppressor genes/proteins. They also direct cellular signaling cascades toward making the cell fate verdict (23, 28). Eventually, these distinct alterations in miRNA expression profile drive a normal cell to transform into a cancer cell and dictate its progression, metastasis, stemness, and responsiveness to therapy (radiotherapy/chemotherapy) (17, 18).

DISTINCT MicroRNA SIGNATURES AS HALLMARKS OF ORAL SQUAMOUS CELL CARCINOMA

The utility of miRNAs as diagnostic and prognostic biomarkers of OSCC has not been convincingly established. Previous studies on miRNA expression profiling mainly focused on differential expression of miRNAs in normal and tumor tissues and body fluids (blood, saliva, serum, or plasma) from OSCC patients (10, 12). These studies have yielded a plethora of dysregulated (upregulated/downregulated) miRNAs in OSCC. Here, we used the miRCancer database, PubMed, and Google to search for relevant data and reevaluate miRNAs as potential biomarkers for the diagnosis, prognosis, and therapeutics of OSCC. miRCancer is an online, up-to-date database (last updated on August 27, 2019) that provides a comprehensive collection of miRNA expression profiles in various human cancers extracted from published literature available in PubMed (31).

MicroRNA PROFILING IN ORAL SQUAMOUS CELL CARCINOMA

Dysregulated miRNA Expression in Tumor Tissues

Tran et al. (32) performed the first high-throughput miRNA profiling in OSCC using nine OSCC cell lines. Subsequently, several investigators have studied miRNA profiles as prognostic biomarkers using primary tumor and paired control tissues from patients with head and neck squamous cell carcinoma (HNSCC) (33–35). The differential expression analysis revealed sets of mature miRNAs that were either upregulated or downregulated in the tumor tissues. Childs et al. (35) showed that miR-21, miR-155, miR-191, and miR-221 were upregulated, whereas miR-1, miR-133a, miR-205, and let-7d were downregulated in primary tumors at diagnosis (35, 36). Another retrospective study on 51 formalin-fixed HNSCC tumor samples revealed consistent expression of mature miRNAs in malignant tissues; miR-21, miR-155, let-7i, miR-142-3p, miR-423, miR-106b, miR-20a, and miR-16 were overexpressed, whereas miR-125b, miR-375, and miR-10a were underexpressed) (37). Lu et al. (38) showed that miR-10b, miR-196a, miR-196b, miR-582-5p, miR-15b, miR-301, miR-148b, and miR-128a were upregulated, whereas miR-503 and miR-31 were downregulated in six oral cancer cell lines compared with those in normal keratinocytes. Specific miRNAs related to the clinicopathological features of site-specific OSCC were investigated, which demonstrated a significant difference in let-7a, miR-200c, miR-34a levels between oropharyngeal and laryngeal cancers (39). In addition, miR-21, miR-200c, and miR-34a were upregulated, and miR-375 was downregulated in tumor tissues of all subsites when compared with those in paired control tissues (39). Studies also suggested that genes associated with the phosphoinositide 3-kinase (PI3K)/AKT and p53 signaling pathways, which are involved in the OSCC carcinogenesis process, were regulated through a set of dysregulated miRNAs, such as let-7a, let-7d, let-7f, miR-16, miR-29b, miR-142-3p, miR-144, miR-203, and miR-223 (40). Lamperska et al. (41) suggested that miR-21 and miR-205 could be used to analyze the clarity of surgical margins, but they failed to find a correlation between miRNA expression and clinical outcome and the course of illness. Here, we considered only those studies that reported targeted or genome-wide miRNA profiling either in cell lines or in tumor samples.

These studies make it obvious that malignant OSCC tumors have distinct miRNA expression profiles. Subsequently, the regulatory network composed of these distinct miRNAs in the malignant cell causes key downstream molecular alteration, which ultimately leads to a distinct patient outcome (17, 28, 42). It is evident from the above studies that the results are not always consistent. The source of the problem could be found within and among the studies. Variations are observed in study design, end point objective, selection of cell lines, use of appropriate controls (in most of the cases, adjacent normal tissues were used which could harbor genomic alterations), methodology, protocol or treatment strategies, and localized patient pools in these studies. Further, purity and availability of tumor tissue, stromal cell contamination, and small sample size may impact study results. In most of the studies, intra/inter tumor heterogeneity, variable etiopathogenesis, and heterogenous genetic constitution of each patient are important factors that lead to variations in results. Despite these limitations, the results of individual studies demonstrate that miRNAs may be useful as potential biomarkers to predict OSCC outcome. The present quantum of knowledge lays the groundwork for logical implementation and execution of large-scale studies with improved, standardized study protocols in the future.

miRNA Expression Signatures Associated With Risk Factors of OSCC

One miRNA profiling study comparing smoker and non-smoker patients reported high miR-155 expression in 58% of OSCC cases and 83% of dysplasia cases and subsequently suggested miR-155 as a driver of oral tumorigenesis in non-smokers (43).

The association of OSCC with betel quid was also analyzed in OSCC specimens by another investigator who discovered 84 betel quid-associated mature miRNAs, of which 19 were located on chromosome 14q32.2 (44). In this context, Hou et al. (45) established that specific polymorphisms in miR-499a are associated with OSCC progression. They discovered that the T/C+C/C genotypes of miR-499a increased the risk of betel quid-associated oral submucosal fibrosis (OSF) but decreased the risk of OSCC. Further, miR-499a T>C (rs3746444) influences the expression of miR-499-5p during OSCC carcinogenesis (45).

Several investigators have also conducted miRNA expression profiling to compare HPV-positive and -negative OSCC tumors and revealed that miR-127-3p, miR-363, miR-20a, miR-34a, let-7c-5p, and miR-9 could effectively distinguish between the two groups (39, 46–49). Different etiological factors causing distinct patterns of miRNA expression have also been well-established by several investigators. Most of the work has been done on HPV-associated OSCC. The studies reveal little effect of tobacco and betel quid on miRNA expression in OSCC compared with that in HPV-associated OSCC.

Dysregulated miRNAs in Tumor Cells Collected Through Non-invasive Brush Biopsy

Recently, the more advanced brush biopsy or other related scraper-based methods have offered non-invasive ways to identify OSCC-specific miRNA biomarkers for diagnosis and prognostication of the disease. Gissi et al., using brush biopsy samples from OSCCs and from regenerative areas after surgical resection and from their respective normal distant mucosa, revealed that miR-146a and miR-191 were significantly altered in the regenerative areas after OSCC resection (50). Studies also claim that brush biopsy samples may be superior to surgically dissected samples (51, 52). In brush biopsy, sampling sites within lesions that are not ulcerated and are non-necrotic and minimally friable make the samples homogeneous, with viable epithelial cells. It must be noted, however, that in case

of smaller tumors (T1, T2), there is a chance of normal epithelial cell contamination in brush biopsy samples (51, 52). For high-throughput technology (next-generation sequencing), obtaining high quality and quantity of total RNA (or enriched miRNA) from brush biopsy samples is the main challenge (51). Quantitative real-time PCR (qRT-PCT) is a reliable method in this case. miRNA profiles in individual brush biopsy OSCC samples show ∼50% overlap with miRNAs enriched in surgically obtained tumor tissue profiles (51). The non-invasive rapid brush biopsy methods are useful in obtaining homogeneous tumor cells. Over the years, given all the limitations, the accuracy in predicting OSCC-associated miRNA expression signature is still to be improved for clinical applications.

CELL-FREE MicroRNA PROFILING: POTENTIAL BIOMARKERS FOR LIQUID BIOPSY

The most fascinating aspect of miRNA biology is the stable presence of cell-free miRNAs in all biological fluids. Previous studies have demonstrated that the stability of circulating cell-free miRNA results from either internalization of miRNAs into exosomes or other microvesicles or formation of complexes between circulating miRNAs and specific proteins and lipids (14–16, 53). These cell-free miRNAs are probably released by cancer cells, necrotic cells, and/or apoptotic cells along with their associated proteins or lipids, such as the RNA-binding protein NPM1 (nucleophosmin), AGO proteins (argonaute 1/2), and high-density lipoprotein (HDL), to avoid RNase degradation in blood circulation (15, 16, 54). Further, the spectrum of these cell-free miRNAs is altered by various pathophysiological conditions, including cancer (42, 54–57). In OSCC, saliva is one of the important sources to identify reliable biomarkers for predicting diagnosis and prognosis. Blood (serum and plasma) is another important sampling source. The sources of these cell-free miRNAs are thought to be directly associated with tumor pathogenesis and/or other related systemic physiological (immune system/metabolic system) conditions (54–56).

Dysregulated Cell-Free miRNAs in Biological Fluids of OSCC Patients

Saliva

Studies using human saliva samples have shown that salivary cell-free miRNAs could be potential diagnostic biomarkers in OSCC patients compared with those in healthy individuals (58–60). Genome-wide expression patterns of miRNAs have revealed that miRNA expression is significantly altered in the saliva of OSCC patients compared with that in healthy controls. miR-125a, miR-136, miR-147, miR-1250, miR-148a, miR-200a, miR-632, miR-646, miR-668, miR-877, miR-503, miR-220a, and miR-323-5p were downregulated, and miR-24 and miR-27b were found to be upregulated. The studies revealed that miR-27b was significantly upregulated in OSCC patients compared with that in healthy controls, patients with OSCC in remission, and patients with oral lichen planus and served as a biomarker to detect OSCC. Finally, the studies concluded that miR-27b could be a valuable cell-free biomarker in saliva for distinguishing OSCC patients (60).

Plasma

A study using plasma samples obtained at different time points showed that plasma miR-146a levels were significantly higher in OSCC patients (sensitivity: >0.72) than in healthy controls, and these levels decreased drastically after tumor resection in these patients (61). Similarly, higher plasma miR-187-3p level was found to be another potential marker of OSCC diagnosis, and the plasma levels of miR-187-3p were significantly reduced after tumor resection in patients who had better prognosis (62). Studies have also suggested that circulating miR-196a, miR-196b, and miR-200b-3p levels in plasma might serve as a panel of plasma biomarkers for the early detection of oral cancer (63–65). In a separate study, three plasma miRNAs—miR-222-3p, miR-150-5p, and miR-423-5p—were identified for early detection of malignant OSCC (66). miR-222-3p and miR-423-5p negatively correlated with T stage, lymph node metastasis status, and clinical stage. A high diagnostic accuracy (area under curve = 0.88) was demonstrated for discriminating oral leukoplakia from OSCC (66).

Serum

A miRNA microarray experiment using serum samples from OSCC patients vs. healthy controls revealed 16 miRNAs were significantly upregulated and 10 were significantly downregulated in the patients. miR-483-5p expression was significantly correlated (sensitivity = 0.853, specificity = 0.746) with lymph node metastasis and shorter survival, suggesting increased miR-483-5p expression in OSCC and suggesting its potential as a novel diagnostic and prognostic biomarker for OSCC (67). Further, low serum miR-9 level correlated with poor prognosis of OSCC (68). Recently, another study compared the circulating miRNA profile with the respective tumor-specific dysregulated miRNA profile and suggested that hsa-miR-32-5p in serum is a potential non-invasive biomarker for OSCC (69).

Whole Blood

Circulating miR-21 level and *PTEN* expression observed in whole blood samples could be possible biomarkers for detection of OSCC (70). Ries et al. (71–73) suggested that whole-blood sample is more reliable than only one specific blood component (serum/plasma/circulating cells) for identifying miRNA biomarkers for OSCC using a minimally invasive method. Microarray-based miRNA expression profiling was performed on 20 whole-blood samples (in a PAXgene blood RNA tube) from OSCC patients and healthy volunteers, and the results were validated through qRT-PCR using another 57 OSCC patient samples and 33 healthy control samples. This study showed that miR-186 was downregulated and miR-3651 and miR-494 were upregulated significantly in OSCC (71). In further studies, the authors evaluated these circulating miRNA biomarkers with diagnostic and prognostic significance in different patient cohorts (72). They also showed that the circulating miRNA expression signature (from whole-blood sample) was different from the miRNA expression in OSCC tissues (73). This is

probably because the changes in miRNA expression in circulation occur as a consequence of pathogenic reactions upon immune-pathogenic interactions in response to cancer.

On the basis of all these studies, we can suggest that liquid biopsy would be a reliable, consistent, rapid, easy, cheap, and minimally invasive method to determine miRNA expression signatures to predict OSCC diagnosis and prognosis (57, 74). Evident challenges persist in terms of quality and quantity (for high-throughput techniques) of RNA and usage of proper endogenous controls for data normalization (75–77). To overcome these issues, recently advanced instruments (Qubit, concentrator, droplet digital PCR) and advanced modified assay protocols (inclusion of exogenous spike-in-control and newly identified endogenous cell-free control miRNA) have been introduced to obtain reliable, potential predictive biomarkers for OSCC (75, 77, 78). We prepared a list of dysregulated miRNAs, in which each miRNA is representative of a particular miRNA expression signature in tumor tissues/cell lines and/or in circulation/other body fluids (**Supplementary Table 1**). Individual studies on the effect of one/two miRNAs with clinical significance were also included in this table. Each miRNA is accountable either for sole or cumulative functions related to OSCC pathogenesis, progression, differential tumor behavior, aggressiveness, invasion, and metastasis, resulting in distinct outcome for each patient with OSCC.

CLINICAL SIGNIFICANCE OF DYSREGULATED MicroRNAs IN THE DIAGNOSIS AND PROGNOSIS OF OSCC

miRNA Signature for Susceptibility to OSCC

A major goal of precision medicine is to assess disease risk based on the genetic makeup of an individual. SNPs in various miRNAs have also been shown to be associated with different cancers. Dysregulation due to distinct polymorphisms in mature miRNAs, particularly miR-196a2 rs11614913 C>T, miR-146a rs2910164 G>C, miR-149 rs2292832 C>T, and miR-499 rs3746444 A>G, are associated with the risk of OSCC (45, 63, 79). In addition, polymorphisms in miR-146a [genotype: CC vs. GG + CG; odds ratio (OR) = 0.874, $p = 0.041$] and miR-196a2 (genotype: TT vs. TC + CC; OR < 1, $p < 0.05$) increase the risk of OSCC, whereas the miR-499 polymorphisms (G allele and the GG genotype; OR > 1, $p < 0.05$) exert protective effects against OSCC risk. In this context, study results on miR-149 polymorphisms are not significant. They are associated with both increased risk of nodal metastasis and poor survival in OSCC, although another research group disclosed that they appeared to have no significant relationship with the risk of OSCC (80, 81).

miRNAs as Early Biomarkers for OSCC Diagnosis

Early detection of OSCC allows clinicians to provide proper administration of curative treatment long before it metastasizes and progresses to the advanced stages. The identification of biomarkers for early detection and prognostication of OSCC through minimally invasive or non-invasive methods acquires major emphasis in current investigative drives. A targeted miRNA expression profiling study (using 22 oral leukoplakia tissue samples with different grades of dysplasia, 17 OSCC samples, and six normal oral mucosa samples) demonstrated the prognostic values of miR-21, miR-181b, and miR-345 in oral leukoplakia with severe dysplasia. Although dysplasia grading is not a very reliable predictor, advanced aggressive dysplasia progresses to OSCC (82). Other studies using tumor tissues revealed that miR-137 and miR-29a/b/c could be potential biomarkers for early diagnosis of OSCC. miR-29s (miR-29a/b/c) were significantly downregulated in OSCC patients (83). Consecutively, circulating miR-223 and miR-10b in plasma were proposed to be potential biomarkers for early detection of oral cancer (38, 84). Further, miR-146a, miR-187-3p, miR-196a, miR-196b, miR-200b-3p, miR-222-3p, miR-223, miR-150-5p, and miR-423-5p levels in plasma could also be potential diagnostic markers for early detection of OSCC (61–66). A separate study described serum miR-32-5p as a potential biomarker for OSCC (69).

miRNAs as Biomarkers for OSCC Prognostication

Lymph Node Invasion and Distant Metastasis in OSCC

Epithelial–mesenchymal transition (EMT) of cancer cells is directly associated with cellular migration/invasion leading to cancer metastasis. In OSCC, ample dysregulated miRNAs have been found to be involved in EMT, invasion, and metastasis, which are primarily responsible for lymph node metastasis and distant metastasis.

In preclinical OSCC cell lines, miR-130b, miR-134, miR-149, miR-181d, miR-146b, miR-491, and miR-27a-3p are associated with EMT and cellular migration through targeting BMI1, MMP9, E-cadherin, and the YAP1-OCT4-Sox2 signaling axis (85, 86). High levels of miR-1275 and low levels of miR-222-3p and miR-423-5p are correlated with induced regional lymph node invasion in OSCC (40). Similarly, other studies have suggested that upregulation of miR-187, miR-196b, miR-372, miR-373, and miR-483 could be potential biomarkers for nodal metastasis in HNSCC (38, 62, 67, 87–90). ZEB1, Twist, and Snail (EMT-related transcription factors) are directly regulated by miR-429 and miR-101 and inversely by let-7d and mediate tumor growth and metastasis in OSCC (35, 91–93). Downregulation of miR-300 is another requirement for EMT initiation and maintenance, mediated through modulation of Twist expression and the transforming growth factor (TGF)β signaling pathway in OSCC (94). Bufalino et al. (95) demonstrated that lymph node metastasis resulted from downregulation of the miR-143/miR-145 cluster and consequent induction of activin-A, which contributed to poor prognosis through induced EMT. Similarly, RUNX2 is directly regulated by miR-376c-3p, which was found to be downregulated and to promote lymph node metastasis in OSCC (96). Other studies also demonstrated that the miR-23b/27b cluster regulates the MET oncogene, whereas miR-29a/b/c regulates the expression of *MMP2*, *LAMC2*, and

ITGA6, responsible for disease invasion and metastasis in OSCC (83, 97, 98). Further, miR-218 is directly correlated with increased invasion and cellular migration mediated through *LAMB3* and *RICTOR* and the focal adhesion and mTOR-Akt signaling pathways (99, 100). *EGFR*, *c-MET*, and *KRAS* are direct targets of miR-1 and miR-206. Both these miRNAs, particularly miR-206, are significantly associated with advanced tumor node metastasis (node positivity in the Tumor Node Metastasis staging system) and shorter overall survival in OSCC (101, 102). Moreover, high expression of miR-196a and miR-149 polymorphisms is associated with increased risk of nodal metastasis (63, 80).

Biomarkers for Locoregional Recurrence in OSCC

The evolution of second primary or locoregional recurrence is unpredictable. In most cases, relapses are detected in late stages, which significantly reduce survival and worsen morbidity. Salvage surgery can cure recurrent tumors effectively if detected early.

Low miR-422a expression in stage III–IV tumors promotes local recurrence *via* targeting oncogenic *CD73* when compared with that in oropharynx stage III–IV tumors, without relapse or with locoregional relapse within 2 years of posttreatment (103). Other studies have shown that miR-196a, miR-205, and miR-675 are significantly associated with locoregional recurrence at diagnosis and treatment in OSCC (35, 80, 103, 104). miR-451 was found to be significantly overexpressed (4.7-fold) in non-relapsed vs. relapsed patients (37). Furthermore, locoregional recurrence in OSCC is also significantly affected by polymorphisms in miR-196a (63). All these indicators could be building blocks for developing meaningful biomarkers for early disease prognostication, recurrence, and/or metastasis in the clinical setting.

Dysregulated miRNAs Associated With Response to Chemoradiation Therapy in OSCC

Until date, cetuximab is the only clinically applied targeted drug used to treat patients with OSCC. However, the occurrence of therapeutic resistance or non-responsiveness has been found during chemotherapy/radiotherapy treatment in patients with OSCC. Several studies identified miRNAs as potential biomarkers to predict the sensitivity/resistance of tumors to chemotherapy or a particular drug used in chemotherapy and radiotherapy for OSCC.

Henson et al. (105) showed that the amplification of chromosomal band 11q13, loss of distal 11q, and downregulation of miR-125b and miR-100 are associated with radioresistance and disease progression (105, 106). In our previous study, we identified six cisplatin resistance-specific signature miRNAs—miR-130b, miR-134, miR-149, miR-181d, miR-146b, and miR-491. These miRNAs function in OSCC mainly through modulating the expression of proteins related to cancer stem cells (augmentation of CD44, c-Myc, and Oct-4), drug resistance (upregulation of P-gp and MRP1), and EMT (increase in BMI1 and MMP9 expression and loss of E-cadherin) (85). Low miR-29a level is reported to be associated with induced drug resistance and invasion (97). High miR-196a and miR-21 levels enhance radioresistance through inhibiting annexin A1 and signal transducer and activator of transcription 3 (STAT3), respectively (107, 108). Moreover, low Dicer expression is associated with resistance to 5-fluorouracil-based chemoradiotherapy and shorter overall survival in patients with OSCC (109). In brief, upregulation of the let-7 family, miR-203, miR-23a, miR-214, miR-518c, and miR-608 and downregulation of miR-21 and miR-342 have been shown to be connected with the manifestation of chemosensitivity/chemoresistance in OSCC (91, 110, 111). Moreover, therapeutic resistance is mediated through EGFR and c-MET, which are further alleviated by low levels of miR-1 and miR-206 in OSCC (102). However, determination of the exact range (single/panel) of these miRNA biomarkers as well as the spectrum of their expression level needs to be extremely accurate, sensitive, and specific in order to predict optimum therapy response in OSCC.

Biomarkers for Prediction of Patient Survival in OSCC

The relation between disease-free survival and overall survival of OSCC patients and aberrant miRNA expression has been studied by several investigators. Early detection and prompt treatment using suitable multidisciplinary protocols could improve survival in OSCC. Earlier evidence has shown that irrespective of tumor size, poor patient survival is significantly correlated with lower expression levels of miR-9, miR-149, miR-150-5p, miR-200b, miR-205, miR-375, miR-483-5p, miR-542-3p, and let-7d (35, 62, 68, 103, 104, 112–118). Concurrently, it was also found that overexpression of miR-1246 and miR-675 and downregulation of miR-187 and miR-134 in plasma are associated with better patient survival in OSCC (35, 62, 67, 68, 103, 104, 112–118). Moreover, other studies discovered that decreased levels of Dicer and miR-206 correlate significantly with lower overall survival in OSCC (101, 109).

ADVANCED THERAPEUTICS BASED ON MicroRNA EXPRESSION IN ORAL SQUAMOUS CELL CARCINOMA

As described above, a variety of tumor-specific dysregulated miRNAs have been identified in OSCC, with either tumor suppressor or oncogenic functions. However, the challenges that remain for therapeutic application of miRNAs in OSCC are as follows: (a) miRNA selection, (b) complex regulatory mechanisms, (c) delivery, (d) pharmacokinetics, and (e) toxicity. Nevertheless, being endogenous molecules, miRNAs exhibit low toxicity in humans. Further, owing to their small size, miRNAs can be introduced into the system through different delivery methods.

In this context, so far, miRNA sponging, locked nucleic acid-mediated suppression of oncogenic miRNAs, and replacement of tumor-suppressive miRNAs using respective mimics/viral vectors/small compounds have already been used for different cancers (17, 119). To this end, the efficacy and accuracy of the miRNA delivery system are very important. Two main miRNA delivery approaches have been described: local (intra-tumor) and systemic. Systemic approaches would be suitable for metastatic or late-stage advanced cancers. The miRNA could

be conjugated with a folate ligand, such as vitamin B9, for selective delivery to treat the cancer (17, 119). In addition, exosome/microvesicle/liposome-mediated delivery of miRNAs could also be used as novel tools for miRNA-based cancer therapy (53). Interestingly, therapeutic delivery of miRNA may be possible just through oral intake of vegetables, since it has been found that humans and animals can acquire plant miRNAs in their sera or body fluids through food intake (120). The first miRNA-based therapy specifically for cancer is MRX34, wherein a synthetic miR-34a mimic is loaded into liposomal nanoparticles (121). Quantification of MRX34 in non-human primates has established a satisfactory 7.7 h half-life in whole blood (122). Currently, only two observational miRNA-based therapies, miR-29b and miR-29, have progressed to clinical trials (Trial ref No.: NCT02009852 and NCT01927354, respectively) for OSCC. Further studies on miRNA-based diagnostics and therapies need to be evaluated extensively for OSCC treatment.

CONCLUSION

This review highlighted the functional landscape of dysregulated miRNAs in OSCC from a clinical perspective. We identified 17 miRNAs (let-7d, miR-1, miR-125b-5p, miR-138-5p, miR-142, miR-145, miR-155, miR-16, miR-196a, miR-196b, miR-200c, miR-20a-5p, miR-21-5p, miR-218, miR-31-5p, miR-34a, and miR-375) commonly dysregulated in OSCC and that have been found to have clinical significance in three or more extensive studies. We also found 22 miRNAs (let-7d, miR-125b-5p, miR-145, miR-146a, miR-150, miR-16, miR-184, miR-191, miR-196a, miR-196b, miR-21-5p, miR-223, miR-24, miR-26a, miR-27b, miR-29a, miR-31-5p, miR-32-5p, miR-375, miR-451, miR-9 and miR-99b-3p) to be significantly dysregulated in two or more clinical sample types (tumor tissues/epithelial cells and one or more circulating body fluid) collected from OSCC patients. These miRNAs could have the potential for clinical application for disease diagnosis, patient stratification, and therapy in OSCC. Six miRNAs (miR-146a, miR-148a, miR-24, miR-438-5p, miR-9, and miR-99b-3p) which are common to different types of biological fluid samples (blood/plasma/serum/saliva) from OSCC patients could be potential biomarkers through minimally invasive or non-invasive methods to predict OSCC more accurately. Logical selection, validation, and confirmation of these potential miRNA biomarkers (single/panel) are very important for augmenting their specific clinical applications in OSCC.

The number of human miRNAs (>2,600) in miRbase significantly increases in every successive version of the database (recent is v22.1) due to continuous inclusion of novel miRNAs (123). In most of the cases, the newer studies came up with new sets of dysregulated miRNA signatures for OSCC detection and prognostication. Therefore, large differences are frequently found in the results of similar older studies and current large-scale data sets. The ethnicity of the recruited patient population is also an important issue in this situation. In the current review, importantly, we summarized the recent progress on elucidating the clinical significance of miRNAs (tumor-associated or circulating), especially with respect to possible ways to develop miRNA-based detection and prognostication methods in conjunction with available techniques. Recent evidence increasingly demonstrates that cell-free miRNAs are evolving as consistent and reliable biomarkers for early detection, disease monitoring, and patient stratification, as well as guides to optimum treatment protocols for patients with OSCC.

In conclusion, a wide variety of dysregulated miRNAs contribute to the OSCC phenotype and differential patient outcomes, including tumor progression, therapy response, recurrence, metastasis, and survival. Moreover, miRNA-mediated regulatory mechanisms are complex and tangled with numerous interconnected physiological events. Here, one of the biggest challenges is to identify the tailor-made potentially relevant key miRNA candidates (single or in spectrum) along with or without their key targets for detection of disease and stratification of each patient with OSCC. Therefore, on the basis of our previous knowledge, careful, logical selection, and functional characterization of signature miRNAs (mentioned above) are very important. Standardized validation studies must be undertaken to ensure the sensitivity, specificity, and robustness of the signature miRNAs for individual patient conditions. Thus, well-designed, multicentered, prospective trials with large patient cohorts would be necessary to mitigate external variations in data sets. This will provide useful information for molecular diagnostics and determination of prognostic information for improved management of OSCC.

AUTHOR CONTRIBUTIONS

RG conceived the idea, collected all data, and designed and wrote the manuscript. SR and AP supervised and contributed with their expert comments and views in the logical presentation of manuscript and checked and edited the manuscript. All authors approved the final manuscript.

FUNDING

This work was supported by HRD WS grant (V.25011/452-HRD/2016-HR) from Department of Health Research (DHR), Govt. of India and a grant support from Lady Tata Memorial Trust, India to RG and J. C. Bose National Fellowship (JCB/2017/000005) to SR.

SUPPLEMENTARY MATERIAL

The Supplementary Material for this article can be found online at: https://www.frontiersin.org/articles/10.3389/fonc.2020.00619/full#supplementary-material

REFERENCES

1. Bray F, Ferlay J, Soerjomataram I, Siegel RL, Torre LA, Jemal A. Global cancer statistics 2018: GLOBOCAN estimates of incidence and mortality worldwide for 36 cancers in 185 countries. *CA Cancer J Clin.* (2018) 68:394–424. doi: 10.3322/caac.21492
2. Ferlay J, Colombet M, Soerjomataram I, Mathers C, Parkin DM, Pineros M, et al. Estimating the global cancer incidence and mortality in 2018: GLOBOCAN sources and methods. *Int J Cancer.* (2019) 144:1941–53. doi: 10.1002/ijc.31937
3. International Agency for Research on Cancer W. *India, Source: Globacon 2018*. The Global Cancer Observatory (2019). Available online at: https://gco.iarc.fr/today/data/factsheets/populations/356-india-fact-sheets.pdf
4. Leemans CR, Braakhuis BJ, Brakenhoff RH. The molecular biology of head and neck cancer. *Nat Rev Cancer.* (2011) 11:9–22. doi: 10.1038/nrc2982
5. Rischin D, Ferris RL, Le QT. Overview of advances in head and neck cancer. *J Clin Oncol.* (2015) 33:3225–6. doi: 10.1200/JCO.2015.63.6761
6. Chinn SB, Myers JN. Oral cavity carcinoma: current management, controversies, and future directions. *J Clin Oncol.* (2015) 33:3269–76. doi: 10.1200/JCO.2015.61.2929
7. Koyfman SA, Ismaila N, Crook D, D'Cruz AL. Management of the neck in squamous cell carcinoma of the oral cavity and oropharynx: ASCO Clinical Practice Guideline. *J Clin Oncol.* (2019) 37:1753–74. doi: 10.1200/JCO.18.01921
8. Wang Z, Jiang L, Huang C, Li Z, Chen L, Gou L, et al. Comparative proteomics approach to screening of potential diagnostic and therapeutic targets for oral squamous cell carcinoma. *Mol Cell Proteomics.* (2008) 7:1639–50. doi: 10.1074/mcp.M700520-MCP200
9. Schaaij-Visser TB, Brakenhoff RH, Leemans CR, Heck AJ, Slijper M. Protein biomarker discovery for head and neck cancer. *J Proteomics.* (2010) 73:1790–803. doi: 10.1016/j.jprot.2010.01.013
10. Kang H, Kiess A, Chung CH. Emerging biomarkers in head and neck cancer in the era of genomics. *Nat Rev Clin Oncol.* (2014) 12:11–26. doi: 10.1038/nrclinonc.2014.192
11. Wang Y, Springer S, Mulvey CL, Silliman N, Schaefer J, Sausen M, et al. Detection of somatic mutations and HPV in the saliva and plasma of patients with head and neck squamous cell carcinomas. *Sci Transl Med.* (2015) 7:293ra104. doi: 10.1126/scitranslmed.aaa8507
12. Cohen JD, Javed AA, Thoburn C, Wong F, Tie J, Gibbs P, et al. Combined circulating tumor DNA and protein biomarker-based liquid biopsy for the earlier detection of pancreatic cancers. *Proc Natl Acad Sci USA.* (2017) 114:10202–7. doi: 10.1073/pnas.1704961114
13. Cohen JD, Li L, Wang Y, Thoburn C, Afsari B, Danilova L, et al. Detection and localization of surgically resectable cancers with a multi-analyte blood test. *Science.* (2018) 359:926–30. doi: 10.1126/science.aar3247
14. Wang K, Zhang S, Weber J, Baxter D, Galas DJ. Export of microRNAs and microRNA-protective protein by mammalian cells. *Nucleic Acids Res.* (2010) 38:7248–59. doi: 10.1093/nar/gkq601
15. Arroyo JD, Chevillet JR, Kroh EM, Ruf IK, Pritchard CC, Gibson DF, et al. Argonaute2 complexes carry a population of circulating microRNAs independent of vesicles in human plasma. *Proc Natl Acad Sci USA.* (2011) 108:5003–8. doi: 10.1073/pnas.1019055108
16. Vickers KC, Palmisano BT, Shoucri BM, Shamburek RD, Remaley AT. MicroRNAs are transported in plasma and delivered to recipient cells by high-density lipoproteins. *Nat Cell Biol.* (2011) 13:423–33. doi: 10.1038/ncb2210
17. Iorio MV, Croce CM. MicroRNA dysregulation in cancer: diagnostics, monitoring and therapeutics. A comprehensive review. *EMBO Mol Med.* (2012) 4:143–59. doi: 10.1002/emmm.201100209
18. Dhawan A, Scott JG, Harris AL, Buffa FM. Pan-cancer characterisation of microRNA across cancer hallmarks reveals microRNA-mediated downregulation of tumour suppressors. *Nat Commun.* (2018) 9:5228. doi: 10.1038/s41467-018-07657-1
19. Lee RC, Feinbaum RL, Ambros V. The C. elegans heterochronic gene lin-4 encodes small RNAs with antisense complementarity to lin-14. *Cell.* (1993) 75:843–54. doi: 10.1016/0092-8674(93)90529-Y
20. Ebert MS, Sharp PA. Roles for microRNAs in conferring robustness to biological processes. *Cell.* (2012) 149:515–24. doi: 10.1016/j.cell.2012.04.005
21. Krol J, Loedige I, Filipowicz W. The widespread regulation of microRNA biogenesis, function and decay. *Nat Rev Genet.* (2010) 11:597–610. doi: 10.1038/nrg2843
22. Djuranovic S, Nahvi A, Green R. miRNA-mediated gene silencing by translational repression followed by mRNA deadenylation and decay. *Science.* (2012) 336:237–40. doi: 10.1126/science.1215691
23. Jonas S, Izaurralde E. Towards a molecular understanding of microRNA-mediated gene silencing. *Nat Rev Genet.* (2015) 16:421–33. doi: 10.1038/nrg3965
24. Redis RS, Calin S, Yang Y, You MJ, Calin GA. Cell-to-cell miRNA transfer: from body homeostasis to therapy. *Pharmacol Ther.* (2012) 136:169–74. doi: 10.1016/j.pharmthera.2012.08.003
25. Fang C, Li Y. Prospective applications of microRNAs in oral cancer. *Oncol Lett.* (2019) 18:3974–84. doi: 10.3892/ol.2019.10751
26. Calin GA, Dumitru CD, Shimizu M, Bichi R, Zupo S, Noch E, et al. Frequent deletions and down-regulation of micro- RNA genes miR15 and miR16 at 13q14 in chronic lymphocytic leukemia. *Proc Natl Acad Sci USA.* (2002) 99:15524–9. doi: 10.1073/pnas.242606799
27. Hanahan D, Weinberg RA. Hallmarks of cancer: the next generation. *Cell.* (2011) 144:646–74. doi: 10.1016/j.cell.2011.02.013
28. Bracken CP, Scott HS, Goodall GJ. A network-biology perspective of microRNA function and dysfunction in cancer. *Nat Rev Genet.* (2016) 17:719–32. doi: 10.1038/nrg.2016.134
29. Anastasiadou E, Jacob LS, Slack FJ. Non-coding RNA networks in cancer. *Nat Rev Cancer.* (2018) 18:5–18. doi: 10.1038/nrc.2017.99
30. Cai Y, Wan J. Competing endogenous RNA regulations in neurodegenerative disorders: current challenges and emerging insights. *Front Mol Neurosci.* (2018) 11:370. doi: 10.3389/fnmol.2018.00370
31. Xie B, Ding Q, Han H, Wu D. miRCancer: a microRNA-cancer association database constructed by text mining on literature. *Bioinformatics.* (2013) 29:638–44. doi: 10.1093/bioinformatics/btt014
32. Tran N, Mclean T, Zhang X, Zhao CJ, Thomson JM, O'brien C, et al. MicroRNA expression profiles in head and neck cancer cell lines. *Biochem Biophys Res Commun.* (2007) 358:12–7. doi: 10.1016/j.bbrc.2007.03.201
33. Chang SS, Jiang WW, Smith I, Poeta LM, Begum S, Glazer C, et al. MicroRNA alterations in head and neck squamous cell carcinoma. *Int J Cancer.* (2008) 123:2791–7. doi: 10.1002/ijc.23831
34. Wong TS, Liu XB, Wong BY, Ng RW, Yuen AP, Wei WI. Mature miR-184 as potential oncogenic microRNA of squamous cell carcinoma of tongue. *Clin Cancer Res.* (2008) 14:2588–92. doi: 10.1158/1078-0432.CCR-07-0666
35. Childs G, Fazzari M, Kung G, Kawachi N, Brandwein-Gensler M, Mclemore M, et al. Low-level expression of microRNAs let-7d and miR-205 are prognostic markers of head and neck squamous cell carcinoma. *Am J Pathol.* (2009) 174:736–45. doi: 10.2353/ajpath.2009.080731
36. Gombos K, Horvath R, Szele E, Juhasz K, Gocze K, Somlai K, et al. miRNA expression profiles of oral squamous cell carcinomas. *Anticancer Res.* (2013) 33:1511–7. Available online at: http://ar.iiarjournals.org/content/33/4/1511.full.pdf
37. Hui AB, Lenarduzzi M, Krushel T, Waldron L, Pintilie M, Shi W, et al. Comprehensive MicroRNA profiling for head and neck squamous cell carcinomas. *Clin Cancer Res.* (2010) 16:1129–39. doi: 10.1158/1078-0432.CCR-09-2166
38. Lu YC, Chen YJ, Wang HM, Tsai CY, Chen WH, Huang YC, et al. Oncogenic function and early detection potential of miRNA-10b in oral cancer as identified by microRNA profiling. *Cancer Prev Res.* (2012) 5:665–74. doi: 10.1158/1940-6207.CAPR-11-0358
39. Kalfert D, Pesta M, Kulda V, Topolcan O, Ryska A, Celakovsky P, et al. MicroRNA profile in site-specific head and neck squamous cell cancer. *Anticancer Res.* (2015) 35:2455–63. Available online at: http://ar.iiarjournals.org/content/35/4/2455.full.pdf
40. Manikandan M, Deva Magendhra Rao AK, Arunkumar G, Manickavasagam M, Rajkumar KS, Rajaraman R, et al. Oral squamous cell carcinoma: microRNA expression profiling and integrative analyses for elucidation of tumourigenesis mechanism. *Mol Cancer.* (2016) 15:28. doi: 10.1186/s12943-016-0512-8
41. Lamperska KM, Kozlowski P, Kolenda T, Teresiak A, Blizniak R, Przybyla W, et al. Unpredictable changes of selected miRNA in expression

profile of HNSCC. *Cancer Biomark.* (2016) 16:55–64. doi: 10.3233/CBM-150540
42. Zeljic K, Jovanovic I, Jovanovic J, Magic Z, Stankovic A, Supic G. MicroRNA meta-signature of oral cancer: evidence from a meta-analysis. *Ups J Med Sci.* (2018) 123:43–9. doi: 10.1080/03009734.2018.1439551
43. Towle R, Gorenchtein M, Garnis C, Dickman C, Zhu Y, Poh CF. Dysregulation of microRNAs across oral squamous cell carcinoma fields in non-smokers. *J Interdiscipl Med Dent Sci.* (2014) 2:131. doi: 10.4172/2376-032X.1000131
44. Shiah SG, Hsiao JR, Chang WM, Chen YW, Jin YT, Wong TY, et al. Downregulated miR329 and miR410 promote the proliferation and invasion of oral squamous cell carcinoma by targeting Wnt-7b. *Cancer Res.* (2014) 74:7560–72. doi: 10.1158/0008-5472.CAN-14-0978
45. Hou YY, Lee JH, Chen HC, Yang CM, Huang SJ, Liou HH, et al. The association between miR-499a polymorphism and oral squamous cell carcinoma progression. *Oral Dis.* (2015) 21:195–206. doi: 10.1111/odi.12241
46. Lajer CB, Garnaes E, Friis-Hansen L, Norrild B, Therkildsen MH, Glud M, et al. The role of miRNAs in human papilloma virus (HPV)-associated cancers: bridging between HPV-related head and neck cancer and cervical cancer. *Br J Cancer*. (2012) 106:1526–34. doi: 10.1038/bjc.2012.109
47. Network TCGA. Comprehensive genomic characterization of head and neck squamous cell carcinomas. *Nature.* (2015) 517:576–82. doi: 10.1038/nature14129
48. Hu J, Ge W, Xu J. HPV 16 E7 inhibits OSCC cell proliferation, invasion, and metastasis by upregulating the expression of miR-20a. *Tumour Biol.* (2016) 37:9433–40. doi: 10.1007/s13277-016-4817-4
49. Bozinovic K, Sabol I, Dediol E, Milutin Gasperov N, Manojlovic S, Vojtechova Z, et al. Genome-wide miRNA profiling reinforces the importance of miR-9 in human papillomavirus associated oral and oropharyngeal head and neck cancer. *Sci Rep.* (2019) 9:2306. doi: 10.1038/s41598-019-38797-z
50. Gissi DB, Morandi L, Gabusi A, Tarsitano A, Marchetti C, Cura F, et al. A noninvasive test for microRNA expression in oral squamous cell carcinoma. *Int J Mol Sci.* (2018) 19:1789. doi: 10.3390/ijms19061789
51. Adami GR, Tang JL, Markiewicz MR. Improving accuracy of RNA-based diagnosis and prognosis of oral cancer by using noninvasive methods. *Oral Oncol.* (2017) 69:62–7. doi: 10.1016/j.oraloncology.2017.04.001
52. Zhou Y, Kolokythas A, Schwartz JL, Epstein JB, Adami GR. microRNA from brush biopsy to characterize oral squamous cell carcinoma epithelium. *Cancer Med.* (2017) 6:67–78. doi: 10.1002/cam4.951
53. Kamerkar S, Lebleu VS, Sugimoto H, Yang S, Ruivo CF, Melo SA, et al. Exosomes facilitate therapeutic targeting of oncogenic KRAS in pancreatic cancer. *Nature.* (2017) 546:498–503. doi: 10.1038/nature22341
54. Redova M, Sana J, Slaby O. Circulating miRNAs as new blood-based biomarkers for solid cancers. *Future Oncol.* (2013) 9:387–402. doi: 10.2217/fon.12.192
55. Mitchell PS, Parkin RK, Kroh EM, Fritz BR, Wyman SK, Pogosova-Agadjanyan EL, et al. Circulating microRNAs as stable blood-based markers for cancer detection. *Proc Natl Acad Sci USA.* (2008) 105:10513–8. doi: 10.1073/pnas.0804549105
56. Turchinovich A, Weiz L, Langheinz A, Burwinkel B. Characterization of extracellular circulating microRNA. *Nucleic Acids Res.* (2011) 39:7223–33. doi: 10.1093/nar/gkr254
57. Rapado-Gonzalez O, Lopez-Lopez R, Lopez-Cedrun JL, Triana-Martinez G, Muinelo-Romay L, Suarez-Cunqueiro MM. Cell-free microRNAs as potential oral cancer biomarkers: from diagnosis to therapy. *Cells.* (2019) 8:1653. doi: 10.3390/cells8121653
58. Park NJ, Zhou H, Elashoff D, Henson BS, Kastratovic DA, Abemayor E, et al. Salivary microRNA: discovery, characterization, and clinical utility for oral cancer detection. *Clin Cancer Res.* (2009) 15:5473–7. doi: 10.1158/1078-0432.CCR-09-0736
59. Yang Y, Li YX, Yang X, Jiang L, Zhou ZJ, Zhu YQ. Progress risk assessment of oral premalignant lesions with saliva miRNA analysis. *BMC Cancer.* (2013) 13:129. doi: 10.1186/1471-2407-13-129
60. Momen-Heravi F, Trachtenberg AJ, Kuo WP, Cheng YS. Genomewide study of salivary microRNAs for detection of oral cancer. *J Dent Res.* (2014) 93:86S−93S. doi: 10.1177/0022034514531018
61. Hung PS, Liu CJ, Chou CS, Kao SY, Yang CC, Chang KW, et al. miR-146a enhances the oncogenicity of oral carcinoma by concomitant targeting of the IRAK1, TRAF6 and NUMB genes. *PLoS ONE.* (2013) 8:e79926. doi: 10.1371/journal.pone.0079926
62. Liu CJ, Lin JS, Cheng HW, Hsu YH, Cheng CY, Lin SC. Plasma miR-187* is a potential biomarker for oral carcinoma. *Clin Oral Investig.* (2016) 21:1131–8. doi: 10.1007/s00784-016-1887-z
63. Liu CJ, Tsai MM, Tu HF, Lui MT, Cheng HW, Lin SC. miR-196a overexpression and miR-196a2 gene polymorphism are prognostic predictors of oral carcinomas. *Ann Surg Oncol.* (2013) 20(Suppl 3):S406–14. doi: 10.1245/s10434-012-2618-6
64. Lu YC, Chang JT, Huang YC, Huang CC, Chen WH, Lee LY, et al. Combined determination of circulating miR-196a and miR-196b levels produces high sensitivity and specificity for early detection of oral cancer. *Clin Biochem.* (2015) 48:115–21. doi: 10.1016/j.clinbiochem.2014.11.020
65. Sun G, Cao Y, Wang P, Song H, Bie T, Li M, et al. miR-200b-3p in plasma is a potential diagnostic biomarker in oral squamous cell carcinoma. *Biomarkers.* (2018) 23:137–41. doi: 10.1080/1354750X.2017.1289241
66. Chang YA, Weng SL, Yang SF, Chou CH, Huang WC, Tu SJ, et al. A three-microRNA signature as a potential biomarker for the early detection of oral cancer. *Int J Mol Sci.* (2018) 19:758. doi: 10.3390/ijms19030758
67. Xu H, Yang Y, Zhao H, Yang X, Luo Y, Ren Y, et al. Serum miR-483-5p: a novel diagnostic and prognostic biomarker for patients with oral squamous cell carcinoma. *Tumour Biol.* (2016) 37:447–53. doi: 10.1007/s13277-015-3514-z
68. Sun L, Liu L, Fu H, Wang Q, Shi Y. Association of decreased expression of serum miR-9 with poor prognosis of oral squamous cell carcinoma patients. *Med Sci Monit.* (2016) 22:289–94. doi: 10.12659/MSM.895683
69. Schneider A, Victoria B, Lopez YN, Suchorska W, Barczak W, Sobecka A, et al. Tissue and serum microRNA profile of oral squamous cell carcinoma patients. *Sci Rep.* (2018) 8:675. doi: 10.1038/s41598-017-18945-z
70. Ren W, Qiang C, Gao L, Li SM, Zhang LM, Wang XL, et al. Circulating microRNA-21 (MIR-21) and phosphatase and tensin homolog (PTEN) are promising novel biomarkers for detection of oral squamous cell carcinoma. *Biomarkers.* (2014) 19:590–6. doi: 10.3109/1354750X.2014.955059
71. Ries J, Vairaktaris E, Agaimy A, Kintopp R, Baran C, Neukam FW, et al. miR-186, miR-3651 and miR-494: potential biomarkers for oral squamous cell carcinoma extracted from whole blood. *Oncol Rep.* (2014) 31:1429–36. doi: 10.3892/or.2014.2983
72. Ries J, Baran C, Wehrhan F, Weber M, Neukam FW, Krautheim-Zenk A, et al. Prognostic significance of altered miRNA expression in whole blood of OSCC patients. *Oncol Rep.* (2017) 37:3467–74. doi: 10.3892/or.2017.5639
73. Ries J, Baran C, Wehrhan F, Weber M, Motel C, Kesting M, et al. The altered expression levels of miR-186, miR-494 and miR-3651 in OSCC tissue vary from those of the whole blood of OSCC patients. *Cancer Biomark.* (2019) 24:19–30. doi: 10.3233/CBM-180032
74. Mazumder S, Datta S, Ray JG, Chaudhuri K, Chatterjee R. Liquid biopsy: miRNA as a potential biomarker in oral cancer. *Cancer Epidemiol.* (2019) 58:137–45. doi: 10.1016/j.canep.2018.12.008
75. Blondal T, Jensby Nielsen S, Baker A, Andreasen D, Mouritzen P, Wrang Teilum M, et al. Assessing sample and miRNA profile quality in serum and plasma or other biofluids. *Methods.* (2013) 59:S1–6. doi: 10.1016/j.ymeth.2012.09.015
76. Buschmann D, Haberberger A, Kirchner B, Spornraft M, Riedmaier I, Schelling G, et al. Toward reliable biomarker signatures in the age of liquid biopsies - how to standardize the small RNA-Seq workflow. *Nucleic Acids Res.* (2016) 44:5995–6018. doi: 10.1093/nar/gkw545
77. Garcia-Elias A, Alloza L, Puigdecanet E, Nonell L, Tajes M, Curado J, et al. Defining quantification methods and optimizing protocols for microarray hybridization of circulating microRNAs. *Sci Rep.* (2017) 7:7725. doi: 10.1038/s41598-017-08134-3
78. Gevaert AB, Witvrouwen I, Vrints CJ, Heidbuchel H, Van Craenenbroeck EM, Van Laere SJ, et al. MicroRNA profiling in plasma samples using qPCR arrays: recommendations for correct analysis and interpretation. *PLoS ONE.* (2018) 13:e0193173. doi: 10.1371/journal.pone.0193173
79. Orsos Z, Szanyi I, Csejtei A, Gerlinger I, Ember I, Kiss I. Association of pre-miR-146a rs2910164 polymorphism with the risk of head and neck cancer.

Anticancer Res. (2013) 33:341–6. Available online at: http://ar.iiarjournals.org/content/33/1/341.full.pdf
80. Tu HF, Liu CJ, Chang CL, Wang PW, Kao SY, Yang CC, et al. The association between genetic polymorphism and the processing efficiency of miR-149 affects the prognosis of patients with head and neck squamous cell carcinoma. *PLoS ONE.* (2012) 7:e51606. doi: 10.1371/journal.pone.0051606
81. Niu YM, Du XY, Lu MY, Xu QL, Luo J, Shen M. Significant association between functional microRNA polymorphisms and head and neck cancer susceptibility: a comprehensive meta-analysis. *Sci Rep.* (2015) 5:12972. doi: 10.1038/srep17149
82. Brito JA, Gomes CC, Guimaraes AL, Campos K, Gomez RS. Relationship between microRNA expression levels and histopathological features of dysplasia in oral leukoplakia. *J Oral Pathol Med.* (2014) 43:211–6. doi: 10.1111/jop.12112
83. Kinoshita T, Nohata N, Hanazawa T, Kikkawa N, Yamamoto N, Yoshino H, et al. Tumour-suppressive microRNA-29s inhibit cancer cell migration and invasion by targeting laminin-integrin signalling in head and neck squamous cell carcinoma. *Br J Cancer.* (2013) 109:2636–45. doi: 10.1038/bjc.2013.607
84. Tachibana H, Sho R, Takeda Y, Zhang X, Yoshida Y, Narimatsu H, et al. Circulating miR-223 in oral cancer: its potential as a novel diagnostic biomarker and therapeutic target. *PLoS ONE.* (2016) 11:e0159693. doi: 10.1371/journal.pone.0159693
85. Ghosh RD, Ghuwalewala S, Das P, Mandloi S, Alam SK, Chakraborty J, et al. MicroRNA profiling of cisplatin-resistant oral squamous cell carcinoma cell lines enriched with cancer-stem-cell-like and epithelial-mesenchymal transition-type features. *Sci Rep.* (2016) 6:23932. doi: 10.1038/srep23932
86. Zeng G, Xun W, Wei K, Yang Y, Shen H. MicroRNA-27a-3p regulates epithelial to mesenchymal transition via targeting YAP1 in oral squamous cell carcinoma cells. *Oncol Rep.* (2016) 36:1475–82. doi: 10.3892/or.2016.4916
87. Lu YC, Chang JT, Liao CT, Kang CJ, Huang SF, Chen IH, et al. OncomiR-196 promotes an invasive phenotype in oral cancer through the NME4-JNK-TIMP1-MMP signaling pathway. *Mol Cancer.* (2014) 13:218. doi: 10.1186/1476-4598-13-218
88. Tu HF, Chang KW, Cheng HW, Liu CJ. Upregulation of miR-372 and−373 associates with lymph node metastasis and poor prognosis of oral carcinomas. *Laryngoscope.* (2015) 125:E365–70. doi: 10.1002/lary.25464
89. Hou YY, You JJ, Yang CM, Pan HW, Chen HC, Lee JH, et al. Aberrant DNA hypomethylation of miR-196b contributes to migration and invasion of oral cancer. *Oncol Lett.* (2016) 11:4013–21. doi: 10.3892/ol.2016.4491
90. Lin SC, Kao SY, Chang JC, Liu YC, Yu EH, Tseng SH, et al. Up-regulation of miR-187 modulates the advances of oral carcinoma by targeting BARX2 tumor suppressor. *Oncotarget.* (2016) 7:61355–65. doi: 10.18632/oncotarget.11349
91. Chang CJ, Hsu CC, Chang CH, Tsai LL, Chang YC, Lu SW, et al. Let-7d functions as novel regulator of epithelial-mesenchymal transition and chemoresistant property in oral cancer. *Oncol Rep.* (2011) 26:1003–10. doi: 10.3892/or.2011.1360
92. Lei W, Liu YE, Zheng Y, Qu L. MiR-429 inhibits oral squamous cell carcinoma growth by targeting ZEB1. *Med Sci Monit.* (2015) 21:383–9. doi: 10.12659/MSM.893412
93. Wu B, Lei D, Wang L, Yang X, Jia S, Yang Z, et al. MiRNA-101 inhibits oral squamous-cell carcinoma growth and metastasis by targeting zinc finger E-box binding homeobox 1. *Am J Cancer Res.* (2016) 6:1396–407. Available online at: http://www.ajcr.us/files/ajcr0026756.pdf
94. Yu J, Xie F, Bao X, Chen W, Xu Q. miR-300 inhibits epithelial to mesenchymal transition and metastasis by targeting Twist in human epithelial cancer. *Mol Cancer.* (2014) 13:121. doi: 10.1186/1476-4598-13-121
95. Bufalino A, Cervigne NK, De Oliveira CE, Fonseca FP, Rodrigues PC, Macedo CC, et al. Low miR-143/miR-145 cluster levels induce activin a overexpression in oral squamous cell carcinomas, which contributes to poor prognosis. *PLoS ONE.* (2015) 10:e0136599. doi: 10.1371/journal.pone.0136599
96. Chang WM, Lin YF, Su CY, Peng HY, Chang YC, Lai TC, et al. Dysregulation of RUNX2/activin-A axis upon miR-376c downregulation promotes lymph node metastasis in head and neck squamous cell carcinoma. *Cancer Res.* (2016) 76:7140–50. doi: 10.1158/0008-5472.CAN-16-1188
97. Lu L, Xue X, Lan J, Gao Y, Xiong Z, Zhang H, et al. MicroRNA-29a upregulates MMP2 in oral squamous cell carcinoma to promote cancer invasion and anti-apoptosis. *Biomed Pharmacother.* (2014) 68:13–9. doi: 10.1016/j.biopha.2013.10.005
98. Fukumoto I, Koshizuka K, Hanazawa T, Kikkawa N, Matsushita R, Kurozumi A, et al. The tumor-suppressive microRNA-23b/27b cluster regulates the MET oncogene in oral squamous cell carcinoma. *Int J Oncol.* (2016) 49:1119–29. doi: 10.3892/ijo.2016.3602
99. Uesugi A, Kozaki K, Tsuruta T, Furuta M, Morita K, Imoto I, et al. The tumor suppressive microRNA miR-218 targets the mTOR component Rictor and inhibits AKT phosphorylation in oral cancer. *Cancer Res.* (2011) 71:5765–78. doi: 10.1158/0008-5472.CAN-11-0368
100. Kinoshita T, Hanazawa T, Nohata N, Kikkawa N, Enokida H, Yoshino H, et al. Tumor suppressive microRNA-218 inhibits cancer cell migration and invasion through targeting laminin-332 in head and neck squamous cell carcinoma. *Oncotarget.* (2012) 3:1386–400. doi: 10.18632/oncotarget.709
101. Lin F, Yao L, Xiao J, Liu D, Ni Z. MiR-206 functions as a tumor suppressor and directly targets K-Ras in human oral squamous cell carcinoma. *Onco Targets Ther.* (2014) 7:1583–91. doi: 10.2147/OTT.S67624
102. Koshizuka K, Hanazawa T, Fukumoto I, Kikkawa N, Matsushita R, Mataki H, et al. Dual-receptor (EGFR and c-MET) inhibition by tumor-suppressive miR-1 and miR-206 in head and neck squamous cell carcinoma. *J Hum Genet.* (2017). 62:113–21. doi: 10.1038/jhg.2016.47
103. Bonnin N, Armandy E, Carras J, Ferrandon S, Battiston-Montagne P, Aubry M, et al. MiR-422a promotes loco-regional recurrence by targeting NT5E/CD73 in head and neck squamous cell carcinoma. *Oncotarget.* (2016) 7:44023–38. doi: 10.18632/oncotarget.9829
104. Liu CJ, Shen WG, Peng SY, Cheng HW, Kao SY, Lin SC, et al. miR-134 induces oncogenicity and metastasis in head and neck carcinoma through targeting WWOX gene. *Int J Cancer.* (2014) 134:811–21. doi: 10.1002/ijc.28358
105. Henson BJ, Bhattacharjee S, O'dee DM, Feingold E, Gollin SM. Decreased expression of miR-125b and miR-100 in oral cancer cells contributes to malignancy. *Genes Chromosomes Cancer.* (2009) 48:569–82. doi: 10.1002/gcc.20666
106. Shiiba M, Shinozuka K, Saito K, Fushimi K, Kasamatsu A, Ogawara K, et al. MicroRNA-125b regulates proliferation and radioresistance of oral squamous cell carcinoma. *Br J Cancer.* (2013) 108:1817–21. doi: 10.1038/bjc.2013.175
107. Zhou X, Ren Y, Liu A, Jin R, Jiang Q, Huang Y, et al. WP1066 sensitizes oral squamous cell carcinoma cells to cisplatin by targeting STAT3/miR-21 axis. *Sci Rep.* (2014) 4:7461. doi: 10.1038/srep07461
108. Suh YE, Raulf N, Gaken J, Lawler K, Urbano TG, Bullenkamp J, et al. MicroRNA-196a promotes an oncogenic effect in head and neck cancer cells by suppressing annexin A1 and enhancing radioresistance. *Int J Cancer.* (2015) 137:1021–34. doi: 10.1002/ijc.29397
109. Kawahara K, Nakayama H, Nagata M, Yoshida R, Hirosue A, Tanaka T, et al. A low Dicer expression is associated with resistance to 5-FU-based chemoradiotherapy and a shorter overall survival in patients with oral squamous cell carcinoma. *J Oral Pathol Med.* (2014) 43:350–6. doi: 10.1111/jop.12140
110. Yu ZW, Zhong LP, Ji T, Zhang P, Chen WT, Zhang CP. MicroRNAs contribute to the chemoresistance of cisplatin in tongue squamous cell carcinoma lines. *Oral Oncol.* (2010) 46:317–22. doi: 10.1016/j.oraloncology.2010.02.002
111. Lin J, Lin Y, Fan L, Kuang W, Zheng L, Wu J, et al. miR-203 inhibits cell proliferation and promotes cisplatin induced cell death in tongue squamous cancer. *Biochem Biophys Res Commun.* (2016) 473:382–7. doi: 10.1016/j.bbrc.2016.02.105
112. Sun L, Yao Y, Liu B, Lin Z, Lin L, Yang M, et al. MiR-200b and miR-15b regulate chemotherapy-induced epithelial-mesenchymal transition in human tongue cancer cells by targeting BMI1. *Oncogene.* (2012) 31:432–45. doi: 10.1038/onc.2011.263
113. Liao L, Wang J, Ouyang S, Zhang P, Wang J, Zhang M. Expression and clinical significance of microRNA-1246 in human oral squamous cell carcinoma. *Med Sci Monit.* (2015) 21:776–81. doi: 10.12659/MSM.892508

114. Guan GF, Zhang DJ, Wen LJ, Xin D, Liu Y, Yu DJ, et al. Overexpression of lncRNA H19/miR-675 promotes tumorigenesis in head and neck squamous cell carcinoma. *Int J Med Sci.* (2016) 13:914–22. doi: 10.7150/ijms.16571
115. Xu P, Li Y, Zhang H, Li M, Zhu H. MicroRNA-340 mediates metabolic shift in oral squamous cell carcinoma by targeting glucose transporter-1. *J Oral Maxillofac Surg.* (2016) 74:844–50. doi: 10.1016/j.joms.2015.09.038
116. Qiao B, Cai JH, King-Yin Lam A, He BX. MicroRNA-542-3p inhibits oral squamous cell carcinoma progression by inhibiting ILK/TGF-beta1/Smad2/3 signaling. *Oncotarget.* (2017) 8:70761–76. doi: 10.18632/oncotarget.19986
117. Zhang B, Li Y, Hou D, Shi Q, Yang S, Li Q. MicroRNA-375 inhibits growth and enhances radiosensitivity in oral squamous cell carcinoma by targeting insulin like growth factor 1 receptor. *Cell Physiol Biochem.* (2017) 42:2105–17. doi: 10.1159/000479913
118. Koshizuka K, Hanazawa T, Kikkawa N, Katada K, Okato A, Arai T, et al. Antitumor miR-150-5p and miR-150-3p inhibit cancer cell aggressiveness by targeting SPOCK1 in head and neck squamous cell carcinoma. *Auris Nasus Larynx.* (2018) 45:854–65. doi: 10.1016/j.anl.2017.11.019
119. Rupaimoole R, Slack FJ. MicroRNA therapeutics: towards a new era for the management of cancer and other diseases. *Nat Rev Drug Discov.* (2017) 16:203–22. doi: 10.1038/nrd.2016.246
120. Zhang L, Hou D, Chen X, Li D, Zhu L, Zhang Y, et al. Exogenous plant MIR168a specifically targets mammalian LDLRAP1: evidence of cross-kingdom regulation by microRNA. *Cell Res.* (2012) 22:107–26. doi: 10.1038/cr.2011.158
121. Bouchie A. First microRNA mimic enters clinic. *Nat Biotechnol.* (2013) 31:577. doi: 10.1038/nbt0713-577
122. Kelnar K, Peltier HJ, Leatherbury N, Stoudemire J, Bader AG. Quantification of therapeutic miRNA mimics in whole blood from nonhuman primates. *Anal Chem.* (2014) 86:1534–42. doi: 10.1021/ac403044t
123. Griffiths-Jones S, Saini HK, Van Dongen S, Enright AJ. miRBase: tools for microRNA genomics. *Nucleic Acids Res.* (2008) 36:D154–8. doi: 10.1093/nar/gkm952

Conflict of Interest: The authors declare that the research was conducted in the absence of any commercial or financial relationships that could be construed as a potential conflict of interest.

frontiers in Oncology

ORIGINAL RESEARCH
published: 22 May 2020
doi: 10.3389/fonc.2020.00681

Identification of Hub Genes Associated With Development of Head and Neck Squamous Cell Carcinoma by Integrated Bioinformatics Analysis

Chia Ying Li[1,2], *Jia-Hua Cai*[3†], *Jeffrey J. P. Tsai*[3] *and Charles C. N. Wang*[3*]

[1] Department of Surgery, Show Chwan Memorial Hospital, Changhua, Taiwan, [2] Ph.D. Program in Tissue Engineering and Regenerative Medicine, National Chung Hsing University, Taichung, Taiwan, [3] Department of Bioinformatics and Medical Engineering, Asia University, Taichung, Taiwan

OPEN ACCESS

Edited by:
Jorge A. R. Salvador,
University of Coimbra, Portugal

Reviewed by:
Lorenzo Lo Muzio,
University of Foggia, Italy
Sheng Li,
Wuhan University, China
Jun Liu,
Sichuan University, China

***Correspondence:**
Charles C. N. Wang
cnwang@asia.edu.tw

[†] These authors have contributed equally to this work

Specialty section:
This article was submitted to Head and Neck Cancer, a section of the journal Frontiers in Oncology

Received: 29 December 2019
Accepted: 09 April 2020
Published: 22 May 2020

Citation:
Li CY, Cai J-H, Tsai JJP and Wang CCN (2020) Identification of Hub Genes Associated With Development of Head and Neck Squamous Cell Carcinoma by Integrated Bioinformatics Analysis. Front. Oncol. 10:681. doi: 10.3389/fonc.2020.00681

Improved insight into the molecular mechanisms of head and neck squamous cell carcinoma (HNSCC) is required to predict prognosis and develop a new therapeutic strategy for targeted genes. The aim of this study is to identify significant genes associated with HNSCC and to further analyze its prognostic significance. In our study, the cancer genome atlas (TCGA) HNSCC database and the gene expression profiles of GSE6631 from the Gene Expression Omnibus (GEO) were used to explore the differential co-expression genes in HNSCC compared with normal tissues. A total of 29 differential co-expression genes were screened out by Weighted Gene Co-expression Network Analysis (WGCNA) and differential gene expression analysis methods. As suggested in functional annotation analysis using the R clusterProfiler package, these genes were mainly enriched in epidermis development and differentiation (biological process), apical plasma membrane and cell-cell junction (cellular component), and enzyme inhibitor activity (molecular function). Furthermore, in a protein-protein interaction (PPI) network containing 21 nodes and 25 edges, the ten hub genes (S100A8, S100A9, IL1RN, CSTA, ANXA1, KRT4, TGM3, SCEL, PPL, and PSCA) were identified using the CytoHubba plugin of Cytoscape. The expression of the ten hub genes were all downregulated in HNSCC tissues compared with normal tissues. Based on survival analysis, the lower expression of CSTA was associated with worse overall survival (OS) in patients with HNSCC. Finally, the protein level of CSTA, which was validated by the Human Protein Atlas (HPA) database, was down-regulated consistently with mRNA levels in head and neck cancer samples. In summary, our study demonstrated that a survival-related gene is highly correlated with head and neck cancer development. Thus, CSTA may play important roles in the progression of head and neck cancer and serve as a potential biomarker for future diagnosis and treatment.

Keywords: head and neck squamous cell carcinoma, differential gene expression analysis, weighted gene co-expression network analysis, the differential co-expression genes, biomarkers

INTRODUCTION

Head and neck squamous cell carcinoma (HNSCC) is one of most common types of cancer in the world. HNSCC includes several malignancies that originate in the mouth, nasopharynx, oropharynx, hypopharynx, larynx, and neck (1). According to the published global cancer statistics report, there were more than an estimated 650,000 new cases and 330,000 deaths diagnosed in 2018 (2). Many lifestyle factors have been investigated, with tobacco use, alcohol consumption, human papillomavirus (HPV), and Epstein-Barr virus (EBV) infection being considered as the risk factors that are associated with the progression of HNSCC (3). However, HPV is currently the one most well-studied and frequently used biomarker in HNSCC (4–6). In the past several years, the treatments for managing head and neck cancer included the following: radiation therapy, surgery, and chemotherapy. Appropriate combinations of the three treatment modalities is selected according to the site of the cancer and the stage of the disease (1, 3). Although there are diverse treatments for HNSCC, patients have a limited survival advantage.

With the development of genomic technologies, bioinformatics has become increasingly popular for gene expression profiles analysis to study the molecular mechanisms of diseases and discover disease-specific biomarkers (7). One important method to understand the gene function and gene association from genome-wide expression is Weighted Gene Co-expression Network Analysis (WGCNA) (8). WGCNA can be used to detect co-expression modules of highly correlated genes and interested modules associated with clinical traits (9), providing great insight into predicting the functions of co-expression genes and finding genes that play key roles in human diseases (10–12). Furthermore, another powerful analysis within transcriptomics is differential gene expression analysis, which provides methods for studying molecular mechanisms underlying genome regulation and discovering quantitative changes in expression levels between experimental groups and control groups (13). Such gene expression differences can lead to the discovery of potential biomarkers for a particular disease. Therefore, using two approaches, the findings from WGCNA and differential gene expression analysis are combined to enhance the discriminating ability of highly related genes that are useful to serve as candidate biomarkers.

In this study, the mRNA expression data of HNSCC from the TCGA and GEO databases were analyzed by WGCNA and differential gene expression analysis to obtain differential co-expression genes. We further explored HNSCC development

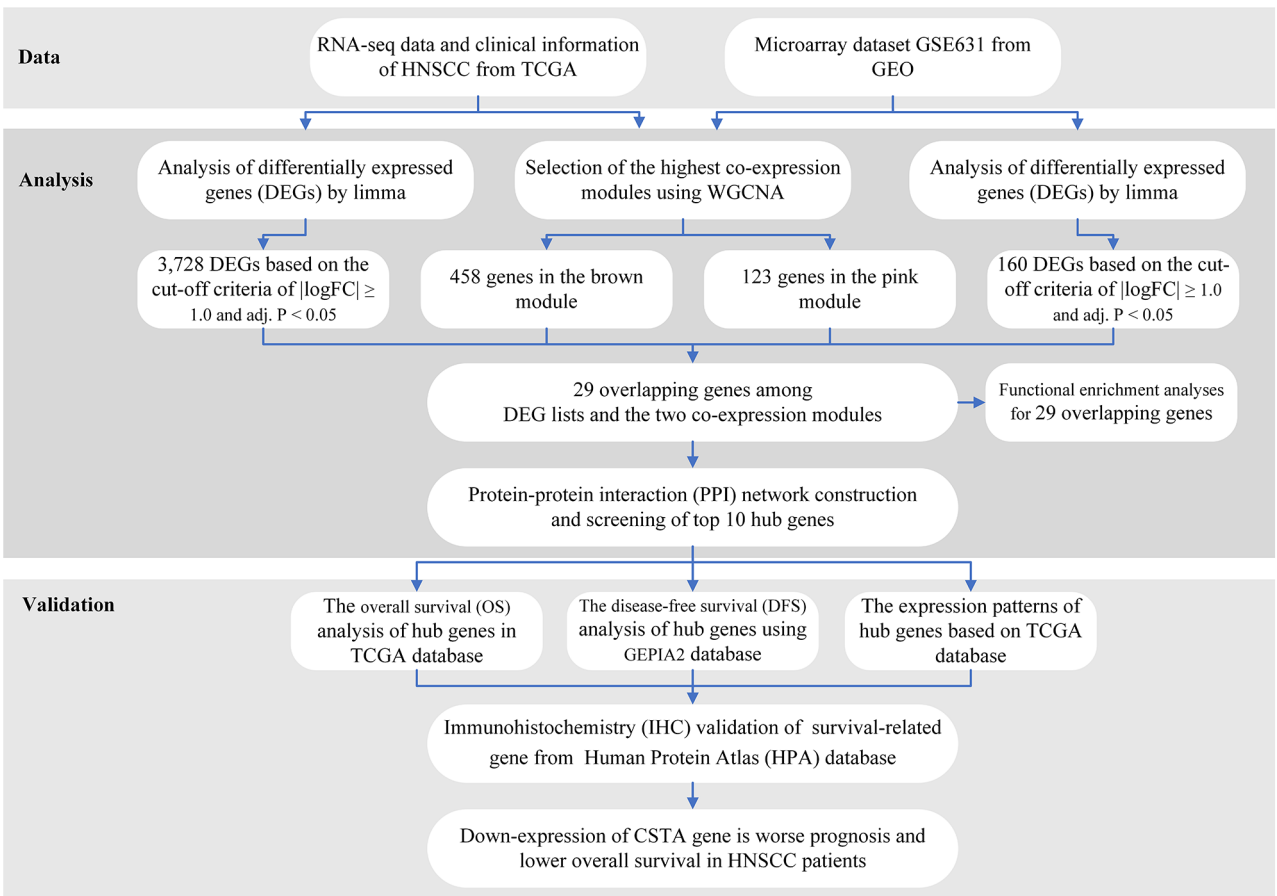

FIGURE 1 | Study design and workflow of this study.

through functional enrichment and protein-protein interaction (PPI) analysis combined with survival analysis. The study provides a potential basis to understand the cause and potential molecular events of HNSCC by analyzing differential co-expression genes for clinical diagnosis or treatment.

MATERIALS AND METHODS

The workflow of the analysis hub gene extraction curation pipeline is shown in **Figure 1**.

We elaborate on each step in the following sub-sections.

Datasets From TCGA and GEO Database

The gene expression profiles of HNSCC were downloaded from TCGA (https://portal.gdc.cancer.gov/) and GEO (https://www.ncbi.nlm.nih.gov/gds). In the TCGA database, all data on HNSCC and corresponding clinical information were freely downloaded by R package *TCGAbiolinks* (14). There were 544 NHSCC samples, including 500 head and neck cancers and 44 normal tissues, and RNAseq count data on 19,430 genes. A total of the data had been generated by using the Illumina HiSeq 2,000 platform, and were annotated to a reference transcript set of Human hg38 gene standard track. As suggested by the *edgeR* package tutorial (15), genes of low

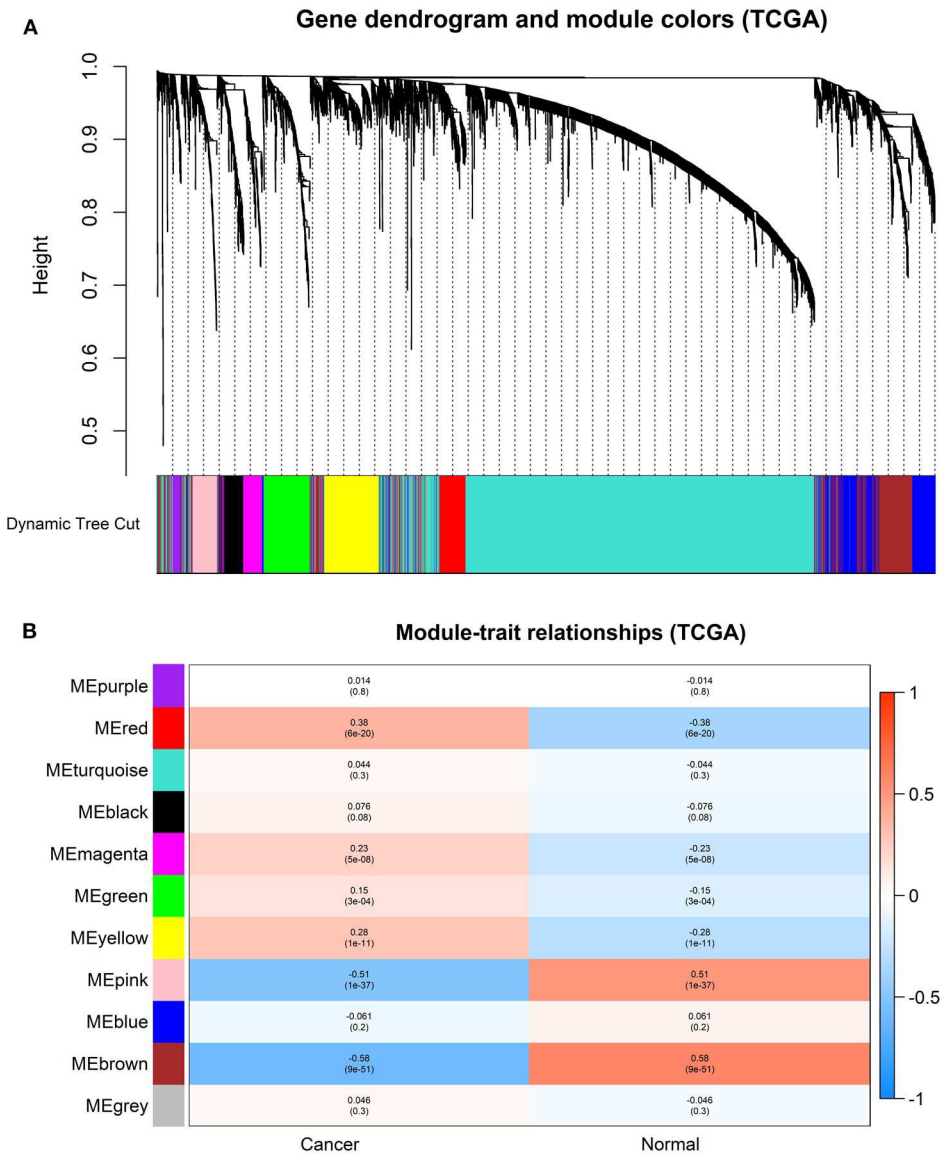

FIGURE 2 | Identification of modules associated with the clinical information in the TCGA-HNSCC dataset. **(A)** The Cluster dendrogram of co-expression network modules was ordered by a hierarchical clustering of genes based on the 1-TOM matrix. Each module was assigned different colors. **(B)** Module-trait relationships. Each row corresponds to a color module and column corresponds to a clinical trait (cancer and normal). Each cell contains the corresponding correlation and *P*-value.

read counts are usually not of interest for further analysis. So, we kept the genes with a cpm (count per million) ≥1 in this study. After filtering using function *rpkm* in *edgeR* package, which is calculated by dividing gene counts by gene length, a total of 15,367 genes with RPKM values were subject to our next analysis.

In addition, the normalized expression profiles of GSE6631, another gene expression profile of HNSCC from GEO, was obtained using R package *GEOquery* (16). GSE6631 consisted of 22 tumor samples and 22 paired normal tissues from patients with HNSCC, which were studied with the GPL8300 platform [HG_U95Av2] Affymetrix Human Genome U95 Version 2 Array. Probes were converted to the gene symbols based on a manufacturer-provided annotation file and duplicated probes for the same gene were removed by determining the median expression value of all its corresponding probes. As a result, a list of 9,203 genes were selected for the subsequent analysis.

Identification of Key Co-expression Modules Using WGCNA

Co-expression networks facilitate methods on network-based gene screening that can be used to identify candidate biomarkers and therapeutic targets. In our study, the gene expression data profiles of TCGA-HNSCC and GSE6631 were constructed to gene co-expression networks using the *WGCNA* package in R (8).

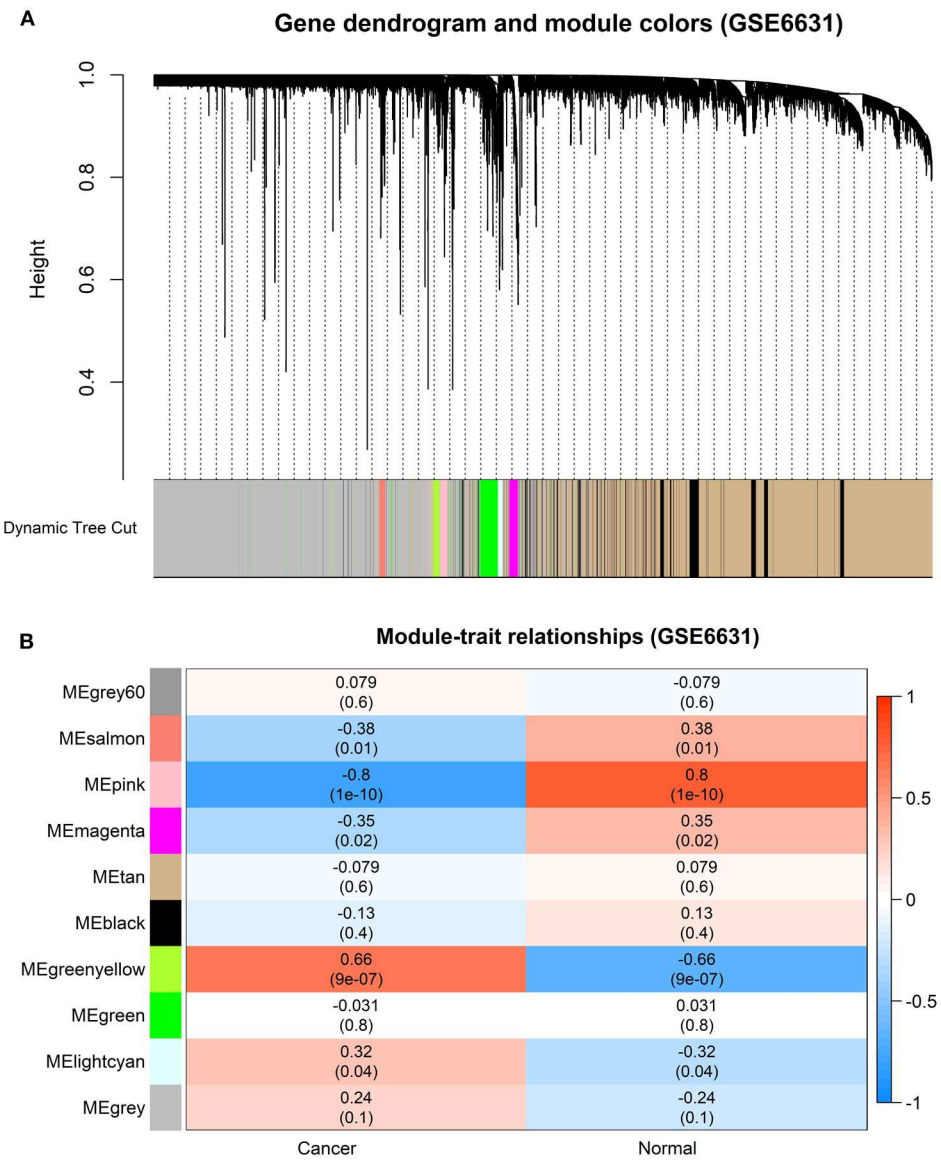

FIGURE 3 | Identification of modules associated with clinical information in the GSE6631 dataset. **(A)** The Cluster dendrogram of co-expression network modules was ordered by a hierarchical clustering of genes based on the 1-TOM matrix. Each module was assigned different colors. **(B)** Module-trait relationships. Each row corresponds to a color module and each column correlates to a clinical trait (cancer and normal). Each cell contains the corresponding correlation and *P*-value.

WGCNA was used to explore the modules of highly correlated genes among samples for relating modules to external sample traits. To build a scale-free network, soft powers $\beta = 3$ and 20 were selected using the function *pickSoftThreshold*. Next, the adjacency matrix was created by the following formula: $a_{ij} = |S_{ij}|^{\beta}$ (a_{ij}: adjacency matrix between gene i and gene j, S_{ij}: similarity matrix which is done by Pearson correlation of all gene pairs, β: softpower value), and was transformed into a topological overlap matrix (TOM) as well as the corresponding dissimilarity (1-TOM). Afterwards, a hierarchical clustering dendrogram of the 1-TOM matrix was constructed to classify the similar gene expressions into different gene co-expression modules. To further identify functional modules in a co-expression network, the module-trait associations between modules, and clinical trait information were calculated according to the previous study (17). Therefore, modules with high correlation coefficient were considered candidates relevant to clinical traits, and were selected for subsequent analysis. A more detailed description of the WGCNA method was reported in our previous study (17).

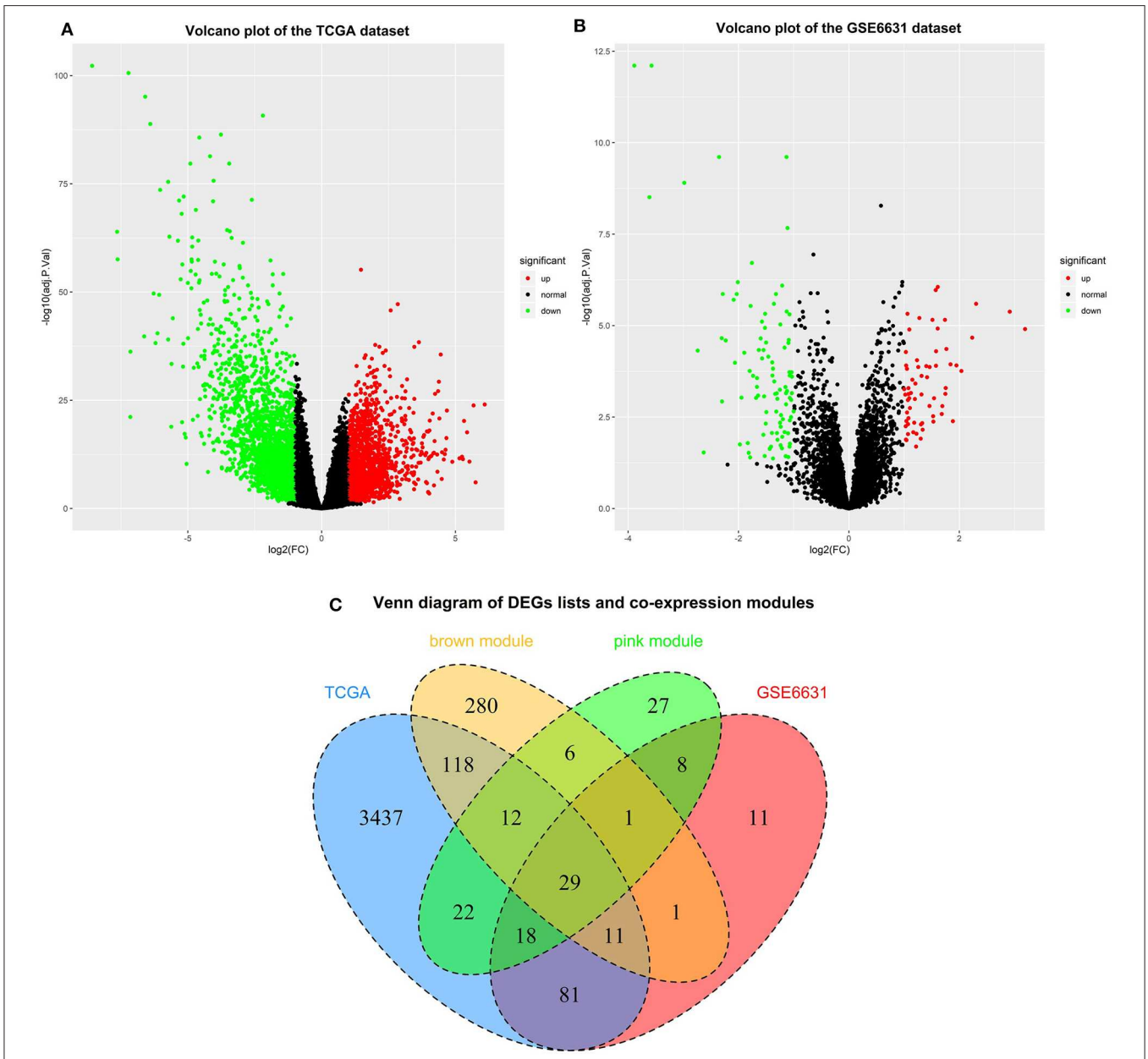

FIGURE 4 | Identification of differentially expressed genes (DEGs) among the TCGA and GSE6631 datasets of HNSCC with the cut-off criteria of |logFC| ≥ 1.0 and adj. $P < 0.05$. **(A)** Volcano plot of DEGs in the TCGA dataset. **(B)** Volcano plot of DEGs in the GSE6631 dataset. **(C)** The Venn diagram of genes among DEG lists and co-expression module. In total, 29 overlapping genes in the intersection of DEG lists and two co-expression modules.

Differential Expression Analysis and Interaction With the Modules of Interest

The R package *limma* (linear models for microarray data) provides an integrated solution for differential expression analyses on RNA-Sequencing and microarray data (18). In order to find the differentially expressed genes (DEGs) between HNSCC and normal tissues, *limma* was applied in the TCGA-HNSCC and GSE6631 dataset, respectively, to screen out DEGs. The *p*-value was adjusted by the Benjamini–Hochberg method to control for the false discovery Rate (FDR). Genes with the cut-off criteria of $|\log FC| \geq 1.0$ and adj. $P < 0.05$ were regarded as DEGs. The DEGs of the TCGA-HNSCC and GSE6631 dataset were visualized as a volcano plot by using the R package *ggplot2* (19). Subsequently, the overlapping genes between DEGs and co-expression genes that were extracted from the co-expression network were used to identify potential prognostic genes, which were presented as a Venn diagram using the R package *VennDiagram* (20).

Functional Annotation for Genes of Interest

To explore Gene Ontology (GO) of selected genes, R package clusterProfiler package (21) was used to explore the functions among genes of interest, with a cut-off criterion of adjusted $p < 0.05$. GO annotation that contains the three sub-ontologies—biological process (BP), cellular component (CC), and molecular function (MF)—can identify the biological properties of genes and gene sets for all organisms (22).

Construction of PPI and Screening of Hub Genes

In our study, we used the STRING (Search Tool for the Retrieval of Interacting Genes) online tool, which is designed for predicting protein–protein interactions (PPI), to construct a PPI network of selected genes (23). Using the STRING database, genes with a score ≥ 0.4 were chosen to build a network model visualized by Cytoscape (v3.7.2) (24). In a co-expression network, Maximal Clique Centrality (MCC) algorithm was reported to be the most

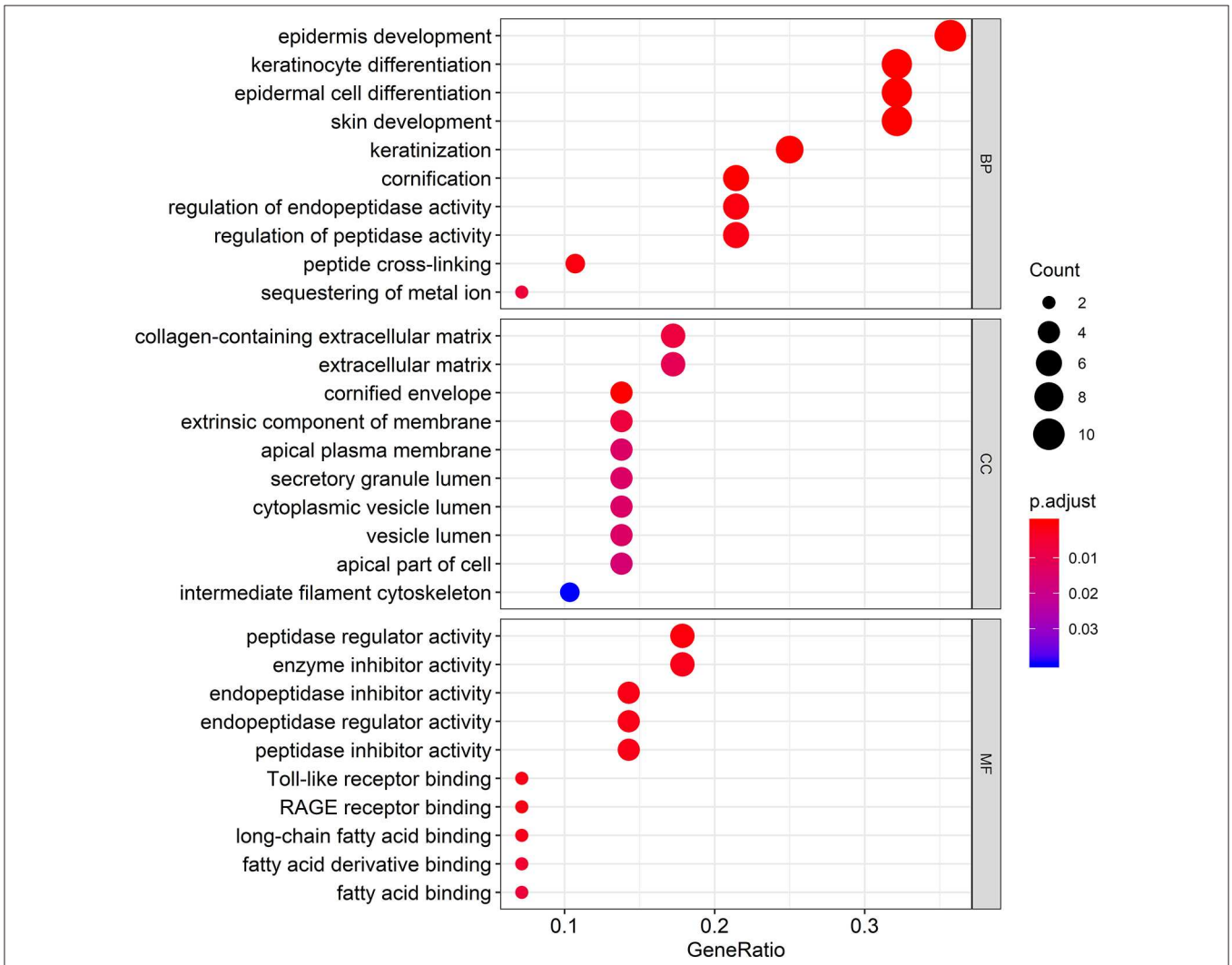

FIGURE 5 | Gene Ontology (GO) enrichment analysis for the genes in the brown module. The color represents the adjusted *p*-values (BH), and the size of the spots represents the gene number.

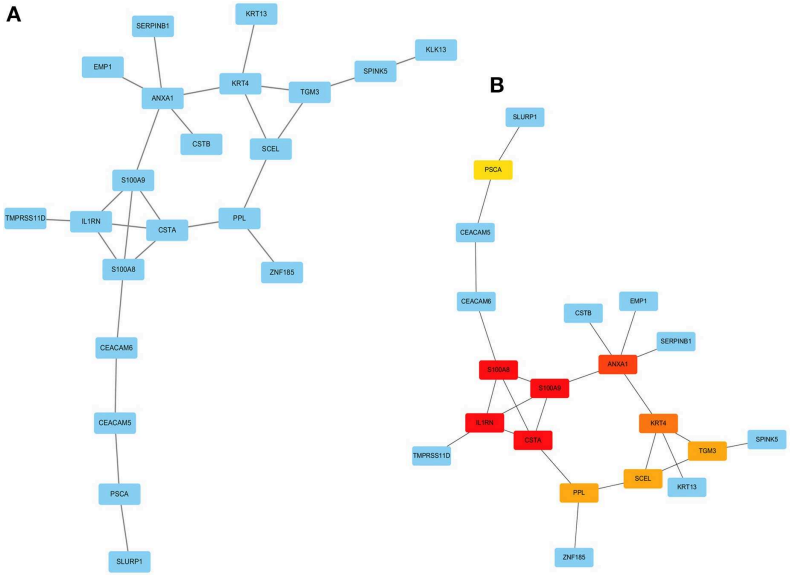

FIGURE 6 | Visualization of the protein-protein interaction (PPI) network and the candidate hub genes. **(A)** PPI network of the genes between DEG lists and two co-expression modules. The blue nodes represent the genes. Edges indicate interaction associations between nodes. **(B)** Identification of the hub genes from the PPI network using maximal clique centrality (MCC) algorithm. Edges represent the protein-protein associations. The red nodes represent genes with a high MCC sores, while the yellow node represent genes with a low MCC sore.

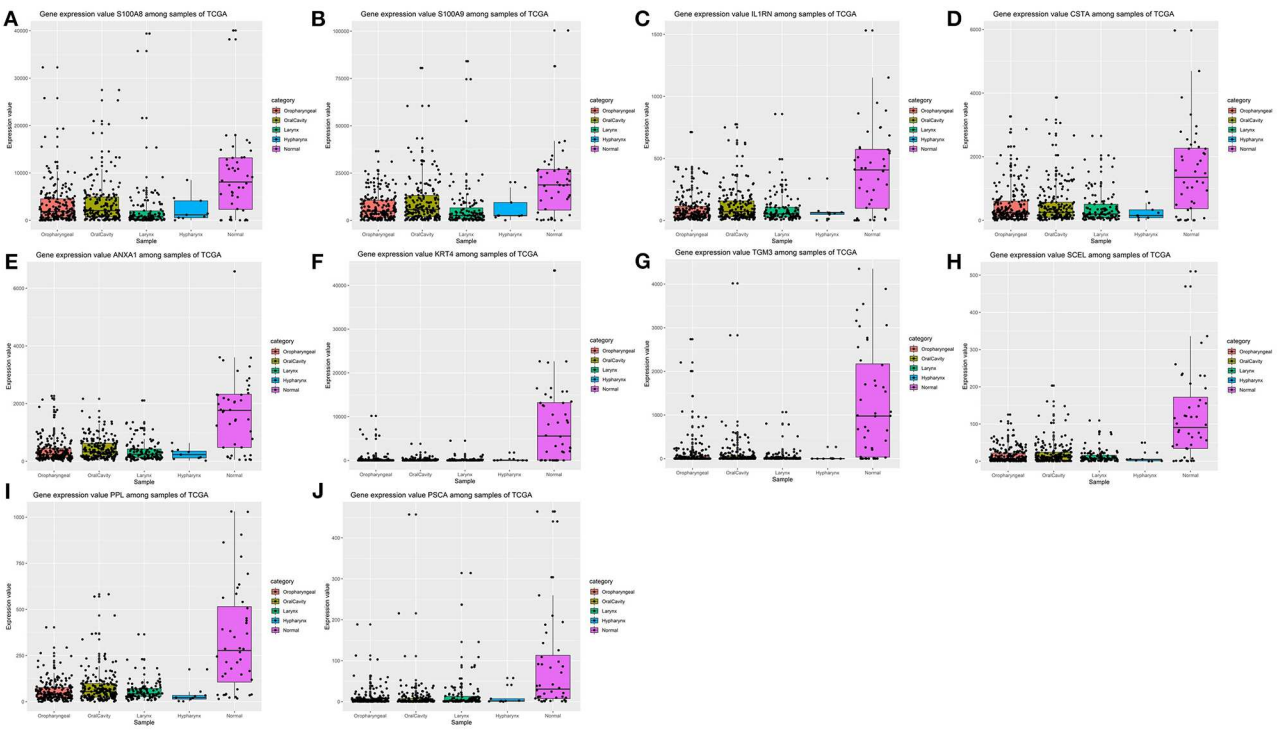

FIGURE 7 | Validation of expression levels of the ten hub genes among HNSCCs and normal tissues from the TCGA database. **(A)** Gene expression value S100A8 among samples of TCGA. **(B)** Gene expression value S100A9 among samples of TCGA. **(C)** Gene expression value IL1RN among samples of TCGA. **(D)** Gene expression value CSTA among samples of TCGA. **(E)** Gene expression value ANXA1 among samples of TCGA. **(F)** Gene expression value KRT4 among samples of TCGA. **(G)** Gene expression value TGM3 among samples of TCGA. **(H)** Gene expression value SCEL among samples of TCGA. **(I)** Gene expression value PPL among samples of TCGA. **(J)** Gene expression value PSCA among samples of TCGA.

effective method of finding hub nodes (25). The MCC of each node was calculated by CytoHubba, a plugin in Cytoscape (25). In this study, the genes with the top 10 MCC values were considered as hub genes.

Verification of the Expression Patterns and the Prognostic Values of Hub Genes

In order to confirm the reliability of the hub genes, we verified the expression patterns of the hub genes in different pathological tumors and normal tissues. The expression level of each hub gene between cancer and normal tissue was plotted as a box plot graph. Based on the data from the TCGA database, Kaplan–Meier univariate survival analysis was performed by using the *survival* package in R software to explore the relationship between overall survival (OS) and hub genes in patients. Moreover, the association between disease-free survival (DFS) and hub genes expressed in HNSCC patients was determined using the online tool GEPIA2 (26). In our study, only patients with completed follow-up times were selected for survival analysis and then divided into two separate groups based on the median expression value of hub genes. The survival-related hub genes with log-rank $p < 0.05$ were regarded as statistically significant.

Validation of Protein Expressions of Survival-Related Hub Genes by the HPA Database

The protein expression of the survival-related genes between HNSCC and normal tissues was determined using immunohistochemistry (IHC) from the Human Protein Atlas database (HPA, https://www.proteinatlas.org/). HPA is a valuable database that provides a large amount of transcriptomics and proteomics data in specific human tissues and cells for

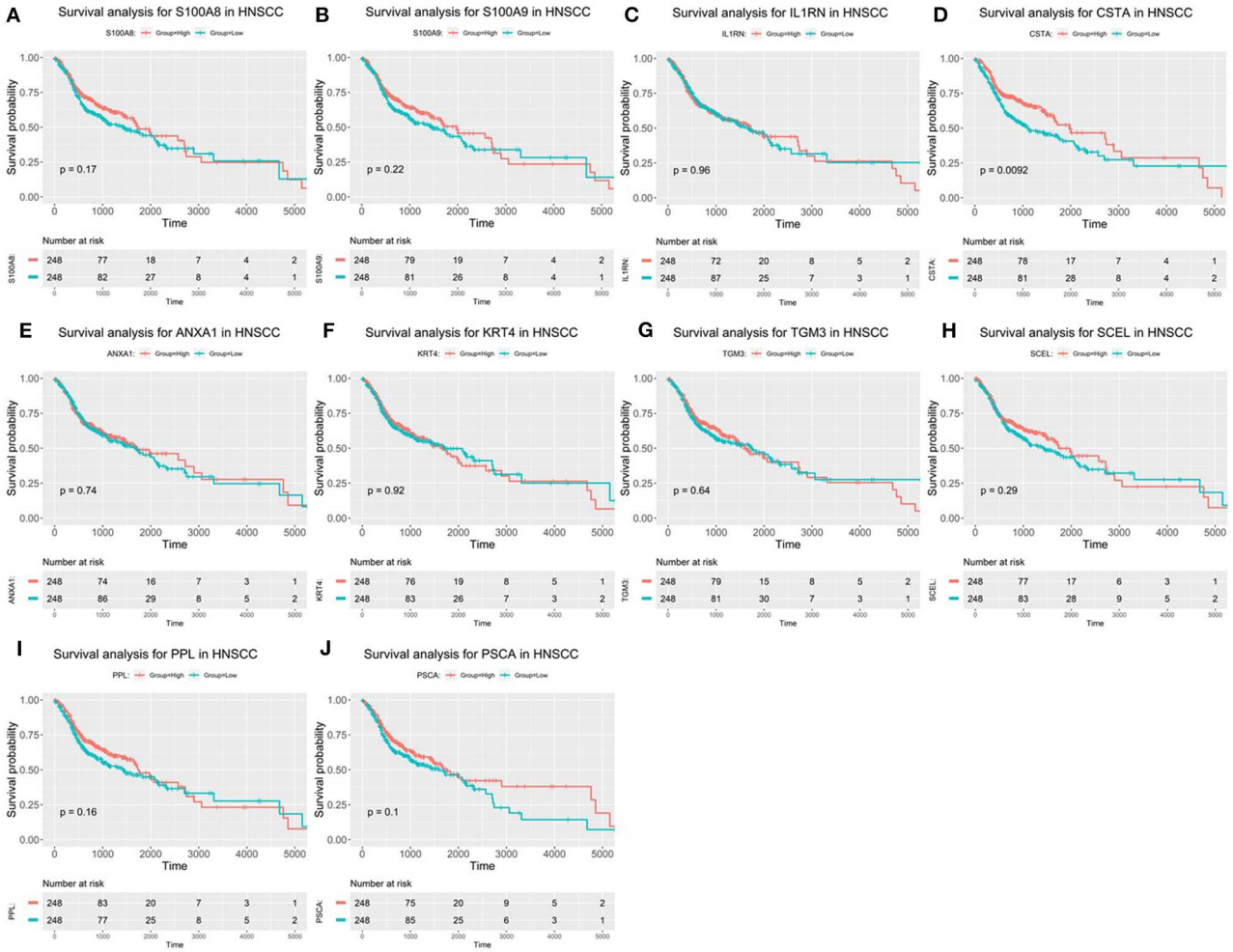

FIGURE 8 | Overall survival (OS) analysis of 10 hub genes in HNSCC patients from the GEPIA2 database. **(A)** Survival analysis for S100A8 in HNSCC. **(B)** Survival analysis for S100A9 in HNSCC. **(C)** Survival analysis for IL1RN in HNSCC. **(D)** Survival analysis for CSTA in HNSCC. **(E)** Survival analysis for ANXA1 in HNSCC. **(F)** Survival analysis for KRT4 in HNSCC. **(G)** Survival analysis for TGM3 in HNSCC. **(H)** Survival analysis for SCEL in HNSCC. **(I)** Survival analysis for PPL in HNSCC. **(J)** Survival analysis for PSCA in HNSCC. The patients were stratified into high-level group (red) and low-level group (green) according to median expression of the gene. Log-rank $P < 0.05$ was considered to be a statistically significant difference.

researchers (27). Moreover, the IHC-based protein expression pattern is the most common application of immunostaining to detect the relative location and abundance of proteins (28).

RESULTS

Construction of Weighted Gene Co-expression Modules

In order to find the functional clusters in HNSCC patients, the gene co-expression networks were constructed from the TCGA-HNSCC and GSE6631 datasets with the *WGCNA* package. With each module assigned a color, a total of 10 modules in the TCGA-HNSCC (**Figure 2A**) and nine modules in the GSE6631 (**Figure 3A**) were identified in the present study (excluding a gray module that was not assigned into any cluster). Then, we plotted the heatmap of module-trait relationships to evaluate the association between each module and two clinical traits (cancer and normal). The results of the module-trait relationships are presented in **Figure 2B**, **3B**, revealing that the brown module in the TCGA-HNSCC and pink module in the GSE6631 were found to have the highest association with normal tissues (brown module: $r = 0.58$, $p = 9e{-}51$; pink module: $r = 0.8$, $p = 1e{-}10$).

Identification of Genes Between the DEG Lists and Co-expression Modules

Based on the cut-off criteria of $|\log FC| \geq 1.0$ and adj. $P < 0.05$, a total of 3,728 DEGs in the TCGA dataset (**Figure 4A**) and 160 DEGs in the GSE6631 dataset (**Figure 4B**) were found to be dysregulated in tumor tissues by the *limma* package. As shown in **Figure 4C**, 458 and 123 co-expression genes were found in the brown module of TCGA dataset and the pink module in GSE6631, respectively. In total, the 29 overlapping genes were extracted for validating the genes of co-expression modules (**Figure 4C**).

Functional Enrichment Analyses for the 29 Genes

To gain further insight into the potential functions of the 29 genes that overlapped with DEG lists and two co-expression modules, gene enrichment analysis was performed by the *clusterProfiler*

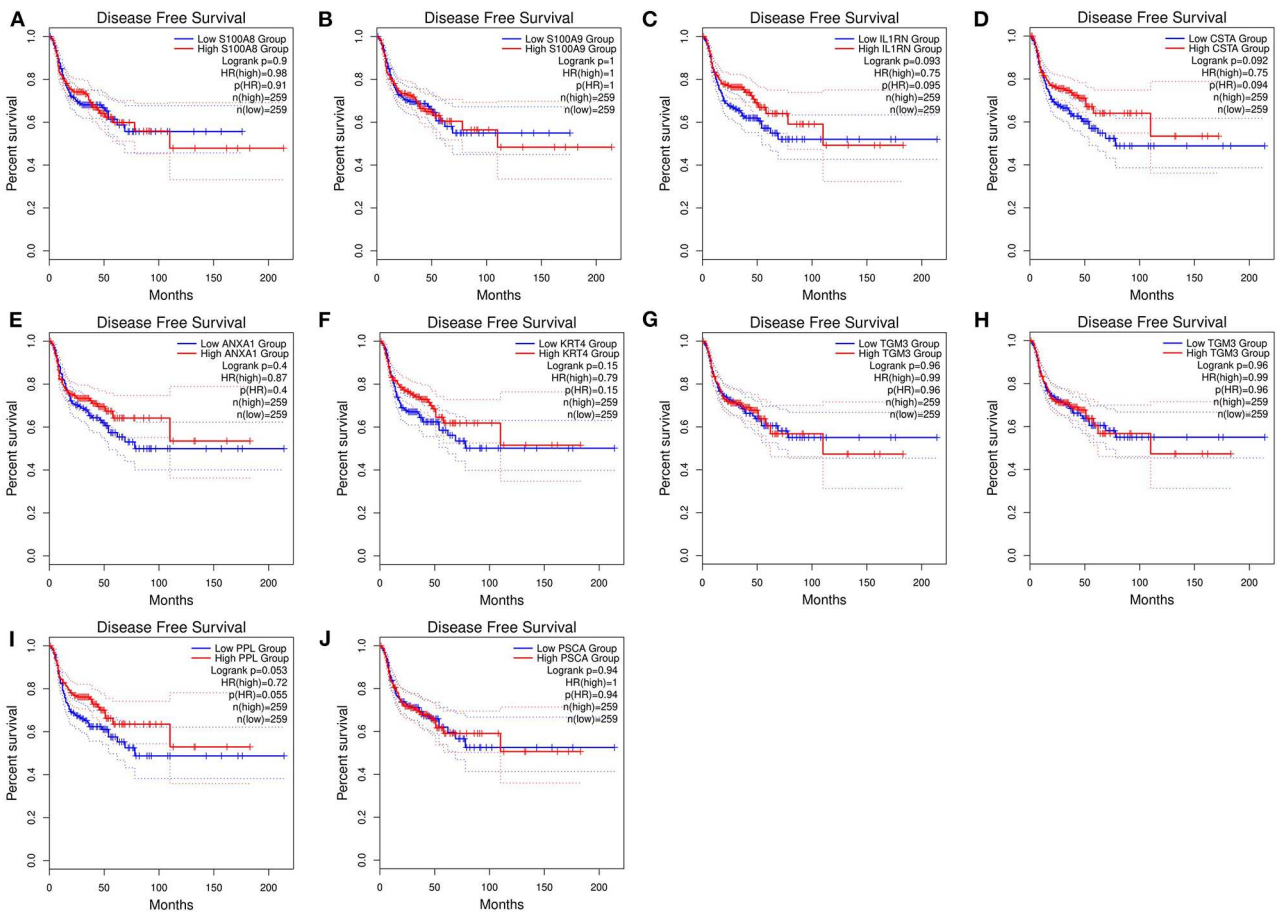

FIGURE 9 | Disease-free survival (DFS) analysis of 10 hub genes in HNSCC patients from the GEPIA2 database. **(A)** Survival analysis for S100A8 in HNSCC. **(B)** Survival analysis for S100A9 in HNSCC. **(C)** Survival analysis for IL1RN in HNSCC. **(D)** Survival analysis for CSTA in HNSCC. **(E)** Survival analysis for ANXA1 in HNSCC. **(F)** Survival analysis for KRT4 in HNSCC. **(G)** Survival analysis for TGM3 in HNSCC. **(H)** Survival analysis for SCEL in HNSCC. **(I)** Survival analysis for PPL in HNSCC. **(J)** Survival analysis for PSCA in HNSCC. The patients were stratified into high-level group (red) and low-level group (green) according to median expression of the gene. Log-rank $P < 0.05$ was considered to be a statistically significant difference.

package. After screening of GO enrichment analysis, we observed several enriched gene sets shown in **Figure 5**. The biological process (BP) of 29 genes are mainly enriched in epidermis development and epidermal cell differentiation. For the result of the cellular component (CC), it was revealed that these genes were mainly involved in apical plasma membrane, apical part of cell, and cell-cell junction. Moreover, in the molecular function (MF) analysis, peptidase regulator activity and enzyme inhibitor activity were suggested to be related to the 29 genes.

PPI Network Construction and Hub Genes Identification

The PPI network among the overlapped genes was established by using the STRING database, with 21 nodes and 25 edges (**Figure 6A**). The hub genes selected from the PPI network using the MCC algorithm of CytoHubba plugin were shown in **Figure 6B**. According to the MCC sores, the top ten highest-scored genes, including S100 calcium-binding protein A8 (S100A8), S100 calcium-binding protein A9 (S100A9), Interleukin-1 receptor antagonist (IL1RN), Cystatin A (CSTA), Annexin-A1 (ANXA1), Keratin 4 (KRT4), Transglutaminase 3 (TGM3), Sciellin (SCEL), Periplakin (PPL), and Prostate Stem Cell Antigen (PSCA), were selected as the hub genes.

Verification of the Expression Patterns, the Prognostic Values, and Protein Expression of Hub Genes

After the ten hub genes (S100A8, S100A9, IL1RN, CSTA, ANXA1, KRT4, TGM3, SCEL, PPL, and PSCA) were screened out by CytoHubba plugin, we verified the expression levels of the hub genes among the patients of the TCGA database. As shown in **Figure 7**, all of the ten hub genes were found to be significantly downregulated in HNSCC carcinoma compared with normal tissues. In addition, OS and DFS analyses of the ten hub genes were performed by Kaplan–Meier plotter using the R *survival* package (**Figure 8**) and the GEPIA2 database (**Figure 9**) for investigating the prognostic values of the hub gens in the HNSCC patients. Of the ten hub genes, the Kaplan–Meier analyses suggested that the lower expression level of CSTA was significantly associated with worse OS of the HNSCC patients ($P < 0.05$) (**Figure 8D**), while with DFS there was no significant difference observed in HNSCC patients with an expression level of CSTA ($P < 0.05$) (**Figure 9D**). Furthermore, the protein levels of the CSTA gene was significantly lower in tumor tissues compared with normal tissues based on the HPA database (**Figure 10**). All the above-mentioned observations confirmed down-expression of CSTA is associated with worse prognosis and lower overall survival in HNSCC patients.

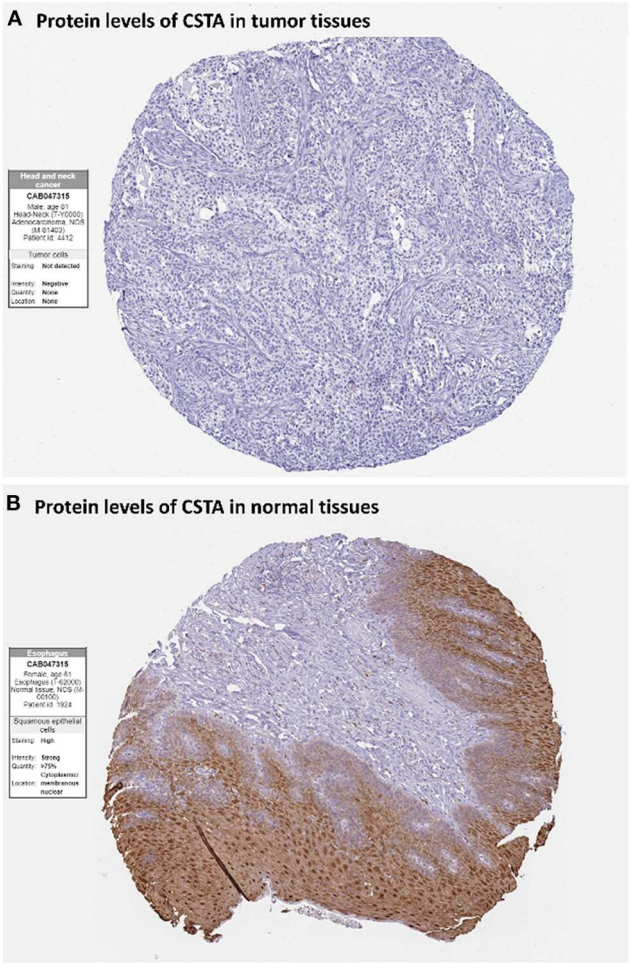

FIGURE 10 | Immunohistochemistry of the CSTA gene in HNSCC and normal tissues from the human protein atlas (HPA) database. **(A)** Protein levels of CSTA in HNSCC tissues (antibody CAB047315; staining: not detected; intensity: negative; quantity: none). **(B)** Protein levels of CSTA in normal oral mucosa tissues (antibody CAB047315; staining: high; intensity: strong; quantity: >75%).

DISCUSSION

Head and neck squamous cell carcinomas (HNSCC) are a group of cancers found in several regions, including the mouth, nose, throat, larynx, sinuses, or salivary glands. Although the treatment of head and neck cancer has improved, the prognosis of patients is generally poor due to the lack of precise molecular targets. Therefore, better biomarkers for specific prognosis and progression of HNSCC are demanded. In this study, a total of 29 significant genes with the same expression trends were identified in the TCGA and GSE6631 databases using integrated bioinformatic analysis. As suggested in functional annotation analysis by the *clusterProfiler* package, these genes were mainly enriched in epidermis development and differentiation, which are basic processes in cell proliferation. Furthermore, according to MCC scores from the CytoHubba plugin in Cytoscape, the top 10 HNSCC-related genes were screened out (namely S100A8, S100A9, IL1RN, CSTA, ANXA1, KRT4, TGM3, SCEL, PPL, and PSCA) and all their expression patterns were found be downregulated in HNSCC tissues compared with the normal controls. Among them, CSTA downexpression was significantly associated with poor overall survival in head and neck cancers. Finally,

survival and immunohistochemical analysis for CSTA was carried out.

CSTA, also known as Cystatin A or stefin A, is a member of the cystatin superfamily. It is an intracellular inhibitor regulating the activities of cystatin proteinase and has an important role in desmosome-mediated cell-cell adhesion (29, 30). Furthermore, lower mRNA levels of CSTA have been reported in breast (31), prostate (32), skin (30), and esophagus tumors (33) as compared to adjacent control tissues (34, 35). In our study, CSTA was down-regulated in tumor tissues compared with normal tissues, showing a significant correlation with HNSCC. Previous studies demonstrated that higher levels of CSTA in tumor tissues have been shown to correlate with a favorable prognosis of patients with HNSCC, that was consistent with our finding of survival analysis (36–39).

As with all research, our study also had limitations about the classification of tumors to different subtypes. Although we provided a comprehensive bioinformatics analysis to identify potential diagnostic genes between cancer and normal tissues, it may not be very accurate for each patient with HNSCC subtypes. Moreover, the molecular mechanisms involved in the survival-related genes that affected the prognosis of HNSCC patients should be further validated through a series of experiments.

In summary, by integrating WGCNA with differential gene expression analysis, our study generated the significant survival-related gene CSTA that has potential for prognosis prediction in HNSCC.

DATA AVAILABILITY STATEMENT

All available data were analyzed in this study. Those can be found here: TCGA (https://portal.gdc.cancer.gov/), GEO (https://www.ncbi.nlm.nih.gov/gds), and HPA (https://www.proteinatlas.org/).

AUTHOR CONTRIBUTIONS

J-HC, CW, and CL: conceptualization and methodology. CW and J-HC: software and data curation. JT and CL: validation. J-HC and CL: writing—original draft preparation. CW and JT: writing—review, editing, and supervision.

FUNDING

This present study was funded by Asia University and Show Chwan Memorial Hospital (Grant no. RD108029).

REFERENCES

1. Marur S, Forastiere AA. Head and neck squamous cell carcinoma: update on epidemiology, diagnosis, and treatment. *Mayo Clin Proc.* (2016) 91:386–96. doi: 10.1016/j.mayocp.2015.12.017
2. Bray F, Ferlay J, Soerjomataram I, Siegel RL, Torre LA, Jemal A. Global cancer statistics 2018: GLOBOCAN estimates of incidence and mortality worldwide for 36 cancers in 185 countries. *CA Cancer J Clin.* (2018) 68:394–424. doi: 10.3322/caac.21492
3. Spitz MR. Epidemiology and risk factors for head and neck cancer. *Semin Oncol.* (1994) 21:281–8.
4. Marur S, D'Souza G, *Westra* WH, Forastiere AA. HPV-associated head and neck cancer: a virus-related cancer epidemic. *Lancet Oncol.* (2010) 11:781–9. doi: 10.1016/S1470-2045(10)70017-6
5. D'Souza G, Dempsey A. The role of HPV in head and neck cancer and review of the HPV vaccine. *Prev Med.* (2011) 53 (Suppl. 1):S5–11. doi: 10.1016/j.ypmed.2011.08.001
6. Ragin CC, Modugno F, Gollin SM. The epidemiology and risk factors of head and neck cancer: a focus on human papillomavirus. *J Dent Res.* (2007) 86:104–14. doi: 10.1177/154405910708600202
7. Can T. Introduction to bioinformatics. *Methods Mol Biol.* (2014) 1107:51–71. doi: 10.1007/978-1-62703-748-8_4
8. Langfelder PS. Horvath WGCNA: an R package for weighted correlation network analysis. *BMC Bioinform.* (2008) 9:559. doi: 10.1186/1471-2105-9-559
9. Zhang B, Horvath S. A general framework for weighted gene co-expression network analysis. *Stat Appl Genet Mol Biol.* (2005) 4:17. doi: 10.2202/1544-6115.1128
10. Li J, Zhou D, Qiu W, Shi Y, Yang JJ, Chen S, et al. Application of weighted gene co-expression network analysis for data from paired design. *Sci Rep.* (2018) 8:622. doi: 10.1038/s41598-017-18705-z
11. Saris CGJ, Horvath S, van Vught WJP, van Es MA, Blauw HM, Fuller TF, et al. Weighted gene co-expression network analysis of the peripheral blood from amyotrophic lateral sclerosis patients. *BMC Genomics.* (2009) 10:405. doi: 10.1186/1471-2164-10-405
12. Yang Y, Han L, Yuan Y, Li J, Hei N, Liang H. Gene co-expression network analysis reveals common system-level properties of prognostic genes across cancer types. *Nat Commun.* (2014) 5:3231. doi: 10.1038/ncomms4231
13. Segundo-Val IS, Sanz-Lozano CS. Introduction to the Gene Expression Analysis. *Methods Mol Biol.* (2016) 1434:29–43. doi: 10.1007/978-1-4939-3652-6_3
14. Colaprico A, Silva TC, Olsen C, Garofano L, Cava C, Garolini D, et al. TCGAbiolinks: an R/Bioconductor package for integrative analysis of TCGA data. *Nucleic Acids Res.* (2016) 44:e71. doi: 10.1093/nar/gkv1507
15. Robinson MD, McCarthy DJ, Smyth GK. edgeR: a Bioconductor package for differential expression analysis of digital gene expression data. *Bioinformatics.* (2010) 26:139–40. doi: 10.1093/bioinformatics/btp616
16. Sean D, Meltzer PS. GEOquery. *Bioinformatics.* (2007) 23:1846–7. doi: 10.1093/bioinformatics/btm254
17. Wang CCN, Li CY, Cai JH, Sheu PC, J.Tsai JP, Wu MY, et al. Identification of prognostic candidate genes in breast cancer by integrated bioinformatic analysis. *J Clin Med.* (2019) 8:1160. doi: 10.3390/jcm8081160
18. Ritchie ME, Phipson B, Wu D, Hu Y, Law CW, Shi W, et al. Limma powers differential expression analyses for RNA-sequencing and microarray studies. *Nucleic Acids Res.* (2015) 43:e47. doi: 10.1093/nar/gkv007
19. Wickham H. *Ggplot2: Elegant Graphics for Data Analysis.* (2009) Dordrecht; New York, NY: Springer.
20. Chen H, and Boutros PC. VennDiagram: a package for the generation of highly-customizable Venn Euler diagrams in R. *BMC Bioinform.* (2011) 12:35. doi: 10.1186/1471-2105-12-35
21. Yu G, Wang LG, Han Y, He QY. clusterProfiler: an R package for comparing biological themes among gene clusters. *Omics.* (2012) 16:284–7. doi: 10.1089/omi.2011.0118
22. Gene Ontology Consortium. The Gene Ontology (GO) project in 2006. *Nucleic Acids Res.* (2006) 34:D322–6. doi: 10.1093/nar/gkj021
23. Szklarczyk D, Gable AL, Lyon D, Junge A, Wyder S, Huerta-Cepas J, et al. STRING v11: protein-protein association networks with increased coverage, supporting functional discovery in genome-wide experimental datasets. *Nucleic Acids Res.* (2019) 47:D607–13. doi: 10.1093/nar/gky1131
24. Shannon P, Markiel A, Ozier O, Baliga NS, Wang JT, Ramage D, et al. Cytoscape: a software environment for integrated models of biomolecular interaction networks. *Genome Res.* (2003) 13:2498–504. doi: 10.1101/gr.1239303
25. Chin CH, Chen SH, Wu HH, Ho CW, Ko MT, Lin CY. cytoHubba: identifying hub objects and sub-networks from complex interactome. *BMC Syst Biol.* (2014) 8(Suppl. 4):S11. doi: 10.1186/1752-0509-8-S4-S11

26. Tang Z, Kang B, Li C, Chen T, Zhang Z. GEPIA2: an enhanced web server for large-scale expression profiling and interactive analysis. *Nucleic Acids Res.* (2019) 47:W556–60. doi: 10.1093/nar/gkz430
27. Thul PJ, Lindskog C. The human protein atlas: a spatial map of the human proteome. *Protein Sci.* (2018) 27:233–44. doi: 10.1002/pro.3307
28. Maity B, Sheff D, Fisher RA. Immunostaining: detection of signaling protein location in tissues, cells and subcellular compartments. *Methods Cell Biol.* (2013) 113:81–105. doi: 10.1016/B978-0-12-407239-8.00005-7
29. Blaydon DC, Nitoiu D, Eckl KM, Cabral RM, Bland P, Hausser I, et al. Mutations in CSTA, encoding Cystatin A, underlie exfoliative ichthyosis and reveal a role for this protease inhibitor in cell-cell adhesion. *Am J Hum Genet*. (2011) 89:564–71. doi: 10.1016/j.ajhg.2011.09.001
30. Gupta A, Nitoiu D, Brennan-Crispi D, Addya S, Riobo NA, Kelsell DP, et al. Cell cycle- and cancer-associated gene networks activated by Dsg2: evidence of cystatin a deregulation and a potential role in cell-cell adhesion. *PLoS ONE*. (2015) 10:e0120091. doi: 10.1371/journal.pone.0120091
31. Duivenvoorden HM, Rautela J, Edgington-Mitchell LE, Spurling A, Greening DW, Nowell CJ, et al. Myoepithelial cell-specific expression of stefin A as a suppressor of early breast cancer invasion. *J Pathol*. (2017) 243:496–509. doi: 10.1002/path.4990
32. Mirtti T, Alanen K, Kallajoki M, Rinne A, Soderstrom KO. Expression of cystatins, high molecular weight cytokeratin, and proliferation markers in prostatic adenocarcinoma and hyperplasia. *Prostate*. (2003) 54:290–8. doi: 10.1002/pros.10196
33. Luo A, Kong J, Hu G, Liew CC, Xiong M, Wang X, et al. Discovery of Ca2+-relevant and differentiation-associated genes downregulated in esophageal squamous cell carcinoma using cDNA microarray. *Oncogene*. (2004) 23:1291–9. doi: 10.1038/sj.onc.1207218
34. Kos J, Lah TT. Cysteine proteinases and their endogenous inhibitors: target proteins for prognosis, diagnosis and therapy in cancer (review). *Oncol Rep*. (1998) 5:1349–61. doi: 10.3892/or.5.6.1349
35. Kos J, Krasovec M, Cimerman N, Nielsen HJ, Christensen IJ, Brunner N. Cysteine proteinase inhibitors stefin A, stefin B, and cystatin C in sera from patients with colorectal cancer: relation to prognosis. *Clin Cancer Res*. (2000) 6:505–11.
36. Ma Y, Chen Y, Li Y, Grün K, Berndt A, Zhou Z, et al. Cystatin A suppresses tumor cell growth through inhibiting epithelial to mesenchymal transition in human lung cancer. *Oncotarget*. (2018) 9:14084–98. doi: 10.18632/oncotarget.23505
37. Strojan P, Budihna M, Smid L, Svetic B, Vrhovec I, Kos J, et al. Prognostic significance of cysteine proteinases cathepsins B and L and their endogenous inhibitors stefins A and B in patients with squamous cell carcinoma of the head and neck. *Clin Cancer Res*. (2000) 6:1052–62.
38. Anicin A, Gale N, Smid L, Kos J, Strojan P. Expression of stefin A is of prognostic significance in squamous cell carcinoma of the head and neck. *Eur Arch Otorhinolaryngol.* (2013) 270:3143–51. doi: 10.1007/s00405-013-2465-5
39. Ralhan R, Desouza LV, Matta A, Tripathi SC, Ghanny S, Datta Gupta S, et al. Discovery and verification of head-and-neck cancer biomarkers by differential protein expression analysis using iTRAQ labeling, multidimensional liquid chromatography, and tandem mass spectrometry. *Mol Cell Proteomics*. (2008) 7:1162–73. doi: 10.1074/mcp.M700500-MCP200

Conflict of Interest: The authors declare that the research was conducted in the absence of any commercial or financial relationships that could be construed as a potential conflict of interest.

frontiers in Oncology

ORIGINAL RESEARCH
published: 29 May 2020
doi: 10.3389/fonc.2020.00718

Analysis of Genetic Alteration Signatures and Prognostic Values of m6A Regulatory Genes in Head and Neck Squamous Cell Carcinoma

Xuanchen Zhou[1], Jie Han[2]*, Xiaoyue Zhen[3], Yiqing Liu[1], Zhaoyang Cui[1], Zhiyong Yue[1], Ling Ding[1] and Shuai Xu[2]*

[1] Department of Otorhinolaryngology Head and Neck Surgery, Shandong Provincial Hospital Affiliated to Shandong First Medical University, Jinan, China, [2] Department of Otorhinolaryngology Head and Neck Surgery, Shandong Provincial Hospital Affiliated to Shandong University, Jinan, China, [3] Minimally Invasive Urology Center, Shandong Provincial Hospital Affiliated to Shandong First Medical University, Jinan, China

Genetic alteration involving N6-methyladenosine (m6A) regulatory genes is a frequent characteristic of multiple tumors. Nevertheless, little is known regarding their genetic alteration signatures and prognostic values in head and neck squamous cell carcinoma (HNSCC). In this study, RNA sequence profiles and copy number variation (CNV) data of 506 HNSCC patients were downloaded from The Cancer Genome Atlas (TCGA) database. Correlation analysis involving alteration of m6A regulatory genes, clinicopathological characteristics, and patient survival was performed using R language. The results suggest that alteration of m6A regulatory genes was correlated with clinical staging. Patients with high expression of *ALKBH5*, *FTO*, *METTL14*, *WTAP*, *YTHDC1*, *YTHDF1*, and *YTHDF2* had poor overall survival (OS) than those with low expression. Univariate and multivariate Cox regression analyses showed that *ALKBH5* and *YTHDC2* were independent risk factors for OS. However, patients with high YTHDC2 expression had better OS. Moreover, according to machine learning results, *YTHDC2* was found to be the most important gene among the 10 m6A regulators. Additionally, high expression of *YTHDC2* was correlated with activation of apoptosis and ubiquitin-mediated proteolysis. Here, we identified alterations to m6A regulatory genes in HNSCC for the first time and found that seven m6A regulators were associated with poor prognosis, especially *ALKBH5*, whereas *YTHDC2* was associated with better prognosis. These m6A-related regulators could act as novel prognostic biomarkers for HNSCC. Our findings provide clues for understanding RNA epigenetic modifications in HNSCC.

Keywords: N6-Methyladenosine, head and neck squamous cell carcinoma, ALKBH5, YTHDC2, prognosis, biomarkers

OPEN ACCESS

Edited by:
Jorge A. R. Salvador,
University of Coimbra, Portugal

Reviewed by:
Ye Fu,
Harvard University, United States
Jingcheng Zhou,
Peking University First Hospital, China

****Correspondence:***
Xuanchen Zhou
xuanchenzhou@163.com
Jie Han
hanjie64@sohu.com

Specialty section:
This article was submitted to Head and Neck Cancer, a section of the journal Frontiers in Oncology

Received: *30 December 2019*
Accepted: *16 April 2020*
Published: *29 May 2020*

Citation:
Zhou X, Han J, Zhen X, Liu Y, Cui Z, Yue Z, Ding L and Xu S (2020) Analysis of Genetic Alteration Signatures and Prognostic Values of m6A Regulatory Genes in Head and Neck Squamous Cell Carcinoma. Front. Oncol. 10:718. doi: 10.3389/fonc.2020.00718

INTRODUCTION

Head and neck squamous cell carcinoma (HNSCC) is a common clinically malignant tumor that mainly occurs on the mucous surface of the upper respiratory digestive tract, such as the nasal cavity, paranasal sinuses, nasopharynx, hypopharynx, larynx, trachea, oral cavity, and oropharynx. According to statistics, there are > 550,000 new cases of squamous cell carcinoma of the head and

neck worldwide every year (1, 2). According to "Cancer statistics in China, 2015," the incidence of new lip, oral, and oropharyngeal cancer in 2015 was 48.1/100,000, and the mortality rate was 22.1/100,000. The incidence of new nasopharyngeal carcinoma (NPC) was 60.6/100,000, and the mortality rate was 34.1/100,000; the incidence of new laryngeal cancer was 26.4/100,000, and the mortality rate was 14.5/100,000 (3). The latest statistics show that, in the United States, HNSCC accounts for 3% of all cancer patients with 60,000 new cases per year and 12,000 deaths per year (4). The five-year survival rate of patients with HNSCC is approximately 40–50%.

At present, tobacco use and alcohol consumption are still the most important risk factors for development of HNSCC (5). There is relatively little information concerning the molecular mechanisms underlying HNSCC progression. However, in order to improve outcomes in HNSCC cases, identifying molecular genetic events during tumor progression is crucial to understanding mechanisms underlying malignancy.

The important role of RNA in biological systems is not only through the flow of genetic information from DNA to protein, but also through the regulation of various biological processes (6). The multiple functions of RNA are accompanied by more than 100 chemical modifications although the functions of most of these RNA modifications remain unclear (6). Among these modifications, adenosine N6 methylation (m6A) is considered to be the most common and conservative internal transcriptional modification in eukaryotic mRNAs (7). RNA m6A is thought to affect RNA transcription, processing, translation, and metabolism (7). The deposition of m6A is encoded by a methyltransferase complex, which involves three homologous factors, namely "writer," "eraser," and "reader" (7).

The "writers" (*METTL3*, *METTL14*, *WTAP*, and *RBM15/15B*) can catalyze the formation of m6A; "erasers" (*FTO* and *ALKBH5*) can selectively remove the methyl code from target mRNAs; "readers" (*YTHDF1*, *YTHDF2*, *YTHDF3*, *YTHDC1*, and *YTHDC2*) can decode methylation of m6A and produce a functional signal (7). m6A RNA modification is a dynamic and reversible process, which involves several biological functions in mammals, such as RNA transcription, processing events, splicing, RNA stability, and translation (8). To date, m6A has been reported to be associated with a variety of disorders, such as infectious diseases, nervous system development, obesity (9), infertility, inflammation, and cancer (10). Emerging evidence shows that m6A modification is related to tumor proliferation, differentiation, occurrence, invasion, and metastasis and plays the role of oncogene or antioncogenes in malignant tumors (7). In acute myeloid leukemia (AML), mimicking FTO depletion, an FTO inhibitor FB23-2 significantly inhibited the proliferation of human AML cell lines and primary cells *in vitro* and promoted cell differentiation/apoptosis (11). HNRNPC has been reported to control the invasiveness of glioblastoma (GBM) cells by regulating PDCD4 (12). In lung cancer, FTO enhances the expression of MZF1 by reducing the mA level and mRNA stability of MZF1 mRNA transcription, then leading to carcinogenic function (13). The deletion of m6A methyltransferase METTL3 leads to selective splicing and gene expression alteration of >20 genes involved in the TP53 signaling pathway in hepatocellular carcinoma (HCC) (14). In breast cancer (BRC), by inhibiting let-7g to upregulate METTL3, HBXIP forms a positive feedback loop of HBXIP/let-7g/METTL3/HBXIP, leading to accelerated proliferation of breast cancer cells (15). Although m6A has been found to be associated with tumorigenesis in various types of cancer, little is known regarding the relationship between m6A regulators and HNSCC. Therefore, we performed a retrospective analysis based on The Cancer Genome Atlas (TGCA) database to analyze genetic alterations involving m6A-related genes, their relationship with clinicopathological characteristics of HNSCC, and the prognostic value.

Abbreviations: m6A, N6-methyladenosine; HNSCC, head and neck squamous cell carcinoma; CNV, copy number variation; TCGA, The Cancer Genome Atlas; GEO, Gene Expression Omnibus; ccRCC, clear cell renal cell carcinoma; AML, acute myeloid leukemia; OS, overall survival; GSEA, gene set enrichment analysis; IHC, immunohistochemistry.

MATERIALS AND METHODS

All TCGA clinical data, copy number variations (CNVs), mutations, and mRNA expression data were retrieved using the UCSC Xena program, which is available to the public under certain guidelines. Therefore, written informed consent was obtained.

SNP and CNV Analysis of 506 HNSCC Samples

All of the TCGA RNA-sequencing data, single nucleotide polymorphisms (SNPs) and CNV data, clinical phenotypes, and survival data of 506 samples from patients with HNSCC were preliminarily integrated and standardized and could then be directly used for subsequent analysis. SNP analysis was based on VarScan2 variant aggregation and masking data in TCGA, in particular for mutation analysis of 10 m6A regulatory genes. These 10 m6A genes were *METTL3*, *METTL14*, *WTAP*, *FTO*, *ALKBH5*, *YTHDF1*, *YTHDF2*, *YTHDF3*, *YTHDC1*, and *YTHDC2*. SNP mutation analysis and results of visualization in this study were performed using the R maftools package (16).

CNV analysis of the 10 m6A regulatory genes was performed using GISTIC 2.0 (17) software with default parameters, and the results were visualized using the R programing language.

Relationship Involving CNVs, m6A Gene Expression, and Clinical Phenotypes

To investigate the relationship between CNVs and gene expression, we used the R package "ggpubr" to visualize the expression levels of the 10 m6A regulatory genes with or without CNVs and performed Kruskal–Wallis *H* tests between different CNV event groups. Here, expression results are represented as box plots.

To study relationships involving CNVs and clinical phenotypes, we performed analysis based on age, gender, clinical stage, tumor node metastasis (TNM) stage, and sample

CNV information. Chi-square testing was performed after grouping the clinical phenotype and CNV information.

Survival Analysis

We performed survival analysis based on regulatory gene expression levels of 10 m6A loci (log2 normalized) and overall survival time (OS) to determine the prognostic value of these 10 genes. Before survival analysis, we removed the gene expression level from the normal control sample from the original data. Samples with survival status of zero (survival) and survival time of <30 days were considered as follow-up failures in this study, and the remaining HNSCC samples were included in the subsequent survival analysis. The optimal cutoff point for gene expression was obtained based on the R package "survminer" (18). After high–low expression ranking of the samples using the optimal cutoff point, survival analysis was performed using the R package "survival" (19), and survival analysis results were visualized by the "ggsurvplot" method.

Construction of an m6A Regulatory Gene Network

We used the geneMANIA (20) database as the main analytical tool to explore the interaction between 10 m6A regulatory genes and other genes using default parameters. Ten m6A regulatory genes were used as analytical background genes, and the functions of the genes enriched in the visualization network results were further analyzed to study the potential main cellular roles of the 10 regulatory genes.

Machine Learning and Gene Set Enrichment Analysis (GSEA)

Based on the R package "caret," we constructed two different machine learning models to investigate features of importance involving 10 m6A regulatory genes. Random forest and neural network models were used to rank the 10 genes by their expression levels in two disease states (tumor and normal). Results were also visualized using R language, and the most important feature of the two models was selected as the key gene.

We then used GSEA software (version 4.0.1) to perform GSEA analysis of key genes and other mRNAs. The Kyoto Encyclopedia of Genes and Genomes (KEGG).v7.0 was used as a gene sets database, and the Pearson method was selected as a metric for ranking genes while other parameters were used at default settings. Among the final enrichment results, $p < 0.05$ was used as the statistically significant cutoff to analyze optimal pathway enrichment results.

Immunohistochemistry (IHC)

According to the Abcam manufacturer's instructions, the *YTHDC2* and *ALKBH5* genes were analyzed by IHC using formalin-fixed, paraffin-embedded tissue blocks. Briefly, paraffin sections were dewaxed, and endogenous peroxidase activity was blocked with 0.3% hydrogen peroxide for 10 min at 37°C. Following antigen retrieval, the tissue sections were incubated with primary antibody *YTHDC2* (1:500; EPR21820-49, AB220160; Abcam, Inc., Cambridge, MA, USA) or *ALKBH5* (1:2000; EPR18958, ab195377, Abcam, Inc.) at 4°C overnight and then with a secondary antibody at room temperature (25°C) overnight. The sections were counterstained with hematoxylin.

RESULTS

SNP Mutation and CNV Results of m6A Regulatory Genes in HNSCC Samples

Of the 506 patients with sequencing data used for SNP mutation analysis, only 41 (8.1%) of the samples had mutation events in any of the 10 m6A regulatory genes as shown in **Figure 1**. For HNSCC samples, the mutation frequency involving the 10 m6A regulatory genes was not high, and each gene was mutated only in several samples (<8), where most of the mutation events were missense mutations. However, it was found that the 10 m6A regulatory genes had different levels of CNV events though analysis using GISTIC, ranging from 23.58 to 57.36%. "Reader" gene *YTHDF3* (57.36%) harbored the most CNV events among the 10 m6A genes (**Figure 2A**). CSMD1 (66.56%) and TP53 (31.61%) were non-m6A genes found to be mutated while

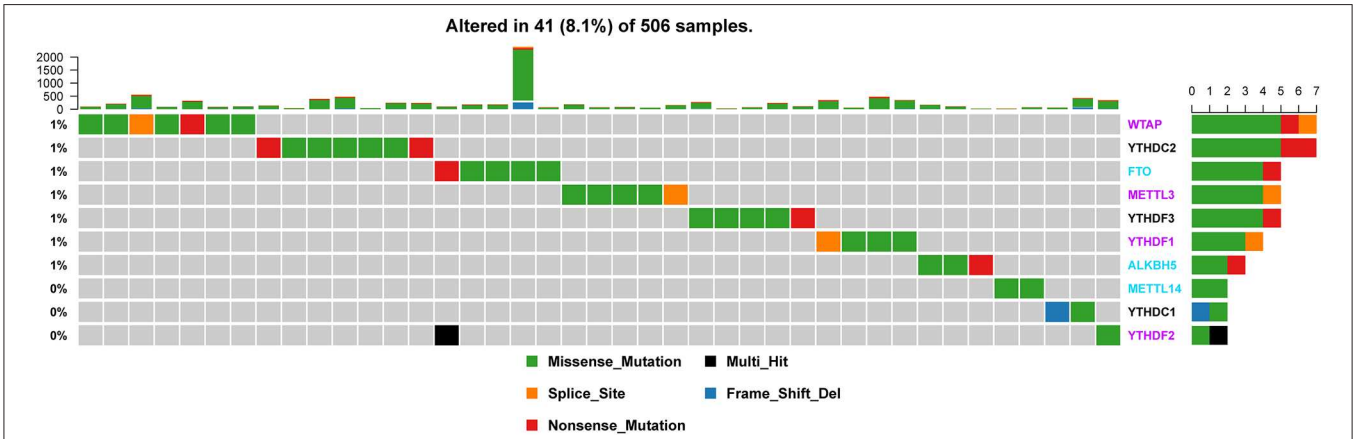

FIGURE 1 | Alteration frequency of m6A regulatory genes in the HNSCC sample based on the TCGA database.

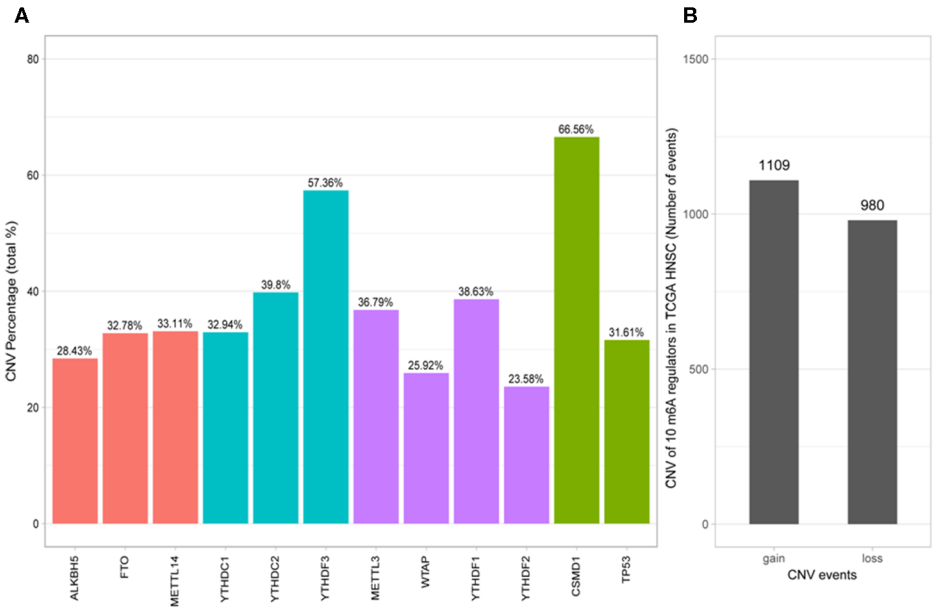

FIGURE 2 | Analysis of 10 m6A regulatory gene mutation data in the TCGA HNSCC sample. **(A)** Percentage of HNSCC samples with CNVs of the m6A regulatory genes from TCGA. **(B)** CNV events of gain or loss of m6A regulators in HNSCCC samples.

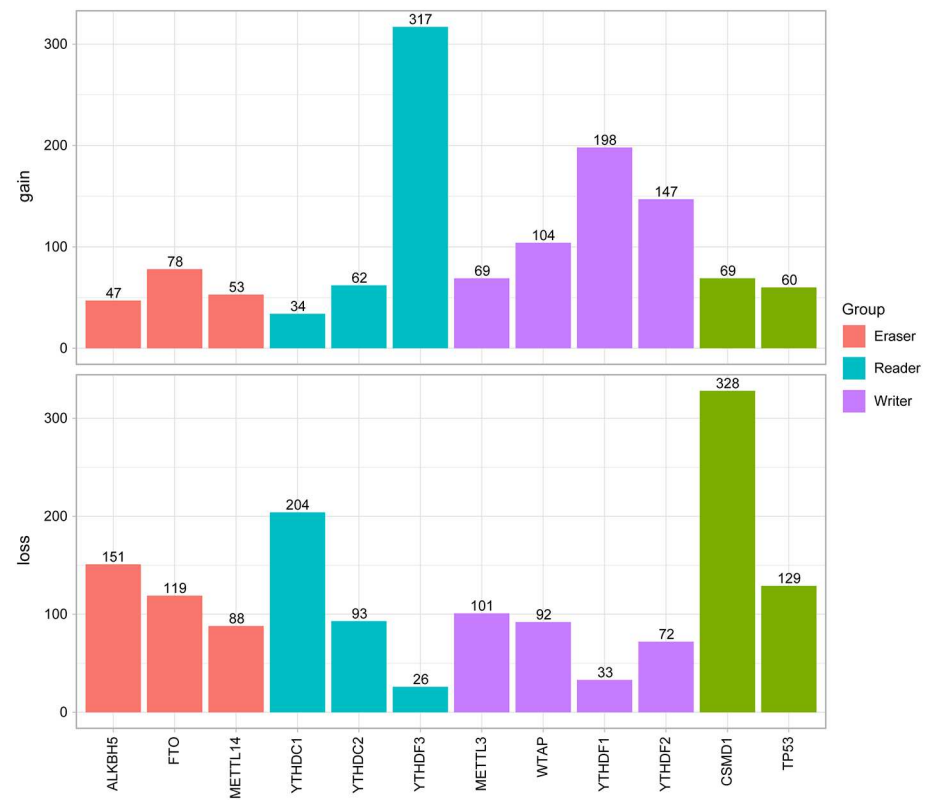

FIGURE 3 | Results of CNV analysis of 10 m6A regulatory genes in the HNSCC cohort.

CSMD1 was the most CNV events and TP53 was the most SNP events in all HNSCC samples. They were analyzed together with 10 m6A regulatory genes as references.

Next, the CNV patterns of the 10 m6A genes in the HNSCC samples were analyzed. It was found that the number of the CNV gain event was larger than that of loss events (1109 > 980) in the 10 m6A regulatory genes (**Figure 2B**). Unlike AML (21) and clear cell renal cell carcinoma (ccRCC) (22), among these 10 m6A regulatory genes, *YTHDF3* exhibited the highest number (317) of CNV gain events. *YTHDC1* had the most CNV loss events with 204 cases (**Figure 3**). Both *YTHDF3* and *YTHDC1* are m6A regulatory "reader" genes.

Additionally, SNP analysis revealed that the most frequent variant classification of m6A regulatory gene mutation was missense mutation, and the largest number of variant types was SNP (**Figure S1**). For SNPs, the most common SNV type was C > T, and the median number of variants per sample was 78. The most obvious mutations involved *TP53* as mentioned before (66%) and *TTN* (35%).

Association Involving CNV Alterations, Clinicopathological Characteristics, and Gene Expression

We then evaluated the relationship between CNV alterations in 10 m6A regulatory genes and clinicopathological features of HNSCC patients. Clinical staging was divided into I–IV according to the HNSCC guidelines of the American Joint Committee on Cancer (23). The results showed that alterations to m6A regulatory genes were significantly related to age, gender, and clinical stage ($P < 0.05$) (**Table 1**). In other words, being aged <60 years, male, with high-grade clinical staging were factors more related to CNV events involving 10 m6A regulatory genes.

Next, we analyzed relationships between CNV patterns and gene expression of the 10 m6A regulatory genes. As can be seen from **Figure 4**, there was a statistically significant relationship between CNV patterns and gene expression. With CNV events from deletion to amplification, gene expression of the 10 m6A regulatory genes also showed an upward trend; that is, gene expression increased with increased CNV amplification and decreased with CNV deletion.

TABLE 1 | Clinical pathological parameters of HNSCC patients with or without CNV of m6A regulatory genes.

Variable		With CNV events	Without CNV events	Total	chi-square value	*P*
Age	<=60	223	13	236	4.205	**0.0402**
	>60	216	27	243		
Gender	Male	329	22	351	6.462	**0.0110**
	Female	110	18	128		
Clinical Stage	Stage I	14	5	19	9.623	**0.0220**
	Stage II	83	9	92		
	Stage III	93	9	102		
	Stage IV	249	17	266		
Stage M	M0	424	39	463	1.63E-29	1
	M1	5	0	5		
	MX	10	1	11		
Stage N	N0	209	26	235	4.620	0.2018
	N1	74	6	80		
	N2	141	8	149		
	N3	7	0	7		
	NX	8	0	8		
Stage T	T1	28	5	33	4.369	0.2243
	T2	125	15	140		
	T3	118	9	127		
	T4	167	11	178		
	TX	1	0	1		

With or without CNV events: Cases have CNV or do not have CNV, confirmed by TCGA database. Ambiguous variables (Nx and Mx) were excluded from chi-square test. Bold values indicate P < 0.05 with significantly statistical difference.

Association Between m6A Regulatory Gene CNVs and HNSCC Patient Survival

We previously studied relationships between CNV patterns and m6A regulatory gene expression. The more extensive the CNV, the more the gene was expressed. We studied relationships between expression levels of m6A regulatory genes and the survival rate of HNSCC patients and explored the prognostic value of m6A regulatory genes. Our analysis revealed that expression of the 10 m6A regulatory genes was mostly related to the prognosis of HNSCC patients. Patients with high expression of *ALKBH5*, *FTO*, *METTL14*, *WTAP*, *YTHDC1*, *YTHDF1*, and *YTHDF2* had lower OS (**Figures 5A–H**), and patients with higher *YTHDC2* expression showed greater OS (**Figure 6A**). Furthermore, when HNSCC patients were grouped with or without CNV events for survival analysis, no statistically significant results were obtained (**Figure 6B**). It could be speculated that the occurrence of CNV events does not directly affect the prognosis of HNSCC patients, but rather that they affect the prognosis of HNSCC patients by influencing the expression of genes. Meanwhile, univariate and multivariate analyses demonstrated that increased expression of *ALKBH5* and *YTHDC2* were independent risk factors for OS in patients with HNSCC (**Table 2**).

Next, by further analysis, no significant differences were observed between different subgroups based on the CNVs of the 10 m6A regulatory genes (**Figure S2**).

Machine Learning and IHC Analysis

To study the important characteristics of the 10 genes, we used a neural network and random forest to build predictive models. As can be seen from **Figure 7**, in both models, the *YTHDC2* gene was consistently ranked the highest among the 10 genes. Combined with the results of the previous analysis (**Figure 2A**), among the 10 genes, the incidence of CNV events involving *YTHDC2* was second only to *YTHDF3*, and *YTHDC2* gene expression and survival prognosis results were also significant. However, association between the expression level of *YTHDF3* and survival prognosis was not statistically significant (**Figure 5I**). Therefore, *YTHDC2* was selected as the most prognostically important locus of the 10 m6A regulatory genes in HNSCC.

Furthermore, we performed IHC staining for *YTHDC2* and *ALKBH5* proteins in 20 pairs of normal and oral squamous cell carcinoma tissues to confirm such findings (**Figure 8**). These

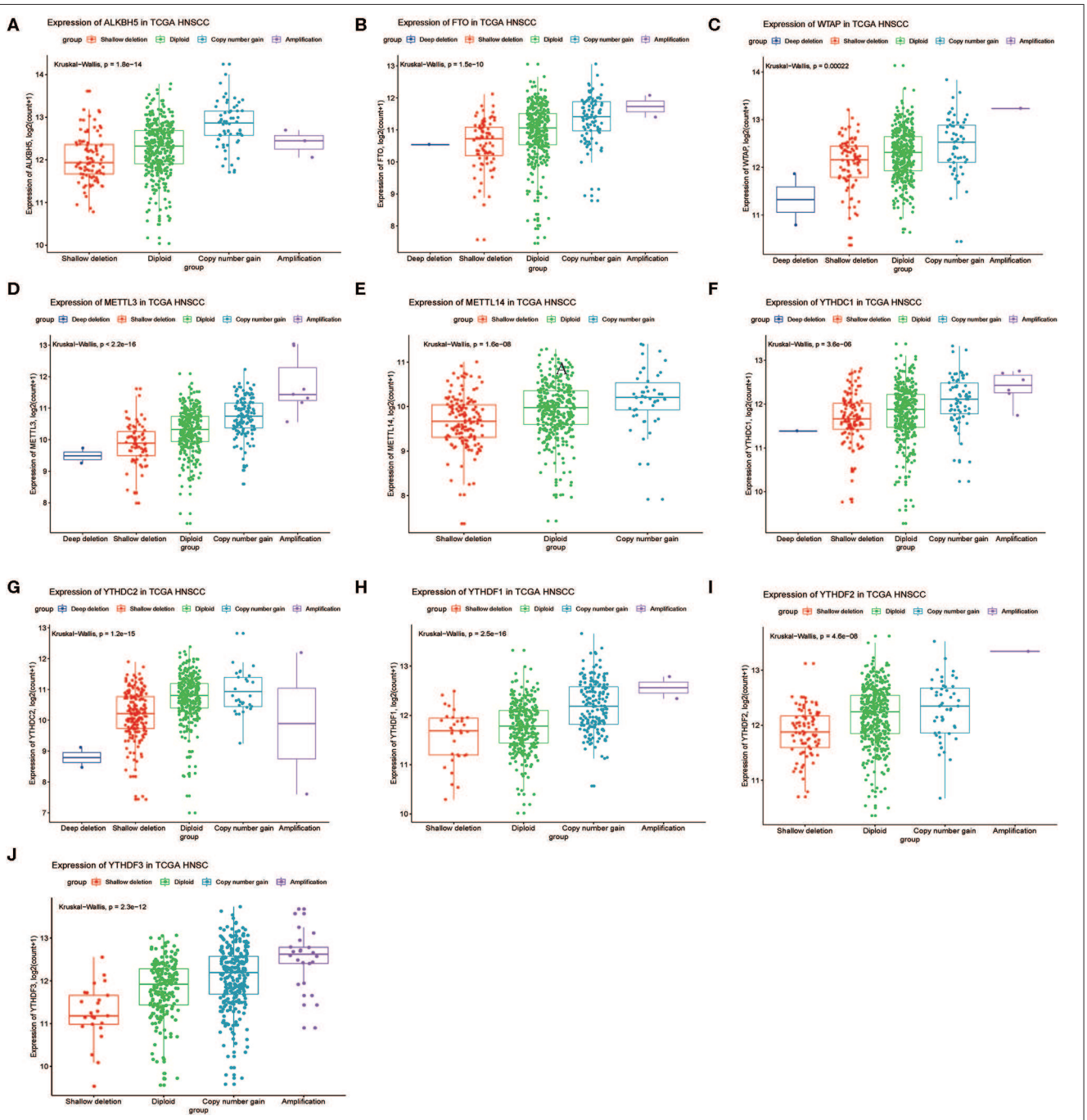

FIGURE 4 | Association between m6A regulatory gene CNV patterns and genetic expression. **(A)** ALKBH5, **(B)** FTO, **(C)** WTAP, **(D)** METTL3, **(E)** METTL14, **(F)** YTHDC1, **(G)** YTHDC2, **(H)** YTHDF1, **(I)** YTHDF2, **(J)** YTHDF3.

results were consistent with our predictions, indicating that *YTHDC2* and *ALKBH5* were expressed more highly in malignant HNSCC tissues than in normal oral tissues.

GSEA Analysis

Considering the importance of *YTHDC2* in the methylation process, we decided to explore the role of *YTHDC2* dysfunction in the pathogenesis of HNSCC. We examined enriched gene sets in samples with different *YTHDC2* mRNA expression levels. GSEA analysis implied that high expression of *YTHDC2* is associated with certain key pathways, such as apoptosis, ubiquitin-mediated proteolysis, long-term potentiation, and rig-i-like receptor signaling pathways, revealing the underlying mechanisms involved in HNSCC pathogenesis (**Figure 9**). To validate our findings, we examined the expression of several genes associated with these pathways. We found that apoptosis-related genes *caps3*, *6*, *8*, *9*, *Bcl-2*, *Bid*, *UBE2S*, and *HERC3* associated with ubiquitin-mediated proteolysis were significantly

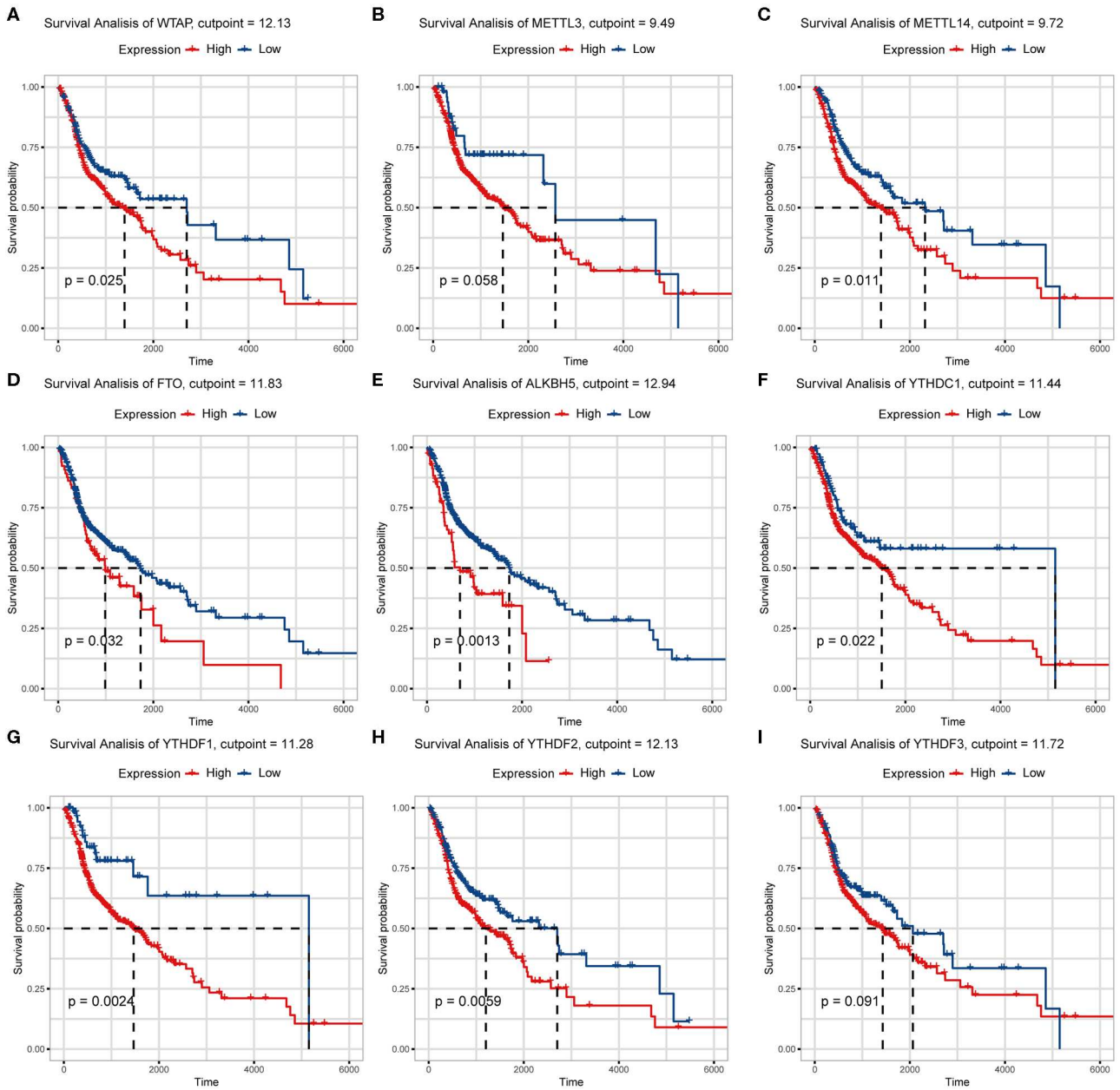

FIGURE 5 | Relationship between expression of nine m6A regulatory genes and overall survival. **(A)** WTAP, **(B)** METTL3, **(C)** METTL14, **(D)** FTO, **(E)** ALKBH5, **(F)** YTHDC1, **(G)** YTHDF1, **(H)** YTHDF2, **(I)** YTHDF3.

different in HNSCC tumor tissues compared to normal tissues (**Figure 10**). The GSEA results were partially validated.

DISCUSSION

m6A is the most abundant chemical modification of mRNA, which is regulated by m6A "writer," "eraser," and "reader" proteins (8, 24, 25). As an important complement to the central dogma, the study of m6A-mediated RNA methylation and its role in cancer has only just commenced. To date, little is known regarding the role of m6A in HNSCC. Only a single study has reported that m6A is associated with nasopharyngeal carcinoma in which m6A-mediated ZNF750 repression facilitates NPC progression (26). Due to the complexity of m6A-Seq and m6A-methylated RNA immunoprecipitation technologies, many studies have chosen alterative methods to assess genetic alterations to m6A regulatory genes, indirectly exploring relationships between m6A status and human disease. In this study, we applied bioinformatics methods to analyze genetic alteration in 10 m6A genes, their relationships with the clinical

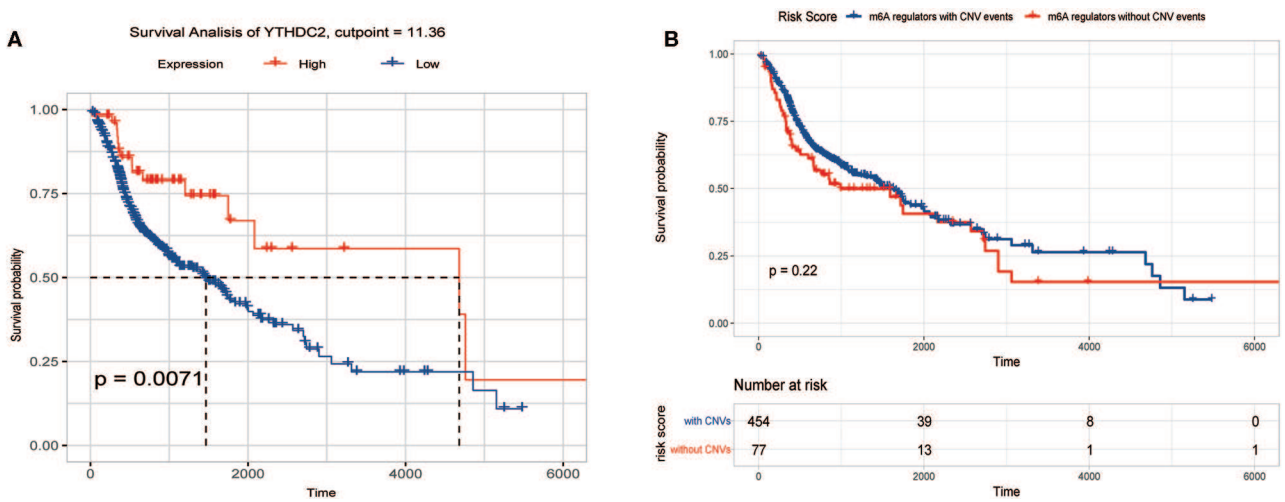

FIGURE 6 | Overall survival of HNSCC patients with or without CNV of m6A regulatory genes and YTHDC2 expression. **(A)** Relation between YTHDC2 expression and overall survival. **(B)** Relation between with or without CNVs and overall survival.

TABLE 2 | Univariate and multivariate COX regression analysis of various prognostic parameters for HNSCC cohort.

Risk factors	Univariate		Multivariate	
	HR(95% CI)	*P*	HR(95% CI)	*P*
Age	1.02(1.01-1.03)	**0.00123**	1.02(1.012-1.0404)	**0.000268**
Gender(male/female)	0.765(0.57-1.03)	0.0747	0.8668(0.6336-1.1858)	0.371157
Clinical M(M0/M1)	4.63(1.71-12.6)	**0.00263**	4.8295(1.744-13.3741)	**0.002444**
Clinical N(N0/N1-N3)	1.24(0.945-1.63)	0.12		
Clinical T(T1-T2/T3-T4)	1.31(0.97-1.76)	**0.0783**	0.7723(0.9535-1.7586)	0.097974
Clinical stage(stage i-ii/stage iii-iv)	1.24(0.889-1.74)	0.203		
METTL3(high/low)	1.617(0.371-1.031)	**0.0655**	1.1450(0.5020-1.5194)	0.631672
WTAP(high/low)	1.478(0.5028-0.9104)	**0.00987**	0.9995(0.6687-1.4971)	0.998031
METTL14(high/low)	1.552(0.4774-0.8693)	**0.00402**	1.3650(0.4864-1.1036)	0.136612
ALKBH5(high/low)	1.726(0.4062-0.8264)	**0.0026**	1.7626(0.3845-0.8371)	**0.004286**
FTO(high/low)	1.437(0.4907-0.9875)	**0.0423**	1.0381(0.6568-1.4128)	0.848160
YTHDF1(high/low)	2.554(0.2183-0.7019)	**0.00164**	1.7128(0.3056-1.1156)	0.103340
YTHDF2(high/low)	1.489(0.5073-0.8896)	**0.00549**	1.0431(0.6480-1.4183)	0.832774
YTHDF3(high/low)	1.251(0.5915-1.08)	0.144		
YTHDC1(high/low)	1.592(0.4346-0.9073)	**0.0132**	1.2575(0.4966-1.2734)	0.340161
YTHDC2(high/low)	0.4903(1.204-3.456)	**0.00806**	0.3896(1.4864-4.4323)	**0.000720**

Ambiguous variables (Nx, Mx, N/A and discrepancy) were deleted. Bold values indicate P < 0.05 with significantly statistical difference.

features of HNSCC, and their prognostic value based on a TCGA database.

In our cohort of 506 HNSCC cases, the CNV frequency involving the 10 m6A regulatory genes was similar to that reported in ccRCC (22), but much higher in AML (21), suggesting that m6A dysfunction may play a more important role in the carcinogenesis of HNSCC than that of AML. Furthermore, "reader" genes *YTHDC2* and *YTHDC3* exhibited higher incidences of CNVs than other genes in our HNSCC samples, which is different from that of ccRCC (22). This suggests that "readers" may be more important than "writers" and "erasers" in HNSCC. However, "erasers" *FTO* and *ALKBH5* have been shown to be more important in glioblastoma (27), AML (28), and BRC (29). This implies tissue specificity of the "writers," "erasers," and "readers" in different tumors. Unlike in AML (21) and ccRCC (22), the CNV events in the HNSCC samples here led to gains in copy number (1109/980). The most obvious gain and loss genes were "readers," which further demonstrated the importance of "reader" genes in m6A processing.

Mutations in CNV are usually associated with different clinicopathological features. In the ccRCC cohort, m6A regulatory gene alterations were significantly related to higher Fuhrman nuclear grading. In AML patients, bone marrow blast numbers, white blood cell count, and cytogenetic risk

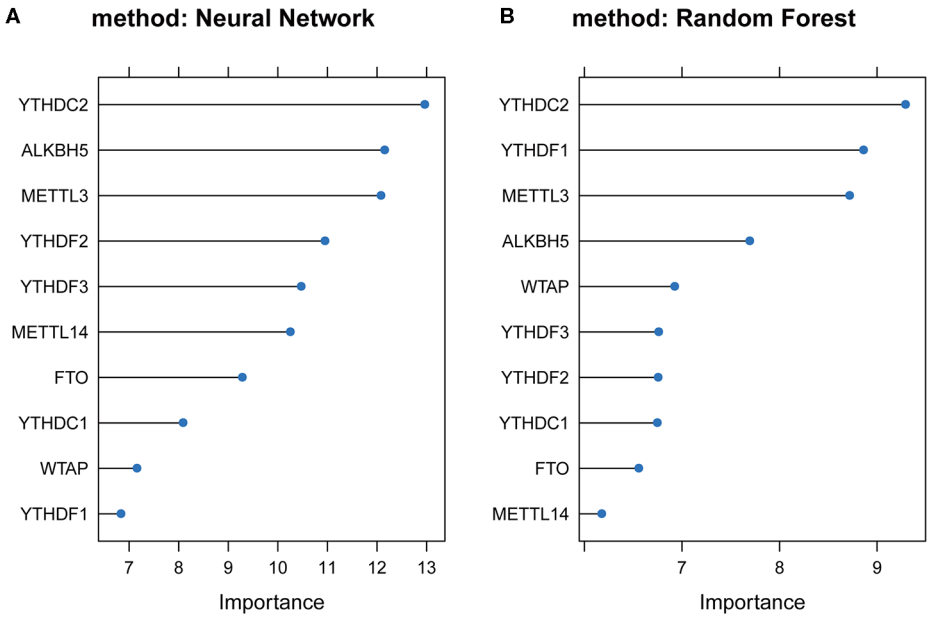

FIGURE 7 | Plots of neural network and random forest for 10 m6A regulatory genes. **(A)** Rank chart for the 10 m6A regulatory genes by Neural network. **(B)** Rank chart of the 10 m6A regulatory genes by Random Forest.

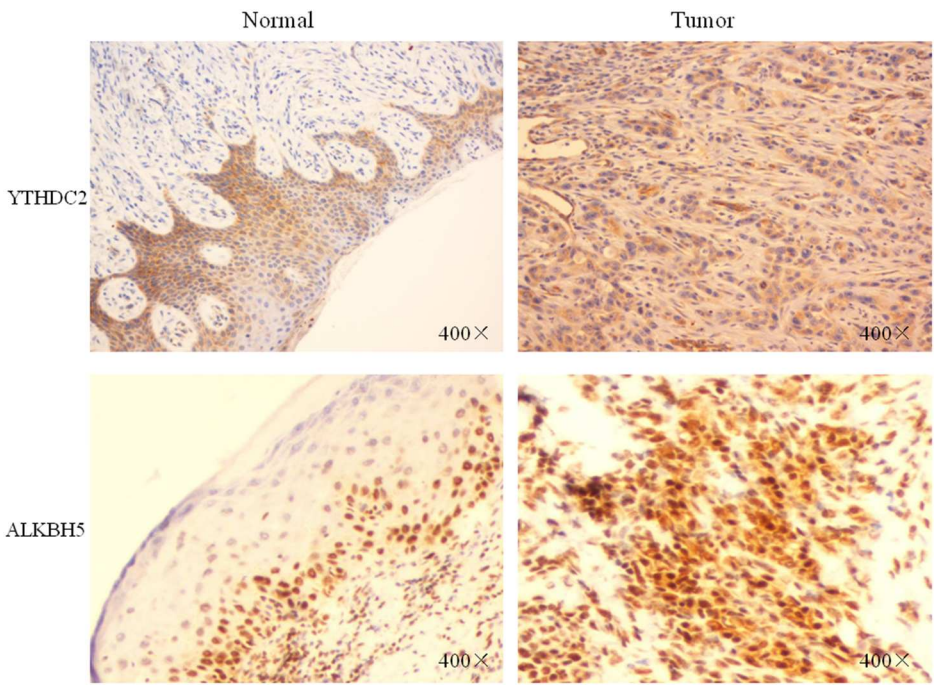

FIGURE 8 | The protein expression of YTHDC2 and ALKBH5 in oral squamous cell carcinoma and normal oral tissues.

are significantly associated with m6A gene alterations. In our HNSCC samples, the alterations to m6A regulatory genes were significantly correlated with age, sex, and clinical stage. This indicated that alterations in m6A CNV may show different clinical characteristics in different tumors. In the future, it will be necessary to study the characteristics of m6A mutations in different malignancies. Similar to ccRCC samples, in our study, copy number gains were correlated with higher mRNA expression and vice versa.

We evaluated the role of m6A regulatory genes in the survival of patients with HNSCC. In contrast toccRCC samples and BRC samples with only two and three m6A genes

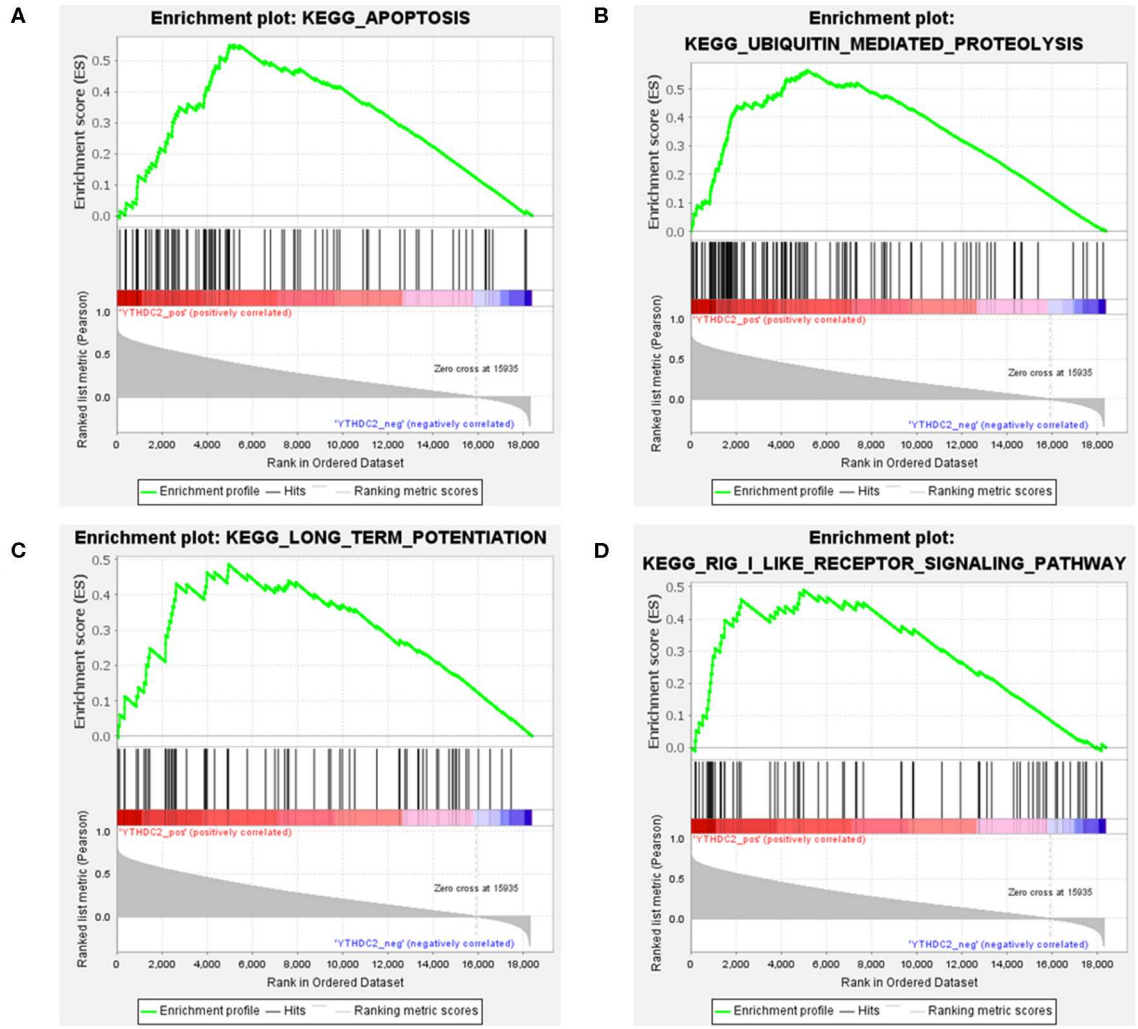

FIGURE 9 | GSEA results of different expression levels of YTHDC2. Gene set enrichment plots of **(A)** apoptosis, **(B)** ubiquitin-mediated proteolysis, **(C)** long-term potentiation, and **(D)** rig-i-like receptor signaling pathways related to low METTL3 mRNA level in the HNSCC samples.

associated with OS, here there were eight m6A regulatory genes that were significantly correlated with patient OS. In our study, patients with high expression of *ALKBH5*, *FTO*, *METTL14*, *WTAP*, *YTHDC1*, *YTHDF1*, and *YTHDF2* predicted poor patient prognosis. In BRC cohort, high expression levels of *YTHDF1*, *YTHDF3*, and *KIAA1429* predicted unfavorable patient prognosis. The two populations presented almost completely different prognostic genes. In the AML cohort, patients without m6A mutation had longer survival times. In HNSCC cases, we observed longer OS with diploid or copy number gain, which is different from the situation in AML but similar to that of ccRCC. These results showed that survival of patients with different types of tumors is related to different CNV patterns and different m6A regulatory gene abundance, which is a very attractive feature of m6A epigenetics.

In addition, the expression level of *ALKBH5* is a promising independent prognostic factor for HNSCC, suggesting that *ALKBH5* can be used as a new biomarker of HNSCC. In agreement with our study, some groups have reported that *ALKBH5* could serve as a novel prognostic biomarker that predicts a poor prognosis in colorectal (30) and pancreatic cancers (31).

Finally, we observed another interesting phenomenon. The HNSCC samples with higher *YTHDC2* expression were associated with longer-term survival, which is in contrast to the other m6A genes. *YTHDC2* has been identified as a frequently mutated gene in pancreatic cancer patients and plays a role in tumor metastasis by increasing the translational efficiency of HIF-1α (32, 33). Our IHC staining showed that the expression of *YTHDC2* in tumors was higher than that in normal tissues (**Figure 8**). Furthermore, by neural network and random forest methods, we found that *YTHDC2* was the most important gene among the 10 m6A regulatory genes. These results suggest that *YTHDC2* might play an

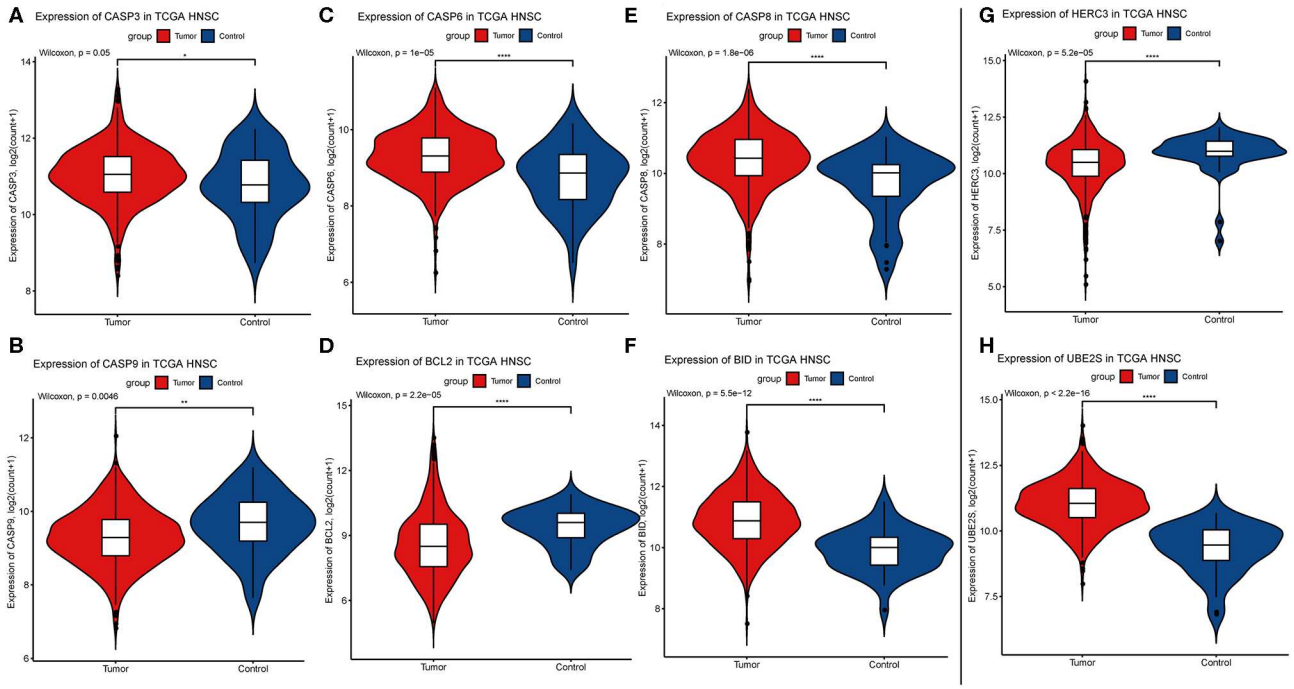

FIGURE 10 | Expression of genes related to apoptosis and ubiquitin-mediated proteolysis. **(A)** CASP3, **(B)** CASP9, **(C)** CASP6, **(D)** BCL2, **(E)** CASP8, **(F)** BID, **(G)** HERC3, **(H)** UBE2S.

important role in HNSCC. However, why did patients with higher *YTHDC2* expression have better prognoses? It has been found that *YTHDC2* is an m6A-binding protein that plays critical roles during spermatogenesis (34). The translation efficiency of *Smc3* (target *YTHDC2* in spermatogenesis) is significantly decreased in *YTHDC2*–/– mice compared to *YTHDC2* +/+ animals. In addition, the testes and epididymis from adult *YTHDC2*–/– mice are smaller in size than wild type (*YTHDC2* +/+). These results show that high *YTHDC2* expression is beneficial for spermatogenesis, which might partly explain why high expression of *YTHDC2* was associated with prolonged OS. However, more work is needed to explore such a mechanism.

The development of HNSCC is related to a series of cancer-related pathways that become uncontrolled. In our HNSCC population, we found that high levels of *YTHDC2* mRNA expression are related to apoptotic activation and the ubiquitin-mediated proteolysis pathway, which are two very important cellular processes in the development of HNSCC. *METTL3* and *METTL14* are the most widely studied m6A regulatory genes in various cancers (24, 35). To date, only one study has reported that m6A is associated with HNSCC, in which *METTL3*-mediated *ZNF750* repression facilitates NPC progression. *METTL3* can promote apoptosis in gastric (36) and breast cancer cells (37) and is associated with ubiquitin-dependent process in pancreatic cancer cells (38). These pathways are similar to those involving *YTHDC2*. Due to the lack of research concerning *YTHDC2*, further studies are needed to verify our findings. However, there is no doubt that our results point out a new direction for the study of m6A in the pathogenesis and progression of HNSCC.

CONCLUSION

In HNSCC patients, a majority of highly expressed m6A regulatory genes is associated with poor OS, in particular *ALKBH5*, whereas *YTHDC2* was associated with better prognosis. We identified, for the first time, the expression characteristics and prognosis of m6A regulatory genes in patients with HNSCC. Our results will provide a direction for further exploration of the pathogenesis of HNSCC.

DATA AVAILABILITY STATEMENT

Publicly available datasets were analyzed in this study. This data can be found here: https://xenabrowser.net/datapages/.

ETHICS STATEMENT

All clinical data, sequence profiles, and CNV data were extracted using UCSC-XENA and the TCGA database, which is open to the public under certain conditions. Therefore, it can be confirmed that all written informed consent forms are available. The study using human oral squamous cell carcinoma tissue and oral mucosa samples for IHC staining was approved by the Ethics Committee of Shandong Provincial Hospital affiliated to Shandong First Medical University. We obtained written informed consent from all participants.

AUTHOR CONTRIBUTIONS

XCZ and XYZ mainly performed experiments and data analysis. LD performed IHC of clinical specimens. JH and YL provided intellectual support and expertise in the field of cancer pathology. XCZ, ZC, and SX wrote the manuscript. JH and ZY designated all experiments in this study. All authors contributed to the critical review of the manuscript.

FUNDING

This present study was supported by funds from the Key Technology Research and Development Program of Shandong (grant no. 2019GSF108257 to JH and 2018GSF118192 to ZY). Funding agencies have no role in research design or manuscript writing.

SUPPLEMENTARY MATERIAL

The Supplementary Material for this article can be found online at: https://www.frontiersin.org/articles/10.3389/fonc.2020.00718/full#supplementary-material

Figure S1 | The types of mutations in the 10 m6A regulatory genes associated with HNSCC and the 10 most common genes.

Figure S2 | Correlations between survival probability and m6A CNV patterns. **(A)** ALKBH5, **(B)** FTO, **(C)** WTAP, **(D)** METTL3, **(E)** METTL14, **(F)** YTHDC1, **(G)** YTHDC2, **(H)** YTHDF1, **(I)** YTHDF2, **(J)** YTHDF3.

REFERENCES

1. Haddad RI, Shin DM. Recent advances in head and neck cancer. *The New England journal of medicine.* (2008) 359:1143–54. doi: 10.1056/NEJMra0707975
2. Bray F, Ferlay J, Soerjomataram I, Siegel RL, Torre LA, Jemal A. Global cancer statistics. *Cancer J Clin.* (2011) 61:69–90. doi: 10.3322/caac.20107
3. Chen W, Zheng R, Baade PD, Zhang S, Zeng H, Bray F, et al. Cancer statistics in China 2015. *Cancer J Clin.* (2016) 66:115–32. doi: 10.3322/caac.21338
4. Siegel RL, Miller KD, Jemal A. Cancer statistics, 2015. *CA Cancer J Clin.* (2015) 65:5–29. doi: 10.3322/caac.21254
5. Hashibe M, Brennan P, Chuang SC, Boccia S, Castellsague X, Chen C, et al. Interaction between tobacco and alcohol use and the risk of head and neck cancer. Pooled analysis in the International Head and Neck Cancer Epidemiology Consortium. *Cancer Epidemiol Biomarkers Prev.* (2009) 18:541–50. doi: 10.1158/1055-9965
6. Fu Y, Dominissini D, Rechavi G, He C. Gene expression regulation mediated through reversible m(6)A RNA methylation. *Nat Rev Genet.* (2014) 15:293–306. doi: 10.1038/nrg3724
7. Chen XY, Zhang J, Zhu JS. The role of m(6)A RNA methylation in human cancer. *Mol Cancer.* (2019) 18:103. doi: 10.1186/s12943-019-1033-z
8. Cao G, Li HB, Yin Z, Flavell RA. Recent advances in dynamic m6A RNA modification. *Open Biol.* (2016) 6:160003. doi: 10.1098/rsob.160003
9. Gallagher EJ, LeRoith D. Obesity and diabetes. The increased risk of cancer and cancer-related mortality. *Physiol Rev.* (2015) 95:727–48. doi: 10.1152/physrev.00030.2014
10. Wei W, Ji X, Guo X, Ji S. Regulatory role of N(6) -methyladenosine (m(6) A) methylation in RNA processing and human diseases. *J Cell Biochem.* (2017) 118:2534–43. doi: 10.1002/jcb.25967
11. Huang Y, Su R, Sheng Y, Dong L, Dong Z, Xu H, et al. Small-Molecule targeting of oncogenic FTO demethylase in acute myeloid leukemia. *Cancer Cell.* (2019) 35:677–91.e610. doi: 10.1016/j.ccell.2019.03.006
12. Cui Q, Shi H, Ye P, Li L, Qu Q, Sun G, et al. m(6)A RNA methylation regulates the self-renewal and tumorigenesis of glioblastoma stem cells. *Cell Rep.* (2017) 18:2622–34. doi: 10.1016/j.celrep.2017.02.059
13. Liu J, Ren D, Du Z, Wang H, Zhang H, Jin Y. m(6)A demethylase FTO facilitates tumor progression in lung squamous cell carcinoma by regulating MZF1 expression. *Biochem Biophys Res Commun.* (2018) 502:456–64. doi: 10.1016/j.bbrc.2018.05.175
14. Ma JZ, Yang F, Zhou CC, Liu F, Yuan JH, Wang F, et al. METTL14 suppresses the metastatic potential of hepatocellular carcinoma by modulating N(6) -methyladenosine-dependent primary MicroRNA processing. *Hepatology.* (2017) 65:529–43. doi: 10.1002/hep.28885
15. Cai X, Wang X, Cao C, Gao Y, Zhang S, Yang Z, et al. HBXIP-elevated methyltransferase METTL3 promotes the progression of breast cancer via inhibiting tumor suppressor let-7g. *Cancer Lett.* (2018) 415:11–19. doi: 10.1016/j.canlet.2017.11.018
16. Mayakonda A, Lin DC, Assenov Y, Plass C, Koeffler HP. Maftools: efficient and comprehensive analysis of somatic variants in cancer. *Genome Res.* (2018) 28:1747–56. doi: 10.1101/gr.239244.118
17. Mermel CH, Schumacher SE, Hill B, Meyerson ML, Beroukhim R, Getz G. GISTIC2.0 facilitates sensitive and confident localization of the targets of focal somatic copy-number alteration in human cancers. *Genome Biol.* (2011) 12:R41. doi: 10.1186/gb-2011-12-4-r41
18. Kassambara. A, Kosinski M. *survminer: Drawing Survival Curves using 'ggplot2'*. R package version 0.4.3. (2018). Available online at: https://CRAN.R-project.org/package=survminer.
19. *A Package for Survival Analysis in S_. version 2.38.* (2015). Available online at: https://CRAN.R-project.org/package=survival.
20. Warde-Farley D, Donaldson SL, Comes O, Zuberi K, Badrawi R, Chao P, et al. The GeneMANIA prediction server. biological network integration for gene prioritization and predicting gene function. *Nucleic acids Res.* (2010) 38(Web Server issue):W214–220. doi: 10.1093/nar/gkq537
21. Kwok CT, Marshall AD, Rasko JE, Wong JJ. Genetic alterations of m(6)A regulators predict poorer survival in acute myeloid leukemia. *J Hematol Oncol.* (2017) 10:39. doi: 10.1186/s13045-017-0410-6
22. Zhou J, Wang J, Hong B, Ma K, Xie H, Li L, et al. Gene signatures and prognostic values of m6A regulators in clear cell renal cell carcinoma - a retrospective study using TCGA database. *Aging.* (2019) 11:1633–47. doi: 10.18632/aging.101856
23. Sridharan S, Thompson LDR, Purgina B, Sturgis CD, Shah AA, Burkey B, et al. Early squamous cell carcinoma of the oral tongue with histologically benign lymph nodes. A model predicting local control and vetting of the eighth edition of the American Joint Committee on Cancer pathologic T stage. *Cancer.* (2019) 125:3198–207. doi: 10.1002/cncr.32199
24. Liu J, Yue Y, Han D, Wang X, Fu Y, Zhang L, et al. A METTL3-METTL14 complex mediates mammalian nuclear RNA N6-adenosine methylation. *Nat Chem Biol.* (2014) 10:93–5. doi: 10.1038/nchembio.1432
25. Ping XL, Sun BF, Wang L, Xiao W, Yang X, Wang WJ, et al. Mammalian WTAP is a regulatory subunit of the RNA N6-methyladenosine methyltransferase. *Cell Res.* (2014) 24:177–89. doi: 10.1038/cr.2014.3
26. Zhang P, He Q, Lei Y, Li Y, Wen X, Hong M, et al. m(6)A-mediated ZNF750 repression facilitates nasopharyngeal carcinoma progression. *Cell Death Dis.* (2018) 9:1169. doi: 10.1038/s41419-018-1224-3
27. Zhang S, Zhao BS, Zhou A, Lin K, Zheng S, Lu Z, et al. m(6)A demethylase ALKBH5 maintains tumorigenicity of glioblastoma stem-like cells by sustaining FOXM1 expression and cell proliferation program. *Cancer Cell.* (2017) 31:591–606 e596. doi: 10.1016/j.ccell.2017.02.013
28. Li Z, Weng H, Su R, Weng X, Zuo Z, Li C, et al. FTO plays an oncogenic role in acute myeloid leukemia as a N(6)-methyladenosine RNA demethylase. *Cancer Cell.* (2017) 31:127–41. doi: 10.1016/j.ccell.2016.11.017
29. Zhang C, Zhi WI, Lu H, Samanta D, Chen I, Gabrielson E, et al. Hypoxia-inducible factors regulate pluripotency factor expression by ZNF217- and ALKBH5-mediated modulation of RNA methylation in breast cancer cells. *Oncotarget.* (2016) 7:64527–42. doi: 10.18632/oncotarget.11743

30. Liu X, Liu L, Dong Z, Li J, Yu Y, Chen X, et al. Expression patterns and prognostic value of m(6)A-related genes in colorectal cancer. *Am J Trans Res.* (2019) 11:3972–91.
31. Cho SH, Ha M, Cho YH, Ryu JH, Yang K, Lee KH, et al. ALKBH5 gene is a novel biomarker that predicts the prognosis of pancreatic cancer: A retrospective multicohort study. *Ann Hepato—Pancr Surg.* (2018) 22:305–9. doi: 10.14701/ahbps.2018.22.4.305
32. Fanale D, Iovanna JL, Calvo EL, Berthezene P, Belleau P, Dagorn JC, et al. Germline copy number variation in the YTHDC2 gene: does it have a role in finding a novel potential molecular target involved in pancreatic adenocarcinoma susceptibility? *Exp Opin Thera Targ.* (2014) 18:841–50. doi: 10.1517/14728222.2014.920324
33. Tanabe A, Tanikawa K, Tsunetomi M, Takai K, Ikeda H, Konno J, et al. RNA helicase YTHDC2 promotes cancer metastasis via the enhancement of the efficiency by which HIF-1alpha mRNA is translated. *Cancer Lett.* (2016) 376:34–42. doi: 10.1016/j.canlet.2016.02.022
34. Hsu PJ, Zhu Y, Ma H, Guo Y, Shi X, Liu Y, et al. Ythdc2 is an N(6)-methyladenosine binding protein that regulates mammalian spermatogenesis. *Cell Res.* (2017) 27:1115–27. doi: 10.1038/cr.2017.99
35. Bokar JA, Shambaugh ME, Polayes D, Matera AG, Rottman FM. Purification and cDNA cloning of the AdoMet-binding subunit of the human mRNA (N6-adenosine)-methyltransferase. *RNA.* (1997) 3:1233–47.
36. He H, Wu W, Sun Z, Chai L. MiR-4429 prevented gastric cancer progression through targeting METTL3 to inhibit m(6)A-caused stabilization of SEC62. *Biochem Biophys Res Commun.* (2019) 517:581–7. doi: 10.1016/j.bbrc.2019.07.058
37. Wang H, Xu B, Shi J. N6-methyladenosine METTL3 promotes the breast cancer progression via targeting Bcl-2. *Gene.* (2020) 722:144076. doi: 10.1016/j.gene.2019.144076
38. Taketo K, Konno M, Asai A, Koseki J, Toratani M, Satoh T, et al. The epitranscriptome m6A writer METTL3 promotes chemo- and radioresistance in pancreatic cancer cells. *Int J Oncol.* (2018) 52:621–9. doi: 10.3892/ijo.2017.4219

Conflict of Interest: The authors declare that the research was conducted in the absence of any commercial or financial relationships that could be construed as a potential conflict of interest.

frontiers in Oncology

ORIGINAL RESEARCH
published: 10 June 2020
doi: 10.3389/fonc.2020.00720

Comparison Between PET-CT–Guided Neck Dissection and Elective Neck Dissection in cT1-2N0 Tongue Squamous Cell Carcinoma

Fengjie Zhu[1]*, *Shuhan Sun*[2] and *Kai Ba*[1]*

[1] Department of Oral Medicine, The First Affiliated Hospital of Zhengzhou University, Zhengzhou, China, [2] Department of Oral Medicine, The Third Affiliated Hospital of Zhengzhou University, Zhengzhou, China

Objective: Neck management in cT1-2N0 tongue squamous cell carcinoma (SCC) remains controversial. Our goal was to compare the survival difference between PET-CT–guided neck dissection and elective neck dissection (END) for the treatment of cT1-2 tongue SCC.

Methods: Patients with surgically treated cT1-2N0 tongue SCC were retrospectively enrolled. These patients were divided into two groups. Group A: The decision of whether to perform neck dissection was mainly based on the results of preoperative PET-CT examinations. Group B: Patients received END treatment without preoperative PET-CT examinations. The study endpoints were regional control (RC) and disease-specific survival (DSS). The Kaplan–Meier method was used to calculate the survival rates.

Results: Group A consisted of 66 patients, and 16 patients underwent neck dissection owing to positive PET-CT results. Group B consisted of 169 patients. The 5-year RC rates in group A and group B were 86 and 87%, respectively, and the difference was not significant ($p = 0.731$). The 5-year DSS rates in group A and group B were 93 and 90%, respectively, and the difference was not significant ($p = 0.583$).

Conclusions: Neck dissection can be safely avoided when the PET-CT scan reveals no neck lymph node involvement.

Keywords: PET-CT, elective neck dissection, survival analysis, early stage tongue cancer, tongue squamous cell carcinoma

OPEN ACCESS

Edited by:
Victor C. Kok,
Asia University, Taiwan

Reviewed by:
Badr Eldin Mostafa,
Ain Shams University, Egypt
Ping-Hung Shen,
Kuang Tien General Hospital, Taiwan

***Correspondence:**
Fengjie Zhu
zhfjhappy@163.com
Kai Ba
k.ba@msn.com

Specialty section:
This article was submitted to Head and Neck Cancer, a section of the journal Frontiers in Oncology

Received: *11 December 2019*
Accepted: *16 April 2020*
Published: *10 June 2020*

Citation:
Zhu F, Sun S and Ba K (2020) Comparison Between PET-CT–Guided Neck Dissection and Elective Neck Dissection in cT1-2N0 Tongue Squamous Cell Carcinoma. Front. Oncol. 10:720. doi: 10.3389/fonc.2020.00720

INTRODUCTION

Tongue squamous cell carcinoma (SCC) is the most common malignancy in the oral cavity, and surgery is usually the first choice of treatment. For cT1-2N0 tongue SCC, its occult metastasis rate varies with different countries and races (1–3). Usually, neck dissection is required if the metastasis rate is greater than 20%. Although current high-quality research has described that routine neck dissection improves the prognosis by distinguishing patients who need adjuvant radiotherapy (1, 4, 5), researchers argue that most patients with cT1-2N0 disease do not have pathologic lymph node metastasis, and they are over-treated and exposed to possible neck dissection–related complications (2, 3); more importantly, the survival benefit associated with routine neck dissection could be contributed to by the late treatment of the metastatic necks at initial treatment. Owing to the development of individualized treatment concepts, it is very important for us to identify patients

with pathologic lymph node metastasis preoperatively to achieve both oncologic and functional outcomes. A number of scholars support the predictive value of the depth of invasion (DOI), perineural invasion (PNI), and lymphovascular invasion (LVI) (6–8). However, these data are not always able to be obtained preoperatively.

PET-CT has been widely used for detecting primary cancer disease and possible metastasis sites. Zhang et al. (9) describe that the overall sensitivity and specificity of PET-CT for predicting lymph node metastasis in cT1-2 oral SCC was 21.4% and 98.4%, respectively, with a negative predictive value of 99.1%. Myers et al. (10) presented an estimated overall sensitivity of PET-CT for the N0 neck of 78% with a specificity of 100%. Similar results were also reported by Zheng et al. (11), Lee et al. (12), and Wong et al. (13). All these findings suggest that there might be high reliability for PET-CT in assessing neck status in cT1-2 tongue SCC. Therefore, our goal was to compare the survival difference between PET-CT–guided neck dissection and elective neck dissection (END) for the treatment of cT1-2 tongue SCC.

PATIENTS AND METHODS

Ethnic Consideration

The Zhengzhou University Institutional Research Committee approved our study, and all patients signed informed consent agreements for medical research before the initial treatment. All methods were performed in accordance with the relevant guidelines and regulations.

Patient Selection

From January 2010 to December 2016, patients with surgically treated primary cT1-2N0 tongue SCC were retrospectively enrolled. Patients without follow-up information were excluded from the analysis. Data regarding demographic and pathologic information as well as follow-up data were extracted. There was no consensus on the standard treatment of a cN0 neck in cT1-2 tongue SCC in China; therefore, in our cancer center, PET-CT was selectively suggested for patients with early stage oral SCC considering the patient's demand and the surgeon's preference from 2008, and our medical team had verified the feasibility of PET-CT in treating early stage tongue SCC (14). Therefore, enrolled patients were divided into two groups. Group A: The decision of whether to perform neck dissection was mainly based on the results of preoperative PET-CT examinations; if a positive result was reported by PET-CT, a neck dissection was performed, and if not, a wait-and-see policy was conducted. Group B: Patients received END treatment without preoperative PET-CT examinations.

Important Variable Definition

Smokers/drinkers were defined as patients who smoked/drank at diagnosis or who had stopped for <1 year prior to diagnosis (15, 16). All pathological sections were re-reviewed by at least two pathologists. PNI was considered to be present if tumor cells were identified within the perineural space and/or nerve bundle; LVI was positive if tumor cells were noted within the lymphovascular channels (17). The pathologic DOI was measured from the level of the adjacent normal mucosa to the deepest point of tumor infiltration regardless of the presence or absence of ulceration (18). The cT1-2 status was defined according to the AJCC 2018 classification, and the cN0 status was defined as no doubt of metastatic lymph nodes after palpation and ultrasound, CT, and MRI examinations.

Treatment Proposal

All patients underwent complete tumor resection with a margin of at least 1 cm, and the sublingual gland as well as the adipose tissue in the floor of the mouth was simultaneously resected. The neck dissection field included levels 1–3. Patients were followed every 3 months within 2 years after the operation and every 6 months for 2 years after the operation until the fifth year after the operation. Immediate interference was performed if disease recurrence was suspected. Adjuvant radiotherapy was suggested if there was pathologic lymph node metastasis, positive margins, PNI, or LVI.

Pathologic Analysis

Surgical specimens were immediately fixed in 10% formalin and then cut into pieces with a thickness of 5 mm and a side length of 1 cm by embedding in paraffin. Sections of a thickness of 5 um were obtained at 0.5-mm intervals and stained with haematoxylin and eosin. All pathologic sections had been reviewed by at least two pathologists. Immunohistochemistry was performed if there was difficulty in identifying malignant disease.

PET-CT Examination

The PET-CT scans (GE Healthcare, Milwaukee, WI) were performed by several technicians. Patients had an empty stomach for at least 6 hours before examination with glucose levels <200 mg/dL, and 10–20 mCi of [^{18}F] FDG dosed according to the weight was given to each patient. Diagnostic CT images and axial PET were obtained from the calvarial vertex through the upper thighs. Emission images were obtained after radiopharmaceutical injection 60 min later. During the CT scan, no contrast medium was used. The images were reconstructed with a 2.5-mm thickness slice. For every suspicious lesion, the isocontour region of interest centered on the maximum value pixel was drawn automatically with workstation tools generating the SUV max of the region. An SUV max cutoff of 2.5 MBq/g was used for FDG-avid primary tumors and lymph nodes on PET-CT.

Statistic Analysis

Student's *t*-tests and chi-square tests were used to compare the clinical and pathologic variables between the two groups, and the Kaplan–Meier method was used to calculate the regional control (RC) rate and disease-specific survival (DSS) rate. The survival time was calculated from the date of surgery to the last follow-up, the date of the first regional recurrence, or the date of cancer-caused death. All statistical analyses were performed using SPSS 20.0, and $p < 0.05$ was considered to be significant.

RESULTS

Demography and Pathologic Data

A total of 235 patients (172 males and 63 females) were included in the analysis, and the mean age was 54.8 (range: 31–79) years. There were 66 patients in group A and 169 patients in group B.

In group A, there were 52 (78.8%) males and 14 (21.2%) females, and the mean age was 55.7 years. A total of 42 (63.6%) and 29 (43.9%) patients were smokers and drinkers, respectively. cT1 and cT2 tumors were present in 25 (37.9%) and 41 (62.1%) patients, respectively. PNI and LVI were reported in eight (12.1%) and seven (10.6%) patients, respectively. The mean pathologic DOI was 4.8 mm. pT1 and pT2 tumors were present in 20 (30.3%) and 46 (69.7%) patients, respectively. Tumor differentiation was well distributed in 22 (33.3%) patients, moderately distributed in 35 (53.0%) patients, and poorly distributed in nine (13.6%) patients. Negative margins were achieved in all patients. Fourteen (21.2%) patients received postoperative radiotherapy (**Table 1**).

In group B, there were 120 (71.0%) males and 49 (29.0%) females, and the mean age was 54.4 years. A total of 111 (65.6%) and 58 (34.3%) patients were smokers and drinkers, respectively. cT1 and cT2 tumors were present in 45 (26.6%) and 124 (73.4%) patients, respectively. PNI and LVI were reported in 22 (13.0%) and 17 (10.1%) patients, respectively. The mean pathologic DOI was 4.7 mm. pT1 and pT2 tumors were present in 40 (23.7%) and 129 (76.3%) patients, respectively. Pathologic lymph node metastasis occurred in 30 (17.8%) patients, and in these patients, N1 was present in 25 cases, and N2a was present in five cases. Tumor differentiation was well distributed in 53 (31.4%) patients, moderately distributed in 99 (58.6%) patients, and poorly distributed in 17 (10.1%) patients. Negative margins were achieved in all patients. Thirty (17.8%) patients received postoperative radiotherapy (**Table 1**).

The two groups had similar distributions regarding age, sex, smoking status, drinking status, clinical, and pathologic tumor stage, PNI, LVI, tumor differentiation, and postoperative radiotherapy (**Table 1**, all $p > 0.05$).

TABLE 1 | Demographic and pathologic information in the two groups.

Variables	Group A ($n = 66$)	Group B ($n = 169$)	p
Age	55.7	54.4	0.884
Sex			
Male	52 (78.8%)	120 (71.0%)	
Female	14 (21.2%)	49 (29.0%)	0.170
Smoker	42 (63.6%)	111 (65.7%)	0.768
Drinker	29 (43.9%)	58 (34.3%)	0.170
Clinical tumor stage			
cT1	25 (37.9%)	45 (26.6%)	
cT2	41 (62.1%)	124 (73.4%)	0.090
Perineural invasion	8 (12.1%)	22 (13.0%)	0.853
Lymphovascular invasion	7 (10.6%)	17 (10.1%)	0.901
Pathologic tumor stage			
pT1	20 (30.3%)	40 (23.7%)	
pT2	46 (69.7%)	129 (76.3%)	0.295
Tumor differentiation			
Well	22 (33.3%)	53 (31.4%)	
Moderate	35 (53.0%)	99 (58.6%)	
Poor	9 (13.6%)	17 (10.1%)	0.649
Postoperative radiotherapy	14 (21.2%)	30 (17.8%)	0.541

PET-CT–Guided Neck Dissection

In group A, 16 (9.5%) patients underwent neck dissection owing to positive PET-CT results, and postoperative pathology confirmed occult metastasis in 14 patients. Of the 14 patients, N1 was present in 12 patients, and N2a was present in two patients.

Survival Analysis

During our follow-up with a mean time of 48.5 months, in group A of the 66 patients, regional recurrence occurred in nine patients: level I occurrence in four patients, level II in three patients, and level III in two patients (**Table 2**). Among these nine patients, seven had a pathologic N+ neck at the initial treatment, two patients had not previously received neck dissection owing to previous negative PET-CT results, there was no local recurrence or distant metastasis, the 5-year RC rate was 86%, recurrent disease was successfully salvaged in six patients with radical operations, four patients died of the disease, and the 5-year DSS rate was 93%. In group B, local recurrence occurred in five patients, and regional recurrence occurred in 20 patients: level I recurrence in nine patients, level II in six patients, level IV in three patients, and level V in two patients (**Table 2**). Among these 20 patients, 14 had a pathologic N+ neck at the initial treatment, there was no distant metastasis, the 5-year RC rate was 87%, patients with local recurrence were all successfully salvaged with radial operations, regional recurrent disease was successfully salvaged in eight patients with radial operations, 14 patients died of the disease, and the 5-year DSS rate was 90%. The two groups had similar RC ($p = 0.731$) and DSS ($p = 0.583$) rates (**Figures 1**, **2**, both $p > 0.05$).

TABLE 2 | Neck recurrence pattern in the two groups.

Metastatic level	Group A ($n = 9$)	Group B ($n = 20$)
Ipsilateral		
I	4 (44.4%)	8 (40.0%)
II	2 (22.2%)	6 (20.0%)
III	2 (22.2%)	0
IV	0	3 (15.0%)
V	0	1 (5.0%)
Contralateral		
I	1 (11.1%)	1 (5.0%)
II	2 (22.2%)	2 (10.0%)
III	0	0
IV	0	1 (5.0%)
V	0	1 (5.0%)

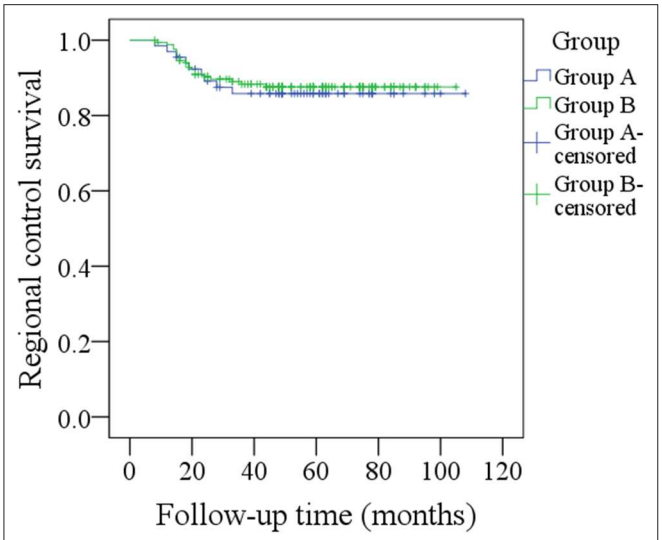

FIGURE 1 | Comparison of regional control between the two groups ($p = 0.731$).

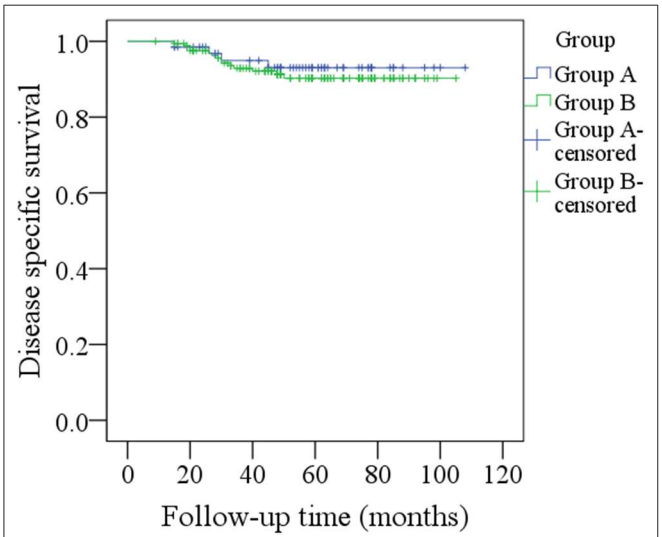

FIGURE 2 | Comparison of disease-specific survival between the two groups ($p = 0.583$).

DISCUSSION

The most significant finding in the current study was that, compared to elective neck dissection, PET-CT–guided neck dissection obtained similar disease control of cT1-2N0 tongue SCC; moreover, there was a higher possibility of successful salvage with PET-CT–guided neck dissection than with elective neck dissection. Our study may provide more suggestions for neck management during early stage tongue SCC treatment, and it provides the first evidence for the high reliability of PET-CT–guided neck dissection.

Neck lymph node status is the most important prognostic factor; usually, the survival rate decreases by half if lymph node metastasis is present (19–21). It is important that surgeons correctly address the neck. However, owing to the varying occult metastasis rates, there is still substantial controversy regarding the best neck management. Canis et al. (4) studied early stage SCC of the upper aerodigestive tract, and the 5-year recurrence-free survival rate was 95% in the neck dissection group and 96% in the wait-and-see group; the authors concluded that a wait-and-see approach was justified in patients with early stage disease. Deganello et al. (22) described that the occult neck disease rate was only 12.5% for laryngeal SCC, and the findings indicated the need to refine the treatment strategy, restricting elective neck dissection only to advanced stage disease. However, tongue SCC was significantly different from SCC in other sites, and the conclusions based on the overall sample of head and neck SCC or laryngeal SCC might not be suitable for tongue SCC. Moratin et al. (23) depicted that regional metastases occurred in 29 of the 97 patients with early stage tongue SCC, and although rare, bilateral cervical metastases could be detected in 2.1% of T1 and 11.8% of T2 disease; therefore, the authors suggested that neck dissection was required in all tongue SCC patients irrespective of tumor stage. Recent evidence showed that, after matched analysis in 1,234 patients, the 5-year overall survival rates were 87.1% in the neck dissection group and 76.2% in the wait-and-see group ($p = 0.0051$), and the DSS rates were 89.2% and 82.2% ($p = 0.0335$), respectively. This finding suggests that routine neck dissection was beneficial for cT1-2N0 tongue SCC (24). A similar viewpoint was also demonstrated by Gad et al. (25), Orabona et al. (26), and D'Cruz et al. (1). However, at least two aspects must be considered seriously when comprehending the conclusions: First, the occult metastasis rate was variable in early stage tongue SCC, and most of the patients would have been over-treated if routine neck dissection was performed; second, the so-called survival difference between elective neck dissection and the wait-and-see policy would have been mainly explained by the undetected real metastatic lymph nodes at the first visit in the wait-and-see group. This raised the point that, if we could identify patients who had real metastatic lymph nodes preoperatively, we might avoid unnecessary neck dissection and achieve similar survival compared to routine neck dissection.

A number of authors have aimed to assess the predictors of occult lymph node metastasis in cT1-2N0 tongue SCC. Jiang et al. (6) introduced a nomogram including the site of the primary lesion, depth of invasion, size of the tumor, and histopathological grade with high consistency for predicting the probability of occult cervical metastasis before surgery. Tam et al. (7) demonstrated that a DOI of 7.25 mm was most predictive for occult nodal disease. Other predictors included PNI and LVI (1). However, the data were always unavailable preoperatively, which greatly limited the clinical application.

PET-CT has been widely used to detect occult lymph node disease in the clinic. Slightly conflicting results have been reported by previous researchers. Stoeckli et al. (27) assessed the value of PET-CT for the staging of cN0 necks in oral and oropharyngeal SCC using sentinel lymph node biopsy and

elective neck dissection as the "gold standard" for comparison, and sentinel lymph node biopsy was accurately feasible in all 12 patients and correctly diagnosed five cases of occult metastasis; however, PET-CT only suggested that two patients had occult metastasis, of whom one turned out to be a false positive case. A similar finding was also reported by Krabbe et al. (28), but both studies did not specifically focus on tongue SCC, which is significantly different from SCC in other sites, and HPV infection might also affect the accuracy of PET-CT. Increasing evidence supports the high reliability of PET-CT for identifying cervical nodal disease. Zhang et al. (9) described that the overall sensitivity and specificity of PET-CT for predicting lymph node metastasis in cT1-2 oral SCC was 21.4 and 98.4%, respectively, with a negative predictive value of 99.1%. Myers et al. (10) presented an estimated overall sensitivity of PET-CT for the N0 neck of 78% with a specificity of 100%. Similar results were also reported by Zheng et al. (11), Lee et al. (12), and Wong et al. (13). A recent important study by Lowe et al. (29) described that PET-CT had a highly negative predictive value for the N0 neck in T2 to T4 SCC of the head and neck and that PET/CT might assist clinicians with the decision of the best therapy for the clinically N0 neck in SCC of the head and neck. Our results supported most of those of other researchers and verified the high reliability of PET-CT for predicting occult metastasis in cT1-2 disease, which could result in similar oncologic outcomes as routine neck dissection. The two groups had comparable important variables except the clinical tumor stage; patients undergoing a PET-CT–guided neck dissection tended to have a smaller tumor, it indicated that we selectively suggested a PET-CT for a small tumor to avoid unnecessary neck dissection and obtain a better functional result previously. Additionally, the tending difference of clinical tumor stage might have led to survival difference between the two groups, but in fact, it was not. It brought some puzzle in comprehending our finding; more high quality research is needed to clarify these questions.

Another heated debated tool of detecting occult metastasis was sentinel lymph node biopsy (SLNB). Moya-Plana et al. (30) compared the reliability between SLNB and END in 229 cT1-2N0 oral SCC patients; the authors reported negative predictive value of SLNB was as high as 92.7%, and the two groups had similar recurrence-free survival and overall survival. Riese et al. (31) described in 36 patients with early oral and oropharynx SCC, all the 12 patients with pathologic metastasis were detected in SLNB, and it showed a sensitivity of 94.4% and a specificity of 100%. All these findings as well as recent research (32–34) confirmed SLNB was a precise diagnostic procedure in oral SCC and superior to PET-CT in melanoma and anal cancer for assessing nodal status. However, comparison between SLNB and PET-CT in oral SCC was never reported, and also application of SLNB in oral cancer was not widely accepted in China. More high-quality studies are needed to clarify these questions.

Salvage operations are important for improving survival, but the rate of successful salvage operations is usually <50% in tongue SCC patients (1–3). A similar finding was also noted in our END group. However, in group A, our salvage operation rate was as high as 66.7%, and it tended to be higher than that in group B. This finding was interesting: The high salvage operation rate might have resulted in improved DSS, but owing to our limited sample size, we could not draw any persuasive conclusions.

It was interesting to note the occult metastasis rate of Group B was just 17.8%; it was a little lower than those of similar studies (35, 36). The difference might be partially explained by different pathologic DOI and races. On the other hand, micrometastasis disease was also partially responsible during standard haematoxylin and eosin; van den Brekel et al. (37) previously presented that 25% of patients with positive lymph nodes had micrometastasis and were at high risk for undetected disease. Similar findings were also reported by Barrera et al. (38) and Rhee et al. (39).

There are some limitations that must be acknowledged. First, this was a retrospective study, it lacked of randomization, and the inherent bias could decrease the statistical power. In our future work, we will perform a prospective study with additional data regarding patient characteristics, especially other preoperative investigations, which could increase the predictive value of negative or positive PET-CT results. Second, our sample size was small, and a study with a larger sample size is needed. Third, some confounding factors might not have been taken into consideration, such as oral hygiene.

In summary, neck dissection could be safely avoided when the PET-CT scan reveals no neck lymph node involvement.

DATA AVAILABILITY STATEMENT

The raw data supporting the conclusions of this article will be made available by the authors, without undue reservation, upon a reasonable request.

ETHICS STATEMENT

The Zhengzhou University Institutional Research Committee approved our study, and all patients signed informed consent agreements for medical research before initial treatment.

AUTHOR CONTRIBUTIONS

All the authors make the contribution in data collection, data analysis, and manuscript writing.

ACKNOWLEDGMENTS

This study was supported by National Natural Science Foundation of China (Grant No. 81500826).

REFERENCES

1. D'Cruz AK, Vaish R, Kapre N, Dandekar M, Gupta S, Hawaldar R, Agarwal JP, et al. Elective versus therapeutic neck dissection in node-negative oral cancer. *N Engl J Med.* (2015) 373:521–9. doi: 10.1056/NEJMoa1506007
2. Abu-Ghanem S, Yehuda M, Carmel NN, Leshno M, Abergel A, Gutfeld O, et al. Elective neck dissection vs observation in early-stage squamous cell carcinoma of the oral tongue with no clinically apparent lymph node metastasis in the neck: a systematic review and meta-analysis. *JAMA Otolaryngol Head Neck Surg.* (2016) 142:857–65. doi: 10.1001/jamaoto.2016.1281
3. Liu JY, Chen CF, Bai CH. Elective neck dissection versus observation in early-stage (cT1/T2N0) Oral squamous cell carcinoma. *Laryngoscope Investig Otolaryngol.* (2019) 4:554–61. doi: 10.1002/lio2.301
4. Canis M, Plüquett S, Ihler F, Matthias C, Kron M, Steiner W. Impact of elective neck dissection vs observation on regional recurrence and survival in cN0-staged patients with squamous cell carcinomas of the upper aerodigestive tract. *Arch Otolaryngol Head Neck Surg.* (2012) 138:650–5. doi: 10.1001/archoto.2012.1026
5. Borgemeester MC, van den Brekel MW, van Tinteren H, Smeele LE, Pameijer FA, van Velthuysen ML, et al. Ultrasound-guided aspiration cytology for the assessment of the clinically N0 neck: factors influencing its accuracy. *Head Neck.* (2008) 30:1505–13. doi: 10.1002/hed.20903
6. Jiang Q, Tang A, Long S, Qi Q, Song C, Xin Y, et al. Development and validation of a nomogram to predict the risk of occult cervical lymph node metastases in cN0 squamous cell carcinoma of the tongue. *Br J Oral Maxillofac Surg.* (2019) 57:1092–7. doi: 10.1016/j.bjoms.2019.09.024
7. Tam S, Amit M, Zafereo M, Bell D, Weber RS. Depth of invasion as a predictor of nodal disease and survival in patients with oral tongue squamous cell carcinoma. *Head Neck.* (2019) 41:177–84. doi: 10.1002/hed.25506
8. Faisal M, Abu Bakar M, Sarwar A, Adeel M, Batool F, Malik KI, et al. Depth of invasion (DOI) as a predictor of cervical nodal metastasis and local recurrence in early stage squamous cell carcinoma of oral tongue (ESSCOT). *PLoS ONE.* (2018) 13:e0202632. doi: 10.1371/journal.pone.0202632
9. Zhang H, Seikaly H, Biron VL, Jeffery CC. Utility of PET-CT in detecting nodal metastasis in cN0 early stage oral cavity squamous cell carcinoma. *Oral Oncol.* (2018) 80:89–92. doi: 10.1016/j.oraloncology.2018.04.003
10. Myers LL, Wax MK, Nabi H, Simpson GT, Lamonica D. Positron emission tomography in the evaluation of the N0 neck. *Laryngoscope.* (1998) 108:232–6. doi: 10.1097/00005537-199802000-00014
11. Zheng D, Niu L, Liu W, Zheng C, Yan R, Gong L, et al. Relationship between the maximum standardized uptake value of fluoro-2-deoxyglucose-positron emission tomography/computed tomography and clinicopathological characteristics in tongue squamous cell carcinoma. *J Cancer Res Ther.* (2019) 15:842–8. doi: 10.4103/jcrt.JCRT_855_18
12. Lee SJ, Choi JY, Lee HJ, Baek CH, Son YI, Hyun SH, et al. Prognostic value of volume-based (18)F-fluorodeoxyglucose PET/CT parameters in patients with clinically node-negative oral tongue squamous cell carcinoma. *Korean J Radiol.* (2012) 13:752–9. doi: 10.3348/kjr.2012.13.6.752
13. Wong WL, Sonoda LI, Gharpurhy A, Gollub F, Wellsted D, Goodchild K, et al. 18F-fluorodeoxyglucose positron emission tomography/computed tomography in the assessment of occult primary head and neck cancers–an audit and review of published studies. *Clin Oncol.* (2012) 24:190–5. doi: 10.1016/j.clon.2011.11.001
14. Zhao G, Sun J, Zhang Y, Ba K. Significance of PET-CT for detecting occult lymph node metastasis and affecting prognosis in early-stage tongue squamous cell carcinoma. *Front Oncol.* (2020) 10:368. doi: 10.3389/fonc.2020.00386
15. Ouyang PY, Su Z, Mao YP, Liang XX, Liu Q, Xie FY. Prognostic impact of family history in southern Chinese patients with undifferentiated nasopharyngeal carcinoma. *Br J Cancer.* (2013) 109:788–94. doi: 10.1038/bjc.2013.343
16. Fang QG, Shi S, Liu FY, Sun CF. Squamous cell carcinoma of the oral cavity in ever smokers: a matched-pair analysis of survival. *J Craniofac Surg.* (2014) 25:934–7. doi: 10.1097/SCS.0000000000000710
17. Skulsky SL, O'Sullivan B, McArdle O, Leader M, Roche M, Conlon PJ, et al. Review of high-risk features of cutaneous squamous cell carcinoma and discrepancies between the American Joint Committee on cancer and NCCN clinical practice guidelines in oncology. *Head Neck.* (2017) 39:578–94. doi: 10.1002/hed.24580
18. Lydiatt WM, Patel SG, O'Sullivan B, Brandwein MS, Ridge JA, Migliacci JC, et al. Head and Neck cancers-major changes in the American Joint Committee on cancer eighth edition cancer staging manual. *Cancer J Clin.* (2017) 67:122–37. doi: 10.3322/caac.21389
19. Fang Q, Li P, Qi J, Luo R, Chen D, Zhang X. Value of lingual lymph node metastasis in patients with squamous cell carcinoma of the tongue. *Laryngoscope.* (2019) 129:2527–30. doi: 10.1002/lary.27927
20. Dai L, Fang Q, Li P, Liu F, Zhang X. Oncologic outcomes of patients with sarcomatoid carcinoma of the hypopharynx. *Front Oncol.* (2019) 9:950. doi: 10.3389/fonc.2019.00950
21. Du W, Fang Q, Wu Y, Wu J, Zhang X. Oncologic outcome of marginal mandibulectomy in squamous cell carcinoma of the lower gingiva. *BMC Cancer.* (2019) 19:775. doi: 10.1186/s12885-019-5999-0
22. Deganello A, Gitti G, Meccariello G, Parrinello G, Mannelli G, Gallo O. Effectiveness and pitfalls of elective neck dissection in N0 laryngeal cancer. *Acta Otorhinolaryngol Ital.* (2011) 31:216–221.
23. Moratin J, Metzger K, Engel M, Hoffmann J, Freudlsperger C, Freier K, et al. The occurrence of cervical metastases in squamous cell carcinoma of the tongue: Is there a rationale for bilateral neck dissection in early-stage tumors? *J Craniomaxillofac Surg.* (2019) 47:1134–8. doi: 10.1016/j.jcms.2019.03.003
24. Otsuru M, Ota Y, Yanamoto S, Okura M, Umeda M, Kirita T, et al. A multicenter retrospective study of elective neck dissection for T1-2N0M0 tongue squamous cell carcinoma: analysis using propensity score-matching. *Ann Surg Oncol.* (2019) 26:555–63. doi: 10.1245/s10434-018-07089-7
25. Gad ZS, El-Malt OA, El-Sakkary MAT, Abdal Aziz MM. Elective neck dissection for management of early- stage oral tongue cancer. *Asian Pac J Cancer Prev.* (2018) 19:1797–803. doi: 10.22034/APJCP.2018.19.7.1797
26. Orabona GD, Bonavolontà P, Maglitto F, Friscia M, Iaconetta G, Califano L. Neck dissection versus "watchful-waiting" in early squamous cell carcinoma of the tongue our experience on 127 cases. *Surg Oncol.* (2016) 25:401–4. doi: 10.1016/j.suronc.2016.09.005
27. Stoeckli SJ, Steinert H, Pfaltz M, Schmid S. Is there a role for positron emission tomography with 18F-fluorodeoxyglucose in the initial staging of nodal negative oral and oropharyngeal squamous cell carcinoma. *Head Neck.* (2002) 24:345–9. doi: 10.1002/hed.10057
28. Krabbe CA, Balink H, Roodenburg JL, Dol J, de Visscher JG. Performance of 18F-FDG PET/contrast-enhanced CT in the staging of squamous cell carcinoma of the oral cavity and oropharynx. *Int J Oral Maxillofac Surg.* (2011) 40:1263–70. doi: 10.1016/j.ijom.2011.06.023
29. Lowe VJ, Duan F, Subramaniam RM, Sicks JD, Romanoff J, Bartel T, et al. Multicenter trial of [18F]fluorodeoxyglucose positron emission tomography/computed tomography staging of head and neck cancer and negative predictive value and surgical impact in the N0 Neck: results from ACRIN 6685. *J Clin Oncol.* (2019) 37:1704–12. doi: 10.1200/JCO.18.01182
30. Moya-Plana A, Aupérin A, Guerlain J, Gorphe P, Casiraghi O, Mamelle G, et al. Sentinel node biopsy in early oral squamous cell carcinomas: Long-term follow-up and nodal failure analysis. *Oral Oncol.* (2018) 82:187–94. doi: 10.1016/j.oraloncology.2018.05.021
31. Riese CGU, Karstadt JA, Schramm A, Güleryüz S, Dressel G, Lorenz KJ, et al. Validity of sentinel node biopsy in early oral and oropharyngeal carcinoma. *J Craniomaxillofac Surg.* (2018) 46:1748–52. doi: 10.1016/j.jcms.2018.07.021
32. Schilling C, Shaw R, Schache A, McMahon J, Chegini S, Kerawala C, et al. Sentinel lymph node biopsy for oral squamous cell carcinoma. Where are we now? *Br J Oral Maxillofac Surg.* (2017) 55:757–62. doi: 10.1016/j.bjoms.2017.07.007
33. El-Maraghi RH, Kielar AZ. PET vs sentinel lymph node biopsy for staging melanoma: a patient intervention, comparison, outcome analysis. *J Am Coll Radiol.* (2008) 5:924–31. doi: 10.1016/j.jacr.2008.02.022
34. De Nardi P, Guarneri G, Canevari C, Tamburini A, Slim N, Passoni P, et al. Prognostic value of fluorodeoxyglucose positron emission tomography/computed tomography and inguinal sentinel lymph node biopsy in patients with anal cancer. *Colorectal Dis.* (2019) 21:1017–24. doi: 10.1111/codi.14691
35. Ahmed SQ, Junaid M, Awan S, Kazi M, Khan HU, Halim S. Frequency of cervical nodal metastasis in early-stage squamous

cell carcinoma of the tongue. *Int Arch Otorhinolaryngol.* (2018) 22:136–40. doi: 10.1055/s-0037-1603626
36. Abbate V, Dell'Aversana Orabona G, Salzano G, Bonavolontà P, Maglitto F, Romano A, et al. Pre-treatment neutrophil-to-lymphocyte ratio as a predictor for occult cervical metastasis in early stage (T1-T2 cN0) squamous cell carcinoma of the oral tongue. *Surg Oncol.* (2018) 27:503–7. doi: 10.1016/j.suronc.2018.06.002
37. van den Brekel MW, van der Waal I, Meijer CJ, Freeman JL, Castelijns JA, Snow GB. The incidence of micrometastases in neck dissection specimens obtained from elective neck dissections. *Laryngoscope.* (1996) 106:987–91. doi: 10.1097/00005537-199608000-00014
38. Barrera JE, Miller ME, Said S, Jafek BW, Campana JP, Shroyer KR. Detection of occult cervical micrometastases in patients with head and neck squamous cell cancer. *Laryngoscope.* (2003) 113:892–6. doi: 10.1097/00005537-200305000-00022
39. Rhee D, Wenig BM, Smith RV. The significance of immunohistochemically demonstrated nodal micrometastases in patients with squamous cell carcinoma of the head and neck. *Laryngoscope.* (2002) 112:1970–4. doi: 10.1097/00005537-200211000-00011

Conflict of Interest: The authors declare that the research was conducted in the absence of any commercial or financial relationships that could be construed as a potential conflict of interest.

frontiers in Oncology

ORIGINAL RESEARCH
published: 30 June 2020
doi: 10.3389/fonc.2020.00870

Myb Immunohistochemical Staining and Fluorescence *in situ* Hybridization in Salivary Rare Basaloid Lesions

Binbin Li[1,2,3], *Weiping Jie*[1,2,3] *and Huiying He*[4]*

[1] Department of Oral Pathology, Peking University School and Hospital of Stomatology, Beijing, China, [2] Research Unit of Precision Pathologic Diagnosis in Tumors of the Oral and Maxillofacial Regions, Chinese Academy of Medical Sciences, Beijing, China, [3] National Clinical Research Center for Oral Diseases, Peking University School and Hospital of Stomatology, Beijing, China, [4] Department of Pathology, School of Basic Medical Sciences, Third Hospital, Peking University Health Science Center, Beijing, China

Objective: Salivary rare basaloid lesions, including cribriform type basal cell adenoma (cBCA), BCA with incomplete capsule (iBCA), sialoblastoma (SB), and intercalated duct hyperplasia (IDH), could easily be misdiagnosed as adenoid cystic carcinoma (AdCC). We aim to identify an approach for differential diagnosis and to establish an optimal workflow concerning the diagnosis of these lesions.

Material and methods: A panel of antibodies (MYB, β-catenin, CD117, SOX10, ki67, P63, calponin) and fluorescence *in situ* hybridization (FISH)-MYB were utilized to distinguish above salivary basaloid diseases from AdCC.

Results: Histologically, the striking diagnostic features of cBCA, iBCA, SB, and IDH are composed of basaloid tumor cells, well-defined encapsulation, or lack of destructive invasion. Immunohistochemically, Myb immune-labeling could effectively make a distinction among cBCA, iBCA, SB, and IDH from AdCC, except in SB. cBCA and iBCA typically expressed β-catenin in the nuclei of tumor cells. There was no statistical significance in the ki67 index between SB and AdCC, but their indices were significantly higher than those of iBCA and IDH ($p < 0.05$, $p < 0.05$, respectively). P63 and calponin immune-expression were observed in the basaloid or myoepithelial cells. CD117 were observed positively in cBCA, iBCA, SB, and AdCC, except in IDH. SOX10 were observed positively in all cases. No cases had fusion of MYB and NFIB detectable by FISH, except in AdCC.

Conclusion: Considering their sensitivity and specificity, FISH-Myb and an immunohistochemical panel of MYB/β-catenin/ki67 would be an optimal choice for the differential diagnosis of these basaloid lesions.

Clinical relevance: Some salivary basaloid tumor or tumor-like lesions have overlapping features with AdCC. Through this present research, we suggested that the panel IHC of MYB, βcatenin, and ki67 combined with FISH-Myb should be an optimal choice for differential diagnosis among those lesions.

Keywords: MYB, immunohistochemistry, fluorescence *in situ* hybridization, salivary basaloid lesions, adenoid cystic carcinoma

OPEN ACCESS

Edited by:
Jorge A. R. Salvador, University of Coimbra, Portugal

Reviewed by:
Nan Xiao, University of the Pacific, United States
Ce Shi, Jilin University, China

***Correspondence:**
Huiying He
hehylibb@aliyun.com

Specialty section:
This article was submitted to Head and Neck Cancer, a section of the journal Frontiers in Oncology

Received: *15 September 2019*
Accepted: *04 May 2020*
Published: *30 June 2020*

Citation:
Li B, Jie W and He H (2020) Myb Immunohistochemical Staining and Fluorescence in situ Hybridization in Salivary Rare Basaloid Lesions. Front. Oncol. 10:870. doi: 10.3389/fonc.2020.00870

INTRODUCTION

Salivary rare basaloid tumor or tumor-like lesions share some features resembling adenoid cystic carcinoma (AdCC), even exhibiting a typical cribriform pattern like that of AdCC. This creates diagnosis pitfalls, especially in fine-needle aspiration testing (FNAT). iBCA and cBCA are usually treated with a conservative treatment strategy (partial or superficial parotidectomy), which is very different from the radical choice of AdCC (radical surgical excision with or without postoperative radiation). No surgical intervention is required for IDH. Most SBs are cured by primary surgical resection. Therefore, it is very important to make a differential diagnosis between them. In addition, these lesions may be less familiar to non-head and neck specialists due to the low incidence. Since exact diagnosis is crucial for an appropriate treatment choice, it is necessary to study the following AdCC mimicking lesions using the specific protein and molecular markers.

Usually, typical basal cell adenoma (BCA) is well-circumscribed and composed of basaloid cells with eosinophilic cytoplasm (1). In practice, there are two types of BCA, cribriform BCA (cBCA) and BCA with incomplete encapsulation (iBCA), which are easily misdiagnosed as AdCC. Because AdCC is mainly characterized by a cribriform growth pattern, the cribriform components apparent in cBCA would mislead pathologists to the diagnosis of AdCC. Our primary study and a recent study both proved that AdCC and cBCA were two distinct tumor entities (2, 3). Some studies suggested that β-catenin mutation was present in up to 52% of BCAs. Thus, the corresponding nuclear expression of β-catenin can be detected in BCA and would be a specific marker to identify cBCA or iBCA from AdCC (4). At the same time, few BCAs have incomplete capsules or could have focal capsule invasion, which are easily mistaken as malignant presentation. In this circumstance it is important to differentiate iBCA from AdCC, despite the capsule of micro-invasion.

Apart from iBCA and cBCA, sialoblastoma (SB), and intercalated duct hyperplasia (IDH) could occasionally resemble AdCC too. SB was ever named as congenital hybrid basal cell adenoma-adenoid cystic carcinoma (5), which suggested that its morphology overlapped with BCA or AdCC. In some instances the cribriform pattern was evident in SB, and it was problematic to distinguish between them. IDH is a salivary ductal proliferation resembling intercalated ducts, which was newly identified as a separate entity in the WHO new classification of Head and Neck Tumors 2017. It is considered as a reactive and hyperplastic process, or a precursor condition for some salivary gland tumors, such as BCA (6). It typically exhibited an idiopathic, focal hypertrophic lesion of intraoral mucous glands with limited growth possibilities (7). Due to its unencapsulation, IDH may also be misdiagnosed as AdCC.

Recent genomic study identified new markers that may be helpful in future investigations. Researchers have shown that the specific translocation *t* (6;9) involving v-myb avian myeloblastosis viral oncogene homolog (MYB) and nuclear factor 1B-type (NFIB) was the most relevant genetic alternation in AdCC (8). MYB immuno-staining was proved to be a useful ancillary test for distinguishing AdCC from other benign and malignant salivary gland neoplasms (9, 10). On the other hand, the transcriptional factor sex-determining region Y (SRY)-related HMG box-containing factor 10 (SOX10), normally only expressed during salivary gland differentiation, was found markedly upregulated in a majority of AdCC cases (11). In addition, it was reported that most AdCCs (90%) exhibited strong and diffuse expression of CD117 (12). Thus, a panel of specific immunomarkers that include MYB, SOX-10, and CD117 could be believed as very effective for the diagnosis of AdCC.

Of course, the typical AdCC is generally recognized by biopsy in HE staining. However, iBCA, cBCA, SB, and IDH are extremely rare lesions, and are much more confusing in microscopic diagnosis. Based on above research progress, genetic abnormalities, and protein expressions may be helpful in their distinction from AdCC. Taken together, it is worth identifying an approach with relatively high sensitivity and high specificity in the histologic diagnosis of salivary basaloid lesions. This study first used a combination of histologic, immunohistochemical, and a FISH test to evaluate MYB, CD117, SOX10, βcatenin, ki67, p63, and calponin in the differential diagnosis of cBCA, iBCA, SB, and IDH from AdCC. It was shown that both SB and AdCC had MYB positive immune-expression, but only AdCC had Myb rearrangement examined by FISH. The positive reaction ofβ-catenin in nuclear was specific in iBCA and cBCA. P63 and calponin immune-expression were observed in the basaloid or myoepithelial cells. CD117 were observed positively in cBCA, iBCA, SB, and AdCC, except in IDH. SOX10 were observed positively in all the cases. The ki67 indices of SB and AdCC were significantly higher than those of iBCA and IDH. Taking account of both sensitivity and specificity, we recommend FISH-Myb and an immunohistochemical panel of MYB/β-catenin/ki67 as an optimal choice for the differential diagnosis of these basaloid lesions.

MATERIALS AND METHODS

Patients

Approved by Institutional Review Board and formally numbered PKUSSIRB-201631121, 64 cases, including 23 cBCAs, 11 iBCAs, 3 SBs, 7 IDHs, and 20 AdCCs (as controls), were collected from the files of Peking University School and Hospital of Stomatology. The criteria for eligibility of AdCC were (i) histologically typical AdCC confirmed by two pathologists (Dr. Li and Dr. He) (ii) presence of adjacent tissue invasion, including muscle, gland, vessel, nerve, and bone infiltration or lung metastasis.

The investigated parameters consisted of gender, age distributions, anatomic location, histologic characteristics, treatment, and postoperative outcomes. Follow-up information was obtained from the medical records or by telephone interview.

Histological Examination

All specimens were fixed in neutral buffered 10% formalin, processed and embedded in paraffin. 4 μm sections were stained with hematoxylin and eosin, and then observed under light microscope.

Immunohistochemical Reaction

All slides were performed with the following seven antibodies by the standard streptavidin-biotin-peroxidase complex technique. The MYB antibody was bought from ABCAM Co. (clone EP769Y, dilution 1:500, ABCAM, Cambridge, MA). CD117 (clone EP10), SOX10 (clone EP268), βcatenin (clone UMAB15), ki67(clone UMAB107), p63 (clone 4A4), and calponin (clone EP63) were obtained from Zymed Co. (Zymed, Carlsbad, CA). The staining was scored qualitatively and assessed on intensity (1+ to 3+) and staining pattern (nuclear, cytoplasm or membrane). Only 2+ or 3+ intensity staining was interpreted as positive.

FISH Test

A commercially available Myb dual-color break-apart probe (ZTV-Z-2143-200, ZytoVision, Bremerhaven, Germany) was utilized for FISH. Before hybridization, 4 μm slides were baked at 65°C overnight, deparaffinized by washing with xylene and ethanol, and rehydrated with deionized water at 90°C for 30 min. Pretreated slides were incubated with a proteinase K solution (100 mg/mL; Sigma-Aldrich, UK) for 10–30 min. Slides and probes were then co-denatured at 73°C for 5 min and hybridized overnight at 37°C using an automated ThermoBrite codenaturation oven (Abbott Molecular) according to the manufacturer's instructions. After hybridization, slides were immersed in a post-hybridization solution, 2xSSC/0.3% NP40 at 73°C for 2 min, and subsequently in 2xSSC/0.1%NP40 at room temperature for 1 min. Slides were dehydrated, dried, and counterstained with 4,6-diamino-2-phenylindole (DAPI; Vysis, USA).

All the FISH slides were reviewed and confirmed by two pathologists, and microscopically scored, respectively.

Statistical Analysis

SPSS 17.0 software was used to perform statistical analysis and draw diagrams. Statistical comparisons of ki67 between all the groups were made using analysis of variance (ANOVA). The LSD *post-doc* assay was used when equal variance was assumed. Otherwise, Dunnetts T3 test was used. Correlation analysis was used to analyze the relation between MYB immuno-analysis and chromosome rearrangement. Differences of $P < 0.05$ were considered significant.

RESULTS

Clinical Features

For all the 44 cases mimicking AdCC, the mean age was 45 years and the male/female ratio was 12/32. Most iBCAs (95%) occurred in the parotid glands. All cBCA and SB occurred in the parotid gland.

All the selected benign salivary diseases have a slow growth process and were well-demarcated. Localized swelling was the main symptom in all cases. All patients underwent complete surgical excision of these lesions and there had been no recurrence at the time when this study was written up (Dec. 2018). The median follow-up time was 87 months.

In particular, three cases of SB were infants or children, including two cases in 1-year-olds, and one case in a 12-years-old. The duration of follow-up for these three patients was 80, 119, and 92 months, respectively (**Table 1**).

Histologic Findings

Generally, all the tumor types included in this study were composed mainly of basal-like cells. These small-to-medium basaloid cells consisted of a series of columnar, cuboidal, or polygonal cells. Cells had hyperchromatic nuclei with little cytoplasm, similar to the basal cells in stratified squamous epithelium. Although these basaloid cells shared similar cellular morphology, the tumors demonstrated different histologic patterns, immunoprofiles, and specific disease behavior.

At low magnification, cBCA was well-demarcated and uniform in parenchyma. These tumors had cribriform patterns with pseudocyst formation containing amorphous and basophilic material, resembling AdCC (**Figure 1A**). At higher magnification, the outermost layers of cells surrounding each cell nest were usually cuboidal with peripheral palisading. Although both BCA and AdCC are thought to arise from the same basal stem cell, BCA had a more distinct pattern with micro-encapsulated areas that were not apparent in AdCC. BCA also displayed a clear separation of epithelium from stroma, which was never seen in AdCC.

For iBCA, the tumor cells may invade the capsule, or there may be no clear boundary between the tumor mass and normal glands (**Figure 1B**). Sometimes, the mass had no definite capsule, but was surrounded by a fibrous pseudocapsule. There existed a limited extension of tumor into normal glandular parenchyma, but this was not a sign of malignancy.

IDH was often accompanied by other benign or malignant lesions. It was usually ill-defined, and lacked destructive invasion, anaplasia, or mitotic activity, and the lobular pattern of normal salivary glands was preserved (**Figure 1C**).

SB showed nests of basaloid cells with a palisading pattern at the periphery, and maturation toward the center. Neither brisk mitotic activity nor necrosis was present (**Figure 2A**). The characteristic morphology and specific age of onset of this tumor were the key points of diagnosis.

In contrast, the AdCCs under study were all typically cribriform, and exhibited invasion such as that into muscle, gland, nerve, or bone. Multiple microcytic spaces divided the nests into numerous cylinders, yielding a "honeycomb" configuration (**Figure 2B**). The nuclei were atypical and appeared hyperchromatic and pleomorphic with increased mitotic activity. The stroma in AdCC appeared more hyalinized and richer than other lesions noted above. Moreover, the separation between the stroma and parenchyma was obvious.

Cytomorphologic Descriptions

Although cancer cells in AdCC were in some instances more pleomorphic and hyperchromatic than cells in benign diseases, cytologic features alone did not serve to distinguish AdCC from its mimics. All the mimics showed overlapping cytological features with AdCC. The nuclei of the mimics were regular in shape and uniformly basophilic. Ductal structures were lined

TABLE 1 | Clinical characteristics of all the basaloid lesions.

Tumor	Median age (years)	Sex (Female/male)	Locations	Current status	Median follow-up duration (months)
cBCA ($n = 23$)	48	16/7	parotid	Alive/No recurrence	110
iBCA ($n = 11$)	47	9/2	parotid	Alive/No recurrence	43
SB ($n = 3$)	5	1/2	parotid	Alive/No recurrence	97
IDH ($n = 7$)	48	6/1	Parotid5/submandibular2	Alive/No recurrence	75
Total ($n = 44$)	45	32/12	Parotid (95%)	Alive/No recurrence	87

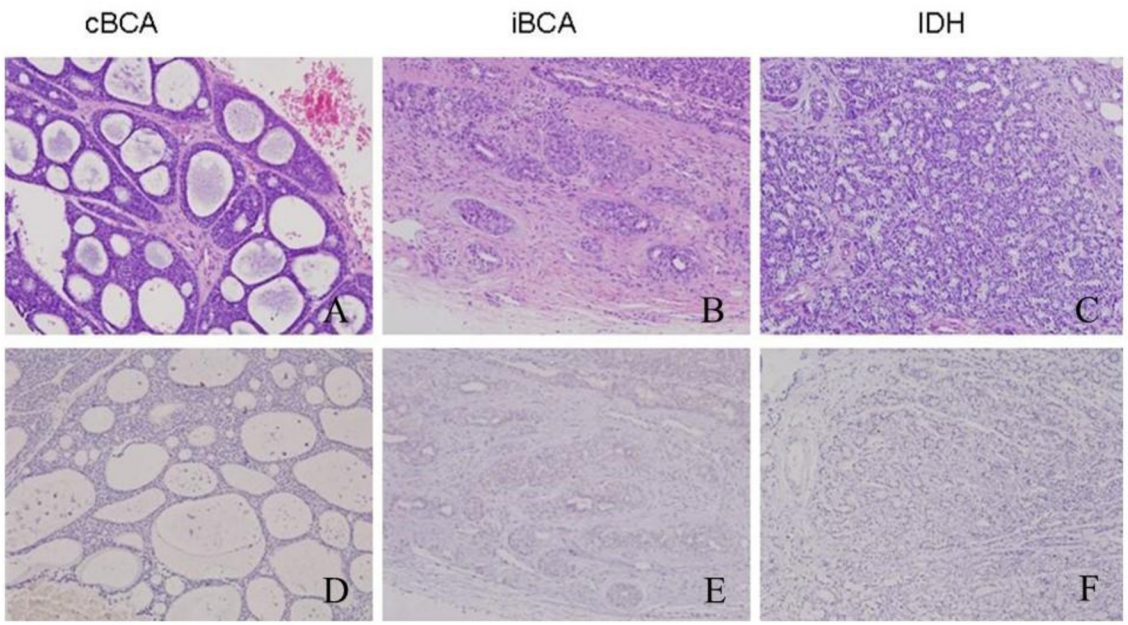

FIGURE 1 | Histology (upper line) and MYB immune-expression (lower line) in cBCA, iBCA, and IDH. cBCA was well-defined and had cribriform patterns with pseudocyst formation **(A)**. Both iBCA and IDH had no definite capsule and presented no clear boundary between the tumor mass and the surrounding tissues **(B,C)**. But iBCA showed typical BCA characteristics of peripheral palisading in parenchyma. No immunoreactivity for MYB antigen was found in these three lesions **(D–F)**.

by cuboidal cells which had uniform nuclei with condensed chromatin. An inner layer of cuboidal cells was surrounded by the outer layer of cells, which exhibited myoepithelial differentiation. Nuclear atypia was absent or minimal, and the mitotic figures were rare.

Immunohistochemistry

The overall results are listed in **Table 2**. iBCA, cBCA, and IDH showed no MYB antigen immunoreactivity (**Figures 1D–F**). However, two cases of SB were MYB positive (**Figure 2C**). As a contrast, all AdCC exhibited strong diffuse nuclear expression of MYB in myoepithelial and partial glandular tumor cells (**Figure 2D**).

Immunomarkers of p63 disclosed the presence of both basaloid and myoepithelial differentiation, while calponin marker indicated only myoepithelial differentiation here. Most tumor cells in all cases were p63-positive in parenchyma. The calponin antigen was detected in the polygonal myoepithelia and was especially prominent in the outer layer of cribriforming.

All tumors showed varied patterns of β-catenin expression: positive iBCA and cBCA staining localized in the nuclei and membrane (7 iBCA and 17cBCA), or nuclear+cytoplasm+membrane staining (4 iBCA and 6 cBCA). However, AdCC showed β-catenin immunoreactivity only in the membrane. Two cases of SB showed positivity only in the membrane, and in one case there was nuclear+cytoplasm+membrane positivity. Four cases of IDH were found to be nuclear+membrane positive, while three cases of IDH showed positivity solely in the membrane (**Figure 3**).

CD117 generally showed a positive trabecular pattern. Five cases of iBCA and three cases of cBCA were positive for CD117. Two cases of SB were positive for CD117. IDH was CD117 negative. CD117 was expressed in 14 cases of AdCC. Sox10 was expressed in all cases.

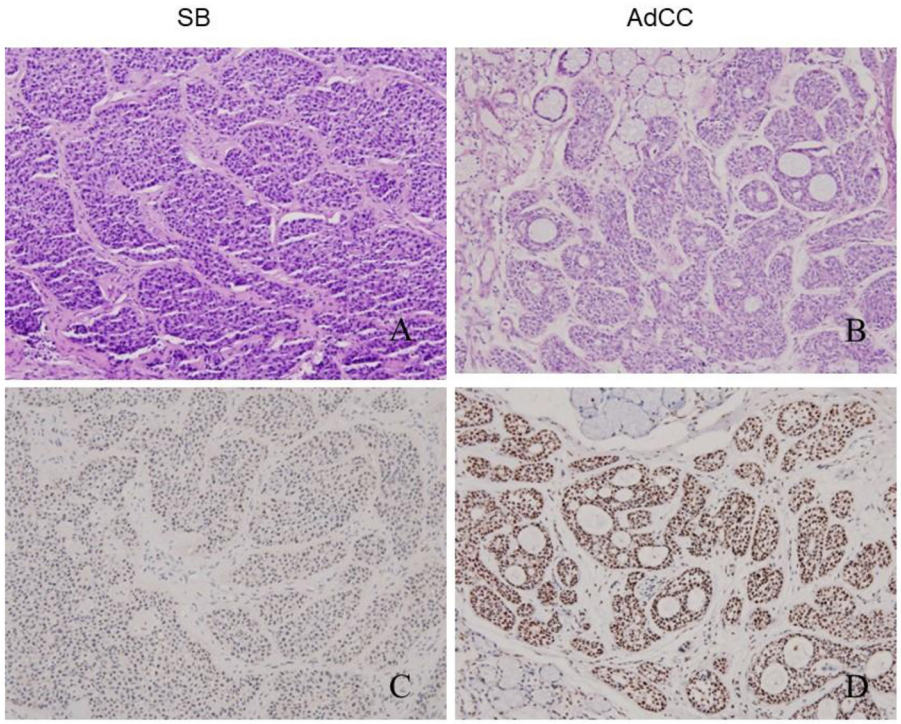

FIGURE 2 | Histology (upper line) and MYB immune-expression (lower line) in SB and AdCC. SB composed of basaloid epithelial nests with a palisading pattern **(A)**. AdCCs in this study were all typically cribriform, and exhibited invasion into normal gland **(B)**. MYB immunostains were strongly and diffusely positive in myoepithelial cells and partial glandular tumor cells of two SBs **(C)** and all the AdCC in this study **(D)**.

TABLE 2 | Immunohistochemical and FISH results of all the basaloid lesions.

Tumor	Myb	βcatenin	CD117	SOX10	ki67 (%)	P63	calponin	FISH-MYB
cBCA	-	+(including nuclear)	+(5/23)	+	0.30%	+	+	-
iBCA	-	+(including nuclear)	+(3/11)	+	2.80%	+	+	-
SB	+	+	+(3/3)	+	37.30%	+	+	-
IDH	-	+	-	+	1.00%	+	+	-
AdCC	+	+(only membrane)	+(14/20)	+	28.25%	+	+	+

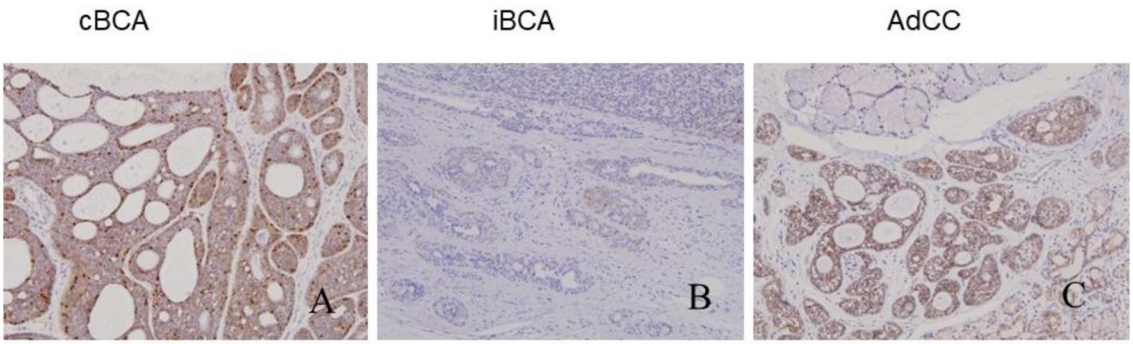

FIGURE 3 | βcatenin immune-expression in cBCA, iBCA, and AdCC. The positive staining of iBCA and cBCA localized in nuclear+membrane or nuclear+cytoplasm+membrane **(A,B)**. AdCC had immuno-activity of β-catenin only in the membrane **(C)**.

The average expression ratio of ki67 in cBCA, iBCA, SB, IDH, and AdCC was 0.3, 2.8, 37.3, 1.0, and 28.25%, respectively. The ki67 indices of SB and AdCC were significantly higher than that of cBCA, iBCA, and IDH ($p < 0.05$, $p < 0.05$, $p < 0.05$, respectively). The ki67 positive index in SB and AdCC was not significantly different.

Evaluation of *Myb* Rearrangement by FISH

None of these lesions under study, including cBCA, iBCA, IDH, and SB, showed *Myb* rearrangement by FISH. One case of cBCA and one case of iBCA did not yield enough evaluable signals due to long storage of blocks and poor probe penetration of nuclei (**Figures 4A–C**). Fourteen cases of 19 AdCC (73.68%) were found to harbor Myb rearrangement (**Figure 4D**). One case of AdCC showed no signal due to poor specimen preparation.

Noticeably, the MYB immunoprofile was significantly related to FISH results ($p = 0.00$, Pearson correlation).

DISCUSSION

Morphologic studies of salivary basaloid lesions have of late received attention (13). This study focused on the differential diagnosis of AdCC and basaloid lesions which mimic AdCC. Our data suggested that an immunoprofile incorporating MYB, ki67, and β-catenin together with FISH was advantageous for diagnosis, and these markers should be considered as first line markers. Alternative markers, including CD117, SOX10, p63, and calponin, were not as specific as MYB, ki67, and β-catenin.

Although AdCC grows comparatively slowly, it should be considered as at least a moderately differentiated cancer because of its predilection for perineural invasion, local recurrence, and distant metastasis even many years after the initial surgery (14). Therefore, its overall prognosis is poor. The recurrent *t* (6; 9) (q22-23; p23-24) translocation has been identified in AdCC (15), resulting in scrutiny of Myb in the diagnosis of AdCC. The poor prognosis of this tumor may be associated with MYB expression (16). However, the MYB expression showed no correlation with traditional prognostic factors such as TNM stage or tumor grade (17). As for the location in which MYB is expressed, it has been reported that MYB immunolabeling is confined mainly in the peripheral myoepithelial cells and has not been identified in ductal cells of tumors with either a tubular or cribriform pattern (16). We chose typical cribriform AdCC as a control and found that these tumors all showed strong MYB expression in both myoepithelial and partial glandular tumor cells. There were also controversies in the choice of immunohistochemistry and FISH to evaluate for MYB antigen or fusion of Myb and NFIB. Poling et al. found that MYB-immunohistochemistry was more sensitive and specific than Myb-FISH (18). Using the FISH technique, West et al. found a balanced translocation between Myb and NFIB was present in 49% of AdCC, while there was no apparent translocation of *Myb* in 35% of the cases (16). Sixteen percent of cases have an abnormal FISH pattern

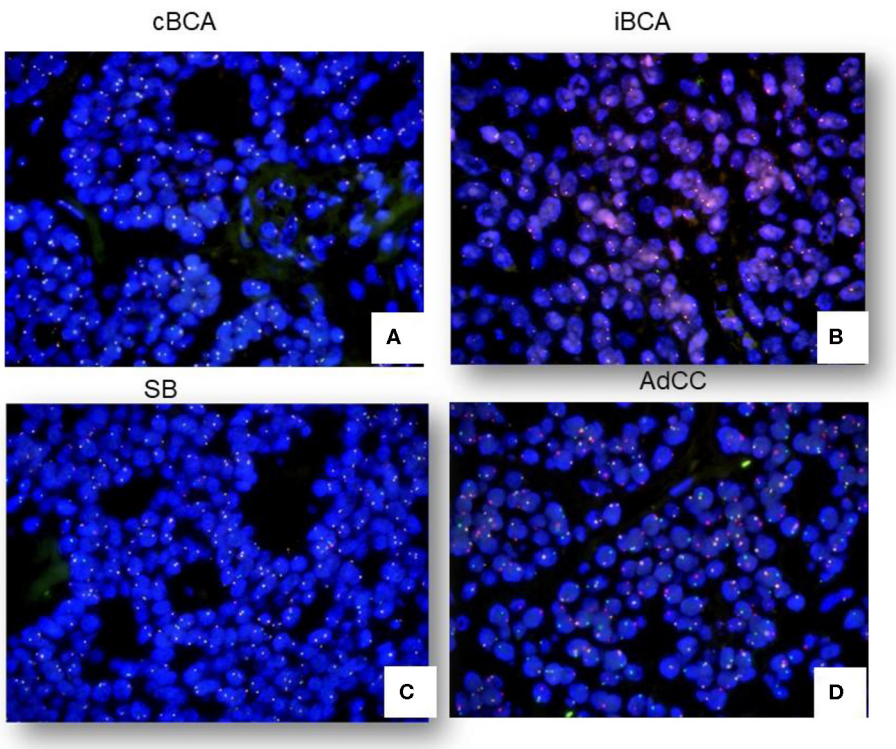

FIGURE 4 | FISH signals in cBCA, iBCA, SB, and AdCC. No cases of cBCA, iBCA, or SB showed Myb rearrangement **(A–C)**. 73.68% of AdCC showed positive signals by FISH **(D)**.

suggestive of a translocation of Myb but not necessarily involving NFIB (Myb 3′, Myb 5′, and NFIB all come together, extra 5′Myb without association with NFIB, and Myb split without association with NFIB). In our study, MYB expression was not observed in iBCA, cBCA, or IDH. MYB immunostain appeared to be a sensitive marker for differentiating AdCC from salivary gland lesions with a similar histology, except SB. However, the positive-MYB SB in immunohistochemistry showed no Myb rearrangement by FISH, while 73.68% of AdCC were found to harbor a Myb rearrangement. This strongly suggested that MYB immunostaining is a specific and cost-effective method in the diagnosis of AdCC, but further confirmation by FISH was recommended.

SB is an extremely rare tumor, and <100 cases have been reported worldwide (19). In most of the reported cases, SB occurred in the parotid, and these cases had all been diagnosed at birth. Our cases of SB involved the parotid gland, but the age of onset was a little older than infancy. There were a few youth cases of 13-years-olds reported in literature (20). The histologic features of these cases were microscopically similar to those in gland embryonic development at the 3rd month. Some pathologists believe IDH is the precursor of BCA. In the current study we found that MYB immuno-expression and the ki67 index overlapped with AdCC. As Myb is the key finding in the diagnosis of AdCC, it is critical to ensure diagnosis by FISH. None of the tumors evaluated in our study showed evidence of fusion of Myb and NFIB by FISH, except AdCC. 73.68% of AdCC showed Myb-NFIB fusion. There was a significant positive correlation of the MYB immunoprofile and Myb rearrangement. As such, we conclude FISH is a reliable diagnostic approach for differentiating basaloid lesions from AdCC.

β-catenin was useful in this study for distinguishing BCA from AdCC, including cBCA and iBCA. Its nuclear expression was typical and specific for BCA. Sato et al. demonstrated that Wnt/β-catenin signal alteration plays a role in the pathogenesis of BCA (4). Our data showed that all the selected AdCCs in our study had membrane immuno-activity of β-catenin. One case of SB was nuclear+cytoplasm+membrane positive, and four cases of IDH were nuclear+membrane positive. The above situations are infrequent but should be kept in mind in differential diagnosis.

Ki67 is widely used as a proliferation marker (21). Generally, benign neoplasms have lower ki67 indices, typically <10%. Although the average positive rates of ki67 in SB and AdCC were 37.3 and 28.25%, respectively, there was no statistic difference between them. This may serve as a reminder that the ki67 index should be taken into consideration in order to make an accurate diagnosis.

CD117 expression in AdCC varies considerably. As a proto-oncogene encoding a transmembrane receptor type tyrosine kinase, early reports suggested that CD117 expression appeared to be restricted to AdCC (22). However, our present study found that it may be expressed in most ductal cells, even including benign salivary gland diseases such as most iBCA, and a small number of cBCA and SB. IDH showed no reactivity to CD117. Therefore, CD117 was of little value in the diagnosis of AdCC. SOX-10 was all positive in our series of cases. Although SOX-10 is a marker for sero-mucinous differentiation (23), our findings demonstrated that it is not a specific marker for AdCC.

Taken together, we first used a combination of histologic, immunohistochemical and FISH test to evaluate MYB, CD117, SOX10, βcatenin, ki67, p63, and calponin in the differential diagnosis of cBCA, iBCA, SB, and IDH from AdCC. Considering their sensitivity and specificity, FISH-Myb and an immunohistochemical panel of MYB/β-catenin/ki67 would be an optimal choice for the differential diagnosis of these basaloid lesions.

DATA AVAILABILITY STATEMENT

All datasets generated for this study are included in the article/supplementary material.

ETHICS STATEMENT

The studies involving human participants were reviewed and approved by Peking University School and Hospital of Stomatology. Written informed consent for participation was not required for this study in accordance with the national legislation and the institutional requirements.

AUTHOR CONTRIBUTIONS

BL: design, IHC test, and writing. WJ: follow-up and data analyse. HH: FISH, writing, and submission. All authors contributed to the article and approved the submitted version.

FUNDING

The work was supported by CAMS Innovation Fund for Medical Sciences (CIFMS) (No. 2019-I2M-5-038) and Adenoid Cystic Carcinoma Research Foundation (ACCRF).

REFERENCES

1. Ogawa I, Nikai H, Takata T, Miyauchi M, Ito H, Ijuhin N. The cellular composition of basal cell adenoma of the parotid gland: an immunohistochemical analysis. *Oral Surg Oral Med Oral Pathol.* (1990) 70:619–26. doi: 10.1016/0030-4220(90)90411-K
2. Tian Z, Li L, Zhang CY. Differences in MYB expression and gene abnormalities further confirm that salivary cribriform basal cell tumors and adenoid cystic carcinoma are two distinct tumor entities. *J Oral Pathol Med.* (2016) 45:698–703. doi: 10.1111/jop.12414
3. Li BB, Zhou CX, Jia SN. Basal cell adenoma of salivary glands with a focal cribriform pattern: clinicopathologic and immunohistochemical study of 19 cases of a potential pitfall for diagnosis. *Ann Diagn Pathol.* (2014) 18:5–9. doi: 10.1016/j.anndiagpath.2013.09.002
4. Sato M, Yamamoto H, Hatanaka Y, Nishijima T, Jiromaru R, Yasumatsu R, et al. Wnt/β-catenin signal alteration and its diagnostic utility in basal cell

adenoma and histologically similar tumors of the salivary gland. *Pathol Res Pract*. (2018) 214:586–92. doi: 10.1016/j.prp.2017.12.016
5. Dardick I, Daley TD, McComb RJ. Sialoblastoma in adults: distinction from adenoid cystic carcinoma. *Oral Surg Oral Med Oral Pathol Oral Radiol Endod*. (2010) 109:109–16. doi: 10.1016/j.tripleo.2009.07.049
6. Chiosea S, Seethala R, Williams MD. Intercalated hyperplasia. In: EI-Naggar AK, Chan JKC, Grandis JR, Takata T, Slootweg PJ, editors. *World Health Organization Classification of Head and Neck Tumours. 4th Edn*. Lyon: IARC Press (2017). p. 197. doi: 10.1007/s12105-017-0785-2
7. Luna MA. Salivary gland hyperplasia. *Adv Anat Pathol*. (2002) 9:251–5. doi: 10.1097/00125480-200207000-00005
8. Wysocki PT, Izumchenko E, Meir J. Adenoid cystic carcinoma: emerging role of translocations and gene fusions. *Oncotarget*. (2016) 7:66239–54. doi: 10.18632/oncotarget.11288
9. Pusztaszeri MP, Sadow PM, Ushiku A. MYB immunostaining is a useful ancillary test for distinguishing adenoid cystic carcinoma from pleomorphic adenoma in fine-needle aspiration biopsy specimens. *Cancer Cytopathol*. (2014) 122:257–65. doi: 10.1002/cncy.21381
10. Bell D, Roberts D, Karpowicz M, Hanna EY, Weber RS, El-Naggar AK. Clinical significance of Myb protein and downstream target genes in salivary adenoid cystic carcinoma. *Cancer Biol Ther*. (2011) 12:569–73. doi: 10.4161/cbt.12.7.17008
11. Ivanov SV, Panaccione A, Nonaka D. Diagnostic Sox10 gene signatures in salivary adenoid cystic and breast basal-like carcinomas. *Br J Cancer*. (2013) 109:444–51. doi: 10.1038/bjc.2013.326
12. Jain A, Shetty DC, Rathore AS, Kumar K. Characterization and localization of c-kit and epidermal growth factor receptor in different patterns of adenoid cystic carcinoma. *J Cancer Res Ther*. (2016) 12:834–9. doi: 10.4103/0973-1482.177504
13. Seethala RR. Basaloid/blue salivary gland tumors. *Mod Pathol*. (2017) 30:S84–95. doi: 10.1038/modpathol.2016.190
14. Stenman G, Licitra L, Said-AI-Naief N, van Zante A, Yarbrough WG. Adenoid cystic carcinoma. In: EI-Naggar AK, Chan JKC, Grandis JR, Takata T, Slootweg PJ, editors. *World Health Organization Classification of Head and Neck Tumours. 4th Edn*. Lyon: IARC Press (2017). p. 164–5.
15. Stenman G, Persson F, Andersson MK. Diagnostic and therapeutic implications of new molecular biomarkers in salivary gland cancers. *Oral Oncol*. (2014) 50:683–90. doi: 10.1016/j.oraloncology.2014.04.008
16. West RB, Kong C, Clarke N. MYB expression and translocation in adenoid cystic carcinomas and other salivary gland tumors with clinicopathologic correlation. *Am J Surg Pathol*. (2011) 35:92–9. doi: 10.1097/PAS.0b013e3182002777
17. Broz M, Steiner P, Salzman R, Hauer L, Starek I. The incidence of MYB gene breaks in adenoid cystic carcinoma of the salivary glands and its prognostic significance. *Biomed Pap Med Fac Univ Palacky Olomouc Czech Repub*. (2016) 160:417–22. doi: 10.5507/bp.2016.027
18. Poling JS, Yonescu R, Subhawong AP, Sharma R, Argani P, Ning Y, et al. MYB labeling by immunohistochemistry is more sensitive and specific for breast adenoid cystic carcinoma than MYB labeling by FISH. *Am J Surg Pathol*. (2017) 41:973–9. doi: 10.1097/PAS.0000000000000878
19. Vidyadhar M1, Amanda C, Thuan Q, Prabhakaran K. Sialoblastoma. *J Pediatr Surg*. (2008) 43:e113. doi: 10.1016/j.jpedsurg.2008.04.035
20. Saravakos P, Hartwein J, Fayyazi A. Sialoblastoma of the parotid gland in a 13-years-old girl with multiple recurrences and long-term follow-up. *Head Neck*. (2016) 38:e13–5. doi: 10.1002/hed.24084
21. Ben-Izhak O, Akrish S, Nagler RM. Ki67 and salivary cancer. *Cancer Invest*. (2008) 26:1015–23. doi: 10.1080/07357900802088968
22. Holst VA, Marshall CE, Moskaluk CA, Frierson HF Jr. KIT protein expression and analysis of c-kit gene mutation in adenoid cystic carcinoma. *Mod Pathol*. (1999) 12:956–60.
23. Panaccione A, Zhang Y, Ryan M, Moskaluk CA, Anderson KS, Yarbrough WG, et al. MYB fusions and CD markers as tools for authentication and purification of cancer stem cells from salivary adenoid cystic carcinoma. *Stem Cell Res*. (2017) 21:160–6. doi: 10.1016/j.scr.2017.05.002

Conflict of Interest: The authors declare that the research was conducted in the absence of any commercial or financial relationships that could be construed as a potential conflict of interest.

frontiers in Oncology

ORIGINAL RESEARCH
published: 29 July 2020
doi: 10.3389/fonc.2020.01088

MMP25 Regulates Immune Infiltration Level and Survival Outcome in Head and Neck Cancer Patients

Yujie Liang[1,2*†], *Chenyu Guan*[1,2†], *Kan Li*[1,2], *Guangsen Zheng*[1,2], *Tao Wang*[1,2], *Sien Zhang*[1,2] *and Guiqing Liao*[1,2*]

[1] *Department of Oral and Maxillofacial Surgery, Guanghua School of Stomatology, Hospital of Stomatology, Sun Yat-sen University, Guangzhou, China,* [2] *Guangdong Province Key Laboratory of Stomatology, Sun Yat-sen University, Guangzhou, China*

Background: MMP25 is a critical gene of matrix metalloproteinases (MMPs). However, the molecular mechanism of MMP25 in head and neck cancer pathogenesis remains unclear.

Methods: MMP25 expression was analyzed using The Cancer Genome Atlas (TCGA) database, and its influence on clinical prognosis was performed using Kaplan–Meier and Cox regression analyses. The correlation between MMP25 and immune infiltration was investigated by CIBERSORT, TIMER, and ESTIMATE. In addition, the relationship between MMP25 expression and molecular mechanisms was analyzed by gene set enrichment analysis (GSEA), gene ontology (GO), and weighted gene co-expression network analysis (WGCNA).

Results: MMP25 expression level correlated with prognosis and immune infiltrating levels, especially activated $CD4^+$ memory T cells, in head and neck cancer. Moreover, MMP25 expression potentially mediated genes, such as IRF8, IKZF1, and DOCK2, and tumor-associated pathways, including p53 signaling, PI3K/AKT/mTOR signaling, and JAK/STAT signaling pathway.

Conclusions: These findings suggested that MMP25 plays a critical role in the prognosis and immune infiltration level of head and neck cancer. In addition, MMP25 expression significantly correlated with the regulation of various oncogenes and tumor-related pathways.

Keywords: MMP25, head and neck cancer, immune infiltration level, TCGA, bioinformatics

OPEN ACCESS

Edited by:
Victor C. Kok,
Asia University, Taiwan

Reviewed by:
ANU R. I.,
MVR Cancer Centre and Research Institute, India
Wen-Wei Chang,
Chung Shan Medical University, Taiwan

***Correspondence:**
Yujie Liang
yujie0350@126.com
Guiqing Liao
drliaoguiqing@hotmail.com

† These authors have contributed equally to this work

Specialty section:
This article was submitted to Head and Neck Cancer, a section of the journal Frontiers in Oncology

Received: *05 September 2019*
Accepted: *01 June 2020*
Published: *29 July 2020*

Citation:
Liang Y, Guan C, Li K, Zheng G, Wang T, Zhang S and Liao G (2020) MMP25 Regulates Immune Infiltration Level and Survival Outcome in Head and Neck Cancer Patients. Front. Oncol. 10:1088. doi: 10.3389/fonc.2020.01088

INTRODUCTION

Head and neck cancer was the seventh most common cancer worldwide (1), originating from multiple anatomical structures:the oral cavity, sinonasal cavity, pharynx, and larynx (2). Advanced disease carries a high risk of local recurrence and metastasis, with poor prognosis (3, 4). Immune checkpoint inhibitors have been considered as a promising strategy for the treatment of head and neck cancer (5). Clinical trials have shown a clear prognostic advantage in head and neck cancer patients treated with immunotherapy (6). However, an increasing number of studies found that some types of head and neck cancer were insensitive to current immunotherapies (7). Moreover, a

recent study has found that tumor-infiltrating immune cells, such as tumor-associated macrophages (TAMs) and regulatory T cells (Tregs) (8), impaired the prognosis and efficacy of immunotherapy in head and neck cancer.

MMPs are calcium-dependent zinc-containing endopeptidases which can degrade the extracellular matrix of tumor tissues and regulate tumor immune environment, and promote cancer invasion and metastasis (9, 10). MMP25 is a member of the matrix metalloproteinase family that is able to degrade collagens, gelatin, and fibrin (11). However, the underlying functions of MMP25 in the head and neck cancer still require further investigation. In this study, we comprehensively analyzed the mechanism by which MMP25 expression influences the prognosis of head and neck cancer patients. Our results showed that MMP25 high expression was related to head and neck cancer patients' better outcome, and that was regulated by oncogenes and cancer-associated pathways. In addition, we found that MMP25 had a significant effect on immune infiltration level in head and neck cancer. The findings shed light on the role of MMP25 in head and neck cancer by providing a potential correlation and a precise mechanism between MMP25 and tumor immune microenvironment.

MATERIALS AND METHODS

Data Source

Expression data and corresponding clinical information of head and neck cancer patients were downloaded from The Cancer Genome Atlas (TCGA) (Tumor samples: $n = 502$, Normal samples: $n = 44$).

Transcriptional Expression of Matrix Metalloproteinases

MMP1, MMP2, MMP3, MMP7, MMP8, MMP9, MMP10, MMP11, MMP12, MMP13, MMP14, MMP15, MMP16, MMP17, MMP19, MMP20, MMP21, MMP23B, MMP24, MMP24OS, MMP25, MMP26, MMP27, and MMP28 were formed with the FPKM of each mRNA expression of samples. Then, comparisons between tumor tissues and normal tissues were analyzed.

Prognostic Analysis of Head and Neck Patients

The clinical outcome of head and neck patients was determined using the Kaplan–Meier method, the log-rank test, and univariate Cox proportional hazards regression. The samples were stratified as high or low expression around the quartile of each MMPs' expression.

Identification of Differentially Expressed Genes

Differentially expressed genes (DEGs) were identified in head and neck cancer tissues by comparison with MMP25 high and low expression groups and using the "edgeR" package in R (R version 3.5.2). $|\text{Fold Change}| > 2$ and adjusted $p < 0.05$ were set as the statistical threshold value of DEGs. The heatmap, volcano plot with clustering for the significantly differentially expressed mRNAs in head and neck cancer between MMP25 high and low expression groups, was generated with the "ggplot2" package in R. GO analysis was constructed by "enrichplot" in R.

Gene Set Enrichment Analysis (GSEA)

The molecular mechanisms underlying the association between MMP25 expression were explored with GSEA. The number of permutations was set at 1,000, and the $p < 0.05$ and a false discovery rate (FDR) <0.25 were considered statistically significant. Multiple GSEA plots were produced by "plyr," "ggplot2," and "grid" packages in R.

The Clinical Features Correlated With MMP25 Expression Level

Clinical information from head and neck cancer patients, including age, gender, tumor grade, and clinical stage, was downloaded from TCGA. Samples were divided into two groups and according to the quartile of MMP25 expression level. Multivariate Cox regression and nomogram were used to analyze the role of MMP25 in the head and neck cancer patients' clinical features.

Immune Landscape Related to MMP25 Expression Level

The samples were analyzed by CIBERSORT to define 22 immune cell subtypes (12). Immune scores were calculated by ESTIMATE algorithm of immune cells (13). The correlations between MMP25 expression levels and immune infiltration level was estimated by TIMER, which is a comprehensive resource for analysis of immune infiltrates of gene expression profiles (14).

Weighted Gene Co-expression Network Analysis

The weighted gene co-expression network analysis (WGCNA) (15, 16) package was used to identify key modules associated with prognosis and clinical stage based on MMP25 expression levels. The module is a cluster of closely interconnected genes, based on the dendrogram height. The module eigengenes of clinical features were hierarchically clustered into different color modules.

Statistical Analysis

The analyses were carried out using "R" software (version 3.5.3), GraphPad Prism 8, and IBM SPSS Statistics 19; $p < 0.05$ was considered statistically significant. $^{***}p < 0.001$, $^{**}p < 0.01$ $^{*}p < 0.05$.

RESULTS

Expression of Matrix Metalloproteinases Family in Head and Neck Cancer

The expression levels of matrix metalloproteinases family genes are shown in **Figure 1**. Except for MMP24OS, the transcription level of other MMP family genes, including MMP1, MMP2, MMP3, MMP7, MMP8, MMP9, MMP10, MMP11, MMP12, MMP13, MMP14, MMP15, MMP16, MMP17, MMP19, MMP20, MMP21, MMP23B, MMP24, MMP25, MMP26, MMP27, and MMP28, in the tumor tissues was significantly higher than those in normal tissues.

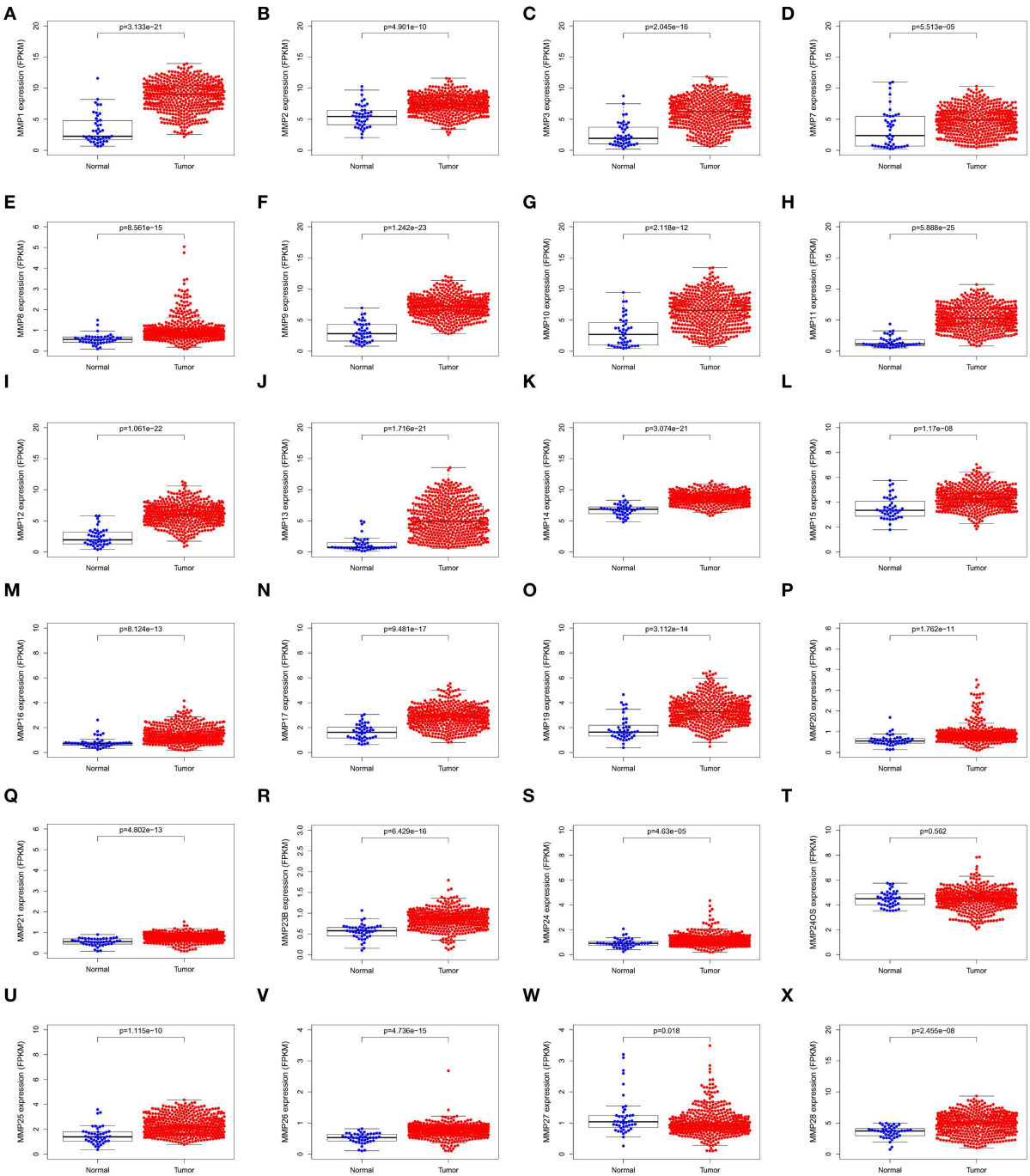

FIGURE 1 | Scatter plots showing the expression levels of matrix metalloproteinases family genes of normal tissues (blue) and tumor tissues (red) in head and neck cancer. **(A)** MMP1; **(B)** MMP2; **(C)** MMP3; **(D)**MMP7; **(E)** MMP8; **(F)** MMP9; **(G)**MMP10; **(H)** MMP11; **(I)** MMP12; **(J)** MMP13; **(K)**MMP14; **(L)**MMP15; **(M)**MMP16; **(N)** MMP17; **(O)** MMP19; **(P)** MMP20; **(Q)** MMP21; **(R)**MMP23B; **(S)** MMP24; **(T)** MMP24OS; **(U)** MMP25; **(V)** MMP26; **(W)** MMP27; **(X)** MMP28.

Analysis of the Prognosis Associated With MMPs Expression Levels in TCGA Cohort of Head and Neck Cancer

Expression levels of MMP10, MMP19, MMP24, and MMP25, which were associated with prognosis in head and neck cancer, were identified using Kaplan–Meier method and log-rank test (**Figure 2**, **Table 1**). Univariate Cox regression analysis showed that there was no significant dereference between expression levels of MMP10 ($p = 0.16$), MMP19 ($p = 0.06$), and MMP24 ($p = 0.30$). Eventually, MMP25 was identified.

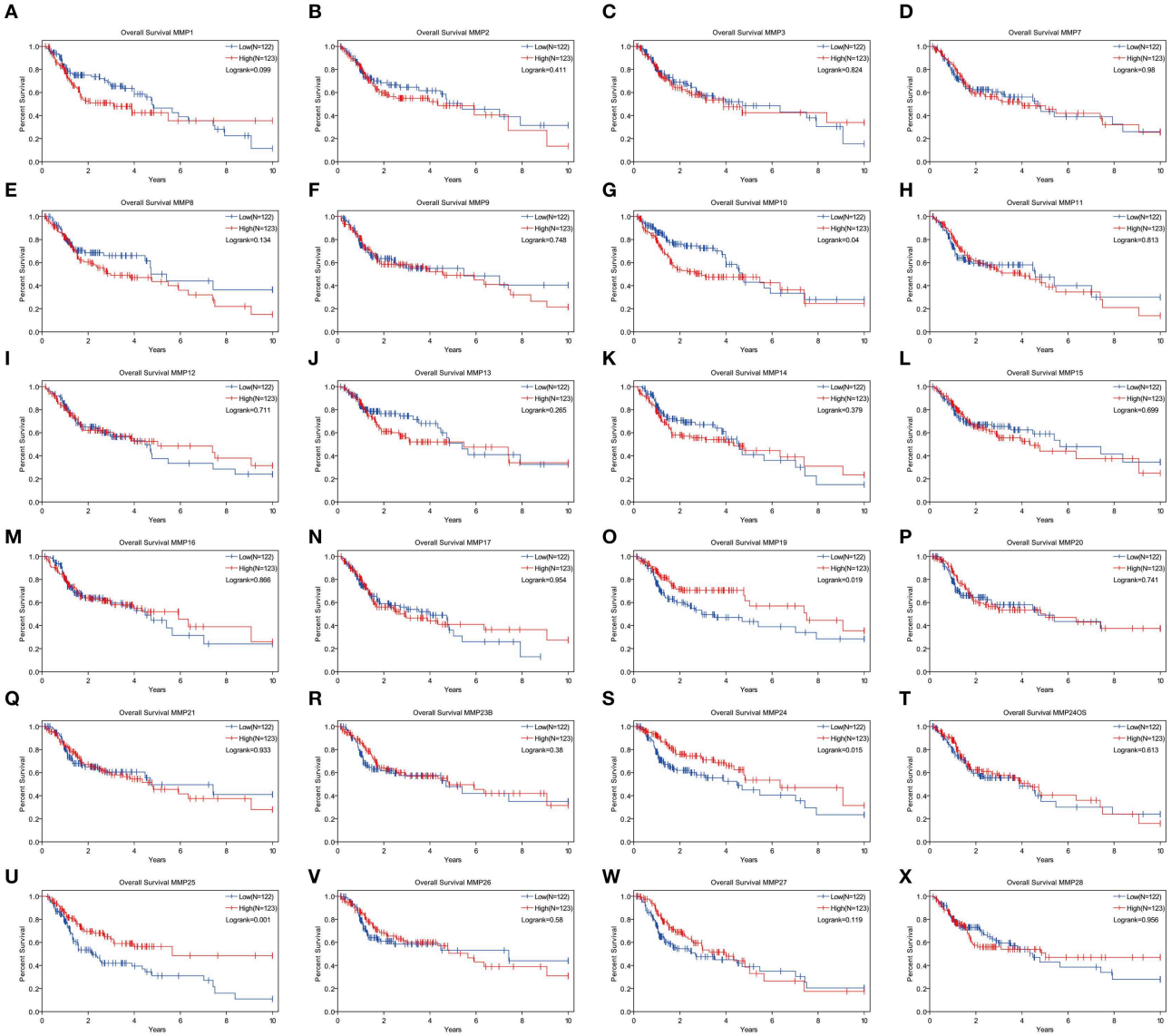

FIGURE 2 | Analysis of the role of MMPs genes in the overall survival in head and neck cancer patients by Kaplan–Meier method and the log-rank test. **(A)** MMP1; **(B)** MMP2; **(C)** MMP3; **(D)** MMP7; **(E)** MMP8; **(F)** MMP9; **(G)**MMP10; **(H)** MMP11; **(I)** MMP12; **(J)** MMP13; **(K)** MMP14; **(L)** MMP15; **(M)** MMP16; **(N)** MMP17; **(O)** MMP19; **(P)** MMP20; **(Q)** MMP21; **(R)** MMP23B; **(S)** MMP24; **(T)** MMP24OS; **(U)** MMP25; **(V)** MMP26; **(W)** MMP27; **(X)** MMP28.

Analysis of the Clinical Features Associated With MMP25 Expression Levels in TCGA Cohort of Head and Neck Cancer

In TCGA cohort, multivariate Cox regression model indicated that MMP25 expression was correlated with clinical stage with prognosis of head and neck cancer patients in terms of overall survival in the TCGA cohort (**Table 2**). In view of the prognostic value of MMP25 in head and neck cancer, we tried to construct the nomogram for predicting 1-, 3-, and 5-year survival. The result illustrated that clinical stages shared the largest contribution to overall survival, followed by MMP25 expression group (**Figure 3**).

Analysis of the Differential Expressed Genes With MMP25 High and Low Expression Group of Head and Neck Cancer

A total of 433 differential expressed genes, including 239 upregulated and 194 downregulated DEGs, was screened with MMP25 high and low expression group ($|\log FC| > 2$ and adjusted $p < 0.05$) (**Figure 4B**). The top 20 differential expressed genes were TIFAB, CLEC6A, PPP1R16B, IRF8, ITGAL, IKZF1, DOCK2, PTPRC, FGL2, MPEG1, IL10RA, ITK, CD226, TLR8, MMP25, LILRB2, PRKCB, SIGLEC10, RHOH, and CXCR6 (**Figure 4A**). The expression levels of

TABLE 1 | Univariate Cox proportional hazards regression analysis of the role of matrix metalloproteinases (MMPs) genes of head and neck cancer (HNSC).

Gene	HR[exp(coef)]	coef	95% CI lower	95% CI upper	*p*-value
MMP25	0.81	−0.21	−0.41	−0.01	0.04
MMP8	1.26	0.23	0.00	0.46	0.05
MMP19	0.88	−0.13	−0.27	0.01	0.06
MMP1	1.06	0.06	−0.01	0.12	0.08
MMP14	1.15	0.14	−0.02	0.29	0.09
MMP10	1.04	0.04	−0.02	0.10	0.16
MMP3	1.04	0.04	−0.02	0.10	0.20
MMP24	0.84	−0.17	−0.50	0.15	0.30
MMP13	1.03	0.03	−0.03	0.08	0.33
MMP7	1.02	0.02	−0.05	0.09	0.52
MMP15	1.05	0.05	−0.12	0.22	0.56
MMP27	0.91	−0.10	−0.45	0.25	0.58
MMP17	0.96	−0.05	−0.22	0.13	0.61
MMP16	0.95	−0.05	−0.27	0.18	0.68
MMP9	1.02	0.02	−0.07	0.10	0.69
MMP20	0.93	−0.07	−0.43	0.29	0.71
MMP12	1.02	0.02	−0.07	0.10	0.71
MMP2	1.02	0.02	−0.08	0.11	0.71
MMP21	1.14	0.13	−0.60	0.85	0.73
MMP11	0.99	−0.01	−0.08	0.07	0.88
MMP23B	1.04	0.04	−0.60	0.69	0.89
MMP26	1.04	0.04	−0.71	0.78	0.92
MMP28	1.00	0.00	−0.09	0.09	0.98
MMP24OS	1.00	0.00	−0.18	0.18	0.98

TABLE 2 | Multivariate Cox regression of clinical characteristics of HNSC patients in The Cancer Genome Atlas (TCGA) cohort.

Variables	MMP25		
	High ($n = 100$)	Low ($n = 101$)	*p*-value
Age			0.91
≤60	46	46	
>60	54	55	
Gender			0.59
Male	64	74	
Female	36	27	
Grade			0.95
Grade (1+2)	70	82	
Grade (3+4)	30	19	
Stage			0.019
Stage (I+II)	32	13	
Stage (III+IV)	68	88	

these genes were positively correlated with the expression level of MMP25. The GO analysis showed that the differentially expressed genes were highly associated with T cell activation, external side of plasma membrane, and receptor ligand activity (**Figure 4C**). The significant pathways for these two groups were mainly enriched in the KRAS signaling pathway, MYC-targets, antigen processing and presentation, and protein export. In addition, tumor-associated pathways, such as apoptosis, PI3K/AKT/mTOR signaling pathway, JAK/STAT signaling pathway, and T cell receptor signaling pathway, were also highly enriched (**Figures 4D,E**).

MMP25 Is Associated With mRNA Subtype Specific Immune Cell Infiltration Patterns in Head and Neck Cancer

The CIBERSORT analysis indicated that the MMP25 high expression group had significantly higher B cells naïve, $CD8^+$ T cells, activated $CD4^+$ memory T cells, resting NK cells, M1 macrophage, and neutrophils, but lower M0 macrophage and eosinophil (**Figures 5A,B**). The TIMER database revealed that MMP25 expression was positively correlated with immune cells infiltration, including B cell, $CD8^+$T cell, $CD4^+$ T cell, and macrophage in head and neck cancers (**Figure 5C**). The graph also showed that there has been an increase of immune scores in the MMP25 high expression group of different clinical stages (**Figures 5D,E**). The Kaplan–Meier method analysis of CIBERSORT data suggested that the infiltration level of activated memory $CD4^+$ T cells was significantly related to the survival outcome of head and neck cancer patients. The infiltration level of activated memory $CD4^+$ T cells was positively correlated with the MMP25 expression level (**Supplemental Figures 1A,B**). These findings showed that a high infiltration level of activated memory $CD4^+$ T cells played an important role in the better prognosis of cancer patients in the MMP25 high expression group.

Identify Key Modules Associated With Head and Neck Cancer Patients' Survival Ratio and Clinical Stage Based on the Expression Levels of MMP25

Gene modules were analyzed using the WGCNA in the MMP25 high and low expression groups, respectively. In the high expression group, soft power 4 and the minimum module size cut-off 30 were chosen as the threshold to identify co-expressed gene modules (**Figure 6A**). Gene color modules that were related to the clinical stage were identified (**Supplemental Figure 2**). These significant gene color modules were further used for GO analysis to display the gene pathway enrichment, gene symbols, and their character in KEGG, as shown in **Supplemental Tables 1, 2**. The genes were related to many pathways in cancer, such as PI3K-Akt signaling pathway, p53 signaling pathway, Ras signaling pathway, MAPK signaling pathway, and TNF signaling pathway. In addition, genes were also enriched in cell cycle, DNA replication, and mismatch in cancer. Hub genes ADCY6, APP, TNC, MFGE8, MFI2, ANO8, APLP2, LTBP1, SERPINA1, and PROC were highly related to the survival outcome of patients. IFIT3, OAS2, OAS1, HLA-C, HLA-E, IRF1, GBP2, IRF2, OAS3, and IFIT1 were closely associated with the patients' clinical stages. However, in the

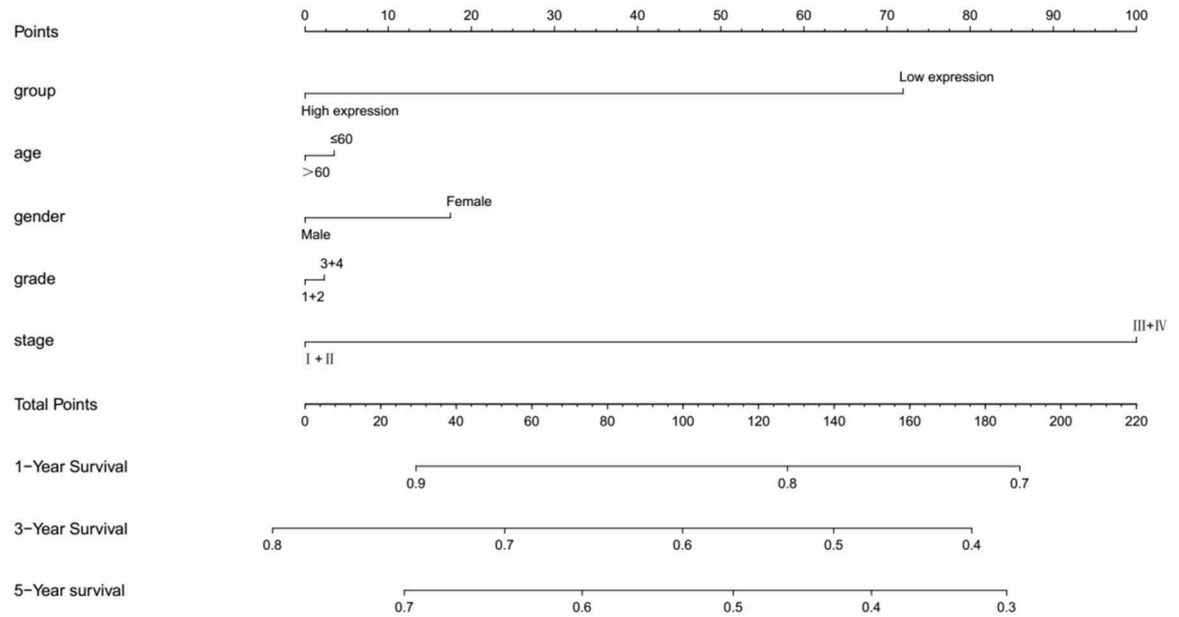

FIGURE 3 | Nomogramfor predicting 1-, 3-, or 5-year survival in head and neck cancer patients. The top row shows the point value for each variable. Rows indicate the variables included in the nomogram. Each variable corresponds to a point value based on head and neck cancer characteristics. The sum of these values is located on the Total Points, and the line drawn downward to the survival axes is used to determine the likelihood of 1-, 3-, or 5-year survival.

low expression group, hub genes CDC34, UBE2D3, GAN, FZR1, CUL3, KLHL2, FBXL8, CDC16, FBXW11, and LMO7 were highly related to the survival outcome. CDSN, LCE1D, LCE3B, LCE1E, LCE3C, LCE1B, LCE2A, LCE1A, LCE2B, and LCE2C were associated with the patients' clinical stages (**Figures 6E–H**).

DISCUSSION

MMP25 is a member of the matrix metalloproteinase family which is frequently connected to embryonic development, reproduction, and tissue remodeling, as well as tumorigenesis. Although MMP25 has not been extensively investigated, research showed that MMP25 could regulate the chemotaxis of neutrophil and monocyte and generate "eat-me" signals to increase the phagocytic removal of neutrophils (17). MMP25 is highly expressed in human cancer cells, such as colon cancer cells and gastric cancer cells (18, 19). In addition, MMP25 was highly expressed and promoted tumor growth in colon cancer (18). Here, we report that the expression level of MMP25 correlated to the activated $CD4^+$ memory T cells and prognosis in head and neck cancer. High expression levels of MMP25 were associated with a better survival outcome. Increased MMP25 expression level could impact the clinical stages of head and neck cancer patients, indicating that MMP25 expression could be used as a potential predictor of clinical stage and prognosis. Moreover, our analysis suggested that immune infiltration levels and diverse tumor-associated pathways were correlated with levels of MMP25 expression. Therefore, our study provides an insight into understanding the role of MMP25 in tumor immune environment and molecular mechanism in head and neck cancer.

In this research, we first analyzed the expression levels of MMPs and prognostic landscape in head and neck cancer. The differential expression between cancer and normal tissues was observed in many matrix metalloproteinase family genes. Expression levels of MMP10, MMP19, MMP24, and MMP25 were associated with prognosis in TCGA cohort of head and neck cancer by Kaplan-Meier analysis. Chongshan Wu demonstrated that the high expression of MMP19 was determined to be a poor prognostic factor in colorectal cancer (20). Trever G Bivona also suggested that MMP24 was a biomarker of tumor progression and worse outcomes in lung and/or gastric cancer patients (21). Univariate Cox proportional hazards regression demonstrated a significant correlation between MMP25 (HR=0.81, $p = 0.04$) and MMP8 (HR=1.26, $p = 0.05$) and prognosis of head and neck cancer patients. Notably, we observed that MMP25 was the only one gene that not only significantly expressed compared to the normal tissues but also played a significant role in the survival outcome of head and neck cancer patients by analysis of Kaplan–Meier method and univariate Cox proportional hazards regression. Likewise, recent evidence also revealed that high MMP25 expression levels were correlated with a better overall survival in ovarian cancer (22). Clinicopathological features from TCGA cohort of head and neck cancer showed that high levels of MMP25 expression were correlated with patients' clinical stages in our study. This important role of MMP25 has not been reported yet so far. Together, these findings suggest that high MMP25 expression levels may be used as a potential prognostic indicator in head and neck cancer.

Differential expressed genes analysis showed that the expression level of MMP25 was related to genes, such as IRF8, IKZF1, and DOCK2. Jason B. Muhitch et al. showed that high

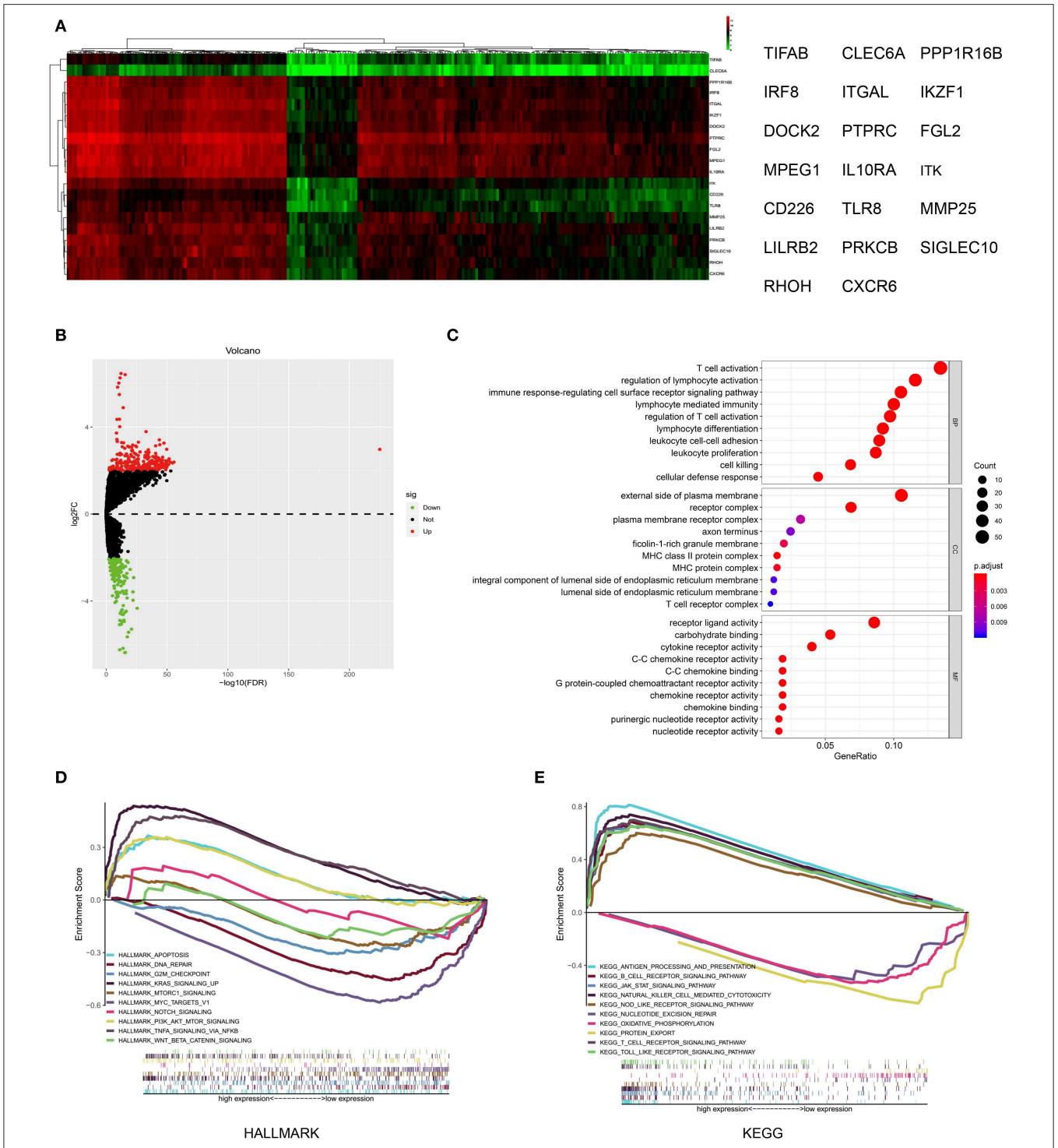

FIGURE 4 | Differential expressed genes and gene set enrichment analysis (GSEA) with MMP25 high and low expression group. **(A)** Heatmap of differential expressed genes analysis by "edgeR" package in R. **(B)** Volcano plot of differential expressed genes with MMP25 high and low expression group. **(C)** GO analysis of differential expressed genes. **(D)** Hallmark enrichment analysis by GSEA. **(E)** KEGG enrichment analysis by GSEA.

expression levels of IRF8 within metastatic sites prolonged overall survival of renal cell carcinoma compared to low levels of IRF8 expression (23). Overexpression of IKZF1 in melanomas enhanced the recruitment of immune infiltration and sensitivity to PD1 and CTLA4 inhibitors (24). Another study also showed that DOCK2 was significantly associated with survival outcome

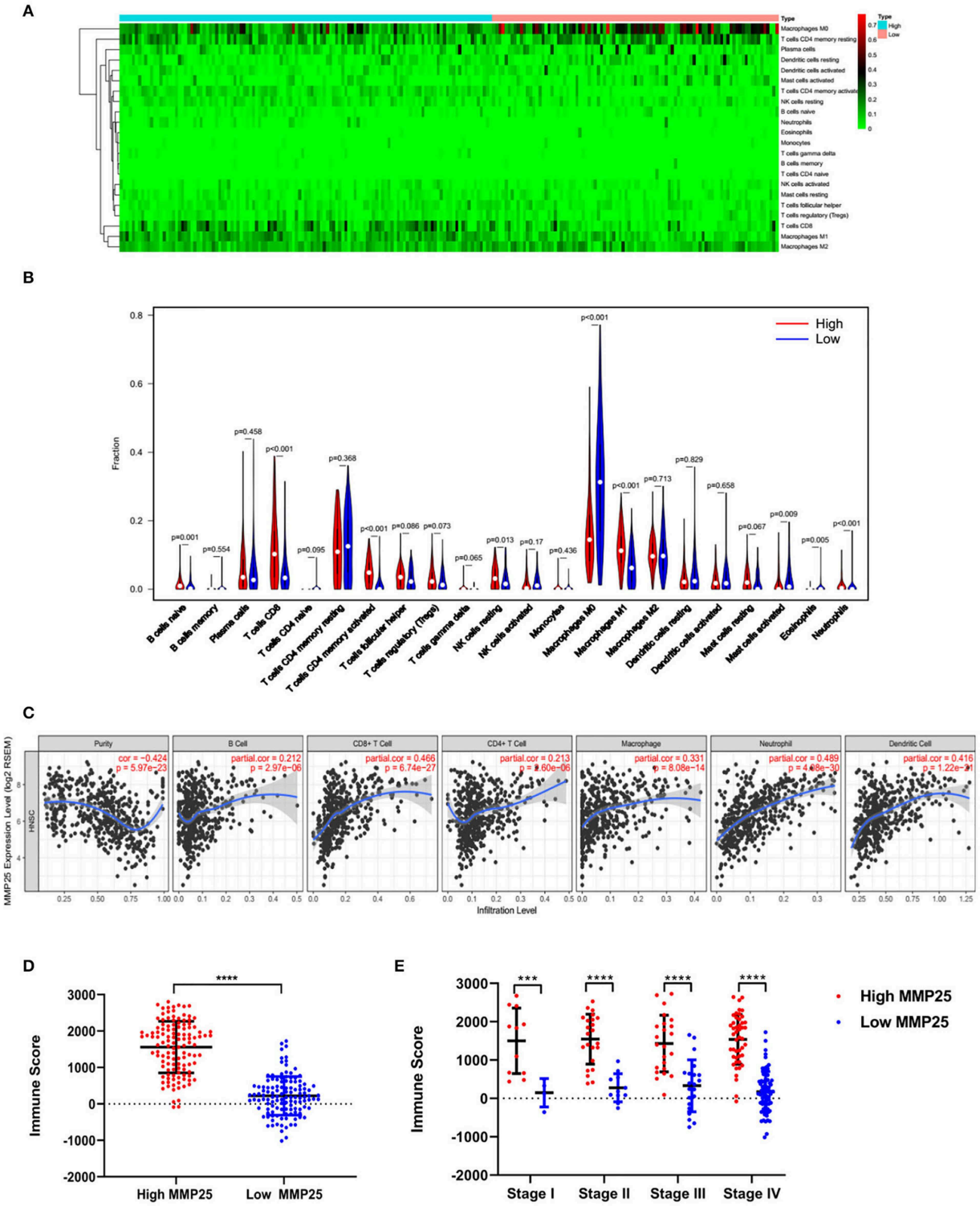

FIGURE 5 | Immune cell infiltration patterns and scores between MMP25 high and low expression group. **(A)** Heatmap of immune infiltration level. **(B)** Violin plot of immune infiltration level between MMP25 high (red) and low (blue) expression group. **(C)** The correlation between the MMP25 expression level and immune infiltration level by TIMER database. **(D)** Difference of immune scores between two groups. **(E)** Difference of immune scores among clinical stages.

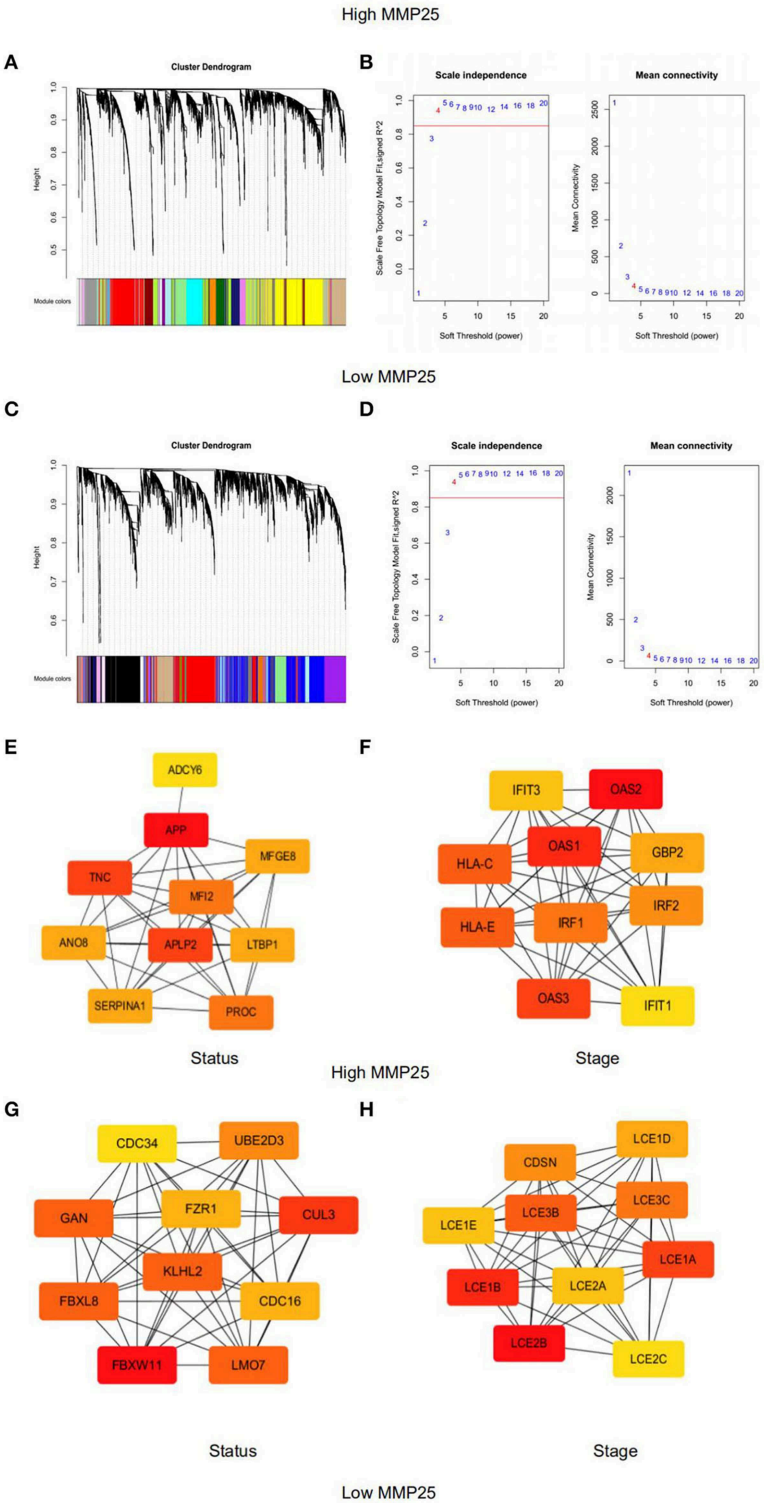

FIGURE 6 | Weighted gene co-expression network analysis of module eigengenes of grade correlated with **(A)** Clustering dendrograms of genes in the MMP25 high expression group. **(B)** The scale-free topology model fit for various soft-thresholding powers (β) in MMP25 high expression group. **(C)** Clustering dendrograms of genes in the MMP25 low expression group. **(D)** The scale-free topology model fit for various soft-thresholding powers (β) in MMP25 low expression group. **(E)** Hub genes protein interaction network of the significant modules for patients' status in MMP25 high expression group. **(F)** Hub genes protein interaction network of the significant modules for patients' stages in MMP25 high expression group. **(G)** Hub genes protein interaction network of the significant modules for patients' status in MMP25 low expression group. **(H)** Hub genes protein interaction network of the significant modules for patients' stages in MMP25 low expression group.

in colorectal cancer (25). In our study, the GO analysis of these differential expressed genes revealed that they were enriched in critical immune biological processes, including T cell activation, regulation of lymphocyte activation, immune response-regulating cell surface receptor signaling pathway, and so on. This partly explained the role of MMP25 in the activation of the $CD4^+$ T memory cell by CIBERSORT analysis. Juric et al. revealed that MMP9 inhibition was able to promote T cell response by disruption of biochemical and physical barriers (26). The MMP23 expression of primary melanoma also demonstrated a trend toward an increased proportion of immunosuppressive Foxp3+ regulatory T cells. These results provided further support for the hypothesis that MMP25 could regulate the immune infiltration level due to the activation of downstream immunological molecules.

Furthermore, high expression levels of MMP25 were associated with many pathways in cancer, for instance, KRAS signaling pathway, apoptosis, PI3K/AKT/mTOR signaling pathway, and JAK/STAT signaling pathway. It has been revealed that JAK/STAT and mTOR pathways were significantly associated with poor overall survival (27, 28). Immune regulatory processes are largely driven by JAK-STAT signaling by a wide range of downstream cellular effectors, including oncogenes, miRNAs, DNA methylation, and other co-regulatory factors (29). Kozaki et al. found that PIK3CA mutations were relatively high in the late stage of oral cancer (30). Recent studies describe that the activation of KRAS signaling on cancer cells extends to the cancer microenvironment (31). Apoptosis is a mechanism that may contribute to cancer. Defects can occur at any point along apoptosis-associated pathways, leading to malignant transformation of the affected cells, tumor metastasis, and resistance (32). In addition, we identified key modules associated with head and neck cancer (HNSCC) patient's survival ratio and clinical stage based on the weighted gene co-expression network analysis (WGCNA). Hub genes have been identified, for example, APLP2, IFIT1, IFIT3, and CDC34. APLP2 expression was significantly related to disease-specific survival in renal cell carcinoma (33). It could be hypothesized that MMP25 was able to interact with multiple key genes to affect the progression of head and neck cancer. Taken together, it is possible that the regulation of cancer-associate genes and signaling pathways may be involved in the regulatory role of MMP25 in the clinical stages and prognosis in HNSCC.

Another important result of this study is that MMP25 expression correlated with diverse immune infiltration levels in head and neck cancer. Our results indicated that there was a correlation between MMP25 expression level and infiltration level of macrophages and B cells naïve, $CD8^+$ T cells, activated $CD4^+$ memory T cells, resting NK cells, M1 macrophage, and neutrophils, but lower M0 macrophage and eosinophil. Univariate Cox proportional hazards regression of these types of immune cells showed that activated $CD4^+$ memory T cells correlated with lower hazard ratio (HR) for better overall survival (OS). Oberg showed that in patients with colon cancer, higher percentages of $CD4^+$ memory T cells may be indicative of a better prognosis (34). Meanwhile, $CD4^+$ memory T cells are associated with tumor cell metastasis to lymph nodes and tumor progression (35). Immune score was an algorithm providing scores of the immune infiltration level by ESTIMATE (13). In the present study, the high expression level of MMP25 showed a strong relationship with the immune scores between tumor tissues and normal tissues, as well as in different clinical stages. It is known that the immune scores could predict patients' clinical outcomes (36).

In summary, increased MMP25 expression correlates with better prognosis and increased immune infiltration levels in head and neck cancer, especially activated CD4+ memory T cells. Moreover, the expression of MMP25 potentially contributes to the regulation of tumor-associated pathway and oncogenes. Therefore, we propose that MMP25 probably plays an integral correlative role in immune cell infiltration and can be a potential prognosis biomarker in head and neck cancer. Further exploration of MMP25 function in clinical cohort study or *in vivo* and *in vitro* model will probably contribute to confirm these results.

DATA AVAILABILITY STATEMENT

Publicly available datasets were analyzed in this study. This data can be found here: https://portal.gdc.cancer.gov, https://cistrome.shinyapps.io/timer/.

AUTHOR CONTRIBUTIONS

YL and CG contributed to conception and design of the study and data analysis. KL, GZ, TW, and SZ contributed to data acquisition. GL and YL critically revised the manuscript. All authors contributed to the article and approved the submitted version.

FUNDING

This work was supported by the National Natural Science Foundation of China (No. 81672679, 81772894, and 81972544) and Science and Technology Program of Guangdong Province (2016B030229003).

SUPPLEMENTARY MATERIAL

The Supplementary Material for this article can be found online at: https://www.frontiersin.org/articles/10.3389/fonc.2020.01088/full#supplementary-material

REFERENCES

1. Bray F, Ferlay J, Soerjomataram I, Siegel RL, Torre LA, Jemal A. Global cancer statistics 2018: GLOBOCAN estimates of incidence and mortality worldwide for 36 cancers in 185 countries. *CA Cancer J Clin.* (2018) 68:394–424. doi: 10.3322/caac.21492
2. Chow LQM. Head and neck cancer. *N Engl J Med.* (2020) 382:60–72. doi: 10.1056/NEJMra1715715
3. Ahmad P, Sana J, Slavik M, Slampa P, Smilek P, Slaby O. MicroRNAs involvement in radioresistance of head and neck cancer. *Dis Markers.* (2017) 2017:8245345. doi: 10.1155/2017/8245345
4. Luo X, Qiu Y, Jiang Y, Chen F, Jiang L, Zhou Y, et al. Long non-coding RNA implicated in the invasion and metastasis of head and neck cancer: possible function and mechanisms. *Mol Cancer.* (2018) 17:14. doi: 10.1186/s12943-018-0763-7
5. Xu B, Jungbluth AA, Frosina D, Alzumaili B, Aleynick N, Slodkowska E, et al. Immune microenvironment and expression of PD-L1, PD-1, cancer testis antigen PRAME and MHC I in salivary duct carcinoma. *Histopathology.* (2019) 75:672–82. doi: 10.1111/his.13944
6. Mandal R, Senbabaoglu Y, Desrichard A, Havel JJ, Dalin MG, Riaz N, et al. The head and neck cancer immune landscape and its immunotherapeutic implications. *JCI Insight.* (2016) 1:e89829. doi: 10.1172/jci.insight.89829
7. Mehra R, Seiwert TY, Gupta S, Weiss J, Gluck I, Eder JP, et al. Efficacy and safety of pembrolizumab in recurrent/metastatic head and neck squamous cell carcinoma: pooled analyses after long-term follow-up in KEYNOTE-012. *Br J Cancer.* (2018) 119:153–9. doi: 10.1038/s41416-018-0131-9
8. Jie HB, Schuler PJ, Lee SC, Srivastava RM, Argiris A, Ferrone S, et al. CTLA-4$^+$ Regulatory T cells increased in cetuximab-treated head and neck cancer patients suppress NK cell cytotoxicity and correlate with poor prognosis. *Cancer Res.* (2015) 75:2200–10. doi: 10.1158/0008-5472.CAN-14-2788
9. Liotta LA, Stetler-Stevenson WG. Metalloproteinases and cancer invasion. *Semin Cancer Biol.* (1990) 1:99–106.
10. Vayrynen O, Astrom P, Nyberg P, Alahuhta I, Pirila E, Vilen ST, et al. Matrix metalloproteinase 9 inhibits the motility of highly aggressive HSC-3 oral squamous cell carcinoma cells. *Exp Cell Res.* (2019) 376:18–26. doi: 10.1016/j.yexcr.2019.01.018
11. English WR, Velasco G, Stracke JO, Knauper V, Murphy G. Catalytic activities of membrane-type 6 matrix metalloproteinase (MMP25). *FEBS Lett.* (2001) 491:137–42. doi: 10.1016/S0014-5793(01)02150-0
12. Newman AM, Liu CL, Green MR, Gentles AJ, Feng W, Xu Y, et al. Robust enumeration of cell subsets from tissue expression profiles. *Nat Methods.* (2015) 12:453–7. doi: 10.1038/nmeth.3337
13. Yoshihara K, Shahmoradgoli M, Martinez E, Vegesna R, Kim H, Torres-Garcia W, et al. Inferring tumour purity and stromal and immune cell admixture from expression data. *Nat Commun.* (2013) 4:2612. doi: 10.1038/ncomms3612
14. Li T, Fan J, Wang B, Traugh N, Chen Q, Liu JS, et al. TIMER: a web server for comprehensive analysis of tumor-infiltrating immune cells. *Cancer Res.* (2017) 77:e108–e110. doi: 10.1158/0008-5472.CAN-17-0307
15. Zhang B, Horvath S. A general framework for weighted gene co-expression network analysis. *Stat Appl Genet Mol Biol.* (2005) 4:Article17. doi: 10.2202/1544-6115.1128
16. Langfelder P, Horvath S. WGCNA: an R package for weighted correlation network analysis. *BMC Bioinformatics.* (2008) 9:559. doi: 10.1186/1471-2105-9-559
17. Starr AE, Bellac CL, Dufour A, Goebeler V, Overall CM. Biochemical characterization and N-terminomics analysis of leukolysin, the membrane-type 6 matrix metalloprotease (MMP25): chemokine and vimentin cleavages enhance cell migration and macrophage phagocytic activities. *J Biol Chem.* (2012) 287:13382–95. doi: 10.1074/jbc.M111.314179
18. Sun Q, Weber CR, Sohail A, Bernardo MM, Toth M, Zhao H, et al. MMP25 (MT6-MMP) is highly expressed in human colon cancer, promotes tumor growth, and exhibits unique biochemical properties. *J Biol Chem.* (2007) 282:21998–2010. doi: 10.1074/jbc.M701737200
19. Wang Y, Yu SJ, Li YX, Luo HS. Expression and clinical significance of matrix metalloproteinase-17 and−25 in gastric cancer. *Oncol Lett.* (2015) 9:671–6. doi: 10.3892/ol.2014.2747
20. Chen Z, Wu G, Ye F, Chen G, Fan Q, Dong H, et al. High expression of MMP19 is associated with poor prognosis in patients with colorectal cancer. *BMC Cancer.* (2019) 19:448. doi: 10.1186/s12885-019-5673-6
21. Okimoto RA, Breitenbuecher F, Olivas VR, Wu W, Gini B, Hofree M, et al. Inactivation of capicua drives cancer metastasis. *Nat Genet.* (2017) 49:87–96. doi: 10.1038/ng.3728
22. Zeng L, Qian J, Zhu F, Wu F, Zhao H, Zhu H. The prognostic values of matrix metalloproteinases in ovarian cancer. *J Int Med Res.* 2019:300060519825983. doi: 10.1177/0300060519825983
23. Muhitch JB, Hoffend NC, Azabdaftari G, Miller A, Bshara W, Morrison CD, et al. Tumor-associated macrophage expression of interferon regulatory factor-8 (IRF8) is a predictor of progression and patient survival in renal cell carcinoma. *J Immunother Cancer.* (2019) 7:155. doi: 10.1186/s40425-019-0630-0
24. Chen JC, Perez-Lorenzo R, Saenger YM, Drake CG, Christiano AM. IKZF1 Enhances immune infiltrate recruitment in solid tumors and susceptibility to immunotherapy. *Cell Syst.* (2018) 7:92–103.e104. doi: 10.1016/j.cels.2018.05.020
25. Yu J, Wu WK, Li X, He J, Li XX, Ng SS, et al. Novel recurrently mutated genes and a prognostic mutation signature in colorectal cancer. *Gut.* (2015) 64:636–45. doi: 10.1136/gutjnl-2013-306620
26. Juric V, O'Sullivan C, Stefanutti E, Kovalenko M, Greenstein A, Barry-Hamilton V, et al. MMP-9 inhibition promotes anti-tumor immunity through disruption of biochemical and physical barriers to T-cell trafficking to tumors. *PLoS ONE.* (2018) 13:e0207255. doi: 10.1371/journal.pone.0207255
27. Marques AE, Elias ST, Porporatti AL, Castilho RM, Squarize CH, De Luca Canto G, et al. mTOR pathway protein immunoexpression as a prognostic factor for survival in head and neck cancer patients: a systematic review and meta-analysis. *J Oral Pathol Med.* (2016) 45:319–28. doi: 10.1111/jop.12390
28. Khanna P, Chua PJ, Bay BH, Baeg GH. The JAK/STAT signaling cascade in gastric carcinoma (review). *Int J Oncol.* (2015) 47:1617–26. doi: 10.3892/ijo.2015.3160
29. Owen KL, Brockwell NK, Parker BS. JAK-STAT signaling: a double-edged sword of immune regulation and cancer progression. *Cancers.* (2019) 11:2002. doi: 10.3390/cancers11122002
30. Kozaki K, Imoto I, Pimkhaokham A, Hasegawa S, Tsuda H, Omura K, et al. PIK3CA mutation is an oncogenic aberration at advanced stages of oral squamous cell carcinoma. *Cancer Sci.* (2006) 97:1351–8. doi: 10.1111/j.1349-7006.2006.00343.x
31. Dias Carvalho P, Guimaraes CF, Cardoso AP, Mendonca S, Costa AM, Oliveira MJ, et al. KRAS oncogenic signaling extends beyond cancer cells to orchestrate the microenvironment. *Cancer Res.* (2018) 78:7–14. doi: 10.1158/0008-5472.CAN-17-2084
32. Wong RS. Apoptosis in cancer: from pathogenesis to treatment. *J Exp Clin Cancer Res.* (2011) 30:87. doi: 10.1186/1756-9966-30-87
33. Gao L, Zhao H, Zhang D, Zhou C, Wang H, Ren C, et al. Role of APLP2 in the prognosis and clinicopathology of renal cell carcinoma. *Oncol Lett.* (2019) 17:508–13. doi: 10.3892/ol.2018.9577
34. Oberg A, Samii S, Stenling R, Lindmark G. Different occurrence of CD8+, CD45R0+, and CD68+ immune cells in regional lymph node metastases from colorectal cancer as potential prognostic predictors. *Int J Colorectal Dis.* (2002) 17:25–29. doi: 10.1007/s003840100337
35. Vahidi Y, Faghih Z, Talei AR, Doroudchi M, Ghaderi A. Memory CD4$^+$ T cell subsets in tumor draining lymph nodes of breast cancer patients: a focus on T stem cell memory cells. *Cell Oncol.* (2018) 41:1–11. doi: 10.1007/s13402-017-0352-6
36. Liu W, Ye H, Liu YF, Xu CQ, Zhong YX, Tian T, et al. Transcriptome-derived stromal and immune scores infer clinical outcomes of patients with cancer. *Oncol Lett.* (2018) 15:4351–7. doi: 10.3892/ol.2018.7855

Conflict of Interest: The authors declare that the research was conducted in the absence of any commercial or financial relationships that could be construed as a potential conflict of interest.

frontiers in Oncology

REVIEW
published: 18 August 2020
doi: 10.3389/fonc.2020.01493

Perineural Invasion in Adenoid Cystic Carcinoma of the Salivary Glands: Where We Are and Where We Need to Go

Xiaohao Liu, Xiaojun Yang, Chaoning Zhan, Yan Zhang, Jin Hou and Xuemin Yin**

Department of Oral and Maxillofacial Surgery, Nanfang Hospital, Southern Medical University, Guangzhou, China

Adenoid cystic carcinoma of the salivary gland (SACC) is a rare malignant tumors of the head and neck region, but it is one of the most common malignant tumors that are prone to perineural invasion (PNI) of the head and neck. The prognosis of patients with SACC is strongly associated with the presence of perineural spread (PNS). Although many contributing factors have been reported, the mechanisms underlying the preferential destruction of the blood-nerve barrier (BNB) by tumors and the infiltration of the tumor microenvironment by nerve fibers in SACC, have received little research attention. This review summarizes the current knowledge concerning the characteristics of SACC in relation to the PNI, and then highlights the interplay between components of the tumor microenvironment and perineural niche, as well as their contributions to the PNI. Finally, we provide new insights into the possible mechanisms underlying the pathogenesis of PNI, with particular emphasis on the role of extracellular vesicles that may serve as an attractive entry point in future studies.

Keywords: adenoid cystic carcinoma, salivary glands, perineural invasion, tumor microenvironment, perineurium barrier

OPEN ACCESS

Edited by:
Victor C. Kok,
Asia University, Taiwan

Reviewed by:
Anxun Wang,
First Affiliated Hospital of Sun Yat-Sen University, China
Moran Amit,
University of Texas MD Anderson Cancer Center, United States

****Correspondence:***
Jin Hou
houjin@smu.edu.cn
Xuemin Yin
yinxuemin1983@163.com

Specialty section:
This article was submitted to Head and Neck Cancer, a section of the journal Frontiers in Oncology

Received: *23 April 2019*
Accepted: *13 July 2020*
Published: *18 August 2020*

Citation:
Liu X, Yang X, Zhan C, Zhang Y, Hou J and Yin X (2020) Perineural Invasion in Adenoid Cystic Carcinoma of the Salivary Glands: Where We Are and Where We Need to Go. Front. Oncol. 10:1493. doi: 10.3389/fonc.2020.01493

INTRODUCTION

There are three main ways by which tumors spread: direct invasion into adjacent tissues, hematogenous metastasis, and lymphatic spread; however, perineural invasion (PNI) is considered a fourth route of dissemination, which can be of great significance in the invasion and metastasis of tumors. PNI has been emerging as a significant pathologic feature of many malignant tumors, including those of the pancreas, prostate, colon, rectum, and head and neck, etc. (1). There is a high incidence of PNI in many of these malignancies, and this feature has become an indicator of poor prognosis and is associated with reduced survival (2).

SACC is one of the most common malignant salivary gland tumors, comprising 10% of all salivary gland neoplasms, which is characterized by PNI, strong invasiveness, and hematogenous metastasis (3). With respect to the primary site of tumor, there are various anatomical locations although most of them arise from the small salivary glands (75.4%). In the major salivary glands, 53.3% of tumors involve the submandibular gland, while 46.7% involve the parotid gland (4). Moreover, SACC comprises 4% of all salivary gland tumors, as well as 7.5% of all epithelial salivary gland malignancies (5). SACC generally has an indolent clinical course; nevertheless, advanced tumors may cause pain and/or nerve paralysis, as SACC has a tendency to directly invade the adjacent nerve sheaths close to the primary tumor and spreads along the nerve, a condition referred to as PNI and perineural spread (PNS), respectively.

The 5-year survival rate is relatively high in SACC patients, in contrast with the poor prognosis associated with other epithelial malignancies (5); however, the recurrence rate is also high in SACC, and closely related to PNI (6). Earlier studies suggested that lymph node involvement is uncommon in SACC, but Amit et al. found that the incidence of occult neck metastases among patients with ACC is 17% by retrospective multicentered study (7). Distant metastases are most frequently detected in the lungs, followed by bones, liver, skin, and breasts. The diagnostic transfer rate of SACC ranges from 25 to 55% (8). Distant metastases from SACC primary tumors can remain asymptomatic for long periods of time (6). Even when the tumor have been completely removed, with no recurrence at the primary tumor site, SACC still has a high tendency to spread to the other body parts over a period of time, which is the major cause of death in patients with SACC. However, outcome in SACC is significantly associated with the involvement of margins. Amit et al. analyzed the data of 507 patients with adenoid cystic carcinoma, and suggested that the positive edge is related to the worst outcome, while the negative edge and the near edge are related to the improved result, but not the distance of the tumor (9).

PNI is significantly correlated with both distant metastasis and unfavorable disease outcomes (10). Notably, in one series of patients with clear surgical margins, 80% of patients harboring PNI eventually progressed to local or distant recurrence, compared with only 27% of patients without PNI (11). Given that microscopic invasion of the cancer cells into the surrounding nerve tissues is assumed to occur via the "path of least resistance" it is often a challenge for a surgeon to detect and determine the resection border during surgery. Due to its microscopic size, CAT (computerized axial tomography), and PET (positron emission tomography) scans may also fail to detect PNI. However, Singh et al. have described that MRI can observe the enlargement and enhancement of the image of nerves that have been invaded by the tumor. This can assess whether the tumor has nerve invasion to a certain extent due to its high soft tissue contrast. Compared with CT, MRI is more sensitive to detect perineural proliferation but CT is complementary to MRI and can be used to assess local skeletal changes (12). There have been several studies concerning the statistical association between margin status and PNI. One such study demonstrated that PNI was the strongest prognostic indicator in their series of patients with SACC; however, no specific *p*-value was presented to support their claims (8). In another study, Jang et al. demonstrated that SACC with PNI subsequently progressed to metastasis, while no distant metastasis was observed in those without PNI (13). Multivariate analysis revealed that PNI was a significant predictive factor in distant metastasis (14). These results indicate that PNI potentiates distant metastatic progression, thus influencing patient outcomes.

Given that PNI is closely related to the prognosis of SACC patients, an in-depth exploration of the underlying mechanisms is needed to identify predictors of this condition, and screen out markers that predict tumor prognosis, which may contribute to the development of novel targeted drugs and reduction in recurrence risk in patients with SACC.

Currently, there are two prominent theories on the pathogenesis of PNI: one is the "path of low resistance" and the other is reciprocal signaling interactions. Due to the anatomical proximity between the salivary glands and some cranial nerves, such as the facial nerve, trigeminal nerve, hypoglossal nerve, and glossopharyngeal nerve, the salivary glands have plenty of neural tissues. Some researchers hypothesize that the tumor cells grow along the eural tissues. Some res" which serves as a conduit for their distant migration, whereas the other researchers believe that there are certain factor-based interactions between tumor cells and nerves, which provide a microenvironment suitable for tumor cell growth and proliferation around the nerves (15). In addition, many recent studies have suggested that cell signaling factors contribute to the interaction between tumor and nerve tissue; for example, by increasing the affinity of tumor cells for neural tissue (8). At present, the occurrence of neurotropic invasion is widely considered to involve a variety of microenvironmental regulatory factors, including chemokines and their receptors, brain-derived neurotrophic factor (BDNF) family proteins and their receptors, nerve growth factor (NGF) family proteins and their receptors, as well as matrix metalloproteinases (MMPs) and PNI-related cells (such as macrophages, astrocytes, and Schwann cells) (16).

In this review, we summarize the current knowledge concerning the characteristics of SACC in relation to the PNI, and then highlight the interplay between components of the tumor microenvironment and perineural niche, as well as their contributions to the PNI. Finally, we provide new insights into the possible mechanisms underlying the pathogenesis of PNI, with particular emphasis on the role of extracellular vesicles that may serve as an attractive candidate pathways in future studies.

ANATOMICAL FACTORS OF SACC PERINEURAL INVASION

PNI is a common clinical manifestation of various tumors, including pancreatic cancer, gastric cancer, prostate cancer, and head and neck cancer (17–20). PNI is distinct from PNS. Specifically, PNI is characterized at the microscopic level by the confined invasion of the tumor mass into nerves, while PNS refers to the clinico-radiological findings of distant distribution via the perineural space, or within the neural sheath and nerve itself (21). In 2009, Liebig et al. proposed that PNI of tumor cells can be defined as tumor cells near peripheral nerve fibers, surrounding them by at least 33%, or tumor cells infiltrating into any layers of nerves–endoneurium, perineurium, and epineurium (1). However, some scholars have divide neural invasion into epineural association, perineural invasion, and endoneural invasion based on the scope of neural invasion. Among them, endoneural invasion is an independent predictor of poor prognosis (22, 23).

The normal peripheral nerve consists of three layers of connective tissue with differing characteristics. The epineurium, the outermost fascial layer, is composed of the dense irregular connective tissues that binds individual nerve fascicles into a nerve trunk; the endoneurium is the innermost layer

surrounding axons along with Schwann cells (SCs); the perineurium, the middle layer, is made of layers of flattened cells forming laminar structures wrapping around single nerve fascicles. Epineurium surrounds the entire nerve trunk, thus contributing to the tensile strength of the nerve, but it does not provide a barrier function. The existence of the tight junction (TJ) structures in perineurium and endoneurial vasculature forms the peripheral nerve barrier (24, 25). These structures have been recognized as shielding barriers to the paracellular diffusion of certain molecules and ions (26, 27). Recently, an increasing number of studies have indicated that TJ may act as a barrier against cancer invasion and metastasis (28–30). Therefore, we speculate that a possible explanation of PNI of malignant tumors may be that when tumor cells begin to invade peripheral never, the TJ structure of perineurium must first be disturbed and dismantled to facilitate penetration of the tumor cells.

THE PERINEURAL NICHE AND TUMOR MICROENVIRONMENT IN PNI

A study of neurological invasion, involving nerve cells, tumor cells, and stromal cells, investigated the neurotropic characteristics of prostate cancer and reported that these cell types could respond to secretory or intracellular cytokines, leading to neurologic attacks by tumors, in which axon growth is an important step (1). Axonal growth is complex and involves multiple factors, the most studied of which include chemokines and their receptors, the GDNF family and their receptors, and the NGF family and their receptors, along with matrix metalloproteinases (MMPs) and PNI-related cells (**Table 1**). Schwann cells are closely associated with the process of neural invasion, both prior to and during tumor invasion, and are therefore important for the initiation and development of PNI (16).

TABLE 1 | Mediators in the perineural niche and tumor microenvironment in PNI.

Factors	Interrelated factors	Role in PNI	References
Perineurial cells	Tight junctions	The tight connections in the perineurial cells are the main players of the neural barrier function	(26, 27)
Other PNI-related cells	Schwann cells	Interact with preneoplastic cells	(31)
	TAMs	Positive correlation with PNI	(32, 33)
	Stellate cells	Induce the proliferation of cancer cell and associated with the generation of neuronal plasticity	(34, 35)
Nerve fibers	NGF secretion	Associated with NGF production and lymph node invasion in cancer	(36)
NGF family and receptors	NGF-TRKA	Positive correlations with PNI and poor prognosis in cancer	(37)
	BDNF-TRKB	Significantly correlated with advanced clinical stage, poor prognosis, PNI, vascular invasion, and distant metastasis in SACC; Have a role in the EMT process in SACC	(38, 39)
GDNF family and receptors	GDNF-GFRα1-RET	Induce tumor cell migration	(40)
Chemokines and receptors	CXCL12/CXCR4	Significantly correlated with PNI and increased secretion of MMPs	(41)
	CX3CL1/CX3CR1	Significant positive correlation with PNI and promote tumor migration and invasion	(42)
MMPs	MMP-2 and MMP-9	Degradation of ECM and basement membrane and involved in NGF–TRKA signaling and GDNF–RET pathway	(43)

Perineurial Cells

A transmission electron microscopy study demonstrated that the thickness of the perineurium is ∼10–25 microns, and that it consists of 8–15 concentric layers of flat perineurial cells (44). Each perineurial cell layer comprises flattened cells, linked by special connections that provide a barrier to diffusion. In addition, some intraneural blood vessels, with diameters of ∼6–10 microns, were found close to the axons; these were composed of 6–8 layers of endothelial cells and formed a blood-neural barrier (BNB) with the perineurium (31). Previous studies have demonstrated that perineurial cells can control the integrity of the BNB by secreting various cytokines and growth factors, such as VEGF, BDNF, GDNF, bFGF, and Angiopoietin-1. Moreover, certain factors secreted by perineurial cells can also contribute to the regulation of the tight junction protein, claudin-5, in BNB endothelial cells, thus strengthening the barrier function of the BNB (32). These findings suggest that various factors in the neural microenvironment may regulate the BNB barrier function by affecting the tight junctions between perineurium cells.

Hence, it is important to fully understand the BNB that may represent the first line of defense against tumor PNI, in order to develop new options for the diagnosis and treatment of tumor PNI.

Other PNI-Related Cells

Schwann cells (SCs) are the most common type of cells in peripheral nerves and, along with glial cells, play a key role in nerve repair and regeneration (33). Recent evidence suggests that the affinity of SCs for specific types of gastrointestinal cancer, as well as their migration in cancer, might precede any invasion of the neural environment, and thus play a role in PNI (34).

Tumor-associated macrophages (TAMs) interact with tumor cells and can modulate tumor growth, proliferation, metastasis, and prognosis via a series of cytokines, which are essential components of the tumor microenvironment (35). Endogenous macrophages also present molecules that participate in the balance and regeneration of peripheral nerves. Moreover, the production of GDNF by endothelial macrophages during PNI

is promoted by CSF-1 secretion by pancreatic cancer (PC) cells. Notably, a clinical study has reported a correlation between macrophages and PNI (45).

Stellate cells are myofibroblasts, which can be activated by hypoxia, inflammation, and interactions with precancerous cells and cancer cells. Activated stellate cells promote PNI in pancreatic carcinoma (PC), and are a key contributor to connective tissue hypertrophy (36). The activation of stellate cells promotes the localized growth of PC in co-cultures of tumor cells and pancreatic astrocytes, as well as the propagation of PC cells in an *in-situ* model of PC (46).

Nerve Fibers

Axons, also called nerve fibers, are thread-like projections that carry electrical signals between nerves and receptors in the skin, muscles, joints, and internal organs (47). Emerging evidence has shown that the invasion of tumor is dependent on the axon structure, and denervation can inhibit the growth and metastasis of tumor (48). Pundavela et al. have found that the presence of nerve fibers in breast cancers is relevant to lymph node invasion and the production of biologically active NGF (49) that can stimulate neuron outgrowth (axonogenesis or neo-neurogenesis), thus promoting PNI (50). Further, in order to investigate interactions between nerve fibers and tumor cells, Liu et al. established an *in vitro* model of PNI by co-culturing rat root ganglia (DRG) and human pancreatic cancer cell line (MIA PaCa-2). They found that these cancer cells could stimulate the outgrowth of neurites from DRG. Of note, while these neurites tended to migrate toward pancreatic cancer cell colonies, cancer cells also exhibited a trend of migrating along the contacting neurites simultaneously (37). This indicates that there may exist a reciprocal regulation loop between nerves and cancer cells. Moreover, it has been suggested that higher densities of nerve fibers within tumors were closely associated with poorer clinical outcomes in prostate cancer patients. However, in a mouse model of gastric cancer, the incidence and progression of tumors could be significantly reduced at denervation sites (either surgically or pharmacologically treated) of the stomach (51), again indicating a crucial role of nerves in the growth and progression of tumors (52). Cancer exosomes induced the innervation of the tumor and the exosomes from patients with head and neck cancer had neurite outgrowth activity, while the exosomes from the healthy control group did not (53). Nonetheless, due to the complexity of the tumor microenvironment, the role of nerve fibers in the tumor microenvironment is so far still an understudied research area that warrants further investigation.

NGF Family and Receptors

The nerve growth factor (NGF) family mainly consists of neurotrophin 3 (NTF3), NGF, neurotrophin 4 (NTF4), and brain-derived neurotrophic factor (BDNF) (54). By binding to diverse receptors, NGFs can trigger multiple signaling pathways, which function in the regulation of cell growth, apoptosis, and neuronal formation. Besides, it not only has many important regulatory functions for the survival, growth and differentiation of nerve cells in the peripheral and central nervous system, but also plays a role in regulating the synthesis of neurotransmitters and neuropeptides in sympathetic and sensory nerve cells effect (38). Each NTF binds to tropomyosin-receptor kinases (TRK) receptor with high affinity, or to p75 neurotrophin receptor (p75NTR), with low affinity; NGF binds with high affinity to TRKA; BDNF and NTF4 both bind to TRKB receptors; and NTF-3 binds preferentially to TRKC (39).

Elevated NGF levels have been identified in PC, relative to adjacent normal tissues, with particular over-expression of TRKA in peripheral nerves. Additionally, there is a significant positive correlation between the expression of NGF and TRKA and the incidence of neural invasion, as well as a poor prognosis, in PC and cell co-culture models of PC (55).

BDNF is thought of as "brain fertilizer," due to its potential roles in promoting the survival of existing neurons, as well as inducing the proliferation and differentiation of new neurons and synapses (56). However, BDNF and TRKB have been recently reported to be involved in the malignant progression of multiple cancers, including colon cancer, hepatocellular carcinoma, prostate cancer, and oral squamous cell carcinoma (40, 57). Jia et al. demonstrated that higher expression levels of BDNF and TRKB were significantly correlated with advanced clinical stage, poor prognosis, PNI, vascular invasion, and distant metastasis of SACC (41). Collectively, these findings implicate the involvement of BDNF/TRKB axis in PNI progression of SACC (58). Furthermore, the BDNF/TRKB axis is also reported to have a role in the epithelial-mesenchymal transition (EMT) process in SACC. And the study by Mei Zhang et al. proposed a correlation between PNI and MIF expression that MIF may promote the PNI of SACC by participating in cytoskeletal reorganization and pseudopod formation induced by Schwann-like cell differentiation of EMT and SACC cells (59). Despite the limited number of studies concerning the association between EMT and PNI, EMT is likely to play an invasive critical role in PNI progression, given the enhanced migration and abilities of cancer cells after EMT (42). Notably, there is a significant negative association between TRKB and E-cadherin expression in SACC specimens, supporting a potential role of the BDNF/TRKB axis in EMT during the development of PNI in SACC (58).

Recently, new evidence suggests that the PIK3K/Akt signaling pathway is associated with PNI in ACC. It has been found that NGF can activate PI3K/AKT pathway through phosphorylating AKT in SACC, thereby potentially stimulating scattering and migration of tumor cells which enhances the progression of PNI (60). Additionally, animal experiments have also shown that a high expression of Akt3 serves as a driving factor of salivary gland tumor progression (43). In addition, the NT-3/TrkC axis promotes the progression of PNI and the poor prognosis of SACC by regulating the interaction between SACC cells and SC. Interrupting the interaction between SACC cells and SC by blocking the NT-3/TrkC axis may be an effective strategy for anti-PNI therapy in SACC (61).

GDNF Family and Receptors

The GDNF family, derived from the glial cell line, a group of neurotrophin polypeptides, which is comprises four members: neurturin (NRTN), persephin (PSPN), artemin (ARTN), and glial

cell line-derived neurotrophic factor (GDNF). The GDNF family is secreted by neural tissues and binds with relevant receptors to trigger the differentiation of neuronal cells of the central and peripheral nervous systems. It works mainly in a paracrine manner and plays an important role in the development and maintenance of the central and peripheral nervous systems, kidney morphogenesis and sperm formation (42). GDNF, NRTN, ARTN, and PSPN bind to GFRA1 (GDNF family receptor alpha-1), GFRA2 (GDNF family receptor alpha-2), GFRA3 (GDNF family receptor alpha-3), and GFRA4 (GDNF family receptor alpha-4), respectively (42). It has been suggested that PNI may be mediated through the secretion of GDNF by nerves and further activation of tumor cell surface Ret proto-oncogene (RET) receptors. GFRA1 functions as a co-receptor with RET, both of which are required for GDNF interaction. He et al. have found that DRG neurons can release soluble GFRA1 that may enhance RET phosphorylation and tumor cell migration toward GDNF, even when tumor cell expression of GFRA1 is absent (62). Moreover, in another previous study, a high level of GDNF expression was detected in SACC cells and adjacent nerve fibers, which was demonstrated to be associated with an increase in matrix-degradation during PNI progression (63).

Chemokines and Receptors

Chemokines and their receptors have critical roles in the growth and invasion of tumor cells. CXCL12/CXCR4 (C-X-C Motif Chemokine Ligand 12/C-X-C Motif chemokine receptor 4) signal transduction is a candidate for participation in inter-tumor interstitial interaction and has various functions, such as the regulation of cell proliferation, invasion, EMT, metastasis, and angiogenesis in multiple types of malignancy (64). In PC cells, MMP-9 secretion in response to CXCR4 stimulation may contribute to the process of PNI, via enhancement of extracellular matrix (ECM) degradation (65). Furthermore, CXCL12 significantly increases the NGF expression in PC cells and promotes neuronal regeneration by binding to the CXCR4 receptor. An *in vitro* model showed that the elimination of the CXCL12/CXCR4 signaling pathway led to the suppression of chemotactic migration between PC cells and nerve cells; by blocking the CXCL12/CXCR4 pathway, PC cell neurotropism decreased significantly (66). Therefore, CXCL12/CXCR4 signaling is significantly correlated with PNI. Moreover, Thomas et al. performed CXCR4 immunohistochemical staining and semiquantitative scoring on the tumor tissue of 73 head and neck adenoid cystic carcinoma (AdCC) patients and found that high CXCR4 expression in AdCC is associated with an increased risk of local recurrence (67).

CX3CL1 (C-X3-C Motif Chemokine Ligand 1) is found to be abundantly produced and released by neurons. An elevated expression level of its receptor, CX3CR1 (C-X3-C Motif Chemokine receptor 1), has been implicated in the development of PNI and earlier recurrence of numerous cancers, such as PC, gastric cancer, and prostate cancer (68–70). Equally important, both *in vitro* co-culture and *in vivo* PNI models demonstrated that nerve cells, including Schwann cells and neurons, express CCL2 (C-C motif chemokine ligand 2) which capable of inducinge the migration of CCR2 (C-C Motif Chemokine receptor 2) expressing cancer cells toward these nerves, ultimately promoting PNI progression (16, 71, 72). Role of CX3CR1/CX3CL1 axis in primary and secondary involvement of the nervous system by cancer.

Matrix Metalloproteinases (MMPs)

MMPs are a family of endopeptidases responsible for the degradation of the ECM and tissue remodeling. The expression of certain types of collagen has been confirmed in peripheral nerves, including collagen IV, the main component of the basement membrane of Schwann cells (73). MMP2, MMP7, MMP9, and all type IV collagenases secreted in response to NGF or GDNF, are likely to be involved in PNI (74). In addition, the overexpression of MMP2 by myofibroblasts has been documented in SACC, exhibiting high-grade PNI.

These results indicate that nerves can indeed provide an appropriate environment for tumor growth and the reciprocal interaction positively influence the growth of both nerves and tumors. Although the accuracy of a "path of low resistance" theory is still up for debate today, emerging evidence indicates that the PNI phenomenon is more like a process of active invasion rather than simple diffusion.

PNI MODELS

As mentioned above, PNI is very closely correlated with the prognosis of patients with SACC. Although it was discovered over a century ago, we still know little about the molecular mechanisms involved in the PNI process. *In vitro* models of these complicated disease processes are very difficult to create. To gain a comprehensive understanding of the contribution of a series of soluble factors to PNI, some researchers have attempted to create *in vitro* models, using highly controlled experimental settings. For example, Ayala et al. established an *in vitro* model, where murine DRGs were co-cultured with prostate cancer cells in Matrigel (75). Once suspended in Matrigel, the axons from the DRGs could spread in all directions. These axons grew toward tumor colonies and were gradually invaded by cancer, which mimics the clinical observation of the typical centripetalism of PNI spread. Using this model, Ayala et al. first described the symbiosis exhibited between cancers and nerves in PNI, in which both gain a growth advantage when co-cultured (76). Although the use of this model can better mimic the invasion of tumor cells into nearby nerves, it is not able to replicate the highly complex microenvironment of *in vivo* perineural niches. Of note, Deborde et al. used Live-imaging technology to investigate the interactions between cancer cells and Schwann cells *in vitro* coculture and *in vivo* murine models of PNI. They found that neither soluble factors secreted by Schwann cells, nor empty tunnels established by Schwann cells were capable of mediating cancer cell invasion, whereas physical contact between Schwann living cells and cancer cells facilitated invasion process. This model provides a new insight into the analysis of the complex *in vivo* characteristics of Schwann cells in enhancing PNI (77). Currently, a murine sciatic nerve model is widely used to explore PNI; tumor cells are injected into the distal sciatic nerve of mice to establish an *in vivo* PNI model. Under gross observation, the sciatic nerve

is seen enlarged; histologically, tumor infiltration of the sciatic nerve can be visualized by hematoxylin and eosin staining and immunohistochemistry of pathological tissue sections. Notably, the effects of PNI can be analyzed by monitoring hind limb motor performance, such as the hind paw width of the mice, as well as sciatic neurological score. More importantly, this model, with the genetic manipulation of mice and/or use of different types of cancer cells, can be applied to study cellular and molecular mechanisms involved in PNI and the effects of therapeutic agents on neural invasion (78). These emerging models of PNI strongly suggested there is an extensive signaling interaction between the nerves and invading tumor cells. Recently, an *in vivo* PNI model has been developed to unravel molecular mechanisms of nerve–tumor interactions. Briefly, rat DRGs are transplanted onto the chick embryo chorioallantoic membrane, followed by the transplantation of human head and neck squamous cell carcinoma (HNSCC) cells adjacent to the DRG. This system can replicate a pro-angiogenic tumor microenvironment observed in carcinogenesis, where the newly formed vasculature provides nourishment for both DRGs and tumor cell grafts (79).

In the past few decades, three-dimensional (3D) printing technology has received widespread attention. Now 3D scaffolds fabricated by 3D bioprinting of biomaterials (bioinks) can be used for the regeneration and reconstruction of complex tissues and organs. Likewise, printed 3D tumor models have also been developed to simulate the *in vivo* tumor microenvironment (80). For instance, using 3D projection printing, an *in vitro* 3D micro-chip in a hydrogel was built, with the objective of simulating 3D vascular morphology of *in vivo* microenvironment, by which the behavior of both cancer and non-cancer cells can be monitored and analyzed (81). In addition, Valentina et al. reported that 3D bioprinting, combined with induced pluripotent stem cells (iPSCs) could effectively control the spatial distribution of cells (e.g., neurons); thus creating a more reliable *in vitro* model (82). Although the applications of this technology in the construction of *in-vitro* 3D tumor and neural tissue models are, so far, in the research stage, they provide some new insights into the study of the underlying mechanisms of PNI pathogenesis and progression.

POSSIBLE MECHANISM OF PNI AND CONCLUSION

Due to its insidious onset, its susceptibility to PNI, and high recurrence rates, SACCs are common malignant neoplasms of head and neck tumors. Furthermore, PNI is closely related to patient prognosis. Although many studies have investigated the mechanisms underlying PNI, the precise details remain unclear. In recent years, researchers have begun to investigate the concept that nerves can reciprocally facilitate cancer invasion and progression (83), representing a paradigm shift in our understanding of the mechanism of PNI. Based on current research, we consider that although anatomical factors, cells, nerve growth factors (NGF, BDNF, etc.), chemokines in the tumor microenvironment are involved in the development of

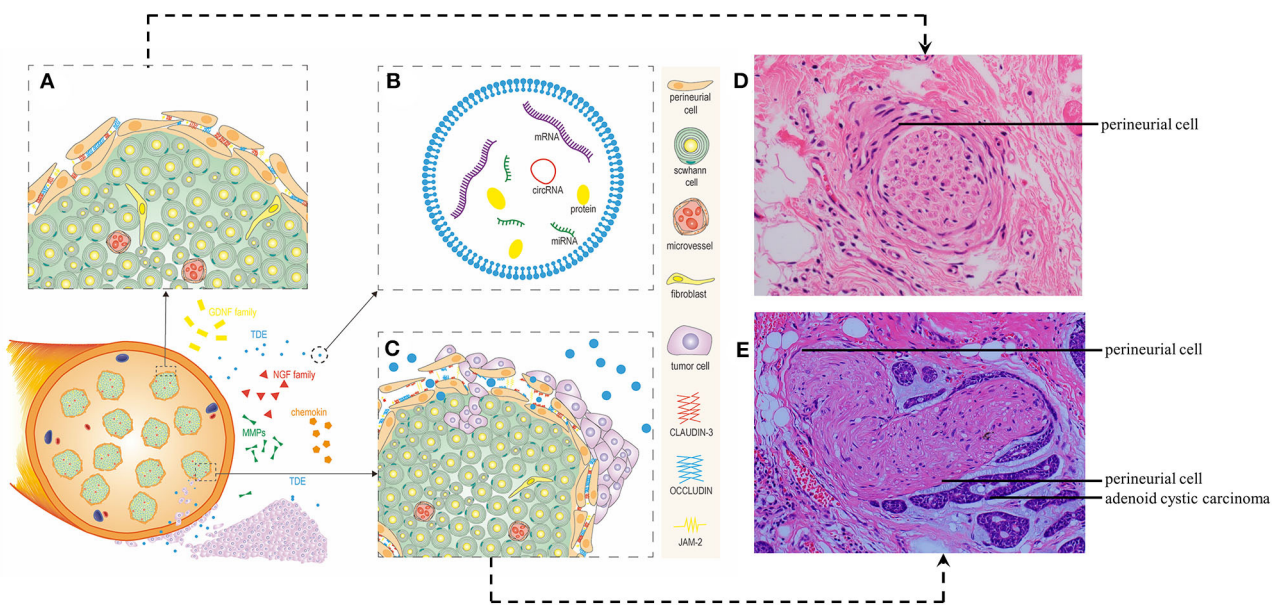

FIGURE 1 | The perineural niche and tumor microenvironment in PNI. **(A)** Diagram showing the architecture and main cellular components of a normal axon. The perineurium that composed of several layers of perineurial cells protects the axon. The perineurium that surrounds individual Schwann cell, micro-vessel, fibroblast. **(B)** Diagram showing the brief structure of tumor derived-exosomes(TDE). TDE contains mRNA, miRNA, protein and other substances, which can be transferred to their target cells, directly or indirectly changing the biological function of recipient cells. **(C)** Diagram showing the architecture and main cellular components of an axon while tumor invades the nerve. After the effect of multiple factors, such as chemokines, GDNF family, NGF family, MMPs and PNI-related cells, the tight connections between the perineurial cells the and the tumor invades the nerve. **(D)** Diagram show the corresponding H&E-stained image of normal nerve. **(E)** Diagram show the corresponding H&E-stained image of tumor infiltrating nerve by the adenoid cystic carcinoma.

PNI, there are other factors that may also contribute to PNI, such as extracellular vesicles (EVs) derived from tumor cells, or other cells in tumor microenvironment and perineural niches (**Figure 1**).

Exosomes, known as the smallest subgroup of EVs, are secreted by cells when multivesicular bodies (MVBs) fuse with the plasma membrane (84). Many previous studies have shown that not only tumor cells produce more exosomes than normal cells, but also tumor-derived exosomes (TDE) containing a diverse set of proteins, mRNA, miRNA, and lipids, can "educate" interstitial cells, endothelial cells, inflammatory cells, and immune cells, in order to regulate the tumor microenvironment and promote tumor growth, invasion, metastasis and angiogenesis (53, 85). Melo et al. (86) found that breast cancer cells can produce mature exosomal miRNAs via a non-cell-dependent pathway, which regulates the phenotype of normal epithelial cells and accelerate their proliferation, and can also be used to generate tumors in nude mice. The development of distant metastases requires primary tumors to break through the basement membrane and penetrate the lymphatic or vascular circulation. Notably, invasive precancerous epithelial cells can overcome this physical constraint by obtaining invasive and migration properties through EMT. Taverna et al. (87) found that exosomal miR-126 derived from chronic myeloid leukemia cells can alter the adhesion and migration ability of recipient cells. Moreover, other studies have confirmed that exosomal miR-105 is specifically expressed and secreted by metastatic breast cancer cells via exosome secretion, and can be transferred to endothelial cells, thereby facilitating cancer metastasis by disrupting the vascular endothelial barrier (88). Hoshino et al. found that tumor-derived exosomes could direct organ-specific metastasis via exosomal integrins (ITGs) (89), based on their intrinsic organotropic homing ability and capacity of initiating pre-metastatic niche formation at foreign sites. Moreover, not only can tumor cells alter the cellular physiology of both surrounding and distant microenvironment through TDE, but other cells in tumor/pre-metastatic microenvironment can also target tumor cells via exosomes, leading to the co-evolution of tumor cells and their microenvironment during tumor dissemination and metastatic outgrowth. A recent study demonstrated that exosomes released by astrocytes could induce an intercellular transfer of PTEN-targeting microRNAs to metastatic tumor cells (90). This finding indicates that exosomes from non-neoplastic cells may also promote the adaptation of disseminated tumor cells to target organs, suggesting the involvement of dynamic bidirectional crosstalk in the pre-metastatic microenvironment. Many previous studies have shown that EVs participate in the dissemination of numerous primary cancer cells, including breast cancer, gastric cancer, colon cancer, liver cancer, malignant melanoma, etc. (91). For instance, one recently published study reported that head and neck tumor-derived exosomes could induce tumor innervation that was enhanced by the exosome-packaged axonal guidance molecule, EphrinB1. This indicates that interventions targeting exosome biogenesis and release may be of therapeutic value against PNI (92). Of particular note, in our previous study, we found that the exosomes derived from the adenoid cystic carcinoma cell line (SACC-83) could be uptaken by human umbilical vein endothelial cells (HUVECs), and destroyed the vascular endothelial barrier (93). Considering that primary tumor-derived EVs can destroy epithelial cell tight junction assembly to induce EMT, and trigger vascular permeability to allow cancer cell dissemination, and "educate" pre-metastatic sites in distant organs, we propose that EVs may also contribute to the disruption of the perineurium barrier and education of the perineural sites into a tumor-promoting microenvironment. It may provide new directions and ideas for further study of PNI pathogenesis in the future. Further, although some research groups have described the involvement of tumor and stroma-derived EVs in the different stages of the metastatic cascade, there is very little information concerning the regulation of tumor cell invasion and metastasis by extracellular vesicles in SACC as well as in PNI.

Of particular note, Galanin is a classic neuropeptide that can function in a variety of physiological processes, such as food intake, nociception, and blood pressure regulation, and it can also act as a growth factor for neurons. Galanin treatment has a tumor-reducing effect in a mouse model of gastrointestinal cancer, and in animal experiments with adenoma formation, galanin appears to be a growth factor that promotes both proliferation and tumor formation (94). In addition, Laminin-5 and insulin-like growth factor-II mRNA binding protein-3 (IMP3) have a good prognostic correlation in various malignancies. Studies have shown that they are also positively expressed in preoperative biopsy specimens of OSCC patients with PNI, implying that preoperative assessment of factors associated with PNI may assist the clinician in the selection of the optimal treatment strategy (95). Nonetheless, whether they can be used as molecular markers of PNI in SACC still needs to be further evaluated.

It's worth mentioning that PNI has been rarely studied in patients with SACC. Emerging evidence for its role as a prognostic factor in SACC is conflicting. Due to the indolent clinical course of SACC, the evaluation of a patient with this malignant tumor is hampered. Furthermore, most previous studies were limited by their small sample size, relatively short follow-up period, mixed pathologies and variable histological sampling of salivary glands, and inadequate reporting of PNI as well (96). Genomic Alterations may also be one of the influencing factors of PNI in SACC. The study found that peripheral nerve invasion was found to be fused with MYB gene with or without copy number changes. MYB-NFIB gene fusion and related GA are associated with ACC peripheral nerve involvement (97). Nonetheless, several studies have found that specific PNI features are indeed closely related to SACC metastasis, locoregional recurrence, long-term survival, and a patient's quality of life (98).

Accordingly, we consider that there are two critical steps in developing strategies for prevention and early therapeutic intervention of PNI: (1) identifying the molecular targets in the microenvironment of perineural niches which are necessary for

PNI development, and (2) finding specific agents against these molecular targets. Therefore, a deeper investigation of underlying mechanisms of PNI should not only clarify the occurrence, proliferation, invasion, recurrence, and metastasis of SACC, but also provide potential targets for the diagnosis and therapy of neurological disorders and diseases.

In conclusion, multiple processes may result in damage at cancer-neural interfaces. There is reciprocity in these interactions, which confers growth and migration advantages to cancer. An in-depth understanding of the molecular mechanism of PNI is essential for developing therapeutic strategies that not only target cancer cells, but also target neural microenvironments as well.

AUTHOR CONTRIBUTIONS

XYi and JH conceived the idea of writing the review. XL wrote the review. XYa assisted to edit. CZ and JZ prepared the Tables and Figures. All authors contributed to the article and approved the submitted version.

FUNDING

This work received support from the Natural Science Foundation of China (Grant No. 81500870) and the Natural Science Foundation of Guangdong Province, China (Grant No. 2016A030313590).

REFERENCES

1. Liebig C, Ayala G, Wilks JA, Berger DH, Albo D. Perineural invasion in cancer: a review of the literature. *Cancer Am Cancer Soc.* (2009) 115:3379–91. doi: 10.1002/cncr.24396
2. Bakst RL, Glastonbury CM, Parvathaneni U, Katabi N, Hu KS, Yom SS. Perineural invasion and perineural tumor spread in head and neck cancer: a critical review. *Int J Radiat Oncol Biol Phys.* (2018) 103:1109–24. doi: 10.1016/j.ijrobp.2018.12.009
3. Bjorndal K, Krogdahl A, Therkildsen MH, Overgaard J, Johansen J, Kristensen CA, et al. Salivary gland carcinoma in Denmark 1990-2005: a national study of incidence, site and histology. Results of the danish head and neck cancer group (DAHANCA). *Oral Oncol.* (2011) 47:677–82. doi: 10.1016/j.oraloncology.2011.04.020
4. Cordesmeyer R, Schliephake H, Kauffmann P, Troltzsch M, Laskawi R, Strobel P, et al. Clinical prognostic factors of salivary adenoid cystic carcinoma: a single-center analysis of 61 patients. *J Craniomaxillofac Surg.* (2017) 45:1784–7. doi: 10.1016/j.jcms.2017.08.004
5. Coca-Pelaz A, Rodrigo JP, Bradley PJ, Vander PV, Triantafyllou A, Hunt JL, et al. Adenoid cystic carcinoma of the head and neck–an update. *Oral Oncol.* (2015) 51:652–61. doi: 10.1016/j.oraloncology.2015.04.005
6. Chang CF, Hsieh MY, Chen MK, Chou MC. Adenoid cystic carcinoma of head and neck: a retrospective clinical analysis of a single institution. *Auris Nasus Larynx.* (2018) 45:831–7. doi: 10.1016/j.anl.2017.10.009
7. Amit M, Na'Ara S, Sharma K, Ramer N, Ramer I, Agbetoba A, et al. Elective neck dissection in patients with head and neck adenoid cystic carcinoma: an international collaborative study. *Ann Surg Oncol.* (2015) 22:1353–9. doi: 10.1245/s10434-014-4106-7
8. Dillon PM, Chakraborty S, Moskaluk CA, Joshi PJ, Thomas CY. Adenoid cystic carcinoma: a review of recent advances, molecular targets, and clinical trials. *Head Neck.* (2016) 38:620–7. doi: 10.1002/hed.23925
9. Amit M, Na'Ara S, Trejo-Leider L, Ramer N, Burstein D, Yue M, et al. Defining the surgical margins of adenoid cystic carcinoma and their impact on outcome: an international collaborative study. *Head Neck.* (2017) 39:1008–14. doi: 10.1002/hed.24740
10. Stelow EB, Bishop JA. Update from the 4th Edition of the world health organization classification of head and neck tumours: tumors of the nasal cavity, paranasal sinuses and skull base. *Head Neck Pathol.* (2017) 11:3–15. doi: 10.1007/s12105-017-0791-4
11. Luksic I, Suton P, Macan D, Dinjar K. Intraoral adenoid cystic carcinoma: is the presence of perineural invasion associated with the size of the primary tumour, local extension, surgical margins, distant metastases, and outcome? *Br J Oral Maxillofac Surg.* (2014) 52:214–18. doi: 10.1016/j.bjoms.2013.11.009
12. Singh FM, Mak SY, Bonington SC. Patterns of spread of head and neck adenoid cystic carcinoma. *Clin Radiol.* (2015) 70:644–53. doi: 10.1016/j.crad.2015.01.013
13. Jang S, Patel PN, Kimple RJ, McCulloch TM. Clinical outcomes and prognostic factors of adenoid cystic carcinoma of the head and neck. *Anticancer Res.* (2017) 37:3045–52. doi: 10.21873/anticanres.11659
14. Ju J, Li Y, Chai J, Ma C, Ni Q, Shen Z, et al. The role of perineural invasion on head and neck adenoid cystic carcinoma prognosis: a systematic review and meta-analysis. *Oral Surg Oral Med Oral Pathol Oral Radiol.* (2016) 122:691–701. doi: 10.1016/j.oooo.2016.08.008
15. Bakst RL, Wong RJ. Mechanisms of perineural invasion. *J Neurol Surg B Skull Base.* (2016) 77:96–106. doi: 10.1055/s-0036-1571835
16. Amit M, Na'Ara S, Gil Z. Mechanisms of cancer dissemination along nerves. *Nat Rev Cancer.* (2016) 16:399–408. doi: 10.1038/nrc.2016.38
17. Gupta A, Veness M, De'Ambrosis B, Selva D, Huilgol SC. Management of squamous cell and basal cell carcinomas of the head and neck with perineural invasion. *Australas J Dermatol.* (2016) 57:3–13. doi: 10.1111/ajd.12314
18. Yang YH, Liu JB, Gui Y, Lei LL, Zhang SJ. Relationship between autophagy and perineural invasion, clinicopathological features, and prognosis in pancreatic cancer. *World J Gastroenterol.* (2017) 23:7232–41. doi: 10.3748/wjg.v23.i40.7232
19. Hwang JE, Hong JY, Kim JE, Shim HJ, Bae WK, Hwang EC, et al. Prognostic significance of the concomitant existence of lymphovascular and perineural invasion in locally advanced gastric cancer patients who underwent curative gastrectomy and adjuvant chemotherapy. *Jpn J Clin Oncol.* (2015) 45:541–6. doi: 10.1093/jjco/hyv031
20. Zareba P, Flavin R, Isikbay M, Rider JR, Gerke TA, Finn S, et al. Perineural invasion and risk of lethal prostate cancer. *Cancer Epidemiol Biomarkers Prev.* (2017) 26:719–26. doi: 10.1158/1055-9965.EPI-16-0237
21. Kuhn FP, Hullner M, Mader CE, Kastrinidis N, Huber GF, von Schulthess GK, et al. Contrast-enhanced PET/MR imaging versus contrast-enhanced PET/CT in head and neck cancer: how much MR information is needed? *J Nucl Med.* (2014) 55:551–8. doi: 10.2967/jnumed.113.125443
22. Amit M, Binenbaum Y, Trejo-Leider L, Sharma K, Ramer N, Ramer I, et al. International collaborative validation of intraneural invasion as a prognostic marker in adenoid cystic carcinoma of the head and neck. *Head Neck.* (2015) 37:1038–45. doi: 10.1002/hed.23710
23. Ihsan Ekin D, Helmut F, Ceyhan GO. Generation and impact of neural invasion in pancreatic cancer. *Pancreatic Cancer.* (2012) 295–312. doi: 10.5772/30117
24. Peltonen S, Alanne M, Peltonen J. Barriers of the peripheral nerve. *Tissue Barriers.* (2013) 1:e24956. doi: 10.4161/tisb.24956
25. Pina-Oviedo S, Ortiz-Hidalgo C. The normal and neoplastic perineurium: a review. *Adv Anat Pathol.* (2008) 15:147–64. doi: 10.1097/PAP.0b013e31816f8519
26. Anderson JM, Van Itallie CM. Physiology and function of the tight junction. *Cold Spring Harb Perspect Biol.* (2009) 1:a2584. doi: 10.1101/cshperspect.a002584
27. Pummi KP, Aho HJ, Laato MK, Peltonen JT, Peltonen SA. Tight junction proteins and perineurial cells in neurofibromas. *J Histochem Cytochem.* (2006) 54:53–61. doi: 10.1369/jhc.5A6671.2005
28. Runkle EA, Mu D. Tight junction proteins: from barrier to tumorigenesis. *Cancer Lett.* (2013) 337:41–48. doi: 10.1016/j.canlet.2013.05.038
29. Anderson JM, Balda MS, Fanning AS. The structure and regulation of tight junctions. *Curr Opin Cell Biol.* (1993) 5:772–8. doi: 10.1016/0955-0674(93)90024-K
30. Martin TA, Jiang WG. Loss of tight junction barrier function and its role in cancer metastasis. *Biochim Biophys Acta.* (2009) 1788:872–91. doi: 10.1016/j.bbamem.2008.11.005

31. Reina MA, Lopez A, Villanueva MC, De Andres JA, Maches F. [The blood-nerve barrier in peripheral nerves]. *Rev Esp Anestesiol Reanim.* (2003) 50:80–86.
32. Shanthaveerappa TR, Bourne GH. The 'perineural epithelium', a metabolically active, continuous, protoplasmic cell barrier surrounding peripheral nerve fasciculi. *J Anat*. (1962) 96:527–37.
33. Kanda T. [Blood-nerve barrier: structure and function]. *Brain Nerve.* (2011) 63:557–69.
34. Demir IE, Boldis A, Pfitzinger PL, Teller S, Brunner E, Klose N, et al. Investigation of schwann cells at neoplastic cell sites before the onset of cancer invasion. *J Natl Cancer Inst.* (2014) 106:dju184. doi: 10.1093/jnci/dju184
35. Zeng L, Guo Y, Liang J, Chen S, Peng P, Zhang Q, et al. Perineural invasion and TAMs in pancreatic ductal adenocarcinomas: review of the original pathology reports using immunohistochemical enhancement and relationships with clinicopathological features. *J Cancer*. (2014) 5:754–60. doi: 10.7150/jca.10238
36. Vonlaufen A, Joshi S, Qu C, Phillips PA, Xu Z, Parker NR, et al. Pancreatic stellate cells: partners in crime with pancreatic cancer cells. *Cancer Res.* (2008) 68:2085–93. doi: 10.1158/0008-5472.CAN-07-2477
37. Liu ZS, Wang Y, Li Q, Zhang SL, Shi YR. *In vitro* interaction of human pancreatic cancer cells and rat dorsal root ganglia: a co-culture model. *Zhonghua Zhong Liu Za Zhi.* (2012) 34:259–63. doi: 10.3760/cma.j.issn.0253-3766.2012.04.005
38. Rocco ML, Soligo M, Manni L, Aloe L. Nerve growth factor: early studies and recent clinical trials. *Curr Neuropharmacol.* (2018) 16:1455–65. doi: 10.2174/1570159X16666180412092859
39. Yamashita N, Kuruvilla R. Neurotrophin signaling endosomes: biogenesis, regulation, and functions. *Curr Opin Neurobiol.* (2016) 39:139–45. doi: 10.1016/j.conb.2016.06.004
40. Yang X, Martin TA, Jiang WG. Biological influence of brain-derived neurotrophic factor on breast cancer cells. *Int J Oncol.* (2012) 41:1541–6. doi: 10.3892/ijo.2012.1581
41. Jia S, Wang W, Hu Z, Shan C, Wang L, Wu B, et al. BDNF mediated TrkB activation contributes to the EMT progression and the poor prognosis in human salivary adenoid cystic carcinoma. *Oral Oncol.* (2015) 51:64–70. doi: 10.1016/j.oraloncology.2014.10.008
42. Fielder GC, Yang TW, Razdan M, Li Y, Lu J, Perry JK, et al. The GDNF family: a role in cancer? *Neoplasia.* (2018) 20:99–117. doi: 10.1016/j.neo.2017.10.010
43. Zboray K, Mohrherr J, Stiedl P, Pranz K, Wandruszka L, Grabner B, et al. AKT3 drives adenoid cystic carcinoma development in salivary glands. *Cancer Med.* (2018) 7:445–53. doi: 10.1002/cam4.1293
44. Joseph NM, Mukouyama YS, Mosher JT, Jaegle M, Crone SA, Dormand EL, et al. Neural crest stem cells undergo multilineage differentiation in developing peripheral nerves to generate endoneurial fibroblasts in addition to schwann cells. *Development.* (2004) 131:5599–612. doi: 10.1242/dev.01429
45. Meng F, Li C, Li W, Gao Z, Guo K, Song S. Interaction between pancreatic cancer cells and tumor-associated macrophages promotes the invasion of pancreatic cancer cells and the differentiation and migration of macrophages. *IUBMB Life.* (2014) 66:835–46. doi: 10.1002/iub.1336
46. Apte MV, Wilson JS, Lugea A, Pandol SJ. A starring role for stellate cells in the pancreatic cancer microenvironment. *Gastroenterology.* (2013) 144:1210–19. doi: 10.1053/j.gastro.2012.11.037
47. Ondicova K, Mravec B. Role of nervous system in cancer aetiopathogenesis. *Lancet Oncol.* (2010) 11:596–601. doi: 10.1016/S1470-2045(09)70337-7
48. Boilly B, Faulkner S, Jobling P, Hondermarck H. Nerve dependence: from regeneration to cancer. *Cancer Cell.* (2017) 31:342–54. doi: 10.1016/j.ccell.2017.02.005
49. Pundavela J, Roselli S, Faulkner S, Attia J, Scott RJ, Thorne RF, et al. Nerve fibers infiltrate the tumor microenvironment and are associated with nerve growth factor production and lymph node invasion in breast cancer. *Mol Oncol.* (2015) 9:1626–35. doi: 10.1016/j.molonc.2015.05.001
50. Jobling P, Pundavela J, Oliveira SM, Roselli S, Walker MM, Hondermarck H. Nerve-cancer cell cross-talk: a novel promoter of tumor progression. *Cancer Res.* (2015) 75:1777–81. doi: 10.1158/0008-5472.CAN-14-3180
51. Zhao CM, Hayakawa Y, Kodama Y, Muthupalani S, Westphalen CB, Andersen GT, et al. Denervation suppresses gastric tumorigenesis. *Sci Transl Med.* (2014) 6:115r−250r. doi: 10.1126/scitranslmed.3009569
52. Magnon C, Hall SJ, Lin J, Xue X, Gerber L, Freedland SJ, et al. Autonomic nerve development contributes to prostate cancer progression. *Science.* (2013) 341:1236361. doi: 10.1126/science.1236361
53. Couto N, Caja S, Maia J, Strano MM, Costa-Silva B. Exosomes as emerging players in cancer biology. *Biochimie.* (2018) 155:2–10. doi: 10.1016/j.biochi.2018.03.006
54. Bapat AA, Munoz RM, Von Hoff DD, Han H. Blocking nerve growth factor signaling reduces the neural invasion potential of pancreatic cancer cells. *PLoS ONE.* (2016) 11:e165586. doi: 10.1371/journal.pone.0165586
55. Ma W, Wang C, Su Y, Tian Y, Zhu H. Expression of nerve growth factor and its receptor, tyrosine kinase receptor A, in rooster testes. *Anim Reprod Sci.* (2015) 161:40–46. doi: 10.1016/j.anireprosci.2015.08.001
56. Benarroch EE. Brain-derived neurotrophic factor: regulation, effects, and potential clinical relevance. *Neurology.* (2015) 84:1693–704. doi: 10.1212/WNL.0000000000001507
57. Tanaka K, Okugawa Y, Toiyama Y, Inoue Y, Saigusa S, Kawamura M, et al. Brain-derived neurotrophic factor (BDNF)-induced tropomyosin-related kinase B (Trk B) signaling is a potential therapeutic target for peritoneal carcinomatosis arising from colorectal cancer. *PLoS ONE.* (2014) 9:e96410. doi: 10.1371/journal.pone.0096410
58. Shan C, Wei J, Hou R, Wu B, Yang Z, Wang L, et al. Schwann cells promote EMT and the schwann-like differentiation of salivary adenoid cystic carcinoma cells via the BDNF/TrkB axis. *Oncol Rep.* (2016) 35:427–35. doi: 10.3892/or.2015.4366
59. Zhang M, Li ZF, Wang HF, Wang SS, Yu XH, Wu JB, et al. MIF promotes perineural invasion through EMT in salivary adenoid cystic carcinoma. *Mol Carcinog.* (2019) 58:898–912. doi: 10.1002/mc.22979
60. Alkhadar H, Macluskey M, White S, Ellis I. Nerve growth factor-induced migration in oral and salivary gland tumour cells utilises the PI3K/Akt signalling pathway: is there a link to perineural invasion? *J Oral Pathol Med.* (2020) 49:227–34. doi: 10.1111/jop.12979
61. Li H, Yang Z, Wang W, Wang J, Zhang J, Liu J, et al. NT-3/TrkC axis contributes to the perineural invasion and the poor prognosis in human salivary adenoid cystic carcinoma. *J Cancer.* (2019) 10:6065–73. doi: 10.7150/jca.33635
62. He S, Chen CH, Chernichenko N, He S, Bakst RL, Barajas F, et al. GFRalpha1 released by nerves enhances cancer cell perineural invasion through GDNF-RET signaling. *Proc Natl Acad Sci USA.* (2014) 111:E2008–17. doi: 10.1073/pnas.1402944111
63. Zheng SC, Zhang YR, Luo SY, Zhang LP. [The effect of GDNF on matrix-degrading and cell-adhesion during perineural invasion of salivary adenoid cystic carcinoma]. *Shanghai Kou Qiang Yi Xue.* (2016) 25:212–16.
64. Luo X, Tai WL, Sun L, Pan Z, Xia Z, Chung SK, et al. Crosstalk between astrocytic CXCL12 and microglial CXCR4 contributes to the development of neuropathic pain. *Mol Pain.* (2016) 12:1744806916636385. doi: 10.1177/1744806916636385
65. Jiang YM, Li G, Sun BC, Zhao XL, Zhou ZK. Study on the relationship between CXCR4 expression and perineural invasion in pancreatic cancer. *Asian Pac J Cancer Prev.* (2014) 15:4893–6. doi: 10.7314/APJCP.2014.15.12.4893
66. Xu Q, Wang Z, Chen X, Duan W, Lei J, Zong L, et al. Stromal-derived factor-1alpha/CXCL12-CXCR4 chemotactic pathway promotes perineural invasion in pancreatic cancer. *Oncotarget.* (2015) 6:4717–32. doi: 10.18632/oncotarget.3069
67. Klein NT, van Es RJJ, Valstar MH, Smeele LE, Smit LA, Klein GR, et al. High CXCR4 expression in adenoid cystic carcinoma of the head and neck is associated with increased risk of locoregional recurrence. *J Clin Pathol.* (2020) 73:476–82. doi: 10.1136/jclinpath-2019-206273
68. Zhang M, Zhu ZL, Gao XL, Wu JS, Liang XH, Tang YL. Functions of chemokines in the perineural invasion of tumors. *Int J Oncol.* (2018) 52:1369–79. doi: 10.3892/ijo.2018.4311
69. Lv CY, Zhou T, Chen W, Yin XD, Yao JH, Zhang YF. Preliminary study correlating CX3CL1/CX3CR1 expression with gastric carcinoma and gastric carcinoma perineural invasion. *World J Gastroenterol.* (2014) 20:4428–32. doi: 10.3748/wjg.v20.i15.4428
70. Marchesi F, Locatelli M, Solinas G, Erreni M, Allavena P, Mantovani A. Role of CX3CR1/CX3CL1 axis in primary and secondary involvement of the nervous system by cancer. *J Neuroimmunol.* (2010) 224:39–44. doi: 10.1016/j.jneuroim.2010.05.007

71. Bakst RL, Xiong H, Chen CH, Deborde S, Lyubchik A, Zhou Y, et al. Inflammatory monocytes promote perineural invasion via CCL2-mediated recruitment and cathepsin B expression. *Cancer Res.* (2017) 77:6400–14. doi: 10.1158/0008-5472.CAN-17-1612
72. He S, He S, Chen CH, Deborde S, Bakst RL, Chernichenko N, et al. The chemokine (CCL2-CCR2) signaling axis mediates perineural invasion. *Mol Cancer Res.* (2015) 13:380–90. doi: 10.1158/1541-7786.MCR-14-0303
73. Mehta P, Piao X. Adhesion G-protein coupled receptors and extracellular matrix proteins: roles in myelination and glial cell development. *Dev Dyn.* (2017) 246:275–84. doi: 10.1002/dvdy.24473
74. Jakubowska K, Pryczynicz A, Januszewska J, Sidorkiewicz I, Kemona A, Niewinski A, et al. Expressions of matrix metalloproteinases 2, 7, and 9 in carcinogenesis of pancreatic ductal adenocarcinoma. *Dis Markers.* (2016) 2016:9895721. doi: 10.1155/2016/9895721
75. Ayala GE, Wheeler TM, Shine HD, Schmelz M, Frolov A, Chakraborty S, et al. *In vitro* dorsal root ganglia and human prostate cell line interaction: redefining perineural invasion in prostate cancer. *Prostate.* (2001) 49:213–23. doi: 10.1002/pros.1137
76. Dai H, Li R, Wheeler T, Ozen M, Ittmann M, Anderson M, et al. Enhanced survival in perineural invasion of pancreatic cancer: an *in vitro* approach. *Hum Pathol.* (2007) 38:299–307. doi: 10.1016/j.humpath.2006.08.002
77. Deborde S, Omelchenko T, Lyubchik A, Zhou Y, He S, McNamara WF, et al. Schwann cells induce cancer cell dispersion and invasion. *J Clin Invest.* (2016) 126:1538–54. doi: 10.1172/JCI82658
78. Deborde S, Yu Y, Marcadis A, Chen CH, Fan N, Bakst RL, et al. An *in vivo* murine sciatic nerve model of perineural invasion. *J Vis Exp.* (2018) 56857. doi: 10.3791/56857
79. Scanlon CS, Banerjee R, Inglehart RC, Liu M, Russo N, Hariharan A, et al. Galanin modulates the neural niche to favour perineural invasion in head and neck cancer. *Nat Commun.* (2015) 6:6885. doi: 10.1038/ncomms7885
80. Gu BK, Choi DJ, Park SJ, Kim YJ, Kim CH. 3D bioprinting technologies for tissue engineering applications. *Adv Exp Med Biol.* (2018) 1078:15–28. doi: 10.1007/978-981-13-0950-2_2
81. Huang TQ, Qu X, Liu J, Chen S. 3D printing of biomimetic microstructures for cancer cell migration. *Biomed Microdevices.* (2014) 16:127–32. doi: 10.1007/s10544-013-9812-6
82. Fantini V, Bordoni M, Scocozza F, Conti M, Scarian E, Carelli S, et al. Bioink composition and printing parameters for 3D modeling neural tissue. *Cells.* (2019) 8:830. doi: 10.3390/cells8080830
83. Saloman JL, Albers KM, Li D, Hartman DJ, Crawford HC, Muha EA, et al. Ablation of sensory neurons in a genetic model of pancreatic ductal adenocarcinoma slows initiation and progression of cancer. *Proc Natl Acad Sci USA.* (2016) 113:3078–83. doi: 10.1073/pnas.1512603113
84. Mathieu M, Martin-Jaular L, Lavieu G, Thery C. Specificities of secretion and uptake of exosomes and other extracellular vesicles for cell-to-cell communication. *Nat Cell Biol.* (2019) 21:9–17. doi: 10.1038/s41556-018-0250-9
85. Tkach M, Thery C. Communication by extracellular vesicles: where we are and where we need to go. *Cell.* (2016) 164:1226–32. doi: 10.1016/j.cell.2016.01.043
86. Tran N. Cancer exosomes as miRNA factories. *Trends Cancer.* (2016) 2:329–31. doi: 10.1016/j.trecan.2016.05.008
87. Taverna S, Giallombardo M, Gil-Bazo I, Carreca AP, Castiglia M, Chacartegui J, et al. Exosomes isolation and characterization in serum is feasible in non-small cell lung cancer patients: critical analysis of evidence and potential role in clinical practice. *Oncotarget.* (2016) 7:28748–60. doi: 10.18632/oncotarget.7638
88. Zhou W, Fong MY, Min Y, Somlo G, Liu L, Palomares MR, et al. Cancer-secreted miR-105 destroys vascular endothelial barriers to promote metastasis. *Cancer Cell.* (2014) 25:501–15. doi: 10.1016/j.ccr.2014.03.007
89. Hoshino A, Costa-Silva B, Shen TL, Rodrigues G, Hashimoto A, Tesic MM, et al. Tumour exosome integrins determine organotropic metastasis. *Nature.* (2015) 527:329–35. doi: 10.1038/nature15756
90. Zhang L, Zhang S, Yao J, Lowery FJ, Zhang Q, Huang WC, et al. Microenvironment-induced PTEN loss by exosomal microRNA primes brain metastasis outgrowth. *Nature.* (2015) 527:100–104. doi: 10.1038/nature15376
91. Becker A, Thakur BK, Weiss JM, Kim HS, Peinado H, Lyden D. Extracellular vesicles in cancer: cell-to-cell mediators of metastasis. *Cancer Cell.* (2016) 30:836–48. doi: 10.1016/j.ccell.2016.10.009
92. Madeo M, Colbert PL, Vermeer DW, Lucido CT, Cain JT, Vichaya EG, et al. Cancer exosomes induce tumor innervation. *Nat Commun.* (2018) 9:4215–84. doi: 10.1038/s41467-018-06640-0
93. Hou J, Wang F, Liu X, Song M, Yin X. Tumor-derived exosomes enhance invasion and metastasis of salivary adenoid cystic carcinoma cells. *J Oral Pathol Med.* (2018) 47:144–51. doi: 10.1111/jop.12654
94. Rauch I, Kofler B. The galanin system in cancer. *Exp Suppl.* (2010) 102:223–41. doi: 10.1007/978-3-0346-0228-0_16
95. Tarsitano A, Asioli S, Morandi L, Monti V, Righi A, Morselli LA, et al. Laminin-5 and insulin-like growth factor-II mRNA binding protein-3 (IMP3) expression in preoperative biopsy specimens from oral cancer patients: their role in neural spread risk and survival stratification. *J Craniomaxillofac Surg.* (2016) 44:1896–902. doi: 10.1016/j.jcms.2016.07.012
96. Gomez DR, Katabi N, Zhung J, Wolden SL, Zelefsky MJ, Kraus DH, et al. Clinical and pathologic prognostic features in acinic cell carcinoma of the parotid gland. *Cancer Am Cancer Soc.* (2009) 115:2128–137. doi: 10.1002/cncr.24259
97. Joseph I, Rooban T, Elizabeth J, Rao UK, Ranganathan K. Genomic alterations landscape in adenoid cystic carcinoma of head and neck. *J Orofac Sci.* (2009) 11:73–78. doi: 10.4103/jofs.jofs_40_19
98. Amit M, Eran A, Billan S, Fridman E, Na'Ara S, Charas T, et al. Perineural spread in noncutaneous head and neck cancer: new insights into an old problem. *J Neurol Surg B Skull Base.* (2016) 77:86–95. doi: 10.1055/s-0036-1571834

Conflict of Interest: The authors declare that the research was conducted in the absence of any commercial or financial relationships that could be construed as a potential conflict of interest.

frontiers in Oncology

ORIGINAL RESEARCH
published: 05 February 2021
doi: 10.3389/fonc.2020.522332

Integrated Analysis Reveals *ENDOU* as a Biomarker in Head and Neck Squamous Cell Carcinoma Progression

Chengzhi Xu[1†], *Yunbin Zhang*[2,3†], *Yupeng Shen*[4], *Yong Shi*[1], *Ming Zhang*[1] *and Liang Zhou*[1*]

[1] Department of Otolaryngology—Head and Neck Surgery, Eye Ear Nose and Throat Hospital, Fudan University, Shanghai, China, [2] Shanghai Institute of Biochemistry and Cell Biology, Chinese Academy of Sciences, University of Chinese Academy of Sciences, Shanghai, China, [3] Department of Respirology, Shanghai Public Health Clinical Center, Fudan University, Shanghai, China, [4] Department of Otolaryngology—Head and Neck Surgery, Bethune International Peace Hospital, Shijiazhuang, China

OPEN ACCESS

Edited by:
Jorge A. R. Salvador,
University of Coimbra, Portugal

Reviewed by:
Wenyue Sun,
National Cancer Institute, United States
Tianrun Liu,
Sun Yat-sen University, China
Yifan Wang,
University of Texas Southwestern Medical Center, United States

***Correspondence:**
Liang Zhou
Zl76856@126.com

[†]These authors have contributed equally to this work

Specialty section:
This article was submitted to Head and Neck Cancer, a section of the journal Frontiers in Oncology

Received: 22 December 2019
Accepted: 07 December 2020
Published: 05 February 2021

Citation:
Xu C, Zhang Y, Shen Y, Shi Y, Zhang M and Zhou L (2021) Integrated Analysis Reveals ENDOU as a Biomarker in Head and Neck Squamous Cell Carcinoma Progression. Front. Oncol. 10:522332. doi: 10.3389/fonc.2020.522332

Background: Head and neck squamous cell carcinoma (HNSCC) is a leading cancer with high morbidity and mortality worldwide. The aim is to identify genes with clinical significance by integrated bioinformatics analysis and investigate their function in HNSCC.

Methods: We downloaded and analyzed two gene expression datasets of GSE6631 and GSE107591 to screen differentially expressed genes (DEGs) in HNSCC. Common DEGs were functionally analyzed by Gene ontology and KEGG pathway enrichment analysis. Protein-protein interaction (PPI) network was constructed with STRING database and Cytoscape. *ENDOU* was overexpressed in FaDu and Cal-27 cell lines, and cell proliferation and migration capability were evaluated with MTT, scratch and transwell assay. The prognostic performance of ENDOU and expression correlation with tumor infiltrates in HNSCC were validated with TCGA HNSCC datasets.

Results: Ninety-eight genes shared common differential expression in both datasets, with core functions like extracellular matrix organization significantly enriched. 15 genes showed prognostic significance, and *COBL* and *ENDOU* serve as independent survival markers in HNSCC. In-vitro *ENDOU* overexpression inhibited FaDu and Cal-27 cells proliferation and migration, indicating its tumor-suppressing role in HNSCC progression. GSEA analysis indicated *ENDOU* down-stream pathways like DNA replication, mismatch repair, cell cycle and IL-17 signaling pathway. *ENDOU* showed relative lower expression in HNSCC, especially HPV-positive HNSCC samples. At last, *ENDOU showed* negative correlation with tumor purity and tumor infiltrating macrophages, especially M2 macrophages.

Conclusion: This study identified *ENDOU* as a biomarker with prognostic significance in HNSCC progression.

Keywords: head and neck squamous cell carcinoma, *ENDOU*, prognosis, tumor suppressor, bioinformatics

INTRODUCTION

HNSCC is a leading cancer with high morbidity and mortality worldwide (1, 2). It can be categorized by the area of the head or neck in which they begin, like oral cavity, pharynx, oropharynx, larynx, paranasal sinuses and nasal cavity and salivary glands. The most important pathogenic risk factors of HNSCC are tobacco and alcohol consumption and at least 75% of head and neck cancers are attributed to them (3). Molecular pathogenesis is still a comprehensive but largely not understood problem in HNSCC. Due to the phenotypic heterogeneity of each individual patient, it is hard to match suitable and effective treatments. Over the past decades, the development of high-throughput sequencing, increasing researchers have focused on the biological genetic functions of genes involved in the tumor-genesis of HNSCC (4–12).They have illustrated a lot of large-scale gene-expression profiles of HNSCC samples. The first successful therapeutic strategy for HNSCC was to inhibit the epidermal growth factor receptor (EGFR). In-depth understanding of the molecular carcinogenesis of HNSCC could help to develop novel and accurate treatment strategies for individual HNSCC patient.

The Cancer Genome Atlas (TCGA) network group of NIH generated comprehensive genomic characterization of HNSCC in 2015 (5). It profiled 279 HNSCC samples and provided a large-scale landscape of genetic and epigenetic characterizations of HNSCC, pointing the pivotal roles of *PIK3CA*, *TRAF3*, *E2F1*, *TP53*, *NOTCH* and other regulators in Wnt signaling pathways in tumor-genesis of HNSCC. Before that, Chen and his colleagues also compared 22-paired samples of HNSCC and normal tissues in 2004 (13). They found critically altered genes in the pathogenic processes of HNSCC through combinatorial analysis of microarray data. However, HNSCC is a cancer with complicated pathogenesis as well as diverse tissue origins. At present, most researches of HNSCC focus on star pathways or molecules, like PI3K signaling pathway or *TP53* protein. Therefore, it's necessary and urgent to dig out more potential targets for HNSCC treatment.

In this study, we downloaded two published and well-generated profiling datasets about HNSCC tumor and normal tissues from the Gene Expression Omnibus (GEO). Then novel potential prognostic markers were dig out to find more avenues to effective clinical treatments of HNSCC *via* multiple bioinformatics analysis, including biological process functional annotation and pathway enrichment analysis, protein-protein interaction network analysis as well as gene expression profiling interactive survival analysis. Gene *ENDOU* showed differential expression, correlation with tumor infiltrates and prognostic significance, and were functionally investigated.

MATERIALS AND METHODS

Data Collection

The expression profiles of RNAs were screened from the National Center of Biotechnology Information Gene Expression Omnibus (http://www.ncbi.nlm.nih.gov/gds/). The GSE6631 dataset is composed of 22 paired HNSCC tumor and normal samples. The platform is GPL8300 [HG_U95Av2] Affymetrix Human Genome U95 Version 2 Array. The GSE107591 dataset contains 23 normal and 24 tumor tissues. The platform is GPL6244 [HuGene-1_0-st] Affymetrix Human Gene 1.0 ST Array.

Identification of Differentially Expressed Genes (DEGs)

We utilized quartile normalization algorithm to subtract and correct background of these downloaded datasets firstly (14). Then we filtered probes without corresponding gene symbols and calculated the average value of gene symbols with multiple probes. We further used *R* software *Limma* package to screen DEGs by filtering *p.adj* value of student's t-test and fold change (FC) (15). Finally, with a threshold of p.adj-value <0.05 and absolute value of FC >2 (16, 17), volcano plot was performed by using R software ggplot2 package to identify the DEGs with statistical significance between two groups. Hierarchical clustering and combined analyses were performed for the DEGs.

Functional Analysis of DEGs in HNSCC Pathogenesis

GO enrichment analyses of differentially expressed mRNAs were implemented with annotation, visualization and integrated discovery (DAVID) (http://david.abcc.ncifcrf.gov/). GO terms (including Molecular Function, Biological Processes and Cellular Components) with p-value less than 0.05 were considered significantly enriched by DEGs. KEGG is a database resource for understanding high-level functions and effects of the biological systems (http://www.genome.jp/kegg/). DAVID was also used to test the significantly statistical enrichment of DEGs in KEGG pathways. Cytoscape (version 3.40) was used to visualize the relationships between biological processes terms and DEGs.

Protein-Protein Interaction (PPI) Network Analysis

Protein-protein interaction analysis was further conducted in STRING database (https://string-db.org/). The higher or larger score protein-protein interaction pairs were selected to construct PPI networks. Then, the regulatory relationships between genes were visualized *via* Cytoscape (version 3.4.0) (18). The sub-networks were extracted from the whole PPI network by using MCODE app.

Survival Analysis and Tumor Filtrating Immune Cells Analysis

To conduct survival analysis, clinical data and RNA expression data from TCGA dataset were downloaded. Univariate and Multivariate Cox analysis was conducted with SPSS, and forest plot was conducted with R. Then Kaplan-Meier survival plot and LogRank analysis was done. The correlation of *ENDOU* expression with tumor infiltrating cells were conducted with TIMER (https://cistrome.shinyapps.io/timer/) (19). For

macrophage markers, *CCL2*, *CD68*, and *IL10* were used for tumor associated macrophages (TAM), *NOS2*, *IRF5*, and *PTGS2* for M1 macrophages and *CD163*, *VSIG4*, and *MS4A4A* for M2 macrophages, referring to previous study (20).

Cells Culture

The FaDu and Cal-27 human carcinoma cell lines were propagated and carefully maintained in our laboratory. FaDu and Cal-27 cells were cultured in Dulbecco's modified Eagle's medium supplemented with 10% fetal bovine serum at 37°C in a humid atmosphere containing 5% CO2.

Lentivirus Mediated *ENDOU* Overexpression

CDS of *ENDOU* (NM_001172440) was inserted into a recombinant lentiviral expression vector (pGSIL) containing green fluorescent proteins (GFP) tag. To generate lentiviral particles, the recombinant expression plasmid was co-transfected with a packaging plasmid system (psPAX2 and pMD2G) into FaDu and Cal-27 cells, and viral particles were collected after 48 h. FaDu and Cal-27 cells were infected with *ENDOU* lentiviral vector or with a negative control (NC) for 24 h. The infection efficiency was preliminarily assessed in each experiment under a fluorescence microscope and then measured by sorting GFP-positive cells by flow cytometry (Beckman Coulter, USA). The stably infected cells were expanded and harvested for further experiments. The overexpression of *ENDOU* was examined with western blotting, using monoclonal antibody (Abcam, Cambridge, MA, USA). GAPDH was used as the house-keeping gene.

MTT Assay

The cell proliferation activity of FaDu and Cal-27 cells was examined with MTT Cell Proliferation and Cytotoxicity Assay Kit (Dojindo Laboratories, Tokyo, Japan). The cells were incubated for 24, 48, 72, and 96 h. After incubation, the MTT solution was removed and replaced with dimethyl sulfoxide (DMSO; 150 μl, 4%; Sigma). A microplate reader (Bio-Tek, Instruments, Neufahrn, Germany) was used to measure the absorbance at 570 nm.

Transwell Assay

Cells in logarithmic growth phase were seeded at the upper transwell chamber insert (Corning, USA) at a density of 2 × 104 cells per well. The chamber was placed in a 24- well plate in which the upper chamber contained serum-free cell culture medium and the lower chamber contained 10% FBS complete medium. The culture was continued for 24 h. The medium was discarded, and stained with a crystal violet solution to observe the number of migrated cells.

Scratch Wound Healing Assay

FaDu and Cal-27 cells were grown in complete growth medium until 90% confluence after transfection. A 3 mm wound was introduced across the diameter of each plate. Cell migration was observed by microscopy at 24 h.

Statistical Analysis

Student's t-test or ANOVA were performed to analyze the differential expression. Kaplan-Meier analysis was used to estimate overall survival rate or time; the differences between the survival curves were analyzed using the log-rank test. In all analyses, $P<0.05$ was considered to indicate a statistically significant result. Continuous data are presented as the mean ± standard deviation.

RESULTS

DEGs Identification in Two HNSCC Datasets

Two GEO datasets of HNSCC, GSE6631 and GSE107591 were first normalized (**Figure S1**) and analyzed to acquire significantly differential expressed genes (DEGs), respectively. Both datasets contains more than twenty tumor and normal samples, and with the same microarray platform of Affymetrix gene expression microarray. The GSE107591 dataset contains 23 normal and 24 tumor tissues. As GSE6631 comprises 22 paired HNSCC tumor and normal samples, we conducted paired comparison. With a threshold of p.adj-value <0.05 and absolute value of FC >2, the expression of DEGs in HNSCC tumor and normal tissues were shown in **Figure 1**. We found 91 genes significantly up-regulated and 121 genes down-regulated in GSE6631 dataset (**Figures 1A, C**). For GSE107591, we found 194 up-regulated and 278 down-regulated genes in HNSCC tumor samples compared with normal tissues (**Figures 1B, D**).

Functional Analysis of 98 Common DEGs Enriched Hub Pathways in HNSCC

To further figure out the roles of these DEGs in HNSCC, we searched the common DEGs both altered in these two datasets. A total of 98 DEGs (37 up-regulated and 61 down-regulated DEGs) showed dysregulation in both datasets (**Figure 2A**). To further detailed unravel the function of these common DEGs in HNSCC, we constructed protein-protein interaction (PPI) network *via* STRING database (https://string-db.org/). The genes with larger scores were selected to construct PPI networks (**Figure 2B**), and their function was uploaded to DAVID database for KEGG pathway and GO enrichment analysis. As shown in **Figure 2C**, biological processes with the largest number of common DEGs and smallest p-value includes extracellular matrix disassemble, collagen catabolic process, extracellular matrix organization, cell adhesion, aging and angiogenesis. As for the KEGG enrichment analysis in **Figure 2C**, not surprisingly, items like Pathways in cancer, ECM-receptor interaction, Focal adhesion and PI3K-Akt signaling pathways are significantly enriched and showed the largest number of common DEGs. The PI3K-Akt signaling was inappropriately activated in many cancers, including head and neck cancer (21). Somatic mutations of *PIK3CA* had been also described before and are found in about 15% of HNSCC (22–24). These findings might help us find more new therapy targets for HNSCC.

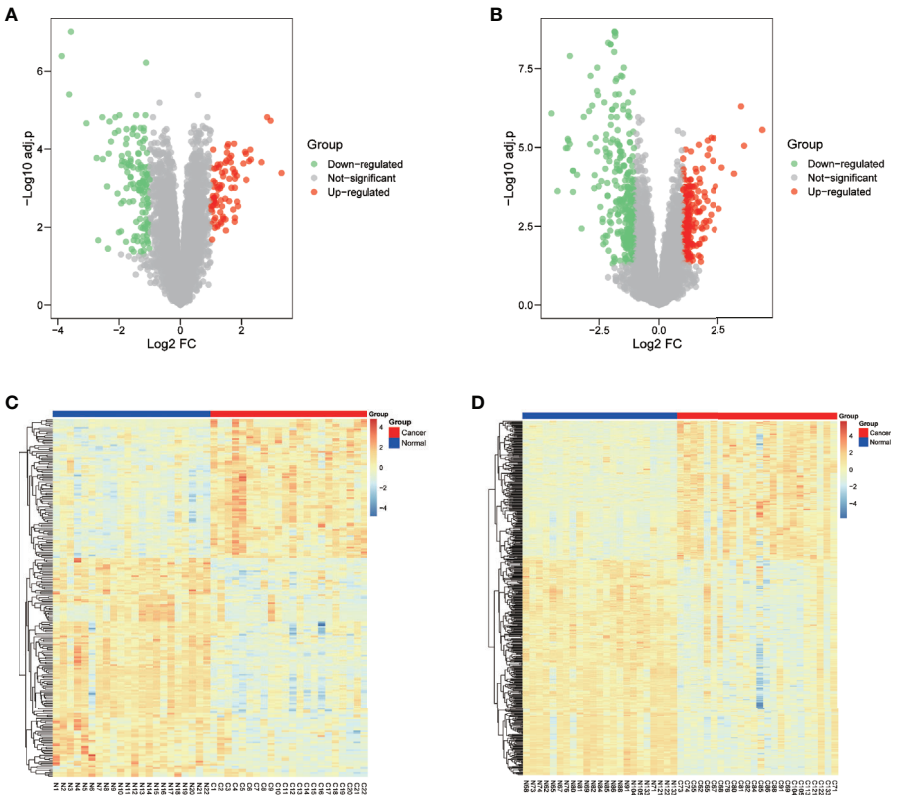

FIGURE 1 | Differentially expressed genes (DEGs) of normal and Head and neck squamous cell carcinoma (HNSCC) tissue from GSE6631 and GSE107591. **(A)** Volcano plot showing significantly deregulated genes in GSE6631; **(B)** Volcano plot showing significantly deregulated genes in GSE107591; **(C)** Heatmap clustering of all DEGs in normal and HNSCC tissue from GSE6631; **(D)** Heatmap clustering of all DEGs in normal and HNSCC tissue from GSE107591; UP, genes with significant increased expression in HNSCC group were labeled in red. DW, genes with significant decreased expression in HNSCC group were labeled in green, genes with no different were in HNSCC group were labelled in grey.

Clinical Significance of 15 Genes Were Analyzed With TCGA HNSCC Datasets

To further explore the clinical significance of DEGs in HNSCC, we first validated the expression of 98 common DEGs with TCGA HNSCC dataset. A total of 2230 DEGs were acquired in HNSCC datasets and 92 genes (in 98 common DEGs, **Table S1**) showed significant dysregulation in all datasets (**Figures 3A, B**). Then the prognostic significance of the 92 DEGs were analyzed with univariate analysis. As shown in **Figure 3C**, 15 genes showed promising performance with HNSCC overall survival. Nine genes of *LAMC2* (HR=1.5, P=0.00319), *SEMA3C* (HR=1.35, P=0.029), *FAP* (HR=1.42, P=0.0112), *COBL* (HR=1.38, P=0.0184), *SERPINE1* (HR=1.61, P=0.000616), *PLAU* (HR=1.49, P=0.00373), *MYO1B* (HR=1.35, P=0.028), *DUSP5* (HR=1.31, P=0.0498), *LAMB3* (HR=1.49, P=0.00407) were hazardous, and 6 genes of *CEACAM1* (HR=0.709, P=0.00049), *CEACAM6* (HR=0.751, P=0.0362), *ALDH3A1* (HR=0.763, P=0.0478), *ENDOU* (HR=0.711, P=0.0135), *SPINK5* (HR=0.736, P=0.0249) and *METTL7A* (HR=0.765, P=0.0494) were potential protective markers. At last, the multivariate analysis was conducted and only *COBL* and *ENDOU* showed significance (**Figure 3D**), indicating *COBL* (HR=1.55, P=0.00233) and *ENDOU* (HR=0.712, P=0.0361) as independent prognostic overall markers in HNSCC, and the Kaplan-Meier overall survival plot of *COBL* and *ENDOU* was shown in **Figures 3E, F**, and other 13 genes were shown in **Figure S2**.

Cordon-Bleu WH2 Repeat Protein (*COBL*) contains WH2 domains (WASP, Wiskott-Aldrich syndrome protein, homology domain-2) and has been reported to play an important role in the reorganization of the actin cytoskeleton (25–27). In acute lymphoblastic leukemia, *COBL* is a hotspot for *IKZF1* deletions (28), and we will study the function of *COBL* in HNSCC in the future. *ENDOU*, also known as *PP11* (Placental Protein 11), encodes uridylate-specific endoribonuclease expressed in the placenta. *ENDOU was reported to* displays RNA binding capability and cleaves single stranded RNA in a Mn (2+)-dependent manner at uridylates (29). Studies of *ENDOU* in cancer dates back to 1980s (30, 31). *ENDOU* was annotated with the function of in proteolysis (Gene Ontology term GO:0006508), and members like matrix metalloproteinases (MMPs) play an important function in cancer progression, by depredating extracellular matrix. Considering the significant enrichment of functional items of extracellular matrix in **Figures 2C, D**, we chose *ENDOU* for the following study.

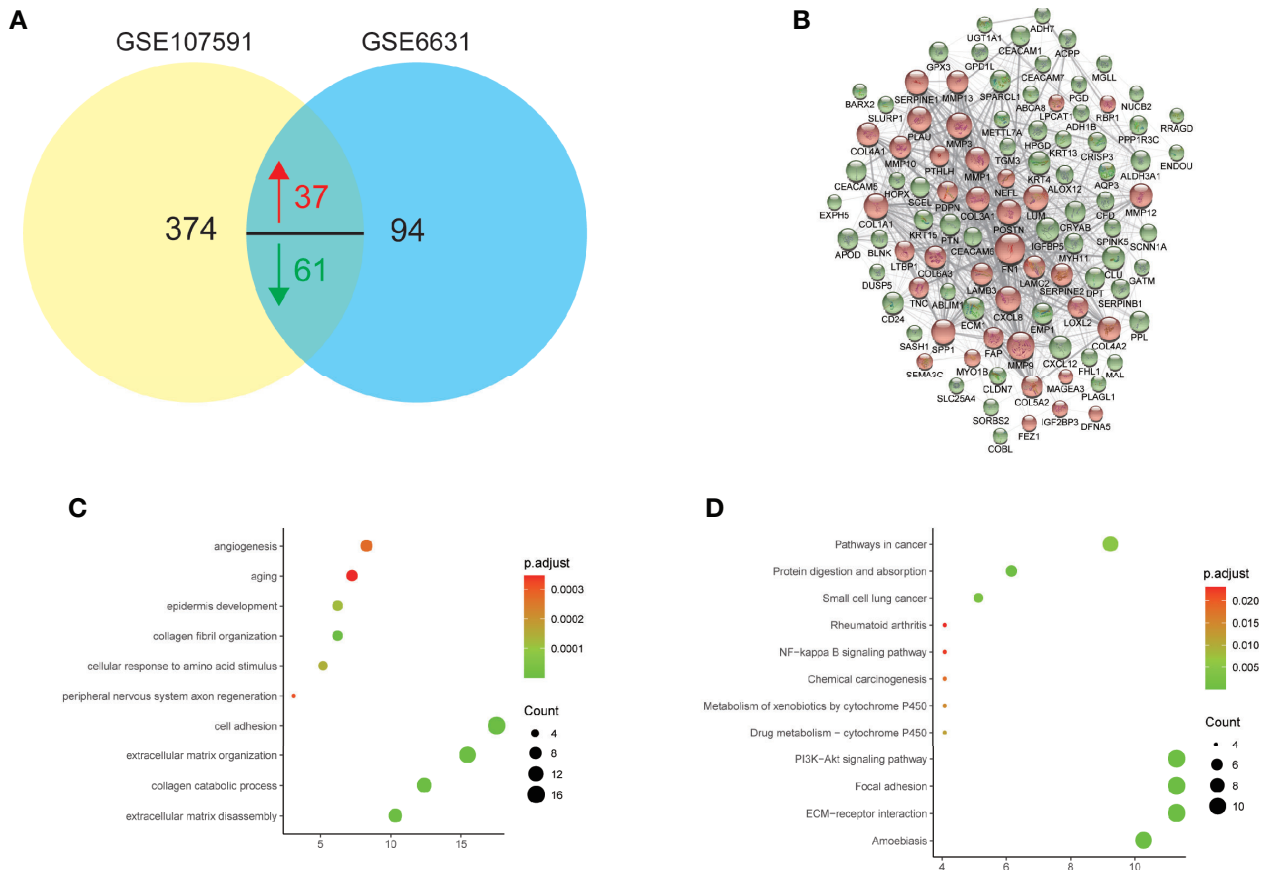

FIGURE 2 | Gene Ontology (GO) and KEGG pathway analysis of 98 commonly deregulated genes in GSE6631 and GSE107591. P value, count and ratio of top 10 enriched functional items were shown. **(A)** Venn plot of 98 commonly deregulated genes in GSE6631 and GSE107591; **(B)** Protein-protein interaction (PPI) network of 98 commonly deregulated genes; **(C)** Top 10 enriched Gene Ontology biological processes, including extracellular matrix disassembly were significantly identified; **(D)** Top 10 enriched KEGG pathways including ECM-receptor interaction were shown.

At last, the clinical association between ENDOU expression and clinicopathological variables in TCGA HNSCC patients was analyzed. As shown in **Table 1**, ENDOU expression showed significant correlation with survival status (P=0.03), gender (P=0.011), alcohol history (P=0.017), clinical N stage (P=0.001), lymphovascular invasion status (P=0.001), neoplasm histologic grade (P<0.001) and pathologic N stage (P<0.001). In sum, *ENDOU* may serve as an independent prognostic marker in HNSCC.

ENDOU Inhibits HNSCC Cancer Cell Proliferation and Migration *In Vitro*

As *ENDOU* shows consistent lower expression and hazardous prognostic significance in HNSCC, to explore the function of *ENDOU* in HNSCC, we conducted in-vitro over-expression (OE) studies in two cell lines of Fadu and Cal-27. The proliferation and migration capability was examined. As shown in **Figure 4A**, the proliferation capability of Fadu and Cal-27cells in *ENDOU* overexpression group was significantly decreased. Then wound healing assay and transwell assay was applied to study the effect of *ENDOU* overexpression on cell migration and invasion. In **Figures 4B, C**, the migration distance of *ENDOU* overexpression group was significantly larger than vector groups, and cells numbers was significantly decreased, implying that *ENDOU* may serve as a tumor suppressor in HNSCC.

To explore the potential mechanism of *ENDOU* as a tumor suppressor in HNSCC, we applied Gene Set Enrichment Analysis (GSEA) analysis to enrich *ENDOU* related KEGG pathways and biological processes. As shown in **Figure 5**, DNA replication, mismatch repair, cell cycle and IL-17 showed significant enrichment, which supported the cellular phenotype of *ENDOU* in HNSCC.

ENDOU Expression Showed Significant Correlation With Macrophages in HNSCC

In addition to HNSCC, we analyzed the expression of *ENDOU* in other cancer types, as shown in **Figure 6A**, decreased expression was also observed in bladder cancer (BLCA), breast cancer (BRCA), liver cancer (LIHC) and other cancer samples, indicating a universal role of *ENDOU in cancer. For HNSCC*, Human papillomavirus (HPV) positive HNSCC has a far better prognosis than HPV negative HNSCC, and HPV infection has

TABLE 1 | Clinical association between ENDOU expression and clinicopathological variables in HNSCC patients.

Characteristics	n	No. of Patients (%)	ENDOU		
			Low	High	*p*
Status	500				0.03
Alive		282(56.4)	129	163	
Death		218(43.6)	121	97	
Gender	500				0.011
Female		133(26.6)	54	79	
Male		367(73.4)	196	171	
Age	499				0.616
<60		220(44.1)	107	113	
≥60		279(55.9)	142	137	
Alcohol_history	489				0.017
No		157(32.1)	66	91	
Yes		332(67.9)	178	154	
Clinical_N	478				0.001
N0		239(50)	101	138	
N1-3		239(50)	139	100	
Clinical_T	485				0.731
T1-2		176(36.3)	86	90	
T3-4		309(63.7)	156	153	
Clinical_stage	486				0.096
I-II		114(23.5)	49	65	
III-IV		372(76.5)	193	179	
Lymph_node_count	407				0.52
Low		203(49.9)	102	101	
High		204(50.1)	96	108	
Lymphovascular_invasion_present	339				0.001
No		219(64.6)	95	124	
Yes		120(35.4)	74	46	
Neoplasm_histologic_grade	481				0
G1-2		360(74.8)	151	209	
G3-4		121(25.2)	88	33	
Recurrence	442				0.39
No		317(71.7)	153	164	
Yes		125(28.3)	66	59	
Pathologic_N	407				0
N0		171(42.0)	63	108	
N1-3		236(58.0)	132	104	
Pathologic_T	444				0.799
T1-2		177(39.9)	84	93	
T3-4		267(60.1)	130	137	
Pathologic_stage	435				0.133
I-II		98(22.5)	41	57	
III-IV		337(77.5)	170	167	
Perineural_invasion	351				0.311
No		186(53.0)	88	98	
Yes		165(47.0)	87	78	
Smoker	490				0.914
No		111(22.7)	56	55	
Yes		379(77.3)	189	190	

been linked with intratumoral immune cell infiltrates (e.g. IL-17 +CD8+T lymphocytes) in HNSCC (32, 33). Then we compared the expression of *ENDOU* in HPV-negative and HPV-positive HNSCC samples, and *ENDOU* showed significant lower expression in HPV-positive HNSCC samples (**Figure 6A**). At last, we analyzed the expression of *ENDOU* with tumor immune infiltrates, in HPV-negative and HPV-positive HNSCC samples. As shown in **Figure 6B**, *ENDOU* showed significant negative correlation with neutrophils, dendritic cells and especially macrophages. As the correlation was most significant in tumor infiltrating macrophages, correlation of TAMs, M1 and M2 macrophages markers with *ENDOU* expression were analyzed. As shown in **Figure 6C**, the markers of M2 macrophages (*CD163*, *VSIG4*, and *MS4A4A*) all showed significant negative correlation coefficient with *ENDOU*, implicating potential role of *ENDOU* in tumor infiltrating M2 macrophages.

DISCUSSION

At present, head and neck cancer is the sixth most common cancer with a poor prognosis and high mortality over the world

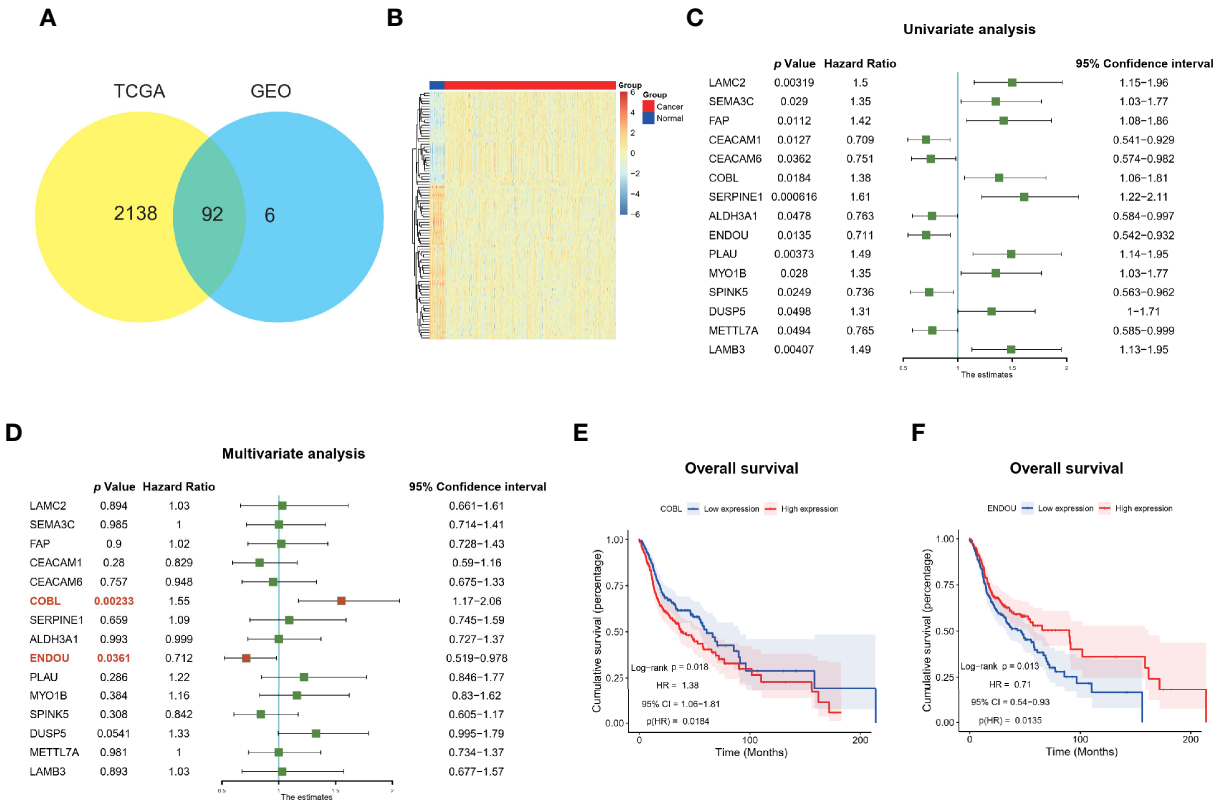

FIGURE 3 | Prognostic significance of genes in The Cancer Genome Atlas (TCGA) HNSCC dataset. **(A)** Ninety-two genes showed consistent dysregulation in TCGA dataset, and were shown with Venn plot; **(B)** Heatmap of the dysregulated 92 genes in TCGA HNSCC cancer and normal samples; **(C)** Univariate analysis identified 15 genes with prognostic significance in TCGA HNSCC datasets; **(D)** Multivariate analysis further identified COBL and ENDOU as independent prognostic markers in HNSCC; **(E, F)** Kaplan-Meier overall survival plot of COBL **(E)** and ENDOU **(F)** in HNSCC.

accounting for approximately 4% of all cancers in the United States (34). HNSCC is a kind of highly heterogeneous malignancy and appropriate clinical treatments remain a major challenge for HNSCC because of heterogeneity. Hence, personalized care for HNSCC patients requires a better understanding of the molecular mechanism of HNSCC. Though some biomarkers in head and neck squamous cell carcinoma progression have been reported yet (35, 36), accepted biomarkers for HNSCC prognosis in the clinic is still raw. Effective prognostic care for HNSCC patients requires a better understanding of the molecular mechanism. With the recent development of next generation sequencing and other "omics" profiling methods, we began to focus on genomic analysis of HNSCC to illustrate the detailed or new causes of HNSCC pathogenesis and to try to develop new markers for treatments of this cancer.

In the present study, gene expression data of HNSCC were downloaded from GEO, which revealed significant differences between survival status and clinical treatments of HNSCC patients. Hence, we reanalyzed two published microarray datasets, GSE6631 and GSE107591 in this study. Finally, we found 98 common DEGs between 45 normal and 46 HNSCC tumor samples. Gene functional annotation and pathway enrichment analysis of these DEGs showed that extracellular matrix disassemble collagen catabolic process, extracellular matrix organization, cell adhesion, aging and angiogenesis were enriched in HNSCC. These results revealed that our bioinformatics analysis may help a better understanding of the regulation of these genes in HNSCC. There are also many researchers focusing on extracellular matrix organization play an important role in HNSCC (37, 38). They pointed out that extracellular matrix organization was one of the most frequently altered pathways in HNSCC, consistent with our results.

By integrating the clinical information in TCGA, we screened 9 hazardous and 6 protective prognostic markers. Of the 15 genes, *LAMC2* (39–41), *SERPINE1* (41–43), *PLAU* (44), *MYO1B* (45), *LAMB3* (46), *CEACAM1* (41, 47), *CEACAM6* (48, 49), *ALDH3A1* (50) and *SPINK5* (51) has been reported as HNSCC prognostic markers, and in this study, we first uncovered the clinical significance of *SEMA3C*, *FAP*, *COBL*, *DUSP5*, *ENDOU* and *METTL7A* with HNSCC survival. Semaphorin 3C (*SEMA3C*) has been reported to play a pivotal role in tumor microenvironment driven neuroblastoma metastasis and progression (52). Fibroblast Activation Protein Alpha (*FAP*) was proven to serve as a marker in metastatic prostate cancer (53), pancreatic cancer (54) and ovarian cancer (55). Cordon-Bleu WH2 Repeat Protein (*COBL*) has been reported to play an

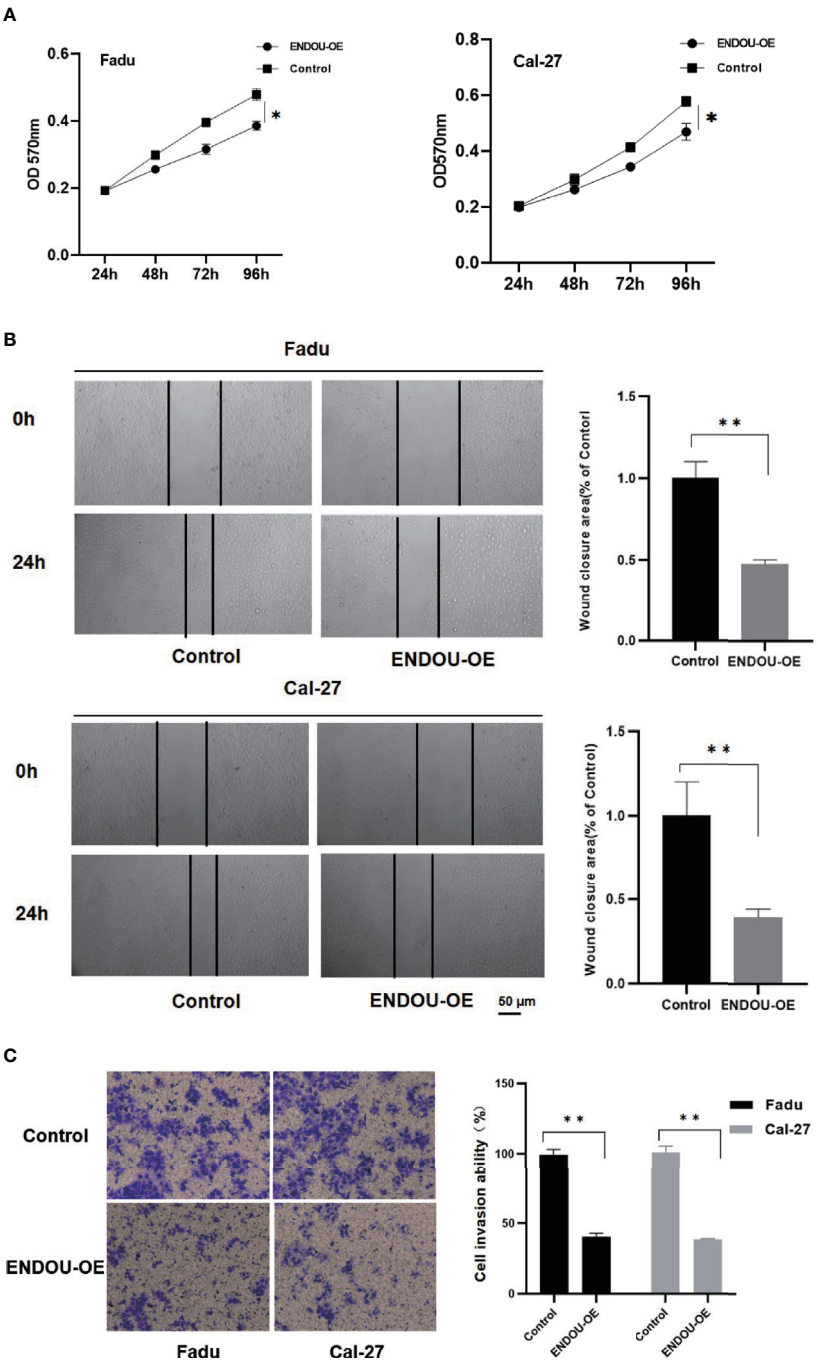

FIGURE 4 | ENDOU overexpression inhibits Fadu and Cal-27 cells proliferation and migration *in vitro*. **(A)** MTT assay results indicated *ENDOU* overexpression (OE) inhibited Fadu and Cal-27 cells proliferation. Each assay was replicated three times. *P < 0.05. **(B)** Scratch healing assay showed decreased migration capability in *ENDOU* overexpressing Fadu and Cal-27 cells. Each assay was replicated three times. *P < 0.05. **(C)** Transwell assay showed that *ENDOU* overexpression (OE) attenuated the invasion capability of Fadu and Cal-27 cells. Each assay was replicated three times. *P < 0.05, **P < 0.01.

important role in the reorganization of the actin cytoskeleton (25–27), and as a hotspot for *IKZF1* deletions (28) in acute lymphoblastic leukemia. Dual Specificity Phosphatase 5 (*DUSP5*) is tumor suppressor in ovarian cancer (56). Methyltransferase Like 7A (*METTL7A*) promoted cell viability and reduced apoptosis following methotrexate in choriocarcinoma (57). Further functional and mechanism studies of *SEMA3C*, *FAP*, *COBL*, *DUSP5*, *ENDOU*, and *METTL7A* may provide more detailed information to reveal their potential role as therapeutic targets in HNSCC.

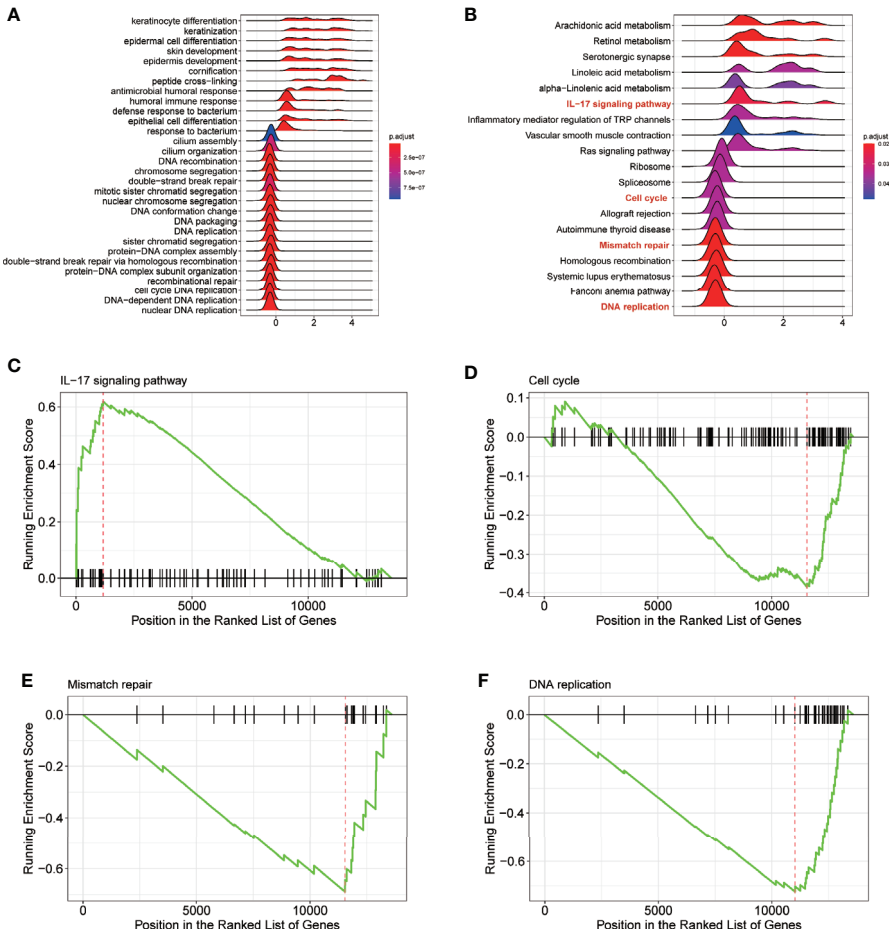

FIGURE 5 | Gene Set Enrichment Analysis (GSEA) analysis reveals DNA replication, Mismatch repair, Cell cycle and IL-17 signaling pathway as potential ENDOU functional mechanism. **(A)** GSEA analysis of Gene ontology enrichment items of ENDOU; **(B)** GSEA analysis of KEGG pathway enrichment items of ENDOU; **(C)** GSEA Enrichment plot of IL-17 signaling pathway in head and neck squamous cell carcinoma (HNSCC); **(D)** GSEA Enrichment plot of Cell cycle in HNSCC; **(E)** GSEA Enrichment plot of Mismatch repair in HNSCC; **(F)** GSEA Enrichment plot of DNA replication in HNSCC.

Then, *ENDOU* not only showed significant lower expression in HNSCC cancer samples (compared with normal samples), but also decreased level in higher stage cancer samples, implicating its tumor suppressing function in HNSCC occurrence and progression. *ENDOU*, also known as *PP11* (Placental Protein 11), encodes uridylate-specific endoribonuclease expressed in the placenta. *ENDOU was reported to* displays RNA binding capability and cleaves single stranded RNA in a Mn (2 +)-dependent manner at uridylates (29). Studies of *ENDOU* in cancer dates back to 1980s (30, 31), and this is the first time investigating the role of *ENDOU* in HNSCC. In this study, *ENDOU* was negatively correlated with tumor purity and then were functionally investigated in cancer cell lines. MTT, scratch healing and transwell assay demonstrated that *ENDOU* indeed inhibited the proliferation and migration capability, supporting it tumor suppressing role in HNSCC cancer cells. Meanwhile, there are several limits in this part. First, the effect of *ENDOU* overexpression can be validated in other HNSCC cell lines, and if possible, the impact of *ENDOU* silencing or mutation on HNSCC cell lines to support the conclusion. Secondly, an *in vivo* study of *ENDOU* would provide more solid evidence, as the function of genes *in vitro* and *in vivo* are not always consistent. Lastly, the underlying mechanism of *ENDOU* inhibiting FaDu cells proliferation and migration may be explored.

At last, tumor infiltrating immune cells in tumor microenvironment plays a pivotal role in HNSCC progression and prognosis prediction (58, 59). In this study, we found *ENDOU* negative correlates with tumor infiltrating neutrophils, dendritic cells and macrophages, especially M2 macrophages. Macrophages were reported to be involved in HNSCC metastasis (60–62), chemotherapy (63) and prognosis (64). Macrophages were polarized into M1 and M2 subtypes depending on their environment (65), and were reported to be functionally distinct in cancer (66). M2 polarized macrophages were found to be correlated with poor prognosis in nasopharyngeal carcinoma patients (67). HNSCC cancer cells were found to contribute to M2 polarization in several ways, like secreting microRNA-21 abundant exosomes (68) and lactic acid (69). Based on the

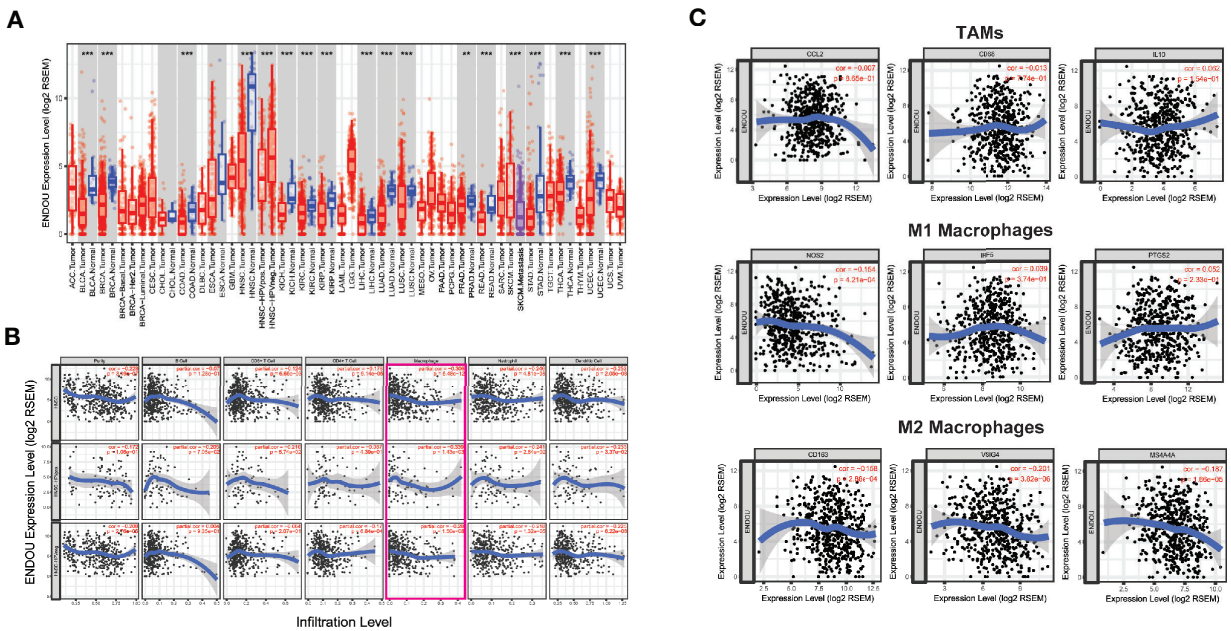

FIGURE 6 | *ENDOU* showed significant down-regulation in head and neck squamous cell carcinoma (HNSCC) development and correlates with tumor infiltrating immune cells. **(A)** *ENDOU* was significantly downregulated in HNSCC samples, compared with normal tissue. *ENDOU* showed significant lower expression in HPV-positive HNSCC samples. Decreased expression was also observed in bladder cancer (BLCA), breast cancer (BRCA), liver cancer (LIHC) and other cancer samples. **P < 0.01; ***P < 0.001; **(B)** The correlation of *ENDOU* expression with tumor infiltrates were analyzed, and *ENDOU* expression showed significant negative correlation with tumor purity, macrophages, neutrophils and dendritic cells; **(C)** *ENDOU* expression showed negative correlation with M2 macrophages markers, including *CD163*, *VSIG4*, and *MS4A4A*.

founding that tumor suppressor gene *ENDOU* was negatively correlated with M2 markers of *CD163*, *VSIG4*, and *MS4A4A*, we speculated that *ENDOU* may also inhibit macrophages M2 polarization in tumor microenvironment.

In sum, our multiple bioinformatics analysis identified 98 genes with core functions like extracellular matrix organization significantly enriched. 15 genes showed prognostic significance, and *COBL* and *ENDOU* serve as independent survival markers in HNSCC. In-vitro *ENDOU* overexpression inhibited FaDu and Cal-27 cells proliferation and migration, indicating its tumor-suppressing role in HNSCC progression. GSEA analysis indicated *ENDOU* down-stream pathways like DNA replication, mismatch repair, cell cycle and IL-17 signaling pathway. *ENDOU* showed relative lower expression in HNSCC, especially HPV-positive HNSCC samples. At last, *ENDOU showed* negative correlation with tumor purity and tumor infiltrating macrophages, especially M2 macrophages. It was the first time that *ENDOU* was identified as a tumor suppressor, with prognostic significance and negative correlation with tumor infiltrating M2 macrophages. However, further biological and basic studies are needed to validate our findings.

DATA AVAILABILITY STATEMENT

All datasets generated for this study are included in the article/ **Supplementary Material**.

ETHICS STATEMENT

The experiment was approved the Ethics Committee of Eye Nose and Throat Hospital, Fudan University.

AUTHOR CONTRIBUTIONS

CX, YZ, and LZ conceived and designed the study. YZ analyzed the data. YPS, YS, and MZ performed the experiments. YZ and LZ wrote the paper. CX and YPS reviewed and edited the manuscript. All authors contributed to the article and approved the submitted version.

FUNDING

This study was supported by Natural Science Foundation ofShanghai (16ZR1419300), the National Natural Science Foundation (81972529) and Science and Technology Commission of Shanghai Municipality (9411961300).

SUPPLEMENTARY MATERIAL

The Supplementary Material for this article can be found online at: https://www.frontiersin.org/articles/10.3389/fonc.2020.522332/full#supplementary-material

Supplementary Figure 1 | Normalization and MDS plot of GSE6631 and GSE107591; **A, B**) Normalization boxplot of GSE6631 and GSE107591; **C, D**) MDS plot of GSE6631 and GSE107591.

Supplementary Figure 2 | Kaplan-Meier survival plot of **(A)** PLAU; **(B)** ALDH3A1; **(C)** SERPINE1; **(D)** CEACAM6; **(E)** CEACAM61; **(F)** LAMB3; **(G)** METTL7A; **(H)** DUSP5; **(I)** SPINK5; **(J)** MYO1B; **(K)** FAP; **(L)** SEMA3C; **(M)** LAMC2 in HNSCC.

REFERENCES

1. Jou A, Hess J. Epidemiology and Molecular Biology of Head and Neck Cancer. *Oncol Res Treat* (2017) 40(6):328–32. doi: 10.1159/000477127
2. Kamangar F, Dores GM, Anderson WF. Patterns of cancer incidence, mortality, and prevalence across five continents: defining priorities to reduce cancer disparities in different geographic regions of the world. *J Clin Oncol* (2006) 24(14):2137–50. doi: 10.1200/JCO.2005.05.2308
3. Moskovitz JM, Moy J, Seiwert TY, Ferris RL. Immunotherapy for Head and Neck Squamous Cell Carcinoma: A Review of Current and Emerging Therapeutic Options. *Oncologist* (2017) 22(6):680–93. doi: 10.1634/theoncologist.2016-0318
4. Agrawal N, Frederick MJ, Pickering CR, Bettegowda C, Chang K, Li RJ. Exome sequencing of head and neck squamous cell carcinoma reveals inactivating mutations in NOTCH1. *Science* (2011) 333(6046):1154–7. doi: 10.1126/science.1206923
5. Cancer Genome Atlas N. Comprehensive genomic characterization of head and neck squamous cell carcinomas. *Nature* (2015) 517(7536):576–82. doi: 10.1038/nature14129
6. Diehn M, Eisen MB, Botstein D, Brown PO. Large-scale identification of secreted and membrane-associated gene products using DNA microarrays. *Nat Genet* (2000) 25(1):58–62. doi: 10.1038/75603
7. El-Naggar AK, Kim HW, Clayman GL, Coombes MM, Le B, Lai S. Differential expression profiling of head and neck squamous carcinoma: significance in their phenotypic and biological classification. *Oncogene* (2002) 21(53):8206–19. doi: 10.1038/sj.onc.1206021
8. Lemaire F, Millon R, Young J, Cromer A, Wasylyk C, Schultz I, et al. Differential expression profiling of head and neck squamous cell carcinoma (HNSCC). *Br J Cancer* (2003) 89(10):1940–9. doi: 10.1038/sj.bjc.6601373
9. Stransky N, Egloff AM, Tward AD, Kostic AD, Cibulskis K, Sivachenko A, et al. The mutational landscape of head and neck squamous cell carcinoma. *Science* (2011) 333(6046):1157–60. doi: 10.1126/science.1208130
10. Emmert-Buck MR, Strausberg RL, Krizman DB, Bonaldo MF, Bonner RF, Bostwick DG, et al. Molecular profiling of clinical tissues specimens: feasibility and applications. *J Mol Diagn* (2000) 2(2):60–6. doi: 10.1016/s1525-1578(10)60617-4
11. Pollack JR, Perou CM, Alizadeh AA, Eisen MB, Pergamenschikov A, Williams CF, et al. Genome-wide analysis of DNA copy-number changes using cDNA microarrays. *Nat Genet* (1999) 23(1):41–6. doi: 10.1038/12640
12. Zhang L, Zhou W, Velculescu VE, Kern SE, Hruban RH, Hamilton SR, et al. Gene expression profiles in normal and cancer cells. *Science* (1997) 276(5316):1268–72. doi: 10.1126/science.276.5316.1268
13. Kuriakose MA, Chen WT, He ZM, Sikora AG, Zhang P, Zhang ZY, et al. Selection and validation of differentially expressed genes in head and neck cancer. *Cell Mol Life Sci* (2004) 61(11):1372–83. doi: 10.1007/s00018-004-4069-0
14. Irizarry RA, Bolstad BM, Collin F, Cope LM, Hobbs B, Speed TP. Summaries of Affymetrix GeneChip probe level data. *Nucleic Acids Res* (2003) 31(4):e15. doi: 10.1093/nar/gng015
15. Diboun I, Wernisch L, Orengo CA, Koltzenburg M. Microarray analysis after RNA amplification can detect pronounced differences in gene expression using limma. *BMC Genomics* (2006) 7:252. doi: 10.1186/1471-2164-7-252
16. Zou Y, Zhang M, Zeng D, Ruan Y, Shen L, Mu Z, et al. Periplaneta americana Extracts Accelerate Liver Regeneration a Complex Network of Pathways. *Front Pharmacol* (2020) 11:1174. doi: 10.3389/fphar.2020.01174
17. Babačić H, Lehtiö J, Pico de Coaña Y, Pernemalm M, Eriksson H. In-depth plasma proteomics reveals increase in circulating PD-1 during anti-PD-1 immunotherapy in patients with metastatic cutaneous melanoma. *J Immunother Cancer* (2020) 8(1). doi: 10.1136/jitc-2019-000204
18. Scardoni G, Petterlini M, Laudanna C. Analyzing biological network parameters with CentiScaPe. *Bioinformatics* (2009) 25(21):2857–9. doi: 10.1093/bioinformatics/btp517
19. Li T, Fan J, Wang B, Traugh N, Chen Q, Liu JS, et al. TIMER: A Web Server for Comprehensive Analysis of Tumor-Infiltrating Immune Cells. *Cancer Res* (2017) 77(21):e108–10. doi: 10.1158/0008-5472.CAN-17-0307
20. Pan JH, Zhou H, Cooper L, Huang JL, Zhu SB, Zhao XX, et al. LAYN Is a Prognostic Biomarker and Correlated With Immune Infiltrates in Gastric and Colon Cancers. *Front Immunol* (2019) 10:6. doi: 10.3389/fimmu.2019.00006
21. Engelman JA. Targeting PI3K signalling in cancer: opportunities, challenges and limitations. *Nat Rev Cancer* (2009) 9(8):550–62. doi: 10.1038/nrc2664
22. Kozaki K, Imoto I, Pimkhaokham A, Hasegawa S, Tsuda H, Omura K, et al. PIK3CA mutation is an oncogenic aberration at advanced stages of oral squamous cell carcinoma. *Cancer Sci* (2006) 97(12):1351–8. doi: 10.1111/j.1349-7006.2006.00343.x
23. Qiu W, Schonleben F, Li X, Ho DJ, Close LG, Manolidis S, et al. PIK3CA mutations in head and neck squamous cell carcinoma. *Clin Cancer Res* (2006) 12(5):1441–6. doi: 10.1158/1078-0432.CCR-05-2173
24. Murugan AK, Hong NT, Fukui Y, Munirajan AK, Tsuchida N. Oncogenic mutations of the PIK3CA gene in head and neck squamous cell carcinomas. *Int J Oncol* (2008) 32(1):101–11. doi: 10.3892/ijo.32.1.101
25. Hou W, Nemitz S, Schopper S, Nielsen ML, Kessels MM, Qualmann B. Arginine Methylation by PRMT2 Controls the Functions of the Actin Nucleator Cobl. *Dev Cell* (2018) 45(2):262–275 e8. doi: 10.1016/j.devcel.2018.03.007
26. Hou W, Izadi M, Nemitz S, Haag N, Kessels MM, Qualmann B. The Actin Nucleator Cobl Is Controlled by Calcium and Calmodulin. *PloS Biol* (2015) 13(9):e1002233. doi: 10.1371/journal.pbio.1002233
27. Schwintzer L, Koch N, Ahuja R, Grimm J, Kessels MM, Qualmann B. The functions of the actin nucleator Cobl in cellular morphogenesis critically depend on syndapin I. *EMBO J* (2011) 30(15):3147–59. doi: 10.1038/emboj.2011.207
28. Lopes BA, Meyer C, Barbosa TC, Poubel CP, Mansur MB, Duployez N, et al. IKZF1 Deletions with COBL Breakpoints Are Not Driven by RAG-Mediated Recombination Events in Acute Lymphoblastic Leukemia. *Transl Oncol* (2019) 12(5):726–32. doi: 10.1016/j.tranon.2019.02.002
29. Laneve P, Gioia U, Ragno R, Altieri F, Di Franco C, Santini T, et al. The tumor marker human placental protein 11 is an endoribonuclease. *J Biol Chem* (2008) 283(50):34712–9. doi: 10.1074/jbc.M805759200
30. Inaba N, Renk T, Daume E, Bohn H. Ectopic production of placenta-"specific" tissue proteins (PP5 and PP11) by malignant breast tumors. *Arch Gynecol* (1981) 231(1):87–90. doi: 10.1007/BF02110028
31. Inaba N, Renk T, Wurster K, Rapp W, Bohn H. Ectopic synthesis of pregnancy specific beta 1-glycoprotein (SP1) and placental specific tissue proteins (PP5, PP10, PP11, PP12) in nontrophoblastic malignant tumours. Possible markers in oncology. *Klin Wochenschr* (1980) 58(15):789–91. doi: 10.1007/BF01478287
32. Song L, Xie H, Tong F, Yan B, Zhang S, Fu E, et al. Association of lnc-IL17RA-11 with increased radiation sensitivity and improved prognosis of HPV-positive HNSCC. *J Cell Biochem* (2019) 120(10):17438–48. doi: 10.1002/jcb.29008
33. Partlova S, Boucek J, Kloudova K, Lukesova E, Zabrodsky M, Grega M, et al. Distinct patterns of intratumoral immune cell infiltrates in patients with HPV-associated compared to non-virally induced head and neck squamous cell carcinoma. *Oncoimmunology* (2015) 4(1):e965570. doi: 10.4161/21624011.2014.965570
34. Siegel RL, Miller KD, Jemal A. Cancer Statistics, 2017. *CA Cancer J Clin* (2017) 67(1):7–30. doi: 10.3322/caac.21387
35. Wicker C, Takiar V, Suganya R, Arnold S, Brill Y, Chen L, et al. Evaluation of antioxidant network proteins as novel prognostic biomarkers for head and neck cancer patients. *Oral Oncol* (2020) 111:104949. doi: 10.1016/j.oraloncology.2020.104949
36. Li W, Chen Y, Nie X. Regulatory Mechanisms of lncRNAs and Their Target Gene Signaling Pathways in Laryngeal Squamous Cell Carcinoma. *Front Pharmacol* (2020) 11:1140. doi: 10.3389/fphar.2020.01140
37. Koontongkaew S, Amornphimoltham P, Monthanpisut P, Saensuk T, Leelakriangsak M. Fibroblasts and extracellular matrix differently modulate MMP activation by primary and metastatic head and neck cancer cells. *Med Oncol* (2012) 29(2):690–703. doi: 10.1007/s12032-011-9871-6

38. Taitz A, Petruzzelli GJ, Lozano Y, Shankar R, Young MR. Bi-directional stimulation of adherence to extracellular matrix components by human head and neck squamous carcinoma cells and endothelial cells. *Cancer Lett* (1995) 96(2):253–60. doi: 10.1016/0304-3835(95)03939-T
39. Ge Y, Li W, Ni Q, He Y, Chu J, Wei P. Weighted Gene Co-Expression Network Analysis Identifies Hub Genes Associated with Occurrence and Prognosis of Oral Squamous Cell Carcinoma. *Med Sci Monit* (2019) 25:7272–88. doi: 10.12659/MSM.916025
40. Mendez E, Houck JR, Doody DR, Fan W, Lohavanichbutr P, Rue TC, et al. A genetic expression profile associated with oral cancer identifies a group of patients at high risk of poor survival. *Clin Cancer Res* (2009) 15(4):1353–61. doi: 10.1158/1078-0432.CCR-08-1816
41. Zhao L, Chi W, Cao H, Cui W, Meng W, Guo W, et al. Screening and clinical significance of tumor markers in head and neck squamous cell carcinoma through bioinformatics analysis. *Mol Med Rep* (2019) 19(1):143–54. doi: 10.3892/mmr.2018.9639
42. Arroyo-Solera I, Pavon MA, Leon X, Lopez M, Gallardo A, Cespedes MV, et al. Effect of serpinE1 overexpression on the primary tumor and lymph node, and lung metastases in head and neck squamous cell carcinoma. *Head Neck* (2019) 41(2):429–39. doi: 10.1002/hed.25437
43. Saleh AD, Cheng H, Martin SE, Si H, Ormanoglu P, Carlson S, et al. Integrated Genomic and Functional microRNA Analysis Identifies miR-30-5p as a Tumor Suppressor and Potential Therapeutic Nanomedicine in Head and Neck Cancer. *Clin Cancer Res* (2019) 25(9):2860–73. doi: 10.1158/1078-0432.CCR-18-0716
44. Yang K, Zhang S, Zhang D, Tao Q, Zhang T, Liu G, et al. Identification of SERPINE1, PLAU and ACTA1 as biomarkers of head and neck squamous cell carcinoma based on integrated bioinformatics analysis. *Int J Clin Oncol* (2019) 24(9):1030–41. doi: 10.1007/s10147-019-01435-9
45. Yamada Y, Koshizuka K, Hanazawa T, Kikkawa N, Okato A, Idichi T, et al. Passenger strand of miR-145-3p acts as a tumor-suppressor by targeting MYO1B in head and neck squamous cell carcinoma. *Int J Oncol* (2018) 52 (1):166–78. doi: 10.3892/ijo.2017.4190
46. Liu L, Jung SN, Oh C, Lee K, Won HR, Chang JW, et al. LAMB3 is associated with disease progression and cisplatin cytotoxic sensitivity in head and neck squamous cell carcinoma. *Eur J Surg Oncol* (2019) 45(3):359–65. doi: 10.1016/j.ejso.2018.10.543
47. Tam K, Schoppy DW, Shin JH, Tay JK, Moreno-Nieves U, Mundy DC, et al. Assessing the Impact of Targeting CEACAM1 in Head and Neck Squamous Cell Carcinoma. *Otolaryngol Head Neck Surg* (2018) 159(1):76–84. doi: 10.1177/0194599818756627
48. Bednarek K, Kostrzewska-Poczekaj M, Szaumkessel M, Kiwerska K, Paczkowska J, Byzia E, et al. Downregulation of CEACAM6 gene expression in laryngeal squamous cell carcinoma is an effect of DNA hypermethylation and correlates with disease progression. *Am J Cancer Res* (2018) 8(7):1249–61.
49. Cameron S, de Long LM, Hazar-Rethinam M, Topkas E, Endo-Munoz L, Cumming A, et al. Focal overexpression of CEACAM6 contributes to enhanced tumourigenesis in head and neck cancer via suppression of apoptosis. *Mol Cancer* (2012) 11:74. doi: 10.1186/1476-4598-11-74
50. Okazaki S, Shintani S, Hirata Y, Suina K, Semba T, Yamasaki J, et al. Synthetic lethality of the ALDH3A1 inhibitor dyclonine and xCT inhibitors in glutathione deficiency-resistant cancer cells. *Oncotarget* (2018) 9(73):33832–43. doi: 10.18632/oncotarget.26112
51. Lv Z, Wu K, Qin X, Yuan J, Yan M, Zhang J, et al. A Novel Tumor Suppressor SPINK5 Serves as an Independent Prognostic Predictor for Patients with Head and Neck Squamous Cell Carcinoma. *Cancer Manag Res* (2020) 12:4855–69. doi: 10.2147/CMAR.S236266
52. Delloye-Bourgeois C, Bertin L, Thoinet K, Jarrosson L, Kindbeiter K, Buffet T, et al. Microenvironment-Driven Shift of Cohesion/Detachment Balance within Tumors Induces a Switch toward Metastasis in Neuroblastoma. *Cancer Cell* (2017) 32(4):427–443 e8. doi: 10.1016/j.ccell.2017.09.006
53. Hintz HM, Gallant JP, Vander Griend DJ, Coleman IM, Nelson PS, LeBeau AM. Imaging Fibroblast Activation Protein Alpha Improves Diagnosis of Metastatic Prostate Cancer with Positron Emission Tomography. *Clin Cancer Res* (2020) 26(18):4882–91. doi: 10.1158/1078-0432.CCR-20-1358
54. Ogawa Y, Masugi Y, Abe T, Yamazaki K, Ueno A, Fujii-Nishimura Y, et al. Three distinct stroma types in human pancreatic cancer identified by image analysis of fibroblast subpopulations and collagen. *Clin Cancer Res* (2020). doi: 10.1158/1078-0432.CCR-20-2298
55. Hussain A, Voisin V, Poon S, Karamboulas C, Bui NHB, Meens J, et al. Distinct fibroblast functional states drive clinical outcomes in ovarian cancer and are regulated by TCF21. *J Exp Med* (2020) 217(8). doi: 10.1084/jem.20191094
56. Hua KT, Wang MY, Chen MW, Wei LH, Chen CK, Ko CH, et al. The H3K9 methyltransferase G9a is a marker of aggressive ovarian cancer that promotes peritoneal metastasis. *Mol Cancer* (2014) 13:189. doi: 10.1186/1476-4598-13-189
57. Jun F, Peng Z, Zhang Y, Shi D. Quantitative proteomic analysis identifies novel regulators of methotrexate resistance in choriocarcinoma. *Gynecol Oncol* (2020) 157(1):268–79. doi: 10.1016/j.ygyno.2020.01.013
58. Badr M, Johrens K, Allgauer M, Boxberg M, Weichert W, Tinhofer I, et al. Morphomolecular analysis of the immune tumor microenvironment in human head and neck cancer. *Cancer Immunol Immunother* (2019) 68 (9):1443–54. doi: 10.1007/s00262-019-02378-w
59. Chimote AA, Hajdu P, Sfyris AM, Gleich BN, Wise-Draper T, Casper KA, et al. Kv1.3 Channels Mark Functionally Competent CD8+ Tumor-Infiltrating Lymphocytes in Head and Neck Cancer. *Cancer Res* (2017) 77 (1):53–61. doi: 10.1158/0008-5472.CAN-16-2372
60. Tsujikawa T, Yaguchi T, Ohmura G, Ohta S, Kobayashi A, Kawamura N, et al. Autocrine and paracrine loops between cancer cells and macrophages promote lymph node metastasis via CCR4/CCL22 in head and neck squamous cell carcinoma. *Int J Cancer* (2013) 132(12):2755–66. doi: 10.1002/ijc.27966
61. Topf MC, Harshyne L, Tuluc M, Mardekian S, Vimawala S, Cognetti DM, et al. Loss of CD169(+) Subcapsular Macrophages during Metastatic Spread of Head and Neck Squamous Cell Carcinoma. *Otolaryngol Head Neck Surg* (2019) 161(1):67–73. doi: 10.1177/0194599819829741
62. She L, Qin Y, Wang J, Liu C, Zhu G, Li G, et al. Tumor-associated macrophages derived CCL18 promotes metastasis in squamous cell carcinoma of the head and neck. *Cancer Cell Int* (2018) 18:120. doi: 10.1186/s12935-018-0620-1
63. Balermpas P, Rodel F, Liberz R, Oppermann J, Wagenblast J, Ghanaati S, et al. Head and neck cancer relapse after chemoradiotherapy correlates with CD163 + macrophages in primary tumour and CD11b+ myeloid cells in recurrences. *Br J Cancer* (2014) 111(8):1509–18. doi: 10.1038/bjc.2014.446
64. Ooft ML, van Ipenburg JA, Sanders ME, Kranendonk M, Hofland I, de Bree R, et al. Prognostic role of tumour-associated macrophages and regulatory T cells in EBV-positive and EBV-negative nasopharyngeal carcinoma. *J Clin Pathol* (2018) 71(3):267–74. doi: 10.1136/jclinpath-2017-204664
65. Wang Y, Smith W, Hao D, He B, Kong L. M1 and M2 macrophage polarization and potentially therapeutic naturally occurring compounds. *Int Immunopharmacol* (2019) 70:459–66. doi: 10.1016/j.intimp.2019.02.050
66. Yuan A, Hsiao YJ, Chen HY, Chen HW, Ho CC, Chen YY, et al. Opposite Effects of M1 and M2 Macrophage Subtypes on Lung Cancer Progression. *Sci Rep* (2015) 5:14273. doi: 10.1038/srep14273
67. Huang H, Liu X, Zhao F, Lu J, Zhang B, Peng X, et al. M2-polarized tumour-associated macrophages in stroma correlate with poor prognosis and Epstein-Barr viral infection in nasopharyngeal carcinoma. *Acta Otolaryngol* (2017) 137(8):888–94. doi: 10.1080/00016489.2017.1296585
68. Hsieh CH, Tai SK, Yang MH. Snail-overexpressing Cancer Cells Promote M2-Like Polarization of Tumor-Associated Macrophages by Delivering MiR-21-Abundant Exosomes. *Neoplasia* (2018) 20(8):775–88. doi: 10.1016/j.neo.2018.06.004
69. Ohashi T, Aoki M, Tomita H, Akazawa T, Sato K, Kuze B, et al. M2-like macrophage polarization in high lactic acid-producing head and neck cancer. *Cancer Sci* (2017) 108(6):1128–34. doi: 10.1111/cas.13244

Conflict of Interest: The authors declare that the research was conducted in the absence of any commercial or financial relationships that could be construed as a potential conflict of interest.

Advantages of publishing in Frontiers

OPEN ACCESS
Articles are free to read for greatest visibility and readership

FAST PUBLICATION
Around 90 days from submission to decision

HIGH QUALITY PEER-REVIEW
Rigorous, collaborative, and constructive peer-review

TRANSPARENT PEER-REVIEW
Editors and reviewers acknowledged by name on published articles

Frontiers
Avenue du Tribunal-Fédéral 34
1005 Lausanne | Switzerland

Visit us: www.frontiersin.org
Contact us: frontiersin.org/about/contact

REPRODUCIBILITY OF RESEARCH
Support open data and methods to enhance research reproducibility

DIGITAL PUBLISHING
Articles designed for optimal readership across devices

FOLLOW US
@frontiersin

IMPACT METRICS
Advanced article metrics track visibility across digital media

EXTENSIVE PROMOTION
Marketing and promotion of impactful research

LOOP RESEARCH NETWORK
Our network increases your article's readership